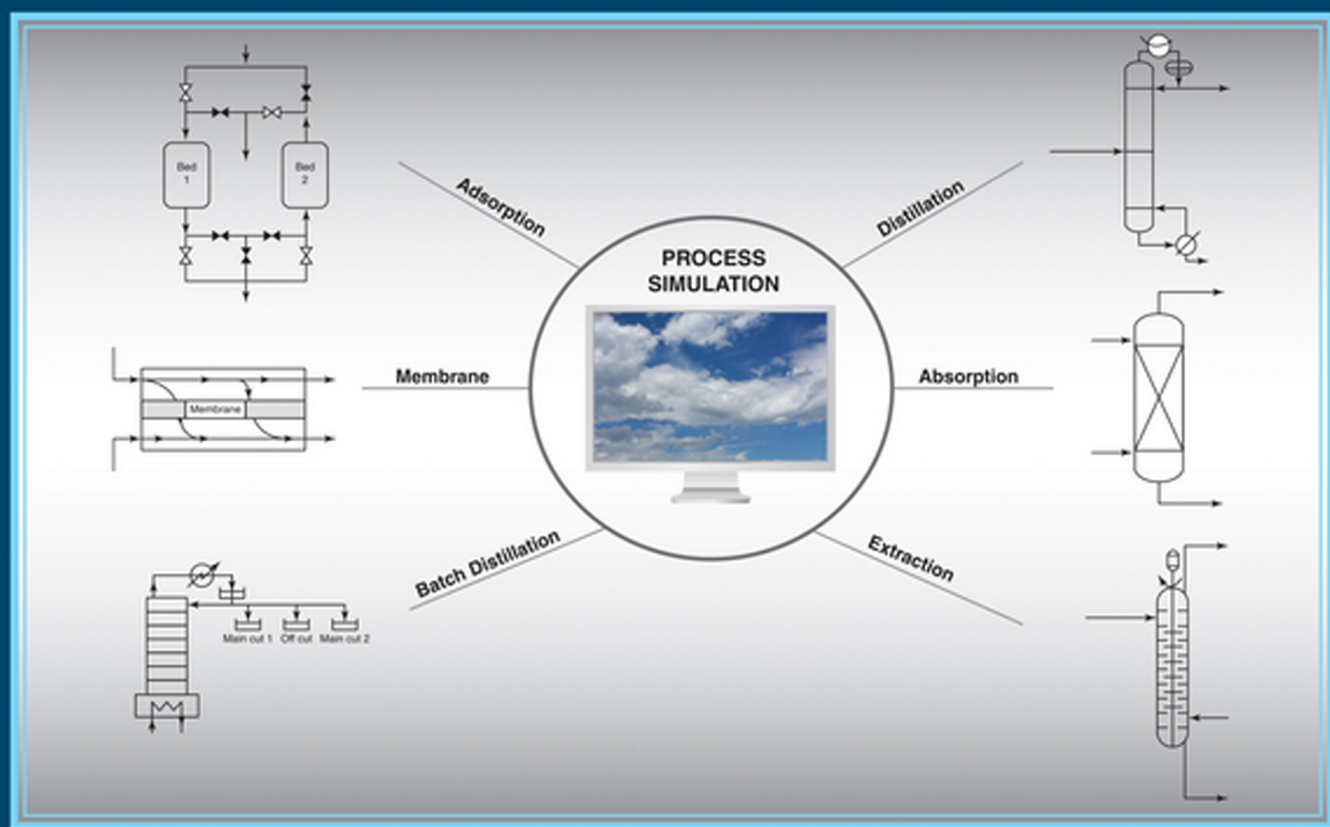


SEPARATION PROCESS PRINCIPLES

with Applications Using Process Simulators

FOURTH EDITION



SEADER • HENLEY • ROPER

WILEY

Factors for Converting AE and CGS Units to SI Units

To convert from	To	Multiply by
Area		
ft ²	m ²	0.0929
in ²	m ²	6.452 × 10 ⁻⁴
Acceleration		
ft/h ²	m/s ²	2.352 × 10 ⁻⁸
Density		
lb _m /ft ³	kg/m ³	16.02
lb _m /gal (US)	kg/m ³	119.8
g/cm ³	kg/m ³ = g/L	1000
Diffusivity, Kinematic Viscosity		
ft ² /h	m ² /s	2.581 × 10 ⁻⁵
cm ² /s	m ² /s	1 × 10 ⁻⁴
Energy, Work, Heat		
ft-lb _f	J	1.356
Btu (IT)	J	1055
cal (IT)	J	4.187
erg	J	1 × 10 ⁻⁷
kW-h	J	3.6 × 10 ⁶
Enthalpy		
Btu (IT)/lb _m	J/kg	2326
cal (IT)/g	J/kg	4187
Force		
lb _f	N	4.448
dyne	N	1 × 10 ⁻⁵
Heat-Transfer Coefficient		
Btu (IT)/h-ft ² -°F	W/m ² -K	5.679
cal (IT)/s-cm ² -°C	W/m ² -K	4.187 × 10 ⁻⁴
Interfacial Tension		
lb _f /ft	kg/s ²	14.59
dyne/cm	kg/s ²	1 × 10 ⁻⁴
Length		
ft	m	0.3048
in	m	0.0254
Mass		
lb _m	kg	0.4536
ton	kg	907.2
tonne (metric ton)	kg	1000

To convert from	To	Multiply by
Mass Flow Rate		
lb _m /h	kg/s	1.26×10^{-4}
lb _m /s	kg/s	0.4536
Mass Flux, Mass Velocity		
lb _m /h-ft ²	kg/s-m ²	1.356×10^{-3}
Power		
ft-lb _f /h	W = J/s	3.766×10^{-4}
ft-lb _f	W = J/s	1.356
hp	W = J/s	745.7
Btu (IT)/h	W = J/s	0.2931
Pressure		
lb _f /ft ²	Pa	47.88
lb _f /in ²	Pa	6895
atm	Pa	1.013×10^5
Bar	Pa	1×10^5
torr = mmHg	Pa	133.3
in Hg	Pa	3386
in H ₂ O	Pa	249.1
Specific Heat		
Btu (IT)/lb _m -°F	J/kg-K	4187
cal/g-°C	J/kg-K	4187
Surface Tension		
lb _f /ft	N/m	14.59
dyne/cm	N/m	0.001
erg/cm ²	N/m	0.001
Thermal Conductivity		
Btu (IT)-ft/h-ft ² -°F	W/m-K = J/s-m-K	1.731
cal (IT)-cm/s-cm ² -°C	W/m-K = J/s-m-K	418.7
Velocity		
ft/h	m/s	8.467×10^{-5}
ft/s	m/s	0.3048
Viscosity		
lb _m /ft-s	kg/m-s	1.488
lb _m /ft-h	kg/m-s	4.134×10^{-4}
cP	kg/m-s	0.001
Volume		
ft ³	kg/m-s	0.001
ft ³	m ³	0.02832
L	m ³	1×10^{-3}
gal (US)	m ³	3.785×10^{-3}

SEPARATION PROCESS PRINCIPLES

with Applications Using Process Simulators

FOURTH EDITION

J. D. Seader

*Department of Chemical Engineering
University of Utah*

Ernest J. Henley

*Department of Chemical Engineering
University of Houston*

D. Keith Roper

*Ralph E. Martin Department of Chemical Engineering
University of Arkansas*

WILEY

VICE PRESIDENT & DIRECTOR	Laurie Rosatone
SENIOR DIRECTOR	Don Fowley
EXECUTIVE EDITOR	Linda Ratts
SPONSORING EDITOR	Mary O'Sullivan
ASSISTANT DEVELOPMENT EDITOR	Adria Giattino
SENIOR ASSISTANT	Courtney Jordan
FREELANCE PROJECT MANAGER	Ellen Keohane
PROJECT SPECIALIST	Nichole Urban
FREELANCE PROJECT ASSISTANT	Anna Melhorn
EXECUTIVE MARKETING MANAGER	Daniel Sayre
ASSISTANT MARKETING MANAGER	Puja Katariwala
ASSOCIATE DIRECTOR	Kevin Holm
SENIOR CONTENT SPECIALIST	Nicole Repasky
PRODUCTION EDITOR	Linda Christina E
PHOTO RESEARCHER	Mary Ann Price
COVER PHOTO CREDIT	Courtesy J.D. Seader

This book was set in 10/12 Times LT Std Roman by SPi Global and printed and bound by Lightning Source Inc.

Founded in 1807, John Wiley & Sons, Inc. has been a valued source of knowledge and understanding for more than 200 years, helping people around the world meet their needs and fulfill their aspirations. Our company is built on a foundation of principles that include responsibility to the communities we serve and where we live and work.

In 2008, we launched a Corporate Citizenship Initiative, a global effort to address the environmental, social, economic, and ethical challenges we face in our business. Among the issues we are addressing are carbon impact, paper specifications and procurement, ethical conduct within our business and among our vendors, and community and charitable support. For more information, please visit our website: www.wiley.com/go/citizenship.

Copyright © 2016, 2011, 2006, 1998 John Wiley & Sons, Inc. All rights reserved. No part of this publication may be reproduced, stored in a retrieval system or transmitted in any form or by any means, electronic, mechanical, photocopying, recording, scanning or otherwise, except as permitted under Sections 107 or 108 of the 1976 United States Copyright Act, without either the prior written permission of the Publisher, or authorization through payment of the appropriate per-copy fee to the Copyright Clearance Center, Inc. 222 Rosewood Drive, Danvers, MA 01923, website www.copyright.com. Requests to the Publisher for permission should be addressed to the Permissions Department, John Wiley & Sons, Inc., 111 River Street, Hoboken, NJ 07030-5774, (201)748-6011, fax (201)748-6008, website <http://www.wiley.com/go/permissions>.

Evaluation copies are provided to qualified academics and professionals for review purposes only, for use in their courses during the next academic year. These copies are licensed and may not be sold or transferred to a third party. Upon completion of the review period, please return the evaluation copy to Wiley. Return instructions and a free of charge return shipping label are available at www.wiley.com/go/returnlabel. Outside of the United States, please contact your local representative.

ISBN: 978-1-119-23959-8 (PBK)
ISBN: 978-1-119-22412-9 (EVALC)

Library of Congress Cataloging-in-Publication Data

Names: Seader, J. D. | Henley, Ernest J. | Roper, D. Keith.
Title: Separation process principles with applications using process simulators / J.D. Seader, Department of Chemical Engineering, University of Utah, Ernest J. Henley, Department of Chemical Engineering, University of Houston, D. Keith Roper, Ralph E. Martin Department of Chemical Engineering, University of Arkansas.
Description: Fourth edition. | Hoboken, NJ : John Wiley & Sons, Inc., 2016. | Includes bibliographical references and index.
Identifiers: LCCN 2015021981 (print) | LCCN 2015022980 (ebook) | ISBN 9781119239598 (pbk.) | ISBN 9781119141303 (pdf) | ISBN 9781119141297 (epub)
Subjects: LCSH: Separation (Technology)—Textbooks.
Classification: LCC TP156.S45 S364 2016 (print) | LCC TP156.S45 (ebook) | DDC 660/.2842—dc23
LC record available at <http://lcn.loc.gov/2015021981>

Printing identification and country of origin will either be included on this page and/or the end of the book. In addition, if the ISBN on this page and the back cover do not match, the ISBN on the back cover should be considered the correct ISBN.

Printed in the United States of America

10 9 8 7 6 5 4 3 2 1

About the Authors

J. D. Seader is Professor Emeritus of Chemical Engineering at the University of Utah. He received B.S. (*summa cum laude*) and M.S. degrees from the University of California at Berkeley and a Ph.D. from the University of Wisconsin–Madison. From 1952 to 1959, he worked for Chevron Research in Richmond, California, where he designed petroleum and petrochemical processes and supervised engineering research, including the development of one of the first computer-aided process simulation programs and the first widely used vapor-liquid equilibrium correlation. From 1959 to 1965, he conducted rocket engine research on all of the engines that took man to the moon for the Rocketdyne Division of North American Aviation in Canoga Park, California. Before joining the faculty at the University of Utah, where he served for 37 years from 1966 until 2003, he was a professor at the University of Idaho. He has authored or coauthored 111 technical articles, nine books, and four patents and also coauthored the section on distillation in the sixth and seventh editions of *Perry's Chemical Engineers' Handbook*. His co-authored textbooks include *FLOWTRAN Simulation—An Introduction* in three editions; *Equilibrium-Stage Separation Operations in Chemical Engineering, Product & Process Design Principles* in four editions; and the previous three editions of *Separation Process Principles*. He was a founding member and trustee of CACHE for 33 years, serving as executive officer from 1980 to 1984. From 1975 to 1978, he served as chairman of the Chemical Engineering Department at the University of Utah. For 20 years, he directed the use and distribution of Monsanto's FLOWTRAN process simulation computer program to 190 chemical engineering departments worldwide, helping to usher in the addition of instruction in computer-aided process design to the chemical engineering curriculum. For 12 years, he served as an associate editor of the journal *Industrial and Engineering Chemistry Research*. He served as a director of AIChE from 1983 to 1985. In 1983, he presented the 35th Annual Institute Lecture of AIChE; in 1988, he received the Computing in Chemical Engineering Award of the CAST Division of AIChE; in 2004, he received the CACHE Award for Excellence in Chemical Engineering Education from the ASEE; and in 2004 he was a co-recipient, with Professor Warren D. Seider, of the Warren K. Lewis Award for Chemical Engineering Education of the AIChE. In 2008, as part of the AIChE Centennial Celebration, he was named one of 30 authors of groundbreaking chemical engineering books.

Ernest J. Henley is Professor of Chemical Engineering at the University of Houston. He received his B.S. degree from the University of Delaware and his Dr. Eng. Sci. from Columbia University, where he served as a professor from 1953 to 1959. Henley also has held professorships at the Stevens Institute of Technology, the University of Brazil, Stanford University, Cambridge University, and the City University of New York. He has authored or coauthored 72 technical articles and 17 books. For 17 years, he was a trustee of CACHE, serving as president from 1975 to 1976 and directing the efforts that produced the seven-volume set of *Computer Programs for Chemical Engineering Education* and the five-volume set, *AIChE Modular Instruction*. An active consultant, Henley holds nine patents and has served on the Board of Directors of 12 industrial corporations and three philanthropies. In 1998, he received the McGraw-Hill Company Award for “Outstanding Personal Achievement in Chemical Engineering” and in 2002, received the CACHE Award of the ASEE for “recognition of his contribution to the use of computers in chemical engineering education.” He is president of the Henley Foundation and his biography appears in *Who's Who in America* and *Who's Who in the World*.

D. Keith Roper is the Charles W. Oxford Professor of Emerging Technologies in the Ralph E. Martin Department of Chemical Engineering at the University of Arkansas. He is also Program Leader for the Engineering Research Centers and Network for Computational Nanotechnology at the National Science Foundation. He received a B.S. degree (*magna cum laude*) from Brigham Young University in 1989 and a Ph.D. from the University of Wisconsin–Madison in 1994. He developed processes for cell culture, fermentation, biorecovery, and analysis of polysaccharide, protein, DNA, and adenoviral-vectored antigens at Merck & Co. (West Point, PA); extraction of photodynamic cancer therapeutics at Frontier Scientific, Inc. (Logan, UT); and virus binding methods for Millipore Corp (Billerica, MA). Previously, he held faculty appointments in chemical engineering and materials science and engineering at the University of Utah. From 2010 to 2013, he served as Assistant Director of the Microelectronics-Photonics graduate program at the University of Arkansas. From 2012 to 2014, he served as Program Director in the Education Engineering and Centers Division at the National Science Foundation. He is an active consultant with industries in biotechnology, biopharmaceuticals,

chemicals, optoelectronics, and energy as well as with universities in translating discovery to disruptive innovation through university–industry partnerships. He has authored or coauthored more than 65 technical articles, one book, two book chapters, three U.S. patents, and six U.S. patent applications. He was instrumental in developing one viral and three bacterial vaccine products, 16 Good Manufacturing Process documents, and multiple bioprocess equipment designs. He is a fellow of the American Institute for Medical and

Biological Engineering and a member of the Arkansas Academy of Science. He holds memberships in Tau Beta Pi, ASEE, ACS, SPIE, and AIChE. His research examines electrodynamics in biochemical and nano-optical material systems important to advanced biomanufacturing, biomedicine, optoelectronics, and sustainable energy, with recent advances in computation, nanolithography, spectroscopy, and electron microscopy of nanoplasmonic metamaterials and polymer thin films.

Preface to the Fourth Edition

INTRODUCTION

Separation Process Principles was first published in 1988 to provide a rigorous and comprehensive treatment of industrial separation processes in the form of a student-friendly textbook format. Both equilibrium-stage and mass-transfer (rate-based) models were covered. Included also were chapters on thermodynamic and mass-transfer theory for separation operations. Five of the 15 chapters began with an example of an industrial separation process and descriptions of how and why modern process design techniques evolved. The 2006 second edition expanded the coverage of mass-transfer-based design methods by adding three new chapters (16, 17, and 18) covering leaching, washing, crystallization, desublimation, evaporation, and drying of solids. In the 2011 third edition, the content was enlarged to include approximately 175 pages on biochemical separations as well as a new Chapter 19 covering mechanical phase separations such as filtration and centrifugation. The title of the third edition, *Separation Process Principles—Chemical and Biochemical Operations*, reflected this expansion.

This new condensed fourth edition focuses on material widely taught in undergraduate separations courses and on process simulations using Aspen Plus, CHEMCAD, and ChemSep to design separation operations. Hence, the new title for the fourth edition: *Separation Process Principles—with Applications Using Process Simulators*. Professor Seader began using process simulation programs in 1957 while engaged in process design in the petroleum industry and was the AIChE Institute Lecturer on this subject in 1984. Professor Henley founded what is now Chemstations and was its first president (when it was named COADE). Professor Roper introduced simulation to vaccine process development in 1997. Authors of this fourth edition believe that students who learn to solve separation problems with process simulators as juniors will be well prepared to tackle difficult process design problems in their senior year. The fourth edition provides comparisons of features of process simulators as well as examples of how they are used to solve industrial-level design problems.

Much of the material removed from the third edition—biochemical separation process principles in: sections of Chapters 1, 2, 3, 8, 14, and 15; Chapters 16, 17, and 18, and Chapter 19 on mechanical phase separations—is being prepared by the authors for inclusion in a volume devoted to bioseparation operations. Meanwhile, this content will remain available from the publisher in the third edition.

STUDENT-FRIENDLY FEATURES

Each chapter begins by stating an average of nine instructional objectives to give the student an introduction to the author's expectations. In chapters that introduce separation technology, this is followed by a flow sheet and description of an industrial process to demonstrate how the technology is used to create saleable products. The theory needed to design equipment or simulate a separation operation is developed and applications are demonstrated by more than 200 examples, many of which make use of process simulators.

Each chapter ends with study questions suitable for class discussion (the inverted classroom) or qualitative examination questions. There are more than 600 homework exercises, many of which require the use of a process simulator. Other examples and exercises involve nonlinear equations with recommendations for using Matlab to solve them. In preparation of the fourth edition, text was clarified based on student feedback, and errors were eliminated. Following a suggestion by some reviewers, chapter-specific nomenclature sections have been added. A general nomenclature lists symbols common to many of the chapters. Each chapter-specific nomenclature keys symbols to equations, figures, or chapter sections. These revisions in the fourth edition reflect our desire to prepare an accessible introduction to chemical separations that includes the methods and equations used by process simulators and the problems and opportunities this has created.

TOPICAL ORGANIZATION

Chapter 1 provides the student with a classification of separation operations and an overview of industrial chemical engineering separations. The next two chapters review thermodynamics and mass transfer, as applied to separation operations, at a level consistent with the level of this book. Chapter 4, which introduces design specifications, and equilibrium flash calculations are a prerequisite for all subsequent chapters. Chapter 5, which is also a prerequisite for all subsequent chapters, extends the single-stage concept to multiple-equilibrium-stage processing units, including a degrees-of-freedom analysis for determining the number of design variables that can be specified for a given separation process. A further prerequisite is Chapter 6, which describes trays and packing, introduces general graphical methods, stage efficiencies, and a transfer unit design method for packed units.

Once the contents of the first six chapters have been mastered, the subsequent chapters can be studied in any order preferred by the reader or the instructor, with a few exceptions: (1) Concepts of minimum stage and minimum reflux are mentioned early in the text, but a quantitative elaboration, using McCabe–Thiele diagrams, resides in Section 7.2. McCabe–Thiele diagrams are used in three other chapters to help readers visualize concepts such as pinch points. (2) Unique technology such as Freundlich and Langmuir isotherms is fully developed in Chapter 15 but applied earlier. (3) Mathematical tools such as solution methods for stiff differential equations and the Newton–Raphson method for solving nonlinear algebraic equations are described where applied. In these three instances, the reader is referred to a book section where the technique is fully developed.

To help students obtain an awareness of a section's complexity, section titles listed in the table of contents include the following symbols as prefixes:

- * Important for a basic understanding of separations and therefore recommended for presentation in class, unless already covered in a previous course.
- Optional because the material is descriptive, probably covered in a previous course, or can be read outside of class with little or no discussion in class.
- Advanced material suitable for an undergraduate course if students are familiar with, and have access to, a process simulator.

NEW TO THIS EDITION

The focus on using process simulators to design separation processes required some rearrangement and revision of Chapters 1, 2, and 4–13, which deal with operations covered in process simulators. Many of the examples and exercises have been revised and new ones added. Some chapters contain correlations that stretch the state of the art. Chapter 7, for example, develops an improved method for obtaining plate efficiencies for sieve-tray columns that is just beginning to appear in process simulators.

HELPFUL WEBSITES In the 1980s, local computer networks began to interconnect in a global system, called the Internet. In late 1990, Tim Berners-Lee at the European Organization for Nuclear Research (CERN), Switzerland, completed all the tools required for sharing information over the Internet. This included the HyperText Transfer Protocol (HTTP), the HyperText Markup Language (HTML), and a document-information system called the World Wide Web (WWW). In early 1991, the first-known web page was sent over the internet by Lee to Paul Jones of UNC-Chapel Hill. Physicists around the world could now quickly and efficiently share data. Later that year, the WWW became available to the public, but its popularity was restrained until the release of the Mosaic web browser in December 1992. Today the

combination of a web browser (e.g., Chrome, Firefox, and Internet Explorer) and a general search engine (e.g., Google, Yahoo, Bing, and Ask) has made it so simple to search for information that the number of internet users has increased from about 400 million in 2000 to almost 3 billion (compared to a world population of 7.2 billion) in 2014.

Some useful websites for the study of separation processes are presented in chapters of this book. However, such websites are sometimes removed from the Internet. Readers of this book are encouraged to conduct their own searches by using key words. Many subjects have articles in the Wikipedia, a free, open-ended encyclopedia on the internet. An initial search, where the word “wiki” is added to the key word(s) is often useful. For example, if the key words “distillation wiki” are entered in the Google search engine, a 13-page article appears that provides excellent background material on a wide spectrum of the subject.

The 15 most-used websites are:

Search engines (Google, Yahoo, Bing, and Ask)

Social networking websites (Facebook, Twitter, Instagram, LinkedIn, and Pinterest)

News, Entertainment, Purchases, and Information (YouTube, Amazon, eBay, MSN)

Blog creation (WordPress)

Students using this book are encouraged to communicate with each other and their instructors via social networking websites to enhance their learning of separation processes.

RESOURCES FOR INSTRUCTORS

The website www.wiley.com/college/seader furnishes the following resources in the Instructor Companion Site:

1. Instructor's Solution Manual
2. Resources for Instructors-An introduction
3. Image Gallery
4. PowerPoint slides
5. Sample Preliminary Examination
6. Suggestions for Completing Homework Exercise
7. Suggested Review of Prerequisite Material

Instructors adopting this book must request a password from their Wiley sales representative.

RESOURCES FOR STUDENTS

Students are encouraged to consult www.wiley.com/college/seader for the following resources in the Student Companion Site:

1. Suggestions for Completing HW Exercises
2. Suggested Review of Prerequisite Material

ACKNOWLEDGEMENTS

Since publication of the 3rd edition of this book, the authors have received valuable comments, corrections, and suggestions from Professor Phillip R. Westmoreland of North Carolina University, Professor Shuguang Deng of New Mexico State University, Professor Daniel E. Rosner of Yale University, and particularly Professor N. Lawrence Ricker of the University of Washington.

The selection of the content for the 4th edition was greatly influenced by the responses of reviewers to two surveys conducted by Wiley.

Dr. D. Keith Roper is currently on intergovernmental personnel assignment with the National Science Foundation. Any opinions, findings, and conclusions or recommendations expressed in this book are those of the authors and do not necessarily reflect the views of the National Science Foundation.

J. D. Seader
Ernest J. Henley
D. Keith Roper

Contents

About the Authors iii

Preface to the Fourth Edition v

General Nomenclature xiii

Dimensions and Units xvii

1. Separation Processes 1

- 1.0* Instructional Objectives 1
- 1.1* Industrial Chemical Processes 1
- 1.2* Basic Separation Techniques 3
- 1.3° Separations by Phase Creation 4
- 1.4° Separations by Phase Addition 6
- 1.5° Separations by Barrier 7
- 1.6° Separations by an External Field or Gradient 7
- 1.7* Brief Comparison of Common Separation Operations 8
- 1.8* Separation Processes, Product Purity, Component Recovery, and Separation Sequences 9
Summary, References, Study Questions, Exercises

2. Thermodynamics of Separation Operations 16

- 2.0* Instructional Objectives 16
- 2.1* Phase Equilibria 16
- 2.2* Ideal-Gas, Ideal-Liquid-Solution Model 20
- 2.3° Graphical Representation of Thermodynamic Properties 21
- 2.4° Nonideal Thermodynamic Property Models 23
- 2.5° P - v - T Equation-of-State (EOS) Models 23
- 2.6° Highly Nonideal Liquid Solutions 27
- 2.7° Gibbs Excess Free-Energy (g^E) Models 29
- 2.8° Predictive Models 34
- 2.9° Electrolyte Solution Models 36
- 2.10° Polymer Solution Models 36
- 2.11* K -Value Methods in Process Simulators 36
- 2.12* Exergy and Second-Law Analysis 37
Nomenclature, Summary, References, Study Questions, Exercises

3. Mass Transfer and Diffusion 46

- 3.0* Instructional Objectives 46
- 3.1* Steady-State, Ordinary Molecular Diffusion 47
- 3.2* Diffusion Coefficients (Diffusivities) 51
- 3.3* Steady-State and Unsteady-State Mass Transfer Through Stationary Media 58
- 3.4* Mass Transfer in Laminar Flow 60
- 3.5* Mass Transfer in Turbulent Flow 68
- 3.6* Models for Mass Transfer in Fluids with a Fluid–Fluid Interface 73
- 3.7* Two-Film Theory and Overall Mass-Transfer Coefficients 76
Nomenclature, Summary, References, Study Questions, Exercises

4. Single Equilibrium Stages and Flash Calculations 87

- 4.0* Instructional Objectives 87
- 4.1* Gibbs' Phase Rule and Degrees of Freedom 88
- 4.2* Binary Vapor–Liquid Systems at Equilibrium 89
- 4.3* Equilibrium Two-Phase Flash Calculations 93
- 4.4* Ternary Liquid–Liquid Systems at Equilibrium 97
- 4.5° Multicomponent Liquid–Liquid Systems 101
- 4.6* Liquid–Solid Systems 102
- 4.7* Gas–Liquid Systems 104
- 4.8* Gas–Solid Systems 105
- 4.9• Three-Phase Equilibrium Systems 107
Nomenclature, Summary, References, Study Questions, Exercises

5. Multistage Cascades and Hybrid Systems 118

- 5.0* Instructional Objectives 118
- 5.1* Cascade Configurations 118
- 5.2* Single-Section Liquid–Liquid Extraction Cascades 119

- 5.3* Two-Section Distillation Cascades 121
- 5.4° Membrane Cascades 123
- 5.5° Hybrid Systems 125
- 5.6* Degrees of Freedom and Specifications for Cascades 125
Nomenclature, Summary, References, Study Questions, Exercises
- 6. Absorption and Stripping 137**
 - 6.0* Instructional Objectives 137
 - 6.1° Equipment for Vapor–Liquid Separations 138
 - 6.2° General Design Considerations 143
 - 6.3* Graphical Method for Trayed Towers 144
 - 6.4* Kremser Group Method for Multicomponent Absorption and Stripping 148
 - 6.5* Stage Efficiency and Column Height for Trayed Columns 154
 - 6.6* Flooding, Column Diameter, and Tray Layout for Trayed Columns 161
 - 6.7* Rate-Based Method for Packed Columns 164
 - 6.8* Packed-Column Liquid Holdup, Diameter, Flooding, Pressure Drop, and Mass-Transfer Efficiency 169
 - 6.9• Reactive (Chemical) Absorption 180
Nomenclature, Summary, References, Study Questions, Exercises
- 7. Distillation of Binary Mixtures 191**
 - 7.0* Instructional Objectives 191
 - 7.1° Equipment and Design Considerations 193
 - 7.2* McCabe–Thiele Graphical Method for Trayed Towers 193
 - 7.3° Extensions of the McCabe–Thiele Method 203
 - 7.4* Estimation of Tray Efficiency for Distillation 208
 - 7.5* Column and Reflux-Drum Diameters 215
 - 7.6* Rate-Based Method for Packed Distillation Columns 216
Nomenclature, Summary, References, Study Questions, Exercises
- 8. Liquid–Liquid Extraction with Ternary Systems 231**
 - 8.0* Instructional Objectives 231
 - 8.1° Equipment for Solvent Extraction 233
 - 8.2° General Design Considerations 239
 - 8.3* Hunter–Nash Graphical Equilibrium-Stage Method 243
 - 8.4° Theory and Scale-Up of Extractor Performance 252
Nomenclature, Summary, References, Study Questions, Exercises
- 9. Approximate Methods for Multicomponent Distillation 267**
 - 9.0* Instructional Objectives 267
 - 9.1* Fenske–Underwood–Gilliland (FUG) Method 267
 - 9.2* Using the Shortcut (FUG) Method with Process Simulators 279
Nomenclature, Summary, References, Study Questions, Exercises
- 10. Equilibrium-Based Methods for Multicomponent Absorption, Stripping, Distillation, and Extraction 284**
 - 10.0* Instructional Objectives 284
 - 10.1* Simple Model for a Vapor–Liquid Equilibrium Stage 284
 - 10.2• Evolution of Methods for Solving the Mesh Equations 286
 - 10.3* Strategies for Applying Process-Simulator Methods 287
 - 10.4* Main Mathematical Procedures 291
 - 10.5* Bubble-Point (BP) and Sum-Rates (SR) Methods 294
 - 10.6* Simultaneous-Correction Method 297
 - 10.7* Inside-Out Method 304
 - 10.8• Rigorous Methods for Liquid–Liquid Extraction 309
Nomenclature, Summary, References, Study Questions, Exercises
- 11. Enhanced Distillation and Supercritical Extraction 320**
 - 11.0* Instructional Objectives 320
 - 11.1* Use of Triangular Graphs 321
 - 11.2* Extractive Distillation 332
 - 11.3• Salt Distillation 335
 - 11.4• Pressure-Swing Distillation 337
 - 11.5• Homogeneous Azeotropic Distillation 339
 - 11.6* Heterogeneous Azeotropic Distillation 343

- 11.7• Reactive Distillation 352
- 11.8• Supercritical-Fluid Extraction 357
Nomenclature, Summary, References, Study
Questions, Exercises
- 12. Rate-Based Models for Vapor–Liquid Separation
Operations 368**
- 12.0• Instructional Objectives 368
- 12.1• Rate-Based Model 370
- 12.2• Thermodynamic Properties and Transport-Rate
Expressions 372
- 12.3• Methods for Estimating Transport Coefficients
and Interfacial Area 375
- 12.4• Vapor and Liquid Flow Patterns 375
- 12.5• Method of Calculation 376
Nomenclature, Summary, References, Study
Questions, Exercises
- 13. Batch Distillation 385**
- 13.0* Instructional Objectives 385
- 13.1* Differential Distillation 385
- 13.2* Binary Batch Rectification 388
- 13.3• Batch Stripping and Complex Batch
Distillation 390
- 13.4• Effect of Liquid Holdup 391
- 13.5* Stage-by-Stage Methods for Batch
Rectification 391
- 13.6* Intermediate-Cut Strategy 400
- 13.7• Optimal Control by Variation of Reflux
Ratio 401
Nomenclature, Summary, References, Study
Questions, Exercises
- 14. Membrane Separations 408**
- 14.0* Instructional Objectives 408
- 14.1° Membrane Materials 410
- 14.2° Membrane Modules 414
- 14.3* Mass Transfer in Membranes 416
- 14.4* Dialysis 430
- 14.5° Electrodialysis 432
- 14.6* Reverse Osmosis 434
- 14.7* Gas Permeation 438
- 14.8° Pervaporation 441
Nomenclature, Summary, References, Study
Questions, Exercises
- 15. Adsorption, Ion Exchange, and
Chromatography 451**
- 15.0* Instructional Objectives 451
- 15.1* Sorbents 453
- 15.2* Equilibrium Considerations 461
- 15.3* Kinetic and Transport Rate
Considerations 470
- 15.4° Equipment for Sorption Operations 475
- 15.5* Slurry and Fixed-Bed Adsorption
Systems 479
- 15.6* Continuous, Countercurrent Adsorption
Systems 494
- 15.7° Ion-Exchange Cycle 502
- 15.8* Chromatographic Separations 503
Nomenclature, Summary, References, Study
Questions, Exercises
- Answers to Selected Exercises 519**
- Index 521**

*Suitable for an UG course

°Optional

•Advanced

General Nomenclature

All symbols are defined in the text where they first appear.

The list below contains only those symbols that are common to two or more chapters.

Other symbols are listed in chapter-specific nomenclatures at the end of each chapter.

Abbreviations and Acronyms

BWR	Benedict–Webb–Rubin EOS, §2.5
CSTR	completely stirred tank or reactor, §3.6.3
CW (cw)	cooling water, Figure 2.11
DAE	differential-algebraic equations, §13.5.2
DDB	Dortmund data bank, §2.5.3
DDBST	DDB software package, §2.5.3
DECHEMA	data bank, §2.5.3
EM	equimolar diffusion, Table 6.5
EOS	equation of state (P - v - T relationship), §2.2
ESA	energy-separation agent, Table 1.1
FUG	Fenske–Underwood–Gilliland method, §9.1
HEPT	height equivalent to a theoretical plate, (6-68)
HETS	height equivalent to a theoretical stage, (6-68)
HHK	heavier than the heavy key, Figure 9.6
HK	heavy key, §9.1
HTU	height of a transfer unit, §6.8.3
LK	light key, §9.1
LKP	Lee–Kessler–Plöcker EOS, §2.11
LLK	lighter than the light key, Figure 9.6
LM	log mean, (3-33)
LW	lost work, Table 2.10
MSA	mass-separation agent, Table 1.2
MW	molecular weight
NRTL	nonrandom, two-liquid model, Table 2.8
NTU	number of transfer units, Table 6.5
ODE	ordinary differential equations, §13.5.2
PR	Peng–Robinson EOS, Table 2.8
PSRK	predictive SRK method, §2.8.2
RK	Redlich–Kwong EOS, §2.8.2
STP	standard conditions, 1 atm, 0°C
SRK	Suave–Redlich–Kwong EOS, Table 2.8
UNIFAC	functional group activity coefficient method, Table 2.8
UM	unimolecular diffusion, Table 6.5

UNIQUAC	universal quasichemical theory method, Table 2.8
VLE	vapor–liquid equilibrium, Figure 4.6
VLLE	vapor–liquid–liquid equilibrium, §11.8
VOC	volatile organic compounds
VTPR	volume-translated P-R EOS, §2.8.3
Wilson	Wilson EOS, Table 2.8

Latin Symbols

Å	Angstrom, §14.1
A	mass-transfer area, (3-13)
\mathcal{A}	absorption factor, L/KV , (5-38)
a	interfacial area per unit volume, (14-5); activity, Table 2.1
B	identifier for bottoms, Figure 1.12
B	bottoms molar flow rate, Figure 5.15
C	identifier for condenser, Figure 1.12
C	components, (4-1)
C_D	drag coefficient, Table 3.9
C_P	heat capacity at constant pressure, (2-38)
c	liquid concentration, moles/volume, (3-40)
D	an identifier for distillate, Figure 1.12
D_{AB}	molecular diffusivity of A in B, (3-3a)
D_i	solute diffusivity, (14-14)
D_K	Knudsen diffusivity, (14-18)
D_e	effective diffusivity, (3-49)
D	distillate flow rate, Figure 5.7; diameter, (3-121)
d_H	hydraulic diameter, (14-5)
d_p	particle diameter, (6-58)
E	extract mass flow rate, Figure 5.2
E	an identifier for extract phase, Figure 5.2
\mathcal{E}	extraction factor, (4-35)
E_{MV}	Murphree vapor tray efficiency, (6-53)
E_o	stage (plate efficiency), (6-41)
E_{OV}	Murphree vapor point efficiency, (6-51)
F	molar feed rate, Example 1.1
F	identifier for feed, Figure 1.2
F	Faraday’s constant, (3-47)
F_D	drag force, (6-57)
f	pure component fugacity, §2.1.1; Fanning friction factor, Table 3.9

f^o	fugacity at standard state, (2-14)	N_D	degrees of freedom, number of design variables, (4-1)
\bar{f}	partial fugacity, (2-7)	N_E	number of independent equations, (4-3)
G	Gibbs free energy, §2.1; mass velocity, (3-145)	N_P	number of phases, (4-1)
g	Gibbs molar free energy, §2.1; gravitational constant, (6-94)	N_V	number of variables, (4-1)
g^E	excess free energy, (2-62)	N_{Fr}	Froude number, Table 3.9
g_c	force to mass conversion factor in AE system of units	N_{Le}	Lewis number, Table 3.9
H	Henry's law constant (2-31); vessel height, Figure 4.18	N_{Nu}	Nusselt number, Table 3.9
ΔH^{vap}	enthalpy of vaporization, (2-43)	N_{Pe}	Peclet number, Table 3.9
H_L	height of a mass-transfer unit (L) liquid or (V) vapor, Table 6.5	N_{Re}	Reynolds number, Table 3.9
H_{OL}	height of an overall mass-transfer unit (L or V), Table 6.5	N_{Sc}	Schmidt number, Table 3.9
h	molar enthalpy, §2.2; heat transfer coefficient, (15-18)	N_{Sh}	Sherwood number, Table 3.9
h^o	ideal gas molar enthalpy, §2.2	N_{St}	Stanton number, Table 3.9
J	molar flux by molecular diffusion relative to mixture, (3-3)	N_{We}	Weber number, Table 3.9
j	mass flux relative to mixture, (3-5)	N_G	number of gas phase (G) or liquid phase (L) mass-transfer units, Table 6.5
j_D, j_H, j_M	Chilton–Colburn factors for mass, heat, and momentum transfer (3-147)	N_{OG}	number of overall gas (G) or liquid phase (L) mass-transfer units, Table 6.5
j -factor	Table 3.9	n	molar flow rate, Example 1.1; mass transfer rate, §6.5.4
K	vapor–liquid equilibrium ratio (K -value), (2-18)	P	pressure, (2-1); product flow rate, Figure 5.3
K	various subscripted overall mass-transfer coefficients, Tables 6.5 and 3.12, §3.7.1	P^s	vapor pressure, (2-13)
K_D	distribution ratio, partition coefficient, (2-19)	P_M	permeability, KD , (14-1), (14-27)
K'_D	liquid–liquid equilibrium ratio in mole or mass ratios (4-33)	$\bar{P}_M = P_M/l_M$	permeance, (14-1)
k	various subscripted individual mass-transfer coefficients, Tables 6.5 and 3.12, §3.7.1	p	partial pressure (for designated component)
k	thermal conductivity, (3-2)	Q	rate of heat transfer, (4-17); volumetric flow rate, (7-51)
L	liquid molar flow rate, Table 1.1; length, (3-82)	q	heat flux, Q/A , (3-2); q -line, (4-11)
L_R	liquid reflux flow rate, Figure 5.8	R	universal gas constant, (3-47); retentate, Example 1.1
\bar{L}	liquid molar flow rate in stripping section, Figure 7.5	R	reflux ratio L/D , Table 7.2; raffinate flow rate, Figure 5.2
l	component liquid flow rate, (6-15); packed height, Figure 6.25	R	identifier for reflux, Example 2.5; raffinate, Figure 4.14
l_M	membrane thickness, (14-1)	r	radius, (3-54)
M	molecular weight	S	entropy (2-2); solvent flow rate, (4-32); side stream, Table 5.4
m	slope of equilibrium curve dy/dx , Figure (3-16)	\mathcal{S}	stripping factor, (5-51)
N	number of moles, (2.1); number of stages (5-7); flux, molar flow/area (3-1)	ΔS_{irr}	irreversible change in entropy, Table 2.11
N_A	Avogadro's number, (3-38)	S	identifier for solvent, §4.4
		s	molar entropy, Table 2.3
		T	temperature, (2-1)
		T_c	critical temperature, Table 15.4
		T_r	reduced temperature, T/T_c , (2-49)
		t	time
		u	liquid velocity, (3-71)
		V	molar vapor flow rate, Table 1.1; volume, (2-2)
		\bar{V}	molar vapor flow in stripping section, Figure 7.5

ν	kinematic viscosity (6-98); vapor component flow rate, (6-13); liquid molar volume, (3-43); pore flow velocity, (14-2)
W_s	shaft work, Table 2.11
w	mass fraction, (3-5)
X	mass or mole ratio in liquid, (4-32)
x	liquid mole fraction
Y	mass or mole ratio in vapor, Figure 4.19
y	vapor mole fraction
z	mole fraction of feed component, Figure 2.9
Z	compressibility factor, (2-49)

Greek Symbols

α_{AB}	relative volatility, K_A/K_B , (4-10)
β	relative selectivity, (2-21), (8-4)
γ	activity coefficient, Table 2.1
Δ	change in value of variable
ϵ	porosity, (15-2)
η	second-law efficiency, Table 2.10
μ	viscosity, (3-38), chemical potential or partial molar Gibbs free energy, (2-2)
ρ	mass density
ρ_L	liquid mass density, (2-41)
ρ_V	vapor mass density, Table 2.3
σ	liquid surface tension, (3-43)
τ	tortuosity, (3-49)
ϕ	pure species fugacity coefficient, Table 2.1
ϕ^s	pure species fugacity coefficient at saturation pressure, (2-30)
$\bar{\phi}$	partial fugacity coefficient, Table 2.1
Φ	local volume fraction, §2.7.1
ω	acentric factor, (2-48)

Subscripts

A,B,C	components, Figure 5.4
B	bottoms, (7-4)
C	condenser, (7-37)
D	distillate, (7-4)
F	feed, (7-6)
c	critical point, §2.5
i	component in a mixture
irr	irreversible
min	minimum
j	stage, Figure 10.1
n	stage, (6-11)
R	reboiler, (7-37)
r	reference component, (9-14)
sat	saturated
x	in the x direction
y	in the y direction
z	in the z direction
o	datum (reference state), 1 atm., 25°C
∞	infinity

Superscripts

F	feed, (4-32)
N	number of stages, (5-7): a stage, (5-15)
R	raffinate, Figure 5.4
s	saturation vapor pressure, (2-28)
o	reference state, Table 2.3
*	phase equilibrium value (with respect to another phase), Figure 3.16
—	average, (3-74); partial molar property, (2-8)
'	derivative, (4-28); mass instead of moles, for K and D values, etc., (4-33); normalized values, §4.5; solute free gas or adsorbent, §6.3

Dimensions and Units

Chemical engineers must be proficient in the use of three systems of units: (1) the International System of Units, **SI** System (Système Internationale d'Unités), which was established in 1960 by the 11th General Conference on Weights and Measures and has been widely adopted; (2) the **AE** (American Engineering) System, which is based largely upon an English system of units adopted when the Magna Carta was signed in 1215 and is a preferred system in the United States; and (3) the **CGS** (centimeter-gram-second) System, which was devised in 1790 by the National Assembly of France, and served as the basis for the development of the SI System. A useful index to units and systems of units is given on the website <http://www.sizes.com/units/index.php>.

Engineers must deal with dimensions units, and values to express numerical quantities. Thus, for 10 gallons of gasoline, the **dimension** is volume, the **unit** is gallons, and the **value** is 10. As detailed in NIST (National Institute of Standards and Technology) *Special Publication 811, Guide for the Use of the International System of Units (SI)*, 2008 edition, which is available at the website <http://www.nist.gov/physlab/pubs/sp811/index.cfm>, units are **base** or **derived**.

BASE UNITS

The base units are those that are independent, cannot be subdivided, and are accurately defined. The base units are for dimensions of length, mass, time, temperature, molar amount, electrical current, and luminous intensity, all of which can be measured independently. Derived units are expressed in terms of base units or other derived units and include dimensions of volume, velocity, density, force, and energy. In this book we deal with the first five of the base dimensions. For these, the base units are:

Base Dimension	SI Unit	AE Unit	CGS Unit
Length	meter, m	foot, ft	centimeter, cm
Mass	kilogram, kg	pound, lb _m	gram, g
Time	second, s	hour, h	second, s
Temperature	kelvin, K	Fahrenheit, °F	Celsius, °C
Molar amount	gram-mole, mol	pound-mole, lbmol	gram-mole, mol

ATOM AND MOLECULE UNITS

atomic weight = atomic mass unit = the mass of one atom

molecular weight (MW) = molecular mass (M) = formula weight* = formula mass* = the sum of the atomic weights of all atoms in a molecule (* also applies to ions)

1 atomic mass unit (amu or u) = 1 universal mass unit = 1 dalton (Da) = 1/12 of the mass of one atom of carbon-12 = the mass of one proton or one neutron

The units of MW are amu, u, Da, g/mol, kg/kmol, or lb/lbmol (the last three are most convenient when MW appears in a formula).

The number of molecules or ions in one mole = Avogadro's number = 6.022×10^{23} .

DERIVED UNITS

Many derived dimensions and units are used in chemical engineering. Some are listed in the following table:

Derived Dimension	SI Unit	AE Unit	CGS Unit
Area = Length ²	m ²	ft ²	cm ²
Volume = Length ³	m ³	ft ³	cm ³
Mass flow rate = Mass/Time	kg/s	lb _m /h	g/s
Molar flow rate = Molar amount/Time	mol/s	lbmol/h	mol/s
Velocity = Length/Time	m/s	ft/h	cm/s
Acceleration = Velocity/Time	m/s ²	ft/h ²	cm/s ²
Force = Mass · Acceleration	newton, N = 1 kg·m/s ²	lb _f	dyne = 1 g·cm/s ²
Pressure = Force/Area	pascal, Pa = 1 N/m ² = 1 kg/m·s ²	lb _f /in. ²	atm
Energy = Force · Length	joule, J = 1 N·m = 1 kg·m ² /s ²	ft·lb _f , Btu	erg = 1 dyne·cm = 1 g·cm ² /s ² , cal
Power = Energy/Time = Work/Time	watt, W = 1 J/s = 1 N·m/s 1 kg·m ² /s ³	hp	erg/s
Density = Mass/Volume	kg/m ³	lb _m /ft ³	g/cm ³

OTHER UNITS ACCEPTABLE FOR USE WITH THE SI SYSTEM

A major advantage of the SI System is the consistency of the derived units with the base units. However, some acceptable deviations from this consistency and some other acceptable base units are given in the following table:

Dimension	Base or Derived SI Unit	Acceptable SI Unit
Time	s	minute (min), hour (h), day (d), year (y)
Volume	m ³	liter (L) = 10 ⁻³ m ³
Mass	kg	metric ton or tonne (t) = 10 ³ kg
Pressure	Pa	bar = 10 ⁵ Pa

PREFIXES

Also acceptable for use with the SI System are decimal multiples and submultiples of SI units formed by prefixes. The following table lists the more commonly used prefixes:

Prefix	Factor	Symbol
tera	10 ¹²	T
giga	10 ⁹	G
mega	10 ⁶	M
kilo	10 ³	k
deci	10 ⁻¹	d
centi	10 ⁻²	c
milli	10 ⁻³	m
micro	10 ⁻⁶	μ
nano	10 ⁻⁹	n
pico	10 ⁻¹²	p

USING THE AE SYSTEM OF UNITS

The AE System is more difficult to use than the SI System because of the units for force, energy, and power. In the AE System, the force unit is the pound-force, lb_f , which is defined to be numerically equal to the pound-mass, lb_m , at sea-level of the earth. Accordingly, Newton's second law of motion is written,

$$F = m \frac{g}{g_c}$$

where F = force in lb_f , m = mass in lb_m , g = acceleration due to gravity in ft/s^2 , and, to complete the definition, the constant $g_c = 32.174 \text{ lb}_m\text{-ft}/\text{lb}_f\text{-s}^2$, where $32.174 \text{ ft}/\text{s}^2$ is the acceleration due to gravity at sea-level of the earth. The constant g_c is not used with the SI System or the CGS System because the former does not define a kg_f and the CGS System does not use a g_f .

Thus, when using AE units in an equation that includes force and mass, incorporate g_c to adjust the units.

EXAMPLE OF UNIT CONVERSIONS

A 5.000-pound-mass weight, m , is held at a height, h , of 4.000 feet above sea-level. Calculate its potential energy above sea-level, $\text{P.E.} = mgh$, using each of the three systems of units. Factors for converting units are given on the inside front cover of this book.

SI System:

$$\begin{aligned} m &= 5.000 \text{ lb}_m = 5.000(0.4536) = 2.268 \text{ kg} \\ g &= 9.807 \text{ m}/\text{s}^2 \\ h &= 4.000 \text{ ft} = 4.000(0.3048) = 1.219 \text{ m} \\ \text{P.E.} &= 2.268(9.807)(1.219) = 27.11 \text{ kg}\cdot\text{m}^2/\text{s}^2 = 27.11 \text{ J} \end{aligned}$$

CGS System:

$$\begin{aligned} m &= 5.000 \text{ lb}_m = 5.000(453.6) = 2268 \text{ g} \\ g &= 980.7 \text{ cm}/\text{s}^2 \\ h &= 4.000 \text{ ft} = 4.000(30.48) = 121.9 \text{ cm} \\ \text{P.E.} &= 2268(980.7)(121.9) = 2.711 \times 10^8 \text{ g}\cdot\text{cm}^2/\text{s}^2 \\ &= 2.711 \times 10^8 \text{ erg} \end{aligned}$$

AE System:

$$\begin{aligned} m &= 5.000 \text{ lb}_m \\ g &= 32.174 \text{ ft}/\text{s}^2 \\ h &= 4.000 \text{ ft} \\ \text{P.E.} &= 5.000(32.174)(4.000) = 643.5 \text{ lb}_m\text{-ft}^2/\text{s}^2 \end{aligned}$$

However, the accepted unit of energy for the AE System is $\text{ft}\cdot\text{lb}_f$, which is obtained by dividing by g_c . Therefore, $\text{P.E.} = 643.5/32.174 = 20.00 \text{ ft}\cdot\text{lb}_f$.

Another difficulty with the AE System is the differentiation between energy as work and energy as heat. As seen in the preceding table, the work unit is $\text{ft}\cdot\text{lb}_f$, while the heat unit is Btu. A similar situation exists in the CGS System with corresponding units of erg and calorie (cal). In older textbooks, the conversion factor between work and heat is often incorporated into an equation with the symbol J , called Joule's constant or the mechanical equivalent of heat, where

$$J = 778.2 \text{ ft}\cdot\text{lb}_f/\text{Btu} = 4.184 \times 10^7 \text{ erg}/\text{cal}$$

Thus, in the previous example, the heat equivalents are

AE System:

$$20.00/778.2 = 0.02570 \text{ Btu}$$

CGS System:

$$2.711 \times 10^8 / 4.184 \times 10^7 = 6.479 \text{ cal}$$

In the SI System, the prefix M, mega, stands for million. However, in the natural gas and petroleum industries of the United States, when using the AE System, M stands for thousand and MM stands for million. Thus, MBtu stands for thousands of Btu, while MM Btu stands for millions of Btu.

It should be noted that the common pressure and power units in use for the AE System are not consistent with the base units. Thus, for pressure, pounds per square inch, psi or lb_f/in^2 , is used rather than lb_f/ft^2 . For power, Hp is used instead of $\text{ft}\text{-lb}_f/\text{h}$, where the conversion factor is

$$1 \text{ hp} = 1.980 \times 10^6 \text{ ft}\text{-lb}_f/\text{h}$$

CONVERSION FACTORS

Physical constants may be found on the inside back cover of this book. Conversion factors are given on the inside front cover. These factors permit direct conversion of AE and CGS values to SI values. The following is an example of such a conversion, together with the reverse conversion.

EXAMPLE

1. Convert 50 psia (lb_f/in^2 absolute) to kPa:

The conversion factor for lb_f/in^2 to Pa is 6,895, which results in

$$50(6,895) = 345,000 \text{ Pa or } 345 \text{ kPa}$$

2. Convert 250 kPa to atm:

250 kPa = 250,000 Pa. The conversion factor for atm to Pa is 1.013×10^5 . Therefore, dividing by the conversion factor,

$$250,000/1.013 \times 10^5 = 2.47 \text{ atm}$$

Three of the units [gallons (gal), calories (cal), and British thermal unit (Btu)] in the list of conversion factors have two or more definitions. The gallons unit cited here is the U.S. gallon, which is 83.3% of the Imperial gallon. The cal and Btu units used here are international (IT). Also in common use are the thermochemical cal and Btu, which are 99.964% of the international cal and Btu.

FORMAT FOR EXERCISES IN THIS BOOK

In numerical exercises throughout this book, the system of units to be used to solve the problem is stated. Then when given values are substituted into equations, units are not appended to the values. Instead, the conversion of a given value to units in the above tables of base and derived units is done prior to substitution into the equation or carried out directly in the equation, as in the following example.

EXAMPLE

Using conversion factors on the inside back cover of this book, calculate a Reynolds number, $N_{\text{Re}} = Dv\rho/\mu$, given $D = 4.0 \text{ ft}$, $v = 4.5 \text{ ft/s}$, $\rho = 60 \text{ lb}_m/\text{ft}^3$, and $\mu = 2.0 \text{ cP}$ (i.e., centipoise).

Using the SI System (kg-m-s),

$$N_{\text{Re}} = \frac{Dv\rho}{\mu} = \frac{[(4.00)(0.3048)][(4.5)(0.3048)][(60)(16.02)]}{[(2.0)(0.001)]} = 804,000$$

Using the CGS System (g-cm-s),

$$N_{\text{Re}} = \frac{Dv\rho}{\mu} = \frac{[(4.00)(30.48)][(4.5)(30.48)][(60)(0.01602)]}{[(0.02)]} = 804,000$$

Using the AE System ($\text{lb}_m\text{-ft-h}$) and converting the viscosity 0.02 cP to $\text{lb}_m/\text{ft-h}$,

$$N_{\text{Re}} = \frac{Dv\rho}{\mu} = \frac{(4.00)[(4.5)(3600)](60)}{[(0.02)(241.9)]} = 804,000$$

Chapter 1

Separation Processes

§1.0 INSTRUCTIONAL OBJECTIVES

After completing this chapter, you should be able to:

- Explain the role of separation operations in the chemical industries.
- Enumerate the four basic separation techniques.
- Explain the uses of energy-separating agents (ESA) and mass-separating agents (MSA).
- Calculate component material balances around a separation operation based on specifications of component recovery and/or product purity.
- Understand the concept of sequencing of separation operations, particularly distillation.

Separation processes for chemical mixtures have been known for millennia. Early civilizations developed processes for: (1) extraction of metals from ores, perfumes from flowers, dyes from plants, and potash from burnt plants; (2) evaporation of seawater to obtain salt; (3) refining of rock asphalt; and (4) distilling of liquors. The human body could not function if it had no kidney to separate water and waste products from blood.

Chemical engineers design large-scale facilities that employ separation methods that most often differ considerably from those used by chemists in laboratories. For example, chemists separate light-hydrocarbon mixtures by chromatography, while a manufacturing plant uses distillation to separate the same mixture. This book discusses methods for the design of large-scale separation operations for processes that manufacture chemical products economically. Included are all of the most common operations, including distillation (both continuous and batch), gas absorption, stripping, liquid–liquid extraction, membrane separations, and gas and liquid adsorption. These design methods are incorporated into commercial computer-aided **process simulators** such as Aspen Plus, Aspen HYSYS, CHEMCAD, ChemSep, ProSimPlus, and UniSim.

Chemical engineers also design small-scale industrial separation systems involving manufacture of specialty chemicals by batch processing; recovery of biological solutes; crystal growth of semiconductors; recovery of chemicals from wastes; and products such as lung oxygenators, espresso machines, and hemodialysis devices. A companion book, *Bioseparation Process Principles*, covers these smaller-scale processes and the principles of bioseparations. Included in that book are membranes and adsorption for bio applications, chromatography, electrophoresis, leaching, crystallization, drying, and mechanical separation operations. Both large- and small-scale operations are illustrated in examples and homework exercises in this book and in *Bioseparation Process Principles*.

§1.1 INDUSTRIAL CHEMICAL PROCESSES

Chemical companies manufacture products that differ from those in the feedstocks. Included can be (1) naturally occurring living or nonliving materials; (2) chemical intermediates that are precursors for producing other chemicals; (3) “chemicals in commerce” that can be purchased from the global market; or (4) waste products that can be processed into valuable products. Especially common are oil refineries, which process crude oil, synthetic crude oil from tar sands, and tight oil from the use of horizontal drilling followed by fracking of shale deposits, to produce a variety of hydrocarbon-based products. For example, starting in 1967, Canada began increasing its oil production dramatically by processing tar sands from the huge Athabasca deposit in the province of Alberta. Figure 1.1 shows the initial products produced by Great Canadian Oil Sands Ltd. (GCOS), now Suncor Energy, from its 1967 plant. The products are the result of numerous separation operations within the plant. By 2013, several Canadian companies produced more than 1.6 million barrels per day (bbl/day) of synthetic crude oil (syncrude). Because Canada produces more oil than it needs, it exports syncrude to the United States by the Keystone Pipeline. If phases 3 and 4 of the pipeline are completed, Canadian syncrude will flow more than 2,000 miles from the Keystone Hardisty Terminal in Alberta, Canada, to the Gulf near Houston, Texas.

Chemical plants operate in a **batchwise, continuous, or semicontinuous** manner. Plant operations may be **key operations** unique to chemical engineering because they involve changes in chemical composition, or **auxiliary operations** that are necessary to the success of the key operations but are often designed by mechanical engineers because they do not involve changes in chemical composition. The key operations involve (1) chemical reactions and (2) separation of chemical mixtures, such as the separation of a mixture of chemicals into pure, or nearly pure, species (components).

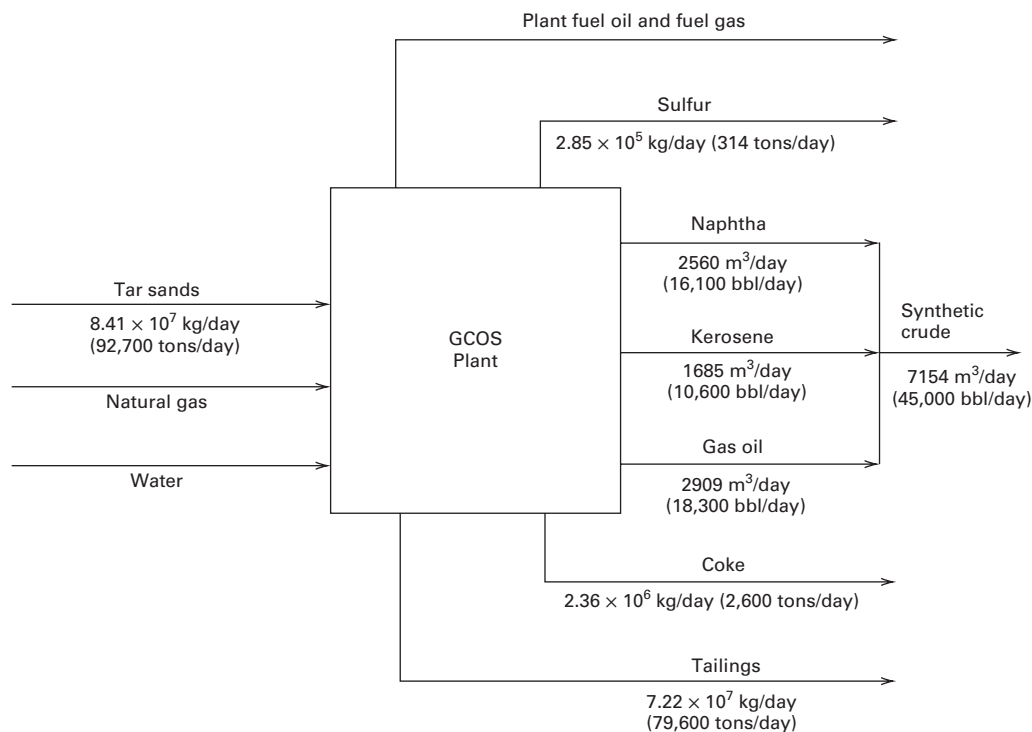


Figure 1.1 GCOS process for producing synthetic crude oil from Canadian Athabasca tar sands.

The auxiliary operations include phase separation (e.g., separation of gas from liquid or separation of two immiscible liquid phases), heat addition or removal (heat exchangers), shaft-work (pumps, compressors, turbines), mixing or dividing of streams, solids agglomeration, size reduction of solids, and separation of solids by size.

Block-flow diagrams can represent key operations in chemical processes. They indicate, by square or rectangular blocks, only the chemical reaction and separation steps and, by connecting lines, the process streams. More detail is shown in **process-flow diagrams**, which also include auxiliary operations and utilize icons that depict the particular type of equipment employed. Figure 1.2 shows a block-flow diagram for manufacturing hydrogen chloride gas from chlorine and hydrogen. Central to the process is a chemical reactor, where the gas-phase combustion reaction, $\text{H}_2 + \text{Cl}_2 \rightarrow 2\text{HCl}$, occurs. In this process, no separation operations are necessary because of the complete conversion of chlorine and the absence of any side reactions. A slight excess of hydrogen is used, and the

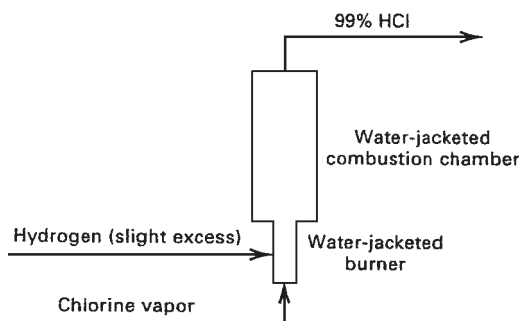


Figure 1.2 Synthetic process for anhydrous HCl production.

product, 99% HCl, with small amounts of H_2 , N_2 , H_2O , CO , and CO_2 , requires no purification. However, simple process flowsheets that do not require separation operations are rare. In most process flowsheets, separation operations dominate.

Most industrial chemical processes involve at least one chemical reactor accompanied by one or more separation operations. An example is the continuous hydration of ethylene with water to produce ethyl alcohol, shown in Figure 1.3. Central to the process is a reactor packed with catalyst particles, in which the reaction $\text{C}_2\text{H}_4 + \text{H}_2\text{O} \rightarrow \text{C}_2\text{H}_5\text{OH}$ occurs. Due to chemical equilibrium limitations, conversion of ethylene is only 5% per pass through the reactor. However, by recovering unreacted ethylene, in a partial condensation separation step, and recycling the ethylene to the reactor, nearly complete overall conversion of the ethylene feed is achieved. Recycling is a common element of chemical processes.

If pure ethylene were available as a feedstock and no side reactions occurred, the simple process in Figure 1.3 could be realized. It utilizes a reactor, a partial condenser for unreacted gaseous ethylene recovery, and distillation to produce an overhead distillate of aqueous ethyl alcohol of near-azeotropic composition (93 wt%), with a wastewater bottoms product. Unfortunately, impurities in the ethylene feed, together with side reactions involving ethylene and the impurities, increase the number of separators required for the process, as shown in Figure 1.4. Also, as shown, an additional reactor may be necessary to convert impurities or by-products to other chemicals that can be more easily separated from the main product. Such an escalation of the need for separation operations is common. Thus, most chemical processes include many more separation operations than chemical reactors.

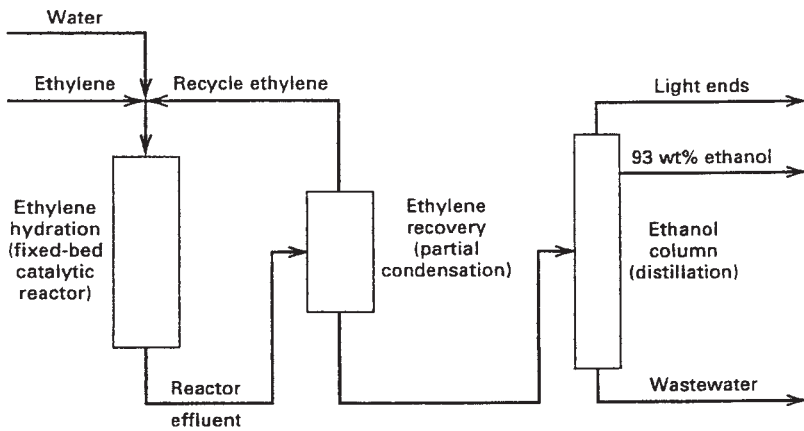


Figure 1.3 Process for hydration of ethylene to ethanol.

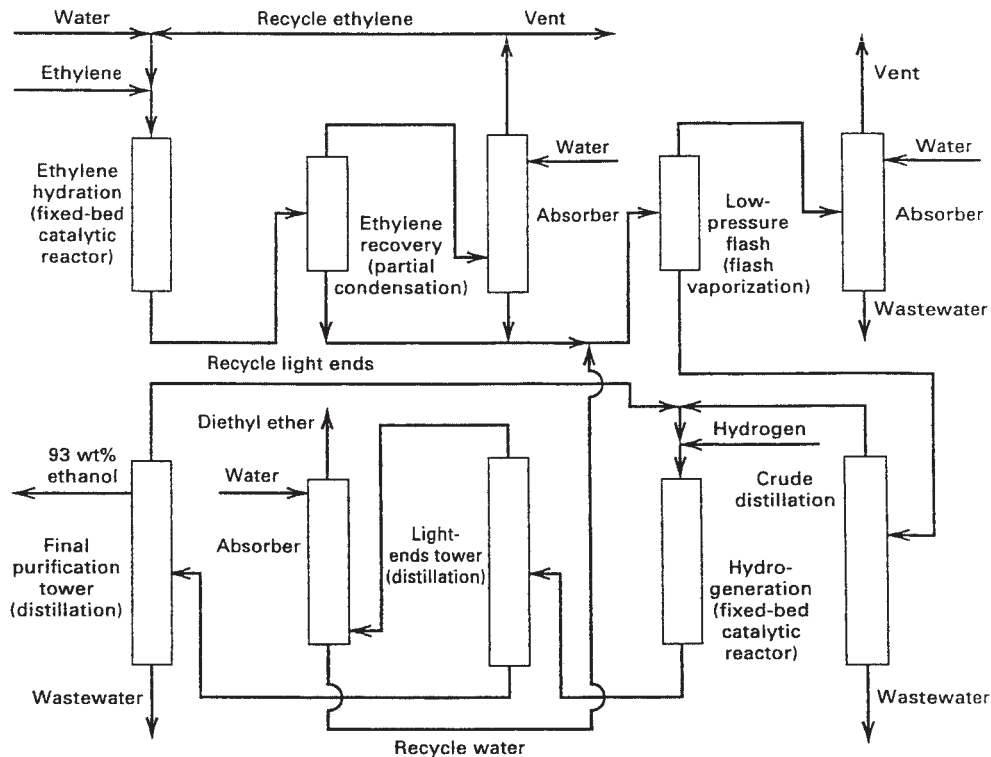


Figure 1.4 Industrial process for hydration of ethylene to ethanol.

Chemical engineers also design products that can involve separation operations. One such product is the espresso coffee machine. Very hot water rapidly leaches desirable chemicals from the coffee bean, leaving behind ingredients responsible for undesirable acidity and bitterness. The resulting cup of espresso has (1) a topping of creamy foam that traps the extracted chemicals, (2) a fullness of body due to emulsification, and (3) a richness of aroma. Typically, 25% of the coffee bean is extracted and the espresso contains less caffeine than filtered coffee. Cussler and Moggridge [1] and Seider, Seader, Lewin, and Widagdo [2] discuss other examples of products designed by chemical engineers that involve the separation of chemical mixtures.

§1.2 BASIC SEPARATION TECHNIQUES

The separation of a chemical mixture into its components is not a spontaneous process, like the mixing by diffusion of soluble components. Separations require energy in some form. A mixture to be separated into its separate chemical species is usually a single, homogeneous phase. If it is multiphase, it is often best to first separate the phases by gravity or centrifugation, followed by the separation of each phase mixture.

A schematic of a general separation process is shown in Figure 1.5. The phase state of the feed can be a **vapor**, **liquid**, or **solid** mixture. The products of the separation differ in composition from the feed and may differ in the state of the

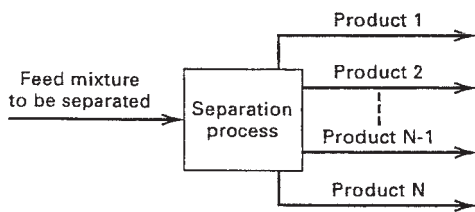


Figure 1.5 General separation process.

phase. The separation is accomplished by inducing the different chemical species in the feed to partition among the different product phases. Four basic methods for doing this are shown in Figure 1.6. Most common is the **phase creation** technique in Figure 1.6a. For example, the feed may be a liquid mixture. By heating the mixture to partially vaporize the liquid, the more-volatile components tend to move to the vapor, while less-volatile components tend to remain in the liquid phase. Alternatively, the feed may be a vapor that is partially condensed.

A second technique, labeled **phase addition**, is shown in Figure 1.6b. For example, a liquid solvent may contact a liquid feed to selectively dissolve certain species from the feed. Less common is the third separation technique that uses a **barrier**, such as a membrane, as shown in Figure 1.6c. The barrier allows passage of certain species in the feed while excluding or slowing other species. Finally, in a fourth technique, an **external force field** or gradient is used to preferentially attract certain species in the feed as indicated in Figure 1.6d. The force field might be electrical or centrifugal.

For the techniques of Figure 1.6, the **rate of separation** is governed by the rates of **mass transfer** of the different components, while the **extent of separation** is limited by **thermodynamic equilibrium**. These two topics are the subject of previous chemical engineering courses, but are reviewed here in Chapters 2 and 3. Also, fluid mechanics and heat transfer play important roles in the separation of mixtures, and their principles are applied, where appropriate, throughout this book.

The extent of separation achieved depends on the exploitation of differences in molecular, thermodynamic, and transport properties of the species in the feed mixture. Of importance are molecular weight, molecular shape, dipole moment, electric charge, vapor pressure, solubility, adsorptivity, and diffusivity. Values of these properties appear in handbooks, reference books, textbooks, and journals. Many can be obtained from physical property models in process-simulation programs. When properties are not available, they are estimated or determined experimentally.

§1.3 SEPARATIONS BY PHASE CREATION

The simplest and most widely used industrial separation technique is phase creation. The feed to the separator is a single-phase vapor, liquid, or solid. The second phase is created by the transfer of energy to or from the feed by an **energy-separating agent (ESA)**. The ESA can be heat transfer or shaft work by means of compression or by the reduction of pressure through a turbine or across a valve. After sufficient time and agitation to approach phase equilibrium, the product phases are separated. The size of the process vessel depends on the flow rate in and out of the vessel and the time for the phases to approach equilibrium.

The most common separation operations using phase creation are listed in Table 1.1. For these operations, design procedures are well established and are included as unit operation models in commercial process simulators.

When the feed mixture is a vapor or a liquid with components that differ widely in volatility (e.g., hydrogen and benzene), **partial condensation** or **partial vaporization**, Operation (1) in Table 1.1, may be adequate to achieve the desired separation. Heat is transferred to or from the feed in a heat exchanger followed by phase separation by gravity in a vessel. Partial vaporization of a liquid occurs in **flash vaporization**, Operation (2), by reducing the feed pressure with a valve or turbine, followed by phase separation. Both of these separation operations are referred to as **single equilibrium stages** because experimental evidence shows that interphase

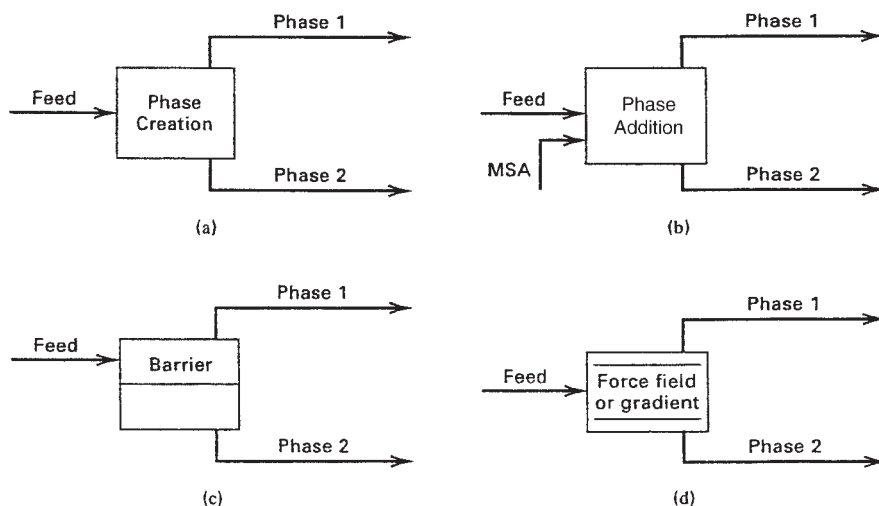
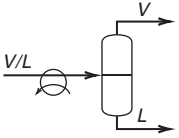
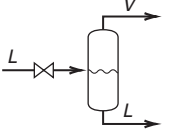
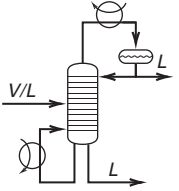


Figure 1.6 Basic separation process techniques: (a) separation by phase creation; (b) separation by phase addition; (c) separation by barrier; (d) separation by external force field or gradient.

Table 1.1 Common Separation Operations Based on Phase Creation

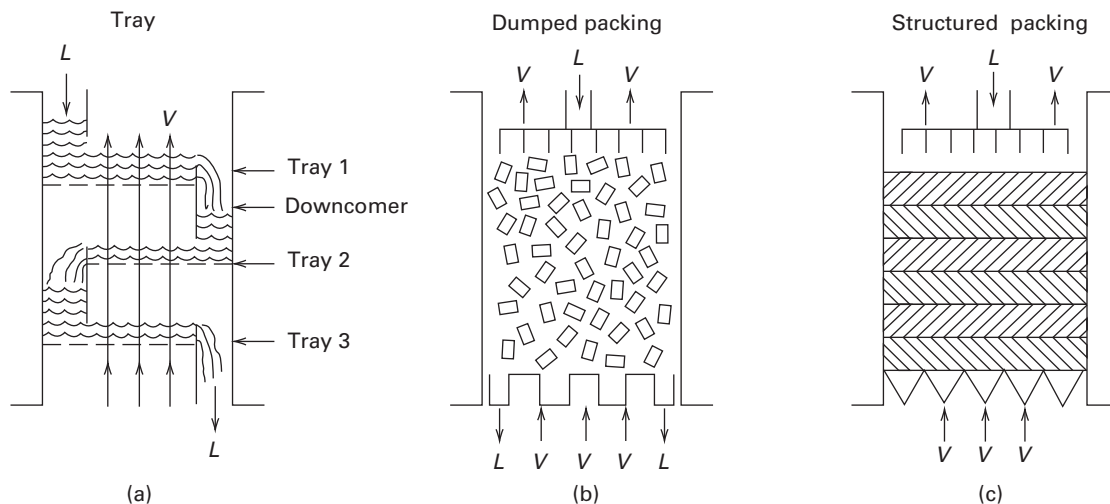
Separation Operation	Symbol	Feed Phase	Created Phase	Separating Agent(s)
(1) Partial condensation or vaporization		Vapor and/or liquid	Liquid or vapor	Heat transfer (ESA)
(2) Flash vaporization		Liquid	Vapor	Pressure reduction
(3) Distillation		Vapor and/or liquid	Vapor and liquid	Heat transfer (ESA) and sometimes shaft work (ESA)

mass transfer of species is so rapid that phase equilibrium is closely approached. The liquid product is enriched with respect to the less volatile species, while the vapor product is enriched with respect to the more volatile species. These operations are discussed in Chapter 4.

When the degree of separation by a single equilibrium stage is inadequate because the volatility differences among key species are insufficiently large (e.g., benzene and toluene), **distillation**, Operation (3) in Table 1.1, with multiple stages, often becomes the separation method of choice. It is and has long been the most widely utilized industrial separation method. Distillation involves vigorous mixing during contacts between countercurrently flowing liquid and vapor phases. Figure 1.7 shows schematics of three widely used phase-contacting methods. Figure 1.7a depicts a series of trays, where the phases are mixed and then disengaged. Each tray is some fraction of an equilibrium stage. In Figures 1.7b

and 1.7c, the phases are in continuous contact with other. In the first case, randomly dumped ceramic, metal, or plastic rings or saddles, called packing, promote turbulence as the vapor follows a tortuous path through the liquid, which flows over and through the packing. In the latter case, stacked, structured packing is used in the form of metal or plastic meshes, grids, or coils. Depending on the efficiency of the packing, inches or feet of packed height are equivalent to an equilibrium stage. In the icon for distillation in Table 1.1, horizontal lines within the column indicate the stages. As vapor flows up the column, it is increasingly enriched with respect to the more volatile species. The liquid flowing down the column is increasingly enriched with respect to the less-volatile species.

Feed to a distillation column enters at a stage somewhere between the top and bottom stages. Any vapor in the feed starts up the column; feed liquid starts down. Liquid is also required for making contacts with vapor above the feed stage, and vapor

**Figure 1.7** Phase-contacting methods in distillation columns.

is also required for making contacts with liquid below the feed stage. Therefore, at the top of the column, vapor is condensed to provide distillate product and down-flowing liquid (**reflux**). Similarly, part of the liquid at the bottom is removed as bottoms product, while the other part passes through a reboiler, where it is heated to provide up-flowing vapor (**boilup**). Continuous distillation is introduced in Chapter 5. The separation of a binary mixture by continuous distillation is discussed in Chapter 7, while the continuous distillation of multicomponent mixtures is discussed in Chapters 9–12. Batch distillation is discussed in Chapter 13.

§1.4 SEPARATIONS BY PHASE ADDITION

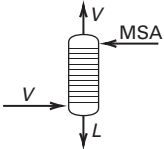
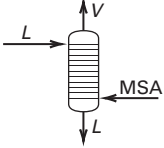
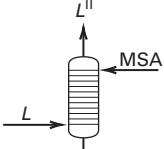
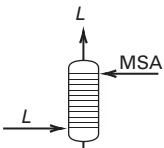
The next most widely used industrial separation technique is phase addition. The feed to the separator is a single-phase vapor, liquid, or solid. The second added phase is called a mass-separating agent (MSA). Certain components in the feed move from the feed phase to the MSA phase. After sufficient time and agitation to approach phase equilibrium, the product phases are separated. Disadvantages of using an MSA are (1) the need for an additional separator to recover the MSA for recycle, (2) the need for MSA makeup, (3) possible product contamination by the MSA, and (4) more complex design procedures. Table 1.2 lists the most common separation operations using phase addition. For these operations, design procedures are well established and are included in process simulators.

When the feed mixture is a vapor, and it is desired to remove the higher molecular weight (heavier) components from the lower molecular weight (lighter) components, **absorption**, Operation (1) in Table 1.2, is used. The feed gas enters at the bottom of a multistage column and flows up the column countercurrent to the MSA, called an absorbent, which enters at the top of the column. Typically, absorbers operate at near-ambient temperature at an elevated pressure. A subsequent separation, often distillation, separates the absorbate from the absorbent, which is then recycled to the absorber.

The inverse of absorption is **stripping**, Operation (2) in Table 1.2. Here, a liquid feed mixture is separated, at elevated temperature and near-ambient pressure, by contacting the feed, which enters at the top of the column, with a gas stripping MSA that enters at the bottom. A second separation operation may be needed if it is necessary to separate the stripping agent from the components stripped from the liquid feed and/or to recycle the stripping agent to the stripper. Absorption and stripping are discussed in Chapter 6. Column internals for absorption and stripping are those of Figure 1.7.

Liquid–liquid extraction, Operation (3) in Table 1.2, using a solvent as the MSA, can be used when distillation is impractical, e.g., because the feed is temperature-sensitive. A solvent (MSA) selectively dissolves only certain components in the feed. The products are an **extract**, L^I , containing the extracted components, and a **raffinate**, L^{II} , containing the unextracted species. Several countercurrently arranged stages may be necessary, either in a staged column with mechanical

Table 1.2 Common Separation Operations Based on Phase Addition

Separation Operation	Symbol	Feed Phase	Added Phase	Separating Agent(s)
(1) Absorption		Vapor	Liquid	Liquid absorbent (MSA)
(2) Stripping		Liquid	Vapor	Stripping vapor (MSA)
(3) Liquid–liquid extraction		Liquid	Liquid	Liquid solvent (MSA)
(4) Adsorption		Vapor or liquid	Solid	Solid adsorbent (MSA)

agitation or in a series of mixing and settling vessels. Additional separation operations, often distillation, are needed to recover the solvent for recycle. Liquid–liquid extraction is described in Chapter 8.

The MSA may be a porous solid, in the form of granules, that selectively removes one or more components from a vapor or liquid feed mixture by **adsorption**, Operation (4) in Table 1.2. Adsorption is confined to the exterior and interior surfaces of the solid adsorbent, unlike absorption, which occurs throughout the liquid absorbent. Adsorption separations are often conducted batchwise or semicontinuously in vessels or columns. However, equipment is available to simulate continuous operation, as in Table 1.2. When the adsorbent, S, becomes saturated with the adsorbed solutes (adsorbate), it must be regenerated to recover the adsorbate and reuse the adsorbent. Alternatively, if the adsorbate is a waste product, the spent adsorbent may be discarded and replaced with fresh adsorbent. Adsorption is described in Chapter 15.

§1.5 SEPARATIONS BY BARRIER

The use of microporous and nonporous membranes as semi-permeable barriers for separating vapor or liquid mixtures is rapidly gaining adherents. The products are the **retentate** (components that do not pass through the membrane) and the **permeate** (components that do pass through the membrane). For microporous membranes, separation is effected by differing rates of species diffusion through the membrane pores. For nonporous membranes, separation is controlled by differences in solubility in the membrane and rates of species diffusion through the membrane material. The most complex and selective membranes are found in the trillions of cells in the human body.

Table 1.3 lists four of the most common industrial membrane separation operations. **Dialysis**, Operation (1) in Table 1.3, is the transport, by a concentration gradient, of small solute molecules through a porous membrane. The molecules unable to pass through the membrane are small, insoluble,

non-diffusible particles. **Reverse osmosis**, Operation (2), is the selective transport of a solvent, for example, water, through a microporous membrane after the pressure of the feed is increased to a value higher than the osmotic pressure of the solution. Solutes in the solvent do not permeate the membrane. It is widely used to produce drinkable water.

Separation of gases by selective **gas permeation** through nonporous membranes, Operation (3), using a pressure driving force, is a process first used by the U.S. government in the 1940s with porous fluorocarbon barriers to separate ²³⁵UF₆ and ²³⁸UF₆. Today, nonporous polymer membranes are employed to enrich mixtures containing hydrogen, recover hydrocarbons from gas streams, and produce oxygen-enriched air.

To achieve high purities, **pervaporation**, Operation (4), can be used. Certain species in the liquid feed diffuse through the nonporous membrane, where they are evaporated before exiting as permeate. This method uses low pressures to enhance vaporization and the heat of vaporization must be supplied. It is used to separate azeotropic mixtures.

All four of the membrane separation operations in Table 1.3 are described in Chapter 14.

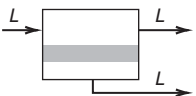
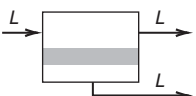
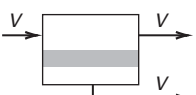
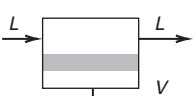
§1.6 SEPARATIONS BY AN EXTERNAL FIELD OR GRADIENT

External fields take advantage of differing degrees of response of certain molecules. **Centrifugation** establishes a pressure field that separates mixtures according to their size, shape, and density. It is used to separate ²³⁵UF₆ from ²³⁸UF₆, and can also separate large polymer molecules according to molecular weight.

If a temperature gradient is applied to a homogeneous solution, concentration gradients induce **thermal diffusion**. It has been used to enhance separation of isotopes in permeation processes.

When water containing 0.000149 atom fraction deuterium is decomposed by **electrolysis** into hydrogen and oxygen, the deuterium concentration in the hydrogen is lower than in water.

Table 1.3 Common Separation Operations Based on Barriers

Separation Operation	Symbol	Feed Phase	Barrier	Separating Agent(s)
(1) Dialysis		Liquid	Microporous membrane	Pressure (ESA)
(2) Reverse osmosis		Liquid	Microporous membrane	Pressure (ESA)
(3) Gas permeation		Vapor	Nonporous membrane	Pressure (ESA)
(4) Pervaporation		Liquid	Nonporous membrane	Pressure and heat transfer (ESA)

Until 1953, this process was the source of heavy water (D₂O). In **electrodialysis**, cation- and anion-permeable membranes carry a fixed charge that prevents migration of species with like charge. This phenomenon is applied to desalinate seawater. A related process is **electrophoresis**, which exploits the different migration velocities of charged colloidal or suspended species in an electric field.

These external field separation operations are not discussed further in this textbook, with the exception of electrodialysis, which is described in Chapter 14.

§1.7 BRIEF COMPARISON OF COMMON SEPARATION OPERATIONS

When selecting among feasible separation techniques for a given application, some major factors to consider are (1) technological maturity, which allows designers to apply prior knowledge; (2) cost; (3) ease of scale-up from laboratory experiments; (4) ease of providing multiple stages; and (5) need for parallel units for large capacities. A survey by Keller [3], Figure 1.8, shows that the degree to which a separation operation is technologically mature correlates with its extent of commercial use. Operations based on membranes are more expensive than those based on phase creation (e.g., distillation) or phase addition (e.g., absorption, extraction, and adsorption). All separation equipment is limited to a maximum size. For capacities requiring a larger size, parallel units must be provided. Except for size constraints or fabrication problems, capacity of a single unit can be doubled for an additional investment cost of about 60%. If two parallel units are installed, the additional investment for the second unit is 100% of the first unit, unless a volume-discount

Table 1.4 Ease of Scale-Up of the Most Common Separations

Operation in Decreasing Ease of Scale-Up	Ease of Staging	Need for Parallel Units
Distillation	Easy	No need
Absorption	Easy	No need
Liquid-liquid extraction	Easy	Sometimes
Membranes	Re-pressurization required between stages	Almost always
Adsorption	Easy	Only for regeneration cycle

applies. Table 1.4 lists operations ranked according to ease of scale-up. Those ranked near the top are frequently designed without pilot-plant or laboratory data. Operations near the middle usually require laboratory data, while those near the bottom require pilot-plant tests. Included in the table is an indication of the ease of providing multiple stages and whether parallel units may be required. Ultimately, the most cost-effective process, based on operating, maintenance, and capital costs, is selected, provided it is controllable, safe, and nonpolluting.

Also of interest are studies by Sherwood, Pigford, and Wilke [4], Dwyer [5], and Keller [3] that show that the cost of recovering and purifying a chemical depends strongly on its concentration in the feed. Keller's correlation, Figure 1.9, shows that the more dilute the feed in the product, the higher the product price. The five highest priced and most dilute chemicals shown are all proteins.

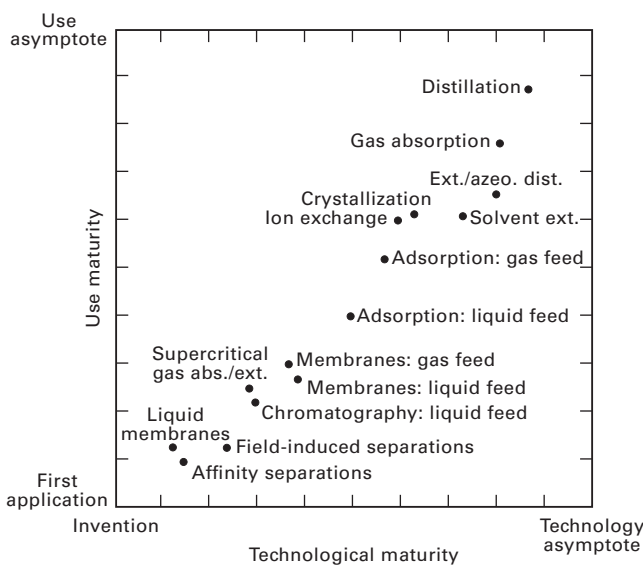


Figure 1.8 Technological and use maturities of separation processes. [Reproduced from [3] with permission of the American Institute of Chemical Engineers.]

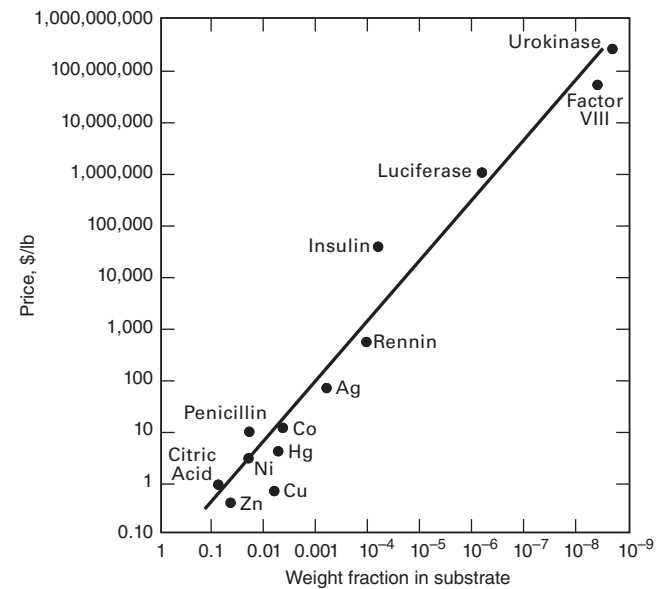


Figure 1.9 Effect of concentration of product in feed material on price. [Reproduced from [3] with permission of the American Institute of Chemical Engineers.]

§1.8 SEPARATION PROCESSES, PRODUCT PURITY, COMPONENT RECOVERY, AND SEPARATION SEQUENCES

Separation processes usually consist of more than one operation and may produce more than one product. The process is designed to meet product specifications, given as **product purities** and compositions. The process strives to do this with high **component recoveries**.

Consider the continuous hydrocarbon recovery process shown in Figure 1.10, which consists of a sequence of three multistage distillation operations (C1, C2, and C3). The feed consists of propane (C_3H_8), iso-butane (iC_4H_{10}), normal-butane (nC_4H_{10}), iso- and normal-pentane (iC_5H_{12} and nC_5H_{12}), higher molecular weight (heavier) hydrocarbons (C_6^+), and a small amount of ethane (C_2H_6). The components in the feed are rank-ordered by decreasing volatility (increasing normal boiling point), with ethane being the most volatile. The distillation columns were designed with the Aspen Plus simulator, using mathematical models described in Chapter 10, to produce four products: a C_5^+ -rich bottoms from C1, a C_3 (propane)-rich distillate from C2, and an iC_4 (isobutane)-rich distillate and an nC_4 (normal butane)-rich bottoms from C3. A material balance for the process is given in Table 1.5. Streams 4, 6, and 7 are final products, while Stream 2 is an intermediate that requires further processing. Specifications for the products are included in Table 1.6. The

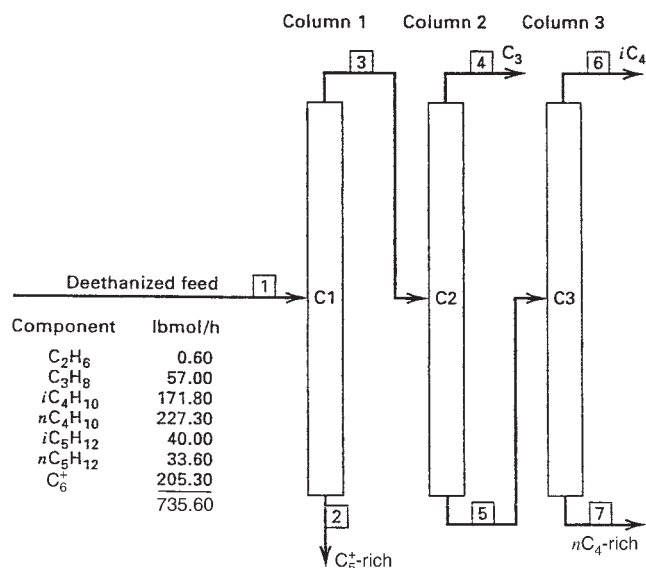


Figure 1.10 Hydrocarbon recovery process using distillation.

C_5^+ -rich component for Stream 2 indicates that all components less volatile than the pentanes are included.

Each column separates two **key components** in the column feed. In Column C1, the separation is between nC_4H_{10} (**light key**) and iC_5H_{12} (**heavy key**). This is indicated by the horizontal line separating the flow rates of these two components

Table 1.5 Material Balance for Hydrocarbon Recovery Process of Figure 1.10

Stream Component	Flow rates in lbmol/h						
	1 Feed to C1	2 C_5^+ -rich Product	3 Feed to C2	4 C_3 -rich Product	5 Feed to C3	6 iC_4 -rich Product	7 nC_4 -rich Product
C_2H_6	0.60	0.00	0.60	0.60	0.00	0.00	0.00
C_3H_8	57.00	0.00	57.00	54.80	2.20	2.20	0.00
iC_4H_{10}	171.80	0.10	171.70	0.60	171.10	162.50	8.60
nC_4H_{10}	227.30	0.70	226.60	0.00	226.60	10.80	215.80
iC_5H_{12}	40.00	11.90	28.10	0.00	28.10	0.00	28.10
nC_5H_{12}	33.60	16.10	17.50	0.00	17.50	0.00	17.50
C_6^+	205.30	205.30	0.00	0.00	0.00	0.00	0.00
Totals	735.60	234.10	501.50	56.00	445.50	175.50	270.00

Table 1.6 Comparison of Process Product Purities with Product Specifications

Component	mol% in Product					
	Propane-Rich		Iso-Butane-Rich		Normal-Butane-Rich	
	Data	Spec	Data	Spec	Data	Spec
C_2H_6	1.07	5 max	0		0	
C_3H_8	97.86	93 min	1.25	3 max	0	1 max
iC_4H_{10}	1.07	2 max	92.59	92 min	83.11	80 min
nC_4H_{10}	0		6.16	7 max		
C_5^+	0		0		16.89	20 max
Total	100.00		100.00		100.00	

in the “Feed to C1” column of Table 1.5. Column C1 produces a C_5^+ -rich product (Stream 2) as bottoms. The distillate from C1 is the feed to C2. Column C2 separates between C_3H_8 (light key) and iC_4H_{10} (heavy key) to produce a C_3 -rich product (Stream 4) as distillate. The bottoms from C2 is the feed to C3, which produces two products by separating between iC_4H_{10} (light key) and nC_4H_{10} (heavy key).

In Table 1.5, it should be noted that an overall material balance equation is satisfied for each of the six components and the C_6^+ multicomponent. For Figure 1.10, that equation in terms of $n_{i,j}$, the lbmol/h flow rate of component i in stream j is

$$n_{i,1} = n_{i,2} + n_{i,4} + n_{i,6} + n_{i,7}$$

For example, for propane (C_3H_8), $57.00 = 0.00 + 54.80 + 2.20 + 0.00$.

From the data in Table 1.5, product purities and component recoveries for the process can be computed. For example, the mol% purity of propane in the C_3 -rich product, Stream 4, is $54.80/56.00 = 0.9786 = 97.86$ mol%. The propane recovery in this product is $54.80/57.00 = 0.9614 = 96.14$ %. Other components in the propane product are ethane and isobutene. Table 1.6 compares the product purities of the final products of Streams 4, 6, and 7 with commercial product specifications. Note that all product specifications are achieved.

The following example illustrates the use of material balances for a separator when product purities and/or component recoveries are specified.

EXAMPLE 1.1 Material balances around a separator

A feed, F , of 100 kmol/h of air containing 21 mol% O_2 (1) and 79 mol% N_2 (2) is to be partially separated by a gas permeation membrane unit, Operation (3) in Table 1.3, according to each of three sets of specifications. Compute the flow rates (n_p and n_R) in kmol/h and compositions in mol% of the two products (retentate, R , and permeate, P). In Figure 1.6(c), Phase 1 is the retentate while Phase 2 is the permeate. The membrane is more permeable to O_2 than to N_2 .

Case 1: 50% recovery of O_2 to the permeate and 87.5% recovery of N_2 to the retentate.

Case 2: 50% recovery of O_2 to the permeate and 50 mol% purity of O_2 in the permeate.

Case 3: 85 mol% purity of N_2 in the retentate and 50 mol% purity of O_2 in the permeate.

Solution

The feed (F) rates of oxygen (1) and nitrogen (2) are

$$n_{1,F} = 0.21(100) = 21 \text{ kmol/h}$$

$$n_{2,F} = 0.79(100) = 79 \text{ kmol/h}$$

Case 1: Because two recoveries are given:

$$n_{1,P} = 0.50(21) = 10.5 \text{ kmol/h}$$

$$n_{2,R} = 0.875(79) = 69.1 \text{ kmol/h}$$

$$n_{1,R} = 21 - 10.5 = 10.5 \text{ kmol/h}$$

$$n_{2,P} = 79 - 69.1 = 9.9 \text{ kmol/h}$$

For the permeate: $n_p = 10.5 + 9.9 = 20.4 \text{ kmol/h}$

$$\text{mol\% } O_2 = 10.5/20.4 = 0.515 = 51.5\%$$

$$\text{mol\% } N_2 = 100 - 51.5 = 48.5\%$$

For the retentate: $n_R = 69.1 + 10.5 = 79.6 \text{ kmol/h}$

$$\text{mol\% } O_2 = 10.5/79.6 = 0.132 = 13.2\%$$

$$\text{mol\% } N_2 = 100 - 13.2 = 86.8\%$$

Case 2: O_2 recovery is given; its distribution to the products is

$$n_{1,P} = 0.50(21) = 10.5 \text{ kmol/h}$$

$$n_{1,R} = 21 - 10.5 = 10.5 \text{ kmol/h}$$

Using the purity of O_2 in the permeate, the total permeate flow rate is

$$n_p = 10.5/0.5 = 21 \text{ kmol/h}$$

By a total permeate material balance:

$$n_{2,P} = 21 - 10.5 = 10.5 \text{ kmol/h}$$

By an overall N_2 material balance:

$$n_{2,R} = 79 - 10.5 = 68.5 \text{ kmol/h}$$

For the permeate: $n_p = 21 \text{ kmol/h}$

$$\text{mol\% } O_2 = 10.5/21 = 0.50 = 50\%$$

$$\text{mol\% } N_2 = 100 - 50 = 50\%$$

For the retentate: $n_R = 100 - 21 = 79 \text{ kmol/h}$

$$\text{mol\% } O_2 = 10.5/79 = 0.133 = 13.3\%$$

$$\text{mol\% } N_2 = 100 - 13.3 = 86.7\%$$

Case 3: Two material-balance equations, one for each component, can be written:

For nitrogen, with a purity of 0.85 in the retentate and $1.00 - 0.50 = 0.50$ in the permeate,

$$n_{2,F} = 0.85n_R + 0.50n_p = 79 \text{ kmol/h} \quad (1)$$

For oxygen, with a purity of 0.50 in the permeate and $1.00 - 0.85 = 0.15$ in the retentate,

$$n_{1,F} = 0.50n_p + 0.15n_R = 21 \text{ kmol/h} \quad (2)$$

Solving (1) and (2) simultaneously for the total flow rates of the products gives

$$n_p = 17.1 \text{ kmol/h} \text{ and } n_R = 82.9 \text{ kmol/h}$$

Therefore, the component flow rates are

$$n_{1,P} = 0.50(17.1) = 8.6 \text{ kmol/h}$$

$$n_{2,R} = 0.85(82.9) = 70.5 \text{ kmol/h}$$

$$n_{1,R} = 82.9 - 70.5 = 12.4 \text{ kmol/h}$$

$$n_{2,P} = 17.1 - 8.6 = 8.5 \text{ kmol/h}$$

For the permeate: $n_p = 17.1 \text{ kmol/h}$

$$\text{mol\% } O_2 = 8.6/17.1 = 0.503 = 50.3\%$$

$$\text{mol\% } N_2 = 100 - 50.3 = 49.7\%$$

For the retentate: $n_R = 100 - 17.1 = 82.9 \text{ kmol/h}$

$$\text{mol\% } O_2 = 12.4/82.9 = 0.150 = 15.0\%$$

$$\text{mol\% } N_2 = 100 - 15.0 = 85.0\%$$

§1.8.1 Purity and Composition Designations

The product purities in Table 1.6 are given in **mol%**, a designation usually restricted to gas mixtures, for which **vol%** is equivalent to mol%. For liquids, purities are more often specified in mass fractions or **wt%**. Although vol% is also common for liquid mixtures, it is not easily calculated when the liquid mixture is a nonideal solution. To meet environmental regulations, the allowable concentration of an impurity in gas, liquid, or solids streams is typically specified in parts of impurity per million parts (**ppm**) or parts of impurity per billion parts (**ppb**), where if a gas, the parts are moles or volumes; if a liquid or solid, then mass or weight. For aqueous solutions, especially those containing acids and bases, common designations for composition are **molarity (M)**, which is the molar concentration in moles of solute per liter of solution; **molality (m)** in moles of solute per kilogram of solvent; and **normality (N)** in number of equivalent weights of solute per liter of solution. Concentrations (c) in mixtures can be in units of moles or mass per volume (e.g., **mol/L**, **g/L**, **kg/m³**, **lbmol/ft³**, **lb/ft³**). For some chemical products, an attribute, such as color, may be used in place of purity in terms of composition.

§1.8.2 Alternative Separation Sequences

The three-distillation-column recovery process shown in Figure 1.10 is only one of five alternative sequences of distillation operations that can separate the process feed into four

products when each column has a single feed that is separated into one distillate and one bottoms. Consider a hydrocarbon feed that consists, in the order of decreasing volatility, propane (C_3), isobutane (iC_4), n -butane (nC_4), isopentane (iC_5), and n -pentane (nC_5). A sequence of distillation columns is used to separate the feed into three nearly pure products of C_3 , iC_4 , and nC_4 ; and one multicomponent product of combined iC_5 and nC_5 . Figure 1.11 shows the five alternative sequences. When two final products are desired, only a single distillation column is needed. For three final products, there are two alternative sequences. As the number of final products increases, the number of alternative sequences grows rapidly as shown in Table 1.7.

For the initial selection of a feasible sequence, the following heuristics (plausible but not infallible rules) are useful and easy to apply, and do not require an economic evaluation:

1. Remove unstable, corrosive, or chemically reactive components early in the sequence. Then the materials of construction used in later columns will be less expensive. Also remove very volatile components early in the sequence so that column pressures can be reduced in later columns.
2. Remove final products one by one, in order of decreasing volatility or increasing boiling point, as overhead distillates.
3. Remove, early in the sequence, those components of greatest molar percentage in the feed. The remaining columns will be smaller in diameter.

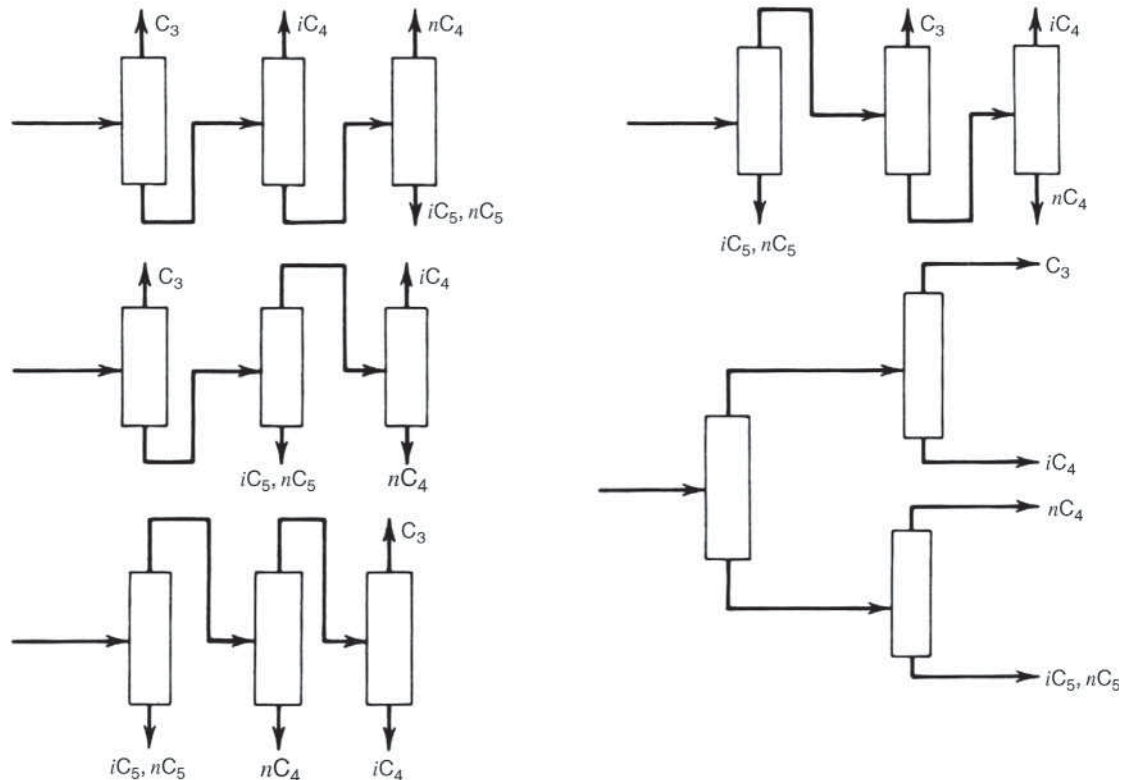


Figure 1.11 Alternative distillation sequences to produce four products.

Table 1.7 Number of Alternative Sequences

Number of Final Products	Number of Columns	Number of Alternative Sequences
2	1	1
3	2	2
4	3	5
5	4	14
6	5	42

4. Make the most difficult separations in the absence of the other components. This will usually lower the diameter of the tallest column.
5. Leave later in the sequence those separations that produce final products of the highest purities. This will also lower the diameter of the tallest column.
6. Select the sequence that favors near-equimolar amounts of distillate and bottoms in each column. Then the two sections of the column will tend to have the same diameter.

Unfortunately, these heuristics sometimes conflict with one another so that one clear choice may not be possible. If applicable, Heuristic 1 should always be employed. The most common industrial sequence is that of Heuristic 2. When energy costs are high, Heuristic 6 is favored because of lower utility costs. When one of the separations is particularly difficult, such as the separation of isomers, Heuristic 4 is usually

SUMMARY

1. Industrial chemical processes include equipment for separating chemical mixtures in process feed(s) and/or produced in reactors within the process.
2. The more widely used separation operations involve transfer of species between two phases, one of which is created by an energy separation agent (ESA) or the introduction of a mass-separating agent (MSA).
3. Less commonly used operations employ a barrier to preferentially pass certain species or a force field to cause species to diffuse to another location at different rates.

REFERENCES

1. CUSSLER, E.L., and G.D. MOGGRIDGE, *Chemical Product Design*, Cambridge University Press, Cambridge, UK (2001).
2. SEIDER, W.D., J.D. SEADER, D.R. LEWIN and S. WIDAGDO, *Product & Process Design Principles* 3rd ed., John Wiley & Sons, Hoboken, NJ (2009).

STUDY QUESTIONS

- 1.1. What are the two key process operations in chemical engineering?
- 1.2. What are the main auxiliary process operations in chemical engineering?

applied. For determining an optimal sequence, Seider et al. [2] present rigorous methods that do require column designs and economic evaluations. They also consider complex sequences that include separators of different types and complexity.

EXAMPLE 1.2 Selection of a Separation Sequence using Heuristics.

A distillation sequence is to produce four final products from five hydrocarbons. Figure 1.11 shows the five possible sequences. The molar percentages in the process feed to the sequence are C_3 (5.0%), iC_4 (15%), nC_4 (25%), iC_5 (20%), and nC_5 (35%). The most difficult separation by far is that between the isomers, iC_4 and nC_4 . Use the heuristics to determine the best sequence(s). All products are to be of high purity.

Solution

Heuristic 1 does not apply. Heuristic 2 favors taking C_3 , iC_4 , and nC_4 as distillates in Columns 1, 2, and 3, respectively, with the multicomponent product of iC_5 and nC_5 taken as the bottoms in Column 3. Heuristic 3 favors the removal of the multicomponent product (55% of the feed) in Column 1. Heuristic 4 favors the separation of iC_4 from nC_4 in Column 3. Heuristics 3 and 4 can be combined with C_3 taken as distillate in Column 2. Heuristic 5 does not apply. Heuristic 6 favors taking the multicomponent product as bottoms in Column 1 (45/55 mole split), nC_4 as bottoms in Column 2 (20/25 mole split), and C_3 as distillate with iC_4 as bottoms in Column 3. Thus, the heuristics lead to three possible sequences as most favorable.

4. Separation operations are designed to achieve product purity and to strive for high recovery.
5. A sequence of separators is usually required when more than two products are to be produced or when the required product purity cannot be achieved in a single separator.
6. The cost of purifying a chemical depends on its concentration in the feed. The extent of industrial use of a particular separation operation depends on its cost and technological maturity.

3. KELLER, G.E., II, *AIChE Monogr. Ser.*, **83**(17) (1987).
4. SHERWOOD, T.K., R.L. PIGFORD, and C.R. WILKE, *Mass Transfer*, McGraw-Hill, New York (1975).
5. DWYER, J.L., *Biotechnology*, **1**, 957 (Nov. 1984).

- 1.3. What are the four general separation techniques and what do they all have in common?
- 1.4. Why is the rate of mass transfer a major factor in separation processes?

- 1.5. What limits the extent to which the separation of a mixture can be achieved?
- 1.6. What are the most common methods used to separate two fluid phases?
- 1.7. What is the difference between an ESA and an MSA? Give three disadvantages of using an MSA.
- 1.8. What is the most widely used industrial separation operation?

EXERCISES

Section 1.1

1.1. Description of the ethanol process.

Considering possible side reactions, describe as best you can what takes place in each block of the process shown in Figure 1.4.

Section 1.2

1.2. Mixing vs. separation.

Explain, using thermodynamic principles, why mixing pure chemicals to form a homogeneous mixture is a spontaneous process, while separation of that mixture into its pure species is not.

1.3. Separation of a mixture requires energy.

Explain, using the laws of thermodynamics, why the separation of a mixture into pure species or other mixtures of differing compositions requires energy transfer to the mixture.

Sections 1.3 and 1.4

1.4. ESA vs. MSA.

Compare the advantages and disadvantages of making separations using an ESA versus using an MSA.

1.5. Differences among distillation and liquid–liquid extraction.

Under what conditions should liquid–liquid extraction be considered over distillation?

Section 1.5

1.6. Osmotic pressure.

The osmotic pressure, π , of seawater is given by $\pi = RTc/M$, where c is the concentration of the dissolved salts (solute) in g/cm^3 , M is the average molecular weight of the solutes as ions, T is temperature in Kelvin, and R is the ideal gas constant. Consider recovering pure water from seawater containing $0.035 \text{ g of salts}/\text{cm}^3$ of seawater and $M = 31.5$, at 298 K. What is the minimum required pressure difference across the membrane in kPa to just overcome the osmotic pressure?

1.7. Basic separation techniques.

For each of the following separation operations, state the basic separation process technique shown in Figure 1.6: absorption, adsorption, dialysis, distillation, flash vaporization, gas permeation, liquid–liquid extraction, pervaporation, reverse osmosis, and stripping.

Section 1.7

1.8. Removing organic pollutants from wastewater.

The need to remove organic pollutants from wastewater is common to many industrial processes. Separation methods to be considered are: (1) adsorption, (2) distillation, (3) liquid–liquid extraction, (4) membrane separation, (5) stripping with air, and (6) stripping with steam. Discuss the advantages and disadvantages of each method. Consider the fate of the organic material.

- 1.9. What is the difference between adsorption and absorption?
- 1.10. The degree of separation in a separation operation is often specified in terms of product purities and component recoveries. How do these two differ?
- 1.11. What is a key component? What is a multicomponent product?
- 1.12. Why are sequences of separators sometimes necessary to separate a feed mixture?

1.9. Removal of VOCs from a wastewater stream.

Many waste gas streams contain volatile organic compounds (VOCs), which must be removed. Recovery of the VOCs may be accomplished by (1) absorption, (2) adsorption, (3) condensation, (4) freezing, (5) membrane separation, or (6) catalytic oxidation. Discuss the pros and cons of each method, paying particular attention to the fate of the VOC. For the case of a stream containing 3 mol% acetone in air, draw a flow diagram for a process based on absorption. Choose a reasonable absorbent and include in your process a means to recover the acetone and recycle the absorbent.

1.10. Separation of air.

Describe three methods suitable for the separation of air into nitrogen and oxygen.

Section 1.8

1.11. Material balance for a distillation sequence.

The feed to Column C3 in Figure 1.10 is given in Table 1.5. The separation is to be altered to produce a distillate of 95 mol% pure isobutane with a recovery in the distillate of 96%. Because of the sharp separation in Column C3 between $i\text{C}_4$ and $n\text{C}_4$, assume all propane goes to the distillate and C_5s to the bottoms.

- (a) Compute the flow rates in lbmol/h of each component in each of the two products leaving Column C3.
- (b) What is the percent purity of the n -butane bottoms product?
- (c) If the isobutane purity in the distillate is fixed at 95%, what percent recovery of isobutane in the distillate will maximize the percent purity of normal butane in the bottoms product?

1.12. Material balance for a distillation sequence.

Five hundred kmol/h of liquid alcohols containing, by moles, 40% methanol (M), 35% ethanol (E), 15% isopropanol (IP), and 10% normal propanol (NP) is distilled in two distillation columns in series. The distillate from the first column is 98% pure M with a 96% recovery of M. The distillate from the second is 92% pure E with a 95% recovery of E from the process feed. Assume no propanols in the distillate from Column C1, no M in the bottoms from Column C2, and no NP in the distillate from Column C2.

- (a) Compute flow rates in kmol/h of each component in each feed, distillate, and bottoms. Draw a labeled block-flow diagram. Include the material balances in a table, similar to Table 1.5.
- (b) Compute the mole-percent purity of the propanol mixture leaving as bottoms from the second column.
- (c) If the recovery of ethanol is fixed at 95%, what is the maximum purity of the ethanol in the distillate from the second column?
- (d) If instead, the purity of the ethanol is fixed at 92%, what is the maximum recovery of ethanol (based on the process feed)?

1.13. Material balance for separation by pervaporation.

Ethanol and benzene are separated in a network of distillation and membrane separation steps. In one step, a near-azeotropic liquid

mixture of 8,000 kg/h of 23 wt% ethanol in benzene is fed to a pervaporation membrane consisting of an ionomeric film of perfluoro-sulfonic polymer cast on a Teflon support. The membrane is selective for ethanol, producing a vapor permeate containing 60 wt% ethanol, while the non-permeate (retentate) liquid contains 90 wt% benzene.

- Draw a flow diagram of the pervaporation using symbols from Table 1.3 and include all process information.
- Compute the component flow rates in kg/h in the feed stream and in the product streams, and enter these results in the diagram.
- What separation operation could be used to purify the vapor permeate?

1.14. Material balance for an absorption-distillation sequence.

1,000 kmol/h of a gas mixture containing 90 mol% acetone and 10% nitrogen is to be processed to recover the acetone. First the gas is fed to a multistage absorber where 95% of the acetone is absorbed with 500 kmol/h of a liquid absorbent of methyl-isobutyl-ketone (MIBK). Two percent of the entering MIBK is lost to the gas leaving the top of the absorber. Nitrogen does not dissolve in the MIBK.

The liquid leaving the bottom of the absorber is sent to a distillation column to separate the acetone from the MIBK. In this column, a distillate of 98 mol% acetone and a bottoms of 99 mol% MIBK is obtained.

- Draw a flow diagram of the separation process and place the above data on the diagram.
- For each stream in the process, calculate by material balances the flow rate of each component and enter your results in a table similar to Table 1.5.

1.15. Separation by Gas Permeation.

The Prism gas permeation process developed by the Monsanto Company is selective for hydrogen when using hollow-fiber membranes made of silicone-coated polysulphone. A feed gas at 16.7 MPa and 40°C containing 42.4 H₂, 7.0 CH₄, and 0.5 N₂ kmol/h is separated by the membrane into a retentate gas at 16.2 MPa and a permeate gas at 4.56 MPa.

- Assume the membrane is non-permeable to nitrogen, the recovery of H₂ is 60.38%, and the mole ratio of CH₄ to H₂ in the permeate is 0.0117. Calculate the total flow rate of the retentate and permeate gases and the flow rates of each component in them.
- Compute the percent purity of the hydrogen in the permeate gas.
- Draw a process-flow diagram that displays pressure and component flow rates.

1.16. Separation by membrane separation and adsorption.

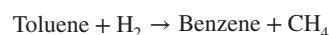
Nitrogen is injected into oil wells to increase the recovery of crude oil (enhanced oil recovery). It mixes with the natural gas that is produced along with the oil. The nitrogen must be separated from the natural gas. A total of 170,000 SCFH (based on 60°F and 14.7 psia) of natural gas containing 18% N₂, 75% CH₄, and 7% C₂H₆ at 100°F and 800 psia is to be processed in two steps to reduce nitrogen content to 3 mol%: (1) membrane separation with a nonporous glassy polyimide membrane, followed by (2) adsorption using molecular sieves to which the permeate gas is fed. The membrane separator is highly selective for N₂ (90.83% recovery), and completely impermeable to ethane. The mole ratio of CH₄ to N₂ in the permeate is 1.756. The adsorption step selectively adsorbs methane, giving 97% pure methane in the adsorbate, with an 85% recovery of CH₄ fed to the adsorber. The non-permeate (retentate) gas from the membrane step and adsorbate from the adsorption step are combined to give a methane stream that contains 3.0 mol% N₂. The pressure drop across the membrane is 760 psia. The permeate at 20°F is compressed to 275 psia and cooled to 100°F before entering

the adsorption step. The adsorbate, which exits the adsorber during regeneration at 100°F and 15 psia, is compressed to 800 psia and cooled to 100°F before being combined with non-permeate gas to give the final pipeline natural gas.

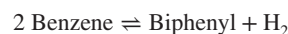
- Draw a process flow diagram of the process using appropriate symbols. Include compressors and heat exchangers. Label the diagram with the data given and number all streams.
- Compute component flow rates of N₂, CH₄, and C₂H₆ in lbmol/h and create a material-balance table similar to Table 1.5.

1.17. Partial condensation of a reactor effluent.

Toluene (methylbenzene) is used as a solvent and a fuel and is a precursor for making benzene by hydrodealkylation; benzene and xylenes by disproportionation; and 2,4,6-trinitrotoluene (TNT)—an explosive used by the military and construction companies—by nitration. Consider a hydrodealkylation process, where the main reaction is:



with an undesirable side reaction:



The reactor effluent is cooled and partially condensed. The liquid phase is then distilled in a sequence of three distillation columns to give the following four products, one of which is recycled back to the reactor.

Component	Off-gas, kmol/h	Benzene Product, kmol/h	Toluene Recycle, kmol/h	Biphenyl By-product, kmol/h
Hydrogen	1.48	0.00	0.00	0.00
Methane	11.07	0.06	0.00	0.00
Benzene	0.80	264.72	1.33	0.00
Toluene	0.00	0.09	88.79	0.45
Biphenyl	0.00	0.00	0.02	4.59
Total	13.35	264.87	90.14	5.04

- Calculate for the sequence the percent recoveries for benzene and biphenyl.
- Calculate the mol% purities for benzene and biphenyl.
- Why is there a toluene recycle stream?
- What would happen if the biphenyl was not separated from the toluene, but was recycled back to the reactor with the toluene?

1.18. Separation by Gas Permeation.

In a hydrodealkylation process of the type stated in Exercises 1.17 and 1.22, a gas rich in hydrogen and methane is separated from the reactor effluent by partial condensation. The gas is then sent to a gas permeation membrane separator (Operation 3 in Table 1.3) to separate the hydrogen from the methane. The permeate is recycled to the reactor and the retentate is used for fuel. The component flow rates for the membrane feed, retentate, and permeate are as follows:

Component	Feed, kmol/h	Retentate, kmol/h	Permeate, kmol/h
Hydrogen	1575.7	157.6	1418.1
Methane	2388.1	2313.5	74.6
Benzene	29.8	29.8	0.0
Toluene	3.5	3.5	0.0
Biphenyl	0.0	0.0	0.0
Total	3997.1	2504.4	1492.7

- (a) Calculate the percent recoveries and mol% purities of hydrogen in the permeate and methane in the retentate. (b) Why not separate hydrogen from methane by distillation or absorption?

1.19. Distillation sequences.

The feed stream in the table below is to be separated into four nearly pure products. None of the components is corrosive and, based on the boiling points, none of the three separations is difficult. As seen in Figure 1.11, five distillation sequences are possible. (a) Determine a suitable sequence of three columns using the heuristics of §1.8.2. (b) If a fifth component were added to give five products, Table 1.7 indicates that 14 alternative distillation sequences are possible. Draw, in a manner similar to Figure 1.10, all 14 of these sequences.

Component	Feed rate, kmol/h	Normal boiling point, K
Methane	19	112
Benzene	263	353
Toluene	85	384
Ethylbenzene	23	409

1.20. Distillation sequence for a solution from fermentation.

Starch from corn or sugarcane can be fermented to an aqueous solution of acetone (A), *n*-butanol (B), and ethanol (E). Typically, the mass ratio of bioproducts is 3(A):6(B):1(E). The solution contains 33 g of bioproducts per liter of water. After removal of solid particles from the broth by centrifugation, the remaining liquid is distilled in a sequence of distillation columns to recover (1) acetone with a maximum of 10 wt% water; (2) ethanol with a maximum of 10 wt% water; (3) *n*-butanol (99.5 wt% purity with a maximum of 0.5% water); and (4) water (W), which can be recycled to the fermenter. If the four products distill according to their normal boiling points in °C of 56.5 (A), 117 (B), 78.4 (E), and 100 (W), devise a suitable distillation sequence using the heuristics of §1.8.2.

1.21. Separation by a distillation sequence.

A light-hydrocarbon feed stream contains 45.4 kmol/h of propane, 136.1 kmol/h of isobutane, 226.8 kmol/h of *n*-butane, 181.4 kmol/h of isopentane, and 317.4 kmol/h of *n*-pentane. This stream is to be separated by a sequence of three distillation columns into four products: (1) propane-rich, (2) isobutane-rich, (3) *n*-butane-rich, and (4) combined pentanes-rich. The first-column distillate is the propane-rich product; the distillate from Column 2 is the isobutane-rich product; the distillate from Column 3 is the *n*-butane-rich product, and the combined pentanes are the Column 3 bottoms. The recovery of the main component in each product is 98%. For example, 98% of the propane in the feed stream appears in the propane-rich product.

- (a) Draw a process-flow diagram for this distillation sequence, similar to Figure 1.10.

- (b) Complete a material balance for each column and summarize the results in a table similar to Table 1.5. To complete the balance, you must make assumptions about the flow rates of: (1) isobutane in the distillates for Columns 1 and 3 and (2) *n*-butane in the distillates for Columns 1 and 2, consistent with the specified recoveries. Assume no propane in the distillate from Column 3 and no pentanes in the distillate from Column 2.

- (c) Calculate the mol% purities of the products and summarize your results as in Table 1.6, but without the specifications.

1.22. Distillation sequence for a wide-boiling mixture.

The effluent from the reactor of a toluene hydrodealkylation process of the type stated in Exercise 1.17 is as follows:

Component	Boiling Point, °C	Flow Rate, kmol/h
Hydrogen	-252.8	1577.1
Methane	-169.0	2399.2
Benzene	80.1	296.6
Toluene	110.6	92.8
Biphenyl	255.2	4.6
Total		4370.3

The reactor effluent at 1265°F and 500 psia is to be separated into four products: (a) a gaseous mixture rich in hydrogen and methane; (b) a benzene-rich product of high purity; (c) a toluene-rich mixture of low purity that is recycled to the reactor; and (d) a biphenyl by-product of high purity. Using the heuristics of §1.8.2, determine one or two favorable sequences. A sequence can contain one single-stage partial condenser in place of one multistage distillation column.

1.23. Distillation sequence for an alcohol mixture.

A mixture of five alcohols is to be separated into nearly pure products in a sequence of distillation columns, each of which produces a distillate and a bottoms. According to Table 1.7, four columns are needed that can be arranged into 14 different sequences. Using the heuristics of §1.8.2, determine one or two feasible sequences. The following table lists the alcohols in the order of volatility. The volatilities relative to the fifth (least volatile) alcohol, 1-hexanol, are shown. Also included are the flow rates of the five alcohols in the feed to the sequence.

Alcohol	Feed flow rate, kmol/h	Volatility relative to 1-hexanol
1-Butanol	360	3.6
2-Methyl-1-Butanol	180	2.5
3-Methyl-2-Butanol	360	2.3
1-Pentanol	2520	1.8
1-Hexanol	3600	1.0
Total	7020	

Thermodynamics of Separation Operations

§2.0 INSTRUCTIONAL OBJECTIVES

After completing this chapter, you should be able to:

- Explain phase equilibria in terms of Gibbs free energy, chemical potential, fugacity, fugacity coefficient, activity, and activity coefficient.
- Understand the usefulness of phase equilibrium ratios (e.g., K -values and distribution ratios) for determining vapor and liquid phase compositions.
- Derive K -value expressions in terms of fugacity coefficients and activity coefficients.
- Explain how computer programs use equation of state (EOS) models to compute thermodynamic properties of vapor and liquid mixtures, including K -values.
- Explain how computer programs use liquid-phase activity-coefficients derived from Gibbs excess free-energy models to compute thermodynamic properties, including K -values.
- Make energy, entropy, and exergy (availability) balances around a separation process.

Thermodynamic properties play a major role in designing and simulating separation operations with respect to energy requirements, phase equilibria, and equipment sizing. This chapter reviews methods for calculating molar volume or density, enthalpy, entropy, exergy (availability), fugacities, activity coefficients, and phase equilibria ratios of ideal and nonideal vapor and liquid mixtures as functions of temperature, pressure, and composition. These thermodynamic properties are used for determining compositions at phase-equilibrium, and for making energy balances, entropy balances, and exergy balances to determine energy efficiency. Emphasis is on the thermodynamic property methods most widely used in process simulators.

Experimental thermodynamic property data should be used, when available, to design and analyze separation operations. When not available, properties can often be estimated with reasonable accuracy by methods discussed in this chapter. The most comprehensive source of thermodynamic properties for pure compounds and nonelectrolyte and electrolyte mixtures—including excess volume, excess enthalpy, activity coefficients at infinite dilution, azeotropes, and vapor–liquid, liquid–liquid, and solid–liquid equilibrium—is the computerized Dortmund Data Bank (DDB), described briefly at www.ddbst.com, and in detail by Gmehling, et al. [1]. It was initiated by Gmehling and Onken in 1973. It is updated annually and widely used by industry and academic institutions on a stand-alone basis or with process simulators via the DDB software package (DDBST). In 2014, the DDB contained more than 6.4 million data sets for more than 49,000 components from more than 65,400 literature references. The DDB contains openly available experimental data from journals, which can be searched free of charge. A large percentage of the

data is from non-English sources, industry, and MS and PhD theses. The DDB also presents comparisons of experimental data with various estimation methods described in this chapter.

§2.1 PHASE EQUILIBRIA

Many separations are determined by the extent to which species are partitioned among two or more phases at equilibrium at a specified T and P . The distribution is determined by application of the **Gibbs free energy**, G . For each phase in a multiphase, multicomponent system, the Gibbs free energy is

$$G = G\{T, P, N_1, N_2, \dots, N_C\} \quad (2-1)$$

where T = temperature, P = pressure, and N_i = moles of species i . At equilibrium, the total G for all phases is a minimum, and methods for determining this are referred to as **free-energy minimization techniques**. Gibbs free energy is also the starting point for the derivation of commonly used equations for phase equilibria. From classical thermodynamics, the total differential of G is

$$dG = -S dT + V dP + \sum_{i=1}^C \mu_i dN_i \quad (2-2)$$

where S = entropy, V = volume, and μ_i is the **chemical potential** or partial molar Gibbs free energy of species i . For a closed system consisting of two or more phases in equilibrium, where each phase is an open system capable of mass transfer with another phase,

$$dG_{\text{system}} = \sum_{p=1}^{N_p} \left[\sum_{i=1}^C \mu_i^{(p)} dN_i^{(p)} \right]_{P,T} \quad (2-3)$$

where superscript (p) refers to each of N_p phases. Conservation of moles of species, in the absence of chemical reaction, requires that

$$dN_i^{(1)} = - \sum_{p=2}^{N_p} dN_i^{(p)} \quad (2-4)$$

which, upon substitution into (2-3), gives

$$\sum_{p=2}^{N_p} \left[\sum_{i=1}^C \left(\mu_i^{(p)} - \mu_i^{(1)} \right) dN_i^{(p)} \right] = 0 \quad (2-5)$$

With $dN_i^{(1)}$ eliminated in (2-5), each $dN_i^{(p)}$ term can be varied independently of any other $dN_i^{(p)}$ term. But this requires that each coefficient of $dN_i^{(p)}$ in (2-5) be zero. Therefore,

$$\mu_i^{(1)} = \mu_i^{(2)} = \mu_i^{(3)} = \dots = \mu_i^{(N_p)} \quad (2-6)$$

Thus, the chemical potential of a species in a multicomponent system is identical in all phases at physical equilibrium. This equation is the basis for the development of all phase-equilibrium calculations.

§2.1.1 Fugacities and Activity Coefficients

Chemical potential is not an absolute quantity, and the numerical values are difficult to relate to more easily understood physical quantities. Furthermore, the chemical potential approaches an infinite negative value as pressure approaches zero. Thus, the chemical potential is not a favored property for phase-equilibria calculations. Instead, **fugacity**, invented by G. N. Lewis in 1901, is employed as a surrogate.

The partial fugacity of species i in a mixture is like a pseudo-pressure, defined in terms of the chemical potential by

$$\bar{f}_i = \mathcal{K} \exp\left(\frac{\mu_i}{RT}\right) \quad (2-7)$$

where \mathcal{K} is a temperature-dependent constant. Regardless of the value of \mathcal{K} , it is shown by Prausnitz, Lichtenthaler, and de Azevedo [2] that (2-6) can be replaced with

$$\bar{f}_i^{(1)} = \bar{f}_i^{(2)} = \bar{f}_i^{(3)} = \dots = \bar{f}_i^{(N_p)} \quad (2-8)$$

where, \bar{f}_i is the **partial fugacity** of species i . Thus, at equilibrium, a given species has the same partial fugacity in each phase. This equality, together with equality of phase temperatures and pressures,

$$T^{(1)} = T^{(2)} = T^{(3)} = \dots = T^{(N_p)} \quad (2-9)$$

$$P^{(1)} = P^{(2)} = P^{(3)} = \dots = P^{(N_p)} \quad (2-10)$$

constitutes the well-accepted conditions for phase equilibria. For a pure component, the partial fugacity, \bar{f}_i , becomes the pure-component fugacity, f_i . For a pure, ideal gas, fugacity equals the total pressure, and for a component in an ideal-gas mixture, the partial fugacity equals its partial pressure, $p_i = y_i P$, such that the sum of the partial pressures equals the total pressure (Dalton's Law). Because of the close

relationship between fugacity and pressure, it is convenient to define a pure-species **fugacity coefficient**, ϕ_i , as

$$\phi_i = \frac{f_i}{P} \quad (2-11)$$

which is 1.0 for an ideal gas. For a mixture, **partial fugacity coefficients** for vapor and liquid phases, respectively, are

$$\bar{\phi}_{iV} \equiv \frac{\bar{f}_{iV}}{y_i P} \quad (2-12)$$

$$\bar{\phi}_{iL} \equiv \frac{\bar{f}_{iL}}{x_i P} \quad (2-13)$$

As ideal-gas behavior is approached, $\bar{\phi}_{iV} \rightarrow 1.0$ and $\bar{\phi}_{iL} \rightarrow P_i^s/P$, where $P_i^s =$ vapor pressure.

At a given temperature, the ratio of the partial fugacity of a component to its fugacity in a standard state, f_i^o , is termed the **activity**, a_i . If the standard state is selected as the pure species at the same pressure and phase condition as the mixture, then

$$a_i \equiv \frac{\bar{f}_i}{f_i^o} \quad (2-14)$$

Since at phase equilibrium, the value of f_i^o is the same for each phase, substitution of (2-14) into (2-8) gives another alternative condition for phase equilibria,

$$a_i^{(1)} = a_i^{(2)} = a_i^{(3)} = \dots = a_i^{(N_p)} \quad (2-15)$$

For an ideal solution, $a_{iV} = y_i$ and $a_{iL} = x_i$.

To represent departure of activities from mole fractions when solutions are nonideal, **activity coefficients** based on concentrations in mole fractions are defined by

$$\gamma_{iV} \equiv \frac{a_{iV}}{y_i} \quad (2-16)$$

$$\gamma_{iL} \equiv \frac{a_{iL}}{x_i} \quad (2-17)$$

For ideal solutions, $\gamma_{iV} = 1.0$ and $\gamma_{iL} = 1.0$

For convenient reference, thermodynamic quantities useful in phase equilibria are summarized in Table 2.1.

§2.1.2 Definitions of K -Values

A **phase-equilibrium ratio** is the ratio of mole fractions of a species in two phases at equilibrium. For vapor–liquid systems, the ratio is called the **K -value** or **vapor–liquid equilibrium ratio**:

$$K_i \equiv \frac{y_i}{x_i} \quad (2-18)$$

For the liquid–liquid case, the ratio is a **distribution ratio**, **partition coefficient**, or **liquid–liquid equilibrium ratio**:

$$K_{D_i} \equiv \frac{x_i^{(1)}}{x_i^{(2)}} \quad (2-19)$$

Table 2.1 Thermodynamic Quantities for Phase Equilibria

Thermodynamic Quantity	Definition	Physical Significance	Limiting Value for Ideal Gas and Ideal Solution
Chemical potential	$\mu_i \equiv \left(\frac{\partial G}{\partial N_i} \right)_{P,T,N_j}$	Partial molar free energy, \bar{g}_i	$\mu_i = \bar{g}_i$
Partial fugacity	$\bar{f}_i \equiv \mathcal{K} \exp\left(\frac{\mu_i}{RT}\right)$	Thermodynamic pressure	$\bar{f}_{iV} = y_i P$ $\bar{f}_{iL} = x_i P_i^S$
Fugacity coefficient of a pure species	$\phi_i \equiv \frac{\bar{f}_i}{P}$	Deviation to fugacity due to pressure	$\phi_{iV} = 1.0$ $\phi_{iL} = \frac{P_i^S}{P}$
Partial fugacity coefficient of a species in a mixture	$\bar{\phi}_{iV} \equiv \frac{\bar{f}_{iV}}{y_i P}$ $\bar{\phi}_{iL} \equiv \frac{\bar{f}_{iL}}{x_i P}$	Deviations to fugacity due to pressure and composition	$\bar{\phi}_{iV} = 1.0$ $\bar{\phi}_{iL} = \frac{P_i^S}{P}$
Activity	$a_i \equiv \frac{\bar{f}_i}{f_i^o}$	Relative thermodynamic pressure	$a_{iV} = y_i$ $a_{iL} = x_i$
Activity coefficient	$\gamma_{iV} \equiv \frac{a_{iV}}{y_i}$ $\gamma_{iL} \equiv \frac{a_{iL}}{x_i}$	Deviation to fugacity due to composition	$\gamma_{iV} = 1.0$ $\gamma_{iL} = 1.0$

For equilibrium-stage calculations, separation factors are defined by forming ratios of equilibrium ratios. For the vapor–liquid case, **relative volatility** $\alpha_{i,j}$ between components i and j is given by

$$\alpha_{i,j} \equiv \frac{K_i}{K_j} \quad (2-20)$$

Separations are easy for very large values of $\alpha_{i,j}$, but become impractical for values close to 1.00.

Similarly for the liquid–liquid case, the **relative selectivity** $\beta_{i,j}$ is

$$\beta_{i,j} \equiv \frac{K_{D_i}}{K_{D_j}} \quad (2-21)$$

Equilibrium ratios are formulated in a variety of ways using the thermodynamic quantities in Table 2.1. The two of most practical interest are formulated next.

§2.1.3 Rigorous K -Value Formulations

For vapor–liquid equilibrium, (2-8) becomes, for each component,

$$\bar{f}_{iV} = \bar{f}_{iL} \quad (2-22)$$

To form an equilibrium ratio, partial fugacities are commonly replaced by expressions involving mole fractions. From the definitions in Table 2.1:

$$\bar{f}_{iL} = \gamma_{iL} x_i f_{iL}^o \quad (2-23)$$

or

$$\bar{f}_{iL} = \bar{\phi}_{iL} x_i P \quad (2-24)$$

and

$$\bar{f}_{iV} = \bar{\phi}_{iV} y_i P \quad (2-25)$$

If (2-24) and (2-25) are used with (2-18), an **equation-of-state (EOS) formulation** of the K -value follows, where the partial fugacity coefficients are obtained from an EOS, as described later in this chapter.

$$K_i = \frac{\bar{\phi}_{iL}}{\bar{\phi}_{iV}} \quad (2-26)$$

If (2-23) and (2-25) are used, an **activity coefficient** or **gamma-phi formulation** of the K -value is obtained:

$$K_i = \frac{\gamma_{iL} f_{iL}^o}{\bar{\phi}_{iV} P} = \frac{\gamma_{iL} \phi_{iL}}{\bar{\phi}_{iV}} \quad (2-27)$$

If the ideal gas EOS, $Pv = RT$ applies—where v = molar volume and R = the ideal-gas constant—and both the vapor and liquid form ideal solutions, then $\gamma_{iL} = 1.0$, $\phi_{iL} = P_i^S/P$, and $\bar{\phi}_{iV} = 1.0$. If these are substituted into (2-27), the result is **Raoult's law** or **ideal K -value** expression:

$$K_i = \frac{P_i^S}{P} \quad (2-28)$$

If, however, the liquid phase is a nonideal solution, $\gamma_{iL} \neq 1.0$ and (2-28) becomes the **modified Raoult's law K-value** expression:

$$K_i = \frac{\gamma_{iL} P_i^s}{P} \quad (2-29)$$

For moderate pressures, the **Poynting correction** is introduced into (2-27) by approximating the pure-component liquid fugacity coefficient in (2-27) by

$$\phi_{iL} = \phi_{iV}^s \frac{P_i^s}{P} \exp\left(\frac{1}{RT} \int_{P_i^s}^P v_{iL} dP\right) \quad (2-30)$$

where ϕ_{iV}^s = pure component vapor fugacity coefficient at the saturation pressure. The exponential term is the Poynting correction. If the liquid molar volume, v , is reasonably constant over the pressure range, the integral in (2-28) becomes $v_{iL}(P - P_i^s)$. For moderate to high pressures, an EOS is used to obtain ϕ_{iV} in (2-27).

For a low-molecular-weight gas species, whose temperature at the critical point, T_c , is less than the system temperature, the **Henry's law** form for the K -value is convenient, provided H_i , the Henry's law coefficient, is available. It depends on composition, temperature, and pressure. At low to moderate pressures, it replaces the vapor pressure in (2-28) to give

$$K_i = \frac{H_i}{P} \quad (2-31)$$

Table 2.2 lists the above-mentioned vapor–liquid K -value expressions and includes recommendations for their application.

Regardless of which thermodynamic formulation in Table 2.2 is used for estimating K -values, its accuracy depends on the correlations used for the thermodynamic properties (vapor pressure, activity coefficient, and fugacity coefficients).

For practical applications, the choice of K -value formulation is a compromise among accuracy, complexity, convenience, and past experience.

For liquid–liquid equilibria, (2-8) becomes

$$\bar{f}_{iL}^{(1)} = \bar{f}_{iL}^{(2)} \quad (2-32)$$

where superscripts (1) and (2) refer to the immiscible liquid phases. A rigorous formulation for the distribution coefficient is obtained by combining (2-23) with (2-19) to obtain an expression involving only activity coefficients:

$$K_{D_i} = \frac{x_i^{(1)}}{x_i^{(2)}} = \frac{\gamma_{iL}^{(2)} f_{iL}^{o(2)}}{\gamma_{iL}^{(1)} f_{iL}^{o(1)}} = \frac{\gamma_{iL}^{(2)}}{\gamma_{iL}^{(1)}} \quad (2-33)$$

For vapor–solid equilibria, if the solid phase consists of just one of the components of the vapor phase, combination of (2-8) and (2-25) gives

$$f_{iS} = \bar{\phi}_{iV} y_i P \quad (2-34)$$

At low pressures, $\bar{\phi}_{iV} = 1.0$ and the fugacity of the solid is approximated by its vapor pressure. Thus, for the vapor-phase mole fraction of the component forming the solid phase:

$$y_i = \frac{(P_i^s)_{\text{solid}}}{P} \quad (2-35)$$

For liquid–solid equilibria, if the solid phase is a pure component, the combination of (2-8) and (2-23) gives

$$f_{iS} = \gamma_{iL} x_i f_{iL}^o \quad (2-36)$$

At low pressure, the fugacity of a solid is approximated by vapor pressure to give, for a component in the solid phase,

$$x_i = \frac{(P_i^s)_{\text{solid}}}{\gamma_{iL} (P_i^s)_{\text{liquid}}} \quad (2-37)$$

Table 2.2 Useful K -Value Expressions for Estimating Vapor–Liquid Equilibria ($K_i = y_i/x_i$)

	Equation	Recommended Application
Rigorous forms:		
(1) Equation-of-state	$K_i = \frac{\bar{\phi}_{iL}}{\bar{\phi}_{iV}}$	Hydrocarbon and light gas mixtures from cryogenic temperatures to the critical region
(2) Activity coefficient	$K_i = \frac{\gamma_{iL} \phi_{iL}}{\bar{\phi}_{iV}}$	All mixtures from ambient to near-critical temperature
Approximate forms:		
(3) Raoult's law (ideal)	$K_i = \frac{P_i^s}{P}$	Ideal solutions at near-ambient pressure
(4) Modified Raoult's law	$K_i = \frac{\gamma_{iL} P_i^s}{P}$	Nonideal liquid solutions at near-ambient pressure
(5) Poynting correction	$K_i = \gamma_{iL} \phi_{iV}^s \left(\frac{P_i^s}{P}\right) \exp\left(\frac{1}{RT} \int_{P_i^s}^P v_{iL} dP\right)$	Nonideal liquid solutions at moderate pressure and below the critical temperature
(6) Henry's law	$K_i = \frac{H_i}{P}$	Low-to-moderate pressures for species at supercritical temperature

EXAMPLE 2.1 K-Values from Raoult's and Henry's Laws.

Estimate K -values and the relative volatility, $\alpha_{M,W}$, of a vapor–liquid mixture of water (W) and methane (M) at $P = 2$ atm, $T = 20$ and 80°C . What is the effect of T on the K -values?

Solution

At these conditions, water exists mainly in the liquid phase and will follow Raoult's law (2-28) if little methane dissolves in the water. Because methane has a critical temperature of -82.5°C , well below the temperatures of interest, it will exist mainly in the vapor phase and follow Henry's law (2-31). The Aspen Plus process simulator is used to make the calculations using the Ideal Properties option with methane as a Henry's law component. The Henry's law constants for the solubility of methane in water are provided in the simulator data bank. The results are as follows:

$T, ^\circ\text{C}$	K_W	K_M	$\alpha_{M,W}$
20	0.01154	18,078	1,567,000
80	0.23374	33,847	144,800

For both temperatures, the mole fraction of methane in the water is less than 0.0001. The K -values for H_2O are low but increase rapidly with temperature. The K -values for methane are extremely high and change much less rapidly with temperature.

§2.2 IDEAL-GAS, IDEAL-LIQUID-SOLUTION MODEL

Classical thermodynamics provides a means for obtaining fluid thermodynamic properties in a consistent manner from P - v - T EOS models. The simplest model applies when both liquid and vapor phases are ideal solutions (all activity coefficients equal 1.0) and the vapor is an ideal gas. Then the thermodynamic properties of mixtures can be computed from pure-component properties of each species using the equations given in Table 2.3. These ideal equations apply only at low pressures—not much above ambient—for components of similar molecular structure.

The vapor molar volume, v_V , and mass density, ρ_V , are computed from (1), the ideal-gas law in Table 2.3. It requires only the mixture molecular weight, M , and the gas constant, R . It assumes that Dalton's law of additive partial pressures and Amagat's law of additive volumes apply.

The molar vapor enthalpy, h_V , is computed from (2) in Table 2.3 by integrating an equation in temperature for the zero-pressure heat capacity at constant pressure, $C_{P_V}^o$, starting from a reference (datum) temperature, T_o , to the temperature of interest, and then summing the resulting species vapor enthalpies on a mole-fraction basis. Typically, T_o is taken as 25°C , although 0 K is also common. Pressure has no effect on the enthalpy of an ideal gas. A number of empirical equations have been used to correlate the effect of temperature on the zero-pressure vapor heat capacity. An example is the fourth-degree polynomial:

$$C_{P_V}^o = [a_0 + a_1T + a_2T^2 + a_3T^3 + a_4T^4] R \quad (2-38)$$

Table 2.3 Thermodynamic Properties for Ideal Mixtures**Ideal gas and ideal-gas solution:**

$$(1) v_V = \frac{V}{\sum_{i=1}^C N_i} = \frac{M}{\rho_V} = \frac{RT}{P}, \quad M = \sum_{i=1}^C y_i M_i$$

$$(2) h_V = \sum_{i=1}^C y_i \int_{T_o}^T (C_{P_V}^o)_{iV} dT = \sum_{i=1}^C y_i h_{iV}^o$$

$$(3) s_V = \sum_{i=1}^C y_i \int_{T_o}^T \frac{(C_{P_V}^o)_{iV}}{T} dT - R \ln \left(\frac{P}{P_o} \right) - R \sum_{i=1}^C y_i \ln y_i,$$

where the first term is s_V^o

Ideal-liquid solution:

$$(4) v_L = \frac{V}{\sum_{i=1}^C N_i} = \frac{M}{\rho_L} = \sum_{i=1}^C x_i v_{iL}, \quad M = \sum_{i=1}^C x_i M_i$$

$$(5) h_L = \sum_{i=1}^C x_i (h_{iV}^o - \Delta H_i^{\text{vap}})$$

$$(6) s_L = \sum_{i=1}^C x_i \left[\int_{T_o}^T \frac{(C_{P_V}^o)_{iV}}{T} dT - \frac{\Delta H_i^{\text{vap}}}{T} \right] - R \ln \left(\frac{P}{P_o} \right) - R \sum_{i=1}^C x_i \ln x_i$$

Vapor–liquid equilibria:

$$(7) K_i = \frac{P_i^s}{P}$$

Reference conditions (datum): h , ideal gas at T_o and zero pressure; s , ideal gas at T_o and $P_o = 1$ atm.

Refer to elements if chemical reactions occur; otherwise refer to components.

where the constants, a , depend on the species. Values of the constants for hundreds of compounds, with T in K , are tabulated by Poling, Prausnitz, and O'Connell [3]. Because $C_p = dh/dT$, (2-38) can be integrated for each species to give the ideal-gas species molar enthalpy:

$$h_V^o = \int_{T_o}^T C_{P_V}^o dT = \sum_{k=1}^5 \frac{a_{k-1}(T^k - T_o^k)R}{k} \quad (2-39)$$

The molar vapor entropy, s_V , is computed from (3) in Table 2.3 by integrating $C_{P_V}^o/T$ from T_o to T for each species; summing on a mole-fraction basis; adding a term for the effect of pressure referenced to a datum pressure, P_o , which is generally taken to be 1 atm (101.3 kPa); and adding a term for the entropy change of mixing. Unlike the ideal vapor enthalpy, the ideal vapor entropy includes terms for the effects of pressure and mixing. The reference pressure is not zero, because

the entropy is infinity at zero pressure. If (2-38) is used for the heat capacity,

$$\int_{T_o}^T \left(\frac{C_{pV}^o}{T} \right) dT = \left[a_0 \ln \left(\frac{T}{T_o} \right) + \sum_{k=1}^4 \frac{a_k (T^k - T_o^k)}{k} \right] R \quad (2-40)$$

The liquid molar volume, v_L , and mass density, ρ_L , are computed from the pure species using (4) in Table 2.3 and assuming additive molar volumes (not densities). The effect of temperature on pure-component liquid density from the freezing point to the near-critical region at saturation pressure is correlated well by the Rackett equation [4]:

$$\rho_L = \frac{A}{B^{(1-T/T_c)^{2/7}}} \quad (2-41)$$

where values of constants A and B , and the critical temperature, T_c , are tabulated for approximately 700 organic compounds by Yaws et al. [5].

The vapor pressure of a liquid species, P^s , is well represented over temperatures from below the normal boiling point to the critical region by an extended Antoine equation:

$$\ln P^s = k_1 + k_2/(k_3 + T) + k_4 T + k_5 \ln T + k_6 T^{k_7} \quad (2-42)$$

where constants k for hundreds of compounds are built into the physical-property libraries of all process simulation programs. At low pressures, the molar enthalpy of vaporization is given in terms of vapor pressure by classical thermodynamics:

$$\Delta H^{\text{vap}} = RT^2 \left(\frac{d \ln P^s}{dT} \right) \quad (2-43)$$

If (2-42) is used for the vapor pressure, (2-43) becomes

$$\Delta H^{\text{vap}} = RT^2 \left(-\frac{k_2}{(k_3 + T)^2} + k_4 + \frac{k_5}{T} + k_7 k_6 T^{k_7-1} \right) \quad (2-44)$$

The molar enthalpy, h_L , of an ideal-liquid mixture is obtained by subtracting the molar enthalpy of vaporization from the ideal molar vapor enthalpy for each species, as given by (2-39), and summing, as shown in (5) in Table 2.3. The molar entropy, s_L , of the ideal-liquid mixture, given by (6), is obtained in a similar manner from the ideal-gas entropy by subtracting the molar entropy of vaporization, $\Delta H^{\text{vap}}/T$.

The final equation in Table 2.3 gives the expression for the ideal K -value, previously included in Table 2.2. It is the K -value based on Raoult's law, using

$$p_i = x_i P_i^s \quad (2-45)$$

and Dalton's law:

$$p_i = y_i P \quad (2-46)$$

Combination of (2-45) and (2-46) gives the Raoult's law K -value:

$$K_i \equiv \frac{y_i}{x_i} = \frac{P_i^s}{P} \quad (2-47)$$

where the extended Antoine equation, (2-42), is used to estimate vapor pressure. The ideal K -value is independent of composition, but exponentially dependent on temperature because of the vapor pressure, and inversely proportional to pressure.

Note that from (2-20), the ideal relative volatility using (2-47) is pressure independent.

EXAMPLE 2.2 Thermodynamic Properties of an Ideal Mixture.

Styrene is manufactured by catalytic dehydrogenation of ethyl benzene, followed by vacuum distillation to separate styrene from unreacted ethyl benzene [6]. Typical conditions for the feed are 77.9°C (351 K) and 100 torr (13.33 kPa), with the following flow rates:

Component	n , kmol/h
	Feed
Ethyl benzene (EB)	103.82
Styrene (S)	90.15

Assuming that the ideal-gas law holds and that vapor and liquid phases exist and are ideal solutions, use a process simulator to determine the feed-stream phase conditions and the thermodynamic properties listed in Table 2.2. Also, compute the relative volatility, $\alpha_{\text{EB,S}}$.

Solution:

The Aspen Plus Simulator with the Ideal Properties option gives the following results where the datum is the elements (not the components) at 25°C and 1 atm.

Property	Vapor	Liquid
EB Flow rate, kmol/h	57.74	46.08
S Flow rate, kmol/h	42.91	47.24
Total Flow rate, kmol/h	100.65	93.32
Temperature, °C	77.9	77.9
Pressure, Bar	0.1333	0.1333
Molar Enthalpy, kJ/kmol	87,200	56,213
Molar Entropy, kJ/kmol-K	-244.4	-350.0
Molar Volume, m ³ /kmol	219.0	0.126
Average MW	105.31	105.15
Vapor Pressure, Bar	0.1546	0.1124
K -Value	1.16 for EB	0.843 for S
Relative Volatility	1.376	

§2.3 GRAPHICAL REPRESENTATION OF THERMODYNAMIC PROPERTIES

Plots of thermodynamic properties are useful not only for the data they contain, but also for the graphical representation, which permits the user to: (1) make general observations about the effects of temperature, pressure, and composition; (2) establish correlations and make comparisons with experimental data; and (3) make extrapolations. All process simulators that calculate thermodynamic properties also allow the user to make property plots. Handbooks and thermodynamic textbooks contain generalized plots of thermodynamic properties as a function of temperature and/or pressure. A typical plot is Figure 2.1, which shows vapor pressure curves of common

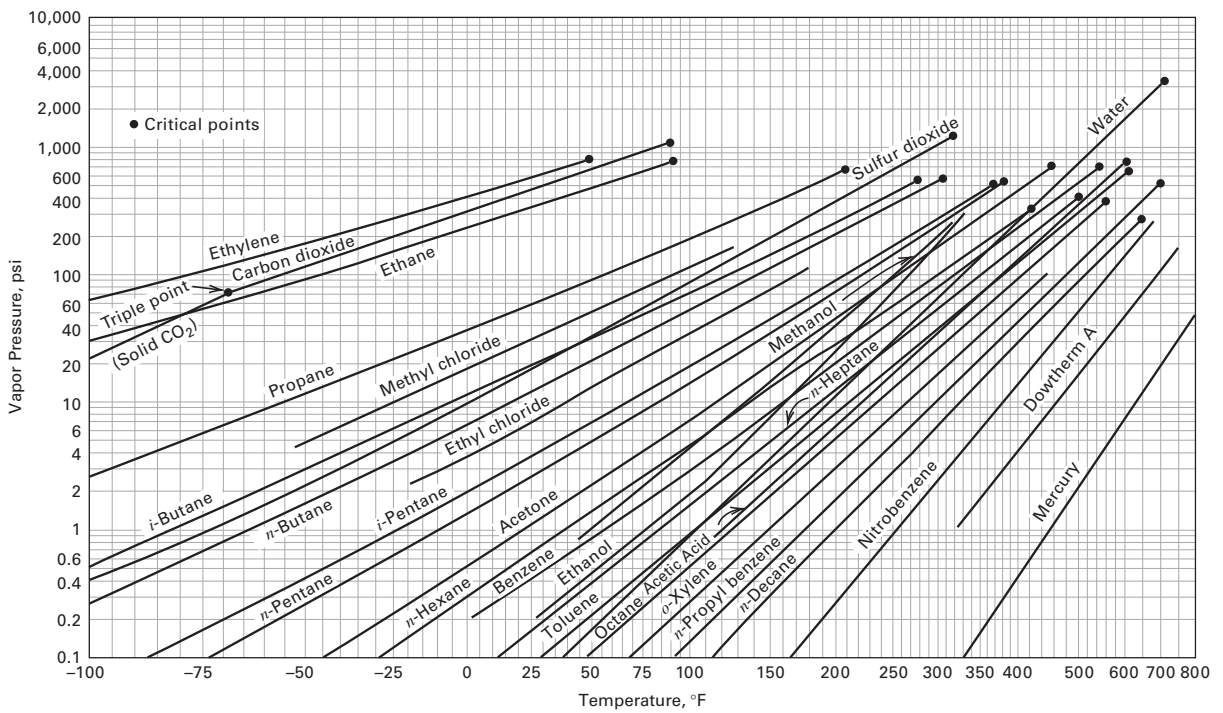


Figure 2.1 Vapor pressure of some common industrial chemicals.
 [Reproduced with permission from A.S. Faust, L.A. Wenzel, C.W. Clump, L. Maus, and L.B. Andersen, *Principles of Unit Operations*, John Wiley & Sons, New York (1960).]

chemicals for temperatures from below their normal boiling point to their critical temperature where the vapor pressure curves terminate. These curves fit the extended Antoine equation (2-42) reasonably well and are useful in establishing the phase of a pure species. If the pressure is above the curve, the phase is liquid, if below it is vapor. Vapor pressures are also used for estimating Raoult's law *K*-values prior to using a process simulator.

Before the advent of digital computers and process simulators, various types of graphs were used for determining effects of temperature and pressure on vapor-liquid *K*-values for hydrocarbons and light gases. These graphs, often in nomograph form, were correlations of experimental phase equilibria data. They were not applicable when mixtures contained sufficiently different hydrocarbons such that liquid-phase activity coefficients were not close to 1.0 and were strongly dependent on composition. With the advent of computers, empirical models that account for effects of composition in addition to temperature and pressure, and can be applied to mixtures of organic chemicals as well as hydrocarbons, displaced graphical correlations. These empirical models are available in all process simulators. Those most widely used are discussed in subsequent sections of this chapter. Some of the models apply to liquid-liquid equilibrium.

§2.4 NONIDEAL THERMODYNAMIC PROPERTY MODELS

Of importance to all separation processes are nonideal thermodynamic properties of mixtures. Models have been formulated to estimate thermodynamic properties of nonideal, nonelectrolyte, electrolyte, and polymer mixtures. Many of these models, together with the constants and parameters needed to apply them to the design and simulation of separation operations, are available in process simulators. In this chapter, emphasis is on the most widely used models of three types: (1) *P-v-T* equation-of-state (EOS) models; (2) Gibbs excess free-energy (g^E) models from which liquid-phase activity coefficients can be calculated; and (3) predictive thermodynamic models. Their applicability depends on the nature of the components in the mixture, the degree of nonideality, the pressure and temperature, and the reliability of the equation constants and parameters.

§2.4.1 Reference State (Datum) for Enthalpy

It is important to note that enthalpy is not an absolute thermodynamic property. It is determined relative to a reference state (datum) and no standard has been accepted. Instead, many different reference states are used in practice. It is important to be aware of the enthalpy reference states used in process simulators.

In the Aspen Plus process simulator, two options, discussed by Felder and Rousseau [47], are available: (1) **elemental**

reference state and (2) **component reference state**. For both states, the reference temperature is 25°C (298.15 K). The default option is the elemental reference state, in which the enthalpy of a pure component is referenced to its standard elements by its standard enthalpy of formation. The component reference state is the pure component as an ideal gas. The advantage of the default option is that an enthalpy balance around a chemical reactor automatically accounts for the heat of reaction because components are referred to the standard elements. The default option must be used for electrolyte systems. As an example, the enthalpy of superheated steam at 300°C and 1 MPa, using the elemental reference state, is -12,920 kJ/kg. If the component reference state is used, the enthalpy becomes 508 kJ/kg. The difference is -13,428 kJ/kg or -241,900 kJ/kmol, which is the value for the standard enthalpy of formation at 25°C for water vapor from the standard elements by the reaction, $\text{H}_{2(g)} + \frac{1}{2}\text{O}_{2(g)} \rightarrow \text{H}_2\text{O}_{(g)}$.

In the ChemSep process simulator, the reference temperature is also 25°C, but the reference phase state can be vapor or liquid. The standard enthalpy of formation can be included or excluded to achieve either the elemental or the component reference state for enthalpy.

In the CHEMCAD process simulator, the reference temperature is also 25°C, but only the elemental reference state is used.

§2.5 *P-v-T* EQUATION-OF-STATE (EOS) MODELS

A relationship between molar volume, temperature, and pressure is a *P-v-T* equation of state. Numerous such equations have been proposed. The simplest is the ideal-gas law, which applies only at low pressures or high temperatures because it neglects intermolecular forces and the volume occupied by the molecules. All other equations of state attempt to correct for these two deficiencies. The most widely used equations of state are listed in Table 2.4.

Not included in Table 2.4 is the van der Waals equation, $P = RT/(v - b) - a/v^2$, where *a* and *b* are species-dependent constants. This equation was the first successful formulation of an equation of state for a nonideal gas. It is now rarely used because of its narrow range of application. However, its development suggested that all species have approximately equal reduced molar volumes, $v_r = v/v_c$ at the same reduced temperature, $T_r = T/T_c$, and reduced pressure, $P_r = P/P_c$, where the subscript *c* refers to the critical point. This finding, referred to as the **law of corresponding states**, was utilized to develop the **generalized equation-of-state**, (2) in Table 2.4, which defines the **compressibility factor**, $Z = Pv/RT$, where *Z* is a function of P_r , T_r , and either the critical compressibility factor, Z_c , or the **acentric factor**, ω . The latter was introduced by Pitzer et al. [7] to account for differences in

Table 2.4 Useful Equations of State

Name	Equation	Equation Constants and Functions
(1) Ideal-gas law	$P = \frac{RT}{v}$	None
(2) Generalized	$P = \frac{ZRT}{v}$	$Z = Z\{P_r, T_r, Z_c \text{ or } \omega\}$ as derived from data
(3) Redlich-Kwong (RK)	$P = \frac{RT}{v-b} - \frac{a}{(v^2 + bv)\sqrt{T}}$	$b = 0.08664RT_c/P_c$ $a = 0.42748R^2T_c^{2.5}/P_c$
(4) Soave-Redlich-Kwong (SRK)	$P = \frac{RT}{v-b} - \frac{a}{v^2 + bv}$	$b = 0.08664RT_c/P_c$ $a = 0.42748R^2T_c^2[1 + f_\omega(1 - T_r^{0.5})]^2/P_c$ $f_\omega = 0.48 + 1.574\omega - 0.176\omega^2$
(5) Peng-Robinson (PR)	$P = \frac{RT}{v-b} - \frac{a}{v^2 + 2bv - b^2}$	$b = 0.07780RT_c/P_c$ $a = 0.45724R^2T_c^2[1 + f_\omega(1 - T_r^{0.5})]^2/P_c$ $f_\omega = 0.37464 + 1.54226\omega - 0.26992\omega^2$

molecular shape and is determined from the vapor pressure curve by:

$$\omega = \left[-\log \left(\frac{P^s}{P_c} \right)_{T_r=0.7} \right] - 1.0 \quad (2-48)$$

The value for ω is zero for symmetric molecules. Some typical values of ω are 0.264, 0.490, and 0.649 for toluene, *n*-decane, and ethyl alcohol, respectively, as taken from the extensive tabulation of Poling et al. [3].

A common empirical P - v - T equation is the virial equation of state due to Thiesen [8] and Onnes [9]. It is a power series for compressibility factor, Z , in terms of $1/v$:

$$Z = 1 + \frac{B}{v} + \frac{C}{v^2} + \dots$$

A modification of the virial equation is the Starling form [10] of the Benedict-Webb-Rubin (BWR) equation for hydrocarbons and light gases. Walas [11] presents a discussion of BWR-type equations, which—because of the large number of terms and species constants (at least 8)—is not widely used except for pure substances at cryogenic temperatures. A more useful modification of the BWR equation is a generalized corresponding-states form developed by Lee and Kesler [12] with an extension to mixtures by Plöcker et al. [13]. All of the constants in the LKP equation are given in terms of the acentric factor and reduced temperature and pressure, as developed from P - v - T data for three simple fluids ($\omega = 0$), methane, argon, and krypton, and a reference fluid *n*-octane ($\omega = 0.398$). The equations, constants, and mixing rules are given by Walas [11]. The LKP equation describes vapor and liquid mixtures of hydrocarbons and/or light gases over wide ranges of T and P .

§2.5.1 The Redlich-Kwong (RK) Model

In 1949, Redlich and Kwong [14] published the **RK equation of state** which, like the van der Waals equation, contains only two constants, a and b , both of which can be determined from T_c and P_c , by applying conditions at the critical point:

$$\left(\frac{\partial P}{\partial v} \right)_{T_c} = 0 \quad \text{and} \quad \left(\frac{\partial^2 P}{\partial v^2} \right)_{T_c} = 0$$

The RK model, given as (3) in Table 2.4 together with the two parameters, is an improvement over the van der Waals equation. When applied to nonpolar compounds, its accuracy is comparable to other EOS models containing many more constants. Furthermore, the RK equation can approximate the liquid-phase region.

A cubic equation in v results when the RK equation is expanded to obtain a common denominator. Alternatively, (2) and (3) in Table 2.4 can be combined to eliminate v to give the more useful compressibility factor, Z , form of the RK equation:

$$Z^3 - Z^2 + (A - B - B^2)Z - AB = 0 \quad (2-49)$$

where

$$A = \frac{aP}{R^2T^2} \quad (2-50)$$

$$B = \frac{bP}{RT} \quad (2-51)$$

Equation (2-49), a cubic in Z , can be solved for the three roots using MATLAB with the Roots function. At supercritical temperatures, where only one phase exists, one real root and a

complex conjugate pair of roots are obtained. Below the critical temperature, where vapor and/or liquid phases can exist, three real roots are obtained, with the largest value of Z applying to the vapor and the smallest root corresponding to the liquid (Z_V and Z_L). The intermediate value of Z is discarded.

To apply the RK model to mixtures, **mixing rules** are used to average the constants a and b for each component. The recommended rules for vapor mixtures of C components are

$$a = \sum_{i=1}^C \left[\sum_{j=1}^C y_i y_j (a_i a_j)^{0.5} \right] \quad (2-52)$$

$$b = \sum_{i=1}^C y_i b_i \quad (2-53)$$

§2.5.2 The Soave–Redlich–Kwong (SRK) Model

Following the work of Wilson [15], Soave [16] replaced the \sqrt{T} term in the RK EOS with a third parameter, the acentric factor, ω , to better represent nonspherical molecules. The resulting Soave–Redlich–Kwong (SRK) or Redlich–Kwong–Soave (RKS) equation, given as (4) in Table 2.4, was quickly accepted for application to mixtures of hydrocarbons and light gases because of its simplicity and accuracy. It makes the constant a a function of ω and T , as shown in Table 2.4, achieving a good fit to vapor pressure data, thereby improving the prediction of liquid-phase properties, and vapor-liquid K -values as discussed below. This is clearly shown in Figure 2.2 where experimental equilibrium data at 250°F for a mixture of 10 components ranging in volatility from N_2 to n -decane is compared to predictions by the SRK EOS over a pressure range of about 250 to 2,500 psi. Note that at a pressure somewhat above 2,500 psi, K -values of all 10 components appear to be approaching a value of 1.0. That point is called the **convergence pressure** for the mixture. It is analogous to the critical pressure for a pure chemical.

The mixing rules for the SRK model are (2-52) and (2-53) except that (2-52) is modified when light gases are present in the mixture to include a binary interaction coefficient, k_{ij} , giving

$$a = \sum_{i=1}^C \left[\sum_{j=1}^C y_i y_j (a_i a_j)^{0.5} (1 - k_{ij}) \right] \quad (2-54)$$

Equation (2-54) is particularly useful for gas mixtures containing N_2 , CO, CO_2 , and H_2S . Values of k_{ij} back-calculated from experimental data are used in process simulators. Generally, k_{ij} is zero for hydrocarbons paired with hydrogen or other hydrocarbons.

§2.5.3 The Peng–Robinson (PR) Model

Four years after the introduction of the SRK equation, Peng and Robinson [17] presented a modification of the RK and

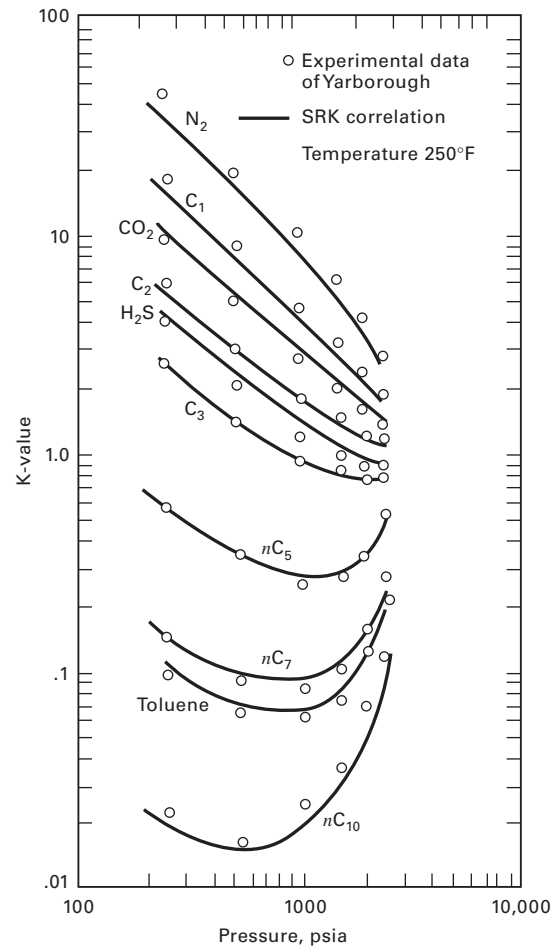


Figure 2.2 Comparison of experimental K -value data and the SRK equation.

SRK equations to achieve improved agreement in the critical region and for liquid molar volume. The Peng–Robinson (PR) EOS is (5) in Table 2.4. The mixing rules for the PR model are (2-52), (2-53), and (2-54). Both the SRK and PR equations are used in process simulators for calculations of vapor–liquid phase equilibrium compositions for mixtures of hydrocarbons and light gases.

§2.5.4 Derived Thermodynamic Properties from EOS Models

If a temperature-dependent, ideal-gas heat capacity or enthalpy equation such as (2-38) or (2-39) is available, along with an EOS, other vapor- and liquid-phase properties can be derived using the integral equations listed in Table 2.5. These equations, in the form of departures from the ideal-gas equations of Table 2.3, apply to both vapor and liquid.

When the ideal-gas law, $P = RT/v$, is substituted into Equations (1) to (4) of Table 2.4, the results for the vapor are $(h - h_v^o) = 0$, $\phi = 1$ and $(s - s_v^o) = 0$, $\phi = 1$.

When the RK equation is substituted into the equations of Table 2.5, the results for the vapor phase are:

$$h_V = \sum_{i=1}^C (y_i h_{iV}^o) + RT \left[Z_V - 1 - \frac{3A}{2B} \ln \left(1 + \frac{B}{Z_V} \right) \right] \quad (2-55)$$

$$s_V = \sum_{i=1}^C (y_i s_{iV}^o) - R \ln \left(\frac{P}{P^o} \right) - R \sum_{i=1}^C (y_i \ln y_i) + R \ln(Z_V - B) \quad (2-56)$$

$$\phi_V = \exp \left[Z_V - 1 - \ln(Z_V - B) - \frac{A}{B} \ln \left(1 + \frac{B}{Z_V} \right) \right] \quad (2-57)$$

$$\bar{\phi}_{iV} = \exp \left[(Z_V - 1) \frac{B_i}{B} - \ln(Z_V - B) - \frac{A}{B} \left(2\sqrt{\frac{A_i}{A}} - \frac{B_i}{B} \right) \ln \left(1 + \frac{B}{Z_V} \right) \right] \quad (2-58)$$

Similar results are obtained with the SRK and PR models.

The results for the liquid phase are identical if y_i and Z_V (but not h_{iV}^o) are replaced by x_i and Z_L , respectively. The liquid-phase forms of (2-55) and (2-56) account for the enthalpy and entropy of vaporization. This is because the RK equation, as well as the SRK and PR equations, are continuous functions through the vapor and liquid regions, as shown for enthalpy in Figure 2.3. Thus, the liquid enthalpy, at temperatures below the critical point, is determined by accounting for four effects. From (1), Table 2.5, and Figure 2.3:

$$h_L = h_V^o + P_V - RT - \int_{\infty}^V \left[P - T \left(\frac{\partial P}{\partial T} \right)_V \right] dV$$

This equation is then divided into four parts as shown in Figure 2.3:

1. Vapor at zero pressure = h_V^o
2. Pressure correction for vapor to saturation pressure =

$$+(P_V)_{V_{\text{sat}}} - RT - \int_{\infty}^{V_{\text{sat}}} \left[P - T \left(\frac{\partial P}{\partial T} \right)_V \right] dV$$

3. Latent heat of vaporization =

$$-T \left(\frac{\partial P}{\partial T} \right)_{\text{sat}} (v_{V_{\text{sat}}} - v_{L_{\text{sat}}})$$

4. Correction to liquid for pressure in excess of saturation pressure =

$$+ \left[(P_V)_L - (P_V)_{L_{\text{sat}}} \right] - \int_{V_{L_{\text{sat}}}}^{V_L} \left[P - T \left(\frac{\partial P}{\partial T} \right)_V \right] dV \quad (2-59)$$

where the subscript “sat” refers to the saturation pressure.

Table 2.5 Integral Departure Equations of Thermodynamics

At a given temperature and composition, the following equations give the effect of pressure above that for an ideal gas.

Mixture enthalpy:

$$(1) (h - h_V^o) = P_V - RT - \int_{\infty}^V \left[P - T \left(\frac{\partial P}{\partial T} \right)_V \right] dV$$

Mixture entropy:

$$(2) (s - s_V^o) = \int_{\infty}^V \left(\frac{\partial P}{\partial T} \right)_V dV - \int_{\infty}^V \frac{R}{V} dV$$

Pure-component fugacity coefficient:

$$(3) \phi_{iV} = \exp \left[\frac{1}{RT} \int_0^P \left(v - \frac{RT}{P} \right) dP \right] = \exp \left[\frac{1}{RT} \int_V^{\infty} \left(P - \frac{RT}{v} \right) dV - \ln Z_V + (Z_V - 1) \right]$$

Partial fugacity coefficient:

$$(4) \bar{\phi}_{iV} = \exp \left\{ \frac{1}{RT} \int_V^{\infty} \left[\left(\frac{\partial P}{\partial N_i} \right)_{T,V,N_j} - \frac{RT}{V} \right] dV - \ln Z_V \right\},$$

$$\text{where } V = v \sum_{i=1}^C N_i$$

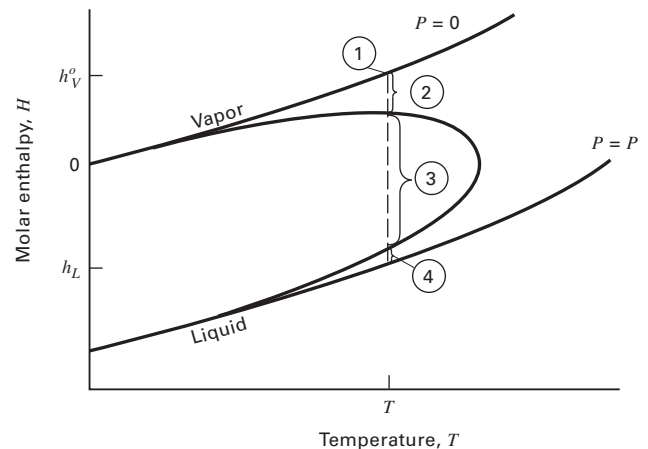


Figure 2.3 Contributions to enthalpy.

The fugacity coefficient, ϕ , of a pure species from the RK equation, as given by (2-57), describes the vapor for $P < P_i^s$. If $P > P_i^s$, ϕ is the liquid fugacity coefficient. Saturation pressure corresponds to the condition of $\phi_V = \phi_L$. Thus, at

a temperature $T < T_c$, the vapor pressure, P_i^s for species, i , can be estimated from the RK equation of state by setting (2-57) for the vapor equal to (2-57) for the liquid and solving for P , which equals P_i^s . Unfortunately, vapor pressure curves calculated by the RK equation do not satisfactorily represent experimental data for a wide range of molecular shapes. This failure is why Soave [16] modified the RK equation by introducing the acentric factor, ω . Thus, while the critical constants T_c and P_c are insufficient to generalize thermodynamic behavior, a substantial improvement results by incorporating a third parameter, ω , that accounts for molecular shape.

Both the SRK and the PR equations are used for estimating thermodynamic properties, including K -values, for hydrocarbon and light-gas mixtures. However, SRK is limited to temperatures above about -140°C , while PR can be used almost to 0 K. The properties are computed from the departure equations in Table 2.5. K -values are computed using the partial fugacity coefficients with (2-26), $K_i = \bar{\phi}_{iL}/\bar{\phi}_{iV}$. Although enhancements to both equations have been made to extend their application to polar organic chemicals, activity-coefficient models, discussed next, are preferred at near ambient conditions.

EXAMPLE 2.3 Use of SRK and PR Equations with a Process Simulator.

In the thermal hydrodealkylation of toluene to benzene ($\text{C}_7\text{H}_8 + \text{H}_2 \rightarrow \text{C}_6\text{H}_6 + \text{CH}_4$), excess hydrogen minimizes cracking of aromatics to light gases. In practice, conversion of toluene per pass through the reactor is only 70%. To separate and recycle hydrogen, hot reactor-effluent vapor of 5,597 kmol/h at 500 psia (3,448 kPa) and 275°F (408.2 K) is cooled to 120°F (322 K) and partially condensed with phases separated in a flash drum. If the composition of the reactor effluent is as given below and the pressure is 485 psia (3,344 kPa), calculate equilibrium compositions and flow rates of vapor and liquid, K -values, and the amount of heat transferred to partially condense the vapor feed, using a process simulation program for both the SRK and PR equations. Compare the results.

Component	Mole Fraction
Hydrogen (H)	0.3177
Methane (M)	0.5894
Benzene (B)	0.0715
Toluene (T)	0.0214
	1.0000

Solution

The computations were made using Aspen Plus with the SRK-ML and PENG-ROB methods. The results are as follows:

	Equation of State	
	SRK	PR
Vapor flows, kmol/h:		
Hydrogen	1,776.1	1,776.2
Methane	3,274.3	3,275.7
Benzene	57.8	59.5
Toluene	6.9	7.1
Total	5,115.1	5,118.5
Liquid flows, kmol/h:		
Hydrogen	2.0	1.9
Methane	24.6	23.2
Toluene	342.4	340.7
Toluene	112.9	112.7
Total	481.9	478.5
K-values:		
Hydrogen	80.93	85.58
Methane	12.54	13.208
Benzene	0.0159	0.0163
Toluene	0.00573	0.00587
Enthalpy change, GJ/h	35.108	34.686
Percent of benzene and toluene condensed	87.4	87.2

Because the K -values for the two methods are reasonably close, the percentage of benzene and toluene condensed by the two methods differ only slightly. Of particular note are the closeness of the K -values estimated by the two methods for H_2 and CH_4 . Both components are far above their critical temperatures. H_2 values are within 15% of experimental values measured by Zhou et al. [18]. Raoult's law K -values for benzene and toluene are 0.01032 and 0.00350, which are considerably lower than the values computed from the two equations of state because deviations to fugacities due to pressure are important.

Because the reactor effluent is mostly hydrogen and methane, the effluent at 275°F and 500 psia, and the equilibrium vapor at 120°F and 485 psia, are nearly ideal gases ($0.98 < Z < 1.00$), despite the moderately high pressures. Thus, the enthalpy change is dominated by vapor heat capacity and latent heat effects, which are independent of which equation of state is used. Consequently, the enthalpy changes differ by only about 1%.

Note that the material balances are accurately satisfied. However, users of simulation programs should never take this as an indication that all results are correct, but instead should always verify outputs in all possible ways.

§2.6 HIGHLY NONIDEAL LIQUID SOLUTIONS

When a liquid contains dissimilar polar species that can form or break hydrogen bonds, the use of EOS models is not recommended unless their mixing rules are modified. Preferred are

activity-coefficient models. Ewell, Harrison, and Berg [19] provide a classification of nonideality based on the potential for association or solvation due to hydrogen-bond formation. If a molecule contains a hydrogen atom attached to a donor atom (O, N, F, and in certain cases C), the active hydrogen atom can form a bond with another molecule containing a donor atom. The classification in Table 2.6 permits qualitative estimates of deviations from Raoult's law for binary pairs when used in conjunction with Table 2.7.

Positive deviations correspond to values of $\gamma_{iL} > 1$. Negative deviations, which are less common, correspond to $\gamma_{iL} < 1$. Nonideality results in variations of γ_{iL} with composition, as shown in Figure 2.4 for several binary systems, where the Roman numerals refer to classification in Tables 2.6 and

2.7. Starting with Figure 2.4a, the following explanations for the nonidealities are offered: *n*-heptane (V) breaks ethanol (II) hydrogen bonds, causing strong positive deviations. In Figure 2.4b, similar, but less positive, deviations occur when acetone (III) is added to formamide (I). Hydrogen bonds are broken and formed with chloroform (IV) and methanol (II) in Figure 2.4c, resulting in an unusual deviation curve for chloroform that passes through a maximum. In Figure 2.4d, chloroform (IV) provides active hydrogen atoms that form hydrogen bonds with oxygen atoms of acetone (III), thus causing negative deviations. For water (I) and *n*-butanol (II) in Figure 2.4e, hydrogen bonds of both molecules are broken, and nonideality is sufficiently strong to cause formation of two immiscible liquid phases.

Table 2.6 Classification of Molecules Based on Potential for Forming Hydrogen Bonds

Class	Description	Example
I	Molecules capable of forming three-dimensional networks of strong H-bonds	Water, glycols, glycerol, amino alcohols, hydroxylamines, hydroxyacids, polyphenols, and amides
II	Other molecules containing both active hydrogen atoms and donor atoms (O, N, and F)	Alcohols, acids, phenols, primary and secondary amines, oximes, nitro and nitrile compounds with α -hydrogen atoms, ammonia, hydrazine, hydrogen fluoride, and hydrogen cyanide
III	Molecules containing donor atoms but no active hydrogen atoms	Ethers, ketones, aldehydes, esters, tertiary amines (including pyridine type), and nitro and nitrile compounds without α -hydrogen atoms
IV	Molecules containing active hydrogen atoms but no donor atoms that have two or three chlorine atoms on the same carbon as a hydrogen or one chlorine on the carbon atom and one or more chlorine atoms on adjacent carbon atoms	CHCl_3 , CH_2Cl_2 , CH_3CHCl_2 , $\text{CH}_2\text{ClCH}_2\text{Cl}$, $\text{CH}_2\text{ClCHClCH}_2\text{Cl}$, and $\text{CH}_2\text{ClCHCl}_2$
V	All other molecules having neither active hydrogen atoms nor donor atoms	Hydrocarbons, carbon disulfide, sulfides, mercaptans, and haloalkanes not in class IV

Table 2.7 Molecule Interactions Causing Deviations from Raoult's Law

Type of Deviation	Classes	Effect on Hydrogen Bonding
Always negative	III + IV	H-bonds formed only
Quasi-ideal; always positive or ideal	III + III III + V IV + IV IV + V V + V	No H-bonds involved
Usually positive, but some negative	I + I I + II I + III II + II II + III	H-bonds broken and formed
Always positive	I + IV (frequently limited solubility) II + IV	H-bonds broken and formed, but dissociation of Class I or II is a more important effect
Always positive	I + V II + V	H-bonds broken only

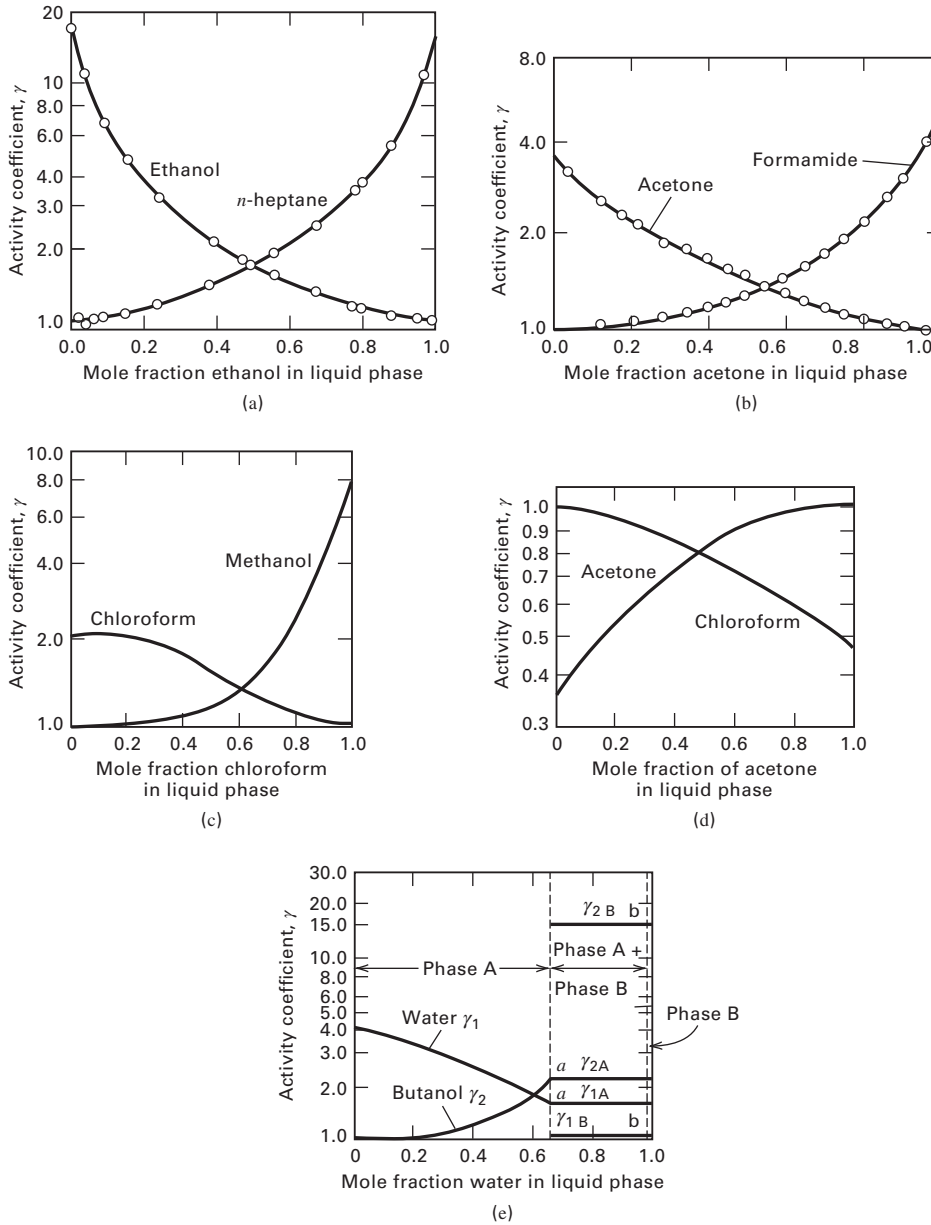


Figure 2.4 Typical variations of activity coefficients with composition in binary liquid systems: (a) ethanol (II)/*n*-heptane (V); (b) acetone (III)/formamide (I); (c) chloroform (IV)/methanol (II); (d) acetone (III)/chloroform (IV); (e) water (I)/*n*-butanol (II).

§2.7 GIBBS EXCESS FREE-ENERGY (g^E) MODELS

Predictions of liquid properties for highly nonideal solutions are based on **Gibbs excess free-energy models** for liquid-phase activity coefficients. From these models, K -values and excess functions, such as volume of mixing and enthalpy of mixing, can be estimated. The more recent and most accurate models, Wilson, NRTL, and UNIQUAC, summarized in Table 2.8, are based on the concept of local composition, introduced by Wilson [20]. These models are in process simulators and are widely used for mixtures containing polar components. They require experimentally determined

binary interaction parameters. Fortunately, many of the available parameters are automatically accessible in process simulators.

The molar Gibbs free energy, g , is the sum of the molar free energy of an ideal solution and an excess molar free energy g^E for nonideal effects. For a liquid,

$$g = \sum_{i=1}^C x_i g_i + RT \sum_{i=1}^C x_i \ln x_i + g^E = \sum_{i=1}^C x_i (g_i + RT \ln x_i + \bar{g}_i^E) \quad (2-60)$$

where $g = h - Ts$ and excess molar free energy, g^E , is the sum of the partial excess molar free energies, \bar{g}_i^E that are related to

Table 2.8 Empirical and Semitheoretical Equations for Correlating Liquid-Phase Activity Coefficients of Binary Pairs

Name	Equation for Species 1	Equation for Species 2
(1) Wilson (two-constant)	$\ln \gamma_1 = -\ln(x_1 + \Lambda_{12}x_2) + x_2 \left(\frac{\Lambda_{12}}{x_1 + \Lambda_{12}x_2} - \frac{\Lambda_{21}}{x_2 + \Lambda_{21}x_1} \right)$	$\ln \gamma_2 = -\ln(x_2 + \Lambda_{21}x_1) - x_1 \left(\frac{\Lambda_{12}}{x_1 + \Lambda_{12}x_2} - \frac{\Lambda_{21}}{x_2 + \Lambda_{21}x_1} \right)$
(2) NRTL (three-constant)	$\ln \gamma_1 = \frac{x_2^2 \tau_{21} G_{21}^2}{(x_1 + x_2 G_{21})^2} + \frac{x_1^2 \tau_{12} G_{12}}{(x_2 + x_1 G_{12})^2}$ $G_{ij} = \exp(-\alpha_{ij} \tau_{ij})$	$\ln \gamma_2 = \frac{x_1^2 \tau_{12} G_{12}^2}{(x_2 + x_1 G_{12})^2} + \frac{x_2^2 \tau_{21} G_{21}}{(x_1 + x_2 G_{21})^2}$ $G_{ij} = \exp(-\alpha_{ij} \tau_{ij})$
(3) UNIQUAC (two-constant)	$\ln \gamma_1 = \ln \frac{\Psi_1}{x_1} + \frac{\bar{Z}}{2} q_1 \ln \frac{\theta_1}{\Psi_1}$ $+ \Psi_2 \left(l_1 - \frac{r_1}{r_2} l_2 \right) - q_1 \ln(\theta_1 + \theta_2 T_{21})$ $+ \theta_2 q_1 \left(\frac{T_{21}}{\theta_1 + \theta_2 T_{21}} - \frac{T_{12}}{\theta_2 + \theta_1 T_{12}} \right)$	$\ln \gamma_2 = \ln \frac{\Psi_2}{x_2} + \frac{\bar{Z}}{2} q_2 \ln \frac{\theta_2}{\Psi_2}$ $+ \Psi_1 \left(l_2 - \frac{r_2}{r_1} l_1 \right) - q_2 \ln(\theta_2 + \theta_1 T_{12})$ $+ \theta_1 q_2 \left(\frac{T_{12}}{\theta_2 + \theta_1 T_{12}} - \frac{T_{21}}{\theta_1 + \theta_2 T_{21}} \right)$

the liquid-phase activity coefficients by

$$\begin{aligned} \frac{\bar{g}_i^E}{RT} = \ln \gamma_i &= \left[\frac{\partial (N_i g^E / RT)}{\partial N_i} \right]_{P,T,N_j} \\ &= \frac{g^E}{RT} - \sum_k x_k \left[\frac{\partial (g^E / RT)}{\partial x_k} \right]_{P,T,x_r} \end{aligned} \quad (2-61)$$

where $j \neq i$, $r \neq k$, $k \neq i$, and $r \neq i$.

The relationship between excess molar free energy and excess molar enthalpy and entropy is

$$g^E = h^E - T s^E = \sum_{i=1}^C x_i \left(\bar{h}_i^E - T \bar{s}_i^E \right) \quad (2-62)$$

Activity-coefficient models use the K -value formulation given by (2-27), $K = \gamma_{iL} \phi_{iL} / \bar{\phi}_{iV}$. For moderate pressures, ϕ_{iL} is approximated by (2-30), which includes the Poynting correction. At near ambient pressures, $\phi_{iL} = P_i^s / P$. The partial fugacity coefficient, $\bar{\phi}_{iV}$, is obtained from Eq. (4) in Table 2.5 using an EOS such as SRK or PR. At near-ambient pressures, $\bar{\phi}_{iV} = 1$ and (2-27) reduces to (2-29), the modified Raoult's law, $K = \gamma_{iL} P_i^s / P$.

§2.7.1 The Local-Composition Concept and the Wilson Model

Following its publication in 1964, the **Wilson equation** [20], Eq. (1) in Table 2.8, received wide acceptance because of its ability to fit strongly nonideal binary systems (e.g., alcohol-hydrocarbon) that do not undergo phase splitting. Figure 2.5 shows the fit of the experimental data of Sinor and Weber [21] by Cukor and Prausnitz [22] for ethanol (1)- n -hexane (2). The binary interaction parameters for the Wilson equation, $\Lambda_{12} = 0.0952$ and $\Lambda_{21} = 0.2713$ from Orye and Prausnitz [23], fit the experimental data well, even in the

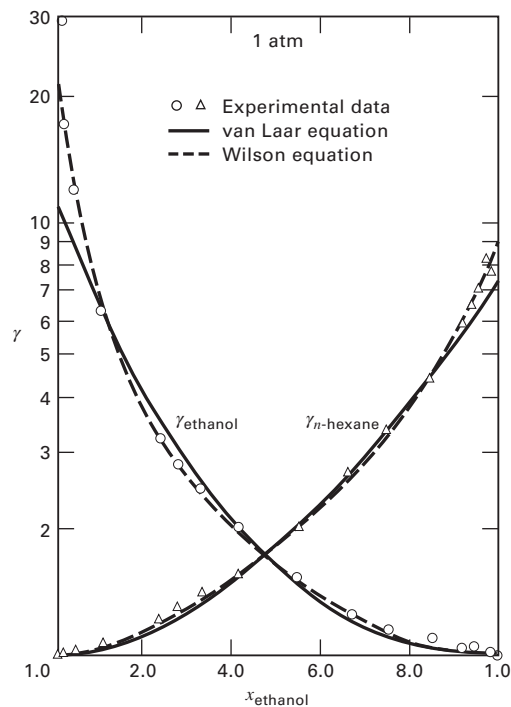


Figure 2.5 Activity coefficients for ethanol/ n -hexane.

[Reprinted from [21] with permission of the American Chemical Society.]

dilute region where the variation of γ_1 becomes exponential. The once-popular van Laar model fails to do so. Corresponding infinite-dilution activity coefficients computed from the Wilson equation are $\gamma_1^\infty = 21.72$ and $\gamma_2^\infty = 9.104$.

The Wilson equation introduced the **concept of local compositions** that differ from overall compositions. The model accounts for differences in both molecular size and intermolecular forces. Local volume fractions, $\bar{\Phi}_i$, related to local-molecule segregations caused by differing energies of interaction between pairs of molecules, are used. This

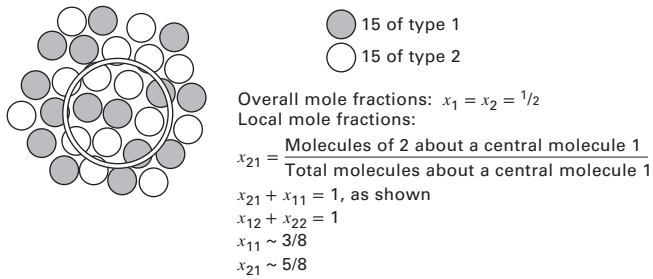


Figure 2.6 The concept of local compositions.
[Reproduced from [22] with permission of the Institution of Chemical Engineers.]

concept is illustrated for an overall equimolar binary solution in Figure 2.6, from Cukor and Prausnitz [22]. About a central molecule of type 1, the local mole fraction of type 2 molecules is shown to be 5/8, while the overall composition is 1/2.

For local-volume fraction in a binary solution, Wilson proposed

$$\bar{\Phi}_i = \frac{v_{iL}x_i \exp[-\lambda_{ii}/RT]}{\sum_{j=1}^C v_{jL}x_j \exp[-\lambda_{ij}/RT]} \quad (2-63)$$

where energies of interaction $\lambda_{ij} = \lambda_{ji}$, but $\lambda_{ii} \neq \lambda_{jj}$. Following Orye and Prausnitz [23], binary interaction parameters are defined by

$$\Lambda_{12} = \frac{v_{2L}}{v_{1L}} \exp \left[-\frac{(\lambda_{12} - \lambda_{11})}{RT} \right] \quad (2-64)$$

$$\Lambda_{21} = \frac{v_{1L}}{v_{2L}} \exp \left[-\frac{(\lambda_{12} - \lambda_{22})}{RT} \right] \quad (2-65)$$

Equations (2-64) and (2-65) lead to the excess free energy, predicted by the Wilson model for a binary system as:

$$\frac{g^E}{RT} = -x_1 \ln(x_1 + \Lambda_{12}x_2) - x_2 \ln(x_2 + \Lambda_{21}x_1) \quad (2-66)$$

The expressions for the two activity coefficients of the binary system (species 1 and 2) in Table 2.8 are obtained by substitution of (2-66) into (2-61).

The Wilson equation is effective for dilute compositions where entropy effects dominate enthalpy effects. Values of $\Lambda_{ij} < 1$ correspond to positive deviations from Raoult's law, while values > 1 signify negative deviations. Ideal solutions result when $\Lambda_{ij} = 1$. Studies indicate that λ_{ii} and λ_{ij} are temperature dependent. Values of v_{iL}/v_{jL} also depend on temperature, but the variation is small compared to the effect of temperature on the exponential terms in (2-64) and (2-65).

The Wilson equation is extended to multicomponent mixtures by neglecting ternary and higher interactions and assuming a pseudo-binary mixture. The following multicomponent Wilson equation involves only binary interaction parameters:

$$\ln \gamma_k = 1 - \ln \left(\sum_{j=1}^C x_j \Lambda_{kj} \right) - \sum_{i=1}^C \left(\frac{x_i \Lambda_{ik}}{\sum_{j=1}^C x_j \Lambda_{ij}} \right) \quad (2-67)$$

where $\Lambda_{ii} = \Lambda_{jj} = \Lambda_{kk} = 1$.

For highly nonideal, but still miscible, multicomponent mixtures, the Wilson equation (2-67) is preferred over the older Margules, van Laar, and regular-solution equations, which are discussed in detail by Walas [11]. The constants in the Wilson equation for many binary systems are tabulated in the DECHEMA collection of Gmehling and Onken [24] and in the Dortmund Data Bank (DDB) and are accessible in process simulators. Two limitations of the Wilson equation are its inability to (1) predict immiscibility, as in Figure 2.4e, and (2) predict maxima and minima in activity coefficient–mole fraction relationships, as in Figure 2.4c.

When insufficient data are available to determine binary parameters from a best fit of activity coefficients, infinite-dilution or single-point values can be used. At infinite dilution, the Wilson equation in Table 2.8 becomes

$$\ln \gamma_1^\infty = 1 - \ln \Lambda_{12} - \Lambda_{21} \quad (2-68)$$

$$\ln \gamma_2^\infty = 1 - \ln \Lambda_{21} - \Lambda_{12} \quad (2-69)$$

If temperatures corresponding to γ_1^∞ and γ_2^∞ are not close or equal, (2-64) and (2-65) should be substituted into (2-68) and (2-69), with values of $(\lambda_{12} - \lambda_{11})$ and $(\lambda_{12} - \lambda_{22})$ determined from estimates of pure-component liquid molar volumes, to estimate Λ_{12} and Λ_{21} .

When the data of Sinor and Weber [21] for *n*-hexane/ethanol, shown in Figure 2.5, are plotted as a *y*-*x* diagram in ethanol (Figure 2.7), the equilibrium curve crosses the 45° line at *y* = *x* = 0.332. The temperature corresponding to this composition is 58°C. This is a minimum-boiling azeotrope for this mixture at 1 atm. The azeotrope temperature is lower than the normal boiling points of ethanol (78.33°C) and *n*-hexane (68.75°C). Nevertheless, ethanol is more volatile than *n*-hexane up to an ethanol mole fraction of *x* = 0.322, the composition of the azeotrope. The azeotrope occurs because of the close boiling points of the two species and the high activity coefficients for ethanol at low concentrations. At the azeotropic composition, *y*_{*i*} = *x*_{*i*}; therefore, *K*_{*i*} = 1.0 and a separation cannot be made by a single or multistage

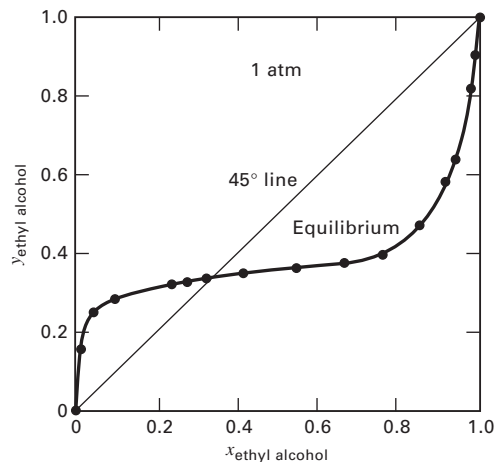


Figure 2.7 Equilibrium curve for *n*-hexane/ethanol.

distillation. Applying the modified Raoult’s law, (2-29), to both species,

$$\gamma_1 P_1^s = \gamma_2 P_2^s \tag{2-70}$$

If pure species 2 is more volatile ($P_2^s > P_1^s$), the criteria for formation of a minimum-boiling azeotrope are

$$\gamma_1 \geq 1 \tag{2-71}$$

$$\gamma_2 \geq 1 \tag{2-72}$$

and

$$\frac{\gamma_1}{\gamma_2} < \frac{P_2^s}{P_1^s} \tag{2-73}$$

for x_1 less than the azeotropic composition. These criteria are most readily applied at $x_1 = 0$. For example, for the *n*-hexane (2)/ethanol (1) system at 1 atm when the liquid-phase mole fraction of ethanol approaches zero, the temperature approaches 68.75°C, the boiling point of pure *n*-hexane. At this temperature, $P_1^s = 10$ psia (68.9 kPa) and $P_2^s = 14.7$ psia (101.3 kPa). Also, from Figure 2.5, $\gamma_1^\infty = 21.72$ when $\gamma_2 = 1.0$. Thus, $\gamma_1^\infty/\gamma_2 = 21.72$, but $P_2^s/P_1^s = 1.47$. Therefore, a minimum-boiling azeotrope will occur.

Maximum-boiling azeotropes are less common. They occur for close-boiling mixtures when negative deviations from Raoult’s law arise, giving $\gamma_i < 1.0$. Criteria are derived in a manner similar to that for minimum-boiling azeotropes. At $x_1 = 1$, where species 2 is more volatile,

$$\gamma_1 = 1.0 \tag{2-74}$$

$$\gamma_2^\infty < 1.0 \tag{2-75}$$

and

$$\frac{\gamma_2^\infty}{\gamma_1} < \frac{P_1^s}{P_2^s} \tag{2-76}$$

For azeotropic binary systems, interaction parameters Λ_{12} and Λ_{21} can be determined by solving Equation (1) of Table 2.8 at the azeotropic composition, as shown in the following example.

EXAMPLE 2.4 Wilson Binary-Interaction Constants from Azeotropic Data.

From measurements by Sinor and Weber [21] of the azeotropic condition for the ethanol (E)/*n*-hexane (H) system at 1 atm (101.3 kPa, 14.696 psia), calculate the binary-interaction constants, Λ_{12} and Λ_{21} for the Wilson model.

Solution

The azeotrope occurs at $x_E = 0.332$, $x_H = 0.668$, and $T = 58^\circ\text{C}$ (331.15 K). At 1 atm, Raoult’s law, (2-29) can be used to approximate K -values. Thus, at azeotropic conditions, with $K_i = 1$ and $\gamma_i = P/P_i^s$. The vapor pressures at 58°C are $P_E^s = 6.26$ psia and $P_H^s = 10.28$ psia. Therefore,

$$\gamma_E = \frac{14.696}{6.26} = 2.348$$

$$\gamma_H = \frac{14.696}{10.28} = 1.430$$

Substituting these values together with the above corresponding values of x_i into the binary form of the Wilson equation in Table 2.8 gives

$$\ln 2.348 = -\ln (0.332 + 0.668\Lambda_{EH}) + 0.668 \left(\frac{\Lambda_{EH}}{0.332 + 0.668\Lambda_{EH}} - \frac{\Lambda_{HE}}{0.332\Lambda_{HE} + 0.668} \right)$$

$$\ln 1.430 = -\ln (0.668 + 0.332\Lambda_{HE}) - 0.332 \left(\frac{\Lambda_{EH}}{0.332 + 0.668\Lambda_{EH}} - \frac{\Lambda_{HE}}{0.332\Lambda_{HE} + 0.668} \right)$$

Solving these two simultaneous nonlinear equations with fsolve of MATLAB gives $\Lambda_{EH} = 0.041$ and $\Lambda_{HE} = 0.281$. From these constants, the activity-coefficient curves can be predicted if the temperature variations of Λ_{EH} and Λ_{HE} are ignored. The results are plotted in Figure 2.8. The fit of experimental data is good, except for near-infinite-dilution conditions, where $\gamma_E^\infty = 49.82$ and $\gamma_H^\infty = 9.28$. The former is considerably greater than the value of 21.72 obtained by Orye and Prausnitz [36] from a fit of all data points. A comparison of Figures 2.5 and 2.8 shows that widely differing γ_E^∞ values have little effect on γ in the region of $x_E = 0.15$ to 1.00, where the Wilson curves are almost identical to the data. For accuracy over the entire composition range, data for at least three liquid compositions per binary are preferred.

§2.7.2 The NRTL Model

The **nonrandom, two-liquid (NRTL)** equation developed by Renon and Prausnitz [25, 26], given for a binary mixture in Table 2.8, is an extension of Wilson’s local composition concept to multicomponent liquid–liquid, and vapor–liquid–liquid systems. The NRTL model assumes that a

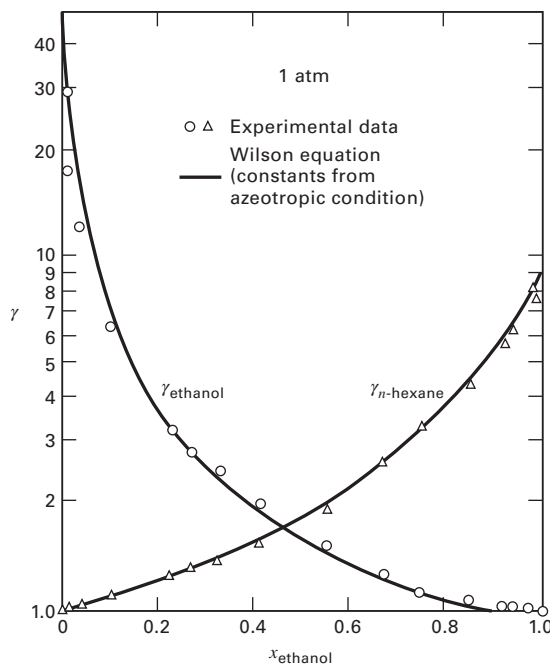


Figure 2.8 Liquid-phase activity coefficients for ethanol/*n*-hexane system.

binary mixture is composed of cells of molecules 1 and 2, each surrounded by assortments of the two molecules, with each of those molecules surrounded in a similar manner. It is widely used for liquid–liquid extraction calculations because unlike the Wilson model, the NRTL model can predict phase splitting. The NRTL equation for the activity coefficient is derived from the following model for the excess Gibbs free energy:

$$g^E = RTx_1x_2 \left[\frac{\tau_{21}G_{21}}{(x_1 + x_2G_{21})} + \frac{\tau_{12}G_{12}}{(x_2 + x_1G_{12})} \right] \quad (2-77)$$

where $G_{ji} = \exp(-\alpha_{ji}\tau_{ji})$, $\tau_{ij} = \frac{g_{ij} - g_{jj}}{RT}$, and $\tau_{ji} = \frac{g_{ji} - g_{ii}}{RT}$

The double-subscripted g values are energies of interaction for molecule pairs. In the equations, $G_{ji} \neq G_{ij}$, $\tau_{ij} \neq \tau_{ji}$, $G_{ii} = G_{jj} = 1$, and $\tau_{ii} = \tau_{jj} = 0$. Often, $(g_{ij} - g_{jj})$ and other constants are linear in temperature. For ideal solutions, $\tau_{ji} = 0$.

For multicomponent systems, only binary-pair parameters from binary-pair experimental data are required, and the NRTL expression for activity coefficients becomes

$$\ln \gamma_i = \frac{\sum_{j=1}^C \tau_{ji} G_{ji} x_j}{\sum_{k=1}^C G_{ki} x_k} + \sum_{j=1}^C \left[\frac{x_j G_{ij}}{\sum_{k=1}^C G_{kj} x_k} \left(\tau_{ji} - \frac{\sum_{k=1}^C x_k \tau_{kj} G_{kj}}{\sum_{k=1}^C G_{kj} x_k} \right) \right] \quad (2-78)$$

Accessible data banks in process simulators include fitted values for τ_{12} and τ_{21} binary interaction parameters, sometimes as a function of temperature.

The third parameter, α_{ji} , characterizes the tendency of species j and i to be distributed nonrandomly. When $\alpha_{ji} = 0$, local mole fractions equal overall solution mole fractions. Generally, α_{ji} is independent of temperature and depends on molecule properties similar to the classifications in Tables 2.6 and 2.7. Fitted values of α_{ji} usually lie between 0.2 and 0.47. When $\alpha_{ji} > 0.426$, phase splitting is predicted. Although α_{ji} can be treated as an adjustable parameter determined from experimental binary-pair data, commonly α_{ji} is set according to the following rules, which are occasionally ambiguous:

1. $\alpha_{ji} = 0.20$ for hydrocarbons and polar, nonassociated species (e.g., *n*-heptane/acetone).
2. $\alpha_{ji} = 0.30$ for nonpolar compounds (e.g., benzene/*n*-heptane), except fluorocarbons and paraffins; nonpolar and polar, nonassociated species (e.g., benzene/acetone); polar species that exhibit negative deviations from Raoult's law (e.g., acetone/chloroform) and moderate positive deviations (e.g., ethanol/water); mixtures of water and polar nonassociated species (e.g., water/acetone).
3. $\alpha_{ji} = 0.40$ for saturated hydrocarbons and homolog perfluorocarbons (e.g., *n*-hexane/perfluoro-*n*-hexane).
4. $\alpha_{ji} = 0.47$ for alcohols or other strongly self-associated species with nonpolar species (e.g., ethanol/benzene; carbon tetrachloride with either acetonitrile or nitromethane; water with either butyl glycol or pyridine).

§2.7.3 The UNIQUAC Model

In an attempt to place calculations of activity coefficients on a more theoretical basis, Abrams and Prausnitz [27] used statistical mechanics to derive an expression for Gibbs excess free energy. Their **UNIQUAC (universal quasichemical) model**, generalizes an analysis by Guggenheim and extends it to molecules that differ in size and shape. As in the Wilson and NRTL models, local concentrations are used. However, rather than local volume fractions or local mole fractions, UNIQUAC uses local area fraction θ_i as the primary concentration variable. As with the NRTL model, the UNIQUAC model predicts phase splitting and is, therefore, applicable to LLE and VLLE, as well as for VLE simulations.

The local area fraction is determined by representing a molecule by a set of bonded segments. Each molecule is characterized by two structural parameters determined relative to a standard segment, taken as an equivalent sphere of a unit of a linear, infinite-length, polymethylene molecule. The two structural parameters are the relative number of segments per molecule, r (volume parameter), and the relative surface area, q (surface parameter). These parameters, computed from bond angles and bond distances, are given for many species by Abrams and Prausnitz [27,28] and Gmehling and Onken [24]. Values can also be estimated by the group-contribution method of Fredenslund et al. [29].

For a multicomponent liquid mixture, the UNIQUAC model gives the Gibbs excess free energy as

$$\begin{aligned} \frac{g^E}{RT} = & \sum_{i=1}^C x_i \ln \left(\frac{\Psi_i}{x_i} \right) + \frac{\bar{Z}}{2} \sum_{i=1}^C q_i x_i \ln \left(\frac{\theta_i}{\Psi_i} \right) \\ & - \sum_{i=1}^C q_i x_i \ln \left(\sum_{j=1}^C \theta_j T_{ji} \right) \end{aligned} \quad (2-79)$$

The first two terms on the right-hand side account for **combinatorial** effects due to differences in size and shape; the last term provides a **residual** contribution due to differences in intermolecular forces, where

$$\Psi_i = \frac{x_i r_i}{\sum_{i=1}^C x_i r_i} = \text{segment fraction} \quad (2-80)$$

$$\theta = \frac{x_i q_i}{\sum_{i=1}^C x_i q_i} = \text{area fraction} \quad (2-81)$$

where \bar{Z} = lattice coordination number set equal to 10, and

$$T_{ji} = \exp \left(\frac{u_{ji} - u_{ii}}{RT} \right) \quad (2-82)$$

Equation (2-79) contains two adjustable parameters for each binary pair, $(u_{ji} - u_{ii})$ and $(u_{ij} - u_{jj})$. Abrams and Prausnitz show that $u_{ji} = u_{ij}$ and $T_{ii} = T_{jj} = 1$. In general, $(u_{ji} - u_{ii})$ and $(u_{ij} - u_{jj})$ are linear functions of absolute temperature.

Table 2.9 Partial Molar Excess Functions

Excess volume:

$$(1) \left(\bar{v}_{iL} - \bar{v}_{iL}^{\text{ID}} \right) \equiv \bar{v}_{iL}^E = RT \left(\frac{\partial \ln \gamma_{iL}}{\partial P} \right)_{T,x}$$

Excess enthalpy:

$$(2) \left(\bar{h}_{iL} - \bar{h}_{iL}^{\text{ID}} \right) \equiv \bar{h}_{iL}^E = -RT^2 \left(\frac{\partial \ln \gamma_{iL}}{\partial T} \right)_{P,x}$$

Excess entropy:

$$(3) \left(\bar{s}_{iL} - \bar{s}_{iL}^{\text{ID}} \right) \equiv \bar{s}_{iL}^E = -R \left[T \left(\frac{\partial \ln \gamma_{iL}}{\partial T} \right)_{P,x} + \ln \gamma_{iL} \right]$$

ID = ideal mixture; E = excess because of nonideality.

If (2-61) is combined with (2-79), the activity coefficient for a species in a multicomponent mixture becomes:

$$\begin{aligned} \ln \gamma_i &= \ln \gamma_i^C + \ln \gamma_i^R \\ &= \underbrace{\ln (\psi_i/x_i) + (\bar{Z}/2)q_i \ln (\theta_i/\psi_i) + l_i - (\psi_i/x_i) \sum_{j=1}^C x_j l_j}_{C, \text{ combinatorial}} \\ &\quad + \underbrace{q_i \left[1 - \ln \left(\sum_{j=1}^C \theta_j T_{ji} \right) - \sum_{j=1}^C \left(\frac{\theta_j T_{ij}}{\sum_{k=1}^C \theta_k T_{kj}} \right) \right]}_{R, \text{ residual}} \end{aligned} \quad (2-83)$$

where

$$l_j = \left(\frac{\bar{Z}}{2} \right) (r_j - a_j) - (r_j - 1) \quad (2-84)$$

For a mixture of species 1 and 2, (2-83) reduces to Eq. (3) in Table 2.8 for $\bar{Z} = 10$.

§2.7.4 Excess Thermodynamic Functions

Values of the excess functions for molar volume, molar enthalpy, and molar entropy are derived from the expressions for the liquid-phase activity coefficient for the Wilson, NRTL, and UNIQUAC equations using the expressions in Table 2.9. These functions are built into process simulators.

§2.8 PREDICTIVE MODELS

The above Gibbs excess free-energy (g^E) models require binary interaction parameters determined from experimental data. When EOS models are applied to slightly nonideal systems, they also perform best when experimentally determined binary interaction parameters are included in the mixing rules. When binary parameters are not available, laboratory experiments can be performed to obtain them or the following

predictive thermodynamic models based on molecular group contributions can be employed.

The lack of a sufficient number of binary interaction parameters for industrial applications is pointed out by Gmehling et al. [1]. Assuming that $N = 1,000$ nonelectrolyte compounds are of industrial interest, then the number of nonelectrolyte binary systems is given by $N(N-1)/2 = 499,500$. As of 2012, the Dortmund Data Bank (DDB) included more than 64,500 VLE data sets for nonelectrolyte systems, but only for 10,300 binary pairs, corresponding to only 2% of the binary systems of interest.

§2.8.1 The UNIFAC Model

In the 1960s, Wilson and Deal [30], and then Derr and Deal [31], developed a predictive method for estimating liquid-phase activity coefficients, called the analytical solution of groups (ASOG) method. It is based on functional group contributions instead of molecular contributions and used the formulation of the Wilson model. For example, in a solution of toluene and acetone, the group contributions might be 5 aromatic CH groups, 1 aromatic C group, and 1 CH₃ group from toluene; and 2 CH₃ groups plus 1 CO carbonyl group from acetone. Alternatively, larger groups could be employed to give 5 aromatic CH groups and 1 CCH₃ group from toluene; and 1 CH₃ group and 1 CH₃CO group from acetone. As larger functional groups are used, the accuracy increases, but the advantage of the group-contribution method decreases because more groups are required. In practice, about 50 functional groups represent thousands of chemicals.

In 1975, concurrently with the development of the UNIQUAC method, Fredenslund, Jones, and Prausnitz [32] published a more advanced group-contribution method called the UNIFAC (UNIQUAC functional-group activity coefficients) method. Its advantages were: (1) it is theoretically based; (2) the parameters are essentially independent of temperature; (3) predictions can be made over a temperature range of 275–425 K and for pressures to a few atmospheres; and (4) extensive comparisons with experimental data are available. All components must be condensable at near-ambient conditions.

For partial molar Gibbs excess free energies, \bar{g}_i^E , and corresponding activity coefficients, size parameters for each functional group and interaction parameters for each pair of groups are required for the UNIFAC method. Size parameters are calculated from theory. Interaction parameters are back-calculated from experimental phase-equilibria data, and used with the size parameters to predict properties of mixtures for which data are unavailable.

The UNIFAC method is based on the UNIQUAC formulation (2-83), wherein the molecular volume and area parameters are replaced by

$$r_i = \sum_k v_k^{(i)} R_k \quad (2-85)$$

$$q_i = \sum_k v_k^{(i)} Q_k \quad (2-86)$$

where $v_k^{(i)}$ is the number of functional groups of type k in molecule i , and R_k and Q_k are the volume and area parameters, respectively, for the type- k functional group.

The residual term in (2-83), which is represented by $\ln \gamma_i^R$, is replaced by the expression

$$\ln \gamma_i^R = \underbrace{\sum_k v_k^{(i)} (\ln \Gamma_k - \ln \Gamma_k^{(i)})}_{\text{all functional groups in mixture}} \quad (2-87)$$

where Γ_k is the residual activity coefficient of group k , and $\Gamma_k^{(i)}$ is the same quantity but in a reference mixture that contains only molecules of type i . The latter quantity is required so that $\gamma_i^R \rightarrow 1.0$ as $x_i \rightarrow 1.0$. Both Γ_k and $\Gamma_k^{(i)}$ have the same form as the residual term in (2-83). Thus,

$$\ln \Gamma_k = Q_k \left[1 - \ln \left(\sum_m \theta_m T_{mk} \right) - \sum_m \frac{\theta_m T_{mk}}{\sum_n \theta_n T_{nm}} \right] \quad (2-88)$$

where θ_m is the area fraction of group m , given by an equation similar to (2-82),

$$\theta_m = \frac{X_m Q_m}{\sum_n X_n Q_n} \quad (2-89)$$

where X_m is the mole fraction of group m in the solution,

$$X_m = \frac{\sum_j v_m^{(j)} x_j}{\sum_j \sum_n (v_n^{(j)} x_j)} \quad (2-90)$$

and T_{mk} is a group interaction parameter given by an equation similar to (2-82),

$$T_{mk} = \exp \left(-\frac{a_{mk}}{T} \right) \quad (2-91)$$

where $a_{mk} \neq a_{km}$. When $m = k$, then $a_{mk} = 0$ and $T_{mk} = 1.0$. For $\Gamma_k^{(i)}$, (2-88) also applies, where θ terms correspond to the pure component i . Although R_k and Q_k differ for each functional group, values of a_{mk} are equal for all subgroups within a main group. For example, main group CH_2 consists of subgroups CH_3 , CH_2 , CH , and C . Accordingly,

$$a_{\text{CH}_3, \text{CHO}} = a_{\text{CH}_2, \text{CHO}} = a_{\text{CH}, \text{CHO}} = a_{\text{C}, \text{CHO}}$$

Thus, the experimental data required to obtain values of a_{mk} and a_{mk} and the size of the corresponding bank of data for these parameters are not as great as might be expected.

Since the publication of the UNIFAC method, a number of updates have been published that add group parameters and interaction parameters for binary group pairs. Unfortunately, it has been found that two sets of parameters were needed, one based on VLE data and the other on LLE data, with the temperature range of application of the latter reduced from 280–420 down to 280–310 K. A major improvement of the

UNIFAC model was published in 1993 by Gmehling et al. [51], referred to as modified UNIFAC (Dortmund). The combinatorial part of (2-83) was modified for mixtures having a range of molecular sizes. For temperature dependence, (2-91) was replaced with a three-coefficient equation. These changes permit reliable predictions of activity coefficients (including dilute solutions and multiple liquid phases), heats of mixing, and azeotropic compositions, with one set of parameters. In 2013, modified UNIFAC (Dortmund) parameters were available for 1,530 binary functional group pairs. These parameters are available to users of most of the process simulators. They can be used within a temperature range of 290 to 420 K.

Despite the many favorable aspects of the modified UNIFAC (Dortmund) model, it has some weaknesses, as described by Gmehling et al. [1]: (1) it cannot differentiate between isomers; (2) it cannot make reliable predictions for large molecules with many different functional groups; and (3) poor results are obtained for the solubilities of some hydrocarbons in water.

§2.8.2 The Predictive Soave–Redlich–Kwong (PSRK) Model

EOS models are mainly useful for mixtures of nonpolar and slightly polar components, such as hydrocarbons and light gases. Gibbs excess free-energy models are suitable for mixtures of subcritical nonpolar and polar organic components. When a mixture contains both polar compounds and supercritical gases, neither method gives satisfactory results. To describe VLE for such mixtures, more theoretically based mixing rules for use with the SRK and PR equations of state have been developed. To broaden the range of applications of these models, Holderbaum and Gmehling [33] formulated a group-contribution equation of state called the predictive Soave–Redlich–Kwong (PSRK) model, which combines the SRK EOS with the UNIFAC model. To improve the ability of the SRK equation to predict vapor pressure of polar compounds, they make the pure-component parameter, a , in Table 2.4 temperature dependent. To handle mixtures of nonpolar, polar, and supercritical components, they use a mixing rule for a that includes the UNIFAC model for non-ideal effects:

$$\frac{a}{bRT} = \sum_i x_i \frac{a_{ii}}{b_i RT} - \frac{1}{0.64663} \left(\frac{g^E}{RT} + \sum_i x_i \frac{b}{b_i} \right) \quad (2-92)$$

where

$$b = \sum_i x_i b_i \quad (2-93)$$

Pure-component and group-interaction parameters for use in the PSRK model are provided by Fischer and Gmehling [34]. In particular, [33] and [34] provide parameters for nine light gases in addition to UNIFAC parameters for 50 groups. The PSRK model can be used up to high temperatures and pressures, but it loses accuracy close to the critical point. The method is available in most process simulators.

§2.8.3 Predictive Peng–Robinson UNIFAC Models

The Peng–Robinson EOS has also been successfully extended to handle mixtures of polar components and light supercritical gases by incorporating the UNIFAC model into mixing rules for the a and b parameters shown in Table 2.4 for the PR model. The result is better estimates of liquid density, heat of mixing, and liquid-phase activity coefficients at infinite dilution. Most popular are the extensions to the PR method that use the mixing rules of Huron and Vidal [35] or those of Wong and Sandler [36], and the Volume-Translated Peng–Robinson (VTPR) model developed by Ahlers and Gmehling [37]. Schmid, Schedemann, and Gmehling [38] increased the number of VTPR group parameters to 252 and suggested that process simulators add the VTPR model to their physical-properties libraries.

§2.9 ELECTROLYTE SOLUTION MODELS

Electrolyte solutions are common in the petroleum, chemical, and biochemical industries. For example, sour water, found in many petroleum plants, consists of water and five dissolved gases: CO, CO₂, CH₄, H₂S, and NH₃. Because of dissociation, the aqueous solution includes ionic as well as molecular species. For sour water, the ionic species include H⁺, OH⁻, HCO₃⁻, CO₃⁼, HS⁻, S⁼, NH₄⁺, and NH₂COO⁻, with the positive and negative ions subject to electron neutrality. For example, while the apparent concentration of NH₃ in the solution might be 2.46 moles per kg of water, the molality is 0.97 when dissociation is taken into account, with NH₄⁺ having a molality of 1.49. All eight ionic species are nonvolatile, while all six molecular species are volatile to some extent. Calculations of vapor–liquid equilibrium for multicomponent electrolyte solutions must consider both chemical and physical equilibrium, both of which involve liquid-phase activity coefficients.

Models are available for predicting activity coefficients in multicomponent systems of electrolytes. Of particular note are those of Pitzer [39] and Chen et al. [40, 41, 42], both of which are included in process simulation programs. Both models can handle dilute to concentrated solutions, but only the model of Chen et al., referred to as the **electrolyte NRTL** model, which is a substantial modification of the NRTL model, can handle mixed-solvent systems.

§2.10 POLYMER SOLUTION MODELS

Polymer processing involves solutions of solvent, monomer, and soluble polymer, thus requiring vapor–liquid and, sometimes, liquid–liquid phase-equilibria calculations, for which activity coefficients of all components are needed. Usually, the polymer is nonvolatile, but the solvent and monomer are volatile. When the solution is dilute in the polymer, activity-coefficient methods of §2.7, such as the NRTL method, are suitable. Of more interest are mixtures with appreciable concentrations of polymer, for which the methods of §2.5 and §2.7 are inadequate. So special-purpose models have been developed. One method, available in process

simulation programs, is the modified NRTL model of Chen [43], which combines a modification of the Flory–Huggins equation for widely differing molecular sizes with the NRTL concept of local composition. Because Chen represents the polymer with segments, solvent–solvent, solvent–segment, and segment–segment binary interaction parameters are required. These are available from the literature and may be assumed to be independent of temperature, polymer chain length, and polymer concentration.

§2.11 K-VALUE METHODS IN PROCESS SIMULATORS

Process simulators include data banks of numerous methods for estimating K -values. Table 2.10 is a list of many of the available methods in Aspen Plus, CHEMCAD, and ChemSep. The methods are grouped under three classifications: hydrocarbon systems, chemical systems, and special types of systems. The most widely selected methods in practice are prefixed with an asterisk. Some of those methods, for example, SRK and UNIFAC, have multiple versions. Process simulators also permit user-specified activity coefficients and K -values in the form of tables or equations. Currently the most extensive set of K -value methods is found in Aspen Plus. For those using Aspen Plus, Sandler [49] presents a step-by-step guide for obtaining thermodynamic properties for VLE, LLE, and VLLE using that process simulator. Four of the chapters cover regression of phase equilibria data to obtain necessary constants.

Table 2.10 K -Value Methods in Process Simulators

Method	Aspen Plus	CHEMCAD	ChemSep
Hydrocarbon Systems:			
BWR	x	x	
CSGS	x	x	x
Lee–Kesler–Plöcker	x		
*PR	x	x	x
*SRK	x	x	x
Chemical Systems:			
Margules	x	x	x
*NRTL	x	x	x
PSRK	x	x	x
Regular solutions	x	x	x
*UNIFAC	x	x	x
*UNIQUAC	x	x	x
*Vapor pressure	x	x	x
van Laar	x	x	x
*Wilson	x	x	x
Special Systems:			
Amines	x	x	
*Electrolyte NRTL	x	x	
Flory–Huggins	x	x	
*Henry’s law	x	x	
Pitzer electrolyte	x	x	
Polymers	x	x	
Sour water	x	x	

§2.11.1 Selecting an Appropriate Model

Design or analysis of a separation process requires a suitable thermodynamic model. Detailed recommendations for selecting appropriate physical-property methods are given by Carlson [44] for users of Aspen Plus. This section presents an abbreviated selection procedure for any process simulator.

The procedure includes a few thermodynamic models not covered in depth in this chapter, but for which a literature reference is given. The procedure begins by characterizing the mixture by chemical type: light gases (LG), hydrocarbons (HC), polar organic compounds (PC), and aqueous solutions (AS), with or without electrolytes (E).

If the mixture is (AS) with no (PC), and if electrolytes are present, select the Pitzer or electrolyte NRTL method. Otherwise, select a special model, such as one for sour water (containing NH_3 , H_2S , CO_2 , etc.) or aqueous amine solutions.

If the mixture contains (HC), with or without (LG), for a wide boiling range, choose the corresponding-states method of Lee–Kesler–Plöcker [12,13]. If the HC boiling range is not wide, selection depends on the pressure and temperature. The Peng–Robinson equation is suitable for all temperatures and pressures. For all pressures and non-cryogenic temperatures, the Soave–Redlich–Kwong equation is applicable. For all temperatures, but not pressures in the critical region, the Benedict–Webb–Rubin–Starling [10, 45, 46] method is viable. For mixtures of environmentally safe refrigerants, use the Lee–Kesler–Plöcker [12,13] method.

If the mixture contains (PC), selection depends on whether (LG) are present. If they are, the VTPR, PSRK, or one of the other PR-UNIFAC methods is recommended. If not, then a Gibbs excess free-energy model should be chosen. If the binary interaction parameters are available and splitting into two liquid phases does not occur, select the Wilson or NRTL equation. Otherwise, if phase splitting is probable, select the NRTL or UNIQUAC equation. If the binary interaction coefficients are not available, select the modified UNIFAC (Dortmann) method.

All process simulators have expert systems that help users choose what the program designers believe to be the optimal thermodynamic package for the chemical species and conditions involved. However, since temperature, composition, and pressure in the various processing units vary, care must be taken in using any expert system.

§2.12 EXERGY AND SECOND-LAW ANALYSIS

Industrial separation operations utilize large quantities of energy in the form of heat and/or shaft work. The distillation of crude oil into its fractions is very energy-intensive, requiring as much as 40% of the total energy used in a petroleum refinery. Thus, it is important to know the energy consumption in a separation process, and to what degree energy requirements might be reduced.

Consider the continuous, steady-state, flow system for a general separation process in Figure 2.9. The process may

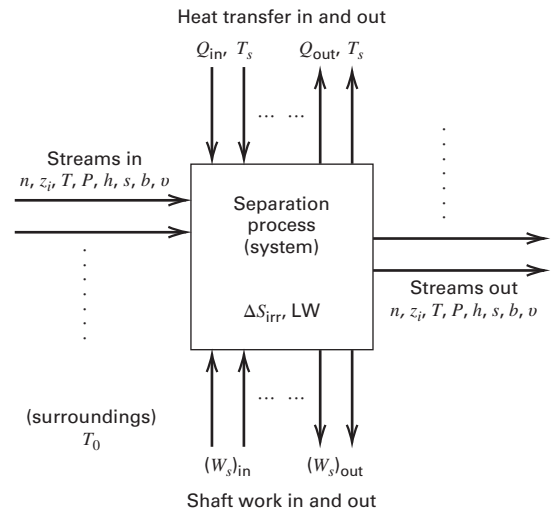


Figure 2.9 General separation system.

include one or more separation operations of the type introduced in Chapter 1. One or more feed streams flowing into the system are separated into two or more product streams. Each stream is characterized by molar flow rates n , component mole fractions z_i , temperature T , pressure P , molar enthalpies h , molar entropies s , and molar volumes v . If chemical reactions occur, enthalpies and entropies are best referred to the elements, as discussed by Felder and Rousseau [47]; otherwise they can be referred to the compounds. Flows of heat in or out are denoted by Q , and shaft work crossing the system boundary of the system is denoted by W_s .

At steady state, if kinetic, potential, and surface energy changes are neglected, the first law of thermodynamics (conservation of energy) states that the sum of energy flows into the system equals the sum of the energy flows leaving the system. The energy balance is given by Eq. (1) in Table 2.1, where all flow-rate, heat-transfer, and shaft-work terms are positive. Molar enthalpies may be positive or negative, depending on the reference state.

The first law of thermodynamics provides no information on energy efficiency, but the second law of thermodynamics, given by Equation (2) in Table 2.11, does. In the entropy balance, the heat sources and sinks in Figure 2.9 are at absolute temperatures, T_s . For example, if condensing steam at 150°C supplies heat, Q , to the reboiler of a distillation column, then $T_s = 150 + 273 = 423$ K. Unlike the energy balance, which states that energy is conserved, the entropy balance predicts the production of entropy, ΔS_{irr} , which is the irreversible increase in the entropy of the universe. This term, which must be positive, is a measure of the thermodynamic inefficiency. In the limit, as a reversible process is approached, ΔS_{irr} tends to zero. Unfortunately, ΔS_{irr} is difficult to relate to energy lost because of inefficiency because it does not have the units of energy/unit time (power).

A more useful measure of process inefficiency is **lost work**, LW, also referred to as loss of exergy or availability.

Table 2.11 Universal Thermodynamic Laws for a Continuous, Steady-State, Flow System

Energy balance:

$$(1) \sum_{\text{out of system}} (nh + Q + W_s) - \sum_{\text{in to system}} (nh + Q + W_s) = 0$$

Entropy balance:

$$(2) \sum_{\text{out of system}} \left(ns + \frac{Q}{T_s} \right) - \sum_{\text{in to system}} \left(ns + \frac{Q}{T_s} \right) = \Delta S_{\text{irr}}$$

Exergy (availability) balance:

$$(3) \sum_{\text{in to system}} \left[nb + Q \left(1 - \frac{T_0}{T_s} \right) + W_s \right] - \sum_{\text{out of system}} \left[nb + Q \left(1 - \frac{T_0}{T_s} \right) + W_s \right] = \text{LW}$$

where $b = h - T_0s =$ exergy (availability) of a stream

Minimum work of separation:

$$(4) W_{\text{min}} = \sum_{\text{out of system}} nb - \sum_{\text{in to system}} nb$$

Second-law efficiency:

$$(5) \eta = \frac{W_{\text{min}}}{\text{LW} + W_{\text{min}}}, \text{ where LW} = T_0 \Delta S_{\text{irr}} = \text{lost work}$$

It is derived by combining Equations (1) and (2) to obtain a combined statement of the first and second laws, given as (3) in Table 2.11. To perform this derivation, it is necessary to define an infinite source or sink available for heat transfer at absolute temperature, T_0 , of the surroundings. This temperature, typically about 300 K, represents the largest source of coolant (heat sink) available. This could be the average temperature of cooling water in a plant, air, or a nearby river, lake, or ocean. Heat transfer associated with this coolant and transferred from (or to) the process is Q_0 . Thus, in both (1) and (2) in Table 2.11, the Q and Q/T_s terms include contributions from Q_0 and Q_0/T_0 .

In the derivation of Equation (3), as shown by de Nevers and Seader [47], any terms in Q_0 are eliminated. The resulting balance is referred to as an exergy (or availability) balance, where the word, exergy, was coined in 1956 by Zoran Rant from the Greek *ex ergon* meaning “from work.” The synonymous word, “availability” means “available for complete conversion to shaft work.” The **availability of a stream**, b , is a derived

thermodynamic property like h and s , defined by

$$b = h - T_0s \tag{2-94}$$

It is a measure of the maximum amount of energy that can be converted into shaft work if the stream is taken to the reference state. It is similar to Gibbs free energy, $g = h - Ts$, but differs in that the infinite source or sink temperature, T_0 , replaces the temperature, T of the pure component or mixture. In (3) of Table 2.11, terms that contain Q are modified to reflect the availability of shaft work from heat. They are multiplied by $(1 - T_0/T_s)$, which, as shown in Figure 2.10, is the reversible Carnot heat-engine cycle efficiency, representing the maximum amount of shaft work producible from Q at T_s , where the residual amount of energy $(Q - W_s)$ is transferred as heat to a sink at T_0 . Shaft work, W_s , has no modifier and is completely available and remains at its full value in (3). It is important to note that in (1) in Table 2.11, energy is never destroyed in a process, and Q and W_s have the same energy value. In the exergy (availability) balance in (3), exergy (availability) is always destroyed in a real process involving a temperature change and heat transfer has less value in (3). Shaft work can be converted completely to heat, but heat cannot be converted completely to shaft work.

The total availability (i.e., ability to produce shaft work) entering a system is always greater than the total availability leaving the system. For that reason, (3) in Table 2.11 is written with the “in to system” terms first. The difference is the lost work, LW, also called the loss of availability or exergy. It can be calculated in either of two ways: (1) from the exergy balance in Table 2.11, or (2) from the irreversible increase in the entropy of the universe:

$$\text{LW} = T_0 \Delta S_{\text{irr}} \tag{2-95}$$

Lost work is always positive. The greater its value, for a given process, the greater the energy inefficiency. In the lower limit, for a reversible process, it is zero. The lost work has units of energy, thus making it easy to attach significance to its numerical value. Its magnitude depends on process

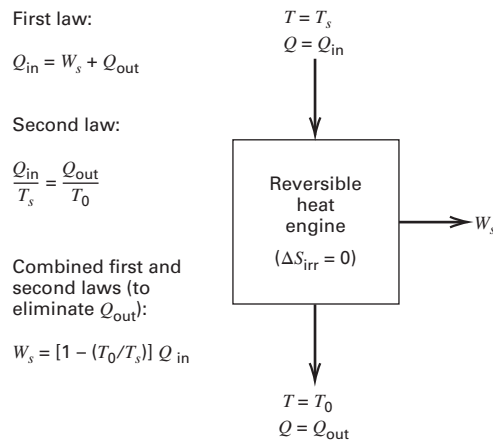


Figure 2.10 Carnot heat-engine cycle for converting heat to shaft work.

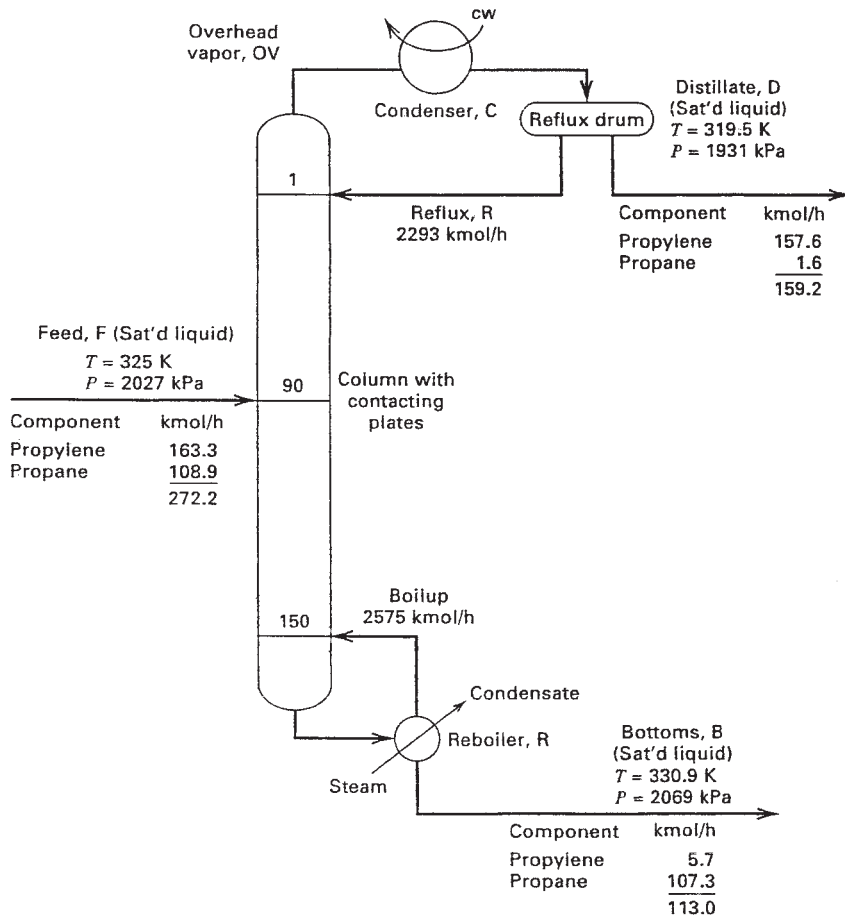


Figure 2.11 Distillation of propylene-propane.

irreversibilities, which include fluid friction, heat transfer due to finite temperature-driving forces, mass transfer due to finite concentration or activity driving forces, chemical reactions proceeding at finite displacements from chemical equilibrium, mixing streams of differing temperature, pressure, and/or composition, etc. To reduce lost work, driving forces for momentum, heat, and mass transfer; and chemical reaction must be reduced. However, economic limits to reduction exist because, as driving forces decrease, equipment sizes increase, tending to infinity as driving forces approach zero.

For a separation without chemical reaction, the availability of streams leaving the process is usually greater than that for streams entering the process. In the limit for a reversible process ($LW = 0$), and (3) of Table 2.11 reduces to (4), where W_{\min} is the minimum shaft work for conducting the separation. It is equivalent to the difference in the heat-transfer and shaft-work terms in (3). This **minimum work of separation** is a property independent of the nature (or path) of the separation process. The actual work of separation for an irreversible process is greater than the minimum value from (4).

Equation (3) of Table 2.11 shows that as a process becomes more irreversible, and thus more energy inefficient, the increasing LW causes the actual work of separation to increase. Thus, the actual work of separation for an irreversible process is the sum of the lost work and the minimum work of separation. The **second-law energy efficiency**, therefore, is defined by (5) in Table 2.11.

EXAMPLE 2.5 Second-Law Efficiency of a Distillation Operation.

For the distillation of propylene-propane shown in Figure 2.11, use the following results from a process simulator to calculate: (a) condenser duty, Q_C ; (b) reboiler duty, Q_R ; (c) irreversible entropy production, assuming 303 K for T_0 , the condenser cooling-water sink, and 378 K for T_s , the reboiler steam source; (d) lost work; (e) minimum work of separation; and (f) second-law efficiency.

Stream	Phase Condition	Enthalpy (h), kJ/kmol	Entropy (s), kJ/kmol-K	Exergy (b), kJ/kmol
Feed (F)	Liquid	13,338	-4.1683	14,601
Overhead Vapor (OV)	Vapor	24,400	24.2609	17,049
Distillate (D) and Reflux (R)	Liquid	12,243	-13.8068	16,426
Bottoms (B)	Liquid	14,687	-2.3886	15,411

Solution

Let Q_C and Q_R cross the system boundary. That is, the cooling water for the condenser and the steam for the reboiler are outside of the system. The following calculations are made using the stream flow rates in Figure 2.11 and the above thermodynamic properties.

- (a) From an energy balance, (1) in Table 2.11, noting that the overhead-vapor molar flow rate is given by $n_{OV} = n_R + n_D$ and $h_R = h_D$, the condenser duty is

$$\begin{aligned} Q_C &= n_{OV}(h_{OV} - h_R) \\ &= (2,293 + 159.2)(24,400 - 12,243) \\ &= 29,811,000 \text{ kJ/h} \end{aligned}$$

- (b) An energy balance around the reboiler cannot be made because data are not given for the boilup rate. From (1), Table 2.11, an energy balance around the entire system is used instead:

$$\begin{aligned} Q_R &= n_D h_D + n_B h_B + Q_C - n_F h_F \\ &= 159.2(12,243) + 113(14,687) \\ &\quad + 29,811,000 - 272.2(13,338) \\ &= 29,789,000 \text{ kJ/h} \end{aligned}$$

- (c) Compute the production of entropy from an entropy balance around the entire system using (2) from Table 2.11:

$$\begin{aligned} \Delta S_{\text{irr}} &= n_D s_D + n_B s_B + Q_C/T_0 - n_F s_F - Q_R/T_s \\ &= 159.2(-13.8068) + 113(-2.3886) \\ &\quad + 29,811,000/303 - 272.2(-4.1683) \\ &= 18,246 \text{ kJ/h-K} \end{aligned}$$

- (d) Compute lost work from its definition at the bottom of Table 2.11:

$$\begin{aligned} \text{LW} &= T_0 \Delta S_{\text{irr}} \\ &= 303(18,246) = 5,529,000 \text{ kJ/h} \end{aligned}$$

Alternatively, compute lost work from an exergy balance around the system. From (3), Table 2.11:

$$\begin{aligned} \text{LW} &= n_F b_F + Q_R(1 - T_0/T_R) \\ &\quad - n_D b_D - n_B b_B - Q_C(1 - T_0/T_C) \\ &= 272.2(14,601) + 29,789,000(1 - 303/378) \\ &\quad - 159.2(16,426) - 113(15,411) \\ &\quad - 29,811,000(1 - 303/303) \\ &= 5,529,000 \text{ kJ/h (same result)} \end{aligned}$$

- (e) Compute the minimum work of separation for the entire system. From (4), Table 2.11,

$$\begin{aligned} W_{\text{min}} &= n_D b_D + n_B b_B - n_F b_F \\ &= 159.2(16,426) + 113(15,411) - 272.2(14,601) \\ &= 382,100 \text{ kJ/h} \end{aligned}$$

- (f) Compute the second-law efficiency for the entire distillation system. From (5), Table 2.11,

$$\begin{aligned} \eta &= \frac{W_{\text{min}}}{\text{LW} + W_{\text{min}}} \\ &= \frac{382,100}{5,529,000 + 382,100} \\ &= 0.0646 \text{ or } 6.46\% \end{aligned}$$

The lost work is much larger than the minimum work. The low second-law efficiency is typical of a difficult distillation separation, which in this case requires 150 theoretical stages with a reflux ratio of almost 15 times the distillate rate.

CHAPTER 2 NOMENCLATURE

Latin Symbols

a	activity, Table 2.1
b	molar availability, exergy, Table 2.11
f	pure component fugacity, Table 2.1
f^o	pure component fugacity in the standard state, (2-14)
\bar{f}	partial fugacity, Table 2.1
G	Gibbs free energy, (2-1)
g^E	Gibbs excess free energy, (2-60)
H	Henry's law coefficient, (2-31)
h	molar enthalpy, Table 2.11
k_{ij}	binary interaction coefficient, (2-54)
s	molar entropy, Table 2.11
Z	compressibility factor, Section 2.5

Greek Symbols

γ	activity coefficient, Table 2.1
μ	chemical potential (partial molar Gibbs free energy), Table 2.1
ϕ	fugacity coefficient, Table 2.1
$\bar{\phi}$	partial fugacity coefficient, Table 2.1
ω	acentric factor, (2-48)

Subscripts

c	critical condition
D	distribution ratio, partition coefficient, liquid-liquid equilibrium ratio
iG	component i as a gas
iL	component i as a liquid
irr	irreversible
min	minimum
o	reference state
r	reduced condition
iS	component i as a solid
0	infinite source or sink

Superscripts

E	excess, Section 2.7
iL	component i as a liquid
iV	component i as a vapor
p	phase
—	partial molar
vap	vaporization

SUMMARY

1. Phase equilibrium is expressed in terms of vapor–liquid and liquid–liquid K -values, which are formulated in terms of fugacity coefficients and activity coefficients.
2. For separation systems involving an ideal-gas and an ideal-liquid solution, thermodynamic properties can be estimated from the ideal-gas law, a vapor heat-capacity equation, a vapor-pressure equation, and an equation for the liquid density.
3. Use of graphical representations of thermodynamic properties have declined because of widespread use of process simulators that can quickly estimate needed thermodynamic properties from complex and more accurate formulations.
4. For non-ideal mixtures containing light gases and hydrocarbons, P - v - T equation-of-state (EOS) models such as SRK, PR, and LKP are used to estimate density, enthalpy, entropy, fugacity, and K -values.
5. For non-ideal liquid solutions of nonpolar and/or polar components, Gibbs excess free-energy (g^E) models, such

as Wilson, NRTL, and UNIQUAC, are used to estimate activity coefficients, volume and enthalpy of mixing, excess entropy of mixing, and K -values when binary interaction parameters derived from experimental phase equilibrium data are available. The Wilson equation is not valid for liquid–liquid equilibrium, but the NRTL and UNIQUAC equations are.

6. Predictive models, such as the UNIFAC model based on group contributions and models that combine an EOS with a g^E model, are used when binary interaction parameters are not available.
7. Special models are available for electrolyte solutions and polymer solutions.
8. Separation processes are energy-intensive. Energy requirements are determined by applying the first law of thermodynamics. Estimates of irreversibility and minimum energy needs use the second law of thermodynamics with an entropy or exergy (availability) balance.

REFERENCES

1. GMEHLING, J., B. KOLBE, M. KLEIBER, and J. RAREY, *Chemical Thermodynamics for Process Simulation*, Wiley-VCH Verlag & Co. KGaA, Weinheim, Germany (2013).
2. PRAUSNITZ, J.M., R.N. LICHTENTHALER, and E.G. DE AZEVEDO, *Molecular Thermodynamics of Fluid-Phase Equilibria*, 3rd ed., Prentice-Hall, Upper Saddle River, NJ (1999).
3. POLING, B.E., J.M. PRAUSNITZ, and J.P. O'CONNELL, *The Properties of Gases and Liquids*, 5th ed., McGraw-Hill, New York (2001).
4. RACKETT, H.G., *J. Chem. Eng. Data*, **15**, 514–517 (1970).
5. YAWS, C.L., H.-C. YANG, J.R. HOPPER, and W.A. CAWLEY, *Hydrocarbon Processing*, **71**(1), 103–106 (1991).
6. FRANK, J.C., G.R. GEYER, and H. KEHDE, *Chem. Eng. Prog.*, **65**(2), 79–86 (1969).
7. PITZER, K.S., D.Z. LIPPMAN, R.F. CURL, JR., C.M. HUGGINS, and D.E. PETERSEN, *J. Am. Chem. Soc.*, **77**, 3433–3440 (1955).
8. THIESEN, M., *Ann. Phys.*, **24**, 467–492 (1885).
9. ONNES, K., *Konink. Akad. Wetens.*, p. 633 (1912).
10. STARLING, K.E., *Fluid Thermodynamic Properties for Light Petroleum Systems*, Gulf Publishing, Houston, TX (1973).
11. WALAS, S.M., *Phase Equilibria in Chemical Engineering*, Butterworth, Boston (1985).
12. LEE, B.I., and M.G. KESLER, *AIChE J.*, **21**, 510–527 (1975).
13. PLÖCKER, U., H. KNAPP, and J.M. PRAUSNITZ, *Ind. Eng. Chem. Process Des. Dev.*, **17**, 324–332 (1978).
14. REDLICH, O., and J.N.S. KWONG, *Chem. Rev.*, **44**, 233–244 (1949).
15. WILSON, G.M., *Adv. Cryogenic Eng.*, **11**, 392–400 (1966).
16. SOAVE, G., *Chem. Eng. Sci.*, **27**, 1197–1203 (1972).
17. PENG, D.Y., and D.B. ROBINSON, *Ind. Eng. Chem. Fundam.*, **15**, 59–64 (1976).
18. ZHOU, Z., Z. CHENG, D. YANG, Z. ZHOU, and W. YUAN, *J. Chem. Eng. Data*, **51**, 972–976 (2006).
19. EWELL, R.H., J.M. HARRISON, and L. BERG, *Ind. Eng. Chem.*, **36**, 871–875 (1944).
20. WILSON, G.M., *J. Am. Chem. Soc.* **86**, 127–130 (1964).
21. SINOR, J.E., and J.H. WEBER, *J. Chem. Eng. Data*, **5**, 243–247 (1960).
22. CUKOR, P.M., and J.M. PRAUSNITZ, *Inst. Chem. Eng. Symp. Ser. No. 32*, **3**, 88 (1969).
23. ORYE, R.V., and J.M. PRAUSNITZ, *Ind. Eng. Chem.*, **57**(5), 18–26 (1965).
24. GMEHLING, J., and U. ONKEN, *Vapor-liquid Equilibrium Data Collection*, DECHEMA Chem. Data Ser., 1–8 (1977–1984).
25. RENON, H., and J.M. PRAUSNITZ, *AIChE J.*, **14**, 135–144 (1968).
26. RENON, H., and J.M. PRAUSNITZ, *Ind. Eng. Chem. Process Des. Dev.*, **8**, 413–419 (1969).
27. ABRAMS, D.S., and J.M. PRAUSNITZ, *AIChE J.*, **21**, 116–128 (1975).
28. ABRAMS, D.S., Ph.D. thesis in chemical engineering, University of California, Berkeley, 1974.
29. FREDENSLUND, A., J. GMEHLING, M.L. MICHELSEN, P. RASMUSSEN, and J.M. PRAUSNITZ, *Ind. Eng. Chem. Process Des. Dev.*, **16**, 450–462 (1977).
30. WILSON, G.M., and C.H. DEAL, *Ind. Eng. Chem. Fundam.*, **1**, 20–23 (1962).
31. DERR, E.L., and C.H. DEAL, *Inst. Chem. Eng. Symp. Ser. No. 32*, **3**, 40–51 (1969).
32. FREDENSLUND, A., R.L. JONES, and J.M. PRAUSNITZ, *AIChE J.*, **21**, 1086–1099 (1975).
33. HOLDERBAUM, T., and J. GMEHLING, *Fluid Phase Equilibria*, **70**, 251–265 (1991).
34. FISCHER, K., and J. GMEHLING, *Fluid Phase Equilibria*, **121**, 185–206 (1996).

35. M.-J. HURON and J. VIDAL, *Fluid Phase Equilibria*, **3**, 255–271 (1979).
36. D. S. WONG and S. I. SANDLER, *AIChE J.*, **38**, 671–680 (1992).
37. AHLERS, J. and J. GMEHLING, *Fluid Phase Equilib.*, **191**, 177–188 (2001).
38. SCHMID, B., A. SCHEDEMANN, and J. GMEHLING, *Ind. Eng. Chem. Research*, **53**, 3393–3405 (2014).
39. PITZER, K.S., *J. Phys. Chem.*, **77**, No. 2, 268–277 (1973).
40. CHEN, C.-C., H.I. BRITT, J.F. BOSTON, and L.B. EVANS, *AIChE Journal*, **28**, 588–596 (1982).
41. CHEN, C.-C., and L.B. EVANS, *AIChE Journal*, **32**, 444–459 (1986).
42. MOCK, B., L.B. EVANS, and C.-C. CHEN, *AIChE Journal*, **28**, 1655–1664 (1986).
43. CHEN, C.-C., *Fluid Phase Equilibria*, **83**, 301–312 (1993).
44. CARLSON, E.C., *Chem. Eng. Progress*, **92**(10) 35–46 (1996).
45. BENEDICT, M., G.B. WEBB, and L.C. RUBIN, *Chem. Eng. Progress*, **47**(8), 419 (1951).
46. BENEDICT, M., G.B. WEBB, and L.C. RUBIN, *Chem. Eng. Progress*, **47**(9), 449 (1951).
47. FELDER, R.M., and R.W. ROUSSEAU, *Elementary Principles of Chemical Processes, 3rd ed.*, John Wiley & Sons, New York, (2000).
48. DE NEVERS, N., and J.D. SEADER, *Latin Am. J. Heat and Mass Transfer*, **8**, 77–105 (1984).
49. SANDLER, S.I., *Using Aspen Plus in Thermodynamics Instruction*, John Wiley & Sons, Hoboken, NJ, (2015).

STUDY QUESTIONS

- 2.1. Why is fugacity used in place of chemical potential to determine phase equilibria? Who invented fugacity?
- 2.2. How is the K -value for vapor–liquid equilibria defined?
- 2.3. How is the distribution coefficient for a liquid–liquid mixture defined?
- 2.4. Define relative volatility and relative selectivity.
- 2.5. What are the three types of models used to estimate thermodynamic properties?
- 2.6. State the limitation of the Redlich–Kwong equation of state. How did Soave modify it to overcome the limitation?
- 2.7. Name the four most widely used methods for estimating liquid-phase activity coefficients.
- 2.8. What very important concept did Wilson introduce in 1964?
- 2.9. What advantage does the NRTL equation have over the Wilson equation?
- 2.10. What is a minimum-boiling azeotrope? What is a maximum-boiling azeotrope? Which type is by far the most common?
- 2.11. Why must electrolyte–solution activity-coefficient models consider both chemical and physical equilibrium?
- 2.12. In an energy balance, what are the two most common references (datums) used for enthalpy and entropy? Does one have an advantage over the other?
- 2.13. In what way does availability differ from Gibbs free energy?

EXERCISES

Section 2.1

2.1. Expressions for computing K -values.

Which of the following K -value expressions are rigorous? For the nonrigorous expressions, cite the assumptions.

- (a) $K_i = \bar{\phi}_{iL}/\bar{\phi}_{iV}$
- (b) $K_i = \phi_{iL}/\phi_{iV}$
- (c) $K_i = \phi_{iL}$
- (d) $K_i = \gamma_{iL}\phi_{iL}/\bar{\phi}_{iV}$
- (e) $K_i = P_i^s/P$
- (f) $K_i = \gamma_{iL}\phi_{iL}/\gamma_{iV}\phi_{iV}$
- (g) $K_i = \gamma_{iL}P_i^s/P$

2.2. Comparison of experimental K -values to Raoult's law predictions.

Experimental measurements of Vaughan and Collins [*Ind. Eng. Chem.*, **34**, 885 (1942)] for the propane–isopentane system, at 167°F and 147 psia, show a propane liquid-phase mole fraction of 0.2900 in equilibrium with a vapor-phase mole fraction of 0.6650. Calculate:

- (a) The K -values for C_3 and iC_5 from the experimental data.
- (b) The K -values of C_3 and iC_5 from Raoult's law, assuming vapor pressures at 167°F of 409.6 and 58.6 psia, respectively.

Compare the results of (a) and (b). Assuming the experimental values are correct, how could better estimates of the K -values be achieved? To respond to this question, compare the rigorous $K_i = \gamma_{iL}\phi_{iL}/\bar{\phi}_{iV}$ to the Raoult's law expression $K_i = P_i^s/P$.

2.3. Distribution coefficients from L/L data.

Mutual solubility data for the isooctane (1)–furfural (2) system at 25°C [*Chem. Eng. Sci.*, **6**, 116 (1957)] are:

	Liquid Phase I	Liquid Phase II
x_1	0.0431	0.9461

Compute:

- (a) The distribution (partition) coefficients for isooctane and furfural
- (b) The selectivity for isooctane relative to that of furfural
- (c) The activity coefficient of isooctane in phase 1 and an activity coefficient of furfural in phase 2, assuming $\gamma_2^{(I)}$ and $\gamma_1^{(II)} = 1.0$

2.4. Activity coefficients of solids dissolved in solvents.

In refineries, alkylbenzene and alkyl-naphthalene streams result from catalytic cracking operations. They can be hydrodealkylated to yield valuable products such as benzene and naphthalene. At 25°C, solid naphthalene (normal melting point = 80.3°C) has the following solubilities in liquid solvents including benzene [*Naphthalene*, API Publication 707, Washington, DC (Oct. 1978)]:

Solvent	Mole Fraction of Naphthalene
Benzene	0.2946
Cyclohexane	0.1487
Carbon tetrachloride	0.2591
<i>n</i> -hexane	0.1168
Water	0.18×10^{-5}

For each solvent, compute the activity coefficient of naphthalene in the solvent phase using the following equations (with T in K) for the vapor pressure in torr of solid and liquid naphthalene:

$$\ln P_{\text{solid}}^s = 26.0708 - 8,712/T$$

$$\ln P_{\text{liquid}}^s = 16.1426 - 3992.01/(T - 71.29)$$

Section 2.2

2.5. Relative volatility from Raoult's law.

The separation of isopentane from n -pentane by distillation is commonly practiced in industry. However, the separation is difficult (approximately 100 trays are required). Using the extended Antoine vapor pressure equation, (2-42), with Raoult's law, calculate relative volatilities for the isopentane/ n -pentane system and compare the values on a plot with the following experimental values [*J. Chem. Eng. Data*, **8**, 504 (1963)]:

Temperature, °F	α_{iC_5, nC_5}
125	1.26
150	1.23
175	1.21
200	1.18
225	1.16
250	1.14

What do you conclude about the applicability of Raoult's law in this temperature range for this binary system? Vapor pressure constants for (2-42) with vapor pressure in kPa and T in K are

Constants in (2-42)	iC_5	nC_5
k_1	13.6106	13.9778
k_2	-2,345.09	-2,554.60
k_3	-40.2128	-36.2529
k_4, k_5, k_6	0	0

2.6. Calculation of condenser duty.

Conditions at the top of a vacuum distillation column for the separation of ethylbenzene from styrene are given below, where the overhead vapor is condensed in an air-cooled condenser to give sub-cooled reflux and distillate. Use a process simulator to estimate the heat-transfer rate (duty) for the condenser in kJ/h, assuming an ideal gas and ideal-gas and liquid solutions. Are these valid assumptions?

	Overhead Vapor	Reflux	Distillate
Phase condition	Saturated vapor	Liquid	Liquid
Temperature	—	5°C subcooled	5°C subcooled
Pressure, kPa	6.69	6.40	6.40
Component flow rates, kg/h:			
Ethylbenzene	77,500	66,960	10,540
Styrene	2,500	2,160	340

2.7. Liquid density of a mixture.

Conditions for the bottoms at 229°F and 282 psia from a depropanizer distillation unit in a refinery are given below, including the pure-component liquid densities. Assuming an ideal-liquid solution (volume of mixing = 0), compute the liquid density in lb/ft³,

lb/gal, lb/bbl (42 gal), and kg/m³. Compare your results to the density obtained with a process simulator.

Component	Flow Rate, lbmol/h	Liquid Density, g/cm ³
Propane	2.2	0.20
Isobutane	171.1	0.40
n -butane	226.6	0.43
Isopentane	28.1	0.515
n -pentane	17.5	0.525

Section 2.3

2.8. Phase condition of a mixture.

Toluene is hydrodealkylated to benzene, with a conversion per pass through the reactor of 70%. The toluene must be recovered and recycled. The conditions for the feed to a commercial distillation unit are 100°F, 20 psia, 415 lbmol/h of benzene, and 131 lbmol/h of toluene. Use Figure 2.1 to determine, if possible, the phase condition of the feed (i.e. superheated vapor, saturated vapor, vapor and liquid phases, saturated liquid, or subcooled liquid).

Section 2.5

2.9. Volumetric flow rates for an adsorber.

Sub-quality natural gas contains an intolerable amount of N₂ impurity. Separation processes that can be used to remove N₂ include cryogenic distillation, membrane separation, and pressure-swing adsorption. For the last-named process, a set of typical feed and product conditions is given below. Assume 90% removal of N₂ and a 97% methane natural-gas product. Using the RK EOS with a process simulator, compute the flow rate in thousands of actual ft³/h for each of the three streams. Stream conditions are:

	Feed (Subquality Natural Gas)	Product (Natural Gas)	Waste Gas
Flow Rate, lbmol/h:			
Nitrogen	174		
Methane	704		
Temperature, °F	70	100	70
Pressure, psia	800	790	280

2.10. K -values from the PR and SRK equations.

Use a process simulation program to estimate the K -values, using the PR and SRK equations of state, of an equimolar mixture of the following two butane isomers and four butene isomers at 220°F and 276.5 psia. Compare the computed values with the following experimental results [*J. Chem. Eng. Data*, **7**, 331 (1962)]:

Component	K -value
Isobutane	1.067
Isobutene	1.024
n -butane	0.922
1-butene	1.024
<i>trans</i> -2-butene	0.952
<i>cis</i> -2-butene	0.876

2.11. Cooling and partial condensation of a reactor effluent.

The disproportionation of toluene to benzene and xylenes is carried out in a catalytic reactor at 500 psia and 950°F. The reactor effluent is cooled in a series of heat exchangers for heat recovery until a

temperature of 235°F is reached at a pressure of 490 psia. The effluent is then further cooled and partially condensed by the transfer of heat to cooling water in a final heat exchanger. The resulting two-phase equilibrium mixture at 100°F and 485 psia is then separated in a flash drum. For the reactor-effluent composition given below, use a process simulation program with the SRK and PR equations of state to compute the component flow rates in lbmol/h in the resulting vapor and liquid streams, the component K -values for the equilibrium mixture, and the rate of heat transfer to the cooling water. Compare the two sets of results.

Component	Reactor Effluent, lbmol/h
H ₂	1,900
CH ₄	215
C ₂ H ₆	17
Benzene	577
Toluene	1,349
<i>p</i> -xylene	508

2.12. Recovery of acetone from air by absorption.

Acetone can be recovered from air by absorption in water. The conditions for the streams entering and leaving are listed below. If the absorber operates adiabatically, obtain the temperature of the exiting liquid phase using a simulation program.

	Feed Gas	Absorbent	Gas Out	Liquid Out
Flow rate, lbmol/h:				
Air	687	0	687	0
Acetone	15	0	0.1	14.9
Water	0	1,733	22	1,711
Temperature, °F	78	90	80	—
Pressure, psia	15	15	14	15
Phase	Vapor	Liquid	Vapor	Liquid

Concern has been expressed about a possible feed-gas explosion hazard. The lower and upper flammability limits for acetone in air are 2.5 and 13 mol%, respectively. Is the feed gas within the explosive range? If so, what can be done to remedy the situation?

Section 2.7

2.13. Condenser duty for two-liquid-phase distillate.

Isopropanol, with 13 wt% water, can be dehydrated to obtain almost pure isopropanol at a 90% recovery by azeotropic distillation with benzene. When condensed, the overhead vapor from the column forms two immiscible liquid phases. Use a process simulator to compute the heat-transfer rate in Btu/h and kJ/h for the condenser.

	Overhead Vapor	Water-Rich Phase Liquid	Organic-Rich Phase Liquid
Phase	Vapor	Liquid	Liquid
Temperature, °C	76	40	40
Pressure, bar	1.4	1.4	1.4
Flow rate, kg/h:			
Isopropanol	6,800	5,870	930
Water	2,350	1,790	560
Benzene	24,600	30	24,570

2.14. Minimum work for separation of a nonideal-liquid mixture.

For a process in which the feed and products are all nonideal solutions at the infinite surroundings temperature, T_0 , Equation (4) of Table 2.11 for the minimum work of separation reduces to

$$\frac{W_{\min}}{RT_0} = \sum_{out} n \left[\sum_i x_i \ln(\gamma_i x_i) \right] - \sum_{in} n \left[\sum_i x_i \ln(\gamma_i x_i) \right]$$

For the separation at ambient conditions (298 K, 101.3 kPa) of a 35 mol% mixture of acetone (1) in water (2) into 99 mol% acetone and 98 mol% water, calculate the minimum work in kJ/kmol of feed. Use a process simulator with the Wilson equation to obtain the activity coefficients. What is the minimum work if acetone and water formed an ideal solution?

2.15. Relative volatility and activity coefficients of an azeotrope.

A sharp separation of benzene (B) and cyclohexane (CH) by distillation is impossible because of an azeotrope at 77.6°C, as shown by the data of K.C. Chao [PhD thesis, University of Wisconsin (1956)]. At 1 atm:

$T, ^\circ\text{C}$	x_B	y_B	γ_B	γ_{CH}
79.7	0.088	0.113	1.300	1.003
79.1	0.156	0.190	1.256	1.008
78.5	0.231	0.268	1.219	1.019
78.0	0.308	0.343	1.189	1.032
77.7	0.400	0.422	1.136	1.056
77.6	0.470	0.482	1.108	1.075
77.6	0.545	0.544	1.079	1.102
77.6	0.625	0.612	1.058	1.138
77.8	0.701	0.678	1.039	1.178
78.0	0.757	0.727	1.025	1.221
78.3	0.822	0.791	1.018	1.263
78.9	0.891	0.863	1.005	1.328
79.5	0.953	0.938	1.003	1.369

- Use the data to calculate and plot the relative volatility of benzene with respect to cyclohexane versus benzene composition in the liquid phase. What happens in the vicinity of the azeotrope?
- Estimate the composition of the azeotrope. Is it a maximum-boiling or minimum-boiling azeotrope?
- Using a process simulator with the Wilson equation to compute and plot the activity coefficients. How well do they compare with the experimental data?

Section 2.12

2.16. Minimum work of separation.

A refinery stream is separated at 1,500 kPa into two products under the conditions shown below. Using the data given, compute the minimum work of separation, W_{\min} , in kJ/h for $T_0 = 298.15$ K.

Component	Flow Rate, kmol/h	
	Feed	Product 1
Ethane	30	30
Propane	200	192
<i>n</i> -butane	370	4
<i>n</i> -pentane	350	0
<i>n</i> -hexane	50	0

	Feed	Product 1	Product 2
Phase condition	Liquid	Vapor	Liquid
Temperature, K	364	313	394
Enthalpy, kJ/kmol	19,480	25,040	25,640
Entropy, kJ/kmol-K	36.64	33.13	54.84

2.17. Minimum work of separation.

In refineries, a mixture of paraffins and cycloparaffins is reformed in a catalytic reactor to produce blending stocks for gasoline and aromatic precursors for petrochemicals. A typical product from catalytic reforming is ethylbenzene with the three xylene isomers. If this mixture is separated, these four chemicals can be processed to make styrene, phthalic anhydride, isophthalic acid, and terephthalic acid. Compute the minimum work of separation in Btu/h for $T_0 = 560^\circ\text{R}$ if the mixture below is separated at 20 psia into three products.

Component	Fraction of Feed to Product			
	Feed, lbmol/h	Product 1	Product 2	Product 3
Ethylbenzene	150	0.96	0.04	0.000
<i>p</i> -xylene	190	0.005	0.99	0.005
<i>m</i> -xylene	430	0.004	0.99	0.006
<i>o</i> -xylene	230	0.000	0.015	0.985

	Feed	Product 1	Product 2	Product 3
Phase condition	Liquid	Liquid	Liquid	Liquid
Temperature, °F	305	299	304	314
Enthalpy, Btu/lbmol	29,290	29,750	29,550	28,320
Entropy, Btu/lbmol-°R	15.32	12.47	13.60	14.68

2.18. Second-law analysis of a distillation.

Column C3 in Figure 1.10 separates stream 5 into streams 6 and 7, according to the material balance in Table 1.5. The separation is carried out at 700 kPa in a distillation column with 70 plates and a condenser duty of 27,300,000 kJ/h. Using the following data and an infinite surroundings temperature T_0 of 298.15 K, compute: (a) the duty of the reboiler in kJ/h; (b) the irreversible production of entropy in kJ/h-K, assuming condenser cooling water at 25°C and reboiler steam at 100°C; (c) the lost work in kJ/h; (d) the minimum work of separation in kJ/h; and (e) the second-law efficiency. Assume the shaft work of the reflux pump is negligible.

	Feed (Stream 5)	Distillate (Stream 6)	Bottoms (Stream 7)
Phase condition	Liquid	Liquid	Liquid
Temperature, K	348	323	343
Pressure, kPa	1,950	700	730
Enthalpy, kJ/mol	17,000	13,420	15,840
Entropy, kJ/kmol-K	25.05	5.87	21.22

2.19. Second-law analysis of membrane separation.

A spiral-wound, nonporous cellulose acetate membrane separator is used to separate a gas containing H_2 , CH_4 , and C_2H_6 . The permeate is 95 mol% pure H_2 and contains no ethane. The relative split ratio for H_2 relative to methane is 47, where the split ratio for each component

is defined as n lbmol/h in the permeate to n lbmol/h in the retentate. Using the following data and an infinite surroundings temperature of 80°F, compute the: (a) irreversible production of entropy in Btu/h-R; (b) lost work in Btu/h; and (c) minimum work of separation in Btu/h. Why is it negative? What other method(s) might be used to make the separation?

Stream flow rates and properties:

Feed Flow Rates, lbmol/h	
H_2	3,000
CH_4	884
C_2H_6	120

	Feed	Permeate	Retentate
Phase condition	Vapor	Vapor	Vapor
Temperature, °F	80	80	80
Pressure, psia	365	50	365
Enthalpy, Btu/lbmol	8,550	8,380	8,890
Entropy, Btu/lbmol-K	1.520	4.222	2.742

2.20. Minimum isothermal work of separation.

An ideal-gas mixture of A and B undergoes an isothermal, isobaric separation at T_0 , the infinite surroundings temperature. Starting with Eq. (4), Table 2.11, derive an equation for the minimum work of separation, W_{\min} , in terms of mole fractions of the feed and products. Use your equation to plot the dimensionless group, W_{\min}/RT_0n_F , as a function of mole fraction of A in the feed for:

- A perfect separation
- A separation with 98% of A to product 1 and 2% of B to product 1.
- A separation with the ratio of moles of A in product 1 to moles of A in product 2 = 9/1 and the same ratio for B = 1/9.

How sensitive is W_{\min} to product purities? Does W_{\min} depend on the separation operation used? Prove, by calculus, that the largest value of W_{\min} occurs for a feed with equimolar quantities of A and B.

2.21. Exergy change for heating and vaporizing water.

Water at 25°C and 1 atm (state 1) is heated and compressed to produce saturated steam at 2 MPa (state 2). Using a process simulator to obtain enthalpies and entropies, and do flash calculations, calculate the change in exergy of the stream in kJ/kmol, assuming an infinite surroundings temperature, $T_0 = 298.15$ K. Would it be more energy-efficient to: (1) first heat and vaporize the water and compress the steam or (2) first pump the water to the higher pressure and then heat and vaporize it? Give reasons for your choice. How could you prove that your choice is correct?

2.22. Exergy change for compression and cooling of methane gas.

100 kmol/h of methane gas is compressed adiabatically from 0.5 MPa and 300 K to 2.0 MPa, after which it is cooled isobarically to 300 K by a large amount of water at 300 K. Assume an infinite surroundings temperature T_0 of 300 K. The mechanical efficiency of the compressor with its motor is 80%. Using a process simulator, determine H_p of the compressor, heat duty of the cooler in kJ/h, and exergies in kJ/h of the entering and exiting methane. For the process determine lost work, LW, in kJ/h, minimum work in kJ/h, irreversible change in entropy in kJ/h-K, and the second-law efficiency.

Chapter 3

Mass Transfer and Diffusion

§3.0 INSTRUCTIONAL OBJECTIVES

After completing this chapter, you should be able to:

- Explain the relationship between mass transfer and phase equilibrium, and why models for both are useful.
- Discuss mechanisms of mass transfer, including bulk flow.
- State Fick's law of diffusion for binary mixtures and discuss its analogy to Fourier's law of heat conduction.
- Estimate, in the absence of data, diffusivities for gas and liquid mixtures.
- Calculate multidimensional, unsteady-state molecular diffusion by analogy to heat conduction.
- Calculate rates of mass transfer by molecular diffusion in laminar flow.
- Define a mass-transfer coefficient and explain its analogy to the heat-transfer coefficient.
- Use analogies, particularly those of Chilton and Colburn, to calculate rates of mass transfer in turbulent flow.
- Calculate rates of mass transfer across fluid–fluid interfaces using two-film theory and penetration theory.

Mass transfer is the net movement of a species in a mixture from one location to another. Different species move at different rates and may move in opposite directions. In separation operations, mass transfer often takes place across an interface between two phases. Absorption by a liquid of a solute from a carrier gas involves transfer of the solute through the gas to the gas–liquid interface, across the interface, and into the liquid. Extraction of a species from a liquid mixture involves transfer of the solute through the liquid to the liquid–liquid solvent interface, across the interface and into the solvent. A component in a gas or liquid may travel to the interior surface of a porous particle, where the species is adsorbed. Mathematical models for these processes, as well as others, are described throughout this book based on the fundamentals of mass transfer presented in this chapter.

Two mechanisms of mass transfer are (1) **molecular diffusion** by random and spontaneous microscopic movement of molecules as a result of thermal motion; and (2) **eddy (turbulent) diffusion** by random, macroscopic fluid motion. Both molecular and eddy diffusion may involve the movement of different species in opposing directions. The total rate of mass transfer of individual species is increased or decreased by a **bulk flow**, which is a third mechanism of mass transfer. However, bulk flow alone does not provide a separation of the species in a mixture.

Molecular diffusion is extremely slow, while eddy diffusion is rapid. Therefore, if industrial separation processes are to be conducted in equipment of reasonable size, the fluids must be agitated and/or interfacial areas maximized. For solids, the particle size is decreased and/or made porous to increase the surface area/volume for mass transfer and decrease the distance for diffusion.

In multiphase systems, the extent of the separation is limited by phase equilibrium (discussed in Chapter 2) because with time, concentrations equilibrate by mass transfer. When mass transfer is rapid, equilibration takes seconds or minutes, and design of separation equipment can be based on phase equilibrium, rather than on mass transfer rates. For separations involving barriers such as membranes, mass-transfer rates govern equipment design.

In binary mixtures, diffusion of species A with respect to B occurs because of driving forces, which include concentration gradients (**ordinary diffusion**), pressure, temperature, and external force fields that act unequally on different species. **Pressure diffusion** requires a large gradient, which is achieved for gas mixtures with a centrifuge. **Thermal diffusion** columns can be employed to separate mixtures by establishing a temperature gradient. Widely applied is **forced diffusion** of ions or charged particles in an electrical field.

This chapter only describes ordinary diffusion driven by composition gradients (e.g., concentration, mole fraction, activity, partial pressure), which is the most common type of diffusion in chemical separation processes. Emphasis is on binary systems, for which diffusion theory is relatively simple and applications are straightforward. Multicomponent ordinary diffusion is introduced in Chapter 12. Taylor and Krishna [1] support advanced study of multicomponent diffusion.

Molecular diffusion occurs in solids and in fluids that are stagnant or in laminar motion. Eddy diffusion occurs in fluids when turbulent motion exists. When both molecular diffusion and eddy diffusion occur, they are additive. When mass transfer occurs under bulk turbulent flow but across a fluid–fluid interface or to a solid surface, flow is generally

laminar or stagnant near the interface or solid surface. Thus, the eddy-diffusion mechanism is dampened or eliminated as the diffusing species approaches the interface or solid surface.

Mass transfer can result in a total net rate of bulk flow or flux in a direction relative to a fixed plane or stationary coordinate system. When a net flux occurs, it carries all species present. Thus, the molar flux of a species can be the sum of all three mechanisms. If N_i is the molar flux of i with mole fraction x_i , and N is the total molar flux in moles per unit time per unit area in a direction perpendicular to a stationary plane across which mass transfer occurs, then the three mechanisms give

$$N_i = \text{molecular diffusion flux of } i \quad (3-1)$$

$$+ \text{eddy diffusion flux of } i + x_i N$$

where $x_i N$ is the bulk-flow flux. Each term in (3-1) is positive or negative depending on the direction of the flux relative to the direction selected as positive. When the molecular and eddy-diffusion fluxes are in one direction and N is in the opposite direction (even though a gradient of i exists), the net species mass-transfer flux, N_i , can be zero.

This chapter covers seven areas: (1) steady-state diffusion in stagnant media, (2) estimation of diffusion coefficients, (3) unsteady-state diffusion in stagnant media, (4) mass transfer in laminar flow, (5) mass transfer in turbulent flow, (6) mass transfer at fluid–fluid interfaces, and (7) mass transfer across fluid–fluid interfaces.

§3.1 STEADY-STATE, ORDINARY MOLECULAR DIFFUSION

Imagine a cylindrical glass vessel partly filled with dyed water. Clear water is carefully added on top so that the dyed solution on the bottom is undisturbed. At first, a sharp boundary exists between layers, but as mass transfer of the dye occurs because of a dye-concentration difference, the upper layer becomes colored and the bottom layer below less colored. The upper layer is more colored near the original interface between the dyed solution and the clear water, and less colored in the region near the top of the liquid contents. During this color change, the motion of each dye molecule is random, undergoing collisions with water molecules and sometimes with dye molecules, moving first in one direction and then in another, with no one direction preferred. This type of motion is sometimes called a **random-walk process**, which yields a mean-square distance of travel in a time interval but not in a direction interval. At a given horizontal plane through the solution, it is not possible to determine whether a particular molecule will cross the plane or not in a given time interval. On the average, a fraction of all (dye and water) molecules in the solution below the plane cross over into the region above, and the same fraction will cross over in the opposite direction. Therefore, if the concentration of dye molecules in the lower region is greater than in the upper region, a net rate of mass transfer of dye takes place from the lower to the upper region. Ultimately, a dynamic equilibrium is achieved and the dye

concentration will be uniform throughout the liquid in the vessel. Based on these observations, it is clear that:

1. Mass transfer by ordinary molecular diffusion in a binary mixture occurs because of a composition gradient; that is, a species diffuses in the direction of decreasing concentration.
2. The mass-transfer rate is proportional to the area normal to the direction of mass transfer. Thus, the rate can be expressed as a flux.
3. Net mass transfer stops when concentrations are uniform throughout.

§3.1.1 Fick's Law of Diffusion

The above three observations were quantified by Fick in 1855. He proposed an analogy to Fourier's 1822 first law of heat conduction,

$$q_z = -k \frac{dT}{dz} \quad (3-2)$$

where q_z is the heat flux by conduction in the z -direction, k is the thermal conductivity, and dT/dz is the temperature gradient, which is negative in the direction of heat conduction.

Fick's first law also features a proportionality between a flux and a gradient. For a mixture of A and B,

$$J_{A_z} = -D_{AB} \frac{dc_A}{dz} \quad (3-3a)$$

and

$$J_{B_z} = -D_{BA} \frac{dc_B}{dz} \quad (3-3b)$$

where J_A is the molar flux (moles per unit perpendicular area and per unit time) of A by ordinary molecular diffusion relative to the molar-average velocity of the mixture in the z -direction, D_{AB} is the **mutual diffusion coefficient** or **diffusivity** of A in B, c_A is the molar concentration of A, and dc_A/dz is the concentration gradient of A, which is negative in the direction of diffusion of A. Similar definitions apply to (3-3b). If the medium through which diffusion occurs is isotropic, then values of k and D_{AB} are independent of direction. Nonisotropic (anisotropic) materials include fibrous and composite solids as well as noncubic crystals.

Alternative composition driving forces can be used in (3-3a) and (3-3b). An example is

$$J_A = -cD_{AB} \frac{dx_A}{dz} \quad (3-4)$$

where the z subscript on J has been dropped, c = total mixture molar concentration, and x_A = mole fraction of A. Two other possible driving forces are partial pressure for a gas and activity for a nonideal liquid.

Equation (3-4) can also be written in an equivalent mass form, where j_A is the mass flux of A relative to the mass-average velocity of the mixture in the positive z -direction, ρ is the mixture mass density, and w_A is the mass fraction of A:

$$j_A = -\rho D_{AB} \frac{dw_A}{dz} \quad (3-5)$$

§3.1.2 Species Velocities in Diffusion

If velocities are based on molar flux, N , and molar diffusion flux, J , then the molar average mixture velocity, v_M , relative to stationary coordinates for the binary mixture, is

$$v_M = \frac{N}{c} = \frac{N_A + N_B}{c} \quad (3-6)$$

Similarly, the velocity of species i in terms of N_i , relative to stationary coordinates, is

$$v_i = \frac{N_i}{c_i} \quad (3-7)$$

Combining (3-6) and (3-7) with $x_i = c_i/c$ gives

$$v_M = x_A v_A + x_B v_B \quad (3-8)$$

Diffusion velocities, v_{iD} , defined in terms of J_i , are relative to molar-average velocity and are defined as the difference between the species velocity and the molar-average mixture velocity:

$$v_{iD} = \frac{J_i}{c_i} = v_i - v_M \quad (3-9)$$

When solving mass-transfer problems involving net mixture movement (bulk flow), fluxes and flow rates based on v_M as the frame of reference are inconvenient to use. It is preferred to use mass-transfer fluxes referred to stationary coordinates. Thus, from (3-9), the total species velocity is

$$v_i = v_M + v_{iD} \quad (3-10)$$

Combining (3-7) and (3-10),

$$N_i = c_i v_M + c_i v_{iD} \quad (3-11)$$

Combining (3-11) with (3-4), (3-6), and (3-7),

$$N_A = \frac{n_A}{A} = x_A N - c D_{AB} \left(\frac{dx_A}{dz} \right) \quad (3-12)$$

and

$$N_B = \frac{n_B}{A} = x_B N - c D_{BA} \left(\frac{dx_B}{dz} \right) \quad (3-13)$$

In (3-12) and (3-13), n_i is the molar flow rate in moles per unit time, A is the mass-transfer area, the first right-hand side terms are the total fluxes resulting from bulk flow, and the second terms are the diffusion fluxes. Two cases are important for a binary mixture: (1) equimolar counter diffusion (EMD) and (2) unimolecular diffusion (UMD).

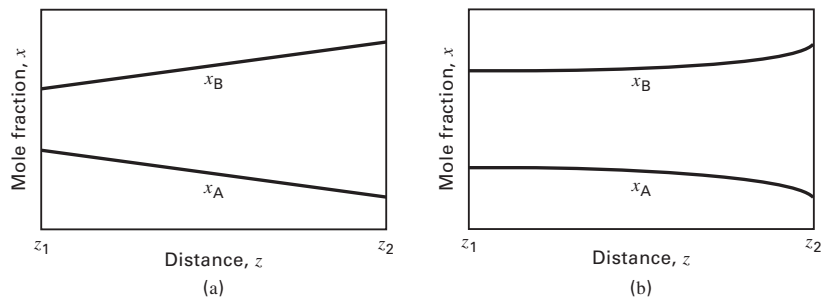


Figure 3.1 Concentration profiles for limiting cases of ordinary molecular diffusion in binary mixtures across a stagnant film: (a) equimolar counter diffusion (EMD); (b) unimolecular diffusion (UMD).

§3.1.3 Equimolar Counter Diffusion (EMD)

In EMD, the molar fluxes in (3-12) and (3-13) are equal but opposite in direction, so

$$N = N_A + N_B = 0 \quad (3-14)$$

Thus, from (3-12) and (3-13), the diffusion fluxes are also equal but opposite in direction:

$$J_A = -J_B \quad (3-15)$$

This idealization is approached in distillation of nearly ideal binary mixtures, as discussed in Chapter 7. From (3-12) and (3-13), in the absence of bulk flow,

$$N_A = J_A = -c D_{AB} \left(\frac{dx_A}{dz} \right) \quad (3-16)$$

and

$$N_B = J_B = -c D_{BA} \left(\frac{dx_B}{dz} \right) \quad (3-17)$$

If the total concentration, pressure, and temperature are constant and the mole fractions are constant (but different) at two sides of a stagnant film between locations z_1 and z_2 , then (3-16) and (3-17) can be integrated from z_1 to any z between z_1 and z_2 to give

$$J_A = \frac{c D_{AB}}{z - z_1} (x_{A1} - x_A) \quad (3-18)$$

and

$$J_B = \frac{c D_{BA}}{z - z_1} (x_{B1} - x_B) \quad (3-19)$$

At steady state, the mole fractions are linear in distance, as shown in Figure 3.1a. Furthermore, because total concentration c is constant through the film, where

$$c = c_A + c_B \quad (3-20)$$

by differentiation,

$$dc = 0 = dc_A + dc_B \quad (3-21)$$

Thus,

$$dc_A = -dc_B \quad (3-22)$$

From (3-3a), (3-3b), (3-15), and (3-22),

$$\frac{D_{AB}}{dz} = \frac{D_{BA}}{dz} \quad (3-23)$$

Therefore, $D_{AB} = D_{BA}$. This equality of diffusion coefficients at a given composition is always true in a binary system.

EXAMPLE 3.1 EMD in a Tube.

Two bulbs are connected by a straight tube, 0.001 m in diameter and 0.15 m in length. Initially, the bulb at End 1 contains N_2 and the bulb at End 2 contains H_2 . Pressure and temperature are constant at 25°C and 1 atm. At a time after diffusion starts, the nitrogen content of the gas at End 1 of the tube is 80 mol% and 25 mol% at End 2. If the binary diffusion coefficient is 0.784 cm²/s, determine:

- The rates and directions of mass transfer of N_2 and H_2 in mol/s.
- The species velocities relative to stationary coordinates, in cm/s.

Solution

- Because the gas system is closed and at constant pressure and temperature, no bulk flow occurs and mass transfer in the connecting tube is EMD.

The area for mass transfer through the tube, in cm², is $A = 3.14(0.1)^2/4 = 7.85 \times 10^{-3}$ cm². By the ideal gas law, the total gas concentration is $c = P/RT = 1/(82.06)(298) = 4.09 \times 10^{-5}$ mol/cm³. Take End 1 as the reference plane of the connecting tube. Applying (3-18) to N_2 over the tube length,

$$\begin{aligned} n_{N_2} &= \frac{cD_{N_2,H_2}}{z_2 - z_1} [(x_{N_2})_1 - (x_{N_2})_2]A \\ &= \frac{(4.09 \times 10^{-5})(0.784)(0.80 - 0.25)}{15} (7.85 \times 10^{-3}) \\ &= 9.23 \times 10^{-9} \text{ mol/s in the positive } z\text{-direction} \\ n_{H_2} &= 9.23 \times 10^{-9} \text{ mol/s in the negative } z\text{-direction} \end{aligned}$$

- For EMD, the molar-average velocity of the mixture, v_M , is 0. Therefore, from (3-9), species velocities are equal to species diffusion velocities. Thus,

$$\begin{aligned} v_{N_2} &= (v_{N_2})_D = \frac{J_{N_2}}{c_{N_2}} = \frac{n_{N_2}}{Acx_{N_2}} \\ &= \frac{9.23 \times 10^{-9}}{[(7.85 \times 10^{-3})(4.09 \times 10^{-5})x_{N_2}]} \\ &= \frac{0.0287}{x_{N_2}} \quad \text{in the positive } z\text{-direction} \end{aligned}$$

Similarly, $v_{H_2} = \frac{0.0287}{x_{H_2}}$ in the negative z -direction

Thus, species velocities depend on mole fractions, as follows:

z , cm	x_{N_2}	x_{H_2}	v_{N_2} , cm/s	v_{H_2} , cm/s
0 (End 1)	0.800	0.200	0.0351	-0.1435
5	0.617	0.383	0.0465	-0.0749
10	0.433	0.567	0.0663	-0.0506
15 (End 2)	0.250	0.750	0.1148	-0.0383

Note that species velocities vary along the length of the tube, but at any location z , $v_M = 0$. For example, at $z = 10$ cm, from (3-8),

$$v_M = (0.433)(0.0663) + (0.567)(-0.0506) = 0$$

§3.1.4 Unimolecular Diffusion (UMD)

In UMD, mass transfer of component A occurs through stagnant B, resulting in a bulk flow. Thus,

$$N_B = 0 \quad (3-24)$$

and

$$N = N_A \quad (3-25)$$

Therefore, from (3-12),

$$N_A = x_A N_A - cD_{AB} \frac{dx_A}{dz} \quad (3-26)$$

which can be rearranged to a Fick's law form by solving for N_A ,

$$N_A = -\frac{cD_{AB}}{(1-x_A)} \frac{dx_A}{dz} = -\frac{cD_{AB}}{x_B} \frac{dx_A}{dz} \quad (3-27)$$

The factor $(1-x_A)$ accounts for the bulk-flow effect. For a mixture dilute in A, this effect is small. But in an equimolar mixture of A and B, $(1-x_A) = 0.5$ and, because of bulk flow, the molar mass-transfer flux of A is twice the ordinary molecular-diffusion flux.

For the stagnant component, B, (3-13) becomes

$$0 = x_B N_A - cD_{BA} \frac{dx_B}{dz} \quad (3-28)$$

or

$$x_B N_A = cD_{BA} \frac{dx_B}{dz} \quad (3-29)$$

Thus, the bulk-flow flux of B is equal to but opposite its diffusion flux.

At quasi-steady-state conditions (i.e., no accumulation of species with time) and with constant molar density, (3-27) in integral form is:

$$\int_{z_1}^z dz = -\frac{cD_{AB}}{N_A} \int_{x_{A1}}^{x_A} \frac{dx_A}{1-x_A} \quad (3-30)$$

which upon integration yields

$$N_A = \frac{cD_{AB}}{z-z_1} \ln \left(\frac{1-x_A}{1-x_{A1}} \right) \quad (3-31)$$

Rearranging (3-31) gives the mole-fraction variation as a function of z .

$$x_A = 1 - (1-x_{A1}) \exp \left[\frac{N_A (z-z_1)}{cD_{AB}} \right] \quad (3-32)$$

Figure 3.1b shows that the mole fractions are nonlinear in z .

A more useful form of (3-31) can be derived from the definition of the log mean, which is often used for the driving force in countercurrent heat exchangers. When $z = z_2$, (3-31) becomes

$$N_A = \frac{cD_{AB}}{z_2-z_1} \ln \left(\frac{1-x_{A2}}{1-x_{A1}} \right) \quad (3-33)$$

The log mean (LM) of $(1 - x_A)$ at the two ends of the stagnant layer is

$$(1 - x_A)_{LM} = \frac{(1 - x_{A_2}) - (1 - x_{A_1})}{\ln \left[\frac{(1 - x_{A_2})}{(1 - x_{A_1})} \right]} = \frac{(x_{A_1} - x_{A_2})}{\ln \left[\frac{(1 - x_{A_2})}{(1 - x_{A_1})} \right]} \quad (3-34)$$

Combining (3-33) with (3-34) gives

$$N_A = \frac{cD_{AB}}{z_2 - z_1} \frac{(x_{A_1} - x_{A_2})}{(1 - x_A)_{LM}} = \frac{cD_{AB}}{(1 - x_A)_{LM}} \frac{(-\Delta x_A)}{\Delta z} = \frac{cD_{AB}}{(x_B)_{LM}} \frac{(-\Delta x_A)}{\Delta z} \quad (3-35)$$

EXAMPLE 3.2 Evaporation from an Open Beaker.

In Figure 3.2, an open beaker, 6 cm high, is filled with liquid benzene (A) at 25°C to within 0.5 cm of the top. Dry air (B) at 25°C and 1 atm is blown across the mouth of the beaker so that evaporated benzene is carried away by convection after it transfers through an air layer within the beaker. The air layer is assumed to be stagnant. The vapor pressure of benzene at 25°C is 0.131 atm. As shown in Figure 3.2, the mole fraction of benzene in the air at the top of the beaker is zero and is at equilibrium at the gas–liquid interface. The diffusion coefficient for benzene in air at 25°C and 1 atm is 0.0905 cm²/s. Compute: (a) the initial rate of evaporation of benzene as a molar flux in mol/cm²-s; (b) initial mole-fraction profiles in the stagnant air layer; (c) initial fractions of the mass-transfer fluxes due to molecular diffusion; (d) initial diffusion velocities, and the species velocities (relative to stationary coordinates) in the stagnant layer; and (e) time for the benzene level in the beaker to drop 2 cm if the specific gravity of benzene is 0.874. Neglect the accumulation of benzene and air in the stagnant layer with time as it increases in height (quasi-steady-state assumption). In this example, x is the mole fraction in the gas.

Solution

The total vapor concentration by the ideal-gas law is:

$$c = P/RT = 1/(82.06)(298) = 4.09 \times 10^{-5} \text{ mol/cm}^3$$

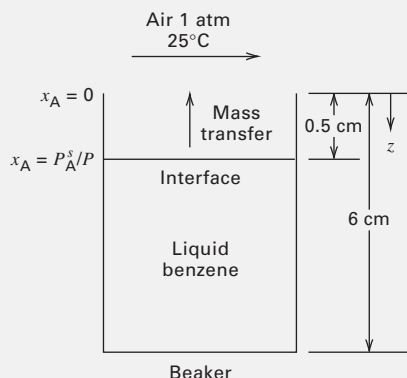


Figure 3.2 Evaporation of benzene from a beaker—Example 3.2.

(a) With z equal to the distance down from the top of the beaker, let $z_1 = 0$ at the top of beaker and $z_2 =$ the distance from the top of the beaker to the gas–liquid interface. Then, initially, the stagnant gas layer thickness is $z_2 - z_1 = \Delta z = 0.5$ cm. From Raoult's and Dalton's laws, assuming equilibrium at the liquid benzene–air interface,

$$x_{A_1} = P_A^s/P = 0.131/1 = 0.131, \quad x_{A_2} = 0$$

$$(1 - x_A)_{LM} = \frac{0.131}{\ln \left[\frac{(1 - 0)}{(1 - 0.131)} \right]} = 0.933 = (x_B)_{LM}$$

From (3-35),

$$N_A = \frac{(4.09 \times 10^{-6})(0.0905)}{0.5} \left(\frac{0.131}{0.933} \right) = 1.04 \times 10^{-6} \text{ mol/cm}^2\text{-s}$$

$$(b) \frac{N_A(z - z_1)}{cD_{AB}} = \frac{(1.04 \times 10^{-6})(z - 0)}{(4.09 \times 10^{-5})(0.0905)} = 0.281z$$

From (3-32),

$$x_A = 1 - 0.869 \exp(0.281z) \quad (1)$$

Using (1), the following results are obtained:

z , cm	x_A	x_B
0.0	0.1310	0.8690
0.1	0.1060	0.8940
0.2	0.0808	0.9192
0.3	0.0546	0.9454
0.4	0.0276	0.9724
0.5	0.0000	1.0000

These profiles are only slightly curved.

(c) Equations (3-27) and (3-29) yield the bulk-flow terms, $x_A N$ and $x_B N$, from which the molecular-diffusion terms are obtained.

z , cm	$x_i N$		J_i	
	Bulk-Flow Flux, mol/cm ² -s $\times 10^6$		Molecular-Diffusion Flux, mol/cm ² -s $\times 10^6$	
	A	B	A	B
0.0	0.1360	0.9040	0.9040	-0.9040
0.1	0.1100	0.9300	0.9300	-0.9300
0.2	0.0840	0.9560	0.9560	-0.9560
0.3	0.0568	0.9832	0.9832	-0.9832
0.4	0.0287	1.0113	1.0113	-1.0113
0.5	0.0000	1.0400	1.0400	-1.0400

Note that the molecular-diffusion fluxes are equal but opposite and the bulk-flow flux of B is equal but opposite to its molecular diffusion flux; thus N_B is zero, making B (air) stagnant.

(d) From (3-6),

$$v_M = \frac{N}{c} = \frac{N_A}{c} = \frac{1.04 \times 10^{-6}}{4.09 \times 10^{-5}} = 0.0254 \text{ cm/s} \quad (2)$$

From (3-9), the diffusion velocities are given by

$$v_{iD} = \frac{J_i}{c_i} = \frac{J_i}{x_i c} \quad (3)$$

From (3-10), species velocities relative to stationary coordinates are

$$v_i = v_{iD} + v_M \quad (4)$$

Using (2) to (4), there follows

z, cm	v_{iD} Molecular-Diffusion Velocity, cm/s		v_i Species Velocity, cm/s	
	A	B	A	B
0.0	0.1687	-0.0254	0.1941	0
0.1	0.2145	-0.0254	0.2171	0
0.2	0.2893	-0.0254	0.3147	0
0.3	0.4403	-0.0254	0.4657	0
0.4	0.8959	-0.0254	0.9213	0
0.5	∞	-0.0254	∞	0

Note that v_B is zero everywhere, because its molecular diffusion velocity is negated by the molar-mean velocity.

(e) The mass-transfer flux for benzene evaporation equals the rate of decrease in the moles of liquid benzene per unit cross-section area of the beaker.

Using (3-35) with $\Delta z = z$,

$$N_A = \frac{cD_{AB}}{z} \frac{(-\Delta x_A)}{(1-x_A)_{LM}} = \frac{\rho_L}{M_L} \frac{dz}{dt} \quad (5)$$

Separating variables and integrating,

$$\int_0^t dt = t = \frac{\rho_L(1-x_A)_{LM}}{M_L c D_{AB} (-\Delta x_A)} \int_{z_1}^{z_2} z dz \quad (6)$$

where z_1 = initial location of the interface and z_2 = location of the interface after it drops 2 cm.

The coefficient of the integral on the RHS of (6) is constant at

$$\frac{0.874(0.933)}{78.11(4.09 \times 10^{-5})(0.0905)(0.131)} = 21,530 \text{ s/cm}^2$$

$$\int_{z_1}^{z_2} z dz = \int_{0.5}^{2.5} z dz = 3 \text{ cm}^2$$

From (6), $t = 21,530(3) = 64,590 \text{ s}$ or 17.94 h, which is a long time because of the absence of turbulence.

§3.2 DIFFUSION COEFFICIENTS (DIFFUSIVITIES)

Diffusion coefficients (diffusivities) are defined for a binary mixture by (3-3) to (3-5). Measurement of diffusion coefficients involves a correction for bulk flow using (3-12) and (3-13), with the reference plane being such that there is no net molar bulk flow. Binary diffusivities, D_{AB} and D_{BA} , are called **mutual** or **binary diffusion coefficients**. Other coefficients include $D_{iM}(D_i)$ the diffusivity of i in a multicomponent mixture; and D_{ii} , the **self-diffusion coefficient**. In this chapter and throughout this book, the focus is on the mutual diffusion coefficient, which will be referred to as the diffusivity or diffusion coefficient. Experimental values of diffusivity are available in handbooks. Diffusivities can also be estimated

from the following correlations and by using methods in process simulators.

§3.2.1 Diffusivity in Gas Mixtures

As discussed by Poling, Prausnitz, and O'Connell [2], equations are available for estimating the value of $D_{AB} = D_{BA}$ in gases at low to moderate pressures. The theoretical equations (based on Boltzmann's kinetic theory of gases, the theorem of corresponding states, and a suitable intermolecular energy-potential function, as developed by Chapman and Enskog) predict D_{AB} to be inversely proportional to pressure, to increase significantly with temperature, and to be almost independent of gas composition. Of greater accuracy and ease of use is the empirical equation of Fuller, Schettler, and Giddings [3], which retains the form of the Chapman-Enskog theory but utilizes empirical constants derived from experimental data:

$$D_{AB} = D_{BA} = \frac{0.00143T^{1.75}}{PM_{AB}^{1/2} \left[(\sum V)_A^{1/3} + (\sum V)_B^{1/3} \right]^2} \quad (3-36)$$

where D_{AB} is in cm^2/s , P is in atm, T is in K,

$$M_{AB} = \frac{2}{(1/M_A) + (1/M_B)} \quad (3-37)$$

and $\sum V$ = summation of atomic and structural **diffusion volumes** from Table 3.1, which includes diffusion volumes of simple molecules.

Experimental values of binary gas diffusivity at 1 atm and near-ambient temperature vary from about 0.10 to 10.0 cm^2/s . Poling et al. [2] compared (3-36) to experimental data for 51 different binary gas mixtures at low pressures over a temperature range of 195–1,068 K. The average deviation was only 5.4%, with a maximum deviation of 25%. Equation (3-36)

Table 3.1 Diffusion Volumes

Atomic Diffusion Volumes and Structural Diffusion-Volume Increments			
C	15.9	F	14.7
H	2.31	Cl	21.0
O	6.11	Br	21.9
N	4.54	I	29.8
Aromatic ring	-18.3	S	22.9
Heterocyclic ring	-18.3		
Diffusion Volumes of Simple Molecules			
He	2.67	CO	18.0
Ne	5.98	CO ₂	26.7
Ar	16.2	N ₂ O	35.9
Kr	24.5	NH ₃	20.7
Xe	32.7	H ₂ O	13.1
H ₂	6.12	SF ₆	71.3
D ₂	6.84	Cl ₂	38.4
N ₂	18.5	Br ₂	69.0
O ₂	16.3	SO ₂	41.8
Air	19.7		

[Reproduced from [3] with permission of the American Chemical Society.]

Table 3.2 Experimental Binary Diffusivities of Gas Pairs at 1 atm

Gas pair, A-B	Temperature, K	D_{AB} , cm ² /s
Air—carbon dioxide	317.2	0.177
Air—ethanol	313	0.145
Air—helium	317.2	0.765
Air— <i>n</i> -hexane	328	0.093
Air—water	313	0.288
Argon—ammonia	333	0.253
Argon—hydrogen	242.2	0.562
Argon—hydrogen	806	4.86
Argon—methane	298	0.202
Carbon dioxide—nitrogen	298	0.167
Carbon dioxide—oxygen	293.2	0.153
Carbon dioxide—water	307.2	0.198
Carbon monoxide—nitrogen	373	0.318
Helium—benzene	423	0.610
Helium—methane	298	0.675
Helium—methanol	423	1.032
Helium—water	307.1	0.902
Hydrogen—ammonia	298	0.783
Hydrogen—ammonia	533	2.149
Hydrogen—cyclohexane	288.6	0.319
Hydrogen—methane	288	0.694
Hydrogen—nitrogen	298	0.784
Nitrogen—benzene	311.3	0.102
Nitrogen—cyclohexane	288.6	0.0731
Nitrogen—sulfur dioxide	263	0.104
Nitrogen—water	352.1	0.256
Oxygen—benzene	311.3	0.101
Oxygen—carbon tetrachloride	296	0.0749
Oxygen—cyclohexane	288.6	0.0746
Oxygen—water	352.3	0.352

[Reproduced from [59] with permission of the American Chemical Society.]

indicates that D_{AB} is proportional to $T^{1.75}/P$, which can be used to adjust experimental diffusivities for T and P . Representative experimental values of binary gas diffusivity are given in Table 3.2.

EXAMPLE 3.3 Estimation of a Gas Diffusivity.

Estimate the diffusion coefficient for oxygen (A) in benzene (B) at 38°C and 2 atm using the method of Fuller et al. (3-36). No experimental value is available.

Solution

$$\text{From (3-37), } M_{AB} = \frac{2}{(1/32) + (1/78.11)} = 45.4$$

$$\text{From Table 3.1, } (\Sigma V)_A = 16.3 \text{ and } (\Sigma V)_B = 6(15.9) + 6(2.31) - 18.3 = 90.96$$

From (3-36), at 2 atm and 311.2 K,

$$D_{AB} = D_{BA} = \frac{0.00143(311.2)^{1.75}}{2(45.4)^{1/2} [(16.3)^{1/3} + (90.96)^{1/3}]^2} = 0.0495 \text{ cm}^2/\text{s}$$

At 1 atm, the predicted diffusivity is 0.0990 cm²/s, which is about 2% below the experimental value in Table 3.2. The theoretical equation of Chapman and Enskog predicts 0.092 cm²/s, while a modification of the theory by Wilke and Lee (see [2]) predicts 0.096 cm²/s. The value for 38°C can be extrapolated to other

temperatures using the $T^{1.75}$ dependency. For example, for a temperature of 200°C, using the experimental value at 38°C,

$$D_{AB} \text{ at } 200^\circ\text{C and 1 atm} = 0.102 \left(\frac{200 + 273.2}{38 + 273.2} \right)^{1.75} = 0.212 \text{ cm}^2/\text{s}$$

For the estimation of binary gas diffusivities at low pressures, Aspen Plus uses the Wilke-Lee modification of the Chapman-Enskog theory, while ChemSep uses (3-36) of Fuller et al. unless the diffusion volumes cannot be estimated. In that case, ChemSep uses the Wilke-Lee modification of the Chapman-Enskog theory. CHEMCAD uses the Fuller et al. method.

For light gases, at pressures to about 10 atm, the pressure dependence on diffusivity is adequately predicted by the inverse relation in (3-36); that is, PD_{AB} = a constant. At higher pressures, deviations are similar to the modification of the ideal-gas law by the compressibility factor, Z , based on the theorem of corresponding states. Takahashi [4] published a corresponding-states correlation, shown in Figure 3.3, patterned after a correlation by Slattery [5]. In the Takahashi plot, $D_{AB}P/(D_{AB}P)_{LP}$ is a function of reduced temperature and pressure, where $(D_{AB}P)_{LP}$ is at low pressure when (3-36) applies. Mixture critical temperature and pressure are molar-average values. Thus, a finite effect of composition is predicted at high pressure. The effect of high pressure on diffusivity is important in separations at supercritical conditions.

EXAMPLE 3.4 Estimation of a Gas Diffusivity at High Pressure.

Estimate the diffusion coefficient for a 25/75 molar mixture of argon and xenon at 200 atm and 378 K. No experimental value is available for these conditions. At this temperature and 1 atm, the experimental diffusion coefficient is 0.180 cm²/s. Critical constants are:

	T_c , K	P_c , atm
Argon	151.0	48.0
Xenon	289.8	58.0

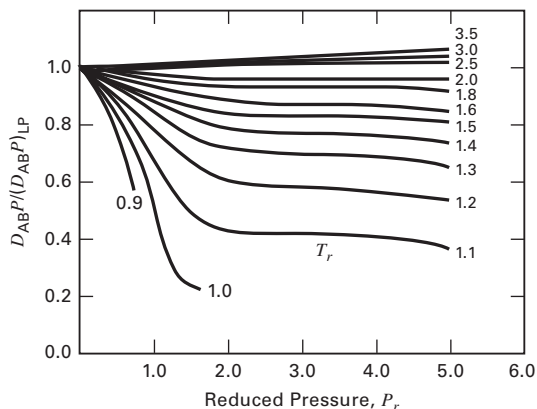


Figure 3.3 Takahashi [4] correlation for effect of high pressure on binary gas diffusivity. Used with permission.

Solution

Calculate reduced conditions:

$$T_c = 0.25(151) + 0.75(289.8) = 255.1 \text{ K}$$

$$T_r = T/T_c = 378/255.1 = 1.48$$

$$P_c = 0.25(48) + 0.75(58) = 55.5 \text{ atm}$$

$$P_r = P/P_c = 200/55.5 = 3.6$$

From Figure 3.3, $\frac{D_{AB}P}{(D_{AB}P)_{LP}} = 0.82$

$$D_{AB} = \frac{(D_{AB}P)_{LP}}{P} \left[\frac{D_{AB}P}{(D_{AB}P)_{LP}} \right] = \frac{(0.180)(1)}{200} (0.82)$$

$$= 7.38 \times 10^{-4} \text{ cm}^2/\text{s}$$

§3.2.2 Diffusivity in Nonelectrolyte Liquid Mixtures

Liquid diffusivities are difficult to estimate because of the lack of a suitable model for the liquid state. An exception is an infinitely dilute solute (A) of large, rigid, spherical molecules diffusing through a solvent (B) of small molecules with no slip at the surface of the solute molecules. The resulting relation, based on the hydrodynamics of creeping flow to describe drag,

is the Stokes–Einstein equation:

$$(D_{AB})_{\infty} = \frac{RT}{6\pi\mu_B R_A N_{AV}} \quad (3-38)$$

where μ_B = the viscosity of the solvent, R_A is the solute-molecule radius, and N_{AV} is Avogadro's number. Equation (3-38) has long served as a starting point for more widely applicable empirical correlations for liquid diffusivity. The Stokes–Einstein equation is restricted to dilute binary mixtures of not more than 10% solutes.

An extension of (3-38) to more concentrated solutions for small solute molecules is the empirical Wilke–Chang [6] equation:

$$(D_{AB})_{\infty} = \frac{7.4 \times 10^{-8} (\phi_B M_B)^{1/2} T}{\mu_B v_A^{0.6}} \quad (3-39)$$

where the units are cm^2/s for D_{AB} ; cP (centipoises) for solvent viscosity, μ_B ; K for T ; and cm^3/mol for v_A , the solute molar volume at its normal boiling point. The parameter ϕ_B is a solvent association factor with a value of 2.6 for water, 1.9 for methanol, 1.5 for ethanol, and 1.0 for unassociated solvents such as hydrocarbons. The effects of temperature and viscosity in (3-39) are identical to the prediction of the Stokes–Einstein equation, while the radius of the solute molecule is replaced by v_A , which can be estimated by summing atomic contributions tabulated in Table 3.3. Some representative experimental values of solute diffusivity in dilute binary liquid solutions are given in Table 3.4.

Table 3.3 Molecular Volumes of Dissolved Light Gases and Atomic Contributions for Other Molecules at the Normal Boiling Point

	Atomic Volume (m^3/kmol) $\times 10^3$		Atomic Volume (m^3/kmol) $\times 10^3$
C	14.8	Ring	
H	3.7	Three-membered, as in	−6
O (except as below)	7.4	ethylene oxide	
Doubly bonded as carbonyl	7.4	Four-membered	−8.5
Coupled to two other elements:		Five-membered	−11.5
In aldehydes, ketones	7.4	Six-membered	−15
In methyl esters	9.1	Naphthalene ring	−30
In methyl ethers	9.9	Anthracene ring	−47.5
In ethyl esters	9.9		
In ethyl ethers	9.9		
In higher esters	11.0		
In higher ethers	11.0		
In acids (—OH)	12.0		
Joined to S, P, N	8.3		
N			
Doubly bonded	15.6		
In primary amines	10.5		
In secondary amines	12.0		
Br	27.0		
Cl in RCHCIR'	24.6		
Cl in RCl (terminal)	21.6		
F	8.7		
I	37.0		
S	25.6		
P	27.0		
		Air	29.9
		O ₂	25.6
		N ₂	31.2
		Br ₂	53.2
		Cl ₂	48.4
		CO	30.7
		CO ₂	34.0
		H ₂	14.3
		H ₂ O	18.8
		H ₂ S	32.9
		NH ₃	25.8
		NO	23.6
		N ₂ O	36.4
		SO ₂	44.8

Source: G. Le Bas, *The Molecular Volumes of Liquid Chemical Compounds*, David McKay, New York (1915).

Table 3.4 Experimental Binary Liquid Diffusivities for Solutes, A, at Low Concentrations in Solvents, B

Solvent, B	Solute, A	Temperature, K	Diffusivity, D_{AB} , $\text{cm}^2/\text{s} \times 10^5$
Water	Acetic acid	293	1.19
	Aniline	293	0.92
	Carbon dioxide	298	2.00
	Ethanol	288	1.00
	Methanol	288	1.26
Ethanol	Allyl alcohol	293	0.98
	Benzene	298	1.81
	Oxygen	303	2.64
	Water	298	1.24
Benzene	Acetic acid	298	2.09
	Cyclohexane	298	2.09
	Ethanol	288	2.25
	<i>n</i> -Heptane	298	2.10
	Toluene	298	1.85
<i>n</i> -Hexane	Carbon tetrachloride	298	3.70
	Methyl ethyl ketone	303	3.74
	Propane	298	4.87
	Toluene	298	4.21
Acetone	Acetic acid	288	2.92
	Formic acid	298	3.77
	Water	298	4.56

EXAMPLE 3.5 Estimation of a Liquid Diffusivity.

Use the Wilke–Chang equation to estimate the diffusivity of aniline (A) in a 0.5 mol% aqueous solution at 20°C. The solubility of aniline in water is 4 g/100 g or 0.77 mol%. Compare the result to the experimental value in Table 3.4.

Solution

$$\mu_B = \mu_{\text{H}_2\text{O}} = 1.01 \text{ cP at } 20^\circ\text{C}$$

v_A = liquid molar volume of aniline at its normal boiling point of 457.6 K = 107 cm³/mol

$$\phi_B = 2.6 \text{ for water; } M_B = 18 \text{ for water; } T = 293 \text{ K}$$

From (3-39),

$$D_{AB} = \frac{(7.4 \times 10^{-8})[2.6(18)]^{0.5}(293)}{1.01(107)^{0.6}} = 0.89 \times 10^{-5} \text{ cm}^2/\text{s}$$

This value is about 3% less than the experimental value of 0.92 × 10⁻⁵ cm²/s in Table 3.4 for an infinitely dilute solution of aniline in water.

More recent liquid diffusivity correlations due to Hayduk and Minhas [7] give better agreement than the Wilke–Chang equation with experimental values for nonaqueous solutions. For a dilute solution of one normal paraffin (C₅ to C₃₂) in another (C₅ to C₁₆),

$$(D_{AB})_\infty = 13.3 \times 10^{-8} \frac{T^{1.47} \mu_B^\varepsilon}{v_A^{0.71}} \quad (3-40)$$

where

$$\varepsilon = \frac{10.2}{v_A} - 0.791 \quad (3-41)$$

and the other variables have the same units as in (3-39). For nonaqueous solutions in general,

$$(D_{AB})_\infty = 1.55 \times 10^{-8} \frac{T^{1.29} (\mathcal{P}_B^{0.5} / \mathcal{P}_A^{0.42})}{\mu_B^{0.92} v_B^{0.23}} \quad (3-42)$$

where \mathcal{P} is the parachor,

$$\mathcal{P}_i = v_i \sigma_i^{1/4} \quad (3-43)$$

When units for liquid molar volume, v , are cm³/mol and for surface tension, σ , are g/s² (dynes/cm), then the units of the parachor are cm³-g^{1/4}/s^{1/2}-mol. Normally, at near-ambient conditions, \mathcal{P} is treated as a constant, for which a tabulation of H.P. Meissner, *Chem. Eng. Prog.*, **45**(2) 149–153 (1949) is given in Table 3.5 from Quayle [8], who also provides in Table 3.6 a group-contribution method for estimating \mathcal{P} for compounds not listed.

Table 3.5 Parachors for Representative Compounds

	Parachor, $\text{cm}^3\text{-g}^{1/4}/\text{s}^{1/2}\text{-mol}$		Parachor, $\text{cm}^3\text{-g}^{1/4}/\text{s}^{1/2}\text{-mol}$		Parachor, $\text{cm}^3\text{-g}^{1/4}/\text{s}^{1/2}\text{-mol}$
Acetic acid	131.2	Chlorobenzene	244.5	Methyl amine	95.9
Acetone	161.5	Diphenyl	380.0	Methyl formate	138.6
Acetonitrile	122	Ethane	110.8	Naphthalene	312.5
Acetylene	88.6	Ethylene	99.5	<i>n</i> -octane	350.3
Aniline	234.4	Ethyl butyrate	295.1	1-pentene	218.2
Benzene	205.3	Ethyl ether	211.7	1-pentyne	207.0
Benzonitrile	258	Ethyl mercaptan	162.9	Phenol	221.3
<i>n</i> -butyric acid	209.1	Formic acid	93.7	<i>n</i> -propanol	165.4
Carbon disulfide	143.6	Isobutyl benzene	365.4	Toluene	245.5
Cyclohexane	239.3	Methanol	88.8	Triethyl amine	297.8

[Reproduced from H.P. Meissner, *Chem. Eng. Prog.*, 45(2) 149–153 (1949) with permission from the AIChE.]

Table 3.6 Structural Contributions for Estimating the Parachor

Carbon–hydrogen:		R—[—CO—]—R'	
		(ketone)	
C	9.0	R + R' = 2	51.3
H	15.5	R + R' = 3	49.0
CH ₃	55.5	R + R' = 4	47.5
CH ₂ in —(CH ₂) _n		R + R' = 5	46.3
n < 12	40.0	R + R' = 6	45.3
n > 12	40.3	R + R' = 7	44.1
		—CHO	66
Alkyl groups			
1-Methylethyl	133.3	O (not noted above)	20
1-Methylpropyl	171.9	N (not noted above)	17.5
1-Methylbutyl	211.7	S	49.1
2-Methylpropyl	173.3	P	40.5
1-Ethylpropyl	209.5	F	26.1
1,1-Dimethylethyl	170.4	Cl	55.2
1,1-Dimethylpropyl	207.5	Br	68.0
1,2-Dimethylpropyl	207.9	I	90.3
1,1,2-Trimethylpropyl	243.5	Ethylenic bonds:	
C ₆ H ₅	189.6	Terminal	19.1
		2,3-position	17.7
		3,4-position	16.3
Special groups:			
—COO—	63.8		
—COOH	73.8	Triple bond	40.6
—OH	29.8		
—NH ₂	42.5	Ring closure:	
—O—	20.0	Three-membered	12
—NO ₂	74	Four-membered	6.0
—NO ₃ (nitrate)	93	Five-membered	3.0
—CO(NH ₂)	91.7	Six-membered	0.8

[Reproduced from [8] with permission of the American Chemical Society.]

EXAMPLE 3.6 Estimation of Solute Liquid Diffusivity.

Estimate the diffusivity of formic acid (A) in benzene (B) at 25°C and infinite dilution, using the appropriate correlation of Hayduk and Minhas.

Solution

Equation (3-42) applies, with $T = 298$ K

From Table 3.5:

$$\mathcal{P}_A = 93.7 \text{ cm}^3\text{-g}^{1/4}/\text{s}^{1/2}\text{-mol}; \quad \mathcal{P}_B = 205.3 \text{ cm}^3\text{-g}^{1/4}/\text{s}^{1/2}\text{-mol}$$

$$\mu_B = 0.6 \text{ cP at } 25^\circ\text{C}; \quad \nu_B = 96 \text{ cm}^3/\text{mol at } 80^\circ\text{C}$$

However, for formic acid, \mathcal{P}_A is doubled to 187.4.

From (3-41),

$$(D_{AB})_\infty = 1.55 \times 10^{-8} \left[\frac{298^{1.29} (205.3^{0.5}/187.4^{0.42})}{0.6^{0.92} 96^{0.23}} \right]$$

$$= 2.15 \times 10^{-5} \text{ cm}^2/\text{s}$$

which is within 6% of the experimental value of $2.28 \times 10^{-5} \text{ cm}^2/\text{s}$.

The restrictions that apply to (3-42) are:

1. Solvent viscosity should not exceed 30 cP.

2. For organic acid solutes and solvents other than water, methanol, and butanols, the acid should be treated as a dimer by doubling the values of \mathcal{P}_A and ν_A .
3. For a nonpolar solute in monohydroxy alcohols, values of ν_B and \mathcal{P}_B should be multiplied by $8 \mu_B$, where viscosity is in cP.

Liquid diffusivities range from 10^{-4} to $10^{-6} \text{ cm}^2/\text{s}$ for solutes of molecular weight up to about 200 and solvents with viscosity up to 10 cP. Thus, liquid diffusivities are five orders of magnitude smaller than diffusivities for gas mixtures at 1 atm. However, diffusion rates in liquids are not necessarily five orders of magnitude smaller than in gases because, as indicated in (3-5), the product of concentration (molar density) and diffusivity determines the rate of diffusion for a given gradient in mole fraction. At 1 atm, the molar density of a liquid is three times that of a gas and, thus, the diffusion rate in liquids is only two orders of magnitude smaller than in gases at 1 atm.

Aspen Plus and CHEMCAD use the Wilke–Chang method, while users of ChemSep can choose from among several models, including Wilke–Chang and Hayduk–Minhas.

Equations (3-39), (3-40), and (3-42) apply only to solute A in a dilute solution of solvent B. Unlike binary gas mixtures in which the diffusivity is almost independent of composition, the effect of composition on liquid diffusivity is complex, sometimes showing strong positive or negative deviations from linearity with mole fraction.

Fick's first law for ordinary molecular diffusion uses a concentration or mole-fraction driving force. While this is adequate for gases, except at very high pressure, and for ideal liquid solutions, experimental evidence sheds doubt on its validity for nonideal solutions. For thermodynamic consistency, a driving force in terms of chemical potential, activities, or activity coefficients should be applied. A modification of (3-5) that utilizes the activity coefficient is:

$$J_A = -cD_{AB} \left(1 + \frac{\partial \ln \gamma_A}{\partial \ln x_A} \right)_{T,P} \frac{dx_A}{dz} \quad (3-44)$$

Vignes [9] has shown that, except for strongly associated binary mixtures, such as chloroform–acetone, which exhibit a rare negative deviation from Raoult's law, infinite-dilution binary diffusivities, $(D)_{\infty}$, can be combined with mixture activity-coefficient data or correlations thereof to predict liquid binary diffusion coefficients over the entire composition range. The Vignes equations are:

$$D_{AB} = (D_{AB})_{\infty}^{x_B} (D_{BA})_{\infty}^{x_A} \left(1 + \frac{\partial \ln \gamma_A}{\partial \ln x_A} \right)_{T,P} \quad (3-45)$$

$$D_{BA} = (D_{BA})_{\infty}^{x_A} (D_{AB})_{\infty}^{x_B} \left(1 + \frac{\partial \ln \gamma_B}{\partial \ln x_B} \right)_{T,P} \quad (3-46)$$

EXAMPLE 3.7 Effect of Composition on Liquid Diffusivities.

At 298 K and 1 atm, infinite-dilution diffusion coefficients for the methanol (A)–water (B) system are $1.5 \times 10^{-5} \text{ cm}^2/\text{s}$ and $1.75 \times 10^{-5} \text{ cm}^2/\text{s}$ for AB and BA, respectively.

Activity-coefficient data over the entire range of compositions as estimated by the UNIFAC method are:

x_A	γ_A	x_B	γ_B
0.0	2.245	1.0	1.000
0.1	1.748	0.9	1.013
0.2	1.470	0.8	1.044
0.3	1.300	0.7	1.087
0.4	1.189	0.6	1.140
0.5	1.116	0.5	1.201
0.6	1.066	0.4	1.269
0.7	1.034	0.3	1.343
0.8	1.014	0.2	1.424
0.9	1.003	0.1	1.511
1.0	1.000	0.0	1.605

Use the Vignes equations to estimate diffusion coefficients over a range of compositions.

Solution

A spreadsheet was used to compute the derivatives in (3-45) and (3-46). They were found to be essentially equal at any composition. The following results are obtained with $D_{AB} = D_{BA}$ at each composition. A minimum diffusivity occurs at a methanol mole fraction of 0.30.

x_A	$D_{AB}, \text{cm}^2/\text{s}$	$D_{BA}, \text{cm}^2/\text{s}$
0.20	1.10×10^{-5}	1.10×10^{-5}
0.30	1.08×10^{-5}	1.08×10^{-5}
0.40	1.12×10^{-5}	1.12×10^{-5}
0.50	1.18×10^{-5}	1.18×10^{-5}
0.60	1.28×10^{-5}	1.28×10^{-5}
0.70	1.38×10^{-5}	1.38×10^{-5}
0.80	1.50×10^{-5}	1.50×10^{-5}

If the diffusivity is assumed to be linear with mole fraction, the value at $x_A = 0.50$ is 1.625×10^{-5} , which is almost 40% higher than the predicted value of 1.18×10^{-5} .

§3.2.3 Diffusivities of Electrolytes

For an electrolyte solute, diffusion coefficients of dissolved salts, acids, and bases depend on the ions present in solution. However, in the absence of an electric potential, only diffusion of the electrolyte is of interest. The infinite-dilution diffusivity in cm^2/s of a salt in an aqueous solution can be estimated from the Nernst–Haskell equation:

$$(D_{AB})_{\infty} = \frac{RT[(1/n_+) + (1/n_-)]}{F^2[(1/\lambda_+) + (1/\lambda_-)]} \quad (3-47)$$

where n_+ and n_- are valences of the cation and anion; λ_+ and λ_- are limiting ionic conductances in $(\text{A}/\text{cm}^2)(\text{V}/\text{cm})$ ($\text{g-equiv}/\text{cm}^3$), with A in amps and V in volts; $F = \text{Faraday's constant} = 96,500 \text{ coulombs}/\text{g-equiv}$; $T = \text{temperature, K}$; and $R = \text{gas constant} = 8.314 \text{ J}/\text{mol}\cdot\text{K}$.

Some values of λ_+ and λ_- at 25°C are listed in Table 3.7. At other temperatures, these values are multiplied by $T/334 \mu_B$,

where T and μ_B are in K and cP, respectively. As the concentration of the electrolyte increases, the diffusivity at first decreases 10% to 20% and then rises to values, at a concentration of 2-N (normal), that approximate the infinite dilution value. Some representative experimental values from Volume V of the International Critical Tables are given in Table 3.8.

Table 3.7 Limiting Ionic Conductance in Water at 25°C , in $(\text{A}/\text{cm}^2)(\text{V}/\text{cm})$ ($\text{g-equiv}/\text{cm}^3$)

Anion	λ_-	Cation	λ_+
OH^-	197.6	H^+	349.8
Cl^-	76.3	Li^+	38.7
Br^-	78.3	Na^+	50.1
I^-	76.8	K^+	73.5
NO_3^-	71.4	NH_4^+	73.4
ClO_4^-	68.0	Ag^+	61.9
HCO_3^-	44.5	Tl^+	74.7

Table 3.8 Experimental Diffusivities of Electrolytes in Aqueous Solutions

Solute	Concentration, mol/L	Temperature, $^\circ\text{C}$	Diffusivity, $D_{AB}, \text{cm}^2/\text{s} \times 10^5$
HCl	0.1	12	2.29
HNO_3	0.05	20	2.62
	0.25	20	2.59
H_2SO_4	0.25	20	1.63
KOH	0.01	18	2.20
	0.1	18	2.15
	1.8	18	2.19
NaOH	0.05	15	1.49
NaCl	0.4	18	1.17
	0.8	18	1.19
	2.0	18	1.23
KCl	0.4	18	1.46
	0.8	18	1.49
	2.0	18	1.58
MgSO_4	0.4	10	0.39
$\text{Ca}(\text{NO}_3)_2$	0.14	14	0.85

EXAMPLE 3.8 Diffusivity of an Electrolyte.

Estimate the diffusivity of KCl in a dilute solution of water at 18.5°C . Compare your result to the experimental value of $1.7 \times 10^{-5} \text{ cm}^2/\text{s}$.

Solution

At 18.5°C , $T/334 \mu_B = 291.7/[(334)(1.05)] = 0.832$. Using Table 3.7, at 25°C , the limiting ionic conductances are:

$$\lambda_+ = 73.5(0.832) = 61.2 \quad \text{and} \quad \lambda_- = 76.3(0.832) = 63.5$$

From (3-47),

$$(D_{AB})_{\infty} = \frac{(8.314)(291.7)[(1/1) + (1/1)]}{96,500^2[(1/61.2) + (1/63.5)]} = 1.62 \times 10^{-5} \text{ cm}^2/\text{s}$$

which is 95% of the experimental value.

§3.2.4 Diffusivity in Solids

Diffusion in solids takes place by mechanisms that depend on the diffusing atom, molecule, or ion; the nature of the solid structure, whether it be porous, nonporous, crystalline, or amorphous; and the kind of solid material, whether it be metallic, ceramic, polymeric, biological, or cellular. Crystalline materials are further classified according to the type of bonding, as molecular, covalent, ionic, or metallic, with most inorganic solids being ionic. Ceramics can be ionic, covalent, or a combination of the two. Molecular solids have relatively weak forces of attraction among the atoms. In covalent solids, such as quartz silica, two atoms share two or more electrons equally. In ionic solids, such as inorganic salts, one atom loses one or more of its electrons by transfer to other atoms, thus forming ions. In metals, positively charged ions are bonded through a field of electrons that are free to move.

Diffusion coefficients in solids cover a range of many orders of magnitude. Despite the complexity of diffusion in solids, Fick's first law can be used if a measured diffusivity is available. However, when the diffusing solute is a gas, its solubility in the solid must be known. If the gas dissociates upon dissolution, the concentration of the dissociated species must be used in Fick's law. The mechanisms of diffusion in solids are complex and difficult to quantify. In the next subsections, examples of diffusion in solids are given, together with measured diffusion coefficients that can be used with Fick's first law.

Polymers

Diffusion through nonporous polymers is dependent on the type of polymer, which may be crystalline or amorphous and, if the latter, glassy or rubbery. Commercial crystalline polymers are about 20% amorphous, and it is through these regions that diffusion occurs. Nonporous polymers are widely used in membrane separations, described in Chapter 14. Mass transfer is characterized by Fick's first law using a **solution-diffusion** mechanism involving the solubility, S , of the component at the polymer surface followed by diffusion throughout the polymer. Accordingly, the concentration of the solute in the membrane when using Fick's law is given by:

$$c_i = S_i P \quad (3-48)$$

This is illustrated in the following example.

EXAMPLE 3.9 Diffusion of Hydrogen through a Nonporous Polymer Membrane.

Hydrogen diffuses through a nonporous polyvinyltrimethylsilane membrane at 25°C. Feed and permeate pressures at the upstream and downstream sides of the membrane are 3.5 MPa (P_1) and 200 kPa (P_2), respectively. The solubility, S , of hydrogen in the polymer is 0.54×10^{-4} mol/m³-Pa. The diffusivity of dissolved hydrogen in the polymer, D_{H_2} , is 160×10^{-11} m²/s. If the membrane thickness, Δz , is 1.6 μ m, calculate the hydrogen flux, N_{H_2} , in kmol/m²-h for a fully developed concentration profile.

Solution

The driving force for diffusion in the membrane is the hydrogen concentration difference across the membrane. At the upstream side of the membrane, the hydrogen concentration is given by (3-48) as

$$c_1 = S P_1 = 0.54 \times 10^{-4} (3.5)(10^6) = 189 \text{ mol/m}^3$$

At the downstream side, the hydrogen concentration is

$$c_2 = S P_2 = 0.54 \times 10^{-4} (200)(10^3) = 11 \text{ mol/m}^3$$

$$\Delta z = 1.6 \mu\text{m} = 1.6 \times 10^{-6} \text{ m}$$

$$D_{H_2} = 160 \times 10^{-11} (3600) = 5.76 \times 10^{-6} \text{ m}^2/\text{h}$$

For a fully developed concentration profile, the integrated concentration form of Fick's first law (3-13) is used:

$$N_{H_2} = D_{H_2} \frac{(c_1 - c_2)_{H_2}}{\Delta z} = 5.76 \times 10^{-6} \left[\frac{(189 - 11)/1000}{1.6 \times 10^{-6}} \right] \\ = 0.641 \text{ kmol/m}^2\text{-h}$$

Membranes must be thin to achieve practical permeation rates.

Porous solids

For porous solids, predictions of the diffusivity of gaseous and liquid solute species in the pores can be made. These methods are considered only briefly here, with details deferred to Chapters 14 and 15, where membrane separations and adsorption are described. Diffusion in pores is also of importance in reactors using porous solid catalysts. Any of the following four mass-transfer mechanisms or combinations thereof take place:

1. Molecular diffusion through pores, which present tortuous paths and hinder movement of molecules when their diameter is more than 10% of the pore
2. Knudsen diffusion, which involves collisions of diffusing gaseous molecules with the pore walls when pore diameter and pressure are such that the molecular mean free path is large compared to pore diameter
3. Surface diffusion involving the jumping of molecules, adsorbed on the pore walls, from one adsorption site to another based on a surface concentration-driving force
4. Bulk flow through or into the pores

When diffusion occurs only in the fluid in the pores, it is common to use an effective diffusivity, D_{eff} , based on (1) total cross-sectional area of the porous solid rather than cross-sectional area of the pore and (2) a straight path, rather than a tortuous pore path. If pore diffusion occurs only by molecular diffusion, Fick's law (3-3) is used with the effective diffusivity replacing the ordinary diffusion coefficient, D_{AB} :

$$D_{\text{eff}} = \frac{D_{AB}\epsilon}{\tau} \quad (3-49)$$

where ϵ is fractional solid porosity (typically 0.5) and τ is pore-path **tortuosity** (typically 1 to 3), which is the ratio of the pore length to the length if the pore were straight.

Effective diffusivity is determined by experiment, or predicted from (3-49) based on measurement of porosity and tortuosity and use of predictive methods for molecular diffusivity. Applications of (3-49) to porous membranes are discussed in Chapter 14.

§3.3 STEADY-STATE AND UNSTEADY-STATE MASS TRANSFER THROUGH STATIONARY MEDIA

Mass transfer occurs in (1) stagnant or stationary media, (2) fluids in laminar flow, and (3) fluids in turbulent flow. Each requires a different calculation procedure. The first flow regime is presented in this section for both steady-state and unsteady-state conditions. Mass transfer in laminar and turbulent flow is covered in subsequent sections.

Fourier's law is used to derive equations for the rate of heat transfer by conduction for steady-state and unsteady-state conditions in stationary media consisting of shapes such as slabs, cylinders, and spheres. Analogous equations are used for mass transfer with Fick's law for diffusion.

In one dimension, the molar flux of A in a binary mixture with stationary B is given by (3-27), which includes bulk flow and molecular diffusion. If the mixture is dilute in A, such that $x_B \approx 1$, the rate of mass transfer of A, $n_A = N_A A$, becomes

$$n_A = -cD_{AB}A \left(\frac{dx_A}{dz} \right) \quad (3-50)$$

which is Fick's first law for one-dimensional diffusion. Alternatively, (3-50) can be written in terms of a concentration gradient:

$$n_A = -D_{AB}A \left(\frac{dc_A}{dz} \right) \quad (3-51)$$

This equation is analogous to Fourier's law for the rate of heat conduction, Q :

$$Q = -kA \left(\frac{dT}{dz} \right) \quad (3-52)$$

§3.3.1 Steady-State Diffusion

For steady-state, one-dimensional diffusion, with constant D_{AB} , (3-51) can be integrated for various geometries, with the results being analogous to heat conduction.

1. Plane wall with a thickness, $z_1 - z_2$:

$$n_A = D_{AB}A \left(\frac{c_{A1} - c_{A2}}{z_1 - z_2} \right) \quad (3-53)$$

2. Hollow cylinder of inner radius r_1 and outer radius r_2 , with diffusion in the radial direction outward:

$$n_A = 2\pi L \frac{D_{AB}(c_{A1} - c_{A2})}{\ln(r_2/r_1)} \quad (3-54)$$

or

$$n_A = D_{AB}A_{LM} \frac{(c_{A1} - c_{A2})}{(r_2 - r_1)} \quad (3-55)$$

where

$$A_{LM} = \text{log mean of areas } 2\pi rL \text{ at } r_1 \text{ and } r_2$$

$$L = \text{length of the hollow cylinder}$$

3. Spherical shell of inner radius r_1 and outer radius r_2 , with diffusion in the radial direction outward:

$$n_A = \frac{4\pi r_1 r_2 D_{AB}(c_{A1} - c_{A2})}{(r_2 - r_1)} \quad (3-56)$$

or

$$n_A = D_{AB}A_{GM} \frac{(c_{A1} - c_{A2})}{(r_2 - r_1)} \quad (3-57)$$

where A_{GM} = geometric mean of the areas, $4\pi r^2$.

When $r_1/r_2 < 2$, the arithmetic mean area is no more than 4% greater than the log mean area. When $r_1/r_2 < 1.33$, the arithmetic mean area is no more than 4% greater than the geometric mean area.

§3.3.2 Unsteady-State Diffusion

Consider one-dimensional molecular diffusion of species A in stationary B through a differential control volume with diffusion in the z -direction only, as shown in Figure 3.4. Assume constant diffusivity and negligible bulk flow. The molar flow rate of species A by diffusion in the z -direction is given by (3-51):

$$n_{A_z} = -D_{AB}A \left(\frac{\partial c_A}{\partial z} \right)_z \quad (3-58)$$

At the plane, $z = z + \Delta z$, the diffusion rate is

$$n_{A_{z+\Delta z}} = -D_{AB}A \left(\frac{\partial c_A}{\partial z} \right)_{z+\Delta z} \quad (3-59)$$

The accumulation of species A in the control volume is

$$A \frac{\partial c_A}{\partial t} \Delta z \quad (3-60)$$

Since rate in - rate out = accumulation,

$$-D_{AB}A \left(\frac{\partial c_A}{\partial z} \right)_z + D_{AB}A \left(\frac{\partial c_A}{\partial z} \right)_{z+\Delta z} = A \left(\frac{\partial c_A}{\partial t} \right) \Delta z \quad (3-61)$$

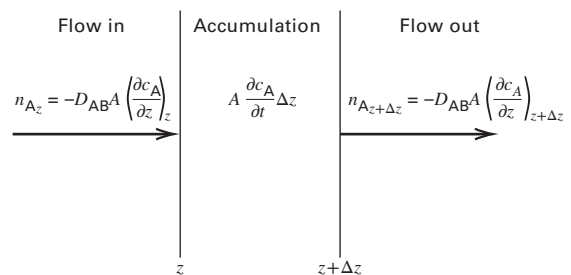


Figure 3.4 Unsteady-state diffusion through a volume $A dz$.

Rearranging and simplifying,

$$D_{AB} \left[\frac{(\partial c_A / \partial z)_{z+\Delta z} - (\partial c_A / \partial z)_z}{\Delta z} \right] = \frac{\partial c_A}{\partial t} \quad (3-62)$$

In the limit, as $\Delta z \rightarrow 0$,

$$\frac{\partial c_A}{\partial t} = D_{AB} \frac{\partial^2 c_A}{\partial z^2} \quad (3-63)$$

Equation (3-63) is Fick's second law for one-dimensional diffusion.

The more general form of **Fick's second law** for three-dimensional rectangular coordinates is

$$\frac{\partial c_A}{\partial t} = D_{AB} \left(\frac{\partial^2 c_A}{\partial x^2} + \frac{\partial^2 c_A}{\partial y^2} + \frac{\partial^2 c_A}{\partial z^2} \right) \quad (3-64)$$

For one-dimensional diffusion in the radial direction only for cylindrical and spherical coordinates, Fick's second law becomes, respectively,

$$\frac{\partial c_A}{\partial t} = \frac{D_{AB}}{r} \frac{\partial}{\partial r} \left(r \frac{\partial c_A}{\partial r} \right) \quad (3-65a)$$

and

$$\frac{\partial c_A}{\partial t} = \frac{D_{AB}}{r^2} \frac{\partial}{\partial r} \left(r^2 \frac{\partial c_A}{\partial r} \right) \quad (3-65b)$$

These two equations are analogous to Fourier's second law of heat conduction, where c_A replaces T , and diffusivity, D_{AB} , replaces thermal diffusivity, $\alpha = k/\rho C_p$.

Analytical solutions to these partial differential equations in the form of either Fick's law or Fourier's law are available for a variety of boundary conditions. They are derived and discussed by Carslaw and Jaeger [10] and Crank [11]. Extensions of these solutions to slabs and cylinders with sealed edges are achieved by the method of Newman [12]. Only the semi-infinite medium solution is presented here, which is particularly instructive for gaining an understanding of the large differences in the rates of diffusion in solids, liquids, and gases.

§3.3.3 Diffusion in a Semi-infinite Medium

The semi-infinite medium shown in Figure 3.5 extends in the z -direction from $z = 0$ to $z = \infty$. The x and y coordinates extend from $-\infty$ to $+\infty$ but are not of interest because diffusion is assumed to take place only in the z -direction. Thus, (3-63) applies to the region $z \geq 0$. At time $t \leq 0$, assume the concentration of c_{A_0} for $z \geq 0$. At $t = 0$, the surface of the semi-infinite medium at $z = 0$ is instantaneously brought to the concentration $c_{A_s} > c_{A_0}$ and held there for $t > 0$, causing diffusion into the medium to occur. Because the medium is infinite in the z -direction, diffusion cannot extend to $z = \infty$ and, therefore, as $z \rightarrow \infty$, $c_A = c_{A_0}$ for all $t \geq 0$.

Because (3-63) and its one initial condition in time and two boundary conditions in distance are linear in the dependent variable, c_A , an exact solution can be obtained by combination

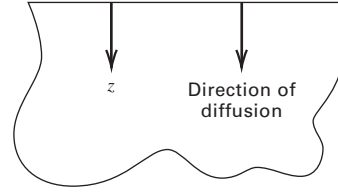


Figure 3.5 One-dimensional diffusion into a semi-infinite medium.

of variables [13] or the Laplace transform method [14]. The result, in terms of fractional concentration change, is

$$\theta = \frac{c_A - c_{A_0}}{c_{A_s} - c_{A_0}} = \text{erfc} \left(\frac{z}{2\sqrt{D_{AB}t}} \right) \quad (3-66)$$

where the complementary error function, **erfc**, is related to the **error function, erf**, by

$$\text{erfc}(x) = 1 - \text{erf}(x) = 1 - \frac{2}{\sqrt{\pi}} \int_0^x e^{-\eta^2} d\eta \quad (3-67)$$

The error function is included in MATLAB and most spreadsheet programs and is tabulated by Abramowitz and Stegun [15]. The variation of $\text{erf}(x)$ and $\text{erfc}(x)$ is:

x	$\text{erf}(x)$	$\text{erfc}(x)$
0	0.0000	1.0000
0.5	0.5205	0.4795
1.0	0.8427	0.1573
1.5	0.9661	0.0339
2.0	0.9953	0.0047
∞	1.0000	0.0000

Equation (3-66) determines the concentration in the semi-infinite medium as a function of time and distance from the surface, assuming no bulk flow. It applies rigorously to diffusion in solids and also to stagnant liquids and gases when the medium is dilute in the diffusing solute.

In (3-66), when $z/2\sqrt{D_{AB}t} = 2$, the complementary error function is only 0.0047, which represents less than a 1% change in the ratio of the concentration change at $z = z$ to the change at $z = 0$. It is common to call $z = 4\sqrt{D_{AB}t}$ the **penetration depth** and to apply (3-66) to media of finite thickness as long as the thickness is greater than the penetration depth.

The instantaneous rate of mass transfer across the medium surface at $z = 0$ can be obtained by taking the derivative of (3-66) with respect to distance and substituting it into Fick's first law applied at the surface of the medium. Then, using the Leibnitz rule for differentiating the integral in (3-67) with $x = z/2\sqrt{D_{AB}t}$,

$$\begin{aligned} n_A &= -D_{AB}A \left(\frac{\partial c_A}{\partial z} \right) \\ &= D_{AB}A \left(\frac{c_{A_s} - c_{A_0}}{\sqrt{\pi D_{AB}t}} \right) \exp \left(-\frac{z^2}{4D_{AB}t} \right) \Bigg|_{z=0} \end{aligned}$$

Thus,

$$n_A|_{z=0} = \sqrt{\frac{D_{AB}}{\pi t}} A (c_{A_s} - c_{A_0}) \quad (3-68)$$

The total number of moles of solute, \mathcal{N}_A , transferred into the semi-infinite medium is obtained by integrating (3-68) with respect to time:

$$\begin{aligned} \mathcal{N}_A &= \int_0^t n_A|_{z=0} dt = \sqrt{D_{AB}/\pi} A (c_{A_s} - c_{A_0}) \int_0^t \frac{dt}{\sqrt{t}} \\ &= 2A (c_{A_s} - c_{A_0}) \sqrt{\frac{D_{AB}t}{\pi}} \end{aligned} \quad (3-69)$$

EXAMPLE 3.10 Rates of Diffusion in Stagnant Media.

Determine how long it will take for the dimensionless concentration change, $\theta = (c_A - c_{A_0})/(c_{A_s} - c_{A_0})$, to reach 0.01 at a depth $z = 100$ cm in a semi-infinite medium. The medium is initially at a solute concentration c_{A_0} after the surface concentration at $z = 0$ increases to c_{A_s} for diffusivities representative of a solute diffusing through a stagnant gas, a stagnant liquid, and a solid.

Solution

For a gas, assume $D_{AB} = 0.1$ cm²/s. From (3-65) and (3-66),

$$\theta = 0.01 = 1 - \operatorname{erf}\left(\frac{z}{2\sqrt{D_{AB}t}}\right)$$

Therefore,

$$\operatorname{erf}\left(\frac{z}{2\sqrt{D_{AB}t}}\right) = 0.99$$

From MATLAB, the value of erf corresponds to $\frac{z}{2\sqrt{D_{AB}t}} = 1.8214$

Solving,

$$t = \left[\frac{100}{1.8214(2)}\right]^2 \frac{1}{0.10} = 7,540 \text{ s} = 2.09 \text{ h}$$

In a similar manner, the times for typical gas, liquid, and solid media are found to be drastically different, as shown below.

Semi-infinite Medium	D_{AB} , cm ² /s	Time for $\theta = 0.01$ at $z = 1$ m
Gas	0.10	2.09 hours
Liquid	1×10^{-5}	2.39 years
Solid	1×10^{-9}	239 centuries

The results show that molecular diffusion is very slow, especially in liquids and solids. For separations involving liquids and gases, the rate of mass transfer is greatly increased by agitation to induce turbulent motion. For separations involving solid particles, it is best to reduce the size of the particles.

§3.4 MASS TRANSFER IN LAMINAR FLOW

Some separations involve diffusion in fluids in laminar flow. As with convective heat-transfer in laminar flow, the calculation of such operations is amenable to well-defined theory.

This is illustrated in this section by three common configurations: (1) a fluid falling as a film down a surface; (2) a fluid flowing slowly along a horizontal, flat surface; and (3) a fluid flowing slowly through a circular tube, where mass transfer occurs, respectively, between a gas and the falling liquid film, from the flat surface into the flowing fluid, and from the inside surface of the tube into the flowing fluid.

§3.4.1 Falling Laminar, Liquid Film

Consider a thin liquid film containing A and nonvolatile B, falling at steady state in a laminar flow down one side of a vertical surface and exposed to pure gas, A, which diffuses into the liquid, as shown in Figure 3.6. The surface is infinitely wide in the x -direction (normal to the page), flow is in the downward y -direction, and mass transfer of A is in the z -direction. Assume that the rate of mass transfer of A into the liquid film is so small that the liquid velocity in the z -direction, u_z , is zero. From fluid mechanics, in the absence of end effects, the equation of motion for the liquid film in fully developed laminar flow in the y -direction is

$$\mu \frac{d^2 u_y}{dz^2} + \rho g = 0 \quad (3-70)$$

Usually, fully developed flow, where u_y is independent of the distance y , is established quickly. If δ is the film thickness and the boundary conditions are $u_y = 0$ at $z = \delta$ (no slip of fluid at the solid surface) and $du_y/dz = 0$ at $z = 0$ (no drag at the gas–liquid interface), (3-70) is readily integrated, giving a parabolic velocity profile:

$$u_y = \frac{\rho g \delta^2}{2\mu} \left[1 - \left(\frac{z}{\delta}\right)^2\right] \quad (3-71)$$

The maximum liquid velocity occurs at $z = 0$,

$$(u_y)_{\max} = \frac{\rho g \delta^2}{2\mu} \quad (3-72)$$

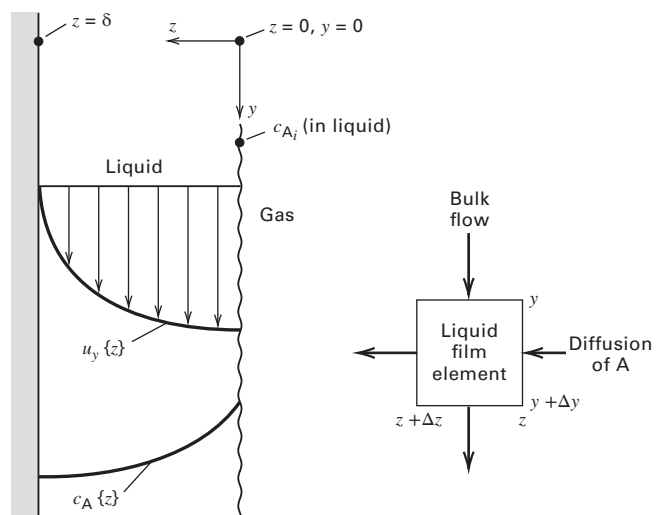


Figure 3.6 Mass transfer from a gas into a falling, laminar liquid film.

The bulk-average velocity in the liquid film is

$$\bar{u}_y = \frac{\int_0^\delta u_y dz}{\delta} = \frac{\rho g \delta^2}{3\mu} \quad (3-73)$$

Thus, with no entrance effects, the film thickness for fully developed flow is independent of location y and is

$$\delta = \left(\frac{3\bar{u}_y \mu}{\rho g} \right)^{1/2} = \left(\frac{3\mu \Gamma}{\rho^2 g} \right)^{1/2} \quad (3-74)$$

where Γ = liquid film flow rate per unit width of film, W . For film flow, the Reynolds number (a dimensionless group), which is the ratio of the inertial force to the viscous force, is

$$N_{Re} = \frac{4r_H \bar{u}_y \rho}{\mu} = \frac{4\delta \bar{u}_y \rho}{\mu} = \frac{4\Gamma}{\mu} \quad (3-75)$$

where r_H = hydraulic radius = (flow cross section)/(wetted perimeter) = $(W\delta)/W = \delta$ and, by continuity (flow rate = velocity \times density \times flow area), $\Gamma = \bar{u}_y \rho \delta$

Grimley [16] found that for $N_{Re} < 8$ to 25, depending on surface tension and viscosity, flow in the film is laminar and the interface between the liquid film and the gas is flat. The value of 25 is obtained with water. For $8 < N_{Re} < 1,200$, the flow is still laminar, but ripples may appear at the interface unless suppressed by the addition of wetting agents.

For a flat interface, I, and a low rate of mass transfer of A, (3-70) to (3-75) hold, and the film velocity profile is given by (3-71). Consider a mole balance on A for an incremental volume of liquid film of constant density, as shown in Figure 3.6. Neglect bulk flow in the z -direction and axial diffusion in the y -direction. Thus, mass transfer of A from the gas into the liquid occurs only by molecular diffusion in the z -direction. Then, at steady state, neglecting accumulation or depletion of A in the incremental volume (quasi-steady-state assumption),

$$\begin{aligned} -D_{AB}(\Delta y)(\Delta x) \left(\frac{\partial c_A}{\partial z} \right) + u_y c_A|_y (\Delta z)(\Delta x) \\ = -D_{AB}(\Delta y)(\Delta x) \left(\frac{\partial c_A}{\partial z} \right)_{z+\Delta z} + u_y c_A|_{y+\Delta y} (\Delta z)(\Delta x) \end{aligned} \quad (3-76)$$

Rearranging and simplifying (3-76),

$$\left[\frac{u_y c_A|_{y+\Delta y} - u_y c_A|_y}{\Delta y} \right] = D_{AB} \left[\frac{(\partial c_A / \partial z)_{z+\Delta z} - (\partial c_A / \partial z)_z}{\Delta z} \right] \quad (3-77)$$

which, in the limit, as $\Delta z \rightarrow 0$ and $\Delta y \rightarrow 0$, becomes

$$u_y \frac{\partial c_A}{\partial y} = D_{AB} \frac{\partial^2 c_A}{\partial z^2} \quad (3-78)$$

Substituting the velocity profile of (3-71) into (3-78),

$$\frac{\rho g \delta^2}{2\mu} \left[1 - \left(\frac{z}{\delta} \right)^2 \right] \frac{\partial c_A}{\partial y} = D_{AB} \frac{\partial^2 c_A}{\partial z^2} \quad (3-79)$$

This linear PDE was solved by Johnstone and Pigford [17] and Olbrich and Wild [18] for the following boundary conditions,

where the initial concentration of A in the liquid film is c_{A_0} :

$$\begin{aligned} c_A &= c_{A_1} \quad \text{at } z = 0 \quad \text{for } y > 0 \\ c_A &= c_{A_0} \quad \text{at } y = 0 \quad \text{for } 0 < z < \delta \\ \partial c_A / \partial z &= 0 \quad \text{at } z = \delta \quad \text{for } 0 < y < L \end{aligned}$$

where L = height of the vertical surface. The solution of Olbrich and Wild is in the form of an infinite series, giving c_A as a function of z and y . Of greater interest, however, is the average concentration of A in the film at the bottom of the wall, where $y = L$, which, by integration, is

$$\bar{c}_{A_y} = \frac{1}{\bar{u}_y \delta} \int_0^\delta u_y c_{A_y} dz \quad (3-80)$$

For the condition $y = L$, the result is

$$\begin{aligned} \frac{c_{A_1} - \bar{c}_{A_L}}{c_{A_1} - c_{A_0}} &= 0.7857e^{-5.1213\eta} + 0.09726e^{-39.661\eta} \\ &+ 0.036093e^{-106.25\eta} \end{aligned} \quad (3-81)$$

where

$$\eta = \frac{2D_{AB}L}{3\delta^2 \bar{u}_y} = \frac{8/3}{N_{Re} N_{Sc} (\delta/L)} = \frac{8/3}{N_{PeM} (\delta/L)} \quad (3-82)$$

$$\begin{aligned} N_{Sc} &= \text{Schmidt number} = \frac{\mu}{\rho D_{AB}} \\ &= \frac{\text{momentum diffusivity, } \mu/\rho}{\text{mass diffusivity, } D_{AB}} \end{aligned} \quad (3-83)$$

$$\begin{aligned} N_{PeM} &= N_{Re} N_{Sc} = \text{Peclet number for mass transfer} \\ &= \frac{4\delta \bar{u}_y}{D_{AB}} \end{aligned} \quad (3-84)$$

The Schmidt number is analogous to the Prandtl number used in heat transfer:

$$N_{Pr} = \frac{C_P \mu}{k} = \frac{(\mu/\rho)}{(k/\rho C_P)} = \frac{\text{momentum diffusivity}}{\text{thermal diffusivity}}$$

The Peclet number for mass transfer is analogous to the Peclet number for heat transfer:

$$N_{PeH} = N_{Re} N_{Pr} = \frac{4\delta \bar{u}_y C_P \rho}{k}$$

Both are ratios of convective to molecular transport.

The total rate of absorption of A from the gas into the liquid film for height L and width W is

$$n_A = \bar{u}_y \delta W (\bar{c}_{A_L} - c_{A_0}) \quad (3-85)$$

§3.4.2 Mass-Transfer Coefficients

Mass-transfer problems involving flowing fluids are often solved using graphical or algebraic correlations of **mass-transfer coefficients**. These are analogous to **heat-transfer coefficients**. For the latter, **Newton's law of cooling** defines a

heat-transfer coefficient, h , by

$$Q = hA\Delta T \quad (3-86)$$

where Q = rate of heat transfer, A = area for heat transfer (normal to the direction of heat transfer), and ΔT = temperature driving force.

For mass transfer, a composition driving force replaces ΔT . Because composition can be expressed in a number of ways, different mass-transfer coefficients apply. If concentration is used, Δc_A is selected as the driving force and

$$n_A = k_c A \Delta c_A \quad (3-87)$$

which defines the mass-transfer coefficient, k_c , in mol/time-area-driving force, for a concentration driving force.

For the falling laminar film, $\Delta c_A = c_{A1} - \bar{c}_A$, where \bar{c}_A is the bulk average concentration of A in the film, which varies with vertical location, y . This is because even though c_{A1} is independent of y , the average film concentration of A increases with y . A theoretical expression for k_c in terms of diffusivity is formed by equating (3-87) to Fick's first law, (3-50), in concentration form at the gas-liquid interface:

$$k_c A (c_{A1} - \bar{c}_A) = -D_{AB} A \left(\frac{\partial c_A}{\partial z} \right)_{z=0} \quad (3-88)$$

Although this is the most widely used approach for defining a mass-transfer coefficient for a falling film, it fails because $\partial c_A / \partial z$ at $z = 0$ is not defined. Therefore, another approach is used. For an incremental height,

$$n_A = \bar{u}_y \delta W d\bar{c}_A = k_c (c_{A1} - \bar{c}_A) W dy \quad (3-89)$$

This defines a local value of k_c , which varies with distance y because \bar{c}_A varies with y . An average value of k_c , over height L , can be defined by separating variables and integrating (3-89):

$$\begin{aligned} k_{c_{\text{avg}}} &= \frac{\int_0^L k_c dy}{L} = \frac{\bar{u}_y \delta}{L} \int_{c_{A0}}^{\bar{c}_{AL}} \frac{d\bar{c}_A}{c_{A1} - \bar{c}_A} \\ &= \frac{\bar{u}_y \delta}{L} \ln \frac{c_{A1} - c_{A0}}{c_{A1} - \bar{c}_{AL}} \end{aligned} \quad (3-90)$$

The argument of the natural logarithm in (3-90) is obtained from the reciprocal of (3-81). For values of η in (3-82) > 0.1 , only the first term in (3-81) is significant (error is less than 0.5%). In that case,

$$k_{c_{\text{avg}}} = \frac{\bar{u}_y \delta}{L} \ln \left[\frac{e^{5.1213\eta}}{0.7857} \right] \quad (3-91)$$

Since $\ln e^x = x$,

$$k_{c_{\text{avg}}} = \frac{\bar{u}_y \delta}{L} (0.241 + 5.1213\eta) \quad (3-92)$$

In the limit for large η , using (3-82) and (3-84), (3-92) becomes

$$k_{c_{\text{avg}}} = 3.414 \frac{D_{AB}}{\delta} \quad (3-93)$$

As suggested by the Nusselt number, $N_{Nu} = h\delta/k$ for heat transfer, where δ is a characteristic length, a Sherwood number for mass transfer is defined for a falling film as

$$N_{\text{Sh}_{\text{avg}}} = \frac{k_{c_{\text{avg}}} \delta}{D_{AB}} \quad (3-94)$$

From (3-93), $N_{\text{Sh}_{\text{avg}}} = 3.414$, which is the smallest value the Sherwood number can have for a falling liquid film. The average mass-transfer flux of A is

$$N_{A_{\text{avg}}} = \frac{n_{A_{\text{avg}}}}{A} = k_{c_{\text{avg}}} (c_{A1} - \bar{c}_A)_{\text{mean}} \quad (3-95)$$

For $\eta < 0.001$ in (3-82), when the liquid-film flow regime is still laminar without ripples, the time of contact of gas with liquid is short and mass transfer is confined to the vicinity of the interface. Thus, the film acts as if it were infinite in thickness. In this limiting case, the downward velocity of the liquid film in the region of mass transfer is $u_{y_{\text{max}}}$, and (3-78) becomes

$$u_{y_{\text{max}}} \frac{\partial c_A}{\partial y} = D_{AB} \frac{\partial^2 c_A}{\partial z^2} \quad (3-96)$$

Since from (3-72) and (3-73) $u_{y_{\text{max}}} = 3\bar{u}_y/2$, (3-96) becomes

$$\frac{\partial c_A}{\partial y} = \left(\frac{2D_{AB}}{3\bar{u}_y} \right) \frac{\partial^2 c_A}{\partial z^2} \quad (3-97)$$

where the boundary conditions are

$$\begin{aligned} c_A &= c_{A0} \text{ for } z > 0 \text{ and } y > 0 \\ c_A &= c_{A1} \text{ for } z = 0 \text{ and } y > 0 \\ c_A &= c_{A1} \text{ for large } z \text{ and } y > 0 \end{aligned}$$

Equation (3-97) and the boundary conditions are equivalent to the case of the semi-infinite medium in Figure 3.6. By analogy to (3-63) and (3-66), the solution is

$$\theta = \frac{c_A - c_{A0}}{c_{A1} - c_{A0}} = \text{erfc} \left(\frac{z}{2\sqrt{2D_{AB}y/3\bar{u}_y}} \right) \quad (3-98)$$

Assuming that the driving force for mass transfer in the film is $c_{A1} - c_{A0}$, Fick's first law can be used at the gas-liquid interface to define a mass-transfer coefficient:

$$N_A = -D_{AB} \left. \frac{\partial c_A}{\partial z} \right|_{z=0} = k_c (c_{A1} - c_{A0}) \quad (3-99)$$

To obtain the gradient of c_A at $z = 0$ from (3-98), note that erfc is defined from (3-67) as

$$\text{erfc}(z) = 1 - \frac{2}{\sqrt{\pi}} \int_0^z e^{-t^2} dt \quad (3-100)$$

Combining (3-100) with (3-98) and applying the Leibnitz differentiation rule,

$$\left. \frac{\partial c_A}{\partial z} \right|_{z=0} = -(c_{A1} - c_{A0}) \sqrt{\frac{3\bar{u}_y}{2\pi D_{AB}y}} \quad (3-101)$$

Substituting (3-101) into (3-99) and introducing the Peclet number for mass-transfer from (3-84), the local mass-transfer coefficient as a function of distance down from the top of the wall is obtained:

$$k_c = \sqrt{\frac{3D_{AB}^2 N_{PeM}}{8\pi y \delta}} = \sqrt{\frac{3D_{AB}\Gamma}{2\pi y \delta \rho}} \quad (3-102)$$

The average value of k_c over the film height, L , is obtained by integrating (3-102) with respect to y , giving

$$k_{c_{avg}} = \sqrt{\frac{6D_{AB}\Gamma}{\pi \delta \rho L}} = \sqrt{\frac{3D_{AB}^2 N_{PeM}}{2\pi \delta L}} \quad (3-103)$$

Combining (3-103) with (3-94) and (3-84),

$$N_{Sh_{avg}} = \sqrt{\frac{3\delta}{2\pi L} N_{PeM}} = \sqrt{\frac{4}{\pi \eta}} \quad (3-104)$$

where, by (3-90), the proper mean concentration driving force to use with $k_{c_{avg}}$ is the log mean. Thus,

$$\begin{aligned} (c_{A1} - \bar{c}_A)_{mean} &= (c_{A1} - \bar{c}_A)_{LM} \\ &= \frac{(c_{A1} - c_{A0}) - (c_{A1} - c_{AL})}{\ln [(c_{A1} - c_{A0}) / (c_{A1} - \bar{c}_{AL})]} \end{aligned} \quad (3-105)$$

When ripples are present on the liquid surface, the surface area increases and values of $k_{c_{avg}}$ and $N_{Sh_{avg}}$ are considerably larger than predicted by the above equations.

The above development shows that asymptotic, closed-form solutions are obtained with relative ease for large and small values of η , as defined by (3-82). These limits, in terms of the average Sherwood number, are shown in Figure 3.7. The general solution for intermediate values of η is not available in closed form. Similar limiting solutions for large and small values of dimensionless groups have been obtained for a large variety of transport and kinetic phenomena (Churchill [19]). Often, the two limiting cases can be patched together to provide an estimate of the intermediate solution, if an intermediate value is available from experiment or the general

numerical solution. The procedure is discussed by Churchill and Usagi [20]. The general solution of Emmert and Pigford [21] to the falling laminar liquid film problem is included in Figure 3.7.

EXAMPLE 3.11 Absorption of CO₂ into a Falling Water Film.

Water (B) at 25°C, in contact with CO₂ (A) at 1 atm, flows as a film down a wall 1 m wide and 3 m high at a Reynolds number of 25. Estimate the rate of absorption of CO₂ into water in kmol/s. Ignore the vaporization of water into the gas. Applicable properties are:

$$D_{AB} = 1.96 \times 10^{-5} \text{ cm}^2/\text{s};$$

$$\rho = 1.0 \text{ g/cm}^3;$$

$$\mu_L = 0.89 \text{ cP} = 0.00089 \text{ kg/m-s}$$

Solubility of CO₂ in water at 1 atm and 25°C = $3.4 \times 10^{-5} \text{ mol/cm}^3$.

Solution

From (3-75),

$$\Gamma = \frac{N_{Re}\mu}{4} = \frac{25(0.89)(0.001)}{4} = 0.00556 \frac{\text{kg}}{\text{m-s}}$$

From (3-83),

$$N_{Sc} = \frac{\mu}{\rho D_{AB}} = \frac{(0.89)(0.001)}{(1.0)(1,000)(1.96 \times 10^{-5})(10^{-4})} = 454$$

From (3-74),

$$\delta = \left[\frac{3(0.89)(0.001)(0.00556)}{1.0^2(1,000)^2(9.807)} \right]^{1/3} = 1.15 \times 10^{-4} \text{ m}$$

From (3-72) and (3-73), $\bar{u}_y = (2/3)u_{y_{max}}$. Therefore,

$$\bar{u}_y = \frac{2}{3} \left[\frac{(1.0)(1,000)(9.807)(1.15 \times 10^{-4})^2}{2(0.89)(0.001)} \right] = 0.0486 \text{ m/s}$$

From (3-82),

$$\eta = \frac{8/3}{(25)(454) [(1.15 \times 10^{-4})/3]} = 6.13$$

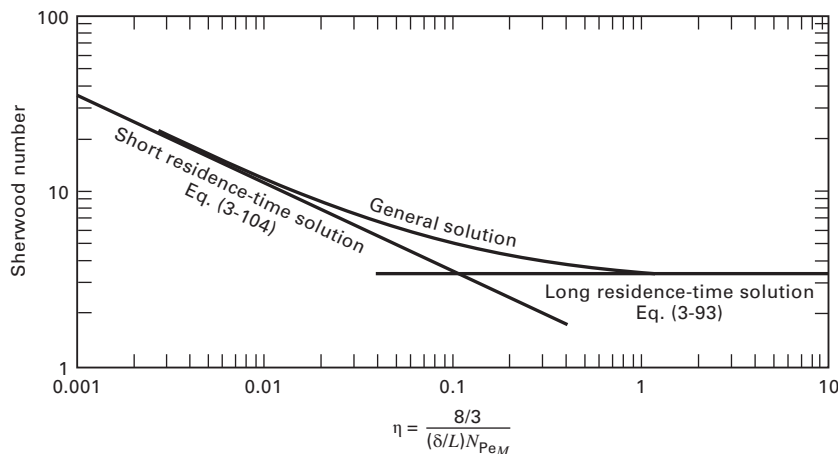


Figure 3.7 Limiting and general solutions for mass transfer to a falling laminar liquid film.

Therefore, (3-93) applies, giving

$$k_{c_{\text{avg}}} = \frac{3.41(1.96 \times 10^{-5})(10^{-4})}{1.15 \times 10^{-4}} = 5.81 \times 10^{-5} \text{ m/s}$$

To obtain the rate of absorption, \bar{c}_{A_L} is determined. From (3-85) and (3-95),

$$n_A = \bar{u}_y \delta W (\bar{c}_{A_L} - c_{A_0}) = k_{c_{\text{avg}}} A \frac{(\bar{c}_{A_L} - c_{A_0})}{\ln \left[\frac{c_{A_1} - c_{A_0}}{c_{A_1} - \bar{c}_{A_L}} \right]}$$

Thus,

$$\ln \left[\frac{c_{A_1} - c_{A_0}}{c_{A_1} - \bar{c}_{A_L}} \right] = \frac{k_{c_{\text{avg}}} A}{\bar{u}_y \delta W}$$

Solving for \bar{c}_{A_L} ,

$$\bar{c}_{A_L} = c_{A_1} - (c_{A_1} - c_{A_0}) \exp \left(-\frac{k_{c_{\text{avg}}} A}{\bar{u}_y \delta W} \right)$$

$$L = 3 \text{ m}, \quad W = 1 \text{ m}, \quad A = WL = (1)(3) = 3 \text{ m}^2$$

$$c_{A_0} = 0, \quad c_{A_1} = 3.4 \times 10^{-5} \text{ kmol/cm}^3 = 3.4 \times 10^{-2} \text{ kmol/m}^3$$

$$\begin{aligned} \bar{c}_{A_L} &= 3.4 \times 10^{-2} \left\{ 1 - \exp \left[-\frac{(5.81 \times 10^{-5})(3)}{(0.0486)(1.15 \times 10^{-4})(1)} \right] \right\} \\ &= 3.4 \times 10^{-2} \text{ kmol/m}^3 \end{aligned}$$

Thus, the exiting liquid film is saturated with CO_2 , which implies equilibrium at the gas–liquid interface. From (3-85),

$$n_A = 0.0486 (1.15 \times 10^{-4}) (3.4 \times 10^{-2}) = 1.9 \times 10^{-7} \text{ kmol/s}$$

§3.4.3 Molecular Diffusion to a Fluid Flowing across a Flat Plate—the Boundary Layer Concept

Figure 3.8 shows a flow of fluid (B) over a thin, horizontal, flat plate. Some possibilities for mass transfer of species A into B are: (1) the plate consists of solid material A, which is slightly soluble in B; (2) A is in the pores of an inert solid plate from which it evaporates or dissolves into B; and (3) the plate is a dense polymeric membrane through which A can diffuse and pass into fluid B. Let the fluid velocity profile upstream of the plate be uniform at a free-system velocity of u_0 . As the fluid passes over the plate, the velocity u_x in the direction x of flow is reduced to zero at the wall, which establishes a velocity profile due to drag. At a certain distance z that is normal to and

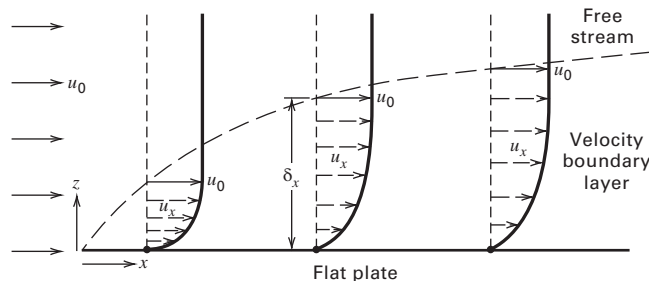


Figure 3.8 Laminar boundary layer for flow across a flat plate.

upward out from the plate surface, the fluid velocity is 99% of u_0 . This distance, which increases with increasing distance x from the leading edge of the plate, is defined as the **velocity boundary-layer thickness**, δ . This thickness is shown as the dashed line in Figure 3.8. Essentially all flow retardation is assumed to occur in the boundary layer, as first suggested by Prandtl [22]. The buildup of this layer, the velocity profile, and the drag force can be determined for laminar flow by solving the Navier–Stokes equations of fluid mechanics.

For a Newtonian fluid of constant density and viscosity, with no pressure gradients in the x - or y -directions, the Navier–Stokes equations for the boundary layer are

$$\frac{\partial u_x}{\partial x} + \frac{\partial u_z}{\partial z} = 0 \quad (3-106)$$

$$u_x \frac{\partial u_x}{\partial x} + u_z \frac{\partial u_x}{\partial z} = \frac{\mu}{\rho} \left(\frac{\partial^2 u_x}{\partial z^2} \right) \quad (3-107)$$

The boundary conditions are

$$u_x = u_0 \text{ at } x = 0 \text{ for } z > 0$$

$$u_x = 0 \text{ at } z = 0 \text{ for } x > 0$$

$$u_x = u_0 \text{ at } z = \infty \text{ for } x > 0$$

$$u_z = 0 \text{ at } z = 0 \text{ for } x > 0$$

A solution of (3-106) and (3-107) was first obtained by Blasius [23], as described by Schlichting [24]. The result in terms of a local friction factor, f_x ; a local shear stress at the wall, τ_{w_x} ; and a local drag coefficient at the wall, C_{D_x} is

$$\frac{C_{D_x}}{2} = \frac{f_x}{2} = \frac{\tau_{w_x}}{\rho u_0^2} = \frac{0.332}{N_{\text{Re}_x}^{0.5}} \quad (3-108)$$

where

$$N_{\text{Re}_x} = \frac{x u_0 \rho}{\mu} \quad (3-109)$$

The drag is greatest at the leading edge of the plate, where the Reynolds number is smallest. Values of the drag coefficient obtained by integrating (3-108) from $x = 0$ to L are

$$\frac{C_{D_{\text{avg}}}}{2} = \frac{f_{\text{avg}}}{2} = \frac{0.664}{N_{\text{Re}_L}^{0.5}} \quad (3-110)$$

As shown in Figure 3.8, the thickness of the velocity boundary layer increases with distance along the plate, as given by

$$\frac{\delta}{x} = \frac{4.96}{N_{\text{Re}_x}^{0.5}} \quad (3-111)$$

A reasonably accurate expression for the velocity profile was obtained by Pohlhausen [25], who assumed the empirical form of the velocity in the boundary layer to be $u_x = C_1 z + C_2 z^3$, where C_1 and C_2 are constants. The boundary conditions are:

$$u_x = 0 \text{ at } z = 0, \quad u_x = u_0 \text{ at } z = \delta, \text{ and } \partial u_x / \partial z = 0 \text{ at } z = \delta.$$

If these conditions are applied to evaluate C_1 and C_2 , the velocity is

$$\frac{u_x}{u_0} = 1.5 \left(\frac{z}{\delta} \right) - 0.5 \left(\frac{z}{\delta} \right)^3 \quad (3-112)$$

This solution is valid only for a laminar boundary layer, which, by experiment, persists up to $N_{Re_x} = 5 \times 10^5$.

When mass transfer of A from the surface of the plate into the boundary layer occurs, a species continuity equation applies:

$$u_x \frac{\partial c_A}{\partial x} + u_z \frac{\partial c_A}{\partial z} = D_{AB} \frac{\partial^2 c_A}{\partial x^2} \quad (3-113)$$

If mass transfer begins at the leading edge of the plate and the concentration in the fluid at the solid–fluid interface, c_{A_1} , is maintained constant, the mass-transfer boundary conditions are

$$\begin{aligned} c_A &= c_{A_0} \text{ at } x = 0 \text{ for } z > 0, \\ c_A &= c_{A_1} \text{ at } z = 0 \text{ for } x > 0, \\ \text{and } c_A &= c_{A_0} \text{ at } z = \infty \text{ for } x > 0 \end{aligned}$$

If the rate of mass transfer is low, the velocity profiles are undisturbed. The analogous heat-transfer problem was first solved by Pohlhausen [26] for $N_{Pr} > 0.5$, as described by Schlichting [27]. The analogous result for mass transfer is

$$\frac{N_{Sh_x}}{N_{Re_x} N_{Sc}^{1/3}} = \frac{0.332}{N_{Re_x}^{0.5}} \quad (3-114)$$

where

$$N_{Sh_x} = \frac{x k_{c_x}}{D_{AB}} \quad (3-115)$$

and the driving force for mass transfer is $c_{A_1} - c_{A_0}$.

The concentration boundary layer, where essentially all of the resistance to mass transfer resides, is defined by

$$\frac{c_{A_1} - c_A}{c_{A_1} - c_{A_0}} = 0.99 \quad (3-116)$$

and the ratio of the concentration boundary-layer thickness, δ_c , to the velocity boundary thickness, δ , is

$$\delta_c / \delta = 1 / N_{Sc}^{1/3} \quad (3-117)$$

Thus, for a liquid boundary layer where $N_{Sc} > 1$, the concentration boundary layer builds up more slowly than the velocity boundary layer. For a gas boundary layer where $N_{Sc} \approx 1$, the two boundary layers build up at about the same rate. By analogy to (3-112), the concentration profile is

$$\frac{c_{A_1} - c_A}{c_{A_1} - c_{A_0}} = 1.5 \left(\frac{z}{\delta_c} \right) - 0.5 \left(\frac{z}{\delta_c} \right)^3 \quad (3-118)$$

Equation (3-114) gives the local Sherwood number. If this expression is integrated over the length of the plate, L , the average Sherwood number is

$$N_{Sh_{avg}} = 0.664 N_{Re_L}^{1/2} N_{Sc}^{1/3} \quad (3-119)$$

where

$$N_{Sh_{avg}} = \frac{L k_{c_{avg}}}{D_{AB}} \quad (3-120)$$

EXAMPLE 3.12 Sublimation of Naphthalene from a Flat Plate.

Air at 100°C and 1 atm with a free-stream velocity of 5 m/s flows over a 3-m-long, horizontal, thin, flat plate of naphthalene, causing it to sublime. Determine: (a) the length over which a laminar boundary layer persists, (b) the average rate of mass transfer over that length, and (c) the thicknesses of the velocity and concentration boundary layers at the point of transition of the boundary layer to turbulent flow. The physical properties are: vapor pressure of naphthalene = 10 torr; viscosity of air = 0.0215 cP; molar density of air = 0.0327 kmol/m³; and diffusivity of naphthalene in air = 0.94×10^{-5} m²/s.

Solution

(a) $N_{Re_x} = 5 \times 10^5$ for transition to turbulent flow. From (3-109),

$$x = L = \frac{\mu N_{Re_x}}{u_\infty \rho} = \frac{[(0.0215)(0.001)](5 \times 10^5)}{(5)[(0.0327)(29)]} = 2.27 \text{ m}$$

at which transition to turbulent flow begins.

(b) $c_{A_0} = 0$, $c_{A_1} = \frac{10(0.0327)}{760} = 4.3 \times 10^{-4}$ kmol/m³.

From (3-83),

$$N_{Sc} = \frac{\mu}{\rho D_{AB}} = \frac{[(0.0215)(0.001)]}{[(0.0327)(29)](0.94 \times 10^{-5})} = 2.41$$

From (3-119),

$$N_{Sh_{avg}} = 0.664(5 \times 10^5)^{1/2}(2.41)^{1/3} = 630$$

From (3-120),

$$k_{c_{avg}} = \frac{630(0.94 \times 10^{-5})}{2.27} = 2.61 \times 10^{-3} \text{ m/s}$$

For a width of 1 m, $A = 2.27$ m²,

$$\begin{aligned} n_A &= k_{c_{avg}} A (c_{A_1} - c_{A_0}) = 2.61 \times 10^{-3} (2.27) (4.3 \times 10^{-4}) \\ &= 2.55 \times 10^{-6} \text{ kmol/s} \end{aligned}$$

(c) From (3-111), at $x = L = 2.27$ m,

$$\delta = \frac{3.46(2.27)}{(5 \times 10^5)^{0.5}} = 0.0111 \text{ m}$$

From (3-117),

$$\delta_c = \frac{0.0111}{(2.41)^{1/3}} = 0.0083 \text{ m}$$

§3.4.4 Molecular Diffusion from the Inside Surface of a Circular Tube to a Flowing Fluid—the Fully Developed Flow Concept

Figure 3.9 shows the development of a laminar velocity boundary layer when a fluid flows from a vessel into a straight circular tube of inside diameter, D . At the entrance, a , the velocity profile is flat. A velocity boundary layer then begins to build up, as shown by the dashed lines from a to e . The

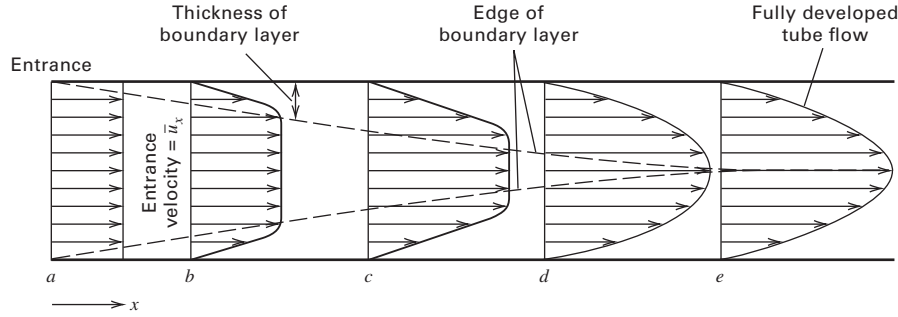


Figure 3.9 Buildup of a laminar velocity boundary layer for flow in a circular tube.

central core outside the boundary layer has a flat velocity profile where the flow is accelerated over the entrance velocity. Finally, at plane e , the boundary layer fills the tube. Now the flow is fully developed. The distance from plane a to plane e is called the entry length L_e . Mathematically, it is the distance from the entrance to the point at which the centerline velocity is 99% of fully developed flow. From Langhaar [27],

$$L_e/D = 0.0575 N_{Re} \quad (3-121)$$

Experiments show that for fully developed laminar flow in a tube, the Reynolds number, $N_{Re} = D \bar{u}_x \rho / \mu < 2,100$, where \bar{u}_x is the flow-average velocity in the axial direction, x . Then the equation of motion in the axial direction is

$$\frac{\mu}{r} \frac{\partial}{\partial r} \left(r \frac{\partial u_x}{\partial r} \right) - \frac{dP}{dx} = 0 \quad (3-122)$$

with boundary conditions:

$$\begin{aligned} r = 0 \text{ (axis of the tube), } & \quad \partial u_x / \partial r = 0 \\ \text{and } r = r_w \text{ (tube wall), } & \quad u_x = 0 \end{aligned}$$

Equation (3-122) was integrated by Hagen in 1839 and Poiseuille in 1841. The resulting equation for the velocity profile, in terms of the flow-average velocity, is

$$u_x = 2\bar{u}_x \left[1 - \left(\frac{r}{r_w} \right)^2 \right] \quad (3-123)$$

or, in terms of the maximum velocity at the tube axis,

$$u_x = u_{x_{\max}} \left[1 - \left(\frac{r}{r_w} \right)^2 \right] \quad (3-124)$$

According to (3-124), the velocity profile is parabolic.

The shear stress, pressure drop, and Fanning friction factor are obtained from solutions to (3-122):

$$\tau_w = -\mu \left. \frac{\partial u_x}{\partial r} \right|_{r=r_w} = \frac{4\mu\bar{u}_x}{r_w} \quad (3-125)$$

$$-\frac{dP}{dx} = \frac{32\mu\bar{u}_x}{D^2} = \frac{2f\rho\bar{u}_x^2}{D} \quad (3-126)$$

with

$$f = \frac{16}{N_{Re}} \quad (3-127)$$

At the upper limit of laminar flow, $N_{Re} = 2,100$, and $L_e/D = 121$, but at $N_{Re} = 100$, L_e/D is only 5.75. In the entry

region, the friction factor is considerably higher than the fully developed flow value given by (3-127). At $x = 0$, f is infinity, but it decreases exponentially with increasing x , approaching the fully developed flow value at L_e . For example, for $N_{Re} = 1,000$, (3-127) gives $f = 0.016$, with $L_e/D = 57.5$. From $x = 0$ to $x/D = 5.35$, the average friction factor from Langhaar is 0.0487, which is three times the fully developed value.

In 1885, Graetz [28] obtained a solution to the problem of convective heat transfer between the wall of a circular tube, at a constant temperature, and a fluid flowing through the tube in fully developed laminar flow. Assuming constant properties and negligible heat conduction in the axial direction, the energy equation, after substituting (3-123) for u_x , is

$$2\bar{u}_x \left[1 - \left(\frac{r}{r_w} \right)^2 \right] \frac{\partial T}{\partial x} = \frac{k}{\rho C_p} \left[\frac{1}{r} \frac{\partial}{\partial r} \left(r \frac{\partial T}{\partial r} \right) \right] \quad (3-128)$$

with boundary conditions:

$$\begin{aligned} x = 0 \text{ (where heat transfer begins), } & \quad T = T_0, \text{ for all } r \\ x > 0, \quad r = r_w, & \quad T = T_1 \text{ and } x > 0, \quad r = 0, \quad \partial T / \partial r = 0 \end{aligned}$$

The analogous species continuity equation for mass transfer, neglecting bulk flow in the radial direction and axial diffusion, is

$$2\bar{u}_x \left[1 - \left(\frac{r}{r_w} \right)^2 \right] \frac{\partial c_A}{\partial x} = D_{AB} \left[\frac{1}{r} \frac{\partial}{\partial r} \left(r \frac{\partial c_A}{\partial r} \right) \right] \quad (3-129)$$

with analogous boundary conditions.

The Graetz solution for (3-129) for the temperature or concentration profile is an infinite series that can be obtained from (3-128) by separation of variables using the method of Frobenius. A detailed solution is given by Sellars, Tribus, and Klein [29]. The concentration profile yields expressions for the mass-transfer coefficient and the Sherwood number. For large x , the concentration profile is fully developed and the local Sherwood number, N_{Sh_x} , approaches a limiting value of 3.656. When x is small, such that the concentration boundary layer is very thin and confined to a region where the fully developed velocity profile is linear, the local Sherwood number is obtained from the classic Leveque [30] solution, presented by Knudsen and Katz [31]:

$$N_{Sh_x} = \frac{k_{c_x} D}{D_{AB}} = 1.077 \left[\frac{N_{PeM}}{x/D} \right]^{1/3} \quad (3-130)$$

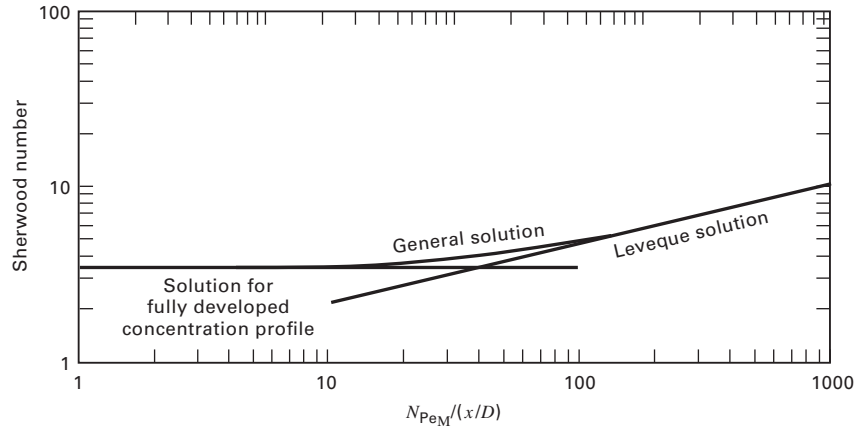


Figure 3.10 Limiting and general solutions for mass transfer to a fluid in laminar flow in a straight, circular tube.

where

$$N_{PeM} = \frac{D\bar{u}_x}{D_{AB}} \quad (3-131)$$

The limiting solutions, together with the general Graetz solution, are shown in Figure 3.10, where $N_{Sh,x} = 3.656$ is valid for $N_{PeM}/(x/D) < 4$ and (3-130) is valid for $N_{PeM}/(x/D) > 100$. These solutions can be patched together if a point from the general solution is available at the intersection like that discussed in §3.4.2. In the region of mass transfer, an average Sherwood number is derived by integrating the general expression for the local Sherwood number. An empirical representation for that average, based on a log-mean concentration driving force, proposed by Hausen [32], is

$$N_{Sh,avg} = 3.66 + \frac{0.0668 [N_{PeM}/(x/D)]}{1 + 0.04 [N_{PeM}/(x/D)]^{2/3}} \quad (3-132)$$

EXAMPLE 3.13 Mass Transfer of Benzoic Acid into Water Flowing in Laminar Motion through a Tube of Benzoic Acid.

Linton and Sherwood [33] dissolved tubes of benzoic acid (A) into water (B) flowing in laminar flow through the tubes. Their data agreed with predictions based on the Graetz and Leveque equations. Consider a 5.23-cm-inside-diameter, 32-cm-long tube of benzoic acid, preceded by 400 cm of straight metal pipe wherein a fully developed velocity profile is established. Water enters at 25°C at a velocity corresponding to a Reynolds number of 100. Based on property data at 25°C, estimate the average concentration of benzoic acid leaving the tube before a significant increase in the inside diameter of the benzoic-acid tube occurs because of dissolution. The properties are: solubility of benzoic acid in water = 0.0034 g/cm³; viscosity of water = 0.89 cP = 0.0089 g/cm-s; and diffusivity of benzoic acid in water at infinite dilution = 9.18×10^{-6} cm²/s.

Solution

$$N_{Sc} = \frac{0.0089}{(1.0)(9.18 \times 10^{-6})} = 970$$

$$N_{Re} = \frac{D\bar{u}_x\rho}{\mu} = 100$$

from which

$$\bar{u}_x = \frac{(100)(0.0089)}{(5.23)(1.0)} = 0.170 \text{ cm/s}$$

From (3-131),

$$N_{PeM} = \frac{(5.23)(0.170)}{9.18 \times 10^{-6}} = 9.69 \times 10^4$$

$$\frac{x}{D} = \frac{32}{5.23} = 6.12$$

$$\frac{N_{PeM}}{(x/D)} = \frac{9.69 \times 10^4}{6.12} = 1.58 \times 10^4$$

From (3-132),

$$N_{Sh,avg} = 3.66 + \frac{0.0668(1.58 \times 10^4)}{1 + 0.04(1.58 \times 10^4)^{2/3}} = 44$$

$$k_{c,avg} = N_{Sh,avg} \frac{D_{AB}}{D} = 44 \left(\frac{9.18 \times 10^{-6}}{5.23} \right) = 7.7 \times 10^{-5} \text{ cm/s}$$

Using a log mean driving force,

$$n_A = \bar{u}_x S (\bar{c}_{A_x} - c_{A_0}) = k_{c,avg} A \frac{(c_{A_1} - c_{A_0}) - (c_{A_1} - \bar{c}_{A_x})}{\ln [(c_{A_1} - c_{A_0}) / (c_{A_1} - \bar{c}_{A_x})]}$$

where S is the cross-sectional area for flow. Simplifying,

$$\ln [(c_{A_1} - c_{A_0}) / (c_{A_1} - \bar{c}_{A_x})] = \frac{k_{c,avg} A}{\bar{u}_x S}$$

$$c_{A_0} = 0 \quad \text{and} \quad c_{A_1} = 0.0034 \text{ g/cm}^3$$

$$S = \frac{\pi D^2}{4} = \frac{(3.14)(5.23)^2}{4} = 21.5 \text{ cm}^2$$

$$A = \pi D x = (3.14)(5.23)(32) = 526 \text{ cm}^2$$

$$\ln [(0.0034 - 0) / (0.0034 - \bar{c}_{A_x})] = \frac{(7.7 \times 10^{-5})(526)}{(0.170)(21.5)} = 0.0111$$

Solving,

$$\bar{c}_{A_x} = 0.0034 - \frac{0.0034}{e^{0.0111}} = 0.000038 \text{ g/cm}^3$$

Thus, the concentration of benzoic acid in the water leaving the benzoic-acid tube is far from saturation.

§3.5 MASS TRANSFER IN TURBULENT FLOW

The two previous sections described mass transfer in stagnant media (§3.3) and laminar flow (§3.4), where in accordance with (3-1), only two mechanisms needed to be considered: molecular diffusion and bulk flow, with the latter being often ignored. For both cases, rates of mass transfer in laminar flow can be calculated theoretically using Fick's law of diffusion. In industrial applications, turbulent flow is more common because it includes eddy diffusion, which results in much

higher heat-transfer and mass-transfer rates, which reduce the size of the processing equipment. Lacking a fundamental theory for eddy diffusion, estimates of mass-transfer rates rely on empirical correlations developed from experimental data. These correlations are comprised of the dimensionless groups of §3.4 and use analogies with heat and momentum transfer. For reference, the most useful dimensionless groups for fluid mechanics, heat transfer, and mass transfer are listed in Table 3.9. Note that most of the dimensionless groups used in empirical equations for mass transfer are analogous

Table 3.9 Some Useful Dimensionless Groups

Name	Formula	Meaning	Analogy
Fluid Mechanics			
Drag Coefficient	$C_D = \frac{2F_D}{Au^2\rho}$	$\frac{\text{Drag force}}{\text{Projected area} \times \text{Velocity head}}$	
Fanning Friction Factor	$f = \frac{\Delta P}{L} \frac{D}{2\bar{u}^2\rho}$	$\frac{\text{Pipe wall shear stress}}{\text{Velocity head}}$	
Froude Number	$N_{Fr} = \frac{\bar{u}^2}{gL}$	$\frac{\text{Inertial force}}{\text{Gravitational force}}$	
Reynolds Number	$N_{Re} = \frac{L\bar{u}\rho}{\mu} = \frac{L\bar{u}}{\nu} = \frac{LG}{\mu}$	$\frac{\text{Inertial force}}{\text{Viscous force}}$	
Weber Number	$N_{We} = \frac{\bar{u}^2\rho L}{\sigma}$	$\frac{\text{Inertial force}}{\text{Surface-tension force}}$	
Heat Transfer			
j -Factor for Heat Transfer	$j_H = N_{StH}(N_{Pr})^{2/3}$		j_M
Nusselt Number	$N_{Nu} = \frac{hL}{k}$	$\frac{\text{Convective heat transfer}}{\text{Conductive heat transfer}}$	N_{Sh}
Peclet Number for Heat Transfer	$N_{PeH} = N_{Re}N_{Pr} = \frac{L\bar{u}\rho C_p}{k}$	$\frac{\text{Bulk transfer of heat}}{\text{Conductive heat transfer}}$	N_{PeM}
Prandtl Number	$N_{Pr} = \frac{C_p\mu}{k} = \frac{\nu}{\alpha}$	$\frac{\text{Momentum diffusivity}}{\text{Thermal diffusivity}}$	N_{Sc}
Stanton Number for Heat Transfer	$N_{StH} = \frac{N_{Nu}}{N_{Re}N_{Pr}} = \frac{h}{C_p G}$	$\frac{\text{Heat transfer}}{\text{Thermal capacity}}$	N_{StM}
Mass Transfer			
j -Factor for Mass Transfer (analogous to the j -Factor for Heat Transfer)	$j_M = N_{StM}(N_{Sc})^{2/3}$		j_H
Lewis Number	$N_{Le} = \frac{N_{Sc}}{N_{Pr}} = \frac{k}{\rho C_p D_{AB}} = \frac{\alpha}{D_{AB}}$	$\frac{\text{Thermal diffusivity}}{\text{Mass diffusivity}}$	
Peclet Number for Mass Transfer (analogous to the Peclet Number for Heat Transfer)	$N_{PeM} = N_{Re}N_{Sc} = \frac{L\bar{u}}{D_{AB}}$	$\frac{\text{Bulk transfer of mass}}{\text{Molecular diffusion}}$	N_{PeH}
Schmidt Number (analogous to the Prandtl Number)	$N_{Sc} = \frac{\mu}{\rho D_{AB}} = \frac{\nu}{D_{AB}}$	$\frac{\text{Momentum diffusivity}}{\text{Mass diffusivity}}$	N_{Pr}
Sherwood Number (analogous to the Nusselt Number)	$N_{Sh} = \frac{k_c L}{D_{AB}}$	$\frac{\text{Convective mass transfer}}{\text{Molecular diffusion}}$	N_{Nu}
Stanton Number for Mass Transfer (analogous to the Stanton Number for Heat Transfer)	$N_{StM} = \frac{N_{Sh}}{N_{Re}N_{Sc}} = \frac{k_c}{\bar{u}}$	$\frac{\text{Mass transfer}}{\text{Mass capacity}}$	N_{StH}

L = characteristic length G = mass velocity = $\bar{u}\rho$, Subscripts: M = mass transfer H = heat transfer

to dimensionless groups used in heat transfer. The Reynolds number from fluid mechanics is used widely in empirical equations of momentum, heat, and mass transfer.

As shown by a famous dye experiment conducted by Osborne Reynolds in 1883 [34], a fluid in laminar flow moves parallel to the solid boundaries in streamline patterns. Every fluid particle moves with the same velocity along a streamline, and there are no normal-velocity components. For a Newtonian fluid in laminar flow, momentum, heat, and mass transfer are by molecular transport, governed by Newton's law of viscosity, Fourier's law of heat conduction, and Fick's law of molecular diffusion.

In turbulent flow, where transport processes are orders of magnitude higher than in laminar flow, streamlines no longer exist, except near a wall, and eddies of fluid (large compared to the mean free path of the molecules in the fluid) mix with each other by moving from one region to another in fluctuating motion. This eddy mixing by velocity fluctuations occurs not only in the direction of flow but also in directions that are normal to flow, with the former referred to as axial transport. The latter are of more interest. Momentum, heat, and mass transfer occur by the two parallel mechanisms given in (3-1): (1) molecular diffusion, which is slow; and (2) turbulent or eddy diffusion, which is rapid except near a solid surface, where the flow velocity accompanying turbulence tends to zero. Superimposed on molecular and eddy diffusion is (3) mass transfer by bulk flow, which may or may not be significant.

In 1877, Boussinesq [35] modified Newton's law of viscosity to add a parallel eddy or turbulent viscosity, μ_t . Analogous expressions were developed for turbulent-flow heat and mass transfer. For flow in the x -direction and transport in the z -direction normal to flow, these expressions are written in flux form (in the absence of bulk flow in the z -direction) as:

$$\tau_{zx} = -(\mu + \mu_t) \frac{du_x}{dz} \quad (3-133)$$

$$q_z = -(k + k_t) \frac{dT}{dz} \quad (3-134)$$

$$N_{A_z} = -(D_{AB} + D_t) \frac{dc_A}{dz} \quad (3-135)$$

where the double subscript zx on the shear stress, τ , stands for x -momentum in the z -direction. The molecular contributions, μ , k , and D_{AB} , are properties of the fluid and depend on chemical composition, temperature, and pressure. The turbulent contributions, μ_t , k_t , and D_t , depend on the mean fluid velocity in the flow direction and on the position in the fluid with respect to the solid boundaries.

In 1925, Prandtl [36] developed an expression for μ_t in terms of an eddy mixing length, l , which is a function of position and is a measure of the average distance that an eddy travels before it loses its identity and mingles with other eddies. The mixing length is analogous to the mean free path of gas molecules, which is the average distance a molecule travels before it collides with another molecule. By analogy, the same mixing length is valid for turbulent-flow heat transfer

and mass transfer. To use this analogy, (3-133) to (3-135) are rewritten in diffusivity form:

$$\frac{\tau_{zx}}{\rho} = -(\nu + \varepsilon_M) \frac{du_x}{dz} \quad (3-136)$$

$$\frac{q_z}{C_p \rho} = -(\alpha + \varepsilon_H) \frac{dT}{dz} \quad (3-137)$$

$$N_{A_z} = -(D_{AB} + \varepsilon_D) \frac{dc_A}{dz} \quad (3-138)$$

where ε_M , ε_H , and ε_D are momentum, heat, and mass eddy diffusivities, respectively; ν is the momentum diffusivity (kinematic viscosity, μ/ρ); and α is the thermal diffusivity, $k/\rho C_p$. As an approximation, the three eddy diffusivities may be assumed equal. This is valid for ε_H and ε_D , but data indicate that $\varepsilon_M/\varepsilon_H = \varepsilon_M/\varepsilon_D$ is sometimes less than 1.0 and as low as 0.5 for turbulence in a free jet.

§3.5.1 Reynolds Analogy

If (3-136) to (3-138) are applied at a solid boundary, they can be used to determine transport fluxes based on transport coefficients, with driving forces from the wall (or interface), I , at $z = 0$, to the bulk fluid condition, designated with an overbar:

$$\frac{\tau_{zx}}{\bar{u}_x} = -(\nu + \varepsilon_M) \left. \frac{d(\rho u_x / \bar{u}_x)}{dz} \right|_{z=0} = \frac{f \rho \bar{u}_x}{2} \quad (3-139)$$

$$q_z = -(\alpha + \varepsilon_H) \left. \frac{d(\rho C_p T)}{dz} \right|_{z=0} = h(T_I - \bar{T}) \quad (3-140)$$

$$N_{A_z} = -(D_{AB} + \varepsilon_D) \left. \frac{dc_A}{dz} \right|_{z=0} = k_c(c_A - \bar{c}_A) \quad (3-141)$$

To develop useful analogies, it is convenient to use dimensionless velocity, temperature, and solute concentration, defined by

$$\theta = \frac{u_x}{\bar{u}_x} = \frac{T_I - T}{T_I - \bar{T}} = \frac{c_{A_I} - c_A}{c_{A_I} - \bar{c}_A} \quad (3-142)$$

If (3-142) is substituted into (3-139) to (3-141),

$$\begin{aligned} \left. \frac{\partial \theta}{\partial z} \right|_{z=0} &= \frac{f \bar{u}_x}{2(\nu + \varepsilon_M)} = \frac{h}{\rho C_p (\alpha + \varepsilon_H)} \\ &= \frac{k_c}{(D_{AB} + \varepsilon_D)} \end{aligned} \quad (3-143)$$

which defines analogies among momentum, heat, and mass transfer. If the three eddy diffusivities are equal and molecular diffusivities are everywhere negligible or equal, i.e., $\nu = \alpha = D_{AB}$, (3-143) simplifies to

$$\frac{f}{2} = \frac{h}{\rho C_p \bar{u}_x} = \frac{k_c}{\bar{u}_x} \quad (3-144)$$

Equation (3-144) defines the Stanton number for heat transfer listed in Table 3.9,

$$N_{St_H} = \frac{h}{\rho C_p \bar{u}_x} = \frac{h}{G C_p} \quad (3-145)$$

where $G = \text{mass velocity} = \bar{u}_x \rho$. The Stanton number for mass transfer is

$$N_{\text{StM}} = \frac{k_c}{\bar{u}_x} = \frac{k_c \rho}{G} \quad (3-146)$$

Equation (3-144) is referred to as the **Reynolds analogy**. Its development is significant, but its application for the estimation of heat-transfer and mass-transfer coefficients from measurements of the Fanning friction factor for turbulent flow is valid only when $N_{\text{Pr}} = \nu/\alpha = N_{\text{Sc}} = \nu/D_{\text{AB}} = 1$. Thus, the Reynolds analogy has very limited practical value and is rarely used. Reynolds postulated its existence in 1874 [37] and derived it in 1883 [34].

§3.5.2 Chilton–Colburn Analogy

A widely used extension of the Reynolds analogy to values of the Prandtl and Schmidt numbers other than 1 was devised in the 1930s by Colburn [38] for heat transfer and by Chilton and Colburn [39] for mass transfer. It is widely applied. Using experimental data, Chilton and Colburn corrected the Reynolds analogy for differences in dimensionless velocity, temperature, and concentration distributions by incorporating the Prandtl number, N_{Pr} , and the Schmidt number, N_{Sc} , into (3-144) to define empirically the following three **j -factors**, two of which are included in Table 3.9. Instead of j_M , the Fanning friction factor is listed in Table 3.9.

$$\boxed{j_M = \frac{f}{2} = j_H = \frac{h}{G C_P} N_{\text{Pr}}^{2/3} = j_D = \frac{k_c \rho}{G} N_{\text{Sc}}^{2/3}} \quad (3-147)$$

Equation (3-147) is the **Chilton–Colburn analogy** or the Colburn analogy for estimating transport coefficients for turbulent flow. For $N_{\text{Pr}} = N_{\text{Sc}} = 1$, (3-147) equals (3-144).

Experiments show that the j -factors depend on the geometric configuration and the Reynolds number, N_{Re} . Based on decades of experimental turbulent-flow transport data, the following representative j -factor correlations for turbulent transport to or from smooth surfaces have evolved. Additional correlations are presented in later chapters. These correlations are reasonably accurate for N_{Pr} and N_{Sc} in the range of 0.5 to 10 and result in average transport coefficients for:

1. Flow through a straight, circular tube of inside diameter D :

$$j_M = j_H = j_D = 0.023(N_{\text{Re}})^{-0.2} \quad (3-148)$$

for $10,000 < N_{\text{Re}} = DG/\mu < 1,000,000$

2. Flow across a flat plate of length L :

$$j_M = j_H = j_D = 0.037(N_{\text{Re}})^{-0.2} \quad (3-149)$$

for $5 \times 10^5 < N_{\text{Re}} = Lu_0 \rho/\mu < 5 \times 10^8$

3. Flow normal to a long, circular cylinder of diameter D , where the drag coefficient includes both form drag and

skin friction, but only the skin friction contribution applies to the analogy:

$$(j_M)_{\text{skin friction}} = j_H = j_D = 0.193(N_{\text{Re}})^{-0.382} \quad (3-150)$$

for $4,000 < N_{\text{Re}} < 40,000$

$$(j_M)_{\text{skin friction}} = j_H = j_D = 0.0266(N_{\text{Re}})^{-0.195} \quad (3-151)$$

for $40,000 < N_{\text{Re}} < 250,000$

with $N_{\text{Re}} = DG/\mu$

4. Flow past a single sphere of diameter D :

$$(j_M)_{\text{skin friction}} = j_H = j_D = 0.37(N_{\text{Re}})^{-0.4} \quad (3-152)$$

for $20 < N_{\text{Re}} = DG/\mu < 100,000$

5. Flow through beds packed with spherical particles of uniform size D_p :

$$j_H = j_D = 1.17(N_{\text{Re}})^{-0.415} \quad (3-153)$$

for $10 < N_{\text{Re}} = D_p G/\mu < 2,500$

The above correlations are plotted in Figure 3.11, where the curves are not widely separated but do not coincide because of necessary differences in Reynolds number definitions. When using the correlations in the presence of appreciable temperature and/or composition differences, Chilton and Colburn recommend that N_{Pr} and N_{Sc} be evaluated at the average conditions from the surface to the bulk stream.

§3.5.3 Other Analogies

A theoretical improvement to the Reynolds analogy was made in 1910 by Prandtl [40], who divided the flow into two regions: (1) a thin laminar-flow **sublayer** of thickness δ next to the wall boundary, where only molecular transport occurs; and (2) a turbulent region dominated by eddy transport, with $\varepsilon_M = \varepsilon_H = \varepsilon_D$. His expression for the Stanton number for heat transfer was less empirical, but less accurate than the later Chilton–Colburn analogy.

Further theoretical improvements to the Reynolds analogy were made by von Karman, Martinelli, and Deissler, as discussed in detail by Knudsen and Katz [31]. The first two investigators inserted a buffer zone between the laminar sublayer and turbulent core. Deissler gradually reduced the eddy diffusivities as the wall was approached. Other advances were made by van Driest [41], who used a modified form of the Prandtl mixing length; Reichardt [42], who eliminated the zone concept by allowing the eddy diffusivities to decrease continuously from a maximum to zero at the wall; and Friend and Metzner [43], who obtained improved accuracy at high Prandtl and Schmidt numbers up to 3,000. Their results for flow through a circular tube are

$$N_{\text{StH}} = \frac{f/2}{1.20 + 11/8 \sqrt{f/2} (N_{\text{Pr}} - 1) N_{\text{Pr}}^{-1/3}} \quad (3-154)$$

$$N_{\text{StM}} = \frac{f/2}{1.20 + 11/8 \sqrt{f/2} (N_{\text{Sc}} - 1) N_{\text{Sc}}^{-1/3}} \quad (3-155)$$

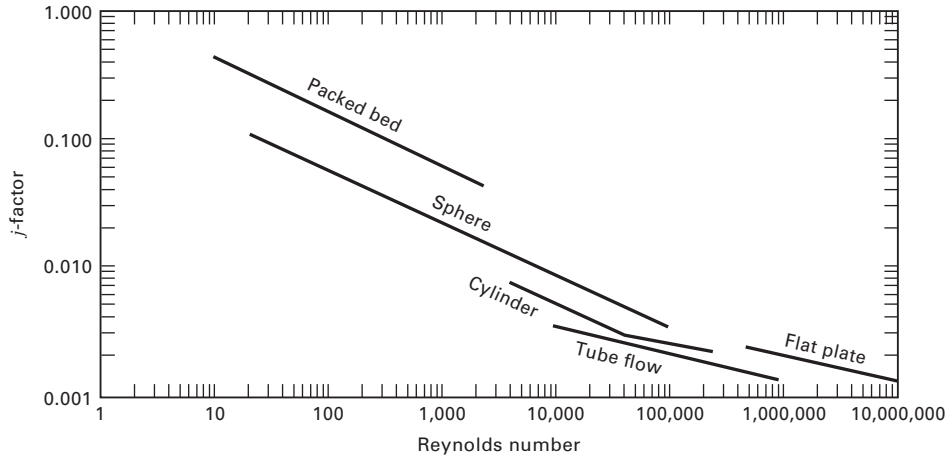


Figure 3.11 Chilton–Colburn j -factor correlations.

where the Fanning friction factor can be estimated for Reynolds numbers from 10,000 to 10,000,000 using the empirical correlation of Drew, Koo, and McAdams [44]:

$$f = 0.00140 + 0.125(N_{Re})^{-0.32} \quad (3-156)$$

which fits the experimental data of Nikuradse [45] and is preferred over (3-147) with (3-148), which is valid only to $N_{Re} = 1,000,000$. For two- and three-dimensional turbulent-flow problems, some success has been achieved with the κ (kinetic energy of turbulence)– ε (rate of dissipation) model of Launder and Spalding [46], which is used in computational fluid dynamics (CFD) computer programs.

A more theoretical alternative to (3-154) to (3-156) for developing equations for turbulent flow is to use **time-averaged** velocities, temperatures, and concentrations in the laws of Newton, Fourier, and Fick. This approach is used in a series of papers by Churchill and co-workers [47] to [52]. The equation of Churchill and Zajic [48] for the Fanning friction for turbulent flow in a straight, smooth cylindrical tube or pipe is:

$$\left(\frac{2}{f}\right)^{1/2} = 3.2 - 227 \left[\frac{\left(\frac{2}{f}\right)^{1/2}}{\frac{N_{Re}}{2}} \right] + 2500 \left[\frac{\left(\frac{2}{f}\right)^{1/2}}{\frac{N_{Re}}{2}} \right]^2 + \frac{1}{0.436} \ln \left[\frac{\left(\frac{2}{f}\right)^{1/2}}{\frac{N_{Re}}{2}} \right]^{-1} \quad (3-157)$$

where the Reynolds number is $N_{Re} = D\bar{u}_x\rho/\mu$.

Equation (3-157) is in agreement with experimental data over a Reynolds number range of 4,000–3,000,000 and can be used up to a Reynolds number of 100,000,000. Table 3.10 is a comparison of the Churchill–Zajic equation, (3-157), with (3-156) of Drew et al. and (3-148) of Chilton and Colburn. Equation (3-156) gives satisfactory agreement for Reynolds numbers from 10,000 to 10,000,000, while (3-148) is useful only for Reynolds numbers from 100,000 to 1,000,000.

Table 3.10 Comparison of Fanning Friction Factors for Fully Developed Turbulent Flow in a Smooth, Straight, Circular Tube

N_{Re}	f , Drew et al. (3-156)	f , Chilton–Colburn (3-148)	f , Churchill–Zajic (3-157)
10,000	0.007960	0.007291	0.008087
100,000	0.004540	0.004600	0.004559
1,000,000	0.002903	0.002902	0.002998
10,000,000	0.002119	0.001831	0.002119
100,000,000	0.001744	0.001155	0.001573

An extension of the Churchill approach by Churchill and Zajic [48] gives an expression for the Nusselt number for turbulent-flow convective heat transfer in a straight, smooth cylindrical tube or pipe:

$$N_{Nu} = \frac{1}{\left(\frac{N_{Pr_t}}{N_{Pr}}\right) \frac{1}{N_{Nu_1}} + \left[1 - \left(\frac{N_{Pr_t}}{N_{Pr}}\right)^{2/3}\right] \frac{1}{N_{Nu_\infty}}} \quad (3-158)$$

where, from Yu, Ozoe, and Churchill [50],

$$N_{Pr_t} = \text{turbulent Prandtl number} = 0.85 + \frac{0.015}{N_{Pr}} \quad (3-159)$$

$$N_{Nu_1} = \text{Nusselt number for } (N_{Pr} = N_{Pr_t})$$

$$= \frac{N_{Re} \frac{f}{2}}{1 + 145 \left(\frac{f}{2}\right)^{-5/4}} \quad (3-160)$$

$$N_{Nu_\infty} = \text{Nusselt number for } (N_{Pr} = \infty)$$

$$= 0.07443 \left(\frac{N_{Pr}}{N_{Pr_t}}\right)^{1/3} N_{Re} \left(\frac{f}{2}\right)^{1/2} \quad (3-161)$$

Table 3.11 is a comparison of the Churchill et al. Nusselt-number correlation (3-158) with those of Friend and Metzner (3-154) and Chilton and Colburn (3-148), where, from Table 3.9, $N_{Nu} = N_{St}N_{Re}N_{Pr}$. At a Prandtl number of 1, which is typical of low-viscosity liquids and close to that of most gases, the Chilton–Colburn correlation is within 10% of

Table 3.11 Comparison of Nusselt Numbers for Fully Developed Turbulent Flow in a Smooth, Straight, Circular Tube

Prandtl number, $N_{Pr} = 1$			
N_{Re}	N_{Nu} , Friend–Metzner (3-154)	N_{Nu} , Chilton–Colburn (3-148)	N_{Nu} , Churchill–Zajic (3-158)
10,000	33.2	36.5	37.8
100,000	189	230	232
1,000,000	1210	1450	1580
10,000,000	8830	9160	11400
100,000,000	72700	57800	86000
Prandtl number, $N_{Pr} = 1000$			
N_{Re}	N_{Nu} , Friend–Metzner (3-154)	N_{Nu} , Chilton–Colburn (3-148)	N_{Nu} , Churchill–Zajic (3-158)
10,000	527	365	491
100,000	3960	2300	3680
1,000,000	31500	14500	29800
10,000,000	267800	91600	249000
100,000,000	2420000	578000	2140000

the Churchill–Zajic equation for Reynolds numbers up to 1,000,000. Beyond that, serious deviations occur (25% at $N_{Re} = 10,000,000$ and almost 50% at $N_{Re} = 100,000,000$). Deviations of the Friend–Metzner correlation vary from 15% to 30% over the entire range of Reynolds numbers. At all Reynolds numbers, the Churchill–Zajic equation predicts higher Nusselt numbers and, therefore, higher heat-transfer coefficients.

At a Prandtl number of 1,000, which is typical of high-viscosity liquids, the Friend–Metzner correlation is in fairly close agreement with the Churchill–Zajic equation. The Chilton–Colburn correlation deviates over the entire range of Reynolds numbers, predicting values ranging from 27 to 74% of those from the Churchill–Zajic equation as the Reynolds number increases. The Chilton–Colburn correlation should not be used at high Prandtl numbers for heat transfer or at high Schmidt numbers for mass transfer.

The Churchill–Zajic equation for predicting the Nusselt number shows an exponent dependence on the Reynolds number. This is in contrast to the typically cited constant exponent of 0.8 for the Chilton–Colburn correlation. For the Churchill–Zajic equation, at $N_{Pr} = 1$, the exponent increases with Reynolds number from 0.79 to 0.88; at a Prandtl number of 1,000, the exponent increases from 0.87 to 0.93.

Extension of the Churchill–Zajic equation to low Prandtl numbers typical of molten metals, and to other geometries is discussed by Churchill [49], who also considers the effect of boundary conditions (e.g., constant wall temperature and uniform heat flux) at low-to-moderate Prandtl numbers.

For calculation of convective mass-transfer coefficients, k_c , for turbulent flow of gases and liquids in straight, smooth circular tubes, it is recommended that the Churchill–Zajic equation be employed by applying the analogy between heat and mass transfer. Thus, as illustrated in the following example, the Sherwood number is substituted for the Nusselt number and the Schmidt number is substituted for the Prandtl number, using Table 3.9 with (3-158) to (3-161).

EXAMPLE 3.14 Analogies for Turbulent Transport in Straight, Smooth, Circular Tubes.

Linton and Sherwood [33] conducted experiments on the dissolution of tubes of cinnamic acid (A) into water (B) flowing turbulently through the tubes. In one run, with a 5.23-cm-i.d. tube, $N_{Re} = 35,800$, and $N_{Sc} = 1,450$, they measured a Stanton number for mass transfer, N_{StM} , of 0.0000351. Compare this value with predictions by the Reynolds, Chilton–Colburn, and Friend–Metzner analogies, as well as the Churchill–Zajic equations.

Solution

From either (3-156) or (3-164), the Fanning friction factor is 0.00576.

Reynolds analogy. From (3-144), $N_{StM} = f/2 = 0.00576/2 = 0.00288$, which, as expected, is in very poor agreement with the experimental value because the effect of the large Schmidt number is ignored.

Chilton–Colburn analogy. From (3-147),

$$N_{StM} = \left(\frac{f}{2}\right) / N_{Sc}^{2/3} = \left(\frac{0.00576}{2}\right) / (1450)^{2/3} = 0.0000225$$

which is 64% of the experimental value.

Friend–Metzner analogy. From (3-155), $N_{StM} = 0.0000350$, which is almost identical to the experimental value.

Churchill–Zajic equation. Using mass-transfer analogies,

$$(3-159) \text{ gives } N_{Sc_r} = 0.850, (3-160) \text{ gives } N_{Sh_1} = 94, \\ (3-161) \text{ gives } N_{Sh_{\infty}} = 1686, \text{ and } (3-158) \text{ gives } N_{Sh} = 1680$$

From Table 3.9,

$$N_{StM} = \frac{N_{Sh}}{N_{Re} N_{Sc}} = \frac{1680}{(35800)(1450)} = 0.0000324,$$

which is an acceptable 92% of the experimental value.

§3.6 MODELS FOR MASS TRANSFER IN FLUIDS WITH A FLUID–FLUID INTERFACE

The three previous sections considered mass transfer mainly between solids and fluids, where the interface was a smooth, solid surface. Applications include adsorption and membrane separations. Of importance in other separation operations is mass transfer across a fluid–fluid interface. Such interfaces exist in absorption, distillation, liquid–liquid extraction, and stripping, where, in contrast to fluid–solid interfaces, turbulence may persist to the interface. The following theoretical models have been developed to describe such phenomena in fluids with a fluid-to-fluid interface. Use of these equations to design equipment is found in many examples in: Chapter 6 on absorption and stripping; Chapter 7 on distillation; and Chapter 8 on liquid–liquid extraction.

§3.6.1 Film Theory

A model for turbulent mass transfer to or from a fluid-phase boundary was suggested in 1904 by Nernst [53], who postulated that the resistance to mass transfer in a turbulent fluid phase is in a thin, relatively stagnant region at the interface, called a film. This is similar to the laminar sublayer that forms when a fluid flows in the turbulent regime parallel to a flat plate. It is shown schematically in Figure 3.12a for a gas–liquid interface, where the gas is component A, which diffuses into non-volatile liquid B. Thus, a process of absorption of A into liquid B takes place. Without vaporization of B, there is no resistance to mass transfer of A in the gas phase, because it is pure A. At the interface, phase equilibrium is assumed, so the concentration of A at the interface, c_{A_i} , is related to the partial pressure of A at the interface, p_A , by a solubility relation like Henry’s law, $c_{A_i} = H_A p_A$. In the liquid film of thickness δ , molecular diffusion occurs with a driving force of $c_{A_i} - c_{A_b}$, where c_{A_b} is the bulk-average concentration of A in the liquid. Since the film is assumed to be very thin, all of the diffusing A is assumed to pass through the film and into

the bulk liquid. Accordingly, integration of Fick’s first law, (3-3a), gives

$$J_A = \frac{D_{AB}}{\delta} (c_{A_i} - c_{A_b}) = \frac{c D_{AB}}{\delta} (x_{A_i} - x_{A_b}) \quad (3-162)$$

If the liquid phase is dilute in A, the bulk-flow effect can be neglected so that (3-162) applies to the total flux, and the concentration gradient is linear, as in Figure 3.12a.

$$N_A = \frac{D_{AB}}{\delta} (c_{A_i} - c_{A_b}) = \frac{c D_{AB}}{\delta} (x_{A_i} - x_{A_b}) \quad (3-163)$$

If the bulk-flow effect is not negligible, then, from (3-31),

$$N_A = \frac{c D_{AB}}{\delta} \ln \left[\frac{1 - x_{A_b}}{1 - x_{A_i}} \right] = \frac{c D_{AB}}{\delta (1 - x_A)_{LM}} (x_{A_i} - x_{A_b}) \quad (3-164)$$

where

$$(1 - x_A)_{LM} = \frac{x_{A_i} - x_{A_b}}{\ln [(1 - x_{A_b}) / (1 - x_{A_i})]} = (x_B)_{LM} \quad (3-165)$$

In practice, the ratios D_{AB}/δ in (3-163) and $D_{AB}/[\delta(1 - x_A)_{LM}]$ in (3-164) are replaced by empirical mass-transfer coefficients k_c and k'_c , respectively, because the film thickness, δ , which depends on the flow conditions, is unknown. The subscript, c , on the mass-transfer coefficient refers to a concentration driving force, and the prime superscript denotes that k'_c includes both diffusion mechanisms and the bulk-flow effect.

The film theory, which is easy to understand and apply, is often criticized because it predicts that the rate of mass transfer is proportional to molecular diffusivity. This dependency is at odds with experimental data, which indicate a dependency of D_{AB}^n , where n ranges from 0.5 to 0.75. However, if D_{AB}/δ is replaced with k_c , which is then estimated from the Chilton–Colburn analogy (3-165), k_c is proportional to $D_{AB}^{2/3}$, which is in better agreement with experimental data. In effect, δ is not a constant but depends on D_{AB} (or N_{Sc}). Regardless

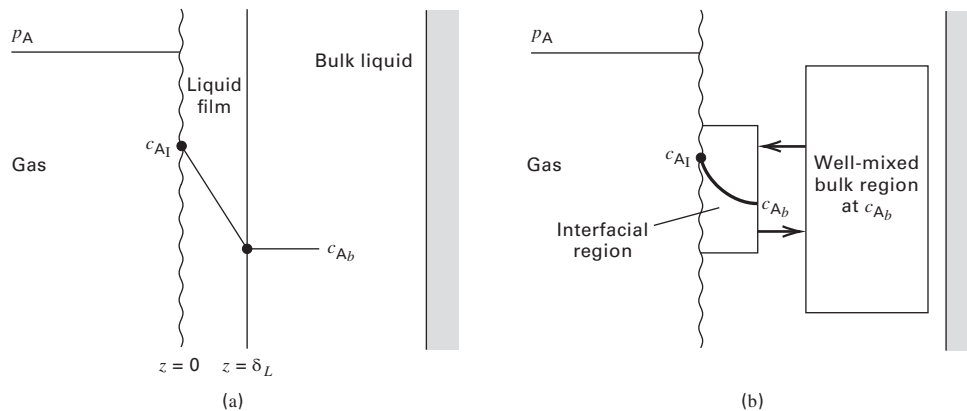


Figure 3.12 Theories for mass transfer from a fluid–fluid interface into a liquid: (a) film theory; (b) penetration and surface-renewal theories.

of whether the criticism is valid, film theory continues to be widely used in design of mass-transfer separation equipment.

EXAMPLE 3.15 Mass-Transfer Flux in a Packed Absorption Tower.

SO₂ is absorbed from air into water in a packed absorption tower. At a location in the tower, the mass-transfer flux is 0.0270 kmol SO₂/m²-h, and the liquid-phase mole fractions are 0.0025 and 0.0003, respectively, at the two-phase interface and in the bulk liquid. If the diffusivity of SO₂ in water is 1.7 × 10⁻⁵ cm²/s, determine the mass-transfer coefficient, k_c , and the corresponding film thickness, neglecting the bulk flow effect.

Solution

$$N_{\text{SO}_2} = \frac{(0.027)(1,000)}{(3,600)(100)^2} = 7.5 \times 10^{-7} \frac{\text{mol}}{\text{cm}^2\text{-s}}$$

For dilute conditions, the concentration of water is

$$c = \left(\frac{1}{18.02} \right) = 5.55 \times 10^{-2} \text{ mol/cm}^3$$

From (3-163),

$$\begin{aligned} k_c &= \frac{D_{AB}}{\delta} = \frac{N_A}{c(x_{A_i} - x_{A_b})} \\ &= \frac{7.5 \times 10^{-7}}{(5.55 \times 10^{-2})(0.0025 - 0.0003)} = 6.14 \times 10^{-3} \text{ cm/s} \end{aligned}$$

Therefore,

$$\delta = \frac{D_{AB}}{k_c} = \frac{1.7 \times 10^{-5}}{6.14 \times 10^{-3}} = 0.0028 \text{ cm}$$

which is small and typical of turbulent-flow processes.

§3.6.2 Penetration Theory

A more realistic mass-transfer model is provided by Higbie's penetration theory [54], shown schematically in Figure 3.12b. The stagnant-film concept is replaced by Boussinesq eddies that: (1) move from the bulk liquid to the interface; (2) stay at the interface for a short, fixed period of time during which they remain static, allowing molecular diffusion to take place in a direction normal to the interface; and (3) leave the interface to mix with the bulk stream. When an eddy moves to the interface, it replaces a static eddy. Thus, eddies are alternately static and moving. Turbulence extends to the interface.

In the penetration theory, unsteady-state diffusion takes place at the interface during the time the eddy is static. This process is governed by Fick's second law, (3-63), with boundary conditions

$$\begin{aligned} c_A &= c_{A_b} & \text{at } t &= 0 & \text{for } 0 \leq z \leq \infty; \\ c_A &= c_{A_i} & \text{at } z &= 0 & \text{for } t > 0; \text{ and} \\ c_A &= c_{A_b} & \text{at } z &= \infty & \text{for } t > 0 \end{aligned}$$

These are the same boundary conditions as in unsteady-state diffusion in a semi-infinite medium. The solution is a rearrangement of (3-66):

$$\frac{c_{A_i} - c_A}{c_{A_i} - c_{A_b}} = \text{erf} \left(\frac{z}{2\sqrt{D_{AB}t_c}} \right) \quad (3-166)$$

where t_c = "contact time" of the static eddy at the interface during one cycle. The corresponding average mass-transfer flux of A, in the absence of bulk flow, is given by the following form of (3-69):

$$N_A = 2\sqrt{\frac{D_{AB}}{\pi t_c}} (c_{A_i} - c_{A_b}) \quad (3-167)$$

or

$$N_A = k_c (c_{A_i} - c_{A_b}) \quad (3-168)$$

Thus, the penetration theory gives

$$k_c = 2\sqrt{\frac{D_{AB}}{\pi t_c}} \quad (3-169)$$

which predicts that k_c is proportional to the square root of the diffusivity, which is at the lower limit of experimental data.

Penetration theory is most useful for describing bubble, droplet, or random-packing interfaces. For bubbles, the contact time, t_c , of the liquid surrounding the bubble is approximated by the ratio of bubble diameter to its rise velocity. An air bubble of 0.4-cm diameter rises through water at a velocity of about 20 cm/s, making the estimated contact time 0.4/20 = 0.02 s. For a liquid spray, when no circulation of liquid occurs inside the droplets, contact time is the total time it takes the droplets to fall through the gas. For a packed tower, where the liquid flows as a film over random packing, mixing is assumed to occur each time the liquid film passes from one piece of packing to another. Resulting contact times are about 1 s. In the absence of any estimate for contact time, the mass-transfer coefficient is sometimes correlated by an empirical expression consistent with the 0.5 exponent on D_{AB} , as in (3-169), with the contact time replaced by a function of geometry and the liquid velocity, density, and viscosity.

EXAMPLE 3.16 Contact Time for Penetration Theory.

For the conditions of Example 3.15, estimate the contact time for Higbie's penetration theory.

Solution

From Example 3.15, $k_c = 6.14 \times 10^{-3}$ cm/s and $D_{AB} = 1.7 \times 10^{-5}$ cm²/s. From a rearrangement of (3-169),

$$t_c = \frac{4D_{AB}}{\pi k_c^2} = \frac{4(1.7 \times 10^{-5})}{3.14(6.14 \times 10^{-3})^2} = 0.57 \text{ s}$$

§3.6.3 Surface-Renewal Theory

Penetration theory assumes a constant contact time for all eddies that reach the surface. This may be unreasonable in some cases, especially for stirred tanks, contactors with random packings, and bubble and spray columns where bubbles and droplets cover a range of sizes. In 1951, Danckwerts [55] suggested an improvement to penetration theory that involves replacement of constant eddy contact time with the assumption of a residence-time distribution, wherein the probability of an eddy at the surface being replaced by a fresh eddy is independent of the age of the surface eddy.

Following Levenspiel's [56] treatment of residence-time distribution, let $F\{t\}$ be the fraction of eddies with a contact time of less than t . For $t = 0$, $F\{t\} = 0$, and $F\{t\}$ approaches 1 as t goes to infinity. A plot of $F\{t\}$ versus t , as shown in Figure 3.13, is a residence-time or age distribution. If $F\{t\}$ is differentiated with respect to t ,

$$\phi\{t\} = dF\{t\}/dt \quad (3-170)$$

where $\phi\{t\}dt$ is the probability that a given surface eddy will have a residence time t . The sum of probabilities is

$$\int_0^{\infty} \phi\{t\}dt = 1 \quad (3-171)$$

Typical plots of $F\{t\}$ and $\phi\{t\}$ are shown in Figure 3.13, where $\phi\{t\}$ is similar to a normal probability curve.

For steady-state flow into and out of a well-mixed vessel, Levenspiel shows that

$$F\{t\} = 1 - e^{-t/\bar{t}} \quad (3-172)$$

where \bar{t} is the average residence time. This function forms the basis, in reaction engineering, of the ideal model of a continuous, stirred-tank reactor (CSTR). Danckwerts selected the same model for his surface-renewal theory, using the corresponding $\phi\{t\}$ function:

$$\phi\{t\} = se^{-st} \quad (3-173)$$

where

$$s = 1/\bar{t} \quad (3-174)$$

is the fractional rate of surface renewal. As shown in Example 3.17 below, plots of (3-172) and (3-173) are much different from those in Figure 3.13.

The instantaneous mass-transfer rate for an eddy of age t is given by (3-167) for penetration theory in flux form as

$$N_{A_t} = 2\sqrt{\frac{D_{AB}}{\pi t}}(c_{A_I} - c_{A_b}) \quad (3-175)$$

The integrated average rate is

$$N_{A_{avg}} = \int_0^{\infty} \phi\{t\}N_{A_t}dt \quad (3-176)$$

Combining (3-173), (3-175), and (3-176) and integrating:

$$N_{A_{avg}} = \sqrt{D_{AB}s}(c_{A_I} - c_{A_b}) \quad (3-177)$$

Thus,

$$k_c = \sqrt{D_{AB}s} \quad (3-178)$$

Surface-renewal theory predicts the same dependency of the mass-transfer coefficient on diffusivity as penetration theory. Unfortunately, s , the fractional rate of surface renewal, is as elusive a parameter as constant contact time, t_c . Toor and Marchello [57] developed a film-penetration theory combining features of the film, penetration, and surface renewal theories.

EXAMPLE 3.17 Application of Surface-Renewal Theory.

For the conditions of Example 3.15, estimate the fractional rate of surface renewal, s , for Danckwerts' theory and determine residence time and probability distributions.

Solution

From Example 3.15,

$$k_c = 6.14 \times 10^{-3} \text{ cm/s} \quad \text{and} \quad D_{AB} = 1.7 \times 10^{-5} \text{ cm}^2/\text{s}$$

From (3-178),

$$s = \frac{k_c^2}{D_{AB}} = \frac{(6.14 \times 10^{-3})^2}{1.7 \times 10^{-5}} = 2.22 \text{ s}^{-1}$$

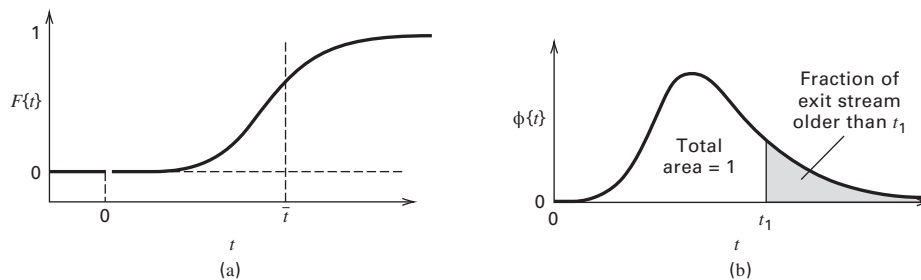


Figure 3.13 Residence-time distribution plots: (a) typical F curve; (b) typical age distribution.

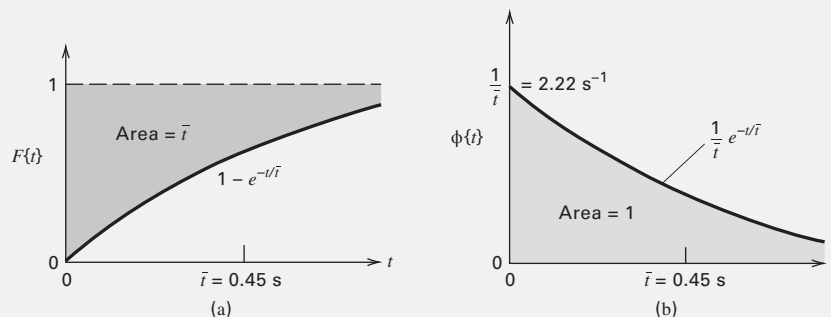


Figure 3.14 Age distribution curves for Example 3.17: (a) F curve; (b) $\phi\{t\}$ curve.

Thus, the average residence time of an eddy at the surface is $1/2.22 = 0.45$ s.

From (3-173),

$$\phi\{t\} = 2.22e^{-2.22t} \quad (1)$$

From (3-172), the residence-time distribution is

$$F\{t\} = 1 - e^{-t/0.45} \quad (2)$$

where t is in seconds. Equations (1) and (2) are plotted in Figure 3.14. These curves differ from the curves of Figure 3.13.

§3.7 TWO-FILM THEORY AND OVERALL MASS-TRANSFER COEFFICIENTS

Gas–liquid and liquid–liquid separation processes involve two fluid phases in contact and require consideration of mass-transfer resistances in both phases. In 1923, Whitman [58] suggested an extension of the film theory to two films in series. Each film presents a resistance to mass transfer, but concentrations in the two fluids at the interface are assumed to be in phase equilibrium. That is, there is no additional interfacial resistance to mass transfer.

The assumption of phase equilibrium at the interface, while widely used, may not be valid when gradients of interfacial tension are established during mass transfer. These gradients give rise to interfacial turbulence, resulting, most often, in considerably increased mass-transfer coefficients. This phenomenon, the **Marangoni effect**, is discussed in detail by Bird, Stewart, and Lightfoot [13], who cite additional references. The effect occurs at vapor–liquid and liquid–liquid interfaces, with the latter having received the most attention. By adding surfactants, which concentrate at the interface, the Marangoni effect is reduced because of interface stabilization, even to the extent that an interfacial mass-transfer resistance (which causes the mass-transfer coefficient to be reduced) results. Unless otherwise indicated, the Marangoni effect is ignored here, and phase equilibrium is assumed at the phase interface.

§3.7.1 Gas (Vapor)–Liquid Systems

Consider steady-state mass transfer of A from a gas of A and B, across an interface, I, and into a liquid containing A and B. It is postulated, as shown in Figure 3.15a, that a thin gas film exists on one side of the interface and a thin liquid film exists on the other side, with a diffusion resistance in each film. In terms of film thicknesses and concentration driving forces, the rate of mass transfer of A is given by:

$$N_A = \frac{(D_{AB})_G}{\delta_G} (c_{A_b} - c_{A_1})_G = \frac{(D_{AB})_L}{\delta_L} (c_{A_1} - c_{A_b})_L \quad (3-179)$$

Alternatively and preferably, the rate of mass transfer can be expressed in terms of mass-transfer coefficients determined from any suitable theory, with the driving-force gradients visualized more realistically as in Figure 3.15b. Any number of different combinations of mass-transfer coefficients and driving forces are used. For the gas phase, under dilute or equimolar counter diffusion (EMD) conditions, the mass-transfer rate in terms of partial pressures is:

$$N_A = k_p (p_{A_b} - p_{A_1}) \quad (3-180)$$

where k_p is a gas-phase mass-transfer coefficient based on a partial-pressure driving force.

For the liquid phase, with molar concentrations:

$$N_A = k_c (c_{A_1} - c_{A_b}) \quad (3-181)$$

At the interface, c_{A_1} and p_{A_1} are in equilibrium. Applying a version of Henry's law,¹

$$c_{A_1} = H_A p_{A_1} \quad (3-182)$$

¹Different forms of Henry's law are found in the literature. They include

$$p_A = H_A x_A, \quad p_A = c_A/H_A, \quad \text{and} \quad y_A = H_A x_A$$

When a Henry's law constant, H_A , is given without citing the defining equation, the equation can be determined from the units of the constant. For example, if the constant has the units of atm or atm/mole fraction, Henry's law is $p_A = H_A x_A$. If the units are mol/L–mmHg, Henry's law is $p_A = c_A/H_A$.

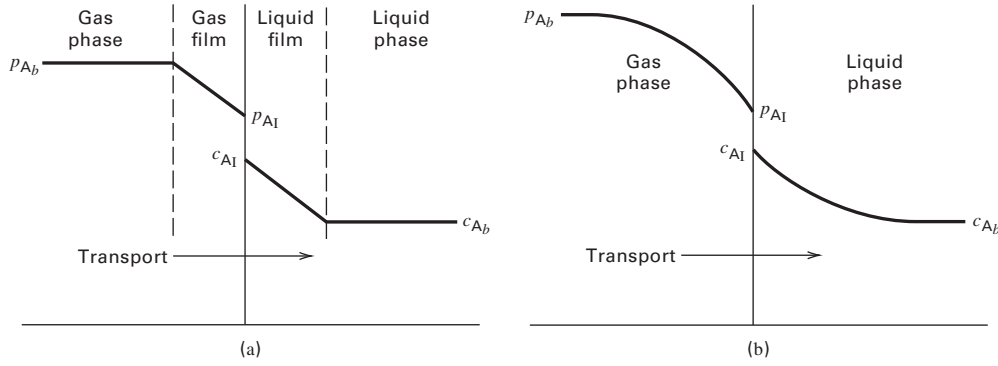


Figure 3.15 Concentration gradients for two-resistance theory: (a) film theory; (b) more realistic gradients.

Equations (3-180) to (3-182) are commonly used combinations for vapor–liquid mass transfer.

Computations of mass-transfer rates are made using bulk concentrations c_{A_b} and p_{A_b} . To obtain an expression for N_A in terms of an overall driving force for mass transfer that includes both fluid phases, (3-180) to (3-182) are combined to eliminate the interfacial compositions, c_{A_i} and p_{A_i} . Solving (3-180) for p_{A_i}

$$p_{A_i} = p_{A_b} - \frac{N_A}{k_p} \quad (3-183)$$

Solving (3-181) for c_{A_i} :

$$c_{A_i} = c_{A_b} + \frac{N_A}{k_c} \quad (3-184)$$

Combining (3-184) with (3-182) to eliminate c_{A_i} and combining the result with (3-183) to eliminate p_{A_i} gives

$$N_A = \frac{p_{A_b} H_A - c_{A_b}}{(H_A/k_p) + (1/k_c)} \quad (3-185)$$

Overall Mass-Transfer Coefficients. It is customary to define: (1) a liquid-phase concentration $c_A^* = p_{A_b}/H_A$, which is a fictitious liquid concentration of A in equilibrium with the partial pressure of A in the bulk gas; and (2) an overall mass-transfer coefficient, K_L . Now (3-185) becomes:

$$N_A = K_L (c_A^* - c_{A_b}) = \frac{(c_A^* - c_{A_b})}{(H_A/k_p) + (1/k_c)} \quad (3-186)$$

where K_L is the **overall mass-transfer coefficient** based on the liquid phase and defined by

$$\frac{1}{K_L} = \frac{H_A}{k_p} + \frac{1}{k_c} \quad (3-187)$$

The corresponding overall driving force for mass transfer is also based on the liquid phase, given by $(c_A^* - c_{A_b})$. The quantities H_A/k_p and $1/k_c$ are measures of gas and liquid

mass-transfer resistances. When $1/k_c \gg H_A/k_p$, the resistance of the gas phase is negligible and the rate of mass transfer is controlled by the liquid phase, with (3-186) simplifying to

$$N_A = k_c (c_A^* - c_{A_b}) \quad (3-188)$$

so that $K_L \approx k_c$. Because resistance in the gas phase is negligible, the gas-phase driving force becomes $(p_{A_b} - p_{A_i}) \approx 0$, so $p_{A_b} \approx p_{A_i}$.

Alternatively, (3-180) to (3-182) combine to define an overall mass-transfer coefficient, K_G , based on the gas phase:

$$N_A = \frac{p_{A_b} - c_{A_b}/H_A}{(1/k_p) + (1/H_A k_c)} \quad (3-189)$$

In this case, it is customary to define: (1) a gas-phase partial pressure $p_A^* = c_{A_b}/H_A$, which is a fictitious partial pressure of A that would be in equilibrium with the concentration of A in the bulk liquid; and (2) an overall mass-transfer coefficient for the gas phase, K_G , based on a partial-pressure driving force. Thus, (3-189) becomes

$$N_A = K_G (p_{A_b} - p_A^*) = \frac{(p_{A_b} - p_A^*)}{(1/k_p) + (1/H_A k_c)} \quad (3-190)$$

where

$$\frac{1}{K_G} = \frac{1}{k_p} + \frac{1}{H_A k_c} \quad (3-191)$$

Now the mass-transfer resistances are $1/k_p$ and $1/H_A k_c$. If $1/k_p \gg 1/H_A k_c$,

$$N_A = k_p (p_{A_b} - p_A^*) \quad (3-192)$$

so $K_G \approx k_p$. Since the resistance in the liquid phase is then negligible, the liquid-phase driving force becomes $(c_{A_i} - c_{A_b}) \approx 0$, so $c_{A_i} \approx c_{A_b}$.

The choice between (3-186) and (3-190) is arbitrary, but is usually made on the basis of which phase has the largest mass-transfer resistance. If it is the liquid, (3-186) is used. If it is the gas, (3-190) is used. If neither is dominant, either equation is suitable.

Another common combination for two-film, vapor–liquid mass transfer uses mole-fraction driving forces, which define another set of mass-transfer coefficients k_y and k_x :

$$N_A = k_y(y_{A_b} - y_{A_i}) = k_x(x_{A_i} - x_{A_b}) \quad (3-193)$$

Equilibrium at the interface can now be expressed in terms of a K -value for vapor–liquid equilibrium instead of as a Henry's law constant. Thus,

$$K_A = y_{A_i}/x_{A_i} \quad (3-194)$$

Combining (3-193) and (3-194) to eliminate y_{A_i} and x_{A_i} ,

$$N_A = \frac{y_{A_b} - x_{A_b}}{(1/K_A k_y) + (1/k_x)} \quad (3-195)$$

Alternatively, fictitious concentrations and overall mass-transfer coefficients can be used with mole-fraction driving forces. Thus, $x_A^* = y_{A_b}/K_A$ and $y_A^* = K_A x_{A_b}$. If the two values of K_A are equal,

$$N_A = K_x(x_A^* - x_{A_b}) = \frac{x_A^* - x_{A_b}}{(1/K_A k_y) + (1/k_x)} \quad (3-196)$$

and

$$N_A = K_y(y_{A_b} - y_A^*) = \frac{y_{A_b} - y_A^*}{(1/k_y) + (K_A/k_x)} \quad (3-197)$$

where K_x and K_y are overall mass-transfer coefficients based on mole-fraction driving forces with

$$\frac{1}{K_x} = \frac{1}{K_A k_y} + \frac{1}{k_x} \quad (3-198)$$

and

$$\frac{1}{K_y} = \frac{1}{k_y} + \frac{K_A}{k_x} \quad (3-199)$$

When using handbook or literature correlations to estimate mass-transfer coefficients, it is important to determine which coefficient (k_p , k_c , k_y , or k_x) is correlated, because often it is not stated. This can be done by checking the units or the form of the Sherwood or Stanton numbers. Coefficients correlated by the Chilton–Colburn analogy are k_c for either liquid or gas phases. The various coefficients are related by the following expressions, which are summarized in Table 3.12.

Liquid phase:

$$k_x = k_c c = k_c \left(\frac{\rho_L}{M} \right) \quad (3-200)$$

Ideal-gas phase:

$$k_y = k_p P = (k_c)_g \frac{P}{RT} = (k_c)_g c = (k_c)_g \left(\frac{\rho_G}{M} \right) \quad (3-201)$$

Typical units are

	SI	AE
k_c	m/s	ft/h
k_p	kmol/s-m ² -kPa	lbmol/h-ft ² -atm
k_y, k_x	kmol/s-m ²	lbmol/h-ft ²

Table 3.12 Relationships among Mass-Transfer Coefficients

Equimolar counter diffusion (EMD):

$$\begin{aligned} \text{Gases: } N_A &= k_y \Delta y_A = k_c \Delta c_A = k_p \Delta p_A \\ k_y &= k_c \frac{P}{RT} = k_p P \text{ if ideal gas} \end{aligned}$$

$$\begin{aligned} \text{Liquids: } N_A &= k_x \Delta x_A = k_c \Delta c_A \\ k_x &= k_c c, \text{ where } c = \text{total molar concentration (A + B)} \end{aligned}$$

Unimolecular diffusion (UMD) with bulk flow:

$$\begin{aligned} \text{Gases: } & \text{Same equations as for EMD with } k \text{ replaced} \\ & \text{by } k' = \frac{k}{(y_B)_{LM}} \end{aligned}$$

$$\begin{aligned} \text{Liquids: } & \text{Same equations as for EMD with } k \\ & \text{replaced by } k' = \frac{k}{(x_B)_{LM}} \end{aligned}$$

When working with concentration units, it is convenient to use:

$$k_G(\Delta c_G) = k_c(\Delta c) \text{ for the gas phase}$$

$$k_L(\Delta c_L) = k_c(\Delta c) \text{ for the liquid phase}$$

When unimolecular diffusion (UMD) occurs under non-dilute conditions, bulk flow must be included. For binary mixtures, this is done by defining modified mass-transfer coefficients, designated with a prime, where the subscript on k depends on the selected driving force for mass transfer.

For the liquid phase, using subscripted k_c or k_x ,

$$k' = \frac{k}{(1 - x_A)_{LM}} = \frac{k}{(x_B)_{LM}} \quad (3-202)$$

For the gas phase, using subscripted k_p , k_y , or k_c ,

$$k' = \frac{k}{(1 - y_A)_{LM}} = \frac{k}{(y_B)_{LM}} \quad (3-203)$$

Expressions for k' are convenient when the mass-transfer rate is controlled mainly by one of the two resistances. Literature mass-transfer coefficient data are generally correlated in terms of k rather than k' . Mass-transfer coefficients estimated from the Chilton–Colburn analogy [e.g., equations (3-148) to (3-153)] are k_c , not k'_c .

§3.7.2 Liquid–Liquid Systems

For mass transfer across two liquid phases, equilibrium is again assumed at the interface. Denoting the two phases by $L^{(1)}$ and $L^{(2)}$, (3-196) and (3-197) become

$$N_A = K_x^{(2)}(x_A^{(2)*} - x_{A_b}^{(2)}) = \frac{x_A^{(2)*} - x_{A_b}^{(2)}}{(1/K_{D_A} k_x^{(1)}) + (1/k_x^{(2)})} \quad (3-204)$$

and

$$N_A = K_x^{(1)}(x_{A_b}^{(1)} - x_A^{(1)*}) = \frac{x_{A_b}^{(1)} - x_A^{(1)*}}{(1/k_x^{(1)}) + (K_{D_A}/k_x^{(2)})} \quad (3-205)$$

where

$$K_{D_A} = \frac{x_{A_I}^{(1)}}{x_{A_I}^{(2)}} \quad (3-206)$$

§3.7.3 Case of Large Driving Forces for Mass Transfer

Previously, phase equilibria ratios such as H_A , K_A , and K_{D_A} have been assumed constant across the two phases. When large driving forces exist, the ratios may not be constant. This commonly occurs when one or both phases are not dilute with respect to the solute, A, in which case, expressions for the mass-transfer flux must be revised. For mole-fraction driving forces, from (3-193) and (3-197),

$$N_A = k_y(y_{A_b} - y_{A_I}) = K_y(y_{A_b} - y_A^*) \quad (3-207)$$

Thus,

$$\frac{1}{K_y} = \frac{y_{A_b} - y_A^*}{k_y(y_{A_b} - y_{A_I})} \quad (3-208)$$

or

$$\frac{1}{K_y} = \frac{(y_{A_b} - y_{A_I}) + (y_{A_I} - y_A^*)}{k_y(y_{A_b} - y_{A_I})} = \frac{1}{k_y} + \frac{1}{k_y} \left(\frac{y_{A_I} - y_A^*}{y_{A_b} - y_{A_I}} \right) \quad (3-209)$$

From (3-193),

$$\frac{k_x}{k_y} = \left(\frac{y_{A_b} - y_{A_I}}{x_{A_I} - x_{A_b}} \right) \quad (3-210)$$

Combining (3-207) and (3-210),

$$\frac{1}{K_y} = \frac{1}{k_y} + \frac{1}{k_x} \left(\frac{y_{A_I} - y_A^*}{x_{A_I} - x_{A_b}} \right) \quad (3-211)$$

Similarly

$$\frac{1}{K_x} = \frac{1}{k_x} + \frac{1}{k_y} \left(\frac{x_A^* - x_{A_I}}{y_{A_b} - y_{A_I}} \right) \quad (3-212)$$

Figure 3.16 shows a curved equilibrium line with values of y_{A_b} , y_{A_I} , y_A^* , x_A^* , x_{A_I} , and x_{A_b} . Because the line is curved, the vapor–liquid equilibrium ratio, $K_A = y_A/x_A$, is not constant. As shown, the slope of the curve and thus, K_A , decrease with increasing concentration of A. Denoting two slopes of the equilibrium curve by

$$m_x = \left(\frac{y_{A_I} - y_A^*}{x_{A_I} - x_{A_b}} \right) \quad (3-213)$$

and

$$m_y = \left(\frac{y_{A_b} - y_{A_I}}{x_A^* - x_{A_I}} \right) \quad (3-214)$$

Substituting (3-213) and (3-214) into (3-211) and (3-212), respectively, gives

$$\frac{1}{K_y} = \frac{1}{k_y} + \frac{m_x}{k_x} \quad (3-215)$$

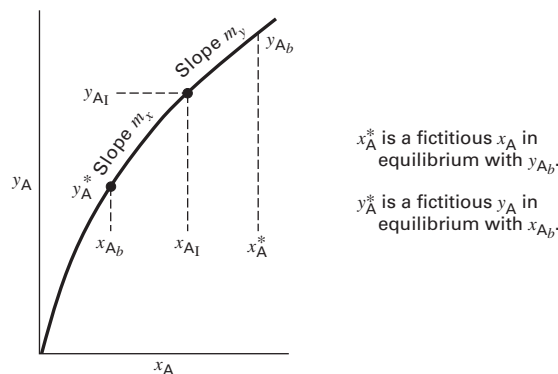


Figure 3.16 Curved equilibrium line.

and

$$\frac{1}{K_x} = \frac{1}{k_x} + \frac{1}{m_y k_y} \quad (3-216)$$

EXAMPLE 3.18 Absorption of SO₂ into Water.

Sulfur dioxide (A) in air is absorbed into water in a packed column, where bulk conditions are 50°C, 2 atm, $y_{A_b} = 0.085$, and $x_{A_b} = 0.001$. Equilibrium data for SO₂ between air and water at 50°C are

p_{SO_2} , atm	c_{SO_2} , lbmol/ft ³
0.0382	0.00193
0.0606	0.00290
0.1092	0.00483
0.1700	0.00676

Experimental values of the mass-transfer coefficients are:

Liquid phase: $k_c = 0.18$ m/h

Gas phase: $k_p = 0.040 \frac{\text{kmol}}{\text{h}\cdot\text{m}^2\cdot\text{kPa}}$

Using mole-fraction driving forces, compute the mass-transfer flux: (a) assuming an average Henry's law constant and a negligible bulk-flow effect; (b) utilizing the actual curved equilibrium line and assuming a negligible bulk-flow effect; (c) utilizing the actual curved equilibrium line and taking into account the bulk-flow effect. In addition, (d) determine the magnitude of the gas and liquid resistances and the values of the mole fractions at the interface that result from part (c).

Solution

Equilibrium data are converted to mole fractions by assuming Dalton's law, $y_A = p_A/P$, for the gas and $x_A = c_A/c$ for the liquid. The concentration of liquid is close to that of water, 3.43 lbmol/ft³ or 55.0 kmol/m³. Thus, the mole fractions at equilibrium are:

y_{SO_2}	x_{SO_2}
0.0191	0.000563
0.0303	0.000846
0.0546	0.001408
0.0850	0.001971

These data are fitted with average and maximum absolute deviations of 0.91% and 1.16%, respectively, by the equation

$$y_{\text{SO}_2} = 29.74x_{\text{SO}_2} + 6,733x_{\text{SO}_2}^2 \quad (1)$$

Differentiating, the slope of the equilibrium curve:

$$m = \frac{dy}{dx} = 29.74 + 13,466x_{\text{SO}_2} \quad (2)$$

The given mass-transfer coefficients are converted to k_x and k_y by (3-200) and (3-201):

$$k_x = k_c c = 0.18(55.0) = 9.9 \frac{\text{kmol}}{\text{h}\cdot\text{m}^2}$$

$$k_y = k_p P = 0.040(2)(101.3) = 8.1 \frac{\text{kmol}}{\text{h}\cdot\text{m}^2}$$

(a) From (1) for $x_{A_b} = 0.001$, $y_{A^*} = 29.74(0.001) + 6,733(0.001)^2 = 0.0365$.

From (1) for $y_{A_b} = 0.085$, solving the quadratic equation yields $x_{A^*} = 0.001975$.

The average slope in this range is

$$m = \frac{0.085 - 0.0365}{0.001975 - 0.001} = 49.7$$

Examination of (3-215) and (3-216) shows that the liquid-phase resistance is controlling because the term in k_x is much larger than the term in k_y . Therefore, from (3-216), using $m = m_x$,

$$\frac{1}{K_x} = \frac{1}{9.9} + \frac{1}{49.7(8.1)} = 0.1010 + 0.0025 = 0.1035$$

or $K_x = 9.66 \frac{\text{kmol}}{\text{h}\cdot\text{m}^2}$

From (3-196),

$$N_A = 9.66(0.001975 - 0.001) = 0.00942 \frac{\text{kmol}}{\text{h}\cdot\text{m}^2}$$

(b) From part (a), the gas-phase resistance is almost negligible. Therefore, $y_{A_1} \approx y_{A_b}$ and $x_{A_1} \approx x_{A^*}$.

From (3-214), the slope m_y is taken at the point $y_{A_b} = 0.085$ and $x_{A^*} = 0.001975$ on the equilibrium line.

By (2), $m_y = 29.74 + 13,466(0.001975) = 56.3$. From (3-216),

$$K_x = \frac{1}{(1/9.9) + \{1/[(56.3)(8.1)]\}} = 9.69 \frac{\text{kmol}}{\text{h}\cdot\text{m}^2}$$

giving $N_A = 0.00945 \text{ kmol/h}\cdot\text{m}^2$. This is a small change from part (a).

(c) Correcting for bulk flow, from the results of parts (a) and (b),

$$y_{A_b} = 0.085, y_{A_1} = 0.085, x_{A_1} = 0.001975, x_{A_b} = 0.001, \\ y_{B_{LM}} = 1.0 - 0.085 = 0.915 \quad \text{and} \quad x_{B_{LM}} \approx 0.9986$$

From (3-202),

$$k'_x = \frac{9.9}{0.9986} = 9.9 \frac{\text{kmol}}{\text{h}\cdot\text{m}^2} \quad \text{and} \quad k'_y = \frac{8.1}{0.915} = 8.85 \frac{\text{kmol}}{\text{h}\cdot\text{m}^2}$$

From (3-216),

$$K_x = \frac{1}{(1/9.9) + \{1/[(56.3)(8.85)]\}} = 9.71 \frac{\text{kmol}}{\text{h}\cdot\text{m}^2}$$

From (3-196),

$$N_A = 9.71(0.001975 - 0.001) = 0.00945 \frac{\text{kmol}}{\text{h}\cdot\text{m}^2}$$

which is only a very slight change from parts (a) and (b), where the bulk-flow effect was ignored. The effect is very small because it is important only in the gas, whereas the liquid resistance is controlling.

(d) The relative magnitude of the two mass-transfer resistances is

$$\frac{1/m_y k'_y}{1/k'_x} = \frac{1/[(56/3)(8.85)]}{1/9.9} = 0.02$$

Thus, the gas-phase resistance is only 2% of the liquid-phase resistance. The interface vapor mole fraction can be obtained from (3-207), after accounting for the bulk-flow effect:

$$y_{A_1} = y_{A_b} - \frac{N_A}{k'_y} = 0.085 - \frac{0.00947}{8.85} = 0.084$$

Similarly,

$$x_{A_1} = \frac{N_A}{k'_x} + x_{A_b} = \frac{0.00947}{9.9} + 0.001 = 0.00196$$

CHAPTER 3 NOMENCLATURE

Abbreviations and Acronyms

EMD	equimolar counter diffusion, §3.1.3
UMD	unimolecular diffusion, §3.1.4
LM	log mean, (3-34)

Latin Symbols

A	area for transport
D_{AB}	diffusivity of A in B, (3-3)
$F\{t\}$	fraction of eddies with contact time $< t$, Figure 3.13
h	heat-transfer coefficient, (3-86)
J	molar flux by ordinary molecular diffusion, (3-3)
j	mass flux relative to mass-average velocity of the mixture, (3-5)
j_D	Chilton–Colburn j -factor for mass transfer, (3-147)
j_H	Chilton–Colburn j -factor for heat transfer, (3-147)
j_M	Chilton–Colburn j -factor for momentum transfer, (3-147)
k	thermal conductivity, (3-2)
k_c, k_p, k_x, k_y	mass-transfer coefficient for different driving forces, (3-200) and (3-201)
L_e	entry length, (3-121)
N_{AV}	Avogadro's number, (3-38)

N_i	total molar mass-transfer flux of component i , (3-1)
n_i	molar rate of mass transfer of component i , (3-12)
Q	rate of heat transfer, (3-86)
q	heat flux, (3-2)
r	inside radius from axis of a tube, (3-122)
S_i	solubility of component i , (3-48)
t_c	contact time of an eddy at an interface, (3-166)
v_i	component velocity relative to stationary coordinates, (3-7)
v_{iD}	difference between species velocity and mixture velocity, (3-9)
v_M	molar-average mixture velocity, (3-6)
W	unit width of liquid film, (3-85)
w	component mass fraction, (3-5)

Non-Latin Symbols

Δ	difference
δ	velocity film thickness, (3-71)
δ_c	concentration film thickness, (3-117)

SUMMARY

1. Mass transfer is the net movement of a species in a mixture from one region to a region of different concentration, often between two phases across an interface. Mass transfer occurs by molecular diffusion, eddy diffusion, and bulk flow. Molecular diffusion occurs by a number of different driving forces, including composition (ordinary), pressure, temperature, and external force fields.
2. Fick's first law for steady-state diffusion states that the mass-transfer flux by ordinary molecular diffusion is equal to the product of the diffusion coefficient (diffusivity) and the concentration gradient.
3. Two limiting cases of mass transfer in a binary mixture are equimolar counter diffusion (EMD) and unimolecular diffusion (UMD). The former is a good approximation for distillation. The latter includes bulk-flow effects.
4. When data are unavailable, diffusivities (diffusion coefficients) in gases and liquids can be estimated. Diffusivities in solids are best measured. For some solids, e.g., wood, diffusivity is anisotropic.
5. Diffusivities vary by orders of magnitude. Typical values are 0.10, 1×10^{-5} , and 1×10^{-9} cm²/s for ordinary molecular diffusion of solutes in a gas, liquid, and an amorphous solid, respectively.
6. Fick's second law for unsteady-state diffusion is readily applied to semi-infinite and finite stagnant media, including anisotropic materials.
7. Molecular diffusion under laminar-flow conditions is determined from Fick's first and second laws, provided

$\varepsilon_D, \varepsilon_H, \varepsilon_M$	eddy diffusivities for mass, heat, and momentum transfer, respectively, (3-136)–(3-138)
\mathcal{N}_A	moles, (3-69)
τ	shear stress (3-125)
Γ	liquid film flow rate per width of film flow, (3-75)
θ	dimensionless, fractional change in u , T , or c , (3-142)

Subscripts

avg	average
b	bulk average, §3.6.1
I	interface, Figure 3.12
LP	low pressure, Figure 3.3
t	turbulent contribution (3-133)
w	wall (3-108)

Superscripts

-	average
---	---------

8. Mass transfer in turbulent flow can be predicted by analogy to heat transfer. The Chilton–Colburn analogy utilizes empirical j -factor correlations with a Stanton number for mass transfer. A more accurate equation by Churchill and Zajic should be used for flow in tubes, particularly at high Reynolds numbers.
9. Models are available for mass transfer near a two-fluid interface. These include film theory, penetration theory, and surface-renewal theory. These predict mass-transfer coefficients proportional to the diffusivity raised to an exponent that varies from 0.5 to 1.0. Most experimental data provide exponents ranging from 0.5 to 0.75.
10. Whitman's two-film theory is widely used to predict the mass-transfer flux from one fluid, across an interface, and into another fluid, assuming phase equilibrium at the interface. One resistance is often controlling. The theory defines an overall mass-transfer coefficient determined from the separate coefficients for each of the phases and the equilibrium relationship at the interface.

REFERENCES

1. TAYLOR, R., and R. KRISHNA, *Multicomponent Mass Transfer*, John Wiley & Sons, New York (1993).
2. POLING, B.E., J.M. PRAUSNITZ, and J.P. O'CONNELL, *The Properties of Liquids and Gases*, 5th ed., McGraw-Hill, New York (2001).
3. FULLER, E.N., P.D. SCHETTLER, and J.C. GIDDINGS, *Ind. Eng. Chem.*, **58**(5), 18–27 (1966).
4. TAKAHASHI, S., *J. Chem. Eng. Jpn.*, **7**, 417–420 (1974).
5. SLATTERY, J.C., *M.S. thesis*, University of Wisconsin, Madison (1955).
6. WILKE, C.R., and P. CHANG, *AIChE J.*, **1**, 264–270 (1955).
7. HAYDUK, W., and B.S. MINHAS, *Can. J. Chem. Eng.*, **60**, 295–299 (1982).
8. QUAYLE, O.R., *Chem. Rev.*, **53**, 439–589 (1953).
9. VIGNES, A., *Ind. Eng. Chem. Fundam.*, **5**, 189–199 (1966).
10. CARSLAW, H.S., and J.C. JAEGER, *Heat Conduction in Solids*, 2nd ed., Oxford University Press, London (1959).
11. CRANK, J., *The Mathematics of Diffusion*, Oxford University Press, London (1956).
12. NEWMAN, A.B., *Trans. AIChE*, **27**, 310–333 (1931).
13. BIRD, R.B., W.E. STEWART, and E.N. LIGHTFOOT, *Transport Phenomena*, 2nd ed., John Wiley & Sons, New York (2002).
14. CHURCHILL, R.V., *Operational Mathematics*, 2nd ed., McGraw-Hill, New York (1958).
15. Abramowitz, M., and I.A. Stegun, Eds., *Handbook of Mathematical Functions*, National Bureau of Standards, Applied Mathematics Series 55, Washington, DC (1964).
16. GRIMLEY, S.S., *Trans. Inst. Chem. Eng. (London)*, **23**, 228–235 (1948).
17. JOHNSTONE, H.F., and R.L. PIGFORD, *Trans. AIChE*, **38**, 25–51 (1942).
18. OLBRICH, W.E., and J.D. WILD, *Chem. Eng. Sci.*, **24**, 25–32 (1969).
19. CHURCHILL, S.W., *The Interpretation and Use of Rate Data: The Rate Concept*, McGraw-Hill, New York (1974).
20. CHURCHILL, S.W., and R. USAGI, *AIChE J.*, **18**, 1121–1128 (1972).
21. EMMERT, R.E., and R.L. PIGFORD, *Chem. Eng. Prog.*, **50**, 87–93 (1954).
22. PRANDTL, L., *Proc. 3rd Int. Math. Congress, Heidelberg* (1904); reprinted in *NACA Tech. Memo 452* (1928).
23. BLASIUS, H., *Z. Math Phys.*, **56**, 1–37 (1908); reprinted in *NACA Tech. Memo 1256* (1950).
24. SCHLICHTING, H., *Boundary Layer Theory*, 4th ed., McGraw-Hill, New York (1960).
25. POHLHAUSEN, E., *Z. Angew. Math Mech.*, **1**, 252 (1921).
26. POHLHAUSEN, E., *Z. Angew. Math Mech.*, **1**, 115–121 (1921).
27. LANGHAAR, H.L., *Trans. ASME*, **64**, A–55 (1942).
28. GRAETZ, L., *Ann. d. Physik*, **25**, 337–357 (1885).
29. SELLARS, J.R., M. TRIBUS, and J.S. KLEIN, *Trans. ASME*, **78**, 441–448 (1956).
30. LEVEQUE, J., *Ann. Mines*, [12], **13**, 201, 305, 381 (1928).
31. KNUDSEN, J.G., and D.L. KATZ, *Fluid Dynamics and Heat Transfer*, McGraw-Hill, New York (1958).
32. HAUSEN, H., *Verfahrenstechnik Beih. z. Ver. Deut. Ing.*, **4**, 91 (1943).
33. LINTON, W.H., Jr., and T.K. SHERWOOD, *Chem. Eng. Prog.*, **46**, 258–264 (1950).
34. REYNOLDS, O., *Trans. Roy. Soc. (London)*, **174A**, 935–982 (1883).
35. BOUSSINESQ, J., *Mem. Pre. Par. Div. Sav.*, XXIII, Paris (1877).
36. PRANDTL, L., *Z. Angew. Math Mech.*, **5**, 136 (1925); reprinted in *NACA Tech. Memo 1231* (1949).
37. REYNOLDS, O., *Proc. Manchester Lit. Phil. Soc.*, **14**, 7 (1874).
38. COLBURN, A.P., *Trans. AIChE*, **29**, 174–210 (1933).
39. CHILTON, T.H., and A.P. COLBURN, *Ind. Eng. Chem.*, **26**, 1183–1187 (1934).
40. PRANDTL, L., *Physik. Z.*, **11**, 1072 (1910).
41. VAN DRIEST, E.R., *J. Aero Sci.*, 1007–1011, 1036 (1956).
42. REICHARDT, H., *Fundamentals of Turbulent Heat Transfer; NACA Report TM-1408* (1957).
43. FRIEND, W.L., and A.B. METZNER, *AIChE J.*, **4**, 393–402 (1958).
44. DREW, T.B., E.C. KOO, and W.H. MCADAMS, *Trans. Am. Inst. Chem. Engrs.*, **28**, 56 (1933).
45. NIKURADSE, J., *VDI-Forschungsheft*, p. 361 (1933).
46. LAUNDER, B.E., and D.B. SPALDING, *Lectures in Mathematical Models of Turbulence*, Academic Press, New York (1972).
47. HENG, L., C. CHAN, and S.W. CHURCHILL, *Chem. Eng. J.*, **71**, 163 (1998).
48. CHURCHILL, S.W., and S.C. ZAJIC, *AIChE J.*, **48**, 927–940 (2002).
49. CHURCHILL, S.W., “Turbulent Flow and Convection: The Prediction of Turbulent Flow and Convection in a Round Tube,” in J.P. Hartnett and T.F. Irvine, Jr., Ser. Eds., *Advances in Heat Transfer*, Academic Press, New York, Vol. 34, pp. 255–361 (2001).
50. YU, B., H. OZOE, and S.W. CHURCHILL, *Chem. Eng. Sci.*, **56**, 1781 (2001).
51. CHURCHILL, S.W., and C. CHAN, *Ind. Eng. Chem. Res.*, **34**, 1332 (1995).
52. CHURCHILL, S.W., *AIChE J.*, **43**, 1125 (1997).
53. NERNST, W., *Z. Phys. Chem.*, **47**, 52 (1904).
54. HIGBIE, R., *Trans. AIChE*, **31**, 365–389 (1935).
55. DANCKWERTS, P.V., *Ind. Eng. Chem.*, **43**, 1460–1467 (1951).
56. LEVENSPIEL, O., *Chemical Reaction Engineering*, 3rd ed., John Wiley & Sons, New York (1999).
57. TOOR, H.L., and J.M. MARCHELLO, *AIChE J.*, **4**, 97–101 (1958).
58. WHITMAN, W.G., *Chem. Met. Eng.*, **29**, 146–148 (1923).
59. MARRERO, T. R., and E. A. MASON, *J. Phys. Chem. Ref. Data*, **1**, 1–118 (1972).

STUDY QUESTIONS

- 3.1. What is meant by diffusion?
- 3.2. Molecular diffusion occurs by any of four driving forces or potentials? Which one is the most common?
- 3.3. What is the bulk-flow effect in mass transfer?
- 3.4. How does Fick's law of diffusion compare to Fourier's law of heat conduction?
- 3.5. What is the difference between equimolar counter diffusion (EMD) and unimolecular diffusion (UMD)?

- 3.6. What is the difference between a mutual diffusion coefficient and a self-diffusion coefficient?
- 3.7. At low pressures, what are the effects of temperature and pressure on the molecular diffusivity of a species in a binary gas mixture?
- 3.8. What is the order of magnitude of molecular diffusivity in cm^2/s for a species in a liquid mixture? By how many orders of magnitude is diffusion in a liquid slower or faster than diffusion in a gas?
- 3.9. By what mechanisms does diffusion occur in porous solids?
- 3.10. What is the effective diffusivity?
- 3.11. Molecular diffusion in gases, liquids, and amorphous solids ranges from slow to extremely slow. What is the best way to increase rate of mass transfer in fluids?
- 3.12. What is the best way to increase the rate of mass transfer in solids?
- 3.13. What is the defining equation for a mass-transfer coefficient? How does it differ from Fick's law?
- 3.14. How is the mass-transfer coefficient analogous to the heat-transfer coefficient?
- 3.15. For laminar flow, can expressions for the mass-transfer coefficient be determined from theory using Fick's law? If so, how?
- 3.16. What is the difference between the Reynolds analogy and the Chilton–Colburn analogy? Which is more useful? Why?
- 3.17. For mass transfer across a phase interface, what is the difference between the film, penetration, and surface-renewal theories, particularly with respect to their dependence on diffusivity?
- 3.18. What is the two-film theory of Whitman? Is equilibrium assumed to exist at the interface of two phases?

EXERCISES

Section 3.1

3.1. Evaporation of liquid from a beaker.

A beaker filled with an equimolar liquid mixture of ethyl alcohol and ethyl acetate evaporates at 0°C into still air at 101 kPa (1 atm). Assuming Raoult's law, what is the liquid composition when half of the ethyl alcohol has evaporated, assuming each component evaporates independently? Also assume that the liquid is always well mixed. The following data are available:

	Vapor Pressure, kPa at 0°C	Diffusivity in Air, m^2/s
Ethyl acetate (AC)	3.23	6.45×10^{-6}
Ethyl alcohol (AL)	1.62	9.29×10^{-6}

3.2. Evaporation of benzene from an open tank.

An open tank, 10 ft in diameter, containing benzene at 25°C is exposed to air. Above the liquid surface is a stagnant air film 0.2 inch thick. If the pressure is 1 atm and the air temperature is 25°C , what is the loss of benzene in lb/day? The specific gravity of benzene at 60°F is 0.877. The concentration of benzene outside the film is negligible. For benzene, the vapor pressure at 25°C is 100 torr, and the diffusivity in air is $0.08 \text{ cm}^2/\text{s}$.

3.3. Countercurrent diffusion across a vapor film.

An insulated glass tube and condenser are mounted on a reboiler containing benzene and toluene. The condenser returns liquid reflux down the wall of the tube. At one point in the tube, the temperature is 170°F , the vapor contains 30 mol% toluene, and the reflux contains 40 mol% toluene. The thickness of the stagnant vapor film is estimated to be 0.1 inch. The molar latent heats of benzene and toluene are assumed equal. Calculate the rate at which toluene and benzene are being interchanged by equimolar countercurrent diffusion at this point in the tube in $\text{lbmol}/\text{h}\cdot\text{ft}^2$, assuming that the rate is controlled by mass transfer in the vapor phase.

Gas diffusivity of toluene in benzene = $0.2 \text{ ft}^2/\text{h}$. Pressure = 1 atm (in the tube). Vapor pressure of toluene at 170°F = 400 torr.

3.4. Rate of drop in water level during evaporation.

Air at 25°C and a dew-point temperature of 0°C flows past the open end of a vertical tube filled with water at 25°C . The tube has an inside diameter of 0.83 inch, and the liquid level is 0.5 inch below the top of the tube. The diffusivity of water in air at 25°C is $0.256 \text{ cm}^2/\text{s}$.

- (a) How long will it take for the liquid level in the tube to drop 3 inches?
- (b) Plot the tube liquid level as a function of time for the time period in part (a).

3.5. Mixing of two gases by molecular diffusion.

Two bulbs are connected by a tube that is 0.002 m in diameter and 0.20 m long. Bulb 1 contains argon, and bulb 2 contains xenon. The pressure and temperature are maintained at 1 atm and 105°C . The binary diffusivity is $0.180 \text{ cm}^2/\text{s}$. At time $t = 0$, diffusion begins for argon and xenon between the two bulbs. At a later time, the argon mole fraction at End 1 of the tube is 0.75, and 0.20 at the other end? Determine at the later time: (a) Rates and directions of mass transfer of argon and xenon; (b) Transport velocity of each species; (c) Molar-average velocity of the mixture.

Section 3.2

3.6. Measurement of diffusivity of toluene in air.

The diffusivity of toluene in air was determined experimentally by allowing liquid toluene to vaporize isothermally into air from a partially filled, 3-mm diameter, vertical tube. At a temperature of 39.4°C , it took $96 \times 10^4 \text{ s}$ for the level of the toluene to drop from 1.9 cm below the top of the open tube to a level of 7.9 cm below the top. The density of toluene is $0.852 \text{ g}/\text{cm}^3$, and the vapor pressure is 57.3 torr at 39.4°C . The barometer reading was 1 atm. Calculate the experimental diffusivity and compare it with the value predicted from (3-36). Neglect the counter diffusion of air.

3.7. Countercurrent molecular diffusion of H_2 and N_2 in a tube.

A tube, 1 mm in inside diameter and 6 inches long, has hydrogen blowing across one end and nitrogen across the other at 75°C .

- (a) For equimolar counter diffusion, what is the rate of transfer of hydrogen into nitrogen in mol/s ? Estimate the diffusivity from (3-36).
- (b) For part (a), plot the mole fraction of hydrogen against distance from the end of the tube past which nitrogen is blown.

3.8. Molecular diffusion of HCl across an air film.

HCl gas diffuses through a film of air 0.1 inch thick at 20°C . The partial pressure of HCl on one side of the film is 0.08 atm and zero on the other. Estimate the rate of diffusion in $\text{mol HCl}/\text{s}\cdot\text{cm}^2$ if the total pressure is (a) 10 atm, (b) 1 atm, (c) 0.1 atm. The diffusivity of HCl in air at 20°C and 1 atm is $0.145 \text{ cm}^2/\text{s}$.

3.9. Estimation of gas diffusivity.

Estimate the diffusion coefficient for a binary gas mixture of nitrogen (A) and toluene (B) at 25°C and 3 atm using the method of Fuller et al. or with a simulator.

3.10. Correction of gas diffusivity for high pressure.

For the mixture of Example 3.3, estimate the diffusion coefficient at 100 atm using the method of Takahashi or the high-pressure method in a simulator.

3.11. Estimation of infinite-dilution liquid diffusivity.

Estimate the diffusivity of carbon tetrachloride at 25°C in a dilute solution of: (a) methanol, (b) ethanol, (c) benzene, and (d) *n*-hexane using the methods of Wilke–Chang and Hayduk–Minhas, either by hand calculations or with a simulator. Compare values with the following experimental observations:

Solvent	Experimental D_{AB} , cm ² /s
Methanol	1.69×10^{-5} cm ² /s at 15°C
Ethanol	1.50×10^{-5} cm ² /s at 25°C
Benzene	1.92×10^{-5} cm ² /s at 25°C
<i>n</i> -Hexane	3.70×10^{-5} cm ² /s at 25°C

3.12. Estimation of infinite-dilution liquid diffusivity.

Estimate the liquid diffusivity of benzene (A) in formic acid (B) at 25°C and infinite dilution from the Hayduk–Minhas equation, either by hand calculations or using a simulator. Compare the estimated value to that of Example 3.6 for formic acid at infinite dilution in benzene.

3.13. Estimation of infinite-dilution liquid diffusivity in solvents.

Estimate the liquid diffusivity of acetic acid at 25°C in a dilute solution of: (a) benzene, (b) acetone, (c) ethyl acetate, and (d) water by manual calculations using the Hayduk–Minhas or Wilke–Chang equation, or with a process simulator. Compare your values with the following experimental data:

Solvent	Experimental D_{AB} , cm ² /s
Benzene	2.09×10^{-5} cm ² /s at 25°C
Acetone	2.92×10^{-5} cm ² /s at 25°C
Ethyl acetate	2.18×10^{-5} cm ² /s at 25°C
Water	1.19×10^{-5} cm ² /s at 20°C

3.14. Vapor diffusion through an effective film thickness.

Water in an open dish exposed to dry air at 25°C vaporizes at a constant rate of 0.04 g/h-cm² of interface area. If the water surface is at the wet-bulb temperature of 11.0°C, calculate the effective gas-film thickness (i.e., the thickness of a stagnant air film that would offer the same resistance to vapor diffusion as is actually encountered).

3.15. Diffusion of alcohol through water and N₂.

Isopropyl alcohol undergoes mass transfer at 35°C and 2 atm under dilute conditions through water, across a phase boundary, and then through nitrogen. Based on the data given below, estimate for isopropyl alcohol: (a) the diffusivity in water using the Wilke–Chang equation; (b) the diffusivity in nitrogen using the Fuller et al. equation; (c) the product, $D_{AB}\rho_M$, in water; and (d) the product, $D_{AB}\rho_M$, in nitrogen, where ρ_M is the mixture molar density.

Compare: (e) the diffusivities in parts (a) and (b); (f) the results from parts (c) and (d). (g) What do you conclude about molecular diffusion in the liquid phase versus the gaseous phase?

Data:	Component	T_c , °R	P_c , psia	Z_c	v_L , cm ³ /mol
	Nitrogen	227.3	492.9	0.289	—
	Isopropyl alcohol	915	691	0.249	76.5

3.16. Estimation of liquid diffusivity over the entire composition range.

Experimental liquid-phase activity-coefficient data are given below in terms of natural log functions for ethanol (1)–benzene (2) at 45°C. Estimate and plot diffusion coefficients for both components of the mixture versus composition using the equations of Vignes. The diffusivities at infinite dilution are 2.51×10^{-5} cm²/s for benzene and 3.4×10^{-5} cm²/s for ethanol.

x_1	$\ln \gamma_1$	$\ln \gamma_2$
0.0374	2.0937	0.0220
0.0972	1.6153	0.0519
0.3141	0.7090	0.2599
0.5199	0.3136	0.5392
0.7087	0.1079	0.8645
0.9193	0.0002	1.3177
0.9591	−0.0077	1.3999

3.17. Estimation of the diffusivity of an electrolyte.

Estimate the diffusion coefficient of NaOH in a 1-M aqueous solution at 25°C with the equation of Nernst and Haskell.

3.18. Estimation of the diffusivity of an electrolyte.

Estimate the diffusion coefficient of NaCl in a 2-M aqueous solution at 18°C using the equation of Nernst and Haskell. The experimental value is 1.28×10^{-5} cm²/s.

3.19. Estimation of effective diffusivity in a porous solid.

Estimate the effective diffusivity of N₂ in H₂ in the pores of a catalyst at 300°C and 20 atm if the porosity is 0.45 and the tortuosity is 2.5. Assume ordinary molecular diffusion in the pores with $D_{AB} = 0.124$ cm²/s from the Fuller et al. equation.

3.20. Diffusion of hydrogen through a steel wall.

Hydrogen at 150 psia and 80°F is stored in a spherical, steel pressure vessel of inside diameter 4 inches and a wall thickness of 0.125 inch. The solubility of hydrogen in steel is 0.094 lbmol/ft³, and the diffusivity of hydrogen in steel is 3.0×10^{-9} cm²/s. If the inner surface of the vessel remains saturated at the existing hydrogen pressure and the hydrogen partial pressure at the outer surface is assumed to be zero, estimate: (a) initial rate of mass transfer of hydrogen through the wall; (b) initial rate of pressure decrease inside the vessel; and (c) time in hours for the pressure to decrease to 50 psia, assuming the temperature stays constant at 80°F.

3.21. Mass transfer of gases through a dense polymer membrane.

A polyisoprene membrane of 0.8-μm (micron) thickness is used to separate methane from H₂. Using data in Table 14.9 and the following partial pressures, estimate the mass-transfer fluxes.

	Partial Pressures, MPa	
	Membrane Side 1	Membrane Side 2
Methane	2.5	0.05
Hydrogen	2.0	0.20

Section 3.3**3.22. Diffusion of NaCl into stagnant water.**

A 3-ft depth of stagnant water at 25°C lies on top of a 0.10-inch thickness of solid NaCl. At time $t < 0$, the water is pure. At time $t = 0$, the salt begins to dissolve and diffuse into the water. If the concentration of salt in the water at the solid–liquid interface is maintained at saturation (36 g NaCl/100 g H₂O) and the diffusivity of NaCl is 1.2×10^{-5} cm²/s, independent of concentration, estimate, by assuming the water to act as a semi-infinite medium, the time and the concentration profile of salt in the water when: (a) 10% of the salt has dissolved; (b) 50% of the salt has dissolved; and (c) 90% of the salt has dissolved.

Section 3.4**3.23. Diffusion of oxygen in a laminar-flowing film of water.**

Estimate the rate of absorption of oxygen at 10 atm and 25°C into water flowing as a film down a vertical wall 1 m high and 6 cm in width at a Reynolds number of 50 without surface ripples. Diffusivity of oxygen in water is 2.5×10^{-5} cm²/s and the mole fraction of oxygen in water at saturation is 2.3×10^{-4} . Viscosity of water = 0.89 cP. Neglect the vaporization of water.

3.24. Diffusion of carbon dioxide in a laminar-flowing film of water.

For Example 3.11, determine at what height the average concentration of CO₂ would correspond to 50% saturation.

3.25. Evaporation of water from a film on a flat plate into flowing air.

Air at 1 atm flows at 2 m/s along a 2-inch-long surface that is covered with a thin film of water. Assume the water surface is not rippled. If the air and water are at 25°C and the diffusivity of water in air is 0.25 cm²/s, estimate the water mass flux for the evaporation of water at the middle of the surface, assuming laminar boundary-layer flow. Is this assumption reasonable? For air, viscosity = 0.018 cP. Vapor pressure of water = 0.46 psi.

3.26. Diffusion of a thin plate of naphthalene into flowing air.

Air at 1 atm and 100°C flows across a thin, flat plate of subliming naphthalene that is 1 m long. The Reynolds number at the trailing edge of the plate is at the upper limit for a laminar boundary layer. Estimate: (a) the average rate of sublimation in kmol/s-m²; and (b) the local rate of sublimation at 0.5 m from the leading edge. Physical properties are given in Example 3.12.

3.27. Sublimation of a circular naphthalene tube into air flowing through it.

Air at 1 atm and 100°C flows through a straight, 5-cm i.d. tube, cast from naphthalene, at a Reynolds number of 1,500. Air entering the tube has an established laminar-flow velocity profile. Properties are given in Example 3.12. If pressure drop is negligible, calculate the length of tube needed for the average mole fraction of naphthalene in the exiting air to be 0.005.

3.28. Evaporation of a spherical water drop into still, dry air.

A spherical water drop is suspended from a fine thread in still, dry air. Show: (a) that the Sherwood number for mass transfer from the surface of the drop into the surroundings has a value of 2 if the characteristic length is the diameter of the drop. If the initial drop diameter is 1 mm, the air temperature is 38°C, the drop temperature is 14.4°C, and the pressure is 1 atm, calculate (b) initial mass of the drop in grams; (c) initial rate of evaporation in grams per second; (d) time in seconds for the drop diameter to be 0.2 mm; and (e) initial rate of heat transfer to the drop. If the Nusselt number is also 2, is the rate of heat transfer sufficient to supply the required heat of vaporization and sensible heat? If not, what will happen? The binary gas diffusion coefficient is 0.273 cm²/s. The vapor pressure of water at 14.4°C is 12.3 torr. The thermal conductivity of air at

38°C is 58×10^{-6} cal/s-cm²-(°C/cm). The specific heat of steam is 0.44 cal/g-°C and the heat of vaporization of water at 14.4°C is 589 cal/g.

Section 3.5**3.29. Dissolution of a tube of benzoic acid into flowing water.**

Water at 25°C flows turbulently at 5 ft/s through a straight, cylindrical tube cast from benzoic acid, of 2-inch i.d. If the tube is 10 ft long, and fully developed, turbulent flow is assumed, estimate the average concentration of acid in the water leaving the tube. Physical properties are in Example 3.13.

3.30. Sublimation of a naphthalene cylinder to air flowing normal to it.

Air at 1 atm flows at a Reynolds number of 50,000 normal to a long, circular, 1-inch-diameter cylinder made of naphthalene. Using the physical properties of Example 3.12 for a temperature of 100°C, calculate the average sublimation flux in kmol/s-m².

3.31. Sublimation of a naphthalene sphere to air flowing past it.

For the conditions of Exercise 3.30, calculate the initial average rate of sublimation in kmol/s-m² for a spherical particle of 1-inch initial diameter. Compare this result to that for a bed packed with naphthalene spheres with a void fraction of 0.5.

Section 3.6**3.32. Stripping of CO₂ from water by air in a wetted-wall tube.**

Carbon dioxide is stripped from water by air in a wetted-wall tube. At a location where pressure is 10 atm and temperature 25°C, the flux of CO₂ is 1.62 lbmol/h-ft². The partial pressure of CO₂ is 8.2 atm at the interface and 0.1 atm in the bulk gas. The diffusivity of CO₂ in air at these conditions is 1.6×10^{-2} cm²/s. Assuming turbulent flow, calculate by film theory the mass-transfer coefficient k_c for the gas phase and the film thickness.

3.33. Absorption of CO₂ into water in a packed column.

Water is used to remove CO₂ from air by absorption in a column packed with Pall rings described in Chapter 6. At a region of the column where the partial pressure of CO₂ at the interface is 150 psia and the concentration in the bulk liquid is negligible, the absorption rate is 0.017 lbmol/h-ft². The CO₂ diffusivity in water is 2.0×10^{-5} cm²/s. Henry's law for CO₂ is $p = Hx$, where $H = 9,000$ psia. Calculate: (a) liquid-phase mass-transfer coefficient and film thickness; (b) contact time for the penetration theory; and (c) average eddy residence time and the probability distribution for the surface-renewal theory.

3.34. Determination of diffusivity of H₂S in water.

Determine an average diffusivity of H₂S in water, using penetration theory, from the data below for absorption of H₂S into a laminar jet of water at 20°C. Jet diameter = 1 cm, jet length = 7 cm, and solubility of H₂S in water = 100 mol/m³. Assume the contact time is the time of exposure of the jet. The average rate of absorption varies with jet flow rate:

Jet Flow Rate, cm ³ /s	Rate of Absorption, mol/s × 10 ⁶
0.143	1.5
0.568	3.0
1.278	4.25
2.372	6.15
3.571	7.20
5.142	8.75

Section 3.7**3.35. Vaporization of water into air in a wetted-wall column.**

In a test on the vaporization of H₂O into air in a wetted-wall column, the following data were obtained: tube diameter = 1.46 cm;

wetted-tube length = 82.7 cm; air rate to tube at 24°C and 1 atm = 720 cm³/s; inlet and outlet water temperatures are 25.15°C and 25.35°C, respectively; partial pressure of water in inlet air is 6.27 torr and in outlet air is 20.1 torr. The diffusivity of water vapor in air is 0.22 cm²/s at 0°C and 1 atm. The mass velocity of air is taken relative to the pipe wall. Calculate: (a) rate of mass transfer of water into the air; and (b) K_G for the wetted-wall column.

3.36. Absorption of NH₃ from air into aq. H₂SO₄ in a wetted-wall column.

The following data were obtained by Chamber and Sherwood [*Ind. Eng. Chem.*, **29**, 1415 (1937)] on the absorption of ammonia from an ammonia-air mixture by a strong acid in a wetted-wall column 0.575 inch in diameter and 32.5 inches long:

Inlet acid (2-N H ₂ SO ₄) temperature, °F	76
Outlet acid temperature, °F	81
Inlet air temperature, °F	77
Outlet air temperature, °F	84
Total pressure, atm	1.00
Partial pressure NH ₃ in inlet gas, atm	0.0807
Partial pressure NH ₃ in outlet gas, atm	0.0205
Air rate, lbmol/h	0.260

The operation was countercurrent with gas entering at the bottom of the vertical tower and the acid passing down in a thin film on the vertical, cylindrical inner wall. The change in acid strength was negligible, and the vapor pressure of ammonia over the liquid is negligible because of the use of a strong acid for absorption. Calculate the mass-transfer coefficient, k_p , from the data.

3.37. Overall mass-transfer coefficient for a packed cooling tower.

A cooling-tower packing was tested in a small column. At two points in the column, 0.7 ft apart, the data below apply. Calculate the overall volumetric mass-transfer coefficient $K_y a$ that can be used to design a large, packed-bed cooling tower, where a is the mass-transfer area, A , per unit volume, V , of tower.

	Bottom	Top
Water temperature, °F	120	126
Water vapor pressure, psia	1.69	1.995
Mole fraction H ₂ O in air	0.001609	0.0882
Total pressure, psia	14.1	14.3
Air rate, lbmol/h	0.401	0.401
Column cross-sectional area, ft ²	0.5	0.5
Water rate, lbmol/h (approximation)	20	20

Chapter 4

Single Equilibrium Stages and Flash Calculations

§4.0 INSTRUCTIONAL OBJECTIVES

After completing this chapter, you should be able to:

- Explain what a single equilibrium stage is and why it may be insufficient to achieve a desired separation.
- Extend Gibbs' phase rule for an equilibrium stage to include extensive variables so that the number of degrees of freedom, which is the number of variables minus the number of independent relations among the variables, can be determined.
- Use T - y - x and y - x diagrams of binary mixtures, in conjunction with a q -line, to determine equilibrium compositions.
- Understand the difference between minimum- and maximum-boiling azeotropes.
- Calculate bubble-point, dew-point, and equilibrium-flash conditions.
- Use triangular phase diagrams for ternary systems with component material balances to determine equilibrium compositions of liquid-liquid mixtures.
- Use distribution coefficients with component material-balance equations to calculate liquid-liquid phase equilibria for multicomponent systems.
- Use equilibrium diagrams together with material balances to determine amounts and compositions for solid-fluid systems (sublimation, desublimation, and adsorption) and for gas absorption in liquids.

When separations require phase creation or phase addition as in Figure 1.6(a) and (b), two questions are pertinent: (1) What is the temperature, pressure, and composition of the phases at equilibrium? (2) How long does it take to closely approach equilibrium? The first question is answered by thermodynamics; the second by the rates of diffusion and chemical kinetics. Thermodynamic equilibrium includes both **physical (phase) equilibrium** and **chemical (reaction) equilibrium**. This textbook considers, with few exceptions, only physical equilibrium. Possible chemical reactions are, in most cases, assumed to be too slow to occur during the interval that mixtures are being separated. This assumption is not an important limitation because with the exception of ionic reactions in aqueous phases or catalyzed chemical reactions, chemical-reaction rates are much slower than mass-transfer rates.

This chapter describes separations by phase creation and phase addition in a single equilibrium step (a stage), as illustrated by separation operations in Tables 1.1 and 1.2. At phase equilibrium, molecules are still moving in both directions across phase boundaries, but no further temperature, pressure, or phase composition changes occur. Thus, the equilibrium is dynamic rather than static. Both the temperature and pressure are equal in each phase, but the phase compositions differ except for azeotropic mixtures. These composition differences allow mixtures to be separated when the phases disengage.

The phases in equilibrium may be gas, liquid, or solid. Most common are (1) a vapor and a liquid, (2) two partially immiscible liquids, and (3) two immiscible liquids and a vapor. Examples of all three are presented in this chapter.

More than two phases can be in physical equilibrium. An extreme example of multiple-phase (multiphase) equilibrium is the seven-component system at near-ambient conditions shown in Figure 4.1. The phase on top is air followed by six partially miscible liquid phases of increasing density. Each of the seven phases contains all seven components. In most of the phases, mole fractions of many of the components range from small to very small. For example, the aniline-rich phase contains on the order of 10 mol% *n*-hexane and 20 mol% water, but much less than 1 mol% each of dissolved air, phosphorous, gallium, and mercury. Even though each phase is not in direct contact with more than two other phases, all are in equilibrium with each other. For example, even though

Air
<i>n</i> -hexane-rich liquid
Aniline-rich liquid
Water-rich liquid
Phosphorous liquid
Gallium liquid
Mercury liquid

Figure 4.1 Seven phases in physical equilibrium.

the *n*-hexane-rich phase is not in direct contact with the water-rich phase, approximately 0.06 mol% water is present in the *n*-hexane-rich phase at physical equilibrium.

§4.1 GIBBS' PHASE RULE AND DEGREES OF FREEDOM

The theoretical foundation for phase equilibrium is the **Gibbs' phase rule**, derived by J. Willard Gibbs at Yale University in 1875. Consider an equilibrium system consisting of one or more phases, N_p , with one or more chemical components, C . In the absence of chemical reactions; and for negligible gravitational, electrical, magnetic, and surface forces, the **intensive thermodynamic variables** (those independent of the mass) are: temperature, T ; pressure, P ; and composition, e.g., in mole fractions. Let N_V = the number of variables and N_E = the number of independent equations that relate the intensive variables. Then, the number of **degrees of freedom** for the system is $N_D = N_V - N_E$, where N_D is the number of variables that must be specified so that the remaining variables can be determined from the independent equations. The Gibbs' phase rule, which is derived below is

$$N_D = C - N_p + 2 \quad (4-1)$$

Consider a one-component system ($C = 1$) of H_2O . The phase diagram is shown in Figure 4.2 in the form of phase boundaries in terms of P and T . Phase boundaries are shown between vapor (water vapor or steam) and liquid (water), vapor and solid (ice), and liquid (water) and solid (ice). If $N_p = 1$, application of (4-1) gives $N_D = 2$. Since the mole fraction is fixed at 1.0, the only intensive variables remaining are T and P , both of which must be specified to fix the state of the system. As shown in Figure 4.2, single phases of water vapor, water, and ice exist over ranges of T and P .

If instead of one phase, $N_p = 2$, (4-1) gives $N_D = 1$. We can only specify T or P , each of which is the same for both phases. As shown in Figure 4.2, the remaining intensive variable must lie on a phase boundary, for example on the vapor pressure

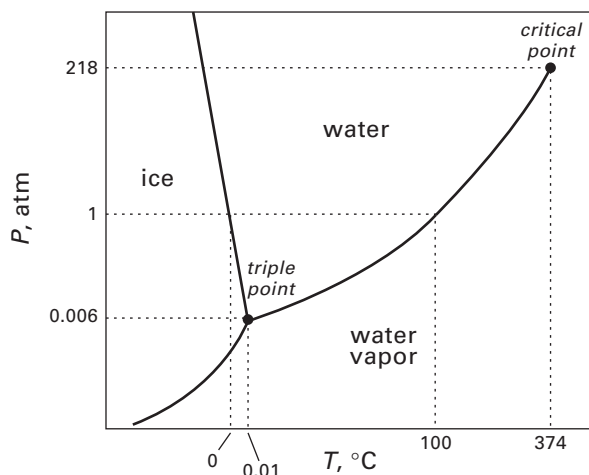


Figure 4.2 Phase diagram for H_2O .

curve for water in equilibrium with steam. Finally, if we let $N_p = 3$, $N_D = 0$ and both T and P are fixed for all three phases, resulting in a unique triple point shown in Figure 4.2.

The application of (4-1) to binary and multicomponent systems is elaborated in the remaining sections of this chapter, after the following derivation of the Gibbs' phase rule. The number of intensive thermodynamic variables in a multiphase, multicomponent system is

$$N_V = N_p(C + 2) \quad (4-2)$$

where $N_p C$ = number of composition variables (e.g., mole fractions) and $2 N_p$ is for T and P of each phase. The number of independent equations is

$$N_E = N_p + (C + 2)(N_p - 1) \quad (4-3)$$

where the first term on the RHS of (4-3) refers to the requirement that the mole fractions in each phase must sum to one. For example, if the phase is a vapor,

$$\sum_{i=1}^C y_i = 1 \quad (4-4)$$

If the phase is a liquid,

$$\sum_{i=1}^C x_i = 1 \quad (4-5)$$

The second term on the RHS of (4-3) accounts for phase equilibrium for $(C + 2)$ conditions, namely C chemical compositions, T , and P . As shown in §2.1 on phase equilibria in Chapter 2, compositions for two phases in equilibrium are commonly and most conveniently expressed by component K -values in terms of ratios of mole fractions in the two phases. For vapor–liquid equilibrium for component i ,

$$K_i = \frac{\text{mole fraction of } i \text{ in the vapor phase}}{\text{mole fraction of } i \text{ in the liquid phase}} = y_i/x_i \quad (4-6)$$

For liquid (1)–liquid (2) phase equilibrium, the K -value is a distribution or partition coefficient, which for component i is

$$K_{D_i} = \frac{\text{mole fraction of } i \text{ in liquid phase 1}}{\text{mole fraction of } i \text{ in liquid phase 2}} = x_i^{(1)}/x_i^{(2)} \quad (4-7)$$

K -values, (4-6) and (4-7), are widely used as a measure of the degree to which a chemical component distributes between two phases. For vapor–liquid equilibrium, high K -values favor the vapor phase, while low K -values favor the liquid phase. K -values are thermodynamic properties and need not be counted as variables because they depend on the intensive variables T , P , and the mole fractions of all components in the system, as discussed in Chapter 2.

For T and P , the equilibrium equations are

$$T_1 = T_2 = \dots = T_{N_p} \quad (4-8)$$

$$P_1 = P_2 = \dots = P_{N_p} \quad (4-9)$$

where the subscripts denote the phase.

Note that in (4-3), the number of conditions, $C + 2$, is multiplied by $(N_p - 1)$ because each condition is in terms of two phases. For example, for three phases at equilibrium: $T_1 = T_2$; $T_2 = T_3$; and $T_1 = T_3$. However, only two of these equations are independent because, for example, the third equation can be derived by combining the first two equations to eliminate T_2 . Subtracting (4-3) from (4-2) gives (4-1), Gibbs' phase rule:

$$N_D = N_V - N_E = N_p(C + 2) - [N_p + (C + 2)(N_p - 1)] \\ = C - N_p + 2$$

EXAMPLE 4.1 Equilibrium Phase Conditions for a Three-Phase System

For three components (A, B, and C), a vapor phase (V) and two liquid phases (L_I and L_{II}) with mole fractions, y_i , x_i^I , and x_i^{II} are at physical equilibrium.

- (a) By Gibbs' phase rule, how many degrees of freedom are there?
 (b) If the temperature and pressure of the vapor phase are specified, can any other intensive variables be specified? If so, what would you specify?
 (c) What are the $N_p(C + 2) = 3(3 + 2) = 15$ intensive variables that apply?
 (d) Write the $N_p + (C + 2)(N_p - 1) = 3 + (3 + 2)(3 - 1) = 13$ independent equations that apply.

Solution

- (a) From (4-1), $N_D = C - N_p + 2 = 3 - 3 + 2 = 2$.
 (b) Since T_V and P_V are specified and $N_p = 2$, no other intensive variables can be specified.
 (c) $T_V, T_{L_I}, T_{L_{II}}, P_V, P_{L_I}, P_{L_{II}}, y_A, y_B, y_C, x_A^I, x_B^I, x_C^I, x_A^{II}, x_B^{II}, x_C^{II}$
 (d) $T_V = T_{L_I}, T_V = T_{L_{II}}, P_V = P_{L_I}, P_V = P_{L_{II}}$ (Why isn't $T_{L_I} = T_{L_{II}}$ included?)

$$\sum_i y_i = 1, \sum_i x_i^I = 1, \sum_i x_i^{II} = 1$$

$$K_i^I = y_i/x_i^I, i = A, B, C; K_i^{II} = y_i/x_i^{II}, i = A, B, C$$

(Why isn't $K_{D_i} = x_i^I/x_i^{II}, i = A, B, C$ included?)

Table 4.1 VLE Data for Three Binary Systems at 1 atm Pressure

a. Water (A)–Glycerol (B) System

$P = 101.3$ kPa

Data of Chen and Thompson, *J. Chem. Eng. Data*, **15**, 471 (1970)

Temperature, °C	y_A	x_A	$\alpha_{A,B}$
100.0	1.0000	1.0000	
104.6	0.9996	0.8846	333
109.8	0.9991	0.7731	332
128.8	0.9980	0.4742	544
148.2	0.9964	0.3077	627
175.2	0.9898	0.1756	456
207.0	0.9804	0.0945	481
244.5	0.9341	0.0491	275
282.5	0.8308	0.0250	191
290.0	0.0000	0.0000	

b. Methanol (A)–Water (B) System

$P = 101.3$ kPa

Data of J.G. Dunlop, M.S. thesis, Brooklyn Polytechnic Institute (1948)

Temperature, °C	y_A	x_A	$\alpha_{A,B}$
64.5	1.000	1.000	
66.0	0.958	0.900	2.53
69.3	0.870	0.700	2.87
73.1	0.779	0.500	3.52
78.0	0.665	0.300	4.63
84.4	0.517	0.150	6.07
89.3	0.365	0.080	6.61
93.5	0.230	0.040	7.17
100.0	0.000	0.000	

c. Para-xylene (A)–Meta-xylene (B) System

$P = 101.3$ kPa

Data of Kato, Sato, and Hirata, *J. Chem. Eng. Jpn.*, **4**, 305 (1970)

Temperature, °C	y_A	x_A	$\alpha_{A,B}$
138.335	1.0000	1.0000	
138.491	0.8033	0.8000	1.0041
138.644	0.6049	0.6000	1.0082
138.795	0.4049	0.4000	1.0123
138.943	0.2032	0.2000	1.0160
139.088	0.0000	0.0000	

§4.2 BINARY VAPOR–LIQUID SYSTEMS AT EQUILIBRIUM

Experimental vapor–liquid equilibrium (VLE) data for binary systems are widely available. The data are for either isobaric or isothermal conditions, with isobaric conditions being most common and useful. The data are presented in the form of (1) tables like Tables 4.1 and 4.2; (2) plots like Figure 4.3; and (3) correlation parameters for equations of state and activity-coefficient equations of the type discussed in Chapter 2. The most complete single source of VLE data is the computerized Dortmund Data Bank (DDB) (www.ddbst.com), started in 1973 under J. Gmehling of the University of Dortmund. The 2013 version of DDB contains 34,116 sets of VLE data. The DDB software package (DDBSP) is designed to be accessed

by process simulators and is available to users of Aspen Plus, CHEMCAD, and ProSimPlus.

§4.2.1 Zeotropic Binary Mixtures

Binary mixtures are **zeotropic** or **azeotropic**. At equilibrium, vapor and liquid phases of a zeotropic mixture never have the same composition. An azeotropic mixture at equilibrium has identical compositions of the vapor and the liquid ($y_i = x_i$). Table 4.1 presents experimental VLE data for three binary systems at 1 atm (101.3 kPa). Each row of data includes the temperature and the phase compositions, y_A and x_A , of, by convention, the more volatile component. By Gibbs' phase rule, (4-1), with two phases and two components,

$N_D = 2 - 2 + 2 = 2$. In Table 4.1, the pressure is specified. Therefore, if x_A is specified, then the temperature and y_A are fixed. Because $y_B = 1 - y_A$ and $x_B = 1 - x_A$, the mole fractions of the less volatile component need not be included in the table.

For each of the three mixtures in Table 4.1, the first row of data corresponds to the boiling-point temperature at the system pressure of A, the more volatile component. The last row of the table corresponds to the boiling-point temperature of the less volatile component. Temperatures in the intermediate rows of data are between the boiling points of the two components.

Table 4.1 also includes in the last column of each row (except when one of the two components is not present) the calculated value of the relative volatility, $\alpha_{A,B}$, defined by

$$\alpha_{A,B} = \frac{K_A}{K_B} = \frac{(y_A/x_A)}{(y_B/x_B)} = \frac{(y_A/x_A)}{(1 - y_A)/(1 - x_A)} \quad (4-10)$$

For example, for the methanol (A)–water (B) system of Table 4.1b, when $x_A = 0.500$, $y_A = 0.779$. Therefore, using (4-6), $K_A = y_A/x_A = 0.779/0.500 = 1.558$ and $K_B = (1 - y_A)/(1 - x_A) = (1 - 0.779)/(1 - 0.500) = 0.442$. From (4-10), $\alpha_{A,B} = 1.558/0.442 = 3.52$.

The relative volatility of a binary mixture, $\alpha_{A,B}$, is a thermodynamic **separation index** that is a measure of the degree of difficulty for the separation of a more volatile component from a less volatile component by the three separation operations in Table 1.1: (1) partial vaporization of the mixture when a liquid, (2) partial condensation of the mixture when a vapor, or (3) multistage distillation. For a mixture, $\alpha_{A,B}$ is a function of pressure, temperature, and phase compositions.

For the water–glycerol system in Table 4.1a, the difference in boiling points is 190°C. Accordingly, $\alpha_{A,B}$ values are very high, and a separation by a single equilibrium stage with Operations (1) or (2) in Table 1.1 may be sufficient. Industrially, the separation is often conducted in an evaporator, which produces nearly pure water vapor and a solute-rich liquid. For example, as seen in the Table 4.1a, at 1 atm and 207°C, a vapor of 98 mol% water is in equilibrium with a liquid containing more than 90 mol% glycerol.

For the methanol–water system, in Table 4.1b, the difference in boiling points is 35.5°C and $\alpha_{A,B}$ values are more than an order of magnitude lower than for the water–glycerol system. A suitable separation cannot be made with a single equilibrium stage. Typically, a 30-stage distillation column is required to obtain a 99 mol% methanol distillate and a 98 mol% water bottoms.

For the paraxylene–metaxylene isomer system in Table 4.1c, the boiling-point difference is only 0.723°C and the relative volatility is very close to 1.0, making separation by distillation economically impractical because about 1,000 stages would be required to produce nearly pure products. Instead, crystallization and adsorption, which have much higher separation indices than the relative volatility, are used commercially.

Phase-equilibrium calculations and visualization of phase conditions using VLE data sets like those in Table 4.1 are

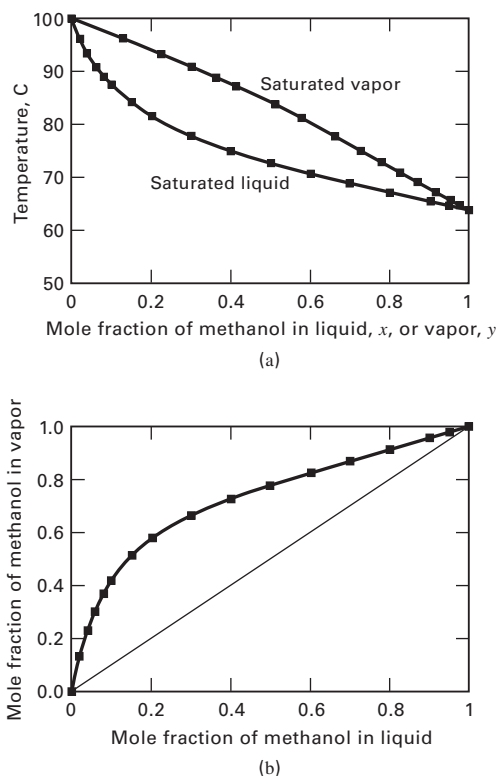


Figure 4.3 Plots of VLE data for methanol–water at 1 atm. (a) T – y – x plot. (b) y – x plot.

conveniently made from plots of the data. Most useful are T – y_A – x_A and y_A – x_A plots for isobaric conditions. Such plots for the methanol–water system in Table 4.1b are shown in Figure 4.3. All of the data appear in the T – y_A – x_A plot of Figure 4.3a, while temperature does not appear in the y_A – x_A plot of Figure 4.3b.

The T – y – x plot is useful for determining phase states, phase-transition temperatures, phase compositions, and phase amounts for a given pressure. Consider the T – y – x plot in Figure 4.4 for the n –hexane (H)– n –octane (O) system at 101.3 kPa.

Figure 4.4 has two curves labeled “Saturated vapor” and “Saturated liquid.” The two curves converge at $x_H = 0$, the normal boiling point of n –octane (258.2°F), and at $x_H = 1$, the boiling point of normal hexane (155.7°F). Mixture conditions above the saturated vapor curve correspond to a **superheated vapor**. Conditions below the saturated liquid curve correspond to a **subcooled liquid**. Two-phase mixtures only exist at conditions on or between the two curves. Temperatures along the saturated vapor curve are called **dew-point temperatures**, while temperatures along the saturated liquid curve are **bubble-point temperatures**.

Consider a mixture of 30 mol% H at 150°F at point A in Figure 4.4. Point A is a subcooled liquid. When this mixture is heated at 1 atm, it remains liquid until a temperature of 210°F, point B, is reached. This is the bubble point where the first bubble of vapor appears. The bubble is a saturated vapor in equilibrium with the liquid at the same temperature. The composition of the bubble is determined by following a dashed **tie line**, BC, from $x_H = 0.3$ to $y_H = 0.7$. This tie

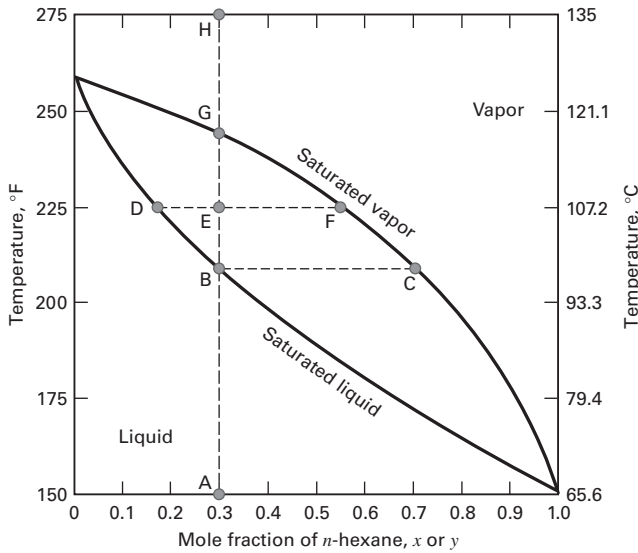


Figure 4.4 T - y , x phase equilibrium diagram for the n -hexane- n -octane system at 1 atm.

line is horizontal because the phase temperatures are equal. If the temperature of the mixture at point B is increased to point E at 225°F, two distinct phases are at equilibrium. From horizontal tie line DEF, the mole fraction of H in the liquid phase decreases to $x_H = 0.17$ (because it is more volatile than O and preferentially vaporizes), and the mole fraction of H in the vapor phase increases to $y_H = 0.55$. It is important to note that throughout the two-phase region, the equilibrium vapor is at its dew point, and the equilibrium liquid is at its bubble point. Of course, the overall composition of the two phases remains at a mole fraction of 0.30 for hexane. At point E, the relative molar amounts of the vapor (V) and liquid (L) phases are determined by the **inverse-lever-arm rule** using the lengths of line segments DE and EF. In Figure 4.4, the molar ratio $V/L = DE/EF$ (not EF/DE). When the temperature is increased to 245°F, point G, the dew point for $y_H = 0.3$, is reached, where the last droplet of liquid evaporates. An increase in temperature to point H at 275°F gives a superheated vapor with $y_H = 0.30$.

Constant-pressure y - x plots like Figure 4.3b are useful because the vapor-and-liquid compositions are points on the equilibrium curve. Such plots usually include a 45° reference line, $y = x$. The y - x plot of Figure 4.5 for H–O at 1 atm is convenient for determining compositions as a function of mole-percent vaporization by geometric constructions.

Consider a feed mixture of F moles, of overall composition $z_H = 0.6$. To determine the phase compositions of the equilibrium vapor (V) and liquid (L) if 60 mol% of the feed is vaporized, make the dashed-line construction in Figure 4.5. Point A on the 45° line represents z_H . Point B is reached on the phase equilibrium curve by extending the dashed line, called the **q -line**, upward and to the left toward the equilibrium curve at a slope equal to $[(V/F) - 1]/(V/F)$. Thus, for 60 mol% vaporization, the slope = $(0.6 - 1)/0.6 = -2/3$. Point B at the intersection of line AB with the equilibrium curve is the equilibrium composition $y_H = 0.76$ and $x_H = 0.37$. The

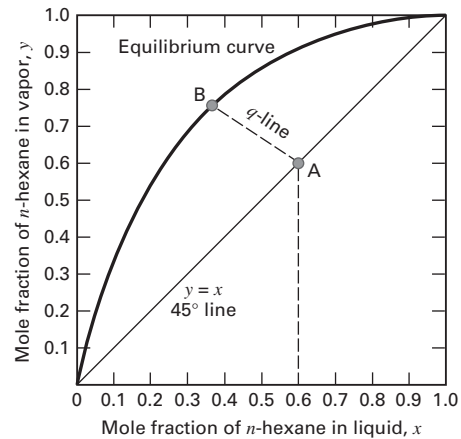


Figure 4.5 y - x phase-equilibrium diagram for the n -hexane- n -octane system at 1 atm.

equation for the slope of the q -line in Figure 4.5 is derived by combining a component material balance

$$Fz_H = Vy_H + Lx_H$$

with the total mole balance,

$$F = V + L$$

to eliminate L , giving the q -line equation:

$$y_H = \left[\frac{(V/F) - 1}{(V/F)} \right] x_H + \left[\frac{1}{(V/F)} \right] z_H \quad (4-11)$$

Thus, the slope of the q -line passing through the equilibrium point (y_H, x_H) is $[(V/F) - 1]/(V/F)$. It is easily verified that the q -line equation does pass through the point $z_H = x_H = y_H$ on the 45° line.

§4.2.2 Azeotropic Binary Mixtures

At vacuum or near-ambient pressures, when the ideal gas law holds, the vapor–liquid equilibrium ratio (K -value) for each component in a mixture can be expressed by the modified Raoult’s law, derived in Chapter 2:

$$K_i = \frac{y_i}{x_i} = \frac{\gamma_{iL} P_i^s}{P} \quad (4-12)$$

where γ_{iL} is the activity coefficient for component i in the liquid phase, P_i^s is the vapor (saturation) pressure of component i , and P is the total pressure. The activity coefficient accounts for nonideal behavior of the components in the liquid solution and typically, but not always, has values greater than 1.0.

If the liquid phase is an ideal solution, liquid-phase activity coefficients of all components are equal to 1.0 and

$$K_i = \frac{y_i}{x_i} = \frac{P_i^s}{P} \quad (4-13)$$

Equation (4-13) is called the **Raoult’s law K -value**, while (4-12) is the **modified Raoult’s law K -value**.

When a liquid solution is ideal and (4-13) applies, azeotropes will only occur when the vapor pressure curves for the two components cross each other in the temperature range between the two boiling points at the system pressure. When the liquid solution is nonideal and (4-12) applies, the variation of activity coefficients with composition often cause azeotrope formation even when the vapor-pressure curves do not cross. The DDB contains more than 53,200 azeotropic data points.

Liquid-phase activity coefficients can be readily estimated from binary VLE data when the system pressure is low enough that (4-12) applies and vapor pressure data are available for the two components. This is illustrated in the following example.

EXAMPLE 4.2 Calculation of Activity Coefficients from Binary VLE Data.

In Table 4.1b, at 101.3 kPa and 66.0°C, methanol equilibrium mole fractions are $y = 0.958$ and $x = 0.900$. From the DDB, the vapor pressures of methanol and water are respectively, 107.2 kPa and 26.08 kPa. Calculate the liquid-phase activity coefficients of methanol and water for these conditions.

Solution

Equation (4-12) applies.

$$\text{For methanol (A), } \gamma_A = \frac{y_A P}{x_A P_A^s} = \frac{0.958(101.3)}{0.900(107.2)} = 1.006$$

$$\text{For water (W), } \gamma_B = \frac{y_B P}{x_B P_B^s} = \frac{(1 - 0.958)(101.3)}{(1 - 0.900)(26.08)} = 1.631$$

Values of γ for the other conditions in Table 4.1b are obtained in the same manner as in Example 4.2. The set of values can then be fitted to liquid-phase activity-coefficient models of the type discussed in §2.6. For example, suppose the two-parameter Wilson equation of Table 2.8 is selected to fit the methanol–water VLE data. The equations are:

$$\begin{aligned} \ln \gamma_A &= -\ln(x_A + \Lambda_{AB}x_B) \\ &+ x_B \left(\frac{\Lambda_{AB}}{x_A + \Lambda_{AB}x_B} - \frac{\Lambda_{BA}}{x_B + \Lambda_{BA}x_A} \right) \\ \ln \gamma_B &= -\ln(x_B + \Lambda_{BA}x_A) \\ &- x_A \left(\frac{\Lambda_{AB}}{x_A + \Lambda_{AB}x_B} - \frac{\Lambda_{BA}}{x_B + \Lambda_{BA}x_A} \right) \end{aligned} \quad (4-14)$$

The Wilson parameters, Λ_{AB} and Λ_{BA} , are determined (from the values of γ_A and γ_B calculated from the experimental VLE data and the corresponding liquid mole fractions) by iterative nonlinear regression, to minimize the objective function (OF):

$$\text{OF} = \sum \left[\left(\frac{\gamma_A^{\text{expt}} - \gamma_A^{\text{calc}}}{\gamma_A^{\text{expt}}} \right)^2 + \left(\frac{\gamma_B^{\text{expt}} - \gamma_B^{\text{calc}}}{\gamma_B^{\text{expt}}} \right)^2 \right]$$

where γ^{expt} values are those from the experimental VLE data as in Example 4.2 and γ^{calc} are the values calculated from (4-14) for a set of parameters Λ_{AB} and Λ_{BA} . Using the `nlinfit` function of MATLAB, the converged parameter set is found by regression to be $\Lambda_{AB} = 0.449748$ and $\Lambda_{BA} = 0.991449$. Many of the experimental VLE data sets in the DDB have been regressed to provide parameters for the more widely used liquid-phase activity-coefficient models. These results are included in the DDBSP available to users of process simulators to predict K -values.

The modified Raoult's law, (4-12), using activity-coefficient models is widely used when separations involve azeotropic mixtures. Binary azeotropic mixtures exhibit mainly **minimum-boiling azeotropes**, where, under isobaric conditions, the azeotrope boils at a temperature below the boiling point of either of the two pure components. At the azeotropic composition, both K -values and the relative volatility are 1.

Figure 4.6 shows y - x and T - y - x plots for the system isopropyl ether (1)–isopropyl alcohol (2) at 1 atm. Their normal boiling points are 68.5°C and 82.5°C, respectively. A minimum-boiling azeotrope forms at 66°C with an isopropyl ether mole fraction of 0.78. The liquid-phase activity coefficients for the system of Figure 4.6 are not less than 1.0 and as high as 3.8 over the composition range. Such behavior constitutes a positive deviation from Raoult's law (4-13).

Less common are **maximum-boiling azeotropes**, where the azeotrope boils at a temperature greater than the pure-component boiling points. Figure 4.7 shows y - x and T - y - x plots for the system acetone (1)–chloroform (2) at 1 atm. Their normal boiling points are 56°C and 61.2°C, respectively. A maximum-boiling azeotrope forms at approximately 66°C with an acetone mole fraction of approximately 0.40. The liquid-phase activity coefficients for the system in Figure 4.7 are not greater than 1.0 and as low as 0.37 over the composition

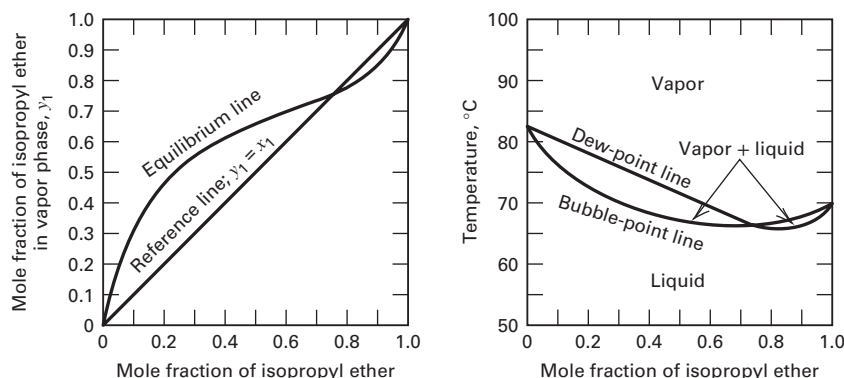


Figure 4.6 VLE diagrams for isopropyl ether (1)–isopropyl alcohol (2) at 1 atm showing a minimum-boiling azeotrope.

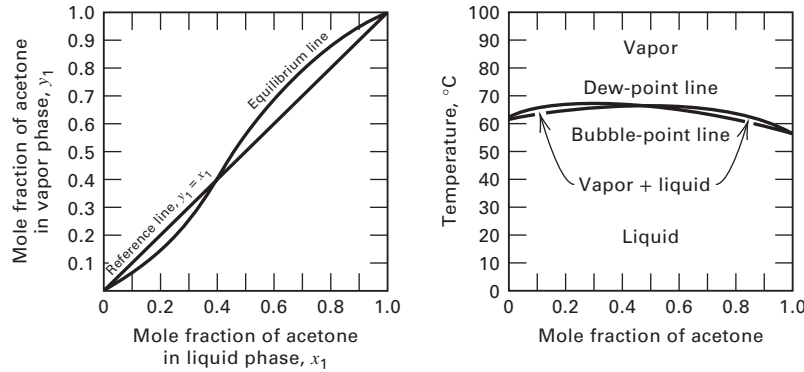


Figure 4.7 VLE diagrams for acetone (1)–chloroform (2) at 1 atm showing a maximum-boiling azeotrope.

range. Such behavior is referred to as a negative deviation from Raoult’s law (4-13).

Azeotropes are not restricted to binary mixtures. Many azeotropes have been observed for systems of more than two components. The two systems of Figures 4.6 and 4.7 form, at equilibrium, **homogeneous azeotropes** with just one liquid phase. Some systems at equilibrium form **heterogeneous azeotropes** with two liquid phases, where the overall mole fractions in the combined liquid phases equal the mole fractions in the vapor. Heterogeneous azeotropes of even three liquid phases and one vapor phase have been observed for some mixtures of three or more components. The separation of azeotropic mixtures is considered in detail in Chapter 11.

§4.3 EQUILIBRIUM TWO-PHASE FLASH CALCULATIONS

As discussed in §4.2, phase-equilibrium calculations for binary vapor–liquid systems are readily made on plots of experimental T – y – x and y – x data without the need to use K -values. This is particularly convenient and accurate when the liquid phase exhibits nonideal behavior. For multicomponent systems of more than two components, graphical methods are not convenient and common practice is to make calculations using (1) component material balances coupled with (2) K -value expressions, such as (4-12) and (4-13), and (3) an energy balance if heat transfer occurs. The calculations, referred to as **flash calculations**, are best made with process simulators, which can provide the necessary thermodynamic properties including vapor pressures, activity coefficients, and enthalpies by accessing property correlations in data banks such as the DDBSP.

A **flash** is a single-equilibrium-stage distillation in which a liquid feed is partially vaporized to give a vapor richer than the feed in the more volatile components. In Figure 4.8, a pressurized liquid feed is heated and flashed adiabatically across a valve to a lower pressure, resulting in creation of a vapor phase that is separated from the remaining liquid in a flash drum. Alternatively, the valve can be omitted and a liquid can be partially vaporized in a heater and then separated into two phases. Also, in Figure 4.9, a vapor feed can be cooled and partially condensed to give, after phase separation, a liquid richer in the

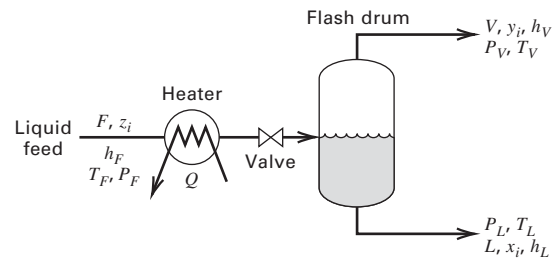


Figure 4.8 Continuous flash vaporization

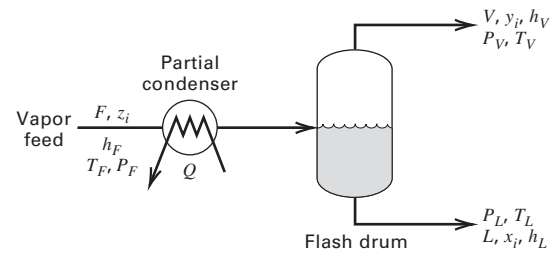


Figure 4.9 Continuous partial condensation.

less volatile components. For properly designed systems, the streams leaving the flash drum will be in phase equilibrium.

Several types of flash calculations are available in process simulators depending upon what variables are specified. Flash calculations are among the most common calculations in chemical engineering. They are used not only for separation operations (1) and (2) in Table 1.1, but also to determine the phase condition of mixtures anywhere in a process, e.g., in a pipeline. To determine how many and which variables can be specified, an extension of Gibbs’ phase rule is useful.

§4.3.1 Extension of Gibbs’ Phase Rule to Include Extensive Variables

Gibbs’ phase rule as discussed in §4.1 does not deal with extensive variables in feed, product, and energy streams, for either a batch or continuous process. However, the rule can be extended for process applications by adding extensive variables for flow rates or amounts in material and energy streams, together with corresponding additional independent equations. To illustrate, consider the extension of a two-phase

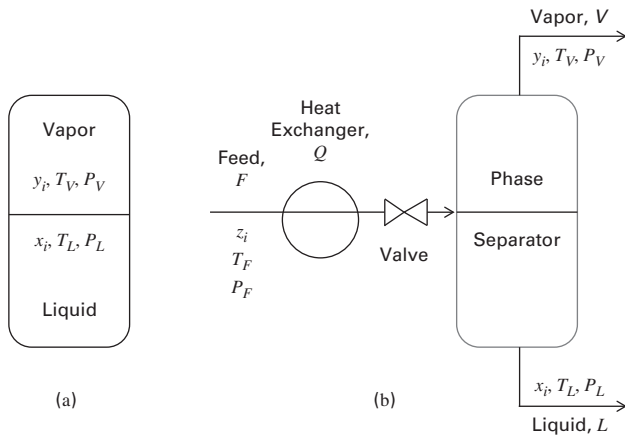


Figure 4.10 Variables for vapor-liquid phase equilibria: (a) Gibbs' Phase Rule for Intensive Variables Only; (b) Extension to Continuous Partial Condensation or Vaporization with both Intensive and Extensive Variables.

(vapor and liquid), multicomponent equilibrium condition (shown in Figure 4.10a), to a continuous, single-stage partial condensation or flash vaporization process as shown in Figure 4.10b. The feed is a vapor, liquid, or mixture of the two. The feed can be heated or cooled in a heat exchanger, and its pressure can be decreased by passing the feed through a valve. The equilibrium phases separate in the phase separator. The vapor phase is enriched in the more volatile components, while the liquid phase is enriched in the less volatile components. For the continuous process in Figure 4.10b, the additional variables are z_i, T_F, P_F , molar feed flow rate, F ; Q for the rate of heat addition or removal in the heat exchanger; and V , and L for the product molar flow rates leaving the phase separator. Thus, $C + 6$ extensive variables are added. An additional $C + 3$ independent equations must be added, as follows:

$(C - 1)$ Component material balances:

$$Fz_i = Vy_i + Lx_i, \quad i = 1 \text{ to } C \quad (4-15)$$

Total material balance:

$$F = V + L \quad (4-16)$$

Energy balance:

$$Fh_F + Q = Vh_V + Lh_L \quad (4-17)$$

Summation of mole fractions in the feed:

$$\sum_{i=1}^C z_i = 1 \quad (4-18)$$

where z_i is the mole fraction of component i in the feed (whether it is vapor, liquid or the mixture of the two); F , V , and L are molar flow rates; Q is the rate of heat transfer [(+) if added to the process, (-) if removed from the process]; and h is the molar enthalpy. In general, for N_p product phases, the additional variables total $(C + N_p + 4)$ and the added equations total $(C + 2)$.

If we revise the degrees of freedom analysis for Gibbs' phase rule, Equations (4-2), (4-3), and (4-1) are extended to:

$$N_V = N_p(C + 2) + (C + N_p + 4) \quad (4-19)$$

$$N_E = N_p + (C + 2)(N_p - 1) + (C + 2) \quad (4-20)$$

and

$$\begin{aligned} N_D &= N_V - N_E \\ &= N_p(C + 2) + [C + N_p + 4] \\ &\quad - [N_p + (C + 2)(N_p - 1) + C + 2] \\ &= C + 4 \end{aligned} \quad (4-21)$$

If we restrict N_p to two phases (vapor and liquid), N_V from (4-19) becomes $(3C + 10)$ and N_E from (4-20) becomes $(2C + 6)$. Note that we could write C instead of $(C - 1)$ component material balances (4-15) and eliminate the total material balance (4-16). However, a procedure for solving the equations favors the former. For process calculations, it is common to completely specify the feed variables: F, T_F, P_F , but only $(C - 1)$ feed mole fractions, because the missing feed mole fraction must satisfy the sum of feed mole fractions, (4-18). This totals $C + 2$ variables, leaving two more variables to specify. Process simulators permit specification of the following combinations of two variables:

T_V, P_V	Isothermal flash
$Q = 0, P_V$	Adiabatic flash
Q, P_V	Nonadiabatic flash
$V/F, P_V$	Percent vaporization flash
$V/F = 0, P_L$	Bubble-point temperature
$V/F = 1, P_V$	Dew-point temperature
$T_L, V/F = 0$	Bubble-point pressure
$T_V, V/F = 1$	Dew-point pressure

With some process simulators, it is also possible to specify one or even two product mole fractions. However, when attempting this, one must be careful to avoid irrational values that can lead to infeasible results. For example, if the components are H_2O, N_2 , and O_2 , and $T_V = 100^\circ F$ and $P_V = 15$ psia are specified, a specification of $x_{N_2} = 0.8$ is not feasible because at these conditions nitrogen is not this soluble if a water-rich phase is formed. It is recommended that all computer-generated results be carefully checked for feasibility.

§4.3.2 Isothermal Flash Calculation

A widely used algorithm for making two-phase flash calculations is the procedure of **Rachford and Rice (RR)** [1], published in 1952 for the case of an **isothermal flash**. They recognized that the $(2C + 6)$ equations constituted a nonlinear system of algebraic equations that could not be solved directly. They developed the following procedure that reduces the number of nonlinear equations that need to be solved to just one.

- (1) Use specified (C-1) feed mole fractions with (4-18) to calculate the remaining feed mole fraction.
- (2) Set $T_V = T_L$ and $P_V = P_L$
- (3) Combine (4-15) and (4-16) to eliminate L and substitute Ψ for V/F . This gives

$$z_i = \Psi y_i + x_i - \Psi x_i \quad (4-22)$$

- (4) Use (4-6) to eliminate y_i in (4-22) and rearrange to give

$$x_i = \frac{z_i}{1 + \Psi(K_i - 1)} \quad (4-23)$$

- (5) Use (4-6) to eliminate x_i in (4-23) and rearrange to give

$$y_i = \frac{z_i K_i}{1 + \Psi(K_i - 1)} \quad (4-24)$$

- (6) Subtract summation (4-5) from summation (4-4) to give

$$\sum_{i=1}^C y_i - \sum_{i=1}^C x_i = 0 \quad (4-25)$$

- (7) Substitute (4-23) and (4-24) into (4-25) to eliminate y_i and x_i to give

$$f\{\Psi\} = \sum_{i=1}^C \frac{z_i(1 - K_i)}{[1 + \Psi(K_i - 1)]} = 0 \quad (4-26)$$

- (8) Equation (4-26) is a nonlinear equation in $\Psi = V/F$ that can be solved directly if $C = 2$, but must be solved iteratively if $C > 2$. If two phases are to be present, $0 < \Psi < 1$.
- (9) With a converged value of Ψ , calculate V from $V = \Psi F$
- (10) Calculate L from (4-16), $L = F - V$
- (11) Calculate C values of x_i from (4-23) and C values of y_i from (4-24)
- (12) If a heat exchanger precedes the phase separator, calculate Q from (4-17)

Before applying the RR procedure, a check should be made to determine whether the mixture is between the bubble and dew points at the specified conditions. However, these checks are only valid for ideal mixtures where Raoult's law (4-13) applies, such that K -values do not depend on the compositions of the liquid and vapor phases.

Check 1: At T_V and P_V , if all $K_i > 1$, only a superheated vapor is present; if all $K_i < 1$, only a subcooled liquid is present and there is no need to apply the RR procedure. Otherwise, try Check 2.

Check 2: If one or more K_i are greater than 1 and one or more K_i are less than 1, calculate $f\{\Psi\}$ from (4-26) with $\Psi = 0$. If $f\{0\} > 0$, the mixture is below the bubble-point temperature. Alternatively, if Ψ is set to 1 and $f\{1\} < 0$, the mixture is above the dew-point temperature.

The single nonlinear equation (4-26) in the RR procedure is most commonly solved by process simulators using Newton's

iterative numerical method. The iterations are made on $\Psi^{(k)}$, where k is the iteration number. For the first iteration, assume $\Psi^{(1)} = 0.5$ (i.e., 50 mol% of the feed becomes vapor). Using this value of Ψ , $f\{\Psi\}$ is calculated from (4-26). In general, $f\{\Psi\}$ will not be 0 and a second iteration, and probably more iterations, will be necessary. In general, for the $k+1$ iteration, the value for $\Psi^{(k+1)}$ is calculated from the recursive relation

$$\Psi^{(k+1)} = \Psi^{(k)} - \frac{f\{\Psi^{(k)}\}}{f'\{\Psi^{(k)}\}} \quad (4-27)$$

where the derivative, $f'\{\Psi^{(k)}\}$, of $f\{\Psi^{(k)}\}$ with respect to Ψ is

$$f'\{\Psi^{(k)}\} = \sum_{i=1}^C \frac{z_i(1 - K_i)^2}{[1 + \Psi^{(k)}(K_i - 1)]^2} \quad (4-28)$$

The iterations are continued until a sufficient degree of accuracy for Ψ is achieved. A reasonable criterion is

$$\frac{|\Psi^{(k+1)} - \Psi^{(k)}|}{\Psi^{(k)}} < 0.0001 \quad (4-29)$$

The RR procedure is illustrated in the following example.

EXAMPLE 4.3 Phase Conditions of a Process Stream.

A 100-kmol/h feed consisting of 10, 20, 30, and 40 mol% of propane (3), *n*-butane (4), *n*-pentane (5), and *n*-hexane (6), respectively, enters a distillation column at 690 kPa and 93°C. Assuming the feed stream is at phase equilibrium, what molar fraction of the feed enters as liquid, and what are the equilibrium liquid and vapor compositions in mole fractions?

Solution

At flash conditions, assume $K_3 = 4.2$, $K_4 = 1.75$, $K_5 = 0.74$, $K_6 = 0.34$, independent of compositions. Because some K -values > 1 and some < 1 , Check 2 is applied to determine if the mixture is partially vaporized.

$$\begin{aligned} f\{0\} &= \frac{0.1(1 - 4.2)}{1} + \frac{0.2(1 - 1.75)}{1} \\ &+ \frac{0.3(1 - 0.74)}{1} + \frac{0.4(1 - 0.34)}{1} = -0.128 \end{aligned}$$

Since $f\{0\}$ is not more than zero, the mixture is above the bubble point. Now compute $f\{1\}$:

$$\begin{aligned} f\{1\} &= \frac{0.1(1 - 4.2)}{1 + (4.2 - 1)} + \frac{0.2(1 - 1.75)}{1 + (1.75 - 1)} \\ &+ \frac{0.3(1 - 0.74)}{1 + (0.74 - 1)} + \frac{0.4(1 - 0.34)}{1 + (0.34 - 1)} = 0.720 \end{aligned}$$

Since $f\{1\}$ is not less than zero, the mixture is below the dew point. Therefore, the mixture is partially vaporized and calculations with the RR equations can proceed by solving (4-26), for Ψ :

$$\begin{aligned} 0 &= \frac{0.1(1 - 4.2)}{1 + \Psi(4.2 - 1)} + \frac{0.2(1 - 1.75)}{1 + \Psi(1.75 - 1)} \\ &+ \frac{0.3(1 - 0.74)}{1 + \Psi(0.74 - 1)} + \frac{0.4(1 - 0.34)}{1 + \Psi(0.34 - 1)} \end{aligned}$$

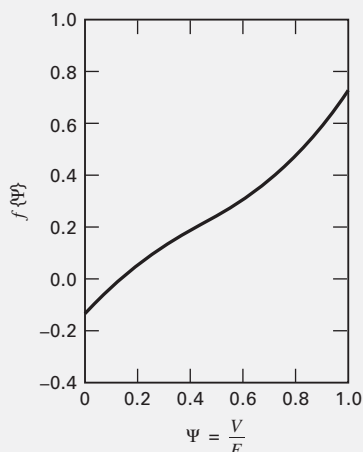


Figure 4.11 Rachford–Rice function for Example 4.3.

This equation can be solved with `fzero` in MATLAB by defining $f\{\Psi\}$ as the function and using any initial value of Ψ between 0 and 1. Alternatively, it is solved by Newton's method. For an initial guess of $\Psi = 0.50$, the following iteration history is computed

k	$\Psi^{(k)}$	$f\{\Psi^{(k)}\}$	$f'\{\Psi^{(k)}\}$	$\Psi^{(k+1)}$	$\left \frac{\Psi^{(k+1)} - \Psi^{(k)}}{\Psi^{(k)}} \right $
1	0.5000	0.2515	0.6259	0.0982	0.8037
2	0.0982	-0.0209	0.9111	0.1211	0.2335
3	0.1211	-0.0007	0.8539	0.1219	0.0065
4	0.1219	0.0000	0.8521	0.1219	0.0000

Convergence is rapid, giving $\Psi = V/F = 0.1219$. The vapor flow rate is $0.1219(100) = 12.19$ kmol/h, and the liquid flow rate is $(100 - 12.19) = 87.81$ kmol/h. Liquid and vapor compositions from (4-23) and (4-24) are:

	x	y
Propane	0.0719	0.3021
<i>n</i> -Butane	0.1833	0.3207
<i>n</i> -Pentane	0.3098	0.2293
<i>n</i> -Hexane	<u>0.4350</u>	<u>0.1479</u>
Total	1.0000	1.0000

A plot of $f\{\Psi\}$ as a function of Ψ is shown in Figure 4.11.

For non-ideal mixtures, when K -values are sensitive to compositions, especially in the liquid phase, K -values must be calculated at each iteration as phase compositions change and the RR procedure may fail to converge. In that case, process simulators use a modified RR procedure, described in §4.5, which can handle even higher nonideality for components in liquid–liquid mixtures.

§4.3.3 Adiabatic, Nonadiabatic, and Percent Vaporization (Ψ) Flash Calculations

When the pressure of a liquid stream is reduced adiabatically across a valve as in Figure 4.8b, an **adiabatic-flash** ($Q = 0$)

calculation determines the resulting phases, temperature, compositions, and flow rates for a specified downstream pressure. The calculation can be made by applying the isothermal-flash calculation procedure of §4.3.2 in an iterative manner. First a guess is made of the flash temperature, T_V . Then Ψ , V , x , y , and L are determined by the RR procedure. The guessed value of T_V (equal to T_L) is then checked by an energy balance (4-17) to determine Q . If Q is not zero to an acceptable degree of accuracy, a new value of T_V is assumed and the RR procedure is repeated. After the first two guesses, a plot of the calculated Q versus the assumed T_V can be made with interpolation or extrapolation used to provide the next guess of T_V . This method is tedious because it involves an inner-loop iteration on Ψ and an outer-loop iteration on T_V . The method is successful for wide-boiling mixtures, but may fail for close-boiling mixtures (e.g., mixtures of isomers). In that case, it is preferable to switch T_V to the inner loop and Ψ to the outer loop. For either case, the method is too tedious for hand calculations and is best made with a process simulator.

The **nonadiabatic flash** ($Q \neq 0$) calculation is identical to the adiabatic-flash calculation except for a non-zero specification of Q . The **percent vaporization flash** can also utilize the RR procedure in the following manner. From two guesses for T_V , two values of Ψ are calculated. From a plot of the calculated values of Ψ versus the assumed values of T_V , interpolation or extrapolation is used to provide the next guess of T_V .

EXAMPLE 4.4 Adiabatic Flash of a Nonideal Mixture.

An equimolar mixture of methanol, ethanol, and water at 5 atm (5.066 bar) and 127°C is flashed adiabatically to 1 atm. Select an appropriate thermodynamic property set and use a process simulator to compute the equilibrium temperature and phase compositions. Compare the K -values to the ideal K -values obtained from vapor pressures at equilibrium conditions.

Solution

Using the ChemSep program with the Wilson equation for activity coefficients, the SRK model for fugacity coefficients, the extended Antoine equation for vapor pressure, and the excess enthalpy equation, the following results were obtained:

Temperature = 76.2°C

Phase mole fractions and K -values

Component	Vapor	Liquid	K -value	Ideal K -value
Methanol	0.4325	0.3123	1.385	1.555
Ethanol	0.3458	0.3307	1.046	0.916
Water	0.2217	0.3570	0.621	0.399
Total	1.0000	1.0000		

In the nonideal solution, methanol is less volatile, while ethanol and water are more volatile than they would be if the mixture were ideal.

§4.3.4 Bubble- and Dew-Point Calculations

At the bubble point, $\Psi = 0$ and (4-26) becomes

$$f\{0\} = \sum_i z_i(1 - K_i) = \sum z_i - \sum z_i K_i = 0$$

However, $\sum_{i=1}^C z_i = 1$. Therefore, the bubble-point equation is

$$\boxed{\sum_i z_i K_i = 1} \quad (4-30)$$

At the dew point, $\Psi = 1$ and (4-26) becomes

$$f\{1\} = \sum_i \frac{z_i(1 - K_i)}{K_i} = \sum \frac{z_i}{K_i} - \sum z_i = 0$$

Therefore, the dew-point equation is

$$\boxed{\sum_i \frac{z_i}{K_i} = 1} \quad (4-31)$$

For a given feed composition, z_i , (4-30) or (4-31) is used to determine T for a specified P or to find P for a specified T .

The bubble- and dew-point equations are nonlinear in temperature, but only moderately nonlinear in pressure, except at high pressures. The latter is especially the case in the region of the convergence pressure, where K -values of very light or very heavy components change drastically with pressure, as discussed in §2.5.2. Therefore, iterative procedures are required to solve for bubble- and dew-point conditions unless Raoult's law is applicable. In that case, a direct calculation of bubble-point pressure for a given temperature can be made with (4-30). Bubble-point and dew-point calculations for ideal and nonideal mixtures are readily made using process simulators.

EXAMPLE 4.5 Bubble- and Dew-Point Calculations for a Nonideal Mixture.

For an equimolar mixture of methanol and water at 1 atm, use a process simulator with the Wilson equation for activity coefficients in the modified Raoult's law K -value to calculate the bubble- and dew-point temperatures and compare the results with Table 4.1b and Figure 4.3a.

Solution

Using the Aspen Plus process simulator with the Wilson property option, the bubble point is 73.1°C and the dew point is 85.0°C. The mole fraction of methanol in the first bubble of vapor is 0.790, while for the first droplet of liquid it is 0.141. These values are in reasonable agreement with Table 4.1b and Figure 4.3a.

§4.3.5 Using a Process Simulator to Estimate Properties of Pure Components and Mixtures.

Frequently, engineers are required to obtain thermodynamic and transport properties of pure components or mixtures. These are readily estimated by executing a run with a flash model in a process simulator. For example, to determine

the thermodynamic and transport properties of an equimolar liquid mixture of acetone and water at 0.2 MPa at the saturation temperature, a percent vaporization flash is made. Specification of the feed to the flash includes an arbitrary total flow rate and composition. The two required specifications for the flash model are the same pressure and the percent vaporized. When the flash is converged, the desired properties are those reported for the feed. For the above acetone–water mixture, the ChemSep results are:

Pressure (MPa)	0.200000
Vapour fraction (–)	0.000000
Temperature (C)	84.4177
Enthalpy (J/kmol)	–2.600E+08
Entropy (J/kmol/K)	159617
Total molar flow (kmol/h)	100.000
Total mass flow (kg/h)	3804.75
Vapour std.vol.flow (m ³ /s)	
Liquid std.vol.flow (m ³ /s)	0.00127308
Mole flows (kmol/h)	
Acetone	50.0000
Water	50.0000
Mole fractions (–)	
Acetone	0.500000
Water	0.500000
Mass flows (kg/h)	
Acetone	2904.00
Water	900.751
Mass fractions (–)	
Acetone	0.763256
Water	0.236744
Combined feed fractions (–)	
Acetone	1.00000
Water	1.00000
Liquid:	
Mole weight (kg/kmol)	38.0475
Density (kg/m ³)	770.710
Std.density (kg/m ³)	830.169
Viscosity (cP)	0.212352
Heat capacity (J/kmol/K)	118158
Thermal cond. (J/s/m/K)	0.396839
Surface tension (dyne/cm)	38.9233

§4.4 TERNARY LIQUID–LIQUID SYSTEMS AT EQUILIBRIUM

In liquid–liquid extraction, nonideal ternary mixtures undergo **phase splitting** to form two liquid phases of different compositions. The simplest case is the single equilibrium stage shown in Figure 4.12a, where only component B, called the **solute**, has any appreciable solubility in either component A, the **carrier**, or component C, the **solvent**. The solute enters the equilibrium stage in the feed, F, with the carrier, but is not present in the fresh solvent, S. In the stage, B is extracted by the solvent C to produce the **extract**, E.

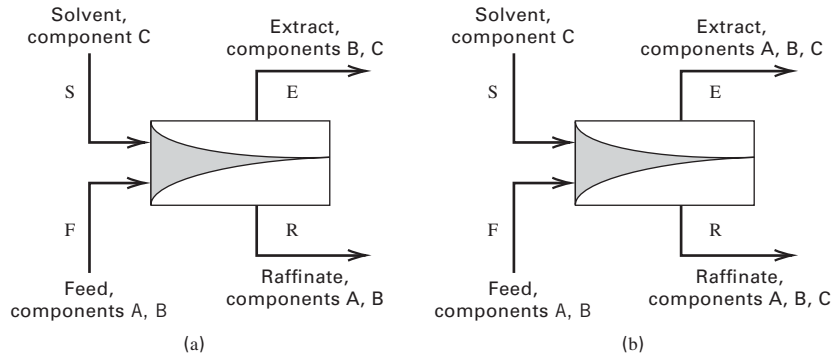


Figure 4.12 Liquid–liquid extraction with ternary mixtures: (a) components A and C are mutually insoluble; (b) components A and C are partially soluble.

The unextracted B leaves the stage with carrier A in the **raffinate**, R. Neither A nor B are assumed to be soluble in each other. Therefore, the flow rate, F_A , of carrier A is the same in the feed and in the raffinate, R; and the flow rate, S , of fresh solvent C is the same in the solvent and in the extract. By convention, the extract is shown leaving from the top of the stage even though it may not have the lower density.

Experimental data for liquid–liquid equilibrium are often reported in mass fractions instead of mole fractions. To illustrate the calculation procedure for Case (a) in Figure 4.12 using mass units, let F_A be the mass flow rate of carrier A in the feed equal to the mass flow rate of carrier A in the raffinate; and S be the mass flow rate of solvent C in the entering solvent equal to the mass flow rate of solvent C in the extract. The calculations are facilitated if compositions are in mass ratios, X_i , instead of mass fractions. Accordingly, let X_B be the ratio of the mass of solute B to the mass of carrier A in the feed (or raffinate) and Y_B be the ratio of the mass of solute B to the mass of solvent C in the extract. A mass balance on solute C is as follows, where the superscript on the mass ratios, X denotes the stream:

$$\begin{aligned} & (\text{solute flow rate in the feed}) \\ &= (\text{solute flow rate in the extract}) \\ &+ (\text{solute flow rate in the raffinate}) \\ X_B^{(F)} F_A &= Y_B^{(E)} S + X_B^{(R)} F_A \end{aligned} \quad (4-32)$$

since the flow rate F_A in the feed is equal to the flow rate of A in the raffinate.

The phase equilibrium ratio for the distribution of B between the extract and raffinate is expressed as

$$Y_B^{(E)} = K'_{D_B} X_B^{(R)} \quad (4-33)$$

where K'_{D_B} is a modified form of the distribution ratio in terms of mass ratios instead of mole fractions as in (4-7). Substituting (4-33) into (4-32) to eliminate $Y_B^{(E)}$,

$$X_B^{(R)} = \frac{X_B^{(F)} F_A}{F_A + K'_{D_B} S} \quad (4-34)$$

A useful parameter is the **extraction factor**, \mathcal{E} , for the solute, B, defined by

$$\mathcal{E} = \frac{K'_{D_B} S}{F_A} \quad (4-35)$$

Substituting (4-35) into (4-34) gives the fraction of B unextracted:

$$\text{Fraction of B unextracted} = \frac{X_B^{(R)}}{X_B^{(F)}} = \frac{1}{1 + \mathcal{E}} \quad (4-36)$$

Thus, large values of \mathcal{E} in (4-36), resulting from large values of K'_{D_B} or of the solvent-to-carrier ratio S/F_A in (4-35), give large degrees of extraction of B.

EXAMPLE 4.6 Single-Stage Extraction of Acetic Acid.

Methyl isobutyl ketone (C) is used as a solvent to remove acetic acid (B) from a 13,500 kg/h feed of 8 wt% acetic acid in water (A), because distillation requires vaporization of large amounts of water. If the raffinate is to contain 1 wt% acetic acid, estimate the kg/h of solvent needed for a single equilibrium stage if C and A are assumed to be insoluble in each other. From experimental data in the literature, $K'_{D_B} = 0.657$.

Solution

$$\begin{aligned} F_A &= 0.92(13,500) = 12,420 \text{ kg/h} \\ X_B^{(F)} &= (13,500 - 12,420)/12,420 = 0.087 \\ X_B^{(R)} &= 0.01/(1 - 0.01) = 0.0101 \end{aligned}$$

From a rearrangement of (4-36),

$$\mathcal{E} = \frac{X_B^{(F)}}{X_B^{(R)}} - 1 = \frac{0.087}{0.0101} - 1 = 7.61$$

From a rearrangement of (4-35),

$$\text{solvent flow rate} = S = \frac{7.61(12,420)}{0.657} = 144,000 \text{ kg/h}$$

This large solvent flow rate can be reduced by using multiple stages or a solvent with a larger distribution coefficient. Using 1-butanol as the solvent, with $K'_{D_B} = 1.613$, reduces the solvent flow rate by 50%.

§4.4.1 Equilibrium Calculations with a Triangular Diagram

In the ternary liquid–liquid system shown in Figure 4.12b, components A and C are partially soluble in each other, and

component B distributes between the extract and raffinate phases. This is the most commonly encountered case. Different types of phase diagrams, constructed from experimental liquid–liquid phase equilibrium data, have been devised for using material balances to calculate equilibrium compositions and phase amounts.

Consider the ternary system water (A)–ethylene glycol (B)–furfural (C) at 25°C and 101 kPa, which is well above the bubble-point pressure. Water–ethylene glycol and furfural–ethylene glycol are completely miscible binary pairs, while furfural–water is a partially miscible binary pair. The solute is ethylene glycol, and furfural is the solvent that removes ethylene glycol from a binary mixture with water. The furfural-rich phase is the extract, and the water-rich phase is the raffinate.

Experimental data for the mixture are given by Conway and Norton [2]. Saturation compositions for a single liquid phase on the verge of splitting into two phases are listed in Table 4.2. The first row of data gives the solubility of water in furfural, while the last row gives the solubility of furfural in water. Intermediate rows include the solute, ethylene glycol. These data are obtained by a cloud-point titration. For example, if water is added slowly to a completely miscible and clear 50–50 wt% mixture of furfural and ethylene glycol until the onset of cloudiness occurs due to the formation of a second liquid phase, the resulting wt% composition of the liquid

Table 4.2 Equilibrium Miscibility Data in Weight Percent for the Furfural–Ethylene Glycol–Water System at 25°C and 101 kPa

Furfural	Ethylene Glycol	Water
95.0	0.0	5.0
90.3	5.2	4.5
86.1	10.0	3.9
75.1	20.0	4.9
66.7	27.5	5.8
49.0	41.5	9.5
44.5	44.5	11.0
34.3	50.5	15.2
27.5	52.5	20.0
13.9	47.5	38.6
11.0	40.0	49.0
9.7	30.0	60.3
8.4	15.0	76.6
7.7	0.0	92.3

saturated with water is: 44.5% furfural, 44.5% ethylene glycol, and 11.0% water.

Several different plots are used to represent liquid–liquid phase equilibrium composition data for ternary mixtures. One uses equilateral triangle graph paper, which can be downloaded from: <http://www.waterproofpaper.com/graph-paper/>. An example is shown as Figure 4.13 for the water (A)–ethylene

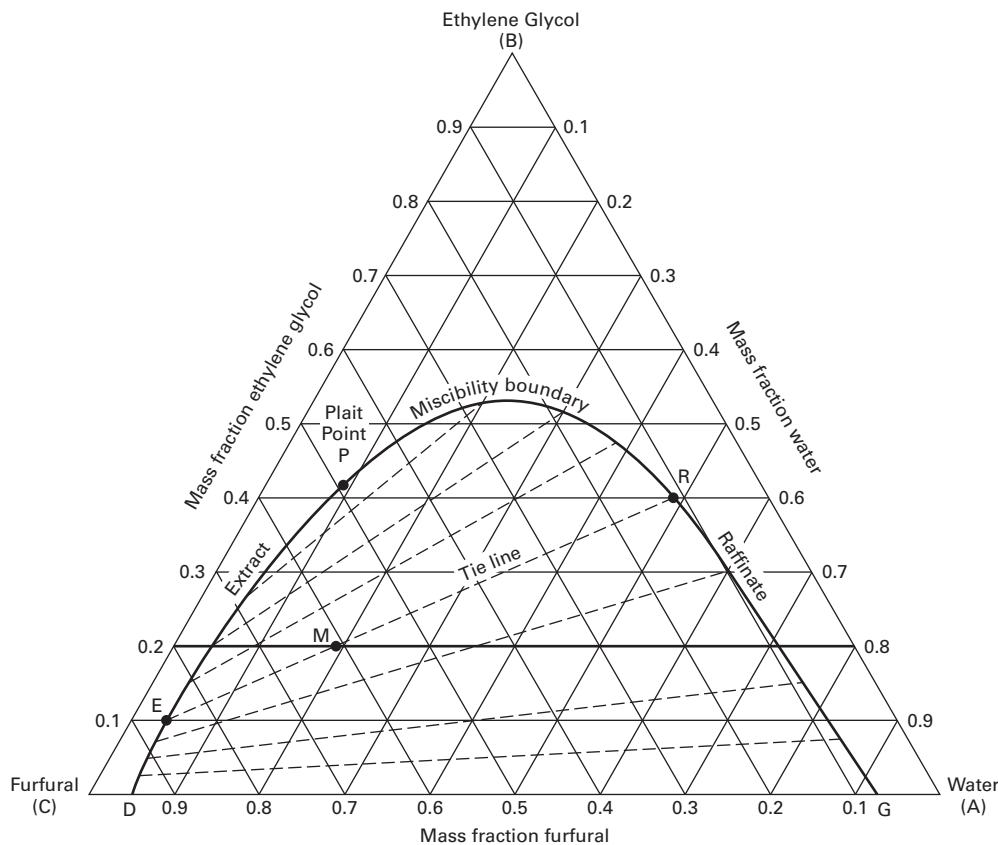


Figure 4.13 Liquid–liquid phase equilibrium for furfural–ethylene glycol–water at 25°C, 1 atm.

glycol (B)–furfural (C) system at 25°C and a pressure of 101.3 kPa. The miscibility data of Table 4.2 are represented by the bold **miscibility boundary curve**, also called the **binodal curve**. Above this curve, only a single liquid phase exists; below the curve, two liquid phases exist.

Each apex of the triangle is a pure component. Each edge is a mixture of the two pure components at the terminal apexes of the side. Any point located within the triangle is a ternary mixture. In this diagram, the sum of the lengths of three perpendicular lines drawn from any interior point to the edges equals the altitude of the triangle. Thus, if each of these three lines is scaled from 0 to 100, the wt% of furfural in the mixture at any point such as M, is simply the length of the line perpendicular to the edge opposite the pure furfural apex. The determination of the composition at an interior point is facilitated by the three sets of parallel lines, where each set is in mass-fraction increments of 0.1 (or 10%) and is parallel to an edge of the triangle opposite the apex of the component, whose mass fraction is given. Thus, the point M in Figure 4.13 represents a two-phase mixture (before phase separation) containing 19 wt% water, 20 wt% ethylene glycol, and 61 wt% furfural.

Also shown in Figure 4.13 are **tie lines** that connect points on the miscibility boundary curve. Each pair of points represents compositions of equilibrium phases. The tie lines are based on experimental data from Conroy and Norton [2] given in Table 4.3. These data were obtained by measuring compositions of different extract (furfural layer) and raffinate (water layer) phases at equilibrium. If a mixture of 20 wt% ethylene glycol, 19 wt% water, and 61 wt% furfural, shown as point M, is brought to equilibrium and the resulting compositions of the equilibrium extract and raffinate phases are measured, the extract, point E, is found to be 10 wt% ethylene glycol, 4 wt% water, and 86 wt% furfural; while the raffinate, point R, is 40 wt% ethylene glycol, 49 wt% water, and 11 wt% furfural. The tie lines converge to point P, called the **plait point**, where the two phases become one. Because the miscibility boundary

Table 4.3 Mutual Equilibrium (Tie-Line) Data for the Furfural–Ethylene Glycol–Water System at 25°C and 101 kPa

Glycol in Water Layer, wt%	Glycol in Furfural Layer, wt%
41.5	41.5
50.5	32.5
52.5	27.5
51.5	20.0
47.5	15.0
40.0	10.0
30.0	7.5
20.0	6.2
15.0	5.2
7.3	2.5

is established by the data of Table 4.2, only ethylene glycol compositions in the two layers at the ends of the tie lines are listed in Table 4.3.

By Gibbs' phase rule, (4-1), there are three degrees of freedom for a three-component, two-liquid-phase system. With T and P specified, the concentration of one component in either phase suffices to define the equilibrium system. As shown in Figure 4.13, one value for wt% ethylene glycol on the miscibility boundary curve fixes that liquid-phase composition and, by means of the corresponding tie line, the composition of the other phase is fixed. Figure 4.13 can be used to solve equilibrium-stage problems by using material balances in conjunction with data in the diagram, as illustrated in the following example.

EXAMPLE 4.7 Single Equilibrium-Stage Extraction of Ethylene Glycol.

Determine (a) equilibrium compositions and (b) amounts of extract, E , and raffinate, R , when a feed, F , of 100 g of 45 wt% ethylene glycol (B)–55 wt% water (A) is contacted with 200 g of solvent, S , of pure furfural (C) at 25°C and 101 kPa, using data in Figure 4.13.

Solution

- (a) The graphical construct is shown in Figure 4.14, where the compositions of feed, F , and solvent, S , are plotted as points and connected by a straight line. A **mixing point**, M , is defined as the sum of the amounts of F and S . The composition of that point corresponds to 45 g of B, 55 g of A, and 200 g of C, which gives 15.0 wt% B, 18.3 wt% A, and 66.7 wt% C.

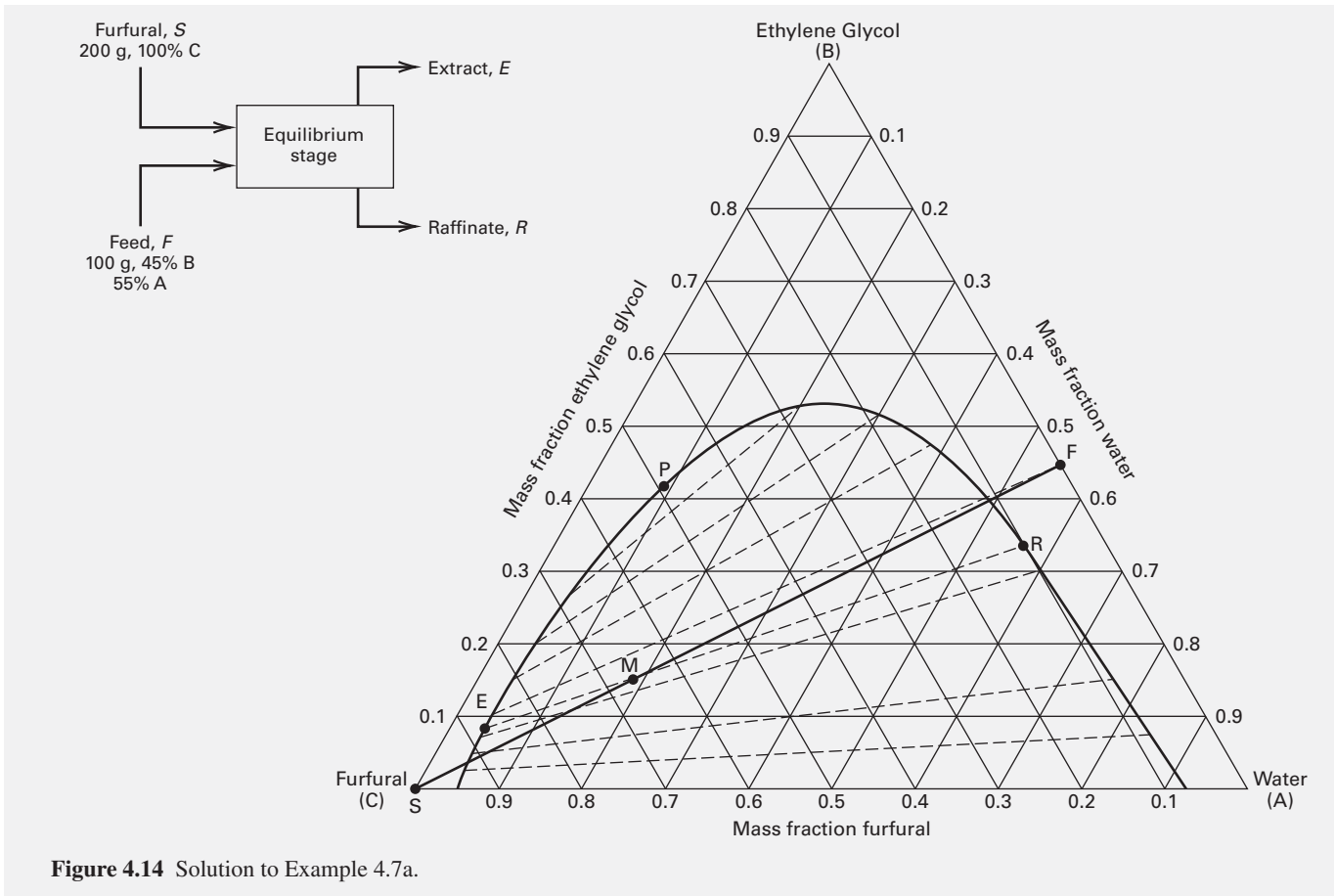
By material balance, the amount of M , is the sum of $E + R = S + F$. Furthermore, as shown, the mixing point is located on an equilibrium tie line. Since it is unlikely that a tie line from experimental data going through point M will already exist, one is drawn by interpolation between the tie lines on either side of point M . An interpolated tie line is included in Figure 4.14 with termination points at the extract, E , at a composition of 8.5 wt% B, 4.5 wt% A, and 87.0 wt% C; and at the raffinate, R , at 34.0 wt% B, 56.0 wt% A, and 10.0 wt% C.

The inverse-lever-arm rule can be used with the tie line that runs through point M to determine the amounts of E and R . Using a ruler to measure line lengths,

$$\frac{E}{F + S} = \frac{E}{E + R} = \frac{\overline{MR}}{\overline{ER}} = 0.733$$

Thus, $E = 0.733(100 + 200) = 220$ g and $R = (100 + 200) - 220 = 80$ g.

- (b) Alternatively, E can be calculated by combining an overall mass balance around the extraction unit with an overall ethylene glycol mass balance, using the wt% values of ethylene glycol determined graphically in part (a).



In Figure 4.13, two pairs of components are mutually soluble, while one pair is only partially soluble. Ternary systems where two pairs and even all three pairs are only partially soluble also exist. Figure 4.15, from Francis [3] and Findlay [4] shows examples of four cases where two pairs of components are only partially soluble. In (a), two separate two-phase regions are formed, while in (c), a three-phase region, RST, exists in addition to the two separate two-phase regions. In (b), the two separate two-phase regions merge. For a ternary mixture, as temperature is reduced, phase behavior may progress from (a) to (b) to (c). In both Figures 4.13 and 4.15, all tie lines slope in the same direction. In some systems **solutropy**, a reversal of tie-line slopes, occurs.

§4.5 MULTICOMPONENT LIQUID-LIQUID SYSTEMS

Quaternary and higher multicomponent mixtures are encountered in extraction processes, particularly if two solvents are used to separate two solutes. Multicomponent liquid-liquid equilibria are complex, and there is no compact, graphical way of representing phase-equilibria data. In addition, few sets of experimental data are available for quaternary and higher multicomponent mixtures. Accordingly, the computation of

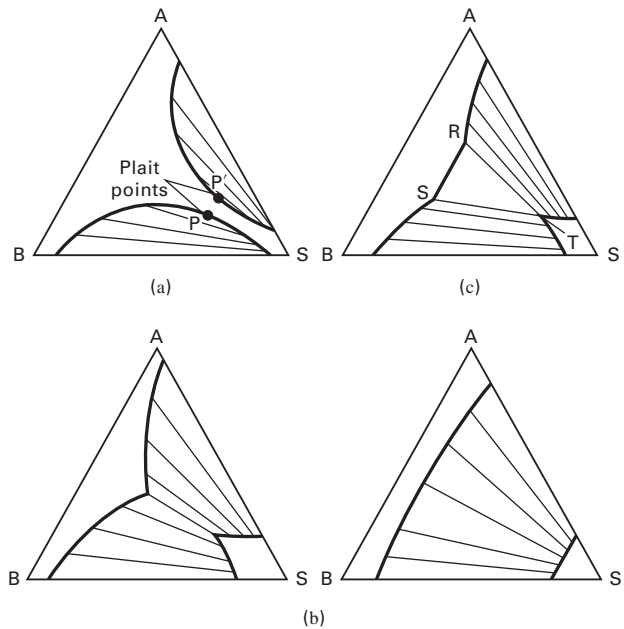


Figure 4.15 Additional types of ternary liquid phase equilibria: (a) miscibility boundaries are separate; (b) miscibility boundaries and tie-line equilibria merge; (c) tie lines do not merge and the three-phase region RST is formed.

single-stage, equilibrium-phase compositions is best made with a process simulator, which uses liquid-phase activity-coefficient models (e.g., NRTL, UNIQUAC, or UNIFAC) from Chapter 2. These models predict multicomponent coefficients from binary data and/or use group-contribution methods when data are not available. When only two liquid phases occur at equilibrium, process simulators use a modification of the Rachford–Rice flash procedure of §4.3.2 for multicomponent vapor–liquid equilibrium. For single-stage liquid–liquid extraction, the following symbol transformations are made, and extraction calculations are typically made with moles.

Vapor–Liquid Equilibria	Liquid–Liquid Equilibria
Feed, F	Feed, F , + solvent, S
Equilibrium vapor, V	Equilibrium Extract, E ($L^{(1)}$)
Equilibrium liquid, L	Equilibrium Raffinate, R ($L^{(2)}$)
Feed mole fractions, z_i	Mole fractions of combined F and S
Vapor mole fractions, y_i	Extract mole fractions, $x_i^{(1)}$
Liquid mole fractions, x_i	Raffinate mole fractions, $x_i^{(2)}$
K -value, K_i	Distribution coefficient, K_{D_i}
$\Psi = V/F$	$\Psi = E/F$

The modified Rachford–Rice algorithm is designed to handle isothermal vapor–liquid or liquid–liquid equilibrium-stage calculations when K -values depend strongly on phase compositions. For application to the liquid–liquid case, the algorithm requires that feed and solvent flow rates and compositions be fixed, and that the system pressure and temperature of one of the products be specified. An initial estimate is made of the equilibrium phase compositions, $x_i^{(1)}$ of the extract and $x_i^{(2)}$ of the raffinate. These values are used to estimate values of the two sets of liquid-phase activity-coefficients $\gamma_i^{(1)}$ and $\gamma_i^{(2)}$ from the NRTL, UNIQUAC, or UNIFAC models discussed in Chapter 2. A modified Raoult’s law, (4-12), applies to each of the two equilibrium liquid phases at near-ambient pressure. If the equations for each phase are combined to eliminate y_i , the following expression is obtained:

$$\gamma_i^{(1)} x_i^{(1)} = \gamma_i^{(2)} x_i^{(2)} \quad (4-37)$$

Substituting (4-37) into the definition of the distribution coefficient, (4-7),

$$K_{D_i} = \frac{\gamma_i^{(2)}}{\gamma_i^{(1)}} \quad (4-38)$$

These K_{D_i} values are then used with (4-26) to iteratively solve for $\Psi = E/(F + S)$, from which new values of $x_i^{(2)}$ and $x_i^{(1)}$ are computed from (4-23) and (4-24) respectively. Resulting values of $x_i^{(2)}$ and $x_i^{(1)}$ will not usually sum to 1 for each phase and are normalized by using equations of the form $x'_i = \frac{C}{x_i / \sum_{i=1}^C x_i}$, where values of x'_i are the normalized values that sum to 1. For the next iteration, normalized values replace previous values. This outer loop is repeated until the compositions, $x_i^{(2)}$ and $x_i^{(1)}$, converge.

EXAMPLE 4.8 Liquid–Liquid Equilibrium for a Four-Component Mixture.

An azeotropic mixture of isopropanol, acetone, and water is dehydrated using ethyl acetate in two distillation columns. Benzene, rather than ethyl acetate was previously used as the dehydrating agent, but legislation has made benzene undesirable because it is carcinogenic. The overhead vapor from the first column, at 20 psia and 80°C with the composition listed below, is condensed and cooled to 35°C, without significant pressure drop, resulting in the formation of two equilibrium liquid phases. Estimate the phase flow rates in kg/h and the equilibrium phase compositions in wt%.

Component	kg/h
Isopropanol	4,250
Acetone	850
Water	2,300
Ethyl acetate	43,700

Note that from §4.3.1, $N_D = C + 4 = 8$, which is satisfied by the specifications.

Solution

This example is solved by a process simulator. The simulator converts mass units to mole units, makes the computations in mole units, and converts the results to mass units. The results using the CHEMCAD process simulator with the UNIFAC method to estimate liquid-phase activity coefficients are as follows:

Component	Weight Fraction	
	Organic-Rich Phase	Water-Rich Phase
Isopropanol	0.0843	0.0615
Acetone	0.0169	0.0115
Water	0.0019	0.8888
Ethyl acetate	<u>0.8969</u>	<u>0.0382</u>
Flow rate, kg/h	48,617	2,483

§4.6 LIQUID–SOLID SYSTEMS

Liquid–solid separations include leaching, crystallization, and adsorption. In leaching (solid–liquid extraction), a multicomponent solid mixture is separated by contacting the solid with a solvent that selectively dissolves some solid species. Although this operation is similar to liquid–liquid extraction, leaching is a more difficult operation to simulate in that diffusion in solids is very slow compared to diffusion in liquids, making it difficult to achieve equilibrium. Also, it is impossible to completely separate a solid phase from a liquid phase. A solids-free liquid phase can be obtained, but the solids will always be accompanied by some liquid. In comparison, complete separation of two liquid phases is easy to achieve by settling vessels with draw-offs or by continuous centrifugation.

Crystallization or precipitation of a component from a liquid mixture is an operation in which equilibrium can be achieved, but a sharp phase separation is again impossible. A drying step is needed because crystals occlude liquid.

Adsorption, a third application of liquid–solid systems, employs porous solid particles that do not undergo phase or composition change. Instead, they selectively adsorb liquid species on their exterior and interior surfaces. After a contact time sufficient to approach equilibrium, adsorbed species are desorbed and the solid adsorbent particles are regenerated. Ion exchange and chromatography are variations of adsorption.

§4.6.1 Liquid Adsorption

When a liquid contacts porous solid particles, adsorption takes place on the external and internal solid surfaces until equilibrium is reached. Solid **adsorbents** are essentially insoluble in the liquid. The adsorbed components are called **solutes** when in the liquid and **adsorbates** when adsorbed. Higher concentrations of solute in the solution result in higher adsorbate concentrations. Other component(s) of the solution are the solvent and carrier, which are assumed not to adsorb.

No theory for predicting adsorption–equilibrium curves, based on molecular properties of the solute and solid, is universally embraced. Laboratory measurements are necessary to provide data for plotting isothermal equilibrium curves, called **adsorption isotherms**. Figure 4.16, from Fritz and Schluender [5], is an equilibrium isotherm for the adsorption of phenol from a very dilute aqueous solution onto activated carbon at 20°C. The ordinate in millimoles of phenol adsorbate per gram of adsorbent is plotted against the concentration of phenol solute in millimoles per liter of aqueous solution. The microporous structure of activated carbon provides a high internal surface area per unit mass of carbon, and therefore a high capacity for adsorption. Activated carbon preferentially adsorbs organic compounds when contacted with water containing dissolved organics. Water is treated as a pure carrier, with negligible adsorption on carbon.

As shown in Figure 4.16, as the concentration of phenol in water increases, the equilibrium adsorption increases rapidly at first and increases slowly as saturation is approached. When the concentration of phenol is 1.0 mmol/L (0.001 mol/L of

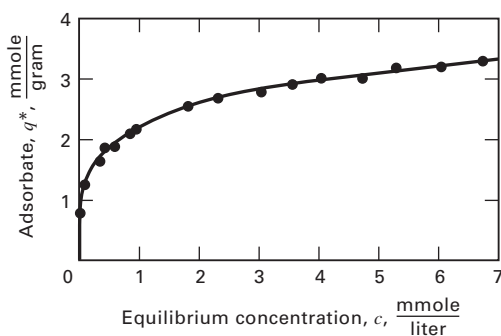


Figure 4.16 Adsorption isotherm for phenol from an aqueous solution with activated carbon at 20°C.

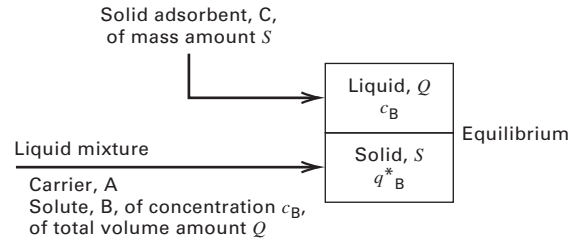


Figure 4.17 Equilibrium stage for liquid adsorption.

aqueous solution or 0.000001 mol/g of aqueous solution), the concentration of phenol on activated carbon is 2.16 mmol/g (0.00216 mol/g of carbon or 0.203 g phenol/g of carbon). The extent of adsorption depends on the adsorption process used and the adsorptivity of the carbon.

Adsorption isotherms are used to determine the amount of adsorbent required to selectively remove solute from a liquid. Consider the ideal, single-stage batch adsorption process of Figure 4.17, where solid adsorbent C and a liquid mixture of carrier A and solute B are charged to a vessel and brought to equilibrium. Let: $c_B^{(F)}$ = concentration of solute in the feed; c_B = concentration of solute in the product liquid; q_B^* = equilibrium concentration of adsorbate on adsorbent; Q = volume of liquid (assumed to remain constant during adsorption); and S = mass of adsorbent particles on a solute-free basis.

A solute material balance, assuming that the entering adsorbent is free of solute and that equilibrium is achieved gives

$$c_B^{(F)}Q = c_B Q + q_B^* S \quad (4-39)$$

Rearrangement of (4-39) into a straight-line form with the coordinates of Figure 4.16 gives:

$$q_B^* = -\frac{Q}{S}c_B + c_B^{(F)}\frac{Q}{S} \quad (4-40)$$

When plotted on Figure 4.16, the slope is $(-Q/S)$ and the intercept is $c_B^{(F)}(Q/S)$. The intersection of the material balance line with adsorption isotherm curve is the equilibrium point. If an equation can be fitted to the adsorption isotherm, the equilibrium point can be determined algebraically as in the following example.

EXAMPLE 4.9 Adsorption of Phenol on Activated Carbon.

A 1.0-L solution of 0.010 mol (10 mmoles) of phenol in water is brought to equilibrium at 20°C with 5 g of activated carbon having the adsorption isotherm shown in Figure 4.16. Determine the percent adsorption and the equilibrium concentration of phenol on and in the carbon by (a) a graphical method, and (b) an algebraic method. For the latter case, the curve of Figure 4.16 is fitted closely by an equation of the form developed by Freundlich using experimental data for adsorption of organic solutes on charcoal:

$$q_i^* = A c_i^{(1/n)} \quad (4-41)$$

where A and n depend on the solute, carrier, and adsorbent. Constant, n , in the exponent is greater than 1, and A is a function of temperature. For the phenol, water, activated carbon system at 20°C, $A = 2.16$ and $n = 4.35$.

Solution

From the data, $c_B^{(F)} = 10$ mmol/L, $Q = 1$ L, and $S = 5$ g.

(a) Graphical method.

Substituting the data into (4-40),

$$q_B^* = -\left(\frac{1}{5}\right)c_B + 10\left(\frac{1}{5}\right) = -0.2c_B + 2 \quad (1)$$

When this equation, with a slope of -0.2 and an intercept of 2 on the ordinate, is plotted on Figure 4.16, it intersects the adsorption isotherm curve at $q_B^* = 1.9$ mmol/g and $c_B = 0.57$ mmol/L. The % adsorption of phenol is

$$\frac{c_B^{(F)} - c_B}{c_B^{(F)}} = \frac{10 - 0.57}{10} = 0.94 \text{ or } 94\%$$

(b) Algebraic method.

The Freundlich equation, (4-41), is

$$q_B^* = 2.16c_B^{(1/4.35)} \quad (2)$$

Combining the solute material balance, (1) with the adsorption isotherm, (2) gives

$$2.16c_B^{0.23} = -0.2c_B + 2 \quad (3)$$

Or rewriting (3) in zero form, $f\{c_B\} = 2.16c_B^{0.23} + 0.2c_B - 2 = 0$. Solving this nonlinear equation in c_B using a nonlinear solver such as zero in MATLAB, $c_B = 0.558$ mmol/L. From (2), $q_B^* = 1.89$ mmol/g, and the % adsorption is 94.4%.

§4.7 GAS-LIQUID SYSTEMS

In the vapor-liquid systems described in §4.2 and §4.3, components in the vapor phase were all condensable at the system temperature. At near ambient pressure, their K -values are determined from Raoult's law, (4-13), if the system is ideal, or by the modified Raoult's law, (4-12), if not. In both cases, the K -value equation requires a value of the vapor pressure of the component. If a component in the vapor has a critical temperature below the system temperature, it is **non-condensable**, its vapor pressure does not exist, and (4-13) and (4-12) do not apply.

If a vapor includes one or more non-condensable components, it is commonly called a **gas**. Non-condensable components can dissolve, to some extent, into a liquid phase containing other components. Equilibrium K -values of non-condensable components cannot be calculated from (4-12) or (4-13). Instead, at near-ambient pressure conditions, it is common practice to apply the following version of Henry's law:

$$K_i = \frac{y_i}{x_i} = \frac{H_i}{P} \quad (4-42)$$

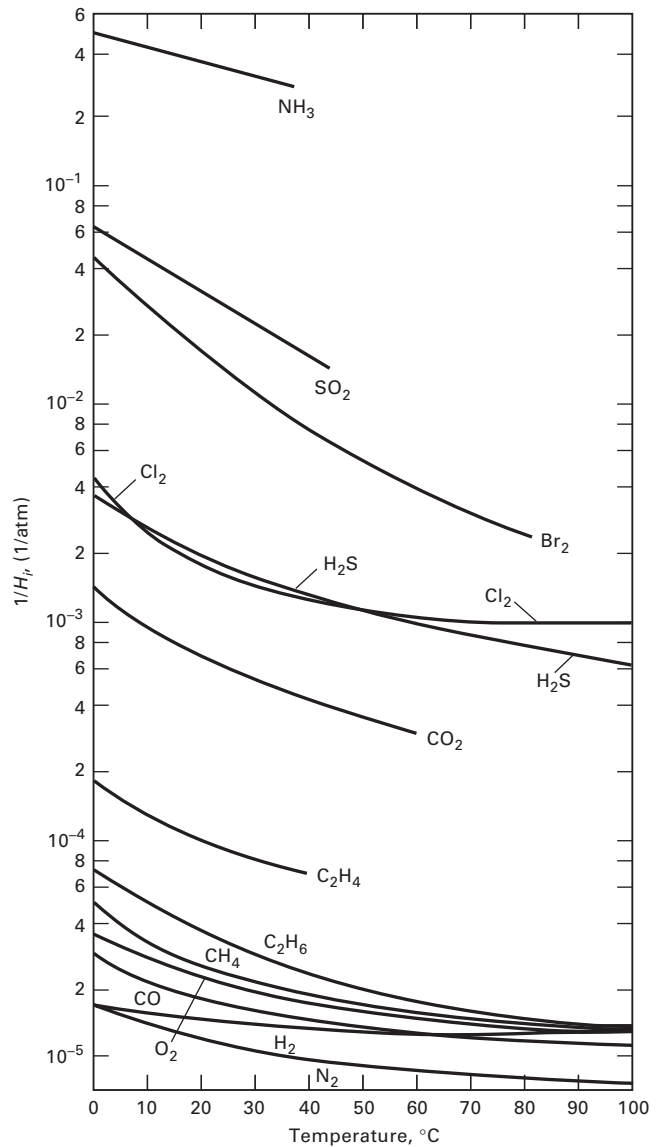


Figure 4.18 Henry's law constant for solubility of gases in water. Adapted from O.A. Hougen, K.M. Watson, and R.A. Ragatz, *Chemical Process Principles. Part I*, 2nd ed., John Wiley and Sons, New York (1954).

where H_i = Henry's law constant for non-condensable component i , which depends mainly on the temperature and liquid-phase composition. H_i has the same units as P . It is analogous to and replaces the term, $\gamma_{iL}P_i^s$, in the modified Raoult's law. Experimental data for the solubility of 13 pure gases in water are plotted in Figure 4.18 over a temperature 0 to 100°C. The ordinate is $(1/H_i)$ in mole fraction/atm. Unfortunately, Henry's law is not applicable to gases at high pressure or for non-condensable components with a high solubility in the liquid phase, e.g., ammonia in water. Then, experimental data at the system T and P are needed.

EXAMPLE 4.10 Absorption of SO₂ with Water.

200 kmol/h of feed gas, *F*, containing 2 mol% SO₂ and 98 mol% air is contacted in a single equilibrium stage with 1,000 kmol/h of pure water, *W*, at 25°C and 10 atm to absorb SO₂. The total flow rates of equilibrium products are *G* and *L*. Determine the fraction of SO₂ absorbed. Neglect the absorption of air and the vaporization of water. Assume the applicability of Henry’s law.

Solution

From Figure 4.18, the reciprocal of the Henry’s law constant for SO₂ at 25°C is 2.7×10^{-2} per atm. Thus, $H_{SO_2} = 37$ atm. At equilibrium from (4-42),

$$y_{SO_2} = \frac{H_{SO_2}}{P} x_{SO_2} = \frac{37}{10} x_{SO_2} = 3.7x_{SO_2} \quad (1)$$

An SO₂ material balance in kmol/h around the equilibrium stage, using mole ratios is

$$0.02F = 0.02(200) = 4.00 = \frac{y_{SO_2}}{1 - y_{SO_2}}(0.98)(200) + \frac{x_{SO_2}}{1 - x_{SO_2}}1000 \quad (2)$$

Solving (1) and (2) simultaneously for SO₂ mole fractions, y_{SO_2} and x_{SO_2} , using solve in MATLAB, gives $y_{SO_2} = 0.00855$ and $x_{SO_2} = 0.00231$.

The kmol/h of SO₂ in the equilibrium liquid = $0.00231(1000) = 2.31$ kmol/h.

Therefore, the fraction SO₂ absorbed = $2.31/4.00 = 0.578$.

EXAMPLE 4.11 Absorption of Ammonia from Air by Water Using an Equilibrium Diagram.

The partial pressure of ammonia (A) in air–ammonia gas mixtures in equilibrium with their aqueous solutions at 20°C is given in Table 4.4. Using these data, and neglecting the vapor pressure of water and the solubility of air in water, construct an equilibrium diagram at 101 kPa using mole ratios $Y_A = \text{mol NH}_3/\text{mol air}$ in the gas phase and $X_A = \text{mol NH}_3/\text{mol H}_2\text{O}$ in the liquid phase as coordinates. Henceforth, the subscript A is dropped. If 10 mol of feed gas of $Y = 0.3$ are contacted with 10 mol of aqueous liquid solution of $X = 0.1$, what are the compositions of the resulting equilibrium phases? The process is assumed to be isothermal at 20°C and 1 atm.

Table 4.4 Partial Pressure of Ammonia over Ammonia–Water Solutions at 20°C

NH ₃ Partial Pressure, kPa	g NH ₃ /g H ₂ O
4.23	0.05
9.28	0.10
15.2	0.15
22.1	0.20
30.3	0.25

Solution

Equilibrium data in Table 4.4 are recalculated in terms of mole ratios and listed in Table 4.5. The equilibrium curve is plotted in Figure 4.19.

Table 4.5 *Y–X* Data for Ammonia–Water, 20°C

<i>Y</i> , mol NH ₃ /mol Air	<i>X</i> , mol NH ₃ /mol H ₂ O
0.044	0.053
0.101	0.106
0.176	0.159
0.279	0.212
0.426	0.265

Mol NH₃ in entering gas = $10[Y_0/(1 + Y_0)] = 10(0.3/1.3) = 2.3$
 Mol NH₃ in entering liquid = $10[X_0/(1 + X_0)] = 10(0.1/1.1) = 0.91$

A material balance for ammonia around the equilibrium stage shown in the insert in Figure 4.19 is

$$GY_0 + LX_0 = GY_1 + LX_1 \quad (1)$$

where *G* = moles of NH₃-free air and *L* = moles of NH₃-free H₂O. Subscript 0 refers to feeds, while 1 refers to equilibrium products. $G = 10 - 2.3 = 7.7$ mol and $L = 10 - 0.91 = 9.09$ mol, as shown in Figure 4.19.

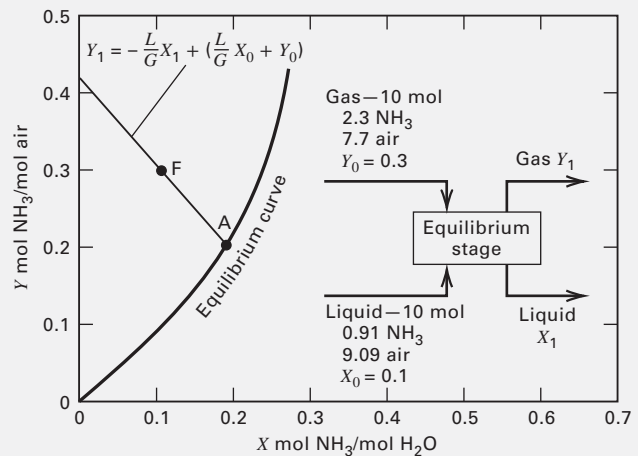


Figure 4.19 Equilibrium for air–NH₃–H₂O at 20°C, 1 atm, in Example 4.11.

Solving for Y_1 from (1),

$$Y_1 = -\frac{L}{G}X_1 + \left(\frac{L}{G}X_0 + Y_0\right) \quad (2)$$

This is an equation of a straight line of slope $(-L/G) = -9.09/7.7 = -1.19$, with an intercept of $(L/G)(X_0) + Y_0 = -(-1.19)(0.1) + 0.3 = 0.42$. The intersection of this material-balance line with the equilibrium curve, as shown in Figure 4.19, gives the ammonia composition of the gas and liquid leaving the stage as $Y_1 = 0.193$ and $X_1 = 0.19$. This result can be checked by an NH₃ balance, since the amount of NH₃ leaving is $(0.193)(7.7) + (0.19)(9.09) = 1.48 + 1.73 = 3.21$, which equals the total moles of NH₃ entering the stage.

§4.8 GAS–SOLID SYSTEMS

Gas–solid systems are encountered in desublimation and gas-adsorption separations.

§4.8.1 Desublimation

In desublimation, one or more components (solutes) in the gas phase are condensed to form a solid phase without passing through a liquid state. At low pressure, desublimation is governed by the solid vapor pressure of the solute. Sublimation of the solid takes place when the partial pressure of the solute in the gas phase is less than the vapor pressure of the solid at the system temperature. When the partial pressure of the solute in the gas phase exceeds the vapor pressure of the solid, desublimation occurs. At phase equilibrium, the vapor pressure of the solid is equal to its partial pressure as a solute in the gas phase.

EXAMPLE 4.12 Desublimation of Phthalic Anhydride.

Ortho-xylene is completely oxidized in the vapor phase with air to produce phthalic anhydride, PA, in a catalytic reactor at about 370°C and 780 torr. A large excess of air is used to keep the xylene concentration below 1 mol% to avoid an explosive mixture. 8,000 lbmol/h of reactor-effluent gas, F , containing 67 lbmol/h of PA and other amounts of N_2 , O_2 , CO , CO_2 , and water vapor, are cooled to separate the PA from the gas by desublimation to a solid at a total pressure of 770 torr. If the gas is cooled to 206°F, where the vapor pressure of solid PA is 1 torr, calculate the number of pounds of PA condensed per hour as a solid, S , and the percent recovery of PA from the gas product, G , if equilibrium is achieved.

Solution

At these conditions, only PA condenses. At equilibrium, the partial pressure of PA in the gas equals the vapor pressure of solid PA, or 1 torr. The partial pressure of PA in the cooled gas, p_{PA} , is given by Dalton's law of partial pressures:

$$n_{PA}^{(G)} = \frac{P_{PA}}{P} G \quad (1)$$

where, $n_{PA}^{(G)}$ = molar flow rate of PA in equilibrium gas.

The equilibrium gas flow rate, G , is

$$G = (8,000 - 67) + n_{PA}^{(G)} \quad (2)$$

Combining (1) and (2),

$$\begin{aligned} n_{PA}^{(G)} &= \frac{P_{PA}}{P} \left[(8,000 - 67) + n_{PA}^{(G)} \right] \\ &= \frac{1}{770} \left[(8,000 - 67) + n_{PA}^{(G)} \right] \end{aligned} \quad (3)$$

Solving this linear equation, $n_{PA}^{(G)} = 10.3$ lbmol/h of PA.

The amount of PA desublimed is $67 - 10.3 = 56.7$ lbmol/h. The percent recovery of PA is $56.7/67 = 0.846$ or 84.6%. It is noteworthy that the PA remaining in the gas is above EPA standards, so a lower temperature or catalytic oxidation is required. At 140°F the recovery is almost 99%.

§4.8.2 Gas Adsorption

As with liquid mixtures, one or more gas components can be adsorbed on the external and internal surfaces of a porous, solid adsorbent. Data for a single solute is represented by an adsorption isotherm of the type shown in Figure 4.16 or similar diagrams. However, when two components of a gas mixture

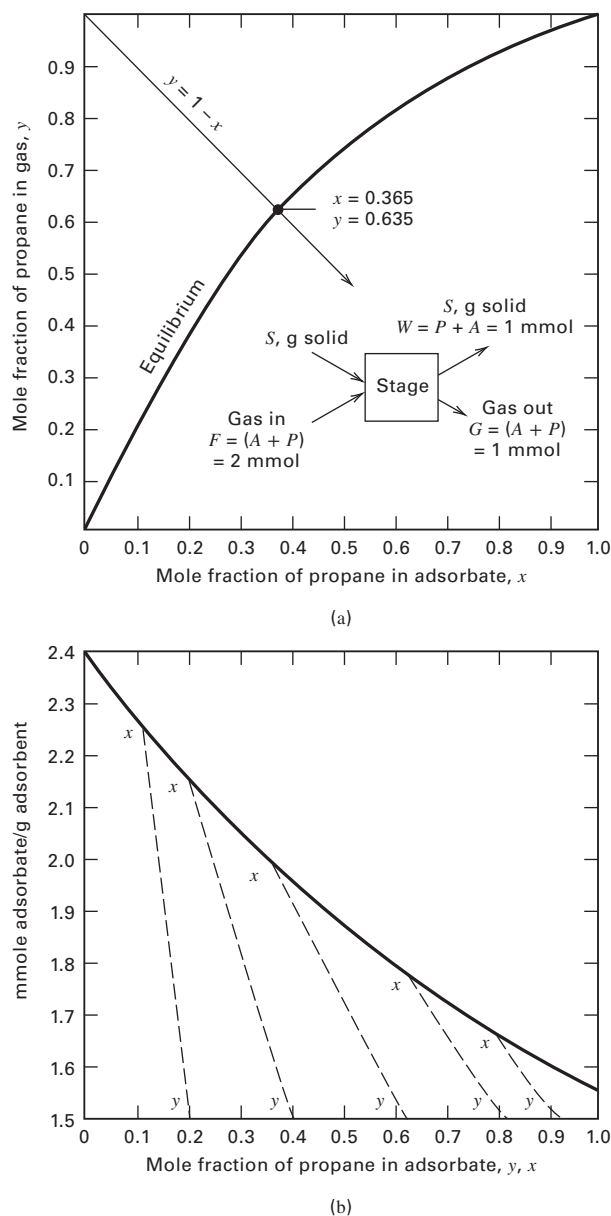


Figure 4.20 Adsorption equilibrium at 25°C and 101 kPa of propane and propylene on silica gel. [Adapted from [6] with permission of the American Chemical Society.]

are adsorbed and the purpose is to separate them, other methods of displaying are preferred. Figure 4.20 shows the data of Lewis et al. [6] for the adsorption of a propane (P)–propylene (A) gas mixture on silica gel at 25°C and 101 kPa. At 25°C, a pressure of at least 1,000 kPa would be required to initiate separation by partial condensation of a mixture of propylene and propane. However, Figure 4.20b shows that in the presence of silica gel, significant amounts of gas are adsorbed at 101 kPa.

Figure 4.20a is similar to a binary vapor–liquid equilibrium plot of the type shown in Figure 4.3b. For propylene–propane mixtures, propane is adsorbed less strongly, so its mole fraction is used in Figure 4.20a. The liquid-phase mole fraction is replaced by the mole fraction of propane in the adsorbate.

On the ordinate axis, the vapor-phase mole fraction has been replaced by the propane mole fraction in the gas. In an equimolar gas-phase mixture, Figure 4.20a shows that the adsorbate contains only 27 mol% propane. An adsorption separation index, similar to the relative volatility used for vapor–liquid equilibrium, is defined by

$$\text{Adsorption separation index} = \frac{y_A/x_A}{(1-y_A)/(1-x_A)}$$

which for the above example is

$$\frac{0.50/0.27}{(1-0.50)/0.27} = 2.70$$

This adsorption separation index is considerably larger than the relative volatility for vapor–liquid equilibrium, defined by (4-10), which is only about 1.13 for the propylene–propane system. Thus, adsorption of propylene from a gas mixture with propane is more thermodynamically favored than distillation.

Figure 4.20b determines the amount of adsorbent needed. It plots the total mmols of adsorbate per gram of adsorbent as a function of the mole fraction, $y = y_P$, of the propane in the gas equilibrated with the adsorbate, on the abscissa. Dashed tie lines connect the gas mole fractions with corresponding liquid mole fractions of propane in the adsorbate, $x = x_P$, on the equilibrium curve. Using the same example, as above, when $x_P = 0.27$, the total mmols of adsorbate per gram of adsorbent = 2.08. Thus, 0.48 grams adsorbent is needed per mmol of adsorbate for an equimolar gas mixture. Inserting a tie line in Figure 4.20b at $x_P = 0.27$ on the equilibrium curve connects to $y_P = 0.50$ on the abscissa (the same value read from the ordinate of Figure 4.20a).

EXAMPLE 4.13 Separation of Propylene–Propane by Adsorption.

Propylene (A) and propane (P) are separated by preferential adsorption on porous silica gel (S) at 25°C and 101 kPa. Two millimoles of a feed gas, F , of 50 mol% P and 50 mol% A are equilibrated with silica gel at 25°C and 101 kPa. Measurements show that 1 mmol of gas is adsorbed. If the data of Figure 4.20 apply, what is the mole fraction of propane in the equilibrium gas and in the adsorbate, and how many grams of silica gel are used?

Solution

The process is included in Figure 4.20a, where W = millimoles of adsorbate, G = millimoles of gas leaving, and z_A = mole fraction of propane in the feed. The propane mole balance is

$$z_A F = W x_A + G y_A \quad (1)$$

Because $F = 2$, $z_A = 0.5$, $W = 1$, and $G = F - W = 1$, substitution in (1) gives $1 = x + y$. This material balance line, $y = 1 - x$ is plotted in Figure 4.20a. It intersects the equilibrium curve at $x = 0.365$, $y = 0.635$. From Figure 4.20b, at the point $x = 0.365$, the equilibrium adsorbate is 2.0 mmol adsorbate/g adsorbent. Therefore, for 1 mmol of adsorbate, $S = 1.0/2 = 0.50$ g silica gel.

§4.9 THREE-PHASE EQUILIBRIUM SYSTEMS

Although in industrial separation processes two-phase systems predominate, three-phase systems are not uncommon. They include vapor–liquid–solid systems in pervaporation membrane separations (separation operation 4 in Table 1.3) and evaporative crystallization. Vapor–liquid–liquid systems occur when partially condensing, partially evaporating, or distilling mixtures of water and organic chemicals that have limited solubility in water.

Although three-phase equilibrium calculations are based on the same principles as two-phase systems (i.e., material balances, physical equilibrium, and, if needed, energy balances), the number of nonlinear equations in the system increases, making the computations more difficult and more demanding in terms of reasonable initial guesses to initiate iterative calculation procedures. These and other rigorous calculations are best made with process simulators.

§4.9.1 Vapor–Liquid–Liquid Flash Procedure

Rigorous computer methods for treating a vapor–liquid–liquid equilibrium system at a given temperature and pressure are called **three-phase isothermal flash** algorithms. As first presented by Henley and Rosen [7], it is analogous to the isothermal two-phase flash algorithm in §4.3. Their procedure, or modifications thereof, is available in all process simulators.

Let the two liquid phases be labeled with superscripts (1) and (2). The following material balances and two phase-equilibrium relations apply for each component:

$$F z_i = V y_i + L^{(1)} x_i^{(1)} + L^{(2)} x_i^{(2)} \quad (4-43)$$

$$K_i^{(1)} = y_i / x_i^{(1)} \quad (4-44)$$

$$K_i^{(2)} = y_i / x_i^{(2)} \quad (4-45)$$

A distribution coefficient relationship that can be substituted for (4-44) or (4-45) is

$$K_{D_i} = x_i^{(1)} / x_i^{(2)} \quad (4-46)$$

These equations are solved by a modification of the Rachford–Rice procedure, where $\Psi = V/F$ and $\xi = L^{(1)} / (L^{(1)} + L^{(2)})$, where $0 \leq \Psi \leq 1$ and $0 \leq \xi \leq 1$.

By combining (4-43), (4-44), and (4-45) with

$$\sum x_i^{(1)} - \sum y_i = 0 \quad (4-47)$$

and

$$\sum x_i^{(1)} - \sum x_i^{(2)} = 0 \quad (4-48)$$

to eliminate y_i , $x_i^{(1)}$, and $x_i^{(2)}$, two simultaneous nonlinear equations in Ψ and ξ are obtained:

$$\sum_i \frac{z_i(1 - K_i^{(1)})}{\xi(1 - \Psi) + (1 - \Psi)(1 - \xi)K_i^{(1)}/K_i^{(2)} + \Psi K_i^{(1)}} = 0 \quad (4-49)$$

and

$$\sum_i \frac{z_i(1 - K_i^{(1)}/K_i^{(2)})}{\xi(1 - \Psi) + (1 - \Psi)(1 - \xi)K_i^{(1)}/K_i^{(2)} + \Psi K_i^{(1)}} = 0 \quad (4-50)$$

Starting guesses are provided for the phase compositions, from which the corresponding K -values are estimated. Values of Ψ and ξ are then computed by solving nonlinear equations (4-49) and (4-50) simultaneously using solve in MATLAB or Newton's method. The results are used to calculate the phase amounts and compositions from

$$V = \Psi F \quad (4-51)$$

$$L^{(1)} = \xi(F - V) \quad (4-52)$$

$$L^{(2)} = F - V - L^{(1)} \quad (4-53)$$

$$y_i = \frac{z_i}{\xi(1 - \Psi)/K_i^{(1)} + (1 - \Psi)(1 - \xi)/K_i^{(2)} + \Psi} \quad (4-54)$$

$$x_i^{(1)} = \frac{z_i}{\xi(1 - \Psi) + (1 - \Psi)(1 - \xi)(K_i^{(1)}/K_i^{(2)}) + \Psi K_i^{(1)}} \quad (4-55)$$

$$x_i^{(2)} = \frac{z_i}{\xi(1 - \Psi)(K_i^{(2)}/K_i^{(1)}) + (1 - \Psi)(1 - \xi) + \Psi K_i^{(2)}} \quad (4-56)$$

If the guessed compositions do not equal the calculated values, the calculations are repeated with new guesses. The procedure is iterated in a manner similar to the Rachford–Rice method, until the phase compositions converge.

Three-phase-flash calculations are difficult, even by the above procedure, because of the strong dependency of activity coefficients in the K -values on liquid-phase compositions when two immiscible liquid phases are present. In addition, although the presence of three phases is assumed initially, realistically there are five possible phase situations: (1) V - $L^{(1)}$ - $L^{(2)}$, (2) V - $L^{(1)}$, (3) $L^{(1)}$ - $L^{(2)}$, (4) V , and (5) $L^{(1)}$. An algorithm used by process simulators for determining phase conditions is shown in Figure 4.21. Process simulators can also perform adiabatic or nonadiabatic three-phase flashes by also iterating on temperature until the enthalpy balance,

$$h_F F + Q = h_V V + h_{L(1)} L^{(1)} + h_{L(2)} L^{(2)} = 0 \quad (4-57)$$

is satisfied. Process simulators also use the three-phase-flash procedure for calculating phase equilibrium for two liquid phases. It is not uncommon for three phases to form on some trays of a distillation column if water is present with certain organic compounds.

EXAMPLE 4.14 Three-Phase Isothermal Flash.

In a process for producing styrene from toluene and methanol, the gaseous reactor effluent is as follows:

Component	kmol/h
Hydrogen	350
Methanol	107
Water	491
Toluene	107
Ethylbenzene	141
Styrene	350

If this stream is brought to equilibrium at 38°C and 300 kPa, compute the amounts and compositions of the phases present.

Solution

Because water, hydrocarbons, an alcohol, and a light gas are present, the possibility of a vapor and two liquid phases exists, with methanol distributed among all three phases. The isothermal three-phase flash module of the CHEMCAD process simulator was used with Henry's law for H_2 and the UNIFAC method for activity coefficients for the other components. The results were:

Component	kmol/h		
	V	$L^{(1)}$	$L^{(2)}$
Hydrogen	349.96	0.02	0.02
Methanol	9.54	14.28	83.18
Water	7.25	8.12	475.63
Toluene	1.50	105.44	0.06
Ethylbenzene	0.76	140.20	0.04
Styrene	1.22	348.64	0.14
Totals	370.23	616.70	559.07

As expected, little H_2 is dissolved in either liquid. The water-rich liquid phase, $L^{(2)}$, contains little of the hydrocarbons, but a greater fraction of the methanol. The organic-rich phase, $L^{(1)}$, contains most of the hydrocarbons, a small amount of water and a lesser fraction of the methanol. Additional calculations at temperatures higher than 38°C and 300 kPa indicate that the organic phase condenses first, with a dew point of 143°C, while the aqueous phase condenses with a secondary dew point of 106°C.

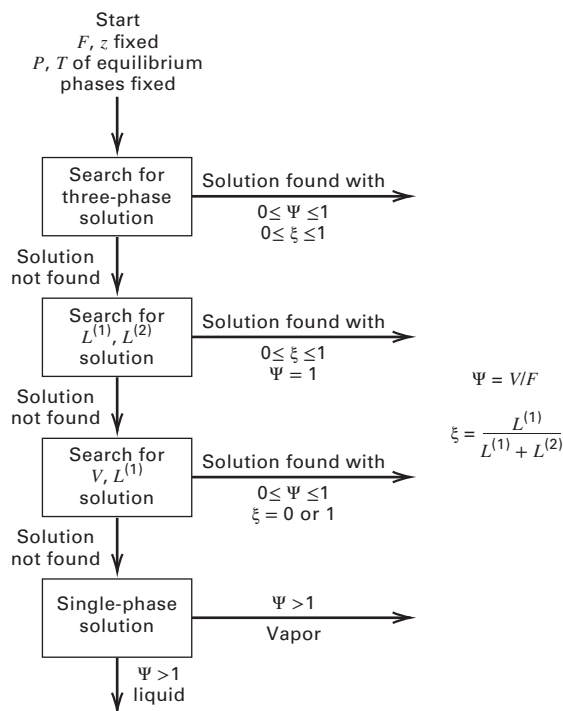


Figure 4.21 Algorithm for an isothermal three-phase flash.

CHAPTER 4 NOMENCLATURE

Abbreviations and Acronyms

RR	Rachford–Rice algorithm
OF	objective function, below (4-14)

Latin Symbols

A	Carrier for solute
A	constant in Freundlich equation, (4-41)
B	solute in liquid–liquid extraction or in liquid adsorption
C	solvent for B, Figure 4.12; adsorbent, Figure 4.17
<i>c</i>	concentration of solute in liquid, Figure 4.17
\mathcal{E}	extraction factor, (4-35)
<i>G</i>	moles of carrier gas (solute free); total gas leaving an adsorption stage, Figure 4.20
K'_D	K_D in terms of mass ratios, (4-33)
<i>L</i>	moles of liquid free of solute; molar flow of liquid
N_E	number of independent equations, (4-3)
N_P	number of phases, (4-3)
N_V	number of variables, (4-3)
<i>Q</i>	total volume of liquid (in adsorption)
q^*	amount adsorbed by adsorbent at equilibrium, (4-41)
S	solvent
S	mass flow rate of solvent (identified as component C in Figure 4.12); adsorbent in Figure 4.20; solid adsorbent, (4-39) and Figure 4.20

W	mass of saturated adsorbate leaving a stage, Figure 4.20
X	mass of solute/mass of carrier (liquid phase), (4-32) and Figure 4.20
<i>x</i>	mass fraction of adsorbate in adsorbent: mole fraction in liquid
Y	mass of solute/mass of carrier (vapor phase), Figure 4.20
<i>y</i>	mole fraction of solute in the gas: mole fraction in vapor

Greek Symbols

Λ	parameters in Wilson equation, (2-63)
Ψ	V/F , (4-22)
ξ	$(L^{(1)})/(L^{(1)} + L^{(2)})$, (4-49)

Subscripts

A	component, carrier for B
B	component, solute adsorbed, absorbed, or extracted

Superscripts

<i>F</i>	feed, (4-39)
<i>G</i>	gas flow or gas phase
<i>n</i>	constant in Freundlich equation, (4-41)
(1)	liquid phase one
(2)	liquid phase two
I, II	liquid phase one, two

SUMMARY

- The Gibbs' phase rule applies to intensive variables at equilibrium. It determines the number of independent variables that specify a system. This rule can be extended to determine the degrees of freedom (number of allowable specifications) for flow systems, which include extensive variables. Intensive and extensive variables are related by material balances, phase-equilibria data or equations, and energy balances.
- Vapor–liquid equilibrium conditions for binary systems can be represented by T – y – x and y – x diagrams. A measure of the comparative ease or difficulty of separating a binary system by partial condensation, partial evaporation, or distillation is the relative volatility.
- Minimum- or maximum-boiling azeotropes formed by nonideal liquid mixtures are represented by the same types of diagrams used for nonazeotropic (zeotropic) binary mixtures. Highly nonideal liquid mixtures can form heterogeneous azeotropes having two liquid phases.
- For multicomponent mixtures, vapor–liquid equilibrium-phase compositions and amounts can be determined by isothermal-flash, adiabatic-flash, partial vaporization, or bubble- and dew-point calculations. For flash calculations, process simulators should be used.
- Liquid–liquid equilibrium conditions for ternary mixtures can be determined graphically from triangular diagrams. Liquid–liquid equilibrium conditions for multicomponent mixtures of four or more components must be determined with process simulators.
- Solid–liquid equilibrium occurs in leaching, crystallization, and adsorption. Adsorption equilibria can be represented algebraically or graphically by adsorption isotherms.
- Solubilities of sparingly soluble gases in liquids are well represented by Henry's law constant that depends on temperature.
- Solid vapor pressure determines equilibrium desublimation conditions for gas–solid systems. Adsorption isotherms and y – x diagrams are useful in calculations for gas mixtures in the presence of a solid adsorbent.
- Calculations of three-phase (vapor–liquid–liquid) equilibrium conditions are readily made with process simulators.

REFERENCES

1. RACHFORD, H.H., Jr. and J.D. RICE, *J. Pet. Tech.*, **4**(10), Section 1, p. 19, and Section 2, p. 3 (Oct. 1952).
2. CONWAY, J.B., and J.J. NORTON, *Ind. Eng. Chem.*, **43**, 1433–1435 (1951).
3. FRANCIS, A.W., *Liquid–Liquid Equilibria*, Interscience, New York (1963).
4. FINDLAY, A., *Phase Rule*, Dover, New York (1951).
5. FRITZ, W., and E.-U. SCHULUENDER, *Chem. Eng. Sci.*, **29**, 1279–1282 (1974).
6. LEWIS, W.K., E.R. GILLILAND, B. CHERTON, and W.H. HOFFMAN, *J. Am. Chem. Soc.*, **72**, 1153–1157 (1950).
7. HENLEY, E.J., and E.M. ROSEN, *Material and Energy Balance Computations*, John Wiley and Sons, New York, pp. 351–353 (1969).

STUDY QUESTIONS

- 4.1. What two types of equations or data are used for single equilibrium stage calculations?
- 4.2. How do intensive and extensive variables differ?
- 4.3. What is meant by the number of degrees of freedom?
- 4.4. What are the limitations of the Gibbs' phase rule? Can it be extended?
- 4.5. When a liquid and a vapor are in physical equilibrium, why is the vapor at its dew point and the liquid at its bubble point?
- 4.6. What is the difference between a homogeneous and a heterogeneous azeotrope?
- 4.7. Why do azeotropes limit the degree of separation achievable in a distillation operation?
- 4.8. What is the difference between an isothermal flash and an adiabatic flash?
- 4.9. Why is the isothermal-flash calculation so useful?
- 4.10. When a binary feed is contacted with a solvent to form two equilibrium liquid phases, which is the extract and which is the raffinate?
- 4.11. Why are triangular diagrams useful for ternary liquid–liquid equilibrium calculations? On such a diagram, what are the miscibility boundary, plait point, and tie lines?
- 4.12. What is the difference between adsorbent and adsorbate?
- 4.13. In adsorption, why should adsorbents have a microporous structure?
- 4.14. Does a solid have a vapor pressure?
- 4.15. What is the maximum number of phases that can exist at physical equilibrium for a given number of components?
- 4.16. In a rigorous vapor–liquid–liquid equilibrium calculation (the so-called three-phase flash), is it necessary to consider all possible phase conditions, i.e., all-liquid, all-vapor, vapor–liquid, liquid–liquid, and vapor–liquid–liquid?

EXERCISES

Section 4.1

4.1. Degrees-of-freedom for three-phase equilibrium.

Consider the equilibrium stage shown in Figure 4.22. Conduct a degrees-of-freedom analysis by performing the following steps:

- (a) list and count the variables,
- (b) write and count the equations relating the variables,

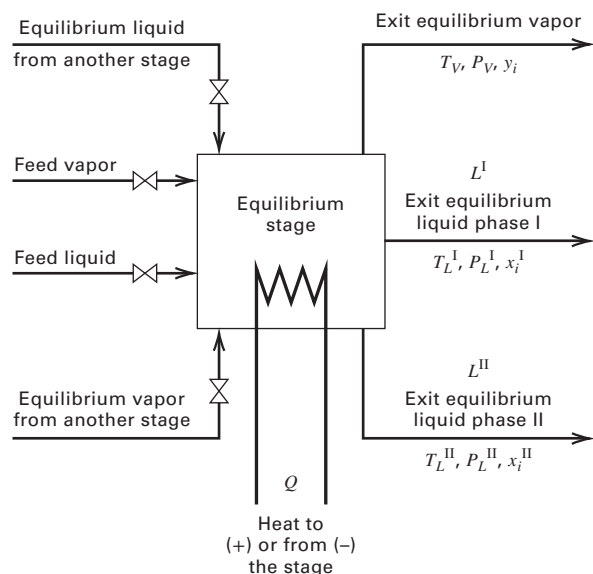


Figure 4.22 Conditions for Exercise 4.1.

- (c) calculate the degrees of freedom, and
 - (d) list a reasonable set of design variables.
- 4.2. **Uniqueness of three different separation operations.**
Can the following problems be solved uniquely?
- (a) The feed streams to an adiabatic equilibrium stage consist of liquid and vapor streams of known composition, flow rate, temperature, and pressure. Given the stage (outlet) temperature and pressure, calculate the compositions and amounts of equilibrium vapor and liquid leaving.
 - (b) The same as part (a), except that the stage is not adiabatic.
 - (c) A vapor of known T , P , and composition is partially condensed. The outlet P of the condenser and the inlet cooling water T are fixed. Calculate the cooling water required.
- 4.3. **Degrees-of-freedom for an adiabatic, two-phase flash.**
Consider an adiabatic equilibrium flash. The variables are all as indicated in Figure 4.8 with $Q = 0$. (a) Determine the number of variables. (b) Write all the independent equations that relate the variables. (c) Determine the number of equations. (d) Determine the number of degrees of freedom. (e) What variables would you prefer to specify in order to solve an adiabatic-flash problem?
- 4.4. **Degrees of freedom for a nonadiabatic, three-phase flash.**
Determine the number of degrees of freedom for a nonadiabatic, three-phase equilibrium flash.
- 4.5. **Application of Gibbs' phase rule.**

For the seven-phase equilibrium system shown in Figure 4.1, assume air consists of N_2 , O_2 , and argon. What is the number of degrees of freedom? What variables might be specified?

Section 4.2

4.6. Partial vaporization of a nonideal binary mixture.

A liquid mixture contains 25 mol% benzene and 75 mol% ethyl alcohol. The components are miscible in all proportions. The mixture is heated at a constant pressure of 1 atm from 60°C to 90°C. Using the following T - y - x experimental data, determine (a) the temperature where vaporization begins; (b) the composition of the first bubble of vapor; (c) the composition of the residual liquid when 25 mol % has evaporated, assuming that all vapor formed is retained in the apparatus and is in equilibrium with the residual liquid. (d) Repeat part (c) for 90 mol% vaporized. (e) Repeat part (d) if, after 25 mol% is vaporized as in part (c), the vapor formed is removed and an additional 35 mol% is vaporized by the same technique used in part (c). (f) Plot temperature versus mol% vaporized for parts (c) and (e).

 T - y - x DATA FOR BENZENE-ETHYL ALCOHOL AT 1 ATM

Temperature, °C:											
78.4	77.5	75	72.5	70	68.5	67.7	68.5	72.5	75	77.5	80.1
Mole percent benzene in vapor:											
0	7.5	28	42	54	60	68	73	82	88	95	100
Mole percent benzene in liquid:											
0	1.5	5	12	22	31	68	81	91	95	98	100

(g) Use the following vapor pressure data with Raoult's and Dalton's laws to construct a T - y - x diagram, and compare it to the answers obtained in parts (a) and (f) with those obtained using the experimental T - y - x data. What are your conclusions?

VAPOR PRESSURE DATA

Vapor pressure, torr:							
20	40	60	100	200	400	760	
Ethanol, °C:							
8	19.0	26.0	34.9	48.4	63.5	78.4	
Benzene, °C:							
-2.6	7.6	15.4	26.1	42.2	60.6	80.1	

4.7. Steam distillation of stearic acid.

Stearic acid is steam distilled at 200°C in a direct-fired still. Steam is introduced into the molten acid in small bubbles, and the acid in the vapor leaving the still has a partial pressure equal to 70% of the vapor pressure of pure stearic acid at 200°C. Plot the kg acid distilled per kg steam added as a function of total pressure from 3.3 kPa to 101.3 kPa at 200°C. The vapor pressure of stearic acid at 200°C is 0.40 kPa.

4.8. Equilibrium plots for benzene-toluene.

The relative volatility, α , of benzene to toluene at 1 atm is 2.5. Construct y - x and T - y - x diagrams for this system at 1 atm. Repeat the construction of the y - x diagram using vapor pressure data for benzene from Exercise 4.6 and for toluene from the table below, with Raoult's and Dalton's laws. Use the diagrams to determine the following: (a) A liquid containing 70 mol% benzene and 30 mol% toluene is heated in a container at 1 atm until 25 mol% of the original liquid is evaporated. Determine the temperature. The phases are then separated mechanically, and the vapors condensed. Determine the composition of the condensed vapor and the liquid residue. (b) Calculate and plot the K -values as a function of temperature at 1 atm.

VAPOR PRESSURE OF TOLUENE

Vapor pressure, torr:							
20	40	60	100	200	400	760	1,520
Temperature, °C:							
18.4	31.8	40.3	51.9	69.5	89.5	110.6	136

4.9. Vapor-liquid equilibrium for heptane-toluene system.

(a) The vapor pressure of toluene is given in Exercise 4.8, and that of *n*-heptane is in the table below. Construct the following plots: (a) a y - x diagram at 1 atm using Raoult's and Dalton's laws; (b) a T - x bubble-point curve at 1 atm; (c) α and K -values versus temperature; and (d) repeat of part (a) using an average value of α . Then, (e) compare your y - x and T - y - x diagrams with the following experimental data of Steinhauser and White [*Ind. Eng. Chem.*, **41**, 2912 (1949)].

VAPOR PRESSURE OF *n*-HEPTANE

Vapor pressure, torr:							
20	40	60	100	200	400	760	1,520
Temperature, °C:							
9.5	22.3	30.6	41.8	58.7	78.0	98.4	124

VAPOR-LIQUID EQUILIBRIUM DATA FOR *n*-HEPTANE/TOLUENE AT 1 ATM

x , <i>n</i> -heptane	y , <i>n</i> -heptane	T , °C
0.025	0.048	110.75
0.129	0.205	106.80
0.354	0.454	102.95
0.497	0.577	101.35
0.843	0.864	98.90
0.940	0.948	98.50
0.994	0.993	98.35

4.10. Continuous, single-stage distillation.

Saturated-liquid feed of $F = 40$ mol/h, containing 50 mol% A and B, is supplied to the apparatus in Figure 4.23. The condensate is split so that reflux/distillate = 1.

(a) If heat is supplied such that $W = 30$ mol/h and $\alpha = 2$, as defined below, what will be the composition of the overhead and the bottoms product?

$$\alpha = \frac{P_A^s}{P_B^s} = \frac{y_A x_B}{y_B x_A}$$

(b) If the operation is changed so that no condensate is returned to the still pot and $W = 3D$, compute the product compositions.

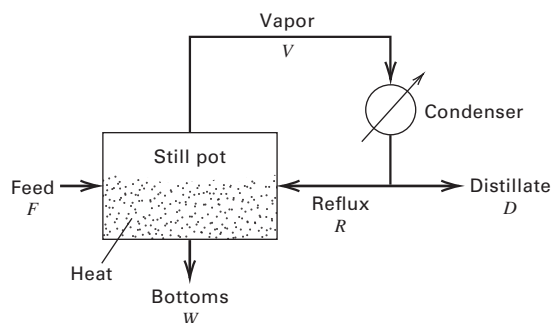


Figure 4.23 Conditions for Exercise 4.10.

4.11. Partial vaporization of feed to a distillation column.

A fractionation tower operating at 101.3 kPa produces a distillate of 95 mol% acetone (A), 5 mol% water, and a residue containing 1 mol% A. The feed liquid is at 125°C and 687 kPa and contains 57 mol% A. Before entering the tower, the feed passes through an expansion valve causing it to be partially vaporized at 60°C. From the data below, determine the molar ratio of liquid to vapor in the feed. Enthalpy and equilibrium data are: molar latent heat of A = 29,750 kJ/kmol; molar latent heat of H₂O = 42,430 kJ/kmol; molar specific heat of A = 134 kJ/kmol-K; molar specific heat of H₂O = 75.3 kJ/kmol-K; enthalpy of high-pressure, hot feed before adiabatic expansion = 0; enthalpies of feed phases after expansion are $h_V = 27,200$ kJ/kmol and $h_L = -5,270$ kJ/kmol. All data except *K*-values, are temperature-independent.

EQUILIBRIUM DATA FOR ACETONE–H₂O AT 101.3 kPa

<i>T</i> , °C	56.7	57.1	60.0	61.0	63.0	71.7	100
Mol% A in liquid:	100	92.0	50.0	33.0	17.6	6.8	0
Mol% A in vapor:	100	94.4	85.0	83.7	80.5	69.2	0

4.12. Enthalpy-concentration diagram.

Using vapor pressure data from Exercises 4.6 and 4.8 and the enthalpy data provided below (a) construct an *h*-*y*-*x* diagram for the benzene–toluene system at 1 atm (101.3 kPa) based on Raoult's and Dalton's laws and (b) calculate the energy required for 50 mol% vaporization of a 30 mol% liquid solution of benzene in toluene at saturation temperature. If the vapor is condensed, what is the heat load on the condenser in kJ/kg of solution if the condensate is saturated, and if it is subcooled by 10°C?

<i>T</i> , °C	Saturated Enthalpy, kJ/kg			
	Benzene		Toluene	
	h_L	h_V	h_L	h_V
60	79	487	77	471
80	116	511	114	495
100	153	537	151	521

4.13. Phase condition for a mixture of alcohols.

For a mixture of 50 mol% 1-propanol, 30 mol% 2-propanol, and 20 mol% ethanol at 5 atm, use a process simulator with the Wilson equation for liquid-phase activity coefficients to calculate the temperature in °C and the phase compositions in mol% for the following conditions: (a) bubble point; (b) dew point; and (c) 50 mol% vaporization.

4.14. Azeotrope of chloroform–methanol.

For the chloroform–methanol system at 1 atm, use a process simulator with the NRTL equation for liquid-phase activity coefficients to prepare plots like those in Figure 4.6. From the plots, determine the azeotrope composition, temperature, and type.

4.15. Azeotrope of water–formic acid.

For the water–formic acid system at 1 atm, use a process simulator with the NRTL equation to prepare plots like those of Figure 4.7 to determine the azeotrope composition, temperature, and type.

4.16. Partial vaporization of water–isopropanol mixture.

Vapor–liquid equilibrium data for mixtures of water and isopropanol at 1 atm are given below. (a) Prepare *T*-*x*-*y* and *x*-*y*

diagrams. (b) When a solution containing 40 mol% isopropanol is slowly vaporized, what is the composition of the initial vapor? (c) If the mixture in part (b) is heated until 75 mol% is vaporized, what are the compositions of the equilibrium vapor and liquid? (d) Calculate *K*-values and values of α at 80°C and 89°C. (e) Compare your answers in parts (a), (b), and (c) to those obtained from *T*-*x*-*y* and *x*-*y* diagrams based on the following vapor pressure data and Raoult's and Dalton's laws. What do you conclude?

VAPOR–LIQUID EQUILIBRIUM DATA FOR ISOPROPANOL AND WATER AT 1 ATM

<i>T</i> , °C	Mol% Isopropanol	
	Liquid	Vapor
93.00	1.18	21.95
84.02	8.41	46.20
83.85	9.10	47.06
81.64	28.68	53.44
81.25	34.96	55.16
80.32	60.30	64.22
80.16	67.94	68.21
80.21	68.10	68.26
80.28	76.93	74.21
80.66	85.67	82.70
81.51	94.42	91.60

Notes: Composition of the azeotrope: $x = y = 68.54\%$.

Boiling point of azeotrope: 80.22°C.

Boiling point of pure isopropanol: 82.5°C.

Vapor Pressures of Isopropanol and Water

Vapor pressure, torr	200	400	760
Isopropanol, °C	53.0	67.8	82.5
Water, °C	66.5	83	100

Section 4.3**4.17. Vaporization of mixtures of hexane and octane.**

Using the *y*-*x* and *T*-*y*-*x* diagrams in Figure 4.4, determine the temperature, amounts, and compositions of the vapor and liquid phases at 101 kPa for the following conditions with a 100 kmol mixture of nC_6 (H) and nC_8 (C). (a) $z_H = 0.5$, $\Psi = V/F = 0.2$; (b) $z_H = 0.4$, $y_H = 0.6$; (c) $z_H = 0.6$, $x_C = 0.7$; (d) $z_H = 0.5$, $\Psi = 0$; (e) $z_H = 0.5$, $\Psi = 1.0$; and (f) $z_H = 0.5$, $T = 200^\circ\text{F}$

4.18. Derivation of equilibrium-flash equations for a binary mixture.

For a binary mixture of components 1 and 2, show that the phase compositions and amounts can be computed directly from the following reduced forms of (4-23, 24, and 26).

$$x_1 = (1 - K_2)/(K_1 - K_2)$$

$$x_2 = 1 - x_1$$

$$y_1 = (K_1 K_2 - K_1)/(K_2 - K_1)$$

$$y_2 = 1 - y_1$$

$$\Psi = \frac{V}{F} = \frac{z_1[(K_1 - K_2)/(1 - K_2)] - 1}{K_1 - 1}$$

4.19. Equilibrium flash using a graph.

A liquid containing 60 mol% toluene and 40 mol% benzene is continuously distilled in a single equilibrium stage at 1 atm. What percent

of benzene in the feed leaves as vapor if 90% of the toluene entering in the feed leaves as liquid? Assume a relative volatility of 2.3 and obtain the solution graphically.

4.20. Flash vaporization of a benzene–toluene mixture.

Solve Exercise 4.19 with a process simulator assuming an ideal solution. Also determine the temperature.

4.21. Equilibrium flash of seven-component mixture.

A seven-component mixture is flashed at a fixed P and T . (a) Using the K -values and feed composition below, make a plot of the Rachford–Rice flash function

$$f\{\Psi\} = \sum_{i=1}^C \frac{z_i(1 - K_i)}{1 + \Psi(K_i - 1)}$$

at intervals of Ψ of 0.1, and estimate the correct root of Ψ . (b) An alternative form of the flash function is

$$f\{\Psi\} = \sum_{i=1}^C \frac{z_i K_i}{1 + \Psi(K_i - 1)} - 1$$

Make a plot of this equation at intervals of Ψ of 0.1 and explain why the Rachford–Rice function is preferred.

Component	z_i	K_i
1	0.0079	16.2
2	0.1321	5.2
3	0.0849	2.6
4	0.2690	1.98
5	0.0589	0.91
6	0.1321	0.72
7	0.3151	0.28

4.22. Equilibrium flash of a hydrocarbon mixture.

One hundred kmol of a feed comprised of 25 mol% n -butane, 40 mol% n -pentane, and 35 mol% n -hexane is flashed at 240°F. Using a process simulator with the RK EOS, determine the pressure and the liquid and vapor compositions if 80% of the hexane is in the liquid.

4.23. Equilibrium-flash vaporization of a hydrocarbon mixture.

An equimolar mixture of ethane, propane, n -butane, and n -pentane is subjected to flash vaporization at 150°F and 205 psia. Using a process simulator with the RK EOS, calculate amounts and compositions of the products? Is it possible to recover 70% of the ethane in the vapor by a single-stage flash at other conditions without losing more than 5% of nC_4 to the vapor?

4.24. Cooling of a reactor effluent with recycled liquid.

Figure 4.24 shows a system to cool reactor effluent and separate light gases from hydrocarbons.

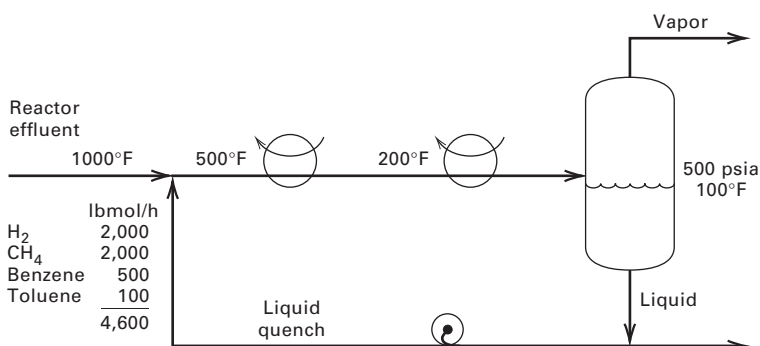


Figure 4.24 Conditions for Exercise 4.24.

The feed pressure is 500 psia and pressure drops are neglected. The first heat exchanger cools the feed to 200°F, while the second reduces it further to 100°F. Using a process simulator with SRK EOS:

- Calculate composition and flow rate of vapor leaving the flash drum.
- Does the liquid-quench flow rate influence the result? Prove your answer analytically.

4.25. Partial condensation of a gas mixture.

The feed in Figure 4.25 is partially condensed. Calculate the amounts and compositions of the equilibrium phases, V and L , using a process simulator with the SRK EOS.

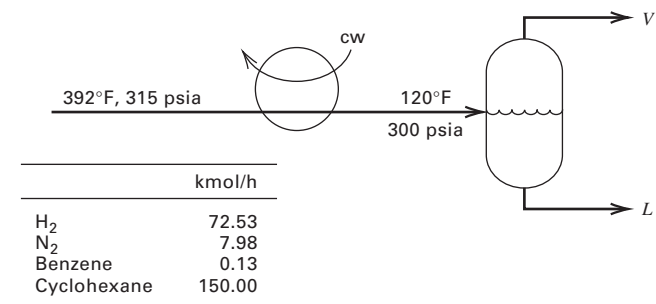


Figure 4.25 Conditions for Exercise 4.25.

4.26. Rapid determination of phase condition.

The following stream is at 200 psia and 200°F. Without making a flash calculation, determine if it is a subcooled liquid or a superheated vapor, or if it is partially vaporized.

Component	lbmol/h	K -value
C ₃	125	2.056
nC_4	200	0.925
nC_5	175	0.520

4.27. Determination of reflux-drum pressure.

Figure 4.26 shows the overhead system for a distillation column. The composition of the total distillates is indicated, with 10 mol% being vapor. Determine reflux-drum pressure if the temperature is 100°F. Use a process simulator with the RK EOS.

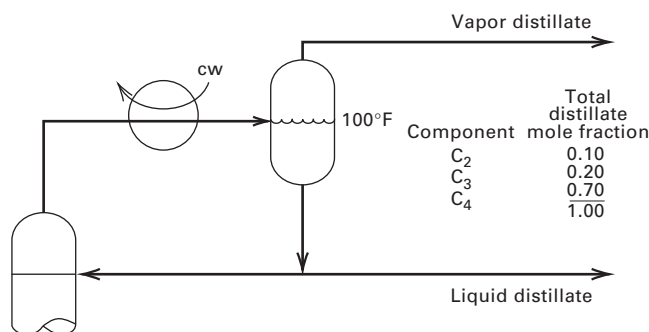


Figure 4.26 Conditions for Exercise 4.27.

4.28. Flash calculations for different K -value correlations.

Determine the phase condition of a stream having the following composition at 7.2°C and 2,620 kPa. Use a process simulator with the SRK and PR options. Does the choice of option influence the results significantly?

Component	kmol/h
N ₂	1.0
C ₁	124.0
C ₂	87.6
C ₃	161.6
<i>n</i> C ₄	176.2
<i>n</i> C ₅	58.5
<i>n</i> C ₆	33.7

4.29. Flash calculations at different values of T and P .

A liquid mixture consisting of 100 kmol of 60 mol% benzene, 25 mol% toluene, and 15 mol% *o*-xylene is flashed at 1 atm and 100°C. Assuming ideal solutions, use vapor pressure data from a process simulator to: (a) Compute kmol amounts and mole-fraction compositions of liquid and vapor products. (b) Repeat the calculation at 100°C and 2 atm. (c) Repeat the calculation at 105°C and 0.1 atm. (d) Repeat the calculation at 150°C and 1 atm.

4.30. Conditions at vapor–liquid equilibrium.

Using the Rachford–Rice flash algorithm, prove that the vapor leaving an equilibrium flash is at its dew point and that the liquid leaving is at its bubble point.

4.31. Bubble-point temperature of feed to a distillation column.

The feed below enters a distillation column as saturated liquid at 1.72 MPa. Calculate the bubble-point temperature using a process simulator.

Compound	kmol/h
Ethane	1.5
Propane	10.0
<i>n</i> -Butane	18.5
<i>n</i> -Pentane	17.5
<i>n</i> -Hexane	3.5

4.32. Bubble- and dew-point pressures of a binary mixture.

An equimolar solution of benzene and toluene is evaporated at a constant temperature of 90°C. What are the pressures at the beginning and end of the vaporization? Assume an ideal solution and use the vapor pressure curves of Figure 2.1, or use a process simulator.

4.33. Bubble point, dew point, and flash of a water–acetic acid mixture.

The following equations are given by Sebastiani and Lacquaniti [*Chem. Eng. Sci.*, **22**, 1155 (1967)] for the liquid-phase activity coefficients of the water (W)–acetic acid (A) system.

$$\log \gamma_W = x_A^2 [A + B(4x_W - 1) + C(x_W - x_A)(6x_W - 1)]$$

$$\log \gamma_A = x_W^2 [A + B(4x_W - 3) + C(x_W - x_A)(6x_W - 5)]$$

$$A = 0.1182 + \frac{64.24}{T(K)}$$

$$B = 0.1735 - \frac{43.27}{T(K)}$$

$$C = 0.1081$$

Find the dew point and bubble point of the mixture $x_W = 0.5, x_A = 0.5$, at 1 atm. Flash the mixture at a temperature halfway between the dew and bubble points.

4.34. Bubble point, dew point, and flash of a mixture.

Use a process simulator with the Wilson equation to find the bubble point and dew point of a mixture of 0.4 mole fraction toluene (1) and 0.6 mole fraction *n*-butanol (2) at 101.3 kPa. If the same mixture is flashed midway between the bubble and dew points and 101.3 kPa, what fraction is vaporized, and what are the phase compositions?

4.35. Bubble point, dew point, and azeotrope of a mixture.

Use a process simulator with the Wilson equation for a solution of a molar composition of ethyl acetate (A) of 80% and ethyl alcohol (E) of 20% to: (a) Calculate the bubble-point temperature at 101.3 kPa and the composition of the corresponding vapor. (b) Find the dew point of the mixture. (c) Determine whether the mixture forms an azeotrope? If it does, predict its temperature and composition.

4.36. Bubble point, dew point, and azeotrope of a mixture.

Use a process simulator with the Wilson equation for a solution at 107°C containing 50 mol% water (W) and 50 mol% formic acid (F) to: (a) Compute the bubble-point pressure. (b) Compute the dew-point pressure. (c) Determine if the mixture forms an azeotrope. If so, predict the azeotropic pressure at 107°C and the composition.

4.37. Bubble point, dew point, and equilibrium flash of a ternary mixture.

For a mixture of 45 mol% *n*-hexane, 25 mol% *n*-heptane, and 30 mol% *n*-octane at 1 atm, use a process simulator to: (a) Find the bubble- and dew-point temperatures. (b) Find the flash temperature, compositions, and relative amounts of liquid and vapor products if the mixture is subjected to a flash distillation at 1 atm so that 50 mol% is vaporized. (c) Find how much octane is taken off as vapor if 90% of the hexane is taken off as vapor. (d) Repeat parts (a) and (b) at 5 atm and 0.5 atm.

4.38. Vaporization of column bottoms in a partial reboiler.

In Figure 4.27, 150 kmol/h of a saturated liquid, L_1 , at 758 kPa of molar composition propane 10%, *n*-butane 40%, and *n*-pentane 50% enters the reboiler from stage 1. Use a process simulator to find the compositions and amounts of V_B and B . What is Q_R , the reboiler duty?

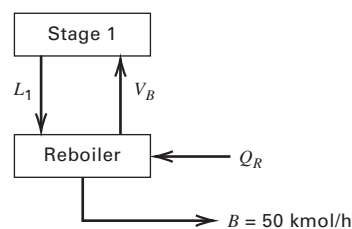


Figure 4.27 Conditions for Exercise 4.38.

4.39. Bubble point and flash temperatures for a ternary mixture.

For a mixture with mole fractions 0.005 methane, 0.595 ethane, and the balance *n*-butane at 50 psia, use a process simulator to: (a) Find the bubble-point temperature. (b) Find the temperature that results in 25% vaporization at this pressure and determine the liquid and vapor compositions in mole fractions.

4.40. Heating and expansion of a hydrocarbon mixture.

In Figure 4.28, a mixture is heated and expanded before entering a distillation column. Calculate, using a process simulator, mole percent vapor and vapor and liquid mole fractions at locations indicated by pressure specifications.

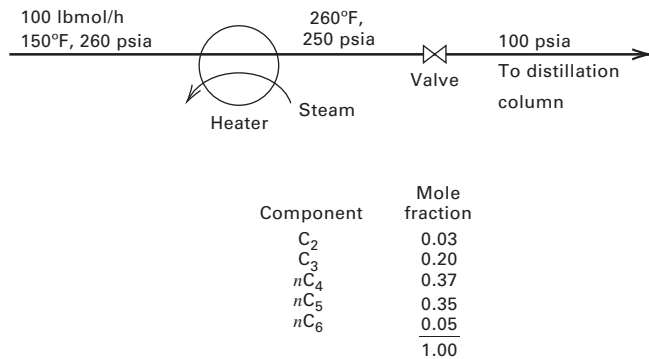


Figure 4.28 Conditions for Exercise 4.40.

4.41. Equilibrium vapor and liquid leaving a feed stage.

Streams entering stage *F* of a distillation column are shown in Figure 4.29. Using a process simulator, find the stage temperature and compositions and amounts of streams *V_F* and *L_F* if the pressure is 785 kPa.

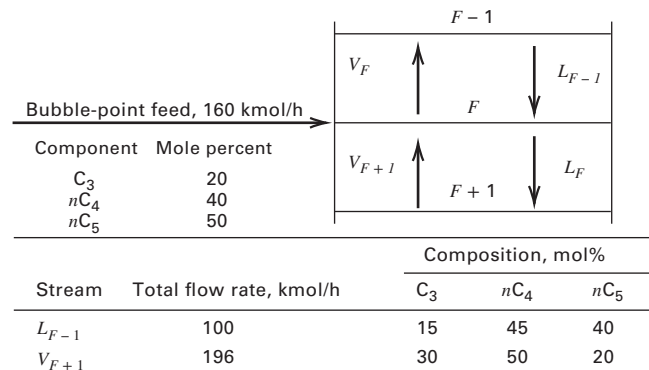


Figure 4.29 Conditions for Exercise 4.41.

4.42. Adiabatic flash across a valve.

The stream below is flashed adiabatically across a valve. Conditions are 250°F and 500 psia upstream and 300 psia downstream. Use

Component	<i>z_i</i>
C ₂ H ₄	0.02
C ₂ H ₆	0.03
C ₃ H ₆	0.05
C ₃ H ₈	0.10
<i>i</i> C ₄	0.20
<i>n</i> C ₄	0.60

a process simulator to compute (a) phase condition upstream of the valve; (b) temperature downstream of the valve; (c) molar fraction vaporized downstream of the valve; and (d) mole-fraction compositions of the vapor and liquid phases downstream of the valve.

4.43. Single-stage equilibrium flash of a clarified broth.

The ABE biochemical process makes acetone (A), *n*-butanol (B), and ethanol (E) by an anaerobic, submerged, batch fermentation at 30°C of corn kernels, using a strain of the bacterium *Clostridia acetobutylicum*. Following fermentation, the broth is separated from the biomass solids by centrifugation. Consider 1,838,600 L/h of clarified broth of S.G. = 0.994, with a titer of 22.93 g/L of ABE in the mass ratio of 3.0:7.5:1.0. A number of continuous bioseparation schemes have been proposed, analyzed, and applied. In particular, the selection of the first separation step needs much study because the broth is so dilute in the bioproducts. Possibilities are single-stage flash, distillation, liquid–liquid extraction, and pervaporation. In this exercise, a single-stage flash is to be investigated. Convert the above data on the clarified broth to component flow rates in kmol/h. Heat the stream to 97°C at 101.3 kPa. Use a process simulator to run a series of equilibrium-flash calculations using the NRTL equation for liquid-phase activity coefficients. Note that *n*-butanol and ethanol both form an azeotrope with water. Also, *n*-butanol may not be completely soluble in water for all concentrations. The specifications for each flash calculation are pressure = 101.3 kPa and *V/F*, the molar vapor-to-feed ratio. A *V/F* is to be sought that maximizes the ABE in the vapor while minimizing the water in the vapor. Because the boiling point of *n*-butanol is greater than that of water, and because of possible azeotrope formation and other nonideal solution effects, a suitable *V/F* may not exist.

4.44. Algorithms for various flash calculations.

Given the isothermal-flash algorithm of Rachford and Rice, propose procedures for the following flash calculations, assuming that expressions for *K*-values and enthalpies are available.

Given	Find
<i>h_F</i> , <i>P</i>	ψ , <i>T</i>
<i>h_F</i> , <i>T</i>	ψ , <i>P</i>
<i>h_F</i> , ψ	<i>T</i> , <i>P</i>
ψ , <i>T</i>	<i>h_F</i> , <i>P</i>
ψ , <i>P</i>	<i>h_F</i> , <i>T</i>
<i>T</i> , <i>P</i>	<i>h_F</i> , ψ

4.45. Flash algorithm for specification of a split of one component.

Develop a procedure, similar to the Rachford–Rice flash algorithm, that is suitable for calculating the mole-fraction compositions of the vapor and the liquid from an equilibrium flash if the pressure and the split fraction, $\psi_i = v_i/f_i$, for one of the components in a multi-component feed is specified, where *v_i* = molar flow rate of *i* in the equilibrium vapor and *f_i* = molar flow rate of *i* in the feed. Assume Raoult's law applies. *Hint*: Start by using material balances, and the definition of α_{ij} , where *j* is the reference component (the one whose split is given), to rewrite (4-26) so that the *K*-values are replaced by α values, which are much less dependent on temperature.

4.46. Equilibrium flash for a specified split.

The mixture of benzene, toluene, and *o*-xylene, listed below, is flashed at a pressure of 1 bar to achieve a split fraction, $\psi_i = v_i/f_i$, for toluene equal to 0.9. Using a flash model in a process simulator, calculate the flash temperature and the component flow rates in

kmol/h in the equilibrium vapor and liquid phases. Assume that Raoult's law applies.

Component	Feed Rate, kmol/h
Benzene	30
Toluene	50
<i>o</i> -xylene	40

Section 4.4

4.47. Comparison of solvents for single-stage extraction.

A feed of 13,500 kg/h is 8 wt% acetic acid (B) in water (A). Removal of acetic acid is to be by liquid–liquid extraction at 25°C. The raffinate is to contain 1 wt% acetic acid. The following four solvents, with accompanying distribution (partition) coefficients in mass-fraction units, are candidates. Water and each solvent (C) can be considered immiscible. For each solvent, estimate the kg/h required if one equilibrium stage is used.

Solvent	K_D
Methyl acetate	1.273
Isopropyl ether	0.429
Heptadecanol	0.312
Chloroform	0.178

4.48. Liquid–liquid extraction of ethylene glycol from water by furfural.

Forty-five kg of a solution of 30 wt% ethylene glycol in water is to be extracted with furfural. Using Figure 4.13, calculate the (a) minimum kg of solvent; (b) maximum kg of solvent; (c) kg of solvent-free extract and raffinate for 45 kg solvent, and the percentage glycol extracted; and (d) maximum purity of glycol in the extract and the maximum purity of water in the raffinate for one stage.

4.49. Representation of a ternary system on a triangular diagram.

Prove that in a triangular diagram where each vertex represents a pure component, the composition of the system at any point inside the triangle is proportional to the length of the respective perpendicular drawn from the point to the side of the triangle opposite the vertex in question. Note that it is not necessary that the triangle be of a right or equilateral type.

4.50. Liquid–liquid extraction of acetic acid from chloroform by water.

A mixture of chloroform (CHCl_3) and acetic acid at 18°C and 1 atm (101.3 kPa) is extracted with water to recover the acid.

LIQUID–LIQUID EQUILIBRIUM DATA FOR CHCl_3 – H_2O – CH_3COOH AT 18°C AND 1 ATM

Heavy Phase (wt%)			Light Phase (wt%)		
CHCl_3	H_2O	CH_3COOH	CHCl_3	H_2O	CH_3COOH
99.01	0.99	0.00	0.84	99.16	0.00
91.85	1.38	6.77	1.21	73.69	25.10
80.00	2.28	17.72	7.30	48.58	44.12
70.13	4.12	25.75	15.11	34.71	50.18
67.15	5.20	27.65	18.33	31.11	50.56
59.99	7.93	32.08	25.20	25.39	49.41
55.81	9.58	34.61	28.85	23.28	47.87

Forty-five kg of 35 wt% CHCl_3 and 65 wt% acid is treated with 22.75 kg of water at 18°C in a one-stage batch extraction. (a) What are the compositions and masses of the raffinate and extract layers? (b) If the raffinate layer from part (a) is extracted again with one-half its weight of water, what are the compositions and weights of the new layers? (c) If all the water is removed from the final raffinate layer of part (b), what will its composition be? Solve this exercise using the given equilibrium data to construct the type of diagram in Figure 4.13.

4.51. Liquid–liquid extraction of acetic acid from water by isopropyl ether.

Isopropyl ether (E) is used to separate acetic acid (A) from water (W). The liquid–liquid equilibrium data at 25°C and 1 atm are given below: (a) One hundred kilograms of a 30 wt% A–W solution is contacted with 120 kg of ether (E). What are the compositions and weights of the resulting extract and raffinate? What would the concentration of acid in the (ether-rich) extract be if all ether were removed? (b) A solution of 52 kg A and 48 kg W is contacted with 40 kg of E. Calculate the extract and raffinate compositions and quantities.

LIQUID–LIQUID EQUILIBRIUM DATA FOR ACETIC ACID (A), WATER (W), AND ISOPROPANOL ETHER (E) AT 25°C AND 1 ATM

Water-Rich Layer			Ether-Rich Layer		
Wt% A	Wt% W	Wt% E	Wt% A	Wt% W	Wt% E
1.41	97.1	1.49	0.37	0.73	98.9
2.89	95.5	1.61	0.79	0.81	98.4
6.42	91.7	1.88	1.93	0.97	97.1
13.30	84.4	2.3	4.82	1.88	93.3
25.50	71.1	3.4	11.4	3.9	84.7
36.70	58.9	4.4	21.6	6.9	71.5
45.30	45.1	9.6	31.1	10.8	58.1
46.40	37.1	16.5	36.2	15.1	48.7

Section 4.5

4.52. Separation of paraffins from aromatics by liquid–liquid extraction.

Diethylene glycol (DEG) is the solvent in the UDEX liquid–liquid extraction process [H.W. GROTE, *Chem. Eng. Progr.*, **54**(8), 43 (1958)] to separate paraffins from aromatics. If 280 lbmol/h of 42.86 mol% *n*-hexane, 28.57 mol% *n*-heptane, 17.86 mol% benzene, and 10.71 mol% toluene is contacted with 500 lbmol/h of 90 mol% aqueous DEG at 325°F and 300 psia, calculate, using a process simulator with the UNIFAC L/L method for liquid-phase activity coefficients, the flow rates and molar compositions of the resulting two liquid phases. Is DEG more selective for the paraffins or the aromatics?

4.53. Liquid–liquid extraction of organic acids from water with ethyl acetate.

A feed of 110 lbmol/h includes 5, 3, and 2 lbmol/h, respectively, of formic, acetic, and propionic acids in water. If the acids are extracted in one equilibrium stage with 100 lbmol/h of ethyl acetate (EA), calculate, with a process simulator using the UNIFAC method, the flow rates and compositions of the resulting liquid phases. What is the selectivity of EA for the organic acids?

Section 4.6

4.54. Adsorption of phenol (B) from an aqueous solution.

Repeat Example 4.9, except determine the grams of activated carbon needed to achieve: (a) 75% adsorption of phenol; (b) 90% adsorption of phenol; and (c) 98% adsorption of phenol.

4.55. Adsorption of a colored substance from an oil by clay particles.

A colored substance (B) is removed from a mineral oil by adsorption with clay particles at 25°C. The original oil has a color index of 200 units/100 kg oil, while the decolorized oil must have an index of only 20 units/100 kg oil. The following are experimental adsorption equilibrium data measurements:

c_B , color units/100 kg oil	200	100	60	40	10
q_B , color units/100 kg clay	10	7.0	5.4	4.4	2.2

(a) Fit the data to the Freundlich equation. (b) Compute the kg of clay needed to treat 500 kg of oil if one equilibrium contact is used.

Section 4.7

4.56. Absorption of acetone (A) from air by water.

Vapor–liquid equilibrium data in mole fractions for the system acetone–air–water at 1 atm (101.3 kPa) are as follows:

y ; acetone in air :	0.004	0.008	0.014	0.017	0.019	0.020
x ; acetone in water :	0.002	0.004	0.006	0.008	0.010	0.012

(a) Plot the data as (1) moles acetone per mole air versus moles acetone per mole water, (2) partial pressure of acetone versus g acetone per g water, and (3) y versus x . (b) If 20 moles of gas containing 0.015 mole-fraction acetone is contacted with 15 moles of water, what are the stream compositions? Solve graphically. Neglect water/air partitioning.

4.57. Separation of air into O₂ and N₂ by absorption into water.

It is proposed that oxygen be separated from nitrogen by absorbing and desorbing air in water. Pressures from 101.3 to 10,130 kPa and temperatures between 0 and 100°C are to be used. (a) Devise a scheme for the separation if the air is 79 mol% N₂ and 21 mol% O₂. (b) Henry's law constants for O₂ and N₂ are given in Figure 4.18. How many batch absorption steps would be necessary to make 90 mol% oxygen? What yield of oxygen (based on the oxygen feed) would be obtained?

4.58. Absorption of ammonia from nitrogen into water.

A vapor mixture of equal volumes NH₃ and N₂ is contacted at 20°C and 1 atm (760 torr) with water to absorb some of the NH₃.

Partial Pressure of NH ₃ in Air, torr	Grams of Dissolved NH ₃ /100 g of H ₂ O
470	40
298	30
227	25
166	20
114	15
69.6	10
50.0	7.5
31.7	5.0
24.9	4.0
18.2	3.0
15.0	2.5
12.0	2.0

If 14 m³ of this mixture is contacted with 10 m³ of water, calculate the % of ammonia in the gas that is absorbed. Both T and P are maintained constant. The partial pressure of NH₃ over water at 20°C is given in the table above.

Section 4.8

4.59. Desublimation of phthalic anhydride from a gas.

Repeat Example 4.12 for temperatures corresponding to vapor pressures for PA of: (a) 0.7 torr, (b) 0.4 torr, and (c) 0.1 torr. Plot the percentage recovery of PA vs. solid vapor pressure for 0.1 torr to 1.0 torr.

4.60. Desublimation of anthraquinone (A) from nitrogen.

Nitrogen at 760 torr and 300°C containing 10 mol% anthraquinone (A) is cooled to 200°C. Calculate the % desublimation of A. Vapor pressure data for solid A are:

T , °C:	190.0	234.2	264.3	285.0
Vapor pressure, torr:	1	10	40	100

These data can be fitted to the Antoine equation (2-42) using the first three constants.

4.61. Separation of a gas mixture by adsorption.

At 25°C and 101 kPa, 2 mol of a gas containing 35 mol% propylene in propane is equilibrated with 0.1 kg of silica gel adsorbent. Using Figure 4.20, calculate the moles and compositions of the adsorbed and unadsorbed gas.

4.62. Separation of a gas mixture by adsorption.

Fifty mol% propylene in propane is separated with silica gel. The products are to be 90 mol% propylene and 75 mol% propane. If 1,000 lb of silica gel/lbmol of feed gas is used, can the desired separation be made in one stage? If not, what separation can be achieved? Use Figure 4.20.

Section 4.9

4.63. Bubble point of a mixture of toluene, ethylbenzene, and water.

A liquid of 30 mol% toluene, 40 mol% ethylbenzene, and 30 mol% water is subjected to a continuous flash distillation at 0.5 atm. Assuming that mixtures of ethylbenzene and toluene obey Raoult's law and that the hydrocarbons are immiscible in water and vice versa, calculate, with a process simulator, the temperature and composition of the vapor phase at the bubble-point temperature.

4.64. Bubble point, dew point, and 50 mol% flash for water–*n*-butanol.

Water (W) and *n*-butanol (B) can form a three-phase system at 101 kPa. For a mixture of overall composition of 60 mol% W and 40 mol% B, use a process simulator with the UNIFAC method to estimate: (a) dew-point temperature and composition of the first drop of liquid; (b) bubble-point temperature and composition of the first bubble of vapor; and (c) compositions and relative amounts of all three phases for 50 mol% vaporization.

4.65. Isothermal flash.

Repeat Example 4.14 for a temperature of 25°C. Are the changes significant?

Multistage Cascades and Hybrid Systems

§5.0 INSTRUCTIONAL OBJECTIVES

After completing this chapter, you should be able to:

- Explain how multiple equilibrium stages arranged in a cascade with countercurrent flow can achieve a significantly better separation than a single equilibrium stage.
- Explain why a two-section countercurrent cascade can achieve a sharp separation between two feed components, while a single-section cascade can only achieve a sharp recovery for a single feed component.
- Configure a membrane cascade to improve a membrane separation.
- Explain the merits and give examples of hybrid separation systems.
- Determine degrees of freedom for multistage cascades and hybrid systems.

Most often, the separation of a mixture by a single equilibrium stage is not sufficient to achieve a desired purity and recovery of a particular component in the feed. For example, consider the separation of a mixture of 48.3 mol% methanol (M) and 51.7 mol% water (W). The mixture is brought to equilibrium at 78°C and 101.3 kPa, using flash vaporization (separation operation 2 of Table 1.1). By calculations, described in Chapter 4 and verified by experiment, a vapor phase with 66.5 mol% M and a liquid phase of 30.0 mol% M are produced, with a 69% recovery of M in the vapor phase. To attain greater degrees of purity and percent recovery of M, multiple equilibrium stages are required. Common configurations of multiple stages in separation cascades, particularly with countercurrent flow, are treated in this chapter. Hybrid separation systems containing two or more different types of separation operations are also considered because they can sometimes save energy. The degrees of freedom analysis of §4.3.1, for a single equilibrium stage, is extended in this chapter to multistage cascades and hybrid systems.

§5.1 CASCADE CONFIGURATIONS

Figure 5.1 shows a **countercurrent cascade** configuration widely used for continuous separations based on phase addition using a mass separating agent, as introduced in §1.4 and shown in Table 1.2 for absorption, stripping, and liquid–liquid extraction. In Figure 5.1, consecutive equilibrium stages are represented by boxes numbered beginning at the feed and connected by passing streams. In Table 1.2, each stage is shown as a line immediately adjacent to the next consecutive stage. Although four stages are shown in Figure 5.1, any number of stages can be arranged vertically in a column. In Figure 5.1, the feed enters at Stage 1, while the MSA enters Stage 4 at the opposite end. The two streams flow countercurrently to each

other, with equilibrium achieved at each stage. If the cascade is for stripping, the feed liquid enters at the top stage, while the stripping gas enters the bottom stage. In an absorption cascade, the feed gas enters at the bottom and the absorbent liquid enters at the top. If the cascade is for liquid–liquid extraction, the feed liquid and solvent liquid enter at opposite ends with the liquid of higher density entering at the top.

Figure 5.2 shows a three-stage **crosscurrent cascade**, which, as will be shown, is not as efficient as the countercurrent cascade but is suited for batch processing, particularly liquid–liquid extraction. The MSA, S , is divided into fractions that are fed individually to each stage of the process. Each box represents an equilibrium stage with a mixer. In Figure 5.2, the feed, F , is added to the first stage, where it is brought to equilibrium with a fraction of the fresh solvent, S . The extracted feed from the first stage is then added to the second stage, where it is again contacted with a fraction of the fresh solvent. In this manner, the feed progresses from stage to stage. Extracted feed, R , leaving the final stage is the raffinate (from the French word *raffiner*, which means “to refine”). The extracts, E , leaving each stage can be processed separately or combined to recover solvent and extracted solutes.

Cascades in Figures 5.1 and 5.2 are **single-section cascades** configured and designed to achieve a desired percent recovery of just one component, called the **key component**, from a feed stream that enters at one end and leaves at the other. When it is desired to achieve a percent purity or percent recovery of two feed components, called **key components**, a **two-section cascade** is necessary. This type of cascade, shown in Figure 5.3, is common for (a) liquid–liquid extraction when two solvents are used that are each selective for one of the two key components, and (b) distillation. The horizontal lines within the two columns in Figure 5.3 delineate consecutive equilibrium stages.

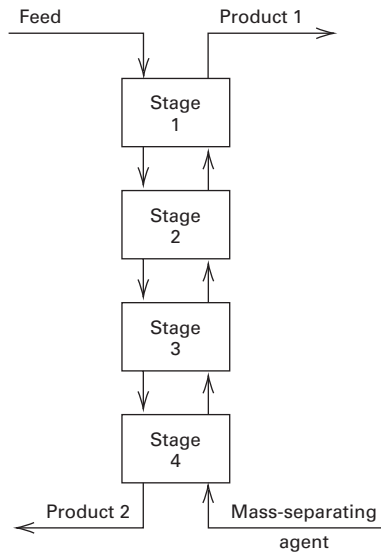


Figure 5.1 Countercurrent cascade of equilibrium stages for a continuous phase-addition separation operation.

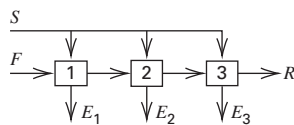


Figure 5.2 Crosscurrent cascade for batchwise liquid-liquid extraction.

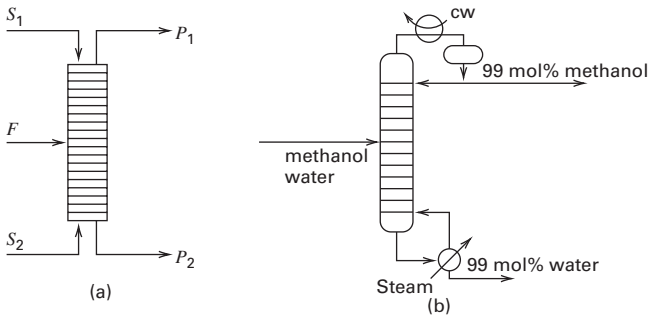


Figure 5.3 Two-section cascades: (a) liquid-liquid extraction with two solvents; (b) distillation.

§5.2 SINGLE-SECTION LIQUID-LIQUID EXTRACTION CASCADES

In §4.4, a single-equilibrium-stage ternary liquid-liquid extraction was considered. In this section, that treatment is extended to multiple stages. First, consider the two-stage cocurrent, crosscurrent, and countercurrent single-section liquid-liquid extraction cascades shown in Figure 5.4, where benzene (*S*) is used to extract *p*-dioxane (*B*) from water (*A*).

The single-stage equations derived in §4.4 can be applied to each two-stage arrangement in Figure 5.4 to derive the overall

degree of extraction. The derivations are extended to any number of equilibrium stages, N .

§5.2.1 Cocurrent Cascade

In Figure 5.4a, the fraction of *B* exiting Stage 1 without being extracted from the aqueous carrier, *A*, is from (4-36),

$$\frac{X_B^{(1)}}{X_B^{(F)}} = \frac{1}{1 + \mathcal{E}} \quad (5-1)$$

where the extraction factor, \mathcal{E} which leverages equilibrium and operational flow rates to achieve the separation, is from (4-35),

$$\mathcal{E} = \frac{K'_{DB} S}{F_A} \quad (5-2)$$

where the distribution ratio, K'_{DB} , modified for mass ratios is, from (4-33),

$$Y_B^{(1)} = K'_{DB} X_B^{(1)} \quad (5-3)$$

Assume that streams leaving a stage are at equilibrium. For the second stage, a material balance for *B* gives

$$X_B^{(1)} F_A + Y_B^{(1)} S = X_B^{(2)} F_A + Y_B^{(2)} S \quad (5-4)$$

with

$$Y_B^{(2)} = K'_{DB} X_B^{(2)} \quad (5-5)$$

However, if equilibrium is reached in Stage 1, no additional extraction takes place when the two exiting streams are recontacted in subsequent stages. Accordingly, a cocurrent cascade has no merit unless required **residence times** are so long that equilibrium is not achieved in a single stage and one or more extra stages are needed to provide additional residence time. Long residence times may be needed to achieve sufficient contacting between feed and solvent, or to accommodate slow mass transfer of solute from feed to solvent. Regardless of the number of cocurrent equilibrium stages, N , the fraction of unextracted *B* in the carrier exiting the terminal stage is

$$\frac{X_B^{(N)}}{X_B^{(F)}} = \frac{1}{1 + \mathcal{E}} \quad (5-6)$$

§5.2.2 Crosscurrent Cascade

For the crosscurrent cascade in Figure 5.4b, the feed progresses through each stage, beginning with Stage 1. The total benzene solvent flow rate, S , is divided into equal fractions, each of which is sent to a consecutive stage. The following mass ratios are obtained for each stage in an N -stage system by application of (4-36), where S is replaced by S/N so that \mathcal{E} is replaced by \mathcal{E}/N :

$$\begin{aligned} X_B^{(1)}/X_B^{(F)} &= 1/(1 + \mathcal{E}/N) \\ X_B^{(2)}/X_B^{(1)} &= 1/(1 + \mathcal{E}/N) \\ &\vdots \\ X_B^{(N)}/X_B^{(N-1)} &= 1/(1 + \mathcal{E}/N) \end{aligned} \quad (5-7)$$

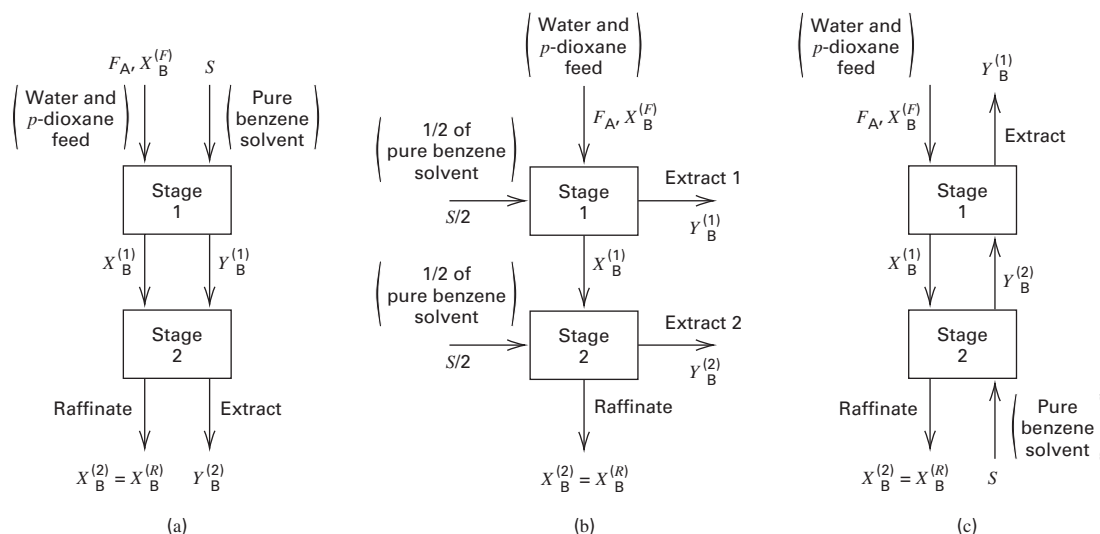


Figure 5.4 Two-stage arrangements: (a) cocurrent cascade; (b) crosscurrent cascade; and (c) countercurrent cascade.

Combining the equations in (5-7) to eliminate intermediate-stage variables, $X_B^{(n)}$, the final raffinate solute mass ratio, corresponding to the fraction of B in the feed that is not extracted is

$$X_B^{(N)}/X_B^{(F)} = X_B^{(R)}/X_B^{(F)} = \frac{1}{(1 + \mathcal{E}/N)^N} \quad (5-8)$$

In contrast to the cocurrent cascade, a crosscurrent cascade decreases the value of X_B in each successive stage. For an infinite number of equilibrium stages, N , (5-8) becomes

$$X_B^{(\infty)}/X_B^{(F)} = \frac{1}{\exp(\mathcal{E})} \quad (5-9)$$

Thus, even for an infinite number of stages, $X_B^{(R)} = X_B^{(\infty)}$ cannot be reduced to zero to completely extract all solute from the feed carrier.

§5.2.3 Countercurrent Cascade

In the countercurrent arrangement in Figure 5.4c, the feed, a carrier-rich liquid phase, initially rich in solute, passes through the cascade countercurrently to the solvent-rich phase, which is initially solute-poor. For a two-equilibrium-stage system, the material-balance and equilibrium equations for solute B for each stage are:

$$\text{Stage 1: } X_B^{(F)}F_A + Y_B^{(2)}S = X_B^{(1)}F_A + Y_B^{(1)}S \quad (5-10)$$

$$K'_{D_B} = \frac{Y_B^{(1)}}{X_B^{(1)}} \quad (5-11)$$

$$\text{Stage 2: } X_B^{(1)}F_A = X_B^{(2)}F_A + Y_B^{(2)}S \quad (5-12)$$

$$K'_{D_B} = \frac{Y_B^{(2)}}{X_B^{(2)}} \quad (5-13)$$

Combining (5-10) to (5-13) with (5-2) to eliminate $Y_B^{(1)}$, $Y_B^{(2)}$, and $X_B^{(1)}$ gives

$$X_B^{(2)}/X_B^{(F)} = X_B^{(R)}/X_B^{(F)} = \frac{1}{1 + \mathcal{E} + \mathcal{E}^2} \quad (5-14)$$

Extending (5-14) to N countercurrent stages,

$$X_B^{(R)}/X_B^{(F)} = 1 / \sum_{n=0}^N \mathcal{E}^n = \frac{\mathcal{E} - 1}{\mathcal{E}^{N+1} - 1} \quad (5-15)$$

Can a perfect extraction be achieved with a countercurrent cascade? For an infinite number of equilibrium stages, the limit of (5-15) gives two results, depending on the value of the extraction factor, \mathcal{E} :

$$X_B^{(\infty)}/X_B^{(F)} = 0, \quad 1 \leq \mathcal{E} \leq \infty$$

$$X_B^{(\infty)}/X_B^{(F)} = (1 - \mathcal{E}), \quad \mathcal{E} \leq 1$$

Thus, complete extraction can be achieved with a countercurrent cascade of an infinite N if the extraction factor $\mathcal{E} > 1$. The countercurrent arrangement is preferred for a continuous process because, as will be shown, this arrangement results in a higher degree of extraction for a given amount of solvent and number of equilibrium stages.

EXAMPLE 5.1 Liquid-Liquid Extraction with Different Cascade Arrangements.

Ethylene glycol is catalytically dehydrated to *p*-dioxane (a cyclic diether) by the reaction $2\text{HOCH}_2\text{CH}_2\text{HO} \rightarrow \text{H}_2\text{CCH}_2\text{OCH}_2\text{CH}_2\text{O} + 2\text{H}_2\text{O}$. Water and *p*-dioxane have normal boiling points of 100°C and 101.1°C, respectively, which precludes using distillation to separate them. Liquid-liquid extraction at 25°C using benzene as a solvent is preferable. A feed of 4,536 kg/h of a 25 wt% solution of *p*-dioxane in water is to be separated continuously with 6,804 kg/h of benzene.

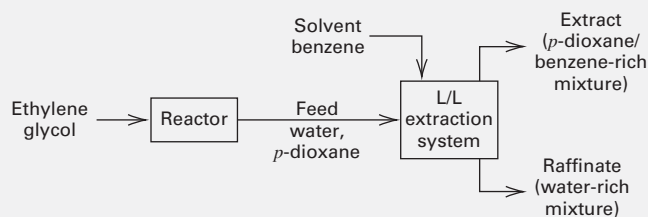


Figure 5.5 Process Flow Diagram for Example 5.1.

Assume that benzene and water are mutually insoluble. Use a constant, average literature value for partitioning of *p*-dioxane between water and benzene. Determine the effect of the number and arrangement of stages on the percent extraction of *p*-dioxane. The process flow diagram is given in Figure 5.5.

Solution

Three arrangements of equilibrium stages are examined: (a) cocurrent, (b) crosscurrent, and (c) countercurrent. Because water and benzene are assumed mutually insoluble, and the partitioning is assumed constant, (5-6), (5-8), and (5-15) can be used to estimate $X_B^{(R)}/X_B^{(F)}$, the fraction of *p*-dioxane not extracted, as a function of N . From the equilibrium data of Berdt and Lynch [1], the distribution coefficient for *p*-dioxane, varies from 1.0 to 1.4 as a function of concentration. Assume a constant value of 1.2. From the given data, $S = 6,804$ kg/h of benzene, $F_A = 4,536(0.75) = 3,402$ kg/h of water, and $X_B^{(F)} = 0.25/0.75 = 1/3$. From (5-2), the extraction factor is $\mathcal{E} = 1.2(6,804)/3,402 = 2.4$.

Single equilibrium stage:

Cocurrent, crosscurrent, and countercurrent arrangements give identical results for a single stage. By (5-6), the fraction of *p*-dioxane remaining unextracted in the raffinate is,

$$X_B^{(1)}/X_B^{(F)} = 1/(1 + 2.4) = 0.294$$

The corresponding fractional extraction into the solvent is

$$1 - X_B^{(R)}/X_B^{(F)} = 1 - 0.294 = 0.706 \text{ or } 70.6\%$$

More than one equilibrium stage:

- (a) Cocurrent: For any number of equilibrium stages, extraction is still only 70.6%.
- (b) Crosscurrent: For any number of equilibrium stages, (5-8) applies. For two stages, assuming equal flow of solvent to each stage,

$$X_B^{(2)}/X_B^{(F)} = \frac{1}{(1 + \mathcal{E}/2)^2} = 1/(1 + 2.4/2)^2 = 0.207$$

and extraction is 79.3%. Results for increasing values of N are in Figure 5.6.

- (c) Countercurrent: For any number of stages, (5-15) applies. For example, for two stages,

$$X_B^{(2)}/X_B^{(F)} = \frac{1}{1 + \mathcal{E} + \mathcal{E}^2} = \frac{1}{1 + 2.4 + 2.4^2} = 0.109$$

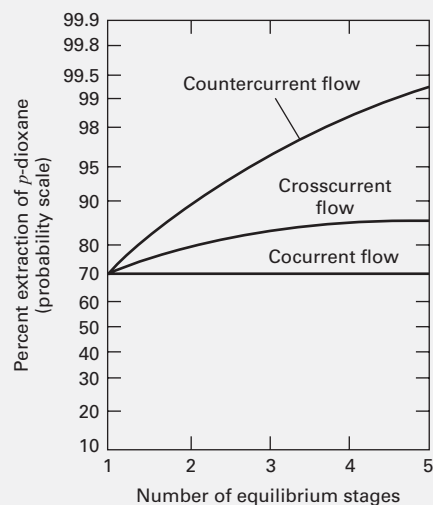


Figure 5.6 Effect of multiple equilibrium stages on extraction efficiency.

and extraction is 89.1%. Results for other discrete values of N are shown in Figure 5.6, where a probability-scale ordinate is convenient because for the countercurrent case with $\mathcal{E} > 1$, 100% extraction is approached as N approaches ∞ . For the crosscurrent arrangement, the maximum extraction from (5.9) is 90.9%, while for five stages, the countercurrent cascade achieves 99.2% extraction.

The single-section cascade is applied to absorption and stripping in Chapters 6 and 10 and to liquid–liquid extraction in Chapters 8 and 10.

§5.3 TWO-SECTION DISTILLATION CASCADES

If the feed to a distillation column is a binary zeotropic mixture, high purity bottoms and distillate can be achieved as shown in Figure 5.3b for a methanol–water separation. To illustrate how recovery of two key components, both at high purity, can be achieved, consider the continuous distillation of 1,000 kmol/h of a 50–50 mol% mixture of *n*-heptane (H) and *n*-octane (O) at 101.3 kPa. The normal boiling points for H and O are 98.4°C and 125.7°C, respectively. This mixture is almost an ideal solution with infinite-dilution liquid-phase activity coefficients, γ_{iL}^{∞} , of 1.03 for O and 1.04 for H. The relative volatility, $\alpha_{H,O}$, varies from 2.277 at the boiling point of H to 2.087 at the boiling point of O.

The column configuration used for the calculations is shown in Figure 5.7. Thermodynamic properties are computed with the SRK EOS, described in §2.5. The feed, F , is a vapor–liquid mixture that has been flashed at the column pressure of 101.3 kPa for a molar vaporization of 50%, as described in §4.3, using the Flash2 model in Aspen Plus. The results of a flash calculation for 1,000 kmol/h of feed mixture is shown in the following table. The degree of separation is minimal.

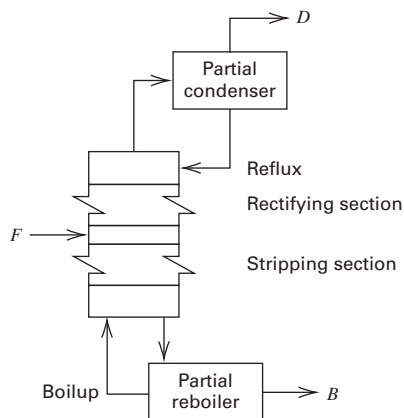


Figure 5.7 Column configuration for distillation of heptane–octane mixture.

Component	Vapor Flow Rate, kmol/h	Liquid Flow Rate, kmol/h	Vapor Mole Fraction	Liquid Mole Fraction
<i>n</i> -Heptane	296.0	204.0	0.592	0.408
<i>n</i> -Octane	204.0	296.0	0.408	0.592
Total	500.0	500.0	1.000	1.000

In Figure 5.7, the flashed feed enters near the middle of the column between the upper (rectifying) and lower (stripping) sections, each consisting of, as yet, an unspecified number of consecutive equilibrium stages. The vapor fraction of the feed rises to the stage above and the liquid fraction flows to the stage below. The vapor exiting the top stage in the column enters a **partial condenser** that produces 500 kmol/h of a vapor **distillate**, *D*, in equilibrium with liquid **reflux**, *R*, that recirculates back to the top stage to provide liquid to contact the vapor rising from stage-to-stage up the column. The *R/D* is set at 3.0, corresponding to a reflux flow rate of 1,500 kmol/h. Stages above the feed entry constitute the **rectifying section**. Increasing the reflux ratio decreases the number of stages required to achieve a given separation. More stages increases the capital cost of a column while increasing the reflux increases the energy cost because more liquid has to be vaporized in the reboiler. This is an optimization problem that is discussed in Chapter 7.

The liquid exiting the bottom stage in the column enters a **partial reboiler** that produces 500 kmol/h of a liquid **bottoms**, *B*, in equilibrium with vapor **boilup** that flows back to and up from the bottom stage to provide vapor to contact the liquid flowing from stage-to-stage down the column. Each stage in the column is assumed to be an equilibrium stage for which the vapor exiting the stage and flowing upward to the next stage is in physical equilibrium with the liquid exiting the stage and flowing downward to the next stage below. Stages below the feed entry constitute the **stripping section**. It should also be noted that the partial condenser and partial reboiler each act as equilibrium stages. Stages in the column are **adiabatic**, while the condenser and reboiler are **diabatic**

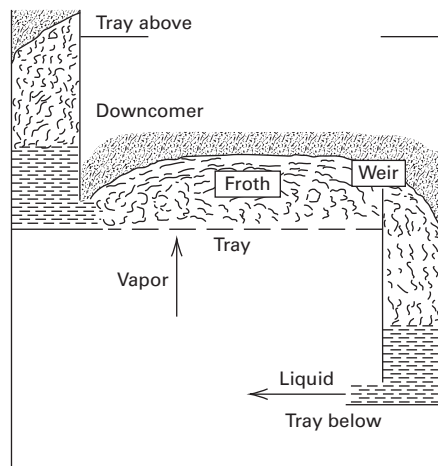


Figure 5.8 Typical vapor-liquid contacting tray.

stages, with heat transfer to the system in the reboiler and from the system in the condenser.

A typical distillation column contains a series of horizontal circular trays, spaced more than 0.3 m apart. The trays are designed for rapidly contacting upflowing vapor with downflowing liquid to approach vapor–liquid equilibrium in the frothy mixture flowing across the tray. Figure 5.8 is a schematic of the details of one type of tray. Vapor rising from the tray below flows through perforations on the tray above into the frothy liquid flowing across the tray. Intimate contact between vapor and frothy liquid enhances component mass-transfer rates. Trays are spaced sufficiently to allow exiting vapor to disentrain from exiting liquid. Liquid leaves the tray by flowing over a weir and into a downcomer that directs it onto the tray below. For mixtures of close-boiling components, physical equilibrium between the vapor and liquid flows leaving a tray is closely approached. Thus, each tray may ideally correspond to one equilibrium stage. However, the efficiency of trays for wide-boiling mixtures can be significantly less than 100% and more than a single tray may be needed to achieve separation equivalent to one equilibrium stage.

A case study of five runs was made with the Aspen Plus process simulator to study the effect of the number of equilibrium stages on percent purity and percent recovery of *n*-heptane in the distillate. Because (1) the feed was a binary mixture with equal molar percentages of H and O; and (2) the molar split between distillate and bottoms was equal, the overall component material balances for the column resulted in the following equalities:

$$\text{mol\% H in the distillate} = \text{mol\% O in the bottoms}$$

$$\% \text{ recovery of H in the distillate} = \% \text{ recovery of O in the bottoms}$$

The calculations were made with the Radfrac model discussed in Chapter 10. In all five simulations, the feed entered the middle of the column, so that the number of rectifying stages and stripping stages were equal. The following table shows the number of equilibrium stages in the column, the total number of equilibrium stages including the partial

condenser and partial reboiler, and the calculated mol% purity of H in the distillate:

Run Number	Column Stages	Total Stages	Mole% Purity of <i>n</i> -Heptane in the Distillate
Feed Flash		1	59.2
1	0	2	66.7
2	2	4	76.8
3	8	10	91.2
4	18	20	98.2
5	28	30	99.7

Figure 5.9 is a plot of the results. The mol% purity of H increases rapidly at first with an increasing number of stages and then asymptotically tends to 100% when the number of stages approaches 30. This increase in mol% purity is due to the use of reflux and boilup to allow countercurrent flow of vapor and liquid. In the rectifying section, the upcoming vapor is enriched in the lighter component by contact with a liquid that has a higher concentration of the lighter component. In the stripping section, the lighter component is stripped out of the downflowing liquid by the vapor originating in the reboiler, which has a lower concentration of the lighter component.

To see more clearly the effect of countercurrent flow, consider the results for the top three stages in the rectifying section for Run 3 as shown in Figure 5.10, where temperature, flow rate and component mole fractions are shown for four streams. Stages 2, 3, and 4 are numbered from the top, progressing downward, where Stage 1 is the partial condenser. Liquid stream, L_2 , exiting Stage 2, and vapor stream, V_4 , exiting Stage 4 are not in equilibrium. Each enters Stage 3 where they are brought into intimate contact in a froth shown in Figure 5.8. Mass transfer of the more volatile component, H, is from the liquid to the vapor, and for the less volatile component, O, is from the vapor to the liquid as the concentrations tend to equilibrium to produce streams L_3 and V_3 that exit Stage 3. The mole fraction of H in the up-flowing vapor is enhanced from a mole fraction of 0.686 to 0.769, while the mole fraction of O in the down-flowing liquid is enhanced from 0.280 to 0.392. Temperatures on each tray are between pure boiling points of H and O and increase at each consecutive stage moving down the column. Liquid streams leaving a stage are at their

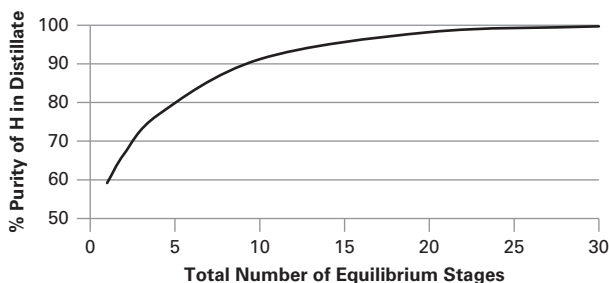


Figure 5.9 Effect of number of stages on mol% product purity.

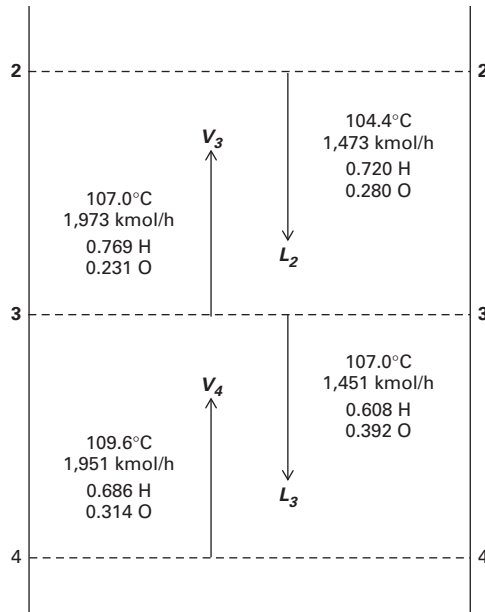


Figure 5.10 Profiles for three stages in a distillation column separating heptane from octane.

bubble point, while vapor streams are at their dew point. Thus, as the up-flowing vapor becomes enriched with H, the temperature decreases. The energy to vaporize H at a stage is almost matched by the energy released by the condensation of O. Energy differences are reflected in the relatively small percentage changes in flows of the vapor and liquid streams. Similar changes occur for other stages. The overall changes in composition depend on the number of stages. In the limit of an infinite number of stages, a two-section distillation cascade could produce a distillate of pure H and a bottoms of pure O.

Two-section distillation cascades are described in depth for binary mixtures in Chapter 7 and for multicomponent mixtures in Chapters 9 and 10.

§5.4 MEMBRANE CASCADES

Membrane systems are typically designed to recover and purify one or more components of a gas or liquid feed by specifying the required membrane area and configuration for a given feed and operating conditions. Most often they consist of multiple, parallel membrane units, called modules, to reduce trans-membrane pressure along the flow path at high feed rates. Figure 5.11a shows four modules of identical size, operating in parallel. Feed that has passed through the membrane in each module (**permeate**) is combined separately from feed retained by the membrane (**retentate**) to give final products. For example, a membrane-separation system for separating hydrogen from methane might require a membrane area of 13,000 ft². If the largest membrane module available has 3,300 ft² of membrane surface, four modules in parallel are required. Ideally, the parallel modules function as a single unit. Membrane modules do not function as equilibrium stages.

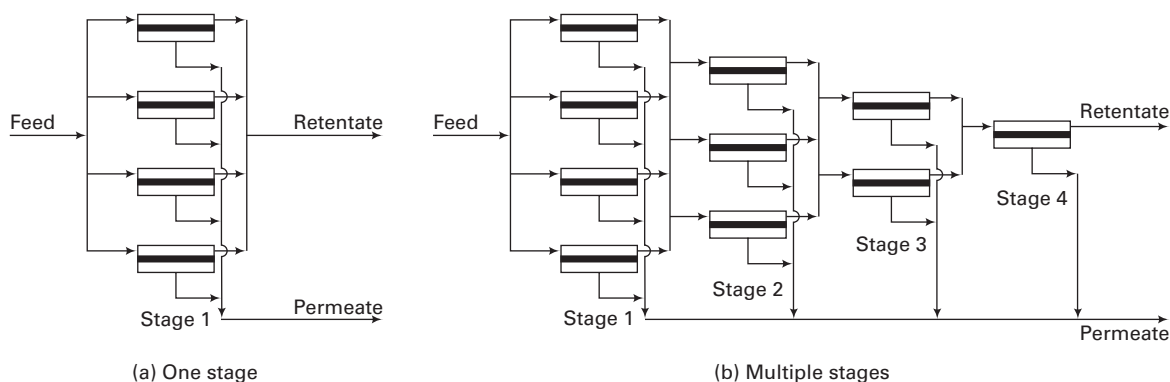


Figure 5.11 Parallel units of membrane separators.

The retentate and permeate leaving a membrane module are not in equilibrium. Instead, the retentate and permeate flow rates and compositions are governed by differing component mass-transfer rates through the membrane. The larger the surface area of a membrane module for a given feed and operating condition the more permeate and the less retentate.

To increase the fraction of a feed component recovered in the permeate, the membrane separation is often conducted in two or more stages, as shown in Figure 5.11b for four stages. Only the combined retentate from each stage is fed to the next stage. The number of modules in parallel is reduced for each successive stage as the flow rate on the feed-retentate side of the membrane decreases. The combined permeates for each stage differ in composition from stage to stage. They are all combined to give the final permeate, as shown in Figure 5.11b. Not shown are required interstage gas compressors and/or liquid pumps to move the streams from stage to stage.

Single-membrane stages are often limited in the degree of separation and recovery achievable. It is rare to obtain a high purity for gas membrane separations, and usually it occurs at the expense of a low recovery. Usually neither a high purity nor a high recovery can be achieved. The following table gives two examples of the separation obtained for a single stage of gas permeation using a commercial membrane.

	Feed Molar Composition	More Permeable Component	Product Molar Composition	Percent Recovery
Example 1	85% H ₂ 15% CH ₄	H ₂	99% H ₂ 1% N ₂ in the permeate	60% of H ₂ in the feed
Example 2	80% CH ₄ 20% N ₄	N ₂	97% CH ₄ 3% N ₂ in the retentate	57% of CH ₄ in the feed

In the first example in the table, the permeate purity is quite high, but the recovery is not. In the second example, the purity of the retentate is reasonably high, but the recovery is not. To improve purity and recovery, membrane modules are cascaded using recycle, similar to the use of reflux in distillation. Shown in Figure 5.12 are three membrane-separation systems,

studied by Prasad et al. [2] for the production of pure nitrogen (retentate) from air, using a membrane material that is more permeable to oxygen. The first system is a single module. The second system is a cascade of two stages, with permeate recycle from the second to the first stage. The third system is a cascade of three stages with permeate recycles from stage 3 to stage 2 and from stage 2 to stage 1. The two cascades are similar to the single-section countercurrent stripping cascade shown in Figure 5.1.

Prasad et al. [2] give the following results for the three configurations in Figure 5.12:

Membrane System	Mol% N ₂ in Retentate	% Recovery of N ₂
Single Stage	98	45
Two Stages	99.5	48
Three Stages	99.9	50

Thus, high purities are obtained with a single-section membrane cascade, but little improvement in the recovery is provided by additional stages. To obtain both high purity and high recovery, a two-section membrane cascade is necessary, as discussed in Chapter 14.

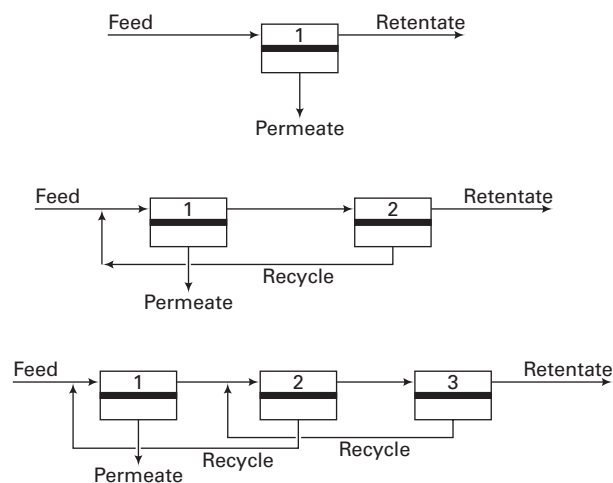


Figure 5.12 Membrane cascades.

§5.5 HYBRID SYSTEMS

Hybrid systems that add two or more different separation operations in series have the potential for reducing energy and raw-material costs and accomplishing difficult separations. Table 5.1 lists some commercial hybrid systems that have received considerable attention. Examples of applications are included. Not listed in Table 5.1 are hybrid systems consisting of distillation combined with extractive distillation, azeotropic distillation, and/or liquid–liquid extraction, which are considered in Chapter 11.

The first example in Table 5.1 combines adsorption, to preferentially remove methane, with a gas permeation membrane operation to remove nitrogen. The permeate is recycled to the adsorption step. Figure 5.13 compares this hybrid system to gas permeation alone and to adsorption alone. Only the hybrid system is capable of making a sharp separation between

Table 5.1 Hybrid Systems

Hybrid System	Separation Example
Adsorption—gas permeation	Nitrogen—Methane
Simulated moving bed adsorption—distillation	Metaxylene—paraxylene with ethylbenzene eluent
Crystallization—liquid–liquid extraction	Sodium carbonate—water
Distillation—adsorption	Ethanol—water
Distillation—gas permeation	Propylene—propane
Distillation—pervaporation	Ethanol—water
Gas permeation—absorption	Dehydration of natural gas
Reverse osmosis—distillation	Carboxylic acids—water
Reverse osmosis—evaporation	Concentration of wastewater
Stripper—gas permeation	Recovery of ammonia and hydrogen sulfide from sour water

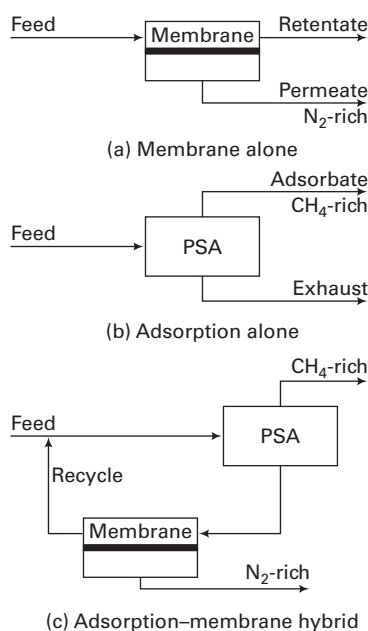


Figure 5.13 Separation of methane from nitrogen.

Table 5.2 Typical Products for Processes in Figure 5.13

	Flow Rate, Mscfh	Mol% CH ₄	Mol% N ₂
Feed gas	100	80	20
Membrane only:			
Retentate	47.1	97	3
Permeate	52.9	65	35
PSA only:			
Adsorbate	70.6	97	3
Exhaust	29.4	39	61
Hybrid system:			
CH ₄ -rich	81.0	97	3
N ₂ -rich	19.0	8	92

methane and nitrogen. Products obtainable from these three processes are compared in Table 5.2 for 100,000 scfh of feed containing 80% methane and 20% nitrogen. For all processes, the methane-rich product contains 97 mol% methane. Only the hybrid system gives a nitrogen-rich product of greater than 90 mol%, and a high recovery of methane (98%). The methane recovery for a membrane alone is only 57%, while the adsorber (PSA) gives 86%.

§5.6 DEGREES OF FREEDOM AND SPECIFICATIONS FOR CASCADES

The solution to a multicomponent, multiphase, multistage separation problem involves a large number of variables in material-balance, energy-balance, and phase-equilibrium equations (relationships). A sufficient number of these variables must be specified so that the number of remaining unknown variables equals the number of independent equations relating the variables. This concept, referred to as a degrees-of-freedom analysis, was presented in §4.3.1 for a single equilibrium stage. In this section, it is extended to single- and multiple-section cascades. Although the extension is for continuous, steady-state processes, similar extensions can be made for batch and semi-continuous processes. Process simulators apply a degrees-of-freedom analysis to every unit operation model to prevent users from under- or over-specifying simulations.

A standard method for finding the number of degrees of freedom, N_D , was developed by Kwauk [3] for an element of an operation, the entire operation, and a process that involves two or more operations. The method involves an enumeration of all variables, N_V , and all independent equations, N_E , that relate the variables. The number of degrees of freedom is then found from

$$N_D = N_V - N_E \quad (5-16)$$

Typically, there are **intensive variables**, such as pressure, composition, and temperature; **extensive variables**, such as flow rates, heat-transfer rates, and rates of shaft work; and equipment parameters, such as number of stages. Physical properties such as enthalpy or K -values are not counted because they are functions of intensive variables. The variables are relatively easy to enumerate for a given operation. More

difficult is the formulation of all independent equations for mass and energy conservations, phase-equilibria restrictions, process specifications, and equipment configurations.

Separation equipment consists of physically identifiable **elements**: equilibrium stages, condensers, reboilers, pumps, etc., as well as **stream dividers** and **stream mixers**. It is helpful to examine each element separately before considering the complete separation operation unit.

§5.6.1 Stream Variables

A complete specification of intensive variables for a single-phase stream consists of C mole fractions plus T and P , or $C + 2$ variables. However, only $C - 1$ of the mole fractions are independent, because the other mole fraction must satisfy the **mole-fraction constraint**:

$$\sum_{i=1}^C \text{mole fractions} = 1.0$$

Thus, only $(C + 1)$ intensive stream variables can be specified. This is in agreement with the Gibbs' phase rule (4-1), which states that, for a single-phase system, the intensive variables are specified by $C - N_p + 2 = C - 1 + 2 = C + 1$ variables. The total flow rate, an extensive variable, is added to this number. Although the missing mole fraction is often treated implicitly, it is preferable to include all mole fractions in the list of stream variables and then to include, in the equations, the above mole-fraction constraint, from which the missing mole fraction is calculated. Thus, for each stream there are $(C + 3)$ variables. For example, for a liquid stream, the variables are liquid mole fractions x_1, x_2, \dots, x_C ; total flow rate L ; temperature T ; and pressure P .

§5.6.2 Adiabatic or Diabatic Equilibrium-Stage Element

A common element in separation operations is an equilibrium-stage with two entering and two exiting streams, as in Figure 5.14. The stage may include heat transfer. The stream variables are those associated with the four streams plus the heat-transfer rate. Thus,

$$N_V = 4(C + 3) + 1 = 4C + 13$$

The exiting streams V_{OUT} and L_{OUT} are in equilibrium, so there are phase equilibrium equations as well as component material balances, a total material balance, an energy balance and mole-fraction constraints. The equations relating the N_V variables are:

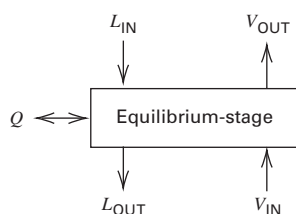


Figure 5.14 Equilibrium-stage element with heat addition or removal.

Equations	Number of Equations
Pressure equality, $P_{V_{OUT}} = P_{L_{OUT}}$	1
Temperature equality, $T_{V_{OUT}} = T_{L_{OUT}}$	1
Phase-equilibrium relationships, $(y_i)_{V_{OUT}} = K_i(x_i)_{L_{OUT}}$	C
Component material balances, $L_{IN}(x_i)_{L_{IN}} = V_{IN}(y_i)_{V_{IN}}$ $= L_{OUT}(x_i)_{L_{OUT}} + V_{OUT}(y_i)_{V_{OUT}}$	$C - 1$
Total material balance, $L_{IN} + V_{IN} = L_{OUT} + V_{OUT}$	1
Energy balance, $Q + h_{L_{IN}}L_{IN} + h_{V_{IN}}V_{IN}$ $= h_{L_{OUT}}L_{OUT} + h_{V_{OUT}}V_{OUT}$	1
Mole-fraction constraints in entering and exiting streams, $\sum_{i=1}^C x_i \text{ or } y_i = 1$	4
	$N_E = 2C + 7$

Alternatively, C , instead of $C - 1$, component material balances can be written. Then, the total material balance becomes a dependent equation that is removed for the list because it can be obtained by summing the component material balances and applying the mole-fraction constraint. Regardless of which two sets of equations are used, N_D from (5-16) becomes

$$N_D = (4C + 13) - (2C + 7) = 2C + 6$$

One must now decide which variables to specify (the **design variables**), leaving the remaining variables to be calculated from the equations. Several different sets of design variables can be specified. The following set, which is a common one, includes a complete specification of the two streams entering the stage, as well as the pressure of the streams leaving the stage and the heat transfer rate.

Variable Specification	Number of Variables
Component mole fractions, x_i , in L_{IN}	$C - 1$
Total flow rate, L_{IN}	1
Component mole fractions, y_i , in V_{IN}	$C - 1$
Total flow rate, V_{IN}	1
Temperature and pressure of L_{IN}	2
Temperature and pressure of V_{IN}	2
Stage pressure, $P_{V_{OUT}}$	1
Heat transfer rate, Q	1
	$N_D = 2C + 6$

Specification of these $2C + 6$ variables leaves the following $2C + 7$ variables to be calculated from the $2C + 7$ independent equations:

$$(x_C)_{L_{IN}}, (y_C)_{V_{IN}}, L_{OUT}, \text{ all } (x_i)_{L_{OUT}}, T_{L_{OUT}}, P_{L_{OUT}}, \text{ all } (y_i)_{V_{OUT}}, \text{ and } T_{V_{OUT}}$$

§5.6.3 Single-Section Countercurrent Cascade Unit

The single-section countercurrent cascade unit in Figure 5.15 contains the N adiabatic or diabatic equilibrium-stage elements from Figure 5.14. To combine elements into a unit, the total number of design variables for the unit is obtained by summing the variables associated with each element, $(N_V)_e$, followed by subtraction of the $(C + 3)$ variables for each of the N_R redundant interconnecting streams that arise when the output of one element becomes the input to another. Also, if the unit contains an unspecified number of repetitions, e.g., stages, an additional variable is added, one for each group of repetitions, giving a total of N_A additional variables. Thus, the number of variables for the unit is

$$(N_V)_{\text{unit}} = \sum_{\text{all elements, } e} (N_V)_e - N_R(C + 3) + N_A \quad (5-17)$$

The number of independent equations for the unit is obtained by summing the values of N_E for the elements and then subtracting the N_R redundant mole-fraction constraints, giving

$$(N_E)_{\text{unit}} = \sum_{\text{all elements, } e} (N_E)_e - N_R \quad (5-18)$$

Applying (5-16) to the unit, gives

$$(N_D)_{\text{unit}} = (N_V)_{\text{unit}} - (N_E)_{\text{unit}} \quad (5-19)$$

which can also be written as

$$(N_D)_{\text{unit}} = \sum_{\text{all elements, } e} (N_D)_e - N_R(C + 2) + N_A \quad (5-20)$$

To determine $(N_D)_{\text{unit}}$ for the N -stage cascade unit of Figure 5.15, note that it consists of N adiabatic or non-adiabatic equilibrium-stage elements with $N_D = 2C + 6$. For N stages, $N_R = 2(N - 1)$. $N_A = 1$ because the unit contains an unknown number of identical elements. Substituting these values into (5-20) gives

$$\begin{aligned} (N_D)_{\text{unit}} &= N(2C + 6) - 2(N - 1)(C + 2) + 1 \\ &= 2N + 2C + 5 \end{aligned}$$

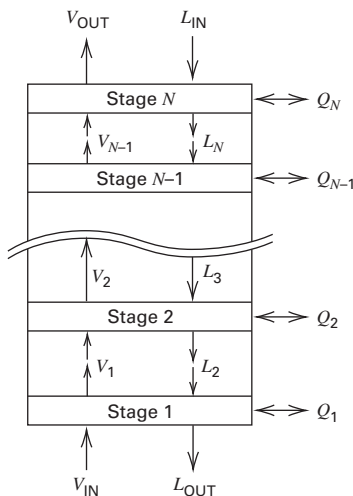


Figure 5.15 N -stage single-section countercurrent cascade unit.

The same result is obtained using (5-17), (5-18), and (5-19). Two features of this result should be noted: (1) The coefficient of C is 2. This corresponds to the number of streams entering the unit. If three streams entered the unit, the coefficient C would be 3. (2) The coefficient of N is 2 and is always this value. It corresponds to the variables Q for heat transfer to or from the stage and P for the pressure of the streams leaving the stage.

The N -stage single-section cascade unit of Figure 5.15 applies to absorbers, strippers, and liquid-liquid extraction units. A common set of design variables is as follows:

Variable Specification	Number of Variables
Heat-transfer rate for each stage (or adiabaticity)	N
Pressure of vapor leaving each stage	N
Stream V_{IN} variables	$C + 2$
Stream L_{IN} variables	$C + 2$
Number of stages	1
	$2N + 2C + 5$

Using these specifications, the following variables are computed from the equations: $(x_C)_{L_{\text{IN}}}$, $(y_C)_{V_{\text{IN}}}$, L_{OUT} , all $(x_i)_{L_{\text{OUT}}}$, $T_{L_{\text{OUT}}}$, $P_{L_{\text{OUT}}}$, V_{OUT} , all $(y_i)_{V_{\text{OUT}}}$, $T_{V_{\text{OUT}}}$, and all other inter-stage stream variables.

§5.6.4 Multiple-Section Countercurrent Cascade Units

Multiple-section countercurrent cascade units, particularly two-section units, are widely used to make industrial separations, e.g., distillation. They consist not only of two or more single-section countercurrent units, but also various elements shown in Table 5.3, including total and partial condensers; partial reboilers; heat exchangers; pumps; compressors; equilibrium stages where a feed, F , enters or where a vapor or liquid sidestream, S , is withdrawn; phase separators; stream mixers; and stream dividers. The elements in Table 5.3 can be combined into any of a number of complex cascades by applying the given element values of N_V , N_E , and N_D to (5-17) through (5-20).

Calculations for multistage separation operations involve solving equations (relationships) for output variables after selecting values of design variables that satisfy the degrees-of-freedom requirement. Two common cases are (1) the **design case**, in which component recoveries and/or purities are specified and the number of required equilibrium stages is determined; and (2) the **simulation case**, in which the number of stages is specified and component separations are computed. The second case is less complex computationally and more widely used in process simulation because the number of stages is specified, thus predetermining the number of equations to be solved. Table 5.4 is a summary of possible variable specifications for each of the two cases for a number of different separation units discussed in later chapters of this book. For all separation units in Table 5.4, it is assumed that inlet streams are completely specified, and that all element and unit pressures and heat-transfer rates (except for condensers and reboilers) are specified. Thus, only variable specifications satisfying the remaining degrees of freedom are listed.

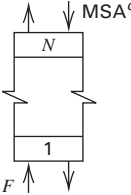
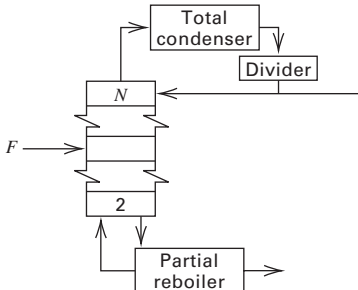
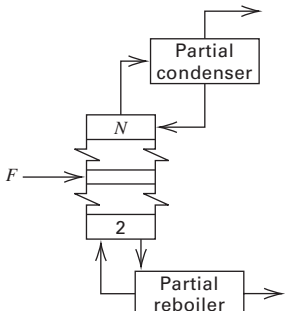
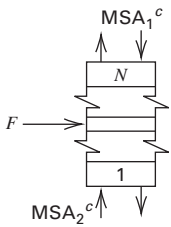
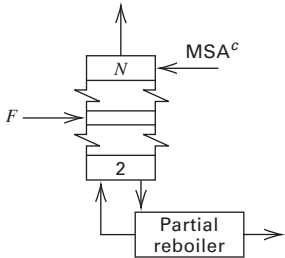
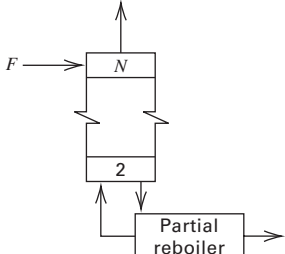
Table 5.3 Degrees of Freedom for Separation Operation Elements and Units

	Schematic	Element or Unit Name	N_V , Total Number of Variables	N_E , Independent Equations	N_D , Degrees of Freedom
(a)		Total boiler (reboiler)	$(2C + 7)$	$(C + 3)$	$(C + 4)$
(b)		Total condenser	$(2C + 7)$	$(C + 3)$	$(C + 4)$
(c)		Partial (equilibrium) boiler (reboiler)	$(3C + 10)$	$(2C + 6)$	$(C + 4)$
(d)		Partial (equilibrium) condenser	$(3C + 10)$	$(2C + 6)$	$(C + 4)$
(e)		Adiabatic equilibrium stage	$(4C + 12)$	$(2C + 7)$	$(2C + 5)$
(f)		Equilibrium stage with heat transfer	$(4C + 13)$	$(2C + 7)$	$(2C + 6)$
(g)		Equilibrium feed stage with heat transfer and feed	$(5C + 16)$	$(2C + 8)$	$(3C + 8)$
(h)		Equilibrium stage with heat transfer and sidestream	$(5C + 16)$	$(3C + 9)$	$(2C + 7)$
(i)		N -connected equilibrium stages with heat transfer	$(7N + 2NC + 2C + 7)$	$(5N + 2NC + 2)$	$(2N + 2C + 5)$
(j)		Stream mixer	$(3C + 10)$	$(C + 4)$	$(2C + 6)$
(k)		Stream divider	$(3C + 10)$	$(2C + 5)$	$(C + 5)$

^aSidestream can be vapor or liquid.

^bAlternatively, all streams can be vapor.

Table 5.4 Typical Variable Specifications for Design Cases

Unit Operation	N_D	Variable Specification ^a		
		Case I, Component Separations Specified	Case II, Number of Equilibrium Stages Specified	
(a) Absorption (two inlet streams)		$2N + 2C + 5$	<ol style="list-style-type: none"> 1. Recovery of one key component 	<ol style="list-style-type: none"> 1. Number of stages
(b) Distillation (one inlet stream, total condenser, partial reboiler)		$2N + C + 9$	<ol style="list-style-type: none"> 1. Condensate at saturation temperature 2. Recovery of light-key component 3. Recovery of heavy-key component 4. Reflux ratio (> minimum) 5. Optimal feed stage^b 	<ol style="list-style-type: none"> 1. Condensate at saturation temperature 2. Number of stages above feed stage 3. Number of stages below feed stage 4. Reflux ratio 5. Distillate flow rate
(c) Distillation (one inlet stream, partial condenser, partial reboiler, vapor distillate only)		$(2N + C + 6)$	<ol style="list-style-type: none"> 1. Recovery of light-key component 2. Recovery of heavy-key component 3. Reflux ratio (> minimum) 4. Optimal feed stage^b 	<ol style="list-style-type: none"> 1. Number of stages above feed stage 2. Number of stages below feed stage 3. Reflux ratio 4. Distillate flow rate
(d) Liquid-liquid extraction with two solvents (three inlet streams)		$2N + 3C + 8$	<ol style="list-style-type: none"> 1. Recovery of key component 1 2. Recovery of key component 2 	<ol style="list-style-type: none"> 1. Number of stages above feed 2. Number of stages below feed
(e) Reboiled absorption (two inlet streams)		$2N + 2C + 6$	<ol style="list-style-type: none"> 1. Recovery of light-key component 2. Recovery of heavy-key component 3. Optimal feed stage^b 	<ol style="list-style-type: none"> 1. Number of stages above feed 2. Number of stages below feed 3. Bottoms flow rate
(f) Reboiled stripping (one inlet stream)		$2N + C + 3$	<ol style="list-style-type: none"> 1. Recovery of one key component 2. Reboiler heat duty^d 	<ol style="list-style-type: none"> 1. Number of stages 2. Bottoms flow rate

(Continued)

Table 5.4 (Continued)

Unit Operation	N_D	Variable Specification ^a	
		Case I, Component Separations Specified	Case II, Number of Equilibrium Stages Specified
(g) Distillation (one inlet stream, partial condenser, partial reboiler, both liquid and vapor distillates)	$2N + C + 9$	<ol style="list-style-type: none"> 1. Ratio of vapor distillate to liquid distillate 2. Recovery of light-key component 3. Recovery of heavy-key component 4. Reflux ratio (> minimum) 5. Optimal feed stage^b 	<ol style="list-style-type: none"> 1. Ratio of vapor distillate to liquid distillate 2. Number of stages above feed stage 3. Number of stages below feed stage 4. Reflux ratio 5. Liquid distillate flow rate
(h) Extractive distillation (two inlet streams, total condenser, partial reboiler, singlephase condensate)	$2N + 2C + 12$	<ol style="list-style-type: none"> 1. Condensate at saturation temperature 2. Recovery of light-key component 3. Recovery of heavy-key component 4. Reflux ratio (> minimum) 5. Optimal feed stage^b 6. Optimal MSA stage^b 	<ol style="list-style-type: none"> 1. Condensate at saturation temperature 2. Number of stages above MSA stage 3. Number of stages between MSA and feed stages 4. Number of stages below feed stage 5. Reflux ratio 6. Distillate flow rate
(i) Liquid-liquid extraction (two inlet streams)	$2N + 2C + 5$	<ol style="list-style-type: none"> 1. Recovery of one key component 	<ol style="list-style-type: none"> 1. Number of stages
(j) Stripping (two inlet streams)	$2N + 2C + 5$	<ol style="list-style-type: none"> 1. Recovery of one key component 	<ol style="list-style-type: none"> 1. Number of stages

^aDoes not include the following variables, which are also assumed specified: all inlet stream variables ($C + 2$ for each stream); all element and unit pressures; all element and unit heat-transfer rates except for condensers and reboilers.

^bOptimal stage for introduction of inlet stream corresponds to minimization of total stages.

^cFor case I variable specifications, MSA flow rate must be greater than minimum values for specified recoveries.

^dFor case I variable specifications, reboiler heat duty must be greater than minimum value for specified recovery.

EXAMPLE 5.2 Degrees of Freedom and Specifications for a Distillation Column.

Consider the multistage distillation column in Figure 5.16, which has one feed, one sidestream, a total condenser, a partial reboiler, and the possibility of heat transfer to or from any stage in the column. Determine the number of degrees of freedom and a reasonable set of specifications.

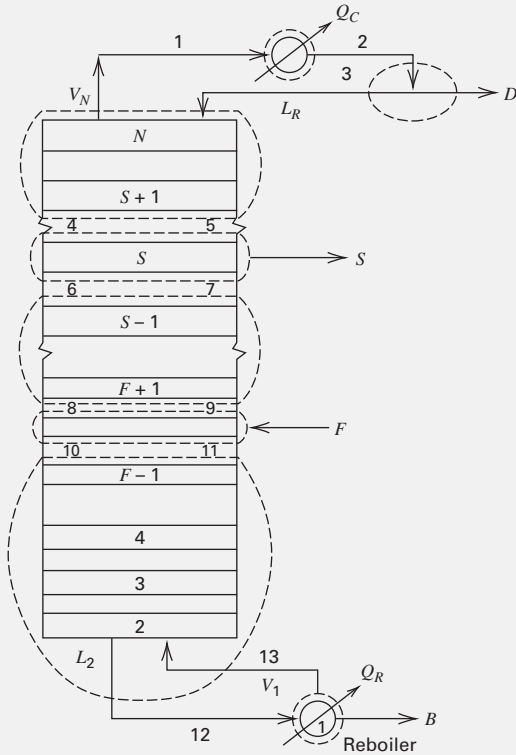


Figure 5.16 Distillation unit with a sidestream.

Solution

The separation unit is assembled from Table 5.3 for the circled elements and units in Figure 5.16. The total variables are determined by summing the variables $(N_V)_e$ for each element from Table 5.3 and subtracting redundant variables due to interconnecting flows. Redundant mole-fraction constraints are subtracted from the sum of independent equations for each element $(N_E)_e$. The stages are numbered as shown in Figure 5.16, with the partial reboiler as the first equilibrium stage. The total condenser is not an equilibrium stage. From Table 5.3, element variables and equations are as follows:

Subtracting $(C + 3)$ redundant variables for 13 interconnecting streams, using (5-17), with $N_A = 0$ (no unspecified repetitions), gives

$$(N_V)_{\text{unit}} = \sum (N_V)_e - 13(C + 3) = 7N + 2NC + 5C + 20$$

Subtracting the corresponding 13 redundant mole-fraction constraints, using (5-18), gives

$$(N_E)_{\text{unit}} = \sum (N_E)_e - 13 = 5N + 2NC + 4C + 9$$

Therefore, from (5-19),

$$N_D = (7N + 2NC + 5C + 20) - (5N + 2NC + 4C + 9) = 2N + C + 11$$

Note that the coefficient of C is only 1, because there is only one feed, and, again, the coefficient of N is 2. From Table 5.4, for the same distillation column, but without a sidestream, the number of degrees of freedom for that unit is $2N + C + 9$. Thus, the sidestream adds two degrees of freedom. One way to rationalize this is that the location of the sidestream adds one degree of freedom and the total flow rate of the sidestream adds another. Similarly, the above example can readily be modified to include a second feed stage. The second feed adds $C + 2$ degrees of freedom, while another variable must be added for the location of the second feed stage. Thus, units (b) and (h) in Table 5.4 differ by $C + 3$ degrees of freedom.

A set of feasible design variable specifications is as follows:

Variable Specification	Number of Variables
1. Pressure at each stage (including partial reboiler)	N
2. Pressure at reflux divider outlet	1
3. Pressure at total condenser outlet	1
4. Heat-transfer rate for each stage (excluding partial reboiler)	$(N-1)$
5. Heat-transfer rate for divider	1
6. Feed mole fractions and total feed rate	C
7. Feed temperature	1
8. Feed pressure	1
9. Condensate temperature (e.g., saturated liquid)	1
10. Total number of stages, N	1
11. Feed stage location	1
12. Sidestream stage location	1
13. Sidestream total flow rate, S	1
14. Total distillate flow rate, D or D/F	1
15. Reflux flow rate, L_R , or reflux ratio, L_R/D	1
$N_D = (2N + C + 11)$	

Element or Unit	$(N_V)_e$	$(N_E)_e$
Total condenser	$(2C + 7)$	$(C + 3)$
Reflux divider	$(3C + 10)$	$(2C + 5)$
$(N - S)$ stages	$[7(N - S) + 2(N - S)C + 2C + 7]$	$[5(N - S) + 2(N - S)C + 2]$
Sidestream stage	$(5C + 16)$	$(3C + 9)$
$(S - 1) - F$ stages	$[7(S - 1 - F) + 2(S - 1 - F)C + 2C + 7]$	$[5(S - 1 - F) + 2(S - 1 - F)C + 2]$
Feed stage	$(5C + 16)$	$(2C + 8)$
$(F - 1) - 1$ stages	$[7(F - 2) + 2(F - 2)C + 2C + 7]$	$[5(F - 2) + 2(F - 2)C + 2]$
Partial reboiler	$(3C + 10)$	$(2C + 6)$
	$\sum (N_V)_e = 7N + 2NC + 18C + 59$	$\sum (N_E)_e = 5N + 2NC + 4C + 22$

In the above table, the first variable specifications are the stage pressures. This refers to the pressure of any one of the streams exiting the stage. The pressures of other streams leaving the same stage are calculated from the pressure equality equation(s).

The condenser and reboiler heat duties, Q_C and Q_R , in Figure 5.16, are not suitable design variables because they are difficult to specify. A poorly specified Q_C might result in a temperature that is not realizable. Similarly, it is much easier to calculate Q_R , knowing the total flow rate and enthalpy of the bottom stream than vice versa. Also, Q_R and Q_C are so closely related that both should never be specified. Preferably, Q_C is fixed by distillate rate and reflux ratio, and Q_R is then calculated from an overall energy balance.

Other specification proxies are possible, but the problem of independence of variables requires careful consideration. Distillate product rate, Q_C , and L_R/D , for example, are closely related. It should also be noted that the equations used to model equilibrium stages are nonlinear and must be solved by iterative numerical methods, e.g. Newton's method as applied in §4.3.2 to calculate an isothermal flash. If recoveries of more than two key species are specified, the result can be non-convergence of the computations because the specified composition may not exist at physical equilibrium.

CHAPTER 5 NOMENCLATURE

Abbreviations and Acronyms

scfh standard cubic feet per hour

Latin Symbols

C number of components
 F_A flow rate of carrier, A, in the feed, (5-2)
 K'_D distribution ratio based on mass ratios, (5-3)

SUMMARY

1. A cascade is a sequence of stages arranged to accomplish a separation not achievable in a single stage.
2. Cascades are single- or multiple-sectioned and configured in cocurrent, crosscurrent, or countercurrent arrays.
3. Calculations for single-section, multistage liquid-liquid extraction with constant distribution coefficients and immiscible solvent and carrier are readily computed for crosscurrent and countercurrent flow. The latter is more efficient.
4. A single-section cascade can achieve a recovery of a single key component but cannot make a split between two key components.
5. A two-section countercurrent cascade can achieve a sharp split between two key components. In distillation, the top (rectifying) section purifies the light components and increases recovery from heavy components. The bottom (stripping) section provides the opposite functions.
6. Single-section membrane cascades increase the purity of one product and the recovery of the main component in that product.
7. Hybrid systems may reduce energy costs and make possible separations that are otherwise difficult and/or improve the degree of separation.
8. The number of degrees of freedom (number of specifications) for a mathematical model of a cascade is the difference between the number of variables and the number of independent equations relating those variables. For a single-section countercurrent cascade, the recovery of one component can be specified. For a two-section countercurrent cascade, two recoveries can be specified.

N number of stages
 N_A number of additional variables, (5-17)
 N_D number of degrees of freedom, (5-16)
 N_E number of independent equations, (5-16)
 N_P number of phases, (5-16)
 N_R number of redundant variables, (5-18)
 N_V number of variables, (5-16)
 Q heat transfer rate
 Q_C condenser heat duty
 Q_R reboiler heat duty
 S liquid sidestream, Table 5.3h
 S solvent flow rate on a solute-free basis, Figure 5.2
 X_B mass ratio of solute to the carrier, (5-3)
 Y_B mass ratio of solute to the solvent, (5-3)

Script Symbols

\mathcal{E} extraction factor, (5-2)

Subscripts

e element, Table 5.3
 B solute
 F feed
 R raffinate, reflux

Superscripts

(1), (2) phase 1 and 2 in (5-7)
 N number of stages

REFERENCES

- BERDT, R.J., and C.C. LYNCH, *J. Am. Chem. Soc.*, **66**, 282–284 (1944).
- PRASAD, R., F. NOTARO, and D.R. THOMPSON, *J. Membrane Science*, **94**, Issue 1, 225–248 (1994).
- KWAUK, M., *AIChE J.*, **2**, 240–248 (1956).

STUDY QUESTIONS

- What is a separation cascade? What is a hybrid system?
- What is the difference between a countercurrent and a cross-current cascade?
- What is the limitation of a single-section cascade? Does a two-section cascade overcome this limitation?
- Which is more efficient, a crosscurrent cascade or a countercurrent cascade?
- Under what conditions can a countercurrent cascade achieve complete liquid–liquid extraction?
- Why is a two-section cascade used for distillation?
- In distillation, what is meant by reflux, boilup, rectification section, and stripping section?
- Why are membrane stages not equilibrium stages?
- Under what conditions is a membrane cascade of multiple stages in series necessary?
- Why are hybrid systems often considered?
- Give an example of a hybrid system that involves recycle.
- When solving a separation problem, are the number and kind of specifications obvious? If not, how can the required number of specifications be determined?
- Can the degrees of freedom be determined for a hybrid system? If so, what is the easiest way to do it?

EXERCISES

Section 5.1

5.1. Batchwise extraction process.

A liquid–liquid extraction process is conducted batchwise as shown in Figure 5.17. The process begins in Vessel 1 (Original),

Organic	Vessel 1				
Aqueous	100 A	100 B			Original
Organic	66.7 A	33.3 B			
Aqueous	33.3 A	66.7 B			Equilibration 1
Organic			Vessel 2		
Aqueous	33.3 A	66.7 B	66.7 A	33.3 B	Transfer
Organic	22.2 A	22.2 B	44.4 A	11.1 B	
Aqueous	11.1 A	44.4 B	22.2 A	22.2 B	Equilibration 2
Organic					Vessel 3
Aqueous	11.1 A	44.4 B	22.2 A	22.2 B	Transfer
Organic	7.4 A	14.8 B	29.6 A	7.4 B	
Aqueous	3.7 A	29.6 B	14.8 A	14.8 B	Equilibration 3
Organic					Vessel 4
Aqueous	3.7 A	29.6 B	7.4 A	14.8 B	Transfer
Organic	2.5 A	9.9 B	14.8 A	14.8 B	
Aqueous	1.2 A	19.7 B	7.4 A	29.6 B	Equilibration 4

Figure 5.17 Liquid–liquid extraction process for Exercise 5.1.

where 100 mg each of solutes A and B are dissolved in 100 mL of water. After adding 100 mL of an organic solvent that is more selective for A than B, the distribution of A and B becomes that shown for Equilibration 1 with Vessel 1. The organic-rich phase is transferred to Vessel 2 (Transfer), leaving the water-rich phase in Vessel 1 (Transfer). The water and the organic are immiscible. Next, 100 mL of water is added to Vessel 2, resulting in the phase distribution shown for Vessel 2 (Equilibration 2). Also, 100 mL of organic is added to Vessel 1 to give the phase distribution shown for Vessel 1 (Equilibration 2). The batch process is continued by adding Vessel 3 and then 4 to obtain the results shown. (a) Study Figure 5.17 and then draw a corresponding cascade diagram, labeled in a manner similar to Figure 5.2. (b) Is the process cocurrent, countercurrent, or cross-current? (c) Compare the separation with that for a batch equilibrium step. (d) How could the cascade be modified to make it countercurrent? [See O. Post and L.C. Craig, *Anal. Chem.*, **35**, 641 (1963).]

5.2. Two-stage membrane cascade.

Nitrogen is removed from a gas mixture with methane by gas permeation (see Table 1.3) using a glassy polymer membrane that is selective for nitrogen. However, the desired degree of separation cannot be achieved in one stage. Draw sketches of two different two-stage membrane cascades that might be used.

Section 5.2

5.3. Batch extraction of acetic acid.

An aqueous acetic acid solution containing 6.0 mol/L of acid is extracted with chloroform at 25°C to recover the acid (B) from chloroform-insoluble impurities in the water. The water (A) and chloroform (C) are immiscible. If 10 L of solution are to be extracted at 25°C, calculate the percent extraction of acid obtained with 10 L of chloroform under the following conditions: (a) the entire quantity of solvent in a single batch extraction; (b) three batch extractions with one-third of the solvent in each batch; (c) three batch extractions with 5 L of solvent in the first, 3 L in the second, and 2 L in the third batch.

Assume the distribution coefficient for the acid = $K''_{DB} = (c_B)_C / (c_B)_A = 2.8$, where $(c_B)_C$ = concentration of acid in chloroform and $(c_B)_A$ = concentration of acid in water, both in mol/L.

5.4. Extraction of uranyl nitrate.

A 20 wt% solution of uranyl nitrate (UN) in water is to be treated with tributyl phosphate (TBP) to remove 90% of the uranyl nitrate in batchwise equilibrium contacts. Assuming water and TBP are mutually insoluble, how much TBP is required for 100 g of solution if, at equilibrium, $(g \text{ UN}/g \text{ TBP}) = 5.5(g \text{ UN}/g \text{ H}_2\text{O})$ and (a) all the TBP is used at once in one stage; (b) half is used in each of two consecutive stages; (c) two countercurrent stages are used; (d) an infinite number of crosscurrent stages is used; and (e) an infinite number of countercurrent stages is used?

5.5. Extraction of uranyl nitrate.

The uranyl nitrate (UN) in 2 kg of a 20 wt% aqueous solution is extracted with 500 g of tributyl phosphate. Using the equilibrium data in Exercise 5.4, calculate and compare the percent recoveries for the following alternative procedures: (a) a single-stage batch extraction; (b) three batch extractions with one-third of the total solvent used in each batch (solvent is withdrawn after contacting the entire UN phase); (c) a two-stage cocurrent extraction; (d) a three-stage countercurrent extraction; (e) an infinite-stage countercurrent extraction; and (f) an infinite-stage crosscurrent extraction.

5.6. Extraction of dioxane.

One thousand kg of a 30 wt% dioxane in water solution is to be treated with benzene at 25°C to remove 95% of the dioxane. The benzene is dioxane-free, and the equilibrium data of Example 5.1 applies. Calculate the solvent requirements for (a) a single batch extraction; (b) two crosscurrent stages using equal amounts of benzene; (c) two countercurrent stages; (d) an infinite number of crosscurrent stages; and (e) an infinite number of countercurrent stages.

5.7. Extraction of benzoic acid.

Chloroform is used to extract benzoic acid from wastewater effluent. The benzoic acid is present at a concentration of 0.05 mol/L in the effluent, which is discharged at 1,000 L/h. The distribution coefficient for benzoic acid is $c^I = K_D^I c^{II}$, where $K_D^I = 4.2$, c^I = molar concentration of solute in solvent, and c^{II} = molar concentration of solute in water. Chloroform and water may be assumed immiscible. If 500 L/h of chloroform is to be used, compare the fraction benzoic acid removed in (a) a single equilibrium contact; (b) three crosscurrent contacts with equal portions of chloroform; and (c) three countercurrent contacts.

5.8. Extraction of benzoic acid.

Repeat Example 5.1 with a solvent for $\mathcal{E} = 0.90$. Display your results in a plot like Figure 5.6. Does countercurrent flow still have a marked advantage over crosscurrent flow? Is it desirable to choose the solvent and solvent rate so that $\mathcal{E} > 1$? Explain.

5.9. Extraction of citric acid from a broth.

A clarified broth from fermentation of sucrose using *Aspergillus niger* consists of 16.94 wt% citric acid, 82.69 wt% water, and 0.37 wt% other solutes. To recover citric acid, the broth would normally be treated first with calcium hydroxide to neutralize the acid and precipitate it as calcium citrate, and then with sulfuric acid to convert calcium citrate back to citric acid. To avoid the need for calcium hydroxide and sulfuric acid, U.S. Patent 4,251,671 describes a solvent-extraction process using N,N-diethyldodecanamide, which is insoluble in water and has a density of 0.847 g/cm³. In a typical experiment at 30°C, 50 g of 20 wt% citric acid and 80 wt% water was contacted with 0.85 g of amide. The resulting organic phase, assumed to be in equilibrium with the aqueous phase, contained 6.39 wt% citric acid and 2.97 wt% water. Determine (a) the partition (distribution) coefficients for citric acid and water, and (b) the solvent flow rate in kg/h needed to extract 98% of the citric

acid in 1,300 kg/h of broth using five countercurrent, equilibrium stages, with the partition coefficients from part (a), but ignoring the solubility of water in the organic phase. In addition, (c) propose a series of subsequent stages to produce near-pure citric acid crystals. In part (b), how serious would it be to ignore the solubility of water in the organic phase?

5.10. Extraction of citric acid from a broth.

A clarified broth of 1,300 kg/h from the fermentation of sucrose using *Aspergillus niger* consists of 16.94 wt% citric acid, 82.69 wt% water, and 0.37 wt% other solutes. To avoid the need for calcium hydroxide and sulfuric acid in recovering citric acid from clarified broths, U.S. Patent 5,426,220 describes a solvent-extraction process using a mixed solvent of 56% tridodecyl lauryl amine, 6% octanol, and 38% aromatics-free kerosene, which is insoluble in water. In one experiment at 50°C, 570 g/min of 17 wt% citric acid in a fermentation liquor from pure carbohydrates was contacted in five countercurrent stages with 740 g/min of the mixed solvent. The result was 98.4% extraction of citric acid. Determine (a) the average partition (distribution) coefficient for citric acid from the experimental data, and (b) the solvent flow rate in kg/h needed to extract 98% of the citric acid in 1,300 kg/h of clarified broth using three countercurrent, equilibrium stages, with the partition coefficient from part (a).

Section 5.6**5.11. Degrees of freedom for reboiler and condenser.**

Verify the values given in Table 5.3 for N_V , N_E , and N_D for a partial reboiler and a total condenser.

5.12. Degrees of freedom for mixer and divider.

Verify the values given in Table 5.3 for N_V , N_E , and N_D for a stream mixer and a stream divider.

5.13. Specifications for a distillation column.

Maleic anhydride with 10% benzoic acid is a by-product of the manufacture of phthalic anhydride. The mixture is to be distilled in a column with a total condenser and a partial reboiler at a pressure of 13.2 kPa with a reflux ratio of 1.2 times the minimum value to give a product of 99.5 mol% maleic anhydride and a bottoms of 0.5 mol% anhydride. Is this problem completely specified?

5.14. Degrees of freedom for distillation.

Verify N_D for the following unit operations in Table 5.4: (b), (c), and (g). How would N_D change if two feeds were used?

5.15. Degrees of freedom for absorber and stripper.

Verify N_D for unit operations (e) and (f) in Table 5.4. How would N_D change if a vapor sidestream were pulled off some stage located between the feed stage and the bottom stage?

5.16. Degrees of freedom for extractive distillation.

Verify N_D for unit operation (h) in Table 5.4. How would N_D change if a liquid sidestream was added to a stage that was located between the feed stage and Stage 2?

5.17. Design variables for distillation.

The following are not listed as design variables for the distillation operations in Table 5.4: (a) condenser heat duty; (b) stage temperature; (c) intermediate-stage vapor rate; and (d) reboiler heat load. Under what conditions might these become design variables? If so, which variables listed in Table 5.4 could be eliminated?

5.18. Degrees of freedom for condenser change.

For distillation, show that if a total condenser is replaced by a partial condenser, the number of degrees of freedom is reduced by 3, provided the distillate is removed solely as a vapor.

5.19. Replacement of a reboiler with live steam.

Unit operation (b) in Table 5.4 is heated by injecting steam into the bottom plate of the column, instead of by a reboiler, for the separation of ethanol and water. Assuming a fixed feed, an adiabatic operation, 1 atm, and a product alcohol concentration: (a) What is the total number of design variables for the general configuration? (b) How many design variables are needed to complete the design? Which variables do you recommend?

5.20. Degrees-of-freedom for a distillation column.

(a) For the distillation column shown in Figure 5.18, determine the number of independent design variables. (b) It is suggested that a feed of 30% A, 20% B, and 50% C, all in moles, at 37.8°C and 689 kPa, be processed in the unit of Figure 5.18, with 15 plates in a 3-m-diameter column, which operates at vapor velocities of 0.3 m/s and an L/V of 1.2. The pressure drop per plate is 373 Pa, and the condenser is cooled by plant water at 15.6°C.

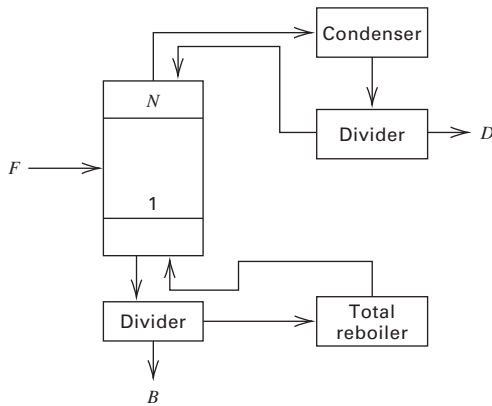


Figure 5.18 Conditions for Exercise 5.20.

The product specifications in terms of the concentration of A in the distillate and C in the bottoms have been set by the process department, and the plant manager has asked you to specify a feed rate for the column. Write a memorandum to the plant manager pointing out why you can't do this and suggest alternatives.

5.21. Degrees of freedom for multistage evaporation.

Calculate the number of degrees of freedom for the mixed-feed, triple-effect evaporator system shown in Figure 5.19. Assume that the steam and all drain streams are at saturated conditions and that the feed is an aqueous solution of a dissolved organic solid. Also, assume all overhead streams are pure steam. If this evaporator system is used to concentrate a feed containing 2 wt% dissolved organic to a product with 25 wt% dissolved organic, using 689-kPa saturated steam, calculate the number of unspecified design variables and suggest likely candidates. Assume perfect insulation against heat loss.

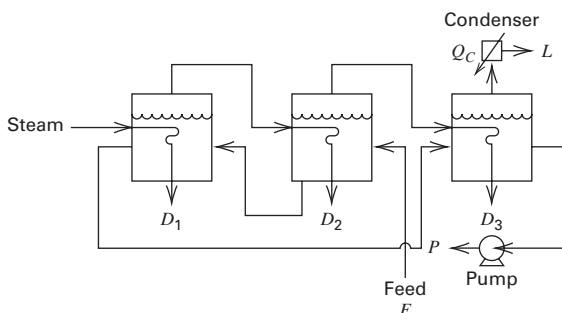


Figure 5.19 Conditions for Exercise 5.21.

5.22. Degrees of freedom for a reboiled stripper.

A reboiled stripper, shown in Figure 5.20, is to be designed. Determine (a) the number of variables; (b) the number of equations relating the variables; and (c) the number of degrees of freedom. Also indicate (d) which additional variables, if any, need to be specified.

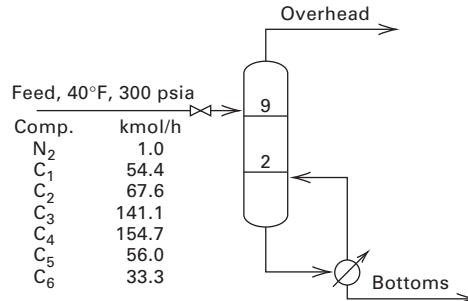


Figure 5.20 Conditions for Exercise 5.22.

5.23. Degrees of freedom of a thermally coupled distillation system.

The thermally coupled distillation system in Figure 5.21 separates a mixture of three components. Determine (a) the number of variables; (b) the number of equations relating the variables; and (c) the number of degrees of freedom. Also propose (d) a reasonable set of design variables.

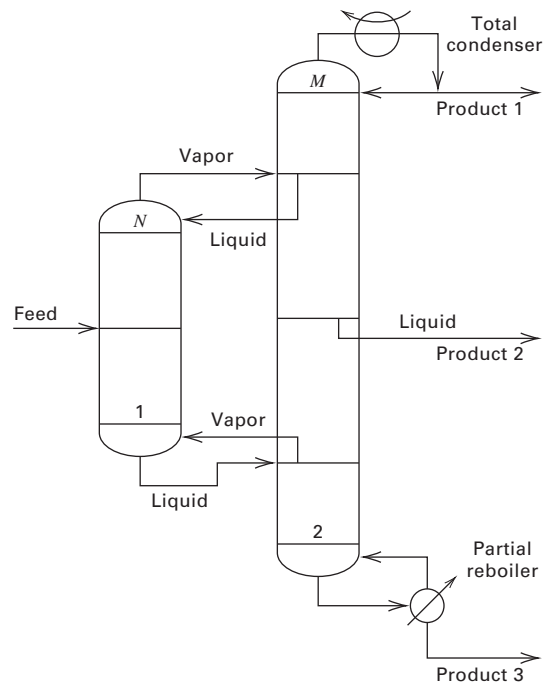


Figure 5.21 Conditions for Exercise 5.23.

5.24. Adding a pasteurization section to distillation column.

When feed to a distillation column contains impurities that are much more volatile than the desired distillate, it is possible to separate the volatile impurities from the distillate by removing the distillate as a liquid sidestream from a stage several stages below the top.

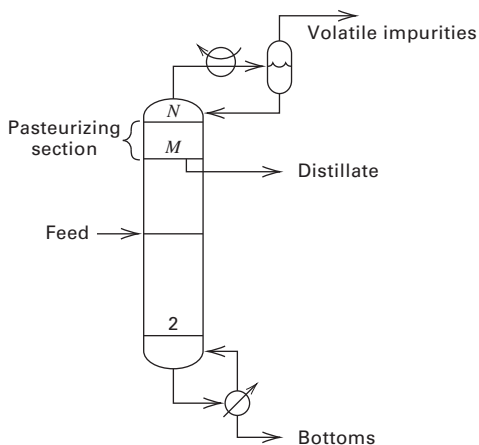


Figure 5.22 Conditions for Exercise 5.24.

As shown in Figure 5.22, this additional section of stages from M to N is referred to as a pasteurizing section. (a) Determine the number of degrees of freedom for the unit. (b) Determine a reasonable set of design variables.

5.25. Degrees of freedom for a two-column system.

A system for separating a feed into three products is shown in Figure 5.23. Determine (a) the number of variables; (b) the number of equations relating the variables; and (c) the number of degrees of freedom. Also propose (d) a reasonable set of design variables.

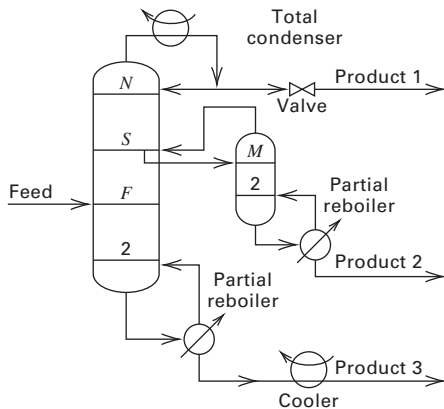


Figure 5.23 Conditions for Exercise 5.25.

5.26. Design variables for an extractive distillation.

Figure 5.24 shows a system for separating a binary mixture by extractive distillation, followed by ordinary distillation for recovery and recycle of the solvent. Are the design variables shown sufficient to specify the problem completely? If not, what additional design variables(s) should be selected?

5.27. Design variables for a three-product distillation column.

A single distillation column for separating a three-component mixture into three products is shown in Figure 5.25. Are the design variables shown sufficient to specify the problem completely? If not, what additional design variable(s) would you select?

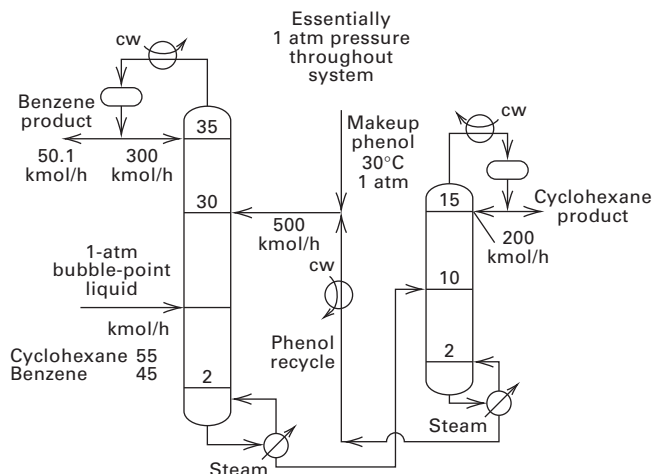


Figure 5.24 Conditions for Exercise 5.26.

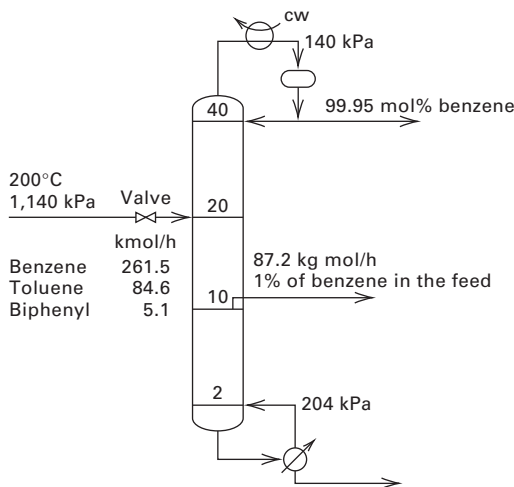


Figure 5.25 Conditions for Exercise 5.27.

5.28. Degrees of freedom for the last column in a three-column sequence.

Table 1.5 includes the material balance for column C3 in Figure 1.10. The key components are $i\text{-C}_4\text{H}_{10}$ and $n\text{-C}_4\text{H}_{10}$. Note that the distillate (Stream 6) contains zero percent $i\text{C}_5$ and there is less than 3.2% $i\text{C}_4$ in the bottoms. This column is to be shut down for maintenance and repair. The plan is to use temporary storage and a smaller spare column containing 12 trays, a total condenser, reflux splitter, and a partial reboiler to supply current customers. In similar applications, this column had a tray efficiency of 85%, so assume it has 11 equilibrium stages, including the reboiler. The condenser has a maximum capacity of 700 lbmol/h of condensate. Management has asked you to provide a report as to what to expect if the feed to the current column is transferred to the smaller column. Table 1.5 lists the product specifications. It has been suggested that an attempt to meet the specifications can be made by varying the reflux ratio and/or amount of distillate. Perform a degrees of freedom analysis to determine if this approach is valid.

Absorption and Stripping

§6.0 INSTRUCTIONAL OBJECTIVES

After completing this chapter, you should be able to:

- Explain the differences among physical absorption, chemical absorption, and stripping.
- Explain why absorbers are best operated at high pressure and low temperature, whereas strippers are best operated at low pressure and high temperature.
- Compare three different types of trays with respect to cost and efficiency.
- Explain the difference between random and structured packing and cite examples of each.
- Derive the operating-line equation used in graphical methods, starting with a component material balance.
- Calculate the minimum mass-separating agent (MSA) flow rate to achieve a specified key-component recovery.
- Determine algebraically or graphically, by stepping off stages, the required number of equilibrium stages in a countercurrent cascade.
- Define and explain the significance of absorption and stripping factors.
- Estimate component recoveries in a single-section, countercurrent cascade, using the Kremser group method.
- Define overall stage efficiency and explain why efficiencies are low for absorbers and moderate for strippers.
- Explain two mechanisms by which a trayed column can flood.
- Estimate column diameter for a trayed column.
- Differentiate between overall tray efficiency and individual tray efficiencies based on the Murphree vapor tray efficiency.
- For a packed column, define the height equivalent to a theoretical (equilibrium) stage (plate or tray), referred to as the HETS or HETP. Explain how the HETS and the number of equilibrium stages differ, respectively, from the height of a transfer unit (HTU) and the number of transfer units (NTU).
- Explain the differences between the loading point and flooding point in a packed column.
- Estimate packed height, packed-column diameter, and pressure drop across the packing.
- Understand how design procedures for strippers and absorbers need modification if chemical reactions between solutes and solvents occur.

Absorption uses a liquid to (1) selectively remove components from a gas mixture; (2) remove impurities, contaminants, pollutants, or catalyst poisons; and (3) recover valuable chemicals. The species of interest in the gas mixture may include all components present in the gas, only the component(s) not absorbed, or only the component(s) absorbed. The species transferred to the liquid **absorbent** are called **solutes**. When the solutes have been absorbed, they are called **absorbates**.

In **stripping (desorption)**, a liquid mixture is brought into contact with a gas that selectively removes components by mass transfer from the liquid to the gas phase. Strippers are frequently coupled with absorbers to permit the recovery and recycling of the absorbent. When water is used as the absorbent, it is common to separate the water from the solute by distillation rather than by stripping.

Industrial Example

Figure 6.1 shows an absorption operation, including stream flow rates, compositions, temperature, and pressure. The feed gas is air containing water vapor and acetone vapor. It comes from a dryer in which water and acetone are evaporated from solid cellulose acetate fibers. The 30-tray (equivalent to 12.5 equilibrium stages) countercurrent absorber is designed to remove 99.5% of the acetone from the feed gas. Scrubbed gas exiting the absorber contains only 143 parts per million (ppm) by weight of acetone. It can be recycled to the dryer, although a small amount must be purged through a pollution-control device to prevent argon buildup. Acetone is the main species absorbed, along with minor amounts of O_2 and N_2 . Water present as vapor in the feed gas and as liquid in the entering absorbent is absorbed and stripped, respectively.

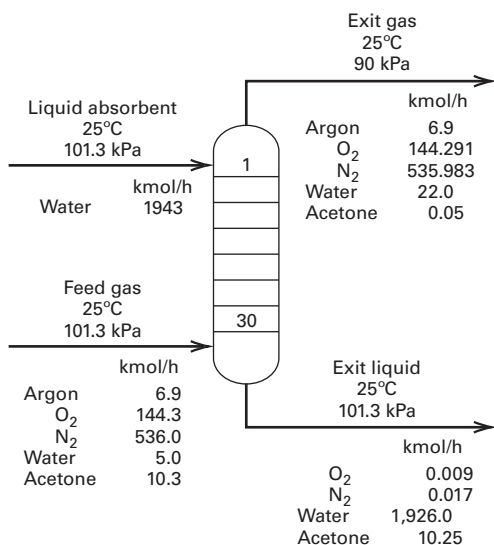


Figure 6.1 Industrial absorption process.

In this example, the net effect is that water is stripped because more water appears in the exit gas than in the feed gas.

The exit gas is almost saturated with water vapor, and the exit liquid is almost saturated with air. As shown in §6.4, the amount of each component absorbed depends on the number of equilibrium stages and the component's **absorption factor**, $A_i = L/K_iV$. For Figure 6.1, K -values and absorption factors based on inlet flow rates are

Component	$A_i = L/K_iV$	K -value
Water	89.2	0.031
Acetone	1.38	2.0
Oxygen	0.00006	45,000
Nitrogen	0.00003	90,000
Argon	0.00008	35,000

For acetone, the K -value is obtained from (4) in Table 2.2, the modified Raoult's law, $K = \gamma P^s/P$, with $\gamma = 6.7$ for acetone in water at 25°C and 101.3 kPa, as determined from the Wilson model in §2.7.1. For oxygen and nitrogen, the K -values are from (6) in Table 2.2, Henry's law, $K = H/P$, using constants from Figure 4.18 at 25°C. For water, the K -value is from (3) in Table 2.2, Raoult's law, $K = P^s/P$, because the mole fraction of water is close to 1. For argon, the Henry's law constant is from the *International Critical Tables of Numerical Data, Physics, Chemistry and Technology* [1].

For absorption and stripping, design procedures are well developed and commercial processes are common. Table 6.1 lists representative applications. Environmental standards for the removal of pollutants have greatly increased the use of gas absorbers.

When water or hydrocarbon oils are used as absorbents and no significant chemical reactions occur between the

absorbent and the solute, the process is referred to as **physical absorption**. When aqueous NaOH is used as the absorbent for an acid gas, absorption is accompanied by a rapid and irreversible reaction in the liquid. This is **chemical absorption** or **reactive absorption**. More complex examples are the processes for absorbing CO₂ and H₂S with aqueous solutions of monoethanolamine (MEA) and diethanolamine (DEA), during which there is a more desirable reversible chemical reaction in the liquid. Chemical reactions can increase the rate of absorption and solvent-absorption capacity and convert a hazardous chemical to an inert compound.

Design procedures for trayed and packed columns for absorption and stripping operations are described in this chapter. Trayed columns are presented in §6.5 and 6.6, while packed columns are covered in §6.7, 6.8, and 6.9. **Equilibrium-based** and **rate-based** (mass-transfer) models, using both graphical and algebraic procedures, for physical absorption and stripping of mainly dilute mixtures are described. The methods also apply to reactive absorption with irreversible and complete chemical reactions of solutes with solvents. Calculations for concentrated mixtures and reactive absorption with reversible chemical reactions are best made with process simulators, as discussed in Chapters 10 and 12.

§6.1 EQUIPMENT FOR VAPOR–LIQUID SEPARATIONS

Methods for designing and analyzing absorption, stripping, and distillation depend on the type of equipment used for contacting vapor and liquid phases. When multiple stages are required, phase contacting is mostly carried out in equipment of the type shown in Figure 6.2. The most common devices are cylindrical, vertical columns containing trays or packing. Less common are spray towers, bubble columns, and centrifugal contactors.

§6.1.1 Trayed Columns

A **trayed tower** is a vertical, cylindrical pressure vessel in which vapor and liquid, flowing countercurrently, are contacted on trays (plates) that provide intimate contact of liquid with vapor in a froth to promote rapid mass transfer. Phase disengagement occurs above the froth and below the tray above. An example of a tray is shown in Figure 6.3. Liquid flows across each tray, over an outlet **weir**, and into a **downcomer**, which takes the liquid by gravity to the tray below. Gas flows upward through openings in each tray, bubbling through the liquid on the tray to produce a froth.

When vapor flows through the holes in the tray, any of five two-phase-flow regimes shown in Figure 6.4 may occur alone, or in combination, as discussed by Lockett [2]. In the **spray regime**, the gas phase is continuous. Jets of vapor rise from the tray openings through the liquid on the tray, entraining and spraying some of the liquid into the space between trays. This regime occurs for low weir heights (low liquid depths) at high gas rates. The most common and favored regime is the **froth**

Table 6.1 Representative Commercial Applications of Absorption

Solute	Absorbent	Type of Absorption
Acetone	Water	Physical
Acrylonitrile	Water	Physical
Ammonia	Water	Physical
Ethanol	Water	Physical
Formaldehyde	Water	Physical
Hydrochloric acid	Water	Physical
Hydrofluoric acid	Water	Physical
Sulfur dioxide	Water	Physical
Sulfur trioxide	Water	Physical
Benzene and toluene	Hydrocarbon oil	Physical
Butadiene	Hydrocarbon oil	Physical
Butanes and propane	Hydrocarbon oil	Physical
Naphthalene	Hydrocarbon oil	Physical
Carbon dioxide	Aq. NaOH	Irreversible chemical
Hydrochloric acid	Aq. NaOH	Irreversible chemical
Hydrocyanic acid	Aq. NaOH	Irreversible chemical
Hydrofluoric acid	Aq. NaOH	Irreversible chemical
Hydrogen sulfide	Aq. NaOH	Irreversible chemical
Chlorine	Water	Reversible chemical
Carbon monoxide	Aq. cuprous ammonium salts	Reversible chemical
CO ₂ and H ₂ S	Aq. monoethanolamine (MEA) or diethanolamine (DEA)	Reversible chemical
CO ₂ and H ₂ S	Diethyleneglycol (DEG) or triethyleneglycol (TEG)	Reversible chemical
Nitrogen oxides	Water	Reversible chemical

regime, in which both liquid-continuous and gas-continuous dispersions can coexist. The gas passes through the froth in the form of jets or a series of bubbles. For low gas rates, the **bubble regime** occurs, in which the liquid is fairly quiescent and bubbles rise in swarms. At high liquid rates, small gas bubbles may be undesirably emulsified. If bubble coalescence is hindered, undesirable foam forms. Ideally, the liquid carries no vapor bubbles (**occlusion**) to the tray below, the vapor carries no liquid droplets (**entrainment**) to the tray above, and there is no **weeping** of liquid through the holes in the tray. With good contacting, equilibrium between the exiting vapor and liquid phases is approached on each tray, unless the liquid is very viscous.

Figure 6.5 shows typical tray openings for vapor passage: (a) perforations, (b) valves, and (c) bubble caps. The simplest is the **sieve or perforated tray** with holes, usually 1/8 to 1/2-inch in diameter. A **valve tray** has openings commonly from 1 to 2 inches in diameter. Each hole is fitted with a valve consisting of a cap that overlaps the hole, with legs or a cage to limit vertical rise, while maintaining the valve cap in a horizontal orientation. Without vapor flow, each valve covers the hole. As the vapor rate increases, the valve rises, providing a larger and larger opening through which the vapor can flow to create a froth.

A **bubble-cap tray** consists of a cap, 3 to 6 inches in diameter, mounted over and above a concentric riser, 2 to 3 inches in diameter. The cap has rectangular or triangular slots cut around its periphery. The vapor flows up through the tray opening into the riser, turns around, and passes out through

the slots and into the liquid, forming a froth. An 11-ft-diameter tray might have 5,000 3/16-inch-diameter perforations, 1,000 2-inch-diameter valve caps, or 500 4-inch-diameter bubble caps. As shown in Figure 6.5(d), trays more than 3 ft in diameter may have removable panels in the center to allow plant operators to climb up the inside of the columns for periodic cleaning and maintenance.

Improvements are constantly being made to increase the efficiency and throughput of sieve and valve trays. Recent changes have increased tray efficiency by several percent and capacity by more than 20%. Sloley [41] discusses these changes in detail. They include: (1) sloping or stepping the downcomer to make the downcomer area smaller at the bottom than at the top, in order to increase the active flow area; (2) vapor flow through the tray section beneath the downcomer, in addition to the normal flow area through the cap; (3) use of staggered, louvered downcomer floor plates to impart horizontal flow to liquid exiting the downcomer, thus enhancing the vapor flow beneath; (4) elimination of vapor impingement from adjacent valves by using bidirectional fixed valves; (5) use of multiple downcomers that terminate in the active vapor space of the tray below, providing very long outlet weirs leading to low crest heights and lower froth heights; (6) directional slotting of sieve trays to impart a horizontal component to the vapor, enhancing the plug flow of the liquid across the tray and eliminating dead areas; and (7) use of mini-valves and fixed valves to achieve higher efficiencies. Typical high-performance trays include SUPERFRACTM and ULTRA-FRACTM produced by Koch-Glitsch.

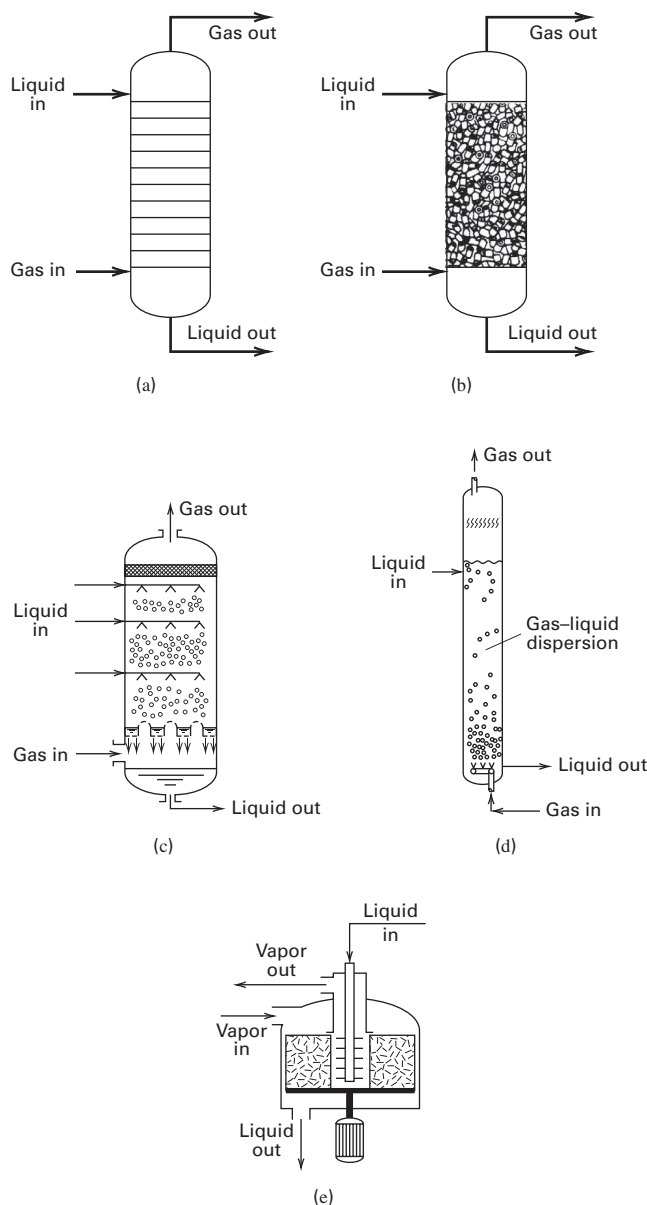


Figure 6.2 Industrial equipment for absorption and stripping: (a) trayed tower; (b) packed column; (c) spray tower; (d) bubble column; (e) centrifugal contactor.

Table 6.2 compares the cost, pressure drop, mass-transfer efficiency, vapor capacity, and flexibility of conventional tray types. Operational flexibility is reported in terms of **turndown ratio** (ratio of maximum-to-minimum vapor flow capacity). At the limiting, **flooding** vapor velocity, liquid-droplet entrainment becomes excessive, causing the liquid flow to exceed the downcomer capacity, thus pushing liquid up the column. At too low a vapor rate, liquid weeping through the tray openings or vapor pulsation becomes excessive. Low cost makes sieve trays preferable unless operational flexibility in throughput is required, in which case valve trays are best. Bubble-cap trays, predominant in pre-1950 installations, are now rarely specified, but may be preferred when liquid holdup must be controlled to provide residence time for a chemical reaction or when weeping must be prevented.

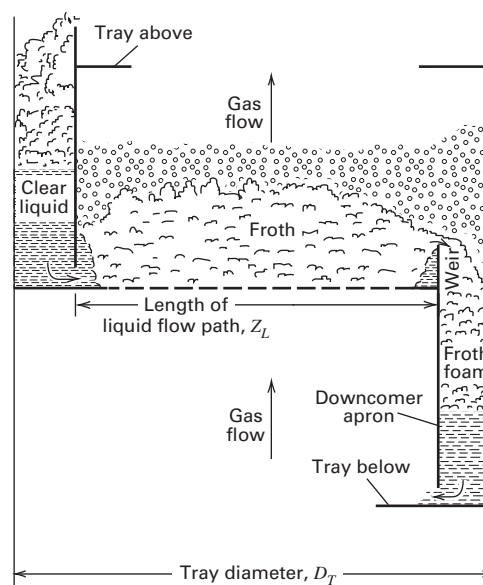


Figure 6.3 Vapor-liquid contact on a tray. [Adapted from B.F. Smith, *Design of Equilibrium Stage Processes*, McGraw-Hill, New York (1963).]

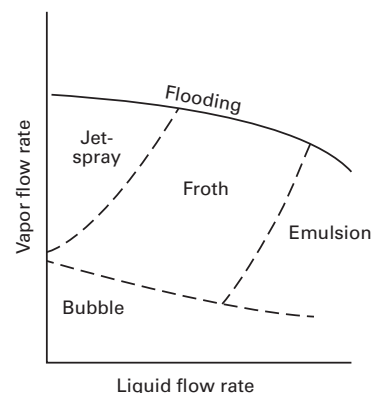


Figure 6.4 Possible vapor-liquid flow regimes for a contacting tray.

Table 6.2 Comparison of Tray Types

	Sieve Trays	Valve Trays	Bubble-Cap Trays
Relative cost	1.0	1.2	2.0
Pressure drop	Lowest	Intermediate	Highest
Efficiency	Lowest	Highest	Highest
Vapor capacity	Highest	Highest	Lowest
Typical turndown ratio	2	4	5

§6.1.2 Packed Columns

A **packed column**, shown schematically in Figure 6.6, is a vertical, cylindrical vessel containing one or more sections of packing over whose surface the liquid flows downward as a film on the packing and walls, or as droplets between packing elements. Feed gas enters at the bottom, passes through a vapor distributor, and flows upward through the wetted packing, thus contacting the liquid and passing out the top. Liquid enters at

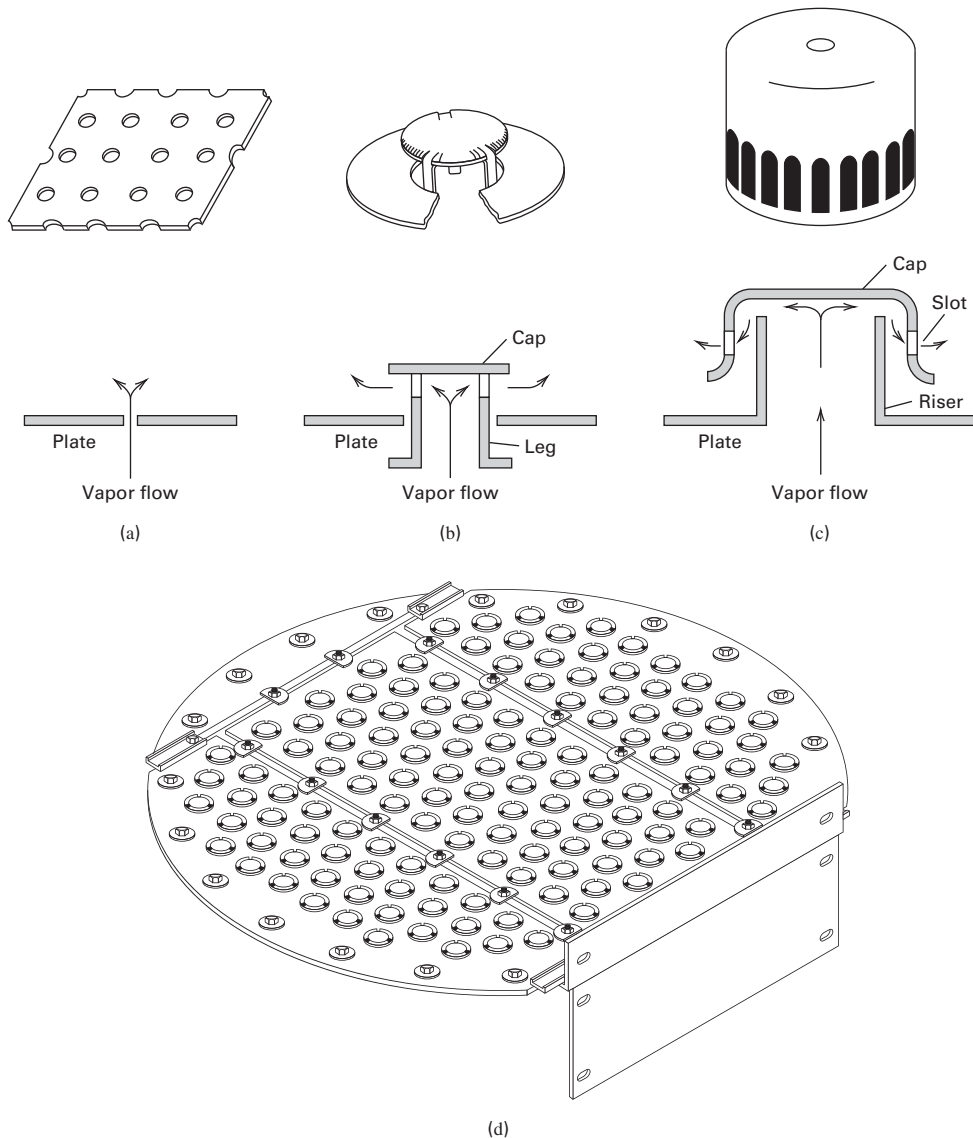


Figure 6.5 Three types of tray openings for the passage of vapor up into the liquid: (a) perforation; (b) valve cap; (c) bubble cap; (d) tray with valve caps.

the top into a **liquid distributor**, flows downward through the packed sections, and leaves at the bottom. Figure 6.6 depicts sections containing **random packings** and **structured packings**. Each packed section is contained between a support plate, which holds the packing, and a bed limiter or hold-down grid, which prevents packing movement. A liquid redistributor ensures uniform distribution of liquid over the cross-sectional area of the column as it enters a packed section. If the packed height between redistributors is more than about 20 ft or 6 m, liquid may **channel** downward near the wall, where resistance is the lowest, while gas flows up the center of the column. Channeling significantly reduces vapor–liquid contact and increases the height equivalent to a theoretical plate (HETP). Some industrial columns contain packed sections as well as trays, as depicted in the bottom third of Figure 6.6.

Commercial packing materials include (1) random (dumped) packings, some of which are shown in Figure 6.7; (2) structured packings of crimped layers of mesh or corrugated sheets, as shown in Figure 6.8; and (3) grid packings that have an open-lattice structure. Grid packings are mainly for heat transfer and washing applications and are not considered here.

Random packings have evolved through four generations of design. Raschig rings and Berl saddles appeared between 1895 and 1950 in ceramic, plastic, metal, and carbon forms, but these packings now see limited use. Metal and plastic Pall rings and ceramic Intalox saddles were introduced in the 1950s to improve capacity, mass-transfer rates, and column pressure drop as compared to Raschig rings and Berl saddles. Metal Intalox IMTP[®] and ceramic, metal, and plastic Cascade

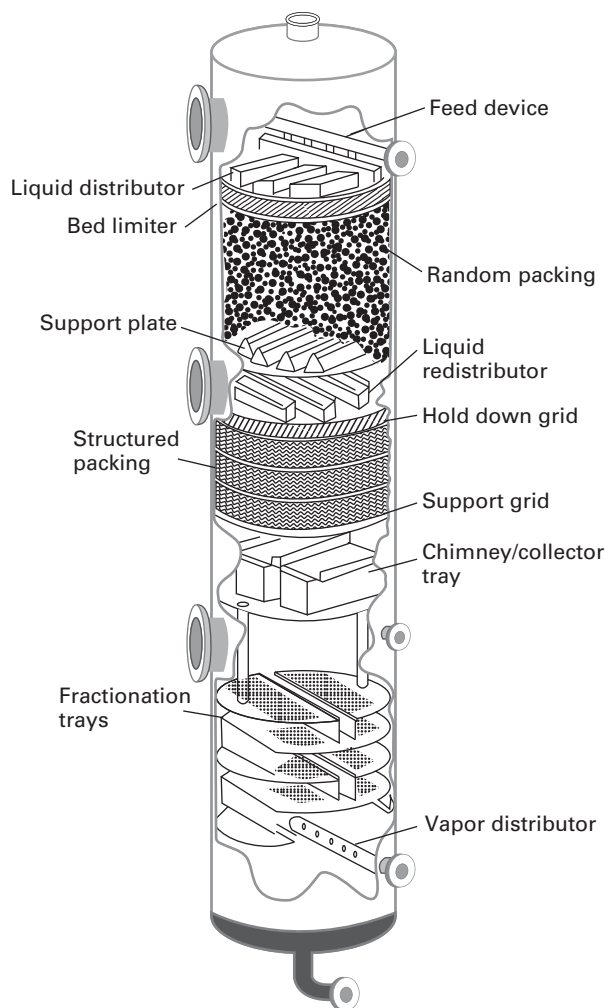


Figure 6.6 Details of internals in a column with packing and trays.

Mini-Rings[®] (CMR) emerged in the 1970s, reducing friction and improving mass transfer. In 1995, open “through-flow design” packings such as Raschig Super-Rings[®] from Raschig-Jaeger, and Intalox[®] Ultra[®] from Koch-Glitsch were launched. These designs provide more surface area for mass transfer, ease of flow through the packing with even higher flow capacity and lower pressure drop through the column.

Many random packings are available in nominal diameters ranging from less than 1 to 3.5 inches. Nominal packing size should be less than one-eighth of the column diameter to minimize liquid channeling. Increased packing diameter decreases pressure drop at the expense of decreased mass-transfer efficiency, resulting in an optimal packing size for a given situation. Packings that feature an open, undulating geometry that promotes uniform wetting with recurrent turbulence promotion are an exception. For those packings, mass-transfer efficiency does not decrease as packing diameter increases, and larger packing height is possible between liquid redistributors.

Metal packings are more expensive, but provide superior strength and good wettability. Ceramic packings have superior

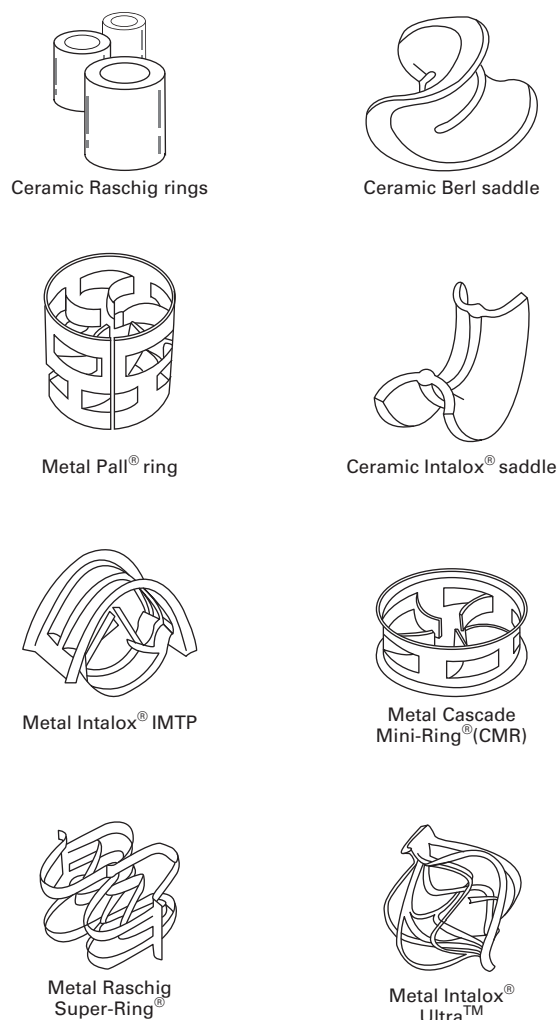


Figure 6.7 Four generations of random packings.

wettability and are used in corrosive environments at elevated temperatures. Plastic packings are inexpensive and have sufficient strength, but may have poor wettability at low liquid rates.

Typical structured packings cover four generations of design evolution. The first, called Panapak, was reported by R.C. Schofield of Pan American Refining Corporation in 1950. It is fabricated from thin metal strips to form a honeycomb. Multiple layers are tacked together. Although it is still available, Panapak never gained popularity because of liquid maldistribution. Representative structured packings of generations 2 to 4 are shown in Figure 6.8. By the early 1960s, the second generation of structured packings, including Goodloe[®] of Koch-Glitsch LP and Sulzer wire gauze[®] of Sulzer Chemtech Ltd., began to gain favor for high vacuum service because of their very low pressure drop. These packings are made of multiple strands of thin wire, knitted together and crimped and coiled or layered. In 1977 a third generation appeared, typified by Mellapak[®] from Sulzer Chemtech Ltd., Flexipac[®] from Koch-Glitsch LP, and Raschig-Pak[®] of Raschig GMBH. These packings are fabricated from thin,

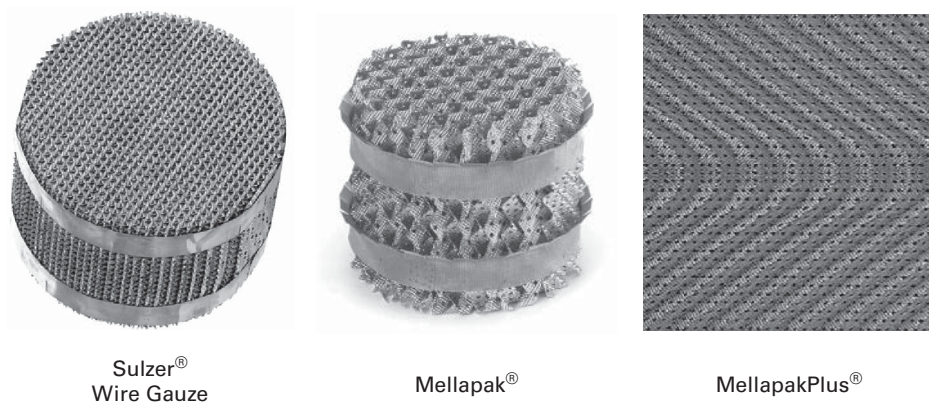


Figure 6.8 Typical structured packings of the last three of four generations. Reproduced with permission of Sulzer Chemtech Ltd.

corrugated and crimped sheets of metal, stacked parallel to each other into elements. Because they exhibit high capacity, high mass-transfer rates, and low pressure drop at a low cost, they have become very popular for vacuum service and tower revamps. The fourth generation was introduced in 1997 with MellapakPlus[®], Flexipac HC[®], and Raschig Super-Pak[®]. These are geometric modifications of the corrugated-sheet packings, designed to direct the vapor to a more vertical orientation and to achieve a smoother vapor flow as it changes directions between sections. Widely used structured packings are available in metals, ceramics, carbon, and plastics.

In Table 6.3, packings are compared using the factors previously considered for trays. The differences between random and structured packings are greater than the differences among the three types of trays in Table 6.2.

§6.1.3 Choice between Trays and Packing

For contacting vapor and liquid streams for absorption, stripping, and distillation, the designer must choose between a trayed column and a packed column. Random packing is favored when the column diameter is less than 2 ft and the packed height is less than 20 ft. Packed columns are favored for (1) corrosive services that tend to use ceramic or plastic materials rather than metals, particularly welded column internals; (2) services that produce foaming too severe for the use of trays; (3) vacuum operations and other services for which pressure drop must be low; and (4) services that benefit from low liquid holdup in the column. Otherwise, trayed towers, which can be designed more reliably, are preferred. Although structured packings are expensive, they are the best

choice for installations when pressure drop is a factor or for replacing existing trays (retrofitting) when a higher capacity or degree of separation is required. Trayed towers are preferred when liquid velocities are low, whereas columns with random packings are best for high liquid velocities. Use of structured packing should be avoided at pressures above 200 psi and liquid flow rates above 10 gpm/ft² (Kister [33]). Turbulent liquid flow is desirable if mass transfer is limiting in the liquid phase, and a continuous, turbulent gas flow is desirable if mass transfer is limiting in the gas phase. Usually, the (continuous) gas phase is mass-transfer-limiting in packed columns and the (continuous) liquid phase is mass-transfer-limiting in tray columns.

§6.2 GENERAL DESIGN CONSIDERATIONS

Absorber and stripper design or analysis requires consideration of the following factors:

1. Entering feed gas (or liquid) flow rate, composition, T , and P
2. Desired degree of recovery of one or more solutes
3. Choice of absorbent (or stripping agent)
4. Column operating P and T , and allowable gas pressure drop
5. Minimum absorbent (or stripping agent) flow rate and actual absorbent (or stripping agent) flow rate
6. Heat effects and need for cooling (or heating)
7. Number of equilibrium stages and stage efficiency
8. Type of absorber (or stripper) equipment (trays or packing)
9. Need for liquid redistributors if packing is used
10. Height of absorber (or stripper)
11. Diameter of absorber (or stripper)

Table 6.3 Comparison of Types of Packing

	Random		Structured
	Raschig Rings and Saddles	“Through Flow”	
Relative cost	Low	Moderate	High
Pressure drop	Moderate	Low	Very low
Efficiency	Moderate	High	Very high
Vapor capacity	Fairly high	High	High
Typical turndown ratio	2	2	2

The ideal absorbent has (a) a high solubility for solute(s); (b) a low volatility to reduce loss; (c) stability and inertness; (d) low corrosiveness; (e) low viscosity and high diffusivity; (f) low foaming proclivities; (g) low toxicity and flammability; (h) availability, if possible, within the process; and (i) low cost. The most widely used absorbents are water,

hydrocarbon oils, and aqueous solutions of acids and bases. The most common stripping agents are steam, air, inert gases, and hydrocarbon gases.

Absorber operating pressure should be high and temperature low in order to minimize stage requirements and/or absorbent flow rate, and to lower the equipment volume required to accommodate the gas flow. Unfortunately, both compression and refrigeration of a gas are expensive. Therefore, most absorbers are operated at feed-gas pressure, which may be greater than ambient pressure, and at ambient temperature, which can be achieved by cooling the feed gas and absorbent with cooling water, unless one or both streams already exist at an ambient or subambient temperature.

Operating pressure should be low and temperature high for a stripper to minimize stage requirements and stripping agent flow rate. However, because the maintenance of a vacuum is expensive, and steam jet exhausts are polluting, strippers are commonly operated at a pressure just above ambient. A high temperature can be used, but it should not be so high as to cause vaporization or undesirable chemical reactions. The possibility of phase changes occurring can be checked by bubble-point and dew-point calculations.

For a given feed-gas (or liquid) flow rate, extent of solute absorption (or stripping), operating P and T , and absorbent (or stripping agent) composition, a **minimum absorbent (stripping agent) flow rate** exists that corresponds to an infinite number of countercurrent equilibrium contacts between phases. In every design problem, a trade-off exists between the number of equilibrium stages and the absorbent (or stripping agent) flow rate, which must be greater than the minimum. The following sections describe graphical and analytical methods for computing the minimum flow rate and this trade-off for mixtures that are dilute in solute(s). For this essentially isothermal case, the energy balance can be ignored. As discussed in Chapters 10 and 11, the use of process simulators is preferred for concentrated mixtures, for which multicomponent phase equilibrium and mass-transfer effects are complex and an energy balance is necessary.

§6.3 GRAPHICAL METHOD FOR TRAYED TOWERS

For absorption in the countercurrent-flow, trayed tower shown in Figure 6.9a, stages are conventionally numbered from the top, where the absorbent enters, to the bottom. For the stripper in Figure 6.9b, stages are numbered from the bottom, where the stripping agent enters, to the top. Phase equilibrium is assumed between the vapor and liquid leaving each tray. Assume for an absorber that only one solute transfers. Let:

L' = molar flow rate of solute-free absorbent

V' = molar flow rate of solute-free gas (carrier gas)

X = mole ratio of solute to solute-free absorbent in the liquid

Y = mole ratio of solute to solute-free gas in the vapor

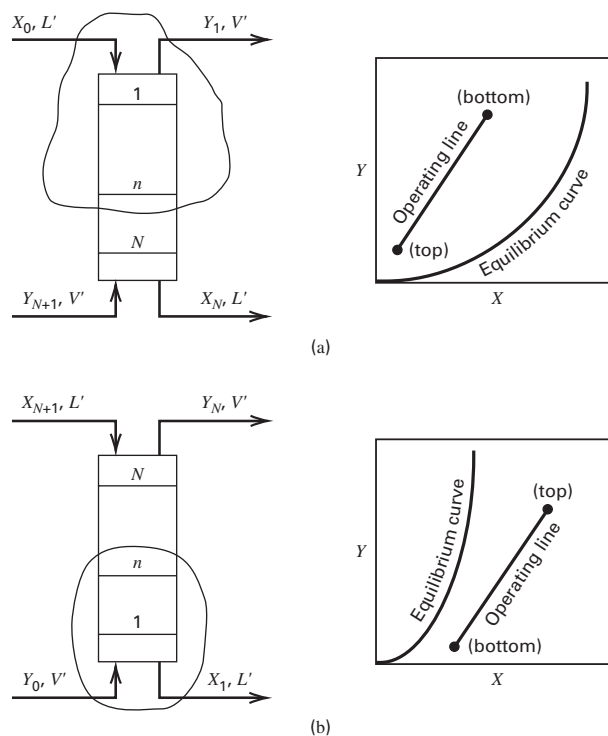


Figure 6.9 Continuous, steady-state operation in a countercurrent cascade with equilibrium stages: (a) absorber; (b) stripper.

With these definitions, the values of L' and V' remain constant throughout the tower because only solute undergoes mass transfer between phases.

§6.3.1 Equilibrium Curves for the Solute

For the solute at any stage n , the K -value is

$$K_n = \frac{y_n}{x_n} = \frac{Y_n/(1+Y_n)}{X_n/(1+X_n)} \quad (6-1)$$

where $Y = y/(1-y)$ and $X = x/(1-x)$.

Figure 6.9 shows representative equilibrium X - Y plots. In general, the equilibrium curve will not be a straight line, but it will pass through the origin. If the solute undergoes an irreversible liquid-phase chemical reaction with the solvent to make a nonvolatile product, the equilibrium curve will be a straight line of zero slope, passing through the origin. For a pure stripping agent, the operating line extends to $Y = 0$ and for a pure absorbent, it goes through $X = 0$.

§6.3.2 Operating Lines (from Solute Material Balances)

In Figure 6.9, the entering and leaving solute compositions and solute-free flow rates are paired. For the absorber, the pairs at the top are (X_0, L') and (Y_1, V') and the pairs at the bottom are (Y_{N+1}, V') and (X_N, L') . For the stripper, (X_{N+1}, L') and (Y_N, V') are at the top, and (Y_0, V') and (X_1, L') are at the bottom. These terminal pairs relate to intermediate pairs for

passing streams between stages by solute material balances for the envelopes shown in Figure 6.9. Solute material balances are written around one end of the tower and an arbitrary intermediate equilibrium stage, n .

For the absorber, the total solute flow rate into the envelope equals the total solute flow rate out of the envelope in Figure 6.9a:

$$X_0 L' + Y_{n+1} V' = X_n L' + Y_1 V' \quad (6-2)$$

Solving for Y_{n+1} ,

$$Y_{n+1} = X_n (L'/V') + Y_1 - X_0 (L'/V') \quad (6-3)$$

Similarly for the stripper in Figure 6.9b,

$$X_{n+1} L' + Y_0 V' = X_1 L' + Y_n V' \quad (6-4)$$

Solving for Y_n ,

$$Y_n = X_{n+1} (L'/V') + Y_0 - X_1 (L'/V') \quad (6-5)$$

Equations (6-3) and (6-5) are the **operating lines** plotted in Figure 6.9. The terminal points represent conditions at the top and bottom of the tower. For absorbers, the operating line is above the equilibrium line because, for a given solute concentration, X , in the liquid, the solute concentration, Y , in the gas is always greater than the equilibrium value, thus providing a mass-transfer driving force for absorption. For strippers, operating lines lie below equilibrium lines, thus enabling desorption. In Figure 6.9, operating lines are straight with a slope of L'/V' .

§6.3.3 Minimum Absorbent Flow Rate (for ∞ Stages)

Operating lines for four different solute-free absorbent flow rates, L' , are shown in Figure 6.10 for a fixed solute-free gas feed rate, V' . In each case, the solute concentration in the exiting gas, Y_1 , is the same. Therefore, each operating line passes through the terminal point, (Y_1, X_0) , at the top of the column. To achieve the desired value of Y_1 for given Y_{N+1} , X_0 , and V' , the solute-free absorbent flow rate L' must be between an ∞ absorbent flow with $L'/V' = \infty$, as represented by operating line 1, and a minimum absorbent rate (corresponding to ∞ stages), L'_{\min} , as represented by operating line 4, with the equilibrium curve and operating line intersecting at Y_{N+1} . Intermediate operating lines 2 and 3, correspond to 2 and 1.5 times L'_{\min} , respectively. The solute concentration in the outlet liquid, X_N , depends on L' . Using a solute material balance over the entire absorber, (6-2) with $n = N$ gives

$$X_0 L' + Y_{N+1} V' = X_N L' + Y_1 V' \quad (6-6)$$

which rearranges to

$$L' = \frac{V'(Y_{N+1} - Y_1)}{(X_N - X_0)} \quad (6-7)$$

Note that the operating line can terminate at the equilibrium line as in operating line 4 of Figure 6.10, but cannot cross it because that would be a violation of the second law of thermodynamics.

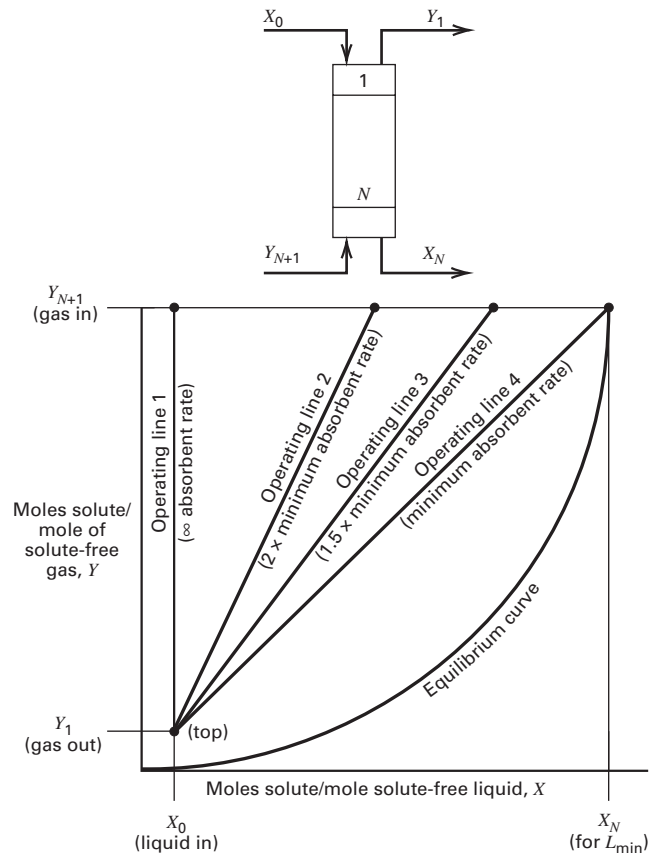


Figure 6.10 Range of operating lines for an absorber.

The minimum absorbent flow rate, L'_{\min} , corresponds to a value of X_N (leaving the bottom of the tower) in equilibrium with Y_{N+1} , the solute concentration in the feed gas. Note that it takes an infinite number of stages for this equilibrium to be achieved. An expression for L'_{\min} of an absorber can be derived from (6-7) as follows. For stage N , (6-1) for the minimum absorbent rate becomes

$$K_N = \frac{Y_{N+1}/(1 + Y_{N+1})}{X_N/(1 + X_N)} \quad (6-8)$$

Solving (6-8) for X_N and substituting the result into (6-7) gives

$$L'_{\min} = \frac{V'(Y_{N+1} - Y_1)}{\{Y_{N+1}/[Y_{N+1}(K_N - 1) + K_N]\} - X_0} \quad (6-9)$$

For dilute solutes, where $Y \approx y$ and $X \approx x$, (6-9) approaches

$$L'_{\min} = V' \left(\frac{Y_{N+1} - Y_1}{\frac{Y_{N+1}}{K_N} - X_0} \right) \quad (6-10)$$

If, for the entering liquid, $X_0 \approx 0$, (6-10) approaches

$$L'_{\min} = V' K_N (\text{fraction solute absorbed}) \quad (6-11)$$

Equation (6-11) confirms that L'_{\min} increases with increasing V' , K , and fraction of solute absorbed.

In practice, the absorbent flow rate is some multiple of L'_{\min} , typically from 1.1 to 2. In Figure 6.10, operating lines 2 and 3

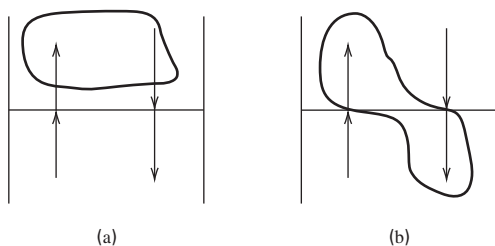


Figure 6.11 Vapor-liquid stream relationships: (a) operating line (passing streams); (b) equilibrium curve (leaving streams).

correspond to 2.0 and 1.5 times L'_{min} , respectively. As the operating line moves from 1 to 4, the number of stages required increases from zero to infinity. Thus, a trade-off exists between L' and N , and an optimal L' exists.

A similar derivation of V'_{min} , for the stripper of Figure 6.9, is analogous to (6-11):

$$V'_{min} = \frac{L'}{K_N} \text{ (fraction solute stripped)} \quad (6-12)$$

In practice, stripping factors, defined by $S = KV/L$, are optimal at about 1.4.

§6.3.4 Number of Equilibrium Stages

As shown in Figure 6.11a, the operating line relates the solute concentration in the vapor passing upward between two stages to the solute concentration in the liquid passing downward between the same two stages. Figure 6.11b illustrates that the equilibrium curve relates the solute concentration in the vapor leaving an equilibrium stage to the solute concentration in the liquid leaving the same stage. This suggests starting at the top of the absorber (at the bottom of the Y - X diagram) and moving to the bottom of the absorber (at the top of the Y - X diagram) by constructing a staircase that alternates between the operating line and the equilibrium curve, as in Figure 6.12a.

Moving up the staircase, steps off the number of stages required for a given solute-free absorbent flow rate corresponding to the slope of the operating line, which in Figure 6.12a is $(L'/V') = 1.5(L'_{min}/V')$. Starting at the point (Y_1, X_0) on

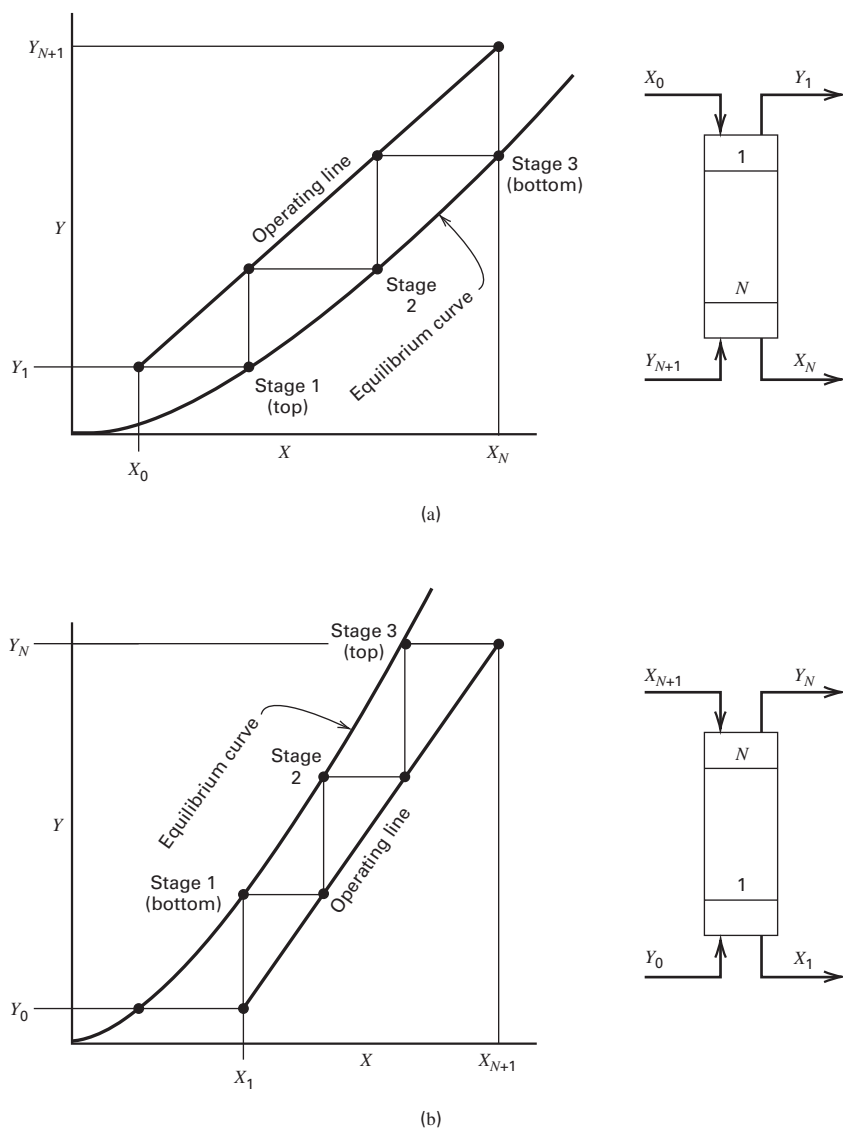


Figure 6.12 Graphical determination of the number of equilibrium stages for (a) absorber and (b) stripper.

the operating line, a horizontal move is made to the right to (Y_1, X_1) on the equilibrium curve. From there, a vertical move is made to (Y_2, X_1) on the operating line. The staircase is climbed until the terminal point (Y_{N+1}, X_N) on the operating line is reached. This point corresponds to the passing streams at the bottom end of the column. As shown in Figure 6.12a, the stages are counted at the points on the equilibrium curve. In this case, $N = 3$. As the operating-line slope L'/V' is increased, fewer equilibrium stages are required. As L'/V' is decreased, more stages are required until L'_{\min}/V' is reached, at which the operating line and the equilibrium curve intersect at a **pinch point** located on the horizontal line for Y_{N+1} . At L'_{\min} , an infinite number of stages is required. Operating line 4 in Figure 6.10 shows a pinch point at (Y_{N+1}, X_N) . If L'/V' is reduced below L'_{\min}/V' the specified extent of absorption cannot be achieved.

The stages required for stripping a solute are determined analogously to absorption. An illustration is shown in Figure 6.12b. For given specifications of Y_0, X_{N+1} , and the extent of stripping of the solute, X_1 , V'_{\min} is determined from the slope of the operating line that passes through the points (Y_0, X_1) and (Y_N, X_{N+1}) . The operating line in Figure 6.12b is for: $V' = 1.5V'_{\min}$ or a slope of $(L'/V') = (L'/V'_{\min})/1.5$. In Figure 6.12, the number of equilibrium stages for both the absorber and stripper is exactly 3. Ordinarily, the result is some fraction above an integer number, and the result is usually rounded to the next highest integer to ensure achievement of the desired composition.

EXAMPLE 6.1 Recovery of Ethyl Alcohol.

In a bioprocess, molasses is fermented to produce a liquor containing ethyl alcohol. A CO_2 -rich vapor with a small amount of ethyl alcohol is evolved. The alcohol is recovered by absorption with water in a sieve-tray tower. Determine the number of equilibrium stages required for countercurrent flow of liquid and gas, assuming isothermal, isobaric conditions and absorption of ethanol only.

Entering gas is 180 kmol/h, 98% CO_2 and 2% ethyl alcohol, 30°C, 110 kPa.

Entering liquid absorbent is 100% water, 30°C, 110 kPa.

Required recovery (absorption) of ethyl alcohol is 97%.

Solution

From §5.6 for a single-section, countercurrent cascade, the number of degrees of freedom is $2N + 2C + 5$. All stages operate adiabatically at a pressure of approximately 110 kPa, thus fixing $2N$ design variables. The entering gas is completely specified by $C + 2$ variables. The entering liquid flow rate is not specified; thus, only $C + 1$ variables are specified for the entering liquid. The recovery of ethyl alcohol is a specified variable; thus, the total degrees of freedom taken by the specification are $2N + 2C + 4$. This leaves one additional specification to be made: the entering liquid absorbent flow rate at 1.5 times the minimum value.

Note that the above degrees-of-freedom analysis assumes an energy balance for each stage. The energy balances are assumed to result in isothermal operation at 30°C. For dilute ethyl alcohol, the K -value is determined from a modified Raoult's law, $K = \gamma P^s/P$.

The ethanol vapor pressure at 30°C is 10.5 kPa, and from infinite dilution in water data at 30°C, the liquid-phase activity coefficient of ethyl alcohol is 6. Thus, $K = (6)(10.5)/110 = 0.57$. The minimum solute-free absorbent rate is given by (6-11), where the solute-free gas rate, V' , is $(0.98)(180) = 176.4$ kmol/h. Thus, the minimum absorbent rate for 97.5% recovery is

$$L'_{\min} = (176.4)(0.57)(0.97) = 97.5 \text{ kmol/h}$$

The solute-free absorbent rate at 50% above the minimum is

$$L' = 1.5(97.5) = 146.2 \text{ kmol/h}$$

The alcohol recovery of 97% corresponds to

$$(0.97)(0.02)(180) = 3.49 \text{ kmol/h}$$

The amount of ethyl alcohol remaining in the exiting gas is

$$(1.00 - 0.97)(0.02)(180) = 0.11 \text{ kmol/h}$$

Alcohol mole ratios at both ends of the operating line are as follows:

$$\begin{aligned} \text{top of the column} & \left\{ X_0 = 0, Y_1 = \frac{0.11}{176.4} = 0.0006 \right\} \\ \text{bottom of the column} & \left\{ Y_{N+1} = \frac{0.11 + 3.49}{176.4} = 0.0204, \right. \\ & \left. X_N = \frac{3.49}{146.2} = 0.0239 \right\} \end{aligned}$$

The equation for the operating line from (6-3), with $X_0 = 0$, is

$$Y_{N+1} = \left(\frac{146.2}{176.4} \right) X_N + 0.0006 = 0.829X_N + 0.0006 \quad (1)$$

This is a dilute system. From (6-1), the equilibrium curve, using $K = 0.57$, is

$$0.57 = \frac{Y/(1+Y)}{X/(1+X)}$$

Solving for Y ,

$$Y = \frac{0.57X}{1 + 0.43X} \quad (2)$$

For the coordinates to cover the entire column, the necessary range of X for a plot of Y versus X is 0 to almost 0.025. From the Y - X equation, (2), the following values are obtained:

Y	X
0.00000	0.000
0.00284	0.005
0.00569	0.010
0.00850	0.015
0.01130	0.020
0.01410	0.025

For this dilute ethyl alcohol system, the maximum error in Y is 1.0%, if Y is taken simply as $Y = KX = 0.57X$. The equilibrium curve in Figure 6.13 is plotted using the Y - X data. It is almost a straight line. The operating line drawn through the terminal points (Y_1, X_0) and (Y_{N+1}, X_N) is straight. The equilibrium stages are stepped off as shown, starting at the top stage (Y_1, X_0) located in the plot near the lower left corner. The required number of equilibrium stages, N , for 97% absorption of ethyl alcohol is between 6 and 7, at about 6.1.

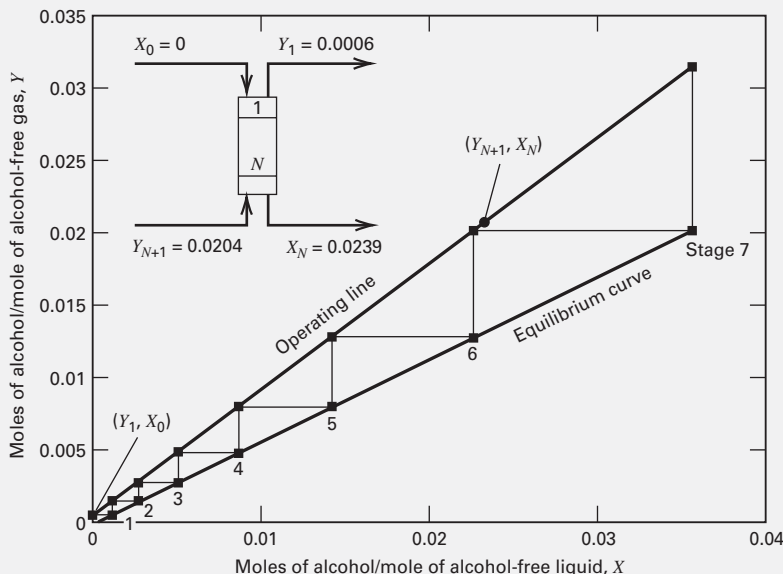


Figure 6.13 Graphical determination of number of equilibrium stages for an absorber.

§6.4 KREMSER GROUP METHOD FOR MULTICOMPONENT ABSORPTION AND STRIPPING

The graphical method of §6.3 for determining N has educational value because a graph provides a visual insight into the phenomena involved. However, the graphical method becomes tedious when the following occurs: (1) problem specifications fix the number of stages rather than the percent recovery of solute, (2) more than one solute is absorbed or stripped, (3) the location of the equilibrium curve is unknown because the optimal operating T and P have not been established, and (4) very low or very high concentrations of solute force the construction to the corners of the diagram so that multiple Y - X diagrams of varying scales are needed to achieve accuracy. When the graphical method is unsuitable, the analytical method of Kremser is useful for obtaining results that can be used to initialize rigorous methods in process simulators.

Kremser [30] introduced a group method that relates the number of equilibrium stages to the recovery of one key component in a single-section, countercurrent cascade used for multicomponent absorption or stripping. The procedure is called a **group method** because it only provides an overall treatment of the group of stages in the cascade. The procedure does not consider detailed changes in temperature, pressure, phase compositions, and flow rates from stage to stage. The treatment here is similar to that of Edmister [31].

Consider a countercurrent absorber of N adiabatic, equilibrium stages, as shown in Figure 6.14a, with stages numbered from top to bottom. The absorbent is pure, and component molar flow rates are v_i and l_i . In the vapor and liquid phases, respectively. The following derivation applies to any component in the vapor feed. Mole fractions are y and x , and total molar flow rates are V and L . A material balance around

the top, including stages 1 through $N - 1$, for any absorbed species is as follows, with the subscript for species, i , dropped for convenience:

$$v_N = v_1 + l_{N-1} \tag{6-13}$$

where

$$v = yV \tag{6-14}$$

and

$$l = xL \tag{6-15}$$

with $l_0 = 0$ for an entering absorbent free of solute.

The equilibrium K -value at stage N is

$$y_N = K_N x_N \tag{6-16}$$

Combining (6-14), (6-15), and (6-16), v_N becomes

$$v_N = \frac{l_N}{L_N / (K_N V_N)} \tag{6-17}$$

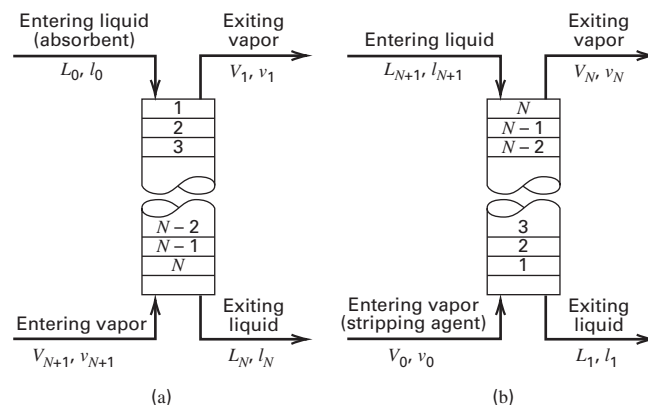


Figure 6.14 Countercurrent cascades of N adiabatic stages: (a) absorber; (b) stripper.

An absorption factor \mathcal{A} , which is analogous to the extraction factor \mathcal{E} , for a given stage and component is defined by

$$\mathcal{A} = \frac{L}{KV} \quad (6-18)$$

Combining (6-17) and (6-18) gives

$$v_N = \frac{l_N}{\mathcal{A}} \quad (6-19)$$

Substituting (6-19) into (6-13),

$$l_N = (l_{N-1} + v_1)\mathcal{A}_N \quad (6-20)$$

The component flow rate, l_{N-1} , is eliminated by successive substitution using material balances around successively smaller sections of the top of the cascade. For stages 1 through $N-2$,

$$l_{N-1} = (l_{N-2} + v_1)\mathcal{A}_{N-1} \quad (6-21)$$

Substituting (6-21) into (6-20),

$$l_N = l_{N-2}\mathcal{A}_{N-1}\mathcal{A}_N + v_1(\mathcal{A}_N + \mathcal{A}_{N-1}\mathcal{A}_N) \quad (6-22)$$

Continuing to the top stage, where $l_1 = v_1\mathcal{A}_1$ expands (6-22) to

$$l_N = v_1(\mathcal{A}_1\mathcal{A}_2\mathcal{A}_3 \cdots \mathcal{A}_N + \mathcal{A}_2\mathcal{A}_3 \cdots \mathcal{A}_N + \mathcal{A}_3 \cdots \mathcal{A}_N + \cdots + \mathcal{A}_N) \quad (6-23)$$

Combining (6-23) with the overall component balance,

$$l_N = v_{N+1} - v_1 \quad (6-24)$$

gives

$$\frac{v_1}{v_{N+1}} = \frac{1}{\mathcal{A}_1\mathcal{A}_2\mathcal{A}_3 \cdots \mathcal{A}_N + \mathcal{A}_2\mathcal{A}_3 \cdots \mathcal{A}_N + \mathcal{A}_3 \cdots \mathcal{A}_N + \cdots + \mathcal{A}_N + 1} \quad (6-25)$$

or (6-25) may be rewritten as

$$v_1 = v_{N+1}\phi_A \quad (6-26)$$

where, ϕ_A is the absorption recovery fraction,

$$\phi_A = \frac{1}{\mathcal{A}_1\mathcal{A}_2\mathcal{A}_3 \cdots \mathcal{A}_N + \mathcal{A}_2\mathcal{A}_3 \cdots \mathcal{A}_N + \mathcal{A}_3 \cdots \mathcal{A}_N + \cdots + \mathcal{A}_N + 1} \quad (6-27)$$

In the Kremser method, an average, effective absorption factor, \mathcal{A}_e , for each component replaces the separate absorption factors for each stage, simplifying (6-27) into

$$\phi_A = \frac{1}{\mathcal{A}_e^N + \mathcal{A}_e^{N-1} + \mathcal{A}_e^{N-2} + \cdots + \mathcal{A}_e + 1} \quad (6-28)$$

When multiplied and divided by $(\mathcal{A}_e - 1)$, (6-28) reduces to the Kremser equation:

$$\phi_A = \frac{\mathcal{A}_e - 1}{\mathcal{A}_e^{N+1} - 1} = \text{fraction of species not absorbed} \quad (6-29)$$

Because each component has a different \mathcal{A}_e , ϕ_A is also component specific. Figure 6.15 from Edmister [31] is a plot of (6-29) with a probability scale for ϕ_A , a logarithmic scale for \mathcal{A}_e , and N as a parameter. By specifying any two of these three quantities, the third can be determined from the plot. Kremser first developed this plot, using linear coordinates [30].

Next, consider the stripper shown in Figure 6.14b. Assume the components stripped from the liquid are not present in the entering vapor, and ignore absorption of the stripping agent. Stages are numbered from bottom to top. The pertinent stripping equations are derived in a manner analogous to the absorber equations. The results are

$$l_1 = l_{N+1}\phi_S \quad (6-30)$$

where

$$\phi_S = \frac{\mathcal{S}_e - 1}{\mathcal{S}_e^{N+1} - 1} = \text{fraction of species not stripped} \quad (6-31)$$

and

$$\mathcal{S} = \frac{KV}{L} = \frac{1}{\mathcal{A}} = \text{stripping factor} \quad (6-32)$$

Figure 6.15 also applies to (6-31). As shown in Figure 6.16, absorbers are frequently coupled with strippers or distillation columns to permit the recovery and recycling of absorbent. Because the stripping action is not perfect, recycled absorbent contains species present in the vapor feed. Up-flowing vapor strips these species, as well as others in the makeup absorbent. A more general absorber equation for handling this situation is obtained by combining (6-26) for absorption with a form of (6-30) for stripping species from the entering liquid. For a species that appears only in the entering liquid of an absorber, with stages numbered from top to bottom, as in Figure 6.14a, (6-30) becomes

$$l_N = l_0\phi_S \quad (6-33)$$

or, because $l_0 = v_1 + l_N$,

$$v_1 = l_0(1 - \phi_S) \quad (6-34)$$

Finally, for a component appearing in both entering vapor and entering liquid, a material balance is obtained by adding (6-26) and (6-34), giving

$$v_1 = v_{N+1}\phi_A + l_0(1 - \phi_S) \quad (6-35)$$

which applies to each component in the entering vapor. The analogous equation to (6-35) for a component appearing in both entering vapor and entering liquid of a stripper is

$$l_1 = l_{N+1}\phi_S + v_0(1 - \phi_A) \quad (6-36)$$

In order to use (6-29) and (6-31) with Figure 6.15, effective values of absorption and stripping factors, \mathcal{A}_e and \mathcal{S}_e , are needed. For preliminary calculations prior to rigorous calculations with a process simulator, as described in Chapter 10, molar L and V flow rates may be taken as entering values. As shown in Chapter 2, K -values depend mainly on T , P ,

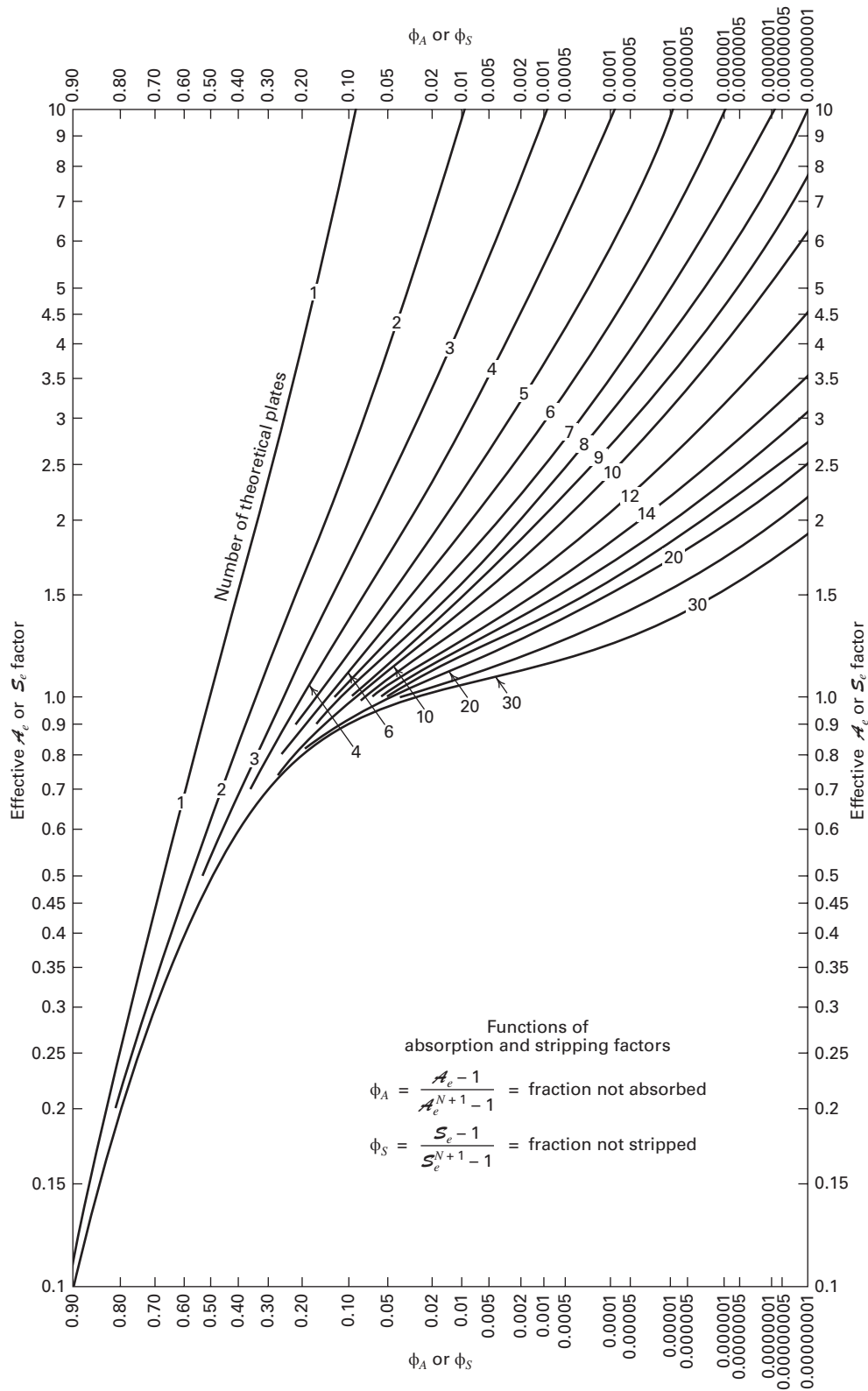


Figure 6.15 Plot of the Kremser equation for a single-section, countercurrent cascade. [From [31] with permission of John Wiley & Sons, Inc.]

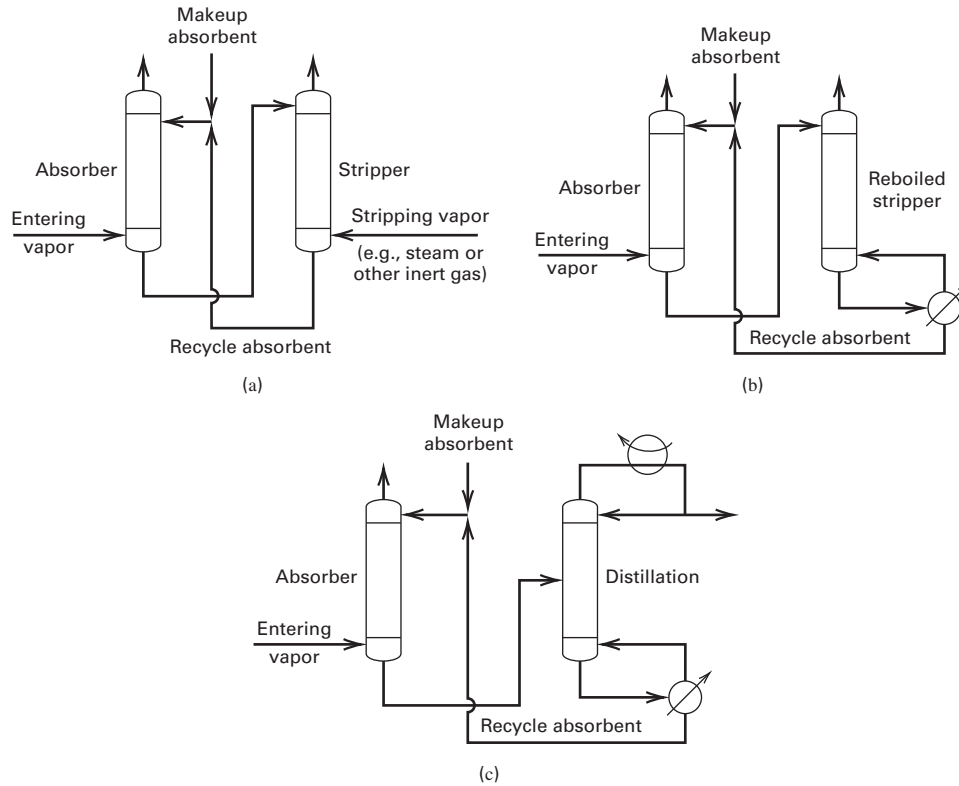


Figure 6.16 Various coupling schemes for absorbent recovery: (a) use of steam or inert gas stripper; (b) use of reboiled stripper; (c) use of distillation.

and liquid-phase composition. At near-ambient pressure, for dilute mixtures, some common expressions are

$$K_i = P_i^s/P \text{ (Raoult's law)} \quad (6-37)$$

$$K_i = \gamma_{iL}^\infty P_i^s/P \text{ (modified Raoult's law)} \quad (6-38)$$

$$K_i = H_i/P \text{ (Henry's law)} \quad (6-39)$$

$$K_i = P_i^s/x_i^s P \text{ (solubility)} \quad (6-40)$$

Raoult's law is for ideal solutions involving solutes at subcritical temperatures. The modified Raoult's law is useful for nonideal solutions for which activity coefficients are known at or near infinite dilution. For solutes at supercritical temperatures, the use of Henry's law may be preferable. For sparingly soluble solutes at subcritical temperatures, (6-40) is preferred when solubility data x_i^s are available. This expression is derived by considering a three-phase system that consists of an ideal vapor containing the solute, carrier vapor, and solvent; a pure or near-pure solute as liquid (1); and a solvent liquid (2) with dissolved solute. In that case, for solute i at equilibrium between the two liquid phases,

$$x_i^{(1)} \gamma_{iL}^{(1)} = x_i^{(2)} \gamma_{iL}^{(2)}$$

But,

$$x_i^{(1)} \approx 1, \gamma_{iL}^{(1)} \approx 1, x_i^{(2)}$$

Therefore,

$$\gamma_{iL}^{(1)} \approx 1/x_i^s$$

From (6-38),

$$K_i^{(2)} = \gamma_{iL}^{(2)} P_i^s/P = P_i^s/(x_i^s P)$$

For moderate to high pressures, vapor fugacity coefficients must be included, as in (2-27).

The plot of the Kremser equation in Figure 6.15 shows a strong dependence for the effect of the number of equilibrium stages, N , (referred to as theoretical plates in Figure 6.15) on the fraction not absorbed, ϕ_A , for a given absorption factor, \mathcal{A} . Components with high absorption factors (i.e., greater than the optimal value of 1.4) show a rapidly decreasing fraction not absorbed for an increasing number of stages. These are components that are easily absorbed, as indicated by their low K -values. As the absorption factor decreases below 1.4, the effect of an increase in the number of stages diminishes rapidly. Below an absorption factor of 0.5, there is little effect on the fraction not absorbed above 3 or 4 stages. These are components that are difficult to absorb, as evidenced by their high K -values. In this region, the maximum value of the fraction that can be absorbed is equal to the absorption factor. That is, $(1-\phi_A)_{\max} = \mathcal{A}$. Because the Kremser plot for absorption is also applicable for stripping, the above analysis applies equally to strippers. This plot of an approximate analytical solution relates the state of a system, $K = K\{T, P, x_i, y_i\}$, and the operability (L, V) and geometry (N) of corresponding equipment to performance (ϕ) in a way that is intuitive and useful to guide design and operation of a separation system.

EXAMPLE 6.2 Recovery of Ethyl Alcohol Using the Kremser Equation.

Repeat Example 6.1 for the recovery of ethyl alcohol from CO₂ by absorption in water, using the Kremser method. Assume the absorber operates at 30°C and 110 kPa. The total entering gas flow rate is 180 kmol/h with 2 mol% ethanol. The absorbent is pure water. The specified recovery of ethanol is 97%. From Example 6.1, the K -value for ethanol is 0.57. Assuming an entering absorbent flow rate of 1.5 times the minimum, determine the following:

- The number of equilibrium stages required
- The fraction of the entering water stripped into the gas
- The fraction of the entering CO₂ absorbed by the water

Solution

To calculate the number of equilibrium stages, (6-29) is used with ethanol as the key component. The ethanol absorption factor, \mathcal{A} , is calculated using $V = 180$ kmol/h, $K = 0.57$, and $L = 1.5 L_{\min}$. To find L_{\min} , note that, if $\mathcal{A}_{\min} < 1.0$ at L_{\min} (i.e., $N = \infty$), then (6-29) reduces to an analog of (6-11):

$$L_{\min} = KV(1 - \phi_A) \quad (1)$$

Using (1), with $\phi_A = (1 - 0.97) = 0.03$, $L_{\min} = 0.57(180)(1 - 0.03) = 99.5$ kmol/h. This value is close to 97.5 kmol/h, which was determined in Example 6.1. The corresponding $\mathcal{A}_{\min} = 99.5 / [(0.57)(180)] = 0.97$. The actual absorbent rate = $L = 1.5 L_{\min} = 1.5(99.5) = 149$ kmol/h.

- To find N from (6-29), compute $\mathcal{A}_e = 149 / [(0.57)(180)] = 1.45$, which is close to the optimal value. From (6-29),

$$\phi_A = 0.03 = \frac{\mathcal{A}_e - 1}{\mathcal{A}_e^{N+1} - 1} = \frac{1.45 - 1}{1.45^{N+1} - 1} \quad (2)$$

Equation (2) is a nonlinear equation in N . Using MATLAB with `fsolve`, $N = 6.46$. This compares to slightly more than 6 stages, as determined graphically in Example 6.1

- For water, use a Raoult's law K -value with a water vapor pressure at 30°C = 4.24 kPa. Therefore, from (6-37), $K = 4.24/110 = 0.0385$. From (6-32), \mathcal{S}_e for water = $0.0385(180)/149 = 0.0465$. From (6-31), with $N = 6.46$, using ethanol as the key component, the fraction of water not stripped = $\frac{\mathcal{S}_e - 1}{\mathcal{S}_e^{N+1} - 1} = \frac{0.0385 - 1}{0.0385^{6.45+1} - 1} = 0.962$, and the fraction of entering water stripped = $1 - 0.962 = 0.038$.

- For CO₂ absorption into water, use the Henry's law K -value from (6-39), with $H_{\text{CO}_2} = 1900$ atm = 195000 kPa from Figure 4.18. From (6-39), K for CO₂ = $295000/110 = 1770$, and from (6-18), $\mathcal{A}_e = 149 / [1770(180)] = 0.00047$. From (6-29),

$$\begin{aligned} \frac{\mathcal{A}_e - 1}{\mathcal{A}_e^{N+1} - 1} &= \frac{0.00047 - 1}{0.00047^{6.45+1} - 1} = 0.9995 \\ &= \phi_A = \text{fraction of CO}_2 \text{ not absorbed} \end{aligned}$$

Therefore, the fraction of CO₂ absorbed = $1 - 0.9995 = 0.0005$.

EXAMPLE 6.3 Absorption of Hydrocarbons by Oil.

In Figure 6.17, the higher-molecular-weight components, normal butane (C₄), and normal pentane (C₅) in hydrocarbon gas are removed by absorption at 400 psia with a high-molecular-weight hydrocarbon oil that is equivalent to normal decane. Trace amounts of each component appear in the entering oil. Estimate the exit vapor and liquid flow rates and compositions via the Kremser method, using estimated component absorption and stripping factors from the entering values of L and V , with the component K -values estimated with a process simulator, based on an average entering temperature of $(90 + 105)/2 = 97.5^\circ\text{F}$.

Solution

From (6-18), $\mathcal{A}_i = L/K_iV = 165/[K_i(800)] = 0.206/K_i$. From (6-32), $\mathcal{S}_i = 1/\mathcal{A}_i = 4.85K_i$; and $N = 6$ equilibrium stages. Figure 6.17 shows $N = 6$. From §2.11, the Lee-Kesler-Plöcker method is preferred for K -values because of the wide boiling range of the combined vapor feed and liquid absorbent. The K -values were estimated by using Aspen Plus to flash the combined feed and absorbent at 97.5°F and 400 psia. The resulting values are listed in the table below. Values of ϕ_A and ϕ_S are from (6-29) and (6-31), or from the Kremser-equation plot in Figure 6.15. The values of $(v_i)_1$ in the exit vapor are from (6-35). The values of $(l_i)_6$ in the exit liquid, are computed from an overall component material balance using Figure 6.14a:

$$(l_i)_6 = (l_i)_0 + (v_i)_7 - (v_i)_1 \quad (1)$$

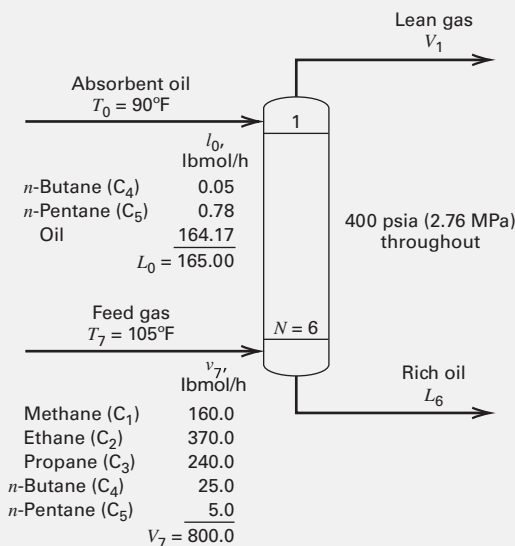


Figure 6.17 Specifications for the absorber in Example 6.3.

The computations, made with a spreadsheet, produce the following results:

Component	K at 97.5°F and 400 psia	A	S	ϕ_A	ϕ_S	v_1	l_6
C_1	7.19	0.0287	—	0.971	—	155.41	4.59
C_2	1.73	0.119	—	0.881	—	325.97	44.03
C_3	0.604	0.341	—	0.659	—	158.24	81.76
nC_4	0.223	0.924	1.082	0.179	0.111	4.52	20.53
nC_5	0.0883	2.33	0.429	0.0035	0.573	0.35	5.43
Oil	0.00080	—	0.00039	—	0.9996	0.064	164.106
						644.554	320.446

The results indicate that approximately 80% of butane and pentane in the entering gas is absorbed. Less than 0.1% of the absorbent oil is stripped.

EXAMPLE 6.4 Stripping Volatile Organic Compounds from Wastewater.

Okoniewski [3] studied the use of air to strip volatile organic compounds (VOCs) from wastewater. At 70°F and 15 psia, 500 gpm of wastewater were stripped with 3,400 scfm of air (60°F and 1 atm) in a 20-plate tower. The wastewater contained three pollutants in the amounts shown in the following table. Included are properties from the 1966 *Technical Data Book—Petroleum Refining* of the American Petroleum Institute. For all compounds, the organic concentrations are less than their solubility values, so only one liquid phase exists.

Organic Compound	Concentration in the Wastewater, mg/L	Solubility in Water at 70°F, mole fraction	Vapor Pressure at 70°F, psia
Benzene	150	0.00040	1.53
Toluene	50	0.00012	0.449
Ethylbenzene	20	0.000035	0.149

It is required that 99.9% of the total VOCs must be stripped. The plate efficiency of the tower is estimated to be from 5% to 20%, so the number of equilibrium stages in the tower is from 1 to 4. Plot the percentage of stripping for each organic compound in this range of equilibrium stages. Under what conditions will the desired degree of stripping be achieved? What do you suggest be done with the exiting air?

Solution

Because the wastewater is dilute in the VOCs, the Kremser equation is applied independently to each organic chemical. The absorption of air by water and the stripping of water by air are ignored. The stripping factor for each compound is $S_i = K_i V/L$, where V and L are taken at entering conditions. K -values are estimated from (6-40) using the given solubility data:

$$K_i = P_i^s/x_i^s P \quad (1)$$

where

$$V = 3,400(60)/(379 \text{ scf/lbmol at } 60^\circ\text{F and } 1 \text{ atm})$$

or 538 lbmol/h, and

$$L = 500(60)(8.33 \text{ lb/gal})/(18.02 \text{ lb/lbmol}) \text{ or } 13,870 \text{ lbmol/h}$$

The applicable K -values and stripping factors are shown in the following table:

Component	K at 70°F, 15 psia	S
Benzene	255	9.89
Toluene	249	9.66
Ethylbenzene	284	11.02

A spreadsheet program using the following modification of (6-31) to give the fraction stripped.

$$\text{Fraction stripped} = 1 - \frac{S - 1}{S^{N+1} - 1} = \frac{S^{N+1} - S}{S^{N+1} - 1} \quad (2)$$

Component	Percent Stripped			
	1 Stage	2 Stages	3 Stages	4 Stages
Benzene	90.82	99.08	99.91	99.99
Toluene	90.62	99.04	99.90	99.99
Ethylbenzene	91.68	99.25	99.93	99.99

The results are sensitive to the number of stages, as shown in Figure 6.18, demonstrating that about 90% of the absorption occurs in just one stage. To achieve 99.9% removal of the VOCs, three stages are needed. This corresponds to 15% stage efficiency in the 20-tray tower.

The exiting air must be processed to destroy the VOCs, particularly the carcinogen benzene [4]. The amount stripped is

$$(500 \text{ gpm})(60 \text{ min/h})(3.785 \text{ liters/gal})(150 \text{ mg/liters})$$

$$= 17,030,000 \text{ mg/h or } 37.5 \text{ lb/h.}$$

If benzene is valued at \$0.65/lb, the annual value is almost \$200,000. This would not justify a recovery technique such as carbon adsorption. It is thus preferable to destroy the VOCs by incineration. For example, the air can be sent to an on-site utility boiler, a waste-heat boiler, or a catalytic incinerator.

The amount of air is arbitrarily given as 3,400 scfm. To complete the design procedure, various air rates should be investigated and column-efficiency calculations made, as discussed in §6.5.

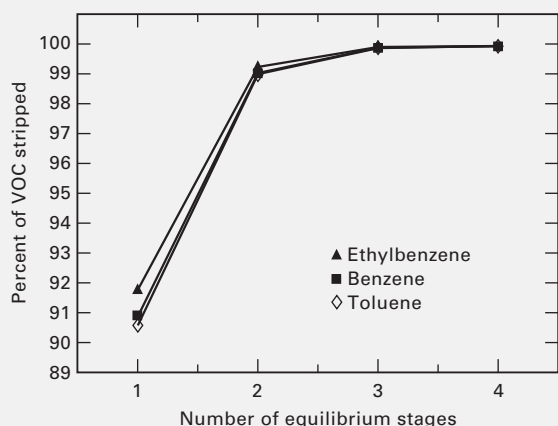


Figure 6.18 Results of Example 6.4 for stripping VOCs from water with air.

§6.5 STAGE EFFICIENCY AND COLUMN HEIGHT FOR TRAYED COLUMNS

Unless temperatures change significantly from stage to stage, it can be reasonably assumed that vapor and liquid phases leaving a tray in a tower are at the same temperature. The assumption of phase composition equilibrium at each tray is not reasonable, however. For streams leaving a tray, vapor-phase mole fractions are not related exactly to liquid-phase mole fractions by thermodynamic K -values. To determine the actual number of required trays in a trayed column, the number of equilibrium stages must be adjusted with an overall stage efficiency, or efficiencies must be estimated for each tray.

Stage efficiency concepts are applicable when phases are contacted and then separated—that is, when discrete stages and interfaces are identified as in trayed columns. This is not the case for packed columns. For these, the efficiency is embedded into equipment- and system-dependent parameters, such as the HETP or HETS (height of packing equivalent to a theoretical stage), as discussed in §6.7.

§6.5.1 Overall Stage Efficiency

A simple approach suitable for preliminary design and evaluation of an existing column is to apply an overall stage efficiency, defined by Lewis [5] as

$$E_o = N_t/N_a \quad (6-41)$$

where E_o is the fractional overall stage efficiency, usually less than 1.0; N_t is the calculated number of theoretical stages; and N_a is the actual number of trays required. Based on the results of extensive research conducted over a period of more than 70 years, the overall stage efficiency has been found to be a

complex function of (a) the geometry and design of the trays, (b) the flow rates and flow paths of vapor and liquid streams, and (c) the compositions and properties of vapor and liquid streams.

For well-designed trays and for flow rates near the column capacity limit discussed in §6.6, E_o depends mainly on the physical properties of the vapor and liquid streams. Values of E_o can be predicted or selected by four methods: (1) comparison with performance data from similar columns, (2) use of empirical efficiency equations derived from data on industrial columns, (3) use of semitheoretical models based on mass-transfer rates, and (4) scale-up from laboratory or pilot-plant columns. The next four subsections discuss the methods for absorbers and strippers. These same methods are applied to distillation in Chapter 7. Suggested correlations of mass-transfer coefficients for trayed towers are deferred to §6.6, following the discussion of tray capacity. A final subsection presents a method for estimating column height based on the number of equilibrium stages, stage efficiency, and tray spacing. Some of the methods discussed form the basis for the column-sizing calculations used in process simulators.

§6.5.2 Tray Efficiencies from Column Performance Data

Performance data from industrial absorption and stripping trayed columns generally include feed and product flow rates and compositions, pressures and temperatures at the bottom and top of the column, details of the tray design, column diameter, tray spacing, average liquid viscosity, and computed overall tray efficiency with respect to one or more components. From these data, particularly if the system is dilute with respect to the solute(s), the graphical or algebraic methods described in §6.3 and 6.4 can estimate the number of equilibrium stages, N_t . Then, knowing N_a , (6-41) can be applied to determine the overall stage efficiency, E_o . Values for absorbers and strippers are typically low, especially for absorption, for which E_o is often less than 50%, especially if the absorbent is a hydrocarbon oil.

Drickamer and Bradford [6] computed the overall stage efficiencies for five hydrocarbon absorbers and strippers with column diameters ranging from 4 to 5 ft and equipped with bubble-cap trays. The overall stage efficiencies for the key component, n -butane in absorbers and n -heptane in strippers, varied from 10.4% to 57%, primarily depending on the molar-average liquid viscosity, which is a key factor for liquid mass-transfer rates.

Individual component overall efficiencies differ because of differences in component physical properties. The data of Jackson and Sherwood [7] for a 9-ft-diameter hydrocarbon absorber equipped with 19 bubble-cap trays on 30-inch tray spacing, operating at 92 psia and 60°F, is summarized in Table 6.4 from O'Connell [8]. Values of E_o vary from 10.3% for ethylene, the most-volatile species, to 33.8% for butylene, the least-volatile species. The molar-average liquid viscosity was 1.90 cP (centipoise).

Table 6.4 Effect of Species on Overall Stage Efficiency

Component	Overall Stage Efficiency, %
Ethylene	10.3
Ethane	14.9
Propylene	25.5
Propane	26.8
Butylene	33.8

Source: H.E. O’Connell [8].

A more dramatic effect of absorbent species solubility on overall stage efficiency was observed by Walter and Sherwood [9], using laboratory bubble-cap tray columns ranging from 2 to 18 inches in diameter. Stage efficiencies varied over a range from less than 1% to 69%. Comparing data for the water absorption of NH₃ (a very soluble gas) and CO₂ (a slightly soluble gas), they found a lower stage efficiency for CO₂, with its low gas solubility (high *K*-value), and a high stage efficiency for NH₃, with its high gas solubility (low *K*-value). Thus, both solubility (or *K*-value) and liquid-phase viscosity are important variables that affect stage efficiency.

§6.5.3 Empirical Correlations for Tray Efficiency

From 20 sets of performance data from industrial absorbers and strippers, Drickamer and Bradford [6] correlated key component overall stage efficiency with just the molar average viscosity of the rich oil (liquid leaving an absorber or liquid entering a stripper) over a viscosity range of 0.19 to 1.58 cP at the column temperature. The empirical equation

$$E_o = 19.2 - 57.8 \log \mu_L, \quad 0.2 < \mu_L < 1.6 \text{ cP} \quad (6-42)$$

where *E_o* is in percent and μ is in cP, fits the data with an average deviation of 10.3%. Equation (6-42) should not be used for non-hydrocarbon liquids and is restricted to the viscosity range of the data.

Mass-transfer theory predicts that, when the solubility or volatility of species being absorbed or stripped covers a wide range, the relative importance of liquid-phase and gas-phase mass-transfer resistances shifts. O’Connell [8] found that the Drickamer–Bradford correlation, (6-42), was inadequate when species cover a wide solubility or *K*-value range. O’Connell obtained a more general correlation by using a parameter that includes not only liquid viscosity, but also liquid density and a Henry’s law constant. Edmister [10] and Lockhart et al. [11] suggested slight modifications to the O’Connell correlation, shown in Figure 6.19, to permit its use with *K*-values (instead of Henry’s law constants). The correlating parameter, $K_i M_L \mu_L / \rho_L$, suggested by Edmister and shown in Figure 6.19, uses *M_L*, liquid average molecular weight in g/mol; μ_L , liquid viscosity in cP; and ρ_L , liquid density in lb/ft³. The data cover the following range of conditions:

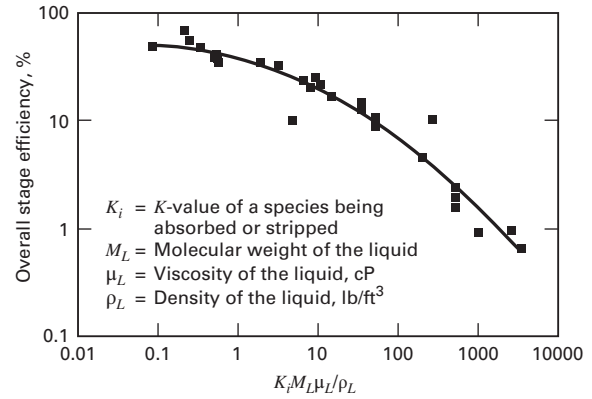


Figure 6.19 O’Connell correlation for plate efficiency of absorbers and strippers.

Column diameter:	2 inches to 9 ft
Average pressure:	14.7 to 485 psia
Average temperature:	60 to 138°F
Liquid viscosity:	0.22 to 21.5 cP
Overall stage efficiency:	0.65 to 69%

The following empirical equation by O’Connell [8] correlates most of the data in Figure 6.19 to within about a 15% deviation for water and hydrocarbon systems:

$$\log E_o = 1.597 - 0.199 \left[\log \left(\frac{K M_L \mu_L}{\rho_L} \right) \right] - 0.0896 \left[\log \left(\frac{K M_L \mu_L}{\rho_L} \right) \right]^2 \quad (6-43)$$

where *E_o* is in percent and other variables have the units shown in Figure 6.19.

The data for Figure 6.19 are mostly for columns having a liquid flow-path length across the tray, shown as *z_L* in Figure 6.3, from 2 to 3 ft. Theory and data show higher efficiencies for longer flow paths. For short liquid flow paths, the liquid flowing across the tray is usually completely mixed. For longer flow paths, the equivalent of two or more successive, completely mixed liquid zones exists. The result is a greater average driving force for mass transfer, leading to a higher stage efficiency—even greater than 100% in some distillation operations! A column with a 10-ft liquid flow path may have an efficiency 25% greater than that predicted by (6-43). However, at high liquid rates, long liquid-path lengths are undesirable because they lead to excessive liquid (hydraulic) gradients. When the height of a liquid on a tray is appreciably higher on the inflow side than at the overflow weir, vapor may prefer to enter the tray in the latter region, leading to nonuniform bubbling. Multipass trays, shown in Figure 6.20a, are used to prevent excessive hydraulic gradients. Estimates of the required number of flow paths can be made with Figure 6.20b, which suggests that a 10-foot-diameter column with a liquid flow rate of 1,000 gpm should use a three-pass tray.

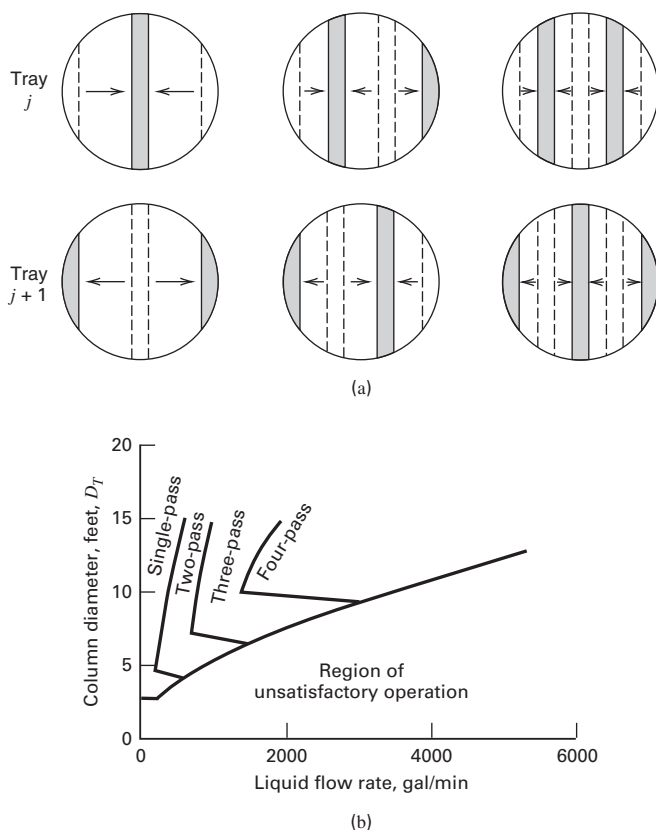


Figure 6.20 Estimation of the number of required liquid flow passes. (a) Multipass trays (2, 3, 4 passes). (b) Flow pass selection. [Based on figure from *Koch Flexitray Design Manual, Bulletin 960*, Koch Engineering Co., Inc., Wichita, KS (1960).]

EXAMPLE 6.5 Prediction of Tray Efficiency for Acetone Absorber.

Use the O'Connell correlation of Figure 6.19 and (6-43) to estimate the percent tray efficiency of the acetone absorber of the industrial example near the beginning of this chapter and the number of actual trays required.

Solution

From Figure 6.19, the correlation parameter is $K_i M_L \mu_L / \rho_L$, with the units in the figure. Because the liquid is dilute in acetone, use the properties of pure water at 25°C:

$$\rho_L = 0.997 \text{ g/cm}^3 = 62.2 \text{ lb/ft}^3, \quad \mu_L = 0.89 \text{ cP}, \quad M_L = 18 \text{ g/mol}$$

Take the K -value for acetone as 2.0.

$$\text{Therefore, } \frac{K_i M_L \mu_L}{\rho_L} = \frac{2(18)(0.89)}{(62.2)} = 0.52$$

Using (6-43), tray efficiency = $E_o = 0.444$ or 44.4%

From (6-41), if the number of equilibrium stages = $N_i = 12.5$, the actual number of trays needed = $N_a = N_i / E_o = 12.5 / 0.444 = 28.2$. The number of trays in the industrial example is 30. The number of trays in industrial columns is sometimes specified in multiples of 5.

EXAMPLE 6.6 Back-Calculation of Tray Efficiency for a Refinery Absorber.

The following table provides performance data for a trayed absorber in a Texas petroleum refinery, as reported by Drickamer and Bradford [6]. Based on these data, back-calculate the overall stage efficiency for *n*-butane and compare the result with the Drickamer–Bradford correlation (6-42). Lean oil and rich gas enter the tower, and rich oil and lean gas leave the tower.

Performance Data

Number of plates	16
Plate spacing, inches	24
Tower diameter, ft	4
Tower pressure, psig	79
Lean oil temperature, °F	102
Rich oil temperature, °F	126
Rich gas temperature, °F	108
Lean gas temperature, °F	108
Lean oil rate, lbmol/h	368
Rich oil rate, lbmol/h	525.4
Rich gas rate, lbmol/h	946
Lean gas rate, lbmol/h	786.9
Lean oil molecular weight, g/mol	250
Lean oil viscosity at 116°F, cP	1.4
Lean oil gravity, °API	21

Stream Compositions, Mol%

Component	Rich Gas	Lean Gas	Rich Oil	Lean Oil
C_1	47.30	55.90	1.33	
C_2	8.80	9.80	1.16	
$C_3^=$	5.20	5.14	1.66	
C_3	22.60	21.65	8.19	
$C_4^=$	3.80	2.34	3.33	
nC_4	7.40	4.45	6.66	
nC_5	3.00	0.72	4.01	
nC_6	1.90		3.42	
Oil absorbent			70.24	100
Totals	100.00	100.00	100.00	100

Solution

First, check the consistency of the plant data by examining the overall material balance and the material balance for each component. From the above stream compositions, it is apparent that the compositions have been normalized to total 100%. The overall material balance is

$$\begin{aligned} \text{Total flow into tower} &= 368 + 946 = 1,314 \text{ lbmol/h, and} \\ \text{Total flow from tower} &= 525.4 + 786.9 = 1,312.3 \text{ lbmol/h} \end{aligned}$$

These totals agree to within 0.13%, which is excellent agreement. The component material balance for the oil absorbent is

$$\begin{aligned} \text{total oil in} &= 368 \text{ lbmol/h and} \\ \text{total oil out} &= (0.7024)(525.4) = 369 \text{ lbmol/h} \end{aligned}$$

These two totals agree to within 0.3%. Again, this is excellent agreement. Component material balances give the following results:

Component	lbmol/h			Total In
	Lean Gas	Rich Oil	Total Out	
C ₁	439.9	7.0	446.9	447.5
C ₂	77.1	6.1	83.2	83.2
C ₃ ⁼	40.4	8.7	49.1	49.2
C ₃	170.4	43.0	213.4	213.8
C ₄ ⁼	18.4	17.5	35.9	35.9
nC ₄	35.0	35.0	70.0	70.0
nC ₅	5.7	21.1	26.8	28.4
nC ₆	0.0	18.0	18.0	18.0
	786.9	156.4	943.3	946.0

Again, there is excellent agreement, except for a difference of 6% for *n*-pentane. Plant data are not always so consistent.

For the back-calculation of stage efficiency from performance data, the Kremser equation is used to compute the number of equilibrium stages required for the measured absorption of *n*-butane:

$$\text{Fraction of } nC_4 \text{ absorbed} = \frac{35}{70} = 0.50$$

From (6-29),

$$1 - 0.50 = \frac{A_e - 1}{A_e^{N+1} - 1} \quad (1)$$

To calculate the number of equilibrium stages, *N*, using Eq. (1), the absorption factor, *A*, for *n*-butane must be estimated from *L/KV*.

Because *L* and *V* vary greatly through the column, arithmetic averages of entering and leaving streams are appropriate:

$$L = \text{average liquid rate} = \frac{368 + 525.4}{2} = 446.7 \text{ lbmol/h, and}$$

$$V = \text{average vapor rate} = \frac{946 + 786.9}{2} = 866.5 \text{ lbmol/h}$$

The average tower temperature = (102 + 126 + 108 + 108)/4 = 111°F. Also assume that the given viscosity of the lean oil at 116°F equals the viscosity of the rich oil at 111°F; in other words, μ = 1.4 cP.

If ambient pressure = 14.7 psia, tower pressure = 79 + 14.7 = 93.7 psia. Using Raoult's law as an approximation for butane at 93.7 psia and 111°F gives *K_{nC4}* = 0.7. Thus,

$$A = \frac{446.7}{(0.7)(866.5)} = 0.736$$

Therefore, from Eq. (1),

$$0.50 = \frac{0.736^{N+1} - 0.736}{0.736^{N+1} - 1} \quad (2)$$

Using *fzero* in MATLAB to solve (2) gives *N* = *N_t* = 1.45. The performance data shows that *N_a* = 16. From (6-41),

$$E_o = \frac{1.45}{16} = 0.091 \text{ or } 9.1\%$$

Equation (6-22) is applicable to *n*-butane because it is about 50% absorbed and is one of the key components. Other possible key components are butenes and *n*-pentane.

From the Drickamer equation (6-42),

$$E_o = 19.2 - 57.8 \log(1.4) = 10.8\%$$

§6.5.4 Semitheoretical Models: Murphree Efficiencies

Tray efficiency models, in order of increasing complexity, have been proposed by Holland [12], Murphree [13], Hausen [14], and Standart [15]. All four models assume that the vapor and liquid streams entering each tray are of uniform composition. The **Murphree vapor efficiency**, which is the oldest and most widely used, is derived with the additional assumptions of (1) a uniform liquid composition on the tray equal to that leaving the tray and (2) a plug flow of the vapor passing up through the liquid, as shown in Figure 6.21. The development presented is applicable to trayed columns for distillation, as well as for absorption and stripping.

For species *i*, let

n = mass-transfer rate for absorption from gas to liquid

K_G = overall gas mass-transfer coefficient based on a partial-pressure driving force

a = vapor-liquid interfacial area per volume of combined gas and liquid holdup (froth or dispersion) on the tray

A_b = active bubbling area of the tray (total cross-sectional area minus liquid downcomer areas)

Z_f = height of combined gas and liquid tray holdup

y_i = bulk mole fraction of *i* in the vapor rising up through the liquid on the tray

y_i^{}* = vapor mole fraction of *i* in equilibrium with the completely mixed liquid mole fraction of *i* on the tray

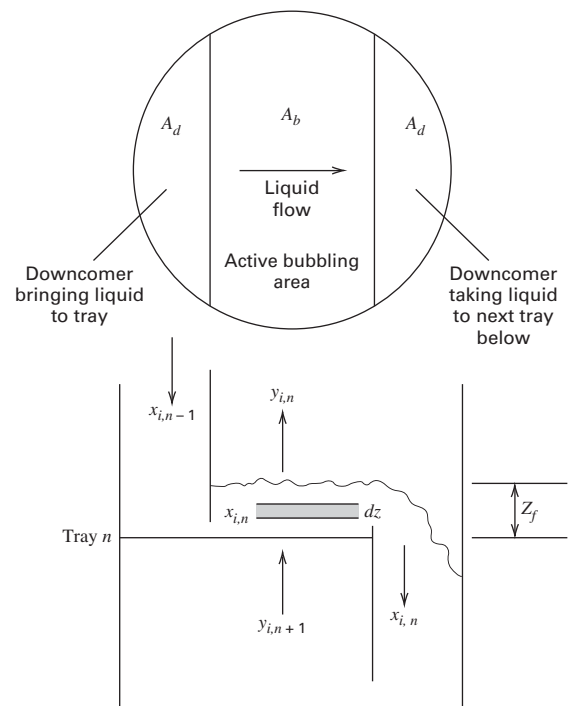


Figure 6.21 Schematic top and side views of tray for derivation of Murphree vapor-tray efficiency.

The bulk vapor mole fraction, y_i , changes as the vapor passes up through the liquid on the tray. The differential rate of mass transfer for a differential height of holdup on the tray is

$$dn_i = K_G a (y_i - y_i^*) P A_b dZ_f \quad (6-44)$$

where, using the two-film theory of mass transfer from §3.7, K_G includes both gas- and liquid-phase resistances to mass transfer, so that

$$\frac{1}{K_G} = \frac{1}{k_G} + \frac{H_i v_L}{k_L} \quad (6-45)$$

For (6-45),

k_G = individual mass-transfer coefficient for the gas phase based on a partial-pressure driving force

k_L = individual mass-transfer coefficient for the liquid phase based on a concentration driving force

H_i = Henry's law coefficient for component i . From (6-39), $K_i = H_i/P$

v_L = liquid molar volume

By material balance, assuming a negligible change in the vapor flow rate, V , across the stage,

$$dn_i = -V dy_i \quad (6-46)$$

where V = the molar gas flow rate up through the tray liquid.

Combining (6-45) and (6-46) to eliminate dn_i , separating variables, and converting to integral form lead to

$$A_b \int_0^{Z_f} \frac{K_G a P}{V} dZ_f = \int_{y_{i,n+1}}^{y_{i,n}} \frac{dy_i}{y_{i,n}^* - y_i} = N_{OG} \quad (6-47)$$

where a second subscript to denote the tray number, n , is added to the vapor mole fraction. The vapor enters tray n as $y_{i,n+1}$ and exits as $y_{i,n}$. This equation defines N_{OG} , which is the number of overall gas-phase mass-transfer units.

The values of K_{OG} , a , P , and V vary somewhat as the gas flows up through the liquid on the tray, but if they, as well as y_i^* , are taken to be constant, (6-47) can be integrated to give

$$N_{OG} = \frac{K_G a P Z_f}{(V/A_b)} = \ln \left(\frac{y_{i,n+1} - y_{i,n}^*}{y_{i,n} - y_{i,n}^*} \right) \quad (6-48)$$

Rearranging (6-48), in terms of the fractional approach of $y_{i,n+1}$ to $y_{i,n}^*$, which is in equilibrium with liquid mole fraction, $x_{i,n}$, defines the fractional Murphree vapor efficiency as

$$E_{MV} = \frac{y_{i,n+1} - y_{i,n}}{y_{i,n+1} - y_{i,n}^*} = 1 - e^{-N_{OG}} \quad (6-49)$$

where

$$N_{OG} = -\ln(1 - E_{MV}) \quad (6-50)$$

If measurements give $y_{i,n+1} = 0.64$, and $y_{i,n} = 0.61$, and phase-equilibrium data yields $y_{i,n}^* = 0.60$, then, from (6-49),

$$E_{MV} = (0.64 - 0.61)/(0.64 - 0.60) = 0.75$$

or a 75% approach to equilibrium. From (6-50),

$$N_{OG} = -\ln(1 - 0.75) = 1.386$$

The Murphree vapor efficiency does not include exiting stream temperatures. However, it does imply that the completely mixed liquid phase is at its bubble point, so the equilibrium vapor-phase mole fraction, $y_{i,n}^*$, can be obtained.

For multicomponent mixtures, values of E_{MV} are component-dependent and vary from tray to tray, but at each tray, the number of independent values of E_{MV} is one less than the number of components. The dependent value of E_{MV} is determined by forcing $\sum y_i = 1$. It is thus possible that a negative value of E_{MV} can result for a component in a multicomponent mixture. Such negative efficiencies are possible because of mass-transfer coupling among concentration gradients in a multicomponent mixture, as discussed in Chapter 12. For a binary mixture, values of E_{MV} are always positive and equal for the two components.

The tray liquid will only satisfy the complete-mixing assumption of (6-49) if it travels a short distance across the tray. For the more general case of incomplete liquid mixing, a local **Murphree vapor-point efficiency** is defined by assuming that liquid composition varies across a tray, but is uniform in the vertical direction. Thus, for species i on tray n , at some horizontal distance from the downcomer, as in Figure 6.22,

$$E_{OV} = \frac{y_{i,n+1} - y_{i,n}}{y_{i,n+1} - y_{i,n}^*} \quad (6-51)$$

Because x_i varies across a tray, y_i^* and y_i also vary. However, the exiting vapor is then assumed to mix to produce a uniform $y_{i,n}$ before entering the tray above. Because E_{OV} is a more fundamental quantity than E_{MV} , E_{OV} serves as the basis for semitheoretical estimates of tray E_{MV} and overall column efficiency. Correlations of experimental data for mass transfer on trays and their application to the estimation of E_{OV} is presented in Chapter 7 in §7.4.3. With E_{OV} known, the Murphree vapor efficiency, E_{MV} , can be calculated using equations from the development.

Lewis [16] integrated E_{OV} over a tray to obtain E_{MV} for several cases. For **complete mixing** of liquid on the tray (uniform $x_{i,n}$),

$$E_{MV} = E_{OV} \quad (6-52)$$

For **plug flow** of liquid across a tray, with no mixing of liquid or diffusion in the horizontal direction, Lewis derived

$$E_{MV} = \frac{1}{\lambda} (e^{\lambda E_{OV}} - 1) \quad (6-53a)$$

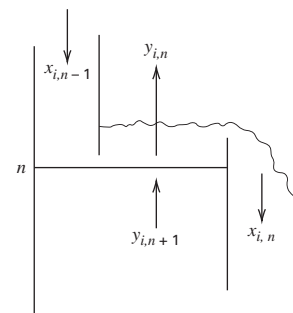


Figure 6.22 Schematic of tray for Murphree vapor-point efficiency.

where

$$\lambda = mV/L \tag{6-53b}$$

and $m = dy/dx$, the slope of the equilibrium line for a species, using the expression $y = mx + b$. If b is taken as zero, then m is the K -value, and for the key component, k ,

$$\lambda = K_k V/L = 1/\mathcal{A}_k$$

If \mathcal{A}_k , the key-component absorption factor, has the optimal or typical value of 1.4, $\lambda = 0.71$.

Suppose the measured or predicted point efficiency is $E_{OV} = 0.25$. From (6-53a), $E_{MV} = 1.4[\exp(0.71 \times 0.25) - 1] = 0.27$, which is only 9% higher than E_{OV} . However, if $E_{OV} = 0.9$, E_{MV} is 1.25, which is 39% higher. This surprising result is due to the liquid concentration gradient across the length of the tray, which allows the vapor to contact a liquid having an average concentration of species k that is appreciably lower than the concentration of k in the liquid leaving the tray.

Equations (6-52) and (6-53) represent extremes between complete mixing and no mixing. Gerster et al. [17] developed

a more realistic, but more complex, model that accounts for **partial liquid mixing**:

$$\frac{E_{MV}}{E_{OV}} = \frac{1 - \exp[-(\eta + N_{Pe})]}{(\eta + N_{Pe}) \{1 + [(\eta + N_{Pe})/\eta]\}} + \frac{\exp(\eta) - 1}{\eta \{1 + [\eta/(\eta + N_{Pe})]\}} \tag{6-54a}$$

where

$$\eta = \frac{N_{Pe}}{2} \left[\left(1 + \frac{4\lambda E_{OV}}{N_{Pe}} \right)^{1/2} - 1 \right] \tag{6-54b}$$

E_{MV}/E_{OV} is plotted as a function of λE_{OV} from 1 to 10 in Figure 6.23b, with a reduced range of λE_{OV} from 0 to 3 in Figure 6.23a. The parameter is a Peclet number for mass transfer, N_{Pe} , listed as N_{PeM} , in Table 3.9. For this case, it is based on the ratio of the velocity of liquid flowing across the tray to the eddy diffusivity, and it is defined by

$$N_{Pe} = Z_L u/D_E \tag{6-55}$$

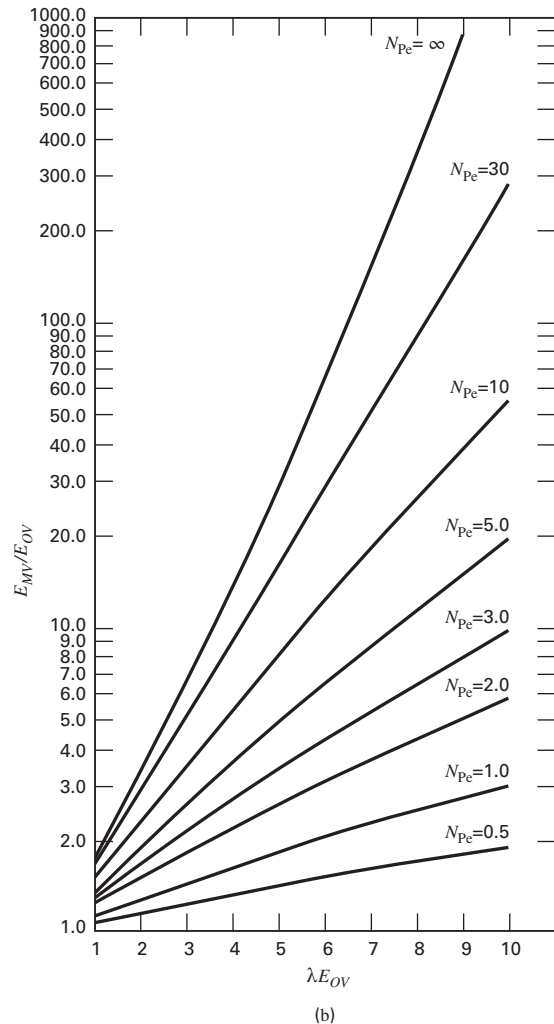
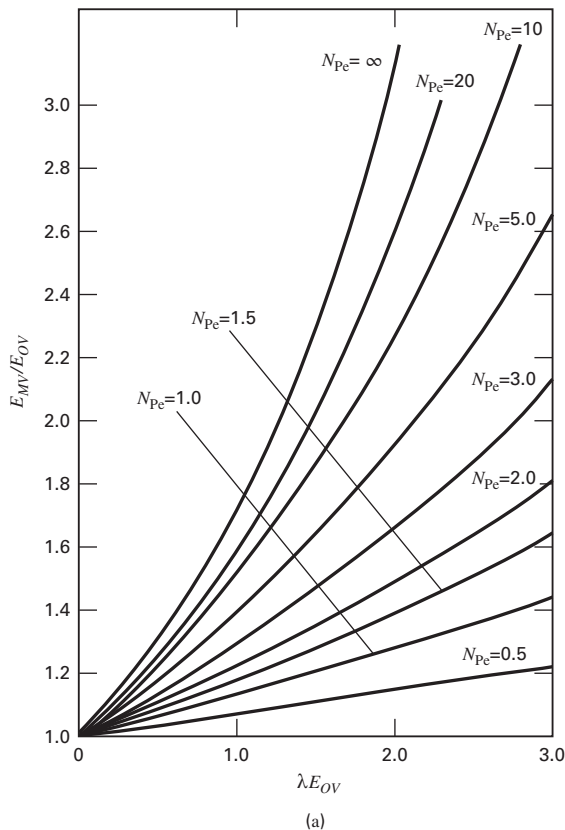


Figure 6.23 (a) Effect of longitudinal mixing on Murphree vapor-tray efficiency. (b) Expanded range for effect of longitudinal mixing on Murphree vapor-tray efficiency.

where, Z_L = liquid flow path length across the tray, as shown in Figure 6.3; D_E = eddy diffusivity in the liquid flow direction; and u = mean liquid velocity across the tray. When $N_{Pe} = 0$, complete liquid mixing is achieved, and (6-52) holds. When $N_{Pe} = \infty$, diffusion across the tray does not occur, and (6-53) holds. From evaluation of experimental measurements of D_E in bubble-cap and sieve-plate columns [18 to 21] N_{Pe} increases from 10 for a 2-ft-diameter column to 30 for a single-pass 6-ft-diameter column.

Lewis [16] showed that, for straight, but not necessarily parallel, equilibrium and operating lines, the overall stage efficiency is related to the Murphree vapor efficiency by

$$E_o = \frac{\log[1 + E_{MV}(\lambda - 1)]}{\log \lambda} \quad (6-56)$$

When the two lines are straight and parallel, $\lambda = 1$, and (6-56) becomes $E_o = E_{MV}$. Also, when $E_{MV} = 1$, $E_o = 1$ regardless of the value of λ .

§6.5.5 Tray Efficiencies by Scale-up of Data with the Oldershaw Column

When vapor–liquid equilibrium data are unavailable, particularly if the system is highly nonideal with possible formation of azeotropes, tray requirements and the feasibility of achieving the desired separation must be verified by laboratory tests. A useful apparatus is the small glass or metal sieve-plate column with center-to-side downcomers developed by Oldershaw [22] and shown in Figure 6.24. Oldershaw columns are typically 1 to 2 inches in diameter and can be assembled with almost any number of sieve plates, which contain 0.035- to 0.043-inch holes with a hole area of approximately 10%. A detailed study by Fair, Null, and Bolles [23] presents the overall tray efficiencies of Oldershaw columns operated over a pressure range of 3 to 165 psia. The data are in conservative agreement with data obtained from sieve-tray, pilot-plant, and industrial-size columns ranging in size from 1.5 to 4 ft in diameter, when operated in the range of 40% to 90% of flooding, as described in §6.6. It may be assumed that similar agreement might be realized for absorption and stripping.

The small-diameter Oldershaw column achieves essentially complete mixing of the liquid on each tray, thus permitting

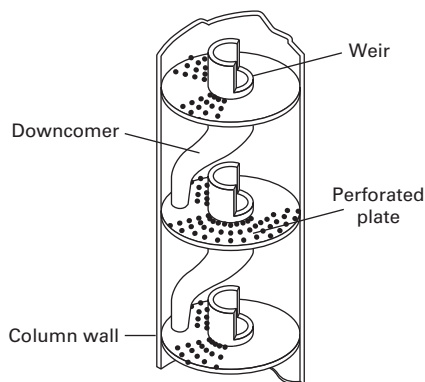


Figure 6.24 Oldershaw column.

the measurement of a Murphree vapor-point efficiency, E_{OV} , from (6-51). Somewhat larger efficiencies may be observed in much-larger-diameter columns, due to incomplete liquid mixing, as described in §6.5.4, resulting in a higher Murphree tray efficiency, E_{MV} , and, therefore, higher overall plate efficiency, E_o .

Fair et al. [23] recommend a scale-up procedure using data from an Oldershaw column: (1) Determine the flooding point, as described in §6.6. (2) Establish operation at about 60% of flooding. (3) Run the system to find a combination of plates and flow rates that gives the desired degree of separation. (4) Assume the commercial column will require the same number of plates for the same ratio of L to V .

If reliable vapor–liquid equilibrium data are available, they can be used with the Oldershaw data to determine the overall column efficiency, E_o . Then (6-56) and Figure 6.23 are used to estimate the average point efficiency. For commercial-size columns, the Murphree vapor efficiency can be determined from the Oldershaw column point efficiency, using Figure 6.23, which corrects for incomplete liquid mixing. In general, the tray efficiency of commercial columns is higher than for the Oldershaw column at the same percentage of flooding.

EXAMPLE 6.7 Murphree Efficiencies.

Assume that the absorber column diameter from Example 6.1 is 3 ft. If the overall stage efficiency, E_o , is 30% for the absorption of ethyl alcohol, estimate the average Murphree vapor efficiency, E_{MV} , and the possible range of the Murphree vapor-point efficiency, E_{OV} .

Solution

For Example 6.1, the system is dilute in ethyl alcohol, the main component undergoing mass transfer. Therefore, the equilibrium and operating lines are essentially straight, and (6-56) is applied. From the data of Example 6.1, $\lambda = KV/L = 0.57(180)/151.5 = 0.68$. Solving (6-56) for E_{MV} , using $E_o = 0.30$, gives

$$E_{MV} = (\lambda^{E_o} - 1) / (\lambda - 1) = (0.68^{0.30} - 1) / (0.68 - 1) = 0.34$$

For a 3-ft-diameter column, the degree of liquid mixing is probably between complete mixing and plug flow. From (6-52) for the former case, $E_{OV} = E_{MV} = 0.34$. From a rearrangement of (6-53a) for the latter case, $E_{OV} = \ln(1 + \lambda E_{MV}) / \lambda = \ln[1 + 0.68(0.34)] / 0.68 = 0.31$. Therefore, E_{OV} lies in the range of 31% to 34%. The differences between E_o , E_{MV} , and E_{OV} for this example are quite small.

§6.5.6 Column Height

The number of trays, N_a , and the tray spacing determine the height of a column between the top tray and bottom tray. The total column height is estimated by adding another 4 ft above the top tray for removal of entrained liquid and 10 ft below the bottom tray for bottoms liquid surge capacity. If the height is greater than 250 ft, two or more columns arranged in series may be preferable to a single column. However, a column at the Shell Chemical Company complex in Deer Park, Texas, stands 338 ft tall [Chem. Eng., 84 (26), 84 (1977)].

§6.6 FLOODING, COLUMN DIAMETER, AND TRAY LAYOUT FOR TRAYED COLUMNS

When trays are designed properly: (1) Vapor flows only up through the open regions of the tray outside the downcomers. (2) Liquid flows from tray to tray only through downcomers. (3) Liquid neither weeps through the tray perforations nor is carried by the vapor as entrainment to the tray above. (4) Vapor is neither carried (occluded) downward by the liquid in the downcomer nor allowed to bubble up through the liquid in the downcomer. Tray layout design determines tray diameter and division of total tray cross-sectional area, A_T , into bubbling area, A_b , and liquid downcomer area, A_d , both from the tray above and to the tray below. In Figure 6.20a, the downcomer area, A_d , from the tray above is bounded by dashed lines and the column perimeter. The downcomer area, A_d , to the tray below is shaded grey and bounded by solid lines and the column perimeter. Tray bubbling area, A_b , lies between these downcomer areas, and arrows in the tray bubbling area show the direction of liquid flow. When the tray layout is fixed, the vapor pressure drop and mass-transfer coefficients can be estimated.

§6.6.1 Flooding and Tray Diameter

Figure 6.25 is a representative plot showing the stable operating limits for a sieve-tray column in terms of vapor and liquid flow rates. Four limits are shown: (1) excessive **liquid entrainment** at low liquid rates, (2) **entrainment (jet) flooding** at high vapor rates, (3) **downcomer (choke) flooding** at high liquid rates, and (4) **weeping** of liquid to the tray below at low vapor rates. As the vapor rate decreases, weeping becomes excessive until all of the liquid on the tray dumps onto the tray below. Entrainment flooding results in a spray, as shown in Figure 6.4a, at low liquid rates, but it progresses to a froth, as shown in Figure 6.4b, as the liquid rate is increased. In the absence of significant entrainment, downcomer flooding takes place at high liquid rates when liquid backup occurs, because the downcomer cross-sectional area, A_d , cannot accommodate the liquid flow. When the aerated liquid backup exceeds the tray spacing, flooding occurs. Typically, downcomer flooding

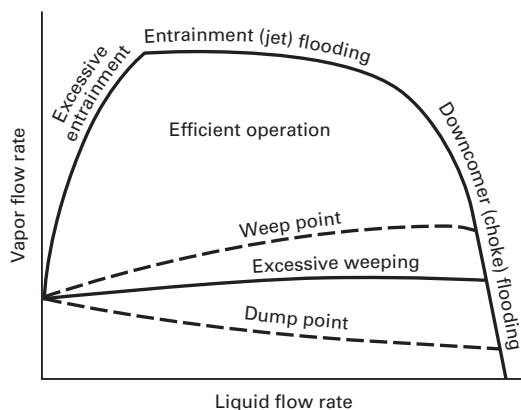


Figure 6.25 Limits of stable operation in a trayed tower.

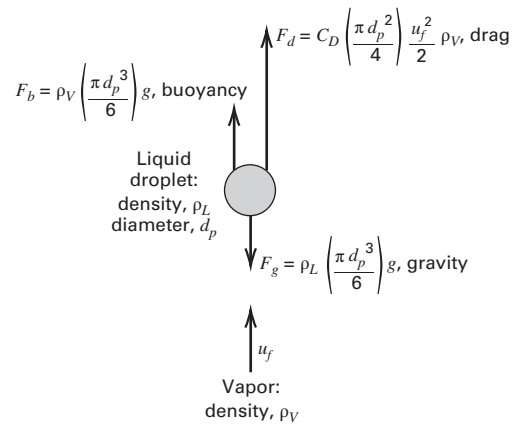


Figure 6.26 Forces acting on a suspended liquid droplet.

is only critical at high pressures, and it rarely dominates if the downcomer cross-sectional area is at least 10% of total column cross-sectional area and if tray spacing is at least 24 inches. The usual design limit is entrainment flooding, particularly at low to moderate pressures. Entrainment flooding is caused by excessive carry-up of liquid, at the molar rate e , by vapor entrainment to the tray above. At incipient flooding, $(e + L) \gg L$ and the downcomer cross-sectional area is inadequate for the excessive liquid load $(e + L)$. Entrainment recycles liquid upward, increasing the downcomer load and eventually causing column flooding. Entrainment rate, e , should be kept below 10% of L .

For well-designed trays, column diameter is determined by entrainment flooding by the carry-up of suspended droplets by rising vapor or the throw-up of liquid by vapor jets at tray perforations, valves, or bubble-cap slots. Souders and Brown [24] correlated entrainment flooding data by assuming that the carry-up of droplets controls entrainment. At low vapor velocity, a droplet settles out; at high vapor velocity, it is entrained. At incipient vapor entrainment velocity (flooding velocity), u_f , the droplet is suspended such that the vector sum of the gravitational, buoyant, and drag forces, F , shown in Figure 6.26, is zero. Thus,

$$\sum F = 0 = F_g - F_b - F_d \quad (6-57)$$

Each term on the RHS of (6-57) can be written in terms of droplet diameter, d_p , as shown in Figure 6.26:

$$\rho_L \left(\frac{\pi d_p^3}{6} \right) g - \rho_V \left(\frac{\pi d_p^3}{6} \right) g - C_D \left(\frac{\pi d_p^2}{4} \right) \frac{u_f^2}{2} \rho_V = 0 \quad (6-58)$$

where C_D is the drag coefficient. Solving (6-58) for the flooding velocity yields

$$u_f = \left(\frac{4d_p g}{3C_D} \right)^{1/2} \left(\frac{\rho_L - \rho_V}{\rho_V} \right)^{1/2} \quad (6-59)$$

Souders and Brown simplified (6-59) to

$$u_f = C \left(\frac{\rho_L - \rho_V}{\rho_V} \right)^{1/2} \quad (6-60)$$

where the parameter, C , in ft/s is determined from flooding data for commercial-size columns, rather than from measuring droplet diameters at flooding. Existing entrainment flooding data covered column pressure from 10 mm Hg to 465 psia, plate spacing from 12 to 30 inches, and liquid surface tension from 9 to 60 dyne/cm. Parameter C increases with surface tension, which increases with d_p . Surface tension influences C because it is a measure of the energy required to break liquid into droplets. Parameter C also increases with tray spacing, because greater spacing allows more time for droplets to agglomerate to a larger d_p , which increases settling rate.

Fair [25] improved the Souders–Brown correlation to produce the general correlation of Figure 6.27, which is applicable to commercial columns with bubble-cap and sieve trays. Fair uses a flooding velocity based on a net vapor flow area, A_n . For a single-pass tray, such as the one shown in Figure 6.21, the net vapor flow area between trays is equal to the total inside column cross-sectional area minus the cross-sectional area blocked by one downcomer; in other words, $A - A_d$. The flooding-factor parameter, C_F , in units of ft/s, in Figure 6.27 depends on tray spacing and the abscissa ratio $F_{LV} = (LM_L/VM_V)(\rho_V/\rho_L)^{0.5}$, which is a kinetic-energy ratio first used by Sherwood, Shipley, and Holloway [26] to correlate packed-column flooding data. Note that LM_L and VM_V are the mass liquid and vapor flow rates, respectively. The value of C in (6-60) is obtained from Figure 6.27 by correcting C_F for surface tension, foaming tendency, and the ratio of vapor hole area A_h to tray active area A_a , according to the empirical relationship

$$C = F_{ST}F_FF_{HA}C_F \tag{6-61}$$

where

$$F_{ST} = \text{surface-tension factor} = (\sigma/20)^{0.2}$$

$$F_F = \text{foaming factor}$$

$$F_{HA} = 1.0 \text{ for } A_h/A_a \geq 0.10 \text{ and } 5(A_h/A_a) + 0.5$$

$$\text{for } 0.06 \leq A_h/A_a \leq 0.1, \text{ and}$$

$$\sigma = \text{liquid surface tension in dyne/cm}$$

For nonfoaming systems, $F_F = 1.0$, but for many absorbers, it is 0.75 or less. A_h is the area open to vapor as it penetrates the liquid on a tray. This area is the total cap slot area for

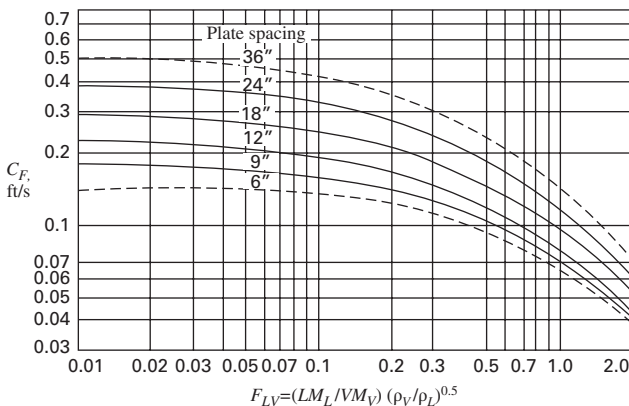


Figure 6.27 Entrainment flooding factor of Fair in a trayed tower.

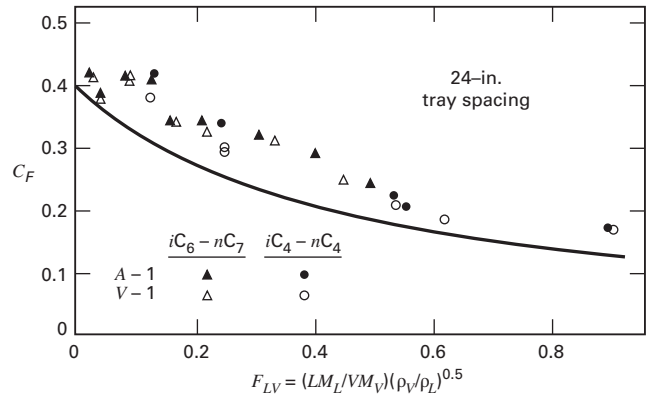


Figure 6.28 Comparison of flooding correlation with data for valve trays.

bubble-cap trays, the perforated area for sieve trays, and the full valve opening through which vapor enters the tray horizontally for valve trays.

Figure 6.27 estimates C_F conservatively, especially for valve trays. This is shown in Figure 6.28, which compares the entrainment-flooding data of Fractionation Research Inc. (FRI) [27, 28] for a 4-ft-diameter column equipped with Koch-Glitsch type A-1 and V-1 valve trays, at 24-inch spacing, to the correlation in Figure 6.27, which is shown as a solid line.

Column (tower) diameter, D_T , is based on a fraction, f , of flooding velocity, u_f , calculated from (6-60), using C from (6-61), based on C_F from Figure 6.27. By the **continuity equation**, molar vapor flow rate = design velocity ($f u_f$) \times flow area \times molar density:

$$V = (f u_f)(A - A_d) \frac{\rho_V}{M_V} \tag{6-62}$$

where A = total column cross-sectional area = $\pi D_T^2/4$. Combining this result with (6-62) gives

$$D_T = \left[\frac{4V M_V}{f u_f \pi (1 - A_d/A) \rho_V} \right]^{0.5} \tag{6-63}$$

Typically, the fraction of flooding, f , is taken to be 0.80.

Oliver [29] suggests that A_d/A can be estimated from F_{LV} in Figure 6.27 by

$$\frac{A_d}{A} = \begin{cases} 0.1, & F_{LV} \leq 0.1 \\ 0.1 + \frac{F_{LV} - 0.1}{9}, & 0.1 \leq F_{LV} \leq 1.0 \\ 0.2, & F_{LV} \geq 1.0 \end{cases}$$

Column diameter is calculated for both top and bottom trays, with the larger of the two used for the entire column, unless the two diameters differ appreciably, in which case the column is swaged. Because of the need for internal access to columns with trays, a packed column, discussed in §6.7, is generally used if the diameter from (6-63) is less than 2 ft.

To use Figure 6.27, tray spacing must be selected. As spacing is increased, the column height increases, but the column diameter is reduced because higher velocities are

tolerated. A 24-inch spacing allows for ease of maintenance, and, as a result, it is common. A smaller spacing is desirable for small-diameter columns with a large number of trays, and larger spacing is used for large columns with few trays.

As shown in Figure 6.25, a minimum vapor rate exists, below which liquid weeps through tray perforations, openings, or risers instead of flowing completely across the active area into the downcomer. Below this minimum, liquid–vapor contact is reduced, causing tray efficiency to decline. The ratio of vapor rate at flooding to the minimum vapor rate is the **turndown ratio**, which is approximately 5 for bubble-cap trays, 4 for valve trays, but only 2 for sieve trays. Thus, valve trays are preferable to sieve trays for operating flexibility.

When vapor and liquid flow rates change appreciably, column diameter, tray spacing, or hole area can be varied to reduce column cost and ensure stable operation at high efficiency. Tray-spacing variation is common for sieve trays because of their low turndown ratio.

EXAMPLE 6.8 Diameter of Column for Ethanol Absorption.

Use the Fair correlation to estimate the diameter of the ethanol absorption column of Example 6.1. Assume a 24-inch tray spacing, a foaming factor of 0.9, and a fraction of flooding of 0.8. The surface tension is 70 dynes/cm.

Solution

Because tower conditions are almost the same at the top and bottom, the column diameter is determined only at the bottom, where gas rate is highest. From Example 6.1,

$$\begin{aligned} T &= 30^\circ\text{C} \\ P &= 110 \text{ kPa} \\ V &= 180 \text{ kmol/h} \\ L &= 151.5 + 3.5 = 155.0 \text{ kmol/h} \\ M_V &= 0.98(44) + 0.02(46) = 44 \\ M_L &= \frac{151.5(18) + 3.5(46)}{155} = 18.6 \\ \rho_V &= \frac{PM}{RT} = \frac{(110)(44)}{(8.314)(303)} = 1.92 \text{ kg/m}^3 \\ \rho_L &= (0.986)(1,000) = 986 \text{ kg/m}^3 \\ F_{LV} &= \frac{(155)(18.6)}{(180)(44)} \left(\frac{1.92}{986} \right)^{0.5} = 0.016 \end{aligned}$$

For tray spacing = 24 inches, Figure 6.27 gives

$$\begin{aligned} C_F &= 0.38 \text{ ft/s,} \\ F_{ST} &= \left(\frac{\sigma}{20} \right)^{0.2} = \left(\frac{70}{20} \right)^{0.2} = 1.285, F_F = 0.90 \end{aligned}$$

Because $F_{LV} < 0.1$, $A_d/A = 0.1$, and $F_{HA} = 1.0$
From (6-61),

$$C = 1.285(0.90)(1.0)(0.38) = 0.44 \text{ ft/s}$$

From (6-60),

$$u_f = 0.44 \left(\frac{986 - 1.92}{1.92} \right)^{0.5} = 10 \text{ ft/s}$$

From (6-63), using SI units and time in seconds, the column diameter is

$$\begin{aligned} D_T &= \left[\frac{4(180/3,600)(44.0)}{(0.80)(10/3.28)(3.14)(1 - 0.1)(1.92)} \right]^{0.5} = 0.82 \text{ m} \\ &= 2.68 \text{ ft} \end{aligned}$$

§6.6.2 High-Performance Trays

Since the 1990s, high-performance trays have been retrofitted and newly installed in many industrial columns. Changes to conventional sieve and valve trays have led to capacity increases of more than 20% of that predicted by Figure 6.27 for sieve and valve trays. Tray efficiencies have also been increased somewhat.

As shown by Stupin and Kister [42], an ultimate superficial vapor velocity, independent of tray design and tray spacing, exists for a countercurrent-flow contactor in which vapor velocity exceeds the settling velocity of droplets. Their formula, based on FRI data, uses the following form of (6-60):

$$u_{V,\text{ult}} = C_{V,\text{ult}} \left(\frac{\rho_L - \rho_V}{\rho_V} \right)^{1/2} \quad (6-64)$$

where $u_{V,\text{ult}}$ is the superficial vapor velocity in m/s, based on the column cross-sectional area. The superficial vapor velocity is defined as the velocity the vapor would have if it filled the column's cross-sectional area. The ultimate capacity parameter, $C_{V,\text{ult}}$ in m/s, is independent of the superficial liquid velocity, L_S in m/s, below a critical value, but above that value, it decreases with increasing L_S . $C_{V,\text{ult}}$ is given by the smaller of C_1 and C_2 , both of which are in m/s:

$$C_1 = 0.445(1 - F) \left(\frac{\sigma}{\rho_L - \rho_V} \right)^{0.25} - 1.4L_S, \text{ and} \quad (6-65)$$

$$C_2 = 0.356(1 - F) \left(\frac{\sigma}{\rho_L - \rho_V} \right)^{0.25} \quad (6-66)$$

where

$$F = \frac{1}{\left[1 + 1.4 \left(\frac{\rho_L - \rho_V}{\rho_V} \right)^{1/2} \right]} \quad (6-67)$$

ρ is in kg/m^3 , and σ is the surface tension in dynes/cm.

EXAMPLE 6.9 Ultimate Superficial Vapor Velocity for Ethanol Absorber.

For the ethanol absorber in Example 6.1, estimate the ultimate vapor superficial velocity. Use the data from Example 6.8.

Solution

From (6.67),

$$F = \frac{1}{\left[1 + 1.4 \left(\frac{986 - 1.92}{1.92} \right)^{1/2} \right]} = 0.0306$$

Assume C_2 is smaller than C_1 . From (6-66),

$$C_2 = 0.356(1 - 0.0306) \left(\frac{70}{986 - 1.92} \right)^{0.25} = 0.178 \text{ m/s}$$

From (6-64),

$$u_{v,\text{ult}} = \left(\frac{986 - 1.92}{1.92} \right)^{1/2} = 4.03 \text{ m/s} = 13.22 \text{ ft/s}$$

Now, check to see if C_1 is smaller than C_2 . To apply (6-65) for C_1 , the value of L_S is required. This is related to the value of the superficial vapor velocity, u_v , as follows:

$$L_S = u_v \frac{\rho_v L M_L}{\rho_L V M_V} = u_v \frac{(1.92)(155)(18.6)}{(986)(180)(44.0)} = 0.000709 u_v$$

With this expression for L_S , (6-65) becomes

$$\begin{aligned} C_1 &= 0.445(1 - 0.0306) \left(\frac{70}{986 - 1.92} \right)^{0.25} - 1.4(0.000709)u_v \\ &= 0.223 - 0.000993 u_v \text{ m/s} \end{aligned}$$

If C_1 is the smaller, then, using (6-64),

$$\begin{aligned} u_{v,\text{ult}} &= (0.223 - 0.000993 u_{v,\text{ult}}) \left(\frac{986 - 1.92}{1.92} \right)^{1/2} \\ &= 5.05 - 0.0225 u_{v,\text{ult}} \end{aligned}$$

Solving with $u_{v,\text{ult}} = 4.94 \text{ m/s}$ yields $C_1 = 0.223 - 0.000993(4.94) = 0.218 \text{ m/s}$. Thus, C_2 is the smaller value, and $u_{v,\text{ult}} = 4.03 \text{ m/s} = 13.22 \text{ ft/s}$. This ultimate velocity is 32% higher than the flooding velocity computed by the Fair correlation in Example 6.8.

§6.6.3 Tray Layout

When the tray diameter is known, the tray layout can be created. The layout consists of the selection of tray type (sieve or valve); the number of liquid passes across the tray, as illustrated in Figure 6.20; the tray spacing; the downcomer area; the downcomer weir height at the top; and the downcomer clearance at the bottom. These parameters are determined so as to keep both weeping and entrainment below 10% of the liquid flow rate. Equivalent clear-liquid height in the downcomer should not exceed 50% of the tray spacing at low to moderate pressures and should be less than 35% at high pressures. Tray pressure drop should be approximately 0.05 psi (0.35 kPa) for vacuum operation and no more than 0.15 psi (1.07 kPa) at high pressures. Weir loading should not be greater than 8 gpm/inch of weir length. For sieve trays, the percent hole area and hole diameter must be selected. For valve trays, the type of valve and valve spacing are needed. Preliminary tray layout calculations are best made with a process simulator, as described in the following example. Final design layouts are best carried out in cooperation with tray vendors.

EXAMPLE 6.10 Tray Layout for Ethanol Absorber.

Use the CHEMCAD simulator to design a tray for the ethanol absorber in Example 6.8.

Solution

Because only a small amount of ethanol is absorbed, all trays in the column have close to the same loadings and compositions of vapor and liquid. The following tray specifications are used with the flow rates and compositions given in Example 6.8.

Input Data:

Tray type: Koch-Glitch A valve Flexitray (formerly Glitsch V-1 ballast tray)

Tray spacing: 24 inches

% Entrainment flooding: 70%

% Hole area (based on tray active area): 15%

Simulation Results:

Weir height: 2.0 inches

Downcomer clearance height at bottom: 1.75 inches

The following results are obtained:

Tower diameter: 36 inches

No. of liquid passes: 1

Weir length: 18.3 inches

Liquid flow path length: 31 inches

Downcomer area: 31 in²

% Active area: 93.9%

Number of A valves: 78

Tray pressure drop: 0.158 psi (1.09 kPa)

Downcomer backup: 6.7 inches

Weir loading: 0.65 gpm/inch

§6.7 RATE-BASED METHOD FOR PACKED COLUMNS

Packed columns are continuous, differential-contacting devices that do not have physically distinguishable, discrete stages. Thus, packed columns are better described by mass-transfer models than by equilibrium-stage concepts. However, in practice, packed-tower performance is often presented on the basis of equivalent equilibrium stages using a packed-height equivalent to a theoretical stage, the HETP or HETS, and defined by the equation

$$\text{HETP} = \frac{\text{packed height}}{\text{number of equivalent equilibrium stages}} = \frac{l_T}{N_t} \quad (6-68)$$

The HETP concept has no theoretical basis. Accordingly, although HETP values can be related to mass-transfer coefficients, such values are best obtained by back-calculation from (6-68), using experimental data. To illustrate the HETP concept, consider Example 6.1, which involves the recovery of ethyl alcohol from a CO₂-rich vapor by absorption with water. From Example 6.2, the required N_t is 6.46. If experience shows that the use of 1.5-inch metal Pall rings will produce an average HETP of 2.25 ft, then the packed height from (6-68) is $l_T = (\text{HETP})N_t = 2.25(6.46) = 13.7 \text{ ft}$. If metal Intalox IMTP #40 random packing has an HETP = 2.0 ft, then $l_T = 12.9 \text{ ft}$. With Mellapak 250Y sheet-metal structured packing, the

HETP might be 1.2 ft, giving $l_T = 7.75$ ft. Usually, the lower the HETP, the more expensive and complex the packing.

It is preferable to determine the packed height from theoretically based methods involving mass-transfer coefficients. Consider the countercurrent-flow packed columns of packed height l_T shown in Figure 6.29. For packed absorbers and strippers, operating-line equations analogous to those in §6.3.2 can be derived. Thus, for the absorber in Figure 6.29a, a molar material balance for the solute, around the upper envelope of packed height, l , gives

$$x_{in}L_{in} + yV_l = xL_l + y_{out}V_{out} \quad (6-69)$$

or, solving for y , assuming dilute solutions such that $V_l = V_{in} = V_{out} = V$ and $L_l = L_{in} = L_{out} = L$,

$$y = x \left(\frac{L}{V} \right) + y_{out} - x_{in} \left(\frac{L}{V} \right) \quad (6-70)$$

Similarly, for the stripper in Figure 6.29b,

$$y = x \left(\frac{L}{V} \right) + y_{in} - x_{out} \left(\frac{L}{V} \right) \quad (6-71)$$

In (6-69) to (6-71), mole fractions y and x represent **bulk compositions** of the gas and liquid in contact at any vertical location in the packing. For the case of absorption, with solute mass transfer from the gas to the liquid stream, the two-film theory of Chapter 3, illustrated in Figure 6.30, applies. A concentration gradient exists in each thin film. At the **interface** between the two phases, physical equilibrium exists. Thus, as with trayed towers, an operating line and an equilibrium line are of great importance for packed towers.

For a given problem specification, the location of the two lines is independent of whether the tower is trayed or packed. Thus, the method for determining the minimum absorbent liquid or stripping vapor flow rates in a packed column is identical to that for trayed towers, as presented in §6.3 and illustrated in Figure 6.10.

The rate of mass transfer for absorption or stripping can be expressed in terms of mass-transfer coefficients for each phase. Coefficients, k , based on a unit area for mass transfer could be used, but the area for interfacial mass transfer in a packed bed is difficult to determine. Accordingly, as with mass

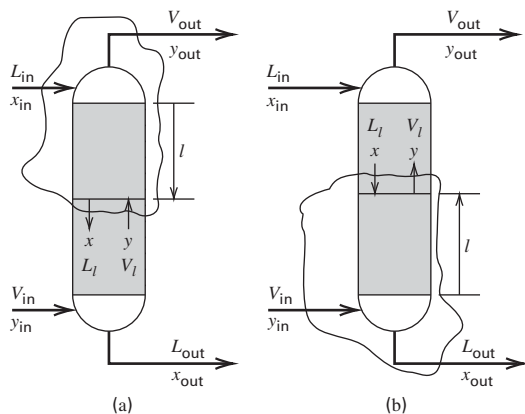


Figure 6.29 Packed columns with countercurrent flow: (a) absorber; (b) stripper.

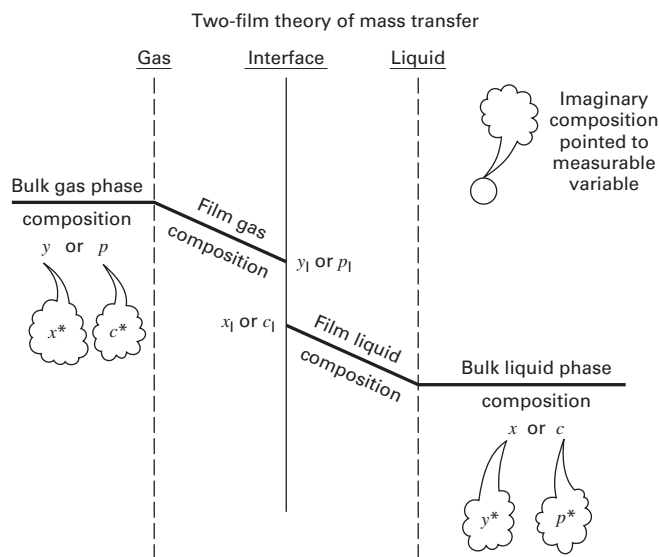


Figure 6.30 Interface properties in terms of bulk properties.

transfer in the froth of a trayed tower, it is common to use **volumetric mass-transfer coefficients**, ka , where the variable a represents the interfacial area for mass transfer between phases per unit volume of packed bed. At steady state, in the absence of chemical reactions, the rate of solute mass transfer through the gas-phase film must equal the rate through the liquid film. If the system is dilute in solute, unimolecular diffusion (UMD) is approximated by the equations for equimolar counter-diffusion (EMD) discussed in Chapter 3. The solute mass-transfer rate per unit volume of packed bed, r , is written in terms of mole-fraction driving forces in each phase (or in terms of a partial-pressure driving force in the gas phase and a concentration driving force in the liquid), as in Figure 6.30. Using mole fractions for absorption, with the subscript I to denote the phase interface, the solute mass-transfer rate is

$$r = k_y a (y - y_1) = k_x a (x_1 - x) \quad (6-72)$$

where $k_y a$ is the volumetric mass-transfer coefficient for the gas phase and $k_x a$ is the volumetric mass-transfer coefficient for the liquid phase. It is assumed that the interface offers no resistance to mass transfer. Thus, at the interface, phase equilibrium exists between y_1 and x_1 . The composition at the interface depends on the ratio $k_x a / k_y a$ because (6-72) can be rearranged to form

$$\frac{y - y_1}{x - x_1} = -\frac{k_x a}{k_y a} \quad (6-73)$$

Thus, as shown in Figure 6.31, a straight line of slope $-k_x a / k_y a$, drawn from the operating line at the bulk composition point (y, x) , intersects the equilibrium curve at (y_1, x_1) .

The slope $-k_x a / k_y a$ determines the relative resistances of the two phases to mass transfer. In Figure 6.31, the distance AE is the gas-phase driving force $(y - y_1)$, while AF is the liquid-phase driving force $(x_1 - x)$. If the resistance in the gas phase is very low, y_1 is approximately equal to y . Then, the resistance resides entirely in the liquid phase. This occurs in the absorption of a slightly soluble solute in the liquid phase

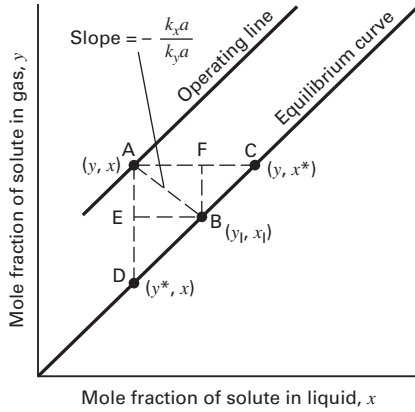


Figure 6.31 Interface composition in terms of the ratio of mass-transfer coefficients.

(a solute with a high K -value, e.g., CO_2) and is referred to as a liquid-film controlling process. Alternatively, if the resistance in the liquid phase is very low, x_1 is nearly equal to x . This occurs in the absorption of a very soluble solute in the liquid phase (a solute with a low K -value, e.g., NH_3) and is referred to as a gas-film controlling process. It is important to know which of the two resistances is controlling, so that its rate of mass transfer can be increased by promoting turbulence and/or increasing the dispersion of the controlling phase.

The composition at the interface between two phases is difficult to measure, so overall volumetric mass-transfer coefficients are defined in terms of overall driving forces between the two phases. Using mole fractions,

$$r = K_y a(y - y^*) = K_x a(x^* - x) \quad (6-74)$$

where $K_y a$ and $K_x a$ are the overall volumetric mass-transfer coefficients, and, as shown in Figure 6.31 and previously discussed in §3.7, y^* is the fictitious vapor mole fraction in equilibrium with the bulk liquid mole fraction, x , and x^* is the fictitious liquid mole fraction in equilibrium with the bulk vapor mole fraction, y . By combining (6-72) to (6-74), overall coefficients can be expressed in terms of separate phase coefficients:

$$\frac{1}{K_y a} = \frac{1}{k_y a} + \frac{1}{k_x a} \left(\frac{y_1 - y^*}{x_1 - x} \right) \quad (6-75)$$

and

$$\frac{1}{K_x a} = \frac{1}{k_x a} + \frac{1}{k_y a} \left(\frac{x^* - x_1}{y - y_1} \right) \quad (6-76)$$

In Figure 6.31, for dilute solutions, when the equilibrium curve is a nearly straight line through the origin,

$$\frac{y_1 - y^*}{x_1 - x} = \frac{\overline{ED}}{\overline{BE}} = K \quad (6-77)$$

and

$$\frac{x^* - x_1}{y - y_1} = \frac{\overline{CF}}{\overline{FB}} = \frac{1}{K} \quad (6-78)$$

where K is the K -value for the solute. Combining (6-75) with (6-77), and (6-76) with (6-78), gives

$$\frac{1}{K_y a} = \frac{1}{k_y a} + \frac{K}{k_x a} \quad (6-79)$$

and

$$\frac{1}{K_x a} = \frac{1}{k_x a} + \frac{1}{K k_y a} \quad (6-80)$$

Column packed height is determined from the overall gas-phase coefficient, $K_y a$, when the liquid has a strong affinity for the solute, so that the resistance to mass transfer is mostly in the gas phase. This is analogous to a trayed tower, for which the tray-efficiency analysis is commonly based on $K_{OG} a$ or N_{OG} . In the countercurrent-flow absorption column in Figure 6.32 for a dilute system, a differential material balance for a solute being absorbed in a differential height of packing dl gives

$$-V dy = K_y a(y - y^*) A_T dl \quad (6-81)$$

where A_T is the inside cross-sectional area of the tower. In integral form, with nearly constant factors placed outside the integral, (6-81) becomes

$$\frac{K_y a A_T}{V} \int_0^{l_T} dl = \frac{K_y a A_T l_T}{V} = \int_{y_{out}}^{y_{in}} \frac{dy}{y - y^*} \quad (6-82)$$

Solving for the packed height,

$$l_T = \frac{V}{K_y a A_T} \int_{y_{out}}^{y_{in}} \frac{dy}{y - y^*} \quad (6-83)$$

Chilton and Colburn [43] suggested that the RHS of (6-83) be written as the product of two terms:

$$l_T = H_{OG} N_{OG} \quad (6-84)$$

where

$$H_{OG} = \frac{V}{K_y a A_T} \quad (6-85)$$

and

$$N_{OG} = \int_{y_{out}}^{y_{in}} \frac{dy}{y - y^*} \quad (6-86)$$

Comparing (6-84) to (6-68) shows that H_{OG} is analogous to HETP, just as N_{OG} is analogous to N_T .

H_{OG} is the **overall height of a (gas) transfer unit (HTU)**. Experimental data show that HTU varies less with V than does

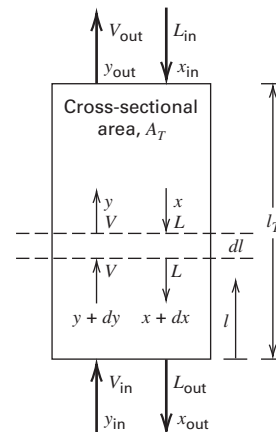


Figure 6.32 Differential contact in a countercurrent-flow, packed absorption column.

$K_y a$. The smaller the HTU, the more efficient the contacting. N_{OG} is the **overall number of (gas) transfer units** (NTU). It represents the overall change in solute mole fraction divided by the average mole-fraction driving force. The larger the NTU, the greater the time or area of contact required.

Equation (6-86) was integrated by Colburn [44], who used a linear equilibrium, $y^* = Kx$, to eliminate y^* and a linear, solute material-balance operating line, (6-70), to eliminate x , yielding

$$\int_{y_{out}}^{y_{in}} \frac{dy}{y - y^*} = \int_{y_{out}}^{y_{in}} \frac{dy}{(1 - KV/L)y + y_{out}(KV/L) - K x_{in}} \tag{6-87}$$

Letting $L/(KV) = \mathcal{A}$, the absorption factor, and integrating (6-87) gives

$$N_{OG} = \frac{\ln\left\{ \left[\frac{(\mathcal{A} - 1)/\mathcal{A}}{(\mathcal{A} - 1)/\mathcal{A}} \right] \left[(y_{in} - K x_{in})(y_{out} - K x_{in}) \right] + (1/\mathcal{A}) \right\}}{(\mathcal{A} - 1)/\mathcal{A}} \tag{6-88}$$

Using (6-88) and (6-85), the packed height, l_T , can be determined from (6-84). However, (6-88) is a very sensitive calculation when $\mathcal{A} < 0.9$.

NTU (N_{OG}) and HTU (H_{OG}) are not equal to the number of equilibrium stages, N_t , and HETP, respectively, unless the operating and equilibrium lines are straight and parallel. Otherwise, NTU is greater than or less than N_t , as shown in Figure 6.33, for the case of absorption. When the operating and equilibrium lines are straight but not parallel,

$$\text{HETP} = H_{OG} \frac{\ln(1/\mathcal{A})}{(1 - \mathcal{A})/\mathcal{A}} \tag{6-89}$$

and

$$N_{OG} = N_t \frac{\ln(1/\mathcal{A})}{(1 - \mathcal{A})/\mathcal{A}} \tag{6-90}$$

Although most applications of HTU and NTU are based on (6-84) to (6-86) and (6-88), alternative groupings have been used, depending on the driving force for mass transfer and whether the resistance to mass transfer is mostly in the gas or the liquid to which H_{OL} and N_{OL} apply. These groupings are summarized in Table 6.5. This table includes driving forces based on partial pressures, p ; mole ratios, X, Y ; concentrations, c ; and mole fractions, x, y . For later reference, Table 6.5 also provides groupings for UMD when solute concentration is not dilute.

Table 6.5 Alternative Mass-Transfer Coefficient Groupings

Driving Force	Height of a Transfer Unit, HTU			Number of a Transfer Unit, NTU		
	Symbol	EM Diffusion ^a or Dilute		Symbol	EM Diffusion or Dilute	
		UM Diffusion	UM Diffusion		UM Diffusion	UM Diffusion
1. $(y - y^*)$	H_{OG}	$\frac{V}{K_y a S}$	$\frac{V}{K'_y a (1 - y)_{LM} S}$	N_{OG}	$\int \frac{dy}{(y - y^*)}$	$\int \frac{(1 - y)_{LM} dy}{(1 - y)(y - y^*)}$
2. $(p - p^*)$	H_{OG}	$\frac{V}{K_{OG} a P S}$	$\frac{V}{K'_{OG} a (1 - y)_{LM} S}$	N_{OG}	$\int \frac{dp}{(p - p^*)}$	$\int \frac{(P - p)_{LM} dy}{(P - p)(p - p^*)}$
3. $(Y - Y^*)$	H_{OG}	$\frac{V'}{K_y a S}$	$\frac{V a}{K_y a S}$	N_{OG}	$\int \frac{dY}{(Y - Y^*)}$	$\int \frac{dY}{(Y - Y^*)}$
4. $(y - y_1)$	H_G	$\frac{V}{k_y a S}$	$\frac{V}{k'_y a (1 - y)_{LM} S}$	N_G	$\int \frac{dy}{(y - y_1)}$	$\int \frac{(1 - y)_{LM} dy}{(1 - y)(y - y_1)}$
5. $(p - p_1)$	H_G	$\frac{V}{k_G a P S}$	$\frac{V}{k'_G a (P - p)_{LM} S}$	N_G	$\int \frac{dp}{(p - p_1)}$	$\int \frac{(P - p)_{LM} dp}{(P - p)(p - p_1)}$
6. $(x^* - x)$	H_{OL}	$\frac{L}{K_x a S}$	$\frac{L}{K'_x a (1 - x)_{LM} S}$	N_{OL}	$\int \frac{dx}{(x^* - x)}$	$\int \frac{(1 - x)_{LM} dx}{(1 - x)(x^* - x)}$
7. $(c^* - c)$	H_{OL}	$\frac{L}{K_{OL} a (\rho_L/M_L) S}$	$\frac{L}{K'_{OL} a (\rho_L/M_L - c)_{LM} S}$	N_{OL}	$\int \frac{dc}{(c^* - c)}$	$\int \frac{(\rho_L/M_L - c)_{LM} dx}{(\rho_L/M_L - c)(c^* - c)}$
8. $(X^* - X)$	H_{OL}	$\frac{L'}{K_X a S}$	$\frac{L'}{K_X a S}$	N_{OL}	$\int \frac{dX}{(X^* - X)}$	$\int \frac{dX}{(X^* - X)}$
9. $(x_1 - x)$	H_L	$\frac{L}{k_x a S}$	$\frac{L}{k'_x a (1 - x)_{LM} S}$	N_L	$\int \frac{dx}{(x_1 - x)}$	$\int \frac{(1 - x)_{LM} dx}{(1 - x)(x_1 - x)}$
10. $(c_1 - c)$	H_L	$\frac{L}{k_L a (\rho_L/M_L) S}$	$\frac{L}{k'_L a (\rho_L/M_L - c)_{LM} S}$	N_L	$\int \frac{dc}{(c_1 - c)}$	$\int \frac{(\rho_L/M_L - c)_{LM} dc}{(\rho_L/M_L - c)(c_1 - C)}$

^a The substitution $K_y = K'_y y_{B,LM}$ or its equivalent can be made.

*In columns 3 and 4 of the table, $S = A_T$

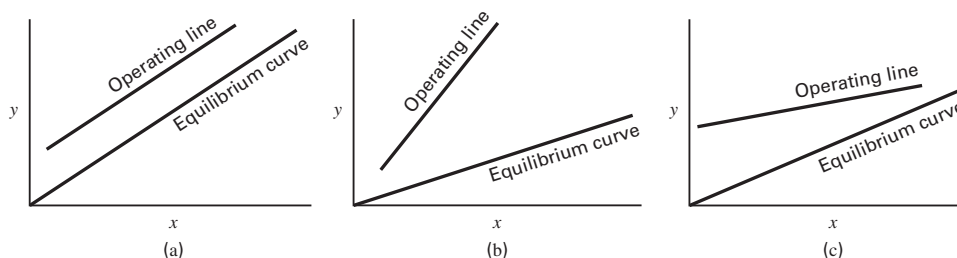


Figure 6.33 Relationship between NTU and the number of theoretical stages N_t : (a) $NTU = N_t$; (b) $NTU > N_t$; (c) $NTU < N_t$.

In the above development, gas and liquid mass-transfer coefficients are based on a mole-fraction driving force. However, other driving forces are often used for packed columns, including partial pressure and mole ratio for a gas, and concentration and mole ratio for a liquid. In those cases, (6-72) for the rate of component mass transfer, r , in moles per unit time per volume of packed bed, is written in terms of these other driving forces as

$$r = k_y a(y - y_1) = k_G a(p - p_1) = k_Y(Y - Y_1)$$

for the gas phase, and

$$r = k_x a(x_1 - x) = k_L a(c_1 - c) = k_X(X_1 - X)$$

for the liquid phase.

Occasionally, a concentration driving force is also used for the gas phase, with the same k_G symbol. When a concentration driving force is used for either the gas or the liquid, the units for the mass-transfer coefficient are length per unit time.

It is frequently necessary to convert a mass-transfer coefficient based on one driving force to another coefficient based on a different driving force. Table 3.12 provides the relationships among the different coefficients. A partial-pressure driving force is common for the gas phase, with k_G being the symbol for the mass-transfer coefficient. A molar concentration driving force is common for the liquid phase, with k_L being the symbol for the mass-transfer coefficient.

In the three examples that follow, the first and second demonstrate processes for which the gas phase resistance is dominant, and the third deals with a system for which both gas and liquid resistances exist.

EXAMPLE 6.11 Height of an Ethanol Absorber.

Repeat Example 6.1 for a tower packed with 1.5-inch metal Pall rings. If $H_{OG} = 2.0$ ft, compute the required packed height.

Solution

From Example 6.1, $V = 180$ kmol/h, $L = 151.5$ kmol/h, $y_{in} = 0.020$, $x_{in} = 0.0$, and $K = 0.57$. For 97% recovery of ethyl alcohol by material balance,

$$y_{out} = \frac{(0.03)(0.02)(180)}{180 - (0.97)(0.02)(180)} = 0.000612$$

$$\mathcal{A} = \frac{L}{KV} = \frac{151.5}{(0.57)(180)} = 1.477$$

$$\frac{y_{in}}{y_{out}} = \frac{0.020}{0.000612} = 32.68$$

From (6-88),

$$N_{OG} = \frac{\ln\{[(1.477 - 1)/1.477](32.68) + (1/1.477)\}}{(1.477 - 1)/1.477} = 7.5 \text{ transfer units}$$

The packed height, from (6-84), is $l_T = 2.0(7.5) = 15$ ft. N_t was determined in Example 6.1 to be 6.1. The 7.5 for N_{OG} is greater than N_t because the operating-line slope, L/V , is greater than the slope of the equilibrium line, K , so that Figure 6.33b applies.

EXAMPLE 6.12 Absorption of SO₂ in a Packed Column.

Air containing 1.6% SO₂ by volume is scrubbed with pure water in a packed column that is 1.5 m² in cross-sectional area and 3.5 m in packed height. Entering gas and liquid flow rates are 0.062 and 2.2 kmol/s, respectively. If the outlet mole fraction of SO₂ in the gas is 0.004 and the column temperature is near-ambient, with $K_{SO_2} = 40$, calculate (a) N_{OG} for the absorption of SO₂, (b) H_{OG} in meters, and (c) $K_y a$ for SO₂ in kmol/m³-s-(Δy).

Solution

(a) The operating line is straight because the system is dilute in SO₂.

$$\mathcal{A} = \frac{L}{KV} = \frac{2.2}{(40)(0.062)} = 0.89$$

$$y_{in} = 0.016, \quad y_{out} = 0.004, \quad x_{in} = 0.0$$

From (6-88), we know that

$$N_{OG} = \frac{\ln\{[(0.89 - 1)/0.89](0.016/0.004) + (1/0.89)\}}{(0.89 - 1)/0.89} = 3.75$$

(b) $l_T = 3.5$ m. From (6-84), $H_{OG} = l_T/N_{OG} = 3.5/3.75 = 0.93$ m.

(c) $V = 0.062$ kmol/s, $A_T = 1.5$ m². From (6-85), $K_y a = V/H_{OG} A_T = 0.062/[(0.93)(1.5)] = 0.044$ kmol/m³-s-(Δy).

EXAMPLE 6.13 Absorption of Ethylene Oxide.

A gaseous reactor effluent of 2 mol% ethylene oxide in an inert gas is scrubbed with water at 30°C and 20 atm. The gas feed rate is 2,500 lbmol/h, and the entering water rate is 3,500 lbmol/h. The column diameter is 4 ft, and the column is packed in two 12-ft-high sections with 1.5-inch metal Pall rings. A liquid redistributor is located between the packed sections. At column conditions, the

K -value for ethylene oxide is 0.85, and the estimated values of $k_y a$ and $k_x a$ are 200 lbmol/h-ft³-Δy and 165 lbmol/h-ft³-Δx. Calculate: (a) $K_y a$ and (b) H_{OG} .

Solution

(a) From (6-79),

$$K_y a = \frac{1}{(1/k_y a) + (K/k_x a)} = \frac{1}{(1/200) + (0.85/165)} = 98.5 \text{ lbmol/h-ft}^3\text{-}\Delta y$$

(b) $A_T = 3.14(4)^2/4 = 12.6 \text{ ft}^2$

From (6-85), $H_{OG} = V/K_y a A_T = 2,500/[(98.5)(12.6)] = 2.02 \text{ ft}$. In this example, both gas- and liquid-phase resistances are important. The value of H_{OG} can also be computed from values of H_G and H_L , using equations in Table 6.5:

$$H_G = V/k_y a A_T = 2,500/[(200)(12.6)] = 1.0 \text{ ft, and}$$

$$H_L = L/k_x a A_T = 3,500/[(165)(12.6)] = 1.68 \text{ ft}$$

Substituting these two expressions and (6-85) into (6-79) yields the following relationship for H_{OG} in terms of H_G and H_L :

$$H_{OG} = H_G = H_L/\mathcal{A} \quad (6-91)$$

$$\mathcal{A} = L/KV = 3,500/[(0.85)(2,500)] = 1.65, \text{ and}$$

$$H_{OG} = 1.0 + 168/1.65 = 2.02 \text{ ft}$$

§6.8 PACKED-COLUMN LIQUID HOLDUP, DIAMETER, FLOODING, PRESSURE DROP, AND MASS-TRANSFER EFFICIENCY

The values of volumetric mass-transfer coefficients and HTUs depend on gas and liquid velocities. These, in turn, depend on gas and liquid flow rates and column diameter. The estimation of column diameter for a given system, packing, and operating conditions requires the consideration of liquid holdup, loading, flooding, and pressure drop. In this section, the correlations for these characteristics stem from the extensive work of Billet and co-workers [35, 37, 38, 39, 45, 47]. In their correlations, the symbol a is the specific packing area (packing surface area per unit volume of packed bed) and not the area for interfacial mass transfer between phases per unit volume of packed bed used in §6.7, as defined in (6-72). Instead, in this section, Billet and co-workers use the symbol a_{ph} for interfacial mass transfer area.

§6.8.1 Liquid Holdup

Figures 6.34 and 6.35 present data taken from Billet [45], and shown by Stichlmair, Bravo, and Fair [46], for pressure drop in the packed bed of an air–water system at 20°C and 1 bar. The 1.5-m-high column is 0.15 m in diameter and packed with 25-mm metal Bialecki rings (similar to Pall rings in Figure 6.7). Figure 6.34 is a plot of specific pressure drop (pressure drop per unit height), $\Delta P/l$, in meters of water per meters of packed height versus the superficial gas velocity,

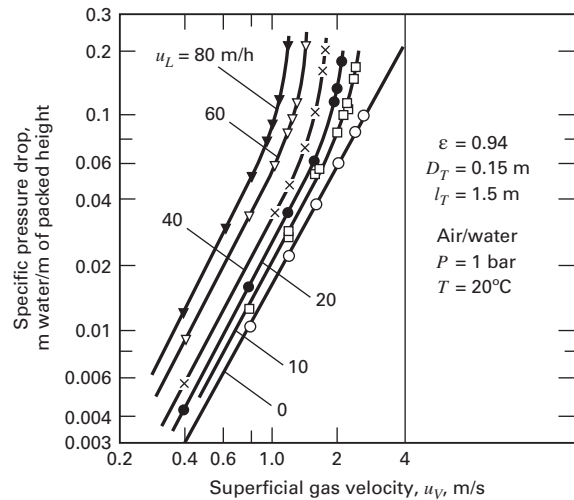


Figure 6.34 Specific pressure drop for dry and irrigated 25-mm metal Bialecki rings.

[From R. Billet, *Packed Column Analysis and Design*, Ruhr-University Bochum (1989) with permission.]

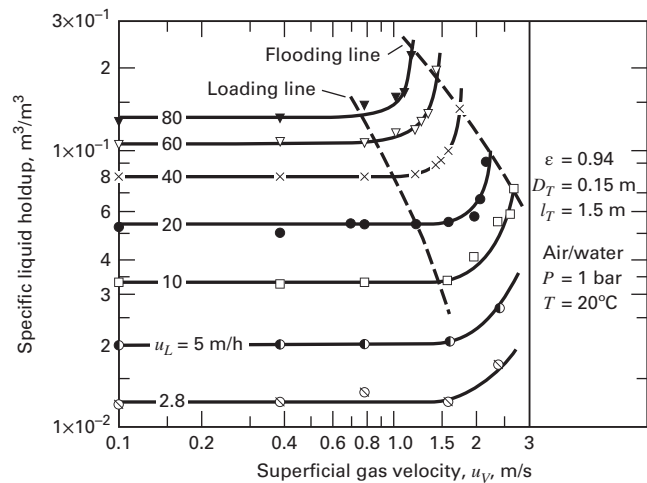


Figure 6.35 Specific liquid holdup for irrigated 25-mm metal Bialecki rings.

[From R. Billet, *Packed Column Analysis and Design*, Ruhr-University Bochum (1989) with permission.]

u_v , in m/s, with a parameter of superficial liquid velocity, u_L , in m/h. Superficial velocity is a term applied to flows in towers, pipes, ducts, and similar structures that may not contain obstructions such as packings. It is the velocity that one of the phases would have if it were the only one flowing and if there were no obstructions (e.g., packing) for a given cross-sectional area. The superficial velocity of a phase is equal to the phase volumetric flow rate divided by the cross-sectional area.

EXAMPLE 6.14 Superficial Velocities in a Packed Bed.

Calculate the superficial liquid and gas velocities for ethanol absorption from CO₂ into water, as described in Example 6.2, assuming the use of a 3-ft-diameter column packed with 50-mm ceramic Pall

rings. Use a process simulator to obtain molecular weights and densities.

Solution

The calculations apply at the top of the packed column.

From Example 6.2, we determine the following values:

$$L = 149 \text{ kmol/h}, V = 180 - 3.5 + 5.7 = 182.2 \text{ kmol/h}$$

$$\text{Molecular weights: } M_L = 18.02, M_V = 43.2$$

$$\text{Densities at column conditions: } \rho_L = 995 \text{ kg/m}^3,$$

$$\rho_V = 1.919 \text{ kg/m}^3$$

$$\text{Volumetric flow rates: } Q_L = 149(18.02)/995 = 2.70 \text{ m}^3/\text{h},$$

$$Q_V = 182.2(43.2)/1.919 = 4,100 \text{ m}^3/\text{h} = 1.14 \text{ m}^3/\text{s}$$

$$\begin{aligned} \text{Column inside cross-sectional area} &= 3.14(3)^2/4 = A_T \\ &= 7.065 \text{ ft}^2 = 0.656 \text{ m}^2 \end{aligned}$$

$$\text{Superficial velocities: } u_L = Q_L/A_T = 2.70/0.656 = 4.12 \text{ m/h},$$

$$u_V = Q_V/A_T = 1.14/0.656 = 1.74 \text{ m/s}$$

The actual velocities are much higher because the ceramic Pall rings occupy approximately 25% of the bed volume and both the liquid and vapor are flowing through the column. A method discussed below for estimating the liquid holdup in the column allows the actual velocities to be calculated.

In Figure 6.34, the lowest curve corresponds to zero liquid flow. Over a 10-fold range of superficial air velocity, pressure drop is proportional to velocity to the 1.86 power. At increasing liquid flows, the gas-phase pressure drop for a given velocity increases. Below a limiting gas velocity, the curve for each liquid velocity is a straight line parallel to the dry pressure-drop curve. In this region, the specific liquid holdup (liquid holdup per unit volume of bed) in the packing for a given liquid velocity remains constant, as seen in Figure 6.35. For a liquid velocity of 40 m/h, the specific liquid holdup is $0.08 \text{ m}^3/\text{m}^3$ of packed bed (8% of the packed volume is liquid), until a superficial gas velocity of 1.0 m/s is reached. The packing of 25-mm metal Bialecki rings has a packed-column void fraction, ϵ , of 0.94 (i.e., the rings occupy only 6% of the packed volume). With a liquid holdup of 8%, the volume available for gas flow is $100 - 6 - 8 = 86$ or 86% of the packed bed volume. From Figure 6.35, as the superficial water velocity is increased from 0 to 40 m/h at a constant superficial gas velocity of 1.0 m/s, the specific gas pressure drop rises from 0.0155 to 0.031 m water/m packed height.

The upper superficial gas velocity limit for a constant liquid holdup is the **loading point**. Below this point, the gas phase is the continuous phase, and liquid trickles down over the surface of the packing, without being influenced by the gas flow. The liquid holdup depends only on the liquid flow. Above the loading point, gas begins to hinder the downward flow of liquid, and liquid holdup begins to load the bed, replacing gas and causing a sharp pressure-drop increase. Finally, the gas reaches a velocity at which the liquid is continuous across the

top of the packing and the column is flooded. At the **flooding point**, the gas drag force is sufficient to entrain all of the liquid. Both loading and flooding lines are shown as dashed lines in Figure 6.35.

In the loading region, column operation is unstable. Typically, the superficial gas velocity at the loading point is approximately 70% of that at the flooding point. Although a packed column can operate in the loading region, a packed column is best designed for operation at or below the loading point, in the **preloading region**.

A dimensionless expression for specific liquid holdup, h_L , in the preloading region was developed by Billet and Schultes [39, 45], using a database of over 3,500 data points for more than 50 test systems and over 70 types of random and structured packings. The liquid holdup depends on packing characteristics, as well as liquid viscosity, density, and superficial velocity. It does not depend on the superficial gas velocity, and it can be expressed as

$$h_L = \left(12 \frac{N_{FrL}}{N_{ReL}} \right)^{1/3} \left(\frac{a_h}{a} \right)^{2/3} \quad (6-92)$$

where

$$N_{ReL} = \text{liquid Reynolds number} = \frac{\text{inertial force}}{\text{viscous force}} = \frac{u_L \rho_L}{a \mu_L} \quad (6-93)$$

$$N_{FrL} = \text{liquid Froude number} = \frac{\text{inertial force}}{\text{gravitational force}} = \frac{u_L^2 a}{g} \quad (6-94)$$

and the ratio of the specific hydraulic area of the packing (hydraulic area per unit volume of packed bed), a_h , to the specific surface area of the packing (area per unit volume of packed bed), a , is given by

$$a_h/a = C_h N_{ReL}^{0.15} N_{FrL}^{0.1}, \quad \text{for } N_{ReL} < 5, \text{ and} \quad (6-95)$$

$$a_h/a = 0.85 C_h N_{ReL}^{0.25} N_{FrL}^{0.1}, \quad \text{for } N_{ReL} \geq 5 \quad (6-96)$$

Values of $a_h/a > 1$ are possible because of droplets and jet flow in addition to the rivulets that cover the packing surface [40].

Table 6.6 lists the values of a and C_h , together with packing void fraction, ϵ , and other constants for both random and structured packings. At low liquid velocities, liquid holdup is low, and it is possible that some of the packing is dry, causing packing efficiency to decrease dramatically, particularly for aqueous systems with high surface tension. For adequate wetting, liquid distributors and redistributors must be used, and superficial liquid velocities should exceed the following values:

Type of Packing Material	$u_{L_{min}}$, m/s
Ceramic	0.0015
Oxidized or etched metal	0.0003
Bright metal	0.0009
Plastic	0.0012

Table 6.6 Characteristics of Packings

Packing	Material	Size	$F_p, \text{ft}^2/\text{ft}^3$	$a, \text{m}^2/\text{m}^3$	$\epsilon, \text{m}^3/\text{m}^3$	C_h	C_L	C_V	
Random:									
Berl saddles	Ceramic	25 mm	110	260.0	0.680	0.620	1.246	0.387	
Berl saddles	Ceramic	13 mm	240	545.0	0.650	0.833	1.364	0.232	
Bialecki rings	Metal	50 mm		121.0	0.966	0.798	1.721	0.302	
Bialecki rings	Metal	35 mm		155.0	0.967	0.787	1.412	0.390	
Bialecki rings	Metal	25 mm		210.0	0.956	0.692	1.461	0.331	
Cascade Mini-Rings	Metal	30 PMK		180.5	0.975	0.930	1.920	0.450	
Cascade Mini-Rings	Metal	30 P		164.0	0.959	0.851	1.577	0.398	
Cascade Mini-Rings	Metal	1.5 inch	24	174.9	0.974	0.935			
Cascade Mini-Rings	Metal	1.5 inch, T		188.0	0.972	0.870			
Cascade Mini-Rings	Metal	1.0 inch	40	232.5	0.971	1.040			
Cascade Mini-Rings	Metal	0.5 inch		356.0	0.952	1.338	2.038	0.495	
Hackettes	Plastic	45 mm		139.5	0.928	0.643			
Hiflow rings	Ceramic	75 mm	15	54.1	0.868		1.377	0.379	
Hiflow rings	Ceramic	50 mm	29	89.7	0.809		1.659	0.464	
Hiflow rings	Ceramic	38 mm	37	111.8	0.788		1.744	0.465	
Hiflow rings	Ceramic	20 mm		286.2	0.758	1.167			
Hiflow rings	Metal	50 mm	16	92.3	0.977	0.876	1.168	0.408	
Hiflow rings	Metal	25 mm	42	202.9	0.962	0.799	1.641	0.402	
Hiflow rings	Plastic	90 mm	9	69.7	0.968				
Hiflow rings	Plastic	50 mm	20	117.1	0.924	1.038	1.487	0.345	
Hiflow rings	Plastic	25 mm	42	194.5	0.918	1.577	1.577	0.390	
Hiflow rings, super	Plastic	50 mm, S		82.0	0.942	0.881	1.219	0.342	
Hiflow saddles	Plastic	50 mm		86.4	0.938				
IMTP	Metal	25 mm	41	207	0.97				
IMTP	Metal	40 mm	24	151	0.97				
IMTP	Metal	50 mm	18	98	0.98				
IMTP	Metal	70 mm	12	60	0.98				
Intalox saddles	Ceramic	50 mm	40	114.6	0.761				
Intalox saddles	Plastic	50 mm	28	122.1	0.908				
Pall rings	Ceramic	50 mm	43	142	0.754	1.066	1.278	0.333	
Pall rings	Metal	90 mm	18	66	0.97				
Pall rings	Metal	50 mm	27	105	0.96	0.784	1.192	0.410	
Pall rings	Metal	38 mm	40	130	0.95	0.644	1.012	0.341	
Pall rings	Metal	25 mm	56	205	0.94	0.719	1.440	0.336	
Pall rings	Metal	16 mm	78	360	0.92	0.590			
Pall rings	Plastic	50 mm	26	111.1	0.919	0.593	1.239	0.368	
Pall rings	Plastic	35 mm	40	151.1	0.906	0.718	0.856	0.380	
Pall rings	Plastic	25 mm	55	225.0	0.887	0.528	0.905	0.446	
Ralu rings	Plastic	50 mm	17	110	0.983	0.640	1.520	0.303	
Ralu rings	Plastic	38 mm	24	150	0.930	0.640	1.320	0.333	
Ralu rings	Plastic	25 mm	41	190	0.940	0.719	1.320	0.333	
Ralu rings	Metal	50 mm	20	105	0.975	0.784	1.192	0.345	
Ralu rings	Metal	38 mm	28	135	0.965	0.644	1.277	0.341	
Ralu rings	Metal	25 mm	48	215	0.960	0.714	1.440	0.336	
Raschig rings	Carbon	25 mm		202.2	0.720	0.623	1.379	0.471	

(Continued)

Table 6.6 (Continued)

Packing	Material	Size	$F_p, \text{ft}^2/\text{ft}^3$	$a, \text{m}^2/\text{m}^3$	$\epsilon, \text{m}^3/\text{m}^3$	C_h	C_L	C_v
Raschig rings	Ceramic	25 mm	179	190.0	0.680	0.577	1.361	0.412
Raschig rings	Ceramic	15 mm	380	312.0	0.690	0.648	1.276	0.401
Raschig rings	Ceramic	10 mm	1,000	440.0	0.650	0.791	1.303	0.272
Raschig rings	Ceramic	6 mm	1,600	771.9	0.620	1.094	1.130	
Raschig rings	Metal	15 mm	170	378.4	0.917	0.455		
Raschig Super-Rings	Metal	No. 0.3		315	0.960	0.750	1.500	0.450
Raschig Super-Rings	Metal	No. 0.5		250	0.975	0.620	1.450	0.430
Raschig Super-Rings	Metal	No. 1		160	0.980	0.750	1.290	0.440
Raschig Super-Rings	Metal	No. 2	28	97.6	0.985	0.720	1.323	0.400
Raschig Super-Rings	Metal	No. 3	15	80	0.982	0.620	0.850	0.300
Raschig Super-Rings	Plastic	No. 2	15	100	0.960	0.720	1.250	0.337
Super Intalox	Ceramic	25 mm	40	207	0.90			
Super Intalox	Ceramic	50 mm	28	108	0.93			
Super Intalox	Ceramic	75 mm	18	59	0.96			
Tellerettes	Plastic	25 mm	40	190	0.930	0.588	0.899	2.913
VSP rings	Metal	50 mm, no. 2	21	104.6	0.980	1.135	1.222	0.420
VSP rings	Metal	25 mm, no. 1	32	199.6	0.975	1.369	1.376	0.405
Structured:								
Euroform®	Plastic	PN-110		110	0.936	0.511	0.973	0.167
Flexeramic	Ceramic	28	40	260	0.66			
Flexeramic	Ceramic	24	24	160	0.77			
Flexeramic	Ceramic	15	15	100	0.86			
Flexipac HC	Metal	700	68	710	0.96			
Flexipac HC	Metal	1Y	25	420	0.98			
Flexipac HC	Metal	1.6Y	17	290	0.99			
Flexipac HC	Metal	2Y	13	220	0.99			
Gempak	Metal	A2 T-304		202	0.977	0.678		
Impulse®	Ceramic	100		91.4				
Impulse	Metal	250		250	0.838	1.900	1.317	0.327
Koch-Sulzer	Metal	CY	70	700	0.85	0.431	0.983	0.270
Koch-Sulzer	Metal	BX	21	492	0.90			
Mellapak	Plastic	250 Y	22	250	0.970			
Mellapak	Metal	2X	7	223	0.99	0.554		
Mellapak	Metal	1.25X	5	125	0.99			
Mellapak	Metal	250X	8	250	0.98			
Mellapak	Metal	500X	25	500	0.98			
Mellapak Plus	Metal	252Y	12	250	0.98			
Mellapak Plus	Metal	452Y	21	350	0.98			
Mellapak Plus	Metal	752Y	40	500	0.98			
Montz	Metal	BI-100		100	0.987			
Montz	Metal	BI-200		200	0.979	0.547	0.971	0.390
Montz	Metal	BI-300	33	300	0.930	0.482	1.165	0.422
Montz	Plastic	CI-200		200	0.954		1.006	0.412
Montz	Plastic	C2-200		200	0.900		0.739	
Ralu Pak®	Metal	YC-250		250	0.945		1.334	0.385
Super-Pak	Metal	250	17	250	0.98			
Super-Pak	Metal	350	21	350	0.98			

EXAMPLE 6.15 Liquid Holdup for Two Packings.

An absorber uses an oil absorbent with a kinematic viscosity, μ/ρ , three times that of water at 20°C. The superficial liquid velocity is 0.01 m/s, which assures good wetting. The superficial gas velocity is in the preloading region. Two packings are considered: (1) randomly packed metal 1.5-inch Cascade Mini-Rings (CMR) and (2) metal Mellapak 250Y structured packing. Estimate the specific liquid holdup for each.

Solution

From Table 6.6,

Packing	$a, \text{m}^2/\text{m}^3$	ϵ	C_h
1.5-inch CMR	174.9	0.974	0.935
Mellapak 250Y	250.0	0.970	0.554

At 20°C for water, the kinematic viscosity, μ/ρ , is $1 \times 10^{-6} \text{ m}^2/\text{s}$. Therefore, for the oil, $\mu/\rho = 3 \times 10^{-6} \text{ m}^2/\text{s}$. From (6-93) and (6-94),

$$N_{\text{Re}_L} = \frac{0.01}{3 \times 10^{-6} a}, \quad N_{\text{Fr}_L} = \frac{(0.01)^2 a}{9.8}.$$

These equations yield the following values:

Packing	N_{Re_L}	N_{Fr_L}
CMR	19.1	0.00178
Mellapak	13.3	0.00255

Use (6-96) for both packings, because $N_{\text{Re}_L} > 5$. For the CMR,

$$a_h/a = (0.85)(0.935)(19.1)^{0.25}(0.00178)^{0.1} = 0.882$$

For Mellapak,

$$a_h/a = 0.85(0.554)(13.3)^{0.25}(0.00255)^{0.10} = 0.495$$

From (6-92) for CMR,

$$h_L = \left(12 \frac{0.00178}{19.1}\right)^{1/3} (0.882)^{2/3} = 0.0955 \text{ m}^3/\text{m}^3$$

From (6-92) for Mellapak,

$$h_L = \left(12 \frac{0.00255}{13.3}\right)^{1/3} (0.495)^{2/3} = 0.0826 \text{ m}^3/\text{m}^3$$

For the CMR random packing, the void fraction available for gas flow is reduced by the liquid holdup from $\epsilon = 0.974$ to $(0.974 - 0.0955) = 0.879 \text{ m}^3/\text{m}^3$. For Mellapak, the reduction is from 0.970 to $(0.970 - 0.0826) = 0.887 \text{ m}^3/\text{m}^3$.

§6.8.2 Pressure Drop, Flooding, and Column Diameter

Liquid holdup, column diameter, and pressure drop in random packed beds are closely related. The diameter must be such that flooding is avoided and pressure drop is not excessive

[below 2 inches of water (equivalent to 0.072 psi)/ft of packed height]. For stable operation, the preloading region is preferred, and the loading region should be avoided. Also, the nominal packing diameter must not be greater than one-eighth of the diameter of the column. Otherwise, poor distribution of liquid and vapor flows can occur.

Flooding data for packed columns were first correlated by Sherwood et al. [26], who used a liquid-to-gas kinetic-energy ratio,

$$F_{LV} = \left(\frac{LM_L}{VM_V}\right) \left(\frac{\rho_V}{\rho_L}\right)^{0.5} \quad (6-97)$$

The superficial gas velocity at flooding, u_V , was embedded in a dimensionless capacity factor, $(u_V^2 a / g \epsilon^3)$, by considering the square of the actual gas velocity, u_V^2 / ϵ^2 ; a hydraulic radius, $r_H = \epsilon/a$, (i.e., the flow volume divided by the surface area of the packing); and the gravitational constant, g . The capacity factor was further multiplied by $(\rho_V / \rho_L) \mu^{0.2}$. The resulting plot of $(u_V^2 a / g \epsilon^3) (\rho_V / \rho_L) \mu$ vs. F_{LV} correlated flooding data over two orders of magnitude of F_{LV} for first-generation packings.

In 1954, Leva [48] used experimental data on Raschig-ring and Berl-saddle packings to extend the work of Sherwood et al. [26] by adding lines of constant pressure drop. To improve accuracy, the group a/ϵ^3 was replaced by a packing factor, F_p , which was back-calculated from experimental pressure-drop data. The resulting chart became known as the generalized pressure-drop correlation (GPDC). A further revision of the correlation was published by Leva [49] in 1992. Leva's GPDC predicts a specific pressure drop at flooding greater than 1.5 inches $\text{H}_2\text{O}/\text{ft}$ of packed height. However, modern random packings are found to flood at lower pressure drops, causing more recent GPDC charts to drop the flooding curve. Also, predicted pressure drops with GPDC charts are not accurate enough for structured packings.

It is now common to use two generalized pressure-drop charts—one for random packings and one for structured packings. Two such charts from Strigle [32] and Kister and Gill [33] are shown in Figures 6.36 and 6.37. The abscissa in both charts is F_{LV} , given by (6-97). The empirical ordinate in both charts is a modified empirical capacity factor given by

$$F_C = u_V F_P^{0.5} \left(\frac{\rho_V}{\rho_L - \rho_V}\right)^{0.5} v_L^{0.05} \quad (6-98)$$

with ρ_L and ρ_V in the same units, u_V in ft/s, F_P in ft^{-1} , and the kinematic viscosity, v_L , in centistokes. Values of F_P are included in Table 6.6.

For modern random and structured packings with packing factors, F_P , between 9 and 60 ft^{-1} , Kister and Gill [50] show that the specific pressure drop at flooding is less than 2 inches $\text{H}_2\text{O}/\text{ft}$, as given by the simple empirical correlation

$$\Delta P_{\text{flood}} = 0.115 F_P^{0.7} \quad (6-99)$$

with ΔP_{flood} in inches $\text{H}_2\text{O}/\text{ft}$ of packed height and F_P in ft^{-1} . For packings with $F_P = 9$, at the limit of the applicability of (6-99), the predicted specific pressure drop at flooding is only

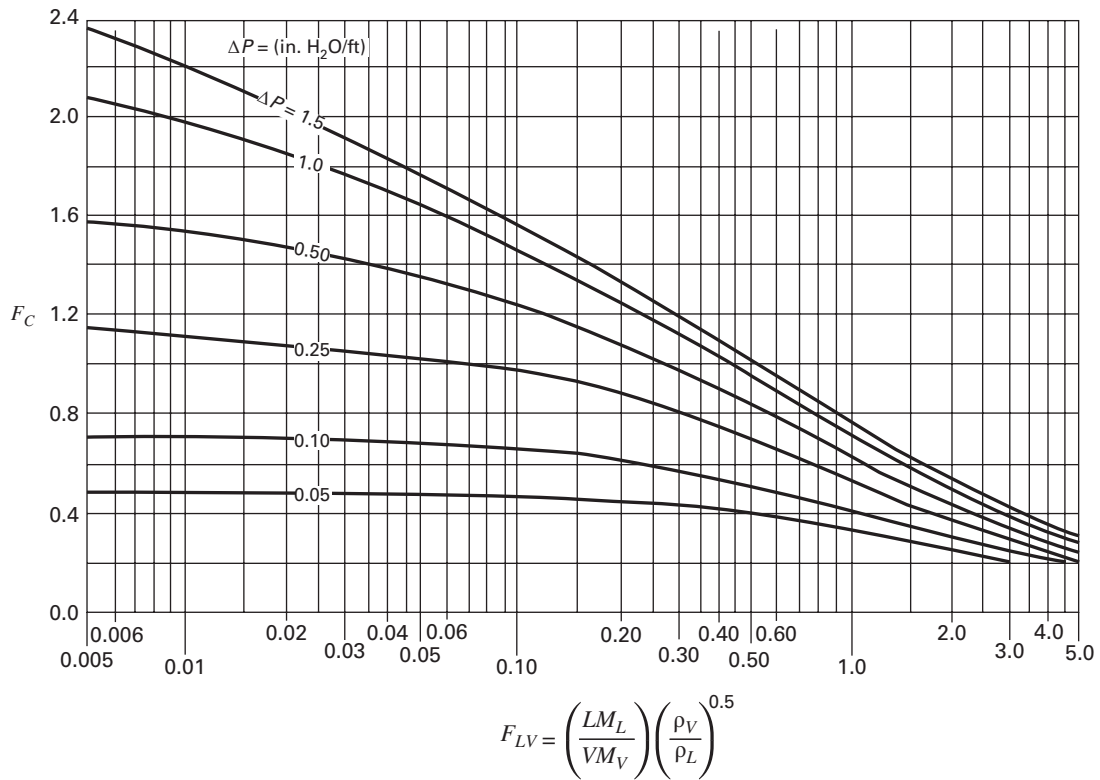


Figure 6.36 Generalized correlation for specific pressure drop for towers with random packing.
 [Reproduced from [32] with permission from Gulf Publishing Company]

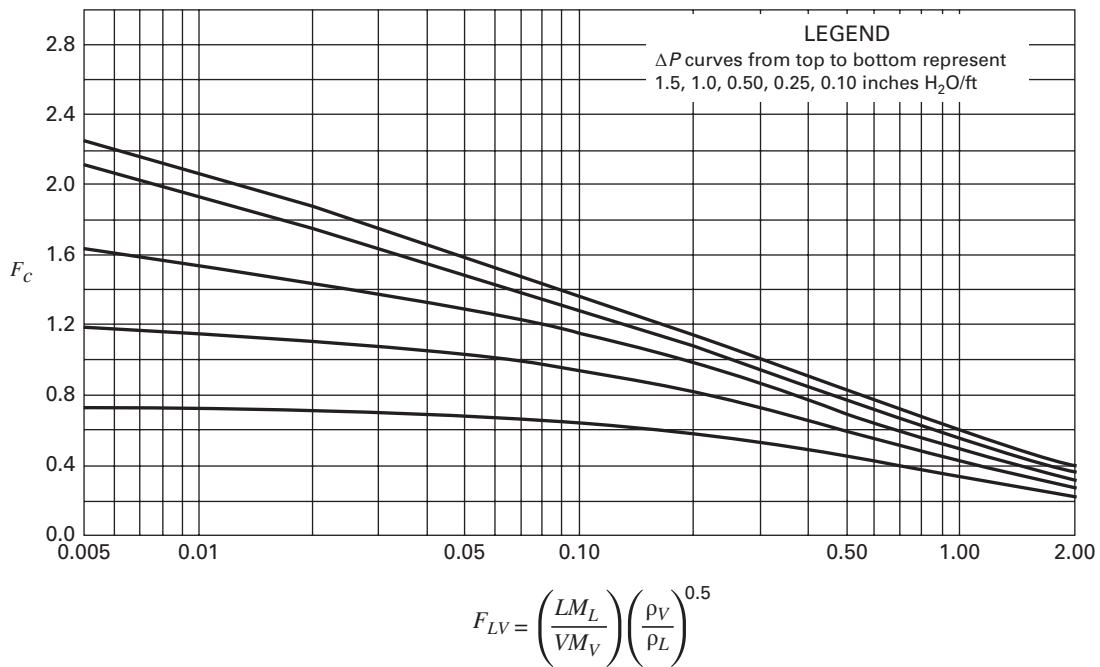


Figure 6.37 Generalized correlation for specific pressure drop for towers with structured packing.
 [Reproduced from [56] with permission from the Institution of Chemical Engineers]

0.54 inches of H₂O/ft of packing. Equation (6-99) is applicable to all packings with exception of first-generation ceramic Raschig rings and Berl saddles, which have values of ΔP_{flood} in inches H₂O/ft ranging from 2.5 for larger sizes to 4 for smaller sizes.

An approximate method for estimating specific pressure drop and packed diameter for packings other than Raschig rings and Berl saddles is as follows:

1. Select a random packing or a structured packing and select its packing factor in Table 6.6.
2. Calculate ΔP_{flood} from (6-99).
3. Calculate F_{LV} from (6-97).
4. For random packings, read F_C from Figure 6.36 for random packings or Figure 6.37 for structured packings.
5. Calculate the superficial vapor velocity from (6-98). This is the estimated flooding velocity, u_{vf} .
6. Select a fraction of flooding, f , from 50 to 70% of the estimated flooding velocity.
7. Calculate the inside diameter of the packed tower from the following modification of (6-63):

$$D_T = \left[\frac{4VM_V}{fu_f \pi \rho_V} \right]^{0.5} \quad (6-100)$$

8. Calculate F_C using $u_V = fu_{vf}$, and for F_{LV} , read off the specific pressure drop from Figure 6.36 or 6.37.

Theoretical models for pressure drop are presented by Stichlmair et al. [46], who used a particle model, and Billet and Schultes [35, 39], who used a channel model. Both extend equations for dry-bed pressure drop to account for the effect of liquid holdup. Billet and Schultes [39] include predictions of superficial vapor velocity at the loading point, which is useful for predicting column diameter for operation at the loading point or some fraction of it. These models are included in some of the process simulators.

EXAMPLE 6.16 Flooding, Diameter, and Pressure Drop for an NH₃ Absorber.

Two hundred lbmol/h of air containing 5 mol% NH₃ enters a column packed with No. 2 Raschig Super Rings at 20°C and 1 atm, so that 90% of the ammonia is scrubbed by a countercurrent flow of 15,000 lb/h of water. Estimate the superficial gas flooding velocity, the column's inside diameter for operation at 70% of flooding, and the pressure drop per foot of packing.

Solution

Calculations are made for the bottom of the column, where the superficial gas velocity is highest.

For the inlet gas,

$$\begin{aligned} M_V &= 0.95(29) + 0.05(17) = 28.4, \quad V = 200 \text{ lbmol/h.} \\ \rho_V &= PM_V/RT = (1)(28.4)/[(0.730)(293)(1.8)] \\ &= 0.0738 \text{ lb/ft}^3 \end{aligned}$$

For the exiting liquid,

$$\begin{aligned} \text{NH}_3 \text{ absorbed} &= 0.90(0.05)(200)(17) = 153 \text{ lb/h or } 9.0 \text{ lbmol/h} \\ \text{Water rate (assumed constant)} &= 15,000 \text{ lb/h or } 834 \text{ lbmol/h} \\ \text{Mole fraction of ammonia} &= 9/(834 + 9) = 0.0106 \\ M_L &= 0.0106(17) + (0.9893)(18) = 17.9 \\ L &= 9 + 834 = 843 \text{ lbmol/h} \end{aligned}$$

From Table 6.6, F_p for No. 2 Raschig Super Rings is 15. From (6-99), $\Delta P_{\text{flood}} = 0.115F_p^{0.7} = 0.115(15)^{0.7} = 0.766$ inches H₂O/ft of packed height.

Let $\rho_L = 62.4$ lb/ft³, $\mu_L = 1.0$ cP, and $\nu_L = 1.0$ centistokes. From (6-97),

$$F_{LV} = \frac{(843)(17.9)}{(200)(28.4)} \left(\frac{0.0738}{62.4} \right)^{0.5} = 0.091$$

From Figure 6.36 for random packings, $F_C = 1.28$

Using (6-98),

$$\begin{aligned} u_{vf} &= \frac{F_C}{F_p^{0.5} \left(\frac{\rho_V}{\rho_L - \rho_V} \right)^{0.5} \nu_L^{0.05}} \\ &= \frac{1.28}{14.9^{0.5} \left(\frac{0.0738}{62.4 - 0.0738} \right)^{0.5} 1^{0.05}} = 9.64 \text{ ft/s} \end{aligned}$$

Assume a fraction of flooding $f = 0.70$. Design superficial vapor velocity = $0.7(9.64) = 6.75$ ft/s, so that

$$D_T = \left[\frac{4VM_V}{fu_{vf} \pi \rho_V} \right]^{0.5} = \left[\frac{4(200/3600)(28.4)}{0.7(9.64)(3.14)(0.0738)} \right]^{0.5} = 2.0 \text{ ft}$$

From (6-100), F_C is directly proportional to the superficial vapor velocity. Therefore, F_C at the design velocity = $1.28(0.7) = 0.90$. From Figure 6.36, $\Delta P = 0.60$ inches H₂O/ft packed height.

§6.8.3 Mass-Transfer Efficiency

Packed-column mass-transfer efficiency is characterized by HETP, HTUs, and volumetric mass-transfer coefficients. Although the HETP concept lacks a theoretical basis, its simplicity, coupled with the relative ease of making equilibrium-stage calculations, has made it a widely used method for estimating packed height. In the preloading region, with good distribution of vapor and liquid, HETP values depend mainly on the packing type and its size, D_p , liquid viscosity, and surface tension. For preliminary estimates, the following relations, taken from Kister [33], can be used.

1. Pall rings and similar high-efficiency random packings with low-viscosity liquids:

$$\text{HETP, ft} = 1.5D_p \text{ (in inches)} \quad (6-101)$$

2. Structured packings at low-to-moderate pressure with low-viscosity liquids:

$$\text{HETP, ft} = 100/a \text{ (in ft}^2\text{/ft}^3\text{)} + 4/12 \quad (6-102)$$

3. Absorption with viscous liquid:

$$\text{HETP} = 5 \text{ to } 6 \text{ ft}$$

4. Vacuum service:

$$\text{HETP, ft} = 1.5D_p \text{ (in inches)} + 0.5 \quad (6-103)$$

5. High-pressure service (> 200 psia):

HETP for structured packings may be greater than predicted by (6-102).

6. Small-diameter towers, $D_T < 2$ ft:

$$\text{HETP (in ft)} = D_T \text{ (in ft)}, \text{ but not less than 1 ft}$$

In general, lower values of HETP are achieved with smaller-size random packings, particularly in small-diameter columns, as well as for through-flow random packings and structured packings with large values of a , which is the packing surface area per packed volume.

Vendors of tower packings often display experimental values of HETP at a constant ratio of L/V as a function of a superficial-vapor-velocity F -factor, F_V , defined by

$$F_V = u_V(\rho_V)^{0.5} \quad (6-104)$$

where F_V has units of $(\text{m/s})(\text{kg/m}^3)^{0.5}$. When liquid and vapor flows are distributed uniformly over the tower cross section in the preloading region, the experimental HETP data exhibit the characteristics shown in Figure 6.38. Point B is the loading point, below which, in the preloading region, the HETP remains relatively constant until point A is reached, after which maldistribution of flow causes a rapid rise in HETP. As the loading region is entered to the right of B, the HETP sometimes drops because of increased liquid holdup, but it then rises rapidly as entrainment increases and flooding is approached at point C. In the preloading region, the turndown ratio corresponds to $(F_V)_B/(F_V)_A$.

Mass-transfer data for packed columns are usually correlated in terms of volumetric mass-transfer coefficients and HTUs, rather than in terms of HETPs. Because the data come from experiments in which either the liquid- or gas-phase mass-transfer resistance is negligible, the dominant resistance can be correlated independently. For applications where both resistances are important, they are added to obtain the overall

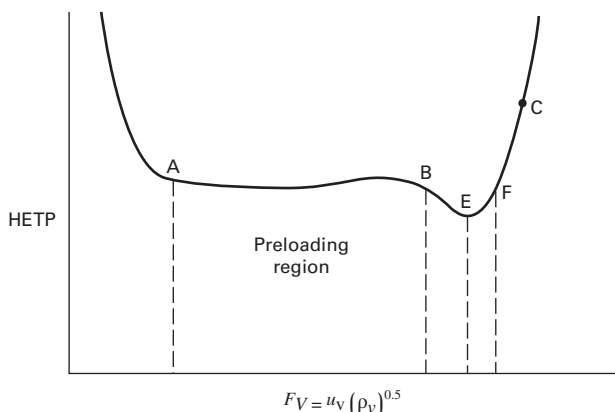


Figure 6.38 Typical variation of HETP with gas capacity factor in packed towers.

resistance, according to the two-film theory discussed in §3.7. This theory assumes equilibrium at the interface of the vapor and liquid phases (i.e., the absence of mass-transfer resistance at the interface).

Equations (6-72) and (6-79) define the overall gas-phase coefficient in terms of the individual volumetric mass-transfer coefficients and the mass-transfer rates in terms of mole-fraction driving forces and the vapor-liquid K -value. In (6-79), the term on the LHS is the overall mass-transfer resistance. The two terms on the RHS from left-to-right are the gas-phase mass-transfer resistance and the liquid-phase mass-transfer resistance, respectively. Often, one of the two phase resistances is significantly larger than the other, and the larger resistance is the controlling one.

Mass-transfer rates can also be expressed in terms of liquid-phase concentrations and gas-phase partial pressure:

$$r = k_G a(p - p_1) = k_L a(c_1 - c) = K_G a(p - p^*) \quad (6-105)$$

For gas partial pressure and liquid concentration driving forces, it is convenient to relate them by Henry's law, (6-39), where $y_i = H_i x_i/P$. Replacing y_i with p_i/P and x_i with $cV_L = cM_L/\rho_L$, and then dropping the component i subscript, gives the modified Henry's law,

$$p = H \left(\frac{M_L}{\rho_L} \right) c = H' c \quad (6-106)$$

At the equilibrium interface between the two phases,

$$p_1 = H' c_1 \quad (6-107)$$

Let

$$p^* = H' c \quad (6-108)$$

Then, (6-105) can be converted to

$$\frac{1}{K_G a} = \frac{1}{k_G a} + \frac{H'}{k_L a} \quad (6-109)$$

Other formulations for the mass-transfer coefficient are given in Table 6.5, with the most common units as follows:

	SI Units	American Engineering Units
r	$\text{mol/m}^3\text{-s}$	$\text{lbmol/ft}^3\text{-h}$
$k_y a, k_x a, K_y a, K_x a$	$\text{mol/m}^3\text{-s}$	$\text{lbmol/ft}^3\text{-h}$
$k_G a, K_G a$	$\text{mol/m}^3\text{-s-kPa}$	$\text{lbmol/ft}^3\text{-h-atm}$
$k_L a, K_L a$	s^{-1}	h^{-1}

As shown in Table 6.5, mass-transfer coefficients are directly related to HTUs, which have the advantages of (1) only one dimension (length), (2) variation with column conditions less than mass-transfer coefficients, and (3) a relationship to an easily understood geometrical quantity, height per equilibrium stage. Definitions of individual and overall HTUs are included in Table 6.5 for the dilute solute case. Substituting these into (6-79) gives

$$(\text{HTU})_G = H_{OG} = H_G + (KV/L)H_L \quad (6-110)$$

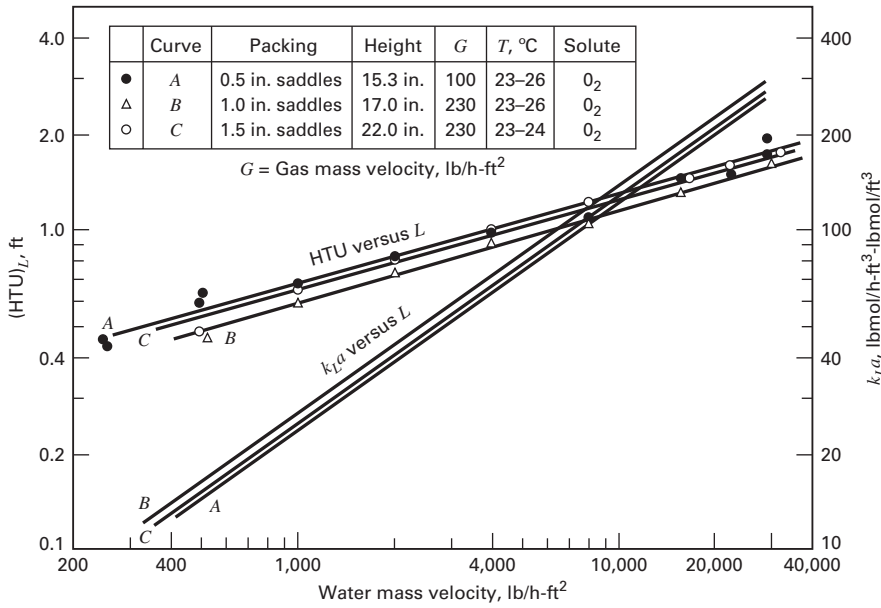


Figure 6.39 Effect of liquid rate on absorption of O₂ from air into water. [Reproduced from [36] with permission of the American Institute of Chemical Engineers]

Alternatively, (6-110) can be written for H_{OL} :

$$(HTU)_L = H_{OL} = H_L + H_G/(KV/L) \quad (6-111)$$

In the absorption or stripping of low-solubility gases (e.g., O₂, N₂, CO, and CO₂), the solute K -value or Henry's law constant, H' , in (6-107), is large, making the liquid-phase resistance in (6-109) to (6-111) large. Then, the gas-phase resistance is negligible, and the rate of mass transfer is liquid-phase-controlled. Such data are used to study the effect of variables on volumetric liquid-phase mass-transfer coefficients and HTUs. Figure 6.39 shows data for three different-size Berl-saddle packings for stripping O₂ from water by air, in a 20-inch-I.D. column operating in the preloading region, as reported in a study by Sherwood and Holloway [36]. The rate of mass transfer is controlled by the liquid phase. The effect of liquid velocity on $k_L a$ is pronounced, with $k_L a$ increasing by the 0.75 power of the liquid mass velocity, $u_L \rho$. Gas velocity has no effect on $k_L a$ in the preloading region. Figure 6.39 also contains data plotted in terms of H_L , where

$$H_L = \frac{M_L L}{\rho_L k_L a A_T} \quad (6-112)$$

Figure 6.39 shows clearly that $H_L = (HTU)_L$ does not depend as strongly on liquid mass velocity as $k_L a$ does.

Another liquid-phase mass-transfer-controlled system is CO₂-air-H₂O. Measurements for Pall rings and Hiflow rings, reported by Billet [45], are shown in Figure 6.40. For the same system, Figure 6.41 shows the effect of gas velocity on $k_L a$ in terms of the F_V -factor at a constant liquid rate. Up to an F_V -factor of about $1.8 \text{ m}^{-1/2}\text{-s}^{-1}\text{-kg}^{1/2}$, which is in the preloading region, no effect of gas velocity is observed. Above the loading limit, $k_L a$ increases with gas velocity because the larger liquid holdup increases interfacial area for mass

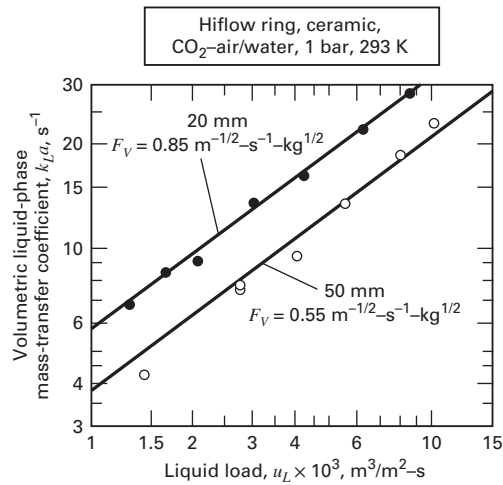


Figure 6.40 Effect of liquid load on liquid-phase mass transfer of CO₂.

[From R. Billet, *Packed Column Analysis and Design*, Ruhr-University Bochum (1989) with permission.]

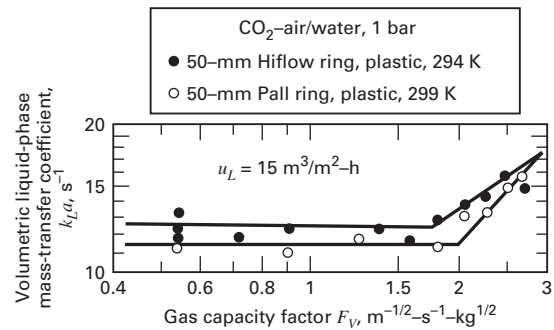


Figure 6.41 Effect of gas rate on liquid-phase mass transfer of CO₂.

[From R. Billet, *Packed Column Analysis and Design*, Ruhr-University Bochum (1989) with permission.]

transfer. Although not illustrated in Figures 6.39 to 6.41, a major liquid-phase factor is the solute diffusivity in water, D_L . Data in the preloading region can usually be correlated by an empirical expression, which includes the liquid velocity and diffusivity:

$$k_L a = C_1 D_L^{0.5} u_L^n \quad (6-113)$$

where n varies from 0.6 to 0.95, with 0.75 being a typical value. The exponent on the diffusivity is consistent with the penetration theory presented in §3.6.2.

A convenient system for studying gas-phase-controlled mass transfer is NH_3 -air- H_2O . The low K -value and high solubility of NH_3 in H_2O make the last terms in (6-79), (6-109), and (6-110) negligible, so that gas-phase resistance controls the rate of mass transfer. Figures 6.42 and 6.43 show a greater effect of vapor velocity compared to liquid loading. In Figure 6.42, the mass-transfer coefficient is proportional to the 0.75 power of F_V , and in Figure 6.43, the coefficient is proportional to only the 0.25 power of the liquid loading. The small effect of liquid loading is due to increases in holdup and interfacial area.

For a given packing, the experimental data on $k_G a$ for different systems in the preloading region is correlated satisfactorily with an empirical relation of the form

$$k_G a = C_2 D_G^{0.67} F_V^{m'} u_L^{n'} \quad (6-114)$$

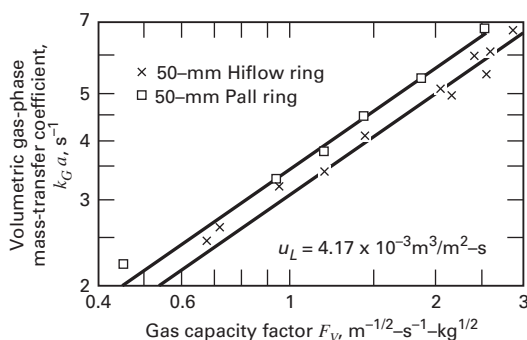


Figure 6.42 Effect of gas rate on gas-phase mass transfer of NH_3 . [From R. Billet, *Packed Column Analysis and Design*, Ruhr-University Bochum (1989) with permission.]

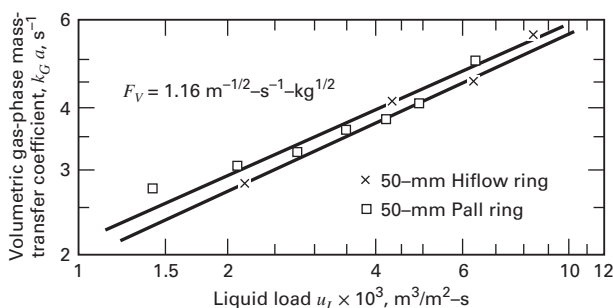


Figure 6.43 Effect of liquid rate on gas-phase mass transfer of NH_3 .

[From R. Billet, *Packed Column Analysis and Design*, Ruhr-University Bochum (1989) with permission.]

where D_G is the gas diffusivity of the solute and m' and n' have been observed by different investigators to vary from 0.65 to 0.85 and from 0.25 to 0.5, respectively, with a typical value for m' being 0.8.

The measurement and correlation of gas- and liquid-phase mass-transfer coefficients and HTUs, as well as volumetric interfacial surface area for mass transfer, are important requirements for modern packed-tower design methods. Since the early investigations of Sherwood and coworkers in 1940, 13 correlations for random packings and 9 correlations for structured packings have been presented in the literature, as reviewed by Wang, Yuan, and Yu [34]. These are largely based on the application of the two-film and penetration theories in Chapter 3. In some cases, the values of k_G and k_L are reported separately from a , and, in others, the combinations $k_G a$ and $k_L a$ are used. The development of such correlations for packed columns is difficult because, as shown by Billet [37], the values of mass-transfer coefficients are significantly affected by the technique used to pack the column and the number of liquid feed-distribution points across the column, which must be more than 25 points.

The Billet and Schultes correlations [39] are widely accepted and included in process simulators. They [38] measured and correlated mass-transfer coefficients and specific surface area for more than 30 different chemical systems in columns with diameters ranging from 2.4 inches to 4.6 ft, packed with more than 60 different types and sizes of random and structured packings, including third-generation Hiflow rings and fourth-generation Raschig Super-Rings. Their semitheoretical mass-transfer theory assumes that the effective void space of the packing is equivalent to a multiplicity of vertical flow channels, wherein the gas flows upward, countercurrent to the liquid trickling down along the channel walls, with continual remixing of the liquid at points of packing contact. The penetration theory is used for mass transfer in both phases and uniform distribution of gas and liquid flows is assumed.

Their correlating equations for the mass-transfer coefficients include factors for the operating conditions, physical properties, and liquid holdup. Two packing-specific constants, C_L and C_V , included in Table 6.6, correct for the actual flow paths.

The systems studied by Billet and Schultes include those for which mass-transfer resistance resides mainly in the liquid phase or mainly in the gas phase. The volumetric mass-transfer coefficient for the liquid phase is defined by

$$r = (k_L a_{ph})(c_{L1} - c_L) \quad (6-115)$$

where a_{ph} is the specific interfacial area (area per unit volume of packed bed) for mass transfer between phases. From the penetration theory,

$$k_L = 2(D_L/\pi t_L)^{1/2} \quad (6-116)$$

where t_L = the time of exposure of the liquid film before remixing. Billet and Schultes assume that this time is based

on a length of travel equal to the **hydraulic diameter** of the packing, resulting in

$$t_L = h_L d_H / u_L \quad (6-117)$$

where the hydraulic diameter $d_H = 4\varepsilon/a$ and h_L is the specific liquid holdup. Their theoretical equation, in the form of an HTU expression, is

$$H_L = \frac{u_L}{k_L a_{ph}} = \frac{\sqrt{\pi}}{2} \left(\frac{4h_L \varepsilon}{D_L a u_L} \right)^{1/2} \frac{u_L}{a_{ph}} \quad (6-118)$$

After modification to include the constant C_L , which appears in Table 6.6 and was back-calculated for each packing to fit the data, the final predictive equation of Billet and Schultes is

$$H_L = \frac{1}{C_L} \left(\frac{1}{12} \right)^{1/6} \left(\frac{4h_L \varepsilon}{D_L a u_L} \right)^{1/2} \frac{u_L}{a} \left(\frac{a}{a_{ph}} \right) \quad (6-119)$$

An analogous equation has been developed by Billet and Schultes for the gas phase, where the time of exposure of the gas between periods of mixing is determined empirically:

$$H_G = \frac{1}{C_V} (\varepsilon - h_L)^{1/2} \left(\frac{4\varepsilon}{a^4} \right) (N_{Re_V})^{-3/4} (N_{Sc_V})^{-1/3} \times \left(\frac{u_V a}{D_G a_{ph}} \right) \quad (6-120)$$

where C_V is included to fit the experimental data,

$$N_{Re_V} = \frac{u_V \rho_V}{a \mu_V}, \text{ and} \quad (6-121)$$

$$N_{Sc_V} = \frac{\mu_V}{\rho_V D_G} \quad (6-122)$$

Equations (6-119) and (6-120) contain a term, a_{ph}/a , the ratio of the phase interface area to the packing surface area, which, from Billet and Schultes [39], is not the same as the hydraulic area ratio, a_h/a , given by (6-95) and (6-96). Instead, they give the following correlation:

$$\frac{a_{ph}}{a} = 1.5(ad_h)^{-1/2} (N_{Re_{L,h}})^{-0.2} (N_{We_{L,h}})^{0.75} (N_{Fr_{L,h}})^{-0.45} \quad (6-123)$$

$$\text{where } d_h = \text{packing hydraulic diameter} = 4 \frac{\varepsilon}{a} \quad (6-124)$$

and the following liquid-phase dimensionless groups use the packing hydraulic diameter as the characteristic length:

$$\text{Reynolds number} = N_{Re_{L,h}} = \frac{u_L d_h \rho_L}{\mu_L} \quad (6-125)$$

$$\text{Weber number} = N_{We_{L,h}} = \frac{u_L^2 \rho_L d_h}{\sigma} \quad (6-126)$$

$$\text{Froude number} = N_{Fr_{L,h}} = \frac{u_L^2}{g d_h} \quad (6-127)$$

After calculating H_L and H_G from (6-119) and (6-120), the overall HTU value, H_{OG} , is obtained from (6-110), N_{OG} is obtained as described in §6.7, and the packed height is from (6-84).

EXAMPLE 6.17 Packed Height from Mass-Transfer Theory.

For the absorption of ethyl alcohol from CO_2 with water, as considered in Example 6.1, a 2.5-ft-I.D. tower, packed with 1.5-inch metal Pall-like rings, is used. It is estimated that the tower will operate in the preloading region with a pressure drop of approximately 1.5-inches $\text{H}_2\text{O}/\text{ft}$ of packed height. From Example 6.11, $N_{OG} = 7.5$. Estimate H_G , H_L , H_{OG} , HETP, and the required packed height in feet, using the following estimates of flow conditions and physical properties at the bottom of the packing:

	Vapor	Liquid
Flow rate, lb/h	17,480	6,140
Molecular weight	44.05	18.7
Density, lb/ft ³	0.121	61.5
Viscosity, cP	0.0145	0.63
Surface tension, dynes/cm	—	101
Diffusivity of ethanol, m ² /s	7.75×10^{-6}	1.82×10^{-9}
Kinematic viscosity, m ² /s	0.75×10^{-5}	0.64×10^{-6}

Solution

Cross-sectional area of tower = $(3.14)(2.5)^2/4 = 4.91 \text{ ft}^2$

Volumetric liquid flow rate = $6,140/61.5 = 99.8 \text{ ft}^3/\text{h}$

u_L = superficial liquid velocity = $99.8/[(4.91)(3,600)]$
 = 0.0056 ft/s or 0.0017 m/s

For this section of the tower, $u_L > u_{L,\min}$, but the velocity is on the low side.

u_V = superficial gas velocity = $17,480/[(0.121)(4.91)(3,600)]$
 = $8.17 \text{ ft/s} = 2.49 \text{ m/s}$

The packing characteristics for the 1.5-inch metal Pall-like rings are as follows (somewhat different from values for Pall rings in Table 6.6):

$$a = 149.6 \text{ m}^2/\text{m}^3, \quad \varepsilon = 0.952$$

$$C_h \approx 0.7, \quad C_L = 1.227, \quad C_V = 0.341$$

Estimation of specific liquid holdup, h_L :

From (6-93),

$$N_{Re_L} = \frac{0.0017}{(0.64 \times 10^{-6})(149.6)} = 17.8$$

From (6-94),

$$N_{Fr_L} = \frac{(0.0017)^2(149.6)}{9.8} = 4.41 \times 10^{-5}$$

From (6-96),

$$\frac{a_h}{a} = 0.85(0.7)(17.8)^{0.25} (4.41 \times 10^{-5})^{0.10} = 0.45$$

$$a_h = 0.45(149.6) = 67.3 \text{ m}^2/\text{m}^3$$

From (6-92),

$$h_L = \left[\frac{12 (4.41 \times 10^{-5})}{17.8} \right]^{1/3} (0.45)^{2/3} = 0.0182 \text{ m}^3/\text{m}^3$$

Estimation of H_L :

First compute a_{ph}/a , the ratio of phase interface area to packing surface area.

From (6-124),

$$d_h = 4 \frac{0.952}{149.6} = 0.0255 \text{ m}$$

From (6-125),

$$N_{Re_{L,h}} = \frac{(0.0017)(0.0255)}{(0.64 \times 10^{-6})} = 67.7$$

From (6-126),

$$N_{We_{L,h}} = \frac{(0.0017)^2 [(61.5)(16.02)](0.0255)}{[(101)(0.001)]} = 0.000719$$

From (6-127),

$$N_{Fr_{L,h}} = \frac{(0.0017)^2}{(9.807)(0.0255)} = 1.156 \times 10^{-5}$$

From (6-123),

$$\frac{a_{ph}}{a} = 1.5(149.6)^{-1/2} (0.0255)^{-1/2} (67.7)^{-0.2}$$

$$(0.000719)^{0.75} (1.156 \times 10^{-5})^{-0.45} = 0.242$$

From (6-119), using consistent SI units,

$$H_L = \frac{1}{1.227} \left(\frac{1}{12} \right)^{1/6} \left[\frac{(4)(0.0182)(0.952)}{(1.82 \times 10^{-9})(149.6)(0.0017)} \right]^{1/2} \times$$

$$\left(\frac{0.0017}{149.6} \right) \left(\frac{1}{0.242} \right) = 0.31 \text{ m} = 1.01 \text{ ft}$$

Estimation of H_G :

From (6-121),

$$N_{Rev} = 2.49 / [(149.6)(0.75 \times 10^{-5})] = 2,220$$

From (6-122),

$$N_{Sc_v} = 0.75 \times 10^{-5} / 7.75 \times 10^{-6} = 0.968$$

From (6-120), using consistent SI units,

$$H_G = \frac{1}{0.341} (0.952 - 0.0128)^{1/2} \left[\frac{(4)(0.952)}{(149.6)^4} \right]^{1/2} \times$$

$$(2220)^{-3/4} (0.968)^{-1/3} \left[\frac{(2.49)}{7.75 \times 10^{-6} (0.242)} \right]$$

$$= 1.03 \text{ m or } 3.37 \text{ ft}$$

Estimation of H_{OG} :

From Example 6.1, the K -value for ethyl alcohol = 0.57,

$$V = 17,480/44.05 = 397 \text{ lbmol/h,}$$

$$L = 6,140/18.7 = 328 \text{ lbmol/h,}$$

$$\text{and } 1/\mathcal{A} = KV/L = (0.57)(397)/328 = 0.69$$

From (6-110),

$$H_{OG} = 3.37 + 0.69(1.01) = 4.07 \text{ ft}$$

The mass-transfer resistance in the liquid phase is less than the gas phase, but not negligible.

Estimation of Packed Height:

From (6-89),

$$l_T = 4.07(7.5) = 30.5 \text{ ft}$$

Estimation of HETP:

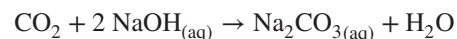
From (6-89), for straight operating and equilibrium lines, with $\mathcal{A} = 1/0.69 = 1.45$,

$$\text{HETP} = 4.07 \left[\frac{\ln(0.69)}{(1 - 1.45)/1.45} \right] = 4.86 \text{ ft}$$

§6.9 REACTIVE (CHEMICAL) ABSORPTION

In **physical absorption**, no significant chemical reactions occur between the solute being absorbed from the gas and the absorbent. Common absorbents in physical absorption, as listed in Table 6.1, are water and hydrocarbon oils. Often, the absorption step is followed by stripping or distillation to recover the solute and recycle the absorbent.

Often, especially when the solute is an acid gas, it is more efficient to use **chemical absorption**. Acid gases include CO_2 , H_2S , N_2O , SO_2 , SO_3 , HCl , and HCN , for which a chemical reaction with the absorbent occurs in the liquid phase. If the absorbent is an aqueous solution of a strong base, such as NaOH or KOH , ionic reactions occur that are irreversible and either fast or instantaneous. For example, if the solute is CO_2 and the absorbent is aqueous sodium hydroxide, the overall reaction is



where the salt, Na_2CO_3 , is soluble in water. The liquid leaving the absorber may require further treatment.

Acid gases, particularly CO_2 and H_2S , are also removed by aqueous amine solutions, including monoethanolamine (MEA), diethanolamine (DEA), diethyleneglycol (DEG), and triethyleneglycol (TEG), with slower, but reversible, chemical reactions occurring in the liquid phase. In this case, the reactions are reversed downstream of the absorber in a subsequent operation to enable the recovery of the acid gases and the recycling of the aqueous amine absorbent.

For both types of chemical absorption, fast chemical reactions increase the rate of absorption by reducing the

mass-transfer resistance of the liquid phase, increasing the absorption capacity of the solvent used in the absorbent, and increasing the selectivity for certain components of the gas. In some cases, a hazardous chemical is converted to a safe one.

Of increasing industrial importance is the need for carbon capture, or the disposal of CO_2 after it has been absorbed and recovered, in cases where it is not further processed for use by the food, oil, or chemical industries. Carbon capture and sequestration is the process of recovering CO_2 from flue gases in large power-generating plants or other industrial sources and then transporting it to and depositing it in an underground geological formation, from which it cannot escape. The goal is to eliminate the release of large amounts of CO_2 into the atmosphere.

Gas-liquid reactions in absorbers are treated in a number of books, including Astarita [51], Danckwerts [52], Sherwood, Pigford, and Wilke [53], Shah [54], and Doraiswamy and Sharma [55]. In this subsection, the subject of reactive absorption is introduced by considering an irreversible reaction occurring mainly in the liquid film adjacent to the two-phase interface in a packed tower. This subject can be extended to more difficult cases involving reversible reactions by the methods in Chapter 12, using process simulators.

Assume the gas fed to an absorber contains component A, which is soluble in the countercurrently flowing nonvolatile absorbent. Except for A, the feed gas is insoluble in the absorbent. The absorbent includes component B, which reacts irreversibly with A to produce nonvolatile products that are soluble in the absorbent by the reaction



Composition profiles for A and B in the fluid films for three cases are shown in the vicinity of the gas-liquid interface, I, in Figure 6.44, where the driving forces for mass transfer are taken as partial pressure in the gas phase and molar concentrations in the liquid phase. In all three cases, the amount of B is in excess of that required for complete reaction of A. Physical equilibrium is assumed at the gas-liquid interface I.

In Case (a), the reaction between A and B is infinitely slow, so no reaction occurs anywhere in the absorber. The absorption is only physical, and the rate of absorption of A depends only on the mass-transfer resistances in the gas and liquid phases. The rate of absorption, in terms of resistances, is obtained by combining (6-105), (6-108), and (6-109) to give the following equation, where all terms without a component subscript apply to component A:

$$r = \frac{p - H'c}{\frac{1}{k_G a} + \frac{H'}{k_L a}} \quad (6-128)$$

The first term in the denominator is the mass-transfer resistance in the gas phase, and the second is the resistance in the liquid phase. If A is very soluble in the liquid phase, the rate of absorption is controlled by the gas phase; otherwise, the liquid phase controls.

At the other extreme is Case (b). The chemical reaction between A and B is instantaneous at the phase interface. Accordingly, the partial pressure and concentration of A at

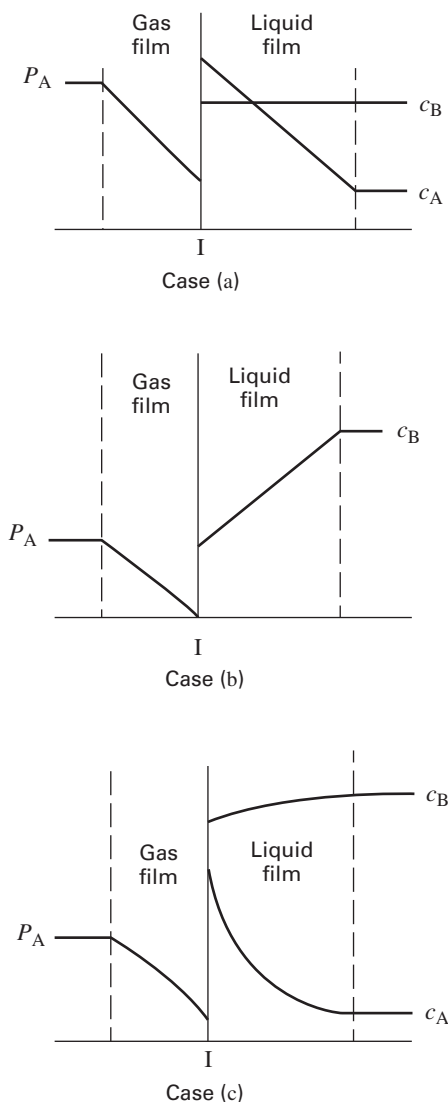


Figure 6.44 Absorption with chemical reaction: (a) Infinitely slow reaction; (b) Instantaneous reaction; (c) Intermediate reaction rate.

the phase interface is zero. The only resistance to the rate of mass transfer of A to the liquid phase is in the gas phase, as given by the following modification of (6-128):

$$r = \frac{p - 0}{\frac{1}{k_G a}} = k_G a p \quad (6-129)$$

In Case (c), the reaction occurs at an intermediate rate, both in the liquid film, adjacent to the phase interface, and in the bulk liquid in the presence of excess B. The rate of mass transfer of A depends on the resistances in the two phases and the rate of the chemical reaction. If it is assumed that the reaction is a pseudo first-order reaction in B, (6-128) is modified, according to the treatment by Hatta, as described by Sherwood et al. [53], to give

$$r = \frac{p}{\frac{1}{k_G a} + \frac{H'}{k_L a E} + \frac{H'}{k c_B h_L}} \quad (6-130)$$

where the mass-transfer resistance in the gas phase is unchanged, but the mass-transfer resistance in the liquid phase is enhanced by the chemical reaction occurring in the liquid film according to an enhancement factor, E , which is > 1 . As shown in Figure 6.45, the enhancement factor is a function of the Hatta number, N_{Ha} , where N_{Ha}^2 is the ratio of the maximum possible chemical conversion in the liquid film to the maximum mass-transfer rate through the film. For the pseudo first-order reaction, where k is the reaction rate constant,

$$N_{Ha} = \frac{(D_A k c_B)^{0.5}}{k_L} \quad (6-131)$$

The enhancement factor is also a function of the parameter E_i , which is the enhancement factor for an instantaneous chemical reaction, as given by

$$E_i = 1 + \frac{D_B c_B H'}{b D_A P I} \quad (6-132)$$

The third term in the denominator of (6-130) accounts for the pseudo first-order reaction in B that occurs in the bulk liquid, where h_L is the fractional volumetric liquid holdup.

For Case (c), if the chemical reaction is fast, and occurs only in the liquid film, and if the concentration of B drops to zero at the phase interface, I, the third term in the denominator of (6-130) is omitted.

As shown in Figure 6.45, the enhancement factor, E , attains very large values (more than one order of magnitude increase) at large values of the Hatta modulus and E_i . In cases where the solute is only slightly soluble in the absorbent, the rate of absorption into a nonreacting absorbent is controlling and low. However, if the solute reacts with a component in the absorbent, the enhancement can be so large that the much lower resistance of the gas phase becomes controlling, with the result that the rate of absorption is much higher. If the reaction is instantaneous, the only resistance is that of the gas phase. For a case of the absorption of CO_2 , Sherwood et al. [53] show that the overall mass-transfer coefficient, K_G , for

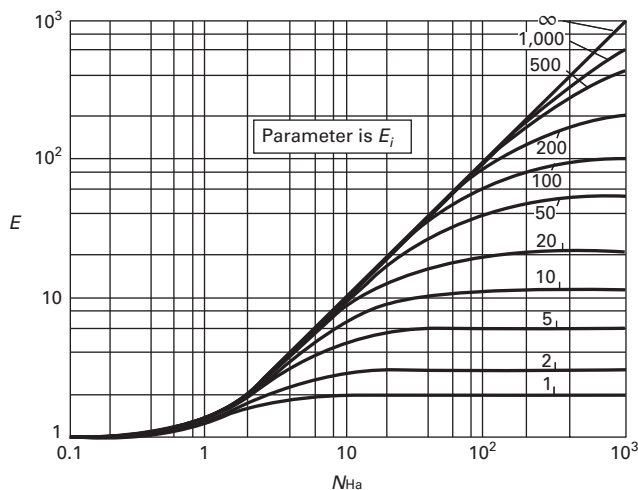


Figure 6.45 Enhancement factor for absorption with chemical reaction.

absorption in 2-N KOH is 76 times greater than for absorption in water.

When the chemical reaction is instantaneous at the phase interface, the required number of equivalent stages or the number of transfer units decreases. Because the concentration and partial pressure of the solute become zero, the equilibrium curve is a horizontal line at an ordinate value of zero:

$$N_{OG} = \int_{p_{out}}^{p_{in}} \frac{dp}{p} = \ln \frac{p_{in}}{p_{out}} \quad (6-133)$$

For a 10-fold decrease, the partial pressure of the solute $N_{OG} = 2.3$. For a 100-fold decrease, $N_{OG} = 4.6$.

CHAPTER 6 NOMENCLATURE

Abbreviations and Acronyms

GPDC generalized pressure drop correlation, §6.8.2

Latin Symbols

- A, A_T column inside cross-sectional area, (6-81)
- A_a, A_b active bubbling area on a tray, (6-44)
- A_d downcomer area, Figure 6.21
- A_h hole area of a sieve tray; hydraulic area per unit volume of packed bed, (6-95)
- A_n net vapor flow area, equal to $A - A_d$ for a single-pass tray
- a vapor-liquid interfacial area per volume of combined gas and liquid holdup (froth or dispersion) on the tray, (6-44); surface area of packing per unit volume of packed bed, (6-95)
- a_{ph} interfacial area per unit volume of packed bed, (6-115)
- C flooding parameter, (6-61)
- C_F flooding factor parameter, (6-61)
- C_h packing parameter to calculate liquid holdup, Table 6.6
- C_L packing factor to calculate H_L , Table 6.6
- C_V packing factor to calculate H_G , Table 6.6
- $C_{V,ult}$ ultimate capacity factor, (6-64)
- d_H packing hydraulic diameter, (6-117)
- D_E eddy diffusivity, (6-55)
- D_L solute diffusivity, (6-113)
- D_p packing diameter, (6-101)
- E enhancement factor, (6-135) and Figure 6.44
- E_i enhancement factor for an instantaneous reaction, (6-137)
- E_o overall stage efficiency, (6-41)
- F sum of gravity F_g , buoyant F_b , and drag F_d forces, (6-57)
- F gas capacity factor, (6-67)
- F_C modified empirical capacity factor, (6-98)

F_F	foaming factor, (6-61)
F_{HA}	ratio of hole area to active tray area, (6-61)
F_{LV}	kinetic energy ratio, Figures 6.27, 6.36, 6.37
F_P	packing factor, Table 6.6
F_{ST}	surface tension factor (6-61)
F_V	superficial-vapor-velocity F -factor, (6-104)
f	fraction of flooding velocity, (6-62)
H'	modified Henry's law, (6-106)
h_L	volumetric liquid holdup per unit volume of packed bed, (6-92)
K'	overall mass-transfer coefficient corrected for bulk flow, Table 6.5
L'	liquid molar flow rate, solute-free, Table 6.5
L_S	superficial liquid velocity, (6-65)
l_T	packed height, (6-68)
m	slope of the equilibrium line, below (6-53b)
N_{Ha}	Hatta number, (6-131)
N_a	actual number of trays required, (6-41)
N_t	number of theoretical stages, (6-41)
ΔP_{flood}	pressure drop per unit of height at flooding, (6-99)
r	rate of mass transfer per volume of packed bed, (6-72)
r_H	hydraulic radius, flow volume per unit of packing surface area, equal to $d_H/4$, below (6-97)
t_L	remixing time in penetration theory, (6-116)
u_L	volumetric liquid flow rate per unit of column cross-sectional area, Figure 6.42
u_f, u_{Vf}	vapor flooding velocity, (6-59)

$u_{V,ult}$	ultimate superficial vapor velocity in a trayed column, (6-64)
V'	vapor molar flow rate, solute free, Table 6.5
x_i^s	mole fraction solubility of solute, (6-40)
Z_f	height of combined gas and liquid holdup, (6-44)
Z_L	length of liquid flow path across a tray, (6-55)

Script Symbols

\mathcal{A}	absorption factor of a component = L/KV , (6-18)
\mathcal{S}	stripping factor of a component = $1/\mathcal{A} = KV/L$, (6-32)

Greek Symbols

ϵ	packed column void fraction, Table 6.6
λ	mV/L , (6-53b)
ϕ_A	fraction of a species not absorbed, (6-29)
ϕ_S	fraction of a species not stripped, (6-31)

Subscripts

k	key component, below (6-53a)
e	effective average for all components, (6-29)

Superscripts

*	composition in equilibrium with bulk phase
---	--

SUMMARY

1. A liquid can selectively absorb components from a gas. A gas can selectively desorb or strip components from a liquid.
2. The fraction of a component that can be absorbed or stripped depends on the number of equilibrium stages and the absorption factor, $\mathcal{A} = L/(KV)$, or the stripping factor, $\mathcal{S} = KV/L$, respectively.
3. Towers with sieve or valve trays, or with random or structured packings, are most often used for absorption and stripping.
4. Absorbers are most effective at high pressure and low temperature. The reverse is true for strippers. However, the high costs of gas compression, refrigeration, and vacuum often preclude operation at the most thermodynamically favorable conditions.
5. For a given gas flow, composition, degree of absorption, choice of absorbent, and operating T and P , there is a minimum absorbent flow rate, given by (6-9) to (6-11), that corresponds to an infinite number of stages. A rate of 1.5 times the minimum typically leads to a reasonable number of stages. A similar criterion, (6-12), holds for a stripper.
6. The equilibrium stages and flow rates for an absorber or stripper can be determined from the equilibrium line, (6-1), and an operating line, (6-3) or (6-5), using graphical, algebraic, or numerical methods. Graphical methods, as shown in Figure 6.12, offer visual insight into the stage-by-stage changes in the compositions of the gas and liquid streams and the effects of those changes on the variables.
7. Estimates of overall stage efficiency for absorbers, defined by (6-41), can be made with the correlations of Drickamer and Bradford (6-42), O'Connell (6-43), and Figure 6.19. More accurate procedures involve the use of a laboratory Oldershaw column or semitheoretical equations to determine a Murphree vapor-point efficiency, (6-51). The Murphree vapor-tray efficiency is obtained from (6-52) to (6-54) and Figure 6.23. The overall efficiency is from (6-56).

8. Tray diameter is determined from (6-63), based on the entrainment flooding considerations shown in Figure 6.27.
9. Packed-column height is determined using HETP, (6-68), or $H_{OG}N_{OG}$ from (6-84), with the latter having a more theoretical basis in the two-film theory of mass transfer. For straight equilibrium and operating lines, HETP is related to H_{OG} by (6-89), and the number of stages to N_{OG} by (6-90).
10. In the preloading region, liquid holdup in a packed column is independent of vapor velocity and is determined from (6-92). The loading point is typically 70% of the flooding point, and most packed columns are designed to operate in the preloading region from 50% to 70% of flooding. The pressure drop at the flooding point is estimated from (6-99). The GPDC charts of Figures 6.36 and 6.37 are used to determine pressure drop and column diameter using (6-100).
11. Numerous rules of thumb for estimating the HETP of packed columns exist. The preferred approach is to estimate H_{OG} from semitheoretical mass-transfer correlations, such as those of (6-118) and (6-119), based on the work of Billet and Schultes.
12. Reactive absorption occurs when the solute absorbed from a gas reacts with the absorbent. The reaction may be reversible or irreversible.
13. Fast chemical reactions increase the rate of absorption by reducing the mass-transfer resistance of the liquid phase.

REFERENCES

1. WASHBURN, E.W., Ed., *International Critical Tables*, McGraw-Hill, New York, Vol. 3, p. 255 (1928).
2. LOCKETT, M., *Distillation Tray Fundamentals*, Cambridge University Press, Cambridge, UK, p. 13 (1986).
3. OKONIEWSKI, B.A., *Chem. Eng. Prog.*, **88**(2), 89–93 (1992).
4. SAX, N.I., *Dangerous Properties of Industrial Materials*, 4th ed., Van Nostrand Reinhold, New York, pp. 440–441 (1975).
5. LEWIS, W.K., *Ind. Eng. Chem.*, **14**, 492–497 (1922).
6. DRICKAMER, H.G., and J.R. BRADFORD, *Trans. AIChE*, **39**, 319–360 (1943).
7. JACKSON, R.M., and T.K. SHERWOOD, *Trans. AIChE*, **37**, 959–978 (1941).
8. O'CONNELL, H.E., *Trans. AIChE*, **42**, 741–755 (1946).
9. WALTER, J.F., and T.K. SHERWOOD, *Ind. Eng. Chem.*, **33**, 493–501 (1941).
10. EDMISTER, W.C., *The Petroleum Engineer*, C45–C54 (Jan. 1949).
11. LOCKHART, F.J., and C.W. LEGGETT, in K.A. Kobe and J.J. McKetta, Jr. Eds., *Advances in Petroleum Chemistry and Refining*, Interscience, New York, Vol. 1, pp. 323–326 (1958).
12. HOLLAND, C.D., *Multicomponent Distillation*, Prentice-Hall, Englewood Cliffs, NJ (1963).
13. MURPHREE, E.V., *Ind. Eng. Chem.*, **17**, 747 (1925).
14. HAUSEN, H., *Chem. Ing. Tech.*, **25**, 595 (1953).
15. STANDART, G., *Chem. Eng. Sci.*, **20**, 611 (1965).
16. LEWIS, W.K., *Ind. Eng. Chem.*, **28**, 399 (1936).
17. GERSTER, J.A., A.B. HILL, N.H. HOCHGRAF, and D.G. ROBINSON, "Tray Efficiencies in Distillation Columns," Final Report from the University of Delaware, American Institute of Chemical Engineers, New York (1958).
18. *Bubble-Tray Design Manual*, AIChE, New York (1958).
19. GILBERT, T.J., *Chem. Eng. Sci.*, **10**, 243 (1959).
20. BARKER, P.E., and M.F. SELF, *Chem. Eng. Sci.*, **17**, 541 (1962).
21. BENNETT, D.L., and H.J. GRIMM, *AIChE J.*, **37**, 589 (1991).
22. OLDERSHAW, C.F., *Ind. Eng. Chem. Anal. Ed.*, **13**, 265 (1941).
23. FAIR, J.R., H.R. NULL, and W.L. BOLLES, *Ind. Eng. Chem. Process Des. Dev.*, **22**, 53–58 (1983).
24. SOUDERS, M., and G.G. BROWN, *Ind. Eng. Chem.*, **26**, 98–103 (1934).
25. FAIR, J.R., *Petro/Chem. Eng.*, **33**, 211–218 (Sept. 1961).
26. SHERWOOD, T.K., G.H. SHIPLEY, and F.A.L. HOLLOWAY, *Ind. Eng. Chem.*, **30**, 765–769 (1938).
27. *Glitsch Ballast Tray, Bulletin No. 159*, Fritz W. Glitsch and Sons, Dallas, TX (from FRI report, Sept. 3, 1958).
28. *Glitsch V-1 Ballast Tray, Bulletin No. 160*, Fritz W. Glitsch and Sons, Dallas, TX (from FRI report, Sept. 25, 1959).
29. OLIVER, E.D., *Diffusional Separation Processes. Theory, Design, and Evaluation*, John Wiley & Sons, New York, pp. 320–321 (1966).
30. KREMSER, A., *Natl. Petroleum News*, **22**(21), 43–49 (May 21, 1930).
31. EDMISTER, W.C., *AIChE J.*, **3**, 165–171 (1957).
32. STRIGLE, R.F., Jr., *Random Packings and Packed Towers*, Gulf Publishing Company, Houston, TX (1987).
33. KISTER, H.Z., *Distillation Design*, McGraw-Hill, New York (1992).
34. WANG, G.Q., YUAN, X.G., and K.T. YU, *Ind. Eng. Chem. Res.*, **44**, 8715–8729 (2005).
35. BILLET, R., and M. SCHULTES, *Chem. Eng. Technol.*, **14**, 89–95 (1991).
36. SHERWOOD, T.K., and F.A.L. HOLLOWAY, *Trans. AIChE.*, **36**, 39–70 (1940).
37. BILLET, R., *Chem. Eng. Prog.*, **63**(9), 53–65 (1967).
38. BILLET, R., and M. SCHULTES, *Beiträge zur Verfahrens-Und Umwelttechnik*, Ruhr-Universität Bochum, pp. 88–106 (1991).
39. BILLET, R., and M. SCHULTES, *Chem. Eng. Res. Des., Trans. IChemE*, **77A**, 498–504 (1999).
40. M. SCHULTES, Private Communication (2004).
41. SLOLEY, A.W., *Chem. Eng. Prog.*, **95**(1), 23–35 (1999).
42. STUPIN, W.J., and H.Z. KISTER, *Trans. IChemE.*, **81A**, 136–146 (2003).
43. CHILTON, T.H., and A.P. COLBURN, *Ind. Eng. Chem.*, **27**, 255–260, 904 (1935).
44. COLBURN, A.P., *Trans. AIChE*, **35**, 211–236, 587–591 (1939).
45. BILLET, R., *Packed Column Analysis and Design*, Ruhr-University Bochum, Germany (1989).
46. STICHLMAIR, J., J.L. BRAVO, and J.R. FAIR, *Gas Separation and Purification*, **3**, 19–28 (1989).
47. BILLET, R., and M. SCHULTES, *Packed Towers in Processing and Environmental Technology*, translated by J.W. Fullarton, VCH Publishers, New York (1995).
48. LEVA, M., *Chem. Eng. Prog. Symp. Ser.*, **50** (10), 51 (1954).
49. LEVA, M., *Chem. Eng. Prog.*, **88**(1), 65–72 (1992).

50. KISTER, H.Z., and D.R. GILL, *Chem. Eng. Prog.*, **87**(2), 32–42 (1991).
51. ASTARITA, G., *Mass Transfer with Chemical Reaction*, Elsevier Publishing Co., New York (1967).
52. DANCKWERTS, P.V., *Gas-Liquid Reactions*, McGraw-Hill, New York (1970).
53. SHERWOOD, T.K., R.L. PIGFORD, and C.R. WILKE, *Mass Transfer*, McGraw-Hill, New York (1975).

54. SHAH, Y.T., *Gas-Liquid-Solid Reactor Design*, McGraw-Hill, New York (1979).
55. DORAISWAMY, L.K., and SHARMA, M.M., *Heterogeneous Reactions*, Vol. 2, John Wiley and Sons, New York (1984).
56. KISTER, H.Z., and D.R. GILL, *ICHEME Symp. Series*, **128**, A109–123 (1992).

STUDY QUESTIONS

- 6.1. What is the difference between physical absorption and chemical (reactive) absorption?
- 6.2. What is the difference between an equilibrium-based and a rate-based calculation method?
- 6.3. What is a trayed column? What is a packed tower?
- 6.4. What are the three most common types of openings in trays for the passage of vapor? Which of the three is rarely specified for new installations?
- 6.5. In a trayed tower, what is meant by flooding and weeping? What are the two types of flooding, and which is more common?
- 6.6. What is the difference between random and structured packings?
- 6.7. For what conditions is a packed column favored over a trayed tower?
- 6.8. In general, why should the operating pressure be high and the operating temperature be low for an absorber, and the opposite for a stripper?
- 6.9. For a given recovery of a key component in an absorber or stripper, does a minimum absorbent or stripping-agent flow rate exist for a tower or column with an infinite number of equilibrium stages?
- 6.10. What is the difference between an operating line and an equilibrium curve?
- 6.11. What is a reasonable value for the optimal absorption factor when designing an absorber? Does that same value apply to the optimal stripping factor when designing a stripper?
- 6.12. When stepping off stages on an Y - X plot for an absorber or a stripper, does the process start and stop with the operating line or the equilibrium curve?
- 6.13. What is the Kremser method? To what type of separation operations is it applicable? What are major assumptions of the method?
- 6.14. What is an absorption factor? What is a stripping factor?
- 6.15. Can the Kremser method be used to determine the required number of equilibrium stages?
- 6.16. Why do longer liquid flow paths across a tray give higher stage efficiencies?
- 6.17. What is the difference between the Murphree tray and point efficiencies?
- 6.18. What is meant by turndown ratio? What type of tray has the best turndown ratio? Which tray has the worst?
- 6.19. Why is the liquid holdup in a packed tower so important?
- 6.20. What is HETP? Does it have a theoretical basis? If not, why is it so widely used?
- 6.21. Why are there so many different kinds of mass-transfer coefficients? How can they be distinguished?
- 6.22. What is the difference between the loading point and the flooding point in a packed column?
- 6.23. In reactive absorption, what are the differences in the consequences of irreversible and reversible reactions?

EXERCISES

Section 6.1

6.1. Stripping in an absorber and absorption in a stripper.

In absorption, the absorbent is stripped to an extent that depends on its K -value. In stripping, the stripping agent is absorbed to an extent that depends on its K -value. Figure 6.1 shows that both absorption and stripping occur. Which occurs to the greatest extent in terms of kmol/h? Should the operation be called an absorber or a stripper? Why?

6.2. Advances in packing.

Prior to 1950, two types of commercial random packings were in common use: Raschig rings and Berl saddles. Since 1950, many new random packings have appeared. What advantages do these newer ones have? By what advances in design and fabrication were achievements made? Why were structured packings introduced?

6.3. Bubble-cap trays.

Bubble-cap trays were widely used in towers prior to the 1950s. Today, sieve and valve trays are favored. However, bubble-cap trays are still specified for operations that require very high turndown ratios or appreciable liquid residence time. What characteristics of

bubble-cap trays make it possible for them to operate satisfactorily at low vapor and liquid rates?

Section 6.2

6.4. Selection of an absorbent.

In Example 6.6, a lean oil of 250 MW is used as the absorbent. Consideration is being given to the selection of a new absorbent. Available streams are:

	Rate, gpm	Density, lb/gal	MW
C ₅ s	115	5.24	72
Light oil	36	6.0	130
Medium oil	215	6.2	180

Which would you choose? Why? Which are unacceptable?

6.5. Stripping of VOCs with air.

Volatile organic compounds (VOCs) can be removed from water effluents by stripping with steam or air. Alternatively, the VOCs can

be removed by carbon adsorption. The U.S. Environmental Protection Agency (EPA) identified air stripping as the best available technology (BAT) for this purpose. What are the advantages and disadvantages of air stripping compared to steam stripping or carbon adsorption?

6.6. Best operating conditions for absorbers and strippers.

Prove by equations why absorbers are most efficiently operated at high P and low T , whereas strippers are best operated at low P and high T . Also prove, by equations, why a trade-off exists between the number of stages and the flow rate of the separating agent.

Section 6.3

6.7. Absorption of CO₂ from air.

The exit gas from an alcohol fermenter consists of an air-CO₂ mixture containing 10 mol% CO₂ that is to be absorbed in a 5.0-N solution of triethanolamine, containing 0.04 mol CO₂ per mol of amine solution. Assume that the column operates isothermally at 25°C, the exit liquid contains 78.4% of the CO₂ in the feed gas to the absorber, and absorption is carried out in a six-theoretical-plate column. Then use the equilibrium data below to calculate (a) exit-gas composition and (b) moles of amine solution required per mole of feed gas.

Equilibrium Data						
Y	0.003	0.008	0.015	0.023	0.032	0.043
X	0.01	0.02	0.03	0.04	0.05	0.06
Y	0.055	0.068	0.083	0.099	0.12	
X	0.07	0.08	0.09	0.10	0.11	

Y = moles CO₂/mole air; X = moles CO₂/mole amine solution

6.8. Absorption of acetone from air.

Ninety-five percent of the acetone vapor in an 85 vol% air stream is to be absorbed by countercurrent contact with pure water in a valve-tray column with an expected overall tray efficiency of 50%. The column will operate at 20°C and 101 kPa. Equilibrium data for acetone-water at these conditions are as follows:

Acetone in water, mol%	3.30	7.20	11.7	17.1
Acetone partial pressure in air, torr	30.00	62.80	85.4	103.0

Calculate (a) the minimum value of L'/V' , the ratio mol H₂O/mol air; (b) the total number of equilibrium stages using a value of L'/V' of 1.25 times the minimum; and (c) the concentration of acetone in the exit water.

From Table 5.3 for N connected equilibrium stages, there are $2N + 2C + 5$ degrees of freedom. The following values are specified in this problem:

Stage pressures (101 kPa)	N
Stage temperatures (20°C)	N
Feed stream composition	$C - 1$
Water stream composition	$C - 1$
Feed stream, T, P	2
Water stream, T, P	2
Acetone recovery	1
L/V	1
	$2N + 2C + 4$

One more specification is needed. Take the gas feed rate at 100 kmol/h.

6.9. Absorber-stripper system.

A solvent-recovery plant consists of an absorber followed by a stripper, with both being trayed columns. Ninety percent of benzene (B) in the inlet gas stream, which contains 0.06 mol B/mol B-free gas, is recovered in the absorber. The oil entering the top of the absorber contains 0.01 mol B/mol pure oil. In the exiting liquid, $X = 0.19$ mol B/mol pure oil. The operating temperature is 77°F (25°C).

Superheated steam is used in the stripper to remove benzene from the benzene-rich oil at 110°C. Concentrations of benzene in the oil = 0.19 and 0.01, in mole ratios, at inlet and outlet, respectively. The oil (pure)-to-steam (benzene-free) flow rate ratio = 2.0. Vapors are condensed, separated, and removed. The additional data are MW oil = 200, MW benzene = 78, and MW gas = 32. The benzene equilibrium data are provided in the following table:

Equilibrium Data at Column Pressures		
X in Oil	Y in Gas, 25°C	Y in Steam, 110°C
0	0	0
0.04	0.011	0.10
0.08	0.0215	0.21
0.12	0.032	0.33
0.16	0.042	0.47
0.20	0.0515	0.62
0.24	0.060	0.795
0.28	0.068	1.05

Calculate (a) the molar ratio of B-free oil to B-free gas in the absorber; (b) the number of theoretical plates for the absorber; and (c) the minimum steam flow rate required to remove benzene from 1 mol of oil under given terminal conditions, assuming the stripper has an infinite number of trays.

6.10. Steam stripping of benzene from oil.

A straw oil used to absorb benzene (B) from coke-oven gas is to be steam-stripped in a sieve-plate column at 1 atm to recover B. Equilibrium at the operating temperature is approximated by Henry's law in the form $p_B = Hx_B$. It is known that, when the oil phase contains 10 mol% B, its partial pressure is 5.07 kPa. The oil is assumed to be nonvolatile, and it enters containing 8 mol% B, 75% of which is to be recovered. The steam leaving is 3 mol% B. (a) How many equilibrium stages are required? (b) How many moles of steam are required per 100 mol of feed? (c) If the benzene recovery is increased to 85% using the same steam rate, how many equilibrium stages are required?

Section 6.4

6.11. Multicomponent, multistage absorption.

Consider the hydrocarbon gas absorption of Example 6.3, with specifications shown in Figure 6.17. (a) Repeat the calculations of Example 6.3 for $N = 1, 3, 10,$ and 30 stages. Plot the percent absorption of each of the five hydrocarbons and the total feed gas, as well as percent stripping of the oil versus the number of stages N . Discuss your results. (b) Solve Example 6.3 for an absorbent flow rate of 330 lbmol/h and three theoretical stages. Compare your results to those of Example 6.3. What is the effect of trading stages for absorbent?

6.12. Minimum absorbent flow.

Estimate the minimum absorbent flow rate required for the separation in Example 6.3, assuming the key component is propane, with an exit flow rate in the vapor measured at 155.4 lbmol/h.

6.13. Isothermal, multistage absorption.

Solve Example 6.3 with the addition of a heat exchanger at each stage, so as to maintain isothermal operation of the absorber at (a) 125°F and (b) 150°F. What is the effect of temperature on absorption in this range of temperature? K -values at these temperatures are as follows, compared to those at 97.5°F:

Component	K -values at 400 psia		
	$T = 97.5^\circ\text{F}$	$T = 125^\circ\text{F}$	$T = 150^\circ\text{F}$
C_1	6.65	8.0	8.8
C_2	1.64	2.0	2.4
C_3	0.584	0.73	0.90
nC_4	0.195	0.26	0.34
nC_5	0.0713	0.098	0.135
Oil	0.0001	0.0002	0.0003

6.14. Multicomponent, multistage absorption.

One million lbmol/day of a gas of the composition below is absorbed by n -heptane at -30°F and 550 psia in an absorber with 10 theoretical stages, so as to absorb 50% of the ethane. Calculate the required flow rate of absorbent and the distribution, in lbmol/h, of all components between the exiting gas and liquid.

Component	Mole Percent in Feed Gas	K -value @ -30°F and 550 psia
C_1	94.9	2.85
C_2	4.2	0.36
C_3	0.7	0.066
nC_4	0.1	0.017
nC_5	0.1	0.004

6.15. Multistage stripper.

A stripper at 50 psia with three equilibrium stages strips 1,000 kmol/h of liquid, at 300°F , with the following molar composition: 0.03% C_1 , 0.22% C_2 , 1.82% C_3 , 4.47% nC_4 , 8.59% nC_5 , and 84.87% nC_{10} . The stripping agent is 1,000 kmol/h of superheated steam at 300°F and 50 psia. Use the Kremser equation to estimate the compositions and flow rates of the stripped liquid and exiting rich gas. Assume that no steam is absorbed. Calculate the dew-point temperature of the exiting gas at 50 psia. If it is above 300°F , what can be done?

Component K -values are as follows:

Component	K
C_1	60
C_2	28
C_3	14
nC_4	6.5
nC_5	3.5
nC_{10}	0.20

6.16. Stripping of VOCs from groundwater with air.

Groundwater, at a rate of 1,500 gpm and containing three volatile organic compounds (VOCs), is to be stripped with air in a trayed tower to produce drinking water that will meet U.S. Environmental Protection Agency (EPA) standards. Relevant data are given below.

Determine the minimum air flow rate in scfm (60°F , 1 atm) and the number of equilibrium stages required if an air flow rate of twice the minimum is used, and the tower operates at 25°C and 1 atm. Determine the composition in parts per million (ppm) for each VOC in the resulting drinking water.

Component	K -value	Concentration, ppm	
		Ground-water	Max. for Drinking water
1,2-Dichloroethane (DCA)	60	85	0.005
Trichloroethylene (TCE)	650	120	0.005
1,1,1-Trichloroethane (TCA)	275	145	0.200

Note: ppm = parts per million by weight.

6.17. Stripping of SO_2 and butadienes with N_2 .

SO_2 and butadienes (B3 and B2) are stripped with nitrogen from the liquid stream shown in Figure 6.46, so that the butadiene sulfone (BS) product contains less than 0.05 mol% SO_2 and less than 0.5 mol% butadienes. Estimate the flow rate of nitrogen, N_2 , and the equilibrium stages required. At 70°C , K -values for SO_2 , B2, B3, and BS are 6.95, 3.01, 4.53, and 0.016, respectively.

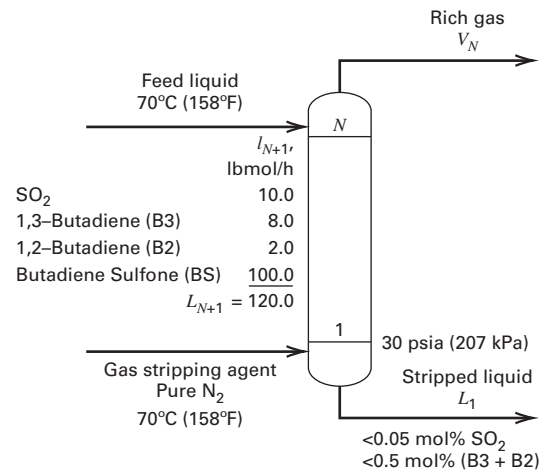


Figure 6.46 Data for Exercise 6.17.

6.18. Trade-off between stages and pressure for absorption.

Determine by the Kremser method the separation that can be achieved for the absorption operation indicated in Figure 6.47 for the following conditions: (a) six equilibrium stages and 75 psia operating pressure, (b) three stages and 150 psia, (c) six stages and 150 psia. Assume an average temperature of 90°F and use the K -values below. What do you conclude about a trade-off between pressure and stages?

Component	K -value at 75 psia	K -value at 150 psia
C_1	2.9	14.0
C_2	6.5	3.5
C_3	1.95	1.05
nC_4	0.61	0.33
nC_5	0.19	0.105
nC_{10}	0.0011	0.00055

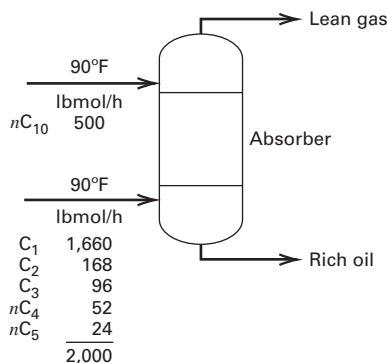


Figure 6.47 Data for Exercise 6.18.

6.19. Absorption of a hydrocarbon gas.

One thousand kmol/h of rich gas at 70°F with 25% C_1 , 15% C_2 , 25% C_3 , 20% nC_4 , and 15% nC_5 by moles is to be absorbed by 500 kmol/h of nC_{10} at 90°F in an absorber operating at 4 atm. Calculate, by the Kremser method, the percent absorption of each component for 4, 10, and 30 theoretical stages. What do you conclude? Use the following K -values:

Component	K -value
C_1	38
C_2	7.6
C_3	2.25
nC_4	0.64
nC_5	0.195
nC_{10}	0.0014

6.20. Absorption of acetone with water.

One mol/s of acetone in 10 mol/s air is fed into an absorber where 95% of the acetone is to be absorbed by water. Assume the absorber operates isothermally at 300 K and isobarically at 10 bar. At 300 K, vapor pressures for water and acetone are 0.035 and 0.33 bars, respectively. For an absorption factor of 1.4 for acetone, calculate the number of equilibrium stages and a complete material balance, taking into account stripping of water, assuming ideal solutions. Is the assumption of ideal solutions reasonable? Prove your response by calculations with a process simulator.

6.21. Stripping of VOCs from wastewater.

A wastewater stream containing benzene and ethylbenzene enters the top of a stripper at 0.0475 m³/s, where 99.9+ wt% of the VOCs at 15°C are to be removed with air entering the bottom at 2.41 m³/s, 15°C, and 103 kPa. For these conditions, the ideal-gas law is applicable and a modified Raoult's law, $K_i = P_i^s/x_i^sP$, can be used to estimate the K -values of the VOCs, as in Example 6.4. Neglecting the stripping of water and the absorption of air, calculate the number of equilibrium stages required using the following data:

Organic Compound	Concentration in the Wastewater, mg/L	Solubility in Water at 15°C, mole fraction	Vapor Pressure at 15°C, kPa
Benzene	150	0.00041	7.85
Ethylbenzene	20	0.000032	0.693

Section 6.5

6.22. Comparison of measured overall stage efficiency with correlations.

Using the data from Example 6.6, back-calculate E_o for propane and compare the result with estimates from the Drickamer–Bradford and O'Connell correlations. Use 2.0 for the K -value of propane, a liquid density of 57.9 lb/ft³, and an average liquid MW of 250.

6.23. Production of 95% H₂ by absorption of HCs from a refinery gas.

Fuel cell automotive systems are being considered that will require hydrogen of 95% purity. A refinery stream of 800,000 scfm (at 32°F, 1 atm), containing 72.5% H₂, 25% CH₄, and 2.5% C₂H₆, is available. To convert this gas to the required purity, oil absorption, activated charcoal adsorption, and membrane separation are being considered. For oil absorption, an available n -octane stream can be used as the absorbent. Because the 95% H₂ must be delivered at not less than 375 psia, the absorber will operate at 400 psia and 100°F. If at least 80% of the hydrogen fed to the absorber is to leave in the exit gas, determine the following: (a) the minimum absorbent rate in gpm; (b) the absorbent rate if 1.5 times the minimum amount is used; (c) the number of theoretical stages; (d) the stage efficiency for each of the three species in the feed gas, using the O'Connell correlation; (e) the number of trays actually required; and (f) the exit gas composition, accounting for octane stripping. For part (g) of the exercise, if the lost octane in part (f) is not recovered, estimate its value if the process operates 7,900 h/year and the octane is valued at \$1.00/gal. Would the use of octane preclude use of this hydrogen in fuel cells? Obtain the necessary properties from a process simulator.

6.24. Scale-up of absorber using Oldershaw-column data.

The absorber of Examples 6.1 and 6.7 is being scaled up by a factor of 15, so a column with an 11.5-ft-diameter will be needed. Because of the 30% efficiency for the original tray, a new design has been developed and tested in an Oldershaw column. The resulting Murphree vapor-point efficiency, E_{OV} , for the new tray design for this system is 55%. Estimate E_{MV} and E_o . To estimate the length of the liquid flow path, Z_L , use Figure 6.20. Assume that $u/D_E = 6 \text{ ft}^{-1}$.

Section 6.6

6.25. Diameter of a valve-tray column.

Figure 6.48 shows the conditions at the bottom tray of a reboiled stripper. If valve trays are used with 24-inch tray spacing, estimate the column diameter for 80% of flooding.

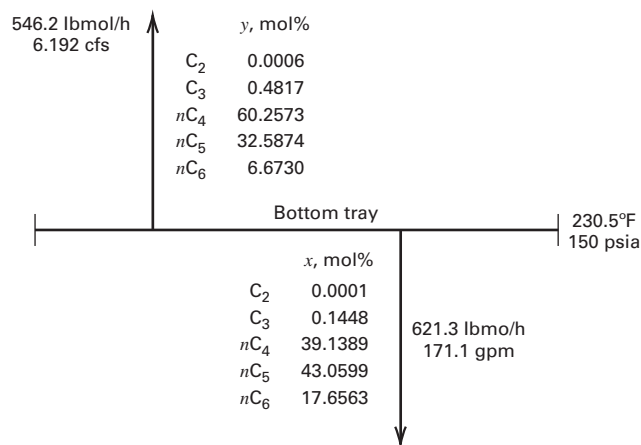


Figure 6.48 Data for Exercise 6.25.

6.26. Flooding velocity and diameter of a valve tray.

Determine the flooding velocity and column diameter at the top tray of a valve-tray absorber, using the following data:

Pressure	400 psia
Temperature	128°F
Vapor rate	530 lbmol/h
Vapor MW	26.6
Vapor density	1.924 lb/ft ³
Liquid rate	889 lbmol/h
Liquid MW	109
Liquid density	41.1 lb/ft ³
Liquid surface tension	18.4 dyne/cm
Foaming factor	0.75
Tray spacing	24 inch
Fraction flooding	0.85

6.27. Sieve-tray column design.

For Exercise 6.23, if an octane absorbent flow rate of 40,000 gpm is used in a sieve-tray column with 24-inch tray spacing, determine, for an 0.80 foaming factor and 0.70 fraction flooding, the column diameter based on conditions near the bottom of the column.

6.28. Trayed-column absorber design.

Repeat the calculations of Example 6.8 for a column diameter corresponding to 40% of flooding.

6.29. Trayed column for acetone absorption.

For the acetone absorber of Figure 6.1, estimate the column diameter for a 0.85 foaming factor and a 0.75 fraction flooding, if sieve trays are used.

6.30. Design of a VOC stripper.

A VOC stripper is to be designed for the flow conditions and separation of Example 6.4, with wastewater and air flow rates twice as high. Determine (a) the number of equilibrium stages required and (b) the column diameter for sieve trays.

Section 6.7**6.31. Absorption of SO₂ in a packed column.**

Air containing 1.6 vol% SO₂ is scrubbed at 1 atm with pure water in a packed column of 1.5-m² cross-sectional area and 3.5-m height, packed with No. 2 plastic Super Intalox saddles. The total gas flow rate is 0.062 kmol/s, the liquid flow rate is 2.2 kmol/s, and the outlet-gas SO₂ concentration is $y = 0.004$. At the column temperature, the equilibrium relationship is $y^* = 40x$. (a) What is L/L_{\min} ? (b) Calculate N_{OG} and compare your answer to that for the number of theoretical stages required. (c) Determine H_{OG} and the HETP from the operating data. (d) Calculate $K_G a$ from the data based on a partial-pressure driving force, as in Item 2 of Table 6.5.

6.32. Absorption of SO₂ in a packed tower.

An SO₂-air mixture is scrubbed with water in a packed tower at 20°C and 1 atm. Solute-free water enters the top at 1,000 lb/h and is well distributed over the packing. The liquor leaving contains 0.6 lb SO₂/100 lb of solute-free water. The partial pressure of SO₂ in the gas leaving is 23 torr. The mole ratio of water to air is 25. The necessary equilibrium data are tabulated below. (a) What percent of the SO₂ in the entering gases is absorbed in the tower? (b) During

operation, it was found that rate coefficients k_p and k_L remained substantially constant throughout the tower at

$$k_L = 1.3 \text{ ft/h, and}$$

$$k_p = 0.195 \text{ lbmol/h-ft}^2\text{-atm}$$

At a point in the tower where the liquid concentration is 0.001 lbmol SO₂ per lbmol of water, what is the liquid concentration at the gas-liquid interface in lbmol/ft³? The solution density is 1 gm/cm³.

Solubility of SO ₂ in H ₂ O at 20°C	
lb SO ₂ 100 lb H ₂ O	Partial Pressure of SO ₂ in Air, torr
0.02	0.5
0.05	1.2
0.10	3.2
0.15	5.8
0.20	8.5
0.30	14.1
0.50	26.0
0.70	39.0
1.0	59

6.33. Stripping of benzene from wastewater in a packed column.

Wastewater at 600 gpm, containing 10 ppm (by weight) of benzene, is to be stripped with air in a packed column, operating at 25°C and 2 atm, to produce water containing 0.005 ppm of benzene. The packing is 2-inch polypropylene Flexirings. The vapor pressure of benzene at 25°C is 95.2 torr. The solubility of benzene in water at 25°C is 0.180 g/100g. An expert in VOC stripping with air suggests the use of 1,000 scfm of air (60°F, 1 atm). At these conditions, for benzene,

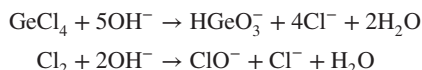
$$k_L a = 0.067 \text{ s}^{-1} \text{ and } k_G a = 0.80 \text{ s}^{-1}$$

Determine: (a) the minimum air-stripping rate in scfm (Is it less than the rate suggested by the expert? If not, use 1.4 times your minimum value.); (b) the stripping factor based on the air rate suggested by the expert; (c) the number of transfer units, N_{OG} ; (d) the overall mass-transfer coefficient, $K_G a$, in units of mol/m³-s-kPa and s⁻¹, and which phase controls mass transfer; and (e) the volume of packing in m³.

Section 6.8**6.34. Scrubbing of GeCl₄ with caustic in a packed column.**

Germanium tetrachloride (GeCl₄) and silicon tetrachloride (SiCl₄) are used in the production of optical fibers. Both chlorides are oxidized at high temperature and converted to glass-like particles. Because the GeCl₄ oxidation is incomplete, the unreacted GeCl₄ is scrubbed from its air carrier with 0.071 kg/s of a dilute caustic solution in a packed column operating at 25°C and 1 atm. The dissolved GeCl₄ has essentially no vapor pressure, and mass transfer is controlled by the gas phase. Thus, the equilibrium curve is a straight line of zero slope. Why? The entering gas is 23,850 kg/day of air containing 288 kg/day of GeCl₄. The air also contains 540 kg/day

of Cl_2 , which, when dissolved, will also have no vapor pressure. The two liquid-phase reactions are as follows:



Ninety-nine percent of both GeCl_4 and Cl_2 must be absorbed in a 2-ft-diameter column packed to a height of 10 ft with 1/2-inch ceramic Raschig rings. The column is to operate at 75% of flooding. For the packing, $\epsilon = 0.63$, $F_p = 580 \text{ ft}^{-1}$, and $D_p = 0.01774 \text{ m}$. The gas-phase mass-transfer coefficients for GeCl_4 and Cl_2 , from empirical equations and properties, are given by

$$\begin{aligned}K_y a &= k_y a \\ \frac{k_y}{(V/A_T)} &= 1.195 \left[\frac{D_p V'}{\mu (1 - \epsilon_o)} \right]^{-0.36} (N_{Sc})^{-2/3} \\ \epsilon_o - \epsilon - h_L & \\ h_L &= 0.03591(L')^{0.331} \\ a &= \frac{14.69(808V'/\rho^{1/2})^n}{(L')^{0.111}} \\ n &= 0.01114L' + 0.148\end{aligned}$$

where A_T = column cross-sectional area in m^2 ; k_y = $\text{kmol}/\text{m}^2\text{-s}$; V = molar gas rate in kmol/s ; D_p = equivalent packing diameter in m ; μ = gas viscosity in $\text{kg}/\text{m-s}$; ρ = gas density in kg/m^3 ; N_{Sc} = Schmidt number = $\mu/\rho D_i$; D_i = molecular diffusivity of component i in the gas in m^2/s ; a = interfacial area for mass transfer in m^2/m^3 of packing; L' = liquid mass velocity in $\text{kg}/\text{m}^2\text{-s}$; and V' = gas mass velocity in $\text{kg}/\text{m}^2\text{-s}$. For the two diffusing species, assume

$$\begin{aligned}D_{\text{GeCl}_4} &= 0.000006 \text{ m}^2/\text{s} \\ D_{\text{Cl}_2} &= 0.000013 \text{ m}^2/\text{s}\end{aligned}$$

- (a) Determine the required packed height in feet based on the controlling species (GeCl_4 or Cl_2). Is the 10 ft of packing adequate? (b) Determine the percent absorption of GeCl_4 and Cl_2 based on the available 10 ft of packing. If the 10 ft of packing is not sufficient, select an alternative packing that is adequate.

6.35. Stripping of VOCs in a packed column.

For the VOC-stripping task of Exercise 6.33, the expert has suggested a tower diameter of 0.80 m with a pressure drop of $500 \text{ N}/\text{m}^2\text{-m}$ of packed height (0.612 inch $\text{H}_2\text{O}/\text{ft}$). Verify the information from the expert by estimating (a) the fraction of flooding using the GPDC chart of Figure 6.36, with $F_p = 24 \text{ ft}^2/\text{ft}^3$; (b) the pressure drop at flooding; and (c) the pressure drop at the operating conditions of Exercise 6.33, using the GPDC chart.

6.36. Mass-transfer coefficients for a packed stripper.

For the VOC stripper of Exercise 6.33, the expert suggested certain mass-transfer coefficients. Check these by using the correlations of Billet and Schultes, assuming that 2-inch plastic Flexiring packing has the characteristics of 2-inch plastic Pall rings.

6.37. Scrubbing of NH_3 with water in a packed column.

A 2 mol% NH_3 -in-air mixture at 68°F and 1 atm is scrubbed with water in a tower packed with 1.5-inch ceramic Berl saddles. The inlet water mass velocity is $2,400 \text{ lb}/\text{h-ft}^2$, and the inlet gas mass velocity is $240 \text{ lb}/\text{h-ft}^2$. The gas solubility follows Henry's law, $p = Hx$, where p is the partial pressure of ammonia, x is the mole fraction of ammonia in the liquid, and $H = 2.7 \text{ atm}/\text{mole fraction}$. (a) Calculate the packed height for 90% NH_3 absorption. (b) Calculate the minimum water mass velocity in $\text{lb}/\text{h-ft}^2$ for absorbing 98% of the NH_3 . (c) The use of 1.5-inch ceramic Hiflow rings rather than Berl saddles has been suggested. What changes would this cause in $K_G a$, maximum liquid rate, $K_L a$, column height, column diameter, H_{OG} , and N_{OG} ?

6.38. Absorption of CO_2 into caustic in a packed column.

Your company, for a carbon-credit exchange program, is considering a packed column to absorb CO_2 from air into a dilute-caustic solution. The air contains 3 mol% CO_2 , and a 97% absorption of CO_2 is mandated. The air-flow rate is $5,000 \text{ ft}^3/\text{minute}$ at 60°F and 1 atm. It may be assumed that the equilibrium curve is $Y^* = 1.75X$, where Y and X are mole ratios of CO_2 to CO_2 -free carrier gas and liquid, respectively. A column diameter of 2.5 ft with 2-inch Intalox saddle packing is assumed for the initial design estimates. Also assume that caustic solution has the properties of water. Calculate (a) the minimum caustic solution-to-air molar flow rate ratio; (b) the maximum possible concentration of CO_2 in the caustic solution; (c) the number of theoretical stages at $L/V = 1.4$ times the minimum; (d) the caustic solution rate; (e) the pressure drop per foot of column height (what does this result suggest?); (f) the overall number of gas transfer units N_{OG} ; and (g) the height of packing, using a $K_G a$ of $2.5 \text{ lbmol}/\text{h-ft}^3\text{-atm}$. Is this a reasonable way to get carbon credits?

6.39. Number of transfer units for an absorber.

A gas stream contains 80 mol% of inerts with a MW of 29 and 20 mol% of propane (MW = 44). An absorber is to be designed to recover 95% of the propane with an HC oil having an average MW of 300. The absorber will be a column with structured packing. The entering-gas mass velocity at the bottom will be $5,000 \text{ lb}/\text{h-ft}^2$. The liquid absorbent will enter the top at a mass velocity of $20,000 \text{ lb}/\text{h-ft}^2$. Equilibrium data for propane at the operating conditions of the column are as follows:

x	0.1	0.2	0.3	0.4	0.5
y^*	0.008	0.028	0.06	0.12	0.2

Determine the number of overall gas transfer units, N_{OG} .

Distillation of Binary Mixtures

§7.0 INSTRUCTIONAL OBJECTIVES

After completing this chapter, you should be able to:

- Explain the need in distillation for a condenser to produce reflux and a reboiler to produce boilup.
- Determine the five construction lines of the McCabe–Thiele method using material balances and vapor–liquid equilibrium relations.
- Distinguish among five possible phase conditions of the feed.
- Apply the McCabe–Thiele method for determining minimum reflux ratio, minimum equilibrium stages, number of stages for a specified reflux ratio greater than minimum, and optimal feed-stage location, given the required split between the two feed components.
- Use a Murphree vapor-stage efficiency to determine the number of actual trays from the number of equilibrium stages.
- Determine the diameter of a trayed tower and the size of the reflux drum.
- Determine packed height and diameter of a packed column for distillation.

In distillation (fractionation), one or more feed mixtures of two or more components are separated into two or more products, including, and often limited to, an overhead distillate and a bottoms product, whose compositions differ from that of the feed(s). Most often, the feed(s) is (are) a liquid or a vapor–liquid mixture. The bottoms product is almost always a liquid, while the distillate may be a liquid, a vapor, or a mixture of the two. The separation requires that (1) a second phase be formed so that both liquid and vapor are present and can make contact while flowing countercurrently to each other in a trayed or packed column; (2) components have different volatilities so that they partition between phases to different extents; and (3) the two phases are separable by gravity or mechanical means. Distillation differs from absorption and stripping in that the second fluid phase is created by thermal means (vaporization and condensation) rather than by introduction of a second phase (mass-separating agent) that may contain an additional component or components not present in the feed mixture(s).

According to Forbes [1], distillation dates back to at least the 1st century A.D. By the 11th century, batch distillation was used in Italy to produce alcoholic beverages. The liquid feed was placed in a heated vessel, causing part of the liquid to evaporate. The vapor passed out of the vessel into a water-cooled condenser and dripped into a product receiver. The word *distillation* is derived from the Latin word *destillare*, which means “dripping.” By the 16th century, it was known that the extent of separation could be improved by providing multiple vapor liquid contacts (stages) in a so-called Rectifierium. The term *rectification* is derived from the Latin words *recte facere*, meaning “to improve.” Today, almost pure products are obtained by continuous, multistage contacting.

Multistage distillation is the most widely used industrial method for separating chemical mixtures, despite the fact that it can be very energy intensive, especially when the relative volatility, α , (2–20), of the key components is low (< 1.50). A recent survey by Pete Sharpe of Emerson Process Experts [http://www.emersonprocessxperts.com/2010/04/reducing_distil/#.U6NG3_ldXAY] reported that more than 40,000 distillation columns are operating in the United States. They account for 40 to 60% of the energy consumed in the chemical and petroleum refining industries, 19% of the energy used by U.S. manufacturers, and 6% of the total U.S. energy consumption. In petroleum refineries, distillation separates crude oil into petroleum fractions, light hydrocarbons, and organic petrochemicals. In the chemical industry, organic alcohols, acids, ketones, etc., are recovered and purified.

The fundamentals of distillation are best understood by the study of continuous **binary distillation**, the separation of a two-component mixture. The more general and mathematically complex cases of continuous multicomponent distillation are covered in Chapters 9 to 12. Batch distillation is described in Chapter 13.

Industrial Example

Figure 7.1 shows a binary distillation for the separation of 620 lbmol/h of a mixture of 46 mol% benzene (the more volatile component) from 54 mol% toluene. The purpose of the 25-sieve-tray column, with a condenser, reflux drum, and reboiler, is to separate the feed into a liquid distillate of 99 mol% benzene and a liquid bottoms product of 98 mol% toluene. The column operates at near-ambient pressure, where benzene and toluene form near-ideal mixtures with a relative

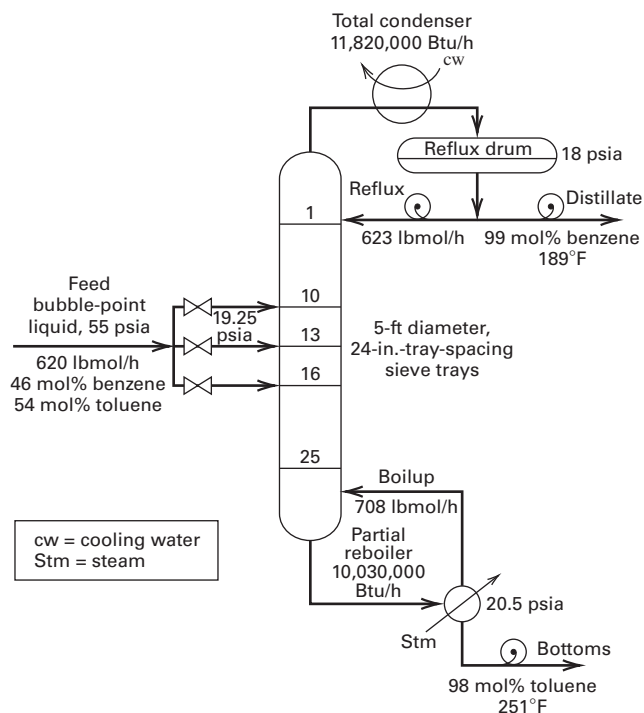


Figure 7.1 Continuous distillation of a binary mixture of benzene and toluene.

volatility, α , in the range from 2.26 at the bottom tray to 2.52 at the top tray, as determined from Raoult’s law, (2-28). The reflux ratio (reflux flow rate to distillate flow rate) is 2.215. This is about 30% higher than the minimum ratio needed to achieve the required separation.

The feed is a saturated (bubble-point) liquid at 55 psia. When flashed adiabatically across the feed valve to the

feed-tray pressure of 19.25 psia, 23.4 mol% of the feed is vaporized. A total condenser is used to obtain saturated liquid reflux and liquid distillate at 189°F and 18 psia. The condenser heat is 11,820,000 Btu/h. At the bottom of the column, a partial reboiler is used to produce vapor boilup and a saturated liquid bottoms product. The reboiler duty is 10,030,000 Btu/h, which is close to the condenser duty.

The inside diameter of the column in Figure 7.1 is a constant 5 ft. At the top, this corresponds to 84% of flooding, while at the bottom, 81%. The column is provided with three alternative feed locations. For the design conditions, the optimal feed entry is between trays 12 and 13. Should the feed composition or product specifications change, one of the other feed trays could become optimal.

Columns similar to that in Figure 7.1 have been built for diameters up to at least 30 ft. With a 24-inch tray spacing, the number of trays in a single column is usually no greater than 150. In many locations, wind loading becomes a limiting factor in the construction of tall columns. For the sharp separation of a binary mixture with an $\alpha < 1.05$, distillation can require many hundreds of trays, so a more efficient separation technique should be sought. Even when distillation is the most economical separation technique, its efficiency, as defined in §2.12, can be less than 10%.

In Figure 1.8, distillation is the most mature of all separation operations. Design and operation procedures are well established (see Kister [3, 4]). Only when vapor–liquid equilibrium, azeotrope formation, or other data are uncertain is a laboratory and/or pilot-plant study necessary prior to the design of a commercial unit. Table 7.1, taken partially from Mix et al. [2], lists representative, industrial, and

Table 7.1 Representative Commercial Binary Distillation Operations

Binary Mixture	Average Relative Volatility	Number of Trays	Typical Operating Pressure, psia	Reflux-to-Minimum-Reflux Ratio
<i>o</i> -Xylene/ <i>m</i> -xylene	1.17	130	15	1.12
Isopentane/ <i>n</i> -pentane	1.30	120	30	1.20
Isobutane/ <i>n</i> -butane	1.35	100	100	1.15
Ethylbenzene/styrene	1.38	34	1	1.71
Propylene/propane	1.40	138	280	1.06
Methanol/ethanol	1.44	75	15	1.20
Water/acetic acid	1.83	40	15	1.35
Ethylene/ethane	1.87	73	230	1.07
Toluene/ethylbenzene	2.15	28	15	1.20
Propane/1,3-butadiene	2.18	40	120	1.13
Ethanol azeotrope/water	2.21	60	15	1.35
Isopropanol/water	2.23	12	15	1.28
Benzene/toluene	3.09	34	15	1.15
Methanol/water	3.27	60	45	1.31
Cumene/phenol	3.76	38	1	1.21
Benzene/ethylbenzene	6.79	20	15	1.14
HCN/water	11.20	15	50	1.36
Ethylene oxide/water	12.68	50	50	1.19
Formaldehyde/methanol	16.70	23	50	1.17
Water/ethylene glycol	81.20	16	4	1.20

continuous binary distillations in decreasing order of difficulty of separation. Included are average values of relative volatility, number of trays, typical column operating pressure, and reflux-to-minimum-reflux ratio. Although the data in Table 7.1 refer to trayed towers, distillation is also carried out in packed columns.

Equilibrium-stage calculations for trayed columns and rate-based calculations for packed columns for continuous binary distillation are covered in this chapter. Column sizing procedures presented in Chapter 6 for absorbers and strippers are applicable here to binary distillation and to multicomponent distillation as well. Methods for estimating tray efficiency are also covered in this chapter and are applicable to both binary and multicomponent distillation.

§7.1 EQUIPMENT AND DESIGN CONSIDERATIONS

Types of trays and packings for distillation are identical to those used in absorption and stripping, as shown in Figures 6.2, 6.5, 6.7, and 6.8 and compared in Tables 6.2 and 6.3.

§7.1.1 Design and Analysis Factors

The following factors that influence the design or analysis of a binary-distillation operation are:

1. Feed flow rate, composition, temperature, pressure, and phase
2. Desired degree of component separation
3. Operating pressure (which must be below the critical pressure of the mixture)
4. Pressure drop, particularly for vacuum operation
5. Reflux ratio
6. Number of equilibrium stages and stage efficiency or HETP
7. Type of condenser (total, partial, or mixed)
8. Degrees of liquid reflux subcooling
9. Type of reboiler (partial or total)
10. Type of trays or packing
11. Column height
12. Feed-entry stage
13. Column diameter
14. Column internals and materials of construction
15. Heat lability and chemical reactivity of feed components
16. Corrosion and materials of construction
17. Toxicity and flammability

§7.1.2 Initial Considerations of Design Factors

Temperature and phase of the feed are determined at the feed-tray pressure by an adiabatic-flash calculation across the

feed valve. As the feed vapor fraction increases, the required reflux rate increases, but the boilup rate decreases.

As column operating pressure is increased, temperatures in the column increase in a manner similar to a vapor-pressure plot. The operating pressure at the top of the column should correspond to a saturated distillate temperature that is somewhat higher (e.g., 10 to 50°F) than the supply temperature of the cooling water to the overhead condenser. However, if this pressure approaches the critical pressure of the more volatile component, then a lower pressure must be used and a refrigerant is required as coolant. For example, in Table 7.1, the separation of ethylene/ethane is conducted at 230 psia, giving a column top temperature of -40°F . Therefore, a refrigerant is required to condense the overhead. Water at 80°F for the condenser cannot be used at any column operating pressure because the critical temperature of ethylene is 48.6°F (282 K).

If the estimated column pressure is less than atmospheric, the operating pressure at the top is often set just above atmospheric to avoid vacuum operation, unless the temperature at the bottom of the column is limited by decomposition, polymerization, excessive corrosion, or other chemical reactions. In that case, vacuum operation is necessary. For example, in Table 7.1, vacuum operation is required for the separation of ethylbenzene from styrene to maintain a temperature low enough to prevent styrene polymerization in the reboiler.

For given (1) feed, (2) desired degree of separation, and (3) operating pressure, a minimum reflux ratio (reflux rate to distillate rate) exists that corresponds to an infinite number of theoretical stages. This is similar to the minimum absorbent to feed flow rate in absorption as described in §6.2. A minimum number of theoretical stages exist that correspond to an infinite reflux ratio. The design trade-off is between the number of stages and the reflux ratio. A graphical method for determining the data needed to establish this trade-off and to determine the optimal feed-stage location is developed in the next section.

§7.2 MCCABE–THIELE GRAPHICAL METHOD FOR TRAYED TOWERS

Figure 7.2 shows a column containing the equivalent of N equilibrium stages, a total condenser, and a partial reboiler. Feed enters the column at an intermediate stage. The overhead vapor leaving the top stage is totally condensed and sent to a reflux drum from which a liquid distillate is withdrawn and a liquid **reflux** is returned to the top stage. In the partial reboiler, liquid from the bottom stage is partially vaporized to give vapor **boilup** that is returned to the bottom stage. The remaining liquid is withdrawn as the bottoms product.

By means of multiple countercurrent stages arranged in a two-section cascade with reflux and boilup, as discussed in §5.3, a sharp separation between the two feed components is possible unless an azeotrope exists, in which case one of the two products will approach the azeotropic composition.

The feed, which contains a more volatile (light) component (the **light key**, LK), and a less volatile (heavy) component (the **heavy key**, HK), enters the column at feed stage f . At feed-stage pressure, the feed of LK mole fraction z_f may be

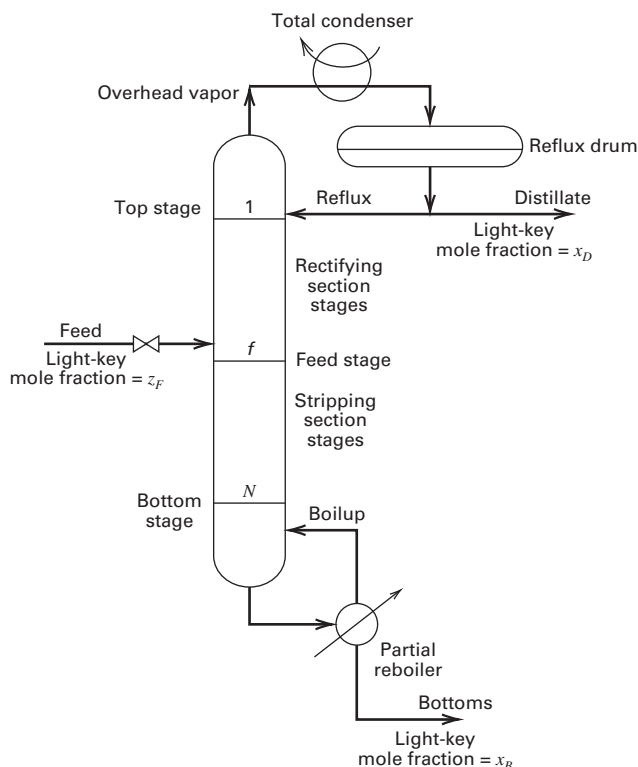


Figure 7.2 Distillation column with a total condenser and partial reboiler.

liquid, vapor, or a mixture of the two. The LK mole fraction is x_D in the distillate and x_B in the bottoms product. Mole fractions of the HK are $(1 - z_F)$, $(1 - x_D)$, and $(1 - x_B)$ in the feed, distillate, and bottoms, respectively.

The goal of distillation is to produce a distillate rich in the LK (i.e., an x_D approaching 1.0) and a bottoms product rich in the HK (i.e., x_B approaching 0.0). Whether the separation is achievable depends on $\alpha_{1,2}$ of the two components (LK = 1 and HK = 2), where

$$\alpha_{1,2} = K_1/K_2 \tag{7-1}$$

If the two components form ideal solutions and follow the ideal-gas law in the vapor phase, Raoult's law (2-28) applies, giving

$$K_1 = P_1^s/P \quad \text{and} \quad K_2 = P_2^s/P$$

and from (7-1), the relative volatility is given by the ratio of vapor pressures, $\alpha_{1,2} = P_1^s/P_2^s$, and is a function only of temperature. As discussed in §4.2, as the temperature (and therefore the pressure) increases, $\alpha_{1,2}$ decreases. At the mixture convergence pressure (e.g., see §2.5.2 and Figure 2.2), $\alpha_{1,2} = 1.0$, and separation cannot be achieved at this or a higher pressure.

The relative volatility in terms of equilibrium vapor and liquid mole fractions from the K -value expressed as $K_i = y_i/x_i$ (2-18) for a binary mixture is

$$\alpha_{1,2} = \frac{y_1/x_1}{y_2/x_2} = \frac{y_1(1-x_1)}{x_1(1-y_1)} \tag{7-2}$$

Solving (7-2) for y_1 ,

$$y_1 = \frac{\alpha_{1,2}x_1}{1 + x_1(\alpha_{1,2} - 1)} \tag{7-3}$$

For components with close boiling points, the temperature change over the column is small and $\alpha_{1,2}$ is almost constant. Figure 7.3 shows a vapor–liquid equilibrium curve for the benzene–toluene system for 1 atm, at which pure benzene and pure toluene boil at 176 and 231°F, respectively. These two components are not close boiling and can be separated by distillation. Using (7-3) with experimental x – y data, α varies from 2.6 at the bottom of the column to 2.35 at the top.

Equilibrium curves for some average values of $\alpha_{1,2}$ are shown in Figure 7.4. The higher the average value of α , the easier the desired separation. Average values of α in Table 7.1 range from 1.17 to 81.2.

In 1925, McCabe and Thiele [5] published a graphical method for combining the equilibrium curve with

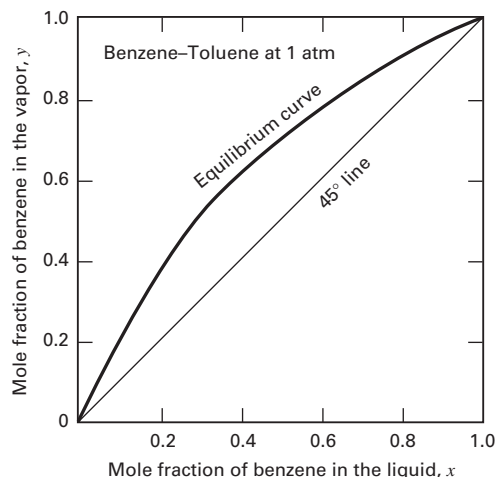


Figure 7.3 Equilibrium curve for benzene–toluene at 1 atm.

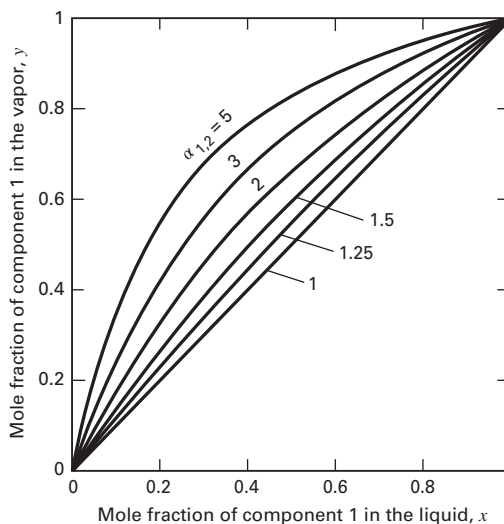


Figure 7.4 Vapor–liquid equilibrium curves for constant values of relative volatility.

material-balance operating lines to estimate, for a binary-feed mixture and selected column pressure, the number of equilibrium stages and reflux required for a specified split of the feed components. The method is an extension of the graphical staircase procedure used for absorbers and strippers described in §6.3.4.

Although computer-aided methods discussed in Chapter 10 are more accurate and rapidly applied, the graphical McCabe–Thiele method greatly facilitates visualization of the fundamentals of multistage distillation, including the effects of specifications such as reflux, feed condition, and feed-stage location. The effort required to learn and apply the method is well justified. Furthermore, as discussed in §5.6.4, the McCabe–Thiele method is representative of the design case. It determines, for a specified separation, the minimum reflux ratio, the minimum number of equilibrium stages, the number of stages for a given reflux ratio, and the optimal feed-stage location. Computer-aided methods are representative of the simulation case. They calculate the separation achieved for a fixed number of equilibrium stages, reflux, feed condition, and feed-stage location. Thus, when a distillation column is to be designed to separate a binary mixture, it is useful to apply the McCabe–Thiele method prior to and during computer-aided calculations with a process simulator. The ChemSep program allows the user to produce McCabe–Thiele plots of computer-produced simulations to facilitate changes to simulation specifications that lead to a desired design.

Typical input specifications and results (outputs) from the McCabe–Thiele construction for a single-feed, two-product distillation are summarized in Table 7.2, where it is required that, for the lighter component, $x_B < z_F < x_D$. The distillate can be a liquid from a total condenser, as shown in Figure 7.2, or a vapor from a partial condenser. The feed-phase condition must be known at column pressure, which is assumed to be uniform throughout the column. The type of condenser and reboiler must be specified, as well as the ratio of reflux to minimum reflux. From the specification of x_D and x_B for the LK, distillate and bottoms rates, D and B , are fixed by material balances, as follows:

By overall material balance for the LK,

$$Fz_F = x_D D + x_B B \quad (7-4)$$

By overall total material balance,

$$F = D + B \quad (7-5)$$

Combine (7-4) and (7-5) to eliminate B and solve for D ,

$$D = F \left(\frac{z_F - x_B}{x_D - x_B} \right) \quad (7-6)$$

and

$$B = F - D \quad (7-7)$$

The graphical McCabe–Thiele construct determines (1) N , the number of equilibrium stages; (2) N_{\min} , the minimum number of equilibrium stages; (3) $R_{\min} = L_{\min}/D$, the minimum reflux ratio; and (4) the optimal feed-stage location. The

Table 7.2 Specifications and Results for the McCabe–Thiele Method for Binary Distillation

Specifications	
F	Total feed rate
z_F	Mole fraction of LK in the feed
P	Column operating pressure (assumed uniform throughout the column)
	Phase condition of the feed at column pressure
	Vapor–liquid equilibrium curve for the binary mixture at column pressure
	Type of overhead condenser (total or partial)
	Type of reboiler (usually partial)
x_D	Mole fraction of LK in the distillate
x_B	Mole fraction of LK in the bottoms
R/R_{\min}	Ratio of reflux to minimum reflux
Results	
D	Distillate flow rate
B	Bottoms flow rate
N_{\min}	Minimum number of equilibrium stages
R_{\min}	Minimum reflux ratio, L_{\min}/D
R	Reflux ratio, L/D
V_B	Boilup ratio, \bar{V}/B
N	Number of equilibrium stages
	Optimal feed-stage location
	Vapor and liquid compositions leaving each stage

remaining variables listed under Results, and the heating and cooling requirements, can then be calculated.

As shown in Figure 7.5, the McCabe–Thiele method includes five construction lines on a plot of y vs. x for the LK. The lines are (1) a **45° reference line**; (2) an **equilibrium curve**; (3) an **operating line for the rectifying section**; (4) an **operating line for the stripping section**; and (5) a feed line,

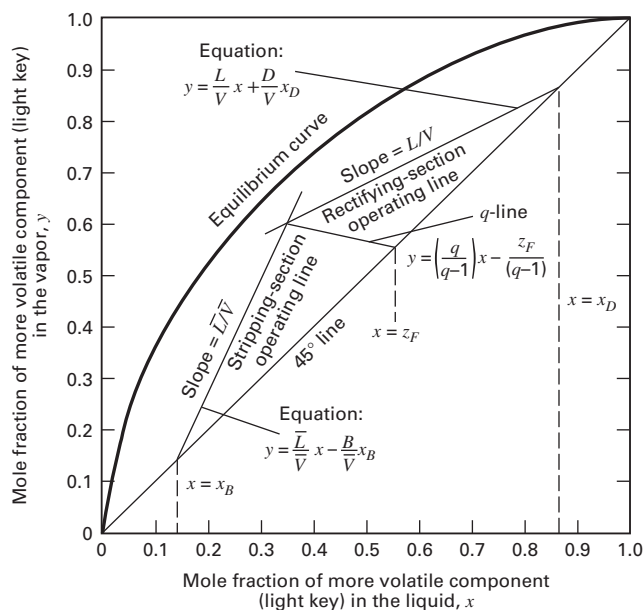


Figure 7.5 Construction lines for McCabe–Thiele graphical method.

called the **q-line**, for the phase or thermal condition of the feed. Typical lines are shown in Figure 7.5, where the ranges of y and x are from 0 to 1. The equilibrium line is obtained from experimental data or calculated from an applicable EOS or g^E method described in Chapter 2. Equations for the lines (3) to (5) are derived next.

§7.2.1 Rectifying-Section Operating Line

Figure 7.2 shows that the rectifying section extends from the top stage, 1, to just above the feed stage, f . Consider a top portion of the rectifying stages, including the total condenser, as shown by the envelope in Figure 7.6a. A material balance for the LK over the envelope for the total condenser and stages 1 to n is as follows, where y and x refer, respectively, to LK vapor and liquid mole fractions. The subscripts on V , L , y , and x refer to the stages from which the streams leave.

$$V_{n+1}y_{n+1} = L_nx_n + Dx_D \quad (7-8)$$

Solving (7-8) for y_{n+1} gives the equation for the rectifying-section operating line:

$$y_{n+1} = \frac{L_n}{V_{n+1}}x_n + \frac{D}{V_{n+1}}x_D \quad (7-9)$$

This equation relates LK compositions y_{n+1} and x_n of **passing streams** V_{n+1} and L_n , respectively.

Equation (7-9) is the locus of LK mole fractions of all passing streams between stages in the rectifying section. To be plotted as a straight line, $y = mx + b$, L and V must not vary from stage to stage in the rectifying section. This is the case if:

1. The two components have equal and constant molar enthalpies of vaporization (latent heats).
2. Component sensible-enthalpy changes ($C_p\Delta T$) and heat of mixing are negligible compared to latent heat changes.

3. The column is insulated, so heat loss is negligible.
4. Column pressure is uniform (no pressure drop).

These are the **McCabe–Thiele assumptions** leading to the condition of **constant molar overflow** in the rectifying section, where total molar flow rates remain constant as liquid overflows each weir from one stage to the next. Since a total material balance for the rectifying-section envelope in Figure 7.6a gives $V_{n+1} = L_n + D$, if L is constant, then V is also constant for a fixed D . Rewriting (7-9) as in Figure 7.5,

$$y = \frac{L}{V}x + \frac{D}{V}x_D \quad (7-10)$$

Thus, the slope of the operating line in the rectifying section is a constant L/V , with $V > L$, giving $L/V < 1$, as in Figure 7.6b.

For constant molar overflow in the rectifying and stripping sections, only material balances and an equilibrium curve are required. Energy balances are needed only to determine condenser and reboiler duties, after completing a McCabe–Thiele calculation, as discussed in §7.3.5.

Liquid entering stage 1 at the top is the **external reflux rate**, L_0 , and its ratio to the distillate rate, L_0/D , is the **reflux ratio** R . Because of constant molar overflow, $R = L/D$ is a constant in the rectifying section. Since $V = L + D$, the slope of the operating line is readily related to the reflux ratio:

$$\frac{L}{V} = \frac{L}{L + D} = \frac{L/D}{L/D + D/D} = \frac{R}{R + 1} \quad (7-11)$$

Similarly,

$$\frac{D}{V} = \frac{D}{L + D} = \frac{1}{R + 1} \quad (7-12)$$

Combining (7-10) to (7-12) produces the most useful form of the rectifying-section operating line:

$$y = \left(\frac{R}{R + 1} \right) x + \left(\frac{1}{R + 1} \right) x_D \quad (7-13)$$

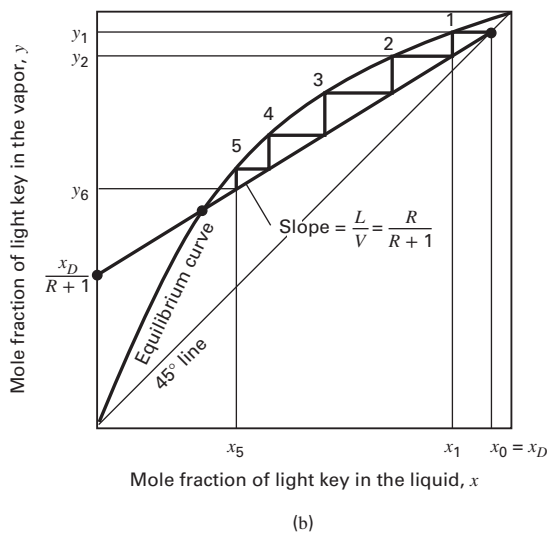
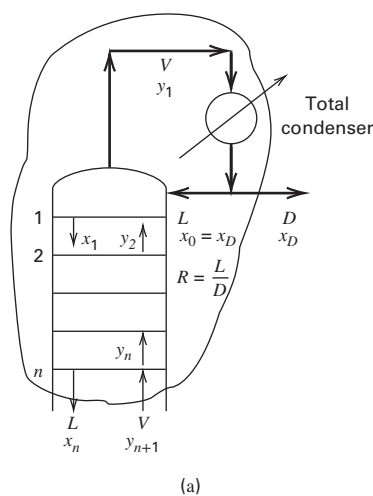


Figure 7.6 McCabe–Thiele operating line for the rectifying section.

If for a total condenser, R and x_D are specified, (7-13) plots as a straight line in Figure 7.6b, with an intersection at $y = x_D$ on the 45° line where $y = x$. The slope of the line is $L/V = R/(R + 1)$, and the intersection is at $y = x_D/(R + 1)$ for $x = 0$.

In Figure 7.6b, the equilibrium stages are stepped off as in §6.3.4 for absorption. Starting from point $(y_1 = x_D, x_0 = x_D)$ on the operating line and the 45° line, a horizontal line is drawn to the left until it intersects the equilibrium curve at (y_1, x_1) , the compositions of the equilibrium phases leaving the top stage. A vertical line is dropped from (y_1, x_1) until it intersects the operating line at (y_2, x_1) , the compositions of the passing streams between stages 1 and 2. Horizontal- and vertical-line constructions are continued, stage-by-stage, down the rectifying section to give a staircase construction, which is arbitrarily terminated in Figure 7.6b at stage 5. The optimal termination stage is considered in §7.2.3.

§7.2.2 Stripping-Section Operating Line

The stripping section extends from the bottom stage to the feed stage. Figure 7.7a shows an envelope around a bottom portion of equilibrium stripping stages. Included is a partial reboiler and stages from N to $m + 1$, below the feed entry. An envelope material balance is,

$$\bar{L}x_m = \bar{V}y_{m+1} + Bx_B \tag{7-14}$$

Solving for y_{m+1} ,

$$y_{m+1} = \frac{\bar{L}}{\bar{V}}x_m - \frac{B}{\bar{V}}x_B \tag{7-15}$$

or

$$y = \frac{\bar{L}}{\bar{V}}x - \frac{B}{\bar{V}}x_B \tag{7-16}$$

where \bar{L} and \bar{V} are total molar flow rates in the stripping section (which will be different from L and V in the rectifying section because of feed addition). They are subject to the same constant-molar-overflow assumption used in the rectifying section and they are not subscripted. The slope of

this stripping-section operating line for the compositions of passing streams is \bar{L}/\bar{V} . Because $\bar{L} > \bar{V}$, $\bar{L}/\bar{V} > 1$, as seen in Figure 7.7b. This is the inverse of the slope of the rectifying-section operating line.

Vapor, \bar{V} , leaving the partial reboiler is assumed to be in equilibrium with the liquid bottoms product, B , making the partial reboiler equivalent to one equilibrium stage. The vapor rate leaving the reboiler is the **boilup**, $\bar{V}_{N+1} = \bar{V}$, and its ratio to the bottoms product rate, $V_B = \bar{V}_{N+1}/B$, is the **boilup ratio**. With the constant-molar-overflow assumption, V_B is constant in the stripping section. Since $\bar{L} = \bar{V} + B$,

$$\frac{\bar{L}}{\bar{V}} = \frac{\bar{V} + B}{\bar{V}} = \frac{V_B + 1}{V_B} \tag{7-17}$$

Similarly,

$$\frac{B}{\bar{V}} = \frac{1}{V_B} \tag{7-18}$$

Combining (7-16) to (7-18), the stripping-section operating-line equation is:

$$y = \left(\frac{V_B + 1}{V_B} \right) x - \left(\frac{1}{V_B} \right) x_B \tag{7-19}$$

If values of V_B and x_B are known, (7-19) can be plotted as a straight line with an intersection at $y = x_B$ on the 45° line and a slope of $\bar{L}/\bar{V} = (V_B + 1)/V_B$ as in Figure 7.7b. The stages are stepped off, in a manner similar to that for the rectifying section construct, starting from the bottom at the intersection of the operating line and the 45° line ($y = x_B, x = x_B$). A vertical line is drawn upward from that point to an intersection with the equilibrium curve at $(y = y_B, x = x_B)$, which represents the vapor and liquid leaving the partial reboiler. From that point, the staircase is constructed by drawing horizontal and then vertical lines between the operating line and equilibrium curve, as in Figure 7.7b, where the staircase is arbitrarily terminated at stage m . The next consideration is the intersection of the two operating lines. This is determined by the selection of the feed stage.

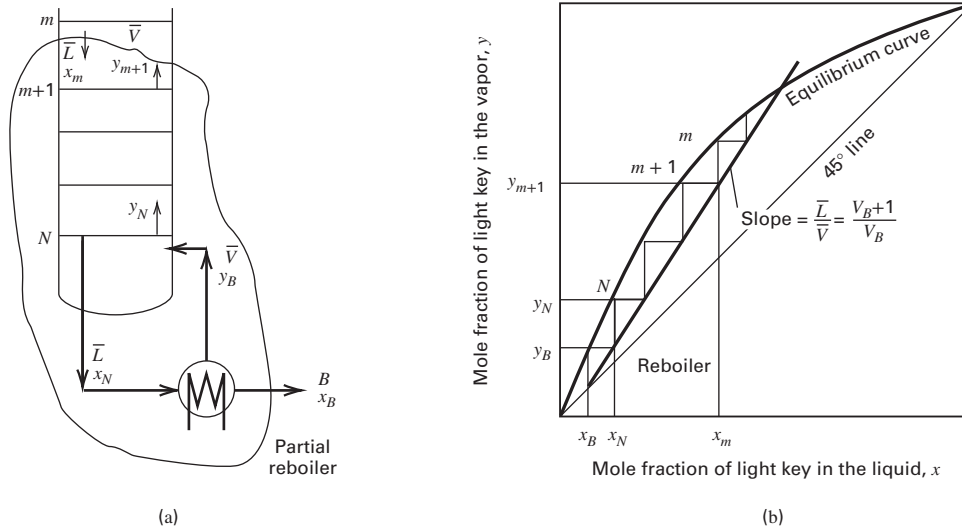


Figure 7.7 McCabe–Thiele operating line for the stripping section.

§7.2.3 Feed-Stage Considerations—the q -Line

When drawing operating lines for the rectifying and stripping sections, x_D and x_B can be selected independently; however, R and V_B are not independent of each other but are related by the feed phase condition.

Figure 7.8 shows five possible feed conditions, where the feed (whose pressure must be, at least, incrementally higher than the column pressure) has been flashed adiabatically to the column pressure at the feed-stage location. In (a), the feed is a bubble-point liquid that adds to the reflux, L , from the stage above, to give $\bar{L} = L + F$. In (b), the feed is a dew-point vapor that adds to the boilup, \bar{V} , coming from the stage below, to give $V = \bar{V} + F$. For the partially vaporized feed in (d), $F = L_F + V_F$, $\bar{L} = L + L_F$ and $V = \bar{V} + V_F$. In (c), the feed is a subcooled liquid that causes some of the boilup, \bar{V} , to condense, giving $\bar{L} > L + F$ and $V < \bar{V}$. In (e), the feed is a superheated vapor that causes a portion of the reflux, L , to vaporize, giving $\bar{L} < L$ and $V > \bar{V} + F$.

Cases (a), (b), and (d) of Figure 7.8, cover well-defined feed conditions from a saturated liquid to a saturated vapor, the boilup \bar{V} is related to the reflux L by the material balance

$$\bar{V} = L + D - V_F \tag{7-20}$$

and the boilup ratio, $V_B = \bar{V}/B$, is

$$V_B = \frac{L + D - V_F}{B} \tag{7-21}$$

Alternatively, the reflux rate can be obtained from the boilup rate by

$$L = \bar{V} + B - L_F \tag{7-22}$$

Although distillations can be specified by reflux ratio, R , or boilup ratio, V_B , by tradition R or R/R_{\min} is used because the distillate is often the more important product.

Cases (c) and (e) in Figure 7.8 are more difficult because V_B and R cannot be related by simple material balances. An energy balance is necessary to convert sensible enthalpy of subcooling or superheating into heat of vaporization. This is conveniently done by defining a parameter, q , equal to the ratio of the increase in molar liquid rate across the feed stage to the molar feed rate:

$$q = \frac{\bar{L} - L}{F} \tag{7-23}$$

or by material balance around the feed stage,

$$q = 1 + \frac{\bar{V} - V}{F} \tag{7-24}$$

Values of q for the five feed conditions of Figure 7.8 are

Feed Condition	q
Subcooled liquid	> 1
Bubble-point liquid	1
Partially vaporized	$L_F/F = 1 - \text{molar fraction vaporized}$
Dew-point vapor	0
Superheated vapor	< 0

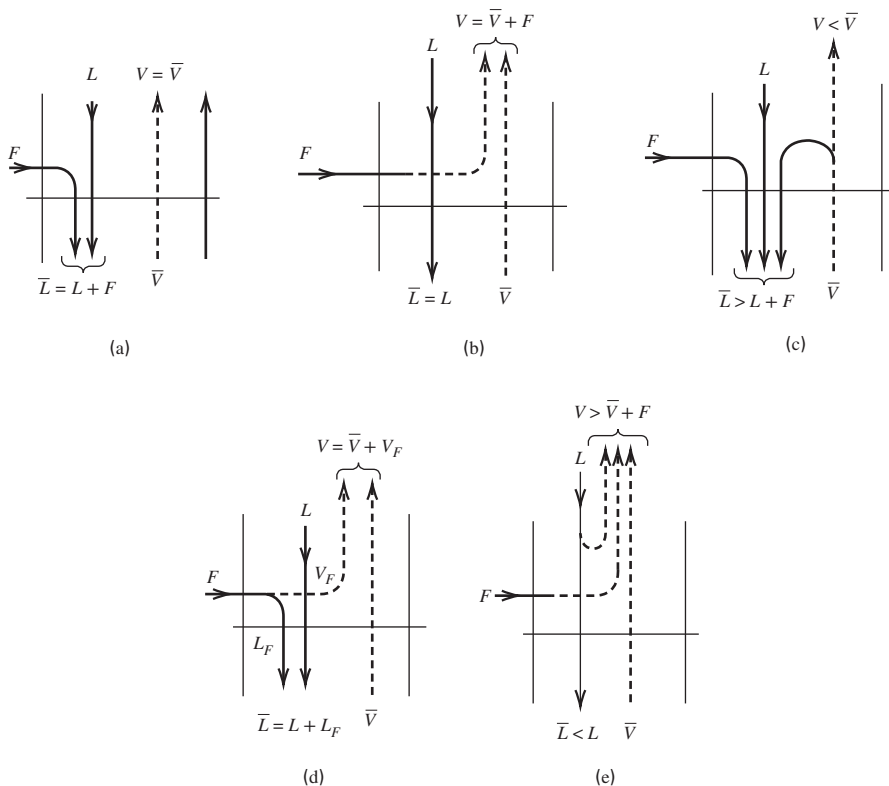


Figure 7.8 Possible feed conditions: (a) bubble-point liquid; (b) dew-point vapor; (c) subcooled liquid; (d) partially vaporized; (e) superheated vapor.

For subcooled liquids and superheated vapors, a more general definition of q is:

$$q = \frac{(h_F)_{\text{sat'd vapor temperature}} - (h_F)_{\text{feed temperature}}}{(h_F)_{\text{sat'd vapor temperature}} - (h_F)_{\text{sat'd liquid temperature}}} \quad (7-25)$$

In words, q = enthalpy change to bring the feed to a dew-point vapor divided by enthalpy of vaporization of the feed (dew-point vapor minus bubble-point liquid); that is:

For a subcooled liquid feed, (7-25) becomes

$$q = \frac{\Delta H^{\text{vap}} + C_{P_L}(T_b - T_F)}{\Delta H^{\text{vap}}} \quad (7-26)$$

For a superheated vapor feed, (7-20) becomes

$$q = \frac{C_{P_V}(T_d - T_F)}{\Delta H^{\text{vap}}} \quad (7-27)$$

where C_{P_L} and C_{P_V} are molar heat capacities of the liquid and vapor; ΔH^{vap} is the molar enthalpy change from the bubble point to the dew point; and T_F , T_d , and T_b are, respectively, feed, dew-point, and bubble-point temperatures of the feed at column operating pressure.

Instead of using (7-19) to locate the stripping-section operating line on the McCabe–Thiele diagram, a q -line can be used as shown in Figure 7.5. One point of this line is where the rectifying- and stripping-section operating lines intersect. It is derived by combining (7-10) with (7-16) to give

$$y(V - \bar{V}) = (L - \bar{L})x + Dx_D + Bx_B \quad (7-28)$$

$$\text{However, overall, } Dx_D + Bx_B = Fz_F \quad (7-29)$$

and a total material balance around the feed stage gives

$$F + \bar{V} + L = V + \bar{L} \quad (7-30)$$

Combining (7-28) to (7-30) with (7-23) gives the q -line equation

$$y = \left(\frac{q}{q-1} \right) x - \left(\frac{z_F}{q-1} \right) \quad (7-31)$$

which is located on the McCabe–Thiele diagram of Figure 7.5 by noting that when $x = z_F$, (7-31) reduces to the point $y = z_F = x$, which lies on the 45° line. From (7-31), the q -line slope is $q/(q-1)$. In Figure 7.5, the q -line is constructed for a partially vaporized feed, where $0 < q < 1$ and $-\infty < [q/(q-1)] < 0$. Following placement of the rectifying-section operating line and the q -line, the stripping-section operating line is located by drawing a line from the point $(y = x_B, x = x_B)$ on the 45° line to and through the intersection of the q -line and rectifying-section operating line, as in Figure 7.5. The point of intersection lies somewhere between the equilibrium curve and the 45° line.

As q changes from > 1 (subcooled liquid) to < 0 (superheated vapor), the q -line slope, $q/(q-1)$, changes from positive to negative and back to positive, as shown in Figure 7.9. For a saturated-liquid feed, the q -line is vertical; for a saturated vapor, the q -line is horizontal.

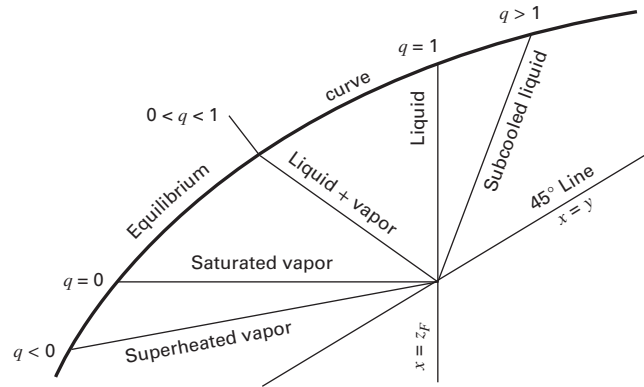


Figure 7.9 Effect of feed condition on the slope of the q -line.

§7.2.4 Number of Equilibrium Stages and Feed-Stage Location

Following construction of the equilibrium curve, the 45° line, the two operating lines, and the q -line, all shown in Figure 7.5, the equilibrium stages required, as well as the location of the feed stage, are determined by stepping off stages from the top down or from the bottom up. An exact integer number of stages is rare; usually fractions of stages arise. Normally the staircase is stepped off from the top and continued to the bottom, starting from the point $(y = x_D, x = x_D)$ on the 45° line, as shown in Figure 7.10a for a partially vaporized feed. In that figure, point P is the intersection of the q -line with the two operating lines. The feed-stage location is the transfer point for stepping off stages between the rectifying-section operating line and the equilibrium curve to stepping off stages between the stripping-section operating line and the equilibrium curve.

The smallest (optimal) number of total equilibrium stages occurs when the transfer is made at the first opportunity after a horizontal line of the staircase passes over point P. In Figure 7.10a, the feed stage is stage 3 from the top and a fortuitous total of exactly five stages is required (four in the column plus a partial reboiler).

In Figure 7.10b, the transfer is delayed and the feed stage is stage 5. But now a total of about 6.4 stages is required. The stepping off of stages in the rectifying section could be continued indefinitely, finally approaching, but never reaching, a feed stage at point K, where the total number of equilibrium stages = ∞ .

In Figure 7.10c, the transfer is made early, at feed stage 2, resulting again in more stages than the optimal number of five. If the stepping off of stages had started from the partial reboiler and proceeded upward, the staircase in the stripping section could have been continued indefinitely, approaching, but never reaching, point R.

When using a process simulator to make calculations of a binary distillation, the required specification of the feed-stage location is difficult. A McCabe–Thiele plot of the results will clearly show if the feed stage specified is optimal. If not, it can be changed and the simulation rerun.

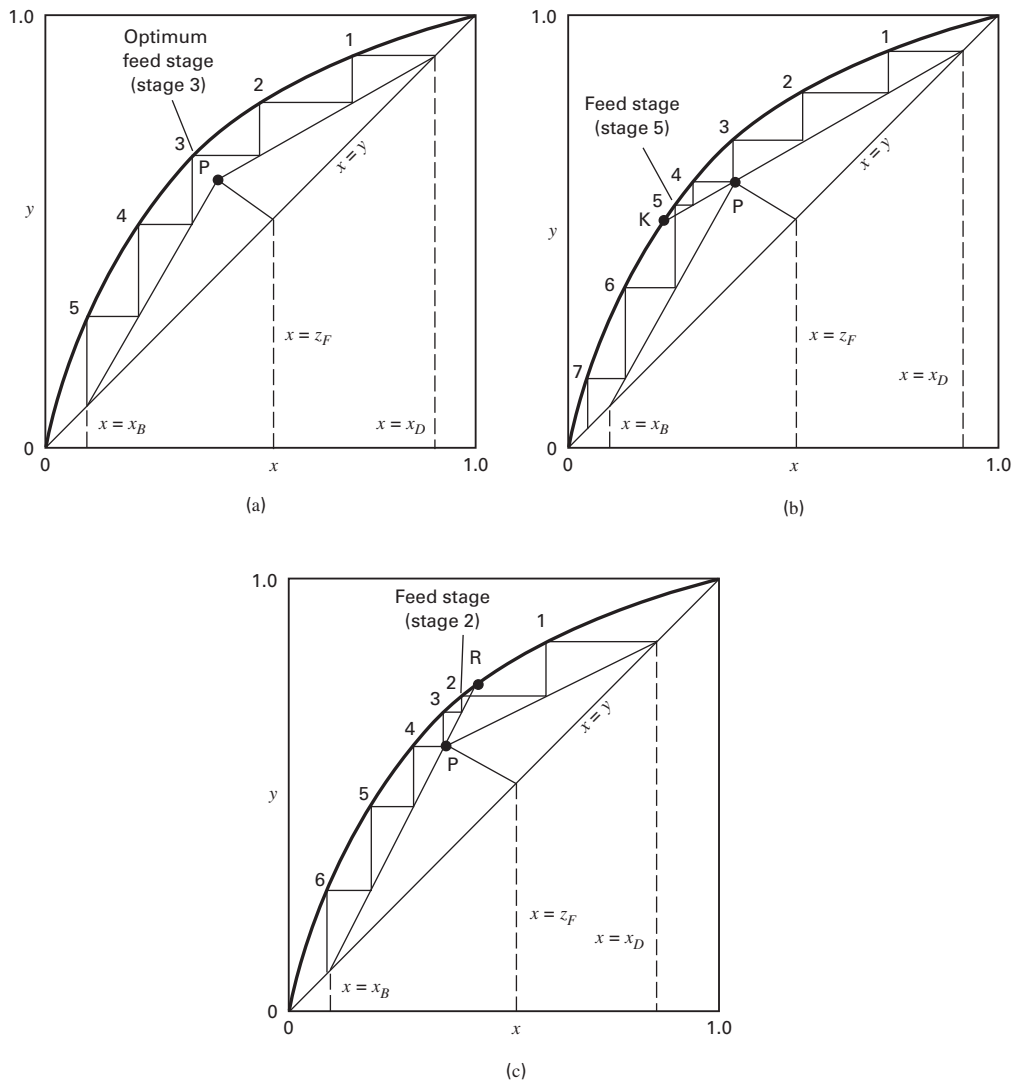


Figure 7.10 Optimal and non-optimal locations of feed stage: (a) optimal feed-stage location; (b) feed-stage location below optimal stage; (c) feed-stage location above optimal stage.

§7.2.5 Limiting Conditions

For a given set of specifications (Table 7.2), a reflux ratio can be selected anywhere from the minimum, R_{\min} , to an infinite value (**total reflux**), where all overhead vapor is condensed and returned to the top stage (thus, neither distillate nor bottoms is withdrawn). As shown in Figure 7.11b, **minimum reflux** corresponds to the need for ∞ stages, while in Figure 7.11a the infinite reflux ratio corresponds to the minimum number of stages. The McCabe–Thiele method can determine the two limits, N_{\min} and R_{\min} . Then, for a practical operation, $N_{\min} < N < \infty$ and $R_{\min} < R < \infty$.

N_{\min} , Minimum Number of Equilibrium Stages

As the reflux ratio increases, the rectifying-section operating-line slope, given by (7-11), increases from $L/V < 1$ to a limiting value of $L/V = 1$. Correspondingly, as the boilup

ratio increases, the stripping-section operating-line slope, given by (7-17), decreases from $\bar{L}/\bar{V} > 1$ to a limiting value of $\bar{L}/\bar{V} = 1$. At this limiting condition, shown in Figure 7.12 for a two-stage column, both the rectifying- and stripping-section operating lines coincide with the 45° line, and neither the feed composition, z_F , nor the q -line influences the staircase construction. This is **total reflux** because when $L = V$, $D = B = 0$. The total condensed overhead is returned as reflux. The liquid leaving the bottom stage is totally vaporized in the reboiler and returned as boilup.

If both distillate and bottoms flow rates are zero, the feed to the column is zero, which is consistent with the lack of influence of the feed condition. A distillation column can be operated at total reflux to measure tray efficiency experimentally because a steady-state operating condition is readily achieved. Figure 7.12 demonstrates that at total reflux, the operating lines are located as far away as possible from the equilibrium curve, resulting in minimum stages.

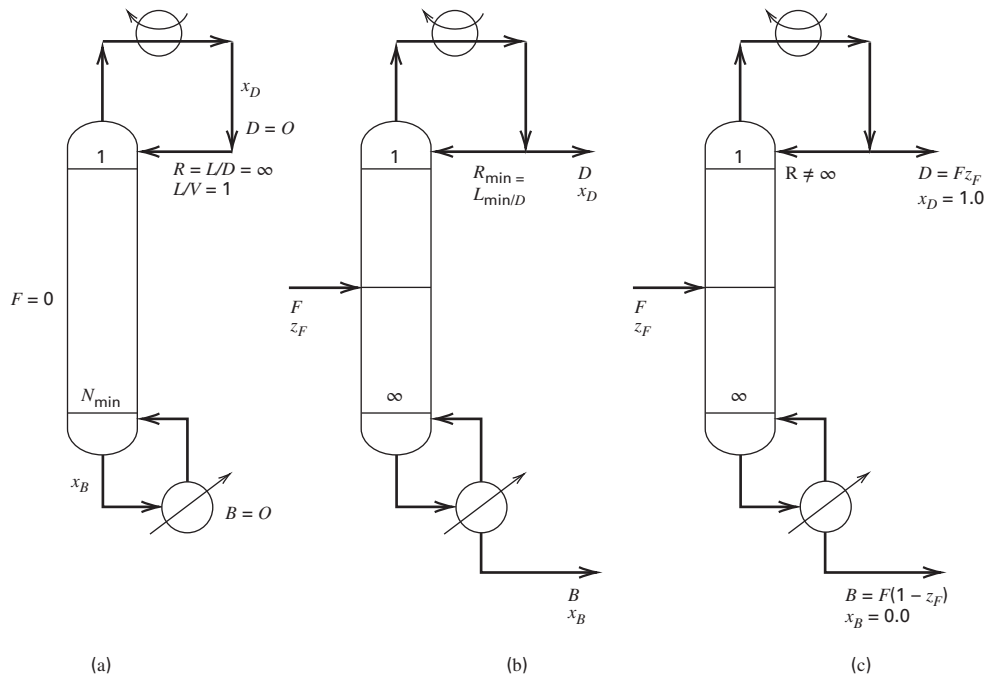


Figure 7.11 Limiting conditions for distillation: (a) total reflux, minimum stages; (b) minimum reflux, infinite stages; (c) perfect separation for nonazeotropic (zeotropic) system.

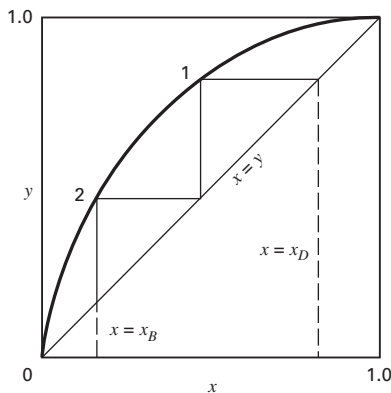


Figure 7.12 Construction for minimum stages at total reflux.

R_{min} , Minimum Reflux Ratio

As the reflux ratio decreases from the limiting case of total reflux, the intersection of the two operating lines and the q -line moves away from the 45° line and toward the equilibrium curve, thus requiring more equilibrium stages for a given LK and HK split. Finally, a limiting condition is reached, if the feed is a nearly ideal mixture, when the intersection of the two operating lines with the q -line is at point P on the equilibrium curve, as in Figure 7.13a. To reach P from the rectifying section or the stripping section, an infinite number of stages is required. P is called a **pinch point** because the two operating lines pinch the equilibrium curve.

For a highly nonideal binary system, the pinch point can occur above or below the feed stage. The former case

is illustrated in Figure 7.13b, where the rectifying-section operating line intersects the equilibrium curve at P. In this case, the intersection of the operating line with the q -line cannot occur on the equilibrium curve. The slope of this rectifying-section operating line cannot be reduced further because the line would then cross the equilibrium curve and thereby violate the second law of thermodynamics. This would require spontaneous mass transfer from a region of low concentration to a region of high concentration, which is impossible in a binary system. This is analogous to a second-law violation by a temperature crossover in a heat exchanger. Now, the pinch point does not occur at the feed stage. Instead, it occurs entirely in the rectifying section, where an infinite number of equilibrium stages exists. A column cannot operate at minimum reflux because it cannot have an infinite number of equilibrium stages.

The minimum reflux ratio can be determined from the slope of the limiting rectifying-section operating line using a rearrangement of (7-11):

$$R_{min} = (L/V)_{min} / [1 - (L/V)_{min}] \quad (7-32)$$

The limiting condition of infinite stages corresponds to a minimum boilup ratio for $(\bar{L}/\bar{V})_{max}$. From (7-17),

$$(V_B)_{min} = 1 / [(\bar{L}/\bar{V})_{max} - 1] \quad (7-33)$$

Perfect Separation

A third limiting condition is the degree of separation. As a perfect split ($x_D = 1$, $x_B = 0$) is approached for $R \geq R_{min}$, the number of stages required near the top and near the bottom of

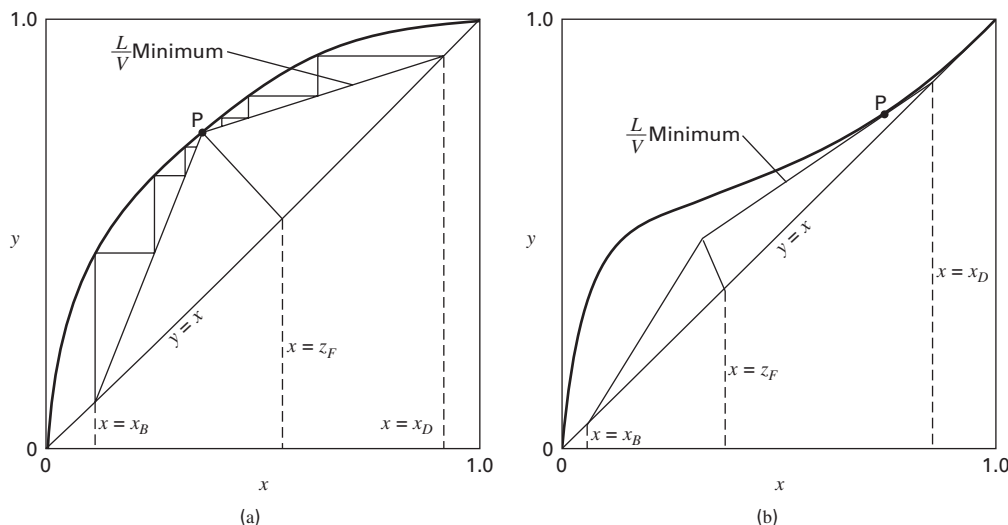


Figure 7.13 Construction for minimum reflux at infinite stages: (a) typical ideal or near-ideal system, pinch point at the feed stage; (b) typical nonideal system, pinch point above the feed stage.

the column increases rapidly and without limit until pinches are encountered at $x_D = 1$ and $x_B = 0$. If there is no azeotrope, a perfect separation requires ∞ stages in both sections of the column. However, this is not the case for the reflux ratio. In Figure 7.13a, as x_D is moved from 0.90 toward 1.0, the slope of the operating line at first increases, but in the range of x_D from 0.99 to 1.0, the slope changes only slightly, so R changes only slightly as it approaches a limiting value. Accordingly, the value of the slope and, therefore, the value of R , is finite for a perfect separation.

If the feed is a saturated liquid ($q = 1$), the combination of (7-3) and (7-13) gives an equation for the minimum reflux of a perfect binary separation ($x_D = 1$):

$$R_{\min} = \frac{1}{z_F(\alpha - 1)} \quad (7-34)$$

If the feed is a saturated vapor ($q = 0$), the result is,

$$R_{\min} = \frac{\alpha}{z_F(\alpha - 1)} - 1 \quad (7-35)$$

where in both cases, relative volatility, α , is at the feed condition.

EXAMPLE 7.1 Distillation of a Mixture of Benzene and Toluene.

Four hundred and fifty lbmol/h (204 kmol/h) of a mixture of 60 mol% benzene (LK) and 40 mol% toluene (HK) is to be separated into a liquid distillate and a liquid bottoms product of 95 mol% and 5 mol% benzene, respectively. The feed enters the column with a molar percent vaporization equal to the distillate-to-feed ratio. Use the McCabe–Thiele method to compute, at 1 atm (101.3 kPa): (a) N_{\min} , (b) R_{\min} , and (c) number of equilibrium stages N , for $R/R_{\min} = 1.3$, and the optimal feed-stage location. Also, compare the results with those from a process simulator. Use Raoult's law to compute vapor–liquid equilibria.

Solution

First calculate D and B . An overall material balance on benzene gives

$$0.60(450) = 0.95D + 0.05B \quad (1)$$

A total balance gives $450 = D + B$ (2)

Combining (1) and (2) and solving, $D = 275$ lbmol/h, $B = 175$ lbmol/h, and $D/F = 0.611$. Thus, the molar vaporization of the feed is 61.1%.

Calculate the slope of the q -line: $V_F/F = D/F = 0.611$, and q for a partially vaporized feed is

$$\frac{L_F}{F} = \frac{(F - V_F)}{F} = 1 - \frac{V_F}{F} = 0.389$$

From (7-31), the slope of the q -line is

$$\frac{q}{q - 1} = \frac{0.389}{0.389 - 1} = -0.637$$

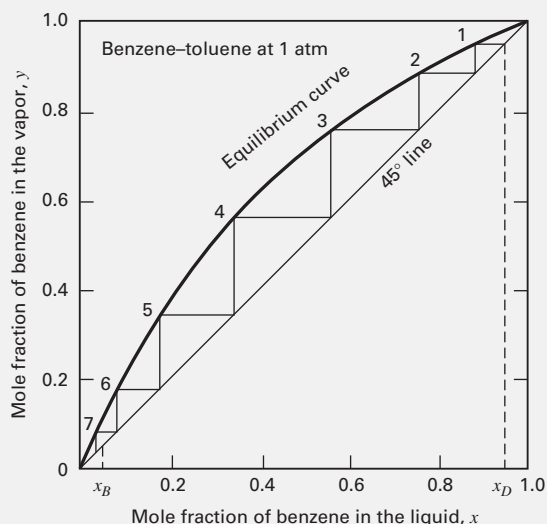
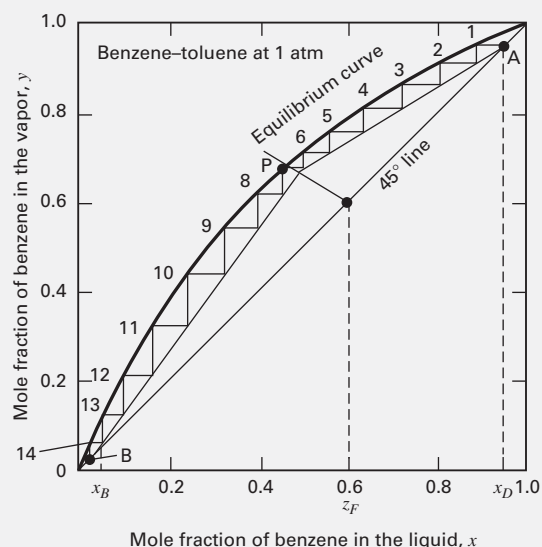
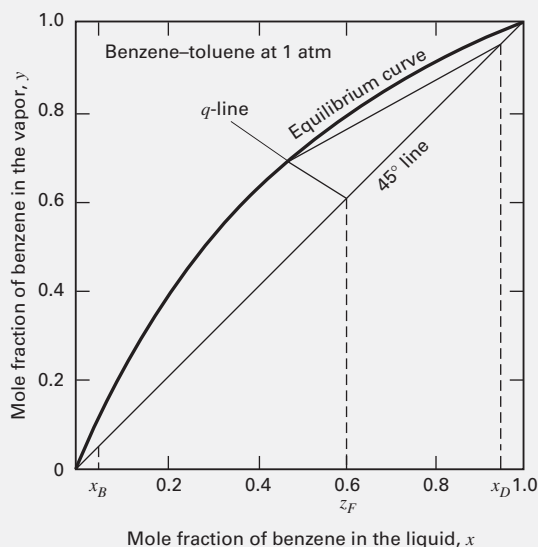
(a) In Figure 7.14, where y and x refer to benzene, $x_D = 0.95$ and $x_B = 0.05$. The minimum stages are stepped off between the equilibrium curve and the 45° line, giving $N_{\min} = 6.7$.

(b) In Figure 7.15, the q -line has a slope of -0.637 and passes through the feed composition ($z_F = 0.60$) on the 45° line. For R_{\min} , an operating line for the rectifying section passes through the point $x = x_D = 0.95$ on the 45° line and through the point of intersection of the q -line and the equilibrium curve ($y = 0.684$, $x = 0.465$). The slope of this operating line is 0.55, which from (7-13) equals $R/(R + 1)$. Solving, $R_{\min} = 1.22$.

(c) The operating reflux ratio is 1.3 $R_{\min} = 1.3(1.22) = 1.59$. From (7-13), the rectifying-section operating-line slope is

$$\frac{R}{R + 1} = \frac{1.59}{1.59 + 1} = 0.614$$

The two operating lines and the q -line are shown in Figure 7.16, where the stripping-section operating line is drawn to pass through the point $x = x_B = 0.05$ on the 45° line and through the


Figure 7.14 Minimum stages for Example 7.1.

Figure 7.16 Number of stages and feed-stage location for Example 7.1.

Figure 7.15 Minimum reflux for Example 7.1.

intersection of the q -line with the rectifying-section operating line. The equilibrium stages are stepped off, first, between the rectifying-section operating line and the equilibrium curve, and then between the stripping-section operating line and the equilibrium curve, starting from point A (distillate composition) and finishing at point B (bottoms composition). For the optimal feed stage, the transfer from the rectifying-section operating line to the stripping-section operating line takes place at point P, giving $N = 13.2$ equilibrium stages, with the feed going into stage 7 from the top. This gives $N/N_{\min} = 13.2/6.7 = 1.97$. The bottom stage is the partial reboiler, leaving 12.2 equilibrium stages in the column. If the plate efficiency were 0.8, 16 trays would be needed.

- (d) The CHEMCAD process simulator was used to verify the McCabe–Thiele results. With a process simulator, the number of stages and the feed-stage location must be specified. The specifications were 13 stages in the column plus a partial reboiler

with the feed stage at 8 from the top, with a reflux ratio of 1.59 and a bottoms flow rate of 175 lbmol/h. Three runs were made with different methods for computing K -values: (1) Raoult's law; (2) Wilson equation; and (3) NRTL equation. The following results were obtained. The product specifications were not quite met, but the three K -value equations gave almost the same results. The specifications could be met by specifying the two product composition specifications and providing initial guesses for the reflux ratio and the bottoms flow rate.

Method	Total Stages	Feed Stage from Top	Benzene x_D	Benzene x_B
McCabe–Thiele	13.2	7	0.950	0.050
Simulator with Raoult's law	14	8	0.957	0.068
Simulator with Wilson equation	14	8	0.955	0.070
Simulator with NRTL equation	14	8	0.956	0.070

§7.3 EXTENSIONS OF THE MCCABE–THIELE METHOD

§7.3.1 Setting Column Operating Pressure

Column pressure and condenser type are set by the algorithm shown in Figure 7.17, which is formulated to achieve, if possible, a reflux-drum pressure, P_D , between 0 and 415 psia (2.86 MPa) at a minimum temperature of 120°F (49°C), corresponding to the use of water as condenser coolant. Pressure and temperature limits depend on economic factors. Columns can operate at a pressure higher than 415 psia provided it is well below the critical or convergence

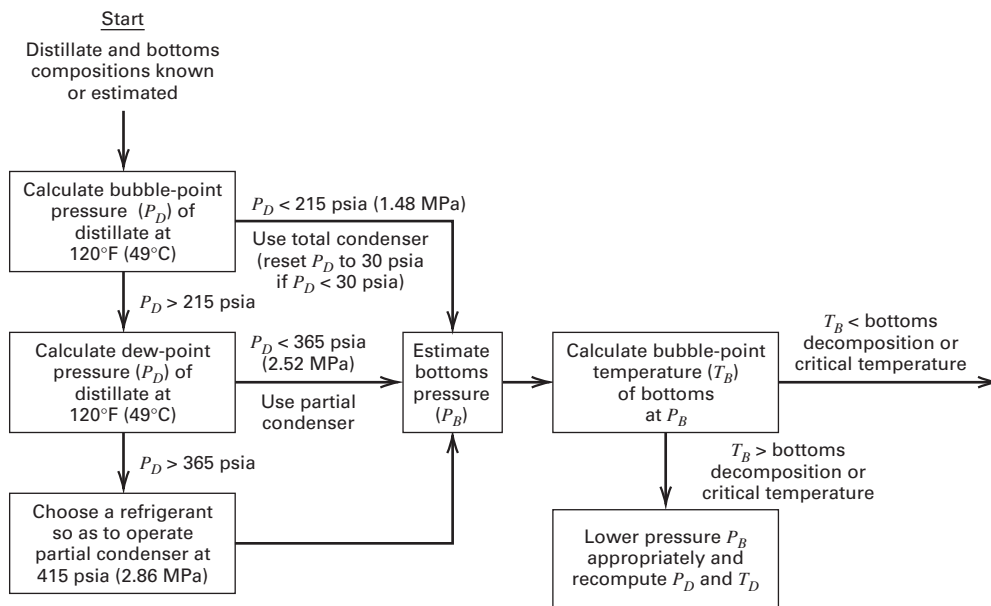


Figure 7.17 Algorithm for setting distillation-column pressure and condenser type.

pressure of the mixture. To obtain the column bottom pressure, a condenser pressure drop of 0 to 2 psi (0 to 14 kPa) and an overall column pressure drop of 5 psi (35 kPa) may be assumed. When the number of trays is known, more refined computations give approximately 0.1 psi/tray (0.7 kPa/tray) pressure drop for atmospheric and super-atmospheric pressure operation, and 0.05 psi/tray (0.35 kPa/tray) pressure drop for vacuum operation. A bubble-point calculation on the bottoms product is made to ensure that conditions are not near-critical or above product-decomposition temperatures. As the algorithm indicates, if the bottoms temperature is too high, a lower temperature is mandated. This is achieved by reducing the pressure in the reflux drum. This may result in vacuum operation and/or the need for a refrigerant, rather than cooling water, for the condenser.

§7.3.2 Condenser Type

Figure 7.18 shows three condenser operating modes. A **total condenser** is suitable for reflux-drum pressures to

215 psia (1.48 MPa). A **partial condenser** is appropriate from 215 psia to 365 psia (2.52 MPa) but is selected below 215 psia if a vapor distillate is desired. A **mixed condenser** can provide both vapor and liquid distillates. A refrigerant is often used as coolant above a condenser pressure of 365 psia when components are difficult to condense. As illustrated in Example 7.2, a partial condenser provides an additional equilibrium stage, based on the assumption that liquid reflux leaving the reflux drum is in equilibrium with the vapor distillate.

§7.3.3 Subcooled Reflux

A distillation column is not always designed to provide reflux at its bubble point. With a total condenser, additional cooling can provide a subcooled liquid that can be divided into reflux and distillate. With partial and mixed condensers, an additional heat exchanger can be added to provide subcooled reflux or, in the case of the mixed condenser, subcooled distillate as well.

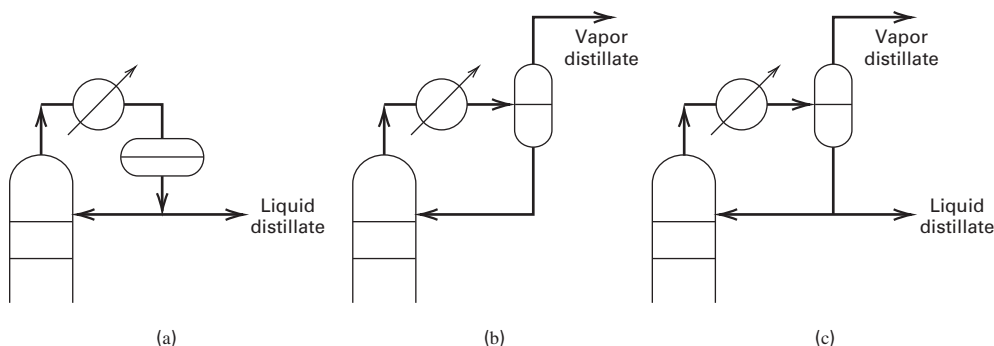


Figure 7.18 Condenser types: (a) total condenser; (b) partial condenser; (c) mixed condenser.

When subcooled reflux enters the top tray, it causes some vapor entering the top tray to condense. The latent enthalpy of condensation of the vapor provides the sensible enthalpy to heat the subcooled reflux to the bubble-point temperature. In that case, the internal reflux ratio within the rectifying section of the column is higher than the external reflux ratio from the reflux drum. The McCabe–Thiele construction should be based on the internal reflux ratio, which can be estimated from the following equation, which is derived from an approximate energy balance around the top tray:

$$R_{\text{internal}} = R \left(1 + \frac{C_{P_L} \Delta T_{\text{subcooling}}}{\Delta H^{\text{vap}}} \right) \quad (7-36)$$

where C_{P_L} and ΔH^{vap} are per mole and $\Delta T_{\text{subcooling}}$ is the degrees of subcooling. The internal reflux ratio replaces R , the external reflux ratio in (7-13). If a correction is not made for subcooled reflux, the calculated number of equilibrium stages is somewhat more than required. Thus, subcooled reflux is beneficial.

EXAMPLE 7.2 McCabe–Thiele Method When Using a Partial Condenser.

One thousand kmol/h of 30 mol% *n*-hexane and 70% *n*-octane is distilled in a column consisting of a partial reboiler, one equilibrium stage, and a partial condenser, all operating at 1 atm. Figure 7.19 shows the y - x equilibrium curve. The feed, a bubble-point liquid, is fed to the reboiler, from which a liquid bottoms is withdrawn. Bubble-point reflux from the partial condenser is returned to the plate. The vapor distillate contains 80 mol% hexane, and the reflux ratio, L/D , is 2. Assume the partial reboiler, plate, and partial condenser are equilibrium stages. Determine if this problem is completely specified. If so, use the McCabe–Thiele method to calculate the bottoms composition and kmol/h of distillate produced.

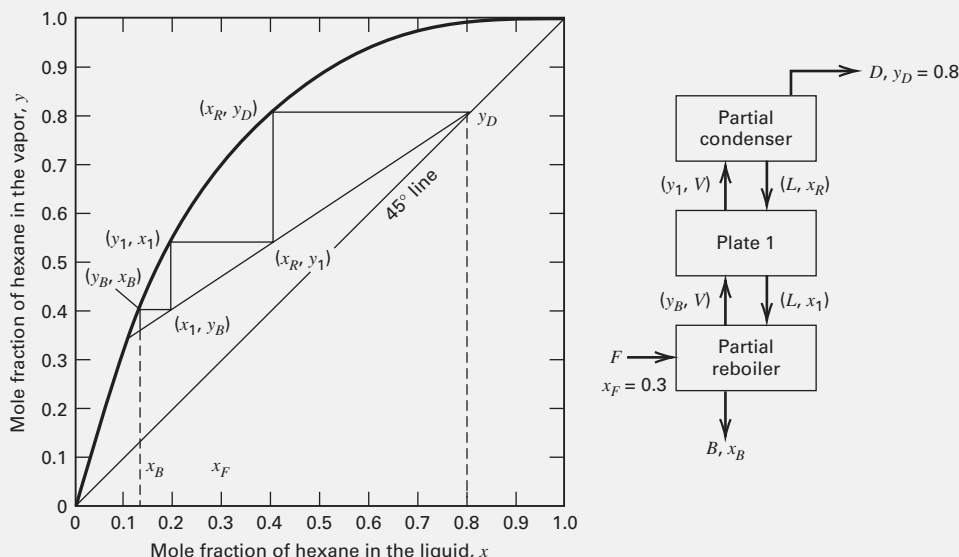


Figure 7.19 Solution to Example 7.2.

Solution

From Table 5.4c, $N_D = C + 2N + 6$ degrees of freedom, where N includes the partial reboiler and the single stage in the column, but not the partial condenser. With $N = 2$ and $C = 2$, $N_D = 12$. Specified are:

Feed stream variables	4
Plate and reboiler pressures	2
Condenser pressure	1
$Q (= 0)$ for plate 1	1
Number of stages	1
Feed-stage location	1
Reflux ratio, L/D	1
Distillate composition	1
Total	12

Thus, the problem is fully specified and can be solved.

The diagram of the separator in Figure 7.19, includes the McCabe–Thiele graphical solution, which is constructed as follows:

1. The point $y_D = 0.8$ at the partial condenser is located on the $x = y$ 45° line.
2. Because x_R (reflux composition) is in equilibrium with y_D , the point (x_R, y_D) is located on the equilibrium curve.
3. Since $(L/V) = 1 - 1/[1 + L/D] = 2/3$, the operating line with slope $L/V = 2/3$ is drawn from the point $y_D = 0.8$ on the 45° line until it intersects the equilibrium curve. Because the feed is introduced into the partial reboiler, there is no stripping section.
4. Three stages (partial condenser, plate 1, and partial reboiler) are stepped off, and the bottoms composition $x_B = 0.135$ is read.

Distillate flow rate is determined from overall material balances. For hexane, $z_F F = y_D D + x_B B$. Therefore, $(0.3)(1,000) = (0.8)D + (0.135)B$. For the total flow, $B = 1,000 - D$. Solving these two equations simultaneously, $D = 248$ kmol/h.

§7.3.4 Reboiler Type

Reboilers for industrial-size distillation columns are usually external heat exchangers of either the **kettle** or **vertical thermosyphon** type shown in Figure 7.20. Either can provide the heat-transfer surface required. In the former case, Figure 7.20a, liquid leaving the sump (reservoir) at the bottom of the column enters the kettle, where it is partially vaporized by transfer of heat from tubes carrying condensing steam or another heat-transfer fluid. The bottoms product liquid leaving the reboiler is assumed to be in equilibrium with the vapor returning to the bottom tray. Thus, a kettle reboiler, which is sometimes located in the bottom of a column, is a partial reboiler equivalent to one equilibrium stage.

Vertical thermosyphon reboilers are shown in Figures 7.20b and 7.20c. In the former, the bottoms product and reboiler feed are both withdrawn from the column bottom sump. Circulation through the reboiler tubes occurs because of a difference in the static heads of the supply liquid and the partially vaporized fluid in the reboiler tubes. The partial vaporization provides enrichment in the exiting vapor. But the exiting liquid is then mixed with liquid leaving the bottom tray, which contains a higher percentage of volatiles. This type of reboiler thus provides only a fraction of a stage, and it is best to take no credit for it.

In the more complex and less common vertical thermosyphon reboiler of Figure 7.20c, reboiler liquid is withdrawn

from the bottom-tray downcomer. Partially vaporized liquid is returned to the column, where the bottoms product from the bottom sump is withdrawn. This type of reboiler functions as an equilibrium stage.

Thermosyphon reboilers are favored when (1) the bottoms product contains thermally sensitive compounds; (2) bottoms pressure is high; (3) only a small ΔT is available for heat transfer; and (4) heavy fouling occurs. Horizontal thermosyphon reboilers may be used in place of vertical types when only small static heads are needed for circulation, when the surface-area requirement is very large, and/or when frequent tube cleaning is anticipated. A pump may be added to a thermosyphon reboiler to improve circulation. Liquid residence time in the column bottom sump should be at least 1 minute and perhaps as much as 5 minutes or more. Large columns may have a 10-foot-high sump.

§7.3.5 Condenser and Reboiler Heat Duties

For a saturated-liquid feed, a total condenser, a partial reboiler, and a column that fulfills the McCabe–Thiele assumptions, reboiler duty and condenser duty are nearly equal. Otherwise they are not, and it is customary to first compute the condenser duty from an energy balance around the condenser and then compute the reboiler duty from an overall energy balance:

$$Fh_F + Q_R = Dh_D + Bh_B + Q_C + Q_{\text{loss}} \quad (7-37)$$

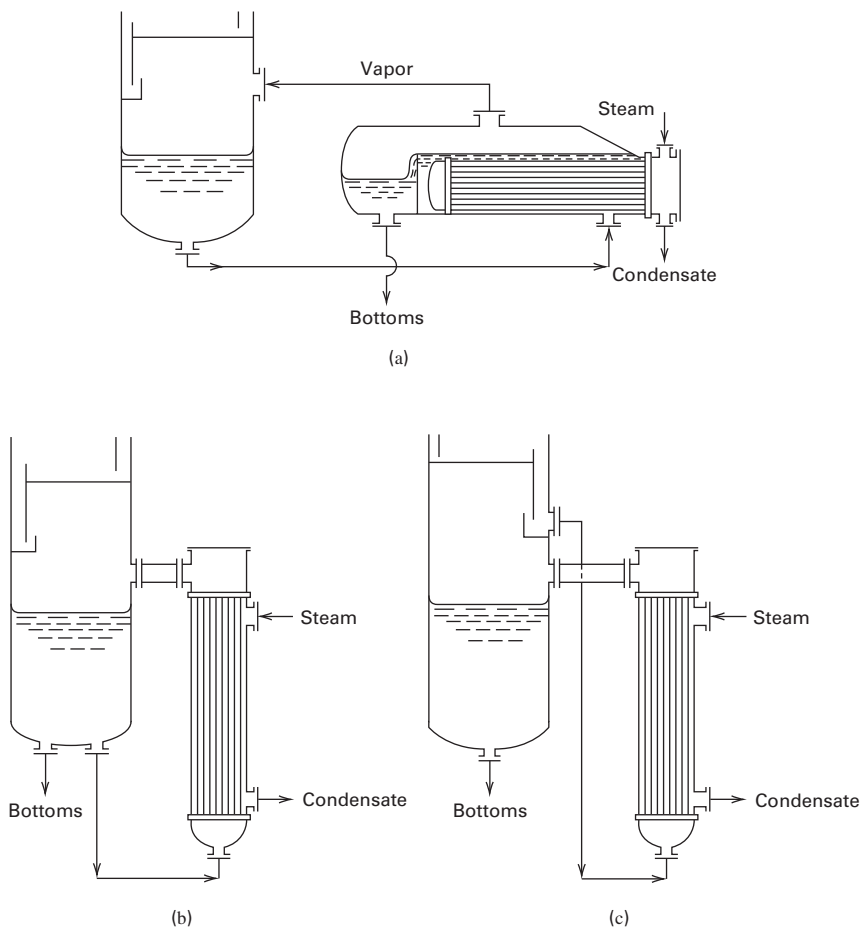


Figure 7.20 Reboilers for plant-size distillation columns: (a) kettle-type reboiler; (b) condensate vertical thermosyphon-type reboiler, reboiler liquid withdrawn from bottom sump; (c) vertical thermosyphon-type reboiler, reboiler liquid withdrawn from bottom-tray downcomer.

where molar flow rates and enthalpies are used with heat transfer rates, Q . Except for small and/or uninsulated distillation equipment, Q_{loss} can be ignored. With the assumptions of the McCabe–Thiele method, an energy balance for a total condenser is

$$Q_C = D(R + 1)\Delta H^{\text{vap}} \quad (7-38a)$$

where ΔH^{vap} = average molar heat of vaporization. For a partial condenser,

$$Q_C = DR\Delta H^{\text{vap}} \quad (7-38b)$$

The reboiler duty, Q_R is computed from (7-37).

For partially vaporized feed and a total condenser, the reboiler duty is less than the condenser duty, given by

$$Q_R = Q_C \left[1 - \frac{V_F}{D(R + 1)} \right] \quad (7-38c)$$

If saturated steam is the reboiler heating medium, the steam rate is given by the energy balance

$$m_s = \frac{M_s Q_R}{\Delta H_s^{\text{vap}}}$$

where m_s = mass flow rate of steam, M_s = molecular weight of steam, and ΔH_s^{vap} = molar enthalpy of vaporization of saturated steam at steam pressure.

The cooling water rate for the condenser is

$$m_{cw} = \frac{Q_C}{C_{P_{\text{H}_2\text{O}}}(T_{\text{out}} - T_{\text{in}})}$$

where m_{cw} = mass flow rate of cooling water, $C_{P_{\text{H}_2\text{O}}}$ = specific heat of water, and T_{out} , T_{in} are cooling water temperature out of and into the condenser, respectively.

§7.3.6 Feed Preheat

Feed pressure must be greater than the pressure in the column at the feed tray. Excess feed pressure is dropped across a valve, which may cause the feed to partially vaporize before entering the column.

Second-law thermodynamic efficiency is highest if the feed temperature equals the temperature in the column at the feed tray. It is best to avoid a subcooled liquid or superheated vapor by supplying a partially vaporized feed. This is achieved by preheating the feed with the bottoms product or a process stream that has a suitably high temperature to ensure a reasonable ΔT driving force for heat transfer and a sufficient available enthalpy.

§7.3.7 Optimal Reflux Ratio

For a specified separation of two key components, a distillation column operates between the limiting conditions of minimum and total reflux. Figure 7.21a shows that as reflux ratio R/D is increased above R_{min}/D , the number of equilibrium stages, N , decreases. Also, the column diameter increases, and reboiler steam and condenser cooling-water

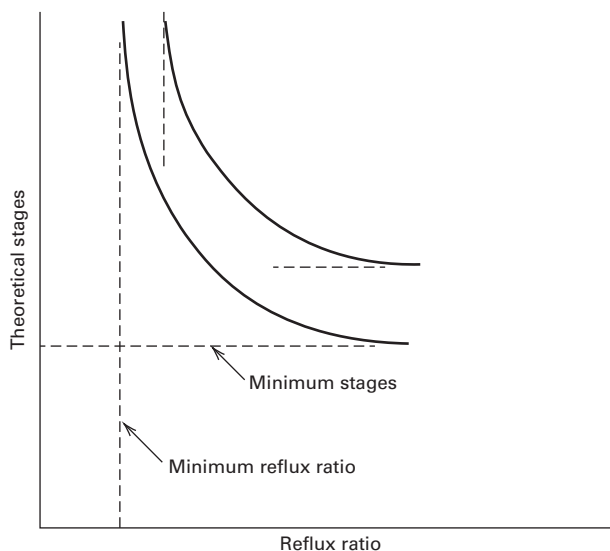


Figure 7.21a Effect of reflux ratio on theoretical (equilibrium) stages for two optimal representative distillation operations showing minimum constraints.

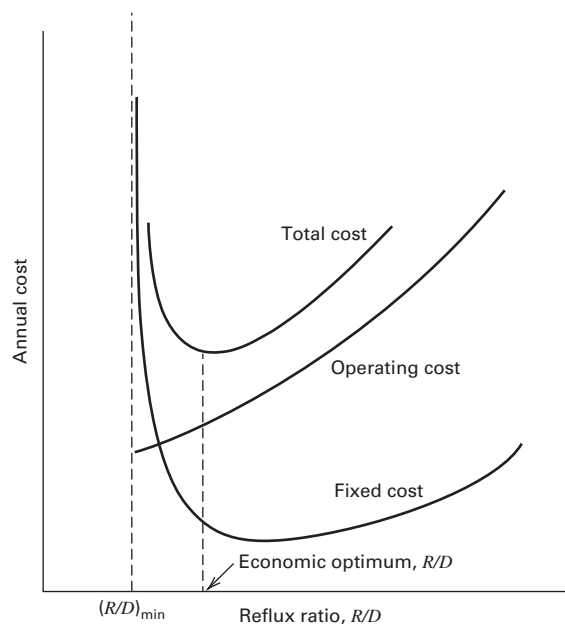


Figure 7.21b Optimal reflux ratio for a representative distillation operation.

requirements increase. When the annualized fixed cost for the column, condenser, reflux drum, reflux pump, and reboiler is added to the operating cost of steam and cooling water to obtain the total annual cost, an optimal reflux ratio of R/R_{min} is determined, as shown for a particular separation in Figure 7.21b.

The accepted range of optimal to minimum reflux ratio is from 1.05 to 1.50, with the lower value applying to a difficult separation (e.g., $\alpha = 1.2$) and the larger value for an easy separation. However, because the optimal ratio is not sharply defined, columns are often designed for flexibility at reflux ratios greater than the optimum.

§7.3.8 Other Extensions

As discussed by Seader et al. [6], the McCabe–Thiele method, described above, can be extended to binary distillations with multiple feeds, vapor and/or liquid sidestreams, and interstage heat transfer. Also, they discuss the use of log–log coordinates and the Kremser equations when product purities result in large numbers of stages. However, these extensions are best handled with process simulators using the methods described in Chapter 10.

§7.4 ESTIMATION OF TRAY EFFICIENCY FOR DISTILLATION

Methods for estimating tray efficiency for binary distillation are analogous to those for absorption and stripping, with one major difference. In absorption and stripping, the liquid phase is often rich in heavy components, and thus liquid viscosity is high and mass-transfer rates are low. This leads to low tray efficiencies, usually less than 50%. For binary distillation, particularly of close-boiling mixtures, both components are near their boiling points and liquid viscosity is low, with the result that tray efficiencies for well-designed trays are often higher than 70% and can even be higher than 100% for large-diameter columns where a crossflow effect is present. A comprehensive treatment of the many factors involved in modeling vapor–liquid contacting in trayed columns is given by Lockett [7].

§7.4.1 Performance Data

Techniques for measuring performance of industrial distillation columns are described in an *AIChE Equipment Testing Procedure* [8]. Overall column efficiencies, E_o , are generally measured at conditions of total reflux to eliminate transients due to fluctuations from steady state due to feed variations, etc. However, as shown by Williams, Stigger, and Nichols [9], efficiency measured at total reflux ($L/V = 1$) can differ from that at design reflux. A significant factor is how closely to flooding the column is operated. Overall efficiencies are calculated from (6-41) and total reflux data. Individual-tray, Murphree vapor efficiencies, E_{MV} , are calculated using (6-49). Here, sampling from downcomers leads to variable results. To mitigate this and other aberrations, it is best to work with near-ideal systems. These and other equipment-specific factors are discussed in §6.5.

Table 7.3, from Gerster et al. [10], lists plant data for the distillation at total reflux of a methylene chloride (MC)–ethylene chloride (EC) mixture in a 5.5-ft-diameter column containing 60 bubble-cap trays on 18-inch tray spacing, operating at 85% of flooding at total reflux. The following example illustrates how such plant data can be used to calculate overall and Murphree vapor efficiency.

Table 7.3 Performance Data for the Distillation of Methylene and Ethylene Chlorides

Company	Eastman Kodak
Location	Rochester, New York
Column diameter	5.5 ft (65.5 inches I.D.)
No. of trays	60
Tray spacing	18 inches
Type tray	10 rows of 3-inch-diameter bubble caps on 4-7/8-inch triangular centers; 115 caps/tray
Bubbling area	20 ft ²
Length of liquid travel	49 inches
Outlet-weir height	2.25 inches
Downcomer clearance	1.5 inches
Liquid rate	24.5 gal/min-ft = 1,115.9 lb/min
Gas F_V -factor, (6-104)	1.31 ft/s (lb/ft ³) ^{0.5}
Percent of flooding	85
Pressure, top tray	33.8 psia
Pressure, bottom tray	42.0 psia
Liquid composition, mole % methylene chloride:	
From tray 33	89.8
From tray 32	72.6
From tray 29	4.64

Source: J.A. Gerster, A.B. Hill, N.H. Hochgrof, and D.B. Robinson, *Tray Efficiencies in Distillation Columns, Final Report from the University of Delaware*, AIChE, New York (1958).

EXAMPLE 7.3 Tray Efficiency from Performance Data.

Using the performance data of Table 7.3, estimate: (a) the overall tray efficiency for the section of trays from 33 to 29 and (b) E_{MV} for tray 32. Assume the following values for $\alpha_{MC,EC}$:

x_{MC}	$\alpha_{MC,EC}$	y_{MC} from (7-3)
0.00	3.55	0.00
0.10	3.61	0.286
0.20	3.70	0.481
0.30	3.76	0.617
0.40	3.83	0.719
0.50	3.91	0.796
0.60	4.00	0.857
0.70	4.03	0.904
0.80	4.09	0.942
0.90	4.17	0.974
1.00	4.25	1.00

Solution

- (a) The above x – α – y data are plotted in Figure 7.22. Four equilibrium stages are stepped off from $x_{33} = 0.898$ to $x_{29} = 0.0464$ for total reflux. Since the actual number of stages is also 4, E_o from (6-41) is 100%.

(b) At total reflux conditions, passing vapor and liquid streams have the same composition, so the operating line is the 45° line. Using this, together with the above performance data and the equilibrium curve in Figure 7.22 for methylene chloride, with trays counted from the bottom up:

$$y_{32} = x_{33} = 0.898 \quad \text{and} \quad y_{31} = x_{32} = 0.726$$

From (6-49), using $x_{32} = 0.726$ and $y_{32}^* = 0.917$ from Figure 7.22,

$$(E_{MV})_{32} = \frac{y_{32} - y_{31}}{y_{32}^* - y_{31}} = \frac{0.898 - 0.726}{0.917 - 0.726} = 0.90 \quad \text{or} \quad 90\%$$

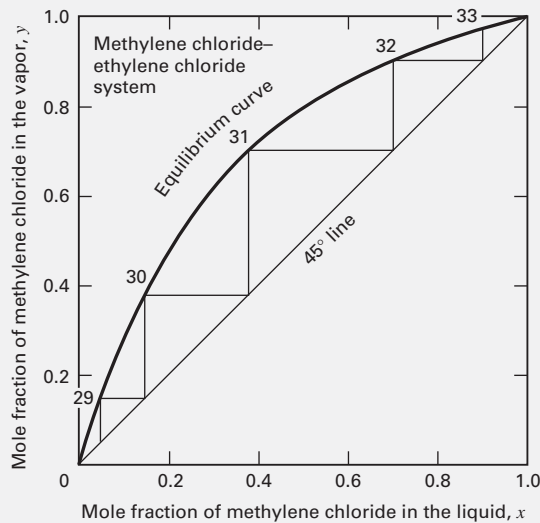


Figure 7.22 McCabe–Thiele diagram for Example 7.3.

§7.4.2 Empirical Correlations of Tray Efficiency

Based on 41 sets of data for bubble-cap-tray and sieve-tray columns distilling hydrocarbons and a few water and miscible organic mixtures, Drickamer and Bradford [11] correlated E_o in terms of the molar-average liquid viscosity, μ , of the tower feed at average tower temperature. The data covered temperatures from 157 to 420°F, pressures from 14.7 to 366 psia, feed liquid viscosities from 0.066 to 0.355 cP, and overall tray efficiencies from 41% to 88%. The equation,

$$E_o = 13.3 - 66.8 \log \mu \quad (7-39)$$

with E_o in percent and μ in cP, fits the data with average and maximum percent deviations of 5.0% and 13.0%. A plot of the Drickamer and Bradford correlation, compared to performance data for distillation, is given in Figure 7.23. Equation (7-39) is restricted to the above range of data and is based mainly on hydrocarbon distillations.

As discussed in §6.5, mass-transfer theory predicts that over a wide range of α , the relative magnitudes of liquid- and gas-phase transfer resistances shifts. O’Connell [12]

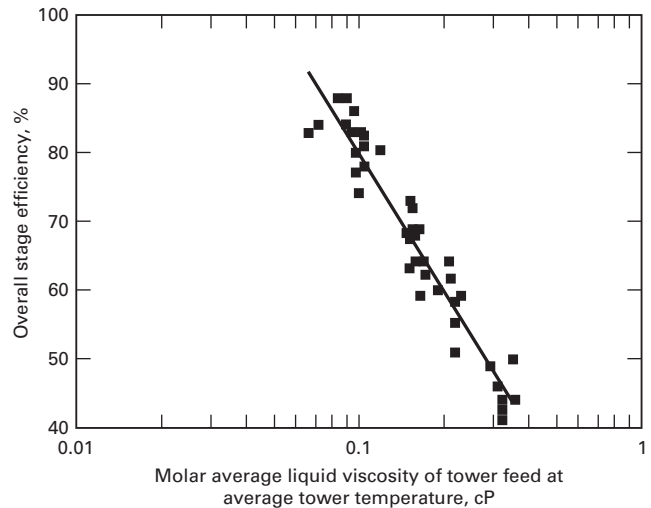


Figure 7.23 Drickamer and Bradford’s correlation for plate efficiency of distillation columns.

found that the Drickamer–Bradford formulation is inadequate for feeds having a large α . O’Connell developed separate correlations in terms of $\mu\alpha$ for fractionators and for absorbers and strippers. As shown in Figure 7.24, Lockhart and Leggett [13] obtained a single correlation using the product of liquid viscosity and an appropriate volatility as the correlating variable. For fractionators, $\alpha_{LK,HK}$ is used; for hydrocarbon absorbers, the volatility is taken as 10 times the K -value of a key component, one that is distributed between top and bottom products. Data used by O’Connell cover a range of α from 1.16 to 20.5. The effect on E_o of the ratio of liquid-to-vapor molar flow rates, L/V , for eight different water and organic binary systems in a 10-inch-diameter column with bubble-cap trays was reported by Williams et al. [9]. While L/V did have an effect, it could not be correlated. For fractionation with L/V nearly equal to 1.0 (i.e., total reflux), their distillation data, which are included in Figure 7.24, are in reasonable agreement with the O’Connell correlation. For the distillation of hydrocarbons in a 0.45-m-diameter column, Zuiderweg, Verburg, and Gilissen [14] found the differences in E_o among bubble-cap, sieve, and valve trays to be insignificant at 85% of flooding. Accordingly, Figure 7.24 is assumed to be applicable to all three tray types, but may be somewhat conservative for well-designed trays. For example, data of Fractionation Research Incorporated (FRI) for valve trays operating with hydrocarbon systems, also included in Figure 7.24, show efficiencies 10% to 20% higher than the correlation.

For just the distillation data plotted in Figure 7.24, the O’Connell correlation fits the empirical equation

$$E_o = 50.3(\alpha\mu)^{-0.226} \quad (7-40)$$

where E_o is in percent, μ is in cP, and α is at average column conditions.

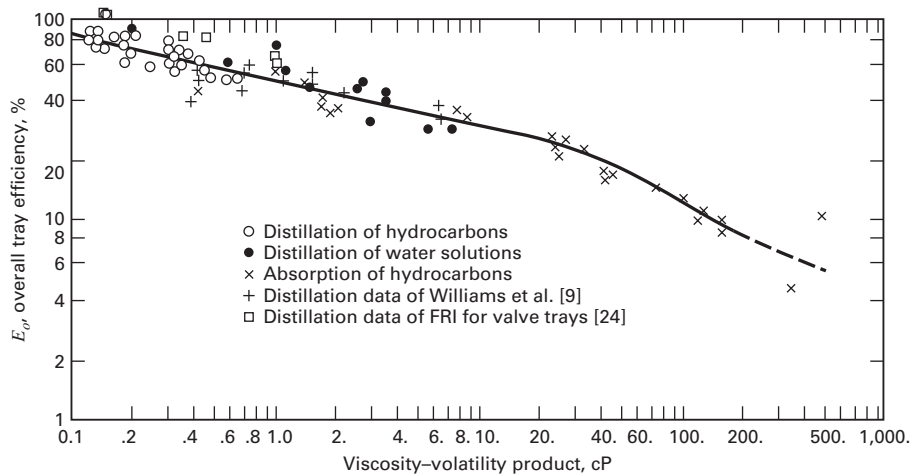


Figure 7.24 Lockhart and Leggett version of the O'Connell correlation for overall tray efficiency of fractionators, absorbers, and strippers. [Based on F.J. Lockhart and C.W. Leggett, in K.A. Kobe and J.J. McKetta Jr. Eds. *Advances in Petroleum Chemistry and Refining*, Journal of Pharmaceutical Sciences, Vol. 1, 323–326 (1958).]

Table 7.4 Correction to Overall Tray Efficiency for Length of Liquid Flow Path ($0.1 \leq \mu\alpha \leq 1.0$)

Length of Liquid Flow Path, ft	Value to Be Added to E_o from Figure 7.24, %
3	0
4	10
5	15
6	20
8	23
10	25
15	27

Source: F.J. Lockhart and C.W. Leggett, in K.A. Kobe and J.J. McKetta Jr. Eds. *Advances in Petroleum Chemistry and Refining*, Journal of Pharmaceutical Sciences, Vol. 1, 323–326 (1958). Reprinted with permission of John Wiley & Sons, Inc.

The data in Figure 7.24 are mostly for columns with liquid flow paths from 2 to 3 ft. Gautreaux and O'Connell [15] showed that higher efficiencies are achieved for longer flow paths because the equivalent of two or more completely mixed, successive liquid zones are present.

Provided that $\mu\alpha$ lies between 0.1 and 1.0, Lockhart and Leggett [13] recommend adding the increments in Table 7.4 to the value of E_o from Figure 7.24 when the liquid flow path is greater than 3 ft. However, at high liquid flow rates, long liquid-path lengths are undesirable because they lead to excessive liquid gradients and cause maldistribution of vapor flow, in which case the multi-pass trays, shown in Figure 6.20a and discussed in §6.5.3, are preferred.

EXAMPLE 7.4 Estimation of Stage Efficiency from Empirical Correlations.

For the benzene–toluene distillation of Figure 7.1, use the Drickamer–Bradford and O'Connell correlations to estimate E_o and the number of actual plates required. Obtain the column height, assuming 24-inch tray spacing with 4 ft above the top tray for removal of

entrained liquid and 10 ft below the bottom tray for bottoms product surge capacity. The separation requires 20 equilibrium stages plus a partial reboiler that acts as an equilibrium stage.

Solution

The liquid viscosity is determined at the feed-stage condition of 220°F, with a liquid composition of 50 mol% benzene; μ of benzene = 0.10 cP; μ of toluene = 0.12 cP; and average $\mu = 0.11$ cP. From Figure 7.3, the average α is

$$\text{Average } \alpha = \frac{\alpha_{\text{top}} + \alpha_{\text{bottom}}}{2} = \frac{2.52 + 2.26}{2} = 2.39$$

From the Drickamer–Bradford correlation (7-39), $E_o = 13.3 - 66.8 \log(0.11) = 77\%$. Therefore, $N_a = 20/0.77 = 26$.

$$\text{Column height} = 4 + 2(26 - 1) + 10 = 64 \text{ ft.}$$

From the O'Connell correlation, (7-40), $E_o = 50.3[(2.39)(0.11)]^{-0.226} = 68\%$.

For a 5-ft-diameter column, the length of the liquid flow path is about 3 ft for a single-pass tray and even less for a two-pass tray. From Table 7.4, the efficiency correction is zero. Therefore, the number of trays required is $N_a = 20/0.68 = 29.4$, or round up to 30 trays. Column height = $4 + 2(30 - 1) + 10 = 72$ ft.

§7.4.3 Models for Tray Efficiency

In the section of Chapter 6 on absorption and stripping, the Murphree vapor-tray efficiency, E_{MV} , (6-49) was defined and related to the overall stage efficiency, E_o , (6-56). A semitheoretical model was developed for the estimation of E_{MV} from the number of overall gas-phase mass-transfer units, N_{OG} , (6-49), in terms of the overall volumetric gas-phase mass-transfer coefficient, $K_G a$, (6-48). The equations are applicable to countercurrent vapor–liquid contacting operations on a tray, including absorption, stripping, and distillation. A more fundamental Murphree vapor-point efficiency, E_{OV} , was also

defined (6-51) and related to E_{MV} for three cases: (1) complete mixing of liquid on the tray (6-52); (2) plug flow of liquid (no mixing) across the tray (6-53); and (3) the general case of partial liquid mixing (6-54). In this section, the semitheoretical model is further developed to enable the estimation of E_{OV} for binary distillation and absorption/stripping in trayed-columns.

After tray specifications are established, E_{OV} can be estimated using correlations for individual mass-transfer coefficients in terms of the numbers of individual transfer units. For a vertical path of vapor flow up through the froth from a point on the bubbling area of the tray, (6-50) can be applied to E_{OV} instead of E_{MV} . Thus,

$$N_{OG} = -\ln(1 - E_{OV}) \quad (7-41)$$

where, from (6-48),

$$N_{OG} = \frac{K_G a P Z_f}{(V/A_b)} \quad (7-42)$$

The overall, volumetric mass-transfer coefficient, $K_G a$ is related to the individual volumetric mass-transfer coefficients by the mass-transfer resistances, which from §3.7 are

$$\frac{1}{K_G a} = \frac{1}{k_G a} + \frac{(m P M_L / \rho_L)}{k_L a} \quad (7-43)$$

where the RHS terms are the gas- and liquid-phase resistances, respectively. In terms of individual transfer units, defined by

$$N_G = \frac{k_G a P Z_f}{(V/A_b)} \quad (7-44)$$

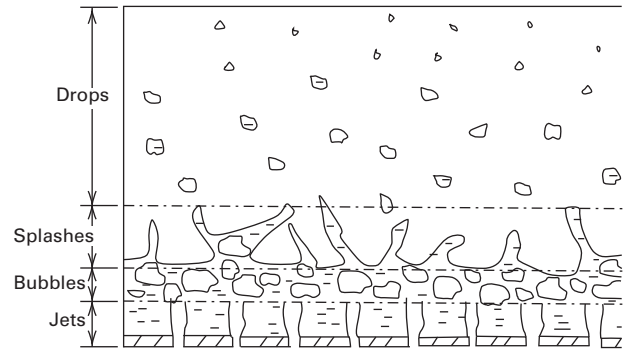
$$N_L = \frac{k_L a \rho_L Z_f}{M_L (L/A_b)} \quad (7-45)$$

From (7-42) and (7-43),

$$\frac{1}{N_{OG}} = \frac{1}{N_G} + \frac{(m V / L)}{N_L} \quad (7-46)$$

Equations (7-41) to (7-46) are the basis for mass-transfer correlations in terms of N_L , N_G , k_L , k_G , and a , for bubble-cap and sieve trays. Important early mass-transfer correlations were published by the AIChE [16] for bubble-cap trays, Chan and Fair [17, 18] for sieve trays, and Scheffe and Weiland [19] for one type of valve tray (Glitsch V-1). The 1984 method of Chan and Fair [17, 18] used a correlation for the liquid phase based on the work of Foss and Gerster [20], as reported by the AIChE [16], and added a separate correlation for the vapor phase based on experimental data. This correlation is available in most process simulators.

More recent tray efficiency correlations for sieve trays are those of Bennett et al., [21]; Chen and Chuang [22], and Garcia and Fair [23, 24], both of which are based on simulating the froth regime shown in Figure 6.4. Garcia and Fair use the dispersion structure of the froth as studied by Prado and Fair [35]. In 2007, Syeda et al. [25] considered both the spray and froth regimes. Their experimental work with methanol and water showed that the transition from the spray to the froth regime was gradual with both occurring simultaneously as shown in the following sketch, where a combination of jets (J), bubbles (large, LB , and small, SB), splashes, and drops occur.



They determined the overall Murphree vapor-point efficiency from contributions by J , LB , and SB with

$$E_{OV} = f_J E_J + (1 - f_J)[f_{SB} E_{SB} + (1 - f_{SB}) E_{LB}] \quad (7-47)$$

where,

f_J = volume fraction of the gas transported as jets

$(1 - f_J)$ = volume fraction of the gas transported as both SB and LB

f_{SB} = volume fraction of SB

$(1 - f_{SB})$ = volume fraction of LB

E_J = Murphree overall point efficiency for J

E_{SB} = Murphree overall point efficiency for SB

E_{LB} = Murphree overall point efficiency for LB

The variables in (7-47) are determined as follows:

f_J , Fraction Jetting Model

Of the three available models for f_J (Prado and Fair [35], Syeda et al. [25], and Vennavelli et al. [26]), the latter model has a phenomenological basis and covers the entire range of fraction jetting. It is based on a modified Froude number, N'_{Fr} , which is proportional to the ratio of the volume of vapor transported as jets, V_J , to the volume of vapor transported as bubbles, V_B , given by:

$$N'_{Fr} = \frac{u_b \rho_V^{0.5}}{(\rho_L g h_{cl})^{0.5}} = \beta \frac{V_J}{V_B} = \beta \frac{f_J}{1 - f_J} \quad (7-48)$$

where,

u_b = vapor velocity based on the tray bubbling area, A_b , m/s

ρ_V, ρ_L = vapor and liquid mass densities, respectively, kg/m³

g = acceleration due to gravity = 9.807 m/s²

h_{cl} = clear liquid height of the liquid holdup on the tray in m

β = a proportionality constant.

The clear liquid height is given by an empirical expression developed from experimental data by Bennett, Agrawal, and Cook [27]:

$$h_{cl} = \alpha_e h_f = \alpha_e \left[h_w + C \left(\frac{Q_L}{L_w \alpha_e} \right)^{2/3} \right] \quad (7-49)$$

where,

α_e = ratio of clear liquid height to froth (dispersion) height, given by,

$$\alpha_e = \exp \left\{ -12.55 \left[u_b \left(\frac{\rho_V}{\rho_L - \rho_V} \right)^{0.5} \right]^{0.91} \right\} \quad (7-50)$$

h_f = froth (dispersion) height, m

h_w = weir height, m

$$C = 0.5 + 0.438 \exp(-137.6 h_w) \quad (7-51)$$

Q_L = volumetric liquid flow rate, m³/s

L_w = weir length, m

Solving (7-48) for f_J as a function of N'_{Fr} and fitting the resulting equation to experimental fraction jetting data of Raper et al. [28] gives,

$$f_J = \frac{N'_{Fr}}{0.0449 + N'_{Fr}} \quad (7-52)$$

f_{SB} , Fraction Small Bubbles Model

Syeda et al. developed the following equation for f_{SB} , the fraction of all bubbles that are small bubbles, using a turbulent bubble-break-up theory:

$$f_{SB} = \frac{2 [1 - \exp(-K_B)]}{2 [1 - \exp(-K_B)] + (d_{32LB}/d_{32SB})^3 \exp(-K_B)} \quad (7-53)$$

where,

K_B is the product of the bubble breakage rate and time, given by,

$$K_B = 0.16 \left[\frac{3.8 \rho_L^{0.1} \rho_V^{0.3}}{\sigma^{0.4}} \right] (u_b g)^{0.6} t_{LB} \quad (7-54)$$

where,

d_{32LB} = Sauter mean diameter of large bubbles, m

d_{32SB} = Sauter mean diameter of small bubbles, m, taken to be $d_{32LB}/5$

σ = surface tension, N/m

t_{LB} = mean residence time of large bubbles in the froth, s

The Sauter mean diameter, d_{32} , is the most appropriate mean diameter for mass-transfer calculations because it is the surface-mean diameter. It is defined as the diameter of a sphere that has the same volume/surface area ratio as the entire population of bubbles of different sizes. The subscript 3 refers to the volume and the subscript 2 to the surface area. The large bubble size in the froth is estimated from,

$$d_{32LB} = 0.887 D_h^{0.846} u_h^{0.21} \quad (7-55)$$

where,

D_h = sieve tray hole diameter, m

u_h = vapor velocity based on hole area, m/s

The mean residence time of the large bubbles in the froth is

$$t_{LB} = \frac{h_f}{U_{LB}} \quad (7-56)$$

where, U_{LB} = rise velocity of the large bubbles through the froth is

$$U_{LB} = 2.5(V_{LB})^{1/6} + u_b \quad (7-57)$$

where, V_{LB} = volume of a spherical bubble of diameter, d_{32LB} , is

$$V_{LB} = \frac{\pi}{6} (d_{32LB})^3 \quad (7-58)$$

Using (7-54) to (7-58), the fraction of bubbles that are SB is calculated from (7-53). The fraction of bubbles that are LB = $f_{LB} = (1 - f_{SB})$.

E_J , Murphree Overall Point Efficiency for the Jets

Syeda et al. [25] use the spray model of Zuiderweg [29] to calculate E_J . If (7-41) is applied to the jets by taking the exponential of both sides,

$$E_J = 1 - \exp(-N_{OGJ}) \quad (7-59)$$

where, N_{OGJ} = number of overall gas-phase transfer units for the jets

$$N_{OGJ} = \frac{a_{ib} K_{OGJ}}{u_b} \quad (7-60)$$

where,

a_{ib} = interfacial area of jets per unit tray bubbling area

K_{OGJ} = overall gas mass-transfer coefficient for the jets, m/s

$$a_{ib} = \frac{40}{f_{HA}^{0.3}} \left(\frac{F_b^2 h_{cl} (\rho_V / \rho_L)^{0.5}}{\sigma} \right)^{0.37} \quad (7-61)$$

where,

f_{HA} = fraction of hole area in the bubbling area

F_b = F-factor based on the bubbling area, (m/s) (kg/m³)^{0.5}

$$F_b = u_b \sqrt{\rho_V} \quad (7-62)$$

$$K_{OGJ} = \frac{1}{\frac{1}{k_{GJ}} + \frac{m}{k_{LJ}} \left(\frac{\rho_V M_L}{\rho_L M_V} \right)} \quad (7-63)$$

where,

k_{GJ} = gas-phase mass-transfer coefficient, m/s

k_{LJ} = liquid-phase mass-transfer coefficient, m/s

m = local slope of the y-x equilibrium line in the case of a binary system

$$k_{GJ} = \frac{0.13}{\rho_V} - \frac{0.065}{\rho_V^2}, \quad \text{for } (1 < \rho_V < 80 \text{ kg/m}^3) \quad (7-64)$$

$$k_{LJ} = \frac{2 \times 10^{-5}}{\mu_L^{0.25}} \quad (7-65)$$

where μ_L = liquid viscosity, kg/m-s

E_j is calculated from (7-59) using (7-60) to (7-65) with (7-49) to (7-51) for h_{cl} .

E_{SB} , Murphree Overall Point Efficiency for SB

Because the diffusion path for SB is very small, they are assumed to reach phase equilibrium in the froth with the surrounding liquid. Thus, $E_{SB} = 1$.

E_{LB} , Model for Murphree Overall Point Efficiency for LB

The calculation of the Murphree overall point efficiency for the LB is based on the application of (7-59):

$$E_{LB} = 1 - \exp(-N_{OGLB}) \quad (7-66)$$

where,

N_{OGLB} = number of overall gas-phase transfer units for the large bubbles

$$N_{OGLB} = \frac{1}{\frac{1}{N_{GLB}} + \frac{\lambda}{N_{LLB}}} \quad (7-67)$$

where,

$$\lambda = mV/L$$

N_{LLB} = number of liquid-phase transfer units for the large bubbles

N_{GLB} = number of gas-phase transfer units for the large bubbles

Syeda et al. use the following modifications of (7-44) and (7-45) to express the dependency of transfer units on interfacial area between phases and residence times:

$$N_{GLB} = k_{GLB} a_{iG} t_G \quad (7-68)$$

$$N_{LLB} = k_{LLB} a_{iL} t_L \quad (7-69)$$

where,

k_{GLB} = gas-phase mass-transfer coefficient for LB, m/s

k_{LLB} = liquid-phase mass-transfer coefficient for LB, m/s

a_{iG} and a_{iL} are the interfacial areas per unit volume of gas and liquid, m^2/m^3

t_G and t_L are the mean residence times of gas and liquid in the froth, s

These four variables above are related by the expression,

$$a_{iL} t_L = \frac{Q_V}{Q_L} a_{iG} t_G \quad (7-70)$$

$$\text{By geometry} \quad a_{iG} = 6/d_{32LB} \quad (7-71)$$

$$t_G = \frac{h_f}{u_b} \quad (7-72)$$

The liquid phase mass-transfer coefficient is given by Higbie [30] using the penetration theory (§3.6.2)

$$k_{LLB} = 2 \left(\frac{D_L}{\pi t_G} \right)^{0.5} \quad (7-73)$$

where, D_L = liquid diffusivity, m^2/s

The gas phase mass-transfer coefficient for the interior of the large bubbles (taking into account circulation), is estimated from the numerical solution of Zaritsky and Calvelo [31], given as an S-shaped plot of a Sherwood number, N_{ShG} , versus a gas-phase Peclet number for mass transfer,

$$N_{ShG} = \frac{d_{32LB} k_{GLB}}{D_G} \quad (7-74)$$

where D_G = gas diffusivity, m^2/s , and

$$N_{PeM} = \frac{d_{32LB} U_{LB}}{D_G} \quad (7-75)$$

At values of $N_{PeM} > 200$, N_{ShG} is asymptotic at a value of 17.9. Syeda et al. obtained the following curve fit for $40 < N_{PeM} < 200$,

$$N_{ShG} = -11.878 + 25.879 \log_{10} N_{PeM} - 5.64 (\log_{10} N_{PeM})^2 \quad (7-76)$$

At values of $N_{PeM} < 4$, N_{ShG} approaches another asymptotic limit of less than 7.

E_{LB} is calculated from (7-66) using (7-67) to (7-76).

Calculation of E_{OV} and E_{MV}

From (7-47), E_{OV} is calculated. From (6-54), E_{MV} is calculated. The Syeda et al. method is applied in the following example.

EXAMPLE 7.5 Estimation of Tray Efficiency Using the Syeda, Afacan, and Chung Method [25].

In 1979, Sakata and Yanagi [32] of FRI reported tray efficiency data for the binary system, isobutane-normal butane, at 1138 kPa for total reflux operation ($L/V = 1$) in a 1.22 m diameter distillation column. Installed in the column were single path cross-flow sieve trays with 0.0127 m diameter holes on 0.0381 m triangular centers. The bubbling area of the tray was $0.859 m^2$, approximately 74% of the column cross-sectional area, making the downcomer area $(100 - 74)/2 = 13\%$ of the column cross-sectional area. The outlet weir was 0.94 m long and 0.0508 m high. The spacing of trays used in the experiments was 0.61 m. The fractional hole area was 0.083 based on the bubbling area.

For one of the data points, the conditions were as follows:

Liquid mass flow rate = 5.94 kg/s	Gas mass flow rate = 5.91 kg/s
Liquid density = 493 kg/m ³	Gas density = 27.8 kg/m
Liquid viscosity = 9 × 10 ⁻⁵ kg/m-s	Gas viscosity = 9.5 × 10 ⁻⁶ kg/m-s
Liquid diffusivity = 1.03 × 10 ⁻⁸ m ² /s	Gas diffusivity = 5.62 × 10 ⁻⁷ m ² /s
Surface tension = 5 × 10 ⁻³ N/m	Molecular weight = 58.12 kg/kgmol
Relative volatility = 1.23	m = 1.0509, λ = 1.0631

From the data, predict the Murphree vapor point efficiency, E_{OV} , using the method of Syeda et al. with the method of Vennavelli et al. for the fraction jetting.

Solution

Calculation of key parameters:

$$\begin{aligned} \text{Column inside total cross-sectional area} &= A_T = \frac{\pi D_T^2}{4} \\ &= \frac{3.14(1.22)^2}{4} = 1.168 \text{ m}^2 \end{aligned}$$

$$\text{Tray bubbling area} = A_b = 0.859 \text{ m}^2$$

$$\text{Tray hole area} = A_h = 0.083(0.859) = 0.0713 \text{ m}^2$$

$$\text{Liquid volumetric flow rate} = Q_L = 5.94/493 = 0.01205 \text{ m}^3/\text{s}$$

$$\text{Gas volumetric flow rate} = Q_G = 5.91/27.8 = 0.2126 \text{ m}^3/\text{s}$$

$$\begin{aligned} \text{Gas velocity based on bubbling area} &= u_b = \frac{Q_G}{A_b} = \frac{0.2126}{0.859} \\ &= 0.2475 \text{ m/s} \end{aligned}$$

$$\begin{aligned} \text{Gas velocity based on hole area} &= u_h = \frac{Q_G}{A_h} = \frac{0.2126}{0.0713} \\ &= 2.982 \text{ m/s} \end{aligned}$$

$$\begin{aligned} \text{F-factor based on the bubbling area} &= F_b = u_b \sqrt{\rho_V} \\ &= 0.2475(27.8)^{0.5} \\ &= 1.305 \text{ (m/s)(kg/m}^3)^{0.5} \end{aligned}$$

Calculation of fraction jetting:

From (7-50), $\alpha_e = 0.3764$; from (7-51), $C = 0.5004$; from (7-49), $h_{cl} = 0.0387 \text{ m}$

From (7-48), $N'_{Fr} = 0.0953$

$$\begin{aligned} \text{From (7-52), fraction jetting} &= f_J = \frac{N'_{Fr}}{0.0449 + N'_{Fr}} \\ &= \frac{0.0953}{0.0449 + 0.0953} = 0.680 \end{aligned}$$

Fraction of small and large bubbles = $1 - 0.680 = 0.320$

Calculation of the fraction of all bubbles that are small bubbles:

From (7.55), $d_{32LB} = 0.0278 \text{ m}$; from (7-58), $V_{LB} = 1.120 \times 10^{-5} \text{ m}^3$

From (7-57), $U_{LB} = 0.6213 \text{ m/s}$; from (7-56), $t_{LB} = 0.1654 \text{ s}$; from (7-54), $K_b = 7.183$

From (7-53), fraction of all bubbles that are small bubbles is,

$$f_{SB} = \frac{2 [1 - \exp(-7.183)]}{2 [1 - \exp(-7.183)] + (5)^3 \exp(-7.183)} = 0.955$$

$$\begin{aligned} \text{Fraction of all bubbles that are large bubbles} &= f_{LB} = 1 - 0.955 \\ &= 0.045 \end{aligned}$$

Calculation of Murphree overall point efficiency for the jets:

From (7-64), $k_{GJ} = 0.00459 \text{ m/s}$; from (7-65), $k_{LJ} = 0.000267 \text{ m/s}$

From (7-63), $K_{OGJ} = 0.00227 \text{ m/s}$; from (7-61), $a_{ib} = 131.2$

From (7-60) the number of overall gas-phase transfer units for the jets is:

$$N_{OGJ} = \frac{a_{ib} K_{OGJ}}{u_b} = \frac{131.2(0.00227)}{0.2475} = 1.203$$

From (7-59), $E_J = 1 - \exp(-N_{OGJ}) = 1 - \exp(-1.203) = 0.700$

Calculation of Murphree overall point efficiencies for large and small bubbles:

For the small bubbles, $E_{SB} = 1$

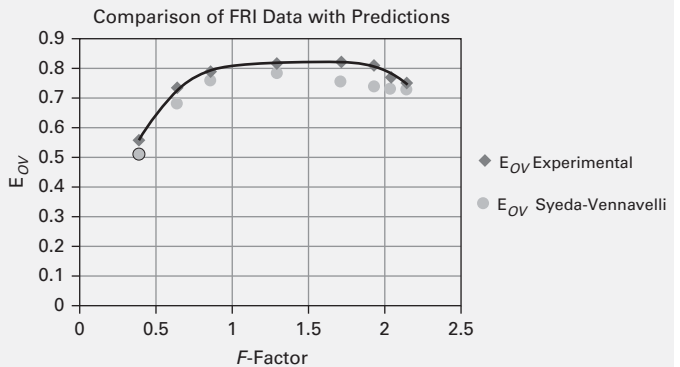
For the large bubbles, the fraction f_{LB} is about 5%. Therefore, it contributes very little. A detailed calculation gives a value of $E_{LB} = 0.012$.

Calculation of overall Murphree vapor point efficiency from combined contributions:

$$\begin{aligned} \text{From (7-47), } E_{OV} &= f_J E_J + (1 - f_J) [f_{SB} E_{SB} + (1 - f_{SB}) E_{LB}] = \\ &= 0.680(0.700) + (1 - 0.680)[0.955(1) + (1 - 0.955)0.012] = 0.782 \end{aligned}$$

This compares to a value of 0.818 from the FRI experimental data.

Calculations were made to compare with FRI data for other operating conditions. The results are shown in the following plot.



As the F -factor increases, the following table shows an increase in the fraction of jetting and a rapid decrease in the fraction of large bubbles.

F-factor	Regime Fractions		
	Jets	Large Bubbles	Small Bubbles
0.394	0.366	0.424	0.210
0.636	0.490	0.180	0.330
0.864	0.573	0.093	0.334
1.305	0.679	0.014	0.307
1.725	0.744	0.002	0.254
1.938	0.769	0.000	0.231
2.037	0.779	0.000	0.221
2.147	0.789	0.000	0.211

Table 7.5 Tray Efficiency Models in Process Simulators

Model	Aspen Plus	CHEMCAD	ChemSep
AIChE method (1958)	x	x	x
Zuiderweg (1982)		x	x
Chan and Fair (1984)	x	x	x
Chen and Chuang (1993)			x
Garcia and Fair (2000)			x
Syeda, Afacan, and Chung (2007)			x
Vennavelli, Whiteley, and Resetarits (2012)			x

§7.4.4 Tray Efficiency Models in Process Simulators

For trayed columns, Aspen Plus, CHEMCAD, and ChemSep have both equilibrium-stage and rate-based (non-equilibrium) models. The rate-based models require tray-efficiency models for estimating mass-transfer coefficients in vapor and liquid phases. Table 7.5 is a list of the models available in the three process simulators. This list could change, as the newer models by Syeda et al. and Vennavelli et al. become better known.

§7.4.5 Scale-up from Laboratory Data

Experimental pilot-plant or laboratory data are rarely necessary prior to the design of columns for ideal or nearly ideal binary mixtures. With nonideal or azeotrope-forming

solutions, use of a laboratory Oldershaw column of the type discussed in §6.5.5 should be used to verify that the desired degree of separation is attainable and to obtain an estimate of E_{OV} . The ability to predict the efficiency of industrial-size sieve-tray columns from measurements with 1-inch glass and 2-inch diameter metal Oldershaw columns is shown in Figure 7.25, from the work of Fair, Null, and Bolles [33]. The measurements are for cyclohexane/*n*-heptane at vacuum conditions (Figure 7.25a) and near-atmospheric conditions (Figure 7.25b), and for the isobutane/*n*-butane system at 11.2 atm (Figure 7.25c). The Oldershaw data are correlated by the solid lines. Data for the 4-ft-diameter column with sieve trays of 8.3% and 13.7% open area were obtained, respectively, by Sakata and Yanagi [32] and Yanagi and Sakata [34], of FRI. The Oldershaw column is assumed to measure E_{OV} . The FRI column measured E_o , but the relations of §6.5.4 were used to convert the FRI data to E_{OV} . The data cover percent flooding from 10% to 95%. Data from the Oldershaw column are in agreement with the FRI data for 14% open area, except at the lower part of the flooding range. In Figures 7.25b and 7.25c, FRI data for 8% open area show efficiencies as much as 10% higher.

§7.5 COLUMN AND REFLUX-DRUM DIAMETERS

As with absorbers and strippers, distillation-column diameters are calculated for conditions at the top and bottom trays of the tower, using the method of §6.6.1. If the diameters differ by

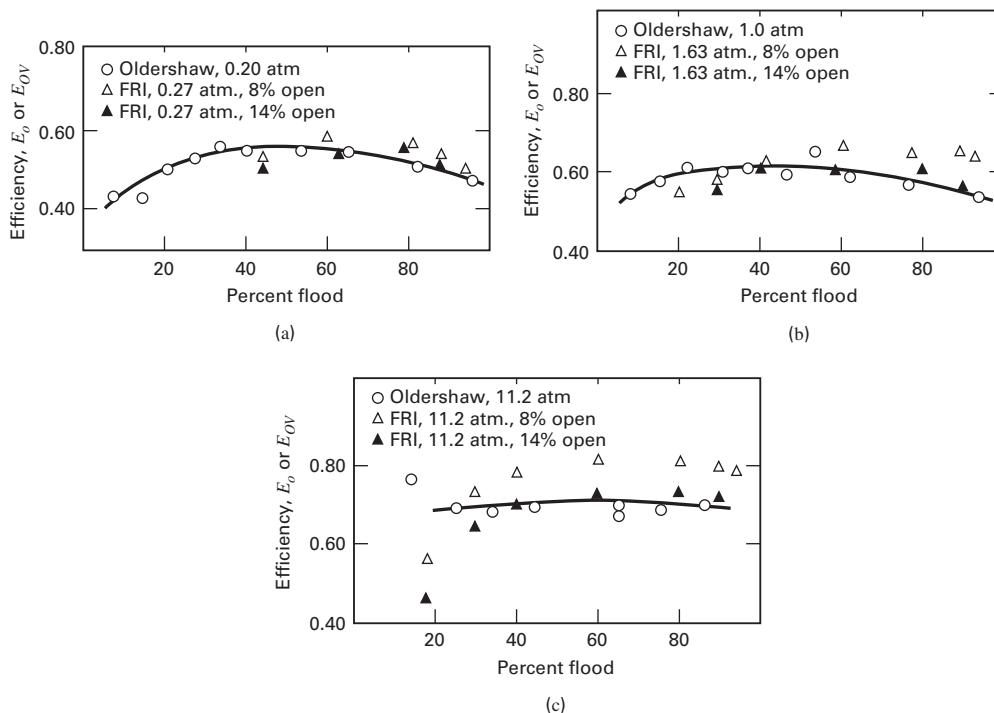


Figure 7.25 Comparison of Oldershaw column efficiency with point efficiency in 4-ft-diameter FRI column with sieve trays: (a) cyclohexane/*n*-heptane system; (b) cyclohexane/*n*-heptane system; (c) isobutane/*n*-butane system.

1 ft or less, the larger diameter is used for the entire column. If the diameters differ by more than 1 ft, it is often more economical to swage the column, using the different diameters computed for the sections above and below the feed.

§7.5.1 Reflux Drums

As shown in Figure 7.1, vapor flows from the top plate to the condenser and then to a cylindrical reflux drum, usually located near ground level. A pump is necessary to lift the reflux to the top of the column. If a partial condenser is used, the drum is oriented vertically to facilitate the separation of vapor from liquid—in effect, acting as a flash drum.

Vertical Drums

Vertical reflux and flash drums are sized by calculating a minimum drum diameter, D_T , to prevent liquid carryover by entrainment, using (6-63) in conjunction with the curve for 24-inch tray spacing in Figure 6.27 and $f = 0.85$ (85% of the flooding velocity), along with values in (6-61) of $F_{ST} = F_{HA} = F_F = 1.0$. To handle process fluctuations and otherwise facilitate control, vessel volume, V_V , is determined on the basis of liquid residence time, t , which should be at least 5 min, with the vessel half full of liquid [20]:

$$V_V = \frac{2LM_L t}{\rho_L} \quad (7-77)$$

where L is the molar liquid flow rate leaving the vessel. Assuming a vertical, cylindrical vessel and neglecting head volume, the vessel height, H , is

$$H = \frac{4V_V}{\pi D_T^2} \quad (7-78)$$

However, if $H > 4D_T$, it is generally preferable to increase D_T and decrease H to give $H = 4D_T$. Then

$$D_T = \frac{H}{4} = \left(\frac{V_V}{\pi} \right)^{1/3} \quad (7-79)$$

A height above the liquid level of at least 4 ft is necessary for feed entry and disengagement of liquid droplets from the vapor. Within this space, it is common to install a wire mesh pad, which serves as a mist eliminator.

Horizontal Drums

When vapor is totally condensed, a cylindrical, horizontal reflux drum is employed to receive the condensate. Equations (7-77) and (7-79) permit estimates of the drum diameter, D_T , and length, H , by assuming a near-optimal value for H/D_T of 4, with the same liquid residence time suggested for a vertical drum. A horizontal drum is also used following a partial condenser when the liquid flow rate is appreciably greater than the vapor flow rate.

EXAMPLE 7.6 Diameter and Height of a Flash Drum.

Equilibrium vapor and liquid streams leaving a flash drum supplied by a partial condenser are as follows:

Component	Vapor	Liquid
Flowrate, lb-mol/hr:		
HCl	49.2	0.8
Benzene	118.5	81.4
Monochlorobenzene	71.5	178.5
Total	239.2	260.7
Flowrate, lb/h:		
T , °F	19,110	26,480
P , psia	270	270
Density, lb/ft ³	35	35
	0.371	57.08

Determine the dimensions of a vertical flash drum.

Solution

Using Figure 6.27,

$$F_{LV} = \frac{26,480}{19,110} \left(\frac{0.371}{57.08} \right)^{0.5} = 0.112$$

giving $C_F = 0.34$ at a 24-inch tray spacing. From (6-63) with $C = C_F$ in (6-60),

$$u_{vf} = 0.34 \left(\frac{57.08 - 0.371}{0.371} \right)^{0.5} = 4.2 \text{ ft/s} = 15,120 \text{ ft/h}$$

From (6-63) with $A_d/A = 0$ and $f = 0.85$,

$$D_T = \left[\frac{(4)(19,110)}{(0.85)(15,120)(3.14)(1)(0.371)} \right]^{0.5} = 2.26 \text{ ft}$$

From (7-77), with $t = 5$ minutes = 0.0833 h,

$$V_V = \frac{(2)(26,480)(0.0833)}{(57.08)} = 77.3 \text{ ft}^3$$

From (7-78),

$$H = \frac{(4)(77.3)}{(3.14)(2.26)^2} = 19.3 \text{ ft}$$

However, $H/D_T = 19.3/2.26 = 8.54 > 4$. Therefore, redimension V_V for $H/D_T = 4$.

From (7-79),

$$D_T = \left(\frac{77.3}{3.14} \right)^{1/3} = 2.91 \text{ ft and } H = 4D_T = (4)(2.91) = 11.64 \text{ ft}$$

Height above the liquid level is $11.64/2 = 5.82$ ft, which is adequate. Alternatively, with a height of twice the minimum disengagement height, $H = 8$ ft and $D_T = 3.5$ ft.

§7.6 RATE-BASED METHOD FOR PACKED DISTILLATION COLUMNS

Improvements in distributors and fabrication techniques, and more economical and efficient packings, have led to increasing use of packed towers in new distillation processes and

Table 7.6 Modified Efficiency and Mass-Transfer Equations for Binary Distillation

$$\lambda = mV/L \quad (7-80)$$

$$m = dy/dx = \text{local slope of equilibrium curve} \quad (7-81)$$

Efficiency:

Equations (6-52) to (6-56) apply if λ is defined by (7-80)

Mass transfer:

$$\frac{1}{N_{OG}} = \frac{1}{N_G} + \frac{\lambda}{N_L} \quad (7-82)$$

$$\frac{1}{K_{OG}} = \frac{1}{k_G a} + \frac{mPM_L/\rho_L}{k_L a} \quad (7-83)$$

$$\frac{1}{K_y a} = \frac{1}{k_y a} + \frac{m}{k_x a} \quad (7-84)$$

$$\frac{1}{K_x a} = \frac{1}{k_x a} + \frac{1}{mk_y a} \quad (7-85)$$

$$H_{OG} = H_G + \lambda H_L \quad (7-86)$$

$$\text{HETP} = H_{OG} \ln \lambda / (\lambda - 1) \quad (7-87)$$

retrofitting of existing trayed towers to increase capacity and reduce pressure drop. Methods in §6.7 and §6.8 for estimating packed-column parameters and packed heights for absorbers are applicable to distillation and are extended here for use in conjunction with the McCabe–Thiele diagram. Both the HETP and HTU methods are covered. Unlike dilute-solution absorption or stripping, where values of HETP and HTU may be constant throughout, values of HETP and HTU vary, especially across the feed entry, where appreciable changes in vapor and liquid traffic occur. Also, because the equilibrium line for distillation is curved, equations of §6.8 must be modified by replacing $\lambda = KV/L$ with

$$\lambda = \frac{mV}{L} = \frac{\text{slope of equilibrium curve}}{\text{slope of operating line}} \quad (7-80)$$

where $m = dy/dx$ varies with location. The efficiency and mass-transfer relationships are summarized in Table 7.6.

§7.6.1 HETP Method for Distillation

In the HETP method, equilibrium stages are first stepped off on a McCabe–Thiele diagram, where equimolar counter-diffusion (EMD) applies. At each stage, T , P , phase-flow ratio, and phase compositions are noted. A suitable packing material is selected, and the column diameter is estimated for operation at, say, 70% of flooding by one of the methods of §6.8. Mass-transfer coefficients for the individual phases are estimated for the stage conditions from correlations in §6.8. From these coefficients, values of H_{OG} and HETP are estimated for each stage and then summed to obtain the packed heights of the rectifying and stripping sections. If experimental values of HETP are available, they are used directly. In computing values of H_{OG} from H_G and H_L , or K_y from k_y and k_x , (6-110)

and (6-75) must be modified because for binary distillation, where the mole fraction of the LK may range from almost 0 at the bottom of the column to almost 1 at the top, the ratio $(y_1 - y^*)/(x_1 - x)$ in (6-77) is no longer a constant equal to the K -value, but the ratio is dy/dx , the slope, m , of the equilibrium curve. The modified equations are given in Table 7.6.

EXAMPLE 7.7 Packed Height by the HETP Method.

For the benzene–toluene distillation of Example 7.1, determine packed heights of the rectifying and stripping sections based on the following values for the individual HTUs (see Table 6.5). Included are the values of molar liquid flow rate to molar vapor flow rate for each section from Example 7.1.

	H_G , ft	H_L , ft	L/V or \bar{L}/\bar{V}
Rectifying section	1.16	0.48	0.62
Stripping section	0.90	0.53	1.40

Solution

Equilibrium-curve slopes, $m = dy/dx$, are from Figure 7.16 and values of λ are from (7-81). H_{OG} for each stage in Table 7.7 is from (7-86), and HETP for each stage is from (7-87). Table 7.7 shows that only 0.2 of stage 13 is needed and that stage 14 is the partial reboiler. From the results in Table 7.7, 10 ft of packing should be used in each section.

Table 7.7 Results for Example 7.7

Stage	m	$\lambda = \frac{mV}{L}$ or $\frac{m\bar{V}}{\bar{L}}$	H_{OG} , ft	HETP, ft
1	0.47	0.76	1.52	1.74
2	0.53	0.85	1.56	1.70
3	0.61	0.98	1.62	1.64
4	0.67	1.08	1.68	1.62
5	0.72	1.16	1.71	1.59
6	0.80	1.29	1.77	1.56
Total for rectifying section:				9.85
7	0.90	0.64	1.32	1.64
8	0.98	0.70	1.28	1.52
9	1.15	0.82	1.34	1.47
10	1.40	1.00	1.43	1.43
11	1.70	1.21	1.53	1.40
12	1.90	1.36	1.62	1.38
13	2.20	1.57	1.73	1.37(0.2) = 0.27
Total for stripping section:				9.11
Total packed height, ft:				18.96

§7.6.2 HTU Method for Distillation in Packed Columns

In the HTU methods, stages are not stepped off on a McCabe–Thiele diagram. Instead, the diagram provides data to perform an integration over the packed height using mass-transfer coefficients or transfer units.

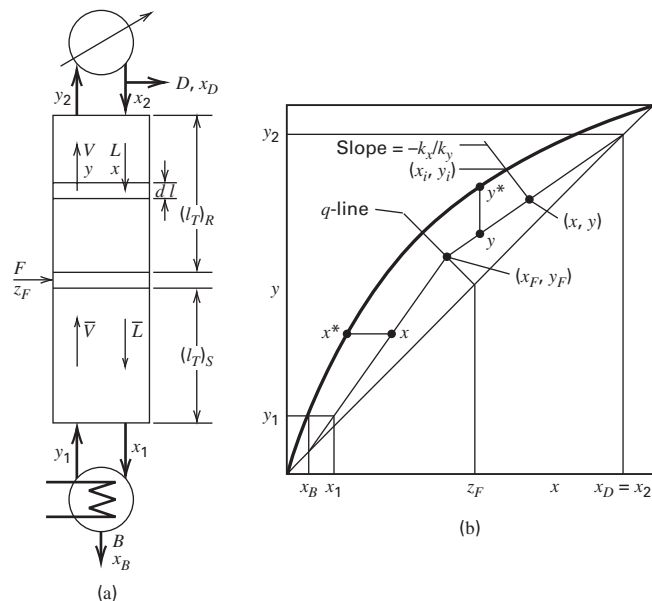


Figure 7.26 Distillation in a packed column.

Consider the packed distillation column and its McCabe–Thiele diagram in Figure 7.26. Assume that V and L in the rectifying section and \bar{V} and \bar{L} in the stripping section are constant.

For equimolar counter diffusion (EMD), the rate of mass transfer of the LK from the liquid to the vapor phase is

$$n = k_x a(x - x_1) = k_y a(y_1 - y) \tag{7-88}$$

Rearranging,

$$-\frac{k_x a}{k_y a} = \frac{y_1 - y}{x_1 - x} \tag{7-89}$$

In Figure 7.26b, for any point (x, y) on the operating line, the interfacial point (x_1, y_1) on the equilibrium curve is obtained by drawing a line of slope $(-k_x a / k_y a)$ from point (x, y) to the point where it intersects the equilibrium curve.

By material balance over an incremental column height, l , with constant molar overflow,

$$V dy = k_y a (y_1 - y) A_T dl \tag{7-90}$$

$$L dx = k_x a (x - x_1) A_T dl \tag{7-91}$$

where A_T is the cross-sectional area of the packed section. Integrating over the rectifying section,

$$(l_T)_R = \int_0^{(l_T)_R} dl = \int_{y_F}^{y_2} \frac{V dy}{k_y a A_T (y_1 - y)} = \int_{x_F}^{x_D} \frac{L dx}{k_x a A_T (x - x_1)} \tag{7-92}$$

or

$$(l_T)_R = \int_{y_F}^{y_2} \frac{H_G dy}{(y_1 - y)} = \int_{x_F}^{x_D} \frac{H_L dx}{(x - x_1)} \tag{7-93}$$

Integrating over the stripping section,

$$(l_T)_S = \int_0^{(l_T)_S} dl = \int_{y_1}^{y_F} \frac{V dy}{k_y a A_T (y_1 - y)} = \int_{x_1}^{x_F} \frac{L dx}{k_x a A_T (x - x_1)} \tag{7-94}$$

or

$$(l_T)_S = \int_{y_1}^{y_F} \frac{H_G dy}{(y_1 - y)} = \int_{x_1}^{x_F} \frac{H_L dx}{(x - x_1)} \tag{7-95}$$

Values of k_y and k_x vary over the packed height, causing the slope $(-k_x a / k_y a)$ to vary. If $k_x a > k_y a$, resistance to mass transfer resides mainly in the vapor and, in using (7-95), it is most accurate to evaluate the integrals in y . For $k_y a > k_x a$, the integrals in x are used. Usually, it is sufficient to evaluate k_y and k_x at three points in each section to determine their variation with x . Then by plotting their ratios from (7-89), a locus of points P can be found, from which values of $(y_1 - y)$ for any value of y , or $(x - x_1)$ for any value of x , can be read for use with (7-92) to (7-95). These integrals can be evaluated either graphically or numerically.

EXAMPLE 7.8 Packed Height by the HTU Method.

Two hundred and fifty kmol/h of saturated-liquid feed of 40 mol% isopropyl ether in isopropanol is distilled in a packed column operating at 1 atm to obtain a distillate of 75 mol% isopropyl ether and a bottoms of 95 mol% isopropanol. This mixture forms an azeotrope at 78 mol% isopropyl ether. The reflux ratio is 1.5 times the minimum and the column has a total condenser and partial reboiler. The mass-transfer coefficients given below have been estimated from empirical correlations in §6.8. Compute the packed volumes of the rectifying and stripping sections.

Solution

From an overall material balance on isopropyl ether,

$$0.40(250) = 0.75D + 0.05(250 - D)$$

Solving,

$$D = 125 \text{ kmol/h and } B = 250 - 125 = 125 \text{ kmol/h}$$

The equilibrium curve at 1 atm is shown in Figure 7.27, where isopropyl ether is the LK.

The distillate composition of 75 mol% is safely below the azeotropic composition. Also shown in Figure 7.27 are the q -line and the rectifying-section operating line for minimum reflux. The slope of the latter is measured to be $(L/V)_{\min} = 0.39$. From (7-32),

$$R_{\min} = 0.39 / (1 - 0.39) = 0.64 \text{ and } R = 1.5 R_{\min} = 0.96$$

$$L = RD = 0.96(125) = 120 \text{ kmol/h}$$

and $V = L + D = 120 + 125 = 245 \text{ kmol/h}$

$$\bar{L} = L + L_F = 120 + 250 = 370 \text{ kmol/h}$$

$$\bar{V} = V - V_F = 245 - 0 = 245 \text{ kmol/h}$$

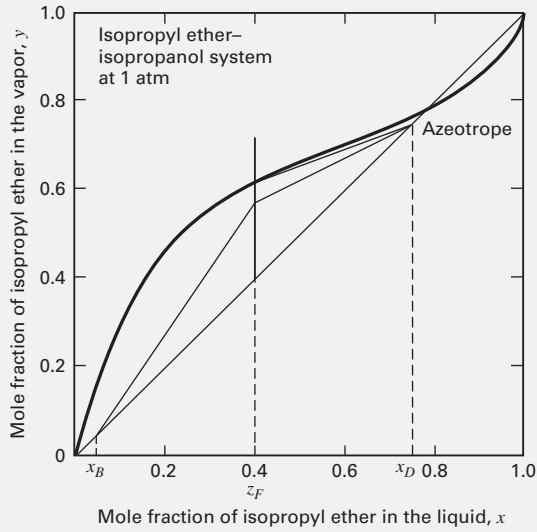


Figure 7.27 Operating lines and minimum reflux line for Example 7.8.

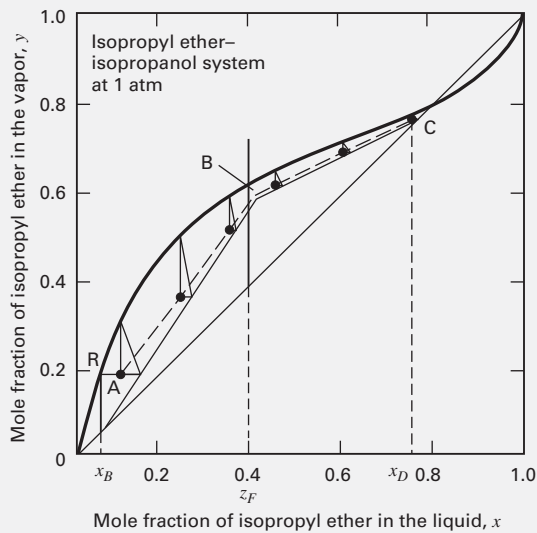


Figure 7.28 Mass-transfer driving forces for Example 7.8.

The rectifying-section operating-line slope = $L/V = 120/245 = 0.49$. This line and the stripping-section operating line are plotted in Figure 7.27. The partial reboiler, R, is stepped off in Figure 7.28 to give the following end points for determining the packed heights of the two sections, where the symbols refer to Figure 7.26a:

	Stripping Section	Rectifying Section
Top	$(x_F = 0.40, y_F = 0.577)$	$(x_2 = 0.75, y_2 = 0.75)$
Bottom	$(x_1 = 0.05, y_1 = 0.18)$	$(x_F = 0.40, y_F = 0.577)$

Mass-transfer coefficients at three values of x are as follows:

x	$k_y a$	$k_x a$
	kmol/m ³ -h-(mole fraction)	kmol/m ³ -h-(mole fraction)
Stripping section:		
0.15	305	1,680
0.25	300	1,760
0.35	335	1,960
Rectifying section:		
0.45	185	610
0.60	180	670
0.75	165	765

Mass-transfer-coefficient slopes are computed for each point x on the operating line using the $-k_x a/k_y a$ ratio according to (7-89), and are drawn from the operating line to the equilibrium line in Figure 7.28. These are tie lines because they tie the operating line to the equilibrium line. Using the tie lines as hypotenuses, right triangles are constructed, as shown in Figure 7.28. Dashed lines, AB and BC, are then drawn through the points at the 90° triangle corners. Additional tie lines can, as needed, be added to the three plotted lines in each section to give better accuracy. From the tie lines, values of $(y_1 - y)$ can be tabulated for operating-line y -values. Column diameter is not given, so the packed volumes are determined from rearrangements of (7-92) and (7-94), with $V = A_T l_T$:

$$V_R = \int_{y_F}^{y_2} \frac{V dy}{k_y a (y_1 - y)} \quad (7-96)$$

$$V_S = \int_{y_1}^{y_F} \frac{V dy}{k_y a (y_1 - y)} \quad (7-97)$$

Values of $k_y a$ are interpolated as necessary.

The results are:

y	$(y_1 - y)$	$k_y a$	$\frac{V(\text{or } \bar{V})}{k_y a (y_1 - y)}, \text{m}^3$
Stripping section:			
0.18	0.145	307	5.5
0.25	0.150	303	5.4
0.35	0.143	300	5.7
0.45	0.103	320	7.4
0.577	0.030	350	23.3
Rectifying section:			
0.577	0.030	187	43.7
0.60	0.033	185	40.1
0.65	0.027	182	49.9
0.70	0.017	175	82.3
0.75	0.010	165	148.5

By numerical integration, $V_S = 3.6 \text{ m}^3$ and $V_R = 12.3 \text{ m}^3$.

CHAPTER 7 NOMENCLATURE

Abbreviations and Acronyms

J	jets, §7.4.3
LB	large bubbles, §7.4.3
SB	small bubbles, §7.4.3

Latin Symbols

d_{32}	Sauter mean diameter, (7-53)
D_T	drum diameter, (7-78)
H	vessel height, (7-78)
m_s	mass flow rate of steam, below (7-38c)
m_{cw}	mass flow rate of cooling water, below (7-38c)
N'_{Fr}	modified Froude number, (7-48)

SUMMARY

1. A binary mixture can be separated into two nearly pure products economically by distillation if $\alpha > \sim 1.05$ and no azeotrope forms.
2. Distillation is the most mature and widely used separation operation, with design and operation practices well established.
3. Product purities depend mainly on the number of equilibrium stages in the rectifying and stripping sections, and to some extent on the reflux ratio. However, both the number of stages and the reflux ratio must be greater than their minimum values corresponding to total reflux and infinite stages, respectively. The optimal R/R_{\min} is usually in the range of 1.10 to 1.50.
4. Distillation is conducted in trayed towers equipped with sieve or valve trays, or in columns packed with random or structured packings. Many older towers are equipped with bubble-cap trays.
5. Most distillation towers have a condenser that provides cooling water, to obtain reflux, and a reboiler, heated with steam, for boilup.
6. When the assumption of constant molar overflow is valid, the McCabe–Thiele graphical method for binary mixtures is convenient for determining stage and reflux

REFERENCES

1. FORBES, R.J., *Short History of the Art of Distillation*, E.J. Brill, Leiden (1948).
2. MIX, T.W., J.S. DWECK, M. WEINBERG, and R.C. ARMSTRONG, *Chem. Eng. Prog.*, **74**(4), 49–55 (1978).
3. KISTER, H.Z., *Distillation Design*, McGraw-Hill, New York (1992).
4. KISTER, H.Z., *Distillation Operation*, McGraw-Hill, New York (1990).
5. MCCABE, W.L., and E.W. THIELE, *Ind. Eng. Chem.*, **17**, 605–611 (1925).
6. SEADER, J.D., E.J. HENLEY, and D.K. ROOPER, *Separation Process Principles*, John Wiley & Sons, Hoboken, NJ (2011).
7. LOCKETT, M.J., *Distillation Tray Fundamentals*, Cambridge University Press, Cambridge (1986).
8. *AIChE Equipment Testing Procedure—Trayed and Packed Columns: A Guide to Performance Evaluation*, 3rd Edition, AIChE, Wiley, New York (2014).
9. WILLIAMS, G.C., E.K. STIGGER, and J.H. NICHOLS, *Chem. Eng. Progr.*, **46**(1), 7–16 (1950).
10. GERSTER, J.A., A.B. HILL, N.H. HOCHGROF, and D.B. ROBINSON, *Tray Efficiencies in Distillation Columns, Final Report from the University of Delaware*, AIChE, New York (1958).

Q_C, Q_R	condenser, reboiler heat duties, below (7-38c)
q	q -line, a line on the McCabe–Thiele diagram, (7-25)
R, R_{\min}	reflux ratio L/D , minimum reflux ratio = L_{\min}/D , Table 7.2
V_B	boilup ratio, \bar{V}/B , (7-18)
V_V	vessel volume, (7-77)
z_F	mole fraction in the feed

Subscripts

B	bottoms product
D	distillate
I	interface between phases
R	rectifying section
S	stripping section

requirements. This method facilitates the visualization of many aspects of distillation and provides a procedure for locating the optimal feed stage.

7. Design of a distillation tower includes selection of operating pressure, type of condenser, degree of reflux subcooling, type of reboiler, and extent of feed preheat.
8. For trayed columns, estimates of overall stage efficiency, defined by (6-41), can be made with the Drickamer and Bradford, (7-39), or O'Connell, (7-40), correlations. More accurate procedures use data from a laboratory Oldershaw column or the semitheoretical mass-transfer equations of Syeda et al.
9. Tray diameter can be estimated by procedures in Chapter 6.
10. Reflux and flash drums are sized by a procedure based on vapor entrainment and liquid residence time.
11. Packed-column diameter and pressure drop are determined by procedures presented in Chapter 6.
12. The height of a packed column is established by the HETP method or, preferably, the HTU method. Application to distillation parallels the methods in Chapter 6 for absorbers and strippers, but differs in the manner in which the curved equilibrium line is handled.

11. DRICKAMER, H.G., and J.R. BRADFORD, *Trans. AIChE*, **39**, 319–360 (1943).
12. O'CONNELL, H.E., *Trans. AIChE*, **42**, 741–755 (1946).
13. LOCKHART, F.J., and C.W. LEGGETT, in K.A. Kobe and J.J. McKetta, Jr., Eds., *Advances in Petroleum Chemistry and Refining*, Vol. 1, Interscience, New York, pp. 323–326 (1958).
14. ZUIDERWEG, F.J., H. VERBURG, and F.A.H. GILISSEN, Proc. *International Symposium on Distillation*, Institution of Chem. Eng., London, 202–207 (1960).
15. GAUTREUX, M.F., and H.E. O'CONNELL, *Chem. Eng. Prog.*, **51**(5) 232–237 (1955).
16. American Institute of Chemical Engineers (AIChE) *Bubble-Tray Design Manual*, AIChE, New York (1958).
17. CHAN, H., and J.R. FAIR, *Ind. Eng. Chem. Process Des. Dev.*, **23**, 814–819 (1984).
18. CHAN, H., and J.R. FAIR, *Ind. Eng. Chem. Process Des. Dev.*, **23**, 820–827 (1984).
19. SCHEFFE, R.D., and R.H. WEILAND, *Ind. Eng. Chem. Res.*, **26**, 228–236 (1987).
20. FOSS, A.S., and J.A. GERSTER, *Chem. Eng. Prog.*, **52**, 28-J to 34-J (Jan. 1956).
21. BENNETT, D.L., D.N. WATSON, and M.A. WIESCINSKI, *AIChE J.*, **43**, 1611 (1997).
22. CHEN, G.X. and CHUANG, K.T., *Ind. Eng. Chem. Res.*, **32**, 701–708 (1993).
23. GARCIA, J.A. and FAIR, J.R., *Ind. Eng. Chem. Res.*, **39**, 1809–1817 (2000).
24. GARCIA, J.A. and FAIR, J.R., *Ind. Eng. Chem. Res.*, **39**, 1818–1825 (2000).
25. SYEDA, S.R., AFACAN, A., and CHUANG, K.T., *Chem. Eng. Res. and Design*, **85**(A2), 269–277 (2007).
26. VENNAVELLI, A.N., J.R. WHITELEY, and M.R. RESEARITS, *Ind. Eng. Chem. Res.*, **51**, 11458–11462 (2012).
27. BENNETT, D.L., R. AGRAWAL, and P.J. COOK, *AIChE J.*, **29**, 434–442 (1983).
28. RAPER, J., M. KEARNEY, J. BURGESS, and C. FELL, *Chem. Eng. Sci.*, **37**, 501–506 (1982).
29. ZUIDERWEG, F. J., *Chem. Eng. Sci.*, **37**, 1441–1464 (1982).
30. HIGBIE, R., *Trans. AIChE*, **31**, 365–388 (1935).
31. ZARITSKY, N., and A. CALVELO, *Can. J. Chem. Eng.*, **57**, 58–64 (1979).
32. SAKATA, M., and T. YANAGI, *I. Chem. E. Symp. Ser.*, **56**, 3.2/21 (1979).
33. FAIR, J.R., H.R. NULL, and W.L. BOLLES, *Ind. Eng. Chem. Process Des. Dev.*, **22**, 53–58 (1983).
34. YANAGI, T., and M. SAKATA, *Ind. Eng. Chem. Process Des. Devel.*, **21**, 712 (1982).
35. PRADO, M., and J.R. FAIR, *Ind. Eng. Chem. Res.*, **29**, 1031 (1990).

STUDY QUESTIONS

- 7.1. What equipment is included in a typical distillation operation?
- 7.2. What determines the operating pressure of a distillation column?
- 7.3. Under what conditions does a distillation column need to operate under vacuum?
- 7.4. Why are distillation columns arranged for countercurrent flow of liquid and vapor?
- 7.5. Why is the McCabe–Thiele graphical method still useful in this era of more rigorous, computer-aided algebraic methods used in process simulators?
- 7.6. Under what conditions does the McCabe–Thiele assumption of constant molar overflow hold?
- 7.7. In the McCabe–Thiele method, between which two lines is the staircase constructed?
- 7.8. What is meant by reflux ratio? What is meant by boilup ratio?
- 7.9. What is the q -line and how is it related to the feed condition?
- 7.10. What are the five possible feed conditions?
- 7.11. In the McCabe–Thiele method, are the stages stepped off from the top down or the bottom up? In either case, when is it best, during the stepping, to switch from one operating line to the other? Why?
- 7.12. Can a column be operated at total reflux? How?
- 7.13. How many stages are necessary for operation at minimum reflux ratio?
- 7.14. What is meant by a pinch point? Is it always located at the feed stage?
- 7.15. What is meant by subcooled reflux? How does it affect the amount of reflux inside the column?
- 7.16. Is it worthwhile to preheat the feed to a distillation column?
- 7.17. Why is the stage efficiency in distillation higher than that in absorption?
- 7.18. What is unique about the Syeda et al. method for predicting plate efficiency for sieve trays?
- 7.19. What small laboratory column is useful for obtaining plate efficiency data?
- 7.20. What is meant by a rate-based design method?

EXERCISES

Note: Unless otherwise stated, the usual simplifying assumptions of saturated-liquid reflux, optimal feed-stage location, no heat losses, steady state, and constant molar liquid and vapor flows apply to each exercise.

Section 7.1

7.1. Differences between absorption, distillation, and stripping.

List as many differences between (1) absorption and distillation and (2) stripping and distillation as you can.

7.2. Popularity of packed columns.

Prior to the 1980s, packed columns were rarely used for distillation unless column diameter was less than 2.5 ft. Explain why, in recent years, some trayed towers are being retrofitted with packing and some new large-diameter columns are being designed for packing rather than trays.

7.3. Use of cooling water in a condenser.

A mixture of methane and ethane is subject to distillation. Why can't water be used as a condenser coolant? What would you use?

7.4. Operating pressure for distillation.

A mixture of ethylene and ethane is to be separated by distillation. What operating pressure would you suggest? Why?

7.5. Laboratory data for distillation design.

Under what circumstances would it be advisable to conduct laboratory or pilot-plant tests of a proposed distillation?

7.6. Economic trade-off in distillation design.

Explain the economic trade-off between trays and reflux.

Section 7.2

7.7. McCabe–Thiele Method.

In the 50 years following the development by Sorel in 1894 of a mathematical model for continuous, steady-state, equilibrium-stage distillation, many manual methods were proposed for solving the equations graphically or algebraically. Today, the only method from that era that remains in widespread use is the McCabe–Thiele graphical method. What attributes of this method are responsible for its continuing popularity?

7.8. Compositions of countercurrent cascade stages.

For the cascade in Figure 7.29a, calculate (a) compositions of streams V_4 and L_1 by assuming 1 atm pressure, saturated-liquid and -vapor feeds, and the vapor–liquid equilibrium data below, where compositions are in mole percent. (b) Given the feed compositions in cascade (a), how many stages are required to produce a V_4 containing 85 mol% alcohol? (c) For the cascade configuration in Figure 7.29b, with $D = 50$ mol/s, what are the compositions of D and L_1 ? (d) For the configuration of cascade (b), how many stages are required to produce a D of 50 mol% alcohol?

EQUILIBRIUM DATA, MOLE-FRACTION ALCOHOL:

x	0.1	0.3	0.5	0.7	0.9
y	0.2	0.5	0.68	0.82	0.94

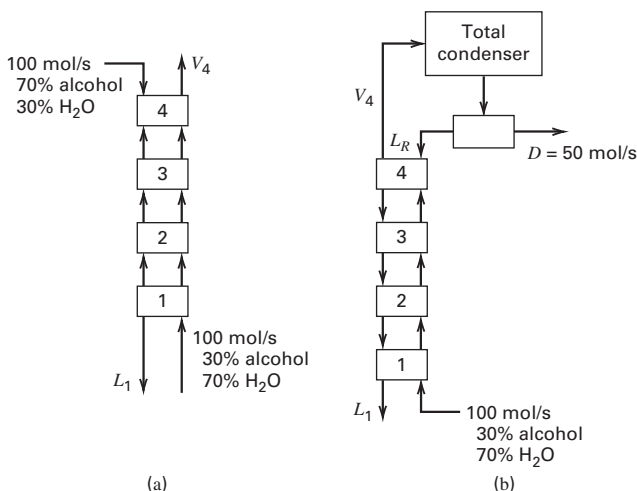


Figure 7.29 Data for Exercise 7.8.

7.9. Stripping of air.

Liquid air is fed to the top of a perforated-tray reboiled stripper operated at 1 atm. Sixty percent of the oxygen in the feed is to be drawn off in the bottoms vapor product, which is to contain 0.2 mol% nitrogen. Based on the assumptions and equilibrium data in the table,

calculate: (a) the mol% N_2 in the vapor from the top stage, (b) the vapor generated in the still per 100 moles of feed, and (c) the number of equilibrium stages required.

Assume constant molar overflow equal to the moles of feed. Liquid air contains 20.9 mol% O_2 and 79.1 mol% N_2 . The equilibrium data [*Chem. Met. Eng.*, **35**, 622 (1928)] at 1 atm are:

Temperature, K	Mole-Percent N_2 in Liquid	Mole-Percent N_2 in Vapor
77.35	100.00	100.00
77.98	90.00	97.17
78.73	79.00	93.62
79.44	70.00	90.31
80.33	60.00	85.91
81.35	50.00	80.46
82.54	40.00	73.50
83.94	30.00	64.05
85.62	20.00	50.81
87.67	10.00	31.00
90.17	0.00	0.00

7.10. Using operating data to determine reflux and distillate composition.

A mixture of A (more volatile) and B is separated in a plate distillation column. In two separate tests run with a saturated-liquid feed of 40 mol% A, the following compositions, in mol% A, were obtained for samples of liquid and vapor streams from three consecutive stages between the feed and total condenser at the top:

Stage	Mol% A			
	Test 1		Test 2	
	Vapor	Liquid	Vapor	Liquid
$M + 2$	79.5	68.0	75.0	68.0
$M + 1$	74.0	60.0	68.0	60.5
M	67.9	51.0	60.5	53.0

Determine the reflux ratio and overhead composition in each case, assuming that the column has more than three stages.

7.11. Determining the best distillation procedure.

A saturated-liquid mixture of 70 mol% benzene and 30 mol% toluene, whose relative volatility is 2.5, is to be distilled at 1 atm to produce a distillate of 80 mol% benzene. Five procedures, described below, are under consideration. For each procedure, calculate and tabulate: (a) moles of distillate per 100 moles of feed, (b) moles of total vapor generated per mole of distillate, and (c) mol% benzene in the bottoms. (d) For each part, construct a $y-x$ diagram. On this, indicate the compositions of the overhead product, the reflux, and the composition of the bottoms. (e) If the objective is to maximize total benzene recovery, which, if any, of these procedures is preferred?

The procedures are as follows:

1. Continuous distillation followed by partial condensation. The feed is sent to the reboiler, from which the bottoms is continuously withdrawn. The overhead vapor enters the top of a helically coiled partial condenser that discharges into a trap. The liquid is returned as reflux to the reboiler, while the vapor is condensed as a distillate containing 80 mol% benzene. The molar ratio of reflux to distillate is 0.5.

- Continuous distillation in a column containing one equilibrium stage. The feed is sent to the reboiler, from which bottoms is withdrawn continuously. The overhead vapor from the stage enters the top of a helically coiled partial condenser that discharges into a trap. The liquid from the trap is returned to the stage, while the uncondensed vapor is condensed to form a distillate containing 80 mol% benzene. The molar ratio of reflux to distillate is 0.5.
- Continuous distillation in a column containing the equivalent of two equilibrium stages. The feed is sent to the reboiler, from which bottoms is withdrawn continuously. The vapors from the top stage enter the top of a helically coiled partial condenser that discharges into a trap. The liquid from the trap is returned to the top stage as reflux, while the uncondensed vapor is condensed to a distillate containing 80 mol% benzene. The molar ratio of reflux to distillate is 0.5.
- The operation is the same as for Procedure 3, except that liquid from the trap is returned to the bottom stage.
- Continuous distillation in a column with the equivalent of one equilibrium stage. The feed at its boiling point is introduced on the stage. The bottoms is withdrawn from the reboiler. The overhead vapor from the stage enters the top of a partial condenser that discharges into a trap. The liquid from the trap is returned to the stage, while the uncondensed vapor is condensed to a distillate of 80 mol% benzene. The molar ratio of reflux to distillate is 0.5.

7.12. Evaluating distillation procedures.

A saturated-liquid mixture of 50 mol% benzene and toluene is distilled at 101 kPa in an apparatus consisting of a reboiler, one equilibrium stage, and a total condenser. The reboiler is equivalent to an equilibrium stage. The apparatus is to produce a distillate of 75 mol% benzene. For each procedure below, calculate, if possible, the moles of distillate per 100 moles of feed. Assume a relative volatility, α , of 2.5.

Procedures: (a) No reflux with feed to the reboiler. (b) Feed to the reboiler with a reflux ratio of 3. (c) Feed to the stage with a reflux ratio of 3. (d) Feed to the stage with a reflux ratio of 3 from a partial condenser. (e) Part (b) using minimum reflux. (f) Part (b) using total reflux.

7.13. Separation of benzene and toluene.

A column at 101 kPa is to separate 30 kg/h of a bubble-point solution of benzene and toluene containing 0.6 mass-fraction toluene into an overhead product of 0.97 mass-fraction benzene and a bottoms product of 0.98 mass-fraction toluene at a reflux ratio of 3.5. The feed is sent to the optimal stage, and the reflux is at saturation temperature. Determine the: (a) top and bottom products and (b) number of stages using the following vapor–liquid equilibrium data.

EQUILIBRIUM DATA IN MOLE-FRACTION BENZENE, 101 kPa:

y	0.21	0.37	0.51	0.64	0.72	0.79	0.86	0.91	0.96	0.98
x	0.1	0.2	0.3	0.4	0.5	0.6	0.7	0.8	0.9	0.95

7.14. Calculation of products.

A mixture of 54.5 mol% benzene in chlorobenzene at its bubble point is fed continuously to the bottom stage of a column containing two equilibrium stages, with a partial reboiler and a total condenser. Sufficient heat is supplied to the reboiler to give $\bar{V}/F = 0.855$, and the reflux ratio L/D in the top of the column is constant at 0.50. Under these conditions using the equilibrium data in the table, what are the compositions of the expected products?

EQUILIBRIUM DATA AT COLUMN PRESSURE, MOLE-FRACTION BENZENE:

x	0.100	0.200	0.300	0.400	0.500	0.600	0.700	0.800
y	0.314	0.508	0.640	0.734	0.806	0.862	0.905	0.943

7.15. Loss of trays in a distillation column.

A continuous distillation with a reflux ratio (L/D) of 3.5 yields a distillate containing 97 wt% benzene (B) and a bottoms of 98 wt% toluene (T). Due to weld failures, the 10 stripping plates in the bottom section of the column are ruined, but the 14 upper rectifying plates are intact. It is suggested that the column still be used, with the feed (F) as saturated vapor at the dew point, with $F = 13,600$ kg/h containing 40 wt% B and 60 wt% T. Assuming that the plate efficiency remains unchanged at 50%: (a) Can this column still yield a distillate containing 97 wt% B? (b) How much distillate is there? (c) What is the residue composition in mole %?

For vapor–liquid equilibrium data, see Exercise 7.13.

7.16. Changes to a distillation operation.

A distillation column having the equivalent of eight theoretical stages (seven stages + partial reboiler + total condenser) separates 100 kmol/h of saturated-liquid feed containing 50 mol% A into a product of 90 mol% A. The liquid-to-vapor molar ratio at the top plate is 0.75. The saturated-liquid feed enters plate 5 down from the top. Determine: (a) the bottoms composition, (b) the \bar{L}/\bar{V} ratio in the stripping section, and (c) the moles of bottoms per hour using the equilibrium data below.

Unknown to the operators, the bolts holding plates 5, 6, and 7 rust through, and the plates fall to the bottom. What is the new bottoms composition?

It is suggested that instead of returning reflux to the top plate, an equivalent amount of liquid product from another column be used as reflux. If that product contains 80 mol% A, what is now the composition of (a) the distillate and (b) the bottoms?

EQUILIBRIUM DATA, MOLE FRACTION OF A:

y	0.19	0.37	0.5	0.62	0.71	0.78	0.84	0.9	0.96
x	0.1	0.2	0.3	0.4	0.5	0.6	0.7	0.8	0.9

7.17. Effect of different feed conditions.

A distillation unit consists of a partial reboiler, a column with seven equilibrium plates, and a total condenser. The feed is a 50 mol% mixture of benzene in toluene. It is desired to produce a distillate containing 96 mol% benzene, when operating at 101 kPa.

(a) With saturated-liquid feed fed to the fifth plate from the top, calculate: (1) minimum reflux ratio $(L/D)_{\min}$; (2) the bottoms composition, using a reflux ratio (L/D) of twice the minimum; and (3) moles of product per 100 moles of feed.

(b) Repeat part (a) for a saturated vapor fed to the fifth plate from the top.

Equilibrium data are in Exercise 7.13.

7.18. Conversion of distillation to stripping.

A valve-tray column containing eight theoretical plates, a partial reboiler, and a total condenser separates a benzene–toluene feed mixture containing 36 mol% benzene at 101 kPa. The reboiler generates 100 kmol/h of vapor. A request has been made for very pure toluene, and it is proposed to run this column as a reboiled stripper, with the saturated-liquid feed to the top plate, employing the same boilup at the still and returning no reflux to the column. Equilibrium data are given in Exercise 7.13. (a) What is the minimum feed rate under the

proposed conditions, and what is the corresponding composition of the liquid in the reboiler at the minimum feed rate? (b) At a feed rate 25% above the minimum, what is the rate of production of toluene, and what are the compositions in mol% of the product and distillate?

7.19. Poor distillation performance.

Fifty mol% methanol in water at 101 kPa is continuously distilled in a seven equilibrium-plate, perforated-tray column, with a total condenser and a partial reboiler heated by steam. Normally, 100 kmol/h of feed is introduced on the third plate from the bottom. The overhead product contains 90 mol% methanol, and the bottoms 5 mol%. One mole of reflux is returned for each mole of overhead product. Recently it has been impossible to maintain the product purity in spite of an increase in the reflux ratio. The following test data were obtained:

Stream	kmol/h	mol% alcohol
Feed	100	51
Bottoms	62	12
Distillate	53	80
Reflux	94	—

What is the most probable cause of this poor performance? What further tests would you make to establish the reason for the trouble? Could some 90% product be obtained by further increasing the reflux ratio, while keeping the vapor rate constant?

Vapor-liquid equilibrium data at 1 atm [Chem. Eng. Prog., 48, 192 (1952)] in mole-fraction methanol are

x	0.0321	0.0523	0.075	0.154	0.225	0.349	0.813	0.918
y	0.1900	0.2940	0.352	0.516	0.593	0.703	0.918	0.963

7.20. Effect of feed rate reduction operation.

A fractionating column equipped with a steam-heated partial reboiler and total condenser (Figure 7.30) separates a mixture of 50 mol% A and 50 mol% B into an overhead product containing 90 mol% A and a bottoms of 20 mol% A. The column has three theoretical (equilibrium) plates, and the reboiler is equivalent to one theoretical plate. When the system is operated at $L/V = 0.75$ with the feed as a saturated liquid to the bottom plate, the desired products are obtained. The steam to the reboiler is controlled and

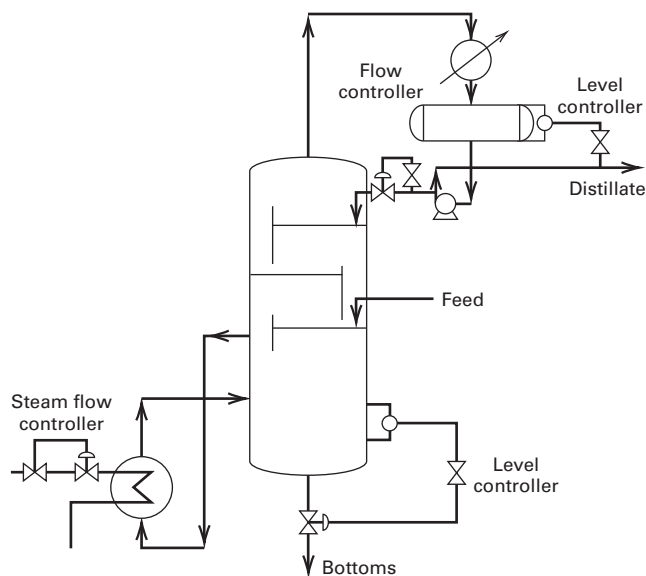


Figure 7.30 Data for Exercise 7.20.

remains constant. The reflux to the column also remains constant. The feed to the column is normally 100 kmol/h, but it was inadvertently cut back to 25 kmol/h. What will be the composition of the reflux and the vapor leaving the reboiler under these new conditions? Assume that the vapor leaving the reboiler is not superheated. Relative volatility is 3.0.

7.21. Stages for a binary separation.

A saturated vapor of maleic anhydride and benzoic acid containing 10 mol% acid is a byproduct of the manufacture of phthalic anhydride. It is distilled under vacuum at 13.3 kPa to give a product of 99.5 mol% maleic anhydride and a bottoms of 0.5 mol%. Calculate the number of equilibrium stages using an L/D of 1.6 times the minimum using the data below.

VAPOR PRESSURE, TORR:

Temperature, °C:	10	50	100	200	400
Maleic anhydride	78.7	116.8	135.8	155.9	179.5
Benzoic acid	131.6	167.8	185.0	205.8	227

7.22. Calculation of stages algebraically.

A bubble-point feed of 5 mol% A in B is to be distilled to give a distillate containing 35 mol% A and a bottoms containing 0.2 mol% A. The column has a partial reboiler and a partial condenser. If $\alpha = 6$, calculate the following algebraically: (a) the minimum number of equilibrium stages; (b) the minimum boilup ratio \bar{V}/B ; and (c) the actual number of equilibrium stages for a boilup ratio equal to 1.2 times the minimum.

7.23. Distillation with a subcooled feed.

Methanol (M) is to be separated from water (W) by distillation, as shown in Figure 7.31. The feed is subcooled: $q = 1.12$. Determine the feed-stage location and the number of equilibrium stages required. Vapor-liquid equilibrium data are given in Exercise 7.19.

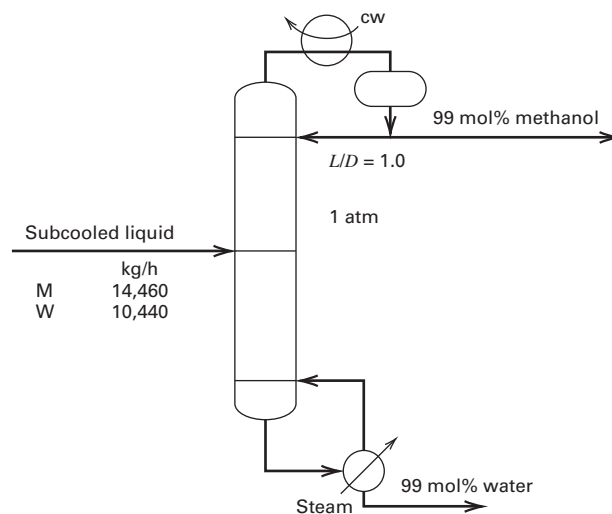


Figure 7.31 Data for Exercise 7.23.

7.24. Calculation of distillation graphically and analytically.

A saturated-liquid feed of 69.4 mol% benzene (B) in toluene (T) is to be distilled at 1 atm to produce a distillate of 90 mol% benzene, with a yield of 25 moles of distillate per 100 moles of feed. The feed is sent to a steam-heated reboiler, where bottoms is withdrawn continuously. The vapor from the reboiler goes to a partial condenser and then to a phase separator that returns the liquid as reflux to the

reboiler. The vapor from the partial condenser is sent to a total condenser to produce distillate. At equilibrium, the mole ratio of B to T in the vapor from the reboiler is 2.5 times the mole ratio of B to T in the bottoms. Calculate analytically and graphically the total moles of vapor generated in the reboiler per 100 mol of feed.

7.25. Operation at total reflux.

A plant has 100 kmol of a liquid mixture of 20 mol% benzene and 80 mol% chlorobenzene, which is to be distilled at 1 atm to obtain bottoms of 0.1 mol% benzene. Assume $\alpha = 4.13$. The plant has a column containing four theoretical plates, a total condenser, a reboiler, and a reflux drum to collect condensed overhead. A run is to be made at total reflux. While steady state is being approached, a finite amount of distillate is held in a reflux trap. When the steady state is reached, the bottoms contain 0.1 mol% benzene. What yield of bottoms can be obtained? The liquid holdup in the column is negligible compared to that in the reboiler and reflux drum.

Section 7.3

7.26. Trays for a known Murphree efficiency.

A 50 mol% mixture of acetone in isopropanol is to be distilled to produce a distillate of 80 mol% acetone and a bottoms of 25 mol%. The feed is a saturated liquid, the column is operated with a reflux ratio of 0.5, and the Murphree vapor efficiency, E_{MV} , is 50%. How many trays are required? Assume a total condenser, partial reboiler, saturated-liquid reflux, and optimal feed stage.

To step off non-equilibrium stages on a McCabe–Thiele diagram, the E_{MV} dictates the fraction of the vertical distance taken from the operating line to the equilibrium line. This is shown in Figure 7.32 for the first two trays from the bottom. For the first tray, $E_{MV} = \overline{EF}/\overline{EG} = 0.7$. The dashed curve for actual exit-phase compositions replaces the thermodynamic equilibrium curve.

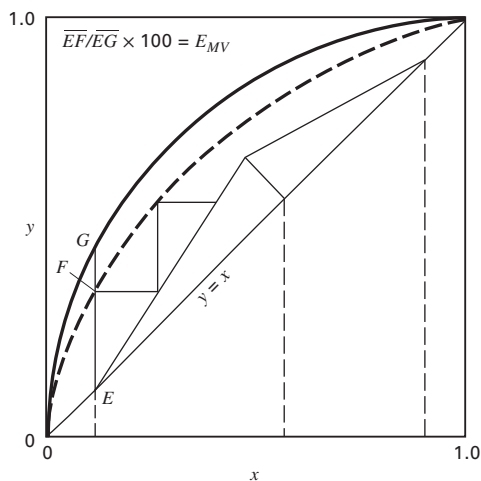


Figure 7.32 Use of E_{MV} with McCabe–Thiele diagram for Exercise 7.26.

The vapor–liquid equilibrium data are:

EQUILIBRIUM DATA, MOLE-PERCENT ACETONE:

Liquid	0	2.6	5.4	11.7	20.7	29.7	34.1	44.0	52.0
Vapor	0	8.9	17.4	31.5	45.6	55.7	60.1	68.7	74.3
Liquid	63.9	74.6	80.3	86.5	90.2	92.5	95.7	100.0	
Vapor	81.5	87.0	89.4	92.3	94.2	95.5	97.4	100.0	

7.27. Minimum reflux, boilup, and number of trays for known efficiency.

A mixture of 40 mol% carbon disulfide (CS_2) in carbon tetrachloride (CCl_4) is continuously distilled. The feed is 50% vaporized ($q = 0.5$). The distillate from a total condenser is 95 mol% CS_2 , and the bottoms from a partial reboiler is 5 mol% CS_2 . The column operates with a reflux ratio, L/D , of 4 to 1. The Murphree vapor efficiency is 80%. See Exercise 7.26 for using E_{MV} with the McCabe–Thiele diagram. (a) Calculate graphically the minimum reflux, the minimum boilup ratio from the reboiler, \bar{V}/B , and the minimum number of stages (including the reboiler). (b) How many trays are required for the actual column at 80% Murphree vapor-tray efficiency by the McCabe–Thiele method? The vapor–liquid equilibrium data at column pressure in terms of CS_2 mole fractions are:

x	0.05	0.1	0.2	0.3	0.4	0.5	0.6	0.7	0.8	0.9
y	0.135	0.245	0.42	0.545	0.64	0.725	0.79	0.85	0.905	0.955

7.28. Reboiler duty for a distillation.

A distillation unit consists of a partial reboiler, a bubble-cap column, and a total condenser. The overall plate efficiency is 65%. The feed is a bubble-point liquid of 50 mol% benzene in toluene, which is fed to the optimal plate. The column is to produce a distillate containing 95 mol% benzene and a bottoms of 95 mol% toluene. Calculate for an operating pressure of 1 atm the: (a) minimum reflux ratio $(L/D)_{\min}$; (b) minimum number of actual plates; (c) number of actual plates needed for a reflux ratio (L/D) of 50% more than the minimum; (d) kg/h of distillate and bottoms, if the feed is 907.3 kg/h; and (e) saturated steam at 273.7 kPa required in kg/h for the reboiler using the enthalpy data below and any assumptions necessary. (f) Make a rigorous enthalpy balance on the reboiler, using the enthalpy data below and assuming ideal solutions. Enthalpies are in Btu/lbmol at reboiler temperature:

	h_L	h_V
Benzene	4,900	18,130
Toluene	8,080	21,830

Vapor–liquid equilibrium data are given in Exercise 7.13.

7.29. Distillation of an azeotrope-forming mixture.

A continuous distillation unit, consisting of a perforated-tray column with a partial reboiler and a total condenser, is to be designed to separate ethanol and water at 1 atm. The bubble-point feed contains 20 mol% alcohol. The distillate is to contain 85 mol% alcohol, and the recovery is to be 97%. (a) What is the molar composition of the bottoms? (b) What is the minimum value of the reflux ratio L/V , the reflux ratio L/D , and the boilup ratio \bar{V}/B ? (c) What is the minimum number of theoretical stages and the number of actual plates, if the overall plate efficiency is 55%? (d) If the L/V is 0.80, how many actual plates will be required?

Vapor–liquid equilibrium for ethanol–water at 1 atm in terms of mole fractions of ethanol are [*Ind. Eng. Chem.*, **24**, 881 (1932)]:

x	y	$T, ^\circ\text{C}$	x	y	$T, ^\circ\text{C}$
0.0190	0.1700	95.50	0.3273	0.5826	81.50
0.0721	0.3891	89.00	0.3965	0.6122	80.70
0.0966	0.4375	86.70	0.5079	0.6564	79.80
0.1238	0.4704	85.30	0.5198	0.6599	79.70
0.1661	0.5089	84.10	0.5732	0.6841	79.30
0.2337	0.5445	82.70	0.6763	0.7385	78.74
0.2608	0.5580	82.30	0.7472	0.7815	78.41
			0.8943	0.8943	78.15

7.30. Multiple feeds and open steam.

Solvent A is to be separated from water by distillation to produce a distillate containing 95 mol% A at a 95% recovery. The feed is available in two saturated-liquid streams, one containing 40 mol% A and the other 60 mol% A. Each stream contains 50 kmol/h of component A. The relative volatility is 3, and since the less volatile component is water, it is proposed to supply the necessary reboiler heat in the form of open steam. For the preliminary design, the operating reflux ratio, L/D , is 1.33 times the minimum, using a total condenser. The overall plate efficiency is estimated to be 70%. How many plates will be required, and what will be the bottoms composition? Determine analytically the points necessary to locate the operating lines. Each feed should enter the column at its optimal location.

The McCabe–Thiele method can be extended to multiple feeds by adding one additional operating line for each feed as shown in Figure 7.33 for two feeds, where F_1 is the uppermost feed and F_2 is the feed below F_1 . The section of stages between the top stage and the feed stage for F_1 has an operating line with a slope L/V as determined from the reflux ratio. The section of stages between the two feed stages has an operating line with a slope L'/V' , where $L' = L + L$ in F_1 and $V' = V - V$ in F_1 . In Figure 7.33, F_1 is a saturated vapor feed, while F_2 is a saturated liquid feed.

The McCabe–Thiele method can also be extended to the use of open steam instead of a reboiler by altering the operating line for the stripping section as shown in Figure 7.34. The lower end of the

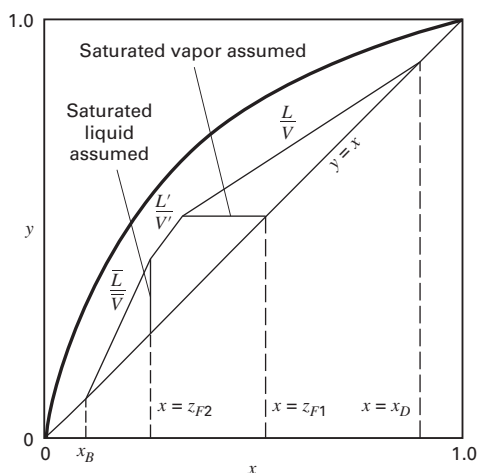


Figure 7.33 Construction for multiple feeds for Exercise 7.30.

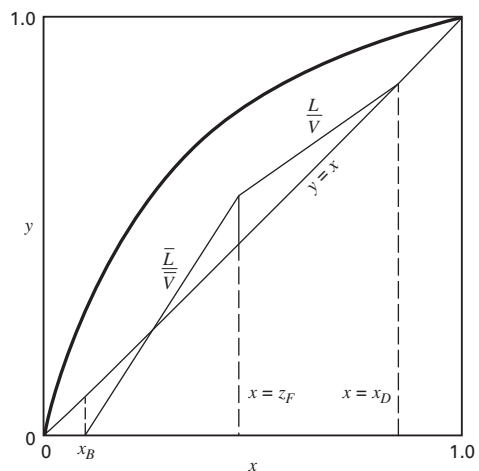


Figure 7.34 Construction for open steam for Exercise 7.30.

operating line for the stripping section is moved to $y = 0$ (pure steam) and $x = x_B$ because now these are the compositions of the passing streams at the bottom of the column.

7.31. Optimal feed plate location.

A saturated-liquid feed of 40 mol% *n*-hexane (H) and 60 mol% *n*-octane is to be separated into a distillate of 95 mol% H and a bottoms of 5 mol% H at 1 atm. The reflux ratio L/D is 0.5, and a cooling coil submerged in the liquid of the second stage from the top removes sufficient heat to condense 50 mol% of the vapor rising from the third stage down from the top. Vapor pressure data are listed below. Use Raoult's law to calculate the equilibrium curve. (a) Derive the equations needed to locate the operating lines. (b) Locate the operating lines and determine the required number of equilibrium stages if the optimal feed stage location is used.

Vapor pressure data in mmHg for *n*-hexane and *n*-octane:

Temperature, °F	155.7	175	200	225	250	258.2
<i>n</i> -hexane	760	1025	1480	2130	3000	3420
<i>n</i> -octane	121	173	278	434	654	760

7.32. Open steam for alcohol distillation.

One hundred kmol/h of a saturated-liquid mixture of 12 mol% ethyl alcohol in water is distilled continuously using open steam at 1 atm introduced directly to the bottom stage. The distillate required is 85 mol% alcohol, representing 90% recovery of the alcohol in the feed. The reflux is saturated liquid with $L/D = 3$. Feed is to the optimal stage. Vapor–liquid equilibrium data are given in Exercise 7.29. Calculate (a) the steam requirement in kmol/h; (b) the number of equilibrium stages; (c) the optimal feed stage; and (d) the minimum reflux ratio, $(L/D)_{\min}$. Because of the closeness of the operating line to the equilibrium curve at ethanol liquid mole fractions above about 0.7, it may be worthwhile to use a supplemental McCabe–Thiele diagram to zero in the y - x region from 0.7 to 1.0. See Exercise 7.30 for extending the McCabe–Thiele method to the use of open steam.

7.33. Distillation of an azeotrope-forming mixture using open steam.

A 10 mol% isopropanol-in-water mixture at its bubble point is to be distilled at 1 atm to produce a distillate containing 67.5 mol% isopropanol, with 98% recovery. At a reflux ratio L/D of 1.5 times the minimum, how many equilibrium stages will be required (a) if a partial reboiler is used and (b) if no reboiler is used and saturated steam at 101 kPa is introduced below the bottom stage? (c) How many stages are required at total reflux? See Exercise 7.30 for extending the McCabe–Thiele method to the use of open steam.

Vapor–liquid data in mole-fraction isopropanol at 101 kPa are:

$T, ^\circ\text{C}$	93.00	84.02	82.12	81.25	80.62	80.16	80.28	81.51
y	0.2195	0.4620	0.5242	0.5686	0.5926	0.6821	0.7421	0.9160
x	0.0118	0.0841	0.1978	0.3496	0.4525	0.6794	0.7693	0.9442

Notes: Composition of the azeotrope is $x = y = 0.6854$.

7.34. Comparison of partial reboiler with live steam.

An aqueous solution of 10 mol% isopropanol at its bubble point is fed to the top stage of a stripping column, operated at 1 atm, to produce a vapor of 40 mol% isopropanol. Two schemes, both involving the same heat expenditure, with V/F (moles of vapor leaving the top of the column/mole of feed) = 0.246, are under consideration. Scheme 1 uses a partial reboiler at the bottom of a stripping column, with heat transfer from steam condensing inside a closed coil. In Scheme 2, live steam is injected directly below the bottom stage.

Determine the number of stages required in each case. Equilibrium data are given in Exercise 7.33. See Exercise 7.30 for extending the McCabe–Thiele method to the use of open steam.

7.35. Optimal feed stages for two feeds.

Determine the optimal-stage location for each feed and the number of equilibrium stages required for the distillation separation shown in Figure 7.35, using the following vapor–liquid data in mole fractions of water. See Exercise 7.30 for extending the McCabe–Thiele method to the use of multiple feeds.

Equilibrium data for water (W)/acetic acid (A), 1 atm

x_W	0.0055	0.053	0.125	0.206	0.297	0.510	0.649	0.803	0.9594
y_W	0.0112	0.133	0.240	0.338	0.437	0.630	0.751	0.866	0.9725

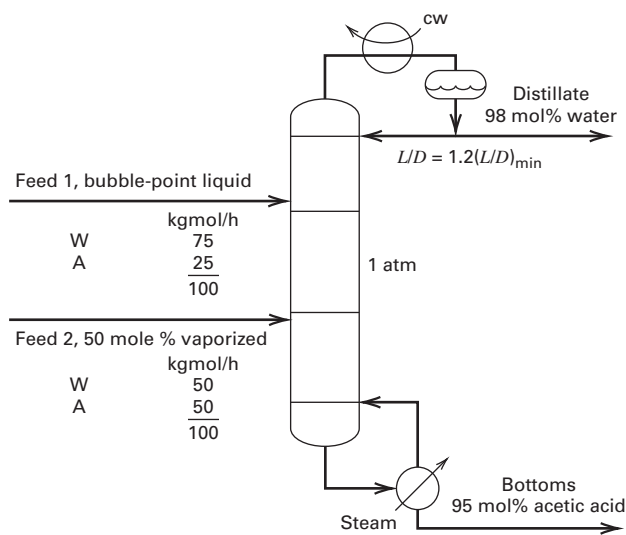


Figure 7.35 Data for Exercise 7.35.

7.36. Optimal sidestream location.

Determine the number of equilibrium stages and optimal-stage locations for the feed and liquid sidestream of the distillation process in Figure 7.36, assuming that methanol (M) and ethanol (E) form an ideal solution, such that relative volatility can be taken as constant at 1.745. Figure 7.37 shows a typical construction for the extension of the McCabe–Thiele method to include a saturated-liquid sidestream withdrawn from the rectifying section. As is the case shown in Exercise 30, there are three operating lines. The slope of the top operating line is determined from the reflux ratio. The middle operating line from the saturated liquid sidestream stage to the feed stage has a slope of L'/V' , where $L' = L - L_s$ and $V' = V$. A similar construction can be made if the saturated liquid sidestream stage lies below the feed stage as in this exercise.

7.37. Use of an interboiler.

A mixture of *n*-heptane (H) and toluene (T) is separated by extractive distillation with phenol (P). Distillation is then used to recover the phenol for recycle, as shown in Figure 7.38a, where the small

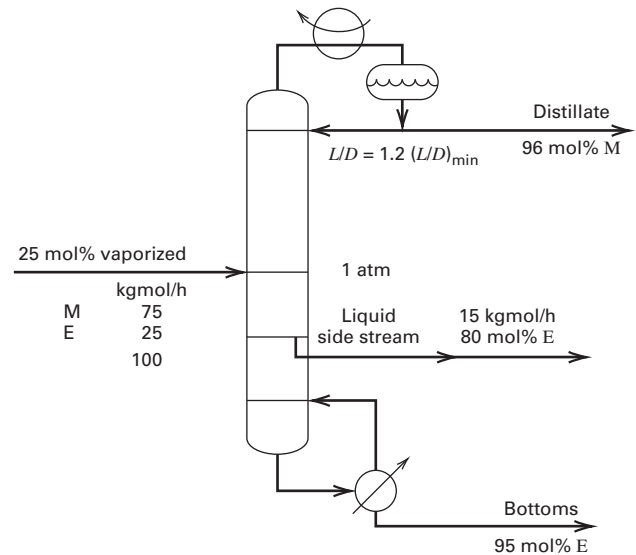


Figure 7.36 Operating data for Exercise 7.36.

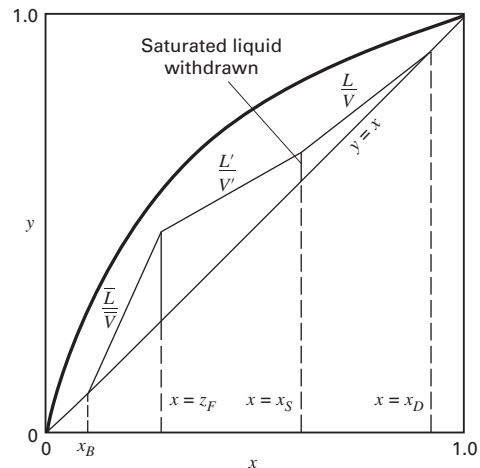


Figure 7.37 Construction for an added liquid sidestream.

amount of *n*-heptane in the feed is ignored. For the conditions shown in Figure 7.38a, determine the number of equilibrium stages required. Note that heat must be supplied to the reboiler at a high temperature because of the high boiling point of phenol, which causes second-law inefficiency. Therefore, consider the scheme in Figure 7.38b, where an interboiler, located midway between the bottom plate and the feed stage, provides 50% of the boilup used in Figure 7.38a. The remainder of the boilup is provided by the reboiler. Determine the number of equilibrium stages required for the case with the interboiler and the temperature of the interboiler stage.

When an interboiler is used, an additional operating line will be required on the McCabe–Thiele diagram. Below the feed stage, one operating line will run from the feed conditions to the interboiler conditions and one from the interboiler conditions to the reboiler conditions. The slopes of the operating lines will differ by the difference between the molar vapor flow rates in the two sections.

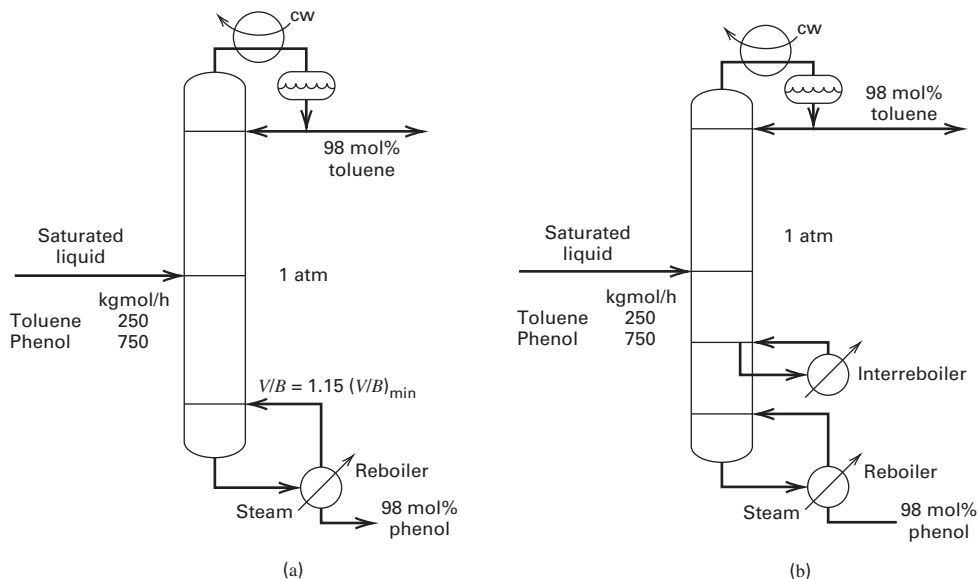


Figure 7.38 Operating data for Exercise 7.37.

Unsmoothed vapor–liquid equilibrium data at 1 atm [Trans. AIChE, 41, 555 (1945)] are:

x_T	y_T	$T, ^\circ\text{C}$	x_T	y_T	$T, ^\circ\text{C}$
0.0435	0.3410	172.70	0.6512	0.9260	120.00
0.0872	0.5120	159.40	0.7400	0.9463	119.70
0.1248	0.6250	149.40	0.8012	0.9545	115.60
0.2190	0.7850	142.20	0.8840	0.9750	112.70
0.2750	0.8070	133.80	0.9394	0.9861	113.30
0.4080	0.8725	128.30	0.9770	0.9948	111.10
0.4800	0.8901	126.70	0.9910	0.9980	111.10
0.5898	0.9159	122.20	0.9973	0.9993	110.50

7.38. Addition of intercondenser and interboiler.

A distillation column to separate *n*-butane from *n*-pentane was recently put on line in a refinery. Apparently, there was a design error because the column did not make the desired separation, as shown below [Chem. Eng. Prog., 61(8), 79 (1965)].

It is proposed to add an intercondenser in the rectifying section to generate more reflux and an interboiler in the stripping section to produce additional boilup. Show by use of a McCabe–Thiele diagram how this might improve the operation. Assume the relative volatility is constant at 2.6. See Exercise 7.37 for comments on extending the McCabe–Thiele method to include an interboiler.

	Design Specification	Actual Operation
Mol% nC_5 in distillate	0.26	13.49
Mol% nC_4 in bottoms	0.16	4.28

7.39. Air separation using a Linde double column.

Air can be partially separated by distillation using the Linde double column, as shown in Figure 7.39. The column consists of a lower section at elevated pressure surmounted by an atmospheric-pressure column. The boiler of the upper column is also the reflux condenser for both columns. Gaseous air, plus enough liquid to compensate for heat leak into the column (more liquid if liquid-oxygen product is withdrawn), enters the heat exchanger at the base of the lower

column and condenses, giving up heat to the boiling liquid and thus supplying the column vapor flow. The liquid air enters an intermediate point in this column. The rising vapors are partially condensed to form the reflux, and the uncondensed vapor passes to an outer row of tubes and is totally condensed, the liquid nitrogen collecting in an annulus, as shown. By operating this column at 4 to 5 atm, the liquid oxygen boiling at 1 atm is cold enough to condense pure nitrogen. The liquid in the bottom section contains about 45 mol% O_2 and

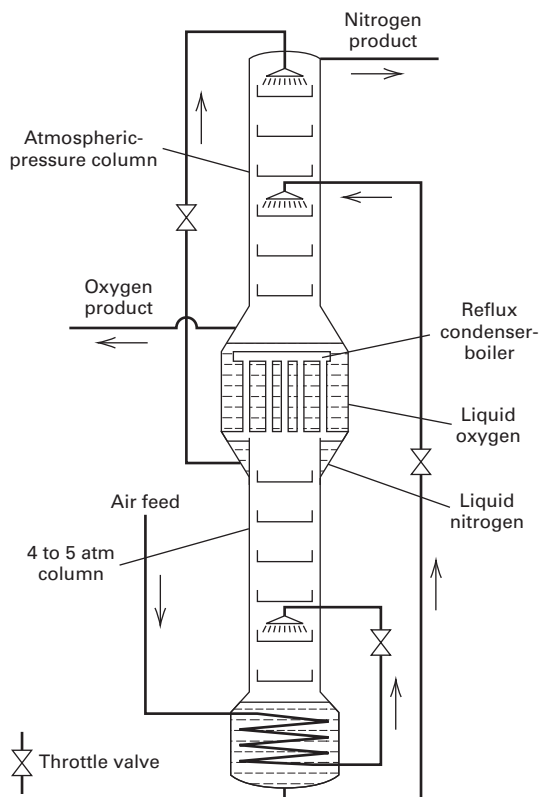


Figure 7.39 Double column for air separation for Exercise 7.39.

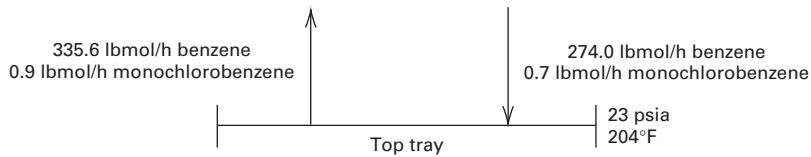


Figure 7.40 Data for Exercise 7.42.

forms the feed for the upper section. This double column can produce very pure O_2 with high O_2 recovery, and relatively pure N_2 . On a single McCabe–Thiele diagram—using equilibrium lines, operating lines, q -lines, a 45° line, stepped-off stages, and other illustrative aids—show qualitatively how stage requirements can be computed. Assume a relative volatility of 2.5 for the lower column section and 4.0 for the upper column section. To use a single McCabe–Thiele diagram, the upper column section can be placed above the 45° line using mole fractions for N_2 (the more volatile component), while the lower column section can be placed below the 45° line using mole fractions for O_2 .

Section 7.4

7.40. Comparison of tray efficiency.

Performance data for a distillation tower separating a 50/50 by weight percent mixture of methanol and water are as follows:

- Feed rate = 45,438 lb/h; feed condition = bubble-point liquid at feed-tray pressure;
- Wt% methanol in distillate = 95.04; Wt% methanol in bottoms = 1.00;
- Reflux ratio = 0.947; reflux condition = saturated liquid;
- Boilup ratio = 1.138; pressure in reflux drum = 14.7 psia;
- Type condenser = total; type reboiler = partial;
- Condenser pressure drop = 0.0 psi; tower pressure drop = 0.8 psi;
- Trays above feed tray = 5; trays below feed tray = 6;
- Total trays = 12; tray diameter = 6 ft; type tray = single-pass sieve tray; flow path length = 50.5 inches;
- Weir length = 42.5 inches; hole area = 10%; hole size = 3/16 inch;
- Weir height = 2 inches; tray spacing = 24 inches;
- Viscosity of feed = 0.34 cP; Surface tension of distillate = 20 dyne/cm;
- Surface tension of bottoms = 58 dyne/cm;
- Temperature of top tray = 154°F ; temperature of bottom tray = 207°F

Vapor–liquid equilibrium data at column pressure in mole fraction of methanol are

y	0.0412	0.156	0.379	0.578	0.675	0.729	0.792	0.915
x	0.00565	0.0246	0.0854	0.205	0.315	0.398	0.518	0.793

Based on the above data: (a) Determine the overall tray efficiency assuming the reboiler is equivalent to a theoretical stage. (b) Estimate the overall tray efficiency from the Drickamer–Bradford correlation. (c) Estimate the overall tray efficiency from the O’Connell correlation, accounting for length of flow path.

7.41. Oldershaw column efficiency.

For the conditions of Exercise 7.40, a laboratory Oldershaw column measures an average Murphree vapor-point efficiency of 65%. Estimate E_{MV} and E_o for (a) complete mixing on the tray, and (b) plug flow of liquid with no longitudinal diffusion.

Section 7.5

7.42. Column diameter.

Figure 7.40 shows conditions for the top tray of a distillation column. Determine the column diameter at 85% of flooding for a valve tray. Use a liquid density of 52 lb/ft^3 and use the ideal gas law to obtain the vapor density. Use a surface tension of 30 dyne/cm and assume a tray spacing of 24 inches. Make any other necessary assumptions.

7.43. Column sizing.

Figure 7.41 depicts a propylene/propane distillation. Equilibrium stages (not actual trays) are shown. Two sieve-tray columns in series are used because a single column would pose structural problems. Determine column diameters, tray efficiency using the O’Connell correlation, number of actual trays, and column heights. Use a relative volatility of 1.14 and a liquid viscosity of 0.4 cP .

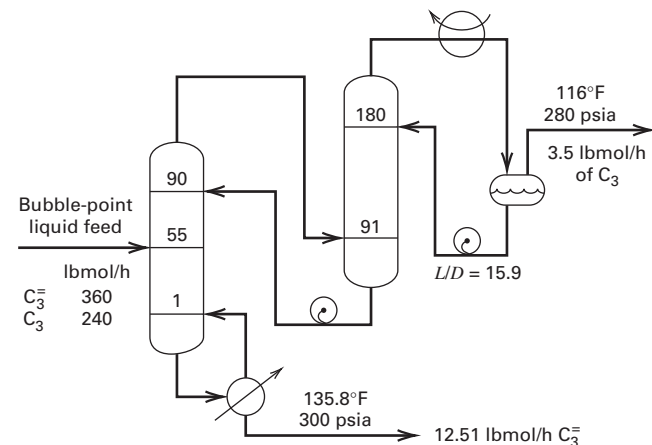


Figure 7.41 Data for Exercise 7.43.

7.44. Sizing a vertical flash drum.

Determine the height and diameter of a vertical flash drum for the conditions shown in Figure 7.42. Use a process simulator to obtain fluid densities.

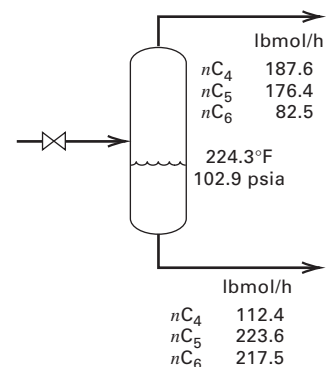


Figure 7.42 Data for Exercise 7.44.

7.45. Sizing a horizontal flash drum.

Determine the length and diameter of a horizontal reflux drum for the conditions shown in Figure 7.43.

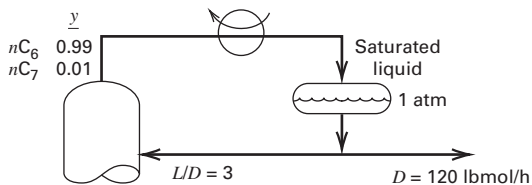


Figure 7.43 Data for Exercise 7.45.

7.46. Possible swaged column.

Results of design calculations for a methanol–water distillation operation are given in Figure 7.44. (a) Calculate the column diameter at the top and at the bottom for 80% of flooding, assuming sieve trays on 24-inch tray spacing. Should the column be swaged? (b) Calculate the length and diameter of the horizontal reflux drum. Use a process simulator to obtain vapor and liquid flow rates and properties at the top and bottom of the column.

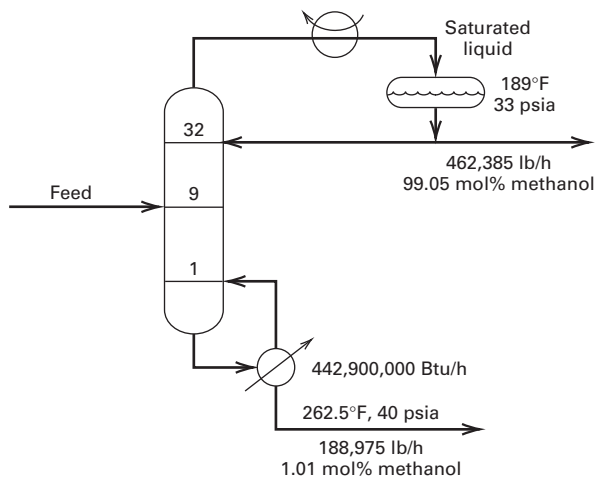


Figure 7.44 Data for Exercise 7.46.

7.47. Tray calculation of flooding.

For the conditions given in Exercise 7.40, estimate the percent of flooding for the top tray and the bottom tray.

7.48. Diameter of a distillation column.

Acetone (A) and water (W) at 100 kPa are to be separated in a 24-stage distillation column with a tray spacing of 24 inches and an $A_d/A = 0.1$, operating at 80% of flooding velocity, with a reflux ratio of 1.025. Given the following information, estimate the column diameter by the method of Example 6.8. Since the vapor velocity is highest at the bottom, and not much lower at the top, the design will be based on the bottom diameter: the top diameter need not be calculated. Feed: 20 mol/s A, 330 mol/s W, at the bubble point, 368 K. Distillate: 19.9 mol/s A, 0.3 mol/s W, at the bubble point, 329 K. Bottoms: 0.1 mol/s A, 329.7 mol/s W, at the bubble point 385 K. Gas density = 870 g/m³ at the bottom. Liquid density at bottom can be taken as 1,000 kg/m³ and all liquid streams can be assumed to have a MW of 18. The surface tension is 70 dynes/cm, the foaming factor is 0.9, and $F_{HA} = 1$.

7.49. Column diameter for the separation of propylene from propane.

The feed to a 198-tray, sieve-plate distillation column is a saturated vapor mixture of 2.14 kg/s of propylene and 1.54 kg/s of propane at a column pressure of 1,670 kPa. The column has been

designed to produce a vapor distillate of about 99 mol% propylene and a liquid bottoms of about 99 mol% propane. The reflux ratio, L/D , is 16. The feed tray is at about the middle of the column. Calculate with a process simulator the inside diameter in feet at the top tray of the column, assuming the following data at the top of the column: liquid density = 482 kg/m³, vapor density = 34.6 kg/m³, surface tension = 4.3 dyne/cm. The plate spacing is 2 ft, with two liquid passes on each tray. The downcomers will occupy 15% of the column cross-sectional area. Assume 80% of flooding. The tray efficiency is 100% and the total tray pressure drop is 70 kPa and the condenser pressure drop is 10 kPa.

Section 7.6

7.50. HETP calculation.

A mixture of benzene and dichloroethane is used to obtain HETP data for a packed column that contains 10 ft of packing and operates adiabatically at atmospheric pressure. The liquid is charged to the reboiler, and the column is operated at total reflux until equilibrium is established. Liquid samples from the distillate and reboiler give for benzene $x_D = 0.653$ and $x_B = 0.298$. Calculate HETP in inches for this packing using a McCabe–Thiele diagram or an algebraic analog of it to obtain the number of equilibrium stages. What are the limitations of using this calculated value for design?

Data for x - y at 1 atm (in benzene mole fractions) are

x	0.10	0.20	0.30	0.40	0.50	0.60	0.70	0.80	0.90
y	0.11	0.22	0.325	0.426	0.526	0.625	0.720	0.815	0.91

7.51. Plate versus packed column.

Consider a distillation column for separating ethanol from water at 1 atm. The feed is a 10 mol% ethanol bubble-point liquid, the bottoms contains 1 mol% ethanol, and the distillate is 80 mol% ethanol. $R/R_{min} = 1.5$. Phase-equilibrium data are given in Exercise 7.29, and constant molar overflow applies. (a) How many equilibrium stages are required above and below the feed if a plate column is used? (b) How many transfer units are required above and below the feed if a packed column is used? (c) Assuming the plate efficiency is 80% and the plate spacing is 18 inches, how high is the plate column? (d) Using an H_{OG} value of 1.2 ft, how high is the packed column? (e) Assuming that HTU data are available only on the benzene–toluene system, how would one go about applying the data to obtain the HTU for the ethanol–water system using the work of Billet et al. in Chapter 6?

7.52. Design of random and structured packed columns.

Plant capacity for the methanol–water distillation of Exercise 7.40 is to be doubled. Rather than installing a second, identical trayed tower, a packed column is being considered. This would have a feed location, product purities, reflux ratio, operating pressure, and capacity identical to the present trayed tower. Two packings are being considered: (1) 50-mm metal Hiflow rings (a random packing), and (2) Montz metal B1-300 (a structured packing).

For each of these packings, design the rectifying section of a column to operate at 70% of flooding at the top of the column by calculating: (a) liquid holdup, (b) column diameter, (c) H_{OG} , and (d) packed height. What are the advantages, if any, of each of the packed-column designs over a second trayed tower? Which packing, if either, is preferable?

7.53. Advantages of a packed column.

For the specifications of Example 7.1, design a packed column using 50-mm metal Hiflow rings and operating at 70% of flooding by calculating for each section: (a) liquid holdup, (b) column diameter, (c) H_{OG} , and (d) packed height. What are the advantages and disadvantages of a packed column as compared to a trayed tower for this service?

Liquid–Liquid Extraction with Ternary Systems

§8.0 INSTRUCTIONAL OBJECTIVES

After completing this chapter, you should be able to:

- List situations where liquid–liquid extraction is preferred to distillation.
- Define the distribution (partition) coefficient and show its relationship to activity coefficients and the selectivity of a solute between carrier and solvent.
- Make a preliminary selection of a solvent using group–interaction rules.
- Distinguish, for ternary mixtures, between Type I and Type II systems.
- For a specified recovery of a solute, calculate with the Hunter and Nash method, using a triangular diagram, minimum solvent requirement and equilibrium stages for multistage ternary liquid–liquid extraction.
- Design a cascade of mixer–settler units based on mass–transfer considerations.
- Make an estimate of the size of an extraction column.

In **liquid–liquid extraction (solvent extraction)**, a liquid feed of two or more components is contacted with a second liquid phase, called the **solvent**, which is immiscible or only partly miscible with one or more feed components and completely or partially miscible with one or more of the other feed components. The solvent is selected to partially dissolve certain species of the liquid feed, effecting at least a partial separation of the feed components. The solvent may be a pure compound or a mixture. If the feed is an aqueous solution, an organic solvent is used; if the feed is organic, the solvent is often water. Important exceptions occur in metallurgy for the separation of metals and in bioseparations for the extraction from aqueous solutions of proteins. **Solid–liquid extraction (leaching)** involves the recovery of substances from a solid by contact with a liquid solvent, such as the recovery of oil from seeds by an organic solvent.

According to Derry and Williams [1], extraction has been practiced since the time of the Romans, who used molten lead to separate gold and silver from molten copper by extraction. This was followed by the discovery that sulfur could selectively dissolve silver from an alloy with gold. However, it was not until the early 1930s that L. Edeleanu invented the first large-scale extraction process, which involved the removal of aromatic and sulfur compounds from liquid kerosene using liquid sulfur dioxide at 10 to 20°F. This resulted in a cleaner-burning kerosene. Liquid–liquid extraction has grown in importance since then because of the demand for temperature-sensitive products, high purity, and availability of better equipment and solvents with higher selectivity.

This chapter introduces liquid–liquid extraction by treating a ternary system consisting of two miscible feed components—the **carrier**, C, and the **solute**, A—plus **solvent**, S, a pure compound. Components C and S are at most only

partially soluble, but solute A is completely or substantially soluble in S. During extraction, mass transfer of A from the feed to the solvent occurs, with less transfer of C to the solvent, or S to the feed. Nearly complete transfer of A to the solvent is seldom achieved in just one equilibrium stage. In practice, a number of stages are used in one- or two-section countercurrent cascades. Most commonly, the stages are provided by mixer–settler units, columns with mechanical agitation, or centrifugal devices. A wealth of information on liquid–liquid extraction is given by Frank et al. in Section 15 of *Perry's Chemical Engineers' Handbook* [2].

Industrial Example

Acetic acid is produced by methanol carbonylation, acetaldehyde oxidation, or as a byproduct of cellulose acetate manufacture. In all cases, a mixture of acetic acid (n.b.p. = 118.1°C) and water (n.b.p. = 100°C) is separated to give glacial acetic acid (99.8 wt% min). When the mixture contains less than 50% acetic acid, separation by distillation is expensive because of the high heat of vaporization of large amounts of water. Thus, a solvent–extraction process becomes attractive. Figure 8.1 shows an implementation of extraction, where two distillation operations are required to recover solvent for recycle. These additional separation operations are common to extraction processes. A feed of 30,260 lb/h of 22 wt% acetic acid in water is sent to a single-section extraction column operating at ambient conditions, where it is contacted with 71,100 lb/h of ethyl–acetate solvent (n.b.p. = 77.1°C), saturated with water. The low-density, solvent-rich stream, called the **extract**, exits from the top of the extractor with 99.8% of the acetic acid in the feed. The high-density, carrier-rich stream, called the **raffinate**, exiting from the extractor bottom,

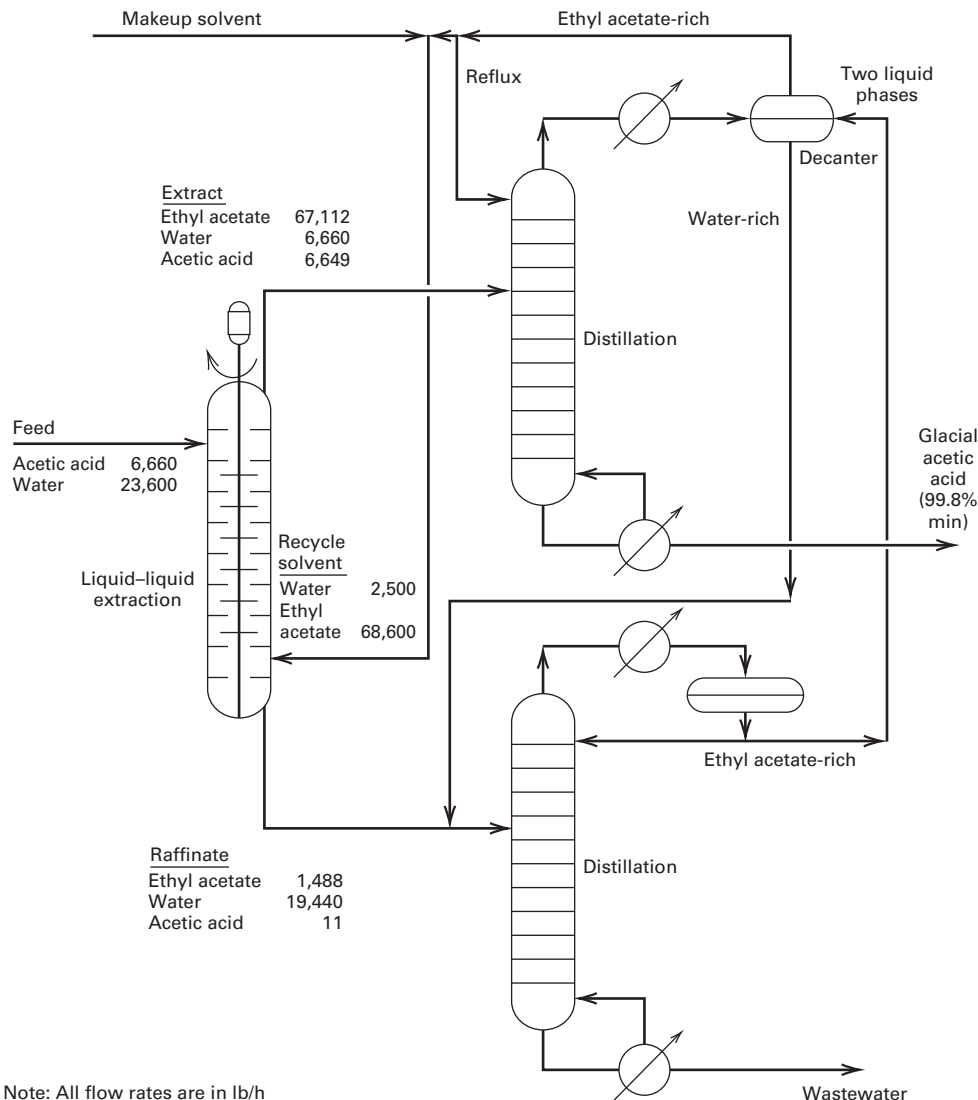


Figure 8.1 Liquid-liquid extraction process for recovering acetic acid.

contains only 0.05 wt% acetic acid. The extract is sent to a distillation column, where glacial acetic acid is the bottoms product. The overhead vapor, which is rich in ethyl acetate but also contains appreciable water vapor, splits into two liquid phases when condensed. These are separated in the decanter by gravity. The lighter ethyl acetate-rich phase is divided into reflux and solvent recycle to the extractor. The water-rich phase from the decanter is sent, together with the raffinate from the extractor, to a second distillation column, where wastewater is the bottoms product and the ethyl-acetate-rich overhead is recycled to the decanter. Makeup ethyl-acetate solvent is provided for solvent losses to the glacial acetic acid and wastewater.

Six equilibrium stages are required to transfer 99.8% of the acetic acid from feed to extract using a solvent-to-feed mass ratio of 2.35; the recycled solvent is water-saturated. A rotating-disk contactor (RDC), described in §8.1.5, is employed within the column to disperse the organic-rich phase into droplets by horizontal, rotating disks, while the water-rich phase is continuous throughout the column. The

column, which contains 40 rotating disks, has an inside diameter of 5.5 ft and a total height of 28 ft. The disks are rotated at 60 rpm by a 5-hp motor. Since the 1930s, thousands of similar extraction columns, with diameters ranging up to at least 25 ft, have been built. As discussed in §8.1, a number of competitive extraction devices are suitable for the process in Figure 8.1.

Liquid-liquid extraction is a reasonably mature operation, although not as mature or as widely applied as distillation, absorption, and stripping. Procedures for determining the number of equilibrium stages to achieve a desired solute recovery are well established. However, for liquid-liquid phase equilibrium, no simple limiting theory, like Raoult's law for vapor-liquid equilibrium, exists. Frequently, experimental data are preferred over predictions based on activity-coefficient correlations. Such data can be correlated and extended by activity-coefficient equations such as NRTL or UNIQUAC, discussed in §2.7. Also, considerable laboratory effort may be required to find an optimal solvent. A variety of industrial

Table 8.1 Representative Industrial Liquid–Liquid Extraction Processes

Solute	Carrier	Solvent(s)
Acetic acid	Water	Ethyl acetate, Isopropyl acetate
Aconitic acid	Molasses	Methyl ethyl ketone
Ammonia	Butenes	Water
Aromatics	Paraffins	Diethylene glycol, Furfural, Sulfur dioxide
Asphaltenes	Hydrocarbon oil	Furfural
Benzoic acid	Water	Benzene
Butadiene	1-Butene	aq. Cuprammonium acetate
Ethylene cyanohydrins	Methyl ethyl ketone	Brine liquor
Fatty acids	Oil	Propane
Formaldehyde	Water	Isopropyl ether
Formic acid	Water	Tetrahydrofuran
Glycerol	Water	High alcohols
Hydrogen peroxide	Anthrahydroquinone	Water
Methyl ethyl ketone	Water	Trichloroethane
Methyl borate	Methanol	Hydrocarbons
Naphthenes	Distillate oil	Nitrobenzene, Phenol
Phenol	Water	Benzene, Chlorobenzene
Penicillin	Broth	Butyl acetate
Sodium chloride	aq. Sodium hydroxide	Ammonia
Vanilla	Oxidized liquors	Toluene
Vitamin A	Fish-liver oil	Propane
Vitamin E	Vegetable oil	Propane
Water	Methyl ethyl ketone	aq. Calcium chloride

equipment is available, making it necessary to consider alternatives before making a final selection. Unfortunately, no generalized capacity and efficiency correlations are available for all equipment types. Often, equipment vendors and pilot-plant tests must be relied on to determine equipment size.

The petroleum industry represents the largest-volume application for liquid–liquid extraction. Extraction processes are well suited to the petroleum industry because of the need to separate heat-sensitive liquid feeds according to chemical type (e.g., aliphatic, aromatic, naphthenic) rather than by molecular weight or vapor pressure. Table 8.1 lists some representative industrial extraction processes. Other applications exist in the biochemical industry, including the separation of antibiotics and recovery of proteins from natural substrates; in the recovery of metals, such as copper from ammoniacal leach liquors; in separations involving rare metals and radioactive isotopes from spent-fuel elements; and in the inorganic chemical industry, where high-boiling constituents such as phosphoric acid, boric acid, and sodium hydroxide need to be recovered from aqueous solutions. In general, extraction is preferred over distillation for:

1. Dissolved or complexed inorganic substances in organic or aqueous solutions.

2. Removal of a contaminant present in small concentrations, such as a color former in tallow or hormones in animal oil.
3. A high-boiling component present in relatively small quantities in an aqueous waste stream, as in the recovery of acetic acid from cellulose acetate.
4. Recovery of temperature-sensitive materials, where extraction may be less expensive than vacuum distillation.
5. Separation of mixtures according to chemical type rather than relative volatility.
6. Separation of close-melting or close-boiling liquids, where solubility differences can be exploited.
7. Separation of mixtures that form azeotropes.

The key to an effective extraction process is a suitable solvent. In addition to being stable, non-toxic, inexpensive, and easily recoverable, a solvent should be relatively immiscible with feed components other than the solute, and have a different density from the feed to facilitate phase separation by gravity. It must have a high affinity for the solute, from which it can be easily separated by distillation, crystallization, or other means. Ideally, the distribution (partition) coefficient (2-19) for the solute between the liquid phases should be greater than one, or a large solvent-to-feed ratio will be required. When the degree of solute extraction is not particularly high and/or when a large extraction factor (4-35) can be achieved, an extractor will not require many stages. This is fortunate because mass-transfer resistance in liquid–liquid systems is high. In this chapter, equipment for liquid–liquid extraction is discussed and equilibrium- and rate-based calculation procedures are presented for extraction in ternary systems. Use of graphical methods is emphasized to gain a visual perspective. Extraction calculations with process simulators are presented in Chapter 10.

§8.1 EQUIPMENT FOR SOLVENT EXTRACTION

Equipment similar to that used for absorption, stripping, and distillation is sometimes used for extraction, but such devices are inefficient unless interfacial tension and liquid viscosities are low and differences in phase density are high. Generally, mechanically agitated or centrifugal devices are preferred, especially if many equilibrium stages are required. During passage through extraction equipment, one phase is the **dispersed phase (discontinuous phase)** in the form of droplets and, the other phase is the **continuous phase**. In static extraction columns of the spray, packed, and sieve tray type, it is preferred to disperse the phase of higher entering volumetric flow rate, unless the other phase has a high viscosity.

§8.1.1 Mixer-Settlers

In mixer-settlers, the two liquid phases are first mixed in a vessel (Figure 8.2) by one of several types of impellers (Figure 8.3) and then separated in a second vessel by

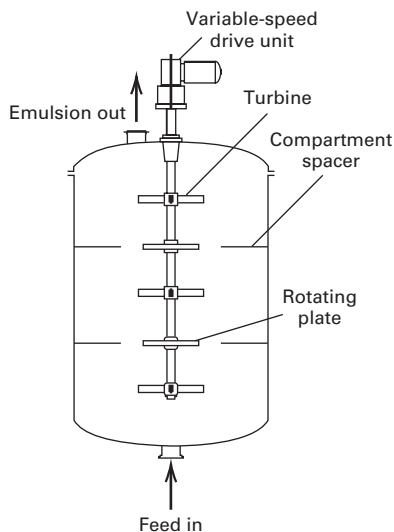


Figure 8.2 Compartmented mixing vessel with turbine agitators.

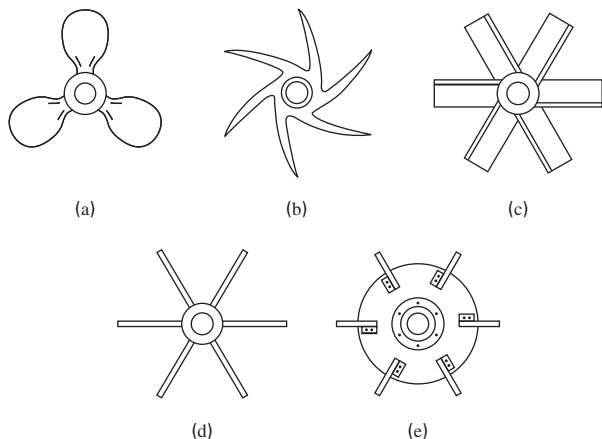


Figure 8.3 Some common types of mixing impellers: (a) marine-type propeller; (b) centrifugal turbine; (c) pitched-blade turbine; (d) flat-blade paddle; (e) flat-blade turbine.

gravity-induced settling (Figure 8.4). Any number of mixer-settler units may be connected together to form a multistage countercurrent cascade. However, floor space can be a major factor. During mixing, one of the liquids is dispersed in the form of small droplets in the other liquid. The dispersed phase may be either the heavier or the lighter phase. The mixing occurs in an agitated vessel with sufficient residence time that a reasonable approach to equilibrium (e.g., 80 to 90%) is achieved. The vessel may be compartmented as in Figure 8.2. If dispersion is easily realized and equilibrium rapidly approached, as with liquids of low interfacial tension and viscosity, mixing can be achieved by (1) impingement in a jet mixer; (2) turbulence in a nozzle mixer, orifice mixer, or other in-line mixing device; (3) shearing action if both phases are fed simultaneously into a centrifugal pump; or (4) injectors, wherein the flow of one liquid is induced by another.

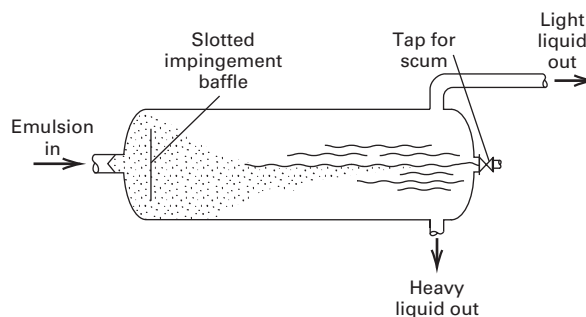


Figure 8.4 Horizontal gravity-settling vessel.

The settling step is by gravity in a **settler (decanter)**. In Figure 8.4, a horizontal vessel, with an impingement baffle to prevent the jet of the entering two-phase dispersion (emulsion) from disturbing the gravity-settling process, is used. Vertical and inclined vessels are also common. A major problem in settlers is emulsification in the mixing vessel, which may occur if the agitation is so intense that the dispersed droplet size falls below 1 to 1.5 μm (micrometers). When this happens, coalescers, separator membranes, meshes, electrostatic forces, ultrasound, chemical treatment, or other ploys are required to speed settling. If the phase-density difference is small, the rate of settling can be increased by substituting centrifugal for gravitational force. Many single stage and multistage mixer-settler units are available as described by Bailes, Hanson, and Hughes [3] and Lo, Baird, and Hanson [4]. As shown in Figure 8.5, the mixer and settler vessels can be combined into one unit or they can be arranged vertically, as in the Lurgi Tower Extractor. Often the settler volume is larger than the mixer volume.

§8.1.2 Spray Columns

The simplest and one of the oldest extraction devices is the spray column. Either the heavy phase or the light phase can be dispersed, as seen in Figure 8.6. The droplets of the dispersed phase are generated at the inlet, usually by spray nozzles. Because of the lack of column internals, combined volumetric

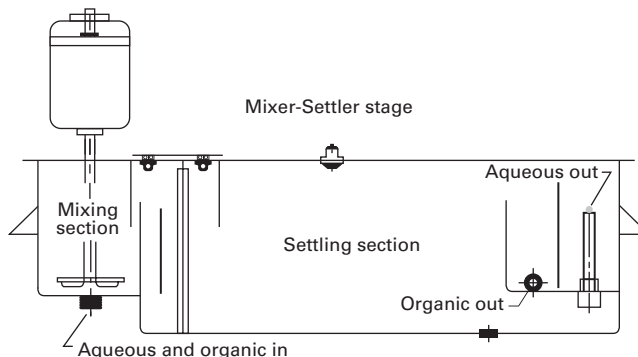


Figure 8.5a Combined Mixer-Settler Unit

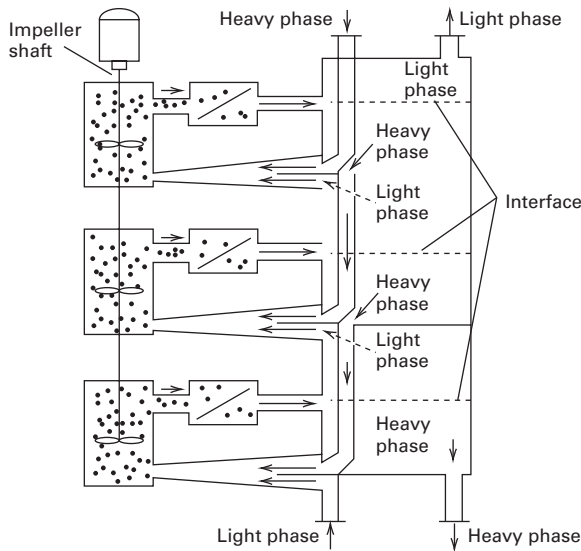


Figure 8.5b Lurgi Tower Extractor.

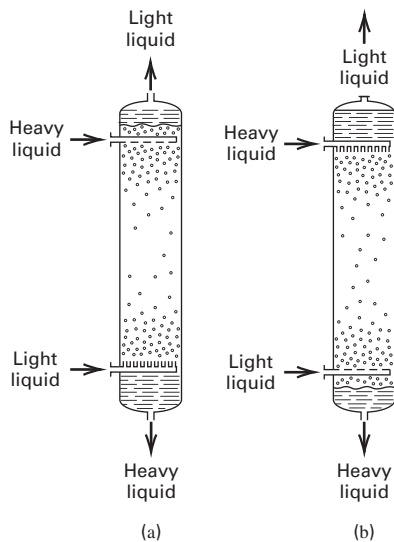


Figure 8.6 Spray columns: (a) light liquid dispersed, heavy liquid continuous; (b) heavy liquid dispersed, light liquid continuous.

throughputs can be large, depending upon phase-density difference and phase viscosities. As in gas absorption, **axial dispersion (backmixing)** in the continuous phase limits these devices to applications where only one or two stages are required.

§8.1.3 Packed Columns

Axial dispersion in a spray column can be reduced, but not eliminated, by packing the column. This also improves mass transfer by breaking up large drops to increase interfacial area and promote mixing in drops by distorting droplet shape. With the exception of Raschig rings [5], the packings used in

distillation and absorption are suitable for liquid–liquid extraction; however, choice of packing material is more critical. For best performance, the packing should be preferentially wetted by the continuous phase. Throughput, especially with newer packings, is large. Because of backmixing, the HETS is generally large, making packed columns suitable only when few equilibrium stages are needed.

§8.1.4 Sieve-Tray Columns

Sieve trays reduce axial mixing and promote a stagewise type of contact. The dispersed phase, which is analogous to vapor bubbles in distillation, flows up the column, with redispersion at each tray. The heavy phase is continuous, flowing at each stage through a **downcomer**, and then across the tray like a liquid in a distillation tower. If the heavy phase is dispersed, **upcomers** are used for the light phase. Columns have been built with diameters larger than 4.5 m. Holes from 0.32 to 0.64 cm (1/8 to 1/4 inches) in diameter, spaced 1.27 to 1.81 cm apart are used, and tray spacings are closer than in distillation—10 to 15 cm for low-interfacial-tension liquids. Plates are usually built without outlet weirs on the downspouts.

If designed and operated properly, extraction rates in sieve-tray columns are high because the dispersed-phase droplets coalesce and re-form on each tray. This destroys concentration gradients, which develop if a droplet passes through the entire column undisturbed. Sieve-tray extractors are subject to the same limitations as distillation columns: flooding, entrainment, and, to a lesser extent, weeping. An additional problem is scum formation at phase interfaces due to small amounts of impurities.

§8.1.5 Columns with Mechanically Assisted Agitation

If (1) interfacial tension is high, (2) density difference between liquid phases is low, and/or (3) liquid viscosities are high, then gravitational forces are inadequate for proper phase dispersal and turbulence creation. In that case, mechanical agitation is necessary to increase interfacial area per unit volume, thus decreasing mass-transfer resistance. For packed and plate columns, agitation can be provided by an oscillating pulse to the liquid, either by mechanical or pneumatic means. Pulsed, perforated-plate columns find considerable application in the nuclear industry. The most prevalent agitated columns are those that employ rotating agitators driven by a shaft extending axially through the column. The agitators create shear mixing zones, which alternate with settling zones. Nine of the more popular mechanically-agitated devices are shown in Figure 8.7a–i.

Agitation can also be induced in a column by moving plates back and forth in a reciprocating motion (Figure 8.7j) or in a novel horizontal contactor (Figure 8.7k). These devices answer the 1947 plea of Fenske, Carlson, and Quiggle [7] for equipment that can efficiently provide large numbers of stages

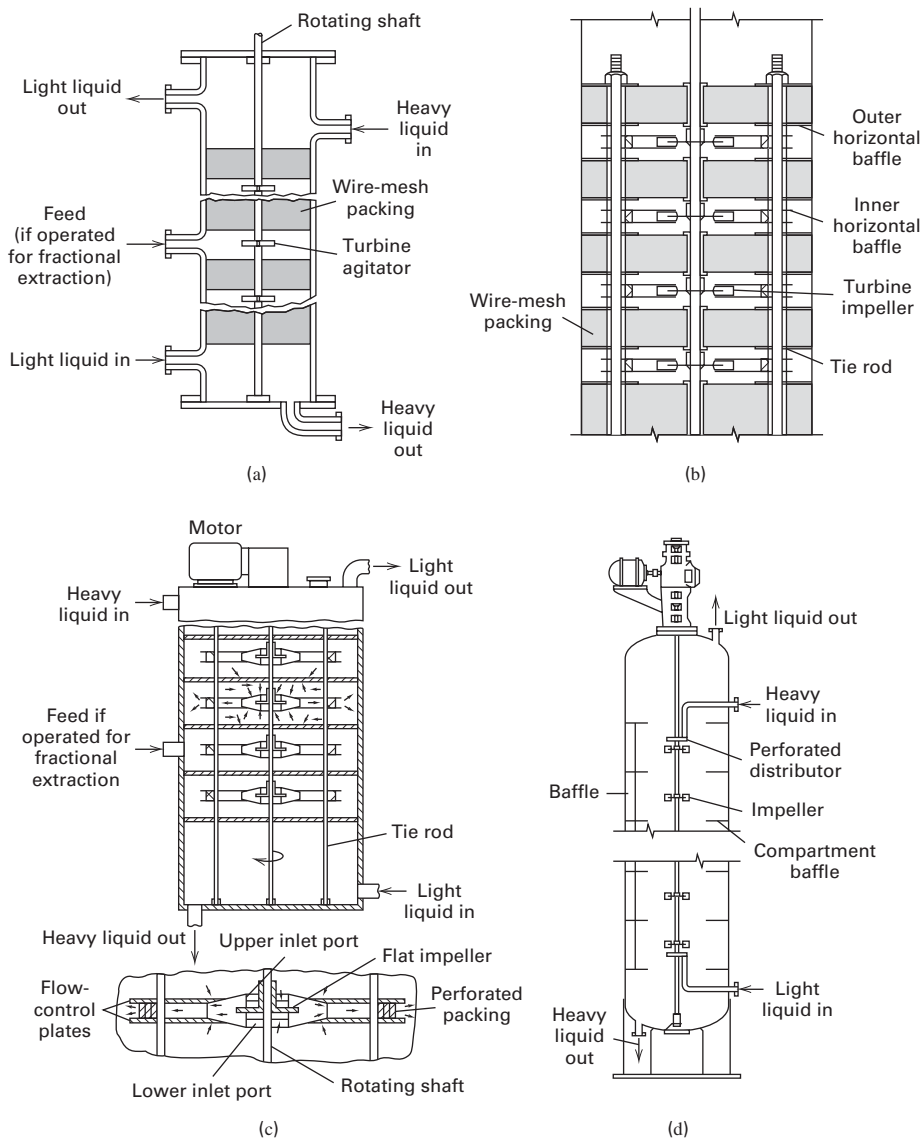


Figure 8.7 Commercial extractors with mechanically assisted agitation: (a) Scheibel column—first design; (b) Scheibel column—second design; (c) Scheibel column—third design; (d) Oldshue-Rushton (Mixco) column; (Continued)

in a device without large numbers of pumps, motors, and piping. They stated, “Despite . . . advantages of liquid-liquid separation processes, the problems of accumulating 20 or more theoretical stages in a small compact and relatively simple countercurrent operation have not yet been fully solved.” In 1946, it was considered impractical to design for more than seven stages, which represented the number of mixer-settler units in the only large-scale, commercial, solvent-extraction process in use.

Perhaps the first mechanically agitated column of importance was the Scheibel column [8] in Figure 8.7a, in which liquid phases are contacted at fixed intervals by unbaffled, flat-bladed, turbine-type agitators (Figure 8.3) mounted on a vertical shaft. In the unbaffled separation zones, located between the mixing zones, knitted wire-mesh packing prevents backmixing between mixing zones, and induces coalescence and settling of drops. The mesh material must be wetted by the dispersed phase. For larger-diameter installations (>1 m),

Scheibel [9] added outer and inner horizontal annular baffles (Figure 8.7b) to divert the vertical flow in the mixing zone and promote mixing. For systems with high interfacial tension and viscosities, the wire mesh is removed. The first two Scheibel designs did not permit removal of the agitator shaft for inspection and maintenance. Instead, the entire internal assembly had to be removed. To permit removal of just the agitator assembly shaft, especially for large-diameter columns (e.g., >1.5 m), and allow an access way through the column for inspection, cleaning, and repair, Scheibel [10] offered a third design, shown in Figure 8.7c. Here the agitator assembly shaft can be removed because it has a smaller diameter than the opening in the inner baffle.

The Oldshue-Rushton extractor [11] (Figure 8.7d) consists of a column with a series of compartments separated by annular outer stator-ring baffles, each with four vertical baffles attached to the wall. The centrally mounted vertical shaft drives a flat-bladed turbine impeller in each compartment.

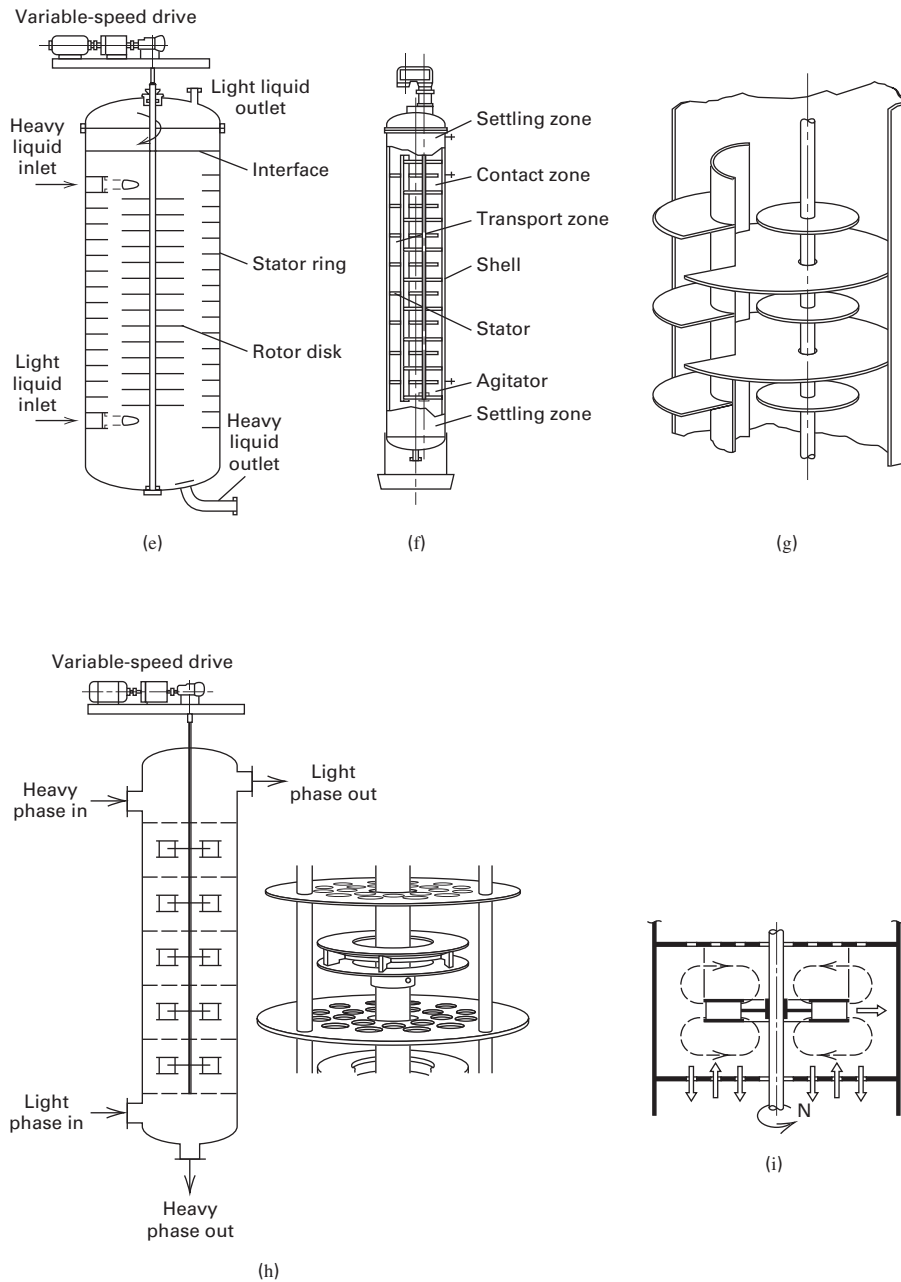


Figure 8.7 (Continued)
 (e) rotating-disk-contactor (RDC);
 (f) asymmetric rotating-disk contactor (ARD); (g) section of ARD contactor;
 (h) Kuhni column; (i) flow pattern in Kuhni column.

A third type of column with rotating agitators that appeared about the same time as the Scheibel and Oldshue–Rushton columns is the rotating-disk contactor (RDC) [12,13] (Figure 8.7e), an example of which is described at the beginning of this chapter and shown in Figure 8.1. It is an extensively used device worldwide [4]. Horizontal disks, mounted on a centrally located rotating shaft, are the agitation elements. The ratio of disk diameter to column diameter is 0.6. The distance, H in m, between disks depends on column diameter, D_T , in m, according to $H = 0.13(D_T)^{0.67}$. Mounted at the column wall are annular stator rings with an opening larger than the agitator-disk diameter, typically 0.7 of D_T . Thus, the agitator assembly shaft is easily removed from the column. Because the rotational speed of the rotor controls the

drop size, the rotor speed can be continuously varied over a wide range.

A modification of the RDC concept is the asymmetric rotating-disk contactor (ARD) [14], which has been in industrial use since 1965. As shown in Figure 8.7f, the contactor consists of a column, a baffled stator, and an offset multi-stage agitator fitted with disks. The asymmetric arrangement, shown in more detail in Figure 8.7g, provides contact and transport zones that are separated by a vertical baffle, to which is attached a series of horizontal baffles. This design retains the efficient shearing action of the RDC, but reduces backmixing because of the separate mixing and settling compartments.

Another extractor based on the Scheibel concept is the Kuhni extraction column [15] in Figure 8.7h, where the

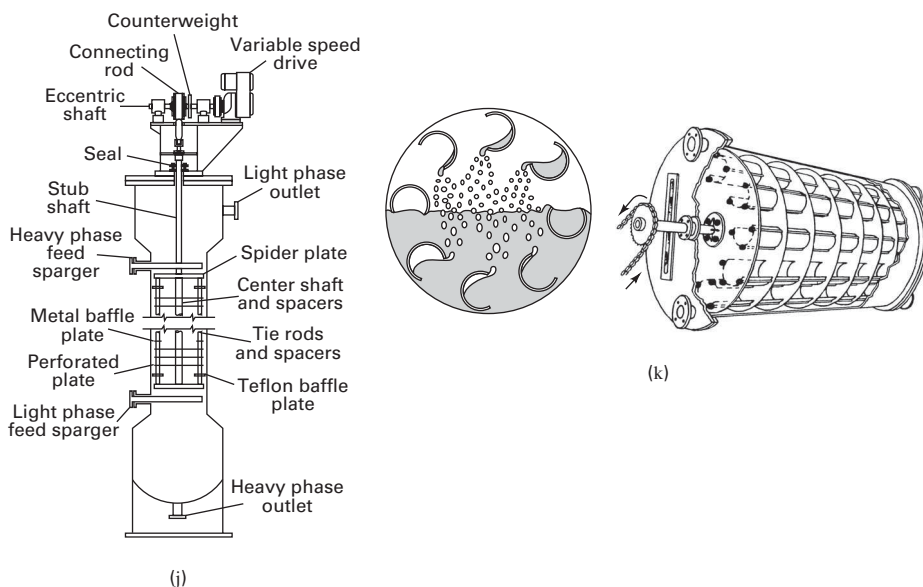


Figure 8.7 (Continued) (j) Karr reciprocating-plate column (RPC); (k) Graesser raining-bucket (RTL) extractor.

column is compartmented by a series of stator disks made of perforated plates. The distance, H in m, between stator disks depends on column diameter, D_T in m, according to $0.2 < H < 0.3 (D_T)^{0.6}$. A centrally positioned shaft has double-entry, radial-flow, shrouded-turbine mixers, which promote, in each compartment, the circulation action shown in Figure 8.7i. The ratio of turbine diameter-to-column diameter ranges from 0.33 to 0.6. For columns of diameter greater than 3 m, three turbine-mixer shafts on parallel axes are normally provided to preserve scale-up.

Rather than providing agitation by impellers on a vertical shaft or by pulsing, Karr [16, 17] devised a reciprocating, perforated-plate extractor column in which plates move up and down approximately 27 times per second with a 6.5–25 mm stroke. This uses less energy than pulsing the entire volume of liquid. Also, the close spacing of the plates (25–50 mm) promotes high turbulence and minimizes axial mixing, thus giving high mass-transfer rates and low HETS. The annular Teflon baffle plates in Figure 8.7j are placed in the plate stack to minimize axial mixing. The perforated plates use large holes (typically 9/16-inch diameter) and a high hole area (typically 58%). The central shaft, which supports both sets of plates, is reciprocated by a drive at the top of the column. Karr columns are particularly useful for bioseparations because residence time is reduced, and they can handle systems that tend to emulsify and feeds that contain particulates.

A modification of the Karr column is the vibrating-plate extractor (VPE) of Prochazka et al. [18], which uses perforated plates of smaller hole size and smaller percent hole area. The small holes provide passage for the dispersed phase, while one or more large holes on each plate provide passage for the continuous phase. Some VPE columns have uniform motion of all plates; others have two shafts for counter-motion of alternate plates.

Another novel device for providing agitation is the Graesser raining-bucket contactor (RTL), developed in the late 1950s [4] primarily for processes involving liquids of small density difference, low interfacial tension, SX and a tendency to form emulsions. Figure 8.7k shows a series of disks mounted inside a shell on a horizontal, rotating shaft with horizontal, C-shaped buckets fitted between and around the periphery of the disks. An annular gap between the disks and the inside shell periphery allows countercurrent, longitudinal flow of the phases. Dispersing action is very gentle, with each phase cascading through the other in opposite directions toward the two-phase interface, which is close to the center.

When fast extraction rates are needed as in bioseparations, high-speed centrifugal extractors are favored, such as the Podbielniak (POD) extractor, used for penicillin extraction [19]. They provide residence times as short as 10 s, and small liquid holdups. PODs can separate liquid phases of density differences as small as 0.01 g/cm^3 without emulsification.

§8.1.6 Comparison of Industrial Extraction Columns

Maximum loadings and sizes for industrial extraction columns, as given by Reissinger and Schroeter [5, 20] and Lo et al. [4], are listed in Table 8.2. As seen, the Lurgi tower, RDC, and Graesser extractors have been built in very large sizes. Combined volumetric throughputs per unit cross-sectional area are highest for the Karr extractor and lowest for the Graesser extractor. Table 8.3 lists the advantages and disadvantages of the various types of extractors, and Figure 8.8 shows a selection scheme for commercial extractors. For example, if only a small number of stages is required, a set of mixer-settler units might be selected. If more than five theoretical stages, a high

Table 8.2 Maximum Size and Loading for Commercial Liquid–Liquid Extraction Columns

Column Type	Maximum Combined Liquid Throughput, m ³ /m ² -h	Maximum Column Diameter, m
Lurgi tower	30	8
Pulsed packed	20	3
Pulsed sieve tray	25	3
Scheibel	25	3
RDC	40	8
ARD	25	5
Kuhni	40	3
Karr	40	3
Graesser	10	7

Above data apply to systems of:

1. High interfacial surface tension (30 to 40 dyne/cm).
2. Viscosity of approximately 1 cP.
3. Volumetric phase ratio of 1:1.
4. Phase-density difference of approximately 0.6 g/cm³.

throughput, and a large load range (m³/m²-h) are needed, and floor space is limited, an RDC or ARD contactor should be considered.

§8.2 GENERAL DESIGN CONSIDERATIONS

Liquid–liquid extraction involves more design variables than distillation. To determine stages, one of the three cascade arrangements in Figure 8.9, or an even more complex arrangement, must be selected. Packed-column configurations are shown in Figure 8.9, but other extraction equipment may be preferred. The single-section cascade of Figure 8.9a, which is similar to that used for absorption and stripping, will transfer solute in the feed to the solvent. The two-section cascade of Figure 8.9b is similar to that used for distillation. Solvent enters at one end and reflux, derived from the extract, enters at the other end. The feed enters in between. With two sections, depending on solubilities, it is sometimes possible to achieve a separation between two feed components; if not, a dual-solvent arrangement with two sections, as in Figure 8.9c, with or without reflux at the ends, may be advantageous. For configurations 8.9b and 8.9c, calculations should be made by a process simulator, as discussed in Chapter 10. For the configuration of Figure 8.9a, it is useful and instructive to make the graphical calculations described in this chapter.

Operative factors are:

1. Entering feed flow rate, composition, temperature, and pressure
2. Type of stage configuration (one- or two-section)

Table 8.3 Advantages and Disadvantages of Different Extraction Equipment

Class of Equipment	Advantages	Disadvantages
Mixer-settlers	Good contacting Handles high viscosity and interfacial tension Handles wide flow ratio Low headroom High stage efficiency Many stages available Reliable scale-up	Large holdup High power costs High investment Large floor space Interstage pumping may be required
Continuous, static counterflow contactors (no mechanical drive)	Low initial cost Low operating cost Simplest construction High throughput except for small density difference	Cannot handle high flow ratio High headroom Low stage efficiency Difficult scale-up
Continuous counterflow contactors with mechanical agitation	Good dispersion Reasonable cost Many stages possible Relatively easy scale-up	Limited throughput with small density difference Cannot handle emulsifying systems Cannot handle high flow ratio
Centrifugal extractors	Handles low-density difference between phases Low holdup volume Short holdup time Low space requirements Small inventory of solvent Avoids emulsification	High initial costs High operating cost High maintenance cost

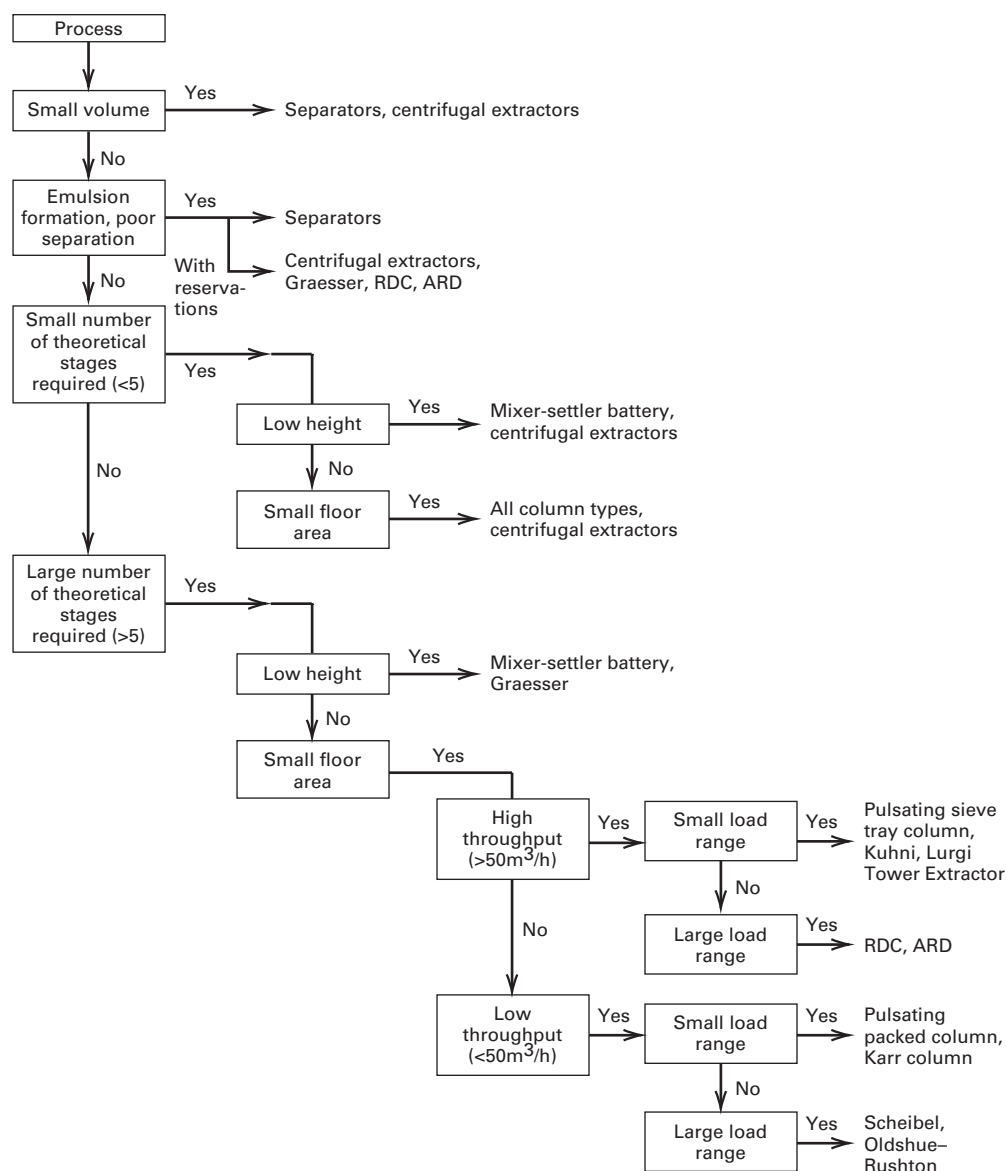


Figure 8.8 Scheme for selecting extractors.

[Reproduced from [5] with permission of Institution of Chemical Engineers.]

3. Desired degree of recovery of one or more solutes for one-section cascades
4. Degree of feed separation for two-section cascades
5. Choice of solvent(s)
6. Operating temperature (often ambient)
7. Operating pressure (greater than the bubble point of both phases)
8. Minimum-solvent flow rate and actual-solvent flow rate as a multiple of the minimum rate for one-section cascades or reflux rate and minimum reflux ratio for two-section cascades
9. Number of equilibrium stages
10. Emulsification and scum-formation tendency
11. Interfacial tension
12. Phase-density difference

13. Maximum residence time to avoid degradation
14. Type of extractor
15. Extractor cost and horsepower requirement

The ideal solvent has:

1. High selectivity for the solute relative to the carrier to minimize the need to recover carrier from the solvent
2. High capacity for dissolving the solute to minimize solvent-to-feed ratio
3. Minimal solubility in the carrier
4. A volatility sufficiently different from the solute that recovery of the solvent can be achieved by distillation, but not so high that a high extractor pressure is needed, or so low that a high temperature is needed if the solvent is recovered by distillation

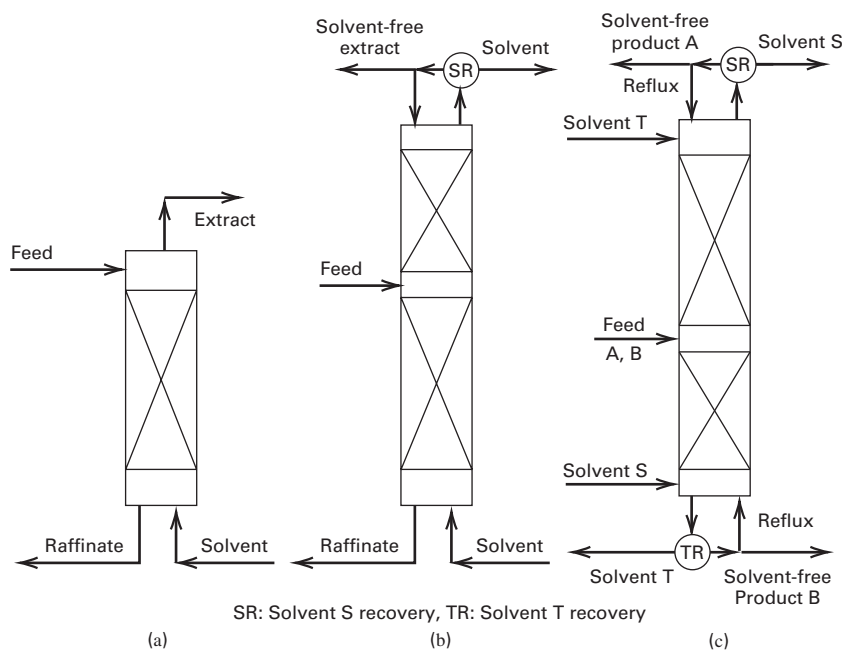


Figure 8.9 Common liquid-liquid extraction cascade configurations: (a) single-section cascade; (b) two-section cascade; (c) dual solvent with two-section cascade. SR is solvent S recovery and TR is solvent T recovery.

5. Stability to maximize the solvent life and minimize the solvent makeup requirement
6. Inertness to permit use of common materials of construction
7. Low viscosity to promote phase separation, minimize pressure drop, and provide a high-solute mass-transfer rate
8. Non-toxic and non-flammable characteristics to facilitate its safe use
9. Availability at a relatively low cost
10. Moderate interfacial tension to balance the ease of dispersion and the promotion of phase separation
11. Large difference in density relative to the carrier to achieve a high capacity in the extractor
12. Compatibility with the solute and carrier to avoid contamination
13. Lack of tendency to form a stable rag or scum layer at the phase interface
14. Desirable wetting characteristics with respect to extractor internals

Solvent selection is a compromise among all these properties. However, first consideration is usually given to selectivity and environmental concerns, and second to capacity and cost. From (2-19) in Chapter 2, the distribution (partition) coefficient, K_D , for solute A between solvent S and carrier C can be applied. Combining (2-19) with (2-15) and (2-17) gives

$$(K_A)_D = (x_A)^{II}/(x_A)^I = (\gamma_A)^I/(\gamma_A)^{II} \quad (8-1)$$

where II is the extract phase, rich in S, and I is the raffinate phase, rich in C. Similarly, for the carrier and the solvent, respectively,

$$(K_C)_D = (x_C)^{II}/(x_C)^I = (\gamma_C)^I/(\gamma_C)^{II} \quad (8-2)$$

$$(K_S)_D = (x_S)^{II}/(x_S)^I = (\gamma_S)^I/(\gamma_S)^{II} \quad (8-3)$$

From (2-21), the relative selectivity, β , of the solute with respect to the carrier is obtained by taking the ratio of (8-1) to (8-2), giving

$$\beta_{AC} = \frac{(K_A)_D}{(K_C)_D} = \frac{(x_A)^{II}/(x_A)^I}{(x_C)^{II}/(x_C)^I} = \frac{(\gamma_A)^I/(\gamma_A)^{II}}{(\gamma_C)^I/(\gamma_C)^{II}} \quad (8-4)$$

For high selectivity, β_{AC} should be high, so at equilibrium there is a high concentration of A and a low concentration of C in the solvent. A first estimate of β_{AC} is made from predictions of activity coefficients $(\gamma_A)^I$, $(\gamma_A)^{II}$, and $(\gamma_C)^{II}$ at infinite dilution where $(\gamma_C)^I = 1$, or by using equilibrium data for the lowest tie line on a triangular diagram of the type discussed in Chapter 4. If A and C form a nearly ideal solution, the value in (8-4) of $(\gamma_A)^I \approx 1$.

For high solvent capacity, $(K_A)_D$ in (8-4) should be high. From (8-2) it is seen that this is difficult to achieve if A and C form nearly ideal solutions such that $(\gamma_A)^I = 1.0$, unless A and S have a great affinity for each other, which would result in a negative deviation from Raoult's law to give $(\gamma_A)^{II} < 1$. Unfortunately, such systems are rare.

For solvent recovery, $(K_S)_D$ should be large and $(K_C)_D$ as small as possible to minimize solvent in the raffinate and carrier in the extract. This will be the case if activity coefficients $(\gamma_S)^I$ and $(\gamma_C)^{II}$ at infinite dilution are large.

If a water-rich feed is to be separated, it is common to select an organic solvent; for an organic-rich feed, an aqueous solvent is preferred. In either case, the solvent chosen should lower the activity coefficient of the solute. Consideration of molecule group interactions can help narrow the search before activity coefficients are estimated or equilibrium data are sought. Organic group interactions for solvent-screening purposes, based on 900 binary systems, as given by Robbins [22], are shown in Table 8.4, where the solute and solvent each belong to any of 12 different chemical groups. In this table, a minus (–) sign for a given solute-solvent pair means the solvent will desirably lower the activity coefficient of the solute relative to its value in the feed.

Table 8.4 Group Interactions for Solvent Selection

Solute Class	H-Donor Groups	Solvent Class											
		1	2	3	4	5	6	7	8	9	10	11	12
1	Phenol	0	0	-	0	-	-	-	-	-	-	+	+
2	Acid, Thiol	0	0	-	0	-	-	0	0	0	0	+	+
3	Alcohol, Water	-	-	0	+	+	0	-	-	+	+	+	+
4	Active-H on Multihalo Paraffin	0	0	+	0	-	-	-	-	-	-	0	+
H-Acceptor Groups													
5	Ketone, Amide with no H on N Sulfone, Phosphine, Oxide	-	-	+	-	0	+	+	+	+	+	+	+
6	Tert Amine	-	-	0	-	+	0	+	+	0	+	0	0
7	Sec Amine	-	0	-	-	+	+	0	0	0	0	0	+
8	Pri Amine, Ammonia, Amide with 2H on N	-	0	-	-	+	+	0	0	+	+	+	+
9	Ether, Oxide, Sulfoxide	-	0	+	-	+	0	0	+	0	+	0	+
10	Ester, Aldehyde, Carbonate, Phosphate, Nitrate, Nitrite, Nitrile, Intra Molecular Bonding, e.g., O-nitro Phenol	-	0	+	-	+	+	0	+	+	0	+	+
11	Aromatic, Olefin, Halogen Aromatic, Multihalo Paraffin without Active-H, Monohalo Paraffin	+	+	+	0	+	0	0	+	0	+	0	0
Non H-Bonding Groups													
12	Paraffin, Carbon Disulfide	+	+	+	+	+	0	+	+	+	+	0	0

(+) Plus sign means that compounds in the column group tend to raise activity coefficients of compounds in the row group.

(-) Minus sign means a lowering of activity coefficients of compounds in the row group.

(0) Zero means little or no effect on activity coefficients of compounds in the row group.

Choose a solvent that lowers the activity coefficient.

[Reproduced from [22] with permission of the American Institute of Chemical Engineers.]

Suppose it is desired to extract acetone from water. In Table 8.4, Group 3 applies for this solute, and desirable solvents are given in Groups 1 and 6. In particular, trichloroethane, a Group 6 compound, is a selective solvent with high capacity for acetone. If the compound is environmentally objectionable, it is rejected.

A sophisticated solvent-selection method, based on the UNIFAC group-contribution method for estimating activity coefficients and utilizing a computer-aided constrained optimization approach, has been developed by Naser and Fournier [23]. A preliminary solvent selection can also be made

using tables of partition coefficients and Godfrey Miscibility Numbers in *Perry's Chemical Engineers Handbook* [2].

§8.2.1 Representation of Ternary Data

Chapter 4 introduced ternary diagrams for representing liquid-liquid equilibrium data at constant temperature. Such diagrams are available for a large number of systems (Humphrey et al. [6]). For ternary systems, the most common diagram is Type I in Figure 8.10a; much less common are Type II systems, in Figure 8.10b, which include (1) *n*-heptane/

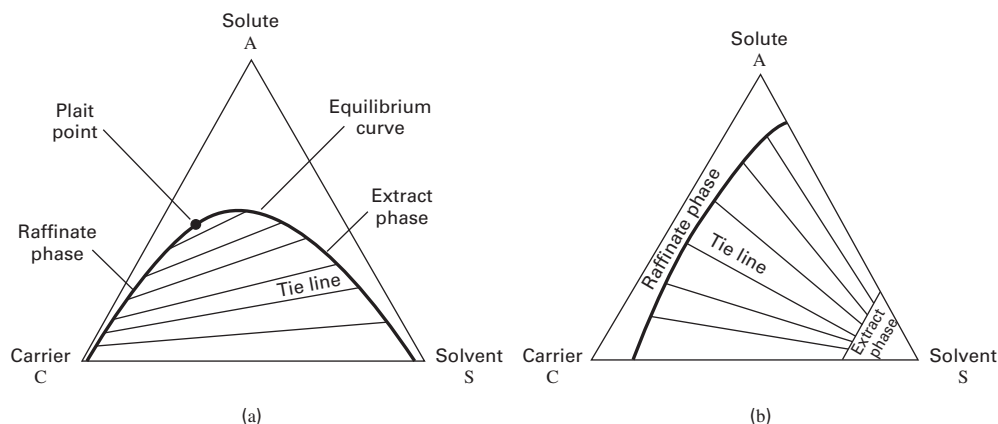


Figure 8.10 Common classes of ternary systems: (a) Type I, one immiscible pair; (b) Type II, two immiscible pairs.

aniline/methylcyclohexane, (2) styrene/ethylbenzene/diethylene glycol, and (3) chlorobenzene/water/methyl ethyl ketone. For Type I, the solute and solvent are miscible in all proportions; in Type II, they are not. For Type I systems, the larger the two-phase region on line \overline{CS} , the greater the immiscibility of carrier and solvent. The closer the top of the two-phase region is to apex A , the greater the range of feed composition along line \overline{AC} that can be separated with solvent S . In Figure 8.11, only feed solutions in the composition range from C to F can be separated because, regardless of how much solvent is added, two liquid phases are not formed in the feed composition range of \overline{FA} (i.e., \overline{FS} does not pass through the two-phase region). Figure 8.11a has a wider range of feed composition than Figure 8.11b. For Type II systems, a high degree of insolubility of S in C and C in S will produce a desirable high relative selectivity, but at the expense of solvent capacity. Solvents that result in Type I systems are thus more desirable.

Whether a system is of Type I or Type II often depends on temperature. Figure 8.12 shows the data of Darwent and Winkler [24] for the ternary system n -hexane (H)–methylcyclopentane (M)–aniline (A) for temperatures of 25, 34.5, and 45°C. At the lowest temperature, 25°C, the system is Type II because both H and M are only partially miscible in the aniline solvent. As temperature increases, the solubility of M in aniline increases more rapidly than the solubility of H in aniline, until 34.5°C, the critical solution temperature for M in aniline, where the system is at the border of Type II and Type I. At 45°C, the system is clearly of Type I, with aniline more selective for M than H. Type I systems have a **plait point** (see Figure 8.10a); Type II systems do not.

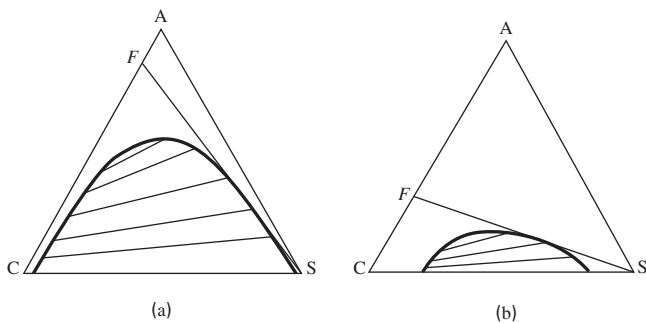


Figure 8.11 Effect of solubility on range of feed composition that can be extracted.

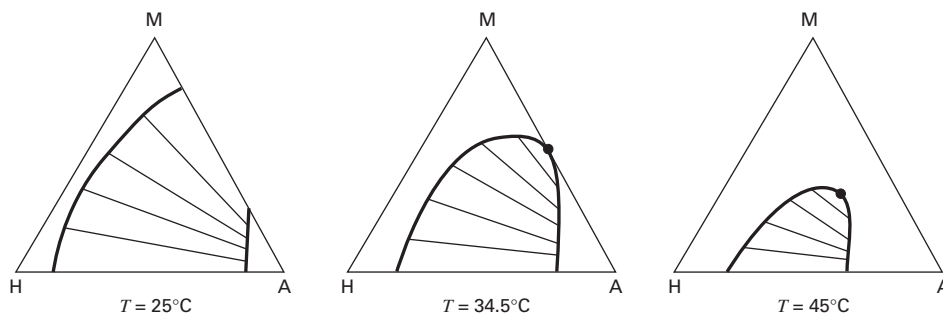


Figure 8.12 Effect of temperature on solubility for the system n -hexane (H)/methylcyclopentane (M)/aniline (A).

Except in the near-critical region, pressure has little effect on liquid–liquid equilibrium because it has little effect on liquid-phase activity coefficients. The operating pressure need only be greater than the bubble-point pressure. Most extractors operate at near-ambient temperature, with the process being nearly isothermal if the heat of mixing is small.

Laboratory or pilot-plant work, using actual plant feed and solvent, is normally necessary to ascertain dispersion and coalescence properties. Although rapid coalescence of drops is desirable, this reduces interfacial area and leads to reduced mass-transfer rates. Thus, compromises are necessary. Coalescence is enhanced when the solvent phase is continuous and mass transfer of solute is from the droplets. This phenomenon, the **Marangoni effect**, is due to a lowering of interfacial tension by a significant solute presence in the interfacial film. If solvent is the dispersed phase, the interfacial film is depleted of solute, causing an increase in interfacial tension and inhibition of coalescence.

For a given (1) feed liquid, (2) degree of solute extraction, (3) operating pressure and temperature, and (4) solvent for a single-section cascade, there is a minimum solvent-to-feed flow-rate ratio that corresponds to an infinite number of countercurrent equilibrium contacts. As with absorption and stripping, a trade-off exists between the number of equilibrium stages and the solvent-to-feed ratio. For a Type I system, this ratio is best determined by a graphical method described next.

§8.3 HUNTER–NASH GRAPHICAL EQUILIBRIUM-STAGE METHOD

For preliminary studies, stagewise extraction calculations for Type I ternary systems are conveniently carried out with equilibrium diagrams. In this section, procedures are developed using the Hunter-Nash method [26] with equilateral-triangle and right-triangle diagrams. Free triangular graph paper can be downloaded from several websites, including <http://www.waterproofpaper.com/graph-paper/ternary-diagram-triangular-graph-paper.shtml>.

Figure 8.13 shows a schematic diagram for a countercurrent, continuous-flow, N -equilibrium-stage extraction cascade operating isothermally at steady state. Each stage includes mixing and phase separation. Stage numbering begins at the feed end, opposite to the end at which the solvent enters. Typically, mass, rather than molar flow rates are used. The final raffinate feed rate is R_N and the final extract feed rate

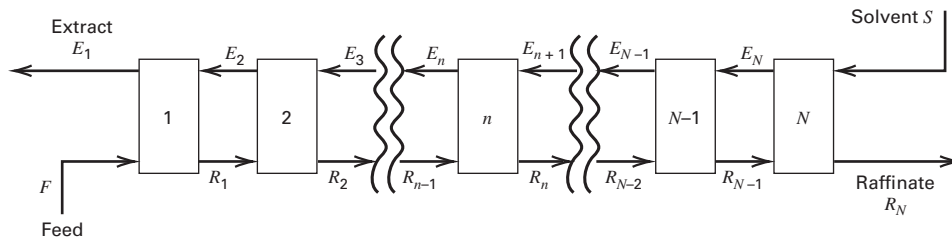


Figure 8.13 Countercurrent-flow, N -equilibrium-stage, liquid–liquid extraction cascade.

is E_1 . Phase equilibrium is assumed at each stage, so for any intermediate stage n , the components in extract E_n and raffinate R_n are in equilibrium. Mass transfer of all species occurs at each stage. The feed, F , contains the carrier, C , and the solute, A . It can also contain solvent, S , up to the solubility limit. Entering solvent flow rate, S , can contain C and A up to the solubility limits, but preferably contains little of either. Because most liquid–liquid equilibrium data are listed and plotted in mass rather than mole concentrations, let: $(y_i)_n$ = mass fraction of species i in extract leaving stage n and $(x_i)_n$ = mass fraction of species i in raffinate leaving stage n .

Although Figure 8.13 implies that the extract is the light phase, either phase can be the light phase. Assume the ternary system is at temperature, T , such that liquid–liquid equilibrium data are as shown in the equilateral-triangle diagram of Figure 8.14, whose coordinates were described in §4.4. The bold line is the equilibrium curve (also called the **binodal curve** because the plait point separates the curve into an extract to the left and a raffinate to the right). The dashed lines are **tie lines** connecting compositions of equilibrium phases lying on the binodal curve. Because the tie lines slope upward from the C side toward the S side, at equilibrium, the solute, A , has a concentration higher in S than in C . This makes S an effective solvent for extracting A from C . If the tie lines slope downward, S is not an effective solvent.

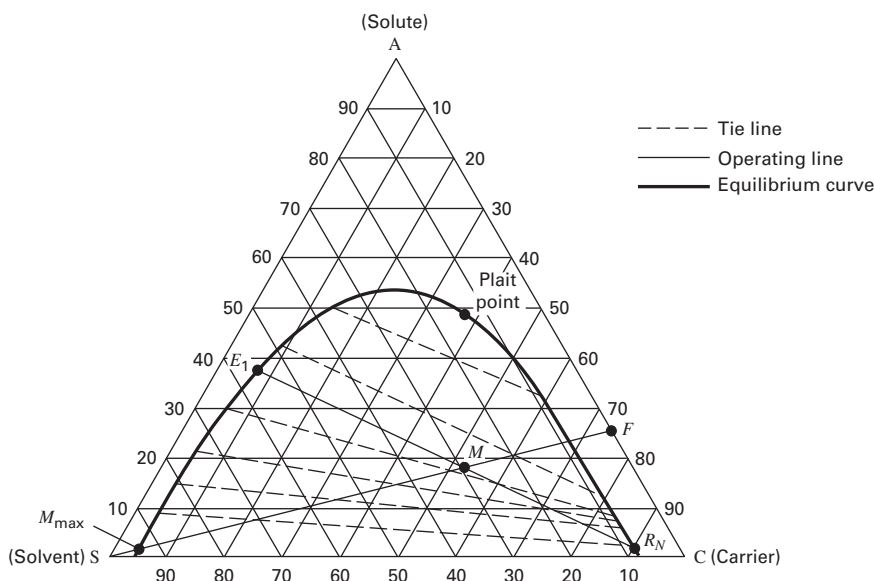


Figure 8.14 Construction 1: Location of product points.

Some systems, such as isopropanol–water–benzene, exhibit a phenomenon called **solutropy**, wherein moving from the plait point into the two-phase region of the diagram, the tie lines first slope in one direction, but then the slope diminishes until an intermediate tie line becomes horizontal. Below that tie line, the remaining tie lines slope in the other direction. Sometimes the solutropy phenomenon disappears if mole-fraction coordinates, rather than mass-fraction coordinates, are used.

§8.3.1 Determining the Number of Equilibrium Stages

A degrees-of-freedom analysis for the ternary system cascade of Figure 8.13 shows there are six variables that must be specified for a ternary system. Four of the variables are F , $(x_i)_F$, $(y_i)_S$, and T . The remaining two variables are selected by choosing one of the following sets.

Set 1. S and $(x_i)_{R_N}$	Set 4. N and $(x_i)_{R_N}$
Set 2. S and $(y_i)_{E_1}$	Set 5. N and $(y_i)_{E_1}$
Set 3. $(x_i)_{R_N}$ and $(y_i)_{E_1}$	Set 6. N and S

where $(x_i)_{R_N}$ and $(y_i)_{E_1}$ and all equilibrium phases lie on the equilibrium curve.

Calculations for sets 1 to 3 involve determination of N and can be made directly using a graphical procedure on a trian-

gular diagram. Process simulators do not allow these three specification sets because N must be specified. Sets 4 to 6 involve a specified N and require a tedious, iterative graphical procedure. Set 6 is often used with process simulators. First, consider Set 1, with the procedures for Sets 2 and 3 being minor modifications. The technique, called the **Hunter–Nash method** [26], involves three construction steps on the triangular diagram. They are more difficult than the McCabe–Thiele staircase-step method for distillation. Although the procedure is illustrated here only for a Type I system, parallel principles apply to a Type II system. The constructions are shown in Figures 8.14, 8.15, and 8.17, where A is the solute, C the carrier, and S the solvent. On the equilibrium curve, extract compositions lie to the left of the plait point, while all raffinate compositions lie to the right. Determination of N is as follows, given feed, F , and solvent, S , flow rates and compositions, and the final raffinate composition:

Construction 1 (Product Composition Points)

On Figure 8.14, locate mixing point M , which represents the combined flow rate and composition of feed F plus entering solvent S . Assume the following feed and solvent specifications, as plotted in Figure 8.14:

Feed	Solvent
$F = 250$ kg	$S = 100$ kg
$(x_A)_F = 0.24$	$(x_A)_S = 0.00$
$(x_C)_F = 0.76$	$(x_C)_S = 0.00$
$(x_S)_F = 0.00$	$(x_S)_S = 1.00$

By total and component material balances, the composition of $M = F + S = 350$ kg is determined as follows:

$$(x_C)_M M = (x_C)_F F + (x_C)_S S \\ = 0.76(250) + 0(100) = 190 \text{ kg}$$

$$(x_C)_M = 190/350 = 0.543$$

$$(x_S)_M M = (x_S)_F F + (x_S)_S S \\ = 0(250) + 1(100) = 100 \text{ kg}$$

$$(x_S)_M = 100/350 = 0.286$$

Note that the component mass fractions for M sum to 1.000.

From these two $(x_i)_M$ values, point M is located, as shown in Figure 8.14. Based on properties of the triangular diagram discussed in §4.4, point M must be located on the straight line connecting F and S . Therefore, M can be located knowing just one value of $(x_i)_M$, say, $(x_S)_M$. Also, the ratio S/F is given by the inverse-lever-arm rule as

$$S/F = \overline{MF}/\overline{MS} = 100/250 = 0.400$$

or

$$S/M = \overline{MF}/\overline{SF} = 100/350 = 0.286$$

Thus, point M can be located by two composition points or by measurement, employing either of these ratios.

The combined flow rates and compositions of entering streams, F and S , must also equal the combined flow rates and compositions of the exiting streams, R_N and E_1 . With point M located, the composition of exiting extract E_1 is determined from overall total and component material balances for the cascade:

$$M = R_N + E_1 = 350 \text{ kg} \\ (x_A)_M M = 60 = (x_A)_{R_N} R_N + (x_A)_{E_1} E_1 \\ (x_C)_M M = 190 = (x_C)_{R_N} R_N + (x_C)_{E_1} E_1 \\ (x_S)_M M = 100 = (x_S)_{R_N} R_N + (x_S)_{E_1} E_1$$

Specify $(x_A)_{R_N} = 0.025$. Because it must lie on the equilibrium curve, R_N can be located and the values of $(x_C)_{R_N}$ and $(x_S)_{R_N}$ can be read from Figure 8.14. A straight line drawn from R_N through M locates E_1 at the equilibrium-curve intersection, from which the composition of E_1 can be read. Values of the flow rates R_N and E_1 can then be determined from the overall material balances above, or from Figure 8.14 by the inverse-lever-arm rule:

$$E_1/M = \overline{MR_N}/\overline{E_1R_N} \\ R_N/M = \overline{ME_1}/\overline{E_1R_N}$$

with $M = 350$ kg. By either method, the results are:

Raffinate Product	Extract Product
$R_N = 198.6$ kg	$E_1 = 151.4$ kg
$(x_A) = 0.025$	$(x_A) = 0.364$
$(x_C) = 0.900$	$(x_C) = 0.075$
$(x_S) = 0.075$	$(x_S) = 0.561$

Again, the composition mass fractions for the two products are seen to sum to 1.000.

Also included in Figure 8.14 is point M_{\max} , which lies on the equilibrium curve along the straight line connecting F to S . M_{\max} corresponds to the maximum possible solvent addition if two liquid phases are to exist. By the inverse-lever-arm rule, it is seen that a very large ratio of S to F exists.

Construction 2 (Operating Point and Operating Lines)

For vapor–liquid cascades, §6.3 and §7.2 describe an operating line that is the locus of passing streams in a cascade. Referring to Figure 8.13, material balances around groups of stages from the feed end can be written as differences:

$$F - E_1 = \cdots = R_{n-1} - E_n = \cdots = R_N - S = P \quad (8-5)$$

Because the passing streams are differenced, P defines a **difference point**, not a **mixing point**, M . From the same geometric considerations that apply to a mixing point, a difference point also lies on a line through the points involved. However, whereas M lies inside the diagram and between the two end points, P usually lies outside the triangular diagram along an extrapolation of the line through a pair of passing-stream points forming differences, such as F and E_1 , R_N and S , and so on.

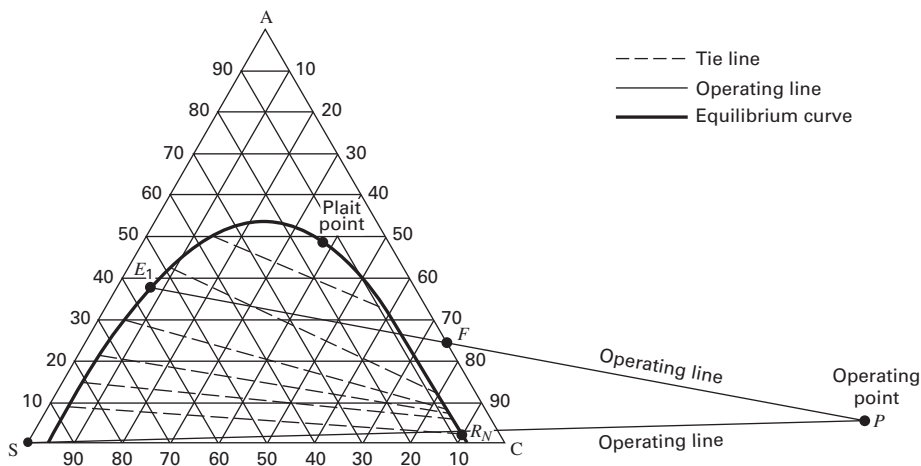


Figure 8.15 Construction 2: Location of operating point.

To locate the difference point, P , two straight lines are drawn through the passing-stream point pairs (E_1, F) and (S, R_N) established by Construction 2, as shown in Figure 8.15. These lines are extrapolated until they intersect at difference (operating) point P . Figure 8.15 shows the intersection at point P . From (8-5), straight lines drawn through points for any other pair of passing streams, such as (E_n, R_{n-1}), must also pass through point P . Thus, the difference point becomes an operating point, and lines drawn through pairs of points for passing streams and extrapolated to point P are operating lines.

The difference point has properties similar to a mixing point. If $F - E_1 = P$ is rewritten as $F = E_1 + P$, F can be interpreted as the mixing point for P and E_1 . Therefore, by the inverse-lever-arm rule, the length of line $\overline{E_1P}$ relative to the length of line \overline{FP} is

$$\frac{\overline{E_1P}}{\overline{FP}} = \frac{E_1 + P}{E_1} = \frac{F}{E_1} \quad (8-6)$$

Thus, point P can be located with a ruler using either pair of feed-product passing streams.

In Figure 8.15, the operating point, P , lies on the feed or raffinate side of the diagram. Depending on the relative amounts of feed and solvent and the slope of the tie lines, point P may lie on the solvent or feed side of the diagram, and inside or outside of the diagram.

Construction 3 (Tie Lines and Equilibrium Lines)

The third type of construction involves the tie lines that define the equilibrium curve, which is divided into the two sides (raffinate and extract) by the plait point. For Type I diagrams, the plait point is the composition of two equilibrium phases that become one phase. A material balance around stage n for any of the three components is

$$(x_i)_{n-1}R_{n-1} + (y_i)_{n+1}E_{n+1} = (x_i)_nR_n + (y_i)_nE_n \quad (8-7)$$

Because R_n and E_n are in equilibrium, their composition points are at the two ends of a tie line. Typically, a diagram will not contain all tie lines needed; however, more tie lines may be added by centering them between existing tie lines, or by using

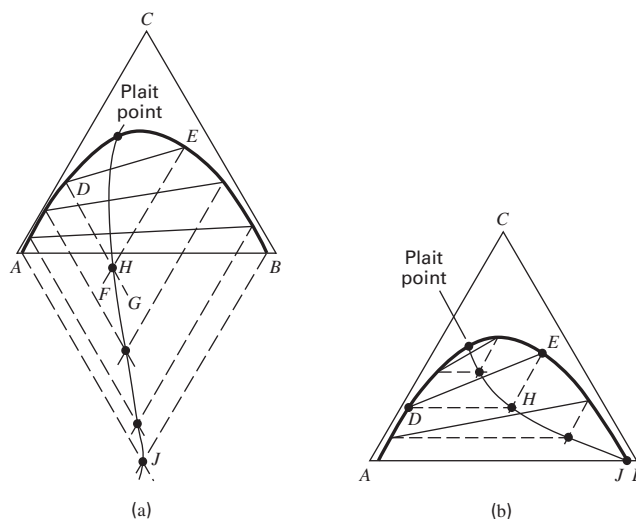


Figure 8.16 Use of conjugate curves to interpolate tie lines: (a) Method 1. (b) Method 2.

either of two interpolation methods illustrated in Figure 8.16. In Figure 8.16a, the conjugate line from the plait point to J is determined from four tie lines and the plait point. From tie line \overline{DE} , lines \overline{DG} and \overline{EF} are drawn parallel to triangle sides \overline{CB} and \overline{AC} , respectively. The intersection at point H gives a second point on the conjugate curve. Subsequent intersections establish additional points from which the conjugate curve is drawn. Then, using the curve, additional tie lines are drawn by reversing the procedure. If it is desired to keep the conjugate curve inside the two-liquid-phase region of the triangular diagram, the method illustrated in Figure 8.16b is used, where lines are drawn parallel to triangle sides \overline{AB} and \overline{AC} .

Stepping Off Stages

In Figure 8.17, equilibrium stages are stepped off by alternate use of tie lines and operating lines. Constructions 1 and 2 have been employed to locate points F, E, S, R_1 , and P . Starting at the feed end of the cascade, Construction 3 is used to draw a tie line from point E_1 to equilibrium phase R_1 . Because R_1

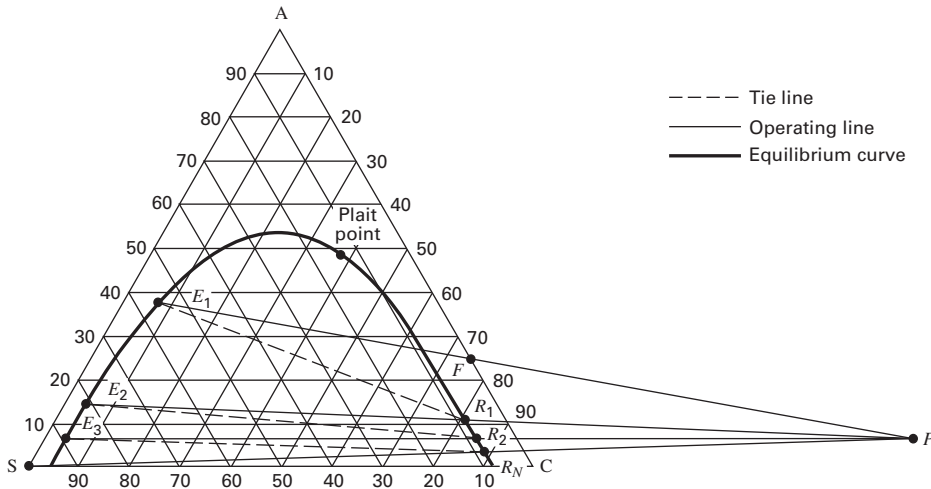


Figure 8.17 Determination of the number of equilibrium stages.

passes E_2 , Construction 2 requires that E_2 lie at the intersection of a straight operating line drawn through points R_1 and P , and back to the extract side of the equilibrium curve. R_2 is located with a tie line from E_2 by Construction 3. From R_2 , E_3 is located with an operating line through P by Construction 2. Continuing in this fashion by alternating between equilibrium tie lines and operating lines, the specified point R_N is reached or passed. If the latter, a fraction of the last stage is taken. In Figure 8.17, 2.8 equilibrium stages are required, where equilibrium stages are counted by the number of equilibrium tie lines used.

Procedures for specification Sets 2 and 3 are similar to that for Set 1. Sets 4 and 5 can be handled by iteration on assumed values for S and following the procedure for Set 1. Set 6 can also use the procedure of Set 1 by iterating on E_1 .

From (8-6), it is seen that if the ratio F/E_1 approaches a value of 1, operating point P will be located at a large distance from the triangular diagram. In that case, by using an arbitrary rectangular-coordinate system superimposed over the triangular diagram, the coordinates of P can be calculated from (8-6) using the equations for the two straight lines established in Construction 2. Operating lines for intermediate stages can

then be located on the triangular diagram so as to pass through P . Details of this procedure are given by Treybal [25].

§8.3.2 Minimum and Maximum Solvent-to-Feed Flow-Rate Ratios

The procedure of §8.3.1 for determining the number of equilibrium stages to achieve a desired solute extraction for a given solvent-to-feed ratio presupposes that this ratio is greater than the minimum ratio, which corresponds to an infinite number of stages, and less than the maximum ratio that would prevent the formation of the required second liquid phase. In practice, the minimum ratio is determined before solving specification Sets 1 or 2. This is done by solving Set 4 with $N = \infty$, where, as in distillation, absorption, and stripping, the infinity of stages occurs at an equilibrium-curve and operating-line pinch point. In ternary systems, the pinch point occurs when a tie line coincides with an operating line. Thus, the pinch point becomes a pinch line. The procedure is involved because the location of the pinch line is not known.

Figure 8.18 shows the previous A–C–S system. The composition points F , S , and R_N are specified, but E_1 is not

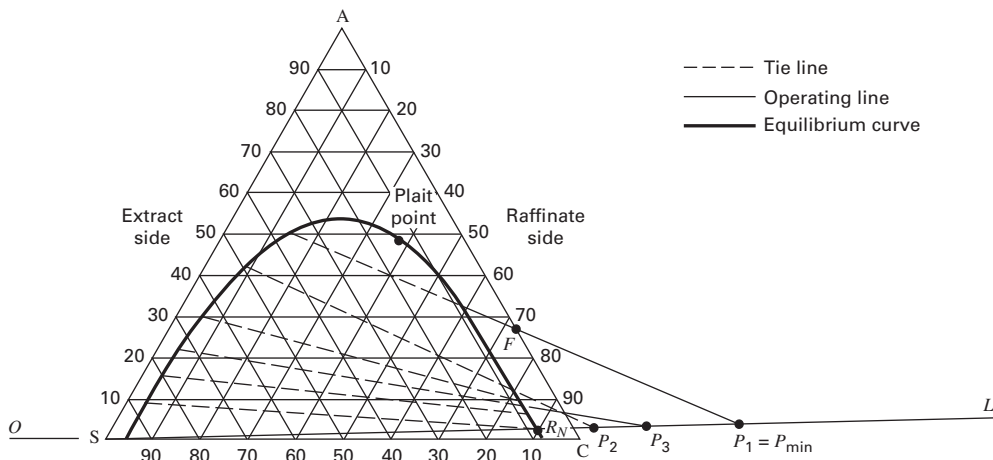


Figure 8.18 Determining minimum solvent-to-feed ratio.

because the solvent rate is not known. The operating line \overline{OL} is drawn through the points S and R_N and extended to the left and right. This line is the locus of all possible material balances determined by adding S to R_N . Each tie line is then assumed to be a pinch line by extending each tie line until it intersects the line \overline{OL} . In this manner, a sequence of intersections P_1, P_2 , etc., is found. If these points lie on the raffinate side of the diagram, as in Figure 8.18, the pinch line corresponds to the line extending to P_{\min} located at the greatest distance from R_N . If the triangular diagram does not have a sufficient number of tie lines to determine that point accurately, additional tie lines are introduced by the method illustrated in Figure 8.16. If it is assumed in Figure 8.18 that no other tie line gives a point P_i that is farther away from R_N than P_1 , then $P_1 = P_{\min}$. With P_{\min} known, the point for the composition of E_1 is at the extract-side end of the tie line coinciding with the pinch line. In Figure 8.18, the composition at that point is 51% A, 13.5% C, and 35.5% S. An operating line can be drawn through point F and extended to E_1 at an intersection with the extract side of the equilibrium curve.

From the compositions of the four points S, R_N, F , and E_1 , the mixing point M can be found and material balances used to solve for S_{\min}/F :

$$F + S_{\min} = R_N + E_1 = M \quad (8-8)$$

$$(x_A)_F F + (x_A)_S S_{\min} = (x_A)_M M \quad (8-9)$$

from which

$$\frac{S_{\min}}{F} = \frac{(x_A)_F - (x_A)_M}{(x_A)_M - (x_A)_S} \quad (8-10)$$

A solvent flow rate greater than S_{\min} is required for extraction in a finite number of stages. In Figure 8.18, such a solvent rate results in an operating point P to the right of P_{\min} , which is a location farther away from R_N . A reasonable value for S might be $1.5 S_{\min}$. From Figure 8.18, the simultaneous solution of (8-8) and (8-9) gives $(x_A)_M = 0.185$, from which, by (8-10), $S_{\min}/F = 0.30$. In Figure 8.17, $S/F = 0.40$, giving $S/S_{\min} = 1.33$.

In Figure 8.18, the tie lines slope downward toward the raffinate side. If the tie lines slope downward toward the extract side of the diagram, the above procedure for finding S_{\min}/F is modified. The sequence of points P_1, P_2 , etc., now occur on the other side of the triangular diagram. However, the pinch line now corresponds to the point, P_{\min} , that is closest to point S , so an operating point, P , must be chosen between points P_{\min} and S . For a system that exhibits solutropy, intersections P_1, P_2 , etc., are found on both sides of the diagram. Those on the extract side determine the minimum solvent-to-feed ratio.

In Figure 8.14, mixing point M lies in the two-phase region. As this point moves along the line \overline{SF} toward S , the ratio S/F increases according to the inverse-lever-arm rule. In the limit, a maximum S/F ratio is reached when $M = M_{\max}$ arrives at the equilibrium curve on the extract side. Now all of the feed is dissolved in the solvent, no raffinate is obtained, and only one stage is required. To avoid this impractical condition, as well

as the other extreme of infinite stages, it is necessary to select a solvent ratio, S/F , such that $(S/F)_{\min} < (S/F) < (S/F)_{\max}$. In Figure 8.14, the mixing point M_{\max} is located as shown, from which $(S/F)_{\max}$ is determined to be about 16.

EXAMPLE 8.1 Equilibrium Stages for Extraction.

Acetone is to be extracted from a 30 wt% acetone (A) and 70 wt% ethyl acetate (C) feed at 30°C, using pure water (S) as the solvent, in the cascade shown at the bottom of Figure 8.19, which establishes the nomenclature for this example. The final raffinate is to contain 5 wt% acetone on a water-free basis. Determine the minimum and maximum solvent-to-feed ratios and the number of equilibrium stages required for two intermediate S/F ratios. The equilibrium data plotted in Figure 8.19 are from Venkataratnam and Rao [28] and correspond to a Type I system, but with tie lines sloping downward toward the extract side. Thus, although water is a convenient solvent, it does not have a high capacity, relative to ethyl acetate, for dissolving acetone. Also determine, for the feed, the maximum wt % acetone that can enter the extractor. This example and Example 8.2 are taken largely from an analysis by Sawistowski and Smith [29].

Solution

Point B represents the solvent-free raffinate. By drawing a straight line from B to S , the intersection with the equilibrium curve on the raffinate side, B' , is the raffinate composition leaving stage N .

Minimum S/F . Because the tie lines slope downward toward the extract side, the extrapolated tie line that intersects the extrapolated line \overline{SF} closest to point S is sought. This tie line, leading to P_{\min} , is shown in Figure 8.20. The intersection is not shown because it occurs far to the left of the diagram. Because this tie line is at the feed end of the extractor, location of extract composition D'_{\min} is found as shown in Figure 8.20. The mixing point, M_{\min} , for $(S/F)_{\min}$ is the intersection of lines $\overline{B'D'_{\min}}$ and \overline{SF} . By the inverse-lever-arm rule, $(S/F)_{\min} = \overline{FM}_{\min} / \overline{SM}_{\min}$.

Maximum S/F . If M in Figure 8.20 is moved along line \overline{FS} toward S , the intersection for $(S/F)_{\max}$ occurs at the point shown on the extract side of the binodal curve. By the inverse-lever-arm rule, using line \overline{FS} , $(S/F)_{\max} = \overline{FM}_{\max} / \overline{SM}_{\max} = 12$.

Equilibrium stages for other S/F ratios. First consider $S/F = 1.75$. In Figure 8.19, the composition of the saturated extract D' is obtained from an extractor material balance,

$$S + F = D' + B' = M$$

For $S/F = 1.75$, point M is located such that $\overline{FM} / \overline{MS} = 1.75$. A straight line must pass through D' , B' , and M . Therefore, D' is located by extending $\overline{B'M}$ to the extract envelope.

The difference point P is located to the left of the diagram. Therefore, $P = S - B' = D' - F$. It is located at the intersection of extensions of lines $\overline{FD'}$ and $\overline{B'S}$.

Step off stages, starting at D' , by following a tie line to L_1 . Then V_2 is located by noting the intersection of the operating line $\overline{L_1P}$ with the phase envelope. Additional stages are stepped off by alternating between the tie lines and operating lines. Only the first stage is shown; four are required.

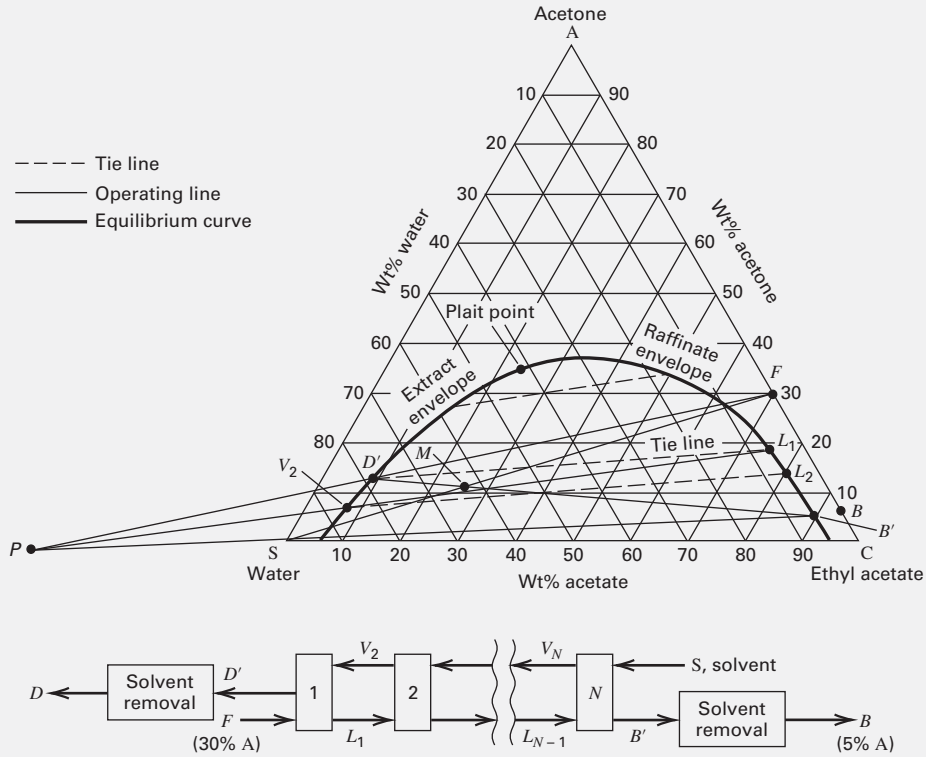


Figure 8.19 Determination of stages for Example 8.1 with $S/F = 1.75$.

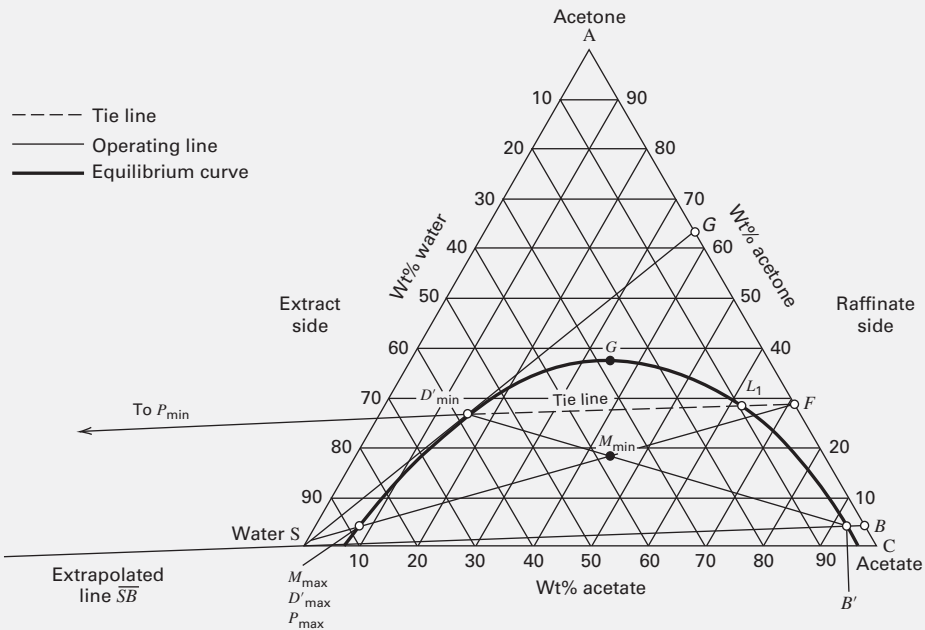


Figure 8.20 Minimum and maximum S/F for Example 8.1.

For $S/F = 5(S/F)_{\min} = 3.0$, M is determined and the stages are stepped off in a similar manner to give two equilibrium stages. In summary, for the countercurrent cascade:

S/F (solvent/feed ratio)	0.60	1.75	3	12
N (equilibrium stages)	∞	4	2	1
x_D (wt% acetone, solvent free)	64	62	50	30

If the wt% acetone in the feed mixture is increased from the base value of 30%, a feed composition will be reached that cannot be extracted because two liquid phases will not form (no phase splitting). This feed composition is determined by extending a line from S , tangent to the equilibrium curve, until it intersects \overline{AC} at point G in Figure 8.20. The feed composition is 64 wt% acetone. Feed mixtures with a higher acetone content cannot be extracted with water.

§8.3.3 Use of Right-Triangle Diagrams

Ternary countercurrent extraction calculations can also be made on a right-triangle diagram, using ordinary graph paper, as shown by Kinney [27]. No new principles are involved. The disadvantage is that mass-percent compositions of only two of the components are plotted; the third is determined, when needed, by the difference from 100%. An advantage of right-triangle diagrams is that either one of the coordinates can be expanded, if necessary, to increase construction accuracy.

Figure 8.21 shows a right-triangle diagram for the A-C-S system as in Figure 8.14. The compositions of S (the solvent) and A (the solute) are plotted in mass fractions, x_i .

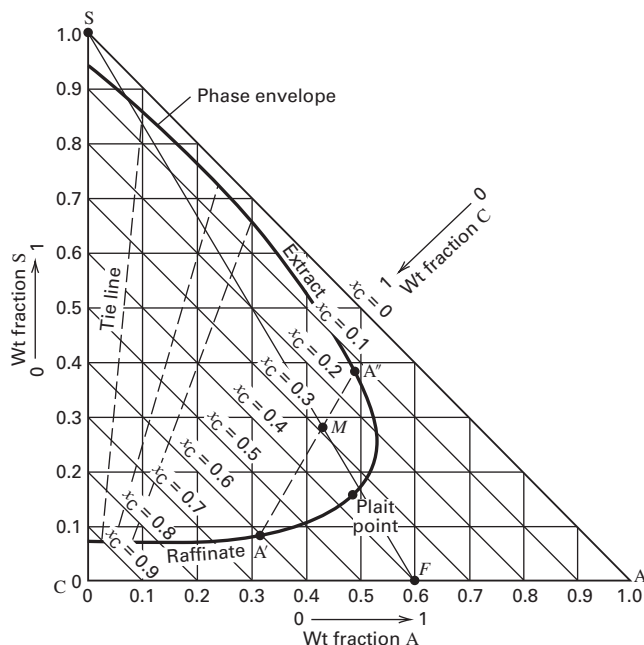


Figure 8.21 Right-triangle diagram for system of Figure 8.14.

For example, point M represents an overall liquid mixture of $(x_A = 0.43, x_S = 0.28)$. By calculation, x_C , which is not included in the diagram, is $1 - 0.43 - 0.28 = 0.29$. Although lines of constant x_C are included in Figure 8.21, they are usually omitted because they clutter the diagram. As with the equilateral-triangle diagram, the binodal curve is shown with extract and raffinate sides, tie lines connecting equilibrium phases, and the plait point.

Because point M falls within the phase envelope, the mixture separates into two liquid phases, given by points A' and A'' at the ends of the tie line passing through M . The extract at A'' is richer in the solute (A) and the solvent (S) than the raffinate at A' . Point M might be the result of mixing a feed, point F , consisting of 26,100 kg/h of 60 wt% A in C ($x_A = 0.6, x_S = 0$), with 10,000 kg/h of pure solvent, point S . The mixture splits into phases A' and A'' . The location of M and the amounts of extract and raffinate are given by the same mixing rule and inverse-lever-arm rule used for equilateral-triangle diagrams. The mixture separates spontaneously into 11,600 kg/h of raffinate ($x_S = 0.08, x_A = 0.32$) and 24,500 kg/h of extract ($x_S = 0.375, x_A = 0.48$).

Figure 8.22 represents the portion of an n -stage, countercurrent-flow cascade, where x and y are weight fractions of solute A in the raffinate and extract, respectively, and L and V are total amounts of raffinate and extract. The feed to stage N is $L_{N+1} = 180$ kg of 35 wt% of solute A in a saturated mixture with carrier C and solvent S (i.e., $x_{N+1} = 0.35$), and the solvent to stage 1 is $V_W = 100$ kg of pure S ($y_W = 0$). Thus, the solvent-to-feed ratio is $100/180 = 0.556$. These points are shown in Figure 8.23. The mixing point for L_{N+1} and V_W is M_1 , as determined by the inverse-lever-arm rule.

Suppose the final raffinate, L_W , leaving stage 1 is to contain $x_W = 0.05$. By an overall balance,

$$M_1 = V_W + L_{N+1} = V_N + L_W \quad (8-11)$$

Because V_W, L_{N+1} , and M_1 lie on a straight line, the mixing rule requires that V_N, L_W , and M_1 also lie on a straight line. Furthermore, because V_N leaves stage N at equilibrium and L_W

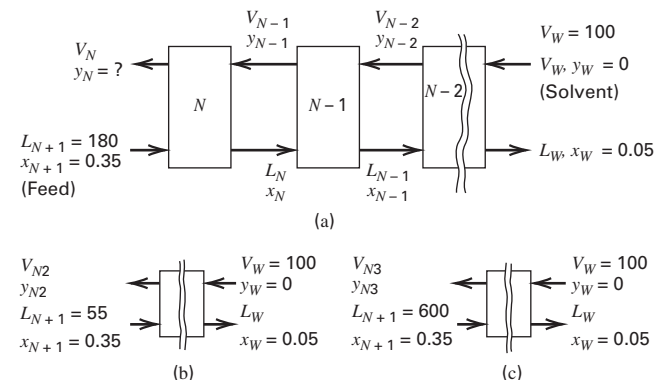


Figure 8.22 Multistage countercurrent contactors.

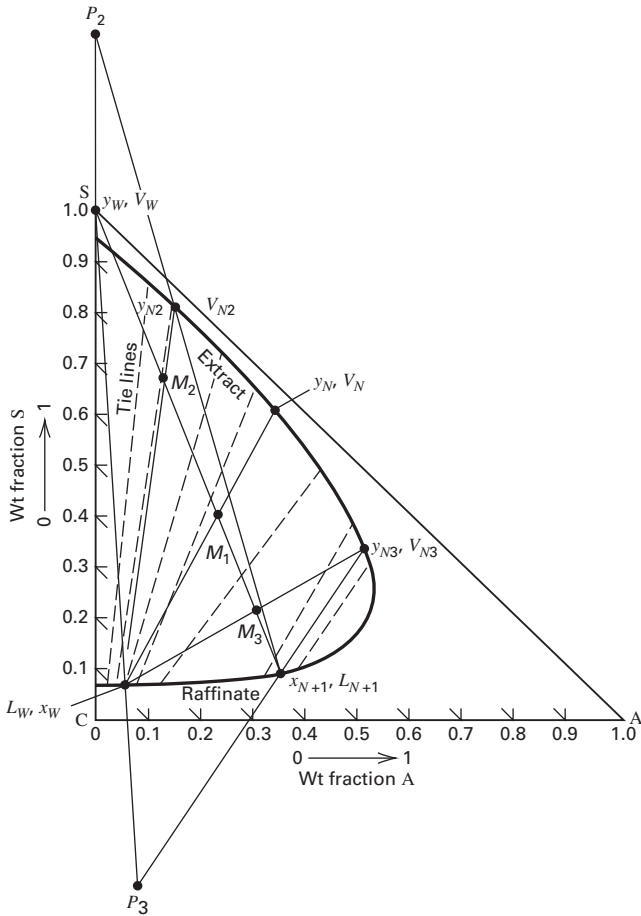


Figure 8.23 Right-triangle diagram constructions for cascade in Figure 8.22.

leaves stage 1 at equilibrium, these streams lie on the extract and raffinate sides, respectively, of the equilibrium curve. The resulting points are shown in Figure 8.23, where it is seen that the solute in the extract is $y_N = 0.34$.

Figures 8.22b and 8.22c include two additional cases of solvent-to-feed ratio, each with the same compositions for the solvent and feed, and the same value for x_W :

Case	Feed L_{N+1} , kg	Solvent, V_W , kg	Solvent-to-Feed Ratio	Extract Designation	Mixing Point
1	180	100	0.556	V_N	M_1
2	55	100	1.818	V_{N2}	M_2
3	600	100	0.167	V_{N3}	M_3

For case 2, a difference point, P_2 , is defined in terms of passing streams, as

$$P_2 = V_{N2} - L_{N+1} = V_W - L_W \quad (8-12)$$

In Figure 8.23, P_2 is at the top of the diagram, where $\overline{L_W V_W}$ and $\overline{L_{N+1} V_{N2}}$ intersect. For case 3, difference point P_3 lies at the bottom, where $\overline{L_W V_W}$ and $\overline{L_{N+1} V_{N3}}$ intersect.

Equilibrium stages for Figure 8.23 are stepped off as before by alternating the use of equilibrium tie lines and operating lines that pass through the difference point. Considering case 2, with a solvent-to-feed ratio of 1.818, and stepping off stages from stage N , a tie line from the point y_{N2} gives $x_N = 0.04$. But this is less than the specified $x_W = 0.05$, so only a fraction of a stage is required.

If stages are stepped off for case 3, starting from y_{N3} , the tie line and operating line coincide, giving a pinch point for a solvent-to-feed ratio of 0.167. Thus, this ratio is the minimum corresponding to ∞ equilibrium stages.

For case 1, where the solvent-to-feed ratio is between that of cases 2 and 3, the required number of stages lies between 1 and ∞ . The difference point and the steps for this case are not shown in Figure 8.23, but the difference point is located at a very large distance from the triangle because lines $\overline{L_W V_W}$ and $\overline{L_{N+1} V_{N2}}$ are nearly parallel. When the stages are stepped off, using operating lines parallel to $\overline{L_W V_W}$ between one and two stages are required.

§8.3.4 Extract Reflux

A two-section extraction cascade can be refluxed with extract, as in Figure 8.24. Stages are numbered from the solvent end of the process. L is used for raffinate flows and V for extract flows. Extract reflux, L_R , is provided by sending the extract, V_N , to a solvent-recovery step, which removes most of the solvent and gives a solute-rich solution, $L_R + D$, divided into product D and extract reflux L_R , which is returned to stage N . Raffinate reflux can also be provided, but its use has been judged to be of little benefit by Skelland [30].

A degrees-of-freedom analysis for a two-section cascade with extract reflux is conveniently carried out by using, as elements, two countercurrent cascades, a feed stage, a splitter, and a divider from Table 5.3. The result is $N_D = 2N + 3C + 13$. All but four of the specifications usually are:

Variable Specification	Number of Variables
Pressure at each stage	N
Temperature for each stage	N
Feed stream flow rate, composition, temperature, and pressure	$C + 2$
Solvent composition, temperature, and pressure	$C + 1$
Split of each component in the splitter (solvent-removal step)	C
Temperature and pressure of the two streams leaving the splitter	4
Pressure and temperature of the divider	2
	$2N + 3C + 9$

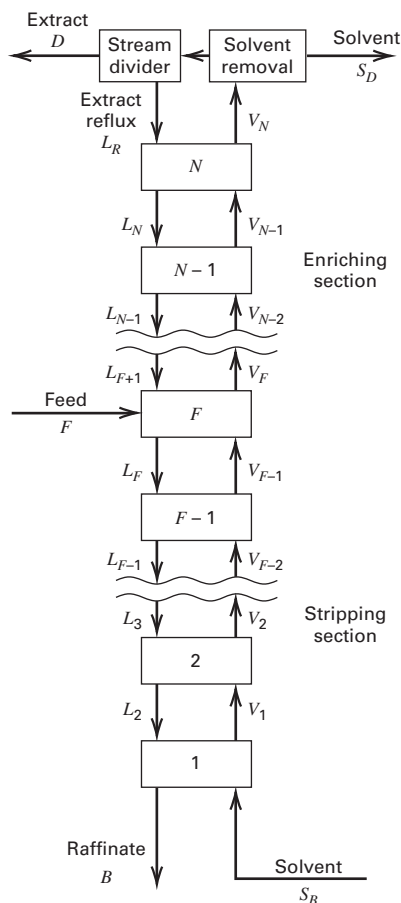


Figure 8.24 Liquid-liquid extraction with extract reflux.

The four additional specifications can be one of the following three sets:

Set 1	Set 2	Set 3
Solvent rate	Reflux ratio	Solvent rate
Solute concentration in extract (solvent-free)	Solute concentration in extract (solvent-free)	Reflux ratio
Solute concentration in raffinate (solvent-free)	Solute concentration in raffinate (solvent-free)	Number of stages
Optimal feed-stage location	Optimal feed-stage location	Feed-stage location

Sets 1 and 2 are of interest in the design of a new extractor because two specifications deal with products of designated purities. Set 2 is analogous to the design of a binary distillation, where purities of the distillate and bottoms, reflux ratio, and optimal feed-stage location are specified. For a single-section cascade, it is not feasible to specify the split of the feed with respect to two components. Instead, as in absorption and

stripping, recovery of just one component in the feed is specified.

A two-section cascade with extract reflux is particularly desirable for Type II ternary systems, as shown in Figure 8.10b. Without a plait point, the two-phase region extends across the entire solute composition. Thus, while solvent-free solute concentrations in the extract are limited for a Type I system, no such limit exists for a Type II system. It is thus possible, with extract reflux, to achieve as sharp a separation as desired between solute (A) and carrier (C). When reflux is used, many stages may be required and triangular diagrams become cumbersome. In that situation, it is preferred to carry out extraction calculations with a process simulator as discussed in Chapter 10.

§8.4 THEORY AND SCALE-UP OF EXTRACTOR PERFORMANCE

Industrial extraction equipment can be selected using the scheme of Figure 8.8. Often in the chemical industry, the choice is between a cascade of mixer-settlers and a multi-compartment column extractor with mechanical agitation, the main considerations being stages required, floor space and headroom available, and capital and operating costs. Methods for estimating size and power requirements for mixer-settler systems are described next. Size and performance of other type extraction equipment is considered only briefly because it is preferable to rely on the experience of vendors, who have pilot-plant equipment. Detailed theory of liquid-liquid extractors is found in Strigle [31], Thornton [32], and Rydberg [33].

§8.4.1 Mixer-Settler Units

Preliminary Sizing

Final mixer-settler unit design is done most accurately by scale-up from laboratory or pilot-plant equipment. However, preliminary sizing can be done using rules-of-thumb and available theory formulated in terms of correlations. Experimental data of Flynn and Treybal [34] show that when viscosities are less than 5 cP and the specific-gravity difference is greater than about 0.10, the average residence time required in the mixing vessel to achieve at least 90% stage efficiency may be as low as 30 s and is usually not more than 5 minutes, when an **agitator-power input of 1,000 ft-lb_f/min-ft³ (4 hp/1,000 gal)** is used.

As reported by Ryan, Daley, and Lowrie [35], the capacity of a settler vessel can be expressed in terms of C gpm of combined extract and raffinate per ft² of phase-disengaging area. For a horizontal, cylindrical vessel of length L and diameter D_T , the economic ratio of L to D_T is approximately 4. Thus, if the phase interface is located at the middle of the vessel, the disengaging area is $D_T L$ or $4D_T^2$. A typical value of C given by Happel and Jordan [36] is about 5. Frequently, the settling vessel will be larger than the mixing vessel, as is the case in the following example.

EXAMPLE 8.2 Preliminary Sizing of a Mixer-Settler Unit Using Rules-of-Thumb.

Benzoic acid is to be continuously extracted from a dilute solution in water using toluene in a series of mixer-settler vessels arranged for countercurrent flow of 500 gpm of feed and 750 gpm of solvent. Assuming a residence time, t_{res} , of 2 minutes in each mixer and a settling vessel capacity of 5 gal/min-ft², estimate: (a) diameter and height of each mixing vessel, assuming $H/D_T = 1$; (b) agitator horsepower for each mixing vessel; (c) diameter and length of each settling vessel, assuming $L/D_T = 4$; and (d) residence time in each settling vessel in minutes.

Solution

- (a) $Q = \text{total flow rate} = 500 + 750 = 1,250 \text{ gal/min}$
 $V = \text{volume} = Qt_{\text{res}} = 1,250(2) = 2,500 \text{ gal} (334 \text{ ft}^3)$
 $V = \pi D_T^2 H / 4$, $H = D_T$, and $V = \pi D_T^3 / 4$
 $D_T = (4V/\pi)^{1/3} = [(4)(334)/3.14]^{1/3}$
 $= 7.52 \text{ ft}$ and $H = 7.52 \text{ ft}$
- (b) Horsepower = $4(2,500/1,000) = 10 \text{ hp}$
- (c) $D_T L = 1,250/5 = 250 \text{ ft}^2$, $D_T^2 = 250/4 = 62.5 \text{ ft}^2$
 $D_T = 7.9 \text{ ft}$, $L = 4(7.9) = 31.6 \text{ ft}$
- (d) Volume of settler = $\pi D_T^2 L / 4 = 3.14(7.9^2)(31.6)/4 = 1,548 \text{ ft}^2$
 or $1,548(7.48) = 11,580 \text{ gal}$
 $t_{\text{res}} = V/Q = 11,580/1,250 = 9.3 \text{ min}$

Power Requirement of a Mixer Unit from a Correlation

Figure 8.25 shows a typical single-compartment mixing tank for liquid–liquid extraction. The vessel is closed, with the two liquid phases entering at the bottom, and the effluent, in the form of a two-phase emulsion, leaving at the top. Rounded heads of the type in Figure 8.2 are preferred, to eliminate stagnant fluid regions. All gas is evacuated from the vessel, so no gas–liquid interface exists.

Mixing is accomplished by an impeller selected from the many types available, some of which are displayed in Figure 8.3. For example, a flat-blade turbine is common, as in Figure 8.25. A single turbine is adequate unless the vessel height is greater than the vessel diameter, in which case a compartmented vessel with two or more impellers are employed. When the vessel is open, vertical side baffles are mandatory to prevent vortex formation at the gas–liquid interface. For closed vessels full of liquid, vortexing will not occur, but it is common to install baffles to minimize swirling and improve circulation. Although no standards exist for vessel and turbine geometry, the following rules of thumb, with reference to Figure 8.25, give good performance in liquid–liquid agitation:

- Number of turbine blades = 6
- Number of vertical baffles = 4
- Vessel height-to-vessel diameter = $H/D_T = 1$

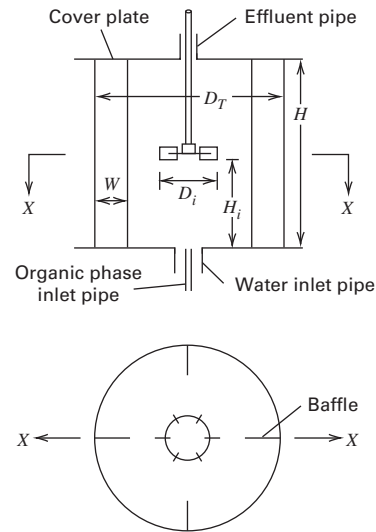


Figure 8.25 Agitated vessel with flat-blade turbine and baffles.

Impeller diameter-to-vessel diameter = $D_i/D_T = 1/3$

Baffle width-to-vessel diameter = $W/D_T = 1/12$

Vertical distance of impeller above vessel bottom-to-vessel height = $H_i/H = 1/2$

To achieve a high extraction efficiency, say, between 90 and 100%, it is necessary to provide vigorous agitation. For a given type of impeller and vessel impeller geometry, the agitator power, P , can be estimated from an empirical correlation in terms of a dimensionless power number, N_{Po} , which depends on an impeller Reynolds number, N_{Re} :

$$N_{Po} = \frac{P g_c}{N^3 D_i^5 \rho_M} \quad (8-13)$$

$$N_{Re} = \frac{D_i^2 N \rho_M}{\mu_M} \quad (8-14)$$

where AE units are: P in ft-lb_f/h; g_c = conversion factor = $4.17 \times 10^8 \text{ lb}_m\text{-ft}/(\text{lb}_f\text{-h}^2)$; N = impeller rotation rate in revolutions/h (rph); D_i = impeller diameter in ft; ρ_M = liquid mixture density in lb_m/ft³; μ_M = liquid mixture viscosity in lb_m/ft-h; with lb_f = lb force and lb_m = lb mass.

The impeller Reynolds number is the ratio of the inertial force to the viscous force, with inertial force proportional to $(ND_i)^2 \rho_M D_i^2$ and viscous force proportional to $\mu_M (ND_i) D_i^2 / D_i$. Thus, the characteristic length in the Reynolds number is the impeller diameter, D_i , and the characteristic velocity is ND_i = impeller peripheral velocity.

The agitator power for a mixer is proportional to the product of volumetric liquid flow produced by the impeller and the applied kinetic energy per unit volume of fluid. The result is: power, P , is proportional to $(ND_i^3)[\rho_M (ND_i)^2 / 2g_c]$, which can be rewritten as (8-13), where the constant of proportionality is $2N_{Po}$. The power number for an agitated vessel serves the same purpose as the friction factor for flow of fluid through a pipe. This is illustrated, over a wide range of impeller Reynolds numbers in Figure 8.26a, taken from

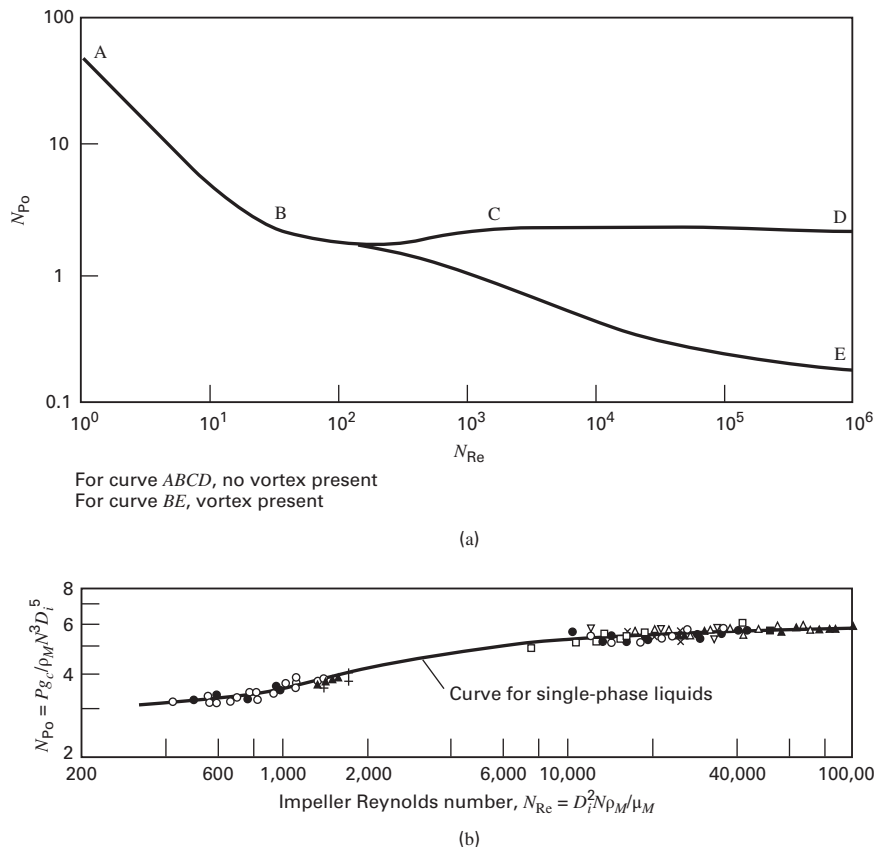


Figure 8.26 Power consumption of agitated vessels. (a) Typical power characteristics. [Reproduced from [37] with permission of John Wiley & Sons.] (b) Power correlation for six-bladed, flat-blade turbines with no vortex. [Reproduced from [38] with permission of the American Institute of Chemical Engineers.]

Rushton and Oldshue [37]. The upper curve, ABCD, is for a vessel with baffles, while the lower curve, ABE, pertains to the same tank with no baffles. In the low Reynolds-number region, AB, viscous forces dominate and the impeller power is proportional to $\mu_M N^2 D_i^3$. Beyond a Reynolds number of about 200, a vortex appears if no baffles are present and the power-number relation is given by BE. In this region, the Froude number, $N_{Fr} = N^2 D_i / g$ (the ratio of inertial to gravitational forces) also becomes a factor. With baffles, and $N_{Re} > 1,000$ for region CD, fully developed turbulence exists, inertial forces dominate, and the power is proportional to $\rho_M N^3 D_i^5$. Baffles greatly increase power requirements.

Figure 8.26b, from Laity and Treybal [38] shows experimental data for liquid–liquid mixing in baffled vessels with six-bladed, flat-blade turbines. The impeller Reynolds number covers only the turbulent-flow region, where there is efficient liquid–liquid mixing. The solid line represents batch mixing of single-phase liquids. The data represent liquid–liquid mixing, where agreement with the single-phase curve is achieved by computing two-phase mixture properties from

$$\rho_M = \rho_C \phi_C + \rho_D \phi_D \quad (8-15)$$

$$\mu_M = \frac{\mu_C}{\phi_C} \left(1 + \frac{1.5 \mu_D \phi_D}{\mu_C + \mu_D} \right) \quad (8-16)$$

where ϕ is the volume fraction of tank holdup, with subscripts C for the continuous phase and D the dispersed phase, such that $\phi_D + \phi_C = 1$. For continuous flow from inlets at the bottom of the vessel to a top outlet for the emulsion and with the

impeller located at a position above the resting interface, the data correlate with Figure 8.26b.

With fully developed turbulent flow, the volume fraction of a dispersed phase in the vessel closely approximates that in the feed; otherwise, the volume fractions may be different, and the residence times of the two phases in the tank will not be identical. At best, spheres of uniform size can pack tightly to give a void fraction of 0.26. Therefore, $\phi_C > 0.26$ and $\phi_D < 0.74$ is quoted, but some experiments have shown a 0.20–0.80 range. At startup, the vessel is filled with the phase to be continuous. Following initiation of agitation, the two feed liquids are introduced at their desired flow ratio.

Based on the work of Skelland and Ramsey [39] and Skelland and Lee [40], a minimum impeller rotation rate, N_{min} , is required for uniform dispersion of one liquid into another. For a flat-blade turbine in a baffled vessel, their equation in terms of dimensionless groups is:

$$\frac{N_{min}^2 \rho_M D_i}{g \Delta \rho} = 1.03 \left(\frac{D_T}{D_i} \right)^{2.76} \phi_D^{0.106} \left(\frac{\mu_M^2 \sigma}{D_i^5 \rho_M g^2 (\Delta \rho)^2} \right)^{0.084} \quad (8-17)$$

where in AE units, $g = 4.17 \times 10^8$ ft/h², $\Delta \rho$ is the absolute value of the density difference in lb_m/ft³, and σ is the interfacial tension between the liquid phases in lb_m/h². The group on the left side of (8-17) is a two-phase Froude number; the group at the far right is a ratio of forces:

$$\frac{(\text{viscous})^2 (\text{interfacial tension})}{(\text{inertial}) (\text{gravitational})^2}$$

EXAMPLE 8.3 Design of a Mixer Extraction Unit.

Furfural is extracted from water by toluene at 25°C in an agitated vessel like the one in Figure 8.25. The feed enters at 20,400 lb/h, while the solvent enters at 11,200 lb/h. For a residence time, t_{res} of 2 minutes, estimate, for either phase as the dispersed phase: (a) dimensions of the mixing vessel and diameter of the flat-blade turbine impeller; (b) minimum rate of rotation of the impeller for complete and uniform dispersion; (c) the power requirement of the agitator at the minimum rotation rate.

Solution

Mass flow rate of feed, $F = 20,400$ lb/h; feed density = 62.3 lb/ft³;

Volumetric flow rate of feed = $Q_F = 20,400/62.3 = 327$ ft³/h;

Mass flow rate of solvent, $S = 11,200$ lb/h; solvent density = 54.2 lb/ft³;

Volumetric flow rate of solvent = $Q_S = 11,200/54.2 = 207$ ft³/h

Because the solute in the feed is dilute and there is sufficient agitation to achieve uniform dispersion, assume that fractional volumetric holdups of raffinate, R , and extract, E , in the vessel are equal to the corresponding volume fractions in the combined feed. Thus,

$$\phi_R = 327/(327 + 207) = 0.612; \phi_E = 1 - 0.612 = 0.388$$

(a) Mixer volume = $(Q_F + Q_S)t_{\text{res}} = V = (327 + 207)(2/60) = 17.8$ ft³.

Assume a cylindrical vessel with $D_T = H$ and neglect the volume of the bottom and top heads and the volume occupied by the agitator and the baffles. Then

$$V = (\pi D_T^2/4)H = \pi D_T^3/4$$

$$D_T = [(4/\pi)V]^{1/3} = [(4/3.14)17.8]^{1/3} = 2.83 \text{ ft}$$

$$H = D_T = 2.83 \text{ ft}$$

Make the vessel 3 ft in diameter by 3 ft high, which gives a volume $V = 21.2$ ft³ = 159 gal. Assume that $D_i/D_T = 1/3$; $D_i = D_T/3 = 3/3 = 1$ ft.

(b) **Case 1—Raffinate phase dispersed:**

$$\phi_D = \phi_R = 0.612; \phi_c = \phi_E = 0.388;$$

$$\rho_D = \rho_R = 62.3 \text{ lb/ft}^3; \rho_C = \rho_E = 54.2 \text{ lb/ft}^3;$$

$$\mu_D = \mu_R = 0.89 \text{ cP} = 2.16 \text{ lb/h-ft};$$

$$\mu_C = \mu_E = 0.59 \text{ cP} = 1.43 \text{ lb/h-ft};$$

$$\Delta\rho = 62.3 - 54.2 = 8.1 \text{ lb/ft}^3;$$

$$\sigma = 25 \text{ dyne/cm} = 719,000 \text{ lb/h}^2$$

where all lb are lb_m.

From (8-15),

$$\rho_M = (54.2)(0.388) + (62.3)(0.612) = 59.2 \text{ lb/h-ft}$$

From (8-16),

$$\mu_M = \frac{1.43}{0.388} \left(1 + \frac{1.5(2.16)(0.612)}{1.43 + 2.16} \right) = 5.72 \text{ lb/h-ft}$$

From (8-17), using AE units, with $g = 4.17 \times 10^8$ ft/h²,

$$\frac{\mu_M^2 \sigma}{D_i^5 \rho_M g^2 (\Delta\rho)^2} = \frac{(5.72)^2 (719,000)}{(1)^5 (59.2) (4.17 \times 10^8)^2 (8.1)^2} = 3.47 \times 10^{-14}$$

$$N_{\text{min}}^2 = 1.03 \left(\frac{g \Delta\rho}{\rho_M D_i} \right) \left(\frac{D_T}{D_i} \right)^{2.76} \phi_D^{0.106} \left(\frac{\mu_M^2 \sigma}{D_i^5 \rho_M g^2 (\Delta\rho)^2} \right)^{0.084}$$

$$= 1.03 \left(\frac{(4.17 \times 10^8) (8.1)}{(59.2)(1)} \right) \left(\frac{3}{1} \right)^{2.76} (0.612)^{0.106} (3.47 \times 10^{-14})^{0.084}$$

$$= 8.56 \times 10^7 \text{ rph}^2$$

$$N_{\text{min}} = 9,250 \text{ rpm} = 155 \text{ rpm}$$

where, rpm = revolutions per minute.

Case 2—Extract phase dispersed:

Calculations similar to Case 1 above result in $N_{\text{min}} = 8,820$ rpm = 147 rpm.

(c) **Case 1—Raffinate phase dispersed:**

From (8-14),

$$N_{\text{Re}} = \frac{(1)^2 (9,250) (59.2)}{5.72}$$

From Figure 8.26b, a fully turbulent flow exists, with the power number given by its asymptotic value of $N_{\text{Po}} = 5.7$.

From (8-13),

$$P = \frac{N_{\text{Po}} N^3 D_i^5 \rho_M}{g_c} = \frac{5.7(9,250)^3 (1)^5 (59.2)}{(4.17 \times 10^5)}$$

$$= 640,000 \text{ ft-lb}_f/\text{h}$$

$$P/V = 0.323(1,000)/159 = 2.0 \text{ hp/1,000 gal}$$

Case 2—Extract phase dispersed:

Calculations as in case 1 result in $P = 423,000$ ft-lb_f/h = 0.214 hp.

$$\text{Power per unit volume} = P/V = 0.214(1,000)/159 = 1.4 \text{ hp/1,000 gal.}$$

Mass-Transfer Efficiency

When dispersion is complete, both phases in the vessel are perfectly mixed, and the solute concentrations in each phase are uniform and equal to the concentrations in the two-phase emulsion leaving the vessel. This is the CFSTR or CSTR (continuous-flow stirred-tank reactor) model used in chemical reactor design, sometimes called the completely back-mixed or perfectly mixed model, first discussed by MacMullin and Weber [41]. The Murphree dispersed-phase efficiency for extraction, based on the raffinate as the dispersed phase, is expressed as the fractional approach to equilibrium. In terms of solute,

$$E_{MD} = \frac{c_{D,\text{in}} - c_{D,\text{out}}}{c_{D,\text{in}} - c_D^*} \quad (8-18)$$

where c_D^* is the fictitious solute concentration in equilibrium with the bulk-solute concentration in the exiting continuous phase, $c_{C,out}$. The molar rate of solute mass transfer, n , from the dispersed phase to the continuous phase is

$$n = K_{OD}a(c_{D,out} - c_D^*)V \quad (8-19)$$

where the mass-transfer driving force is uniform throughout the vessel and equal to the driving force based on exit concentrations; a is the interfacial area for mass transfer per unit volume of liquid phases; V is the total volume of liquid in the vessel; and K_{OD} is the overall mass-transfer coefficient based on the dispersed phase, given in terms of the resistances of the dispersed and continuous phases by

$$\frac{1}{K_{OD}} = \frac{1}{k_D} + \frac{1}{mk_C} \quad (8-20)$$

where equilibrium is assumed at the interface between the phases and m = the slope of the equilibrium curve for the solute, plotted as c_C versus c_D :

$$m = dc_C/dc_D \quad (8-21)$$

For dilute solutions, changes in volumetric flow rates of raffinate and extract are small, and the rate of solute mass transfer, n , based on the change in solute concentration in the dispersed phase is:

$$n = Q_D (c_{D,in} - c_{D,out}) \quad (8-22)$$

where Q_D is the volumetric flow rate of the dispersed phase. To obtain an expression for E_{MD} in terms of $K_{OD}a$, (8-18), (8-19), and (8-22) are combined to give

$$\frac{E_{MD}}{1 - E_{MD}} = \frac{c_{D,in} - c_{D,out}}{c_{D,out} - c_D^*} \quad (8-23)$$

Equating (8-19) and (8-22), and noting that the RHS of (8-23) is the number of dispersed-phase transfer units for a perfectly mixed vessel with $c_D = c_{D,out}$

$$N_{OD} = \int_{c_{D,out}}^{c_{D,in}} \frac{dc_D}{c_D - c_D^*} = \frac{c_{D,in} - c_{D,out}}{c_{D,out} - c_D^*} = \frac{K_{OD}aV}{Q_D} \quad (8-24)$$

Combining (8-23) and (8-24) and solving for E_{MD} ,

$$E_{MD} = \frac{K_{OD}aV/Q_D}{1 + K_{OD}aV/Q_D} = \frac{N_{OD}}{1 + N_{OD}} \quad (8-25)$$

When $N_{OD} = K_{OD}aV/Q_D \gg 1$, $E_{MD} = 1$.

Drop Size and Interfacial Area

Estimates of E_{MD} require experimental data for interfacial area, a , and mass-transfer coefficients k_D and k_C . The droplets in an agitated vessel cover a range of sizes and shapes; hence, it is useful to define d_e , the equivalent diameter of a spherical drop, using the method of Lewis, Jones, and Pratt [42],

$$d_e = (d_1^2 d_2)^{1/3} \quad (8-26)$$

where d_1 and d_2 are major and minor axes of an ellipsoidal-drop image. For a spherical drop, d_e is simply the drop diameter. For the drop population, it is necessary to define

an average drop diameter as weight-mean, mean-volume, surface-mean, mean-surface, length-mean, or mean-length diameter [43]. For mass transfer calculations, the surface-mean diameter, d_{vs} (also called the **Sauter mean diameter**), is appropriate because it is the mean drop diameter that gives the same interfacial surface area as the entire population of drops for the same mass of drops. It is determined from drop-size distribution data for N drops by:

$$\frac{\pi d_{vs}^2}{(\pi/6)d_{vs}^3} = \frac{\pi \sum_N d_e^2}{(\pi/6) \sum_N d_e^3}$$

which, when solved for d_{vs} , gives

$$d_{vs} = \frac{\sum_N d_e^3}{\sum_N d_e^2} \quad (8-27)$$

With this definition, the interfacial surface area per unit volume of a two-phase mixture is

$$a = \frac{\pi N d_{vs}^2 \phi_D}{(\pi/6) N d_{vs}^3} = \frac{6\phi_D}{d_{vs}} \quad (8-28)$$

Equation (8-28) is used to estimate the interfacial area, a , from a measurement of d_{vs} or vice versa. Early experimental investigations, such as those of Vermeulen, Williams, and Langlois [44], found that d_{vs} depends on a Weber number:

$$N_{We} = \frac{(\text{inertial force})}{(\text{interfacial tension force})} = \frac{D_i^3 N^2 \rho_C}{\sigma} \quad (8-29)$$

High Weber numbers give small droplets and high interfacial areas. Gnanasundaram, Degaleesan, and Laddha [45] correlated d_{vs} over a wide range of N_{We} . Below $N_{We} = 10,000$, d_{vs} depends on dispersed-phase holdup, ϕ_D , because of coalescence effects. For $N_{We} > 10,000$, inertial forces dominate so that coalescence effects are less prominent and d_{vs} is almost independent of holdup up to $\phi_D = 0.5$. The correlations are

$$\frac{d_{vs}}{D_i} = 0.052(N_{We})^{-0.6} e^{4\phi_D}, N_{We} < 10,000 \quad (8-30)$$

$$\frac{d_{vs}}{D_i} = 0.39(N_{We})^{-0.6}, N_{We} > 10,000 \quad (8-31)$$

Typical values of N_{We} for industrial extractors are less than 10,000, so (8-30) applies. Values of d_{vs}/D_i are frequently in the range of 0.0005 to 0.01.

Studies like those of Chen and Middleman [46] and Sprow [47] show that dispersion in an agitated vessel is dynamic. Droplet breakup by turbulent pressure fluctuations dominates near the impeller blades, while for a reasonable dispersed-phase holdup, coalescence of drops by collisions dominates away from the impeller. Thus, there is a distribution of drop sizes, with smaller drops in the vicinity of the impeller and larger drops elsewhere. When both drop breakup and coalescence occur, the drop-size distribution is such that $d_{\min} \approx d_{vs}/3$ and $d_{\max} \approx 3 d_{vs}$. Thus, the drop size varies over about a 10-fold range, approximating a Gaussian distribution.

EXAMPLE 8.4 Droplet Size and Interfacial Area.

For the conditions and results of Example 8.3, with the extract phase dispersed, estimate the Sauter mean drop diameter, the range of drop sizes, and the interfacial area.

Solution

$$D_i = 1 \text{ ft}; N = 147 \text{ rpm} = 8,820 \text{ rpm}; \\ \rho_C = 62.3 \text{ lb/ft}^3; \sigma = 718,800 \text{ lb/h}^2$$

From (8-29),

$$N_{We} = (1)^3(8,820)^2(62.3)/718,800 = 6,742; \phi_D = 0.338$$

From (8-30),

$$d_{vs} = (1)(0.052)(6,742)^{-0.6} \exp[4(0.338)] = 0.00124 \text{ ft}$$

and

$$(0.00124)(12)(25.4) = 0.38 \text{ mm}$$

$$d_{\min} = d_{vs}/3 = 0.126 \text{ mm}; \quad d_{\max} = 3d_{vs} = 1.134 \text{ mm}$$

From (8-28),

$$a = 6(0.388)/0.00124 = 1,880 \text{ ft}^2/\text{ft}^3$$

Mass-Transfer Coefficients

Mass transfer in agitated liquid–liquid systems is complex. It must take into account what is happening (1) in the dispersed-phase droplets, (2) in the continuous phase, and (3) at the interface. The magnitude of k_D depends on drop diameter, solute diffusivity, and fluid motion within the drop. According to Davies [48], when drop diameter is small (less than 1 mm), interfacial tension is high (> 15 dyne/cm), and trace amounts of surface-active agents are present, droplets are rigid (internally stagnant) and behave like solids. As droplets enlarge, interfacial tension decreases, surface-active agents become ineffective, and internal toroidal fluid circulation patterns, caused by viscous drag of the continuous phase, appear within the drops. For larger-diameter drops, the shape of the drop oscillates between spheroid and ellipsoid or other shapes.

Continuous-phase mass-transfer coefficients, k_C , depend on the motion between the droplets and the continuous phase, and whether the drops are forming, breaking, or coalescing. Interfacial movements or turbulence, called Marangoni effects, occur due to interfacial-tension gradients, which induce increases in mass-transfer rates.

A conservative estimate of the overall mass-transfer coefficient, K_{OD} , in (8-20) can be made from estimates of k_D and k_C by assuming rigid drops, the absence of Marangoni effects, and a stable drop size. For k_D , the asymptotic steady-state solution for mass transfer in a rigid sphere with negligible surrounding resistance is given by Treybal [25] as

$$(N_{Sh})_D = \frac{k_D d_{vs}}{D_D} = \frac{2}{3} \pi^2 = 6.6 \quad (8-32)$$

where D_D is the solute diffusivity in a dispersed phase droplet and N_{Sh} is the Sherwood number.

Exercise 3.28 in Chapter 3 for diffusion from the surface of a sphere into an infinite, quiescent fluid gives the continuous-phase Sherwood number as:

$$(N_{Sh})_C = \frac{k_C d_{vs}}{D_C} = 2 \quad (8-33)$$

where d_{vs} is the surface-mean droplet diameter from (8-27) and D_C is the solute diffusivity in the continuous-phase. However, if other spheres of equal diameter are located near the sphere of interest, $(N_{Sh})_C$ may decrease to a value as low as 1.386, according to Cornish [49]. In an agitated vessel, $(N_{Sh})_C > 1.386$. An estimate can be made with the correlation of Skelland and Moeti [50], which fits data for three different solutes, three different dispersed organic solvents, and water as the continuous phase. Mass transfer was from the dispersed phase to the continuous phase, but only for $\phi_D = 0.01$. They assumed a proportionality of the form

$$(N_{Sh})_C \propto (N_{Re})_C^y (N_{Sc})_C^x \quad (8-34)$$

where

$$(N_{Sh})_C = k_C d_{vs} / D_C \quad (8-35)$$

$$(N_{Sc})_C = \mu_C / \rho_C D_C \quad (8-36)$$

For the Reynolds number, they assume the characteristic velocity to be the square root of the mean-square, local fluctuating velocity in the droplet vicinity based on the theory of local isotropic turbulence of Batchelor [51], who uses the following proportionality:

$$\bar{u}^2 \propto \left(\frac{Pg_C}{V} \right)^{2/3} \left(\frac{d_{vs}}{\rho_C} \right)^{2/3} \quad (8-37)$$

Thus,

$$(N_{Re})_C = \frac{(\bar{u}^2)^{1/2} d_{vs} \rho_C}{\mu_C} \quad (8-38)$$

Combining (8-37) and (8-38) and dropping the proportionality constant, \propto ,

$$(N_{Re})_C = \frac{d_{vs}^{4/3} \rho_C^{2/3} (Pg_C/V)^{1/3}}{\mu_C} \quad (8-39)$$

where P = power and V = volume of the mixing vessel.

As discussed previously in conjunction with Figure 8.26, in the turbulent-flow region, the following proportionalities exist:

$$Pg_C \propto \rho_M N^3 D_i^5 \text{ or for low } \phi_D, Pg_C/V \propto \rho_C N^3 D_i^5 D_T^3$$

Thus,

$$(N_{Re})_C = \frac{d_{vs}^{4/3} \rho_C N D_i^{5/3}}{\mu_C D_T} \quad (8-40)$$

Skelland and Moeti correlated the mass-transfer coefficient data with

$$(N_{Sh})_C = \frac{k_C d_{vs}}{D_C} = 1.237 \times 10^{-5} \left(\frac{\mu_C}{\rho_C D_C} \right)^{1/3} \\ \times \left(\frac{D_i^2 N \rho_C}{\mu_C} \right)^{2/3} \phi_D^{-1/2} \left(\frac{D_i N^2}{g} \right)^{5/12} \\ \times \left(\frac{D_i}{d_{vs}} \right)^2 \left(\frac{d_{vs}}{D_T} \right)^{1/2} \left(\frac{\rho_D d_{vs}^2 g}{\sigma} \right)^{5/4} \quad (8-41)$$

Where the last dimensionless group on the RHS is a droplet Eotvos number, N_{Eo} , = gravitational force/surface tension force. Equation (8-41) correlates 180 data points for an average deviation of 19.71%.

EXAMPLE 8.5 Mass Transfer in a Mixer.

For the system, conditions, and results of Examples 8.3 and 8.4, with the extract as the dispersed phase, estimate the:

- dispersed-phase mass-transfer coefficient, k_D ;
- continuous-phase mass-transfer coefficient, k_C ;
- Murphree dispersed-phase efficiency, E_{MD} ; and
- fractional extraction of furfural.

The molecular diffusivities of furfural in toluene (dispersed) and water (continuous) at dilute conditions are $D_D = 8.32 \times 10^{-5}$ ft²/h and $D_C = 4.47 \times 10^{-5}$ ft²/h. The slope of the distribution coefficient for dilute conditions is $m = 0.0985$.

Solution

- From (8-32), $k_D = 6.6(D_D)/d_{vs} = 6.6(8.32 \times 10^{-5})/0.00124 = 0.44$ ft/h.
- To apply (8-41) to the estimation of k_C , first compute each dimensionless group:

$$N_{Sc} = \mu_C/\rho_C D_C = 2.156/[(62.3)(4.47 \times 10^{-5})] = 777$$

$$N_{Re} = D_i^2 N \rho_C/\mu_C = (1)^2(8,820)(62.3)/2.165 = 254,000$$

$$N_{Fr} = D_i N^2/g = (1)(8,820)^2/(4.17 \times 10^8) = 0.187$$

$$D_i/d_{vs} = 1/0.00124 = 806; d_{vs}/D_T = 0.00124/3 = 0.000413$$

$$N_{Eo} = \rho_D d_{vs}^2 g/\sigma = (54.2)(0.00124)^2(4.17 \times 10^8)/718,800 = 0.0483$$

From (8-41), the Sherwood number for the continuous phase is,

$$N_{Sh} = 1.237 \times 10^{-5}(777)^{1/3}(254,000)^{2/3}(0.388)^{-1/2}(0.187)^{5/12} \times (806)^2(0.000413)^{1/2}(0.0483)^{5/4} = 109$$

which is much greater than 2 for a quiescent fluid.

$$k_C = N_{Sh} D_C/d_{vs} = (109)(4.47 \times 10^{-5})/0.00124 = 3.93 \text{ ft/h}$$

- From (8-20) and the results of Example 8.4,

$$K_{OD} a = \left\{ \frac{1}{1/0.44 + 1/[(0.0985)(3.93)]} \right\} 1,880 = 387 \text{ h}^{-1}$$

From (8-24), with $V = \pi D_T^2 H/4 = (3.14)(3)^2(3)/4 = 21.2$ ft³,

$$N_{OD} = K_{OD} a V/Q_D = 387(212)/207 = 39.6$$

From (8-25),

$$E_{MD} = N_{OD}/(1 + N_{OD}) = 39.6/(1 + 39.6) = 0.975 = 97.5\%$$

- By material balance,

$$Q_C(c_{C,in} - c_{C,out}) = Q_D c_{D,out} \quad (1)$$

From (8-18),

$$E_{MD} = c_{D,out}/c_D^* = m c_{D,out}/c_{C,out} \quad (2)$$

Combining (1) and (2) to eliminate $c_{D,out}$ gives

$$\frac{c_{C,out}}{c_{C,in}} = \frac{1}{1 + Q_D E_{MD}/(Q_C m)} \quad (3)$$

and

$$f_{\text{extracted}} = \frac{c_{C,in} - c_{C,out}}{c_{C,in}} = 1 - \frac{c_{C,out}}{c_{C,in}} = \frac{Q_D E_{MD}/(Q_C m)}{1 + Q_D E_{MD}/(Q_C m)}$$

$$\frac{Q_D E_{MD}}{Q_C m} = \frac{(207)(0.975)}{(327)(0.0985)} = 6.27$$

Thus,

$$f_{\text{extracted}} = \frac{6.27}{1 + 6.27} = 0.862 \text{ or } 86.2\%$$

§8.4.2 Column Extractors

An extraction column, with or without mechanical agitation, is sized by determining its diameter and height. Column diameter must be large enough to permit the liquid phases to flow through the column countercurrently without flooding. Column height must be equivalent to the number of required equilibrium stages to achieve the desired extraction. In this section, only preliminary sizing is considered. Final sizing is best determined by the vendor supplying the extraction column.

For small columns, preliminary estimates of the diameter and height can be made using the results of Stichlmair [52] with toluene–acetone–water for $Q_D/Q_C = 1.5$. Typical ranges of 1/HETS and the operating capacity equal to the sum of the superficial phase velocities for extraction columns are given in Table 8.5. The typical operating capacities in Table 8.5 are considerably lower than the maximum capacities given in Table 8.2. Note that m³ of combined liquid phases per hour per m² of inside cross-sectional area of the column, as listed in Table 8.2, is the same as the sum of the superficial velocities $U_D + U_C$ of the two liquid phases, as listed in Table 8.5.

Column Diameter. An accurate assessment of column diameter for liquid–liquid extractors is more difficult than that for

Table 8.5 Performance of Several Types of Column Extractors

Extractor Type	1/HETS, m ⁻¹	$U_D + U_C$, m/h
Packed column	1.5–2.5	12–30
Pulsed packed column	3.5–6	17–23
Sieve-tray column	0.8–1.2	27–60
Pulsed-tray column	0.8–1.2	25–35
Scheibel column	5–9	10–14
RDC	2.5–3.5	15–30
Kuhni column	5–8	8–12
Karr column	3.5–7	30–40
RTL contactor	6–12	1–2

[Reproduced from [52] with permission of John Wiley & Sons.]

vapor–liquid contactors because of the importance of additional factors, including phase-density differences, interfacial tension, rotating or reciprocating speed of internal agitation devices, and the geometry of these internals. Column diameter is best determined by scale-up from laboratory or pilot-plant units. In general, the sum of the absolute superficial velocities of the liquid phases in the test unit is assumed to hold for commercial units.

EXAMPLE 8.6 Diameter of an RDC.

Estimate the diameter of an RDC to extract acetone from a dilute mixture with toluene into water at 20°C. The flow rates for the dispersed organic and continuous aqueous phases are 12,250 and 11,300 kg/h, respectively. Assume the liquid densities are $\rho_C = 1,000 \text{ kg/m}^3$, $\rho_D = 867 \text{ kg/m}^3$.

Solution

The volumetric flow rates are:

$$Q_C = 11,300/1,000 = 11.3 \text{ m}^3/\text{h}, \quad Q_D = 12,250/867 \\ = 14.1 \text{ m}^3/\text{h}$$

$$Q_C + Q_D = 11.3 + 14.1 = 25.4 \text{ m}^3/\text{h}$$

From Table 8.5, the RDC typical operating capacity is from 15 to 30 $\text{m}^3/\text{m}^2\text{-h}$.

From Table 8.2, the maximum RDC capacity = 40 $\text{m}^3/\text{m}^2\text{-h}$.

Column cross-sectional area in $\text{m}^2 = A_T = 25.4/\text{Capacity}$.

For typical operation, $A_T = 25.4/15$ to $25.4/30 = 1.693$ to 0.847 m^2 .

Column diameter for typical operation = $D_T = \sqrt{\frac{4A_T}{\pi}}$ = from 1.468 to 1.038 m or 4.82 ft to 3.41 ft

Minimum column cross-sectional area = $A_T = 25.4/40 = 0.635 \text{ m}^2$

Minimum column diameter = 0.900 m = 2.95 ft

A vendor suggested a diameter of 4 ft.

Column Height. Despite compartmentalization, mechanically assisted liquid–liquid extraction columns, such as the RDC and Karr columns, operate more like differential devices than staged contactors. Therefore, it is common to consider stage efficiency for such columns in terms of height equivalent to a theoretical stage (HETS). While not theoretically based, HETS is preferred because it can be used to determine column height from the number of equilibrium stages.

The large number of variables that influence efficiency have made general correlations for HETS difficult to develop. However, for well-designed and efficiently operated columns, data indicate that the dominant physical properties influencing HETS are interfacial tension, viscosities, and density difference between the phases. In addition, observations by Reman [59] for RDC units, and by Karr and Lo [60] for Karr columns, show that HETS increases with increasing column diameter because of axial mixing.

A prudent procedure for determining column height is to obtain values of HETS from small-scale laboratory experiments and scale these values to commercial-size columns by assuming that HETS varies with column diameter D_T raised to an exponent that may vary from 0.2 to 0.4, depending on the system.

EXAMPLE 8.7 HETS for an RDC Extractor.

Estimate HETS for the conditions of Example 8.6, assuming five equilibrium stages are required to achieve the desired degree of extraction of acetone.

Solution

Because toluene has a viscosity of approximately 0.6 cP, this is a low-viscosity system. However, the interfacial tension of 32 dyne/cm is high. From Table 8.5, HETS for an RDC varies from 0.29 to 0.40 m. For five equilibrium stages, the estimated compartmented portion of the height is from 1.45 m to 2.0 m.

A vendor suggested a compartmented height of 3 m because of concern for the possibility of appreciable axial dispersion.

CHAPTER 8 NOMENCLATURE

Abbreviations and Acronyms

ARD	asymmetric rotating disk contactor, Figure 8.7
CFSTR, CSTR	continuous flow stirred tank reactor
RDC	rotating-disk contactor, Figure 8.7
RPC	reciprocating plate column, Figure 8.7
VPE	vibrating plate extractor, Section 8.1.5
rph, rpm, rps	revolutions per hour, minute, second
RTL	raining-bucket contactor, Figure 8.7

Latin Symbols

A	solute, (8-4)
A_T	column cross-sectional area, Example 8.6
C	mass flow rate of carrier, (8-2)
c	concentration
c_D^*	fictitious solute dispersed phase concentration in equilibrium with bulk solute in the exiting continuous phase, $c_{D,\text{out}}$, (8-18)
D_i	impeller diameter, Figure 8.25
D_T	column or vessel diameter
d_e	equivalent diameter of a spherical drop, (8-26)
d_{vs}	surface-mean (Sauter) diameter, (8-27)
E	extract mass flow rate, Figure 8.13
E_{MD}	Murphree dispersed phase extraction efficiency, (8-18)
F	feed mass flow rate, Figure 8.13
H	mixing vessel height, Figure 8.25
H_i	vertical distance of impeller above vessel bottom

$(K_i)_D$	distribution coefficient of component i , (8-1)
K_{OD}	overall mass-transfer coefficient based on the dispersed phase, (8-19)
$K_{OD}a$	overall volumetric mass-transfer coefficient based on the dispersed phase, (8-19)
k_D	individual mass-transfer coefficient for the dispersed phase, (8-20)
k_C	individual mass-transfer coefficient for the continuous phase, (8-20)
L	settling vessel length, Example 8.2
L	raffinate mass flow rate, Figure 8.24
M	mixing point, Figure 8.14
N	number of equilibrium stages, Figure 8.13; number of drops, (8-27), rate of impeller rotation, (8-13)
N_{Eo}	Eotvos number, below (8-41)
N_{OD}	number of overall dispersed phase transfer units, (8-24)
N_{Po}	power number, (8-13)
P	difference point, (8-5); agitator power, (8-13)
Q	volumetric flow rate, (8-22)
R	raffinate mass flow rate
R_n	mass flow rate of raffinate leaving stage n , Figure 8.13
S	solvent, (8-3)
S	solvent mass flow rate
t_{res}	residence time, Example 8.2
U	superficial phase velocities, Table 8.5
\bar{u}	mean local fluctuating velocity (8-37)
V	volume, (8-19)
V	extract mass flow rate, Figure 8.24

V_W	pure solvent feed (8-11)
W	baffle width, Figure 8.25
(x_i)	mass fraction of i in the raffinate, (8-7)
(y_i)	mass fraction of i in the extract, (8-7)

Greek Symbols

β_{ij}	relative selectivity of i with respect to j , (8-4)
ϕ_C	volume fraction of continuous phase, (8-15)
ϕ_D	volume fraction of dispersed phase, (8-15)

Subscripts

A	solute
C	carrier
C	continuous phase
D	dispersed phase
E	extract, Example 8.3
e	equivalent, (8-26)
i	impeller, Figure 8.25
M	mixing point, Figure 8.14
n	stage number, Figure 8.13
R	raffinate, Example 8.3
w	final raffinate, (8-11)

Superscripts

I, II	phase I, phase II, (8-1)
–	line segment

SUMMARY

1. A solvent can be used to selectively extract one or more components from a liquid mixture.
2. Although liquid–liquid extraction is a reasonably mature separation operation, considerable experimental effort is often needed to find a solvent and residence-time requirements or values of HETS or mass-transfer coefficients.
3. Mass-transfer rates in extraction are lower than in vapor–liquid systems. Column efficiencies are frequently low, especially when no mechanical agitation is provided.
4. Commercial extractors range from simple columns with no mechanical agitation to centrifugal devices that spin at several thousand revolutions per minute. The selection scheme in Table 8.3 is useful for choosing suitable extractors for a given separation.
5. Solvent selection is facilitated by considering chemical and physical factors given in Tables 8.4 and 8.2.
6. For extraction with ternary mixtures, phase equilibrium is conveniently represented on equilateral- or right triangle diagrams for both Type I (solute and solvent completely miscible) and Type II (solute and solvent not completely miscible) systems.
7. For determining equilibrium-stage requirements of single-section countercurrent cascades for ternary systems, the graphical methods of Hunter and Nash (equilateral triangle diagram) or Kinney (right triangle diagram) are useful. These methods can also determine minimum and maximum solvent requirements.
8. A two-section countercurrent cascade with extract reflux can be employed with a Type II ternary system to enable a sharp separation of a binary-feed mixture.
9. When few equilibrium stages are required, mixer-settler cascades are attractive because each mixer can be

designed to approach an equilibrium stage. With many ternary systems, the residence-time requirement may be only a few minutes for a 90% approach to equilibrium using an agitator input of approximately 4 hp/1,000 gal. Adequate phase-disengaging area for the settlers may be estimated from the rule of 5 gal of combined extract and raffinate per minute per square foot of disengaging area.

10. For mixers utilizing a six-flat-bladed turbine in a closed vessel with side vertical baffles, extractor design correlations are available for estimating, for a given extraction,

mixing-vessel dimensions, minimum impeller rotation rate for uniform dispersion, impeller horsepower, mean droplet size, range of droplet sizes, interfacial area per unit volume, dispersed- and continuous-phase mass-transfer coefficients, and stage efficiency.

11. For column extractors, with and without mechanical agitation, preliminary sizing of equipment is quickly carried out. For final extractor selection and design, recommendations of equipment vendors and scale-up procedures based on data from pilot-size equipment are desirable.

REFERENCES

- DERRY, T.K., and T.I. WILLIAMS, *A Short History of Technology*, Oxford University Press, New York (1961).
- GREEN, D.W., and R.H. PERRY, Eds., *Perry's Chemical Engineers' Handbook*, 8th ed., McGraw-Hill, New York (2008).
- BAILES, P.J., C. HANSON, and M.A. HUGHES, *Chem. Eng.*, **83**(2), 86–100 (1976).
- LO, T.C., M.H.I. BAIRD, and C. HANSON, Eds., *Handbook of Solvent Extraction*, Wiley-Interscience, New York (1983).
- REISSINGER, K.-H., and J. SCHROETER, "Alternatives to Distillation," *I. Chem. E. Symp. Ser. No. 54*, 33–48 (1978).
- HUMPHREY, J.L., J.A. ROCHA, and J.R. FAIR, *Chem. Eng.*, **91**(19), 76–95 (1984).
- FENSKE, M.R., C.S. CARLSON, and D. QUIGGLE, *Ind. Eng. Chem.*, **39**, 1932 (1947).
- SCHEIBEL, E.G., *Chem. Eng. Prog.*, **44**, 681 (1948).
- SCHEIBEL, E.G., *AIChE J.*, **2**, 74 (1956).
- SCHEIBEL, E.G., U.S. Patent 3,389,970 (June 25, 1968).
- OLDSHUE, J., and J. RUSHTON, *Chem. Eng. Prog.*, **48**(6), 297 (1952).
- REMAN, G.H., *Proceedings of the 3rd World Petroleum Congress*, The Hague, Netherlands, Sec. III, 121 (1951).
- REMAN, G.H., *Chem. Eng. Prog.*, **62**(9), 56 (1966).
- MISEK, T., and J. MAREK, *Br. Chem. Eng.*, **15**, 202 (1970).
- FISCHER, A., *Verfahrenstechnik*, **5**, 360 (1971).
- KARR, A.E., *AIChE J.*, **5**, 446 (1959).
- KARR, A.E., and T.C. LO, *Chem. Eng. Prog.*, **72**(11), 68 (1976).
- PROCHAZKA, J., J. LANDAU, F. SOUHRADA, and A. HEYBERGER, *Br. Chem. Eng.*, **16**, 42(1971).
- BARSON, N., and G.H. BEYER, *Chem. Eng. Prog.*, **49**(5), 243–252 (1953).
- REISSINGER, K.-H., and J. SCHROETER, "Liquid-Liquid Extraction, Equipment Choice," in J.J. MCKETTA and W.A. CUNNINGHAM, Eds., *Encyclopedia of Chemical Processing and Design*, Vol. **21**, Marcel Dekker, New York (1984).
- CUSACK, R.W., P. FREMEAUX, and D. GLATZ, *Chem. Eng.*, **98**(2), 66–76 (1991).
- ROBBINS, L.A., *Chem. Eng. Prog.*, **76**(10), 58–61 (1980).
- NASER, S.F., and R.L. FOURNIER, *Comput. Chem. Eng.*, **15**, 397–414 (1991).
- DARWENT, B., and C.A. WINKLER, *J. Phys. Chem.*, **47**, 442–454 (1943).
- TREYBAL, R.E., *Liquid Extraction*, 2nd ed., McGraw-Hill, New York (1963).
- HUNTER, T.G., and A.W. NASH, *J. Soc. Chem. Ind.*, **53**, 95T–102T (1934).
- KINNEY, G.F., *Ind. Eng. Chem.*, **34**, 1102–1104 (1942).
- VENKATARATNAM, A., and R.J. RAO, *Chem. Eng. Sci.*, **7**, 102–110 (1957).
- SAWISTOWSKI, H., and W. SMITH, *Mass Transfer Process Calculations*, Interscience, New York (1963).
- SKELLAND, A.H.P., *Ind. Eng. Chem.*, **53**, 799–800 (1961).
- STRIGLE, R.F., Jr., *Random Packings and Packed Towers*, Gulf Publishing Company, Houston, TX (1987).
- THORNTON, J.D., *Science and Practice of Liquid-Liquid Extraction*, Vol. 1, Clarendon Press, Oxford (1992).
- RYDBERG, J., "Introduction to Solvent Extraction," in J. RYDBERG, C. MUSIKAS, and G.R. CHOPPIN, Eds., *Principles and Practices of Solvent Extraction*, pp. 117., Dekker, New York (1992).
- FLYNN, A.W., and R.E. TREYBAL, *AIChE J.*, **1**, 324–328 (1955).
- RYON, A.D., F.L. DALEY, and R.S. LOWRIE, *Chem. Eng. Prog.*, **55**(10), 7075 (1959).
- HAPPEL, J., and D.G. JORDAN, *Chemical Process Economics*, 2nd ed., Marcel Dekker, New York (1975).
- RUSHTON, J.H., and J.Y. OLDSHUE, *Chem. Eng. Prog.*, **49**(4) 161–168 (1953).
- LAITY, D.S., and R.E. TREYBAL, *AIChE J.*, **3**, 176–180 (1957).
- SKELLAND, A.H.P., and G.G. RAMSEY, *Ind. Eng. Chem. Res.*, **26**, 7781 (1987).
- SKELLAND, A.H.P., and J.M. LEE, *Ind. Eng. Chem. Process Des. Dev.*, **17**, 473–478 (1978).
- MACMULLIN, R.B., and M. WEBER, *Trans. AIChE*, **31**, 409–458 (1935).
- LEWIS, J.B., I. JONES, and H.R.C. PRATT, *Trans. Inst. Chem. Eng.*, **29**, 126 (1951).
- COULSON, J.M., and J.F. RICHARDSON, *Chemical Engineering*, Vol. 2, 4th ed., Pergamon, Oxford (1991).
- VERMUELEN, T., G.M. WILLIAMS, and G.E. LANGLOIS, *Chem. Eng. Prog.*, **51**, 85F (1955).
- GNANASUNDARAM, S., T.E. DEGALEESAN, and G.S. LADDHA, *Can. J. Chem. Eng.*, **57**, 141–144 (1979).
- CHEN, H.T., and S. MIDDLEMAN, *AIChE J.*, **13**, 989–995 (1967).
- SPROW, F.B., *AIChE J.*, **13**, 995–998 (1967).

48. DAVIES, J.T., *Turbulence Phenomena*, Academic Press, New York, p. 311 (1978).
49. CORNISH, A.R.H., *Trans. Inst. Chem. Eng.*, **43**, T332–T333 (1965).
50. SKELLAND, A.H.P., and L.T. MOETI, *Ind. Eng. Chem. Res.*, **29**, 2258–2267 (1990).
51. BATCHELOR, G.K., *Proc. Cambridge Phil. Soc.*, **47**, 359–374 (1951).

52. STICHLMAIR, J., *Chemie-Ingenieur-Technik*, **52**, 253 (1980).
53. REMAN, G.H., *Chem. Eng. Prog.*, **62**(9), 56–61 (1966).
54. KARR, A.E., and T.C. LO, “Performance of a 36-inch Diameter Reciprocating-Plate Extraction Column,” *Proc. International Solvent Extraction Conf ISEC*, **77**, 355–361 (1979).

STUDY QUESTIONS

- 8.1. When liquid–liquid extraction is used, are other separation operations needed? Why?
- 8.2. Under what conditions is extraction preferred to distillation?
- 8.3. What are the important characteristics of a good solvent?
- 8.4. Can a mixer–settler unit be designed to closely approach phase equilibrium?
- 8.5. Under what conditions is mechanically assisted agitation necessary in an extraction column?
- 8.6. What are the advantages and disadvantages of mixer–settler extractors?
- 8.7. What are the advantages and disadvantages of continuous counterflow mechanically assisted extractors?
- 8.8. What is the difference between a Type I and a Type II ternary system? Can a system transition from one type to the other by changing the temperature? Why?
- 8.9. What is meant by the mixing point? For a multi-stage extractor, is the mixing point on a triangular diagram the same for the feeds and the products?
- 8.10. What happens if more than the maximum solvent rate is used? What happens if less than the minimum solvent rate is used?
- 8.11. What are extract and raffinate reflux? Which one is of little value?
- 8.12. What is the typical range of residence time for approaching equilibrium in an agitated mixer when the liquid-phase viscosities are less than 5 cP?
- 8.13. When continuously bringing together two liquid phases in an agitated vessel, are the residence times of each of the two phases in the vessel necessarily the same? If not, are there any conditions where they would be the same?
- 8.14. Why is liquid–liquid mass transfer so complex in agitated systems?
- 8.15. What are Marangoni effects? How do they influence mass transfer?

EXERCISES

Section 8.1

8.1. Extraction versus distillation.

Explain why it is preferable to separate a dilute mixture of benzoic acid in water by solvent extraction rather than by distillation.

8.2. Liquid–liquid extraction versus distillation.

Why is liquid–liquid extraction preferred over distillation for the separation of a mixture of formic acid and water?

8.3. Selection of extraction equipment.

Based on Table 8.3 and the selection scheme in Figure 8.8, is an RDC appropriate for extraction of acetic acid from water by ethyl acetate in the process of Figure 8.1? What other types of extractors might be considered?

8.4. Extraction devices.

What is the major advantage of the ARD over the RDC? What is the disadvantage of the ARD compared to the RDC?

8.5. Selection of extraction devices.

Under what conditions is a cascade of mixer–settler units probably the best choice of extraction equipment?

8.6. Selection of extraction device.

A petroleum reformat stream of 4,000 bbl/day is to be contacted with diethylene glycol to extract aromatics from paraffins. The ratio of solvent to reformat volume is 5. It is estimated that eight theoretical stages are needed. Using Tables 8.2 and 8.3 and Figure 8.8, which extractors would be suitable?

Section 8.2

8.7. Selection of extraction solvents.

Using Table 8.4, select possible liquid–liquid extraction solvents for separating the following mixtures: (a) water–ethyl alcohol, (b) water–aniline, and (c) water–acetic acid. For each case, indicate which of the two components should be the solute.

8.8. Selection of extraction solvents.

Using Table 8.4, select liquid–liquid extraction solvents for removing the solute from the carrier in the following cases:

	Solute	Carrier
(a)	Acetone	Ethylene glycol
(b)	Toluene	<i>n</i> -Heptane
(c)	Ethyl alcohol	Glycerine

8.9. Characteristics of an extraction system.

For extracting acetic acid (A) from a dilute water (C) solution into ethyl acetate (S) at 25°C, estimate or obtain data for $(K_A)_D$, $(K_C)_D$, $(K_S)_D$, and β_{AC} . Does this system exhibit (a) high selectivity, (b) high solvent capacity, and (c) easy solvent recovery? Using a process simulator, try to find a better solvent than ethyl acetate.

8.10. Estimation of interfacial tension.

Very low values of interfacial tension result in stable emulsions that are difficult to separate, while very high values require large energy inputs to form the dispersed phase. It is best to measure the interfacial tension for the two-phase mixture of interest. However, in the absence of experimental data, propose a method for estimating the interfacial tension of a ternary system using only the compositions of the equilibrium phases and the values of surface tension in air for each of the three components.

Section 8.3

8.11. Extraction of acetone by trichloroethane.

One thousand kg/h of a 45 wt% acetone-in-water solution is to be extracted at 25°C in a continuous countercurrent system with pure 1,1,2-trichloroethane solvent to obtain a raffinate containing 10 wt% acetone. Using the following equilibrium and tie-line data, determine with an equilateral-triangle diagram: (a) the minimum flow rate of solvent; (b) the number of stages required for a solvent rate equal to 1.5 times minimum; and (c) the flow rate and composition of each stream leaving each stage. Alternatively, use a ternary phase diagram calculated from a suitable method for estimating activity coefficients with a process simulator using the database of the simulator.

	Acetone, Weight Fraction	Water, Weight Fraction	Trichloroethane, Weight Fraction
Extract	0.60	0.13	0.27
	0.50	0.04	0.46
	0.40	0.03	0.57
	0.30	0.02	0.68
	0.20	0.015	0.785
	0.10	0.01	0.89
Raffinate	0.55	0.35	0.10
	0.50	0.43	0.07
	0.40	0.57	0.03
	0.30	0.68	0.02
	0.20	0.79	0.01
	0.10	0.895	0.005

The tie-line data are:

Raffinate, Weight Fraction Acetone	Extract, Weight Fraction Acetone
0.44	0.56
0.29	0.40
0.12	0.18

8.12. Using a right-triangle diagram for extraction.

Solve Exercise 8.11 with a right-triangle diagram using the given equilibrium and tie-line data, or use a process simulator.

8.13. Extraction of isopropanol with water.

A distillate of 45 wt% isopropyl alcohol, 50 wt% diisopropyl ether, and 5 wt% water is obtained from an isopropyl alcohol finishing unit. The ether is to be recovered by liquid-liquid extraction in a column extractor. Water, the solvent, enters the top and the feed enters the bottom, so as to produce an ether-rich raffinate containing <2.5 wt% alcohol, and an extract containing at least 20 wt% alcohol. The unit

will operate at 25°C and 1 atm. Find the number of equilibrium stages required. Is it possible to obtain an extracted alcohol composition of 25 wt%? Use the equilibrium data below or a phase diagram printed from a process simulator that uses a suitable method for computing activity coefficients.

Equilibrium data are as follows:

PHASE-EQUILIBRIUM (TIE-LINE) DATA AT 25°C, 1 ATM

Ether phase			Water phase		
Wt% Alcohol	Wt% Ether	Wt% Water	Wt% Alcohol	Wt% Ether	Wt% Water
2.4	96.7	0.9	8.1	1.8	90.1
3.2	95.7	1.1	8.6	1.8	89.6
5.0	93.6	1.4	10.2	1.5	88.3
9.3	88.6	2.1	11.7	1.6	86.7
24.9	69.4	5.7	17.5	1.9	80.6
38.0	50.2	11.8	21.7	2.3	76.0
45.2	33.6	21.2	26.8	3.4	69.8

ADDITIONAL POINTS ON THE PHASE BOUNDARY

Wt% Alcohol	Wt% Ether	Wt% Water
45.37	29.70	24.93
44.55	22.45	33.00
39.57	13.42	47.01
36.23	9.66	54.11
24.74	2.74	72.52
21.33	2.06	76.61
0	0.6	99.4
0	99.5	0.5

8.14. Extraction of trimethylamine from benzene with water.

Benzene and trimethylamine (TMA) are to be separated in a three-equilibrium-stage liquid-liquid extraction column using pure water as the solvent. If the solvent-free extract and raffinate products are to contain, respectively, 70 and 3 wt% TMA, find the original feed composition and the water-to-feed ratio with a right-triangle diagram. There is no reflux. Equilibrium data are as follows:

TRIMETHYLAMINE-WATER-BENZENE COMPOSITIONS ON THE PHASE BOUNDARY

Extract, wt%			Raffinate, wt%		
TMA	H ₂ O	Benzene	TMA	H ₂ O	Benzene
5.0	94.6	0.4	5.0	0.0	95.0
10.0	89.4	0.6	10.0	0.0	90.0
15.0	84.0	1.0	15.0	1.0	84.0
20.0	78.0	2.0	20.0	2.0	78.0
25.0	72.0	3.0	25.0	4.0	71.0
30.0	66.4	3.6	30.0	7.0	63.0
35.0	58.0	7.0	35.0	15.0	50.0
40.0	47.0	13.0	40.0	34.0	26.0

The tie-line data are:

Extract, wt% TMA	Raffinate, wt% TMA
39.5	31.0
21.5	14.5
13.0	9.0
8.3	6.8
4.0	3.5

8.15. Extraction of diphenylhexane from docosane with furfural.

The system docosane-diphenylhexane (DPH)-furfural is representative of complex systems encountered in the solvent refining of lubricating oils. Five hundred kg/h of a 40 wt% mixture of DPH in docosane are to be extracted in a countercurrent system with 500 kg/h of a solvent containing 98 wt% furfural and 2 wt% DPH to produce a raffinate of 5 wt% DPH. Calculate, with a triangular diagram, the stages required and the kg/h of DPH in the extract at 45°C and 80°C.

BINODAL CURVES IN DOCOSANE-DIPHENYLHEXANE-FURFURAL SYSTEM [IND. ENG. CHEM., 35, 711 (1943)].

Wt% at 45°C			Wt% at 80°C		
Docosane	DPH	Furfural	Docosane	DPH	Furfural
96.0	0.0	4.0	90.3	0.0	9.7
84.0	11.0	5.0	50.5	29.5	20.0
67.0	26.0	7.0	34.2	35.8	30.0
52.5	37.5	10.0	23.8	36.2	40.0
32.6	47.4	20.0	16.2	33.8	50.0
21.3	48.7	30.0	10.7	29.3	60.0
13.2	46.8	40.0	6.9	23.1	70.0
7.7	42.3	50.0	4.6	15.4	80.0
4.4	35.6	60.0	3.0	7.0	90.0
2.6	27.4	70.0	2.2	0.0	97.8
1.5	18.5	80.0			
1.0	9.0	90.0			
0.7	0.0	99.3			

The tie lines in the docosane-diphenylhexane-furfural system are:

Docosane Phase Composition, wt%			Furfural Phase Composition, wt%		
Docosane	DPH	Furfural	Docosane	DPH	Furfural
Temperature, 45°C:					
85.2	10.0	4.8	1.1	9.8	89.1
69.0	24.5	6.5	2.2	24.2	73.6
43.9	42.6	13.3	6.8	40.9	52.3
Temperature, 80°C:					
86.7	3.0	10.3	2.6	3.3	94.1
73.1	13.9	13.0	4.6	15.8	79.6
50.5	29.5	20.2	9.2	27.4	63.4

8.16. Selection of extraction method.

For each ternary system in Figure 8.27, indicate which one would be the most economical: (a) simple countercurrent extraction, (b) countercurrent extraction with extract reflux, (c) countercurrent extraction with raffinate reflux, or (d) countercurrent extraction with both extract and raffinate reflux.

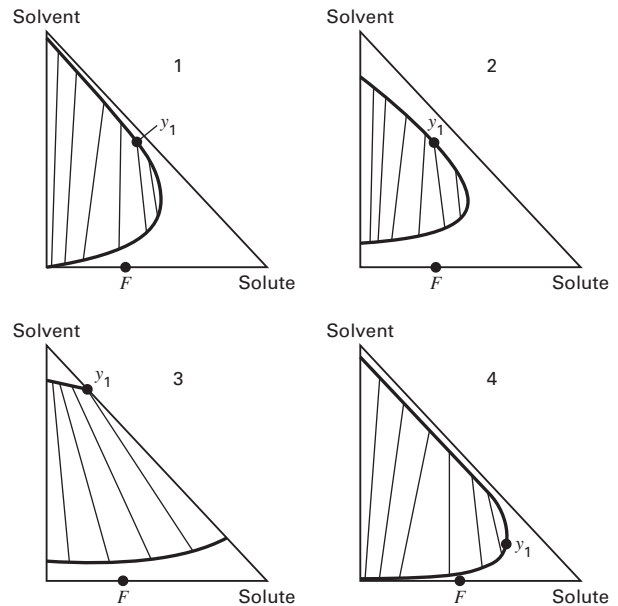


Figure 8.27 Data for Exercise 8.16.

8.17. Extraction of acetone from two feeds.

Two feeds— F_1 at 7,500 kg/h containing 50 wt% acetone and 50 wt% water, and F_2 at 7,500 kg/h containing 25 wt% acetone and 75 wt% water—are to be extracted with 5,000 kg/h of 1,1,2-trichloroethane at 25°C to give a 10 wt% acetone raffinate. Calculate the equilibrium stages required and the stage to which each feed should be introduced using a triangular diagram. Equilibrium data are in Exercise 8.11.

8.18. Extraction in a three-stage unit.

The three-stage extractor shown in Figure 8.28 is used to extract the amine from a feed consisting of 40 wt% benzene (B) and 60 wt% trimethylamine (T). The solvent (water) flow to stage 3 is 5,185 kg/h and the feed flow rate is 10,000 kg/h. Solvent also is fed to stages 1 and 2. On a solvent-free basis, V_1 is to contain 76 wt% T, and L_3 is to contain 3 wt% T. Determine the required solvent flow rates S_1 and S_2 using a triangular diagram. Solubility data are in Exercise 8.14.

8.19. Analysis of a multiple-feed countercurrent extraction cascade.

The extraction process shown in Figure 8.29 is conducted without reflux. Feed F' is composed of solvent and solute, and is an extract-phase feed. Feed F'' is composed of unextracted raffinate and solute and is a raffinate-phase feed. Derive the equations required to establish the three reference points needed to step off the stages in the extraction column. Show the graphical determination of these points on a triangular diagram.

8.20. Extraction of acetone from water.

A 45% acetone (A)-55% water (by weight) feed is to be extracted with 1,1,2-dichloroethane (TCE), the solvent, to reduce the concentration of acetone below 10 wt%. Use 32 kg of solvent per 100 kg of feed. Using a triangular diagram, how many equilibrium stages are

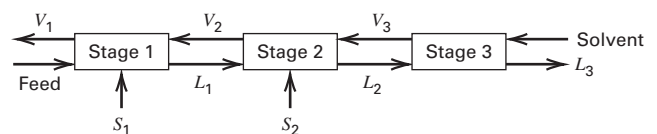


Figure 8.28 Data for Exercise 8.18.

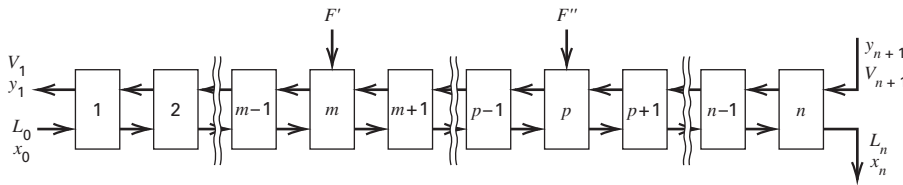


Figure 8.29 Data for Exercise 8.19.

required? Use the following tie-line data where for each of five experiments, compositions are given in weight percent for the TCE-rich (I) and water-rich (II) phases at equilibrium.

	I	II	I	II	I	II	I	II	I	II
A	58	49	52	40	39	30	37	23	21	15
Water	7	46	5	55	4	66	3	74	2	84
TCE	36	6	41	5	57	4	61	2	77	1

8.21. Extraction of hafnium from zirconium.

Zirconium (Zr), which is used in nuclear reactors, is associated with hafnium (Hf), which has a high neutron-absorption cross section and must be removed. Refer to Figure 8.30 for a proposed liquid–liquid extraction process wherein tributyl phosphate (TBP) is used as a solvent for the separation. One L/h of 5.1-N HNO₃ containing 127 g of dissolved Hf and Zr oxides per liter is fed to stage 5 of the 14-stage extraction unit. The feed contains 22,000 g Hf per million g of Zr. Fresh TBP enters at stage 14, while scrub water is fed to stage 1. Raffinate is removed at stage 14, while the organic extract phase removed at stage 1 goes to a stripping unit. The stripping operation consists of a single contact between fresh water and the organic phase. (a) Use the data below to complete a material balance for the process. (b) Check the data for consistency. (c) What is the advantage of running the extractor as shown? Would you recommend that all stages be used?

STAGewise ANALYSES OF MIXER-SETTLER RUN

Stage	Organic Phase			Aqueous Phase		
	g oxide/ liter	N HNO ₃	(Hf/Zr) × (100)	g oxide/ liter	N HNO ₃	(Hf/Zn) × (100)
1	22.2	1.95	<0.010	17.5	5.21	<0.010
2	29.3	2.02	<0.010	27.5	5.30	<0.010
3	31.4	2.03	<0.010	33.5	5.46	<0.010
4	31.8	2.03	0.043	34.9	5.46	0.24
5	32.2	2.03	0.11	52.8	5.15	3.6
6	21.1	1.99	0.60	30.8	5.15	6.8
7	13.7	1.93	0.27	19.9	5.05	9.8
8	7.66	1.89	1.9	11.6	4.97	20
9	4.14	1.86	4.8	8.06	4.97	8.06
10	1.98	1.83	10	5.32	4.75	67
11	1.03	1.77	23	3.71	4.52	110
12	0.66	1.68	32	3.14	4.12	140
13	0.46	1.50	42	2.99	3.49	130
14	0.29	1.18	28	3.54	2.56	72
Stripper		0.65		76.4	3.96	<0.01

[Data from R.P. Cox, H.C. Peterson, and C.H. Beyer, *Ind. Eng. Chem.*, **50**(2), 141 (1958). Exercise adapted from E.J. Henley and H. Bieber, *Chemical Engineering Calculations*, McGraw-Hill, New York, p. 298 (1959).]

8.22. Extraction of diphenylhexane from docosane with furfural.

At 45°C, 5,000 kg/h of a mixture of 65 wt% docosane, 7 wt% furfural, and 28 wt% diphenylhexane is to be extracted with pure furfural to obtain a raffinate with 12 wt% diphenylhexane in a continuous, countercurrent, multi-stage liquid–liquid extraction system. Phase-equilibrium data are given in Exercise 8.15. Determine (a) minimum solvent flow, (b) flow rate and composition of the extract at the minimum solvent flow, and (c) number of equilibrium stages if a solvent flow rate of 1.5 times minimum is used.

8.23. Extraction of diphenylhexane from docosane with furfural.

At 45°C, 1,000 kg/h of a mixture of 0.80 mass fraction docosane and 0.20 mass fraction diphenylhexane is extracted with pure furfural to remove some diphenylhexane from the feed. Phase-equilibrium data are given in Exercise 8.15. Determine: (a) composition and flow rate of the extract and raffinate from a single equilibrium stage for solvent flow rates of 100, 1,000, and 10,000 kg/h; (b) minimum solvent flow rate to form two liquid phases; (c) maximum solvent flow rate to form two liquid phases; and (d) composition and flow rate of the extract and raffinate if a solvent flow rate of 2,000 kg/h and two equilibrium stages are used in a countercurrent-flow system.

8.24. Extraction of acetone from water by 1,1,2-trichloroethane.

A liquid of 27 wt% acetone and 73 wt% water is to be separated at 25°C into a raffinate and extract by multistage countercurrent liquid–liquid extraction with a solvent of pure 1,1,2-trichloroethane. Equilibrium data are given in Exercise 8.11. Determine (a) minimum solvent-to-feed ratio to obtain a raffinate essentially free of acetone; (b) composition of extract at the minimum solvent-to-feed ratio; and (c) composition of the extract stream exiting stage 2 (see Figure 8.13), if a very large number of equilibrium stages is used with the minimum solvent.

Section 8.4

8.25. Design of a mixer-settler unit for extraction.

Acetic acid is extracted from a 3 wt% dilute solution in water with a solvent of isopropyl ether in a mixer-settler unit. The flow rates of the feed and solvent are 12,400 and 24,000 lb/h, respectively. Assuming a residence time of 1.5 minutes in the mixer and a settling vessel capacity of 4 gal/min-ft² of disengagement area, estimate: (a) diameter and height of the mixing vessel, assuming $H/D_T = 1$; (b) agitator horsepower for the mixing vessel; and (c) diameter, length, and residence time in minutes of the settling vessel, assuming $L/DT = 4$.

8.26. Extraction in an available unit.

A countercurrent cascade of six mixer-settler units is available, each unit consisting of a 10-ft-diameter by 10-ft-high mixing vessel equipped with a 20-hp agitator, and a 10-ft-diameter by 40-ft-long settling vessel. If this cascade is used for the acetic acid extraction described in the introduction to this chapter, how many lb/h of feed can be processed?

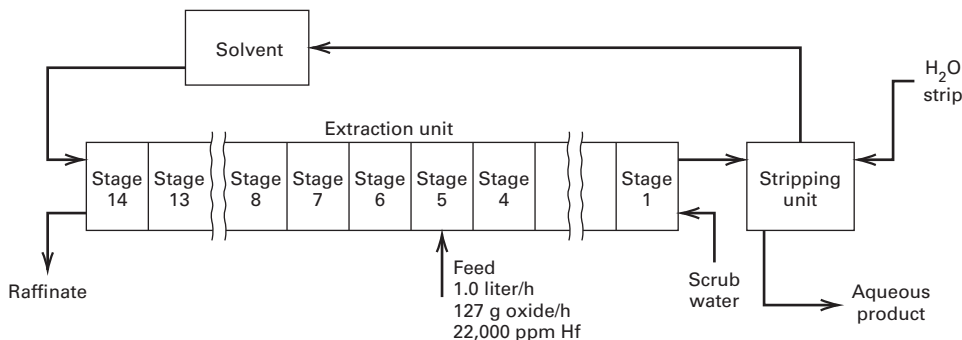


Figure 8.30 Data for Exercise 8.21.

8.27. Agitator size for extraction of acetic acid.

Acetic acid is extracted from a dilute aqueous solution with isopropyl ether at 25°C in a countercurrent cascade of mixer-settler units. In one unit, the following conditions apply:

	Raffinate	Extract
Flow rate, lb/h	21,000	52,000
Density, lb/ft ³	63.5	45.3
Viscosity, cP	3.0	1.0

Interfacial tension = 13.5 dyne/cm. If the raffinate is the dispersed phase and the mixer residence time is 2.5 minutes, estimate for the mixer: (a) dimensions of a closed, baffled vessel; (b) diameter of a flat-bladed impeller; (c) minimum rate of impeller rotation in rpm for uniform dispersion; and (d) agitator power requirement at the minimum rate of rotation.

8.28. Droplet characteristics for extraction of acetic acid.

For Exercise 8.27, estimate (a) Sauter mean drop size, (b) range of drop sizes, and (c) interfacial area of the two-phase liquid-liquid emulsion.

8.29. Mass-transfer coefficient for extraction of acetic acid.

For the conditions of Exercises 8.27 and 8.28 and the data below, estimate (a) dispersed-phase mass-transfer coefficient, (b) continuous-phase mass-transfer coefficient, (c) Murphree dispersed-phase efficiency, and (d) fraction of acetic acid extracted.

Diffusivity of acetic acid in the raffinate is 1.3×10^{-9} m²/s and in the extract is 2.0×10^{-9} m²/s. The distribution coefficient for acetic acid between the two phases is $c_D/c_C = 2.7$.

8.30. Design of a mixer unit.

For the conditions and results of Example 8.2, determine the following when using a flat-six-bladed turbine impeller in a closed vessel with baffles and with the extract phase dispersed: (a) minimum rate of rotation of the impeller for complete and uniform dispersion; (b) agitator power requirement at the minimum rotation rate; (c) Sauter mean droplet diameter; (d) interfacial area; (e) overall mass-transfer coefficient, K_{OD} ; (f) overall transfer units, N_{OD} ; (g) Murphree efficiency, E_{MD} ; and (h) fractional benzoic acid extraction. Use the following properties:

Interfacial tension = 22 dyne/cm, and distribution coefficient for benzoic acid = $c_D/c_C = 21$.

	Raffinate Phase	Extract Phase
Density, g/cm ³	0.995	0.860
Viscosity, cP	0.95	0.59
Diffusivity of benzoic acid, cm ² /s	2.2×10^{-5}	1.5×10^{-5}

8.31. Diameter of an RDC column.

Estimate the diameter of an RDC column to extract acetic acid from water with isopropyl ether for Exercises 8.25 and 8.27, using Table 8.5.

8.32. Diameter of a Karr column.

Estimate the diameter of a Karr column to extract benzoic acid from water with toluene for the conditions of Exercise 8.30 using Table 8.5.

8.33. HETS of an RDC column.

Estimate HETS for an RDC column operating under the conditions of Exercise 8.31 using Table 8.5.

8.34. HETS of a Karr column.

Estimate HETS for a Karr column operating under the conditions of Exercise 8.32 using Table 8.5.

8.35. Scale-up of a Karr extraction column.

A Karr column is to be sized to extract 99.95% of the methyl vanillin in water using *o*-xylene. The feed rate is 6 m³/h with a vanillin concentration of 40 kg/m³. The average partition coefficient is 5.6, defined as the concentration of vanillin in xylene to its concentration in water. Experiments with a Karr column of 2-inch diameter and 1.5 meter plate-stack height give the optimal conditions as 610 mL/min of feed and 270 mL/min of xylene, for a stroke height of 19.1 mm and 250 strokes/min. Scale up this data to determine the diameter of a commercial Karr column. In addition, the vendor's experience is that the HETS varies with the 0.38 exponent of the column diameter. Using this information, estimate the height of the commercial Karr column.

Approximate Methods for Multicomponent Distillation

§9.0 INSTRUCTIONAL OBJECTIVES

After completing this chapter, you should be able to:

- Select two key components, operating pressure, and a condenser type for a multicomponent distillation.
- Estimate the minimum number of equilibrium stages and distribution of non-key components by the Fenske equation, minimum reflux ratio by the Underwood method, number of equilibrium stages for a reflux ratio greater than minimum by the Gilliland correlation, and determine a feed-stage location for a specified separation between two key components.

Although rigorous methods are available for solving multicomponent separation problems, approximate methods continue to be useful for preliminary design, parametric studies to establish optimal design conditions, process synthesis studies to determine optimal separation sequences, and to obtain initial input approximations for rigorous, iterative methods.

The approximate method of Kremser [1] and Edmister [2] for single-section cascades used in absorption and stripping was presented in Chapter 6. This chapter develops an additional approximate method for preliminary design of multicomponent distillations, called the **Fenske–Underwood–Gilliland (FUG, Shortcut)** method. It continues to be useful in early stages of designing a distillation column. It can quickly provide estimates of operating pressure, equilibrium stages, and reflux ratio for a desired separation between two key components. These estimates are required inputs for rigorous calculations performed by process simulators. The method is available in process simulators or it can be applied by hand calculations.

§9.1 FENSKE–UNDERWOOD–GILLILAND (FUG) METHOD

Figure 9.1 gives an algorithm for the FUG method, named after the authors of the three main steps in the procedure. These steps are applied to the distillation column in Figure 9.3. Most commonly, the method is applied to a column with one feed, a total condenser, and a partial reboiler. From Table 5.4, the number of degrees of freedom for such a column is $2N + C + 9$. For a design case, the variables below are generally specified, with the partial reboiler counted as an equilibrium stage:

	Number of Specifications
Feed flow rate	1
Feed mole fractions	$C - 1$
Feed temperature ¹	1
Feed pressure ¹	1
Adiabatic stages (excluding reboiler)	$N - 1$
Stage pressures (including reboiler)	N
Split of LK component	1
Split of HK component	1
Feed-stage location	1
Reflux ratio ($> R_{\min}$)	1
Reflux temperature	1
Adiabatic reflux divider	1
Pressure of total condenser	1
Pressure at reflux divider	1
Total	$2N + C + 9$

Note: Similar specifications can be written for a column with a partial condenser.

¹Feed temperature and pressure may correspond to known stream conditions leaving the previous piece of equipment.

§9.1.1 Selection of Two Key Components

For the design case of Table 5.4, the specification of two key components and their distribution between distillate and bottoms is required for multicomponent feeds. Preliminary guesses of the distribution of non-key components can, at times, be sufficiently difficult to require the iterative procedure indicated in Figure 9.1. However, generally only two and seldom more than three iterations are necessary.

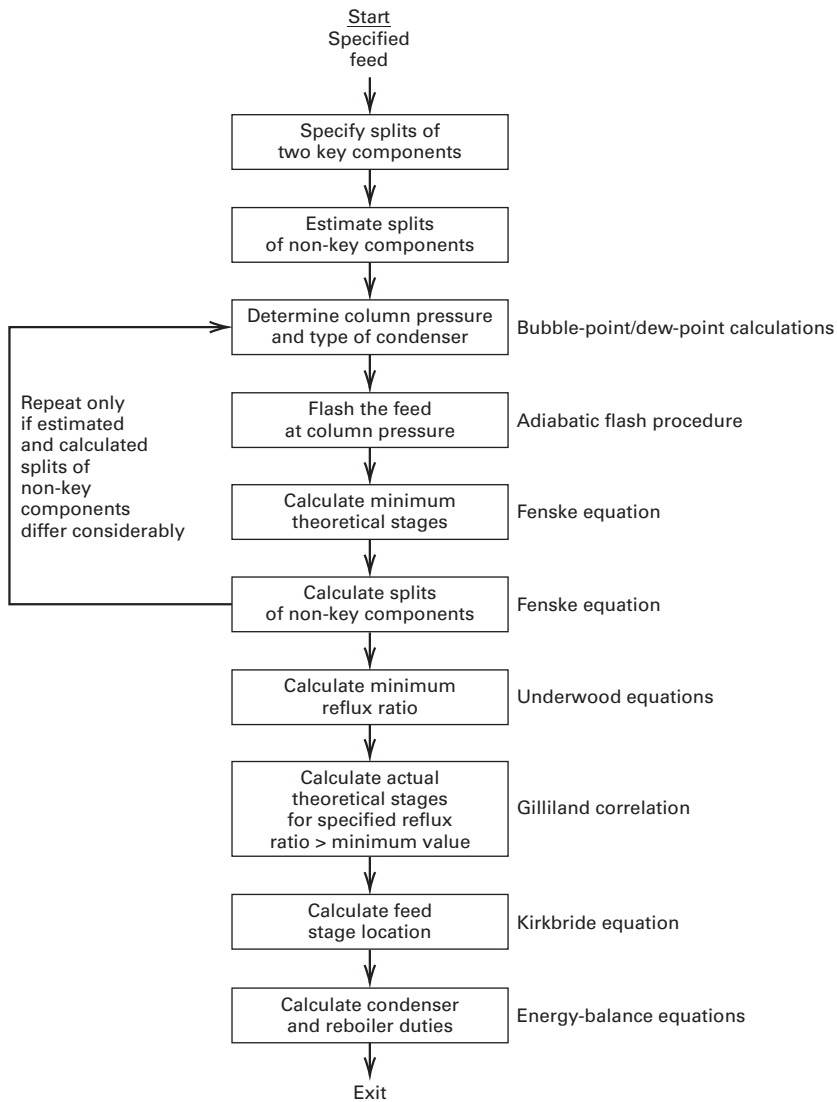
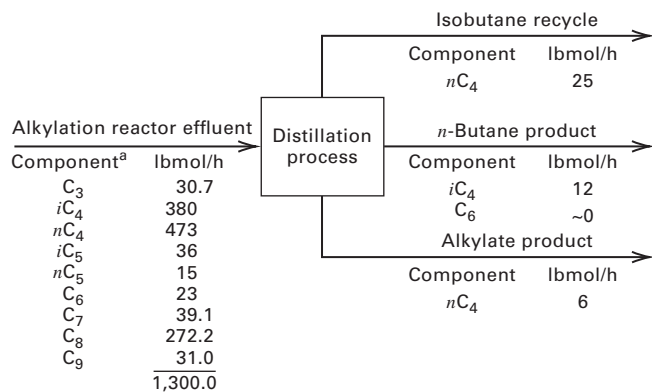


Figure 9.1 Algorithm for multicomponent distillation calculations by FUG method.



^aC₆, C₇, C₈, C₉ are taken as normal paraffins.

Figure 9.2 Separation specifications for alkylation-reactor effluent.

Figure 9.2 shows a typical multicomponent hydrocarbon feed to the recovery section of a petroleum refinery alkylation unit [3], where C₄ hydrocarbons are combined to produce

C₈ hydrocarbons for gasoline. Feed components are listed in order of decreasing volatility. As described in §1.8.2, the distillation process uses a sequence involving a deisobutanizer to separate isobutane, *i*C₄, from *n*-butane, *n*C₄, in series with a debutanizer to separate *n*C₄ from heavier (higher molecular weight) hydrocarbons. Case 1 of Table 9.1 puts the deisobutanizer first. Maximum allowable flow rates specified for *n*C₄ in the isobutane recycle and *i*C₄ in the *n*-butane product indicate that *i*C₄ is the LK and *n*C₄ is the HK. These two keys are adjacent in volatility. Since a fairly sharp separation between these two keys is specified and non-key components are much less volatile than the butanes, the non-key component separations are initially considered to be perfect.

Cases 2 and 3 put the debutanizer first and select *n*C₄ as the LK. Because no recovery or purity is specified for any component less volatile than *n*-butane, *i*C₅ or any heavier hydrocarbon could be selected as HK for the debutanizer. Case 2 of Table 9.1 selects *i*C₅, which is adjacent to *n*-butane. Setting a limit of 13 lbmol/h of *i*C₅ in the distillate produces a non-sharp split between *n*-butane and *i*C₅. Since *n*C₅ is close

Table 9.1 Specifications of Key Component Splits and Preliminary Estimation of Non-Key Component Splits for Alkylation Reactor Effluent

Component	Feed lbmol/h	Case 1, Deisobutanizer Column First, lbmol/h		Case 2, Debutanizer Column First (<i>i</i> C ₅ is HK), lbmol/h		Case 3, Debutanizer Column First (C ₆ is HK), lbmol/h	
		Distillate	Bottoms	Distillate	Bottoms	Distillate	Bottoms
C ₃	30.7	(30.7)	(0)	(30.7)	(0)	(30.7)	(0)
<i>i</i> C ₄	380	368 ^a	12 ^b	(380.0)	(0)	(380.0)	(0)
<i>n</i> C ₄	473	25 ^b	448 ^a	467 ^a	6 ^b	467 ^a	6 ^b
<i>i</i> C ₅	36	(0)	(36)	13 ^b	23 ^a	(13)	(23)
<i>n</i> C ₅	15	(0)	(15)	(1)	(14)	(1)	(14)
C ₆	23	(0)	(23)	(0)	(23)	0.01 ^b	22.99 ^a
C ₇	39.1	(0)	(39.1)	(0)	(39.1)	(0)	(39.1)
C ₈	272.2	(0)	(272.2)	(0)	(272.2)	(0)	(272.2)
C ₉	31.0	(0)	(31.0)	(0)	(31.0)	(0)	(31.0)
	1,300.0	423.7	876.3	891.7	408.3	891.71	408.29

^aBy material balance.^bSpecification

(Preliminary estimate.)

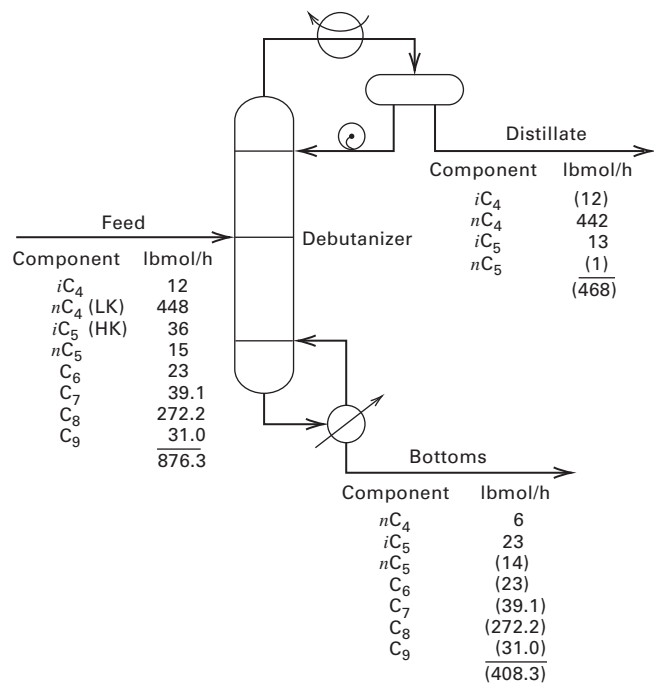
in volatility to *i*C₅, a non-negligible amount of *n*C₅ will also likely appear in the distillate. Case 2 estimates distributions of remaining non-key components, including a value of zero for *i*C₄ in the debutanizer bottoms product.

Case 3 in Table 9.1 selects C₆ as the HK rather than *i*C₅ as in Case 2. The HK is estimated to appear at a rate of 0.01 lbmol/h in the distillate. Consequently, *i*C₅ and *n*C₅, which fall between the LK and HK, will distribute between the distillate and bottoms. Initially, the distributions for *i*C₅ and *n*C₅ are estimated to be the same as for Case 2.

Separation of close-boiling butane isomers in the deisobutanizer is more difficult than separating *i*C₅ from *n*C₄ in the debutanizer. From §1.8.2, Heuristic 2 favors Case 1, while Heuristics 3 and 4 favor Cases 2 and 3. In practice, the deisobutanizer is placed first in the sequence, and the bottoms for Case 1 becomes the debutanizer feed. Selecting *n*C₄ and *i*C₅ as the key components produces the separations indicated in Figure 9.3, where preliminary estimates for non-key components appear in parentheses. This separation has been treated by Bachelor [4] and the FUG method is applied to it in this chapter. Because *n*C₄ and C₈ make up 82.2 mol% of the feed to the debutanizer in Figure 9.3, and differ widely in volatility, the temperature difference between distillate and bottoms is likely to be large. A feed of this type where the major components are separated by small amounts of components that are intermediate in volatility is often referred to as a **dumbbell feed**. Furthermore, the LK split is rather sharp, but the HK split is not. It will be shown that this case provides a severe test of the FUG shortcut design procedure.

§9.1.2 Column Operating Pressure, Condenser Type, and Feed Flash.

Figure 7.17 is useful for establishing a reasonable column operating pressure in the third step of the shortcut design

**Figure 9.3** Specifications for debutanizer.

procedure of Figure 9.1. This step is necessary because column pressure must be specified before design calculations can be made with a process simulator. If the outcome of a distillation design is unsatisfactory, a new pressure is assumed, and the calculations are repeated.

A condenser is selected from the types shown in Figure 7.18. The choice depends on the pressure, as indicated in Figure 7.17, unless a particular distillate phase condition is desired.

The feed sent to the column may be at, below, or above column pressure at the column feed entry. If above, the feed

is flashed to column pressure. If below, a pump is required to bring a liquid feed to column pressure or a compressor is required for a vapor feed. When a liquid feed is flashed to column pressure, the result may be a partially or completely vaporized feed. If a particular feed phase condition is necessary, it can be achieved by adding a feed heat exchanger. Also, as an energy-conservation measure, a feed heat exchanger might be provided to recover heat from a column bottoms product.

EXAMPLE 9.1 Column Pressure and Condenser Type.

Determine column operating pressure, type of condenser, and feed condition for the debutanizer of Figure 9.3. The feed sent to the column is a saturated liquid at a pressure of 105 psia. The component feed flow rates are in Figure 9.3.

Solution

The calculations are conveniently made with a process simulator. For this example, CHEMCAD was used, with the SRK EOS for K -values and enthalpies. Applying the first step in Figure 7.17, the bubble-point pressure at 120°F (assumed condenser exit temperature) was determined for the distillate composition in Figure 9.3. The result was 70 psia, assuming a saturated liquid leaving the condenser. This indicates the use of a total condenser. The column bottoms pressure was estimated by assuming a 2 psi drop in the condenser and a 5 psi drop in the column. Thus, the column bottoms pressure is assumed to be $70 + 2 + 5 = 77$ psia. The bubble-point temperature of the bottoms product at this pressure is 334°F, which is acceptable for hydrocarbons.

The feed tray pressure is between 72 and 77 psia. Assume a pressure of 74 psia. Because the feed is at 105 psia, it is flashed adiabatically across a valve before entering the column. By a bubble-point calculation, the temperature of the feed upstream of the valve is 201.8°F. After the flash across the valve, the temperature is 181.4°F with 13.4 mol% vaporization. The component molar flows of the vapor and liquid feed entering the column, together with the calculated K -values of the feed, distillate, and bottoms using the SRK EOS, are given in the following table.

Component	Feed Vapor 181.4°F, 74 psia lbmol/h	Feed Liquid 181.4°F, 74 psia lbmol/h	Feed K -Values 181.4°F, 74 psia	Distillate K -Values 120°F, 70 psia	Bottoms K -Values 334°F, 77 psia
Isobutane	3.31	8.69	2.467	1.354	6.314
<i>n</i> -butane	102.59	345.41	1.922	1.009	5.425
Isopentane	4.72	31.28	0.977	0.458	3.440
<i>n</i> -pentane	1.67	13.33	0.810	0.366	3.073
<i>n</i> -hexane	1.18	21.82	0.348	0.136	1.755
<i>n</i> -heptane	0.90	38.20	0.152	0.051	1.029
<i>n</i> -octane	2.79	269.41	0.067	0.019	0.602
<i>n</i> -nonane	0.14	30.86	0.029	0.0072	0.352
Total	117.30	759.00			

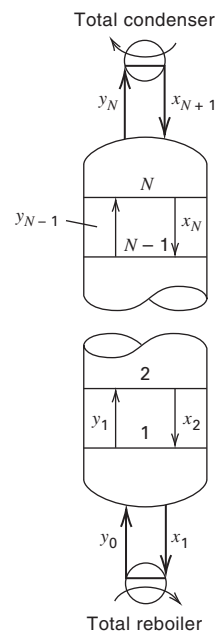


Figure 9.4 Distillation column operation at total reflux.

§9.1.3 Fenske Equation for Minimum Equilibrium Stages

A minimum number of equilibrium stages, N_{\min} , corresponds to a condition of total reflux. In practice, this is achieved by charging the column with feedstock and bringing it to steady state without addition of further feed or withdrawal of products, as shown in Figure 9.4.

To facilitate derivation of the Fenske equation, stages are numbered from the bottom up, instead of top down. All vapor leaving top stage N is condensed and returned to stage N as reflux. All liquid leaving bottom stage 1 is vaporized in the reboiler and returned to stage 1 as boilup. For steady-state operation within the column, heat input to the reboiler and heat output from the condenser are made equal (assuming no heat

losses). Then, by a material balance, vapor and liquid streams passing between any pair of adjacent stages have equal molar flow rates and compositions, for example, $V_{N-1} = L_N$ and $y_{i,N-1} = x_{i,N}$. However, molar vapor and liquid flow rates change from stage to stage unless constant molar overflow (L/V) occurs, as discussed in §7.2.

Derivation of an exact equation for the minimum number of equilibrium stages involves only the definition of the K -value and the mole-fraction vapor–liquid equality between stages. For component i at stage 1 in Figure 9.4,

$$y_{i,1} = K_{i,1}x_{i,1} \quad (9-1)$$

For passing streams,

$$y_{i,1} = x_{i,2} \quad (9-2)$$

Combining these two equations to eliminate y ,

$$x_{i,2} = K_{i,1}x_{i,1} \quad (9-3)$$

Similarly, for stage 2,

$$y_{i,2} = K_{i,2}x_{i,2} \quad (9-4)$$

Combining (9-3) and (9-4),

$$y_{i,2} = K_{i,2}K_{i,1}x_{i,1} \quad (9-5)$$

Equation (9-5) is readily extended in this fashion to give

$$y_{i,N} = K_{i,N}K_{i,N-1} \cdots K_{i,2}K_{i,1}x_{i,1} \quad (9-6a)$$

Similarly, for component j ,

$$y_{j,N} = K_{j,N}K_{j,N-1} \cdots K_{j,2}K_{j,1}x_{j,1} \quad (9-6b)$$

Dividing (9-6a) by (9-6b),

$$\frac{y_{i,N}}{y_{j,N}} = \alpha_N \alpha_{N-1} \cdots \alpha_2 \alpha_1 \left(\frac{x_{i,1}}{x_{j,1}} \right) \quad (9-7)$$

Noting that $y_{i,N} = x_{i,N+1}$ and $y_{j,N} = x_{j,N+1}$ and rearranging (9-7), gives

$$\left(\frac{x_{i,N+1}}{x_{i,1}} \right) \left(\frac{x_{j,1}}{x_{j,N+1}} \right) = \prod_{k=1}^{N_{\min}} \alpha_k \quad (9-8)$$

where $\alpha_k = K_{i,k}/K_{j,k}$, the relative volatility between components i and j at stage k . Equation (9-8) relates the relative enrichments of any two components i and j over N equilibrium stages to the relative volatilities of i to j . If these two enrichments are specified, then $N = N_{\min}$. Although (9-8) is exact, it is not used to calculate N_{\min} because the conditions at each stage must be known to compute the relative volatilities. Instead, a mean relative volatility, $(\alpha_{i,j})_m$ is used, and (9-8) simplifies to

$$\left(\frac{x_{i,N+1}}{x_{i,1}} \right) \left(\frac{x_{j,1}}{x_{j,N+1}} \right) = (\alpha_{i,j})_m^N \quad (9-9)$$

Taking the log to base 10 of both sides of (9-9), and rearranging the result gives,

$$N_{\min} = \frac{\log \left\{ \left[\frac{(x_{i,N+1})/x_{i,1}}{(x_{j,N+1})/x_{j,1}} \right] \right\}}{\log (\alpha_{i,j})_m^N} \quad (9-10)$$

Equation (9-10) is the useful **Fenske equation** [5]. When i = the LK and j = the HK, the minimum number of equilibrium stages is influenced by the non-key components only by their effect (if any) on the relative volatility between the key components.

Equation (9-10) permits a rapid estimation of N_{\min} when the split between two key components is specified. A more convenient form of (9-10) is obtained by (1) replacing $(\alpha_{i,j})_m$ by a geometric mean of the top- and bottom-stage values, and (2) replacing the product of the mole-fraction ratios by the equivalent product of mole-distribution ratios in terms of component distillate and bottoms flow rates d and b , respectively (even though distillate and bottoms products are not withdrawn from the column). Thus,

$$N_{\min} = \frac{\log \left[\frac{(d_i/d_j) (b_j/b_i)}{(\alpha_{i,j})_N (\alpha_{i,j})_1} \right]}{\log \left[(\alpha_{i,j})_N (\alpha_{i,j})_1 \right]^{1/2}} \quad (9-11)$$

The Fenske equation can also be written in terms of **split ratios**, $s_i = d_i/f_i$ where $f_i = d_i + b_i$ and $s_j = d_j/f_j$ where $f_j = d_j + b_j$:

$$N_{\min} = \frac{\log \left[\left(\frac{s_i}{1-s_i} \right) \left(\frac{1-s_j}{s_j} \right) \right]}{\log \left[(\alpha_{i,j})_N (\alpha_{i,j})_1 \right]^{1/2}} \quad (9-12)$$

In both (9-11) and (9-12), N_{\min} is determined by using specified separations for i = LK and j = HK. N_{\min} depends on the degree of separation of the two key components and their mean α . It is independent of feed-phase condition because at total reflux, there is no feed to the column. Equations (9-11) and (9-12) are exact for $N_{\min} = 2$. For one stage, they are equivalent to the equilibrium-flash equation for a single stage.

The Fenske equation is exact only if α does not vary and/or the mixture forms ideal solutions. A good approximation of the optimal number of equilibrium stages for a given split of two components is twice the N_{\min} computed by the Fenske equation. This rule is a useful starting point for rigorous stage-calculations with process simulators as described in Chapter 10. However, the Fenske equation should be applied with caution when applied to mixtures that are not close to ideal, especially if azeotropes form.

When the mixture forms nearly ideal solutions, but relative volatilities vary appreciable from the top to the bottom stage of the column because the feed contains components that cover a wide range of boiling point, a modification of the Fenske

equation by Winn [24] is more accurate. It is based on the assumption that pairs of K -values fit the expression

$$K_i = \zeta_{i,j} K_j^{\varphi_{i,j}}$$

where $\zeta_{i,j}$ and $\varphi_{i,j}$ are constants over the temperature and pressure range of the column. Dividing each side of (9-6a) by the φ power of (9-6b), and combining with the above equation gives the Winn equation for the LK and the HK:

$$N_{\min} = \frac{\log \left[\left(\frac{x_{LK,N+1}}{x_{LK,1}} \right) \left(\frac{x_{HK,1}}{x_{HK,N+1}} \right)^{\varphi_{LK,HK}} \right]}{\log \zeta_{LK,HK}} \quad (9-13)$$

EXAMPLE 9.2 Minimum Stages by the Fenske Equation.

For the debutanizer shown in Figure 9.3 and considered in Example 9.1, estimate N_{\min} by the Fenske equation. Calculate the mean relative volatility from the K -values in Example 9.1.

Solution

The LK is n -C₄ and the HK is i C₅. Figure 9.3 specifies distillate and bottoms flow rates for n -C₄ as 442 and 6 lbmol/h and for i C₅ as 13 and 23, respectively. From the solution to Example 9.1, their relative volatilities in the distillate and bottoms are, respectively: $1.009/0.459 = 2.203$ and $5.425/3.446 = 1.577$

$$(\alpha_{LK,HK})_m = [(2.203)(1.577)]^{1/2} = 1.864$$

From (9-11),

$$N_{\min} = \frac{\log[(442/6)(23/13)]}{\log [1.864]} = \frac{2.115}{0.2704} = 7.82$$

§9.1.4 Distribution of Non-Key Components at Total Reflux

The derivation of the Fenske equation in §9.1.3 is not restricted to key components. Therefore, once N_{\min} is calculated for the split of the two key components, (9-11) can be used to calculate splits of all non-key components using that value of N_{\min} . As discussed in §9.1.8, these values provide an approximation to the product distribution when using a process simulator to develop a design using more stages than N_{\min} .

Let i = a non-key component and j = the HK denoted by r . Then (9-11) becomes

$$\left(\frac{d_i}{b_i} \right) = \left(\frac{d_r}{b_r} \right) (\alpha_{i,r})_m^{N_{\min}} \quad (9-14)$$

Substituting $f_i = d_i + b_i$ in (9-14) gives

$$b_i = \frac{f_i}{1 + (d_r/b_r) (\alpha_{i,r})_m^{N_{\min}}} \quad (9-15)$$

or

$$d_i = \frac{f_i (d_r/b_r) (\alpha_{i,r})_m^{N_{\min}}}{1 + (d_r/b_r) (\alpha_{i,r})_m^{N_{\min}}} \quad (9-16)$$

Equations (9-15) and (9-16) give the distribution of a non-key component at total reflux as a function of N_{\min} , the split of the HK, and the mean relative volatility of the non-key with respect to the HK.

For accurate calculations, (9-15) and (9-16) are best used to compute the smaller of b_i and d_i . The other quantity is then obtained by an overall material balance, $f_i = d_i + b_i$. The Winn equation, (9-13), can also be applied to non-key components to calculate their distributions.

EXAMPLE 9.3 Distribution of Non-Key Components.

Estimate the product distributions for non-key components by the Fenske equation for the conditions of Example 9.2.

Solution

Using the K -values from the solution to Example 9.1, the geometric mean relative volatilities of all components with respect to the HK, isopentane, are calculated as in Example 9.2, with the following results:

Component	$(\alpha_{i,HK})_m$
isobutane	2.329
n -butane	1.864
isopentane	1.000
n -pentane	0.845
n -hexane	0.389
n -heptane	0.1825
n -octane	0.0852
n -decane	0.0401

The distillate and bottoms flow rates for n -butane and isopentane are fixed because they are the two key components. For isobutane, (9-15) is used to compute the bottoms flow rate:

$$\begin{aligned} b_{iC_4} &= \frac{f_{iC_4}}{1 + (d_{iC_5}/b_{iC_5}) (\alpha_{iC_4,iC_5})_m^{N_{\min}}} \\ &= \frac{12}{1 + (13/23)(2.329)^{7.82}} = 0.028 \text{ lbmol/h} \end{aligned}$$

from which, $d_{iC_4} = 12 - 0.028 = 11.972$ lbmol/h.

For n -pentane, which distributes primarily to the bottoms product, (9-16) is used to compute the distillate rate:

$$d_{nC_5} = \frac{f_{nC_5} (d_{iC_5}/b_{iC_5}) (\alpha_{nC_5,iC_5})_m^{N_{\min}}}{1 + (d_{iC_5}/b_{iC_5}) (\alpha_{nC_5,iC_5})_m^{N_{\min}}} = \frac{15(13/23)(0.845)^{7.82}}{1 + (13/23)(0.845)^{7.82}} = 1.97$$

from which, $b_{nC_5} = 15 - 1.97 = 13.03$ lbmol/h.

The distribution of the additional four non-key components is calculated by the same method as for n -pentane. The results for the distribution of components at N_{\min} are:

Component	Distillate, lbmol/h	Bottoms, lbmol/h
isobutane	11.972	0.028
n -butane	442.0	6.0
isopentane	13.0	23.0
n -pentane	1.97	13.03
n -hexane	0.00811	22.99
n -heptane	3.69E-05	39.10
n -octane	6.66E-07	272.20
n -decane	2.09E-10	31.00
Total	468.95	407.35

§9.1.5 Underwood Equations for Minimum Reflux

The minimum reflux ratio is also a useful limiting condition. Unlike minimum stages, there is a feed, and products are withdrawn, but the column has ∞ equilibrium stages.

For distillation of an ideal binary mixture at minimum reflux, as shown in Figure 7.13a, most of the stages are crowded into a constant-composition zone that bridges the feed stage. In this zone, all vapor and liquid streams have compositions essentially identical to those of the flashed feed. This zone constitutes a single **pinch point** (infinity of stages) as shown in Figure 9.5a. If nonideal phase conditions are such as to create a point of tangency between the equilibrium curve and the operating line in the rectifying section, as shown in Figure 7.12b, the pinch point occurs within the rectifying section as in Figure 9.5b. Alternatively, the single pinch point can occur in the stripping section (not shown in Figure 9.5).

Multicomponent systems are classified by Shiras, Hanson, and Gibson [6] as having one (Class 1) or two (Class 2) pinch points. For Class 1 separations, all components in the feed distribute to both the distillate and bottoms products. Then a single pinch point bridges the feed stage, as shown in Figure 9.5c. Class 1 separations occur with narrow-boiling-range mixtures or when the degree of separation between key components is not sharp.

For Class 2 separations, one or more components appear in only one of the products because some stripping or enriching takes place before the pinch zone is encountered. If neither distillate nor bottoms product contains all feed components, two pinch points occur away from the feed stage, as in Figure 9.5d. Stages between the feed stage and the rectifying-section pinch point remove heavy non-key (HHK) components that do not appear in the distillate. Light non-key (LLK) components that do not appear in the bottoms are removed by the stages between the feed stage and the stripping-section pinch point. However, if all feed components appear in the bottoms, the stripping-section pinch point moves to the feed stage, as shown in Figure 9.5e. The equations that predict the minimum

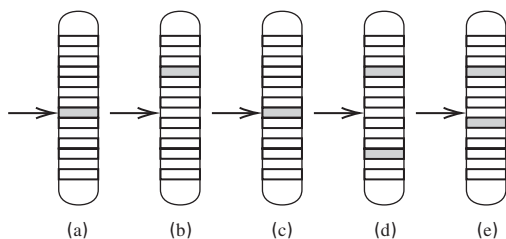


Figure 9.5 Location of pinch-point zones at minimum reflux: (a) ideal binary system; (b) nonideal binary system with conditions giving a point of tangency; (c) multicomponent system, all components distributed (Class 1); (d) multicomponent system, not all LLK and HHK distributing (Class 2); (e) multicomponent system, all LLK, if any, distributing, but not all HHK distributing (Class 2). (LLK = lighter than light key; HHK = heavier than heavy key.)

reflux ratio for Class 1 separations differ from and are less complex than those for Class 2 separations.

Consider the general case of a rectifying-section pinch point at or away from the feed stage as shown in Figure 9.6. A component material balance for component i , over all stages gives

$$y_{i,\infty}V_\infty = x_{i,\infty}L_\infty + x_{i,D}D \quad (9-17)$$

A total balance over all stages is

$$V_\infty = L_\infty + D \quad (9-18)$$

Since phase compositions do not change in the pinch zone, the phase-equilibrium relation is

$$y_{i,\infty} = K_{i,\infty}x_{i,\infty} \quad (9-19)$$

Writing (9-17) to (9-19) for component j and combining them with (9-17) to (9-19) for component i to eliminate $y_{i,\infty}$, $y_{j,\infty}$, and V_∞ gives the following equation for the internal reflux ratio at the pinch point, after replacing $K_{i,\infty}/K_{j,\infty}$ with $(\alpha_{i,j})_\infty$.

$$\frac{L_\infty}{D} = \frac{[(x_{i,D}/x_{i,\infty}) - (\alpha_{i,j})_\infty (x_{j,D}/x_{j,\infty})]}{(\alpha_{i,j})_\infty - 1} \quad (9-20)$$

Class 1 Separations

For Class 1 separations, flashed feed-and pinch-zone compositions are identical provided that the feed is neither subcooled nor superheated. Thus, $x_{i,\infty} = x_{i,F}$ and (9-20), with $i = \text{LK}$ and $j = \text{HK}$, becomes

$$\frac{(L_\infty)_{\min}}{F} = \frac{(L_F/F) [(Dx_{\text{LK},D}) / (L_F x_{\text{LK},F}) - (\alpha_{\text{LK},\text{HK}})_F (Dx_{\text{HK},D}) / (L_F x_{\text{HK},F})]}{(\alpha_{\text{LK},\text{HK}})_F - 1} \quad (9-21)$$

This equation is attributed to Underwood [7] and can be applied to subcooled-liquid or superheated-vapor feeds by using fictitious values of L_F and $x_{i,F}$ computed by making a flash calculation outside the two-phase region. As with the Fenske equation, (9-21) applies to non-key components. Therefore, for a specified split of two key components, the distribution of non-key components is obtained by combining

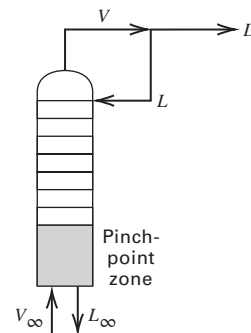


Figure 9.6 Rectifying-section pinch-point zone.

(9-21) with the analogous equation for component i in place of the light key to give

$$\frac{Dx_{i,D}}{L_F x_{i,F}} = \left[\frac{(\alpha_{i,\text{HK}})_F - 1}{(\alpha_{\text{LK},\text{HK}})_F - 1} \right] \left(\frac{Dx_{\text{LK},D}}{L_F x_{\text{LK},F}} \right) + \left[\frac{(\alpha_{\text{LK},\text{HK}})_F - (\alpha_{i,\text{HK}})_F}{(\alpha_{\text{LK},\text{HK}})_F - 1} \right] \left(\frac{Dx_{\text{HK},D}}{L_F x_{\text{HK},F}} \right) \quad (9-22)$$

For a Class 1 separation,

$$0 < \left(\frac{Dx_{i,D}}{F x_{i,F}} \right) < 1$$

for all non-key components. If so, the external reflux ratio (entering the column) is obtained from the internal reflux ratio by an enthalpy balance around the rectifying section in the form

$$\frac{(L_{\min})_{\text{external}}}{D} = (R_{\min})_{\text{external}} = \frac{(L_{\min})_{\infty} (h_{V_{\infty}} - h_{L_{\infty}}) + D (h_{V_{\infty}} - h_V)}{D (h_V - h_L)} \quad (9-23)$$

where h is molar enthalpy and subscripts V and L refer to vapor leaving the top stage and external liquid reflux sent to the top stage, respectively. For conditions of constant molar overflow,

$$(R_{\min})_{\text{external}} = (R_{\min})_{\infty} = (L_{\infty})_{\min}/D$$

Even when (9-21) is invalid because all feed components do not distribute, it is useful because, as shown by Gilliland [8], R_{\min} computed by assuming a Class 1 separation is \geq the true minimum. This is because the distributing non-key components in the pinch-point zones increase the separation difficulty, thus increasing the reflux requirement.

EXAMPLE 9.4 Minimum Reflux for a Class 1 Separation.

Calculate the minimum internal reflux-to-feed ratio for Example 9.2 assuming a Class 1 separation. Check the validity of this assumption.

Solution

From Example 9.1, $\alpha_{\text{LK},\text{HK}} = \alpha_{n\text{C}_4,i\text{C}_5}$ at column feed-stage conditions is $1.922/0.977 = 1.967$. Feed liquid and distillate quantities are given in Figure 9.3 and Example 9.1. From (9-21),

$$\frac{(L_{\infty})_{\min}}{F} = \frac{759}{876.3} \frac{[(442/345.41) - 1.967(13/31.28)]}{1.967 - 1} = 0.414$$

Assuming the distillate rate is that of Figure 9.3, $(L_{\infty})_{\min}/D = 0.414(976.3/468) = 0.864$

Because the feed contains components covering a wide range of boiling point, it is very unlikely that the assumption of a Class 1 separation is valid. Using (9-22), this is found to be the case. Calculated distillate flow rates of hexane to nonane are negative. The distillate rate of $i\text{C}_4$ is greater than its feed rate. Only $n\text{C}_5$ distributes, probably because it boils closely to the HK, for which the split is not sharp.

Class 2 Separations

For Class 2 separations, (9-17) to (9-20) still apply. However, (9-20) cannot be used directly to compute the internal minimum reflux ratio because values of $x_{i,\infty}$ are not easily relatable to feed composition for Class 2 separations. Underwood [9] devised a procedure to overcome this limitation. For the rectifying section pinch-point zone, he defined a quantity Φ by

$$\sum_i \frac{(\alpha_{i,r})_{\infty} x_{i,D}}{(\alpha_{i,r})_{\infty} - \Phi} = 1 + (R_{\infty})_{\min} \quad (9-24)$$

where subscript r is a reference component (e.g. the HK). Similarly, for the stripping section, Underwood defined Φ' by

$$\sum_i \frac{(\alpha'_{i,r})_{\infty} x_{i,B}}{(\alpha'_{i,r})_{\infty} - \Phi'} = 1 - (R'_{\infty})_{\min} \quad (9-25)$$

where $R'_{\infty} = L'_{\infty}/B$ and the prime refers to the stripping-section pinch-point zone. Underwood assumed that α values are constant in the region between the two pinch-point zones and that $(R_{\infty})_{\min}$ and $(R'_{\infty})_{\min}$ are related by the assumption of constant molar overflow between the feed entry and the rectifying-section pinch point and between the feed entry and the stripping-section pinch point. Hence,

$$(L'_{\infty})_{\min} - (L_{\infty})_{\min} = qF \quad (9-26)$$

where q is the feed condition given by (7-25). It is 1.0 for a saturated liquid feed and 0.0 for a saturated vapor feed. With these two critical assumptions, Underwood showed that at least one common root θ (where $\theta = \Phi = \Phi'$) exists between (9-24) and (9-25).

Equation (9-24) is analogous to the following equation derived from (9-19) and the relation $\alpha_{i,r} = K_i/K_r$,

$$\sum_i \frac{(\alpha_{i,r})_{\infty} x_{i,D}}{(\alpha_{i,r})_{\infty} - L_{\infty}/[V_{\infty}(K_r)_{\infty}]} = 1 + (R_{\infty})_{\min} \quad (9-27)$$

where $L_{\infty}/[V_{\infty}(K_r)_{\infty}]$ is the absorption factor for a reference component in the rectifying-section pinch-point zone. Although Φ is analogous to the absorption factor, a different root of Φ is used to solve for $(R_{\infty})_{\min}$ (Shiras et al. [6]).

The common root θ is determined by multiplying (9-24) and (9-25) by D and B , respectively, adding the equations, substituting (9-25) to eliminate $(R'_{\infty})_{\min}$ and $(R_{\infty})_{\min}$, and utilizing the component balance $z_{i,F}F = x_{i,D}D + x_{i,B}B$ to obtain

$$\sum_i \frac{(\alpha_{i,r})_{\infty} f_i}{(\alpha_{i,r})_{\infty} - \theta} = F(1 - q) \quad (9-28)$$

When only the two key components distribute, (9-28) is applied to the LK and HK and solved iteratively for a root of θ in the region, $\alpha_{\text{LK},\text{HK}} > \theta > 1$. The following modification of (9-24) is then solved for the internal reflux ratio $(R_{\infty})_{\min}$:

$$\sum_i \frac{(\alpha_{i,r})_{\infty} d_i}{(\alpha_{i,r})_{\infty} - \theta} = D + (L_{\infty})_{\min} \quad (9-29)$$

If any non-key components are suspected of distributing, estimated values of $x_{i,D}$ cannot be used directly in (9-29). This is particularly true when non-key components are intermediate in volatility between the keys or isomers of the keys. In this case, (9-28) is solved for m roots of θ , where m is one less than the number of distributing components. Each root of θ lies between an adjacent pair of relative volatilities of the distributing species. In Example 9.4, nC_5 distributes at minimum reflux, but nC_6 and heavier do not and iC_4 does not. Thus, it is only necessary to compute two roots of θ from (9-28), where, using $r = \text{HK}$,

$$\alpha_{nC_4, iC_5} > \theta_1 > 1.0 > \theta_2 > \alpha_{nC_5, iC_5}$$

With these two roots, (9-29) is written twice (once for $i = \text{LK}$ and once for $i = nC_5$) and solved simultaneously to yield $(R_\infty)_{\min}$ and the unknown value of d_{nC_5} . The solution must satisfy the condition $\sum_i d_i = D$.

With the internal reflux ratio $(R_\infty)_{\min}$ known, the external reflux ratio is computed by an enthalpy balance with (9-23). This requires a knowledge of the rectifying-section pinch-point compositions. Underwood [9] shows that

$$x_{i,\infty} = \frac{\theta x_{i,D}}{(R_\infty)_{\min}[(\alpha_{i,r})_\infty - \theta]} \quad (9-30)$$

with $y_{i,\infty}$ given by (9-17). The value of θ to be used in (9-30) is the root of (9-29) satisfying the inequality,

$$(\alpha_{\text{HNK},r})_\infty > \theta > 0$$

where HNK refers to the heaviest non-key in the distillate at minimum reflux. This root is equal to $L_\infty/[V_\infty(K_r)_\infty]$ in (9-27). With wide-boiling feeds, the external reflux can be higher than the internal reflux. Bachelor [4] cites a case where the external reflux rate is 55% greater.

For the stripping-section pinch-point composition, Underwood obtains

$$x'_{i,\infty} = \frac{\theta x_{i,B}}{[(R'_\infty)_{\min} + 1][(\alpha_{i,r})_\infty - \theta]} \quad (9-31)$$

where, here, θ is the root of (9-29) satisfying the inequality $(\alpha_{\text{HNK},r})_\infty > \theta > 0$, where HNK refers to the heaviest non-key in the bottoms product at minimum reflux.

The Underwood minimum reflux equations are widely used, but often without examining the possibility of non-key distribution. In addition, the assumption is frequently made that $(R_\infty)_{\min}$ equals the external reflux ratio. When the assumptions of constant α and constant molar overflow between the two pinch-point zones are not valid, values of the Underwood minimum reflux ratio for Class 2 separations can be appreciably in error because of the sensitivity of (9-28) to the value of q , as will be demonstrated in Example 9.5. When the Underwood assumptions appear valid and a negative minimum reflux ratio is computed, a rectifying section may not be needed for the separation. The Underwood equations show that the minimum reflux depends mainly on feed condition and α and, to a lesser extent, on degree of separation, as is

the case with binary distillation, as shown in Chapter 7. As with binary distillation, a minimum reflux ratio exists in a multicomponent system for an assumed perfect separation between the LK and HK.

An extension of the Underwood method for multiple feeds is given by Barnes et al. [10]. Exact methods for determining minimum reflux are also available [11]. For calculations at actual reflux conditions with a process simulator, knowledge of R_{\min} is useful, but not essential because R can be varied during the simulation. This is not the case for N_{\min} . It must be known so that a fixed value of $N > N_{\min}$ can be specified to make the specified split between two key components.

EXAMPLE 9.5 Minimum Reflux for a Class 2 Separation.

Repeat Example 9.4 assuming a Class 2 separation and using the Underwood equations.

Solution

Use the component feed rates and relative volatilities at feed conditions from Example 9.1. Assume $1-q$ = molar fraction vaporized = $117.3/876.3 = 0.134$. From Example 9.4, assume that the only distributing non-key component is n -pentane. Applying (9-28),

$$\begin{aligned} & \frac{2.329(12)}{2.329 - \theta} + \frac{1.864(448)}{1.864 - \theta} + \frac{1.00(36)}{1.00 - \theta} \\ & + \frac{0.845(15)}{0.845 - \theta} + \frac{0.389(23)}{0.389 - \theta} + \frac{0.1825(39.1)}{0.1825 - \theta} \\ & + \frac{0.0852(272.2)}{0.0852 - \theta} + \frac{0.0401(31)}{0.0401 - \theta} = 876.3(0.134) \end{aligned}$$

Solving with fzero of MATLAB for two roots of θ that satisfy

$$\begin{aligned} \alpha_{nC_4, iC_5} > \theta_1 > \alpha_{iC_5, iC_5} > \theta_2 > \alpha_{nC_5, iC_5} \\ & = 1.864 > \theta_1 > 1.00 > \theta_2 > 0.845 \\ \theta_1 & = 1.0443 \text{ and } \theta_2 = 0.8587 \end{aligned}$$

These two values of θ are used with (9-29) along with the sum of the component distillate rates to compute D , d_{nC_5} , and $(L_\infty)_{\min}$. Because the three equations are linear, they are solved with linsolve of MATLAB, assuming that $d_i = 12$ lbmol/h for isobutane and 0 for components heavier than n -pentane.

$$\begin{aligned} D + (L_\infty)_{\min} &= \frac{2.329(12)}{2.329 - 1.0443} + \frac{1.864(442)}{1.864 - 1.0443} \\ &+ \frac{1.00(13)}{1.00 - 1.0443} + \frac{0.845(d_{nC_5})}{0.845 - 1.0443} \\ D + (L_\infty)_{\min} &= \frac{2.329(12)}{2.329 - 0.8587} + \frac{1.864(442)}{1.864 - 0.8587} \\ &+ \frac{1.00(13)}{1.00 - 0.8587} + \frac{0.845(d_{nC_5})}{0.845 - 0.8587} \\ D &= 12 + 442 + 13 + (d_{nC_5}) \end{aligned}$$

Solving these three equations gives

$$\begin{aligned} d_{nC_5} &= 3.5 \text{ lbmol/h} \\ D &= 470.5 \text{ lbmol/h} \\ (L_\infty)_{\min} &= 244 \text{ lbmol/h} \end{aligned}$$

and

$$(L_{\infty})_{\min}/D = 244/468 = 0.521$$

The internal minimum reflux ratio of 0.521 at the rectifying pinch point is considerably less than the value of 0.864 computed in Example 9.4 for the invalid application of the Class 1 Underwood method. Using a rigorous method, Bachelor [4] computes an internal reflux ratio of 0.637. The reason for the discrepancy between 0.521 and the rigorous value of 0.637 is the invalidity of the constant molar overflow assumption used by Underwood to obtain an analytical solution. Using somewhat different K -values, Bachelor computes an average temperature between the two pinch regions of 152°F, which is appreciably lower than the flashed-feed temperature 181.4°F. The relatively hot feed causes vaporization across the feed zone. More vapor flows up the column in the rectifying section and less liquid flows down in the stripping section. The value of q is decreased significantly, causing a need for a higher minimum reflux ratio. Bachelor also computes a minimum external reflux ratio of 0.624 (very close to the internal value) with an enthalpy balance.

§9.1.6 Gilliland Correlation for Actual Reflux Ratio and Equilibrium Stages

Capital, and interest-on-capital costs, are related to the number of stages, whereas operating costs are tied to reflux ratio and thus to fuel costs for providing heat to the reboiler. Less reflux is needed if more stages are added, so operating costs decrease as capital costs increase. The Gilliland correlation [13] provides an approximate relationship between the number of equilibrium stages and the reflux ratio so that an optimal reflux ratio can be readily determined.

For an industrial separation, the reflux ratio and equilibrium stages must be greater than their minimum values. An operating reflux ratio is established by economic considerations at a reflux $>$ minimum reflux. The optimal number of stages could be established at some value $>$ minimum stages, but the former choice is preferred because the reflux to R_{\min} is much closer to 1.0 than is the ratio N/N_{\min} . The corresponding number of equilibrium stages is then determined with the shortcut (FUG) method using the empirical Gilliland correlation. As shown in Figure 9.7, from studies by Fair and Bolles [12], an optimal

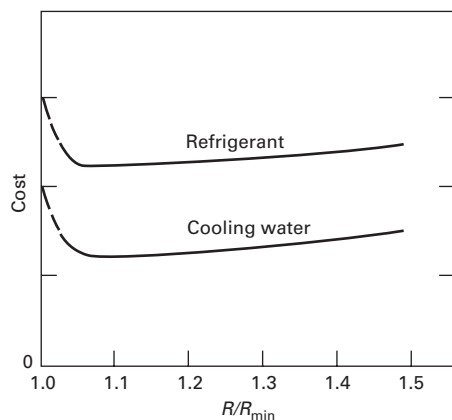


Figure 9.7 Effect of reflux ratio on cost.

value of R/R_{\min} , based on relative operating cost at the time of their study, was 1.05, for either cooling water or a refrigerant for the condenser. However, near-optimal conditions are not sharply defined, but extend over a relatively broad range of larger values of R/R_{\min} . Superfractionators requiring many stages commonly use a value of R/R_{\min} of approximately 1.10, while columns requiring a small number of stages are designed for a value of R/R_{\min} of approximately 1.50. For intermediate cases, a common rule of thumb is $R/R_{\min} = 1.30$.

The number of equilibrium stages required for the separation of a binary mixture assuming constant relative volatility and constant molar overflow depends on $z_{i,F}$, $x_{i,D}$, $x_{i,B}$, q , R , and α . From (9-11), for a binary mixture, N_{\min} depends on $x_{i,D}$, $x_{i,B}$, and α , while R_{\min} depends on $z_{i,F}$, $x_{i,D}$, q , and α . Accordingly, studies have assumed correlations of the form

$$N = N \left\{ N_{\min} \{ x_{i,D}, x_{i,B}, \alpha \}, R_{\min} \{ z_{i,F}, x_{i,D}, q, \alpha \}, R \right\} \quad (9-32)$$

Furthermore, studies have assumed that such a correlation might exist for nearly ideal multicomponent systems even though additional feed composition variables and values of α for non-key components also influence the value of R_{\min} .

A simple, successful correlation is that of Gilliland [13], which was modified later by Robinson and Gilliland [14]. The correlation is shown in Figure 9.8, where three sets of data points, all based on accurate calculations, are the original points from Gilliland [13], with added points of Brown and Martin [15] and Van Winkle and Todd [16]. The 61 data points cover the following ranges:

- | | |
|----------------------------------|------------------------------|
| 1. Number of components: 2 to 11 | 4. α : 1.11 to 4.05 |
| 2. q : 0.28 to 1.42 | 5. R_{\min} : 0.53 to 9.09 |
| 3. Pressure: vacuum to 600 psig | 6. N_{\min} : 3.4 to 60.3 |

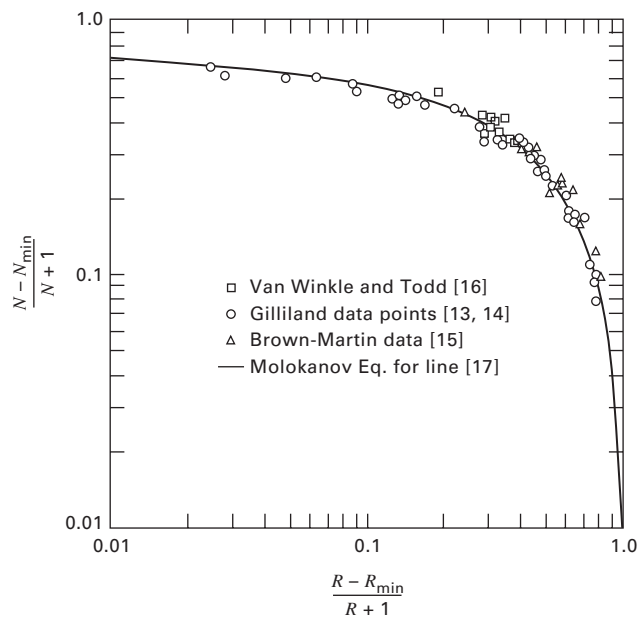


Figure 9.8 Comparison of rigorous calculations with Gilliland correlation.

The line drawn through the data represents the equation developed by Molokanov et al. [17]:

$$Y = \frac{N - N_{\min}}{N + 1} = 1 - \exp \left[\left(\frac{1 + 54.4X}{11 + 117.2X} \right) \left(\frac{X - 1}{X^{0.5}} \right) \right] \quad (9-33)$$

where

$$X = \frac{R - R_{\min}}{R + 1} \quad (9-34)$$

Equation (9-33) satisfies the end points ($Y = 0, X = 1$) and ($Y = 1, X = 0$). At a value of R/R_{\min} near the optimum of 1.3, Figure 9.9 predicts an optimal ratio for N/N_{\min} of approximately 2. The value of N includes one stage for a partial reboiler and one stage for a partial condenser, if used. Alternatively, a simpler equation by Eduljee [25] fits the Gilliland correlation well except at the end points:

$$Y = 0.75(1 - X^{0.5668}) \quad (9-35)$$

The Gilliland correlation is appropriate only for preliminary exploration of design variables. Although it was never intended for final design, the correlation was widely used for final designs of hydrocarbon distillation columns before digital computers were available to make accurate equilibrium-stage calculations. Robinson and Gilliland [14] state that a more accurate correlation should utilize a parameter involving the feed condition q . This effect is shown in Figure 9.9 using data points for the sharp separation of benzene–toluene mixtures from Guerreri [18]. The data, which cover feed conditions ranging from subcooled liquid to superheated vapor ($q = 1.3$ to -0.7), show a trend toward decreasing stage requirements with increasing feed vaporization. The Gilliland correlation is conservative for feeds having low values of q . Donnell and Cooper [19] state that this effect of q is important only when the $\alpha_{LK,HK}$ is high, or when the feed is low in volatile components.

A serious problem with the Gilliland correlation can occur when stripping is more important than rectification, because the correlation is based on reflux and not boilup.

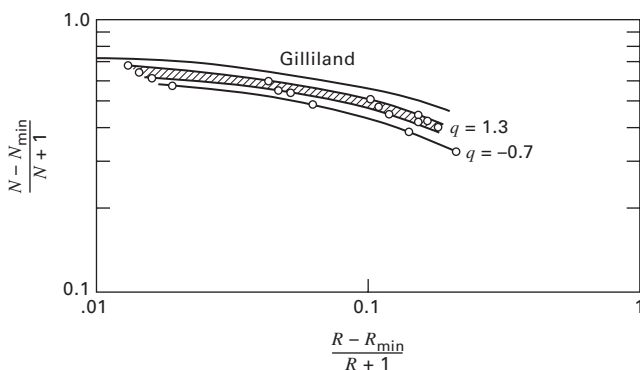


Figure 9.9 Effect of feed condition on Gilliland correlation. [Reproduced from [18] with permission from the Gulf Publishing Company.]

For example, Oliver [20] considers a fictitious binary case with specifications of $z_F = 0.05$, $x_D = 0.40$, $x_B = 0.001$, $q = 1$, $\alpha = 5$, $R/R_{\min} = 1.20$, and constant molar overflow. By exact calculations, $N = 15.7$. From the Fenske equation, $N_{\min} = 4.04$. From the Underwood equation, $R_{\min} = 1.21$. From (9-32) for the Gilliland correlation, $N = 10.3$. This is 34% lower than the exact value. This limitation, caused by ignoring boilup, is discussed by Strangio and Treybal [21].

EXAMPLE 9.6 Use of the Gilliland Correlation.

Use the Gilliland correlation to estimate the equilibrium-stage requirement for the debutanizer of Examples 9.1 to 9.5 for a reflux ratio 30% higher than the minimum value.

Solution

From Example 9.2, $N_{\min} = 7.82$. From results in Examples 9.4 and 9.5, three values of R_{\min} may be considered:

Underwood Class 1: 0.864

Underwood Class 2: 0.521

Rigorous: 0.637

Although all three of these are internal ratios in the pinch zone, they will be used because the rigorous result of Bachelor [4] for the external ratio is within 2% of the internal ratio.

The calculation is made with (9-33), which fits the Gilliland correlation well. For example, using the Class 2 value of $R_{\min} = 0.521$,

$$X = \frac{R - R_{\min}}{R + 1} = \frac{1.3(0.521) - 0.521}{1.3(0.521) + 1} = 0.0932$$

$$Y = \frac{N - N_{\min}}{N + 1} = 1 - \exp \left[\left(\frac{1 + 54.4(0.0932)}{11 + 117.2(0.0932)} \right) \left(\frac{0.0932 - 1}{0.0932^{0.5}} \right) \right] = 0.5607$$

Solving, $N = 19.1$ and $N/N_{\min} = 19.1/7.82 = 2.44$

Equilibrium stages for the other two R_{\min} values are calculated in the same manner, with the following results:

R_{\min} Method	Underwood Case 1	Underwood Case 2	Rigorous
R_{\min}	0.864	0.521	0.637
N	17.8	19.1	18.6

Although the estimates of R_{\min} vary widely, the values of N do not.

§9.1.7 Feed-Stage Location

Implicit in the application of the Gilliland correlation is the specification that stages be distributed optimally between rectifying and stripping sections. Brown and Martin [15] suggest that the optimal feed stage be located by assuming that the ratio of stages above the feed to stages below is the same as the ratio determined by applying the Fenske equation to the separate sections at total reflux conditions. Thus, using feed

conditions at the bottom of the rectifying section and at the top of the stripping section,

$$\frac{N_R}{N_S} \approx \frac{(N_R)_{\min}}{(N_S)_{\min}} = \frac{\log \left[\frac{(x_{LK,D}/z_{LK,F}) (z_{HK,F}/x_{HK,D})}{(\alpha_B \alpha_F)^{1/2}} \right]}{\log \left[\frac{(z_{LK,F}/x_{LK,B}) (x_{HK,B}/z_{HK,F})}{(\alpha_D \alpha_F)^{1/2}} \right]} \quad (9-36)$$

Where the subscripts *R* and *S* refer to the rectifying and stripping sections, respectively and the relative volatilities are for the LK with respect to the HK. Unfortunately, (9-36) is not reliable except for fairly symmetrical feeds and separations.

A better approximation of the optimal feed-stage location can be made with the Kirkbride [22] empirical equation:

$$\frac{N_R}{N_S} = \left[\left(\frac{z_{HK,F}}{z_{LK,F}} \right) \left(\frac{x_{LK,B}}{x_{HK,D}} \right)^2 \left(\frac{B}{D} \right) \right]^{0.206} \quad (9-37)$$

A severe test of both equations is provided by a fictitious binary-mixture problem of Oliver [20] cited in the previous section. Exact calculations by Oliver and calculations using (9-36) and (9-37) give the following results:

Method	N_R/N_S
Exact	0.0827
Kirkbride (9-37)	0.1971
Fenske ratio (9-36)	0.6408

Although the Kirkbride result is not very satisfactory, the result from the Fenske ratio method is much worse. In practice, distillation columns are provided with several feed entry locations, leaving the task of selecting the optimal feed location to the equipment operators.

EXAMPLE 9.7 Feed-Stage Location.

Use the Kirkbride equation to determine the feed-stage location for the debutanizer of Example 9.1, assuming 19.1 total equilibrium stages, 18.1 in the column and 1 for a partial reboiler.

Solution

Assume that the product distribution, computed in Example 9.3 for total-reflux conditions, is a good approximation to the distillate and bottoms compositions at actual reflux conditions. Then

$$B = 407.35 \text{ lbmol/h}, \quad x_{nC_4,B} = \frac{6.0}{407.35} = 0.0147$$

$$D = 468.95 \text{ lbmol/h}, \quad x_{iC_5,D} = \frac{13}{468.95} = 0.0278$$

From Figure 9.3,

$$z_{nC_4,F} = 448/876.3 = 0.5112$$

and $z_{nC_5,F} = 36/876.3 = 0.0411$

From (9-37),

$$\frac{N_R}{N_S} = \left[\left(\frac{0.0411}{0.5112} \right) \left(\frac{0.0147}{0.0278} \right)^2 \left(\frac{407.35}{468.95} \right) \right]^{0.206} = 0.444$$

Therefore, $N_R = (0.444/1.444)(18.1) = 5.6$ stages and $N_S = 18.1 - 5.6 = 12.5$ stages. Rounding the estimated stage requirements leads to one stage as a partial reboiler, 13 stages below the feed, and 6 stages above the feed. Because the split of the LK is much sharper than that of the HK, it is reasonable that more stages are needed in the stripping section.

§9.1.8 Distribution of Non-Key Components at Actual Reflux

As shown in §9.1.3 to 9.1.5 for multicomponent mixtures, all components distribute between distillate and bottoms at total reflux; while at minimum reflux conditions, none or only a few of the non-key components distribute. Distribution ratios for these two limiting conditions are given in Figure 9.10 for the previous debutanizer example. For total reflux, the Fenske-equation results from Example 9.3 plot as a straight line on log–log coordinates. For minimum reflux, Underwood-equation results from Example 9.5 are a dashed line.

Product–distribution curves for a reflux ratio between the minimum and infinity might be expected to lie between lines for total and minimum reflux. However, as shown by Stupin and Lockhart [23] in Figure 9.11, this is not the case. Near R_{\min} , product distribution (curve 3) lies between the two limits (curves 1 and 4). However, for a high reflux ratio, non-key distributions (curve 2) may lie outside the limits, thus causing inferior separations.

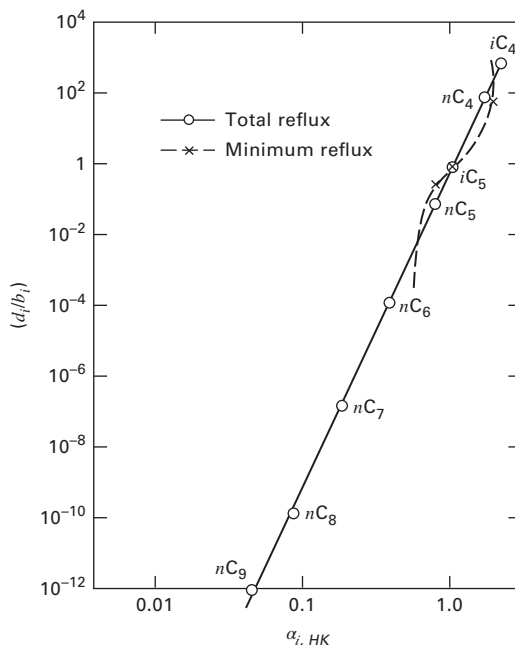


Figure 9.10 Component distribution ratios at extremes of distillation operating conditions.

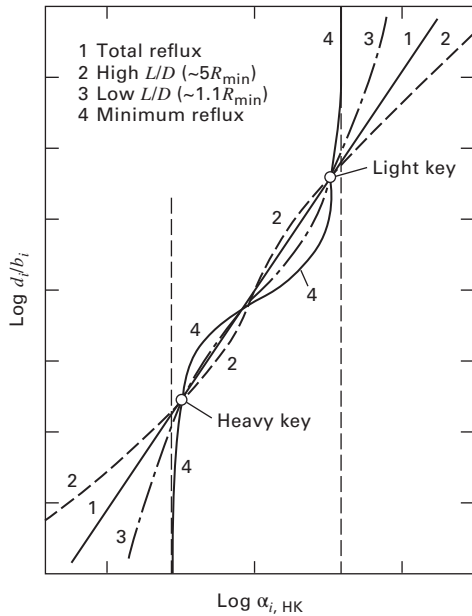


Figure 9.11 Component distribution ratios at various reflux ratios.

Stupin and Lockhart provide explanations for Figure 9.11 consistent with the Gilliland correlation. As the reflux ratio is decreased from total reflux while maintaining the key-component splits, stage requirements increase slowly at first, but then rapidly as minimum reflux is approached. Initially, large decreases in reflux cannot be compensated for by increasing stages. This causes inferior non-key distributions. As R_{min} is approached, small decreases in reflux are compensated for by large increases in stages; and the separation of non-key components becomes superior to that at total reflux. It appears reasonable to assume that, at a near-optimal R/R_{min} -ratio of 1.3, non-key-component distribution is close to that estimated by the Fenske equation for total-reflux conditions.

§9.2 USING THE SHORTCUT (FUG) METHOD WITH PROCESS SIMULATORS

Because the shortcut (FUG) method is so useful for making preliminary multicomponent distillation calculations prior to rigorous ones, it is included in all process simulators. The method is particularly useful for the design of distillation columns for the separation of hydrocarbon mixtures. In the following example, the FUG method is applied with three process simulators to the debutanizer in Figure 9.3.

EXAMPLE 9.8 FUG Method by Process Simulators.

Use Aspen Plus, CHEMCAD, and ChemSep to apply the FUG method with the following specifications taken from Figure 9.3 and Example 9.1. Compare the results with those of the hand calculations in Examples 9.2 to 9.7:

- Component feed flow rates in Figure 9.3
- LK and HK selection and splits in Figure 9.3

Feed temperature of 181.4°F and pressure of 74 psia at column entry point
 Pressure leaving condenser = 70 psia.
 Pressure at column top stage = 72 psia
 Pressure at column bottom stage = 77 psia
 Total condenser and partial reboiler
 $R/R_{min} = 1.3$
 SRK model for thermodynamic properties

Solution

Input for the three simulators differ somewhat, as shown in the table below. In the ChemSep simulator, the FUG method is part of a rigorous simulation and is accessible only after a successful simulation run:

	Aspen Plus	CHEMCAD	ChemSep
Model	DSTWU	SHOR	FUG
LK and HK splits	By recoveries	By split fractions to distillate	By recoveries
Pressure	Distillate and bottoms pressures	Distillate pressure and column pressure drop	Condenser, top, and bottoms pressures
Method for N_{min}	Winn	Fenske	Fenske
Method for feed stage location	Kirkbride	Fenske or Kirkbride	Kirkbride
Can specify a range of R/R_{min} values	Yes	Yes	Yes
Can specify N/N_{min} instead of R/R_{min}	Yes	No	No

Results of calculations from the process simulators are as follows for $R/R_{min} = 1.3$:

	Aspen Plus	CHEMCAD	ChemSep	Hand calculations
Model	DSTWU	SHOR	FUG	FUG
N_{min}	7.6	8.8	7.8	7.8
R_{min}	0.608	0.553	0.545	0.521
R	0.791	0.719	0.709	0.677
N	16.2	19.9	18.7	19.1
Feed stage from top	4.6	4.9 (Kirkbride) 6.8 (Fenske)	5.9 (Kirkbride)	5.6 (Kirkbride)
Condenser duty, Btu/h	7,536,000	6,953,000	6,095,000	—
Reboiler duty, Btu/h	9,864,000	9,263,000	9,163,000	—

Figure 9.12, from CHEMCAD results for Example 9.8, shows the variation of the number of equilibrium stages with R/R_{min} covering the range from 1.05 to 1.50. The optimal R/R_{min} is always within this range, while as shown in Figure 9.12, the corresponding optimal N/N_{min} is near the value of two.

This example is solved rigorously by a process simulator in Chapter 10.

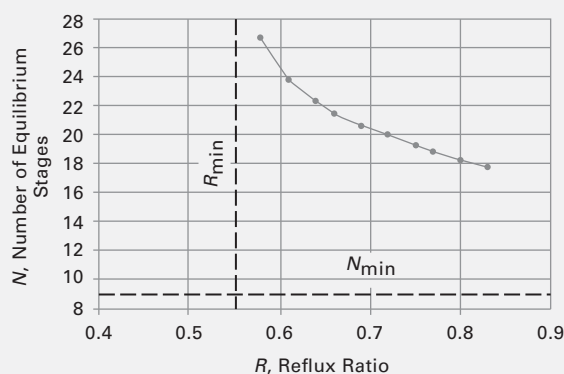


Figure 9.12 Variation of N with R for debutanizer of Figure 9.3.

CHAPTER 9 NOMENCLATURE

Abbreviations and Acronyms

HNK heaviest non-key in the bottoms product, (9-30) and (9-31)

Latin Symbols

b_i moles of component i in the bottoms, (9-11)
 d_i moles of component i in the distillate, (9-11)
 f_i moles of component i in the feed, (9-12)
 k stage number, (9-8)

SUMMARY

1. The Fenske–Underwood–Gilliland (FUG) method for distillation of ideal and nearly ideal multicomponent mixtures is useful for preliminary estimates of stage and reflux requirements, prior to rigorous calculations with a process simulator. The FUG method is available in most process simulators.
2. Based on a specified split of two key components in the feed mixture, the Fenske equation is used to determine N_{\min} at

REFERENCES

1. KREMSER, A., *Natl. Petroleum News*, **22**(21), 43–49 (1930).
2. EDMISTER, W.C., *AIChE J.*, **3**, 165–171 (1957).
3. KOBE, K.A., and J.J. MCKETTA, Jr., Eds, *Advances in Petroleum Chemistry and Refining*, Interscience, New York, Vol. 2, pp. 315–355 (1959).
4. BACHELOR, J.B., *Petroleum Refiner.*, **36**(6), 161–170 (1957).
5. FENSKE, M.R., *Ind. Eng. Chem.*, **24**, 482–485 (1932).
6. SHIRAS, R.N., D.N. HANSON, and C.H. GIBSON, *Ind. Eng. Chem.*, **42**, 871–876 (1950).
7. UNDERWOOD, A.J.V., *Trans. Inst. Chem. Eng.*, **10**, 112–158 (1932).
8. GILLILAND, E.R., *Ind. Eng. Chem.*, **32**, 1101–1106 (1940).
9. UNDERWOOD, A.J.V., *J. Inst. Petrol.*, **32**, 614–626 (1946).

L_{∞} molar liquid flow rate at the rectifying section pinch point, (9-26)
 L'_{∞} molar liquid flow rate at the stripping section pinch point, (9-26)
 R_{∞} reflux ratio the rectifying section pinch point = L_{∞}/D , (9-24)
 R'_{\min} reflux ratio at the stripping section pinch point = L'_{∞}/B , (9-25)
 s_i, s_j split ratios, d_i/f_i and d_j/f_j respectively, (9-12)
 $x_{i,\infty}$ mole fraction of component i at the rectifying section pinch point, (9-30)
 $x'_{i,\infty}$ mole fraction of component i at the stripping section pinch point, (9-31)

Greek Symbols

ζ, φ constants in the Winn equation, (9-13)
 Φ, Φ', θ roots of the Underwood equation, (9-24) and (9-28)

Subscripts

m mean value, (9-9)
 i, j components, (9-8); $i = LK, j = HK$, (9-12)
 R rectifying section, (9-36)
 r reference component in the Fenske equation, (9-14)
 S stripping section, (9-36)

total reflux. The Underwood equations are used to determine R_{\min} for an infinite number of stages. The empirical Gilliland correlation relates N_{\min} and R_{\min} to estimate the actual R and N .

3. Distribution of non-key components and feed-stage location can be estimated with the Fenske and Kirkbride equations, respectively.

10. BARNES, F.J., D.N. HANSON, and C.J. KING, *Ind. Eng. Chem., Process Des. Dev.*, **11**, 136–140 (1972).

11. TAVANA, M., and D.N. HANSON, *Ind. Eng. Chem., Process Des. Dev.*, **18**, 154–156 (1979).

12. FAIR, J.R., and W.L. BOLLES, *Chem. Eng.*, **75**(9), 156–178 (1968).

13. GILLILAND, E.R., *Ind. Eng. Chem.*, **32**, 1220–1223 (1940).

14. ROBINSON, C.S., and E.R. GILLILAND, *Elements of Fractional Distillation*, 4th ed., McGraw-Hill, New York, pp. 347–350 (1950).

15. BROWN, G.G., and H.Z. MARTIN, *Trans. AIChE*, **35**, 679–708 (1939).

16. VAN WINKLE, M., and W.G. TODD, *Chem. Eng.*, **78**(21), 136–148 (1971).

17. MOLOKANOV, Y.K., T.P. KORABLINA, N.I. MAZURINA, and G.A. NIKIFOROV, *Int. Chem. Eng.*, **12**(2), 209–212 (1972).

18. GUERRERI, G., *Hydrocarbon Processing*, **48**(8), 137–142 (1969).
19. DONNELL, J.W., and C.M. COOPER, *Chem. Eng.*, **57**, 121–124 (1950).
20. OLIVER, E.D., *Diffusional Separation Processes: Theory, Design, and Evaluation*, John Wiley & Sons, New York, pp. 104–105 (1966).
21. STRANGIO, V.A., and R.E. TREYBAL, *Ind. Eng. Chem., Process Des. Dev.*, **13**, 279–285 (1974).

STUDY QUESTIONS

- 9.1. Rigorous, computer-based methods for multicomponent distillation are readily available in process simulators. Why, then, is the FUG method still useful and widely applied for distillation of multicomponent mixtures?
- 9.2. When calculating multicomponent distillation, why is it best to list the components in order of decreasing volatility? In such a list, do the two key components have to be adjacent?
- 9.3. What does the Fenske equation compute? What assumptions are made in its derivation?
- 9.4. For what conditions should the Fenske equation be used with caution?
- 9.5. Is use of the Fenske equation restricted to the two key components? If not, what else can the Fenske equation be used for besides the estimation of the minimum number of equilibrium stages, corresponding to total reflux? What is a near-optimal value of N/N_{\min} .

EXERCISES

Section 9.1

9.1. Type of condenser and operating pressure.

A mixture of propionic and *n*-butyric acids, which can be assumed to form ideal solutions, is to be separated by distillation into a distillate containing 95 mol% propionic acid and a bottoms of 98 mol% *n*-butyric acid. Select an appropriate type condenser and estimate the distillation operating pressure. The normal boiling points are 141.1°C for propionic acid and 163.5°C for *n*-butyric acid.

9.2. Type of condenser and operating pressure.

Two distillation columns are used to produce the products indicated in Figure 9.13. Establish the type of condenser and an operating pressure for each column for: (a) direct sequence (C_2/C_3 separation first) and (b) indirect sequence (C_3/nC_4 separation first). See Section 1.8.2 for a discussion of sequences. Use a process simulator with the SRK EOS to determine bubble-points and dew-points.

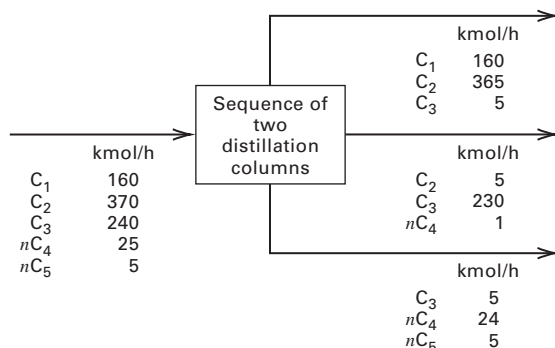


Figure 9.13 Data for Exercise 9.2.

22. KIRKBRIDE, C.G., *Petroleum Refiner*, **23**(9), 87–102 (1944).
23. STUPIN, W.J., and F.J. LOCKHART, “The Distribution of Non-Key Components in Multicomponent Distillation,” presented at the 61st Annual Meeting of the AIChE, Los Angeles, CA, December 1–5, 1968.
24. WINN, F.W., *Petroleum Refiner*, **37**(5), 216–218 (1958).
25. EDULJEE, H.E., *Hydrocarbon Processing*, **54**(9), 120 (1975).

- 9.6. What is a pinch point or pinch-point zone? For multicomponent distillation, under what conditions is the pinch point at the feed location? What conditions cause the pinch point to migrate away from the feed location?
- 9.7. What is the difference between a Class 1 and a Class 2 separation? Why is the Class 1 Underwood equation useful even if the separation is Class 2?
- 9.8. What is internal reflux? How does it differ from external reflux? Does the Underwood equation compute internal or external reflux? How can one be determined from the other?
- 9.9. What is the optimal range of values for R/R_{\min} ?
- 9.10. What key parameter is missing from the Gilliland correlation?
- 9.11. When can a serious problem arise with the Gilliland correlation?
- 9.12. What is the best method for estimating the distribution of non-key components at the actual (operating) reflux?

9.3. Type of condenser and operating pressure.

For each of the distillations *D*-1 and *D*-2 in Figure 9.14, establish the type of condenser and an operating pressure. Use a process simulator with the SRK EOS to determine bubble-points and dew-points.

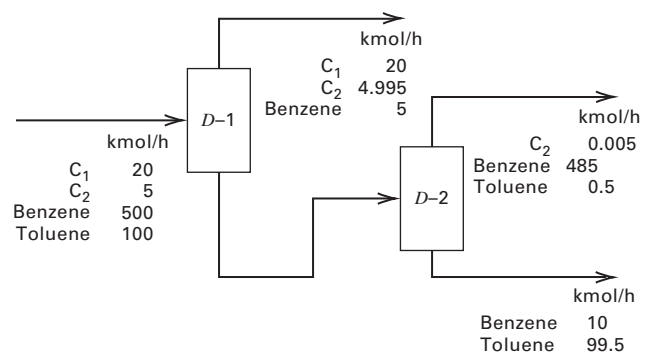


Figure 9.14 Data for Exercise 9.3.

9.4. Stages for a deethanizer.

For the deethanizer in Figure 9.15, estimate the number of equilibrium stages, assuming it is equal to 2.5 times N_{\min} .

9.5. Fenske equation for a column with a vapor sidestream.

For the complex distillation in Figure 9.16, use the Fenske equation to determine N_{\min} between the: (a) distillate and feed, (b) feed and sidestream, and (c) sidestream and bottoms. Use a process simulator with Raoult's law K -values to obtain bubble- and dew-points and relative volatilities.

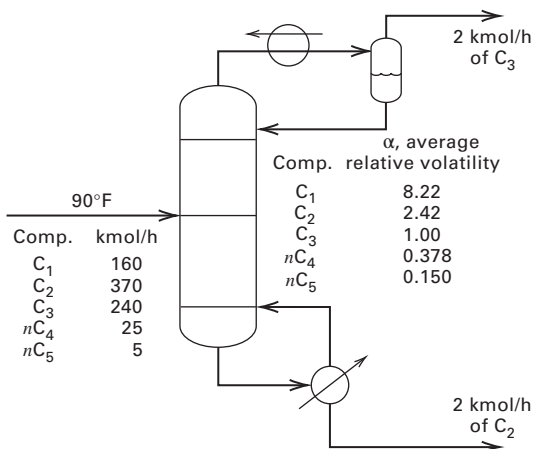


Figure 9.15 Data for Exercise 9.4.

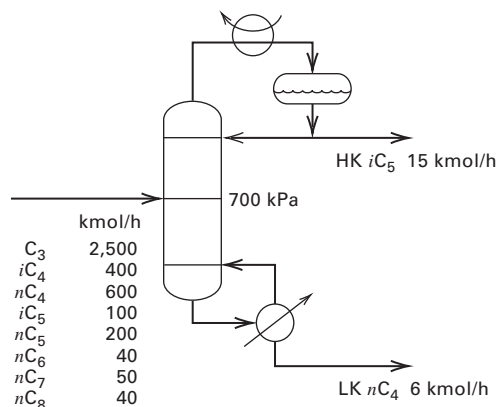


Figure 9.17 Data for Exercise 9.7.

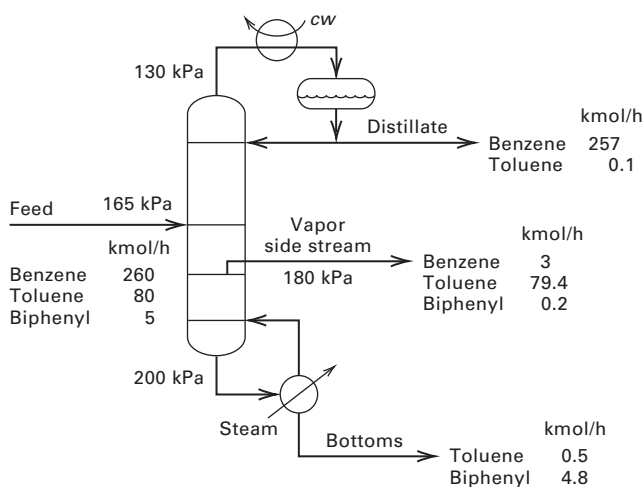


Figure 9.16 Data for Exercise 9.5.

9.6. Fenske equation for a binary distillation.

A 25 mol% mixture of acetone (A) in water (W) is to be separated by distillation at 130 kPa into a liquid distillate containing 95 mol% acetone and a liquid bottoms of 2 mol% acetone. Calculate N_{min} by the Fenske equation. Use a process simulator with the Wilson equation for liquid-phase activity coefficients to obtain bubble points and relative volatilities.

9.7. Distribution of non-keys and minimum stages.

For the distillation in Figure 9.17, calculate N_{min} and the distribution of the non-key components by the Fenske equation, using a process simulator with the SRK EOS to make bubble-point calculations and obtain relative volatilities.

9.8. Type of condenser, operating pressure, non-key distribution, and N_{min} .

For the distillation in Figure 9.18, establish the condenser type and operating pressure, calculate N_{min} , and estimate the distribution of the non-key components. Use a process simulator with the SRK EOS to make bubble and dew point calculations and obtain K -values for using the Fenske equation.

9.9. Effect of distillate rate on key-component recovery.

For $N_{min} = 15$ at 250 psia, calculate and plot the percent recovery of C₃ in the distillate as a function of distillate flow rate for the distillation of 1,000 lbmol/h of a feed containing by moles: 3% C₂,

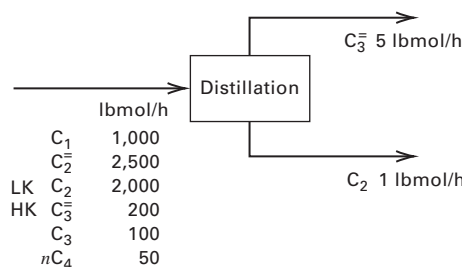


Figure 9.18 Data for Exercise 9.8.

20% C₃, 37% nC₄, 35% nC₅, and 5% nC₆. Use a process simulator with the SRK EOS to make bubble- and dew-point calculations and obtain K -values for using the Fenske equation.

9.10. Class 1 Underwood equations.

Use the Underwood equations to estimate the minimum external reflux ratio for the separation by distillation of 30 mol% propane in propylene to obtain 99 mol% propylene and 98 mol% propane, if the feed condition at a column pressure of 300 psia is: (a) bubble-point liquid, (b) 50 mol% vaporized, and (c) dew-point vapor. For all three cases, use a relative volatility of 1.125.

9.11. Class 2 Underwood equations.

For the conditions of Exercise 9.7, with bubble-point liquid feed at column pressure, compute the minimum external reflux and non-key distribution at R_{min} by the Class 2 Underwood equations.

Use a process simulator with the SRK EOS to calculate the bubble-point for the feed and obtain K -values at the feed condition. Use MATLAB to solve the Class 2 Underwood equations.

9.12. R_{min} and N_{min} as functions of product purity.

Calculate and plot the external R_{min} and N_{min} against % product purity for the separation by distillation of an equimolar bubble-point liquid feed of isobutane/*n*-butane at 100 psia. The distillate is to have the same iC₄ purity as the bottoms is to have nC₄ purity. Consider purities from 90% to 99.99%. Discuss the results. Use a relative volatility of 1.35.

Section 9.2

9.13. Reflux ratio by the FUG method.

Use a process simulator with the SRK EOS to determine by the FUG method the reflux ratio required for the distillation in Figure 9.19 for $N/N_{min} = 2.0$. The column pressures are 19 atm in the condenser, 20 atm at the feed plate, and 20.5 atm in the reboiler.

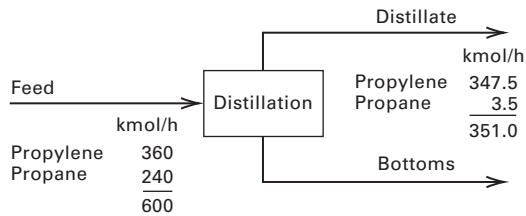


Figure 9.19 Data for Exercise 9.13.

The feed is at the bubble-point temperature at feed-tray pressure. Assume that external reflux equals internal reflux at the upper pinch zone. A total condenser and a partial reboiler are used.

9.14. Equilibrium stages by the FUG method.

A feed of 62 mol% *para*-dichlorobenzene in *ortho*-dichlorobenzene is separated by distillation at atmospheric pressure into a distillate containing 98 mol% *para* isomer and a bottoms of 96 mol% *ortho* isomer. A total condenser and partial reboiler are used and the feed is 10 mol% vaporized at the feed tray. Use a process simulator with Raoult's law to determine by the FUG method the number of equilibrium stages required for $R/R_{\min} = 1.15$.

9.15. Limitation of the Gilliland correlation.

Explain why the Gilliland correlation can give erroneous results when the ratio of rectifying to stripping stages is small.

9.16. FUG method for HC distillation.

The hydrocarbon feed to a distillation column is a bubble-point liquid at 300 psia with mole fractions: $C_2 = 0.08$, $C_3 = 0.15$, $nC_4 = 0.20$, $nC_5 = 0.27$, $nC_6 = 0.20$, and $nC_7 = 0.10$. Determine, using a process simulator with the SRK EOS: (a) column pressure and type of condenser, if condenser outlet temperature is 120°F, for a sharp separation between nC_4 and nC_5 ; (b) at total reflux, the separation for eight equilibrium stages overall, for 0.01 mole fraction nC_4 in the bottoms product; (c) R_{\min} for the separation in part (b); and (d) the number of equilibrium stages, at $R/R_{\min} = 1.5$, using the Gilliland correlation.

9.17. FUG method for HC distillation.

The following bubble-point feed mixture is to be separated by ordinary distillation at 120 psia to obtain 92.5 mol% of the nC_4 in the liquid distillate and 82.0 mol% of the iC_5 in the bottoms.

Component	lbmol/h
C_3	5
iC_4	15
nC_4	25
iC_5	20
nC_5	35
	100

Use a process simulator with the SRK EOS to (a) estimate N_{\min} by the Fenske equation; (b) use the Fenske equation to determine the distribution of non-key components between distillate and bottoms; (c) use the Underwood method to estimate R_{\min} ; (d) determine N by the Gilliland correlation assuming $R/R_{\min} = 1.2$, a partial reboiler, and a total condenser; (e) estimate feed-stage location.

9.18. FUG method for a chlorination effluent.

Consider the separation by distillation of a chlorination effluent to recover C_2H_5Cl . The feed is a bubble-point liquid at the column pressure of 240 psia with the following composition.

Component	Mole Fraction
C_2H_4	0.05
HCl	0.05
C_2H_6	0.10
C_2H_5Cl	0.80

Specifications are (x_D/x_B) for $C_2H_5Cl = 0.01$ and (x_D/x_B) for $C_2H_6 = 75$. Use a process simulator with an appropriate thermodynamic method to calculate by the FUG method: product distribution, N_{\min} , R_{\min} , N at $R = 1.5R_{\min}$, feed-stage location. The column is to have a partial condenser and a partial reboiler.

9.19. Number of stages by FUG method and feed-stage location.

The feed given below enters the feed tray of a sieve-plate column as a saturated vapor. The column pressure may be assumed constant at 1668 kPa. The column is designed to produce a propylene distillate of 99.6 mol% and a bottoms product of 99.8 mol% of propane. Use a process simulator with the SRK EOS to estimate by the FUG method the number of equilibrium stages and the feed stage location for $R = 1.2R_{\min}$.

Component	kg/s
Acetylene	1.3×10^{-6}
Ethylene	1.3×10^{-6}
Ethane	3.3×10^{-4}
Propylene	6.41
Propane	4.62
1,3 Butadiene	3.7×10^{-4}
<i>i</i> -Butene	1.9×10^{-4}
1-Butene	1.2×10^{-4}

9.20. Distillation calculation by the approximate FUG method.

A feed at its bubble-point at 100 psia is fractionated at 100 psia to produce a distillate containing 5% of the isobutane (HK) in the feed and 3.5% of the propane (LK) in the bottoms. Use a process simulator with the SRK EOS to calculate N_{\min} , R_{\min} , N for $R/R_{\min} = 1.2$ and the feed stage by the FUG method. The feed is as follows:

Component	kmol/h in the feed
Ethane	60
Propene	90
Propane	180
Isobutane	180
Isobutene	250
<i>n</i> -Butane	240

9.21. Minimum reflux ratio by the Underwood equation.

An ideal ternary mixture A, B, and C, for which average α -values and distillate and bottoms compositions are given, is to be fractionated. Calculate the minimum reflux by the Underwood equation for both Class 1 and Class 2 cases if the feed is a saturated liquid. Note that the data given indicate that only the HK and the LK distribute. However, at minimum reflux, this may not be so. Do your results indicate that this is just a Class 1 separation?

Component		x_F	α	x_D	x_B
	A	0.047	2.50	0.1263	0.0000
LK	B	0.072	1.57	0.1913	0.0013
HK	C	0.881	1.00	0.6824	0.9987

Equilibrium-Based Methods for Multicomponent Absorption, Stripping, Distillation, and Extraction

§10.0 INSTRUCTIONAL OBJECTIVES

After completing this chapter, you should be able to:

- Write MESH equations for an equilibrium stage in a multicomponent vapor–liquid cascade.
- Explain how equilibrium stages can be combined to form a countercurrent cascade of N equilibrium stages that can be used to model absorption, stripping, distillation, and liquid–liquid extraction.
- Discuss the use of the tridiagonal-matrix algorithm used in equilibrium-based methods.
- Solve rigorously, with a process simulator, countercurrent-flow, multistage, multicomponent separation problems by the sum-rates method, the inside-out method, and the simultaneous correction method.

Except for simple cases, such as binary distillation and ternary liquid–liquid extraction, or when physical properties or stage efficiencies are not well known, the design methods described in the previous chapters are suitable only for preliminary design and parameter studies. Final design of multistage, multicomponent separation equipment requires rigorous determination of temperatures, pressures, stream flow rates, stream compositions, and heat-transfer rates at each stage by solving material-balance, energy-balance, and equilibrium relations for each stage. Unfortunately, these relations consist of strongly interacting nonlinear algebraic equations, for which manual solution procedures are difficult and tedious. However, once the procedures are programmed for a high-speed digital computer, solutions are usually achieved rapidly and almost routinely. This chapter discusses the mathematical techniques and algorithms used in process simulators, with applications to absorption, stripping, distillation, and liquid–liquid extraction. Applications to the more difficult operations of extractive, azeotropic, and reactive distillation are covered in Chapter 11.

This chapter begins with the development of a mathematical model for a vapor–liquid or liquid–liquid equilibrium stage. The model includes component Material balances, phase Equilibrium relations, mole-fraction Sums, and enthalpy (H) balances, referred to as the MESH equations. Collectively, they represent a countercurrent-flow cascade of stages. Because the collection constitutes a nonlinear set of algebraic equations, their solution must be obtained by an iterative procedure. A number of such procedures have been developed specifically for solving the MESH equations. These are mentioned in §10.2. All utilize an algorithm for solving a tridiagonal-matrix equation, described in §10.4.1.

The three most widely used procedures are described in detail, with applications to absorption, stripping, distillation, and more complex vapor–liquid separators in §10.5.2 (sum-rates method), §10.6 (simultaneous-correction method), and §10.7 (inside-out method). A strategy for solving liquid–liquid extractors is offered in §10.8.

§10.1 SIMPLE MODEL FOR A VAPOR–LIQUID EQUILIBRIUM STAGE

For any vapor–liquid or liquid–liquid equilibrium stage in a countercurrent-flow cascade, assume (1) phase equilibrium is achieved at each stage, (2) no chemical reactions occur, and (3) negligible entrainment of liquid drops in vapor, negligible occlusion of vapor bubbles in liquid, and complete separation of two liquid phases in the case of extraction. Figure 10.1 represents such a stage, where stages are numbered down from the top. The same representation applies to liquid–liquid extraction if the higher-density liquid phases are represented by liquid stream symbols and the lower-density liquid phases are represented by vapor stream symbols.

Entering stage j is a single- or two-phase feed of molar flow rate F_j , with overall composition in mole fractions $z_{i,j}$ of component i , temperature T_{Fj} , pressure P_{Fj} , and corresponding overall molar enthalpy h_{Fj} . Feed pressure is equal to or greater than stage pressure P_j . If greater, $(P_F - P_j)$ is reduced to zero adiabatically across Valve F .

Also entering stage j is interstage liquid from stage $j - 1$ above, if any, of molar flow rate L_{j-1} , with composition in mole fractions $x_{i,j-1}$, enthalpy h_{Lj-1} , temperature T_{j-1} , and pressure P_{j-1} , which is equal to or less than the pressure of stage j . Pressure of liquid from stage $j - 1$ is increased adiabatically by a

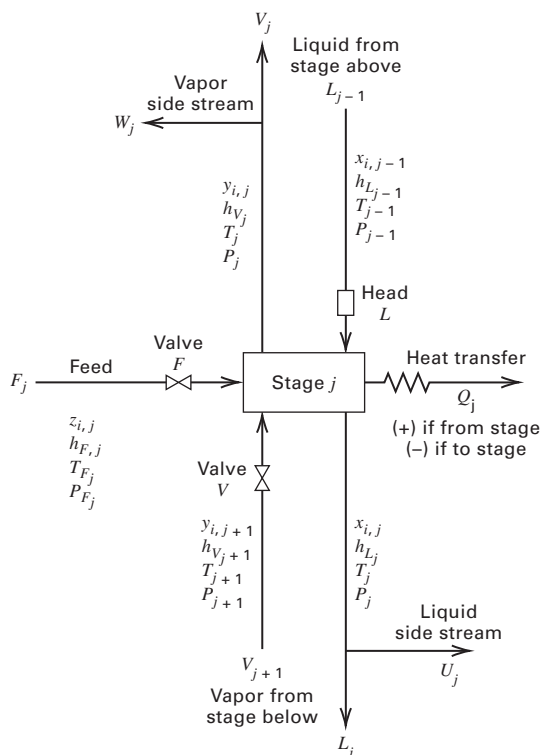


Figure 10.1 Simple equilibrium stage.

hydrostatic head change across Head L (downcomer liquid), as shown in Figure 10.1.

Similarly, from stage $j + 1$ below, interstage vapor of molar flow rate V_{j+1} , with composition in mole fractions $y_{i,j+1}$, enthalpy $h_{V,j+1}$, temperature T_{j+1} , and pressure P_{j+1} enters stage j . Any excess pressure ($P_{j+1} - P_j$) is reduced to zero adiabatically across Valve V (tray holes).

Leaving stage j is vapor of intensive properties $y_{i,j}$, $h_{V,j}$, T_j , and P_j . This stream can be divided into a vapor sidestream of molar flow rate W_j and an interstage stream of molar flow rate V_j to be sent to stage $j - 1$ or, if $j = 1$, to leave as a product. Also leaving stage j is liquid of intensive properties $x_{i,j}$, $h_{L,j}$, T_j , and P_j , in equilibrium with vapor ($V_j + W_j$). This liquid is divided into a sidestream of molar flow rate U_j and an interstage stream of molar flow rate L_j to be sent to stage $j + 1$ or, if $j = N$, to leave as a product.

Heat can be transferred at a rate Q_j from (+) or to (–) stage j to simulate stage intercoolers, interheaters, intercondensers, interreboilers, condensers, or reboilers.

Associated with each **simple equilibrium stage** are the following indexed **MESH equations** expressed in terms of the variable set in Figure 10.1. However, variables other than those shown in Figure 10.1 can be used, e.g., component flow rates can replace mole fractions and sidestream flow rates can be expressed as fractions of interstage flow rates.

1. M equations—Material balance for each component (C equations for each stage).

$$M_{i,j} = L_{j-1}x_{i,j-1} + V_{j+1}y_{i,j+1} + F_j z_{i,j} - (L_j + U_j)x_{i,j} - (V_j + W_j)y_{i,j} = 0 \quad (10-1)$$

2. E equations—phase-Equilibrium relation for each component (C equations for each stage),

$$E_{i,j} = y_{i,j} - K_{i,j}x_{i,j} = 0 \quad (10-2)$$

3. S equations—mole-fraction Summations (one for each stage),

$$(S_y)_j = \sum_{i=1}^C y_{i,j} - 1.0 = 0 \quad (10-3)$$

$$(S_x)_j = \sum_{i=1}^C x_{i,j} - 1.0 = 0 \quad (10-4)$$

4. H equation—energy (enthalpy) balance (one for each stage).

$$H_j = L_{j-1}h_{L,j-1} + V_{j+1}h_{V,j+1} + F_j h_{F,j} - (L_j + U_j)h_{L,j} - (V_j + W_j)h_{V,j} - Q_j = 0 \quad (10-5)$$

where kinetic, potential, and other forms of energy changes are ignored.

Unlike the treatment in §5.6, here all C component material balances are included and the total material balance is omitted. Also, the separate but equal temperature and pressure of the equilibrium phases are replaced by the stage temperature and pressure.

A total material-balance equation can be used in place of (10-3) or (10-4). It is derived by combining these two equations and $\sum z_{i,j} = 1.0$ with (10-1) summed over the C components and over stages 1 through j to give

$$L_j = V_{j+1} + \sum_{m=1}^j (F_m - U_m - W_m) - V_1 \quad (10-6)$$

In general, $K_{i,j} = K_{i,j}\{T_j, P_j, \mathbf{x}_j, \mathbf{y}_j\}$, $h_{V,j} = h_{V,j}\{T_j, P_j, \mathbf{y}_j\}$, and $h_{L,j} = h_{L,j}\{T_j, P_j, \mathbf{x}_j\}$, where \mathbf{x}_j and \mathbf{y}_j (in bold) are vectors of component mole fractions in streams leaving stage j . Because these property relations are not counted as equations and the three properties are not counted as variables, each equilibrium stage is defined only by the $2C + 3$ MESH equations.

A **countercurrent cascade of N equilibrium stages**, as shown in Figure 10.2, is represented by $N(2C + 3)$ such equations in $[N(3C + 10) + 1]$ variables. If N and all F_j , $z_{i,j}$, $T_{F,j}$, $P_{F,j}$, P_j , U_j , W_j , and Q_j are specified, the model is represented by $N(2C + 3)$ simultaneous algebraic equations in $N(2C + 3)$ unknown variables. These comprise all $x_{i,j}$, $y_{i,j}$, L_j , V_j , and T_j variables, where the M , E , and H equations are nonlinear (because they include terms that are products of unknowns) and must be solved by an iterative technique.

If the simple cascade of Figure 10.2 is applied to an absorber, the only input streams to the cascade are F_1 (absorbent feed) and F_N (gas in). The only output streams are V_1 (gas out) and L_N (liquid out). All other F , Q , U , and W streams have zero values.

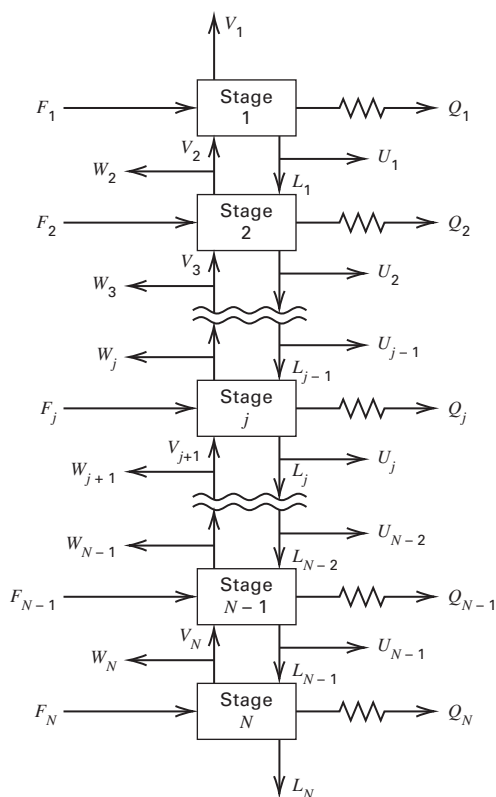


Figure 10.2 Simple countercurrent cascade of N stages.

If the cascade in Figure 10.2 is applied to a reboiled stripper, the only input streams are F_1 (liquid in) and Q_N (with a negative value for heat input), where Stage N is a partial reboiler. The only output streams are V_1 (vapor out) and L_N (liquid out). All other F , Q , U , and W streams have zero values.

For an ordinary distillation column with a total condenser and a partial reboiler, the only input streams are, say, F_j , and Q_N (with a negative value for heat input), where Stage N is a partial reboiler. There are three output streams: U_1 (distillate liquid), L_N (bottoms liquid), and Q_1 (heat output), where Stage 1 is a total condenser. All other F , Q , U , and W streams have zero values. The reflux is L_1 and the boilup is V_N .

More complicated column configurations can have multiple feed streams, vapor sidestreams, liquid sidestreams, and intermediate heat exchangers.

§10.2 EVOLUTION OF METHODS FOR SOLVING THE MESH EQUATIONS

A wide variety of iterative solution procedures for solving nonlinear, algebraic equations have appeared in the literature. Many of these procedures make use of equation partitioning in conjunction with equation tearing and/or linearization by Newton–Raphson techniques, which are described by Myers and Seider [2]. Equation tearing was applied in §4.3 to a flash computation.

Early, pre-digital computer attempts to solve (10-1) to (10-5) or equivalent forms of these equations resulted in the classical stage-by-stage, equation-by-equation calculation

procedures of Lewis–Matheson [3] in 1932 and Thiele–Geddes [4] in 1933 based on equation tearing for solving ordinary fractionators with one feed and two products. Composition-independent K -values and component enthalpies were generally employed. The Thiele–Geddes method was formulated to handle the Case II variable specification in Table 5.4 wherein the number of equilibrium stages above and below the feed, the reflux ratio, and the distillate flow rate are specified, and stage temperatures and interstage vapor (or liquid) flow rates were the iteration (tear) variables. Although widely used for hand calculations in the years following its development, the Thiele–Geddes method was often found to be numerically unstable when attempts were made to program it for a computer. However, Holland [5] developed a Thiele–Geddes procedure called the **theta method**, which was programmed and applied with considerable success.

The Lewis–Matheson method was formulated for the Case I variable specification in Table 5.4 to determine stage requirements when given the specifications for the separation of two key components, a reflux ratio and a feed-stage location. Both outer and inner iterations were required. The outer-loop tear variables were the mole fractions or flow rates of non-key components in the products. The inner-loop tear variables were the interstage vapor (or liquid) flows. The Lewis–Matheson method was widely used for hand calculations, but was often unstable when implemented on a computer.

Rather than an equation-by-equation solution procedure, Amundson and Pontinen [6], in a significant development in 1958, showed that (10-1), (10-2), and (10-6) of the MESH equations for a Case II specification could be combined and solved component-by-component from simultaneous-linear-equation sets for all N stages by an equation-tearing procedure using the same tear variables as the Thiele–Geddes method. Although tedious for hand calculations, the equation sets are readily solved by a digital computer.

In a study in 1964, Friday and Smith [7] systematically analyzed a number of tearing techniques for solving the MESH equations. They considered the choice of output variable for each equation and showed that no one tearing technique could solve all problem types. For separators where the feed(s) contain(s) only components of similar volatility (narrow-boiling case), a modified Amundson–Pontinen approach was suggested. It was termed the **bubble-point (BP) method** and was published by Wang and Henke [1] in 1966. It was successful for near-ideal systems when implemented on a digital computer. For a feed containing components of widely different volatility (wide-boiling case), the BP method was subject to failure and a so-called **sum-rates (SR) method** was suggested. An implementation of the SR method was published by Burningham and Otto [11] in 1967. For intermediate cases, the equation-tearing technique may fail to converge; in that case, Friday and Smith indicated that either a **simultaneous-correction (SC) method** or a combined tearing and SC technique was necessary.

Boston and Sullivan [8] in 1974 presented an alternative, robust approach to obtain a solution to the MESH equations. They tackled the problem of handling the variation of K -values

and enthalpies with temperature and composition. To do this, they defined volatility and energy parameters, which are used as the primary successive-approximation variables. A third parameter, which is a combination of the phase flow rates and temperature at each stage, was employed to iterate on the primary variables. This two-tier approach was named the **inside-out method**.

Current practice in process simulators is based mainly on the SR, inside-out, and SC methods, all of which are treated in this chapter. The SR method is designed specifically to handle wide-boiling systems of the type in absorption and stripping. The inside-out method is widely used in practice because it is fast and provides flexibility in the choice of specified variables. For the most difficult nonideal systems, the slower SC method is employed but convergence may require good initial guesses of the unknowns.

§10.3 STRATEGIES FOR APPLYING PROCESS-SIMULATOR METHODS

Iterative methods employed in process simulators for solving large sets of nonlinear algebraic equations are not 100% successful. However if the recommendations given in this subsection are followed, chances are excellent that a solution to the MESH equations will be achieved.

§10.3.1 Aspen Plus Models

The first consideration is the selection of the model to be used for a particular problem. Aspen Plus includes the three

rigorous equilibrium-stage vapor–liquid models listed in Table 10.1. The RadFrac model handles almost all configurations for single columns, including every absorber, stripping, and distillation configuration in Table 5.4. A column can have (1) multiple feeds, sidestreams, and interstage heat exchangers, as shown for example in Figure 10.3; (2) pumparounds of the type shown in Figure 10.4; (3) condensers of all types shown in Figure 7.18, including subcooling with a total condenser; and (4) kettle or thermosyphon reboilers in Figure 7.20. Feeds to the column can enter between stages or on a stage. Chemical reactions, solids, electrolyte streams, and a second liquid phase can all be handled.

Although **RadFrac** is an equilibrium-stage model, Murphree vapor tray efficiencies can be specified to obtain actual tray conditions. Tray or packing internals can be specified and column diameter calculated, together with pressure drop across a tray or packing. Because RadFrac includes all three (SR, inside-out, and SC) of the most widely used methods for converging the MESH equations, it can handle narrow-boiling to wide-boiling feeds and ideal to highly nonideal systems. For most problems, the inside-out method, or a modification of it, is the default method. **MultiFrac** and **PetroFrac** handle interlinked columns.

§10.3.2 CHEMCAD Models

Table 10.2 lists the options and methods for the three, rigorous, equilibrium-stage vapor–liquid models in the CHEMCAD process simulator. The SCDS model handles single columns, of almost every configuration imaginable,

Table 10.1 Aspen Plus Rigorous Vapor–Liquid Equilibrium-Stage Models

Model	Options	Methods	Applications
RadFrac	multiple feeds, sidestreams, interstage heat exchangers, pumparounds, decanters, free-water, feed-stream entry to (on) or between stages, condenser with subcooling, kettle or thermosyphon reboiler, three-phase (VLL) systems, strong liquid-phase nonideality, solids, chemical reactions (equilibrium, conversion, or rate-controlled), electrolyte systems (including reactions and salt precipitation), Murphree tray efficiencies, sizing of trayed and packed columns	SR, inside-out, SC	Single Columns , ordinary distillation, absorption, stripping, narrow to wide boiling systems, reboiled absorption, reboiled stripping, extractive distillation, azeotropic distillation, three-phase distillation, reactive distillation
MultiFrac	multiple feeds, sidestreams, interstage heat exchangers, pumparounds and bypasses, solids, free water, feed-stream entry to (on) or above a stage, condenser with subcooling, decanters, connecting streams between columns or within each column, flow splitting, mixing and heat exchange of connecting streams, Murphree tray efficiencies, sizing of trayed and packed columns	SR, inside-out, SC	Interlinked Columns , absorber-stripper combination, heat-integrated columns, air separation, Petlyuk towers, separated-wall columns
PetroFrac	multiple feeds, sidestreams, interstage heat exchangers, kettle reboiler, pumparounds, free-water, side strippers, connecting streams, external heat exchangers, condenser with subcooling, feed furnace, Murphree tray efficiencies, sizing of trayed and packed columns	SR, inside-out, SC	Complex Petroleum Columns , atmospheric crude unit with side strippers, vacuum unit, catalytic cracker main fractionator

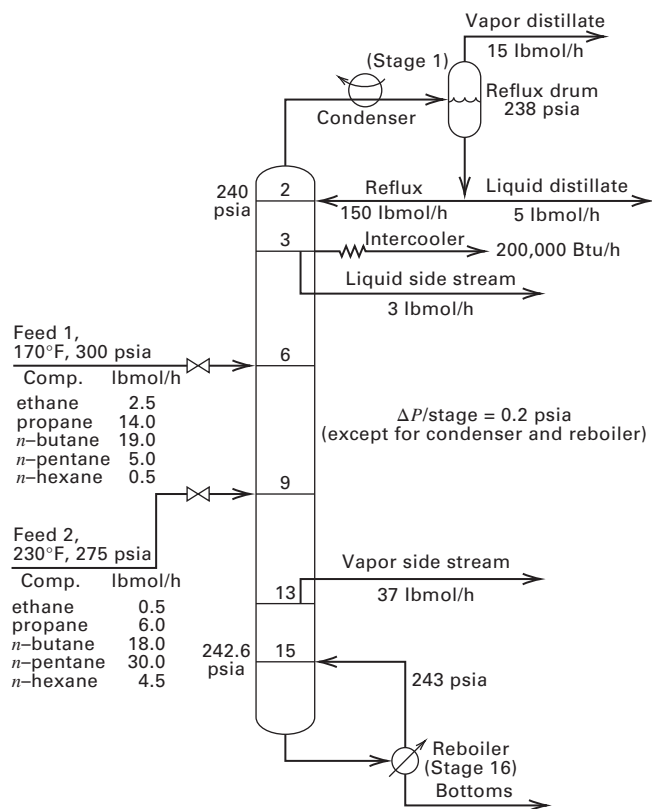


Figure 10.3 Distillation column with multiple feeds, sidestreams, and an interstage heat exchanger.

including all absorber, stripping, and distillation configurations in Table 5.4. A column can have (1) multiple feeds, sidestreams, and interstage heat exchangers, as shown for

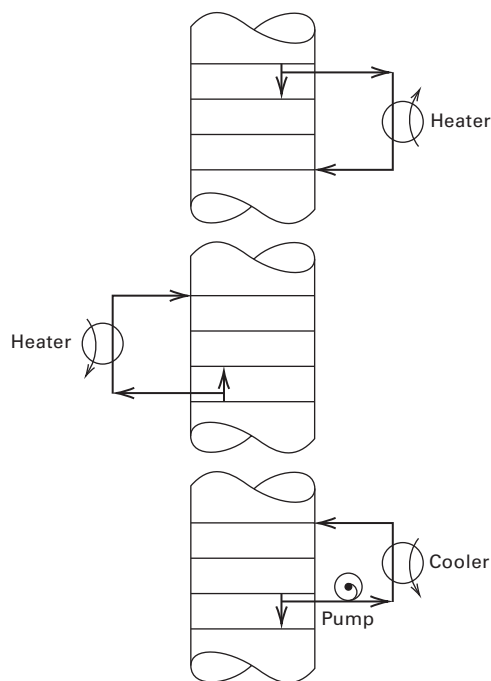


Figure 10.4 Sections of a distillation column showing bypasses and pumparounds.

example in Figure 10.3; (2) condensers of all types, as shown in Figure 7.18, including subcooling in a total condenser; and (3) kettle or thermosyphon reboilers, shown in Figure 7.20. Chemical reactions and a second liquid stream can be handled. The TOWR model is more restricted, but is preferred for hydrocarbon systems that use equation-of-state models for K -values and enthalpies. All three models can be applied with

Table 10.2 CHEMCAD Rigorous Vapor-Liquid Equilibrium-Stage Models

Model	Options	Methods	Applications
TOWR	multiple feeds, sidestreams, interstage heat exchangers, condenser with subcooling, free-water, kettle or thermosyphon reboiler, solids, electrolyte systems (including reactions and salt precipitation), Murphree tray efficiencies, sizing of trayed and packed columns	inside-out	Single Columns , ordinary distillation, absorption, stripping, narrow to wide boiling systems, reboiled absorption, reboiled stripping
SCDS	multiple feeds, sidestreams, interstage heat exchangers, decanter, condenser with subcooling, kettle or thermosyphon reboiler, three-phase (VLL) systems, strong liquid-phase nonideality, solids, electrolyte systems (including reactions and salt precipitation), chemical reactions (equilibrium, conversion, or rate-controlled), Murphree tray efficiencies, sizing of trayed and packed columns	SC	Single Columns , ordinary distillation, absorption, stripping, narrow to wide boiling systems, reboiled absorption, reboiled stripping, extractive distillation, azeotropic distillation, three-phase distillation, reactive distillation, heat-integrated columns, divided-wall columns
TOWR PLUS	multiple feeds, sidestreams, interstage heat exchangers, decanter, condenser with subcooling, solids, electrolyte systems (including reactions and salt precipitation), kettle or thermosyphon reboiler, pumparounds and bypasses, free-water, side strippers, Murphree tray efficiencies, sizing of trayed and packed columns	inside-out	Single or Column with Side Strippers, Complex Petroleum Columns , atmospheric crude unit with side strippers, vacuum unit, catalytic cracker main fractionator, divided-wall columns

tray efficiencies and can calculate column diameter and pressure drop for trayed and packed columns. TOWER PLUS handles divided-wall columns, petroleum refinery crude units, vacuum units, and other fractionators with side strippers. All models handle solids and electrolyte systems.

§10.3.3 CHEMSEP Model

Table 10.3 lists the options and the method used by the equilibrium-stage model in the ChemSep program of H.A. Kooijman and R. Taylor, which was first used by students in the Netherlands in 1988 and offered for licensing to universities through the CACHE Corporation in 1992. The equilibrium-stage model handles columns, of almost all configurations, including all absorber, stripping, and distillation configurations in Table 5.4. A column can have (1) multiple feeds, sidestreams, and interstage heat exchangers, as shown in Figure 10.3; (2) pumparounds of the type in Figure 10.4; (3) condensers of all types, as shown in Figure 7.18, including subcooling in a total condenser; and (4) reboilers of all types shown in Figure 7.20, and a total reboiler. Chemical reactions based on kinetics can be handled. The model can handle tray efficiencies and can calculate column diameter and pressure drop for trayed and packed columns.

§10.3.4 Degrees of Freedom and Specification of Variables

All models in process simulators automatically perform a degrees-of-freedom analysis. A run cannot be executed until the correct number of input design variables are specified. In effect, the number of variables that can and must be specified is fixed. Nevertheless, a user must avoid making specifications that are impossible. Some of the more common specifications that lead to failure or incorrect solutions are:

1. Column temperature and/or pressure outside of the range of the selected thermodynamic model.
2. Column pressure exceeds the convergence pressure of the system (§2.5.2).
3. Unexpected phase splitting of a highly nonideal mixture when using a model that does not handle VLL systems.
4. Use of an absorbent that is more volatile than the component to be absorbed.

5. Use of a stripping agent that is less volatile than the component to be stripped.
6. Insufficient reflux resulting in the disappearance of liquid before reaching the feed stage or the reboiler.
7. Insufficient boilup flow rate resulting in the disappearance of vapor before reaching the feed stage or the condenser.
8. Number of stages or reflux ratio less than the minimum when specifying the splits of two key components.
9. Impossible partial condenser specification for a feed mixture containing hydrogen or methane.
10. Impossible key-component splits for mixtures that form azeotropes.
11. Too large a sidestream flow rate resulting in the withdrawal of all vapor or liquid at that stage.

The user is forced to make the following required specifications:

1. Type of condenser or “no condenser.”
2. Type of reboiler or “no reboiler.”
3. Total number, N , of equilibrium stages (numbered from the top down), with the condenser (if present) numbered 1 even if it is not an equilibrium stage (i.e., a partial condenser), and the reboiler (if present) numbered N .
4. Stage location for every feed, sidestream, and external, intermediate heat exchanger.
5. For each feed stream, the composition and two of the three feed conditions (T , P , and fraction vaporized).
6. Stream pressure leaving the condenser (top pressure), pressure drop across the condenser, and column pressure drop in order that all stage pressures are fixed.

Depending upon the type separation, other specifications may be mandatory. For the most common separators, the remaining specifications that can be user-selected include:

1. Absorption—None.
2. Stripping—None.
3. Ordinary distillation—Two from distillate or bottoms flow rate; reflux ratio or boilup ratio; split of LK; split of HK. If a partial condenser: ratio of vapor distillate to liquid distillate. If a total condenser: degrees of subcooling if any.

Table 10.3 ChemSep Rigorous Vapor–Liquid Equilibrium-Stage Model

Model	Options	Methods	Applications
ChemSep Equilibrium-Stage Model	multiple feeds, sidestreams, interstage heat exchangers, pumparounds and bypasses, feed-stream entry to (on) or between stages, condenser with subcooling, strong liquid-phase nonideality, chemical reactions (rate-controlled), Murphree tray efficiencies, sizing of trayed and packed columns	SC	Single Columns , ordinary distillation, absorption, stripping, narrow to wide boiling systems, reboiled absorption, reboiled stripping, extractive distillation, azeotropic distillation, reactive distillation total reflux operation

4. Reboiled absorption—One: bottoms flow rate or recovery of a key component.
5. Reboiled stripping—One: bottoms flow rate or recovery of a key component.

The design goal of a single-section separator, such as an absorber or stripper, is the recovery of a key component. The recovery is a function of the number of equilibrium stages, N , and the ratio of the absorbent (stripping agent) flow rate to the feed flow rate, both of which must be specified. No degrees of freedom remain to specify the recovery of a key component. A solution to this dilemma is to apply the Kremser method of §6.4 with Figure 6.15 to make preliminary calculations to establish a near optimal L/V or V/L ratio and corresponding N .

For a two-section separator, such as ordinary distillation, the splits between two key components can be specified. However, if the system is near-ideal, it is preferable to first use the FUG method of Chapter 9 to estimate minimum reflux ratio, minimum equilibrium stages, actual number of equilibrium stages as a function of reflux-to-minimum reflux, and feed-stage location. These values are then used as specifications and initial guesses to help a rigorous method achieve a successful solution. If the system is highly nonideal, the FUG method is not reliable, but can be used to make rough estimates. Then, instead of specifying the two key-component splits for the rigorous method, the user can input rough estimates to specify the reflux ratio and a bottoms flow rate consistent with the desired key-components split. It is then possible to execute the rigorous method, examine the results, and keep revising the specifications until the desired split is approached. Then, specify the split.

§10.3.5 Rigorous-Method Steps

The SR, inside-out, and SC rigorous equilibrium-stage methods involve the following steps: (1) initialization, (2) iteration, (3) damping or acceleration, and (4) convergence. Different approaches are used for these steps depending on the method selected.

Initialization

To solve the nonlinear system of equations, initial guesses (estimates) are required of all unspecified variables. These are the T , V , L , $x_{i,j}$, and $y_{i,j}$ at each stage. Several default techniques are applied depending upon the nature of the feed (narrow boiling or wide boiling) and the degree of nonideality of the system or the user can enter values or profiles. These techniques include:

1. Flash calculation on the feed (or combined feeds) to obtain vapor and liquid mole fractions that are assumed the same for every stage (constant composition profile). This method should not be used for wide-boiling feeds.

2. Linear temperature profile based on a bubble- or dew-point calculation of estimated distillate and bottoms compositions.
3. Linear vapor and liquid flow-rate profiles in the rectifying and stripping sections based on a feed flash and estimated reflux, distillate, and bottoms flow rates.
4. The first iteration of the sum-rates (SR) method for wide-boiling feeds.
5. The first iteration of the bubble-point (BR) method for narrow-boiling feeds.
6. User-provided estimates from experience or results of previous runs on similar separations.

Iteration

Using the initial estimates, generated by default or supplied by the user, calculations by a given method are performed iteratively by updating the iteration results from the previous iteration and repeating the calculations in the next iteration. However, before proceeding with the next iteration, the results are examined to determine if they have converged to within a certain tolerance of a correct solution. If not, they are examined to see if they have improved compared to the previous iteration.

Damping and Acceleration

At the end of each iteration, an **error** is calculated and compared to a **tolerance**. If the error < tolerance, the problem is converged and the results accepted. If the problem is not converged and the error is greater than the error of the previous iteration, the update is damped. The updates are usually in the form of delta corrections (plus or minus) to the unspecified variables. For T , V , and L , the calculated corrections are damped by multiplying them by a factor that is some fraction (often between 0.3 and 0.7). In rare cases, where a line search is made to determine an optimal multiplying factor, the rate of convergence can be accelerated by multiplying by a factor >1. For mole-fractions, corrections may result in unacceptable values less than zero or greater than 1. If so, a fraction of the correction is made, so the new value is some fraction of the distance between the old value and zero or one. The damping and acceleration techniques are usually opaque to users.

Convergence

A converged solution is achieved when the error < tolerance. Different methods use different definitions of the error and different ways to compute the tolerance. One method is to substitute the computed values at the end of an iteration and substitute them into the right-hand sides of the MESH equations (10-1) to (10-5) to calculate the residuals, $M_{i,j}$, $E_{i,j}$, $(S_y)_j$, $(S_x)_j$, and H_j . The residuals are normalized, squared, and summed to give the error. Each method has its own procedure for determining a tolerance, which is usually based on the number of stages and components.

§10.4 MAIN MATHEMATICAL PROCEDURES

Two main mathematical procedures are used by the three rigorous equilibrium-stage methods. One is an equation-tearing (decoupling) approach where the MESH equations are solved one or one group at a time. The other is a simultaneous-correction approach, where the MESH equations are solved simultaneously. The former involves solving a triadiagonal sparse matrix for the liquid-phase mole fractions. The latter involves solving for all of the unspecified variables using a Newton–Raphson (NR) method.

§10.4.1 Tridiagonal Matrix Algorithm

Equation-tearing procedures are widely used in process simulators because they are easy to implement, rapid in execution, and require a minimum of computer memory. They are applied to a wide variety of multicomponent, multistage separation problems.

Because the system of equations to be solved is nonlinear, user-provided initial guesses of unspecified variables ($x_{i,j}$, $y_{i,j}$, L_j , V_j , and T_j) or a default method for generating them must be supplied. An oft-applied initialization procedure begins by guessing vectors \mathbf{V} and \mathbf{T} (called tear variables). Next, (10-2) is substituted into (10-1) to eliminate the vector of \mathbf{y} , followed by the substitution into the resulting equation to eliminate \mathbf{L} . In this manner, equations for calculating \mathbf{y} and \mathbf{L} are decoupled from the other equations. We now have C sets of N modified M equations, one for each component. The equations are linear in component mole fractions, if estimated K -values are provided.

$$A_j x_{i,j-1} + B_{i,j} x_{i,j} + C_{i,j} x_{i,j+1} = D_{i,j} \quad (10-7)$$

where

$$A_j = V_j + \sum_{m=1}^{j-1} (F_m - W_m - U_m) - V_1, \quad 2 \leq j \leq N \quad (10-8)$$

$$B_{i,j} = - \left[V_{j+1} + \sum_{m=1}^j (F_m - W_m - U_m) - V_1 + U_j + (V_j + W_j) K_{i,j} \right], \quad 1 \leq j \leq N \quad (10-9)$$

$$C_{i,j} = V_{j+1} K_{i,j+1}, \quad 1 \leq j \leq N - 1 \quad (10-10)$$

$$D_{i,j} = -F_j z_{i,j}, \quad 1 \leq j \leq N \quad (10-11)$$

From an inspection of Figure 10.2, $x_{i,0} = 0$, $V_{N+1} = 0$, $W_1 = 0$, and $U_N = 0$. Equations (10-7) to (10-11) are grouped by component and partitioned into a series of separate sets, one for each component. The output variable for each matrix equation is x_i over the entire N -stage cascade.

The set of equations for each component can be written as follows in the form of an $N \times N$ **tridiagonal matrix equation** that is solved by a modified Gaussian elimination algorithm due to Thomas as described by Wang and Henke [1]. Note that for convenience, the i subscripts have been dropped from $B_{i,j}$, $C_{i,j}$, and $D_{i,j}$.

$$\begin{bmatrix}
 B_1 & C_1 & 0 & 0 & 0 & \dots & \dots & 0 \\
 A_2 & B_2 & C_2 & 0 & 0 & \dots & \dots & 0 \\
 0 & A_3 & B_3 & C_3 & 0 & \dots & \dots & 0 \\
 \dots & \dots & \dots & \dots & \dots & \dots & \dots & \dots \\
 \dots & \dots & \dots & \dots & \dots & \dots & \dots & \dots \\
 \dots & \dots & \dots & \dots & \dots & \dots & \dots & \dots \\
 \dots & \dots & \dots & \dots & \dots & \dots & \dots & \dots \\
 \dots & \dots & \dots & \dots & \dots & \dots & \dots & \dots \\
 0 & \dots & \dots & \dots & 0 & A_{N-2} & B_{N-2} & C_{N-2} & 0 \\
 0 & \dots & \dots & \dots & 0 & 0 & A_{N-1} & B_{N-1} & C_{N-1} \\
 0 & \dots & \dots & \dots & 0 & 0 & 0 & A_N & B_N
 \end{bmatrix}
 \times
 \begin{bmatrix}
 x_{i,1} \\
 x_{i,2} \\
 x_{i,3} \\
 \dots \\
 \dots \\
 \dots \\
 \dots \\
 \dots \\
 x_{i,N-2} \\
 x_{i,N-1} \\
 x_{i,N}
 \end{bmatrix}
 =
 \begin{bmatrix}
 D_1 \\
 D_2 \\
 D_3 \\
 \dots \\
 \dots \\
 \dots \\
 \dots \\
 \dots \\
 D_{N-2} \\
 D_{N-1} \\
 D_N
 \end{bmatrix} \quad (10-12)$$

The tridiagonal matrix algorithm of Thomas for solving the linearized equation set (10-12) for each component is a Gaussian elimination procedure involving forward elimination, starting from Stage 1 and working toward Stage N to finally isolate $x_{i,N}$. Other values of $x_{i,j}$ are then obtained, starting with $x_{i,N-1}$ by backward substitution. Figure 10.5 shows, for

$$\begin{bmatrix}
 B_1 & C_1 & 0 & 0 & 0 \\
 A_2 & B_2 & C_2 & 0 & 0 \\
 0 & A_3 & B_3 & C_3 & 0 \\
 0 & 0 & A_4 & B_4 & C_4 \\
 0 & 0 & 0 & A_5 & B_5
 \end{bmatrix}
 \cdot
 \begin{bmatrix}
 x_1 \\
 x_2 \\
 x_3 \\
 x_4 \\
 x_5
 \end{bmatrix}
 =
 \begin{bmatrix}
 D_1 \\
 D_2 \\
 D_3 \\
 D_4 \\
 D_5
 \end{bmatrix} \quad (a)$$

$$\begin{bmatrix}
 1 & p_1 & 0 & 0 & 0 \\
 0 & 1 & p_2 & 0 & 0 \\
 0 & 0 & 1 & p_3 & 0 \\
 0 & 0 & 0 & 1 & p_4 \\
 0 & 0 & 0 & 0 & 1
 \end{bmatrix}
 \cdot
 \begin{bmatrix}
 x_1 \\
 x_2 \\
 x_3 \\
 x_4 \\
 x_5
 \end{bmatrix}
 =
 \begin{bmatrix}
 q_1 \\
 q_2 \\
 q_3 \\
 q_4 \\
 q_5
 \end{bmatrix} \quad (b)$$

$$\begin{bmatrix}
 1 & 0 & 0 & 0 & 0 \\
 0 & 1 & 0 & 0 & 0 \\
 0 & 0 & 1 & 0 & 0 \\
 0 & 0 & 0 & 1 & 0 \\
 0 & 0 & 0 & 0 & 1
 \end{bmatrix}
 \cdot
 \begin{bmatrix}
 x_1 \\
 x_2 \\
 x_3 \\
 x_4 \\
 x_5
 \end{bmatrix}
 =
 \begin{bmatrix}
 r_1 \\
 r_2 \\
 r_3 \\
 r_4 \\
 r_5
 \end{bmatrix} \quad (c)$$

Figure 10.5 The coefficient matrix for the M equations of a component at various steps in the Thomas algorithm for five stages. The i subscript is deleted from x . (a) Initial matrix. (b) Matrix after forward elimination. (c) Matrix after backward substitution.

five stages, the matrix equations for a given component at the beginning, middle, and end of the procedure.

The details of the procedure are as follows. For Stage 1, (10-7) is $B_1x_{i,1} + C_1x_{i,2} = D_1$, which can be solved for $x_{i,1}$ in terms of unknown $x_{i,2}$ to give

$$x_{i,1} = (D_1 - C_1x_{i,2}) / B_1$$

Let
$$p_1 = \frac{C_1}{B_1} \quad \text{and} \quad q_1 = \frac{D_1}{B_1}$$

Then
$$x_{i,1} = q_1 - p_1x_{i,2} \quad (10-13)$$

Thus, the coefficients in the matrix become $B_1 \leftarrow 1$, $C_1 \leftarrow p_1$, and $D_1 \leftarrow q_1$, where \leftarrow means “is replaced by.”

For Stage 2, (10-7) can be combined with (10-13) and solved for $x_{i,2}$ to give

$$x_{i,2} = \frac{D_2 - A_2q_1}{B_2 - A_2p_1} - \left(\frac{C_2}{B_2 - A_2p_1} \right) x_{i,3}$$

Let
$$q_2 = \frac{D_2 - A_2q_1}{B_2 - A_2p_1} \quad \text{and} \quad p_2 = \frac{C_2}{B_2 - A_2p_1}$$

Then
$$x_{i,2} = q_2 - p_2x_{i,3}$$

Thus, $A_2 \leftarrow 0$, $B_2 \leftarrow 1$, $C_2 \leftarrow p_2$, and $D_2 \leftarrow q_2$. Only values for p_2 and q_2 need be stored in memory.

In general,

$$p_j = \frac{C_j}{B_j - A_jp_{j-1}} \quad (10-14)$$

$$q_j = \frac{D_j - A_jq_{j-1}}{B_j - A_jp_{j-1}} \quad (10-15)$$

Then
$$x_{i,j} = q_j - p_jx_{i,j+1} \quad (10-16)$$

with $A_j \leftarrow 0$, $B_j \leftarrow 1$, $C_j \leftarrow p_j$, and $D_j \leftarrow q_j$. Thus, starting with Stage 1, values of p_j and q_j are computed recursively in the order $p_1, q_1, p_2, q_2, \dots, p_{N-1}, q_{N-1}, q_N$. For Stage N , (10-16) isolates $x_{i,N}$ as

$$x_{i,N} = q_N \quad (10-17)$$

Successive values of x_i are computed recursively by backward substitution from (10-16) in the form

$$x_{i,j-1} = q_{j-1} - p_{j-1}x_{i,j} = r_{j-1} \quad (10-18)$$

Equation (10-18) corresponds to the identity matrix.

The tridiagonal matrix algorithm avoids buildup of computer truncation errors because none of the steps involve subtraction of nearly equal quantities. Furthermore, computed values of $x_{i,j}$ are almost always positive. The algorithm is superior to alternative matrix-inversion routines. A modified algorithm for difficult cases is given by Boston and Sullivan [9]. Such cases can occur for columns with large numbers of equilibrium stages and components whose absorption factors, $A = L/KV$, are less than unity in one section and greater than unity in another.

EXAMPLE 10.1 Using the Tridiagonal Matrix Algorithm for a First Iteration of Equilibrium-Stage Calculations.

For the distillation specifications in Figure 10.6, initialize the stage calculations using the tridiagonal matrix algorithm.

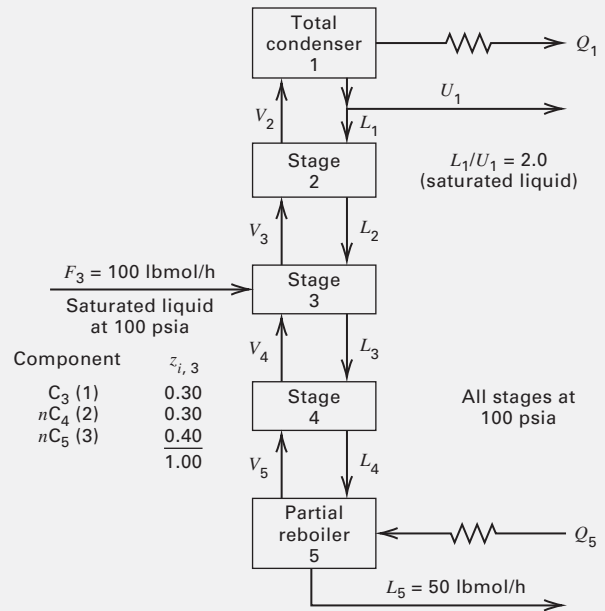


Figure 10.6 Specifications for distillation column of Example 10.1.

Solution

By an overall total material balance

$$\text{Liquid distillate} = U_1 = F_3 - L_5 = 100 - 50 = 50 \text{ lbmol/h}$$

Then,
$$L_1 = (L_1/U_1) U_1 = (2) (50) = 100 \text{ lbmol/h}$$

By a total material balance around the total condenser,

$$V_2 = L_1 + U_1 = 100 + 50 = 150 \text{ lbmol/h}$$

Initial guesses of tear variables are:

Stage j	V_j , lbmol/h	T_j , °F
1	(Fixed at 0 by specifications)	65
2	(Fixed at 150 by specifications)	90
3	150	115
4	150	140
5	150	165

At 100 psia, the estimated K -values, at column pressure and the assumed stage temperatures, are:

Stage	K_{ij}				
	1	2	3	4	5
C_3 (1)	1.23	1.63	2.17	2.70	3.33
nC_4 (2)	0.33	0.50	0.71	0.95	1.25
nC_5 (3)	0.103	0.166	0.255	0.36	0.49

The matrix equation (10-12) for the first component C_3 is developed as follows. From (10-8) with $V_1 = 0, W = 0,$

$$A_j = V_j + \sum_{m=1}^{j-1} (F_m - U_m)$$

Thus, $A_5 = V_5 + F_3 - U_1 = 150 + 100 - 50 = 200$ lbmol/h. Similarly, $A_4 = 200, A_3 = 100,$ and $A_2 = 100$ in the same units. From (10-9) with $V_1 = 0, W = 0,$

$$B_j = - \left[V_{j+1} + \sum_{m=1}^j (F_m - U_m) + U_j + V_j K_{i,j} \right]$$

Thus, $B_5 = -[F_3 - U_1 + V_5 K_{1,5}] = -[100 - 50 + (150)3.33] = -549.5$ lbmol/h. Similarly, $B_4 = -605, B_3 = -525.5, B_2 = -344.5,$ and $B_1 = -150$ in the same units. From (10-10), $C_j = V_{j+1} K_{1,j+1}.$ Thus, $C_1 = V_2 K_{1,2} = 150(1.63) = 244.5$ lbmol/h.

Similarly, $C_2 = 325.5, C_3 = 405,$ and $C_4 = 499.5$ in the same units.

From (10-11), $D_j = -F_j z_{1,j}.$ Thus, $D_3 = -100(0.30) = -30$ lbmol/h. Similarly, $D_1 = D_2 = D_4 = D_5 = 0.$ Substitution of the above values into (10-7) gives the tridiagonal matrix equation:

$$\begin{bmatrix} -150 & 244.5 & 0 & 0 & 0 \\ 100 & -344.5 & 325 & 0 & 0 \\ 0 & 100 & -525.5 & 405 & 0 \\ 0 & 0 & 200 & -605 & 499.5 \\ 0 & 0 & 0 & 200 & -549.5 \end{bmatrix} \begin{bmatrix} x_{1,1} \\ x_{1,2} \\ x_{1,3} \\ x_{1,4} \\ x_{1,5} \end{bmatrix} = \begin{bmatrix} 0 \\ 0 \\ -30 \\ 0 \\ 0 \end{bmatrix}$$

Using (10-14) and (10-15), the forward step of the Thomas algorithm becomes

$$p_1 = \frac{C_1}{B_1} = 244.5/(-150) = -1.630$$

$$q_1 = \frac{D_1}{B_1} = 0/(-150) = 0$$

$$p_2 = \frac{C_2}{B_2 - A_2 p_1} = \frac{325.5}{-344.5 - 100(-1.630)} = -1.793$$

By similar calculations, the matrix equation after the forward elimination procedure is

$$\begin{bmatrix} 1 & -1.630 & 0 & 0 & 0 \\ 0 & -1 & -1.793 & 0 & 0 \\ 0 & 0 & 1 & -1.170 & 0 \\ 0 & 0 & 0 & 1 & -1.346 \\ 0 & 0 & 0 & 0 & 1 \end{bmatrix} \begin{bmatrix} x_{1,1} \\ x_{1,2} \\ x_{1,3} \\ x_{1,4} \\ x_{1,5} \end{bmatrix} = \begin{bmatrix} 0 \\ 0 \\ 0.0867 \\ 0.0467 \\ 0.0333 \end{bmatrix}$$

Applying the backward steps of (10-17) and (10-18) gives

$$x_{1,5} = q_5 = 0.0333$$

$$x_{1,4} = q_4 - p_4 x_{1,5} = 0.0467 - (-1.346)(0.0333) = 0.0915$$

Similarly,

$$x_{1,3} = 0.1938, x_{1,2} = 0.3475, x_{1,1} = 0.5664$$

The matrix equations for nC_4 and nC_5 are solved similarly to give

Stage	x_{ij}				
	1	2	3	4	5
C_3	0.5664	0.3475	0.1938	0.0915	0.0333
nC_4	0.1910	0.3820	0.4483	0.4857	0.4090
nC_5	0.0191	0.1149	0.3253	0.4820	0.7806
$\sum x_{ij}$	0.7765	0.8444	0.9674	1.0592	1.2229

§10.4.2 Simultaneous-Correction Algorithm

Several methods can be employed to simultaneously solve for all unknowns in a set of nonlinear algebraic equations. They include the Newton–Raphson (NR) method, which is limited to finding one solution, and the α branch-and-bound, global-terrain, homotopy-continuation, and interval-Newton methods, which strive to find all solutions. The NR method is applied most widely in **simultaneous-correction algorithms** for equilibrium-stage calculations in process simulators.

In the NR algorithm, n simultaneous equations, subscripted with $i,$ in terms of n generic variables, $x_j,$ subscripted with $j,$ are written in zero form:

$$f_i \{x_1, x_2, \dots, x_n\} = 0, \quad i = 1, 2, \dots, n \quad (10-19)$$

Initial guesses, marked by asterisks, are provided for the n variables, and each of the n functions is expanded about these guesses in a Taylor’s series that is terminated after the first derivatives to give

$$0 = f_i \{x_1, x_2, \dots, x_n\}$$

$$\approx f_i \{x_1^*, x_2^*, \dots, x_n^*\}$$

$$+ \left. \frac{\partial f_i}{\partial x_1} \right|^* \Delta x_1 + \left. \frac{\partial f_i}{\partial x_2} \right|^* \Delta x_2 + \dots + \left. \frac{\partial f_i}{\partial x_n} \right|^* \Delta x_n \quad (10-20)$$

where the corrections are $\Delta x_j = x_j - x_j^*$ (10-21)

The n equations of (10-20) and (10-21) are linear and can be solved directly for the corrections $\Delta x_j.$ If all are zero, the guesses are correct and (10-19) has been solved; if not, the corrections are added to the guesses to provide a new set of guesses for (10-20). The procedure is repeated, for r iterations, until all corrections, and thus all the functions, become zero to within some tolerance. In recursion form, (10-20) and (10-21) are

$$\sum_{j=1}^n \left[\left(\frac{\partial f_i}{\partial x_j} \right)^{(r)} \Delta x_j^{(r)} \right] = -f_i^{(r)}, \quad i = 1, 2, \dots, n \quad (10-22)$$

$$x_j^{(r+1)} = x_j^{(r)} + \Delta x_j^{(r)}, \quad j = 1, 2, \dots, n \quad (10-23)$$

EXAMPLE 10.2 Newton–Raphson Algorithm.

Solve the simultaneous, nonlinear equations

$$\begin{aligned} x_1 \ln x_2 + x_2 \exp(x_1) &= \exp(1) \\ x_2 \ln x_1 + 2x_1 \exp(x_2) &= 2 \exp(1) \end{aligned}$$

for x_1 and x_2 to within ± 0.001 , by the Newton–Raphson algorithm.

Solution

In the form of (10-19), the two equations are

$$\begin{aligned} f_1\{x_1, x_2\} &= x_1 \ln x_2 + x_2 \exp(x_1) - \exp(1) = 0 \\ f_2\{x_1, x_2\} &= x_2 \ln x_1 + 2x_1 \exp(x_2) - 2 \exp(1) = 0 \end{aligned}$$

From (10-22), the linearized recursive form of these equations is

$$\begin{aligned} \left(\frac{\partial f_1}{\partial x_1}\right)^{(r)} \Delta x_1^{(r)} + \left(\frac{\partial f_1}{\partial x_2}\right)^{(r)} \Delta x_2^{(r)} &= -f_1^{(r)} \\ \left(\frac{\partial f_2}{\partial x_1}\right)^{(r)} \Delta x_1^{(r)} + \left(\frac{\partial f_2}{\partial x_2}\right)^{(r)} \Delta x_2^{(r)} &= -f_2^{(r)} \end{aligned}$$

The form of the solution of these two equations is readily obtained by the method of determinants to give

$$\Delta x_1^{(r)} = \frac{\begin{bmatrix} f_2^{(r)} \left(\frac{\partial f_1}{\partial x_2}\right)^{(r)} - f_1^{(r)} \left(\frac{\partial f_2}{\partial x_2}\right)^{(r)} \end{bmatrix}}{D}$$

and

$$\Delta x_2^{(r)} = \frac{\begin{bmatrix} f_1^{(r)} \left(\frac{\partial f_2}{\partial x_1}\right)^{(r)} - f_2^{(r)} \left(\frac{\partial f_1}{\partial x_1}\right)^{(r)} \end{bmatrix}}{D}$$

where $D = \left(\frac{\partial f_1}{\partial x_1}\right)^{(r)} \left(\frac{\partial f_2}{\partial x_2}\right)^{(r)} - \left(\frac{\partial f_1}{\partial x_2}\right)^{(r)} \left(\frac{\partial f_2}{\partial x_1}\right)^{(r)}$

and the derivatives as obtained from the equations are

$$\left(\frac{\partial f_1}{\partial x_1}\right)^{(r)} = \ln(x_2^{(r)}) + x_2^{(r)} \exp(x_1^{(r)})$$

$$\left(\frac{\partial f_2}{\partial x_1}\right)^{(r)} = \frac{x_2^{(r)}}{x_1^{(r)}} + 2 \exp(x_2^{(r)})$$

$$\left(\frac{\partial f_1}{\partial x_2}\right)^{(r)} = \frac{x_1^{(r)}}{x_2^{(r)}} + \exp(x_1^{(r)})$$

$$\left(\frac{\partial f_2}{\partial x_2}\right)^{(r)} = \ln(x_1^{(r)}) + 2x_1^{(r)} \exp(x_2^{(r)})$$

As initial guesses, let $x_1^{(1)} = 2, x_2^{(1)} = 2$. Application of the Newton–Raphson algorithm gives the following results, where, at the sixth iteration, convergence is achieved with values of $x_1 = 1.0000$ and $x_2 = 1.0000$, which correspond closely to values of 0 for f_1 and f_2 .

§10.5 BUBBLE-POINT (BP) AND SUM-RATES (SR) METHODS

The **bubble-point (BP) method** found wide use for equilibrium-stage calculations for the distillation of narrow-boiling, near-ideal mixtures until the availability of the inside-out method. The BP method is no longer available in process simulators except for initialization. Its counterpart, the **sum-rates (SR) method**, developed for wide-boiling, near-ideal mixtures, is still available in some process simulators and also finds use in initialization. Common to both methods is the tridiagonal matrix formulation in §10.4.1, as illustrated in Example 10.1. That example concludes with a table of liquid-phase mole fraction summations of the three components for the five stages. The summations do not equal 1.0. The BP and SR methods deviate at this point in the manner in which the variables are updated to begin the next iteration.

§10.5.1 Initialization using the BP Method

In the BP method, the liquid-phase mole fractions are normalized at each stage so as to sum to 1.0, using the equation,

$$(x_{i,j})_{\text{normalized}} = \frac{x_{i,j}}{\sum_{i=1}^C x_{i,j}} \quad (10-24)$$

Then, updated stage temperatures are obtained by bubble-point temperature calculations using normalized $x_{i,j}$ values. Friday and Smith [7] showed that bubble-point calculations are effective for mixtures having a narrow range of K -values because temperatures are not sensitive to composition. At the other extreme, bubble-point calculations are sensitive to composition for wide-boiling systems and are not recommended.

The bubble-point equation is obtained by combining (10-2) and (10-3) to eliminate $y_{i,j}$, giving

$$\sum_{i=1}^C K_{i,j} x_{i,j} - 1.0 = 0 \quad (10-25)$$

which is solved iteratively by the method described in §4.3.4.

r	$x_1^{(r)}$	$x_2^{(r)}$	$f_1^{(r)}$	$f_2^{(r)}$	$(\partial f_1 / \partial x_1)^{(r)}$	$(\partial f_1 / \partial x_2)^{(r)}$	$(\partial f_2 / \partial x_1)^{(r)}$	$(\partial f_2 / \partial x_2)^{(r)}$	$\Delta x_1^{(r)}$	$\Delta x_2^{(r)}$
1	2.0000	2.0000	13.4461	25.5060	15.4731	8.3891	15.7781	30.2494	-0.5743	-0.5436
2	1.4247	1.4564	3.8772	7.3133	6.4354	5.1395	9.6024	12.5880	-0.3544	-0.3106
3	1.0713	1.1457	0.7720	1.3802	3.4806	3.8541	7.3591	6.8067	-0.0138	-0.1878
4	1.0575	0.9579	-0.0059	0.1290	2.7149	3.9830	6.1183	5.5679	-0.0591	0.0417
5	0.9984	0.9996	-0.0057	-0.0122	2.7126	3.7127	6.4358	5.4244	0.00159	0.000368
6	1.0000	1.0000	5.51×10^{-6}	2.86×10^{-6}	2.7183	3.7183	6.4366	5.4366	12.1×10^{-6}	-3.0×10^{-6}
7	1.0000	1.0000	0.0	-2×10^{-9}	2.7183	3.7183	6.4366	5.4366	—	—

Corresponding, updated values of $y_{i,j}$ are determined from (10-2). With a consistent set of values for $x_{i,j}$, T_j , and $y_{i,j}$, molar enthalpies are computed for each liquid and vapor stream leaving a stage. Then (10-5) and (10-6) are used to compute the condenser and reboiler heat duties and updated values of V_j and L_j . This first iteration of the BP method serves as the initialization step for other more robust methods.

§10.5.2 The SR Method

For wide-boiling systems, such as for most absorbers and strippers, stage energy balances, (10-5), are much more sensitive to stage temperatures than to interstage flow rates. In this case, Friday and Smith [7] showed that an alternative procedure, called the sum-rates (SR) method, devised by Sujata [10], could be used to update the MESH equation variables. This method was further developed to make use of the tridiagonal-matrix formulation for the modified M equations by Burningham and Otto [11].

Problem specifications consist of conditions and stage locations for feeds, stage pressures, sidestream stage locations and flow rates, interstage locations and heat-transfer rates, and number of stages. The SR method is identical to the BP method up to the solution of the tridiagonal matrix equation for $x_{i,j}$ values that do not sum to 1.0 at each stage, as at the end of Example 10.1. Instead of normalizing these values as in the BP method, they are used directly to produce updated values of L_j by applying (10-4) in a form referred to as the sum-rates equation:

$$L_j^{(k+1)} = L_j^{(k)} \sum_{i=1}^C x_{i,j} \quad (10-26)$$

where k is the iteration number.

Corresponding updated values of $V_j^{(k+1)}$ are obtained from a total material balance derived by summing (10-1) over the C components, combining the result with (10-3) and (10-4), and summing that result over stages j through N to give

$$V_j = L_{j-1} - L_N + \sum_{m=j}^N (F_m - W_m - U_m) \quad (10-27)$$

Normalized $x_{i,j}$ values are calculated from (10-19). Corresponding values of $y_{i,j}$ are computed from (10-2).

An updated set of T_j values is obtained by solving the energy-balance relations (10-5) simultaneously for the N stages. The temperatures are embedded in the specific enthalpies for the unspecified vapor and liquid flow rates. Typically, these enthalpies are nonlinear in temperature.

To obtain a new set of T_j from the energy equation (10-5), the Newton–Raphson recursion equation is

$$\left(\frac{\partial H_j}{\partial T_{j-1}} \right)^{(r)} \Delta T_{j-1}^{(r)} + \left(\frac{\partial H_j}{\partial T_j} \right)^{(r)} \Delta T_j^{(r)} + \left(\frac{\partial H_j}{\partial T_{j+1}} \right)^{(r)} \Delta T_{j+1}^{(r)} = -H_j^{(r)} \quad (10-28)$$

where

$$\Delta T_j^{(r)} = T_j^{(r+1)} - T_j^{(r)} \quad (10-29)$$

$$\frac{\partial H_j}{\partial T_{j-1}} = L_{j-1} \frac{\partial h_{L_{j-1}}}{\partial T_{j-1}} \quad (10-30)$$

$$\frac{\partial H_j}{\partial T_j} = -(L_j + U_j) \frac{\partial h_{L_j}}{\partial T_j} - (V_j + W_j) \frac{\partial h_{V_j}}{\partial T_j} \quad (10-31)$$

$$\frac{\partial H_j}{\partial T_{j+1}} = V_{j+1} \frac{\partial h_{V_{j+1}}}{\partial T_{j+1}} \quad (10-32)$$

The partial derivatives depend upon the temperature dependence of the enthalpy correlations.

Updates for T_j are then determined from

$$T_j^{(r+1)} = T_j^{(r)} + t \Delta T_j^{(r)} \quad (10-33)$$

where t is a damping factor that is useful when initial guesses and true values are not reasonably close. Generally, t is taken as 1, but an optimal value can be determined at each iteration to minimize the sum of the squares of the functions,

$$\sum_{j=1}^N \left[H_j^{(r+1)} \right]^2$$

When corrections $\Delta T_j^{(r)}$ approach zero, the resulting values of T_j are used with criteria, such as the sum of the squares of temperature differences between iterations, to determine if convergence has been achieved. Convergence is rapid for absorbers and strippers with the SR method.

EXAMPLE 10.3 SR Method for an Absorber.

Use the SR method to design the hydrocarbon absorber of Example 6.3, as shown in Figure 6.17.

Solution

From Table 10.1, it is seen that the SR method is an option with the rigorous RadFrac model in Aspen Plus. It is particularly suitable for hydrocarbon absorbers in petroleum refineries because the system is near-ideal. The six components are selected by entering their names, using all normal paraffins, including n -decane for the oil. The SRK EOS is selected from Methods/Specifications for thermodynamic properties and the default binary-interaction Parameters were and must be accepted from Methods/Parameters/Binary Interaction. The temperature and component molar flow rates of the absorbent are entered, using the data in Figure 6.17, for a stream entering the top stage of the absorber, together with a pressure of 400 psia. The feed gas temperature and component molar flow rates are entered for the inlet gas to the bottom stage, together with a pressure of 403 psia. This bottoms pressure is assumed on the basis of a 30-tray absorber with a pressure drop of 0.1 psi per tray. For the 6 equilibrium-stage absorber block in Aspen Plus, the two allowable specifications under Configuration are mandatory: no condenser (duty = 0) and no reboiler (duty = 0). The SR option is selected for the absorber block by choosing Setup/Convergence from the drop-down menu Petroleum/wide-boiling. Convergence of the absorber was achieved after four iterations in less than one second, despite very poor starting guesses for $x_{i,j}$, $y_{i,j}$, L_j , V_j , and T_j . Values for the ratio of

error-to-tolerance after each iteration were as follows, where it is seen that the initial error was very large because of the poor guesses for the initialization.

Iteration	Error/Tolerance After Iteration
1	407.22
2	17.299
3	1.6185
4	0.082834

The converged summary for the two inlet and two exiting streams is as follows.

	Feed Gas	Absorbent	Lean Gas	Rich Oil
Temperature, °F	105	90	151.4	145.6
Pressure, psia	403	400	400	403
Component flow rates, lbmol/h:				
Methane	160.0	0.0	146.53	13.47
Ethane	370.0	0.0	270.50	99.50
Propane	240.0	0.0	99.96	140.04
<i>n</i> -Butane	25.0	0.05	1.41	23.64
<i>n</i> -Pentane	5.0	0.78	0.24	5.54
<i>n</i> -Decane (absorbent oil)	0.0	164.17	0.83	163.34
Total	800.0	165.00	519.47	445.53

From the above flow rates, it is seen that an appreciable amount of absorption occurs. The molar ratio of leaving rich oil to-entering lean oil is $445.53/165.0 = 2.7$. The % of feed gas absorbed is approximately $(800 - 519.47)/800 = 0.35 = 35\%$. Absorption is an exothermic process. In effect, condensation occurs, releasing heat. This is clearly shown both in the absorber temperature profile of Figure 10.7, plotted with Aspen Plus, and the above outlet stream

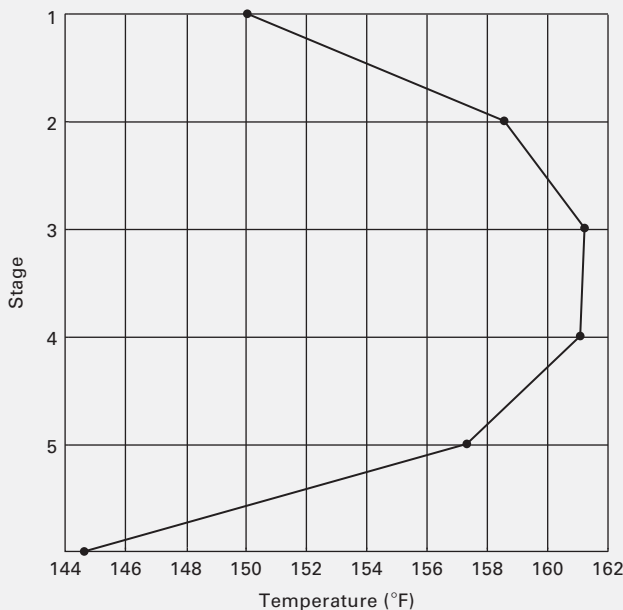


Figure 10.7 Temperature profile for absorber of Example 10.3.

summary. Although the absorbent enters at 90°F and the feed gas enters at 105°F, the rich oil leaves at 145.6°F and the lean gas leaves at 151.4°F. However all four intermediate-stage (2 to 5) temperatures are even higher, as high as 161.2°F. It is not uncommon to provide an interstage cooler on an absorber to reduce interstage temperatures and, thereby, increase the amount of absorption. This is the subject of one of the exercises.

Figure 10.8 is a plot of the vapor and liquid molar flow rate profiles. The vapor flow rate entering Stage 6 is the feed gas flow rate of 800 lbmol/h. It decreases by about 70 lbmol/h across the bottom stage (6). The changes are then small until the top stage (1) is reached where the vapor flow rate decreases by about 150 lbmol/h to 519.4 lbmol/hr. Thus, most of the absorption occurs at the top and bottom stages.

The following table lists the percent and amount of each component absorbed, and the arithmetic average absorption factor ($A = L/KV$) for the top and bottom stages. Only a small amount of methane is absorbed, in agreement with the Kremser equation (6-29). Large amounts of ethane and propane are absorbed, mainly at the top and bottom stages, where the largest changes in stage temperatures occur. The results in the table for these two components are very close to those calculated from the Kremser equation. As shown in Figure 10.9, the absorption of *n*-butane is spread out over all stages. The absorption of *n*-pentane occurs mainly at the bottom three stages. For *n*-butane and *n*-pentane, the results in the table are also in agreement with the Kremser equation, when their flow rates in the absorbent oil and feed gas are considered separately as in Example 6.3. However, the results in Example 6.3 differ markedly from those in this example because (1) the absorption factors were estimated using the ratio $L/V =$ entering molar liquid flow rate/entering molar vapor flow rate and (2) K -values were determined at the average entering temperature. Because of the large absorption rate, both were poor assumptions. When the effect of the absorption factor on the fraction not absorbed, as shown in the plot of the Kremser equation in Figure 6.15,

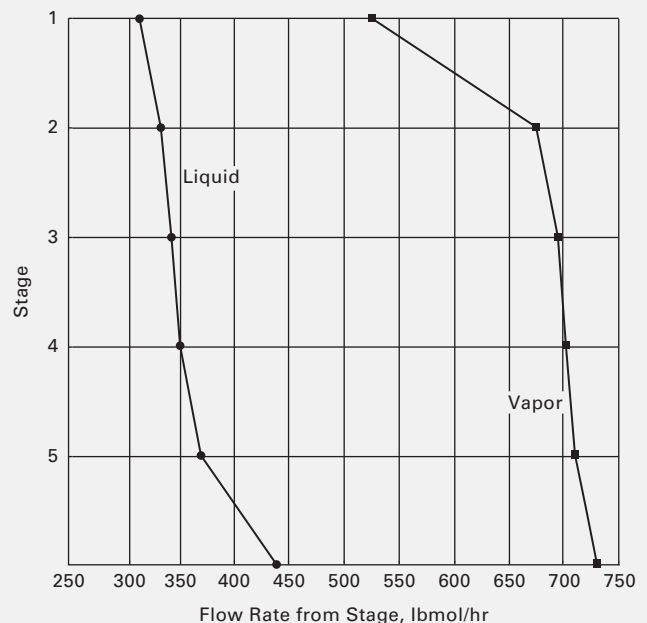


Figure 10.8 Vapor and liquid flow rate profiles for absorber of Example 10.3.

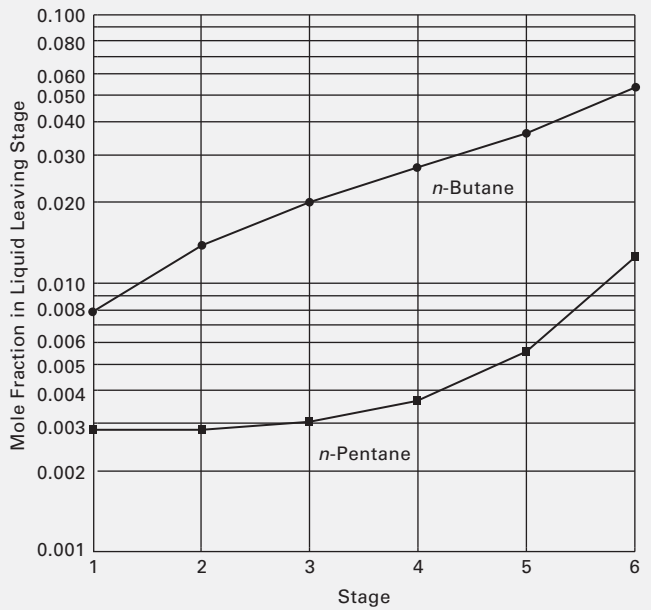


Figure 10.9 Liquid mole-fraction profiles of *n*-butane and *n*-pentane for absorber of Example 10.3.

is applied to the components in this example, the following conclusions can be drawn:

1. Regardless of the number of stages, the % absorption of methane remains constant at about the value in the table.
2. As the average absorption factor for the other four components increases, the effect of increasing or decreasing the number of stages changes from a small effect to a very large effect as shown dramatically in Figure 6.15.

Component	% Absorbed	Amount Absorbed, lbmol/h	Average Absorption Factor
Methane	8.4	13.47	0.0875
Ethane	26.9	99.50	0.290
Propane	58.4	140.04	0.700
<i>n</i> -Butane	94.4	23.59	1.69
<i>n</i> -Pentane	95.2	4.76	3.94

§10.6 SIMULTANEOUS-CORRECTION METHOD

Rigorous BP and SR methods are relatively simple and easy to implement on a computer. However, for highly nonideal systems, they converge with difficulty or not at all. Fortunately, other, more robust, procedures have been developed that are much more robust. One such procedure applies the simultaneous-correction (SC) technique.

To develop an SC procedure, it is necessary to select and order the unspecified variables and corresponding functions (MESH equations) in a matrix. Goldstein and Stanfield [16] group the functions by type to efficiently handle problems involving many components, but few stages. Typical applications are crude units, vacuum units, and catalytic cracking

main fractionators in petroleum refineries. For problems involving many equilibrium stages but relatively few components, it is more efficient to group the functions according to stage location. The latter grouping, described here, was devised by Naphtali and Sandholm [17]. Their procedure utilizes an extension of the tridiagonal-matrix mathematical procedure presented in §10.4.1. A computer program for their method is given by Fredenslund et al. [18]. However, implementations of the SC method in process simulators have more flexible specifications.

The stage model of Figures 10.1 and 10.2 is again employed. However, rather than solving the $N(2C + 3)$ MESH equations simultaneously, (10-3) and (10-4) are combined with the other MESH equations to eliminate $2N$ variables and thus reduce the problem to the simultaneous solution of $N(2C + 1)$ equations. This is done by first multiplying (10-3) and (10-4) by V_j and L_j , respectively to give

$$V_j = \sum_{i=1}^C v_{i,j} \tag{10-34}$$

$$L_j = \sum_{i=1}^C l_{i,j} \tag{10-35}$$

where mole-fraction definitions are used:

$$y_{i,j} = \frac{v_{i,j}}{V_j} \tag{10-36}$$

$$x_{i,j} = \frac{l_{i,j}}{L_j} \tag{10-37}$$

Equations (10-34) to (10-37) are substituted into (10-1), (10-2), and (10-5) to eliminate V_j , L_j , $y_{i,j}$, and $x_{i,j}$ and introduce component flow rates $v_{i,j}$ and $l_{i,j}$. As a result, the following $N(2C + 1)$ equations are obtained, where $s_j = U_j/L_j$ and $S_j = W_j/V_j$ are dimensionless sidestream flow rates.

Material Balance

$$M_{i,j} = l_{i,j}(1 + s_j) + v_{i,j}(1 + S_j) - l_{i,j-1} - v_{i,j+1} - f_{i,j} = 0 \tag{10-38}$$

Phase Equilibria

$$E_{i,j} = K_{i,j} l_{i,j} \frac{\sum_{k=1}^C v_{k,j}}{C} - v_{i,j} = 0 \tag{10-39}$$

Energy Balance

$$H_j = h_{L_j}(1 + s_j) \sum_{i=1}^C l_{i,j} + h_{V_j}(1 + S_j) \sum_{i=1}^C v_{i,j} - h_{L_{j-1}} \sum_{i=1}^C l_{i,j-1} - h_{V_{j+1}} \sum_{i=1}^C v_{i,j+1} - h_{F_j} \sum_{i=1}^C f_{i,j} - Q_j = 0 \tag{10-40}$$

where $f_{i,j} = F_j z_{i,j}$.

$$\bar{C}_j = \frac{\partial \bar{F}_j}{\partial \mathbf{X}_{j+1}} = \begin{matrix} \text{Functions} \\ \left[\begin{array}{c} H_j \\ M_{1,j} \\ \vdots \\ M_{C,j} \\ E_{1,j} \\ \vdots \\ E_{C,j} \end{array} \right] \end{matrix} \begin{matrix} \text{Output variables} \\ \left[\begin{array}{c} v_{1,j+1} \cdots v_{C,j+1} \\ T_{j+1} \\ l_{1,j+1} \cdots l_{C,j+1} \end{array} \right] \end{matrix} \quad (10-50)$$

Thus, (10-45) consists of a set of $N(2C + 1)$ simultaneous, linear equations in the $N(2C + 1)$ corrections $\Delta \mathbf{X}$. For example, the $2C + 2$ equation in the set is obtained by expanding function H_2 (10-40) into a Taylor series like (10-21) around the $N(2C + 1)$ output variables. The result is as follows after the usual truncation of terms involving derivatives of order greater than one:

$$\begin{aligned} & 0(\Delta v_{1,1} + \dots + \Delta v_{C,1}) - \frac{\partial h_{L_1}}{\partial T_1} \sum_{i=1}^C l_{i,j}(\Delta T_1) \\ & - \left(\frac{\partial h_{L_1}}{\partial l_{1,1}} \sum_{i=1}^C l_{i,1} + h_{L_1} \right) \Delta l_{1,1} - \dots \\ & - \left(\frac{\partial h_{L_1}}{\partial l_{C,1}} \sum_{i=1}^C l_{i,1} + h_{L_1} \right) \Delta l_{C,1} - \dots \\ & + \left[\left(\frac{\partial h_{V_2}}{\partial v_{1,2}} \right) (1 + S_2) \sum_{i=1}^C v_{i,2} + h_{V_2} (1 + S_2) \right] \Delta v_{1,2} + \dots \\ & + \left[\left(\frac{\partial h_{V_2}}{\partial v_{C,2}} \right) (1 + S_2) \sum_{i=1}^C v_{i,2} + h_{V_2} (1 + S_2) \right] \Delta v_{C,2} \\ & + \left[\left(\frac{\partial h_{L_2}}{\partial T_2} \right) (1 + s_2) \sum_{i=1}^C l_{i,2} + \left(\frac{\partial h_{V_2}}{\partial T_2} \right) (1 + S_2) \sum_{i=1}^C v_{i,2} \right] \Delta T_2 \\ & + \left[\left(\frac{\partial h_{L_2}}{\partial l_{1,2}} \right) (1 + s_2) \sum_{i=1}^C l_{i,2} + h_{L_2} (1 + s_2) \right] \Delta l_{1,2} + \dots \\ & + \left[\left(\frac{\partial h_{L_2}}{\partial l_{C,2}} \right) (1 + s_2) \sum_{i=1}^C l_{i,2} + h_{L_2} (1 + s_2) \right] \Delta l_{C,2} \\ & - \left(\frac{\partial h_{V_3}}{\partial v_{1,3}} \sum_{i=1}^C v_{i,3} + h_{V_3} \right) \Delta v_{1,3} - \dots \\ & - \left(\frac{\partial h_{V_3}}{\partial v_{C,3}} \sum_{i=1}^C v_{i,3} + h_{V_3} \right) \Delta v_{C,3} \\ & - \frac{\partial h_{V_3}}{\partial T_3} \sum_{i=1}^C v_{i,3} \Delta T_3 + 0(\Delta l_{1,3} + \dots + \Delta l_{C,3}) = -H_2 \end{aligned} \quad (10-51)$$

Partial derivatives of enthalpies and K -values depend on the property correlations and are sometimes simplified by including only the dominant terms.

Because the tridiagonal matrix algorithm can be applied to the block-tridiagonal structure of (10-47), submatrices of partial derivatives are computed only as needed. The solution of (10-45) follows the scheme in §10.4.1, given by (10-13) to (10-18) and represented in Figure 10.5, where matrices and vectors $\bar{A}_j, \bar{B}_j, \bar{C}_j, -\mathbf{F}_j$, and $\Delta \mathbf{X}_j$ correspond to variables A_j, B_j, C_j, D_j , and x_j , respectively. However, the multiplication and division operations in §10.4.1 are changed to matrix multiplication and inversion, respectively. The steps are:

Starting at stage 1, $\bar{C}_1 \leftarrow (\bar{B}_1)^{-1} \bar{C}_1, \mathbf{F}_1 \leftarrow (\bar{B}_1)^{-1} \mathbf{F}_1$, and $\bar{B}_1 \leftarrow \mathbf{I}$ (the identity submatrix). Only \bar{C}_1 and \mathbf{F}_1 are saved.

For stages j from 2 to $(N - 1)$, $\bar{C}_j \leftarrow (\bar{B}_j - \bar{A}_j \bar{C}_{j-1})^{-1} \bar{C}_j, \mathbf{F}_j \leftarrow (\bar{B}_j - \bar{A}_j \bar{C}_{j-1})^{-1} (\mathbf{F}_j - \bar{A}_j \mathbf{F}_{j-1})$. Then $\bar{A}_j \leftarrow 0$, and $\bar{B}_j \leftarrow \mathbf{I}$. Save \bar{C}_j and \mathbf{F}_j for each stage.

For the last stage, $\mathbf{F}_N \leftarrow (\bar{B}_N - \bar{A}_N \bar{C}_{N-1})^{-1} (\mathbf{F}_N - \bar{A}_N \mathbf{F}_{N-1}), \bar{A}_N \leftarrow 0, \bar{B}_N \leftarrow \mathbf{I}$, and therefore, $\Delta \mathbf{X}_N = -\mathbf{F}_N$. This completes the forward steps. Remaining values of $\Delta \mathbf{X}$ are obtained by successive, backward substitution from $\Delta \mathbf{X}_j = -\mathbf{F}_j \leftarrow -(\mathbf{F}_j - \bar{C}_j \mathbf{F}_{j+1})$

This procedure is illustrated by the following example.

EXAMPLE 10.4 Block-Tridiagonal-Matrix Equation.

Solve the following block-tridiagonal-matrix equation using the functions in MATLAB.

$$\begin{bmatrix} 1 & 2 & 1 & 2 & 2 & 1 & 0 & 0 & 0 \\ 2 & 1 & 1 & 2 & 1 & 0 & 0 & 0 & 0 \\ 1 & 2 & 2 & 1 & 2 & 0 & 0 & 0 & 0 \\ \hline 0 & 1 & 3 & 1 & 2 & 1 & 1 & 2 & 1 \\ 0 & 0 & 1 & 2 & 2 & 0 & 1 & 2 & 0 \\ 0 & 0 & 2 & 2 & 1 & 1 & 1 & 1 & 0 \\ \hline 0 & 0 & 0 & 0 & 1 & 2 & 2 & 1 & 1 \\ 0 & 0 & 0 & 0 & 0 & 2 & 1 & 1 & 1 \\ 0 & 0 & 0 & 0 & 0 & 1 & 2 & 1 & 2 \end{bmatrix} \cdot \begin{bmatrix} \Delta x_1 \\ \Delta x_2 \\ \Delta x_3 \\ \Delta x_4 \\ \Delta x_5 \\ \Delta x_6 \\ \Delta x_7 \\ \Delta x_8 \\ \Delta x_9 \end{bmatrix} = \begin{bmatrix} 9 \\ 7 \\ 8 \\ 12 \\ 8 \\ 8 \\ 7 \\ 5 \\ 6 \end{bmatrix}$$

Solution

The matrix equation is in the form

$$\begin{bmatrix} \bar{B}_1 & \bar{C}_1 & 0 \\ \bar{A}_2 & \bar{B}_2 & \bar{C}_2 \\ 0 & \bar{A}_3 & \bar{B}_3 \end{bmatrix} \cdot \begin{bmatrix} \Delta \mathbf{X}_1 \\ \Delta \mathbf{X}_2 \\ \Delta \mathbf{X}_3 \end{bmatrix} = - \begin{bmatrix} \mathbf{F}_1 \\ \mathbf{F}_2 \\ \mathbf{F}_3 \end{bmatrix}$$

Following the procedure just given, starting at the first block row,

$$\bar{B}_1 = \begin{bmatrix} 1 & 2 & 1 \\ 2 & 1 & 1 \\ 1 & 2 & 2 \end{bmatrix}, \quad \bar{C}_1 = \begin{bmatrix} 2 & 2 & 1 \\ 2 & 1 & 0 \\ 1 & 2 & 0 \end{bmatrix}, \quad \mathbf{F}_1 = \begin{bmatrix} -9 \\ -7 \\ -8 \end{bmatrix}$$

By standard matrix inversion

$$(\bar{B}_1)^{-1} = \begin{bmatrix} 0 & 2/3 & -1/3 \\ 1 & -1/3 & -1/3 \\ -1 & 0 & 1 \end{bmatrix}$$

By standard matrix multiplication

$$(\bar{\mathbf{B}}_1)^{-1}(\bar{\mathbf{C}}_1)^{-1} = \begin{bmatrix} 1 & 0 & 0 \\ 1 & 1 & 1 \\ -1 & 0 & -1 \end{bmatrix}$$

which replaces $\bar{\mathbf{C}}_1$, and

$$(\bar{\mathbf{B}}_1)^{-1}(\mathbf{F}_1) = \begin{bmatrix} -2 \\ -4 \\ 1 \end{bmatrix}$$

which replaces \mathbf{F}_1 . Also

$$\mathbf{I} = \begin{bmatrix} 1 & 0 & 0 \\ 0 & 1 & 0 \\ 0 & 0 & 1 \end{bmatrix} \text{ replaces } \bar{\mathbf{B}}_1$$

For the second block row

$$\bar{\mathbf{A}}_2 = \begin{bmatrix} 0 & 1 & 3 \\ 0 & 0 & 1 \\ 0 & 0 & 2 \end{bmatrix}, \bar{\mathbf{B}}_2 = \begin{bmatrix} 1 & 2 & 1 \\ 2 & 2 & 0 \\ 2 & 1 & 1 \end{bmatrix}$$

$$\bar{\mathbf{C}}_2 = \begin{bmatrix} 1 & 2 & 1 \\ 1 & 2 & 0 \\ 1 & 1 & 0 \end{bmatrix}, \bar{\mathbf{F}}_2 = \begin{bmatrix} -12 \\ -8 \\ -8 \end{bmatrix}$$

By matrix multiplication and subtraction

$$(\bar{\mathbf{B}}_2 - \bar{\mathbf{A}}_2\bar{\mathbf{C}}_1) = \begin{bmatrix} 3 & 1 & 3 \\ 3 & 2 & 1 \\ 4 & 1 & 3 \end{bmatrix}$$

which upon inversion becomes

$$(\bar{\mathbf{B}}_2 - \bar{\mathbf{A}}_2\bar{\mathbf{C}}_1)^{-1} = \begin{bmatrix} -1 & 0 & 3 \\ 1 & 3/5 & -6/5 \\ 1 & -1/5 & -3/5 \end{bmatrix}$$

By multiplication

$$(\bar{\mathbf{B}}_2 - \bar{\mathbf{A}}_2\bar{\mathbf{C}}_1)^{-1}\bar{\mathbf{C}}_2 = \begin{bmatrix} 0 & -1 & -1 \\ 2/5 & 2 & 1 \\ 1/5 & 1 & 1 \end{bmatrix}$$

which replaces $\bar{\mathbf{C}}_2$. In a similar manner, the remaining steps for this and the third block row are carried out to give

$$\begin{bmatrix} \begin{bmatrix} 1 & 0 & 0 \\ 0 & 1 & 0 \\ 0 & 0 & 1 \end{bmatrix} & \begin{bmatrix} 1 & 0 & 0 \\ 1 & 1 & 1 \\ -1 & 0 & -1 \end{bmatrix} & \begin{bmatrix} 0 & 0 & 0 \\ 0 & 0 & 0 \\ 0 & 0 & 0 \end{bmatrix} \\ \begin{bmatrix} 0 & 0 & 0 \\ 0 & 0 & 0 \\ 0 & 0 & 0 \end{bmatrix} & \begin{bmatrix} 1 & 0 & 0 \\ 0 & 1 & 0 \\ 0 & 0 & 1 \end{bmatrix} & \begin{bmatrix} 0 & -1 & -1 \\ 2/5 & 2 & 1 \\ 1/5 & 1 & 1 \end{bmatrix} \\ \begin{bmatrix} 0 & 0 & 0 \\ 0 & 0 & 0 \\ 0 & 0 & 0 \end{bmatrix} & \begin{bmatrix} 0 & 0 & 0 \\ 0 & 0 & 0 \\ 0 & 0 & 0 \end{bmatrix} & \begin{bmatrix} 1 & 0 & 0 \\ 0 & 1 & 0 \\ 0 & 0 & 1 \end{bmatrix} \end{bmatrix} \cdot \begin{bmatrix} \Delta X_1 \\ \Delta X_2 \\ \Delta X_3 \\ \Delta X_4 \\ \Delta X_5 \\ \Delta X_6 \\ \Delta X_7 \\ \Delta X_8 \\ \Delta X_9 \end{bmatrix} = - \begin{bmatrix} -2 \\ -4 \\ +1 \\ +1 \\ -22/5 \\ -16/5 \\ -1 \\ -1 \\ -1 \end{bmatrix}$$

Thus, $\Delta X_7 = \Delta X_8 = \Delta X_9 = 1$. The remaining backward steps begin with the second block row, where

$$\bar{\mathbf{C}}_2 = \begin{bmatrix} 0 & -1 & -1 \\ 2/5 & 2 & 1 \\ 1/5 & 1 & 1 \end{bmatrix}, \mathbf{F}_2 = \begin{bmatrix} 1 \\ -22/5 \\ -16/5 \end{bmatrix}$$

$$(\mathbf{F}_2 - \bar{\mathbf{C}}_2 \mathbf{F}_3) = \begin{bmatrix} -1 \\ -1 \\ -1 \end{bmatrix}$$

Thus, $\Delta X_4 = \Delta X_5 = \Delta X_6 = 1$. Similarly, for the first block row,

$$\Delta X_1 = \Delta X_2 = \Delta X_3 = 1$$

Problem specifications for the SC method are flexible. However, number of stages, stage pressures, compositions, flow rates, and stage locations for all feeds, sidestreams, and interstage heat exchangers are necessary specifications. For distillation columns, the specification of condenser and/or reboiler duties is not desirable. Alternative specifications are accomplished by removing heat-balance functions H_1 and/or H_N from the simultaneous equation set and replacing them with discrepancy functions. For example, the bottoms flow rate, B , can be specified in place of the reboiler duty by replacing the H_N function with $\sum l_{i,N} - B = 0$.

If desired, (10-39) can be modified to accommodate actual rather than equilibrium stages. Values of the Murphree vapor tray efficiency, E_{MV} , (§6.5.4) must then be specified. These are related to phase compositions by the definition

$$(E_{MV})_j = \eta_j = \frac{y_{i,j} - y_{i,j+1}}{K_{i,j}x_{i,j} - y_{i,j+1}} \quad (10-52)$$

In terms of component flow rates, (10-52) becomes the following discrepancy function, which replaces (10-39).

$$(E_{i,j})_{MV} = \frac{\eta_j K_{i,j} l_{i,j} \sum_{\kappa=1}^C v_{\kappa,j}}{\sum_{\kappa=1}^C l_{\kappa,j}} - v_{i,j} + \frac{(1 - \eta_j) v_{i,j+1} \sum_{\kappa=1}^C v_{\kappa,j}}{\sum_{\kappa=1}^C v_{\kappa,j+1}} \quad (10-53)$$

The SC method is readily extended to staged separators involving three coexisting phases (e.g., three-phase distillation), two liquid phases (e.g., liquid-liquid extraction), reactive absorption and distillation, and to interlinked separators.

EXAMPLE 10.5 Distillation of a Methanol–Water Mixture.

A common industrial distillation is the separation of a methanol–water mixture. Unlike ethanol and isopropanol, methanol does not form an azeotropic mixture with water at near-ambient pressure. Also, unlike ethanol and isopropanol, methanol is toxic. A 1,000 kmol/h saturated feed of 60 mol% methanol and 40 mol% water at 160 kPa

is to be distilled to produce a saturated liquid distillate of 95 mol% methanol and a bottoms product containing only 1 mol% methanol. From past experience, set column pressures of 150 kPa at the top and 165 kPa at the bottom, with negligible pressure drop through the condenser. Use the SCDS model of CHEMCAD to complete a process design of the distillation column, including the number of equilibrium stages, feed-stage location, reflux ratio, duties of the total condenser and partial reboiler, and a stream summary. In addition, track the error-to-tolerance ratio of the iterations, starting with the default initialization.

Solution

The following two approaches are employed:

1. Specify a reflux ratio and a bottoms flow rate (consistent with the desired product purities) and obtain a converged solution. Hopefully, the results of the run will not be far from the desired solution. Using the converged solution as the starting point, the two initial specifications are replaced by the two purity specifications so as to achieve the desired solution. This approach is useful for nonideal mixtures because it is almost always possible to achieve a converged solution when specifying a reflux ratio and a bottoms flow rate, provided that the reflux flow rate is large enough that the liquid flow rate in the rectifying section does not decrease to zero as it approaches the feed stage.
2. Specify the two product purities and seek a converged solution, using the default initialization. If the run fails, provide initial guesses and try again.

For both approaches, a final converged solution that meets the product purity specifications is only possible if the number of equilibrium stages and the reflux ratio exceed the minimum values by some margin. Also, the feed-stage location must not be far from the optimum. The number of equilibrium stages and the feed-stage location must be specified when using SCDS. The preferred way to obtain these two values is to use the Fenske and Kirkbride equations from Chapter 9.

Distillate and bottoms flow rates

$$\text{Methanol molar material balance: } 600 = 0.95D + 0.01B$$

$$\text{Total molar material balance: } D + B = 1,000$$

$$\text{Solving, } B = 372.34 \text{ lbmol/h and } D = 627.66 \text{ lbmol/h}$$

$$\text{Also, methanol flow rate in distillate} = 0.95(627.66) = 596.28 \text{ lbmol/h}$$

$$\text{water flow rate in distillate} = 0.05(627.66) = 31.38 \text{ lbmol/h}$$

$$\text{methanol flow rate in bottoms} = 0.01(372.34) = 3.72 \text{ lbmol/h}$$

$$\text{water flow rate in bottoms} = 0.99(372.34) = 368.62 \text{ lbmol/h}$$

Average Relative Volatility

The relative volatility at the top of the column is determined from a distillate bubble-point calculation at 150 kPa. Because the methanol–water system is nonideal, but far from exhibiting phase

splitting, the Wilson method is selected for estimating liquid-phase activity coefficients. Using CHEMCAD, the result is a relative volatility of $1.029/0.451 = 2.28$ at a temperature of 75.5°C . The calculation is repeated for the bottoms composition at a pressure of 165 kPa, giving a relative volatility of $6.397/0.946 = 6.76$ at a temperature of 112.5°C . The geometric mean relative volatility = 3.93.

Results from the Shortcut (FUG) Method (SHOR) of CHEMCAD

Using the shortcut model of CHEMCAD (SHOR) gives $N_{\min} = 6.40$ and $R_{\min} = 0.3555$.

$$\text{For } R/R_{\min} = 1.5, N = 13.9.$$

Try a column with 13 equilibrium stages with a partial reboiler counted as an additional equilibrium stage, and a reflux ratio of $1.5(0.3555) = 0.533$. Thus, since the total condenser counts as Stage 1 in CHEMCAD, even though it is not an equilibrium stage, the column top stage is 2, the column bottom stage is 14, and the reboiler is Stage 15.

The feed stage location is difficult to select. Because the relative volatility is much larger in the stripping section than in the rectifying section, try a location of Stage 9 from the column top stage, which is Stage 10 in the CHEMCAD input specification.

Run Results Using Approach 1

In this approach, a reflux ratio of 0.533 and a bottoms molar flow rate of 372.34 lbmol/h were specified and the simulator provided the default initialization, which was a linear temperature profile and constant liquid molar flow rates leaving the stages in the rectifying and stripping sections. The default damping factor and default tolerance of 3.87×10^{-3} for convergence were taken. The calculations converged in 7 iterations with the following error sequence:

Iteration	Error at End of Iteration
Initialization	4.10×10^6
1	2.74×10^5
2	1.58×10^5
3	1.27×10^5
4	1.15×10^5
5	1.11×10^4
6	6.88
7	2.17×10^{-5}

The default initialization resulted in a large error. By the end of 4 iterations, convergence was in doubt. However, iteration 5 was a distinct improvement and was followed by major improvements in the final two iterations. The converged product purities were 93.1 mol% methanol in the distillate and 4.26 mol% methanol in the bottoms.

A second run was made using the profiles from the first run, with the two desired purity specifications replacing the reflux ratio and the bottoms molar flow rate. Convergence was achieved in

17 iterations using damping factors that were automatically generated as follows:

Iteration(s)	Damping Factor	Error at End of Iteration(s)
1	0.03125	$1.36 \times 10^{+2}$
2-11	0.125	$4.93 \times 10^{+1}$
12-14	0.25	$3.13 \times 10^{+1}$
15	0.50	$2.56 \times 10^{+1}$
16	1.00	$1.15 \times 10^{+1}$
17	1.00	2.60×10^{-4}

During the 17 iterations, the SC method resulted in a gradual increase in the reflux ratio from the initial value of 0.533 to the final converged value of 0.678.

To determine whether the feed-stage location is near optimal, a McCabe–Thiele diagram in Figure 10.10 was plotted using the Tray Composition report generated from the converged run based on the purity specifications.

The McCabe–Thiele diagram shows that the feed stage is not optimal. Two stages can be removed from the rectifying section and one stage added to the stripping section.

Run Results Using Approach 2

The run was executed using Approach 2, but with 14 stages that included the total condenser and the partial reboiler. The feed stage was relocated to Stage 8 from the top. The two methanol purities were specified and the default initialization was used.

The default initialization gave a poor result with an error of $1.58 \times 10^{+6}$ using a reflux ratio of 2.227. Damping factors as low as 0.0156 were used in early iterations, resulting in a rapid decline in the reflux ratio. After 8 iterations, convergence was achieved with

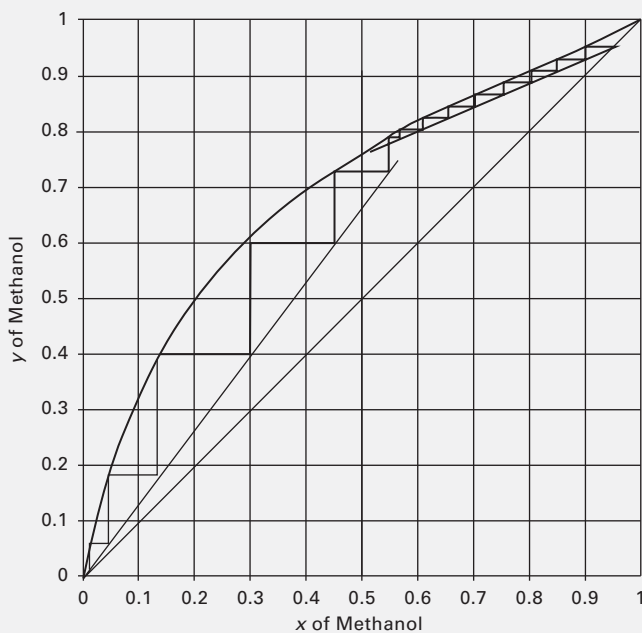


Figure 10.10 McCabe–Thiele plot of run results from approach 1 of Example 10.5.

an error of 9.98×10^{-6} compared to a tolerance of 3.87×10^{-3} . The converged reflux ratio was 0.706. The condenser and reboiler duties were 37,200 MJ/h and 37,100 MJ/h, respectively. Calculated column diameters for 70 to 75% flooding ranged from 7 ft at the top to 5 ft at the bottom.

Convergence was achieved with both approaches despite poor default initializations by damping the Newton–Raphson corrections in early iterations.

EXAMPLE 10.6 Reboiled Absorber Using the SC Method.

Figure 10.11 shows a reboiled absorber for the separation of a hydrocarbon vapor feed. The absorbent oil is equivalent to *n*-decane. The 770 lbmol/h (349 kmol/h) of bottoms product corresponds to the amount of C_3 and heavier in the two feeds, so the column is designed as a deethanizer. Calculate stage temperatures, interstage vapor and liquid flow rates and compositions, and reboiler duty by the SC method.

Solution

This example can be solved with RadFrac of Aspen Plus, SCDS of CHEMCAD or ChemSep. Here, the example is solved with the digital computer program of Sandholm and Naphtali [17], who developed the SC method. The convergence criterion was 2.856×10^{-2} based on the sum-of-squares of the discrepancy functions of (10-38) to (10-40).

Initialization was by a crude method and was called the first iteration. The combined feeds were flashed at 400 psia and a *V/L* ratio

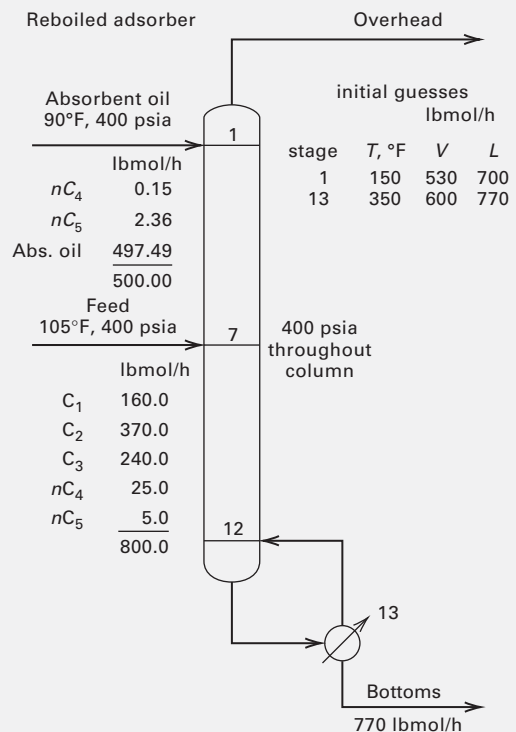


Figure 10.11 Specifications for reboiled absorber of Example 10.6.

of $0.688 = 530/770 =$ ratio of overhead-to-bottoms flow rates. The computed vapor and liquid mole fractions below were the initial values used for every stage.

Species	y	x
C_1	0.2603	0.0286
C_2	0.4858	0.1462
C_3	0.2358	0.1494
nC_4	0.0153	0.0221
nC_5	0.0025	0.0078
nC_{10}	<u>0.0003</u>	<u>0.6459</u>
	1.0000	1.0000

Figure 10.12 shows the convergence pattern. The corresponding sum of squares of the discrepancy functions, was 2.865×10^7 , a very large error to begin iteration 2. At each iteration an optimal damping factor, t , was determined that corresponded to the smallest error. For iteration 2, the optimal value, 0.34, caused only a moderate reduction in the sum of squares. The optimal value was 0.904 for iteration 3, with an error reduction of one order of magnitude. As shown in Figure 10.9, each subsequent iteration produced at least two orders of magnitude reduction in the sum-of squares error, with damping factors close to or at 1.0. Convergence was achieved after 7 iterations.

In Figures 10.13 and 10.14, converged temperature and V/L profiles are compared to the initial profiles. In Figure 10.13, converged stage temperatures with respect to stage number are far from the linear initialization. Above the feed stage, the temperature increases from the top down in a gradual, declining manner. The cold feed causes a small temperature drop from Stage 6 to 7. Temperature also increases from Stage 7 to 13. A dramatic increase occurs in moving from the bottom stage to the reboiler. In Figure 10.14, the converged V/L profile is far from the initial guess.

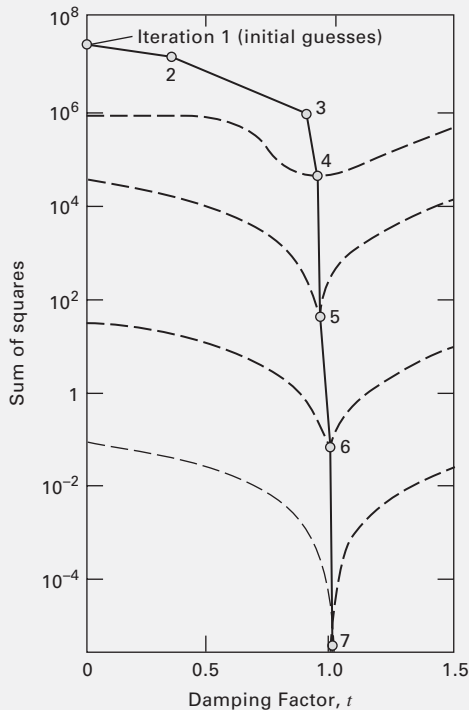


Figure 10.12 Convergence pattern for Example 10.8.

Figure 10.15 shows component flow-rate profiles for the key components (ethane vapor, propane liquid). As expected, the values from the initialization are in very poor agreement with converged values.

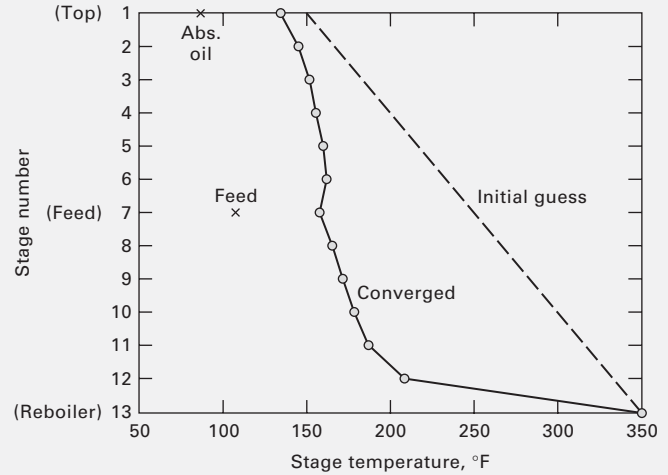


Figure 10.13 Converged temperature profile for reboiled absorber in Figure 10.8.

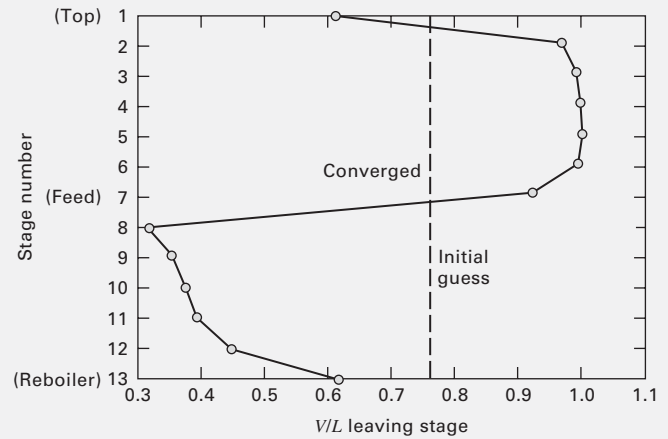


Figure 10.14 Vapor-liquid ratio profile for reboiled absorber in Figure 10.8.

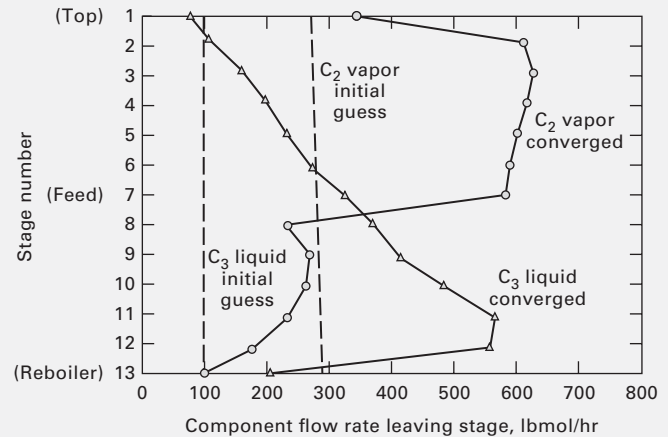


Figure 10.15 Converged flow rates for key components in Example 10.8.

Table 10.4 Product Compositions and Reboiler Duty for Reboiled Absorber of Figure 10.8

	Soave–Redlich–Kwong Equation
Overhead component flow rates, lbmol/h	
C_1	159.99
C_2	341.57
C_3	28.12
nC_4	0.04
nC_5	0.18
Abs. oil	<u>0.10</u>
	530.00
Bottoms component flow rates, lbmol/h	
C_1	0.01
C_2	28.43
C_3	211.88
nC_4	25.11
nC_5	7.18
Abs. oil	<u>497.39</u>
	770.00
Reboiler duty, Btu/h	15,640,000
Bottoms temperature, °F	380.8

The converged propane–liquid profile is regular except at the bottom, where a large decrease occurs because of vaporization in the reboiler. The converged ethane–vapor profile has changes at the top, where entering oil absorbs ethane, and at the feed stage, where substantial ethane vapor is introduced.

Converged values for the reboiler duty, and overhead and bottoms compositions, are given in Table 10.4 based on the SRK EOS for thermodynamic properties.

EXAMPLE 10.7 HCN Absorber Using the SC Method with Electrolyte Thermodynamics.

An off-gas located downstream from the main fractionator of a fluid-catalytic cracker unit in a petroleum refinery contains 200 ppm of HCN, a poisonous chemical. The gas flow rate is 1,000 kmol/h at 25°C and 150 psia. The HCN concentration must be reduced to 5 ppm. HCN is soluble in water with a K -value of approximately 0.5 at these conditions. In water, it partially ionizes to hydrogen and cyanide ions. Determine a suitable absorbent water flow rate and the number of equilibrium stages required for an absorber

To meet the specification of 5 ppm, the fraction of HCN to be absorbed is $195/200 = 0.975$ or the fraction not absorbed = 0.025. The plot of the Kremser equation in Figure 6.15 shows that this degree of absorption can only be achieved with an absorption factor greater than 1.0 and preferably about 1.4. Let, $A = L/KV = 1.4 = L/[0.45(1,000)]$. Solving $L = 630$ lbmol/h of water. To be safe, because of uncertainties in the K -value and the effect of ionization of the HCN, let $L = 750$ lbmol/h of water at 25°C and 150 psia. Two runs were made with the SCDS model of CHEMCAD using the electrolyte NRTL method with Henry's law for K -values. In both runs, the default initialization was used. Five equilibrium stages were specified for the first run. The calculations converged in 8 iterations with 6.5 ppm of HCN leaving in the

off-gas. The number of equilibrium stages was increased to 6 for the second run. The calculations converged in 8 iterations with 4.7 ppm, which meets the goal. In both runs, the amount of absorbed HCN that ionized was negligible because of the very small dissociation constant for HCN (a weak acid). In a third run, 0.2 lbmol/h of HCl (same flow rate as HCN), a strong acid, was added to the off-gas. Again convergence was achieved in 8 iterations. All of the HCl was absorbed and was completely ionized in the absorbent.

§10.7 INSIDE-OUT METHOD

In the BP, SR, and SC methods, the major computational effort is expended in calculating K -values and enthalpies from rigorous thermodynamic-property models because property calculations are made at each iteration. Furthermore, at each iteration, derivatives are required of (1) all properties with respect to temperature and compositions of both phases for the SC method; (2) K -values with respect to temperature for the BP method, and (3) vapor and liquid enthalpies with respect to temperature for the SR method.

In 1974, Boston and Sullivan [19] presented an algorithm designed to reduce the time spent computing thermodynamic properties when making equilibrium-stage calculations. As shown in Figure 10.16, two sets of thermodynamic-property models are employed: (1) a simple, approximate, empirical set used frequently to converge inner-loop calculations, and (2) a rigorous set used less often in the outer loop. The MESH equations are always solved in the inner loop with the approximate set. The parameters in the empirical equations for the inner-loop set are updated only infrequently in the outer loop using the rigorous equations. The distinguishing Boston–Sullivan feature is the inner and outer loops, hence the name inside-out method.

Another feature of the inside-out method shown in Figure 10.16 is the choice of iteration variables. For the SC method, the iteration variables are $l_{i,j}$, $v_{i,j}$, and T_j . For the BP and SR methods, the choice is $x_{i,j}$, $y_{i,j}$, T_j , L_j , and V_j . For the inside-out method, the iteration variables for the outer loop are the parameters in the approximate equations for the thermodynamic properties. The iteration variables for the inner loop are related to stripping factors, $S_{i,j} = K_{i,j}V_j/L_j$.

The inside-out method takes advantage of the following characteristics of the iterative calculations:

1. Component relative volatilities vary much less than component K -values.
2. Enthalpy of vaporization varies less than phase enthalpies.
3. Component stripping factors combine effects of temperature and liquid and vapor flow rates at each stage.

The inner loop of the inside-out method uses relative volatility, energy, and stripping factors to improve stability and reduce computing time. A widely used implementation is that of Russell [21], which is described here together with further refinements suggested and tested by Jelinek [22].

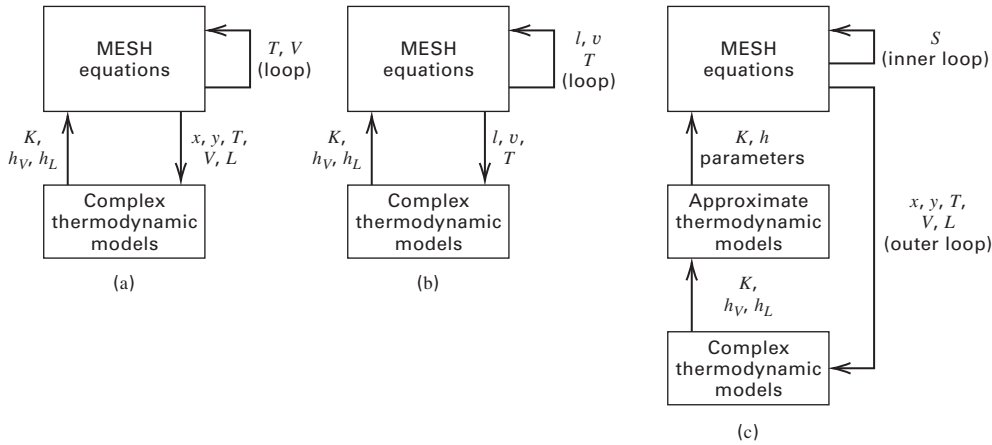


Figure 10.16 Incorporation of thermodynamic-property correlations into interactive loops. (a) BP and SR methods. (b) SC method. (c) inside-out method.

§10.7.1 MESH Equations for Inside-Out Method

As with the BP, SR, and SC methods, the equilibrium-stage model of Figures 10.1 and 10.2 is employed. The form of the equations is similar to the SC method in that component flow rates are utilized. However, in addition, the following inner-loop variables are defined:

$$\alpha_{i,j} = K_{i,j}/K_{b,j} \quad (10-54)$$

$$\mathcal{S}_{b,j} = K_{b,j}V_j/L_j \quad (10-55)$$

$$R_{L_j} = 1 + U_j/L_j \quad (10-56)$$

$$R_{V_j} = 1 + W_j/V_j \quad (10-57)$$

where K_b is the K -value for a base or hypothetical reference component, $\mathcal{S}_{b,j}$ is the stripping factor for the base component, R_{L_j} is a liquid-phase withdrawal factor, and R_{V_j} is a vapor-phase withdrawal factor. For stages without side-streams, R_{L_j} and R_{V_j} reduce to 1. The defined variables in (10-54) to (10-57) and (10-34) to (10-37) still apply, but the MESH equations, (10-38) to (10-40), become as follows, where (10-59) results from the use of (10-56) to (10-58) to eliminate variables in V and the sidestream ratios s and S :

Phase Equilibria:

$$v_{i,j} = \alpha_{i,j}\mathcal{S}_{b,j}l_{i,j}, \quad i = 1 \text{ to } C, \quad j = 1 \text{ to } N \quad (10-58)$$

Component Material Balance:

$$\begin{aligned} l_{i,j-1} - (R_{L_j} + \alpha_{i,j}\mathcal{S}_{b,j}R_{V_j})l_{i,j} + (\alpha_{i,j+1}\mathcal{S}_{b,j+1})l_{i,j+1} \\ = -f_{i,j}, \quad i = 1 \text{ to } C, \quad j = 1 \text{ to } N \end{aligned} \quad (10-59)$$

Energy Balance:

$$\begin{aligned} H_j = h_{L_j}R_{L_j}L_j + h_{V_j}R_{V_j}V_j - h_{L_{j-1}}L_{j-1} - h_{V_{j+1}}V_{j+1} \\ -h_{F_j}F_j - Q_j = 0, \quad j = 1 \text{ to } N \end{aligned} \quad (10-60)$$

where $\mathcal{S}_{i,j} = \alpha_{i,j}\mathcal{S}_{b,j}$.

In addition, discrepancy functions can be added to the MESH equations to permit any reasonable set of product specifications.

§10.7.2 Rigorous and Complex Thermodynamic-Property Models

The complex thermodynamic models referred to in Figure 10.16 can include any of the models discussed in Chapter 2, including those based on P - v - T equations of state and those based on free-energy models for liquid-phase activity coefficients. These generate parameters in the approximate thermodynamic-property models of the form

$$K_{i,j} = K_{i,j}\{P_j, T_j, \mathbf{x}_j, \mathbf{y}_j\} \quad (10-61)$$

$$h_{V_j} = h_{V_j}\{P_j, T_j, \mathbf{y}_j\} \quad (10-62)$$

$$h_{L_j} = h_{L_j}\{P_j, T_j, \mathbf{x}_j\} \quad (10-63)$$

§10.7.3 Approximate Thermodynamic-Property Models

The approximate property models in the inside-out method are designed to facilitate calculation of stage temperatures and stripping factors.

K -values

The approximate K -value model of Russell [21] and Jelinek [22], which differs slightly from that of Boston and Sullivan [19] and originated from a proposal in Robinson and Gilliland [23], is (10-54) combined with

$$K_{b,j} = \exp(A_j - B_j/T_j) \quad (10-64)$$

where A and B are parameters. Either a feed component or a hypothetical reference component can be selected as the base, b , with the latter preferred. It is determined from vapor-composition weighting using the following relations:

$$K_{b,j} = \exp\left(\sum_i w_{i,j} \ln K_{i,j}\right) \quad (10-65)$$

where $w_{i,j}$ are weighting functions given by

$$w_{i,j} = \frac{y_{i,j} [\partial \ln K_{i,j} / \partial (1/T)]}{\sum_i y_{i,j} [\partial \ln K_{i,j} / \partial (1/T)]} \quad (10-66)$$

A unique K_b model and values of $\alpha_{i,j}$ in (10-54) are derived for each stage j from values of $K_{i,j}$ from the rigorous model. At the top stage, the base component will be close to a light component, while at the bottom stage, the base component will be close to a heavy one. The derivatives in (10-66) are obtained numerically or analytically from the rigorous model. To obtain values of A_j and B_j in (10-64), two temperatures must be selected for each stage. For example, the estimated or current temperatures of the two adjacent stages, $j-1$ and $j+1$, might be selected. Calling these T_1 and T_2 and using (10-64) at each stage:

$$B = \frac{\ln (K_{bT_1} / K_{bT_2})}{\left(\frac{1}{T_2} - \frac{1}{T_1} \right)} \quad (10-67)$$

and
$$A = \ln K_{bT_1} + B/T_1 \quad (10-68)$$

For highly nonideal-liquid solutions, it is advisable to separate the rigorous K -value expression of (2-27) into two factors

$$K_i = \gamma_{iL} (\phi_{iL} / \bar{\phi}_{iV}) \quad (10-69)$$

Then, $(\phi_{iL} / \bar{\phi}_{iV})$ is used to determine K_b and, as proposed by Boston [20], values of γ_{iL} at each stage are fitted at a reference temperature, T^* , to the liquid-phase mole fraction by the linear function

$$\gamma_{iL}^* = a_i + b_i x_i \quad (10-70)$$

with parameters a and b , to obtain the approximate estimates of γ_{iL}^* . Equation (10-59) is then modified by replacing $\alpha_{i,j}$ with $\alpha_{i,j} \gamma_{iL}^*$, where

$$\alpha_{i,j} = \frac{(\phi_{iL} / \bar{\phi}_{iV})_j}{K_{b,j}} \quad (10-71)$$

rather than the $\alpha_{i,j}$ given by (10-54).

Enthalpies

Boston and Sullivan [19] and Russell [21] employ the same approximate enthalpy models. Jelinek [22] does not use approximate enthalpy models, because the additional complexity involved in the use of two enthalpy models may not always be justified to the extent that approximate and rigorous K -value models are justified.

The basis for the enthalpy calculations is the same as for the rigorous equations discussed in Chapter 2. Thus, for either phase, from Table 2.5,

$$h = h_V^\circ + (h - h_V^\circ) = h_V^\circ + \Delta H \quad (10-72)$$

where h_V° is the ideal-gas mixture enthalpy, as given by the polynomial equations (2-38) and (2-39), based on the vapor-phase composition for h_V and the liquid-phase composition for h_L . The ΔH term is the enthalpy departure, $\Delta H_V = (h_V - h_V^\circ)$, for the vapor phase, which accounts for the effect of pressure, and $\Delta H_L = (h_L - h_V^\circ)$ for the liquid

phase, which accounts for the enthalpy of vaporization and the effect of pressure on both liquid and vapor phases, as indicated in (2-59). The enthalpy of vaporization dominates the ΔH_L term. The time-consuming parts of the enthalpy calculations are the two enthalpy-departure terms, which are complex when an equation of state is used. Therefore, in the approximate enthalpy equations, the rigorous enthalpy departures are replaced by the simple linear functions

$$\Delta H_{V_j} = c_j - d_j(T_j - T^*) \quad (10-73)$$

and
$$\Delta H_{L_j} = e_j - f_j(T_j - T^*) \quad (10-74)$$

where the departures are modeled in terms of enthalpy per unit mass instead of per unit mole, and T^* is a reference temperature. The parameters c , d , e , and f are evaluated from rigorous models at each outer-loop iteration.

§10.7.4 Inside-Out Algorithm

The inside-out algorithm of Russell [21] involves an initialization procedure, inner-loop iterations, and outer-loop iterations.

Initialization Procedure

First, it is necessary to provide reasonably good estimates of stage values of $x_{i,j}$, $y_{i,j}$, T_j , V_j , and L_j . Boston and Sullivan [19] suggest the following procedure:

1. Specify the number of theoretical stages, conditions of all feeds, feed-stage locations, and pressure profile.
2. Specify stage locations for each product withdrawal (including sidestreams) and for each heat exchanger.
3. Provide an additional specification for each product and each intermediate heat exchanger.
4. If not specified, estimate each product-withdrawal rate, and estimate each value of V_j . Obtain values of L_j from the total material-balance equation, (10-6).
5. Estimate an initial temperature profile, T_j , by combining all feed streams (composite feed) and determining bubble-and dew-point temperatures at average column pressure. The dew-point temperature is the top-stage temperature, T_1 , whereas the bubble-point temperature is the bottom-stage temperature, T_N . Intermediate-stage temperatures are estimated by interpolation. Reference temperatures T^* for use with (10-70), (10-73), and (10-74) are set equal to T_j .
6. Flash the composite feed isothermally at the average column pressure and temperature. The resulting vapor and liquid compositions, y_i and x_i , are the estimated stage compositions.
7. With the initial estimates from Steps 1 through 6, use the complex thermodynamic-property correlation to determine values of the stagewise outside-loop K and h parameters A_j , B_j , $a_{i,j}$, $b_{i,j}$, c_j , d_j , e_j , f_j , $K_{b,j}$, and $\alpha_{i,j}$ of the approximate models.
8. Compute initial values of $\mathcal{S}_{b,j}$, R_{L_j} , and R_{V_j} from (10-55), (10-56), and (10-57).

Inner-Loop Calculation Sequence

An iterative sequence of inner-loop calculations begins with values for the outside-loop parameters listed in Step 7, obtained initially from the initialization procedure and later from outer-loop calculations, using results from the inner loop, as shown in Figure 10.16c.

9. Compute component liquid flow rates, $l_{i,j}$, from the set of N equations (10-59) for each of the C components by the tridiagonal-matrix algorithm.
10. Compute component vapor flows, $v_{i,j}$, from (10-58).
11. Compute a revised set of flow rates, V_j and L_j , from the component flow rates by (10-34) and (10-35).
12. To calculate a revised set of stage temperatures, T_j , compute a set of x_i values for each stage from (10-37), then a revised set of $K_{b,j}$ values from a combination of the bubble-point equation, (10-25), with (10-54), which gives

$$K_{b,j} = 1 / \sum_{i=1}^C (\alpha_{i,j} x_{i,j}) \quad (10-75)$$

From this new set of $K_{b,j}$ values, compute a set of stage temperatures from a rearrangement of (10-64):

$$T_j = \frac{B_j}{A_j - \ln K_{b,j}} \quad (10-76)$$

At this point in the inner-loop iterative sequence, there is a revised set of $v_{i,j}$, $l_{i,j}$, and T_j , which satisfy the component material-balance and phase-equilibria equations for the estimated properties. However, these values do not satisfy the energy-balance and specification equations unless the estimated base-component stripping factors and product withdrawal rates are correct.

13. Select inner-loop iteration variables as

$$\ln \mathcal{S}_{b,j} = \ln(K_{b,j} V_j / L_j) \quad (10-77)$$

together with any other iteration variables. For an ordinary distillation column, no other inner loop iteration variables are needed if the condenser and reboiler duties are specified. If reflux ratio (L/D) and bottoms flow rate (B) are specified rather than the two duties (which is the more common situation), the two (10-60) equations for H_1 and H_N are replaced by two discrepancy functions D_1 and D_2 in terms of L/D and B :

$$D_1 = L_1 - (L/D)V_1 = 0 \quad (10-78)$$

$$D_2 = L_N - B = 0 \quad (10-79)$$

For each sidestream, a withdrawal factor is added as an inner-loop iteration variable, e.g., $\ln(U_j/L_j)$ and $\ln(W_j/V_j)$, together with a specification on purity or some other variable.

14. Compute stream enthalpies from (10-72) to (10-74).
15. Compute normalized discrepancies of H_j , D_1 , D_2 , etc., from the energy balances (10-60) and (10-78), (10-79), etc., but compute Q_1 from H_1 , and Q_N from H_N where appropriate. A typical normalization is (10-24).

16. Compute the Jacobian of partial derivatives of H_j , D_1 , D_2 , etc., with respect to the iteration variables of (10-77), etc., by perturbation of each iteration variable and recalculation of the discrepancies through Steps 9 to 15, numerically or by differentiation.
17. Compute corrections to the inner-loop iteration variables by a SC iteration of the type discussed for the SR and SC methods in §10.5.2 and 10.6.
18. Compute new values of the iteration variables from the sum of the previous values and the corrections with (10-46), using damping if necessary to reduce the sum of squares of the normalized discrepancies.
19. Check whether the sum-of-squares is sufficiently small. If so, proceed to the outer-loop calculation procedure given next. If not, repeat Steps 15 to 18 using the latest iteration variables. For any subsequent cycles through Steps 15 to 18, Russell [21] uses Broyden [24] updates to avoid re-estimation of the Jacobian partial derivatives, whereas Jelinek [22] recommends the standard SC method of recalculating the partial derivatives for each inner-loop iteration.
20. Upon convergence of Steps 15 to 19, Steps 9 through 12 will have produced an improved set of primitive variables $x_{i,j}$, $v_{i,j}$, $l_{i,j}$, T_j , V_j , and L_j . From (10-36), corresponding values of $y_{i,j}$ can be computed. The values of these variables are not correct until the approximate thermodynamic properties are in agreement with the properties from the rigorous models. The primitive variables are input to the outer-loop calculations to bring the approximate and complex models into successively better agreement.

Outer-Loop Calculation Sequence

Each outer loop proceeds as follows:

21. Using the values of the primitive variables from Step 20, compute relative volatilities and stream enthalpies from the complex thermodynamic models. If they are in close agreement with previous values used to initiate a set of inner-loop iterations, both outer-and inner-loop iterations are converged, and the problem is solved. If not, proceed to Step 22.
22. Determine values of the stagewise outside-loop K and h parameters of the approximate models from the complex models, as in initialization Step 7.
23. Compute values of $\mathcal{S}_{b,j}$, R_{L_j} , and R_{V_j} , as in initialization Step 8.
24. Repeat the inner-loop calculation of Steps 9–20.

Although convergence of the inside-out method is not guaranteed for all problems, the method is quite robust and rapid. Convergence difficulties arise because of poor initial estimates, which result in negative or zero flow rates at certain locations in the column. To counteract this tendency, all component stripping factors use a scalar multiplier, S_b , called a base stripping factor, to give

$$\mathcal{S}_{i,j} = S_b \alpha_{i,j} \mathcal{S}_{b,j} \quad (10-80)$$

The value of \mathcal{S}_b is initially chosen to force the results of the initialization procedure to give a reasonable distribution of component flows throughout the column. Russell [21] recommends that \mathcal{S}_b be chosen only once, but Boston and Sullivan [19] compute a new \mathcal{S}_b for each new set of $\mathcal{S}_{b,j}$ values.

For highly nonideal-liquid mixtures, the inside-out method may fail to converge. If so, the SC method should be tried. If the SC method also fails to converge, relaxation or continuation methods, described by Kister [25], are usually successful, but computing time may be an order of magnitude longer than that for similar problems converged successfully with the inside-out method.

EXAMPLE 10.8 Five-Stage Distillation by the Inside-Out Method.

For the conditions of the ordinary distillation column shown in Figure 10.6, track the results of the loops while obtaining a converged solution by the inside-out method. Use the SRK equation of state for thermodynamic properties.

Solution

The TOWR model (an inside-out method) of the CHEMCAD process simulator was used. The only initial assumptions were a condenser outlet temperature of 65°F and a bottoms-product temperature of 165°F. The bubble-point temperature of the feed was 123.5°F. In the initialization procedure, the parameters A and B in (10-64), with T in °R, were determined from the SRK equation, with the following results:

Stage	T , °F	A	B	K_b
1	65	6.870	3708	0.8219
2	95	6.962	4031	0.7374
3	118	7.080	4356	0.6341
4	142	7.039	4466	0.6785
5	165	6.998	4576	0.7205

Values of the enthalpy coefficients c , d , e , and f in (10-73) and (10-74) are not tabulated here but were computed for each stage, based on the initial temperature distribution.

In the inner-loop calculation sequence, component liquid flow rates were obtained from (10-59) by the tridiagonal-matrix method of §10.4.1. The resulting bottoms-product flow rate deviates somewhat from the specified value of 50 lbmol/h. By modifying the component stripping factors with a base stripping factor, \mathcal{S}_b , in (10-80) of 1.1863, the error in the bottoms flow rate is reduced to 0.73%.

The initial inside-loop error from the solution of the normalized energy-balance equations, (10-60), was only 0.04624. This reduced to 0.000401 after two iterations through the inner loop.

At this point in the inside-out method, the revised column profiles of temperature and phase compositions were used in the outer loop with the SRK thermodynamic models to compute updates for the approximate K and h parameters. Only one inner-loop iteration was required to obtain satisfactory convergence of the energy equations. The K and h parameters were again updated in the outer loop. After one inner-loop iteration, the approximate K and h values were found to be sufficiently close to the SRK values for overall convergence. Thus, a total of only three outer-loop iterations and four inner-loop iterations were required.

To illustrate the efficiency of the inside-out method, results from each of the three outer-loop iterations were:

Outer-Loop Iteration	Stage Temperatures, °F				
	T_1	T_2	T_3	T_4	T_5
Initial guess	65	—	—	—	165
1	82.36	118.14	146.79	172.66	193.20
2	83.58	119.50	147.98	172.57	192.53
3	83.67	119.54	147.95	172.43	192.43

Outer-Loop Iteration	Total Liquid Flows, lbmol/h				
	L_1	L_2	L_3	L_4	L_5
Specification	100	—	—	—	—
1	100.00	89.68	187.22	189.39	50.00
2	100.03	89.83	188.84	190.59	49.99
3	100.0	89.87	188.96	190.56	50.00

Outer-Loop Iteration	Component Flows in Bottoms Product, lbmol/h			
	C_3	nC_4	nC_5	L_5
1	0.687	12.045	37.268	50.000
2	0.947	12.341	36.697	49.985
3	0.955	12.363	36.683	50.001

It is seen that stage temperatures and total liquid flow rates are already close to the converged solution after one outer-loop iteration. However, the composition of the bottoms product with respect to the lightest component, C_3 , is not close to the converged solution until after two iterations. The inside-out method does not always converge so dramatically but is usually efficient, as shown in the following table for four exercises in this chapter.

Problem	Total Number of Inner Loops	Number of Outer-Loop Iterations
Exercise 10.9	7	6
Exercise 10.20	6	3
Exercise 10.31	17	9
Exercise 10.35	16	5

Computing time on a PC for each of these four exercises was less than 1 second.

EXAMPLE 10.9 Distillation with Multiple Feeds, Sidestreams, and Interstage Heat Exchangers by the Inside-Out Method.

Use the RadFrac model in Aspen Plus with the inside-out method to solve the complex distillation column shown in Figure 10.3. Use the Peng–Robinson EOS for thermodynamic properties.

Solution

The specifications are included in Figure 10.3. Note that both vapor and liquid distillates are produced. The molar flow rates for the vapor distillate, liquid distillate, and liquid sidestream sum to molar flow rates of ethane and propane in the two feeds. The molar flow rate of the vapor sidestream equals the sum of the n -butane molar flow rates in the two feeds. By material balance, the bottoms molar flow rate is

40 lbmol/h. This equals the sum of the molar feed rates for *n*-pentane and *n*-hexane in the two feeds.

With the Peng–Robinson method, the default interaction parameters in Aspen Plus were applied. However, the user must accept this default. A partial vapor–liquid condenser was specified because both vapor and liquid distillates are produced. The fraction of vapor distillate was 0.75. A kettle reboiler, counted as an equilibrium stage, was accepted by default. The total number of stages was 16, counting the partial condenser and the partial reboiler. The two feeds, both liquids, were sent to Stages 6 and 9. The two specifications for the column were a reflux flow rate of 150 lbmol/h and a combined distillate flow rate of 20 lbmol/h. The liquid sidestream was located at Stage 3 with a flow rate of 3 lbmol/h. The vapor sidestream was located at Stage 13 with a flow rate of 37 lbmol/h. An interstage cooler with a duty of –200,000 Btu/h was located at Stage 3 using the specification sheet found under Blocks/B1/Configuration/Side Duties. Initialization of the iterations was by default.

Convergence of the RadFrac block using the standard inside-out method was achieved almost instantaneously in 5 outer-loop iterations with the following error/tolerance sequence:

Outer Loop Iteration	Error/Tolerance
1	51.605
2	6.788
3	2.989
4	1.001
5	0.026

Thus, because of the complexity of the distillation and the use of the default initialization, the initial error was very high. However, the error was quickly reduced by the inside-out method to a value below the default tolerance.

The converged stream summary with flow rates in lbmol/h was as follows:

Component	Feed 1	Feed 2	Vapor Distillate	Liquid Distillate	Liquid Side-stream	Vapor Side-stream	Bottoms
Ethane	2.5	0.5	2.6	0.4	0.0	0.0	0.0
Propane	14.0	6.0	12.1	4.4	2.4	1.1	0.0
<i>n</i> -Butane	19.0	18.0	0.3	0.2	0.6	25.5	10.4
<i>n</i> -Pentane	5.0	30.0	0.0	0.0	0.0	10.0	25.0
<i>n</i> -Hexane	0.5	4.5	0.0	0.0	0.0	0.4	4.6
Total	41.0	59.0	15.0	5.0	3.0	37.0	40.0

The attempt to obtain a near-pure *n*-butane product in the vapor sidestream was a failure. In general, it is very difficult to obtain near-pure sidestream products. Either the component must have a *K*-value much different from adjacent components or a very large reflux or boilup ratio is required.

The temperature of the distillates and reflux was 108.6°F. The bottoms temperature was 283.9°F. Feed 1 at 300 psia was flashed across a valve to column pressure of 241 psia, causing 4.3 mol% of it to vaporize. The boilup flow rate leaving the reboiler was 212.7 lbmol/h. The condenser duty was 900,000 Btu/h, while the reboiler duty was 1,566,000 Btu/h.

This example was also solved, using the same specifications, with the TOWR (inside-out) model of CHEMCAD. Convergence was rapid and the results were almost identical to RadFrac.

EXAMPLE 10.10 Carbon Capture by Absorption of CO₂ by an Aqueous Amine Solution.

A gas stream at 56°C and 1.07 bar has a composition in kmol/h of 200 CO₂, 400 H₂O, 4,000 N₂, and 600 H₂. It is to be scrubbed with aqueous monoethanolamine (MEA) at 50°C and 1.05 bar in an absorber to capture CO₂. The absorbent flow rate is 750 kmol/h of MEA in 5,700 kmol/h of water. Determine the percent capture of CO₂ as a function of the number of equilibrium stages.

Solution

The TOWR model of CHEMCAD was used with the Amine option for thermodynamic properties. For one equilibrium stage, an adiabatic flash of the combined gas and absorbent streams resulted in 97.1% CO₂ absorbed. For two equilibrium stages, the TOWR model converges in 9 iterations with a % capture of CO₂ of 99.999.

§10.8 RIGOROUS METHODS FOR LIQUID–LIQUID EXTRACTION

Rigorous equilibrium-stage models for multicomponent liquid–liquid extraction include modifications of the sum-rates (SR), simultaneous-correction (SC), and inside-out models for vapor–liquid separation operations. The SR model is simpler, but initialization is critical because of the highly nonideal nature of the system. Reasonable initial guesses of stage compositions may be necessary to converge the calculations. Convergence is more likely with the inside-out model or the SC model, especially if damping is used.

§10.8.1 The Isothermal Sum-Rates (ISR) Method

In industry, liquid–liquid extraction is usually adiabatic, entering streams are often at ambient temperature, and heat of mixing is negligible, resulting in a nearly isothermal operation. If stage temperatures are specified, as discussed by Friday and Smith [7] and Tsuboka and Katayama [12], a simplified isothermal version of the sum-rates method (ISR) is applicable. It is based on the equilibrium-stage model in §10.1. For application to a liquid–liquid system, liquid-phase and vapor-phase symbols correspond to raffinate and extract, respectively and *K*-values become distribution (partition) coefficients. With all stage temperatures specified, the equilibrium-stage energy balances are ignored. However, close attention must be paid to the possibility that phase compositions may strongly influence *K*_{*D*,*i*} values.

For the Tsuboka–Katayama ISR method, problem specifications are feed flow rates and compositions; feed-stage locations; stage temperatures (frequently all equal); total flow rates of side-streams; and the number of equilibrium stages, *N*. Stage pressures must be greater than corresponding bubble-point pressures to prevent vaporization.

With stage temperatures specified, the only tear variables are *V_j* (extract flow rates). An initial set is obtained by assuming a perfect separation for feed components and neglecting

solvent mass transfer to the raffinate phase. This fixes approximate values for exiting raffinate and extract flow rates. Intermediate V_j values are obtained by linear interpolation.

The effect of compositions on K_D -values can be considerable. It is best to provide initial estimates of $x_{i,j}$ and $y_{i,j}$ from which values of $K_{D,i,j}$ are computed. Initial values of $x_{i,j}$ are obtained by linear interpolation using the compositions of the known entering and assumed exit streams. Corresponding values of $y_{i,j}$ are obtained by material balance from (10-1). Values of $\gamma_{iL,j}$ and $\gamma_{iV,j}$ are determined using an appropriate activity-coefficient correlation from Chapter 2. Selection of the NRTL equation is often preferred. Corresponding K_D -values are from an equation equivalent to (2-33).

$$K_{i,j} = \frac{\gamma_{iL,j}}{\gamma_{iV,j}} \quad (10-81)$$

New $x_{i,j}$ values come from solving (10-12) by the tridiagonal matrix algorithm. These are compared to the assumed values by

$$\text{error} = \sum_{j=1}^N \sum_{i=1}^C \left| x_{i,j}^{(r-1)} - x_{i,j}^{(r)} \right| \quad (10-82)$$

where r is an inner-loop index. If the error is greater than the tolerance, where, for example, the tolerance might be 0.01 NC , an inner loop is used to improve the K_D values by using normalized values of $x_{i,j}$ and $y_{i,j}$ to compute new values of $\gamma_{iL,j}$ and $\gamma_{iV,j}$.

When the inner loop is converged, values of $x_{i,j}$ are used to compute new values of $y_{i,j}$ from (10-2). A new set of tear variables V_j is then obtained from the sum-rates relation

$$V_j^{(k+1)} = V_j^{(k)} \sum_{i=1}^C y_{i,j} \quad (10-83)$$

where k is an outer-loop index. Values of $L_j^{(k+1)}$ are obtained from (10-6). The outer loop is converged when

$$\text{error} = \sum_{j=1}^N \left(\frac{V_j^{(k)} - V_j^{(k-1)}}{V_j^{(k)}} \right)^2 \leq \text{tolerance} \quad (10-84)$$

where the tolerance may be 0.01 N . Convergence of the ISR method depends on the effect of composition on the K_D values.

EXAMPLE 10.11 Separation of Benzene from *n*-Heptane by Extraction with Aqueous Dimethylformamide (DMF).

The separation of benzene (B) from *n*-heptane (H) by distillation is difficult, even though the normal boiling points differ by 18.3°C, because of liquid-phase nonideality. The relative volatility decreases to less than 1.15 at high benzene concentrations [13]. Alternatively, liquid-liquid extraction with a mixture of dimethylformamide (DMF) and water [14] can be used. The solvent is more selective

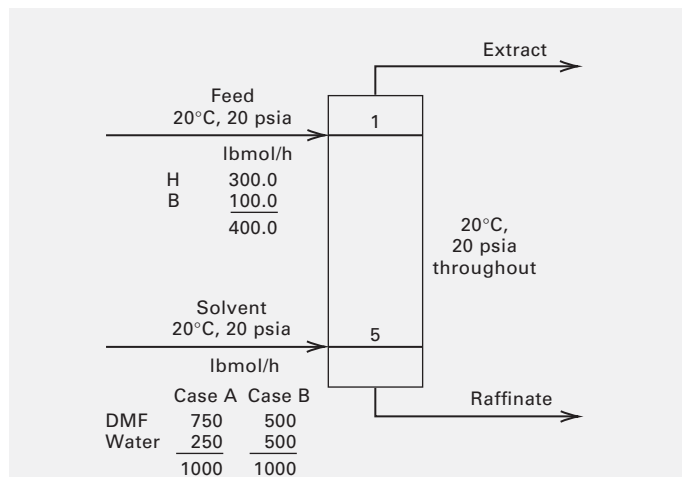


Figure 10.17 Specifications for Example 10.11.

for benzene than for *n*-heptane at 20°C. For the two different solvent compositions, shown in Figure 10.17, calculate interstage flow rates and product compositions by the ISR method for a five equilibrium-stage liquid-liquid extraction cascade.

Solution

Experimental phase-equilibrium data for the quaternary system [19] were fitted to the NRTL equation by Cohen and Renon [15]. The resulting binary-pair constants in (2-77) to (2-78) are

Binary Pair, ij	τ_{ij}	τ_{ji}	α_{ji}
DMF, H	2.036	1.910	0.25
Water, H	7.038	4.806	0.15
B, H	1.196	-0.355	0.30
Water, DMF	2.506	-2.128	0.253
B, DMF	-0.240	0.676	0.425
B, Water	3.639	5.750	0.203

For Case A, estimates of V_j (the extract phase), $x_{i,j}$, and $y_{i,j}$, based on a perfect separation and linear interpolation by stage, are

Stage j	V_j	$y_{i,j}$				$x_{i,j}$			
		H	B	DMF	Water	H	B	DMF	Water
1	1100	0.0	0.0909	0.6818	0.2273	0.7895	0.2105	0.0	0.0
2	1080	0.0	0.0741	0.6944	0.2315	0.8333	0.1667	0.0	0.0
3	1060	0.0	0.0566	0.7076	0.2359	0.8824	0.1176	0.0	0.0
4	1040	0.0	0.0385	0.7211	0.2404	0.9375	0.0625	0.0	0.0
5	1020	0.0	0.0196	0.7353	0.2451	1.0000	0.0	0.0	0.0

The converged solution for Case A gives the following stage flow rates and compositions:

Stage j	V_j	$y_{i,j}$				$x_{i,j}$			
		H	B	DMF	Water	H	B	DMF	Water
1	1113.1	0.0263	0.0866	0.6626	0.2245	0.7586	0.1628	0.0777	0.0009
2	1104.7	0.0238	0.0545	0.6952	0.2265	0.8326	0.1035	0.0633	0.0006
3	1065.6	0.0213	0.0309	0.7131	0.2347	0.8858	0.0606	0.0532	0.0004
4	1042.1	0.0198	0.0157	0.7246	0.2399	0.9211	0.0315	0.0471	0.0003
5	1028.2	0.0190	0.0062	0.7316	0.2432	0.9438	0.0125	0.0434	0.0003

Computed products for the two cases are:

	Extract, lbmol/h		Raffinate, lbmol/h	
	Case A	Case B	Case A	Case B
H	29.3	5.6	270.7	294.4
B	96.4	43.0	3.6	57.0
DMF	737.5	485.8	12.5	14.2
Water	<u>249.9</u>	<u>499.7</u>	<u>0.1</u>	<u>5.0</u>
	1113.1	1034.1	286.9	365.9

On a percentage extraction basis, the results are:

	Case A	Case B
Percent of benzene feed extracted	96.4	43.0
Percent of <i>n</i> -heptane feed extracted	9.8	1.87
Percent of solvent transferred to raffinate	1.26	1.45

Thus, the solvent with 75% DMF extracts a much larger percentage of the benzene, but the solvent with 50% DMF is more selective between benzene and *n*-heptane. For Case A, the stage variations of K -values and the relative selectivity are shown in Figure 10.18, where the relative selectivity is $\beta_{B,H} = K_{D_B} / K_{D_H}$. The distribution coefficient for *n*-heptane varies by a factor of almost 1.75 from Stage 5 to Stage 1, while the coefficient for benzene is almost constant. The relative selectivity varies by a factor of almost 2.

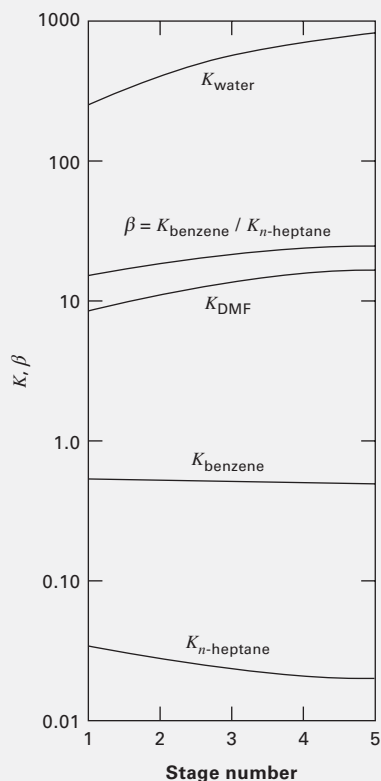


Figure 10.18 Distribution coefficient and relative selectivity profiles for Example 10.11, Case A.

§10.8.2 The Simultaneous-Correction (SC) and Inside-Out Methods

The SC method is used by the EXTR model of CHEMCAD and the Extraction model of ChemSep. For EXTR, the user has the option to include derivatives of the distribution coefficient with respect to composition if convergence fails.

The inside-out algorithm is used in the EXTRACT model of Aspen Plus. That model allows for side feeds and product sidestreams. It consists of two nested iteration loops. The K -value and enthalpy models are evaluated only in the outside loop to determine parameters of simplified local models used in the inner loop. The local model parameters are the outside loop iteration variables. Convergence of the outer loop is achieved by a combination of the bounded Wegstein method and the Broyden quasi-Newton method. In the inside loop, the MESH equations are expressed in terms of the local physical property models. Convergence of the inner loop uses one of the following methods, depending on difficulty: bounded Wegstein, Broyden quasi-Newton, Schubert quasi-Newton, and Newton. The tolerance for convergence becomes tighter as the outside loop converges. These convergence methods are included in MATLAB.

EXAMPLE 10.12 Extraction of Acetic Acid from Water with Ethyl Acetate.

Use the EXTRACT model of Aspen Plus to determine the effect of the number of equilibrium stages, from 2 to 8, on the percent extraction of acetic acid from water by ethyl acetate, using the feed and recycle solvent flow rates in Figure 8.1. Assume both streams enter the extraction unit at 30°C and 1 bar. The operation is adiabatic. Use the UNIFAC-LL method for estimating the distribution coefficients. From the results for 8 stages, calculate the average molar flow rates of the two countercurrently flowing streams and the average distribution coefficient for acetic acid between ethyl acetate and water. Compare the Aspen Plus results with predictions by the Kremser plot of Figure 6.15, assuming the extract phase is analogous to the vapor and the raffinate phase is analogous to the liquid, such that a stripping factor applies. If 99.8% extraction of acetic acid is desired, does the Kremser plot indicate that the solvent flow rate could be appreciably reduced, without a large increase in the required number of equilibrium stages?

Solution

The feed to the top stage of the EXTRACT model is the feed (1st liquid phase), with the raffinate leaving at the bottom. The recycle solvent (2nd liquid phase) enters the bottom stage, with the extract leaving at the top. The key component of the 1st liquid phase is water. The key component of the 2nd liquid phase is ethyl acetate. Initial estimates of stage temperatures and stage pressures are those of the feed and recycle solvent. Calculations converged in 9 iterations or

less. Results for the % acetic acid extraction as a function of the number of equilibrium stages are as follows:

Number of Equilibrium Stages	Percent Extraction of Acetic Acid	Fraction of Acetic Acid not Extracted
2	94.62	0.0538
3	98.44	0.0156
4	99.53	0.00472
5	99.85	0.00146
6	99.95	0.000455
7	99.986	0.000143
8	99.995	0.000045

Thus, 5 equilibrium stages are required.

From the 8-stage result, the average molar flow rate of the feed/raffinate stream (L) is 1318 lbmol/h. The average molar flow rate of the recycle solvent/extract stream (V) is 1020 lbmol/h. The average distribution coefficient (K_D) on a mole fraction basis is close to 4.5. The stripping factor, \mathcal{S} , is $K_D V/L = 4.5(1020)/1318 = 3.5$. This is a high stripping factor. Using it with the Kremser plot gives results that agree well with values computed by Aspen Plus. If the stripping factor is reduced to 2.0, the number of stages required for 99.98% extraction (0.0002 fraction of acetic acid not extracted) is 12.3, which is an unfavorably large increase.

CHAPTER 10 NOMENCLATURE

Abbreviations and Acronyms

BP	bubble-point (method)
ISR	isothermal sum-rates (method)
MESH	equations for modeling an equilibrium stage
NR	Newton–Raphson (method)
SC	simultaneous-correction (method)
SR	sum-rates (method)

Latin Symbols

A_j	defined by (10-8)
$B_{i,j}$	defined by (10-9)
$C_{i,j}$	defined by (10-10)
$D_{i,j}$	defined by (10-11)
D_1, D_2	discrepancy functions, (10-78)
$E_{i,j}$	phase equilibrium relation, (10-2) and (10-39)
$(E_{i,j})_{MV}$	discrepancy function based on Murphree Vapor efficiency, (10-53)
\mathbf{F}_j	vector of functions for stage j , (10-42)
$f_{i,j}$	$f_{i,j} = F_j z_{i,j}$, below (10-40)
H_j	energy balance equation for stage j , (10-5)
ΔH	enthalpy departure ($h - h^o$) mixture enthalpy minus ideal mixture enthalpy, (10-72)
$K_{b,j}$	base K -value relation defined by (10-64)

$l_{i,j}$	liquid flow rate of component i at stage j , (10-37)
$M_{i,j}$	material balance equation for component i , stage j , (10-1)
m	index for stages, (10-9)
p, q	tridiagonal matrix coefficients, section 10.4.1
R_{L_j}	liquid phase withdrawal factor = $1 + U_j/L_j$, (10-56)
R_{V_j}	vapor-phase withdrawal factor = $1 + W_j/U_j$, (10-57)
r	iteration number, (10-22); inner-loop index, (10-82)
S_j	vapor sidestream ratio = W_j/V_j , (10-38)
$(S_y)_j$	mole fraction summation equation for vapor on stage j , (10-3)
$(S_x)_j$	mole fraction summation equation for liquid on stage j , (10-4)
$\mathbf{S}_{b,j}$	inner-loop variable for inside-out method = $K_{b,j} V_j/L_j$, (10-55)
s_j	liquid sidestream ratio = U_j/L_j , (10-38)
t	damping factor, (10-46)
U	liquid sidestream flow rate, Fig. 10.1
$v_{i,j}$	vapor flow rate of component i at stage j , (10-36)
W	vapor sidestream flow rate, Fig. 10.1
$w_{i,j}$	weighting function for inside-out method, (10-66)
\mathbf{X}	vector of output variables for stage j , (10-41)

Note that bold letters indicate vectors and over-barred vectors denote a matrix.

Greek Symbols

$\alpha_{i,j}$	inner-loop variable for inside-out method = $K_{i,j}/K_{b,j}$, (10-54)
Δ	correction (difference), below (10-21)

Subscripts

b	reference component, (10-55)
k	iteration number, (10-45)
n	number of equations, (10-19)

Superscripts

*	initial guesses for variables, (10-21); reference values, (10-70)
k	outer loop index, (10-83)
r	iteration number, (10-22)
T	transposed vector, (10-41)
–	a matrix when placed over a (bold) vector, §10.6

SUMMARY

1. Rigorous methods are readily available for computer-solution of equilibrium-based models for multicomponent, multistage absorption, stripping, distillation, and liquid–liquid extraction.
2. The equilibrium-based model for a countercurrent-flow cascade provides for multiple feeds, vapor sidestreams, liquid sidestreams, and intermediate heat exchangers. Thus, the model can handle almost any type of column configuration.
3. The model equations include component and total material balances, phase-equilibria relations, and energy balances.
4. Some or all of the model equations can be grouped to obtain tridiagonal-matrix equations, for which an efficient solution algorithm is available.
5. Widely used for iteratively solving the model equations are the sum-rates (SR) method, the simultaneous-correction (SC) method, and the inside-out method.
6. The bubble-point method is sometimes useful for initializing the other methods.
7. The SR method is generally restricted to absorption and stripping problems involving wide-boiling feed mixtures or, in the ISR form, to extraction problems.
8. The SC and inside-out methods are designed to solve any type of column configuration for any type of feed mixture. Because of its computational efficiency, the inside-out method is often the method of choice; however, it may fail to converge for highly nonideal-liquid mixtures, in which case the slower SC method should be tried. Both permit considerable flexibility in specifications.
9. When the SC and inside-out methods fail, slower relaxation and continuation methods, not covered here, are a last resort.

REFERENCES

1. WANG, J.C., and G.E. HENKE, *Hydrocarbon Processing*, **45**(8), 155–163 (1966).
2. MYERS, A.L., and W.D. SEIDER, *Introduction to Chemical Engineering and Computer Calculations*, Prentice-Hall, Englewood Cliffs, NJ, pp. 484–507 (1976).
3. LEWIS, W.K., and G.L. MATHESON, *Ind. Eng. Chem.*, **24**, 496–498 (1932).
4. THIELE, E.W., and R.L. GEDDES, *Ind. Eng. Chem.*, **25**, 290 (1933).
5. HOLLAND, C.D., *Multicomponent Distillation*, Prentice-Hall, Englewood Cliffs, NJ (1963).
6. AMUNDSON, N.R., and A.J. PONTINEN, *Ind. Eng. Chem.*, **50**, 730–736 (1958).
7. FRIDAY, J.R., and B.D. SMITH, *AIChE J.*, **10**, 698–707 (1964).
8. BOSTON, J.F., and S.L. SULLIVAN, JR., *Can. J. Chem. Eng.*, **52**, 52–63 (1974).
9. BOSTON, J.F., and S.L. SULLIVAN, JR., *Can. J. Chem. Eng.*, **50**, 663–669 (1972).
10. SUJATA, A.D., *Hydrocarbon Processing*, **40**(12), 137–140 (1961).
11. BURNINGHAM, D.W., and F.D. OTTO, *Hydrocarbon Processing*, **46**(10), 163–170 (1967).
12. TSUBOKA, T., and T. KATAYAMA, *J. Chem. Eng. Japan*, **9**, 40–45 (1976).
13. HÁALA, E., I. WICHTERLE, J. POLAK, and T. BOUBLIK, *Vapor-Liquid Equilibrium Data at Normal Pressures*, Pergamon, Oxford, p. 308 (1968).
14. STEIB, V.H., *J. Prakt. Chem.*, **4**, Reihe, Bd. 28, 252–280 (1965).
15. COHEN, G., and H. RENON, *Can. J. Chem. Eng.*, **48**, 291–296 (1970).
16. GOLDSTEIN, R.P., and R.B. STANFIELD, *Ind. Eng. Chem., Process Des. Develop.*, **9**, 78–84 (1970).
17. NAPHTALI, L.M., and D.P. SANDHOLM, *AIChE J.*, **17**, 148–153 (1971).
18. FREDENSLUND, A., J. GMEHLING, and P. RASMUSSEN, *Vapor-Liquid Equilibria Using UNIFAC, A Group Contribution Method*, Elsevier, Amsterdam (1977).
19. BOSTON, J.F., and S.L. SULLIVAN, JR., *Can. J. Chem. Engr.*, **52**, 52–63 (1974).
20. BOSTON, J.F., *ACS Symp. Ser. No. 124*, 135–151 (1980).
21. RUSSELL, R.A., *Chem. Eng.*, **90**(20), 53–59 (1983).
22. JELINEK, J., *Comput. Chem. Engng.*, **12**, 195–198 (1988).
23. ROBINSON, C.S., and E.R. GILLILAND, *Elements of Fractional Distillation*, 4th ed., McGraw-Hill, New York, pp. 232–236 (1950).
24. BROYDEN, C.G., *Math Comp.*, **19**, 577–593 (1965).
25. KISTER, H. Z., *Distillation Design*, McGraw-Hill, Inc., New York (1992).

STUDY QUESTIONS

- 10.1. Why are rigorous solution procedures difficult and tedious for multicomponent, multistage separation operations?
- 10.2. In the equilibrium-stage model, can each stage have a feed, a heat exchanger, a vapor sidestream, and/or a liquid sidestream? How many independent equations apply to each stage for C components?
- 10.3. In the equilibrium-stage model equations, are K -values and enthalpies counted as variables? Are the equations used to compute these properties counted as equations?
- 10.4. For a cascade of N countercurrent equilibrium stages, what is the number of variables, number of equations, and number of degrees of freedom? What are typical specifications, and

what are the typical computed (output) variables? Why is it necessary to specify the number of equilibrium stages and the locations of all sidestream withdrawals and heat exchangers?

- 10.5.** Early attempts to solve the MESH equations by hand calculations were the Lewis–Matheson and Thiele–Geddes methods. Why are they not favored for computer calculations?
- 10.6.** What are the three methods most widely used to solve the MESH equations?
- 10.7.** How do equation-tearing and simultaneous-correction procedures differ?
- 10.8.** What is a tridiagonal-matrix (TDM) equation? How is it developed from the MESH equations? In the matrix equation, what are the variables and what are the tear variables? What is a tear variable? Is there one TDM equation for each component? If so, can each equation be solved independently of the others?

- 10.9.** What is meant by normalization of a set of variables?
- 10.10.** Does the SR method use tridiagonal-matrix equations? What are the tear variables in the SR method?
- 10.11.** What limitation of the SR method is overcome by the SC method? How does the SC method differ from the SR method?
- 10.12.** What is the difference between a tridiagonal-matrix (TDM) equation and a block-tridiagonal-matrix (BTDM) equation? How do the algorithms for solving these two types of equations differ?
- 10.13.** What is a Jacobian matrix? How is the Jacobian formulated?
- 10.14.** What types of calculations consume the most time in the SR and SC methods? How does the inside-out method reduce this time?
- 10.15.** For a given problem, would it be expected that the SC and inside-out methods converge to the same result?

EXERCISES

Exercises for this chapter are divided into two groups: (1) those that can be solved manually or with MATLAB and (2) those that are best solved with a process simulator. The first group is referenced to chapter section numbers. The second group of problems follows the first group and is referenced to the type of separation operation.

Section 10.1

10.1. Interdependency of the MESH equations.

Show mathematically that (10-6) is not independent of (10-1), (10-3), and (10-4).

10.2. Revision of MESH equations.

Revise the MESH equations to account for entrainment of drops in the vapor, occlusion of bubbles in the liquid, and chemical reactions.

Section 10.4

10.3. Revision of MESH equations.

Revise the MESH equations (10-1) to (10-6) to allow for pumparounds of the type shown in Figure 10.4. Pumparounds are discussed by Bannon and Marple [*Chem. Eng. Prog.*, **74**(7), 41–45 (1978)] and Huber [*Hydrocarbon Processing*, **56**(8), 121–125 (1977)]. Combine the equations to obtain modified M equations similar to (10-7). Can these equations still be partitioned in a series of C tridiagonal-matrix equations?

10.4. The Thomas algorithm.

Use the Thomas algorithm to solve the following matrix equation by manual calculations for x_1, x_2 , and x_3 . Verify your result with MATLAB.

$$\begin{bmatrix} -160 & 200 & 0 \\ 50 & -350 & 180 \\ 0 & 150 & -230 \end{bmatrix} \cdot \begin{bmatrix} x_1 \\ x_2 \\ x_3 \end{bmatrix} = \begin{bmatrix} 0 \\ -50 \\ 0 \end{bmatrix}$$

10.5. The Thomas algorithm.

Use the Thomas algorithm to solve the following tridiagonal-matrix equation by manual calculations for the x vector. Verify your result with MATLAB.

$$\begin{bmatrix} -6 & 3 & 0 & 0 & 0 \\ 3 & -4.5 & 3 & 0 & 0 \\ 0 & 1.5 & -7.5 & 3 & 0 \\ 0 & 0 & 4.5 & -7.5 & 0 \\ 0 & 0 & 0 & 4.5 & -4.5 \end{bmatrix} \cdot \begin{bmatrix} x_1 \\ x_2 \\ x_3 \\ x_4 \\ x_5 \end{bmatrix} = \begin{bmatrix} 0 \\ 0 \\ 100 \\ 0 \\ 0 \end{bmatrix}$$

10.6. Substituting component flow rates for mole fractions.

Derive an equation similar to (10-7), but with $v_{i,j} = y_{i,j}V_j$ as variables instead of liquid mole fractions. Can the equations still be partitioned into a series of C tridiagonal-matrix equations?

10.7. Newton–Raphson method.

Solve by the Newton–Raphson method with manual calculations the simultaneous, nonlinear equations

$$\begin{aligned} x_1^2 + x_2^2 &= 17 \\ (8x_1)^{1/3} + x_2^{1/2} &= 4 \end{aligned}$$

for x_1 and x_2 to within ± 0.001 . As initial guesses, assume:

- (a) $x_1 = 2, x_2 = 5$; (b) $x_1 = 4, x_2 = 5$;
(c) $x_1 = 1, x_2 = 1$; (d) $x_1 = 8, x_2 = 1$.

Verify your results by using the `fsolve` function of MATLAB.

10.8. Newton–Raphson method.

Solve by the Newton–Raphson method the simultaneous, nonlinear equations

$$\begin{aligned} \sin(\pi x_1 x_2) - \frac{x_2}{2} - x_1 &= 0 \\ \exp(2x_1) \left[1 - \frac{1}{4\pi} \right] + \exp(1) \left[\frac{1}{4\pi} - 1 - 2x_1 + x_2 \right] &= 0 \end{aligned}$$

for x_1 and x_2 to within ± 0.001 . As initial guesses, assume (a) $x_1 = 0.4, x_2 = 0.9$; (b) $x_1 = 0.6, x_2 = 0.9$; (c) $x_1 = 1.0, x_2 = 1.0$. Use the `fsolve` function of MATLAB.

Section 10.5

10.9. First iteration of the BP method.

One thousand kmol/h of a saturated-liquid mixture of 60 mol% methanol (M), 20 mol% ethanol (E), and 20 mol% *n*-propanol (P) is fed to the middle stage of a distillation column having three equilibrium stages, a total condenser, a partial reboiler, and an operating pressure of 1 atm. The distillate rate is 600 kmol/h, and the external reflux rate is 2,000 kmol/h of saturated liquid. Equilibrium stage calculations using (10-1) to (10-6) are to be initialized with the BP method. To initiate the iteration, assume a linear-temperature profile based on a distillate temperature equal to the normal boiling point of methanol (64.7°C) and a bottoms temperature equal to the arithmetic average of the normal boiling points of the other two

alcohols (88.1°C). Assuming ideal solutions with K -values from vapor pressures, the following K -values apply to the five stages:

Stage	1	2	3	4	5
Temperature, K	337.9	343.7	349.6	355.4	361.3
K -values:					
M	1.0086	1.2639	1.5702	1.9350	2.3665
E	0.5705	0.7309	0.9272	1.1654	1.4521
P	0.2505	0.3294	0.4281	0.5504	0.7002

Assume constant molar overflow such that the vapor rate leaving the reboiler and each stage is 2,600 kmol/h. Use MATLAB to solve the three tridiagonal matrix equations (one set for each component) for an initial set of liquid-phase mole fractions. Then, normalize them for each stage so as to sum to one.

Section 10.6

10.10. Block-tridiagonal-matrix equation.

Solve the nine simultaneous linear equations below, which have a block-tridiagonal-matrix structure, using the Thomas algorithm with manual calculations. Verify your result with MATLAB.

$$\begin{aligned}x_2 + 2x_3 + 2x_4 + x_6 &= 7 \\x_1 + x_3 + x_4 + 3x_5 &= 6 \\x_1 + x_2 + x_3 + x_5 + x_6 &= 6 \\x_4 + 2x_5 + x_6 + 2x_7 + 2x_8 + x_9 &= 11 \\x_4 + x_5 + 2x_6 + 3x_7 + x_9 &= 8 \\x_5 + x_6 + x_7 + 2x_8 + x_9 &= 8 \\x_1 + 2x_2 + x_3 + x_4 + x_5 + 2x_6 + 3x_7 + x_8 &= 13 \\x_2 + 2x_3 + 2x_4 + x_5 + x_6 + x_7 + x_8 + 3x_9 &= 14 \\x_3 + x_4 + 2x_5 + x_6 + 2x_7 + x_8 + x_9 &= 10\end{aligned}$$

10.11. Matrix structure for equations ordered by type.

Naphtali and Sandholm group the $N(2C + 1)$ equations by stage. Instead, group the equations by type (i.e., enthalpy balances, component balances, and equilibrium relations). Using a three-component, three-stage example, show whether the resulting matrix structure is still block tridiagonal.

10.12. Thermally coupled distillation.

Revise (10-38) to (10-40) to allow two interlinked columns of the type shown in Figure 10.19 to be solved simultaneously by the SC method. Is the matrix equation that results from the SC procedure still block tridiagonal?

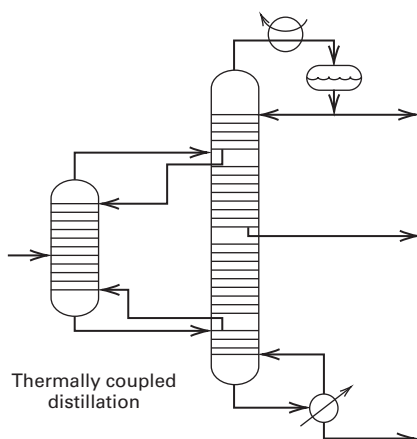


Figure 10.19 Data for Exercise 10.12.

10.13. Ordering of variables and equations in SC method.

In (10-43), why is the variable order selected as v, T, l ? What would be the consequence of changing the order to l, v, T ? In (10-44), why is the function order selected as H, M, E ? What would be the consequence of changing the order to E, M, H ?

Section 10.7

10.14. Scalar multiplier in the inside-out method.

Suggest in detail a method for determining the scalar multiplier, S_b , in (10-80).

Distillation Problems

10.15. Rigorous equilibrium-stage calculation for distillation.

Calculate product compositions, stage temperatures, interstage vapor and liquid flow rates and compositions, reboiler duty, and condenser duty with a process simulator for the following column specifications.

Feed (bubble-point liquid at 250 psia and 213.9°F):

Component	lbmol/h
Ethane	3.0
Propane	20.0
<i>n</i> -Butane	37.0
<i>n</i> -Pentane	35.0
<i>n</i> -Hexane	5.0

Column pressure = 250 psia; partial condenser and partial reboiler; Distillate rate = 23.0 lbmol/h; reflux rate = 150.0 lbmol/h; Number of equilibrium stages (exclusive of condenser and reboiler) = 15; Feed is sent to middle stage.

For this system at 250 psia, K -values and enthalpies may be computed by the SRK EOS.

10.16. Optimal feed-stage location.

Find the optimal feed-stage location for Exercise 10.15.

10.17. Distillation with a vapor sidestream.

Revise Exercise 10.15 so as to withdraw a vapor sidestream at a rate of 37.0 lbmol/h from the fourth stage from the bottom.

10.18. Distillation with intercooler and interheater.

In Exercise 10.15, provide a 200,000 Btu/hr intercooler on the fourth stage from the top and a 300,000 Btu/h interheater on the fourth stage from the bottom.

10.19. Distillation with two feeds.

Using the PR EOS for thermodynamic properties, calculate with a process simulator the product compositions, stage temperatures, interstage vapor and liquid flow rates and compositions, reboiler duty, and condenser duty for the following multiple-feed distillation column, which has 30 equilibrium stages exclusive of a partial condenser and a partial reboiler and operates at 250 psia.

Feeds (both bubble-point liquids at 250 psia):

Component	lbmol per Hour	
	Feed 1 to Stage 15 from the Bottom	Feed 2 to Stage 6 from the Bottom
Ethane	1.5	0.5
Propane	24.0	10.0
<i>n</i> -Butane	16.5	22.0
<i>n</i> -Pentane	7.5	14.5
<i>n</i> -Hexane	0.5	3.0

Distillate rate = 36.0 lbmol/h; Reflux rate = 150.0 lbmol/h
Determine whether the feed locations are optimal.

10.20. Effect of property methods on distillation calculations.

Use the Grayson–Streed correlation and the PR EOS for thermodynamic properties to calculate product compositions, stage temperatures, interstage flow rates and compositions, reboiler duty, and condenser duty for the distillation specifications in Figure 10.20. Compare your two sets of results with those in the *Chemical Engineers Handbook*, 8th Edition, pp. 13–35. Why do the three solutions differ?

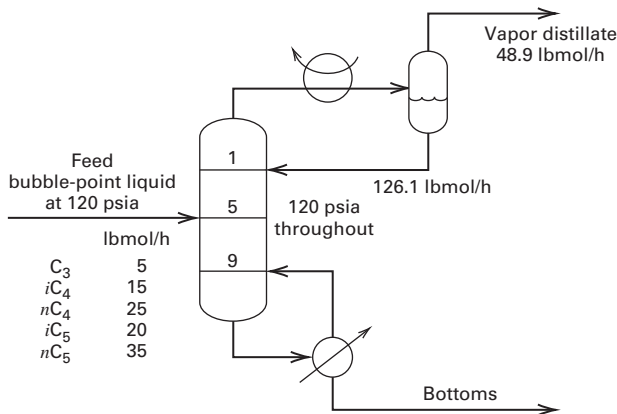


Figure 10.20 Data for Exercise 10.20.

10.21. Distillation of a light alcohol mixture.

Obtain a converged solution with a process simulator for the specifications in Exercise 10.9 using the UNIFAC method for K -values.

10.22. Distillation with two sidestreams.

Calculate with a process simulator using the PR EOS for properties, the product compositions, stage temperatures, interstage flow rates and compositions, reboiler duty, and condenser duty for the distillation specifications in Figure 10.21, which represents an attempt to obtain four nearly pure products from a single distillation operation. Reflux is a saturated liquid. Why is such a high reflux ratio required?

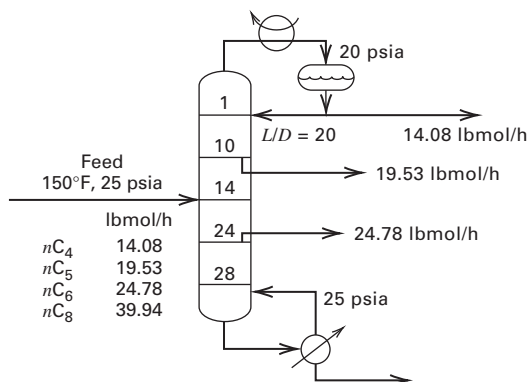


Figure 10.21 Data for Exercise 10.22.

10.23. Distillation of a hydrocarbon mixture.

Repeat Exercise 10.20, but substitute the following specifications for vapor distillate rate and reflux rate: recovery of nC_4 in distillate = 98% and recovery of iC_5 in bottoms = 98%. If the calculations fail to converge, the number of stages may be less than the minimum value. If so, increase the number of stages, revise the feed location, and repeat until convergence is achieved.

10.24. Distillation with a specified split.

A saturated liquid feed at 125 psia contains 200 lbmol/h of 5 mol% iC_4 , 20 mol% nC_4 , 35 mol% iC_5 , and 40 mol% nC_5 . This

feed is to be distilled at 125 psia in a column equipped with a total condenser and partial reboiler. The distillate is to contain 95% of the nC_4 in the feed, and the bottoms is to contain 95% of the iC_5 in the feed. Use a process simulator with the SRK equation for thermodynamic properties to determine a suitable design. You may wish to first use the FUG method discussed in Chapter 9 to establish the minimum number of equilibrium stages and the minimum reflux ratio. Twice the minimum number of stages, as estimated by the Fenske equation should provide a reasonable number of actual equilibrium stages.

10.25. Design of a depropanizer.

A depropanizer distillation column is to be designed with a process simulator to operate at a feed stage pressure of 315 psia for separating a feed into distillate and bottoms for the following flow rates:

	lbmol/h		
	Feed	Distillate	Bottoms
Methane (C_1)	26	26	
Ethane (C_2)	9	9	
Propane (C_3)	25	24.6	0.4
<i>n</i> -Butane (C_4)	17	0.3	16.7
<i>n</i> -Pentane (C_5)	11		11
<i>n</i> -Hexane (C_6)	12		12
Totals	100	59.9	40.1

The feed is 66 mol% vapor at tower pressure. Steam at 315 psia and cooling water at 65°F are available for the reboiler and condenser. Assume a 2-psi column pressure drop. (a) Should a total condenser be used for this column? (b) What are the feed temperature, K -values, and relative volatilities (with reference to C_3) at the feed temperature and pressure? (c) If the reflux ratio is 1.3 times the minimum reflux, what is the actual reflux ratio? How many theoretical plates are needed in the rectifying and stripping sections? (d) Compute the separation of species. How will the separation differ if a reflux ratio of 1.5, 15 theoretical plates, and feed at the ninth plate are chosen? (e) For part (c), compute the temperature and concentrations on each stage. What is the effect of feed plate location? How will the results differ if a reflux ratio of 1.5 and 15 theoretical plates are used?

10.26. Separation of toluene from biphenyl.

Toluene is to be separated from biphenyl by ordinary distillation. The specifications for the separation are:

	lbmol/h		
	Feed	Distillate	Bottoms
Benzene	3.4		
Toluene	84.6		2.1
Biphenyl	5.1	1.0	

Temperature = 264°F; pressure = 37.1 psia for the feed; reflux ratio = 1.3 times minimum reflux with total condenser; top pressure = 36 psia; bottom pressure = 38.2 psia. Use a process simulator with the SRK EOS, the FUG method of Chapter 9, and a rigorous method of this chapter to: (a) determine the actual reflux ratio and the number of theoretical trays in the rectifying and stripping sections and (b) compute, for a D/F ratio of $(3.4 + 82.5 + 1.0)/93.1$, the separation of components. Compare the results to the preceding specifications. (c) If the separation of components computed in part (b) is not sufficiently close to the specified split, adjust the reflux ratio to achieve the specified toluene flow in the bottoms.

10.27. Comparison of two distillation sequences.

A feed at 100°F and 480 psia is to be separated by two ordinary distillation columns into the indicated products.

Species	lbmol/h			
	Feed	Product 1	Product 2	Product 3
H ₂	1.5	1.5		
CH ₄	19.3	19.2	0.1	
C ₆ H ₆ (benzene)	262.8	1.3	258.1	3.4
C ₇ H ₈ (toluene)	84.7		0.1	84.6
C ₁₂ H ₁₀ (biphenyl)	5.1			5.1

Two distillation sequences (see §1.8.2) are to be examined. In the first sequence, CH₄ is the LK in the first column. In the second sequence, toluene is the HK in the first column. Use a process simulator with the SRK EOS to compute the two sequences by estimating the actual reflux ratio and stage requirements for both sequences by the FUG method of Chapter 9. Using a rigorous method of this chapter, specify a reflux ratio of 1.3 times the minimum. Adjust isobaric column pressures to obtain distillate temperatures of about 130°F; however, no column pressure should be less than 20 psia. Specify total condensers, except that a partial condenser should be used when methane is taken overhead.

10.28. Separation of propylene from propane.

A process for the separation of a propylene–propane mixture to produce 99 mol% propylene and 95 mol% propane is shown in Figure 10.22. As shown, because of the high product purities and the low α , 200 stages may be required. A tray efficiency of 100% and tray spacing of 24 inches will necessitate two columns in series,

because a single tower would be too tall. Assume a vapor distillate pressure of 280 psia, a pressure drop of 0.1 psi per tray, and a 2-psi drop through the condenser. The stage numbers and reflux ratio shown are only approximate. Use a process simulator with the SRK EOS and a rigorous method to determine the necessary reflux ratio for the stage numbers shown. Pay close attention to the determination of the proper feed-stage location to avoid pinch or near-pinch conditions wherein several adjacent trays may not be accomplishing any separation.

10.29. Design of stabilizer to remove hydrogen.

Stabilizers are distillation columns used in the petroleum industry to perform relatively easy separations between light components and considerably heavier components when one or two single-stage flashes are inadequate. An example of a stabilizer is shown in Figure 10.23 for the separation of H₂, methane, and ethane from benzene, toluene, and xylenes. Such columns can be difficult to calculate because a purity specification for the vapor distillate cannot be readily determined. Instead, it is more likely that the designer will be told to provide a column with 20 to 30 actual trays and a water-cooled partial condenser to provide 100°F reflux at a rate that will provide sufficient boilup at the bottom of the column to meet the purity specification there. It is desired to more accurately design the stabilizer column. The number of theoretical stages shown is just a first approximation and may be varied. A desirable bottoms product has no more than 0.05 mol% methane plus ethane and the vapor distillate temperature should be about 100°F. These specifications may be achieved by varying the distillate rate and the reflux ratio. Reasonable initial estimates for these two quantities are 49.4 lbmol/h and 2, respectively. Assuming a tray efficiency of 70% and SRK EOS for properties, use a process simulator to make the calculations.

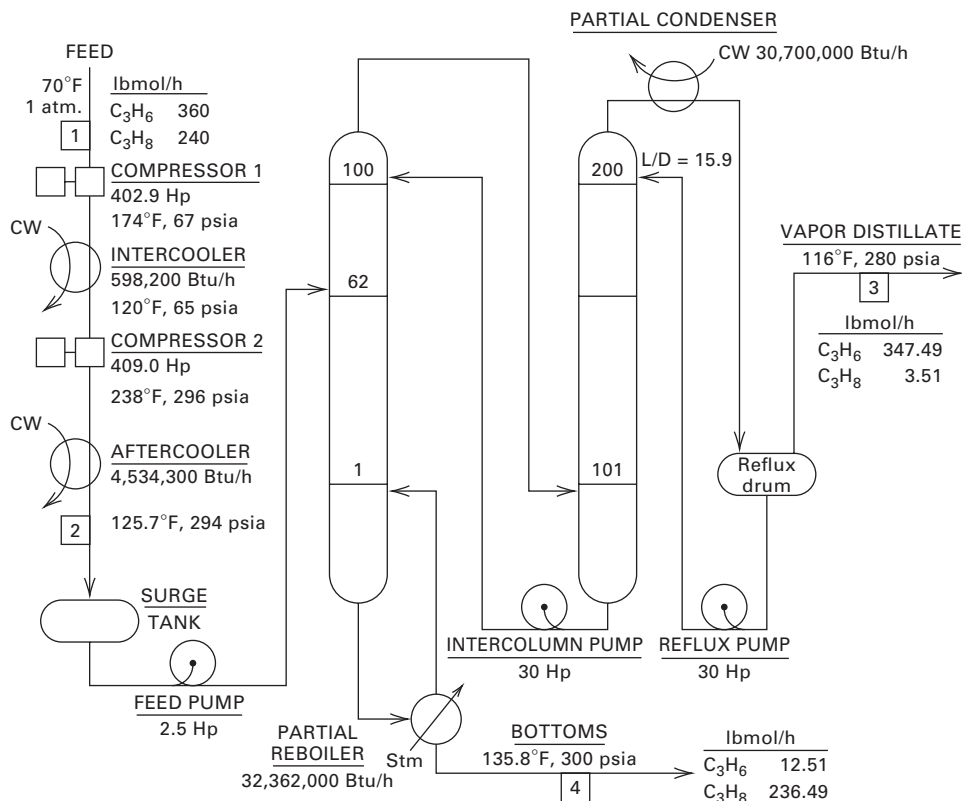


Figure 10.22 Data for Exercise 10.28.

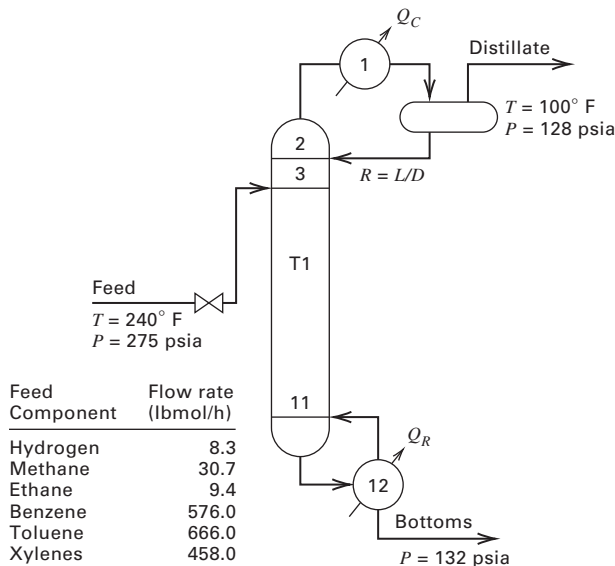


Figure 10.23 Data for Exercise 10.29.

Absorber and Stripper Problems

10.30. Absorber design.

An absorber is to be designed for a pressure of 75 psia to handle 2,000 lbmol/h of gas at 60°F having the following composition:

Component	Mole Fraction
Methane	0.830
Ethane	0.084
Propane	0.048
<i>n</i> -Butane	0.026
<i>n</i> -Pentane	0.012

The absorbent is an oil, which can be treated as *n*-undecane (C₁₁H₂₄). Using a process simulator with the SRK EOS, calculate product rates and compositions, stage temperatures, and interstage vapor and liquid flow rates and compositions for the following conditions:

	Number of Equilibrium Stages	Entering Absorbent Flow Rate lbmol/h	Entering Absorbent Temperature, °F
(a)	6	500	90
(b)	12	500	90
(c)	6	1,000	90
(d)	6	500	60

10.31. Absorption of a hydrocarbon gas.

Use a process simulator with the SRK EOS to calculate product rates and compositions, stage temperatures, and interstage vapor and liquid flow rates and compositions for an absorber having four equilibrium stages with the specifications in Figure 10.24. Assume the oil is *n*C₁₀.

10.32. An intercooler for an absorber.

In Example 10.3, temperatures of the gas and oil, as they pass through the absorber, increase substantially. This limits the extent of absorption. Use a process simulator to repeat the calculations with

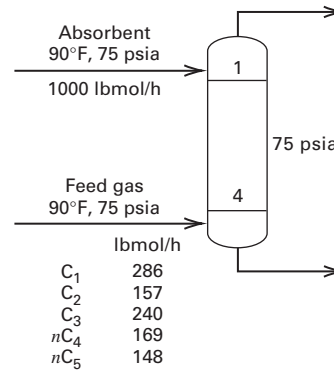


Figure 10.24 Data for Exercise 10.31.

a heat exchanger that removes 500,000 Btu/h from: (a) Stage 2; (b) Stage 3; and (c) Stage 4. How effective is the intercooler? Which stage is the preferred location for the intercooler? Should the duty of the intercooler be increased or decreased, assuming that the minimum-stage temperature is 100°F when using cooling water? The absorber oil is *n*C₁₀.

10.33. Absorber with two feeds.

Using a process simulator with the SRK EOS, calculate product rates and compositions, stage temperatures, and interstage vapor and liquid flow rates and compositions for the absorber shown in Figure 10.25. Assume the oil has the properties of *n*C₁₂.

10.34. Reboiled absorber.

Using a process simulator with the SRK EOS, determine product compositions, stage temperatures, interstage flow rates and compositions, and reboiler duty for the reboiled absorber in Figure 10.26. Repeat the calculations without the interreboiler. Is the interreboiler worthwhile? Should an intercooler in the top section of the column be considered?

10.35. Reboiled stripper.

Using a process simulator with the SRK EOS, calculate the product compositions, stage temperatures, inter-stage flow rates and compositions, and reboiler duty for the reboiled stripper shown in Figure 10.27.

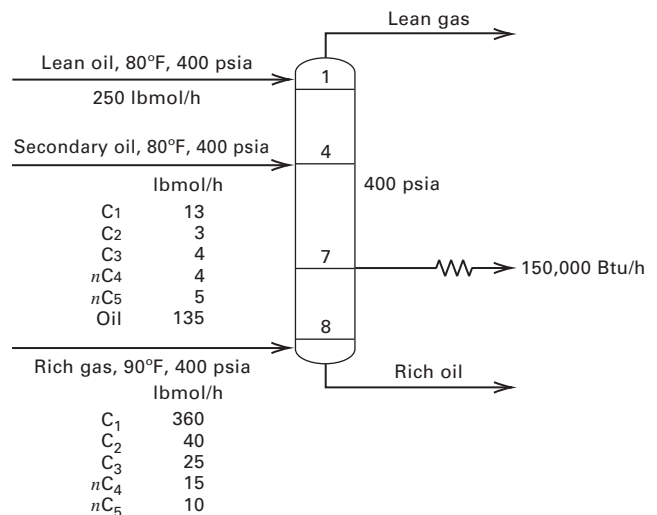


Figure 10.25 Data for Exercise 10.33.

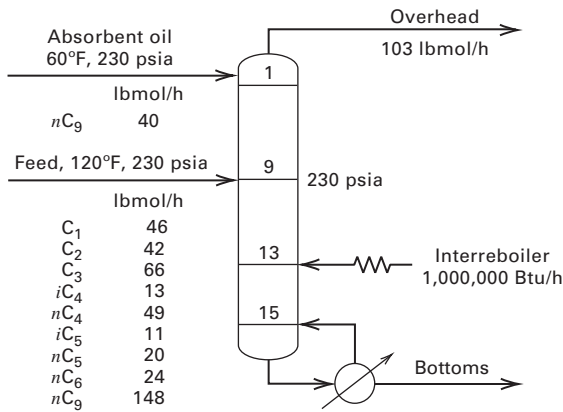


Figure 10.26 Data for Exercise 10.34.

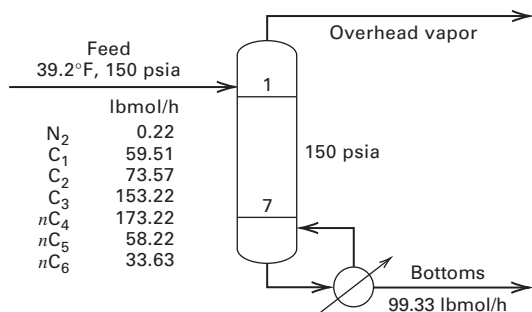


Figure 10.27 Data for Exercise 10.35.

Liquid-Liquid Extraction Problems

10.36. Liquid-liquid extraction with methanol.

A mixture of cyclohexane and cyclopentane is to be separated by liquid-liquid extraction at 25°C with methanol. Phase equilibria for

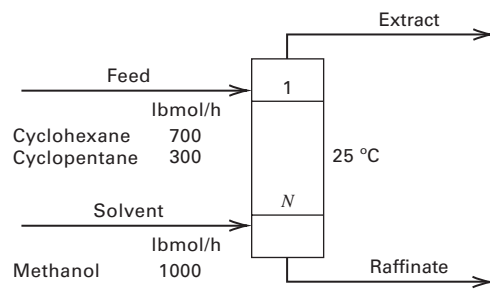


Figure 10.28 Data for Exercise 10.36.

this system may be predicted by the NRTL equation. Using a process simulator, calculate product rates and compositions and interstage flow rates and compositions for the conditions in Figure 10.28 with 1, 2, 5, and 10 equilibrium stages.

10.37. Liquid-liquid extraction of acetic acid with water.

The liquid-liquid extractor in Figure 8.1 operates at 100°F and a nominal pressure of 15 psia. For the feed and solvent flows shown, use a process simulator to determine the number of equilibrium stages to extract 99.5% of the acetic acid, using the NRTL equation for activity coefficients. The NRTL constants may be taken as follows, with ethyl acetate (1), water (2), and acetic acid (3). Alternatively, the databank of the process simulator may be used.

I	J	B_{ij}	B_{ji}	α_{ij}
1	2	166.36	1190.1	0.2
1	3	643.30	-702.57	0.2
2	3	-302.63	-1.683	0.2

Compare the computed compositions of the raffinate and extract products to those of Figure 8.1.

Enhanced Distillation and Supercritical Extraction

§11.0 INSTRUCTIONAL OBJECTIVES

After completing this chapter, you should be able to:

- Explain how enhanced-distillation methods work and how they differ from ordinary distillation.
- Explain how supercritical-fluid extraction differs from liquid–liquid extraction.
- Describe what residue-curve maps and distillation-curve maps represent on triangular diagrams for a ternary mixture.
- Explain how residue-curve maps limit feasible product-composition regions in ordinary and enhanced distillation.
- Calculate, with a simulation program, a separation by extractive distillation.
- Explain how pressure-swing distillation is used to separate a binary azeotropic mixture.
- Calculate, with a process simulator using a residue-curve map, a separation by homogeneous azeotropic distillation.
- Calculate, with a process simulator, using a residue-curve map and a binodal curve, a separation by heterogeneous azeotropic distillation.
- Calculate, with a process simulator, a separation by reactive distillation.
- Explain why enormous changes in properties occur in the critical region.
- Calculate, with a process simulator, a separation by supercritical-fluid extraction.

When $\alpha < 1.10$, separation by ordinary distillation may be uneconomical and even impossible if an azeotrope forms. In that event, techniques referred to by Stichlmair, Fair, and Bravo [1] as **enhanced distillation**, should be explored:

- 1. Extractive Distillation:** A method for separating a close-boiling mixture by adding large amounts of a relatively high-boiling solvent to alter the liquid-phase activity coefficients (§2.6) so that the relative volatility, α , of key components becomes more favorable. Solvent enters the column a few trays below the top and exits from the bottom without forming any azeotropes. If the column feed is an azeotrope, the solvent breaks it and may also reverse key-component volatilities.
- 2. Salt Distillation:** A variation of extractive distillation in which α of the key components is altered by adding to the top reflux, a soluble, nonvolatile ionic salt, which stays in the liquid phase as it passes down the column.
- 3. Pressure-Swing Distillation:** A method for separating a mixture that forms a pressure-sensitive azeotrope by utilizing two columns in sequence at different pressures.
- 4. Homogeneous Azeotropic Distillation:** A method for separating a mixture by adding an entrainer that forms a homogeneous minimum- or maximum-boiling azeotrope with feed component(s). Where the entrainer is added depends on whether the azeotrope is removed from the top or the bottom of the column.
- 5. Heterogeneous Azeotropic Distillation:** A method for separating a mixture by forming a minimum-boiling heterogeneous azeotrope with an entrainer. The azeotrope splits into two liquid phases in the overhead condenser. One liquid phase is sent back as reflux; the other is sent to another separation step or taken off as a product.
- 6. Reactive Distillation:** A separation method involving the addition of a chemical that reacts selectively and reversibly with one or more feed constituents. The reaction product is then distilled from the nonreacting components. The reaction is later reversed to recover the separating agent and reacting component. This operation, referred to as **catalytic distillation** if a catalyst is used, is suited to reactions limited by equilibrium constraints, since the product is continuously separated. Reactive distillation also refers to chemical reaction and distillation conducted simultaneously in the same apparatus.

For ordinary multicomponent distillation, determination of feasible distillation sequences, as well as column design and optimization, is relatively straightforward. In contrast, determining and optimizing enhanced-distillation sequences are considerably more difficult. Rigorous calculations may fail to converge because of liquid–solution nonidealities and/or the difficulty of specifying feasible separations. To significantly reduce the chances of failure, especially for ternary systems, graphical techniques—described by Partin

[2] and developed largely by Doherty and co-workers, and by Stichlmair and co-workers, as referenced later—provide guidance for the feasibility of enhanced-distillation sequences prior to making rigorous column calculations. This chapter presents an introduction to these graphical methods and applies them to enhanced distillation. Doherty and Malone [94], Stichlmair and Fair [95], and Siirola and Barnicki [96] extend the treatment given here.

Also discussed in this chapter is **supercritical extraction**, which differs considerably from conventional liquid–liquid extraction because of strong nonideal effects, and requires considerable care in the development of an optimal system. The principles and techniques in this chapter are largely restricted to ternary systems; enhanced distillation and supercritical extraction are commonly applied to ternary mixtures because the expense of these operations often requires that a multicomponent mixture first be reduced, by distillation or other means, to a binary or ternary system.

§11.1 USE OF TRIANGULAR GRAPHS

Figure 11.1 shows two isobaric vapor–liquid equilibrium curves for a binary mixture in terms of the mole fractions of the lowest-boiling component (A). All possible equilibrium compositions are located on the diagrams. In Figure 11.1a, compositions of the distillate and bottoms cover the range from pure B to pure A for a **zeotropic** (nonazeotropic) system. Temperatures, although not shown, range from the boiling point of A to the boiling point of B. As the composition changes from pure B to pure A, the temperature decreases.

In Figure 11.1b, a minimum-boiling azeotrope forms at C, dividing the plot into two regions. For Region 1, distillate and bottoms compositions vary from pure B (isopropyl alcohol) to azeotrope C; in Region 2, they vary from azeotrope C to pure A (isopropyl ether). The minimum-boiling azeotrope is 78 mol% isopropyl ether at 66°C and 1 atm. In Region 2, the temperature also decreases as the composition changes from

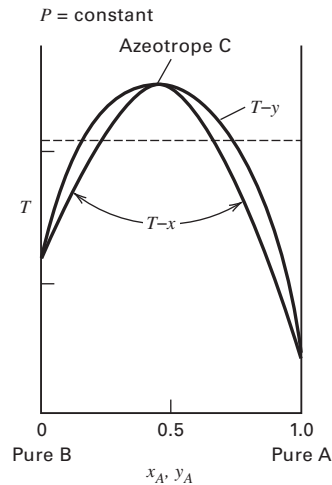


Figure 11.2 Multiple equilibrium solutions for an azeotropic system.

pure A to azeotrope C. A distillation column at 1 atm cannot separate the mixture into two nearly pure products. Depending upon whether the feed composition lies in Region 1 or 2, the column, at best, can produce only a distillate of azeotrope C and a bottoms of either pure B or pure A. However, all equilibrium compositions still lie on the equilibrium curve. From Gibbs phase rule (4-1), with two components and two phases, there are two degrees of freedom. Thus, if the pressure and temperature are fixed, the equilibrium vapor and liquid compositions are fixed. However, as shown in Figure 11.2 for the case of an azeotrope-forming binary mixture, two feasible solutions exist within a certain temperature range. The solution observed depends on the overall composition of the two phases.

In the distillation of a ternary mixture, possible equilibrium compositions do not lie uniquely on a single, isobaric equilibrium curve because the Gibbs phase rule gives an additional degree of freedom. The other compositions are determined only if the temperature, pressure, and composition of one component in one phase are fixed.

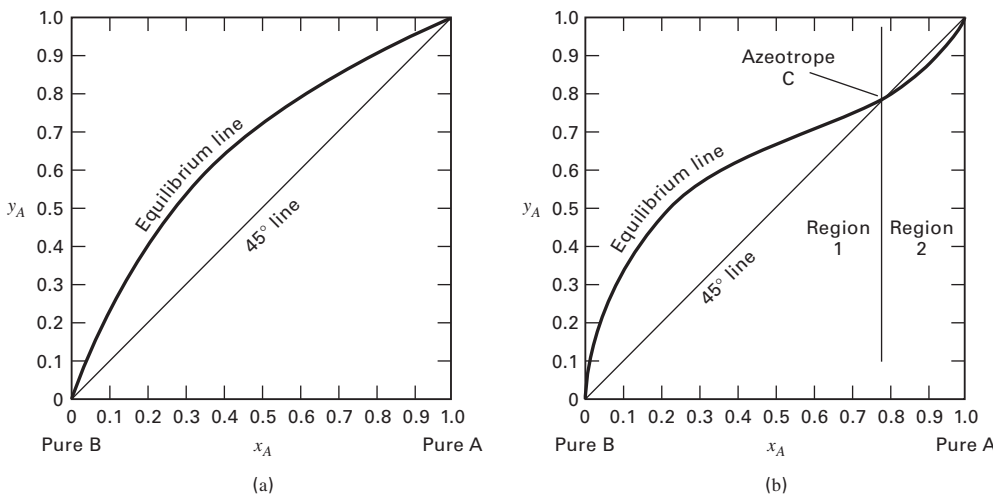


Figure 11.1 Vapor–liquid equilibria for binary systems. (a) Zeotropic system. (b) Azeotropic system.

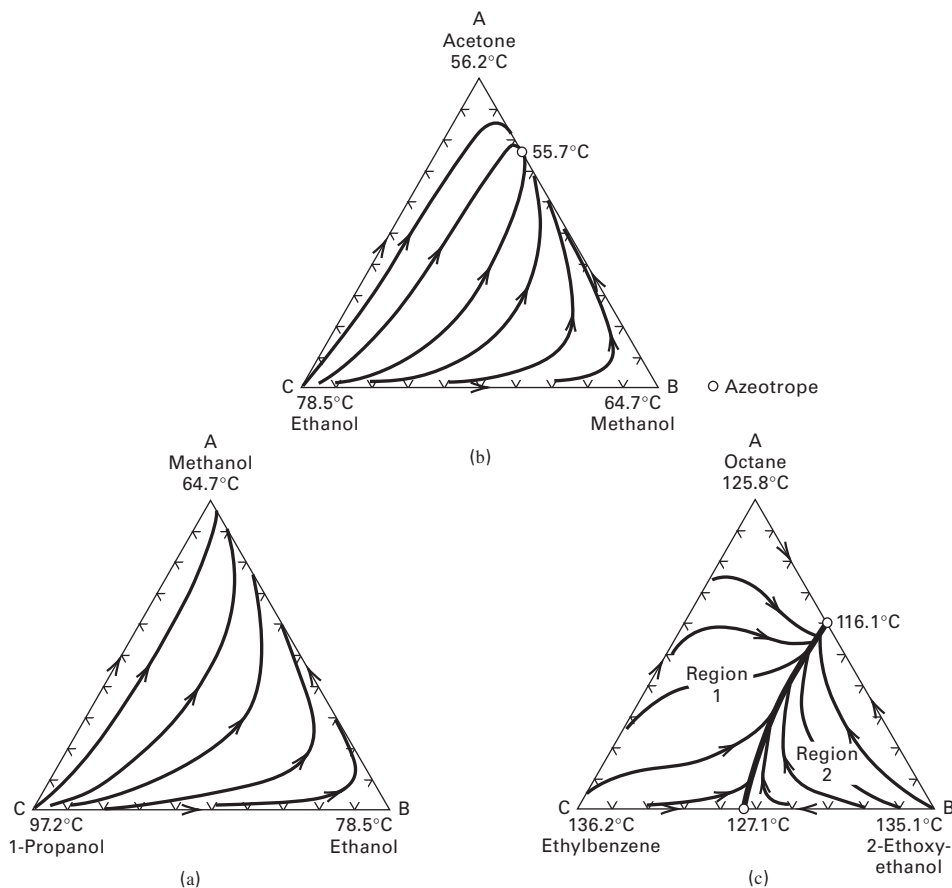


Figure 11.3 Distillation curves for liquid-phase compositions of ternary systems at 1 atm. (a) Mixture not forming an azeotrope. (b) Mixture forming one minimum-boiling azeotrope. (c) Mixture forming two minimum-boiling azeotropes.

§11.1.1 Distillation Regions and Boundaries

As discussed in Chapters 4 and 8, the composition of a ternary mixture can be represented on a triangular diagram, either equilateral or right, where the three apexes represent pure components. Although Stichlmair [3] shows that vapor–liquid phase equilibria at a fixed pressure can be plotted by letting the triangular grid represent the liquid phase, with superimposed lines of constant equilibrium-vapor composition for two of the three components, this representation is seldom used. It is more useful, when developing a feasible-separation process for a ternary mixture, to plot only equilibrium-liquid-phase compositions on the triangular diagram. Figure 11.3, where compositions are in liquid mole fractions, shows plots of this type for three different ternary mixtures. Each curve is the locus of possible equilibrium-liquid-phase compositions during distillation of a mixture, starting from any point on the curve. The boiling points of the three components and their binary and/or ternary azeotropes at 1 atm are included on the diagrams. The zeotropic alcohol system of Figure 11.3a does not form any azeotropes. If a mixture of these three alcohols is distilled, there is only one **distillation region**, similar to the binary system of Figure 11.1a. Accordingly, the distillate can be nearly pure methanol (A), or the bottoms can be nearly pure 1-propanol (C). However, nearly pure ethanol (B), the intermediate-boiling component, cannot be produced as a distillate or bottoms. To separate this ternary mixture into the three components, a sequence of two columns is used, as shown in Figure 11.4, where the feed, distillate,

and bottoms product compositions must lie on a straight, total-material-balance line within the triangular diagram. In the **direct sequence** of Figure 11.4a, the feed, F, is first separated into distillate A and a bottoms of B and C; then B is separated from C in the second column. In the **indirect sequence** of Figure 11.4b, a distillate of A and B and a bottoms

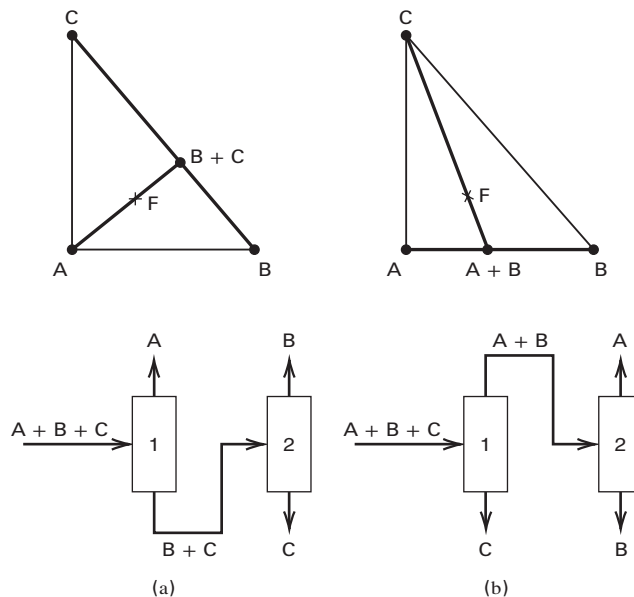


Figure 11.4 Distillation sequences for ternary zeotropic mixtures. (a) Direct sequence. (b) Indirect sequence.

of C are produced in the first column, followed by the separation of A from B in the second column.

When a ternary mixture forms an azeotrope, the products from a single distillation column depend, as for a binary mixture, on the feed composition. However, unlike the case of the binary mixture, where the two distillation regions, shown in Figure 11.1b, are well defined, determination of distillation regions for azeotrope-forming ternary mixtures is complex. Consider first the example of Figure 11.3b, for a mixture of acetone (A), methanol (B), and ethanol (C), which are in the order of increasing boiling point. The only azeotrope formed at 1 atm is a minimum-boiling binary azeotrope, at 55.7°C, of the two lower-boiling components, acetone and methanol. The azeotrope contains 78.4 mol% acetone. For this type of system, as will be shown later, no distillation boundaries for the ternary mixture exist, even though an azeotrope is present. A feed composition located within the triangular diagram can be separated into two binary products, consistent with the total-material-balance line. Ternary distillate or bottoms products can be avoided if the column split is properly selected. For example, the following five feed compositions can all produce, at a high reflux ratio and a large number of stages, a distillate of the minimum-boiling acetone-methanol azeotrope, and a bottoms product of methanol and ethanol. That is, little or no ethanol will be in the distillate and little or no acetone will be in the bottoms.

Case	Feed		Distillate		Bottoms	
	x_{acetone}	x_{methanol}	x_{acetone}	x_{methanol}	x_{acetone}	x_{methanol}
1	0.1667	0.1667	0.7842	0.2158	0.0000	0.1534
2	0.1250	0.3750	0.7837	0.2163	0.0000	0.4051
3	0.2500	0.2500	0.7837	0.2163	0.0000	0.2658
4	0.3750	0.1250	0.7837	0.2163	0.0000	0.0412
5	0.3333	0.3333	0.7837	0.2163	0.0000	0.4200

Alternatively, the column split can be a bottoms of nearly pure ethanol and a distillate of acetone and methanol. For either split, the straight, total-material-balance line passing through the feed point can extend to the sides of the triangle.

A more complex case is the ternary mixture of *n*-octane (A), 2-ethoxyethanol (B), and ethylbenzene (C) presented in Figure 11.3c. A and B form a minimum-boiling binary azeotrope at 116.1°C, and B and C do the same at 127.1°C. A triangular diagram for this system is separated by a **distillation boundary** (shown as a bold curved line) into Regions 1 and 2. A material-balance line connecting the feed to the distillate and bottoms cannot cross this distillation boundary, thus restricting the possible distillation products. For example, a mixture with a feed composition inside Region 2 cannot produce a bottoms of ethylbenzene, the highest-boiling component in the mixture. It can be distilled to produce a distillate of the A–B azeotrope and a bottoms of a mixture of B and C, or a bottoms of B and a distillate of all three components. If the feed lies in Region 1 of Figure 11.3c, it is possible to produce the A–B azeotrope and a bottoms of a mixture of A and C, or a bottoms of C and a distillate of an A and B mixture. Thus, each region produces unique products.

To further illustrate the restriction in product compositions caused by a distillation boundary, consider a feed mixture of 15 mol% A, 70 mol% B, and 15 mol% C. For this composition in Figure 11.3a or b, a bottoms product of nearly pure C, the highest-boiling component, is obtained with a distillate-to-bottoms ratio of 85/15. If, however, the mixture is that in Figure 11.3c, the same feed split ratio results in a bottoms of nearly pure B, the second-highest-boiling component.

In conclusion, when distillation boundaries are present, products of a ternary mixture cannot be predicted from component and azeotrope compositions and a specified distillate-to-bottoms ratio. These distillation boundaries, as well as the mappings of distillation curves in the ternary plots of Figure 11.3, can be determined using the two methods described in §11.1.2 and §11.1.4.

§11.1.2 Residue-Curve Maps

Consider the simple batch distillation (no trays, packing, or reflux) shown schematically in Figure 13.1. For any ternary-mixture component, a material balance for its vaporization from the still, assuming that the liquid is perfectly mixed and at its bubble point, is given by (13-1), which can be written as

$$\frac{dx_i}{dt} = (y_i - x_i) \frac{dW}{Wdt} \quad (11-1)$$

where x_i = mole fraction of component i in W moles of a perfectly mixed liquid residue in the still, and y_i = mole fraction of component i in the vapor leaving the still (instantaneous distillate) in equilibrium with x_i .

Because W decreases with time, t , it is possible to combine W and t into a single variable. Following Doherty and Perkins [4], let this variable be ξ , such that

$$\frac{dx_i}{d\xi} = x_i - y_i \quad (11-2)$$

Combining (11-1) and (11-2) to eliminate $dx_i/(x_i - y_i)$:

$$\frac{d\xi}{dt} = -\frac{1}{W} \frac{dW}{dt} \quad (11-3)$$

Let the initial condition be $\xi = 0$ and $W = W_0$ at $t = 0$. Then the solution to (11-3) for ξ at time t is

$$\xi\{t\} = \ln[W_0/W\{t\}] \quad (11-4)$$

Because $W\{t\}$ decreases monotonically with time, $\xi\{t\}$ must increase monotonically with time and is considered a dimensionless, warped time. Thus, for the ternary mixture, the distillation process can be modeled by the following set of **differential-algebraic equations** (DAEs), assuming that a second liquid phase does not form:

$$\frac{dx_i}{d\xi} = x_i - y_i, \quad i = 1, 2 \quad (11-5)$$

$$\sum_{i=1}^3 x_i = 1 \quad (11-6)$$

$$y_i = K_i x_i, \quad i = 1, 2, 3 \quad (11-7)$$

$$\sum_{i=1}^3 K_i x_i = 1 \quad (11-8)$$

where, in the general case, $K_i = K_i(T, P, \mathbf{x}, \mathbf{y})$.

Thus, the system consists of seven equations in nine variables: P , T , x_1 , x_2 , x_3 , y_1 , y_2 , y_3 , and ξ . With the pressure fixed, the next seven variables can be computed from (11-5) to (11-8) as a function of the ninth variable, ξ , from a specified initial condition. The calculation can proceed in the forward or backward direction of ξ . The results, when plotted on a triangular graph, are **residue curves** because the plot follows, with time, the liquid-residue composition in the still. A collection of residue curves, at a fixed pressure, is a **residue-curve map**. A simple, but inefficient, procedure for calculating a residue curve is illustrated in Example 11.1. Better, but more elaborate, procedures are given by Doherty and Perkins [4] and Bossen, Jørgensen, and Gani [5]. The latter procedure is also applicable when two separate liquid phases form, as is a procedure by Pham and Doherty [6].

EXAMPLE 11.1 Residue-Curve Calculation.

Plot a portion of a residue curve for *n*-propanol (1), isopropanol (2), and benzene (3) at 1 atm, starting from a bubble-point liquid with 20 mol% each of 1 and 2, and 60 mol% of component 3. For K -values, use a process simulator with a modified Raoult's law (Table 2.2) and the Wilson equation to estimate the liquid-phase activity coefficients. The normal boiling points of the three components in °C are 97.3, 82.3, and 80.1, respectively. Minimum-boiling azeotropes are formed at 77.1°C for components 1, 3 and at 71.7°C for 2, 3.

Solution

A bubble-point calculation, using (11-7) and (11-8), gives starting values of y of 0.1437, 0.2154, and 0.6409, respectively, and a value of 79.07°C for the starting temperature, from the ChemSep program of Taylor and Kooijman [7].

For an increment in dimensionless time, ξ , the differential equations (11-5) can be solved for x_1 and x_2 using Euler's method with a spreadsheet. Then x_3 is obtained from (11-6). The corresponding values of y and T are from (11-7) and (11-8). This

procedure is repeated for the next increment in ξ . Thus, from (11-5) for component 1:

$$\begin{aligned} x_1^{(1)} &= x_1^{(0)} + (x_1^{(0)} - y_1^{(0)})\Delta\xi \\ &= 0.2000 + (0.2000 - 0.1437)0.1 = 0.2056 \end{aligned}$$

where superscripts (0) indicate starting values and superscript (1) indicates the value after the first increment in ξ .

The value of 0.1 for $\Delta\xi$ gives reasonable accuracy, since the change in x_1 is only 2.7%. Similarly:

$$x_2^{(1)} = 0.2000 + (0.2000 - 0.2154)0.1 = 0.1985$$

From (11-6):

$$x_3^{(1)} = 1 - x_1^{(1)} - x_2^{(1)} = 1 - 0.2056 - 0.1985 = 0.5959$$

From a bubble-point calculation using (11-7) and (11-8),

$$y^{(1)} = [0.1474, 0.2134, 0.6392]^T \text{ and } T^{(1)} = 79.14^\circ\text{C}$$

The calculations are continued in the forward direction of ξ only to $\xi = 1.0$, and in the backward direction only to $\xi = -1.0$. The results are in the table below, and that portion of the partial residue curve is plotted in Figure 11.5a. The complete residue-curve map for this system is given on a right-triangle diagram in Figure 11.5b.

ξ	x_1	x_2	y_1	y_2	$T, ^\circ\text{C}$
-1.0	0.1515	0.2173	0.1112	0.2367	78.67
-0.9	0.1557	0.2154	0.1141	0.2344	78.71
-0.8	0.1600	0.2135	0.1171	0.2322	78.75
-0.7	0.1644	0.2117	0.1201	0.2300	78.79
-0.6	0.1690	0.2099	0.1232	0.2278	78.83
-0.5	0.1737	0.2081	0.1264	0.2256	78.87
-0.4	0.1786	0.2064	0.1297	0.2235	78.91
-0.3	0.1837	0.2047	0.1331	0.2214	78.95
-0.2	0.1889	0.2031	0.1365	0.2194	79.00
-0.1	0.1944	0.2015	0.1401	0.2173	79.05
0.0	0.2000	0.2000	0.1437	0.2154	79.07
0.1	0.2056	0.1985	0.1474	0.2134	79.14
0.2	0.2115	0.1970	0.1512	0.2115	79.19
0.3	0.2175	0.1955	0.1550	0.2095	79.24
0.4	0.2237	0.1941	0.1589	0.2076	79.30
0.5	0.2302	0.1928	0.1629	0.2058	79.34
0.6	0.2369	0.1915	0.1671	0.2041	79.41
0.7	0.2439	0.1902	0.1714	0.2023	79.48
0.8	0.2512	0.1890	0.1758	0.2006	79.54
0.9	0.2587	0.1878	0.1804	0.1989	79.61
1.0	0.2665	0.1867	0.1850	0.1973	79.68

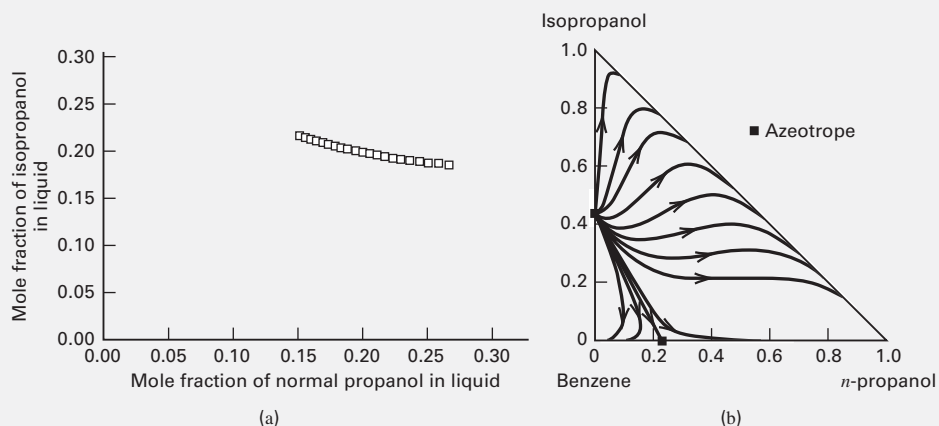


Figure 11.5 Residue curves for the normal propanol-isopropanol-benzene system at 1 atm for Example 11.1. (a) Calculated partial residue curve. (b) Residue-curve map.

The residue-curve map in Figure 11.5b shows an arrow on each residue curve. The arrows point from a lower-boiling component or azeotrope to a higher-boiling component or azeotrope. In Figure 11.5b, all residue curves originate from the isopropanol–benzene azeotrope (lowest boiling point, 71.7°C). One of the curves terminates at the other azeotrope (*n*-propanol–benzene, which has a higher boiling point, 77.1°C) and is a special residue curve, called a **simple distillation boundary** because it divides the ternary region into two separate regions. All residue curves lying above and to the right of this distillation boundary terminate at the *n*-propanol apex, which has the highest boiling point (97.3°C) for that region. All residue curves lying below and to the left of the distillation boundary are deflected to the benzene apex, whose boiling point of 80.1°C is the highest for this second region.

On a triangular diagram, all pure-component vertices and azeotropic points whether binary azeotropes on the borders of the triangle, as in Figure 11.5b, or a ternary azeotrope within the triangle are **singular or fixed points** of the residue curves because at these points, $dx/d\xi = 0$. In the vicinity of these points, the behavior of a residue curve depends on the two

eigenvalues of (11-5). At each pure-component vertex, the two eigenvalues are identical. At each azeotropic point, the two eigenvalues are different. Three cases, illustrated by each of three pattern groups in Figure 11.6a, b, and c are possible:

Case 1: Both eigenvalues are negative. This is the point reached as ξ tends to ∞ , and is where all residue curves in a given region terminate. Thus, it is the component or azeotrope with the highest boiling point in the region. This point is a **stable node** because it is like the low point of a valley, in which a rolling ball finds a stable position. In Figure 11.6b, the stable node is pure *n*-propanol.

Case 2: Both eigenvalues are positive. This is the point where all residue curves in a region originate, and is the component or azeotrope with the lowest boiling point in the region. This point is an **unstable node** because it is like the top of a mountain from which a ball rolls toward a stable position. In Figure 11.6b, the unstable node is the isopropanol–benzene azeotrope.

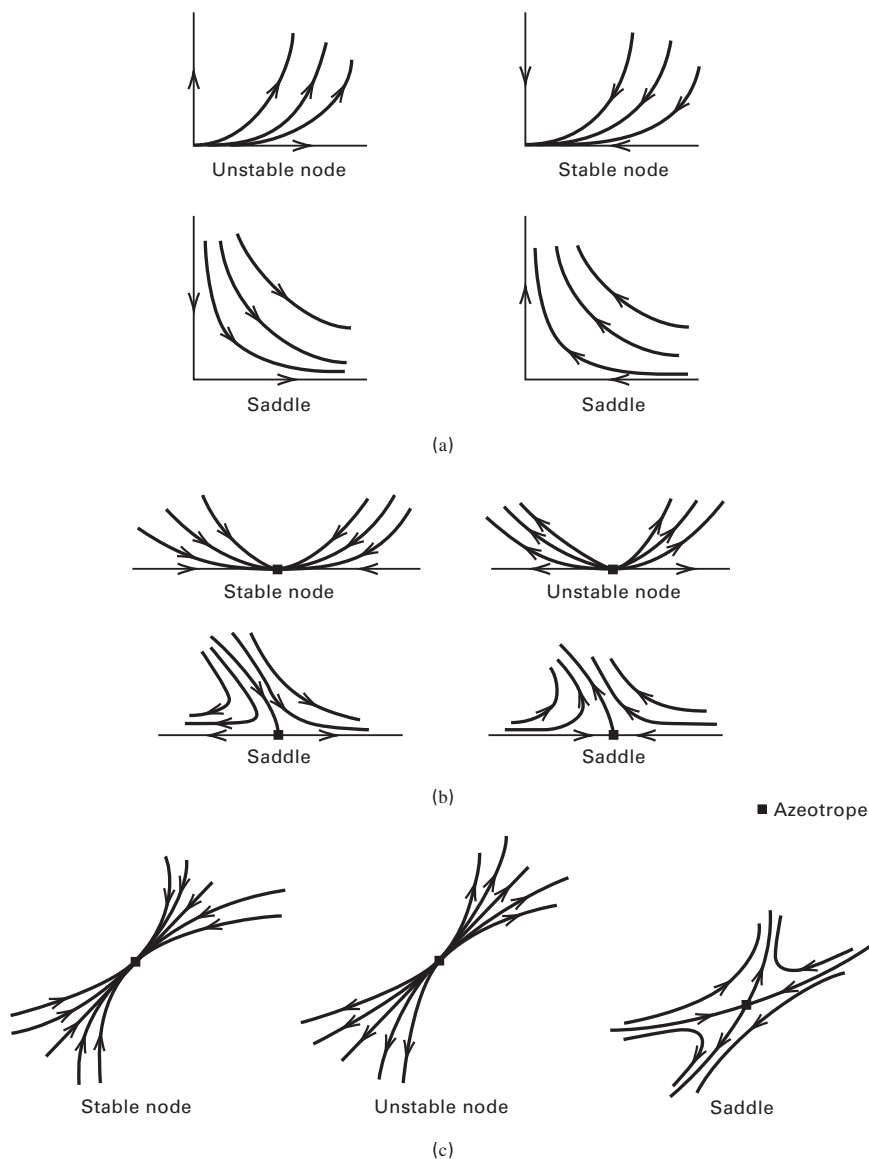


Figure 11.6 Residue-curve patterns: (a) near pure-component vertices; (b) near-binary azeotropes; (c) near-ternary azeotropes. [Reproduced from [16] with permission from the American Chemical Society.]

Case 3: One eigenvalue is positive and one is negative. Residue curves within the triangle move toward and then away from such **saddle points**. For a given region, all pure components and azeotropes intermediate in boiling point between the stable node and the unstable node are saddles. In Figure 11.5b, the upper region has one saddle at the isopropanol vertex and another saddle at the *n*-propanol–benzene azeotrope.

§11.1.3 Approximate Residue-Curve Maps

From Example 11.1, it is clear that manual calculations of a residue-curve map require a considerable effort. However, process simulators such as Aspen Plus [9] and CHEMCAD compute residue maps rapidly. Alternatively, Doherty and Perkins [10] and Doherty [8] have shown that the classification of singular points as stable nodes, unstable nodes, and saddles provides a rapid method for approximating a residue-curve map, including approximate distillation boundaries, from just the pure-component boiling points and azeotrope boiling points and compositions. Boiling points of pure substances are available in handbooks and databases, and extensive listings of binary azeotropes are found in Horsley [11] and Gmehling et al. [12]. The former lists more than 1,000 binary azeotropes. The latter includes experimental data for more than 20,000 systems involving approximately 2,000 compounds, as well as material on selecting enhanced-distillation systems. The listings of ternary azeotropes are incomplete; however, in lieu of experimental data, a homotopy-continuation method for estimating homogeneous azeotropes of a multicomponent mixture from a thermodynamic model (e.g., Wilson, NRTL, UNIQUAC, UNIFAC) has been developed by Fidkowski, Malone, and Doherty [13]. Eckert and Kubicek [97] present an extension for computing heterogeneous azeotropes.

Based on experimental evidence for ternary mixtures, with very few exceptions there are at most three binary azeotropes and one ternary azeotrope. Accordingly, the following set of restrictions applies to a ternary system:

$$N_1 + S_1 = 3 \quad (11-9)$$

$$N_2 + S_2 = B \leq 3 \quad (11-10)$$

$$N_3 + S_3 = 1 \text{ or } 0 \quad (11-11)$$

where N is the number of stable and unstable nodes, S is the number of saddles, B is the number of binary azeotropes, and the subscript is the number of components at the node (stable or unstable) or saddle. Thus, S_2 is the number of binary azeotrope saddles. Doherty and Perkins [10] give a topological relationship among N and S :

$$2N_3 - 2S_3 + 2N_2 - B + N_1 = 2 \quad (11-12)$$

For Figure 11.5b, where there is no ternary azeotrope, $N_1 = 2$, $N_2 = 1$, $N_3 = 0$, $S_1 = 1$, $S_2 = 1$, $S_3 = 0$, and $B = 2$.

Applying (11-12) gives $0 - 0 + 2 - 2 + 2 = 2$. Equation (11-9) gives $2 + 1 = 3$; (11-10) gives $1 + 1 = 2$; and (11-11) gives $0 + 0 = 0$. Thus, all four relations are satisfied.

The topological relationships are useful for rapidly sketching, on a ternary diagram, an approximate residue-curve map, including distillation boundaries, as described in detail by Foucher, Doherty, and Malone [14]. Their nine-step procedure is illustrated by an example from their article, shown in Figure 11.7 that uses the flow chart in Figure 11.8. Approximate maps are usually developed from data at 1 atm.

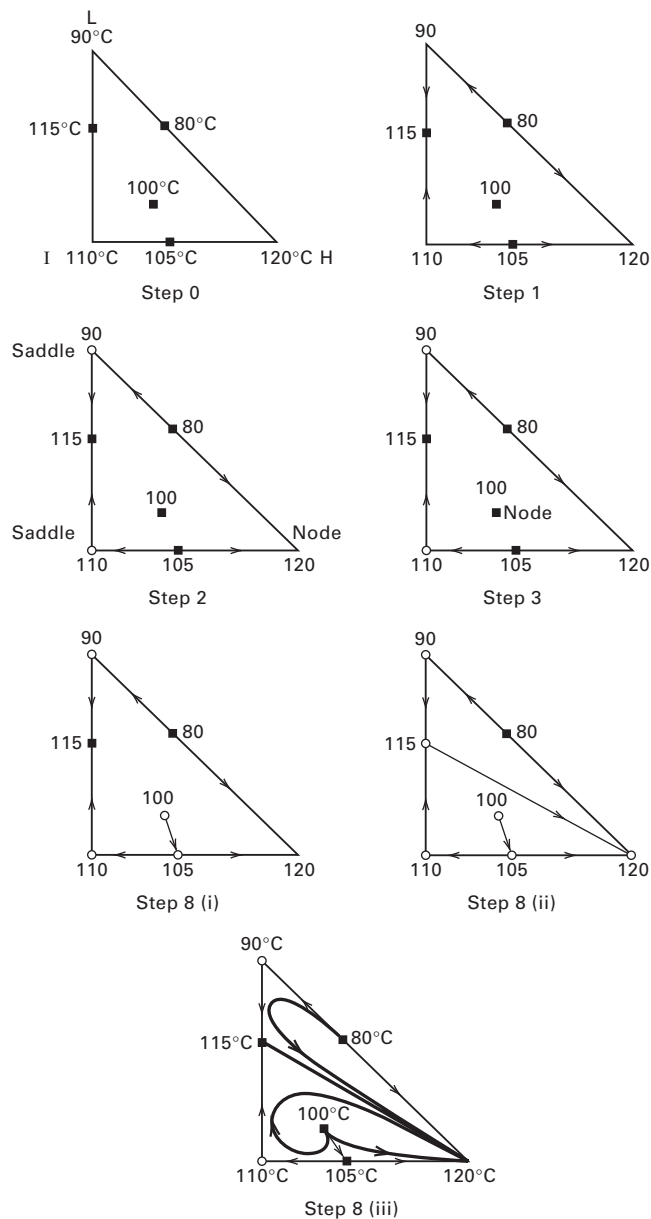


Figure 11.7 Step-by-step development of an approximate residue-curve map for a hypothetical system with two minimum-boiling binary azeotropes, one maximum-boiling binary azeotrope, and one ternary azeotrope. [Reproduced from [14] with permission from the American Chemical Society.]

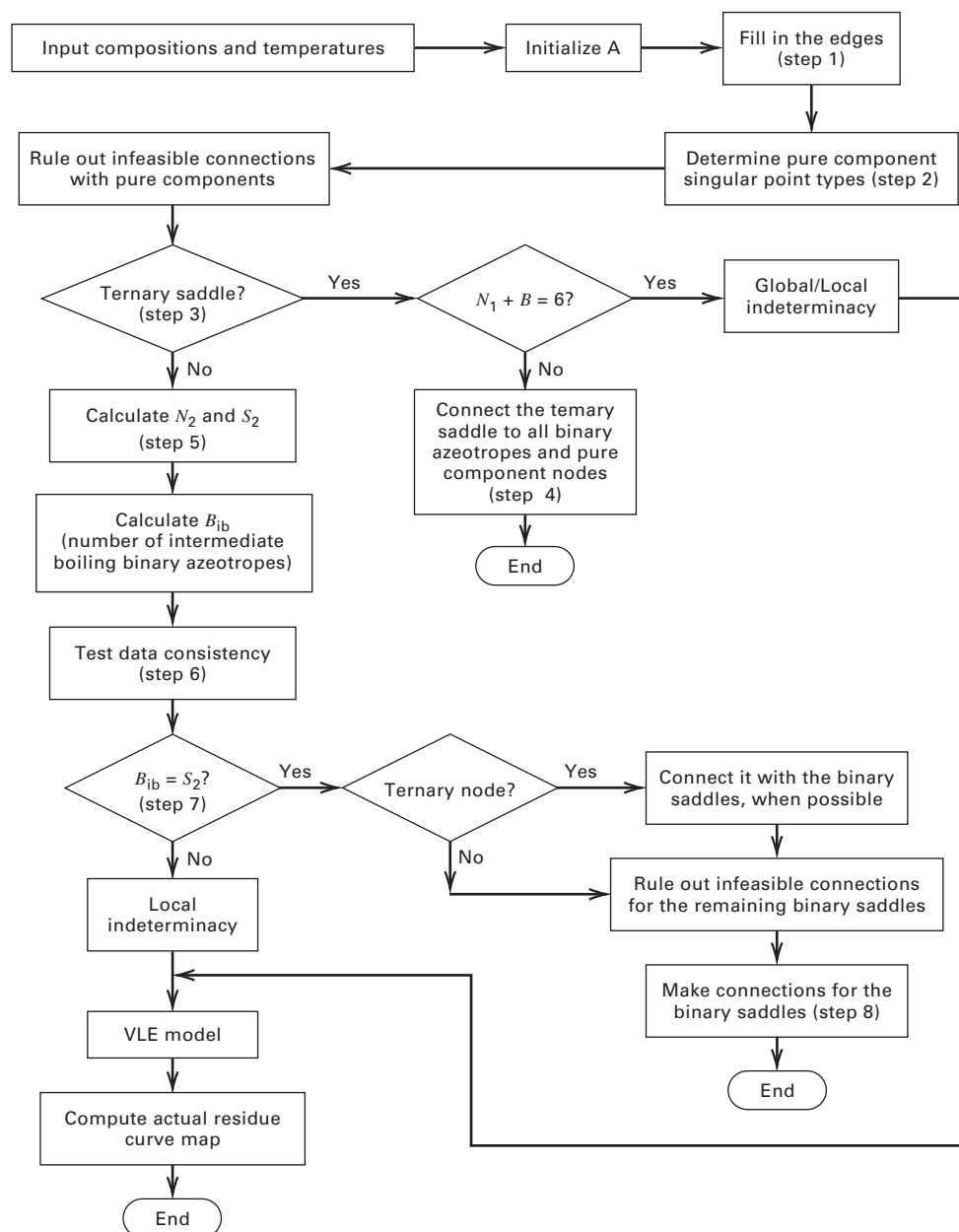


Figure 11.8 Flowchart of algorithm for sketching an approximate residue-curve map. [Reproduced from [14] with permission from the American Chemical Society.]

In the description, the term species refers to both pure components and azeotropes.

Step 0 Label the ternary diagram with the pure-component, normal-boiling-point temperatures. It is preferable to designate the top vertex of the triangle as the low boiler (L), the bottom-right vertex as the high boiler (H), and the bottom-left vertex as the intermediate boiler (I). Plot composition points for the binary and ternary azeotropes and add labels for their normal boiling points. This determines the value of B . See Figure 11.7, Step 0, where two minimum-boiling and one maximum-boiling binary azeotropes and one ternary azeotrope are designated by filled square markers. Thus, $B = 3$.

Step 1 Draw arrows on the edges of the triangle, in the direction of increasing temperature, for each pair of adjacent species. See Figure 11.7, Step 1, where six species are on the edges of the triangle and six arrows have been added.

Step 2 Determine the type of singular point for each pure-component vertex using Figure 11.6 with the arrows drawn in Step 1 of Figure 11.7. This determines the values for N_1 and S_1 . If a ternary azeotrope exists, go to Step 3; if not, go to Step 5. In Figure 11.7, Step 2, L is a saddle because one arrow points toward L and one points away from L; H is a stable node because both arrows point toward H, and I is a saddle. Therefore, $N_1 = 1$ and $S_1 = 2$.

Step 3 (for a ternary azeotrope): Determine the type of singular point for the ternary azeotrope, if one exists. The point is a node if (a) $N_1 + B < 4$, and/or (b) excluding the pure-component saddles, the ternary azeotrope has the highest, second-highest, lowest, or second-lowest boiling point of all species. Otherwise, the point is a saddle. This determines the values for N_3 and S_3 . If the point is a node, go to Step 5; if a saddle, go to Step 4. In Figure 11.7, Step 3, $N_1 + B = 1 + 3 = 4$.

However, excluding L and I because they are saddles, the ternary azeotrope has the second-lowest boiling point. Therefore, the point is a node, and $N_3 = 1$ and $S_3 = 0$. The type of node, stable or unstable, is still to be determined.

Step 4 (for a ternary saddle): Connect the ternary saddle, by straight lines, to all binary azeotropes and to all pure-component nodes (but not to pure-component saddles), and draw arrows on the lines to indicate the direction of increasing temperature. Determine the type of singular point for each binary azeotrope, by using Figure 11.6 with the arrows drawn in this step. This determines the values for N_2 and S_2 . These values should be consistent with (11-10) and (11-12). This completes the development of the approximate residue-curve map, with no further steps needed. However, if $N_1 + B = 6$, then special checks must be made, as given in detail by Foucher, Doherty, and Malone [14]. This step does not apply to the example in Figure 11.7, because the ternary azeotrope is not a saddle.

Step 5 (for a ternary node or no ternary azeotrope): Determine the number of binary nodes, N_2 , and binary saddles, S_2 , from (11-10) and (11-12), where (11-12) can be solved for N_2 to give

$$N_2 = (2 - 2N_3 + 2S_3 + B - N_1)/2 \quad (11-13)$$

For the example of Figure 11.7, $N_2 = (2 - 2 + 0 + 3 - 1)/2 = 1$. From (11-10), $S_2 = 3 - 1 = 2$.

Step 6 Count the binary azeotropes that are intermediate boilers (i.e., that are not the highest-or the lowest-boiling species), and call that number B_{ib} . Make the following two data-consistency checks: (a) The number of binary azeotropes, B , less B_{ib} , must equal N_2 , and (b) S_2 must be $\leq B_{ib}$. For the system in Figure 11.7, both checks are satisfied because $B_{ib} = 2$, $B - B_{ib} = 1$, $N_2 = 1$, and $S_2 = 2$. If these two consistency checks are not satisfied, one or more of the boiling points may be in error.

Step 7 If $S_2 \neq B_{ib}$, this procedure cannot determine a unique residue-curve-map structure, which therefore must be computed from (11-5) to (11-8). If $S_2 = B_{ib}$, there is a unique structure, which is

completed in Step 8. For the example in Figure 11.7, $S_2 = B_{ib} = 2$; therefore, there is a unique map.

Step 8 In this final step for a ternary node or no ternary azeotrope, the distillation boundaries (connections), if any, are determined and entered on the triangular diagram as straight lines, and, if desired, one or more representative residue curves are sketched as curved lines within each distillation region. This step applies to cases of $S_3 = 0$, $N_3 = 0$ or 1, and $S_2 = B_{ib}$. In all cases, the number of distillation boundaries equals the number of binary saddles, S_2 . Each binary saddle must be connected to a node (pure component, binary, or ternary). A ternary node must be connected to at least one binary saddle. Thus, a pure-component node cannot be connected to a ternary node, and an unstable node cannot be connected to a stable node. The connections are made by determining a connection for each binary saddle such that (a) a minimum-boiling binary saddle connects to an unstable node that boils at a lower temperature and (b) a maximum-boiling binary saddle connects to a stable node that boils at a higher temperature.

It is best to first consider connections with the ternary node and then examine possible connections for the remaining binary saddles. In the example of Figure 11.7, $S_2 = 2$, with these saddles denoted as L-I, a maximum-boiling azeotrope at 115°C, and as I-H, a minimum-boiling azeotrope at 105°C. Therefore, two connections are made to establish two distillation boundaries. The ternary node at 100°C cannot connect to L-I because 100°C is not greater than 115°C. The ternary node can, however, connect, as shown in Step 8 (i), to I-H because 100°C is lower than 105°C. This marks the ternary node as unstable. The connection for L-I can only be to H, as shown in Step 8 (ii), because it is a node (stable), and 120°C is greater than 115°C. This completes the connections. Finally, as shown in Step 8 (iii) of Figure 11.7, three typical, but approximate, residue curves are added to the diagram. These curves originate from unstable nodes and terminate at stable nodes.

Residue-curve maps are used to determine feasible distillation sequences for nonideal ternary systems. Matsuyama and Nishimura [15] showed that the topological constraints just discussed limit the number of possible maps to about 113. However, Siirola and Barnicki [96] show 12 additional maps; all 125 maps are called distillation region diagrams (DRD). Doherty and Caldarola [16] provide sketches of 87 maps that contain at least one minimum-boiling binary azeotrope and also cover industrial applications, since minimum-boiling azeotropes are much more common than maximum-boiling azeotropes.

§11.1.4 Distillation-Curve Maps

Residue curves represent the changes in residue composition with time as the result of a simple, one-stage batch distillation. The curve points in the direction of increasing time, from a lower-boiling state to a higher-boiling state. An alternative representation for distillation on a ternary diagram is a **distillation curve** for continuous, rather than batch, distillation. The curve is most readily obtained for total reflux (§9.1.3, the Fenske method) at a constant pressure, usually 1 atm. The calculations are made down or up the column, starting from any composition. Consider making the calculations by moving up the column, starting from a stage designated as Stage 1. Between equilibrium stages j and $j + 1$, at total reflux, passing vapor and liquid streams have the same composition. Thus,

$$x_{i,j+1} = y_{i,j} \quad (11-14)$$

Also, since liquid and vapor streams leaving the same stage are in equilibrium,

$$y_{i,j} = K_i x_{i,j} \quad (11-15)$$

To calculate a distillation curve, an initial liquid-phase composition, $x_{i,1}$, is assumed. This liquid is at its bubble-point temperature, which is determined from (11-8), which also gives the equilibrium-vapor composition, $y_{i,1}$ in agreement with (11-15). The composition, $x_{i,2}$, of the passing liquid stream is equal to $y_{i,1}$ by (11-14). The process is then repeated to obtain $x_{i,3}$, then $x_{i,4}$, and so forth. The sequence of liquid-phase compositions, which corresponds to the operating line for total reflux, is plotted on the triangular diagram and is analogous to the 45° line on a McCabe–Thiele diagram (§7.2). Calculation of a portion of a distillation curve is illustrated next.

EXAMPLE 11.2 Calculation of a Distillation Curve.

Calculate and plot a portion of a distillation curve for the starting conditions in Example 11.1.

Solution

The starting values, $\mathbf{x}^{(1)}$, are 0.2000, 0.2000, and 0.6000 for components 1, 2, and 3, respectively. From Example 11.1, the bubble-point calculation gives a temperature of 79.07°C and $\mathbf{y}^{(1)}$ values of 0.1437, 0.2154, and 0.6409. From (11-14), values of $\mathbf{x}^{(2)}$ are 0.1437, 0.2154, and 0.6409. A bubble-point calculation for this composition gives $T^{(2)} = 78.62^\circ\text{C}$ and $\mathbf{y}^{(2)} = 0.1063, 0.2360, \text{ and } 0.6577$. Subsequent calculations are summarized in the following table:

Equilibrium Stage	x_1	x_2	y_1	y_2	$T, ^\circ\text{C}$
1	0.2000	0.2000	0.1437	0.2154	79.07
2	0.1437	0.2154	0.1063	0.2360	78.62
3	0.1063	0.2360	0.0794	0.2597	78.29
4	0.0794	0.2597	0.0592	0.2846	78.02
5	0.0592	0.2846	0.0437	0.3091	77.80

Figure 11.9 is the resulting distillation curve, where points represent equilibrium stages and are connected by straight lines.

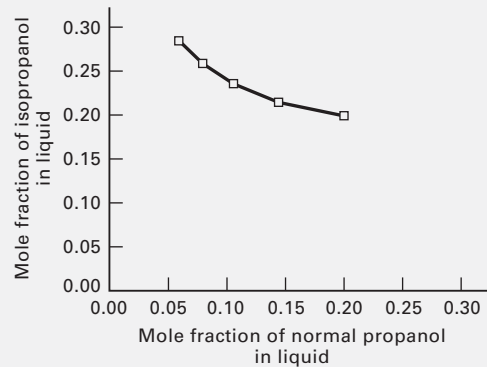


Figure 11.9 Calculated distillation curve for the normal propanol–isopropanol–benzene system at 1 atm for Example 11.2.

Distillation curves can be computed more rapidly than residue curves, and closely approximate them for reasons noted by Fidkowski, Doherty, and Malone [17]. If (11-5) (which must be solved numerically as in Example 11.1) is written in a forward-finite-difference form,

$$(x_{i,j+1} - x_{i,j})/\Delta\xi = x_{i,j} - y_{i,j} \quad (11-16)$$

In Example 11.1, $\Delta\xi$ was set to +0.1 for calculations that give increasing values of T and to -0.1 to give decreasing values. If the latter direction is chosen to be consistent with the direction used in Example 11.2 and $\Delta\xi$ is set equal to -1.0 , (11-16) becomes identical to (11-14). Thus, residue curves (which are true continuous curves) are equal to distillation curves (which are discrete points through which a smooth curve is drawn), when the residue curves are approximated by a crude forward-finite-difference formulation, using $\Delta\xi = -1.0$.

A collection of distillation curves, including lines for distillation boundaries, is a **distillation-curve map**, an example of which, from Fidkowski et al. [17], is given in Figure 11.10. The Wilson equation was used to compute liquid-phase activity coefficients. The dashed lines are the distillation curves, which approximate the solid-line residue curves. This system has two minimum-boiling binary azeotropes, one maximum-boiling binary azeotrope, and a ternary saddle azeotrope. The map shows four distillation boundaries, designated by A, B, C, and D. These computed boundaries, which define four distillation regions (1 to 4), are all curved lines rather than the approximately straight lines in the sketches of Figure 11.7.

Distillation-curve maps have been used by Stichlmair and associates [1, 3, 18] for the development of feasible-distillation sequences. In their maps, arrows are directed toward the lower-boiling species, rather than toward the higher-boiling species as in residue-curve maps.

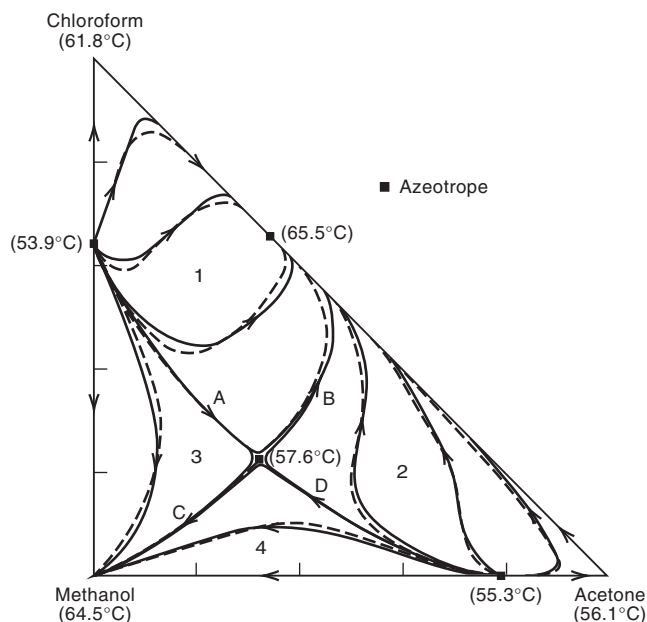


Figure 11.10 Comparison of residue curves to distillation curves. [Reproduced from [17] with permission from the American Institute of Chemical Engineers.]

§11.1.5 Feasible Product-Composition Regions at Total Reflux (Bow-Tie Regions)

The feasible-distillation regions for azeotrope-forming ternary mixtures are not obvious. Fortunately, residue-curve maps and distillation-curve maps can be used to make preliminary estimates of regions of **feasible-product compositions** for non-ideal ternary systems. These regions are determined by superimposing a column material-balance line on either type of curve-map diagram. Consider first the zeotropic ternary system in Figure 11.11a, which shows an isobaric residue-curve map with three residue curves. Assume this map is identical to a corresponding distillation-curve map for total-reflux conditions and to a map for a finite, but very high reflux, ratio. Suppose ternary feed F in Figure 11.11a is continuously distilled isobarically, at a high R , to produce distillate D and bottoms B . A straight line that connects distillate and bottoms compositions must pass through the feed composition at some intermediate point to satisfy material-balance equations. Three **material-balance lines** are included in the figure. For

a given line, D and B composition points, designated by open squares, lie on the same distillation curve. This causes the material-balance line to intersect the distillation curve at these two points and be a chord to the distillation curve.

The limiting distillate-composition point for this zeotropic system is pure low-boiling component, L . From the material-balance line passing through F , as shown in Figure 11.11b, the corresponding bottoms composition with the least amount of component L is point B . At the other extreme, the limiting bottoms-composition point is high-boiling component H . A material-balance line from this point, through feed point F , ends at D . These two lines and the distillation curve define the feasible product-composition regions, shown shaded. Note that, because for a given feed both the distillate and bottoms compositions must lie on the same distillation curve, shaded feasible regions lie on the convex side of the distillation curve that passes through the feed point. Because of its appearance, the feasible-product-composition region is called a **bow-tie region**.

For azeotropes, where distillation boundaries are present, a feasible-product-composition region exists for each distillation region. Two examples are shown in Figure 11.12. Figure 11.12a has two distillation regions caused by two minimum-boiling binary azeotropes. A curved distillation boundary connects the minimum-boiling azeotropes. In the lower, right-hand distillation region (1), the lowest-boiling species is the n -octane/2-ethoxy-ethanol minimum-boiling azeotrope, while the highest-boiling species is 2-ethoxy-ethanol. Accordingly, for feed $F1$, straight lines are drawn from the points for each of these two species, through the point $F1$, and to a boundary (either a distillation boundary or a side of the triangle). Shaded, feasible-product-composition regions are then drawn on the outer side of the distillation curve that passes through the feed point. The result is that distillate compositions are confined to shaded region $D1$ and bottoms compositions are confined to shaded region $B1$. For a given $D1$, $B1$ must lie on a straight line that passes through $D1$ and $F1$. At total reflux, $D1$ and $B1$ must also lie on the same distillation curve.

A more complex distillation-curve map, with four distillation regions bounded by thick solid lines, is shown in Figure 11.12b for the acetone-methanol-chloroform system. This system has two minimum-boiling binary azeotropes, one maximum-boiling binary azeotrope, and one ternary

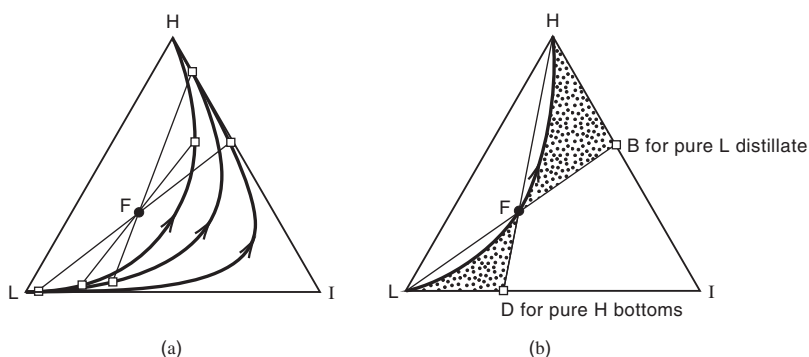


Figure 11.11 Product-composition regions for a zeotropic system. (a) Material-balance lines and distillation curves. (b) Product-composition regions shown shaded.

[Reproduced from [19] with permission from the American Institute of Chemical Engineers.]

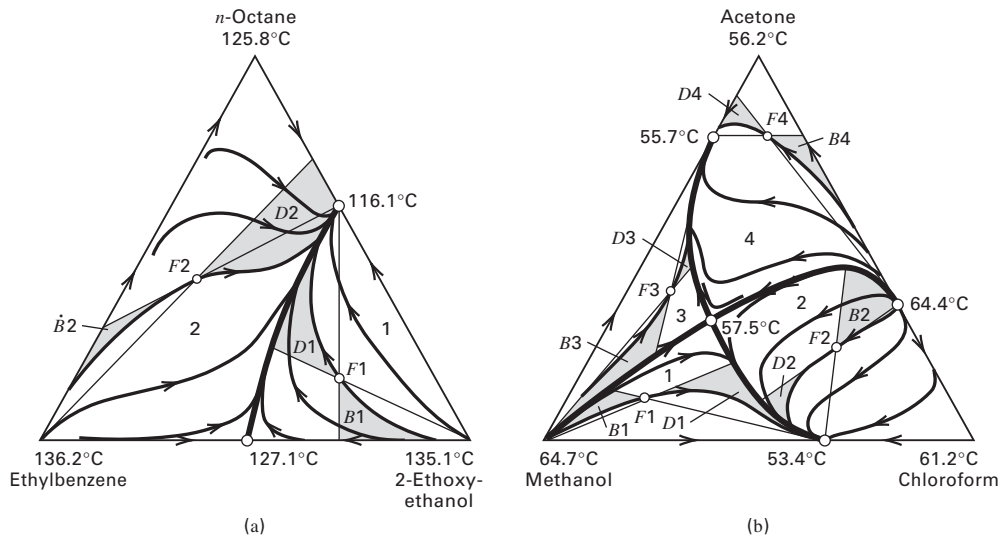


Figure 11.12 Product composition regions for given feed compositions. (a) Ternary mixture with two minimum-boiling binary azeotropes at 1 atm. (b) Ternary mixture with three binary and one ternary azeotrope at 1 atm.

azeotrope. One shaded bow-tie region, determined in the same way as for Region 1 in Figure 11.12a, is present for each distillation region. For this system, feasible-product composition regions are highly restricted.

A complicated situation is observed in distillation Region 2 on the left side of Figure 11.12a, where the lowest-boiling species is the binary azeotrope of octane and 2-ethoxy-ethanol, while the highest-boiling species is ethylbenzene. The complicating factor in Region 1 is that feed F_2 lies on or close to an inflection point of an S-shaped distillation curve. In this case, as discussed by Wahnschafft et al. [20], feasible-product composition regions may lie on either side of the distillation curve passing through the feed point. The feasible regions shown are similar to those determined by Stichlmair et al. [1], while other feasible regions are shown for this system by Wahnschafft et al. [20]. As they point out, mass-balance lines of the type drawn in Figure 11.12b do not limit feasible regions. Hoffmaster and Hauan [98] provide a method for determining extended-product-feasibility regions for S-shaped distillation curves.

In Figures 11.11b, 11.12a, and 11.12b, each bow-tie region is confined to its distillation region, as defined by the distillation boundaries. In all cases, the feed, distillate, and bottoms points on the material-balance line lie within a distillation region, with the feed point between the distillate and bottoms points. The material-balance lines do not cross the distillation-boundary lines. Is this always so? The answer is no! Under conditions where the distillation-boundary line is highly curved, it can be crossed by material-balance lines to obtain feasible-product compositions. That is, a feed point can be on one side and the distillate and bottoms points on the other side of the distillation-boundary line.

Consider the example in Figure 11.13, from Widagdo and Seider [19]. The highly curved distillation-boundary line extends from a minimum-boiling azeotrope K of components H and I to pure component L. This line divides the

triangular diagram into two distillation regions, 1 and 2. Feed F_1 can be separated into products D_1 and B_1 , which lie on distillation curve (a). In this case, the material-balance line and the distillation curve are both on the convex side of the distillation-boundary line. However, because feed point F_1 lies close to the highly curved boundary line, F_1 can also be separated into D_2 and B_2 (or B_3), which lie on a distillation curve in Region 2 on the concave side of the boundary. Thus, the material-balance line crosses the boundary from the convex to the concave side. Feed F_2 can be separated into D_4 and B_4 , but not into D and B. In the latter case, the material-balance line cannot cross the boundary from the concave to the convex side, because the point F_2 does not lie between D and B on the material-balance line. The determination of the feasible-product-composition regions for Figure 11.13 is left for an exercise at the end of this chapter.

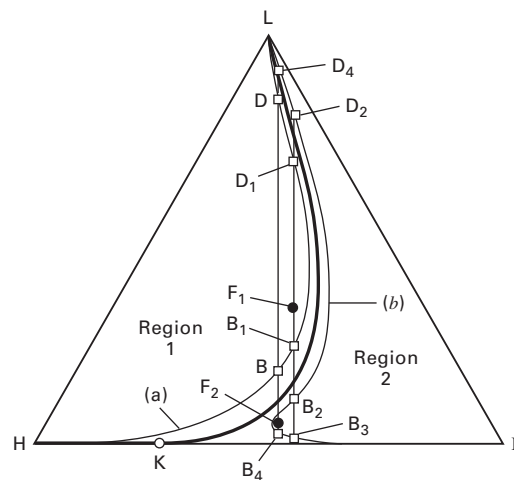


Figure 11.13 Feasible and infeasible crossings of distillation boundaries for an azeotropic system

[Reproduced from [19] with permission from the American Institute of Chemical Engineers.]

A detailed treatment of product-composition regions is given by Wahnschafft et al. [20].

§11.2 EXTRACTIVE DISTILLATION

Extractive distillation is used to separate azeotropes and close-boiling mixtures. If the feed is a minimum-boiling azeotrope, a solvent, with a lower volatility than the key components of the feed mixture, is added just a few trays below the top of the column so that (1) the solvent is present in the down-flowing liquid, and (2) little solvent is stripped and lost to the overhead vapor. If the feed is a maximum-boiling azeotrope, the solvent enters the column with the feed. The components in the feed must have different solvent affinities so that the solvent causes an increase in the relative volatility of the key components, to the extent that separation becomes feasible and economical. The solvent should not form azeotropes with any feed components. Usually, a molar ratio of solvent to feed on the order of 1 is required. The bottoms are processed to recover the solvent for recycle and complete the separation. The name **extractive distillation** was introduced by Dunn et al. [21] in connection with the commercial separation of toluene from a paraffin-hydrocarbon mixture, using phenol as solvent.

Table 11.1 lists industrial applications of extractive distillation. Consider the case of the acetone-methanol system. At 1 atm, acetone (nbp = 56.2°C) and methanol (nbp = 64.7°C) form a minimum-boiling azeotrope of 80 mol% acetone at a temperature of 55.7°C. Using UNIFAC (§2.8.1) to predict vapor-liquid equilibria for this system at 1 atm, the azeotrope is estimated to occur at 55.2°C with 77.1 mol% acetone, reasonably close to measured values. At infinite dilution with respect to methanol, $\alpha_{A,M}$ for acetone (A) with respect

to methanol (M), is predicted to be 0.74 by UNIFAC, with a liquid-phase activity coefficient for methanol of 1.88. At infinite dilution with respect to acetone, $\alpha_{A,M}$ is 2.48; by coincidence, the liquid-phase activity coefficient for acetone is also 1.88.

Water is a possible solvent for the system because at 1 atm (1) it does not form a binary or ternary azeotrope with acetone and/or methanol, and (2) it boils (100°C) at a higher temperature. The resulting residue-curve map with arrows directed from the azeotrope to pure water, computed by Aspen Plus using UNIFAC, is shown in Figure 11.14, where it is seen that no distillation boundaries exist. As discussed by Doherty and Calderola [16], this is an ideal situation for the selection of an extractive distillation process. Their residue-curve map for this type of system (designated 100) is included as an insert in Figure 11.14

Ternary mixtures of acetone, methanol, and water at 1 atm give the following separation factors, estimated from the UNIFAC equation, when appreciable solvent is present.

Mol% Water	Relative Volatility, $\alpha_{A,M}$			Liquid-Phase Activity Coefficient at Infinite Dilution	
	Methanol-rich	Acetone-rich	Equimolar	Acetone	Methanol
40	2.48	2.57	2.03	2.12	0.70
50	2.56	2.86	2.29	2.41	0.72

The presence of appreciable water increases the liquid-phase activity coefficient of acetone and decreases that of methanol; thus, over the entire concentration range of acetone and methanol, $\alpha_{A,M}$ is at least 2.0. This makes it possible, with extractive distillation, to obtain a distillate of acetone and a bottoms of methanol and water. The α values of acetone to water and methanol to water average 4.5 and 2.0, respectively, making it relatively easy to prevent water from reaching the distillate, and, in subsequent operations, to separate methanol from water by distillation.

Table 11.1 Some Industrial Applications of Extractive Distillation

Key Components in Feed Mixture	Solvent
Acetone-methanol	Aniline, ethylene glycol, water
Benzene-cyclohexane	Aniline
Butadienes-butanes	Acetone
Butadiene-butene-1	Furfural
Butanes-butenes	Acetone
Butenes-isoprene	Dimethylformamide
Cumene-phenol	Phosphates
Cyclohexane-heptanes	Aniline, phenol
Cyclohexanone-phenol	Adipic acid diester
Ethanol-water	Glycerine, ethylene glycol
Hydrochloric acid-water	Sulfuric acid
Isobutane-butene-1	Furfural
Isoprene-pentanes	Acetonitrile, furfural
Isoprene-pentenes	Acetone
Methanol-methylene bromide	Ethylene bromide
Nitric acid-water	Sulfuric acid
n-Butane-butene-2s	Furfural
Propane-propylene	Acrylonitrile
Pyridine-water	Bisphenol
Tetrahydrofuran-water	Dimethylformamide, propylene glycol
Toluene-heptanes	Aniline, phenol

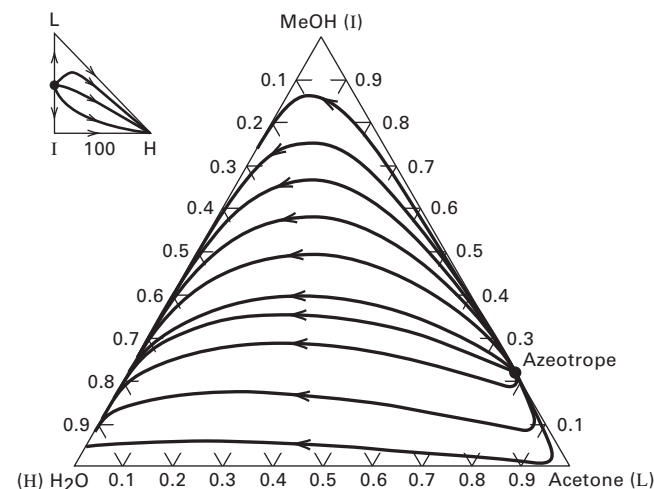


Figure 11.14 Residue-curve map for acetone-methanol-water system at 1 atm.

EXAMPLE 11.3 Extractive Distillation of Acetone and Methanol.

Forty mol/s of a bubble-point mixture of 75 mol% acetone and 25 mol% methanol at 1 atm is separated by extractive distillation, using water as the solvent, to produce an acetone product of not less than 95 mol% acetone, a methanol product of not less than 98 mol% methanol, and a water stream for recycle of at least 99.9 mol% purity. Prepare a preliminary process design using the traditional three-column sequence consisting of ordinary distillation followed by extractive distillation, and then ordinary distillation to recover the solvent, as shown for a different system in Figure 11.15.

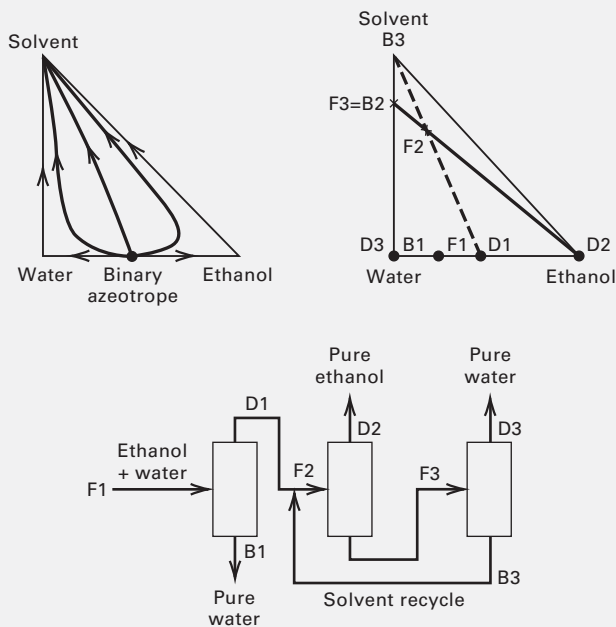


Figure 11.15 Distillation sequence for extractive distillation. [Reproduced from [16] with permission from the American Chemical Society.]

Solution

Usually, in the first column, the feed mixture of acetone and methanol would be partially separated by ordinary distillation, where the distillate composition would approach that of the binary azeotrope. The bottoms would be nearly pure acetone or nearly pure methanol, depending upon whether the feed contains more or less than 80 mol% acetone. In this example, the feed composition is already close to the azeotrope composition; therefore, the first column is not required, and the acetone–methanol feed is sent to the second column, an extractive-distillation column equipped with a total condenser and a partial reboiler, to produce a distillate of at least 95 mol% acetone.

The ChemSep and CHEMCAD programs were used to make the calculations, with the UNIFAC method for activity coefficients. Number of stages, feed-stage location, solvent-entry stage, solvent flow rate, and reflux-ratio requirements were manipulated until a satisfactory design was achieved. The resulting material and energy balances are summarized in Table 11.2.

For the extractive-distillation column, a solvent flow rate of 60 mol/s of water is suitable. Using 28 theoretical trays, a 50°C solvent entry at tray 6 from the top, a feed entry at tray 12 from the top, and a reflux ratio of 4, a distillate composition of 95.6 mol% acetone is achieved. The impurity is mainly water. The acetone recovery is 99.5%. A 6-ft-diameter column with 60 sieve trays on 2-ft tray spacing is adequate. A liquid-phase composition profile is shown in Figure 11.16. The mole fraction of water (the solvent) is appreciable, at least 0.35 for all stages below the solvent-entry stage.

Figure 11.17 shows distillation curves for the extractive distillation, where vapor and liquid curves are plotted. Arrows are directed from the column bottom to the top.

For the water-recovery column, 16 theoretical stages, a bubble-point feed-stage location of stage 11, and $R = 2$ are adequate for a methanol distillate of 98.1 mol% purity and a water bottoms, suitable for recycle, of 99.9 mol% purity. A McCabe–Thiele diagram in Figure 11.18 shows the locations of the theoretical stages. As seen, the feed stage is optimally located. Water makeup is less than 1.5 mol/s. A 2.5-ft-diameter column packed with 48 feet of 50-mm metal Pall rings is suitable.

Table 11.2 Material and Energy Balances for Extractive-Distillation Process of Example 11.3

Material Balances						
Species	Flow Rate, mol/s: Column 2 Feed	Column 2 Solvent	Column 2 Distillate	Column 2 Bottoms	Column 3 Distillate	Column 3 Bottoms
Acetone	30	0	29.86	0.14	0.14	0.0
Methanol	10	0	0.016	9.984	9.926	0.058
Water	0	60	1.35	58.65	0.06	58.59
Total	40	60	31.226	68.774	10.126	58.648
Energy Balances						
	Column 1	Column 2				
Condenser duty, MW	4.71	1.07				
Reboiler duty, MW	4.90	1.12				

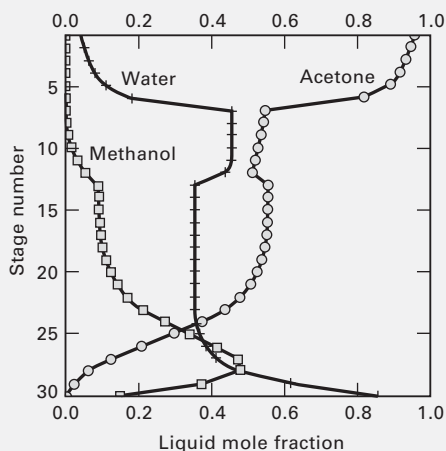


Figure 11.16 Liquid composition profile for extractive-distillation column of Example 11.3.

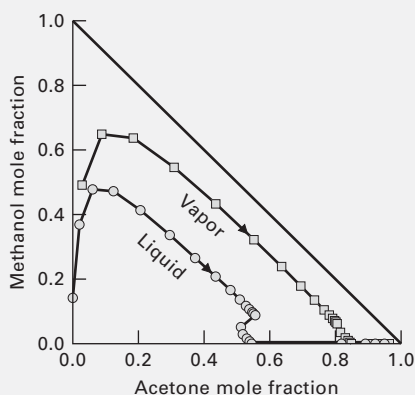


Figure 11.17 Distillation-curve map for Example 11.3. Data points are for theoretical stages.

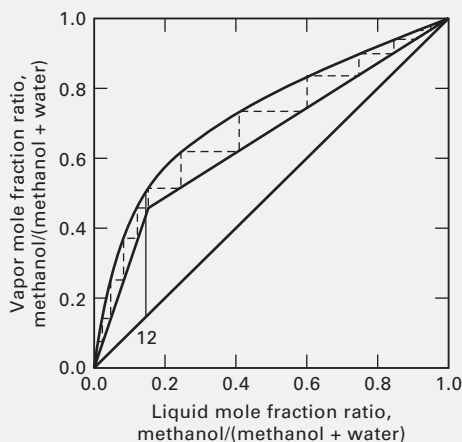


Figure 11.18 McCabe-Thiele diagram for methanol-water distillation in Example 11.3.

One unfortunate aspect of the extractive-distillation column in Example 11.3 is the relatively low boiling point of water. With a solvent-entry point of tray 6 from the top, 1.35 mol/s (2.25% of the water solvent) is stripped from the liquid into the distillate. Use of two other, higher-boiling solvents listed in Table 11.1, aniline (nbp = 184°C) or ethylene glycol (nbp = 198°C), results in far less solvent stripping. Other possible solvents include methylethylketone (MEK) and ethanol. MEK behaves in a fashion opposite to that of water, causing the volatility of methanol to be greater than acetone. Thus, methanol is the distillate, leaving acetone to be separated from MEK.

In selecting a solvent for extractive distillation, factors to be considered include availability, cost, corrosivity, vapor pressure, thermal stability, heat of vaporization, reactivity, toxicity, infinite-dilution activity coefficients in the solvent of the components to be separated, and ease of solvent recovery for recycle. In addition, the solvent should not form azeotropes. Initial screening is based on the measurement or prediction of infinite-dilution activity coefficients. Berg [22] discusses selection of separation agents for both extractive and azeotropic distillation. He points out that all successful solvents for extractive distillation are highly hydrogen-bonded liquids (Table 2.6), such as (1) water, amino alcohols, amides, and phenols that form three-dimensional networks of strong hydrogen bonds; and (2) alcohols, acids, phenols, and amines that are composed of molecules containing both active hydrogen atoms and donor atoms (oxygen, nitrogen, and fluorine). It is unusual to find a solvent to separate components having the same functional groups.

Extractive distillation is also used to separate binary mixtures that form a maximum-boiling azeotrope, as shown in the following example.

EXAMPLE 11.4 Extractive Distillation of Acetone and Chloroform.

Acetone (nbp = 56.16°C) and chloroform (nbp = 61.10°C) form a maximum-boiling homogeneous azeotrope at 1 atm and 64.43°C that contains 37.8 mol% acetone. They cannot be separated by ordinary distillation at 1 atm. Instead, extractive distillation in a two-column sequence, shown in Figure 11.19, with benzene (nbp = 80.24°C) as the solvent, is to be used. Benzene does not form azeotropes with the feed components.

In the first column, feed, blended with recycled solvent, produces a distillate of 99 mol% acetone. The bottoms is sent to the second column, where 99 mol% chloroform leaves as distillate, and the bottoms, rich in benzene, is recycled to the first column with makeup benzene. If the fresh feed is 21.89 mol/s of 54.83 mol% acetone, with the balance chloroform, design a feasible two-column system using a ratio of 3.1667 moles of benzene per mole of acetone plus chloroform in the combined feed to the first column. Both columns operate at 1 atm with total condensers, saturated-liquid reflux, and partial reboilers. Use the UNIFAC method for estimating activity coefficients. The combined feed to the first column is brought to the bubble point before entering the column.

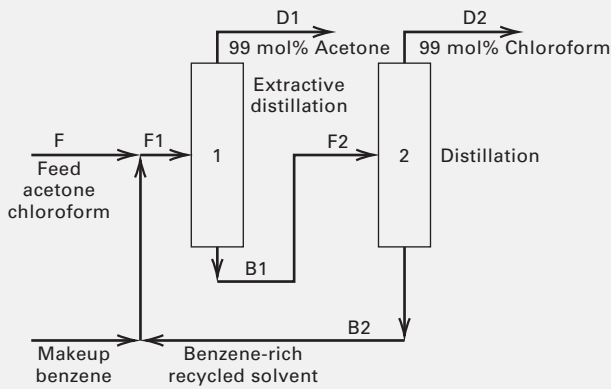


Figure 11.19 Process for the separation of acetone and chloroform in Example 11.4.

Solution

Figure 11.20 shows the residue-curve map for the ternary system acetone–chloroform–benzene at 1 atm. The only azeotrope is that of acetone and chloroform. A curved distillation boundary extending from that azeotrope to the pure-benzene apex divides the diagram into two distillation regions. The first column, which produces nearly pure acetone, operates in Region 1; the second column operates in Region 2.

This ternary system was studied in detail by Fidkowski, Doherty, and Malone [17]. A design based on their studies that uses the CHEMCAD process simulator is summarized in Table 11.3. The first column contains 65 theoretical stages, with the combined feed entering stage 30 from the top. For a reflux ratio, R , of 10, acetone distillate purity is achieved with an acetone recovery of better than 99.95%. In Column 2, which contains 50 theoretical stages with feed entering at stage 30, an R of 11.783 gives the required chloroform purity in the distillate but with a recovery of only 82.23%. This is not serious because the chloroform leaving in the bottoms is recycled with benzene to Column 1, resulting in a 98.9% overall recovery of chloroform. The benzene makeup rate is 0.1141 mol/s. Feed, distillate, and bottoms compositions are designated in Figure 11.20.

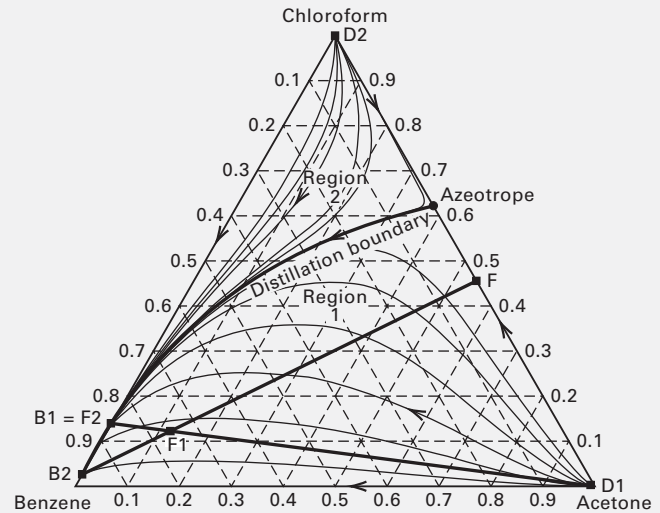


Figure 11.20 Residue-curve map for Example 11.4.

§11.3 SALT DISTILLATION

Water, used as a solvent in the extractive distillation of acetone and methanol in Example 11.3, has the disadvantages that a large amount is required to adequately alter the relative volatility, α , and, even though the solvent is introduced into the column several trays below the top, enough water is stripped into the distillate to reduce the acetone purity to 95.6 mol%. The water vapor pressure can be lowered, and thus the purity of acetone distillate increased, by using an aqueous inorganic-salt solution as the solvent. A 1927 patent by Othmer [23] describes use of a concentrated calcium chloride brine. Not only does calcium chloride, which is highly soluble in water, reduce the volatility of water, but it also has a strong affinity for methanol. Thus, α of acetone with respect to methanol is enhanced. The separation of brine solution from methanol is easily accommodated in the subsequent distillation, with the brine solution recycled to the extractive-distillation column. The vapor pressure of the dissolved salt is so small that it never enters the vapor, provided entrainment is avoided.

Table 11.3 Material and Energy Balances for Homogeneous Azeotropic Distillation of Example 11.4

Material Balances with Flows in mol/s						
Species	F	F_1	D_1	$B_1 = F_2$	D_2	B_2
Acetone	12.0000	12.0000	11.9948	0.0052	0.0052	0.0000
Chloroform	9.8858	12.0000	0.1046	11.8954	9.7812	2.1142
Benzene	0.0000	76.0000	0.0207	75.9793	0.0934	75.8859
Energy Balances						
Heat duty, kcal/h	Column 1		Column 2			
Condenser	950,000		891,600			
Reboiler	958,400		1,102,000			

An even earlier patent by Van Raymbeke [24] describes the extractive distillation of ethanol from water using solutions of calcium chloride, zinc chloride, or potassium carbonate in glycerol.

Salt can be added as a solid or melt into the column by dissolving it in the reflux before it enters the column. This was demonstrated by Cook and Furter [25] in a 4-inch-diameter, 12-tray rectifying column with bubble caps, separating ethanol from water using potassium acetate. At salt concentrations below saturation and between 5 and 10 mol%, an almost pure ethanol distillate was achieved. The salt, which must be soluble in the reflux, is recovered from the aqueous bottoms by evaporation and crystallization.

Salt distillation is accompanied by several problems. First and foremost is corrosion, particularly with aqueous chloride-salt solutions, which may require stainless steel or a more expensive corrosion-resistant material. Feeding and dissolving a salt into the reflux poses problems described by Cook and Furter [25]. The solubility of salt will be low in

the reflux because it is rich in the more-volatile component, the salt being most soluble in the less-volatile component. Salt must be metered at a constant rate and the salt-feeding mechanism must avoid bridging and prevent the entry of vapor, which could cause clogging when condensed. The salt must be rapidly dissolved, and the reflux must be maintained near the boiling point to avoid precipitation of already-dissolved salt. In the column, presence of dissolved salt may increase foaming, requiring addition of antifoaming agents and/or an increased column diameter. Concern has been voiced for the possibility of salt crystallization within the column. However, the concentration of the less-volatile component (e.g., water) increases down the column, so the solubility of salt increases down the column while its concentration remains relatively constant. Thus, the possibility of clogging and plugging due to solids formation is unlikely.

In aqueous alcohol solutions, both **salting out** and **salting in** have been observed by Johnson and Furter [26], as shown in the vapor-liquid equilibrium data in Figure 11.21. In

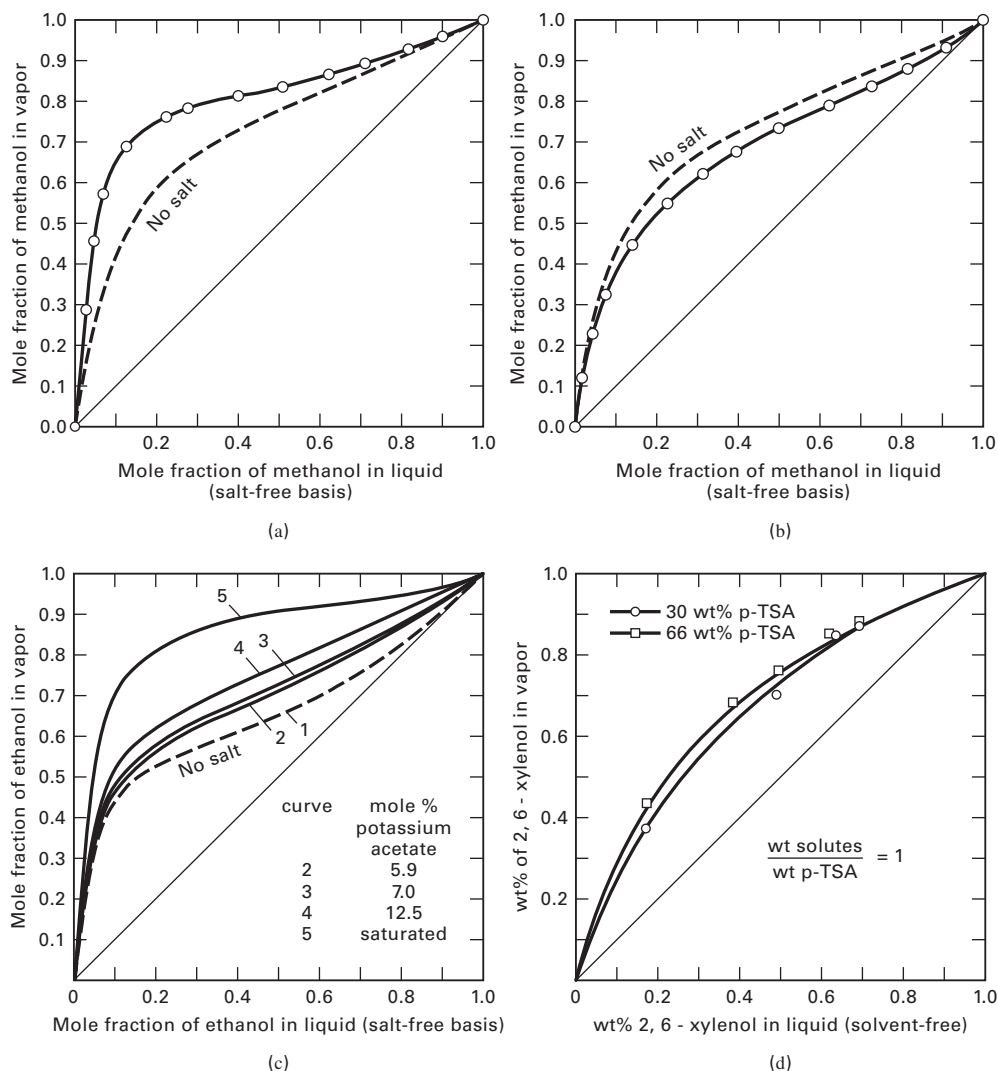


Figure 11.21 Effect of dissolved salts on vapor-liquid equilibria at 1 atm. (a) Salting-out of methanol by saturated aqueous sodium nitrate. (b) Salting-in of methanol by saturated aqueous mercuric chloride. (c) Effect of salt concentration on ethanol-water equilibria. (d) Effect of *p*-toluenesulfonic acid (*p*-TSA) on phase equilibria of 2,6-xyleneol-*p*-cresol.

[Reproduced from [26] with permission of John Wiley & Sons, Inc.]

(a), sodium nitrate salts out methanol, but in (b), mercuric chloride salts in methanol. Even low concentrations of potassium acetate can eliminate the ethanol–water azeotrope, as shown in Figure 11.21c. Mixed potassium-and sodium-acetate salts were used in Germany and Brazil from 1930 to 1965 for the separation of ethanol and water.

Surveys of the use of inorganic salts for extractive distillation, including effects on vapor–liquid equilibria, are given by Johnson and Furter [27], Furter and Cook [28], and Furter [29, 30]. A survey of methods for predicting the effect of inorganic salts on vapor–liquid equilibria is provided by Kumar [31]. Column-simulation results, using the Newton–Raphson method, are presented by Llano-Restrepo and Aguilar-Arias [99] for the ethanol–water–calcium chloride system and by Fu [100], for the ethanol–water–ethanediol–potassium acetate system, who shows simulation results that compare favorably with those from an industrial column.

Salt distillation can be applied to organic compounds that have little capacity for dissolving inorganic salts by using organic salts called **hydrotropes**. Typical are alkali and alkaline-earth salts of the sulfonates of toluene, xylene, or cymene, and the alkali benzoates, thiocyanates, and salicylates. Mahapatra, Gaikar, and Sharma [32] found that the addition of aqueous solutions of 30 and 66 wt% *p*-toluenesulfonic acid to 2, 6-xyleneol and *p*-cresol at 1 atm increased the α from approximately 1 to about 3, as shown in Figure 11.21d. Hydrotropes can also enhance liquid–liquid extraction, as shown by Agarwal and Gaikar [33].

§11.4 PRESSURE-SWING DISTILLATION

The temperature and composition of a binary azeotrope shifts with a change in pressure. If a binary azeotrope disappears at some pressure, or changes composition by 5 mol% or more over a moderate range of pressure, consideration should be given to using two ordinary distillation columns operating in series at different pressures. This process is referred to as **pressure-swing distillation**. Knapp and Doherty [34] list 36 pressure-sensitive, binary azeotropes, mainly from the compilation of Horsley [11]. The effect of pressure on the composition

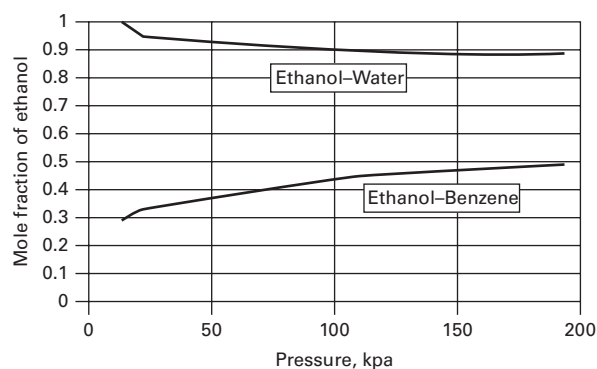


Figure 11.22 Effect of pressure on azeotrope composition.

of two minimum-boiling azeotropes is shown in Figure 11.22. The mole fraction of ethanol in the ethanol–water azeotrope is 0.895 at 101.3 kPa. Below about 10 kPa, the azeotrope disappears. An opposite change in composition with pressure is seen in Figure 11.22 for the ethanol–benzene system. It forms a minimum-boiling azeotrope at 44 mol% ethanol at 101.3 kPa. The percent ethanol in the azeotrope decreases with decreasing pressure. Applications of pressure-swing distillation, first noted by Lewis [35] in a 1928 patent, include separations of the minimum-boiling azeotrope of tetrahydrofuran–water and maximum-boiling azeotropes of hydrochloric acid–water and formic acid–water.

Van Winkle [36] shows the effect of pressure on a minimum-boiling azeotrope for A and B, with the T - y - x curves shown in Figure 11.23a. As pressure is decreased from P_2 to P_1 , the azeotropic composition moves toward a smaller percentage of A in the azeotrope. An operable pressure-swing sequence is shown in Figure 11.23b. The total feed, F_1 , to Column 1, operating at lower pressure P_1 , is the sum of fresh feed, F , which is richer in A than the azeotrope, and recycled distillate, D_2 , whose composition is close to that of the azeotrope at pressure P_2 . D_2 and, consequently, F_1 are both richer in A than the azeotrope at P_1 . The bottoms, B_1 , leaving Column 1 is almost pure A. Distillate, D_1 , which is slightly richer in A than the azeotrope, but less rich in A than

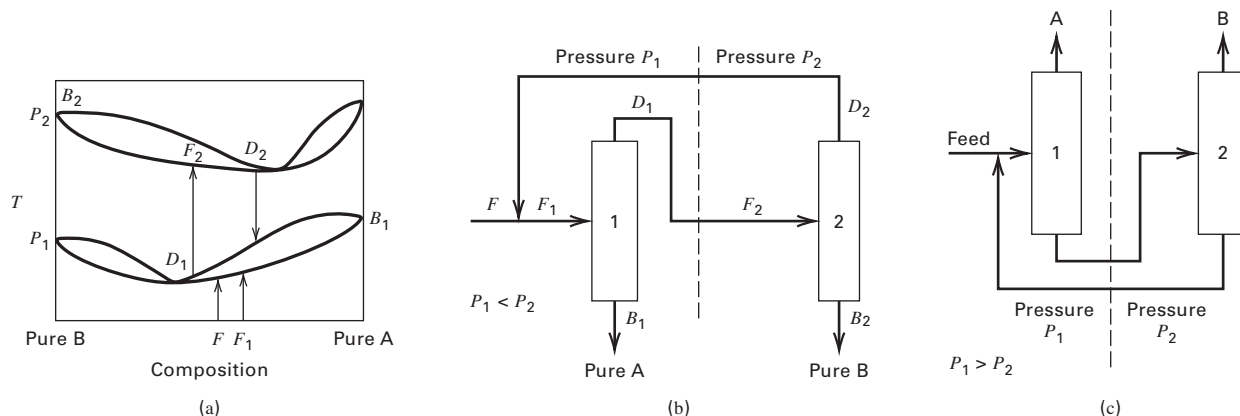


Figure 11.23 Pressure-swing distillation. (a) T - y - x curves at pressures P_1 and P_2 for minimum boiling azeotrope. (b) Distillation sequence for minimum-boiling azeotrope. (c) Distillation sequence for maximum-boiling azeotrope.

the azeotrope at P_2 , is fed to Column 2, where the bottoms, B_2 , is almost pure B. Robinson and Gilliland [37] discuss the separation of ethanol and water, where the fresh feed is less rich in ethanol than the azeotrope. For that case, products are still removed as bottoms, but nearly pure B is taken from the first column and A from the second.

Pressure-swing distillation can also be used to separate less-common maximum-boiling binary azeotropes. A sequence is shown in Figure 11.23c, where both products are withdrawn as distillates, rather than as bottoms. In this case, the azeotrope becomes richer in A as pressure is decreased. Fresh feed, richer in A than the azeotrope at the higher pressure, is first distilled in Column 1 at higher pressure P_1 , to produce a distillate of nearly pure A and a bottoms slightly richer in A than the azeotrope at the higher pressure. The bottoms is fed to Column 2, operating at lower pressure P_2 , where the azeotrope is richer in A than the feed to that column. Accordingly, distillate is nearly pure B, while recycled bottoms from Column 2 is less rich in A than the azeotrope at the lower pressure.

For pressure-swing-distillation sequences, because of the high cost of gas compression, recycle ratio is a key design factor, and depends on the variation in azeotropic composition with column pressure. The next example illustrates the importance of the recycle stream.

EXAMPLE 11.5 Pressure-Swing Distillation.

Ninety mol/s of a mixture of 2/3 by moles ethanol and 1/3 benzene at the bubble point at 101.3 kPa is to be separated into 99 mol% ethanol and 99 mol% benzene. The mixture forms a minimum-boiling azeotrope of 44.8 mol% ethanol at 101 kPa and 68°C. If the pressure is reduced to 27 kPa, as shown in Figure 11.22, the azeotrope shifts to 36 mol% ethanol at 35°C. This is a candidate for pressure-swing distillation.

Apply the sequence shown in Figure 11.23b with the first column operating at a top-tray pressure at 30 kPa (225 torr). Because the feed composition is greater than the azeotrope composition at the column pressure, the distillate composition approaches the

minimum-boiling azeotrope at the top-tray pressure, and the bottoms is 99 mol% ethanol. The distillate is sent to the second column, which has a top-tray pressure of 106 kPa. Feed to this column has an ethanol content less than the azeotrope at the second-column pressure, so the distillate approaches the azeotrope at the top-tray pressure, and the bottoms is 99 mol% benzene. The distillate is recycled to the first column. Design a pressure-swing distillation system for this separation.

Solution

For the first column, which operates under vacuum, reflux-drum and reboiler pressures are set at 26 and 40 kPa, respectively. For the second column, operating slightly above ambient pressure, reflux-drum and reboiler pressures are set at 101.3 and 120 kPa, respectively. Bottoms compositions are specified at the required purities. The distillate for the first column is set at 37 mol% ethanol, slightly greater than the azeotrope composition at 30 kPa. Distillate composition for the second column is 44 mol% ethanol, slightly less than the azeotrope composition at 106 kPa. Material-balance calculations on ethanol and benzene give the following flow rates in mol/s.

Component	F	D_2	F_1	B_1	D_1	B_2
Ethanol	60.0	67.3	127.3	59.7	67.6	0.3
Benzene	30.0	85.6	115.6	0.6	115.0	29.4
Totals:	90.0	152.9	242.9	60.3	182.6	29.7

Equilibrium-stage calculations for the columns were made with the ChemSep program, using total condensers and partial reboilers. For Column 1, runs were made to find optimal feed-tray locations for the fresh feed and the recycle, using a reflux rate that avoided any near-pinch conditions. The selected design uses seven theoretical trays (not counting the partial reboiler), with the recycle stream, at a temperature of 68°C, sent to tray 3 from the top and the fresh feed to tray 5 from the top. An $R = 0.5$ is sufficient to meet specifications. The resulting liquid-phase composition profile is shown in Figure 11.24a, where the desired lack of pinch points is observed. The McCabe–Thiele diagram for Column 1 in Figure 11.24b has three operating lines, and the optimal-feed locations are indicated.

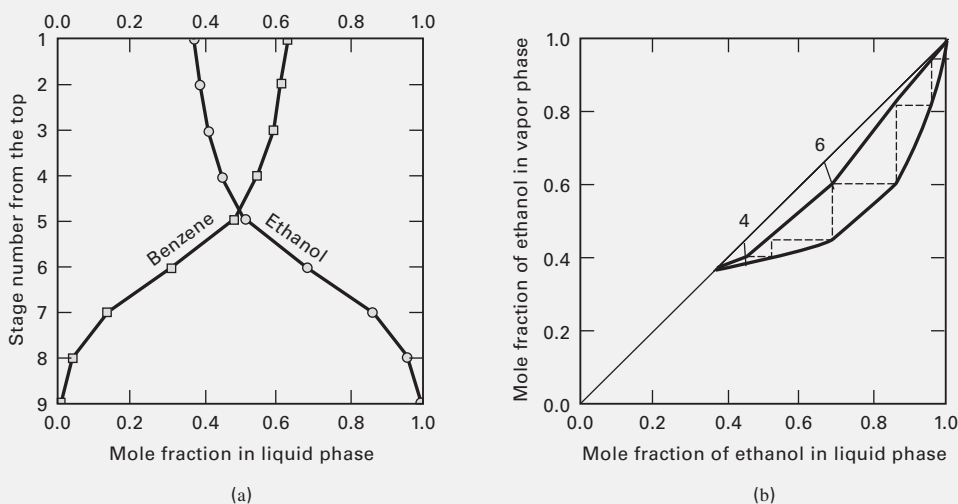


Figure 11.24 Computed results for Column 1 of pressure-swing distillation system in Example 11.5. (a) Liquid composition profiles. (b) McCabe–Thiele diagram.

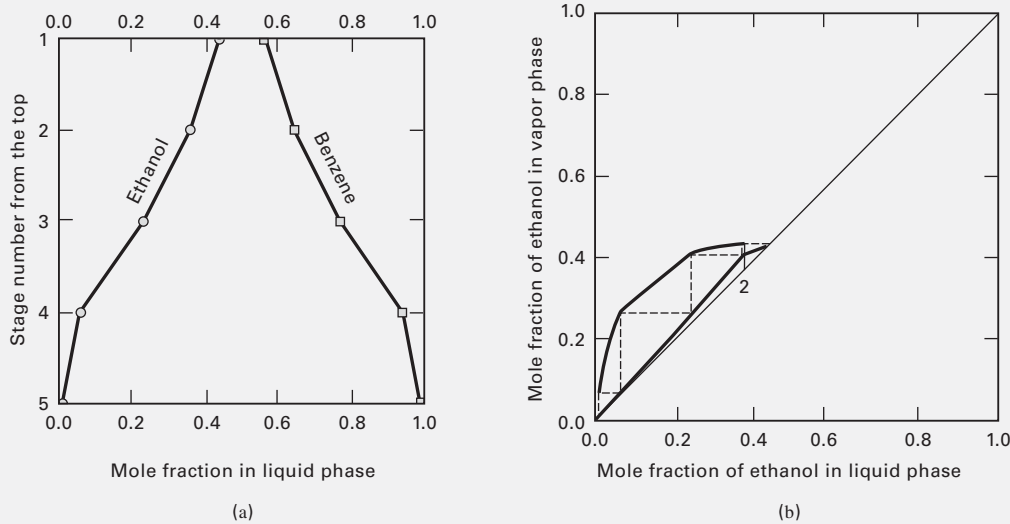


Figure 11.25 Computed results for Column 2 of pressure-swing distillation system in Example 11.5. (a) Liquid composition profiles. (b) McCabe–Thiele diagram.

Because of the azeotrope, the operating lines and equilibrium curve all lie below the 45° line. The condenser duty is 9.88 MW, while the reboiler duty is 8.85 MW. The bottoms temperature is 56°C . This column was sized with the CHEMCAD program for sieve trays on 24-inch tray spacing and a 1-inch weir height to minimize pressure drop. The resulting diameter is 3.2 meters (10.5 ft). A tray efficiency of about 47% is predicted, so 15 trays are required.

A similar procedure was used to establish the optimal-feed tray, total trays, and reflux ratio for Column 2. The selected design turned out to be a refluxed stripper with only three theoretical stages (not counting the partial reboiler). A reflux rate of only 25.5 mol/s achieves the product specifications, with most of the liquid traffic in the stripper coming from the feed. The resulting liquid-phase composition profile is shown in Figure 11.25a, where, again, no composition pinches are evident.

The McCabe–Thiele diagram for Column 2 is given in Figure 11.25b, where an optimal-feed location is indicated. The condenser and reboiler duties are 6.12 MW and 7.07 MW. The bottoms temperature is 84°C . This column was sized like Column 1, resulting in a column diameter of 2.44 meters (8 ft). A tray efficiency of 50% results in 6 actual trays.

§11.5 HOMOGENEOUS AZEOTROPIC DISTILLATION

An azeotrope can be separated by extractive distillation, using a solvent that is higher boiling than the feed components and does not form any azeotropes. Alternatively, the separation can be made by **homogeneous azeotropic distillation**, using an **entrainer** not subject to such restrictions. Like extractive distillation, a sequence of two or three columns is used. Alternatively, the sequence is a hybrid system that includes operations other than distillation, such as solvent extraction.

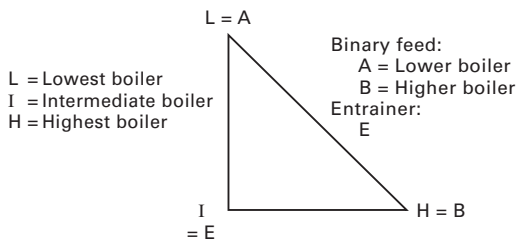
The conditions that a potential entrainer must satisfy have been studied by Doherty and Caldarola [16]; Stichlmair, Fair, and Bravo [1]; Foucher, Doherty, and Malone [14]; Stichlmair and Herguijuela [18]; Fidkowski, Malone, and Doherty [13];

Wahnschafft and Westerberg [38]; and Laroche, Bekiaris, Andersen, and Morari [39]. If it is assumed that a distillation boundary, if any, of a residue-curve map is straight or cannot be crossed, the conditions of Doherty and Caldarola apply. These are based on the rule that for entrainer E, the two components, A and B, to be separated, or any product azeotrope, must lie in the same distillation region of the residue-curve map. Thus, a distillation boundary cannot be connected to the A–B azeotrope. Furthermore, A or B, but not both, must be a saddle.

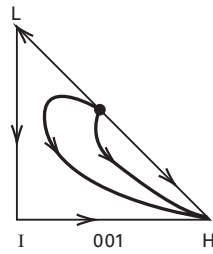
The maps suitable for a sequence that includes homogeneous azeotropic distillation together with ordinary distillation are classified into the five groups illustrated in Figure 11.26a, b, c, d, and e, where each group includes applicable residue-curve maps and the sequence of separation columns used to separate A from B and recycle the entrainer. For all groups, the residue-curve map is drawn, with the lowest-boiling component, L, at the top vertex; the intermediate-boiling component, I, at the bottom-left vertex; and the highest-boiling component, H, at the bottom-right vertex. Component A is the lower-boiling binary component and B the higher. For the first three groups, A and B form a minimum-boiling azeotrope; for the other two groups, they form a maximum-boiling azeotrope.

In Group 1, the intermediate boiler, I, is E, which forms no azeotropes with A and/or B. As shown in Figure 11.26a, this case, like extractive distillation, involves no distillation boundary. Both sequences assume that fresh feed F, of A and B, as fed to Column 1, is close to the azeotropic composition. This feed may be distillate from a previous column used to produce the azeotrope from the original A and B mixture. Either the **direct sequence** or the **indirect sequence** may be used. In the former, Column 2 is fed by the bottoms from Column 1 and the entrainer is recovered as distillate from Column 2 and recycled to Column 1. In the latter, Column 2 is fed by the distillate from Column 1 and the entrainer is recovered as bottoms from Column 2 and recycled to Column 1. Although both sequences

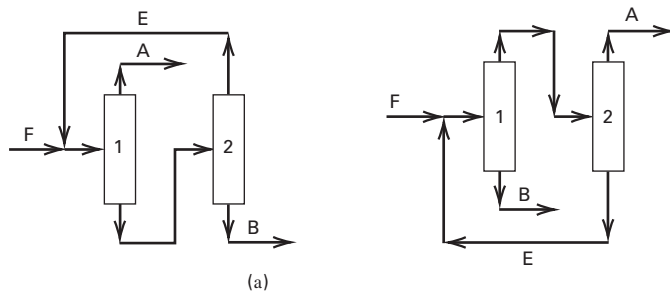
Residue-curve map arrangement



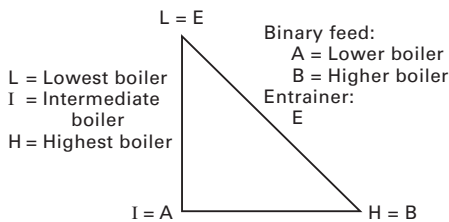
Applicable residue-curve map



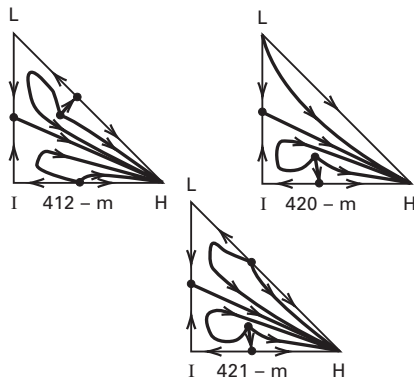
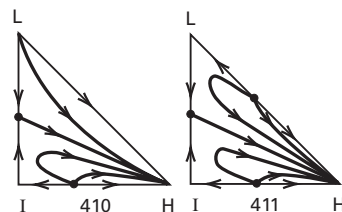
Sequences



Residue-curve map arrangement



Applicable residue-curve maps



Typical sequence

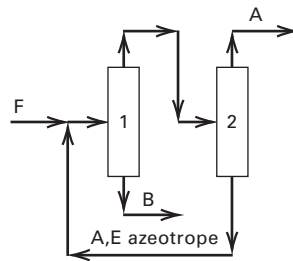


Figure 11.26 Residue-curve maps and distillation sequences for homogeneous azeotropic distillation. (a) Group 1: A and B form a minimum-boiling azeotrope, I = E, E forms no azeotropes. (b) Group 2: A and B form a minimum-boiling azeotrope, L = E, E forms a maximum-boiling azeotrope with A. (Continued)

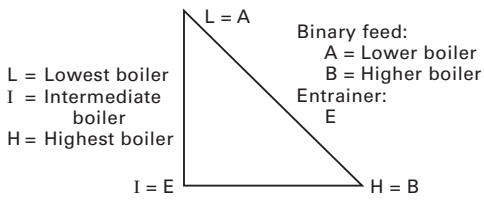
show entrainer combined with fresh feed before Column 1, fresh feed and recycled entrainer can be fed to different trays to enhance the separation.

In Group 2, low boiler L is E, which forms a maximum-boiling azeotrope with A. Entrainer E may also form a minimum-boiling azeotrope with B, and/or a minimum-boiling (unstable node) ternary azeotrope. Thus, in Figure 11.26b, any of the five residue-curve maps may apply. In all cases, a distillation boundary exists, which is directed from the maximum-boiling azeotrope of A–E to pure B, the high boiler. A feasible indirect or direct sequence is restricted to the subtriangle bounded by the vertices of pure components A, B, and the binary A–E azeotrope. An example of an

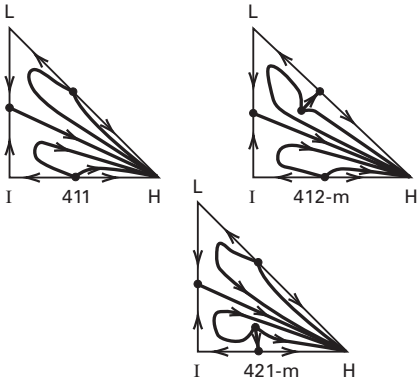
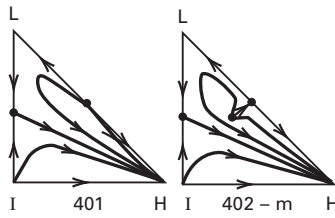
indirect sequence is included in Figure 11.26b. Here, the A–E azeotrope is recycled to Column 1 from the bottoms of Column 2. Alternatively, as in Figure 11.26c for Group 3, A and E may be switched to make A the low boiler and E the intermediate boiler, which again forms a maximum-boiling azeotrope with A. All sequences for Group 3 are confined to the same subtriangle as for Group 2.

Groups 4 and 5, in Figures 11.26d and e, are similar to Groups 2 and 3. However, A and B now form a maximum-boiling azeotrope. In Group 4, the entrainer is the intermediate boiler, which forms a minimum-boiling azeotrope with B. The entrainer may also form a maximum-boiling azeotrope with A, and/or a maximum-boiling (stable node) ternary azeotrope.

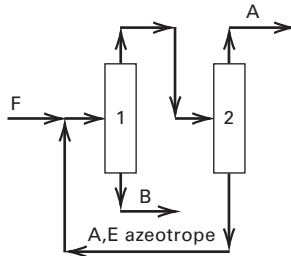
Residue-curve map arrangement



Applicable residue-curve maps

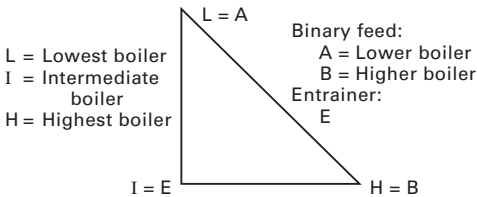


Typical sequence

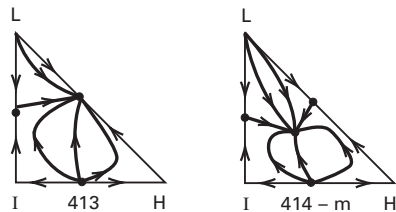
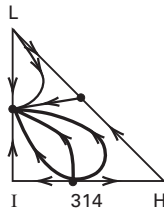


(c)

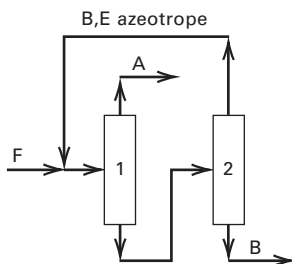
Residue-curve map arrangement



Applicable residue-curve maps



Sequence



(d)

Figure 11.26 (Continued) (c) Group 3: A and B form a minimum-boiling azeotrope, I = E, E forms a maximum-boiling azeotrope with A. (d) Group 4: A and B form a maximum-boiling azeotrope, I = E, E forms a minimum-boiling azeotrope with B.

A feasible sequence is restricted to the subtriangle formed by vertices A, B, and the B–E azeotrope. In the sequence, the distillate from Column 2, which is the minimum-boiling B–E azeotrope, is mixed with fresh feed to Column 1, which produces a distillate of pure A. The bottoms from Column 1 has a composition such that when fed to Column 2, a bottoms of pure B can be produced. Although a direct sequence is shown, the indirect sequence can also be used. Alternatively, as shown in Figure 11.26e for Group 5, B and E may be switched to make E the high boiler. In the sequence shown, as in that of Figure 11.26d, the bottoms from Column 1 is

such that, when fed to Column 2, a bottoms of pure B can be produced. The other conditions and sequences are the same as for Group 4.

The distillation boundaries for the hypothetical ternary systems in Figure 11.26 are shown as straight lines. When a distillation boundary is curved, it may be crossed, provided that both the distillate and bottoms products lie on the same side of the boundary.

It is often difficult to find an entrainer for a sequence involving homogeneous azeotropic distillation and ordinary distillation. However, azeotropic distillation can also be

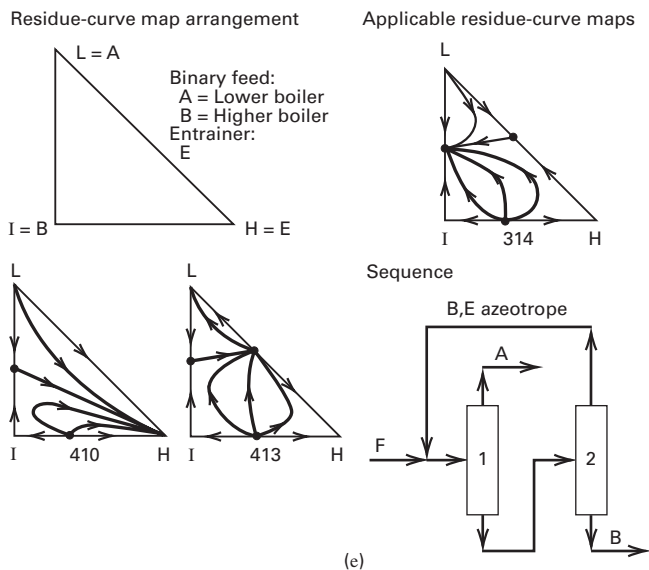


Figure 11.26 (Continued) (e) Group 5: A and B form a maximum-boiling azeotrope, H = E, E forms a minimum-boiling azeotrope with B.

incorporated into a hybrid sequence involving separation operations other than distillation. In that case, some of the restrictions for the entrainer and resulting residue-curve map may not apply. For example, the separation of the close-boiling and minimum-azeotrope-forming system of benzene and cyclohexane using acetone as the entrainer violates the restrictions for a distillation-only sequence because the ternary system involves only two minimum-boiling binary azeotropes. However, the separation can be made by the sequence shown in Figure 11.27. It involves (1) homogeneous azeotropic distillation with acetone entrainer to produce a bottoms product of nearly pure benzene and a distillate close in composition to the minimum-boiling binary azeotrope of acetone and cyclohexane; (2) solvent extraction of distillate

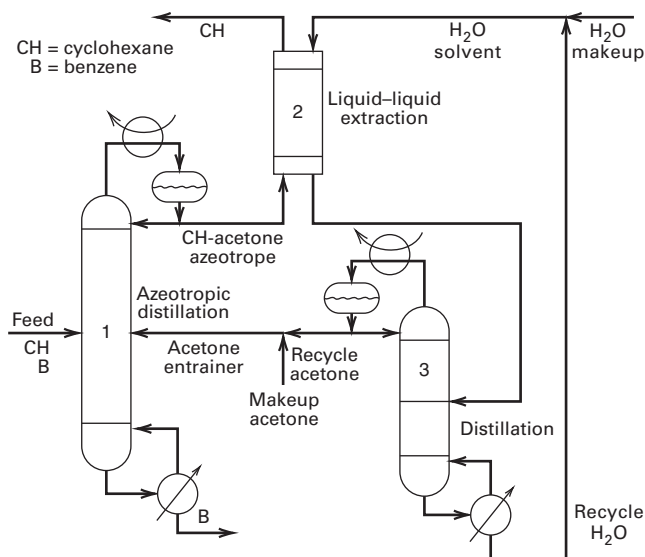


Figure 11.27 Sequence for separating cyclohexane and benzene using homogeneous azeotropic distillation with acetone entrainer.

with water to give a raffinate of cyclohexane and an extract of acetone and water; and (3) ordinary distillation of extract to recover acetone for recycle. In Example 11.6, the azeotropic distillation is subject to product-composition-region restrictions.

EXAMPLE 11.6 Homogeneous Azeotropic Distillation.

Benzene (nbp = 80.13°C) and cyclohexane (nbp = 80.64°C) form a minimum-boiling homogeneous azeotrope at 1 atm and 77.4°C of 54.2 mol% benzene. Since they cannot be separated by distillation at 1 atm, it is proposed to separate them by homogeneous azeotropic distillation using acetone as entrainer in the sequence shown in Figure 11.27. The azeotropic-column feed consists of 100 kmol/h of 75 mol% benzene and 25 mol% cyclohexane. Determine a feasible acetone-addition rate so that nearly pure benzene is obtained as bottoms product. Acetone (nbp = 56.14°C) forms a minimum-boiling azeotrope with cyclohexane at 53.4°C and 1 atm at 74.6 mol% acetone. Figure 11.28 is the residue-curve map at 1 atm.

Solution

The residue-curve map shows a slightly curved distillation boundary connecting the two azeotropes and dividing the diagram into distillation regions 1 and 2. Fresh feed is designated in Figure 11.28 by a filled-in box labeled F. If a straight line is drawn from F to the pure acetone apex, A, the mixture of fresh feed and acetone entrainer must lie somewhere on this line in Region 1. Suppose 100 kmol/h of fresh feed is combined with an equal flow rate of entrainer. The mixing point, M, is located at the midpoint of the line connecting F and A. If a line is drawn from the benzene apex, B, through M, to the side that connects the acetone apex to the cyclohexane apex, it does not cross the distillation boundary separating the two regions, but lies completely in Region 1. Thus, the separation into a nearly pure benzene bottoms and a distillate mixture of mainly acetone and cyclohexane is possible. This is confirmed with the Aspen Plus process simulator for a column operating at 1 atm with 38 theoretical stages, a total condenser, a partial reboiler, reflux ratio = 4, B = 75 kmol/h (equivalent to the benzene flow rate in the feed), and a bubble-point

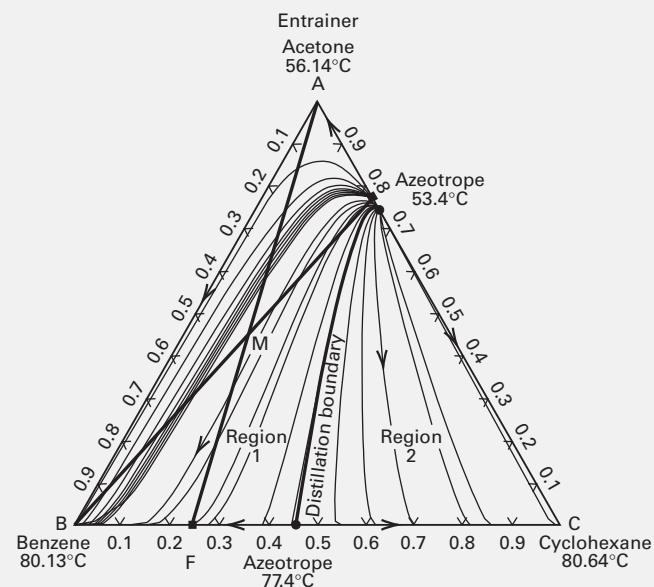


Figure 11.28 Residue-curve map for Example 11.6.

Table 11.4 Effect of Acetone-Entrainer Flow Rate on Benzene Purity for Example 11.6

Case	Acetone Flow Rate, kmol/h	Benzene Purity in Bottoms, %
1	50	88.69
2	75	94.21
3	100	99.781
4	125	99.779

combined feed to stage 19 from the top. The product flow rates are listed in Table 11.4 as Case 3, where bottoms of 99.8 mol% benzene is obtained with a benzene recovery of the same value. A higher entrainer flow rate of 125 kmol/h, included as Case 4, also achieves a high benzene-bottoms-product purity and recovery. However, if only 75 kmol/h (Case 2) or 50 kmol/h (Case 1) of entrainer is used, a nearly pure benzene bottoms is not achieved because of the distillation boundary restriction.

§11.6 HETEROGENEOUS AZEOTROPIC DISTILLATION

Homogeneous azeotropic distillation requires that A and B lie in the same distillation region of the residue-curve map as entrainer E. This is so restrictive that it is difficult, if not impossible, to find a feasible entrainer. The Group 1 map in Figure 11.26a requires that the entrainer not form an azeotrope but yet be the intermediate-boiling component, while the other two components form a minimum-boiling azeotrope. Such systems are rare, because most intermediate-boiling entrainers form an azeotrope with one or both of the other two components. The other four groups in Figure 11.26 require formation of at least one maximum-boiling azeotrope. However, such azeotropes are far less common than minimum-boiling azeotropes. Thus, sequences based on homogeneous azeotropic distillation are rare and a better alternative is needed.

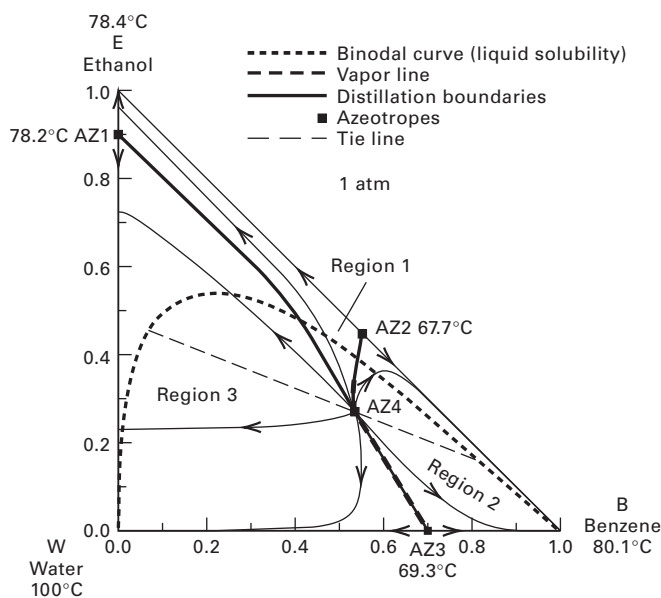
A better, alternative technique that finds wide use is **heterogeneous azeotropic distillation** to separate close-boiling binaries and minimum-boiling binary azeotropes by employing an entrainer that forms a binary and/or ternary heterogeneous (two-phase) azeotrope. As discussed in §4.2.2, a heterogeneous azeotrope has two or more liquid phases. If it has two, the overall, two-liquid-phase composition is equal to that of the vapor phase. Thus, all three phases have different compositions. The overhead vapor from the column is close to the composition of the heterogeneous azeotrope. When condensed, two liquid phases form in a decanter. After separation, most or all of the entrainer-rich liquid phase is returned to the column as reflux, while most or all of the other liquid phase is sent to the next column for further processing. Because these two liquid phases usually lie in different distillation regions of the residue-curve map, the restriction that dooms homogeneous azeotropic distillation is overcome. In heterogeneous azeotropic distillation, the components to be separated need not lie in the same distillation region.

Heterogeneous azeotropic distillation has been practiced for a century, first by batch and then by continuous processing.

Two of the most widely used applications are (1) the use of benzene or another entrainer to separate the minimum-boiling azeotrope of ethanol and water, and (2) use of ethyl acetate or another entrainer to separate the close-boiling mixture of acetic acid and water. Other applications, cited by Widagdo and Seider [19], include dehydrations of isopropanol with isopropylether, *sec*-butyl-alcohol with *disec*-butylether, chloroform with mesityl oxide, formic acid with toluene, and acetic acid with toluene. Also, tanker-transported feedstocks such as benzene and styrene, which become water-saturated during transport, are dehydrated using heterogeneous azeotropic distillation.

Consider separation of the ethanol–water azeotrope by heterogeneous azeotropic distillation. The two most widely used entrainers are benzene and diethyl ether, but others are feasible—including *n*-pentane. In 1902, Young [40] discussed the use of benzene as an entrainer for a batch process, in perhaps the first application of heterogeneous azeotropic distillation. In 1928, Keyes obtained a patent [41] for a continuous process, discussed in a 1929 article [42].

A residue-curve map, computed by Bekiaris, Meski, and Morari [43] for the ethanol (E)–water (W)–benzene (B) system at 1 atm, using the UNIQUAC equation (§2.7.3) for liquid-phase activity coefficients (with parameters from Aspen Plus), is shown in Figure 11.29. Superimposed on the map is a bold-dashed binodal curve for the two-liquid-phase-region boundary. The normal boiling points of E, W, and B are 78.4, 100, and 80.1°C, respectively. The UNIQUAC equation predicts that homogeneous minimum-boiling azeotropes AZ1 and AZ2 are formed by E and W at 78.2°C and 10.0 mol% W, and by E and B at 67.7°C and 44.6 mol% E, respectively. A heterogeneous minimum-boiling azeotrope AZ3 is predicted for W and B at 69.3°C, with a vapor composition of 29.8 mol% W. The overall two-liquid-phase composition is the same as that of the vapor, but each liquid phase is


Figure 11.29 Residue-curve map for the ethanol water benzene system at 1 atm.

almost pure. The B-rich liquid phase is predicted to contain 0.55 mol% W, while the W-rich liquid phase contains only 0.061 mol% B. A ternary minimum-boiling heterogeneous azeotrope AZ4 is predicted at 64.1°C, with a vapor composition of 27.5 mol% E, 53.1 mol% B, and 19.4 mol% W. The overall two-liquid-phase composition of the ternary azeotrope equals that of the vapor, but a thin, dashed tie line through AZ4 shows that the benzene-rich liquid phase contains 18.4 mol% E, 79.0 mol% B, and 2.6 mol% W, while the water-rich liquid phase contains 43.9 mol% E, 6.3 mol% B, and 49.8 mol% W.

In Figure 11.29, the map is divided into three distillation regions by three thick, solid-line distillation boundaries that extend from AZ4 to binary azeotropes at AZ1, 2, and 3. Each distillation region contains one pure component. Because the ternary azeotrope is the lowest-boiling azeotrope, it is an unstable node. Because all three binary azeotropes boil below the boiling points of the three pure components, the binary azeotropes are saddles and the pure components are stable nodes. Accordingly, all residue curves begin at the ternary azeotrope and terminate at a pure-component apex. Liquid–liquid solubility (binodal curve) is shown as a thick, dashed, curved line. However, this curve is not like the usual ternary solubility curve, because it is for isobaric, not isothermal, conditions. Thick dashes that represent vapor composition in equilibrium with two liquid phases are superimposed on the distillation boundary that separates Regions 2 and 3. Compositions of the two equilibrium-liquid phases for a particular vapor composition are obtained from the two ends of the straight tie line that passes through the vapor composition point and terminates at the liquid solubility curve. The only tie line shown in Figure 11.29 is a thin, dashed line that passes through AZ4. Other tie lines, representing other temperatures, could be added; however, in all distillations,

a strenuous attempt is made to restrict the formation of two liquid phases to the decanter because when two liquid phases form on a tray, the tray efficiency decreases.

Figure 11.29 shows how a distillation boundary is crossed by the tie line through AZ4 to form two liquid phases in the decanter. This phase split is utilized in a typical operation, where the tower is treated as a column with no condenser, a main feed that enters a few trays below the top of the column, and the reflux of benzene-rich liquid as a second feed. The composition of the combined two feeds lies in Region 1. Thus, from the residue-curve directions, products of the tower can be a bottoms of nearly pure ethanol and an overhead vapor approaching the AZ4 composition. When that vapor is condensed, phase splitting occurs to give a water-rich phase that lies in Region 3 and an entrainer-rich phase in Region 2. If the water-rich phase is sent to a reboiled stripper, the residue curves indicate that a nearly pure-water bottoms can be produced, with the overhead vapor, rich in ethanol, recycled to the decanter. When the entrainer-rich phase in Region 2 is added to the main feed in Region 1, the overall composition lies in Region 1.

To avoid formation of two liquid phases on the top trays of the azeotropic tower, the composition of the vapor leaving the top tray must have an equilibrium liquid that lies outside of the two-phase-liquid region in Figure 11.29. Shown in Figure 11.30, from Prokopakis and Seider [44], are 18 vapor compositions that form two liquid phases when condensed, but are in equilibrium with only one liquid phase on the top tray, as restricted to the very small expanded window. That window is achieved by adding to the entrainer-rich reflux a portion of the water-rich liquid or some condensed vapor prior to separation in the decanter.

Figure 11.31, taken from Ryan and Doherty [45], shows three proposed heterogeneous azeotropic distillation schemes

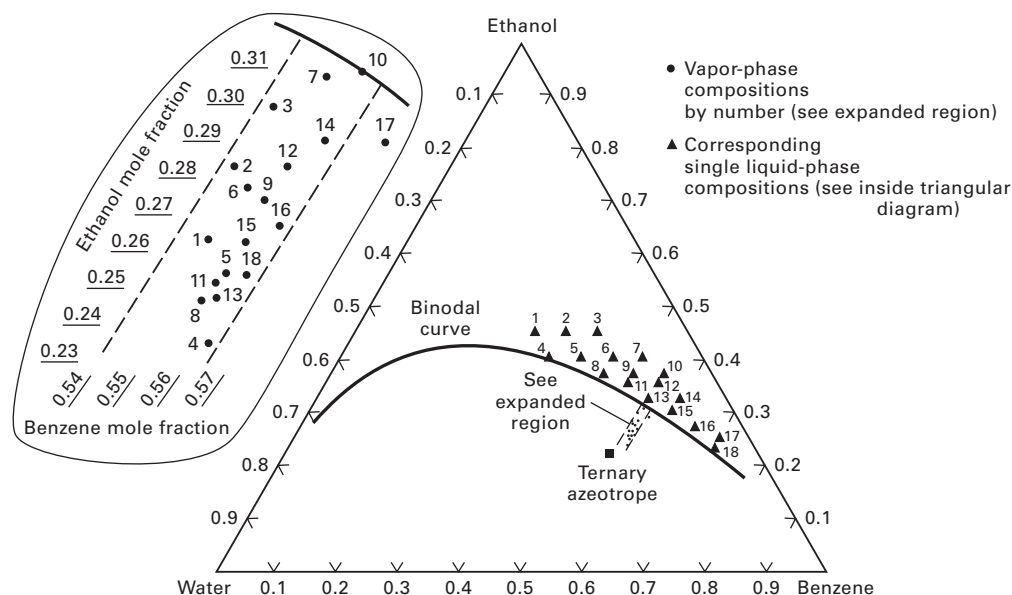


Figure 11.30 Overhead vapor compositions not in equilibrium with two liquid phases.

[Reproduced from [44] with permission from John Wiley & Sons, Inc.]

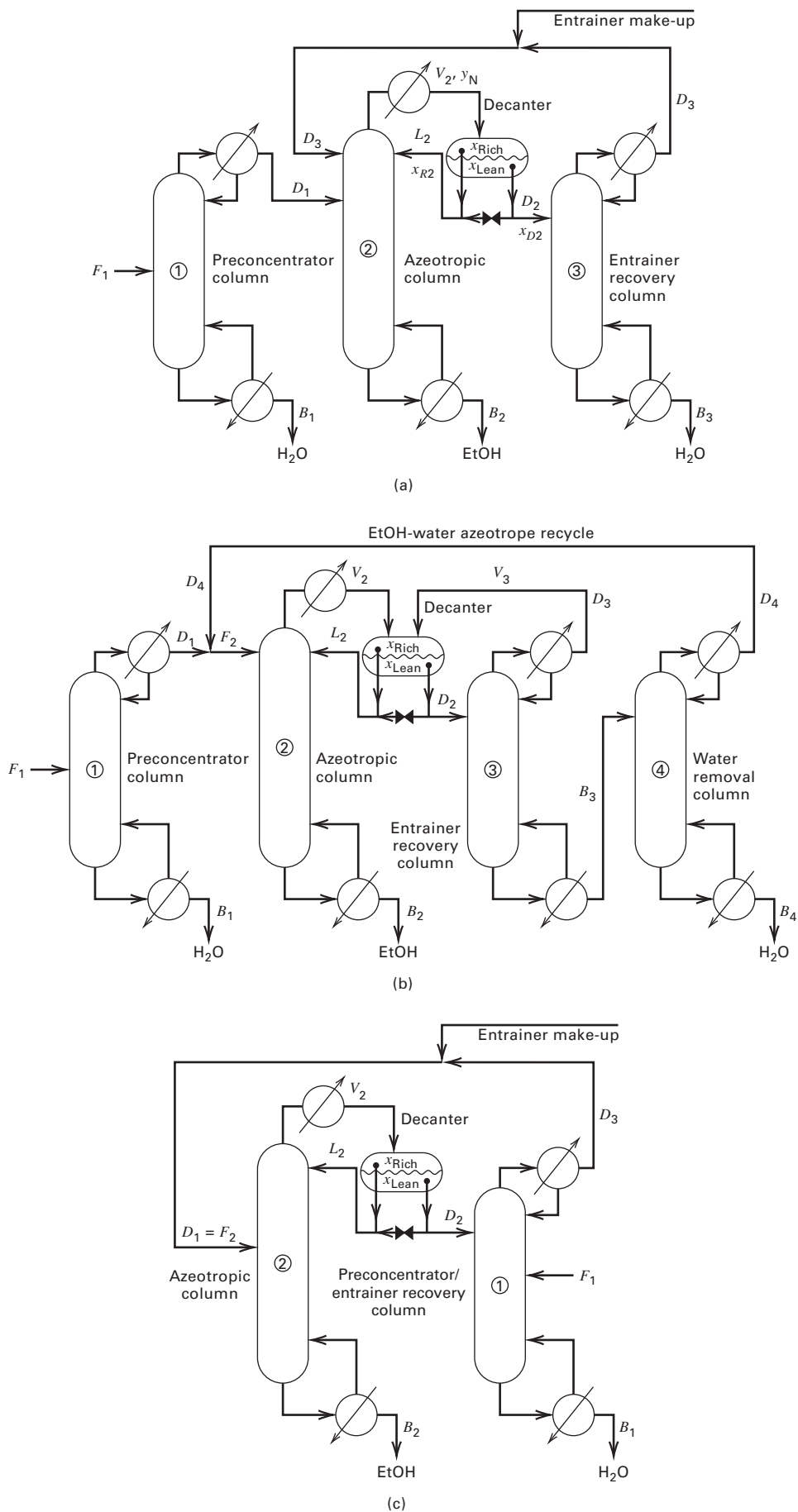


Figure 11.31 Distillation sequences for heterogeneous azeotropic distillation: (a) three-column sequence; (b) four-column sequence; (c) two-column sequence. [Reproduced from [45] with permission from John Wiley & Sons, Inc.]

that utilize only distillation for the other column(s). Most common is the three-column sequence in Figure 11.31a, in which an aqueous feed, dilute in ethanol, is preconcentrated in Column 1 to obtain a nearly pure-water bottoms product and distillate close in composition to the binary azeotrope. The latter is fed to the azeotropic tower, Column 2, where nearly pure ethanol is recovered as bottoms. The tower is refluxed by most or all of the entrainer-rich liquid from the decanter. The water-rich phase, which contains ethanol and a small amount of entrainer, is sent to the entrainer-recovery column, which is a distillation column or a stripper. Distillate from the recovery column is recycled to the azeotropic column. Alternatively, the distillate from Column 3 could be recycled to the decanter. As shown in all three sequences of Figure 11.31, portions of either liquid phase from the decanter can be returned to the azeotropic tower or to the next column in the sequence to control phase splitting on the top trays of the azeotropic tower.

A four-column sequence is shown in Figure 11.31b. The first column is identical to the first column of the three-column sequence of Figure 11.31a. The second column is the azeotropic column, which is fed by the near-azeotrope distillate of ethanol and water from Column 1 and by a recycle distillate, of about the same composition, from Column 4. The purpose of Column 3 is to remove, as distillate, entrainer from the water-rich liquid leaving the decanter and recycle it to the decanter. Ideally, the composition of this distillate is identical to that of the vapor distillate from Column 2. The bottoms from Column 3 is separated in Column 4 into a bottoms of nearly pure water, and a distillate that approaches the ethanol–water azeotrope and is therefore recycled to the feed to Column 2. Pham and Doherty [46] found no advantage of the four-column over the three-column sequence.

A novel two-column sequence, described by Ryan and Doherty [45], is shown in Figure 11.31c. The feed is sent to Column 2, a combined preconcentrator and entrainer-recovery

column. The distillate from this column is feed for the azeotropic column. The bottoms from Column 1 is nearly pure ethanol, while Column 2 produces a bottoms of nearly pure water. For feeds dilute in ethanol, Ryan and Doherty found that the two-column sequence has a lower investment cost, but a higher operating cost, than a three-column sequence. For ethanol-rich feeds, the two sequences are economically comparable.

The ethanol–benzene–water residue-curve map of Figure 11.29 is one of a number of residue-curve maps that can lead to feasible distillation sequences that include heterogeneous azeotropic distillation. Pham and Doherty [46] note that a feasible entrainer is one that causes phase splitting over a portion of the three-component region, but does not cause the two feed components to be placed in different distillation regions. Figure 11.32 shows two other such maps, where the dashed lines are liquid–liquid solubility (binodal) curves.

Convergence of computer simulations for heterogeneous azeotropic distillation columns by the methods described in Chapter 10 is difficult, especially when convergence of the entire sequence is attempted. It is preferable to uncouple the columns by using a residue-curve map to establish, by material-balance calculations, flow rates and compositions of feeds and products for each column. This procedure is illustrated for a three-column sequence in Figure 11.33, where the dash-dot lines separate the three distillation regions, the short-dash line is the liquid–liquid solubility curve, and the remaining lines are material-balance lines. Each column in the sequence is computed separately. Even then, the calculations can fail because of nonidealities in the liquid phase and possible phase splitting, making it necessary to use more robust methods such as the boundary-value, tray-by-tray method of Ryan and Doherty [45], the homotopy-continuation method of Kovach and Seider [47], or the collocation method of Swartz and Stewart [48].

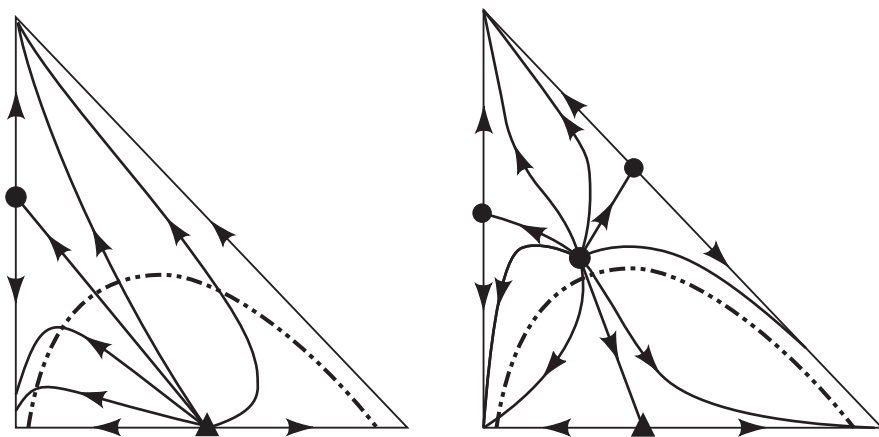


Figure 11.32 Two additional residue-curve maps for heterogeneous azeotropic distillations that lead to feasible distillation sequences for the separation of ethanol–water with benzene.

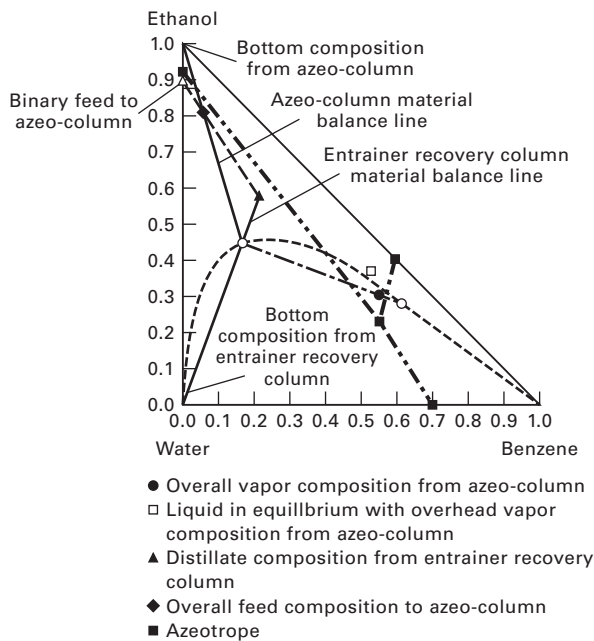


Figure 11.33 Material-balance lines for the three-column sequence of Figure 11.31a.

[Reproduced from [45] with permission from John Wiley and Sons.]

§11.6.1 Multiplicity of Solutions

Solutions to nonlinear mathematical models are not always unique. The existence of multiple, steady-state solutions for continuous, stirred-tank reactors has been known since at least 1922 and is described in textbooks on chemical reaction engineering, where typically one or more of the multiple solutions are unstable and, therefore, inoperable. The existence of multiplicity in steady-state separation problems is a relatively new discovery. Gani and Jørgensen [49] define three types of multiplicity, all of which can occur in distillation simulations:

- 1. Output multiplicity**, where all input variables are specified and more than one solution for the output variables, typically sets of product compositions and temperature profiles, are found.
- 2. Input multiplicity**, where one or more output variables are specified and multiple solutions are found for the unknown input variables.
- 3. Internal-state multiplicity**, where multiple sets of internal conditions or profiles are found for the same values of the input and output variables.

Output multiplicity for azeotropic distillation was first observed by Shewchuk [50] in 1974. With different starting guesses, two steady-state solutions for the dehydration of ethanol by heterogeneous azeotropic distillation with benzene were found. In a more detailed study, Magnussen, Michelsen, and Fredenslund [51] found, with difficulty, for a narrow range of ethanol flow rate in the top feed to the column, three steady-state solutions, one of which was unstable. One of the two stable solutions predicts a far purer ethanol bottoms

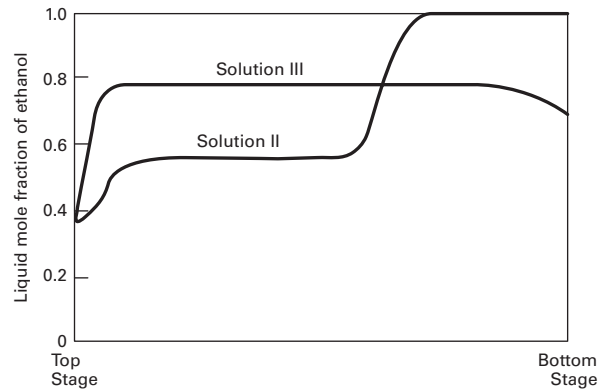


Figure 11.34 Two multiple solutions for a heterogeneous distillation operation.

product than the other stable solution. Thus, from a practical standpoint, it is important to obtain all stable solutions when more than one exists. Subsequent studies, some contradictory, show that multiple solutions persist only over a narrow range of D or B , but may exist over a wide range of R , provided there are sufficient stages. Figure 11.34 shows composition profiles for ethanol from two of five solutions found by Kovach and Seider [47] for a 40-tray ethanol–water–benzene heterogeneous azeotropic distillation. Solution II provides almost pure ethanol; Solution III gives only 70 mol% ethanol. It is important to compute all solutions; process simulators compute only one solution. Finding these solutions is difficult because (1) azeotropic columns are difficult to converge by process simulators to even one solution, (2) multiple solutions may exist only in a restricted range of input variables, (3) multiple solutions can be found with process simulators only by changing initial-composition guesses, and (4) the choice of an activity-coefficient correlation and interaction parameters can be crucial. The best results are obtained when advanced mathematical techniques such as continuation and bifurcation analysis are employed, as described by Kovach and Seider [47]; Widagdo and Seider [19]; Bekiaris, Meski, Radu, and Morari [52]; and Bekiaris, Meski, and Morari [43]. The last two articles provide explanations why multiple solutions occur in azeotropic distillations. The following example illustrates a technique using a process simulator to find one solution. Black and co-workers [53–56] present a similar approach for the design of a two-column system for heterogeneous azeotropic distillation of an ethanol–water mixture using n -pentane as the entrainer.

EXAMPLE 11.7 Separation of Acetic Acid and Water Using Heterogeneous Azeotropic Distillation with an Entrainer of n -Propyl Acetate.

Design a distillation system with a process simulator to separate 1,000 kmol/h of a 20 mol% aqueous acetic acid into nearly pure acetic acid and water, using heterogeneous azeotropic distillation at 1 atm with n -propyl acetate as the entrainer. Select the UNIQUAC method for calculating liquid-phase activity coefficients.

Solution

The phase behavior of the acetic acid (AA)/water (W)/*n*-propyl acetate (NPA) system at 1 atm was explored with Aspen Plus using UNIQUAC for activity coefficients. The normal boiling points in °C are 118.1 for AA, 100 for W, and 101.4 for NPA. Only one azeotrope is predicted, a heterogeneous one, at 82.9°C. The composition of the azeotrope is 52.4 mol% W and 47.6 mol% NPA. W and AA, as well as NPA and AA, are completely soluble in each other.

Figure 11.35a is a residue curve map from Aspen Plus for the AA-W-NPA system at 1 atm. It shows that only two different products can leave a distillation column: (1) a nearly pure AA bottoms product and (2) an overhead vapor having the composition of the azeotrope. Figure 11.35b from Aspen Plus shows a ternary liquid-liquid triangular diagram for the system at 82.9°C. Both the binodal curve and tie lines are included. Of interest are the compositions of the two liquid phases after total condensation of the heterogeneous azeotrope. The water-rich phase contains less than 1 mol% NPA, while the NPA-rich phase contains approximately 15 mol% water.

Figure 11.31 depicts three common distillation sequences for heterogeneous azeotropic distillation. They all include a pre-concentration column. This column can be omitted here because the feed is already concentrated in water. Furthermore, only an

azeotropic column is necessary because Figure 11.35a indicates that with a sufficient number of equilibrium stages and reflux, it is possible to produce a nearly pure bottoms product of acetic acid and a nearly pure water-rich product from the decanter that separates the condensed azeotrope into two liquid phases.

The design of the azeotropic column can be made with Aspen Plus, CHEMCAD, or ChemSep. The Aspen Plus flowsheet is shown in Figure 11.35c. The feed, stream 1, enters B1, which is modeled with a RadFrac block, using the Azeotropic Distillation algorithm with the SC method to converge the calculations. The acetic acid product leaves the partial reboiler at the bottom of the column in stream 5. B1 does not include a condenser. Instead the overhead vapor, stream 2, which may be close in composition to the heterogeneous azeotrope, flows to B2, a Heater block that condenses the overhead vapor to produce stream 3, comprised of two liquid phases at the bubble point. That stream enters B3, a Decanter block, which separates the two equilibrium liquid phases into a water-rich product, stream 4, and an NPA-rich reflux, stream 6, which is recycled as reflux to B1. Although the reflux (stream 6 in Figure 11.35c) appears to enter the column with the feed, it enters the top tray of the column. All three blocks use an option to check for the presence of two equilibrium liquid phases on every tray in the distillation column.

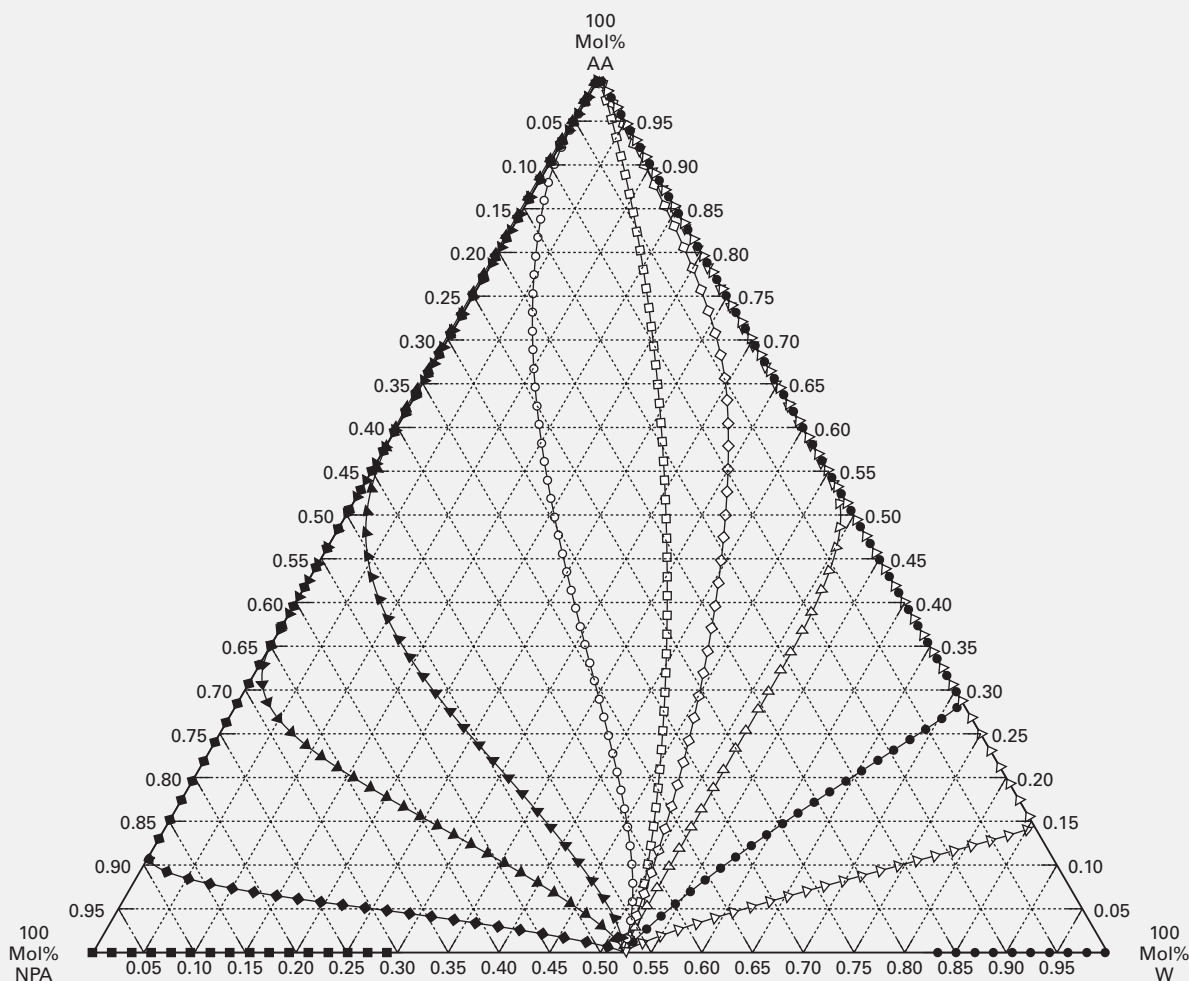


Figure 11.35a Residue curve map for the acetic acid (AA)—water (W)—*n*-propyl acetate (NPA) system at 1 atm.

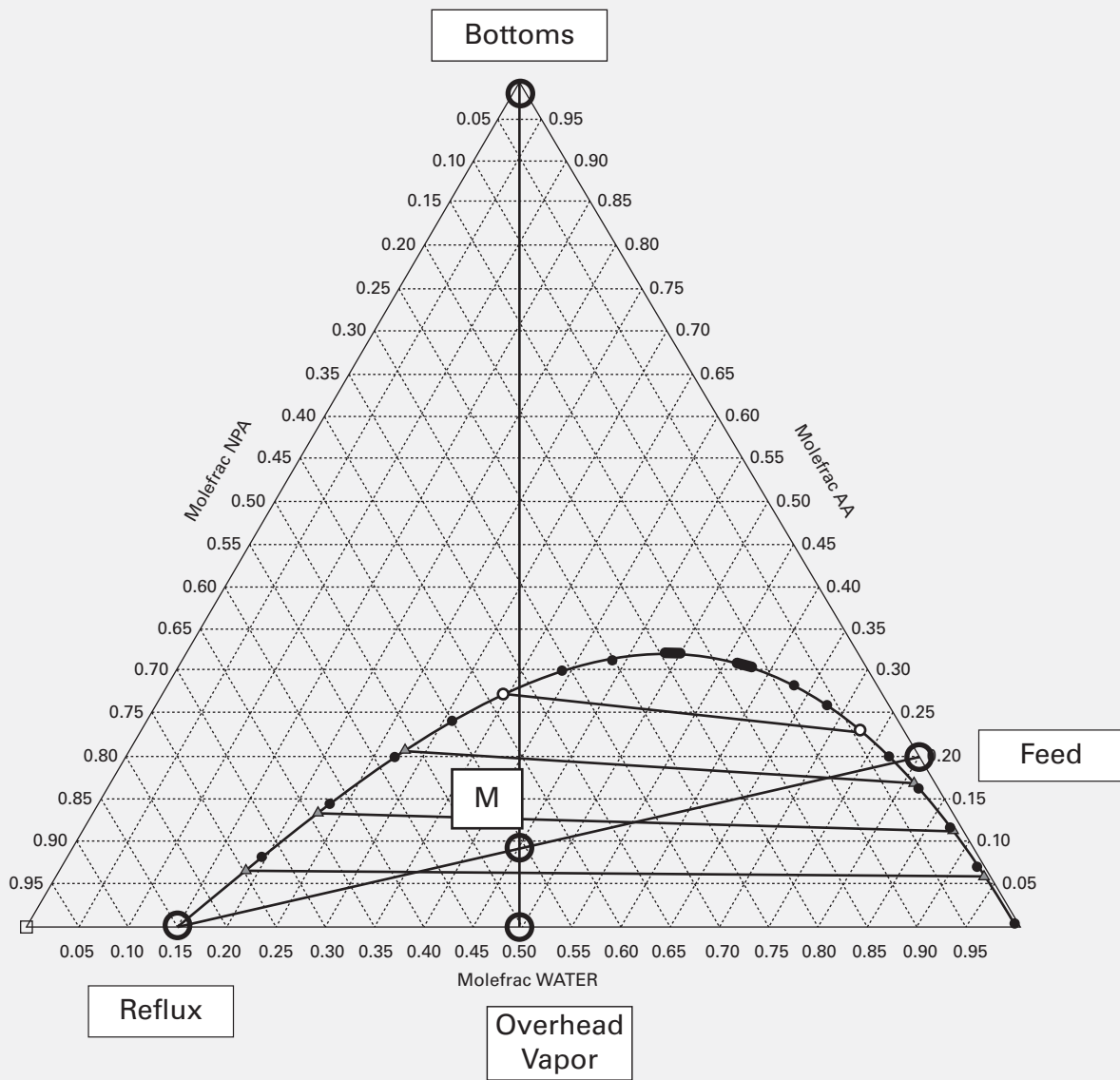


Figure 11.35b Ternary Liquid-Liquid Equilibrium Diagram for the Acetic Acid-Water-*n*-Propyl Acetate System at 82.9°C.

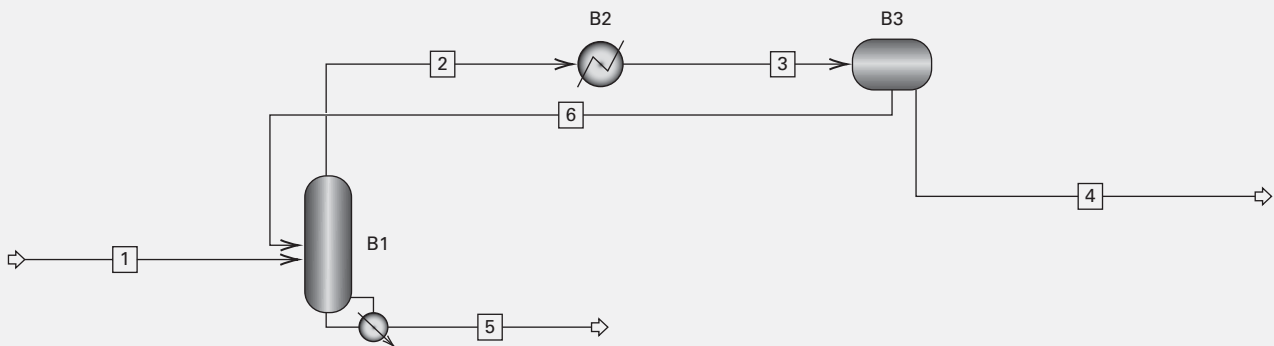


Figure 11.35c Aspen Plus Flowsheet for Heterogeneous Azeotropic Distillation to Separate Acetic Acid from Water Using *n*-Propyl Acetate as the Entrainer.

Aspen Plus uses the sequential modular method to calculate the three blocks, one-at-a-time, in sequence. However, in the flowsheet of Figure 11.35c, B1 cannot be calculated because stream 6 is not known. The flowsheet has one recycle loop that involves streams 2, 3, and 6. A calculation sequence can be initiated from anyone of these three streams. If stream 2 is selected and provided an initial guess for its pressure, temperature, flow rate, and composition, it becomes a “tear stream.” The calculation sequence becomes B2, B3, and B1. If stream 2, calculated from B1, does not match the guess, to within some tolerance, the sequence is repeated until convergence is achieved.

Figure 11.35b can be used to obtain an initial guess for the flow rate and composition of stream 2 by the mixing-point concept discussed in §8.3. Assuming a perfect separation in B1, the construction lines for finding a mixing point, M , are included in Figure 11.35b. These two lines are based on the total molar material-balance equation,

$$M = F + R = OH + B \quad (1)$$

where, M = mixing point, F = feed, R = reflux, OH = overhead vapor, and B = bottoms. Assuming 1 atm pressure throughout the process, the given and assumed stream conditions are:

	F , Stream 1	R , Stream 6	OH , Stream 2	B , Stream 5
Vapor Fraction	0 (Bubble Point)	0 (Bubble Point)	1 (Dew Point)	0 (Bubble Point)
Mole fraction:				
Water	0.80	0.15	0.52	0.00
Acetic acid	0.20	0.00	0.00	1.00
<i>n</i> -Propyl acetate	0.00	0.85	0.48	0.00
Total kmol/h	1000			200

where the mole fractions in R and OH are shown in Figure 11.35b. To obtain the approximate total flow rates of R and OH , the following two component molar material balances are solved with mole fractions from the above table.

$$\text{NPA balance: } 0.48 OH = 0.85 R \quad (2)$$

$$\text{W balance: } 800 + 0.15 R = 0.52 OH \quad (3)$$

Solving (2) and (3), $OH = 1840$ kmol/h and $R = 1040$ kmol/h.

Note that NPA is not in the feed to the process, but is internal to the process. However, because a perfect separation will not be obtained in B1, a very small amount may be lost to the distillate product, stream 4. Assume it to be 4 kmol/h and add it to the feed. Also, a small amount of AA appears in the overhead vapor. Assume it to be 15 kmol/h. The only two streams needed for the input to Aspen Plus are the feed, stream 1, and the tear stream, stream 2.

Input for the three blocks, B1, B2, and B3, are:

Block B1: Number of stages = 30; No condenser; Bottoms flow rate = 200 kmol/h; Feed F sent to stage 7 (from the top); Reflux, stream 6, sent to stage 1 (the top stage in the column); stages 1 to 5 checked for phase splitting.

Block B2: Outlet vapor fraction = 0 (bubble-point liquid from the three-phase flash)

Block B3: Heat duty = 0; second liquid stream out is rich in NPA

The Aspen Plus run must achieve convergence of B1 and convergence of the tear stream. Convergence of the latter depends on the accuracy of the guess for the make-up flow rate of NPA in feed stream 1. B1 was converged for each loop through the process, but convergence of the NPA makeup was not achieved. The final unconverged loss of NPA after 30 loops was 2.32 kmol/h. The initially assumed value of 4 was replaced with 2.32 and the run was repeated. After repeating this procedure two more times, a final assumed NPA make-up flow rate of 2.38 gave a reasonable convergence of the tear stream. Phase splitting did not occur on any tray within the distillation column. Table 11.5 lists the converged material balance.

Figures 11.36a and 11.36b are plots of the temperature profile and the molar liquid flow rate column profiles, respectively. Figure 11.36c is a plot of the liquid-phase mole fraction column profiles for the three components. Below the feed stage, the NPA mole fraction in the liquid phase is negligible and the temperature and liquid flow profiles are similar. At the top stage, the liquid phase is concentrated in NPA, but its concentration drops rapidly to a negligible level by stage 4, while the temperature increases dramatically and the liquid flow rate is relatively constant until the feed enters the column at stage 7.

The three Figure 11.36 plots can be used to determine if any pinch points occur in the column. This is the subject of Exercise 11.21, which also requires a study of the effect of the number of stages and location of the feed stage on the product purities. That exercise also considers the addition of an Aspen Plus MULT block and a design specification to automatically determine the make-up NPA flow rate, where the make-up is added to the reflux instead of to the feed.

Table 11.5 Converged Material Balance for Heterogeneous Azeotropic Distillation Process of Figure 11.35c

	Feed, Stream 1	Overhead Vapor, Stream 2	Decanter Feed, Stream 3	Distillate, Stream 4	Bottoms, Stream 5	Reflux, Stream 6
Temperature, °C	101.3	83.7	83.0	83.0	117.8	83.0
kmol/h:						
Water	800.0	959.9	959.9	797.5	2.5	162.4
Acetic Acid	200.0	6.2	6.2	2.5	197.5	3.7
<i>n</i> -Propyl Acetate	2.4	897.9	897.9	2.4	0.0	895.5
Total	1002.4	1864.0	1864.0	802.4	200.0	1061.6

The purity of the acetic acid bottoms product is 98.7 mol%.

The purity of the water distillate product is 99.4 mol%.

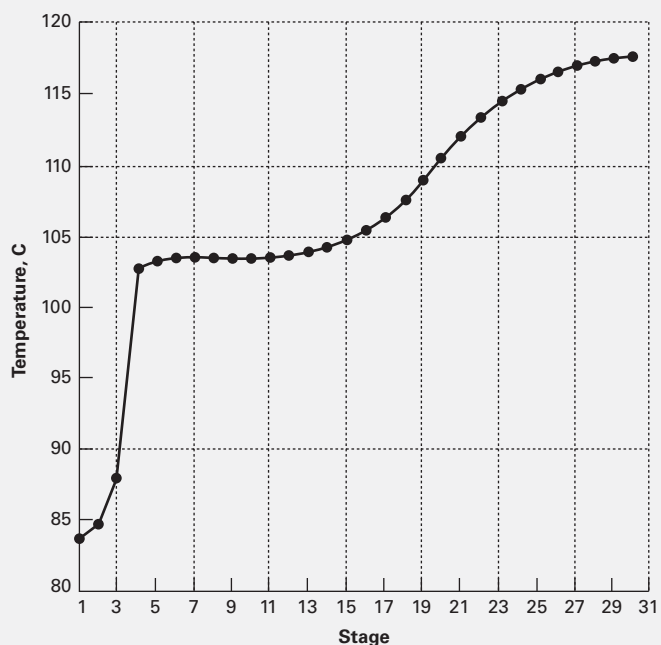


Figure 11.36a Temperature Profile for Azeotropic Distillation Column of Example 11.7

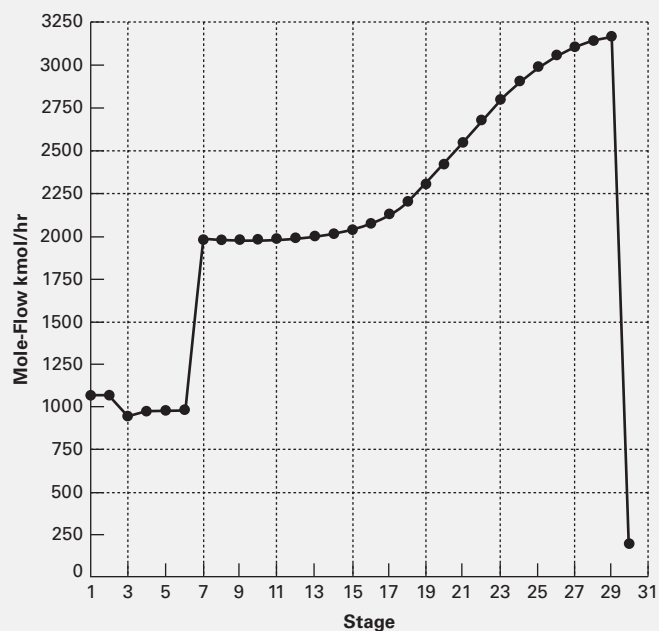


Figure 11.36b Liquid Molar Flow Rate Profile for Azeotropic Distillation Column of Example 11.7.

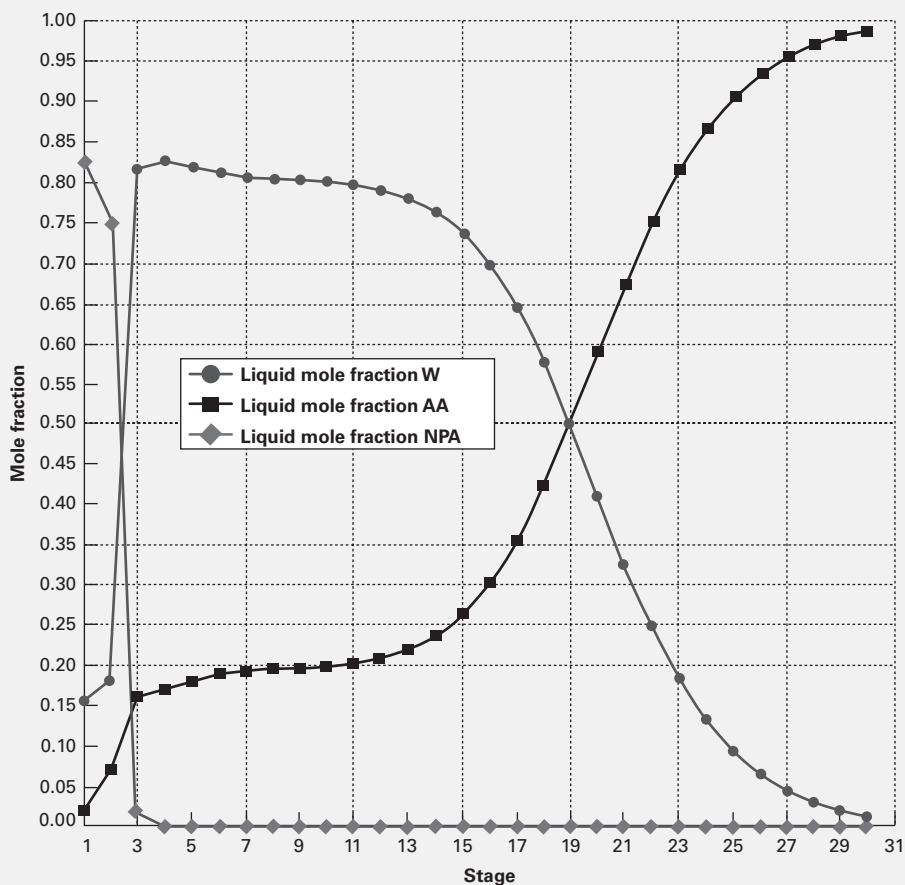


Figure 11.36c Liquid Mole Fraction Profiles for Azeotropic Distillation Column of Example 11.7.

§11.7 REACTIVE DISTILLATION

Reactive distillation denotes simultaneous chemical reaction and distillation. The reaction usually takes place in the liquid phase or at the surface of a solid catalyst in contact with the liquid. One application of reactive distillation, described by Terrill, Sylvestre, and Doherty [57], is the separation of a close-boiling or azeotropic mixture of components A and B, where a chemically reacting entrainer E is introduced into the column. If A is the lower-boiling component, it is preferable that E be higher boiling than B and that it react selectively and reversibly with B to produce reaction product C, which also has a higher boiling point than component A and does not form an azeotrope with A, B, or E. Component A is removed as distillate, and components B and C, together with any excess E, are removed as bottoms. Components B and E are recovered from C in a separate distillation, where the reaction is reversed ($C \rightarrow B + E$); B is taken off as distillate, and E is taken off as bottoms and recycled to the first column.

Terrill, Sylvestre, and Doherty [57] discuss the application of reactive entrainers to the separation of mixtures of *p*-xylene and *m*-xylene, whose normal boiling points differ by only 0.8°C, resulting in a relative volatility of only 1.029. Separation by ordinary distillation is impractical because, to produce 99 mol% pure products from an equimolar feed, more than 500 theoretical stages are required. By reacting the *m*-xylene with a reactive entrainer such as *tert*-butylbenzene using a solid aluminum chloride catalyst, or chelated sodium *m*-xylene dissolved in cumene, stage requirements are drastically reduced.

Closely related to the use of reactive entrainers in distillation is the use of reactive absorbents in absorption, which is widely practiced. For example, sour natural gas is sweetened by the removal of H₂S and CO₂ acid gases by absorption into aqueous alkaline solutions of mono- and di-ethanolamines. Fast, reversible reactions occur to form soluble-salt complexes such as carbonates, bicarbonates, sulfides, and mercaptans. The rich solution leaving the absorber is sent to a reboiled stripper, where the reactions are reversed at higher temperatures and often at lower pressures to regenerate the amine solution as the bottoms and deliver the acid gases as overhead vapor.

A second application of reactive distillation involves undesirable reactions that may occur during distillation. Robinson and Gilliland [58] discuss the separation of cyclopentadiene from C₇ hydrocarbons, where cyclopentadiene dimerizes. The more volatile cyclopentadiene is taken overhead as distillate, but a small amount dimerizes in the lower section of the column and leaves in the bottoms with the C₇s. Alternatively, the dimerization can be facilitated, in which case the dicyclopentadiene is removed as bottoms.

Reactive distillation can involve combining desirable chemical reaction(s) and separation by distillation in a single distillation apparatus. This idea was first proposed by Backhaus, who, starting in 1921 [59], obtained patents for esterification reactions in a distillation column. This concept was verified experimentally by Leyes and Othmer [60] for the esterification of acetic acid with an excess of *n*-butanol in the presence of sulfuric acid catalyst to produce butyl acetate and water.

Reactive distillation should be considered whenever the following hold:

1. The chemical reaction occurs in the liquid phase, in the presence or absence of a homogeneous catalyst, or at the interface of a liquid and a solid catalyst.
2. Feasible temperature and pressure for the reaction and distillation are the same to ensure that reaction rates and distillation rates are of the same order of magnitude.
3. The reaction is equilibrium-limited so that if one or more of the products can be removed by distillation, the reaction can be driven to completion; thus, a large reactant excess is not necessary for a high conversion. This is particularly advantageous when excess reagent recovery is difficult because of azeotrope formation. For reactions that are irreversible, it is more economical to take the reactions to completion in a reactor and then separate the products in a distillation column. In general, reactive distillation is not attractive for supercritical conditions, gas-phase reactions, reactions at high temperatures and pressures, and/or reactions with solids.

Careful consideration must be given to the configuration of reactive distillation columns. Important factors are feed entry and product-removal stages, the possible need for intercoolers and interheaters when the heat of reaction is appreciable, and obtaining required residence time for the liquid phase. In the following ideal cases, it is possible, as shown by Belck [61] and others, for several two-, three-, and four-component systems to produce the desired products without the need for a separate distillation.

Case 1: The reaction $A \leftrightarrow R$ or $A \leftrightarrow 2R$, where R has a higher volatility than A. In this case, only a reboiled rectification section is needed. Feed A is sent to the column reboiler where the reaction takes place. As R is produced, it is vaporized, passing to the rectification column, where it is purified. Overhead vapor from the column is condensed, with part of the condensate returned as reflux. Chemical reaction may also take place in the column. If A and R form a maximum-boiling azeotrope, this configuration is still applicable if the mole fraction of R in the reboiler is greater than the azeotropic composition.

Case 2: The reaction $A \leftrightarrow R$ or $2A \leftrightarrow R$, where A has the higher volatility. In this case, only a stripping section is needed. Liquid A is sent to the top of the column, from which it flows down, reacting to produce R. The column is provided with a total condenser and partial reboiler. Product R is withdrawn from the reboiler. This configuration requires close examination because, at a certain location in the column, chemical equilibrium may be achieved, and if the reaction is allowed to proceed beyond that point, the reverse reaction can occur.

Case 3: The reactions $2A \leftrightarrow R + S$ or $A + B \leftrightarrow R + S$, where A and B are intermediate in volatility to R and S, and R has the highest volatility. Feed enters an ordinary distillation column somewhere near the middle. R is withdrawn as distillate and S as bottoms. If B is less

volatile than A, then B may enter the column separately and at a higher level than A.

Commercial applications of reactive distillation include the following:

1. Esterification of acetic acid with ethanol to produce ethyl acetate and water
2. Reaction of formaldehyde and methanol to produce methylal and water, using a solid acid catalyst [62]
3. Esterification of acetic acid with methanol to produce methyl acetate and water, using a sulfuric acid catalyst, as patented by Agreda and Partin [63], and described by Agreda, Partin, and Heise [64]
4. Reaction of isobutene with methanol to produce methyl-*tert*-butyl ether (MTBE), using a solid, strong-acid ion-exchange resin catalyst, as patented by Smith [65–67] and further developed by DeGarmo, Parulekar, and Pinjala [68]

Consider the esterification of acetic acid (A) with ethanol (B) to produce ethyl acetate (R) and water (S). The respective normal boiling points in °C are 118.1, 78.4, 77.1, and 100. Also, minimum-boiling, binary homogeneous azeotropes are formed by B–S at 78.2°C with 10.57 mol% B, and by B–R at 71.8°C with 46 mol% B. A minimum-boiling, binary heterogeneous azeotrope is formed by R–S at 70.4°C with 24 mol% S, and a ternary, minimum-boiling azeotrope is formed by B–R–S at 70.3°C with 12.4 mol% B and 60.1 mol% R. Thus, this system is exceedingly complex and nonideal. A number of studies, both experimental and computational, have been published, many of which are cited by Chang and Seader [69], who developed a robust computational procedure for reactive distillation based on a homotopy-continuation method. More recently, other algorithms have been reported by Venkataraman, Chan, and Boston [70] and Simandl and Svrcek [71]. Kang, Lee, and Lee [72] obtained binary interaction parameters for the UNIQUAC equation (§2.7.3) by fitting experimental data simultaneously for vapor–liquid equilibrium and liquid-phase chemical equilibrium.

In all of the computational procedures, a reaction-rate term must be added to the stage material balance. Chang and Seader [69] modified (10-38) of the SC method (§10.6) to include a reaction-rate source term for the liquid phase, assuming the liquid is completely mixed:

$$M_{i,j} = l_{i,j}(1 + s_j) + v_{i,j}(1 + S_j) - l_{i,j-1} - v_{i,j+1} - f_{i,j} - (V_{LH})_j \sum_{n=1}^{NRX} \varsigma_{i,n} r_{j,n}, \quad i = 1, \dots, C \quad (11-17)$$

where

$(V_{LH})_j$ = volumetric liquid holdup on stage j ;

$\varsigma_{i,n}$ = stoichiometric coefficient for component i and reaction n using positive values for products and negative values for reactants

$r_{j,n}$ = reaction rate for reaction n on stage j , as the increase in moles of a reference reactant per unit time per unit volume of liquid phase

NRX = number of reversible and irreversible reactions

Typically, each reaction rate is expressed in a power-law form with liquid molar concentrations (where the n subscript is omitted):

$$r_j = \sum_{p=1}^2 k_p \prod_{q=1}^{NRC} c_{j,q}^m = \sum_{p=1}^2 A_p \exp\left(-\frac{E_p}{RT_j}\right) \prod_{q=1}^{NRC} c_{j,q}^m \quad (11-18)$$

where

$c_{j,q}$ = concentration of component q at stage j

k_p = reaction-rate constant for the p th term, where $p = 1$ indicates the forward reaction and $p = 2$ indicates the reverse reaction, with k_1 positive and k_2 negative

m = exponent on the concentration

NRC = number of components in the power-law expression

A_p = pre-exponential (frequency) factor

E_p = activation energy

With (11-17) and (11-18), a reaction may be treated as irreversible ($k_2 = 0$), reversible (k_2 negative and not equal to zero), or at equilibrium. The latter can be achieved by using very large values for the volumetric liquid holdup at each stage in the case of a single, reversible reaction, or by multiplying each of the two frequency factors, A_1 and A_2 , by the same large number. This greatly increases the forward and backward reactions, but maintains the correct value for the chemical-reaction equilibrium constant. For equilibrium reactions, it is important that the power-law expression for the backward reaction be derived from the power-law expression for the forward reaction and the reaction stoichiometry, so as to be consistent with the expression for the chemical-reaction equilibrium constant. The volumetric liquid holdup for a stage, when using a trayed tower, depends on (1) the active bubbling area, (2) height of the froth as influenced by the weir height, and (3) liquid-volume fraction of the froth. In general, the liquid backup in the downcomer is not included in the estimate of liquid holdup. When large holdups are necessary, bubble-cap trays are preferred because they do not weep. When the chemical reaction is in the reboiler, a large liquid holdup can be provided.

The following example deals with the esterification of acetic acid with ethanol to produce ethyl acetate and water. Here, the single, reversible chemical reaction is assumed to reach chemical equilibrium at each stage. Thus, no estimate of liquid holdup is needed. In a subsequent example, chemical equilibrium is not achieved, so holdup estimates are made, and a tower diameter assumed.

EXAMPLE 11.8 Ethanol by Reactive Distillation.

A reactive-distillation column with 13 theoretical stages and equipped with a total condenser and partial reboiler is used to produce ethyl acetate (R) at 1 atm. A saturated-liquid feed of 90 lbmol/h of acetic acid (A) enters stage 2 from the top, while 100 lbmol/h of a saturated liquid of 90 mol% ethanol (B) and 10 mol% water (S) (close to the azeotropic composition) enters stage 9 from the top. Thus, the acetic acid and ethanol are in stoichiometric ratio for esterification. Other specifications are $R = 10$ and $D = 90$ lbmol/h, in the hope that complete conversion to ethyl acetate (the low boiler)

will occur. Data for the homogeneous reaction are given by Izarraraz et al. [73], in terms of the rate law:

$$r = k_1 c_A c_B - k_2 c_R c_S$$

with $k_1 = 29,000 \exp(-14,300/RT)$ and $k_2 = 7,380 \exp(-14,300/RT)$, both in L/(mol-minute) with T in K. Because the activation energies for the forward and backward steps are identical, the chemical-equilibrium constant is independent of temperature and equal to $k_1/k_2 = 3.93$. Assume that chemical equilibrium is achieved at each stage. Thus, very large values of liquid holdup are specified for each stage. Binary interaction parameters for all six binary pairs, for predicting liquid-phase activity coefficients from the UNIQUAC equation (§2.7.3), are as follows, from Kang et al. [72]:

Components in Binary Pair, $i-j$	Binary Parameters	
	$u_{i,j}/R, K$	$u_{j,i}/R, K$
Acetic acid–ethanol	268.54	-225.62
Acetic acid–water	398.51	-255.84
Acetic acid–ethyl acetate	-112.33	219.41
Ethanol–water	-126.91	467.04
Ethanol–ethyl acetate	-173.91	500.68
Water–ethyl acetate	-36.18	638.60

Vapor-phase association of acetic acid and possible formation of two liquid phases on the stages must be considered. Calculate compositions of distillate and bottoms products and determine the liquid-phase-composition and reaction-rate profiles.

Solution

Calculations were made with the SC method of the CHEMCAD process simulation program, where the total condenser is counted as the first stage. The only initial estimates provided were 163 and 198°F for the temperatures of the distillate and the bottoms, respectively. Calculations converged in 17 iterations to the values below:

Component	Product Flow Rates, lbmol/h	
	Distillate	Bottoms
Ethyl acetate	49.52	6.39
Ethanol	31.02	3.07
Water	6.73	59.18
Acetic acid	2.73	31.36
Total	90.00	100.00

All four components appear in both products. The overall conversion to ethyl acetate is only 62.1%, with 88.6% of this going to the distillate. The distillate is 55 mol% acetate; the bottoms is 59.2 mol% water. Only small composition changes occur when feed locations are varied. Two factors in the failure to achieve high conversion and nearly pure products are (1) the highly nonideal nature of the quaternary mixture, accompanied by the large number of azeotropes, and (2) the tendency of the reverse reaction to occur on certain stages. The former is shown in Figure 11.37a, where the α values between ethyl acetate and water and between ethanol and water in the top section are no greater than 1.25, making the separations difficult.

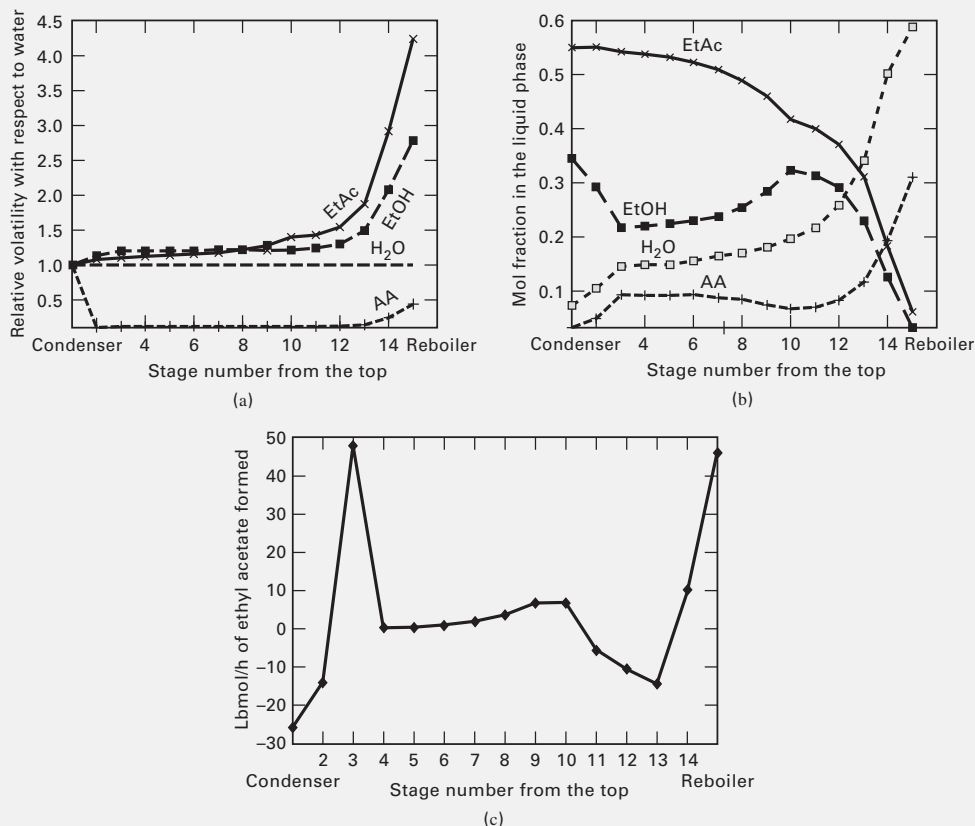


Figure 11.37 Profiles for reactive distillation in Example 11.8. (a) Relative volatility profiles. (b) Liquid-phase mole-fraction profiles. (c) Reaction-rate profile.

The liquid-phase mole-fraction distribution is shown in Figure 11.37b, where, between feed points, compositions change slowly despite the esterification reaction. In Figure 11.37c, the reaction-rate profile is unusual. Above the upper feed stage (now stage 3), the reverse reaction is dominant. From that feed point down to the second feed entry (now stage 10), the forward reaction dominates mainly at the upper feed stage. The reverse reaction is dominant for stages 11–13, whereas the forward reaction dominates at Stages 14 and 15 (the reboiler). The largest extents of forward reaction occur at stages 3 and 15. Even with 60 stages, and with the reaction confined to Stages 25 to 35, the distillate contains appreciable ethanol and the bottoms contains a substantial fraction of acetic acid. For this example, development of a reactive-distillation scheme for achieving a high conversion and nearly pure products represents a significant challenge.

EXAMPLE 11.9 Reactive Distillation to Produce MTBE.

Following the ban on addition of tetraethyl lead to gasoline by the U.S. Amendment to the Clean Air Act of 1990, refiners accelerated the addition of methyl-*tert*-butyl ether (MTBE) to gasoline to boost octane number and reduce unburned hydrocarbons and CO₂ in automobile exhaust. More than 50 MTBE plants were constructed, with many using reactive distillation to produce MTBE from methanol. However, by 2002, MTBE also fell into disfavor in the U.S. because when it leaked from an underground tank at a gas station, it dissolved easily and traveled quickly in groundwater, causing contamination in wells and cancer in animals.

Using thermodynamic and kinetic data from Rehfinger and Hoffmann [74] for the formation of methyl-*tert*-butyl ether (MTBE) from methanol (MeOH) and isobutene (IB), in the presence of *n*-butene (NB), both Jacobs and Krishna [75] and Nijhuis, Kerkhof, and Mak [76] found drastically different IB conversions when the feed stage for methanol was varied. An explanation for these multiple solutions is given by Hauan, Hertzberg, and Lien [77].

Compute a converged solution, taking into account the reaction kinetics but assuming vapor–liquid equilibrium at each stage. The column has a total condenser, a partial reboiler, 15 stages at *V/L* equilibrium, and operates at 11 bar. The total condenser is numbered stage 1 even though it is not an equilibrium stage. The mixed butenes feed, consisting of 195.44 mol/s of IB and 353.56 mol/s of NB, enters stage 11 as a vapor at 350 K and 11 bar. The methanol, at a flow rate of 215.5 mol/s, enters stage 10 as a liquid at 320 K and 11 bar. $R = 7$ and $B = 197$ mol/s. The catalyst is provided only for stages 4 through 11, with 204.1 kg of catalyst per stage. The catalyst is a strong-acid, ion-exchange resin with 4.9 equivalents of acid groups per kilogram of catalyst. Thus, the equivalents per stage are 1,000, or a total of 8,000 for the eight stages. Compute the product compositions and column profiles.

Solution

The RADFRAC model in Aspen Plus was used. Because NB is inert, the only chemical reaction considered is



For the forward reaction, the rate law is formulated in terms of mole-fraction concentrations as in Rehfinger and Hoffmann [74]:

$$r_{\text{forward}} = 3.67 \times 10^{12} \exp(-92,440/RT) x_{\text{IB}} / x_{\text{MeOH}} \quad (1)$$

The corresponding backward rate law, consistent with chemical equilibrium, is

$$r_{\text{backward}} = 2.67 \times 10^{17} \exp(-134,450/RT) x_{\text{MTBE}} / x_{\text{MeOH}}^2 \quad (2)$$

where r is in moles per second per equivalent of acid groups, $R = 8.314$ J/mol-K, T is in K, and x_i is liquid mole fraction.

The Redlich–Kwong equation of state (§2.5.1) is used to estimate vapor-phase fugacities with the UNIQUAC equation (§2.7.3) to estimate liquid-phase activity coefficients. The UNIQUAC binary interaction parameters are as follows, where it is important to include the inert NB in the system by assuming it has the same parameters as IB and that the two butenes form an ideal solution. The parameters are defined as follows, with all $a_{ij} = 0$.

$$T_{ij} = \exp\left(-\frac{u_{ij} - u_{ji}}{RT}\right) = \exp\left(a_{ij} + \frac{b_{ij}}{T}\right) \quad (3)$$

Components in Binary Pair, ij	Binary Parameters	
	b_{ij} , K	b_{ji} , K
MeOH–IB	35.38	–706.34
MeOH–MTBE	88.04	–468.76
IB–MTBE	–52.2	24.63
MeOH–NB	35.38	–706.34
NB–MTBE	–52.2	24.63

The only initial guesses provided are temperatures of 350 and 420 K, for stages 1 and 17, respectively; liquid-phase mole fractions of 0.05 for MeOH and 0.95 for MTBE leaving stage 17; and vapor-phase mole fractions of 0.125 for MeOH and 0.875 for MTBE leaving stage 17. The Aspen Plus input data are listed in the first and second editions of this book. The converged temperatures for stages 1 and 17 are 347 and 420 K. Converged products are:

Component	Flow Rate, mol/s	
	Distillate	Bottoms
MeOH	28.32	0.31
IB	7.27	1.31
NB	344.92	8.64
MTBE	0.12	186.74
Total	380.63	197.00

The combined feeds contained a 10.3% mole excess of MeOH over IB. Therefore, IB was the limiting reactant and the preceding product distribution indicates that 95.6% of the IB, or 186.86 mol/s, reacted to form MTBE. The percent purity of the MTBE in the bottoms is 94.8%. Only 2.4% of the inert NB and 1.1% of the unreacted MeOH are in the bottoms. The condenser and reboiler duties are 53.2 and 40.4 MW.

Seven iterations gave a converged solution. In Figure 11.38a, most of the reaction occurs in a narrow temperature range of 348.6 to 353K. Figure 11.38b shows that vapor traffic above the two feed entries changes by less than 11% because of small changes in temperature. Below the two feed entries, temperature increases rapidly from 353 to 420K, causing vapor traffic to decrease by about 20%. In Figure 11.38c, composition profiles show that the liquid is dominated by NB from the top down to stage 13, thus drastically reducing

the reaction driving force. Below stage 11, liquid becomes richer in MTBE as mole fractions of other components decrease because of increasing temperature. Above the reaction zone, the mole fraction of MTBE quickly decreases as it moves to the top stage. These changes are due mainly to the large differences between the K -values for MTBE and those for the other three components. The relative volatility of MTBE with any of the other components ranges from about 0.24 at the top stage to about 0.35 at the bottom. Nonideality in the liquid influences mainly MeOH, whose liquid-phase activity coefficient varies from a high of 10 at stage 5 to a low of 2.6 at stage 17. This causes the unreacted MeOH to leave mainly with the NB in the distillate rather than with MTBE in the bottoms. The rate-of-reaction profile in Figure 11.38d shows that the forward reaction dominates in the reaction section; however, 56% of the reaction occurs on stage 10, the MeOH feed stage. The least amount of reaction is on stage 11.

The literature indicates that conversion of IB to MTBE depends on the MeOH feed stage. In the range of MeOH feed stages from about 8 to 11, both low- and high-conversion solutions exist. This is shown in Figure 11.39, where the high-conversion solutions are in the 90+ % range, while the low-conversion solutions are all less than 10%. However, if component activities rather than mole fractions are used in the rate expressions, the low-conversion solutions are higher because of the large MeOH activity coefficient. The results in Figure 11.39 were obtained starting with the MeOH feed entering stage 2. The resulting profiles were used as the initial guesses for the run with MeOH entering stage 3. Subsequent runs were performed

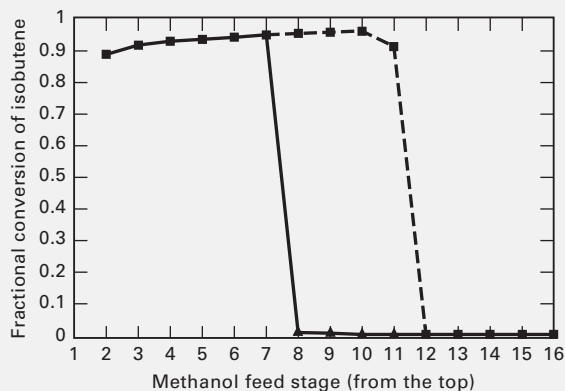


Figure 11.39 Effect of MeOH feed-stage location on conversion of IB to MTBE.

in a similar manner, increasing the MeOH feed stage by 1 each time and initializing with the results of the previous run.

High-conversion solutions were obtained for each run, until the MeOH feed stage was lowered to stage 12, at which point conversion decreased dramatically. Further lowering of the MeOH feed stage to stage 16 also resulted in a low-conversion solution. However, when the direction of change to the MeOH feed stage was reversed starting from stage 12, a low conversion was obtained until the feed stage was decreased to stage 9, at which point the conversion jumped back to the high-conversion result.

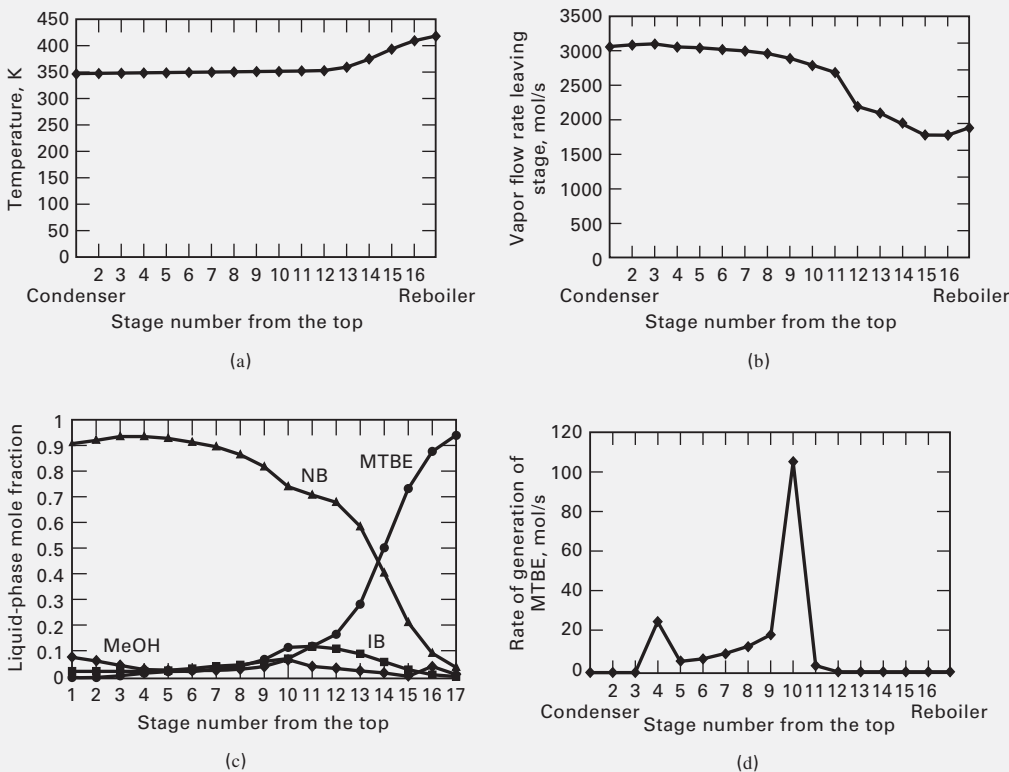


Figure 11.38 Profiles for reactive distillation in Example 11.9. (a) Temperature profile. (b) Vapor traffic profile. (c) Liquid-phase mole-fraction profiles. (d) Reaction-rate profile.

Huss et al. [101] present a study of reactive distillation for the acid-catalyzed reaction of acetic acid and methanol to produce methyl acetate and water, including the side reaction of methanol dehydration, using simulation models and experimental measurements. They consider both finite reaction rates and chemical equilibrium, coupled with phase equilibrium. The results include reflux limits and multiple solutions.

§11.8 SUPERCRITICAL-FLUID EXTRACTION

Solute extraction from a liquid or solid mixture is usually accomplished with a liquid solvent at conditions of temperature and pressure substantially below the solvent critical point, as discussed in Chapter 8. Following extraction, solvent and dissolved solute are subjected to subsequent separations to recover solvent for recycle and to purify the solute.

In 1879, Hannay and Hogarth [78] reported that solid potassium iodide could be dissolved in ethanol, as a dense gas, at supercritical conditions of $T > T_c = 516$ K and $P > P_c = 65$ atm. The iodide could then be precipitated from the ethanol by reducing the pressure. This process was later called **supercritical-fluid extraction (SFE)**, **supercritical-gas extraction**, and, most commonly, **supercritical extraction**. By the 1940s, as chronicled by Williams [79], proposed applications of SFE began to appear in the patent and technical literature. Figure 11.40 shows the supercritical-fluid region for CO_2 , a common solvent for SFE, which has a critical point of 304.2 K and 73.83 bar.

The solvent power of a compressed gas can undergo an enormous increase in the vicinity of its critical point, as shown for the solubility of *p*-iodochlorobenzene (*p*ICB) in ethylene in Figure 11.41, at 298 K for pressures from 2 to 8 MPa. This temperature is 1.05 times the critical temperature of ethylene (283 K), and the pressure range straddles the critical pressure of ethylene (5.1 MPa). At 298 K, *p*ICB is a solid (melting point = 330 K) with a vapor pressure of the order of 0.1 torr. At 2 MPa, if *p*ICB formed an ideal-gas

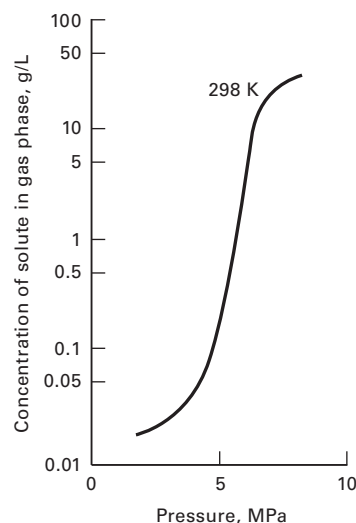


Figure 11.41 Effect of pressure on solubility of *p*ICB in supercritical ethylene.

solution with ethylene, the concentration of *p*ICB in the gas in equilibrium with pure, solid *p*ICB would be 0.00146 g/L. But the concentration from Figure 11.41 is 0.015 g/L, an order of magnitude higher. If the pressure is increased from 2 MPa to almost the critical pressure at 5 MPa (an increase by a factor of 2.5), the equilibrium concentration of *p*ICB is increased about 10-fold to 0.15 g/L. At 8 MPa, the concentration is 40 g/L, 2,700 times higher than predicted for an ideal-gas solution. It is this dramatic increase in solubility of a solute at near-critical solvent conditions that makes SFE of interest.

Why does the solvent power increase so dramatically in the region of the critical pressure? The explanation lies in the change of solvent density while the solute solubility increases. A pressure–enthalpy diagram for ethylene is shown in Figure 11.42, which includes the specific volume (reciprocal of the density) as a parameter. The range of variables and parameters straddles the critical point of ethylene.

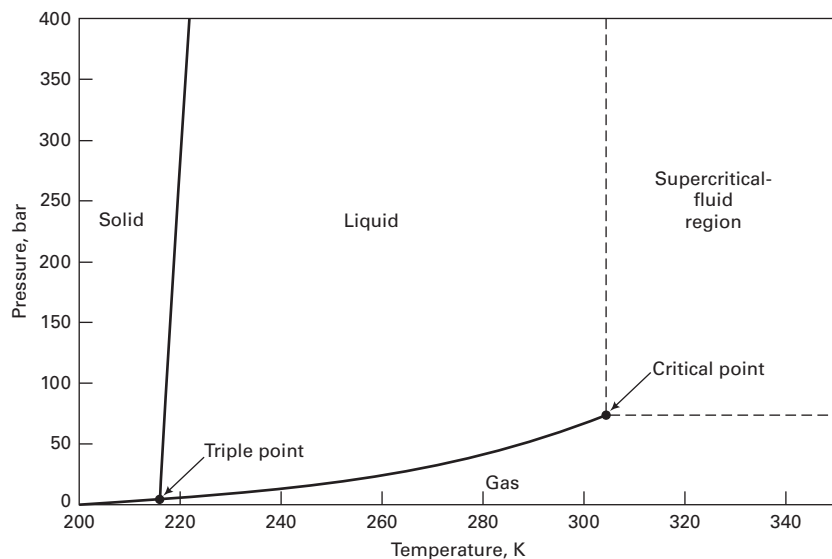


Figure 11.40 Supercritical-fluid region for CO_2 .

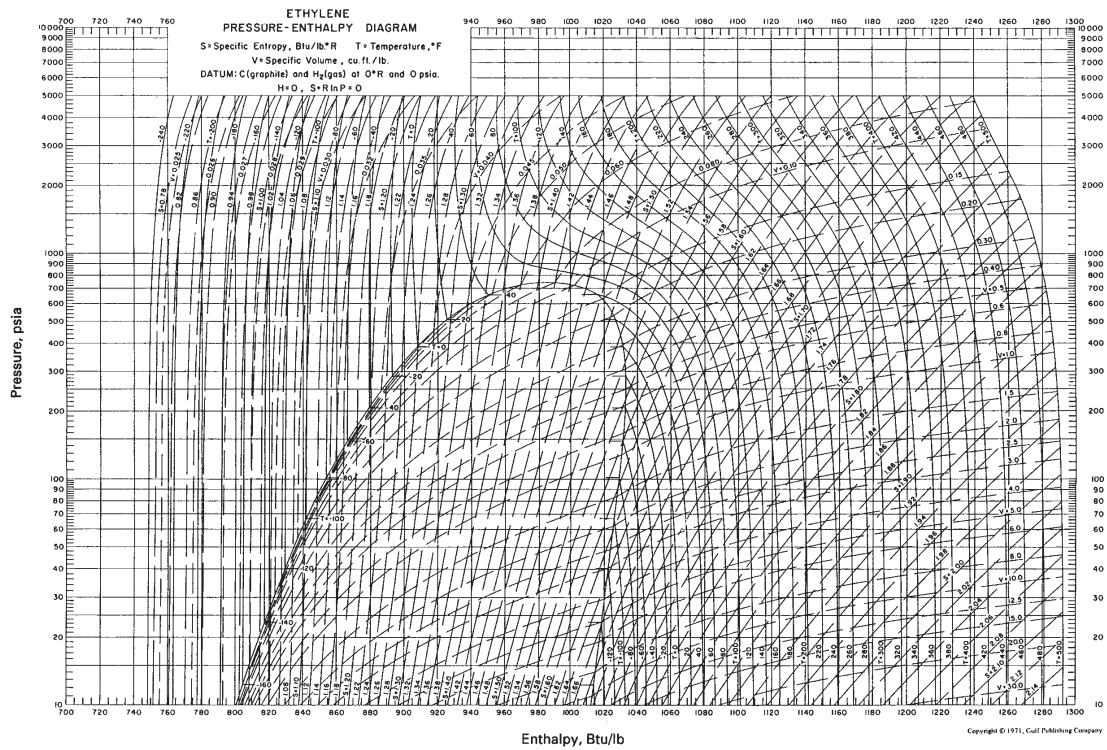


Figure 11.42 Pressure-enthalpy diagram for ethylene.
[Reproduced from K.E. Starling, *Fluid Thermodynamic Properties for Light Petroleum Systems*, Gulf Publishing, Houston (1973). With permission.]

The density of ethylene compared to the solubility of *p*ICB is as follows at 298 K:

Pressure, MPa	Ethylene Density, g/L	Solubility of <i>p</i> ICB, g/L
2	25.8	0.015
5	95	0.15
8	267	40

Although far from a 1:1 correspondence for the increase of *p*ICB solubility with ethylene density over this range of pressure, there is a meaningful correlation. As the pressure increases, closer packing of the solvent molecules allows them to surround and trap solute molecules. This phenomenon is most useful at reduced temperatures from about 1.01 to 1.12.

Two other effects in the supercritical region are favorable for SFE. Molecular diffusivity of a solute in an ambient-pressure gas is about four orders of magnitude higher than in a liquid. For a near-critical fluid, the diffusivity of solute molecules is usually one to two orders of magnitude higher than in a liquid solvent, thus resulting in a lower mass-transfer resistance in the solvent phase. In addition, the viscosity of the supercritical fluid is about an order of magnitude lower than that of a liquid solvent.

Industrial applications for SFE have been the subject of many studies, patents, and venture capital proposals. However, when other techniques are feasible, SFE usually cannot compete because of high solvent-compression costs. SFE is most favorable for extraction of small amounts of large, relatively nonvolatile and expensive solutes, as in bioextraction. Applications are also cited by Williams [79] and McHugh and Krukonic [80].

Solvent selection depends on the feed mixture. If only the chemical(s) to be extracted is (are) soluble in a potential solvent, then high solubility is a key factor. If a chemical besides the desired solute is soluble in the potential solvent, then solvent selectivity becomes as important as solubility. A number of gases and low-MW chemicals, including the following, have received attention as solvents.

Solvent	Critical Temperature, K	Critical Pressure, MPa	Critical Density, kg/m ³
Methane	192	4.60	162
Ethylene	283	5.03	218
Carbon dioxide	304	7.38	468
Ethane	305	4.88	203
Propylene	365	4.62	233
Propane	370	4.24	217
Ammonia	406	11.3	235
Water	647	22.0	322

Solvents with $T_c < 373$ K have been well studied. Most promising, particularly for extraction of undesirable, valuable, or heat-sensitive chemicals from natural products, is CO₂, with its moderate P_c , high critical density, low supercritical

viscosity, high supercritical molecular diffusivity, and T_c close to ambient. Also, it is nonflammable, noncorrosive, inexpensive, nontoxic in low concentrations, readily available, and safe. Separation of CO₂ from the solute is often possible by simply reducing the extract pressure. According to Williams [79], supercritical CO₂ has been used to extract caffeine from coffee, hops oil from beer, piperine from pepper, capsaicin from chilis, oil from nutmeg, and nicotine from tobacco. However, the use of CO₂ for such applications in the U.S. may be curtailed in the future because of an April 2009 endangerment finding by the Environmental Protection Agency (EPA) that CO₂ is a pollutant that threatens public health and welfare, and must be regulated.

CO₂ is not always a suitable solvent, however. McHugh and Krukonic [81] cite the energy crisis of the 1970s that led to substantial research on an energy-efficient separation of ethanol and water. The goal, which was to break the ethanol-water azeotrope, was not achieved by SFE with CO₂ because, although supercritical CO₂ has unlimited capacity to dissolve pure ethanol, water is also dissolved in significant amounts. A supercritical-fluid phase diagram for the ethanol–water–CO₂ ternary system at 308.2 K and 10.08 MPa, based on the data of Takishima et al. [82], is given in Figure 11.43. These conditions correspond to $T_r = 1.014$ and $P_r = 1.366$ for CO₂. For the mixture of water and CO₂, two phases exist: a water-rich phase with about 2 mol% CO₂ and a CO₂-rich phase with about 1 mol% water. Ethanol and CO₂ are mutually soluble. Ternary mixtures containing more than 40 mol% ethanol are completely miscible.

If a near-azeotropic mixture of ethanol and water, say, 85 mol% ethanol and 15 mol% water, is extracted by CO₂ at the conditions of Figure 11.43, a mixing line drawn between this composition and a point for pure CO₂ does not cross into the two-phase region, so no separation is possible at these conditions. Alternatively, consider an ethanol–water broth from a fermentation reactor with 10 wt% (4.17 mol%) ethanol. If this mixture is extracted with supercritical CO₂, complete dissolution will not occur and a modest degree of separation of ethanol from water can be achieved, as shown in the next

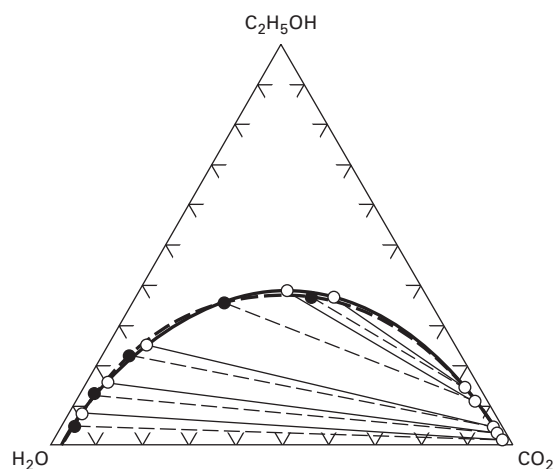


Figure 11.43 Liquid–fluid equilibria for CO₂–C₂H₅OH–H₂O at 308–313.2 K and 10.1–10.34 MPa.

example. The separation can be enhanced by a cosolvent (e.g., glycerol) to improve selectivity, as shown by Inomata et al. [83].

When CO₂ is used as a solvent, it must be recovered and recycled. Three schemes, discussed by McHugh and Krukonis [81], are shown in Figure 11.44. In the first scheme for separation of ethanol and water, the ethanol–water feed is pumped to the pressure of the extraction column, where it is contacted with supercritical CO₂. The raffinate leaving

the extractor bottom is enriched with respect to water and is sent to another location for further processing. The top extract stream, containing most of the CO₂, some ethanol, and a smaller amount of water, is expanded across a valve to a lower pressure. In a flash drum downstream of the valve, ethanol–water condensate is collected and the CO₂-rich gas is recycled through a compressor back to the extractor. Unless pressure is greatly reduced across the valve, which results in high compression costs, little ethanol condenses.

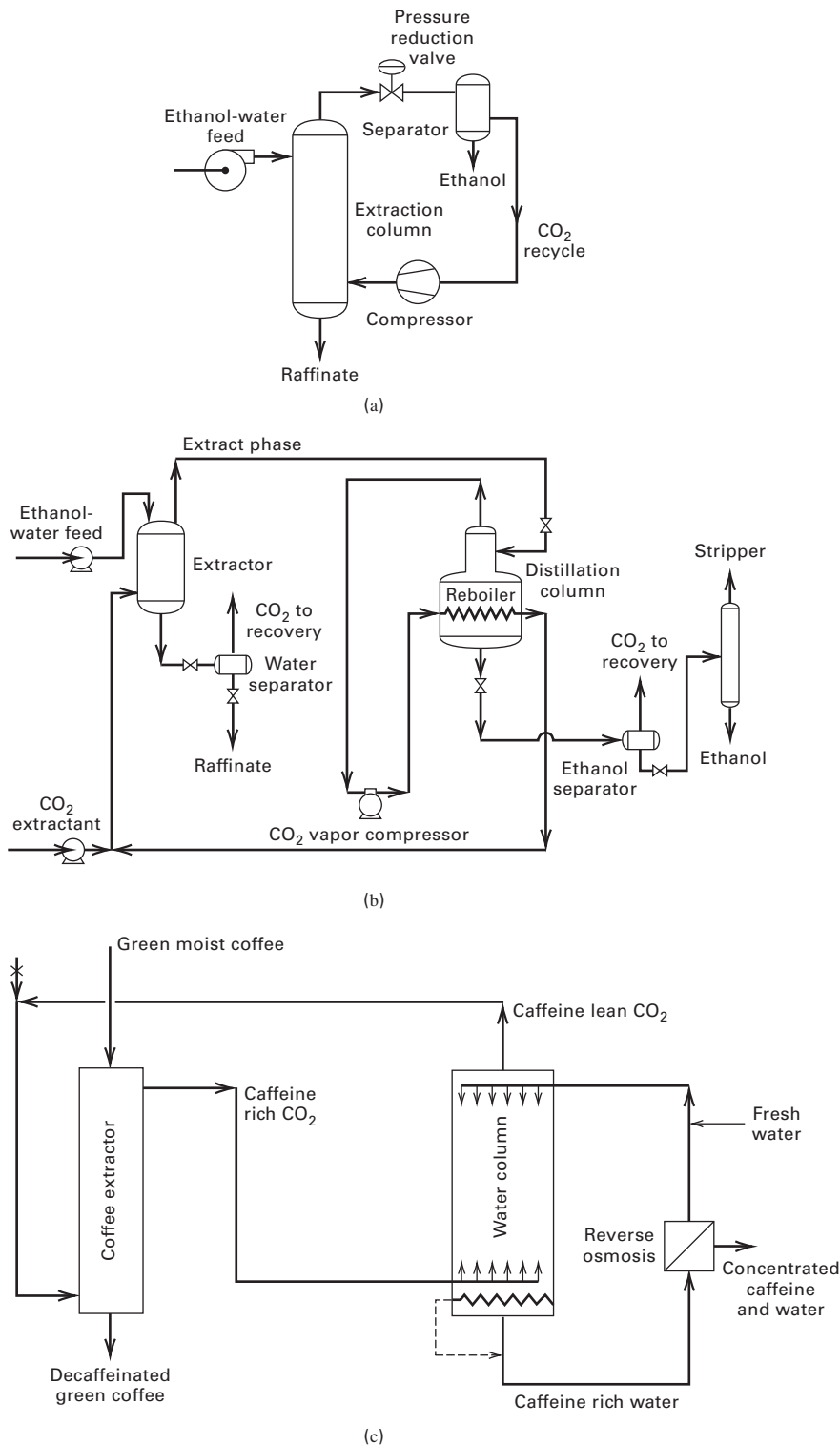


Figure 11.44 Recovery of CO₂ in supercritical extraction processes. (a) Pressure reduction. (b) High-pressure distillation. (c) High-pressure absorption with water.

A second CO₂ recovery scheme, due to de Filippi and Vivian [84], is given in Figure 11.44b. The flash drum is replaced by high-pressure distillation, at just below the pressure of the extraction column, to produce a CO₂-rich distillate and an ethanol-rich bottoms. The distillate is compressed and recycled through the reboiler back to the extractor. Both raffinate and distillate are flashed to recover CO₂. This scheme, though more complicated than the first, is more versatile.

A third CO₂-recovery scheme, due to Katz et al. [85] for coffee decaffeination, is shown in Figure 11.44c. In the extractor, green, wet coffee beans are mixed with supercritical CO₂ to extract caffeine. The extract is sent to a second column, where the caffeine is recovered with water. The CO₂-rich raffinate is recycled through a compressor (not shown) back to the first column, from which the decaffeinated coffee leaves from the bottom and is sent to a roaster. The caffeine-rich water leaving the second column is sent to a reverse-osmosis unit, where the water is purified and recycled to the water column. All three separation steps operate at high pressure. The concentrated caffeine-water mixture leaving the osmosis unit is sent to a crystallizer.

Multiple equilibrium stages are generally needed to achieve the desired extent of extraction. A major problem in determining the number of stages is the estimation of liquid supercritical-fluid phase-equilibrium constants. Most commonly, cubic-equation-of-state methods, such as the Soave-Redlich-Kwong (SRK) or Peng-Robinson (PR) equations are used, but they have two shortcomings. First, their accuracy diminishes in the critical region. Second, for polar components that form a nonideal-liquid mixture, appropriate mixing rules that provide a correct bridge between equation-of-state methods and activity-coefficient methods must be employed, e.g., Wong and Sandler [86], described next.

First consider the SRK and PR equations, discussed in §2.5.2 and §2.5.3. For pure components, they contain two parameters, a and b , computed from critical constants. They are extended to mixtures by **mixing rules** for computing values of a_m and b_m from values for the pure components. The simplest mixing rules, due to van der Waals, are:

$$a_m = \sum_{i=1}^C \sum_{j=1}^C x_i x_j a_{ij} \quad (11-19)$$

$$b_m = \sum_{i=1}^C \sum_{j=1}^C x_i x_j b_{ij} \quad (11-20)$$

where x is a mole fraction in the vapor or liquid. Although these two mixing rules are identical in form, the following **combining rules** for a_{ij} and b_{ij} are different, with the former being a geometric mean and the latter an arithmetic mean:

$$a_{ij} = (a_i a_j)^{1/2} \quad (11-21)$$

$$b_{ij} = (b_i + b_j)/2 \quad (11-22)$$

As stated by Sandler, Orbey, and Lee [87], (11-19) to (11-22) are usually adequate for nonpolar mixtures of hydrocarbons

and light gases when critical temperature and/or size differences between molecules are not large.

Molecular-size differences and/or modest degrees of polarity are better handled by the following combining rules:

$$a_{ij} = (a_i a_j)^{1/2} (1 - k_{ij}) \quad (11-23)$$

$$b_{ij} = [(b_i + b_j)/2] (1 - l_{ij}) \quad (11-24)$$

where k_{ij} and l_{ij} are binary interaction parameters back-calculated from vapor-liquid equilibrium and/or density data. Often the latter parameter is set equal to zero. Values of k_{ij} suitable for use with the SRK and PR equations when the mixture contains hydrocarbons with CO₂, H₂S, N₂, and/or CO are given by Knapp et al. [88]. In a study by Shibata and Sandler [89], using experimental phase-equilibria and phase-density data for the nonpolar binary system nitrogen-*n*butane at 410.9 K over a pressure range of 30 to 70 bar, good predictions, except in the critical region, were obtained using (11-19) and (11-20), with (11-23) and (11-24), and values of $k_{ij} = -0.164$ and $l_{ij} = -0.233$ in conjunction with the PR equation. Similar good agreement with experimental data was obtained for the systems N₂-cyclohexane, CO₂-*n*butane, and CO₂-cyclohexane, and the ternary systems N₂-CO₂-*n*butane and N₂-CO₂-cyclohexane.

For high pressures and mixtures with one or more strongly polar components, the preceding rules are inadequate, and it is desirable to combine the equation-of-state method with the activity-coefficient method to handle liquid nonidealities. The following theoretically based mixing rule of Wong and Sandler [86] provides the combination. If the PR equation of state and the NRTL activity-coefficient equation are used, the Wong and Sandler mixing rule leads to the following expressions for computing a_m and b_m for the PR equation:

$$a_m = RTQD/(1 - D) \quad (11-25)$$

$$b_m = Q/(1 - D) \quad (11-26)$$

$$Q = \sum_{i=1}^C \sum_{j=1}^C x_i x_j \left(b - \frac{a}{RT} \right)_{ij} \quad (11-27)$$

$$D = \sum_{i=1}^C x_i \frac{a_i}{b_i RT} + \frac{G^{ex}(x_i)}{\sigma RT} \quad (11-28)$$

$$\left(b - \frac{a}{RT} \right)_{ij} = \frac{1}{2} \left[\left(b_i - \frac{a_i}{RT} \right) + \left(b_j - \frac{a_j}{RT} \right) \right] (1 - k_{ij}) \quad (11-29)$$

$$\sigma = \frac{1}{\sqrt{2}} \left[\ln(\sqrt{2} - 1) \right] \quad (11-30)$$

$$\frac{G^{ex}}{RT} = \sum_{i=1}^C x_i \left(\frac{\sum_{j=1}^C x_j \tau_{ji} g_{ji}}{\sum_{k=1}^C x_k g_{ki}} \right) \quad (11-31)$$

$$g_{ij} = \exp(-\alpha_{ij} \tau_{ij}) \quad (11-32)$$

with $a_{ij} = a_{ji}$.

Table 11.6 Calculated Flow and Composition Profiles for Example 11.10

Leaving Streams	Stage 1		Stage 2		Stage 3		Stage 4		Stage 5	
	Extract Mole Fraction	Raffinate Mole Fraction	Extract Mole Fraction	Raffinate Mole Fraction	Extract Mole Fraction	Raffinate Mole Fraction	Extract Mole Fraction	Raffinate Mole Fraction	Extract Mole Fraction	Raffinate Mole Fraction
Carbon dioxide	0.98999	0.02870	0.99002	0.02870	0.99012	0.02870	0.99043	0.02870	0.99138	0.02874
Ethanol	0.00466	0.04053	0.00463	0.04023	0.00452	0.03929	0.00419	0.03645	0.00319	0.02775
Water	0.00535	0.93077	0.00535	0.93107	0.00536	0.93201	0.00538	0.93485	0.00543	0.94351
Total flow, mol/s	3.0013	1.0298	3.0311	1.0294	3.0308	1.0285	3.0298	1.0255	3.0268	0.9987

Equations (11-25) to (11-32) show that for a binary system using the NRTL equation, there are four adjustable binary interaction parameters (BIPs): k_{ij} , α_{ij} , τ_{ij} , and τ_{ji} . For a temperature and pressure range of interest, these parameters are best obtained by regression of experimental binary-pair data for VLE, LLE, and/or VLLE. The parameters can be used to predict phase equilibria for ternary and higher multicomponent mixtures. However, Wong, Orbey, and Sandler [90] show that when values of the latter three parameters are already available, even at just near-ambient temperature and pressure conditions from a data source such as Gmehling and Onken [91], those parameters can be assumed independent of temperature and used to make reasonably accurate predictions of phase equilibria, even at temperatures to at least 200°C and pressures to 200 bar. Regression of experimental data to obtain a value of k_{ij} is also not necessary, because Wong, Orbey, and Sandler show that it can be determined from the other three parameters by choosing its value so that the excess Gibbs free energy from the equation of state matches that from the activity-coefficient model. Thus, application of the Wong–Sandler mixing rule to supercritical extraction is facilitated.

Another phase-equilibrium prediction method applicable to wide ranges of pressure, temperature, molecular size, and polarity is the group-contribution equation of state (GC-EOS) of Skjold-Jørgensen [92]. This method, which combines features of the van der Waals equation of state, the Carnahan-Starling expression for hard spheres, the NRTL activity-coefficient equation, and the group-contribution principle, has been applied to SFE conditions, and is useful when all necessary binary data are not available.

When experimental K -values are available, or when the Wong–Sandler mixing rule or the GC-EOS can be applied, stage calculations for supercritical extraction can be made using process simulators, as in the next example.

EXAMPLE 11.10 SFE of Ethanol with CO₂.

One mol/s of 10 wt% ethanol in water is extracted by 3 mol/s of carbon dioxide at 305 K and 9.86 MPa in a countercurrent-flow extraction column with five equilibrium stages. Determine the flow rates and compositions of the exiting extract and raffinate.

Solution

This problem, taken from Colussi et al. [93], who used the GC-EOS method, was solved with the Tower Plus model of the CHEMCAD process simulator, at constant T and P , where composition changes were small enough that K -values were constant and are defined as the extract mole fraction divided by the raffinate mole fraction. They are in good agreement with experimental data:

Component	K -Value
CO ₂	34.5
Ethanol	0.115
Water	0.00575

The extraction of ethyl alcohol is 33.6%, with an extract of 69 wt% pure ethanol (solvent-free basis) and a raffinate containing 93 wt% water (solvent-free basis). Calculated stagewise flow rates and component mole fractions are listed in Table 11.6, where stages are numbered from the feed end.

CHAPTER 11 NOMENCLATURE

Abbreviations and Acronyms

DAEs	differential algebraic equations, Section 11.1.2
DRD	distillation region diagram, Section 11.1.3
NRC	number of components, (11-18)
nbp	normal boiling point, (1 atm)
NRX	number of reactions, (11-17)
SFE	supercritical fluid extraction, Section 11.8

Latin Symbols

A_p	pre-exponential factor, (11-18)
B	number of binary azeotropes, (11-10)
B_{ib}	number of intermediate-boiling binary azeotropes, Section 11.1.3
$c_{j,q}$	concentration of component q at stage j , (11-18)
E	entrainer, Section 11.5
E_p	activation energy, (11-18)

k_p	reaction rate constant, (11-18)
m	exponent on concentration, (11-18)
N	number of nodes, (11-9)
r	reaction rate, (11-17)
S	number of stable and unstable saddles, (11-9)
(V_{LH})	volumetric liquid holdup, (11-17)
W	moles of liquid residue, (11-1)

SUMMARY

1. Extractive distillation, salt distillation, pressure-swing distillation, homogeneous azeotropic distillation, heterogeneous azeotropic distillation, and reactive distillation are enhanced-distillation techniques to be considered when separation by ordinary distillation is uneconomical or unfeasible. Reactive distillation can be used to conduct, simultaneously and in the same equipment, a chemical reaction and a separation.
2. For ternary systems, a composition plot on a triangular graph is very useful for finding feasible separations, especially when binary and ternary azeotropes form. With such a diagram, distillation paths, called residue curves or distillation curves, are readily tracked. The curves may be restricted to certain regions of the triangular diagram by distillation boundaries. Feasible-product compositions at total reflux are readily determined.
3. Extractive distillation, using a low-volatility solvent that enters near the top of the column, is widely used to separate azeotropes and very close-boiling mixtures. Preferably, the solvent should not form an azeotrope with any feed component.
4. Certain salts, when added to a solvent, reduce the solvent volatility and increase the relative volatility between the two feed components. In this process, called salt distillation, the salt is dissolved in the solvent or added as a solid or melt to the reflux.
5. Pressure-swing distillation, utilizing two columns operating at different pressures, can be used to separate an azeotropic mixture when the azeotrope can be made to disappear at some pressure. If not, it may still be practical

Greek Symbols

ξ	dimensionless time, (11-2)
ζ	stoichiometric coefficient, (11-17)

Subscripts

o	at $t = 0$
-----	------------

if the azeotropic composition changes by 5 mol% or more over a moderate range of pressure.

6. In homogeneous azeotropic distillation, an entrainer is added to a stage, usually above the feed stage. A minimum- or maximum-boiling azeotrope, formed by the entrainer with one or more feed components, is removed from the top or bottom of the column. Applications of this technique for difficult-to-separate mixtures are not common because of limitations due to distillation boundaries.
7. A more common and useful technique is heterogeneous azeotropic distillation, in which the entrainer forms, with one or more components of the feed, a minimum-boiling heterogeneous azeotrope. When condensed, the overhead vapor splits into organic-rich and water-rich phases. The azeotrope is broken by returning one liquid phase as reflux, with the other sent on as distillate for further processing.
8. A growing application of reactive distillation is to combine chemical reaction and distillation in one column. To be effective, the reaction and distillation must be feasible at the same pressure and range of temperature, with reactants and products favoring different phases so that an equilibrium-limited reaction can go to completion.
9. Liquid-liquid or solid-liquid extraction can be carried out with a supercritical-fluid solvent at temperatures and pressures just above critical because of favorable values for solvent density and viscosity, solute diffusivity, and solute solubility in the solvent. An attractive supercritical solvent is carbon dioxide, particularly for extraction of certain chemicals from natural products.

REFERENCES

1. STICHLMAIR, J., J.R. FAIR, and J.L. BRAVO, *Chem. Eng. Progress*, **85**(1), 63–69 (1989).
2. PARTIN, L.R., *Chem. Eng. Progress*, **89**(1), 4348 (1993).
3. STICHLMAIR, J., Distillation and Rectification, in *Ullmanns Encyclopedia of Industrial Chemistry*, 5th ed., VCH Verlagsgesellschaft Weinheim Vol. B3, pp. 4–1 to 4–94 (1988).
4. DOHERTY, M.F., and J.D. PERKINS, *Chem. Eng. Sci.*, **33**, 281–301 (1978).
5. BOSSEN, B.S., S.B. JØRGENSEN, and R. GANI, *Ind. Eng. Chem. Res.*, **32**, 620–633 (1993).
6. PHAM, H.N., and M.F. DOHERTY, *Chem. Eng. Sci.*, **45**, 1837–1843 (1990).
7. TAYLOR, R., and H.A. KOIJMAN, *CACHE News*, No. **41**, 13–19 (1995).
8. DOHERTY, M.F., *Chem. Eng. Sci.*, **40**, 1885–1889 (1985).
9. ASPEN PLUS, What's New in Release 9, Aspen Technology, Cambridge, MA (1994).
10. DOHERTY, M.F., and J.D. PERKINS, *Chem. Eng. Sci.*, **34**, 1401–1414 (1979).
11. HORSLEY, L.H., "Azeotropic Data III," in *Advances in Chemistry Series*, American Chemical Society, Washington, D.C., Vol. 116 (1973).
12. GMEHLING, J., J. MENKE, J. KRAFCZYK, and K. FISCHER, *Azeotropic Data*, 2nd ed. in 3 volumes, Wiley-VCH, Weinheim, Germany (2004).
13. FIDKOWSKI, Z.T., M.F. MALONE, and M.F. DOHERTY, *Computers Chem. Engng.*, **17**, 1141–1155 (1993).

14. FOUCHER, E.R., M.F. DOHERTY, and M.F. MALONE, *Ind. Eng. Chem. Res.*, **30**, 760772 (1991) and **30**, 23–64 (1991).
15. MATSUYAMA, H., and H.J. NISHIMURA, *J. Chem. Eng. Japan*, **10**, 181 (1977).
16. DOHERTY, M.F., and G.A. CALDAROLA, *Ind. Eng. Chem. Fundam.*, **24**, 474–485 (1985).
17. FIDKOWSKI, Z.T., M.F. DOHERTY, and M.F. MALONE, *AIChE J.*, **39**, 1303–1321 (1993).
18. STICHLMAIR, J.G., and J.-R. HERGUIJUELA, *AIChE J.*, **38**, 1523–1535 (1992).
19. WIDAGDO, S., and W.D. SEIDER, *AIChE J.*, **42**, 96–130 (1996).
20. WAHNSCHAFFT, O.M., J.W. KOEHLER, E. BLASS, and A.W. WESTERBERG, *Ind. Eng. Chem. Res.*, **31**, 2345–2362 (1992).
21. DUNN, C.L., R.W. MILLAR, G.J. PIEROTTI, R.N. SHIRAS, and M. SOUDERS, Jr., *Trans. AIChE*, **41**, 631–644 (1945).
22. BERG, L., *Chem. Eng. Progress*, **65**(9), 52–57 (1969).
23. OTHMER, D.F., *AIChE Symp. Series*, **235**(79), 90–117 (1983).
24. VAN, RAYMBEKE U.S. Patent 1, 474, 216 (1922).
25. COOK, R.A., and W.F. FURTER, *Can. J. Chem. Eng.*, **46**, 119–123 (1968).
26. JOHNSON, A.I., and W.F. FURTER, *Can. J. Chem. Eng.*, **43**, 356–358 (1965).
27. JOHNSON, A.I., and W.F. FURTER, *Can. J. Chem. Eng.*, **38**, 78–87 (1960).
28. FURTER, W.F., and R.A. COOK, *Int. J. Heat Mass Transfer*, **10**, 23–36 (1967).
29. FURTER, W.F., *Can. J. Chem. Eng.*, **55**, 229–239 (1977).
30. FURTER, W.F., *Chem. Eng. Commun.*, **116**, 35 (1992).
31. KUMAR, A., *Sep. Sci. and Tech.*, **28**, 1799–1818 (1993).
32. MAHAPATRA, A., V.G. GAIKAR, and M.M. SHARMA, *Sep. Sci. and Tech.*, **23**, 429–436 (1988).
33. AGARWAL, M., and V.G. GAIKAR, *Sep. Technol.*, **2**, 79–84 (1992).
34. KNAPP, J.P., and M.F. DOHERTY, *Ind. Eng. Chem. Res.*, **31**, 346–357 (1992).
35. LEWIS, W.K., U.S. Patent 1, 676, 700 (1928).
36. VAN WINKLE, M., *Distillation*, McGraw-Hill, New York (1967).
37. ROBINSON, C.S., and E.R. GILLILAND, *Elements of Fractional Distillation*, 4th ed., McGraw-Hill, New York (1950).
38. WAHNSCHAFFT, O.M., and A.W. WESTERBERG, *Ind. Eng. Chem. Res.*, **32**, 1108 (1993).
39. LAROCHE, L., N. BEKIARIS, H.W. ANDERSEN, and M. MORARI, *AIChE J.*, **38**, 1309 (1992).
40. YOUNG, S., *J. Chem. Soc. Trans.*, **81**, 707–717 (1902).
41. KEYES, D.B., U.S. Patent 1, 676, 735 (1928).
42. KEYES, D.B., *Ind. Eng. Chem.*, **21**, 998–1001 (1929).
43. BEKIARIS, N., G.A. MESKI, and M. MORARI, *Ind. Eng. Chem. Res.*, **35**, 207–217 (1996).
44. PROKOPAKIS, G.J., and W.D. SEIDER, *AIChE J.*, **29**, 49–60 (1983).
45. RYAN, P.J., and M.F. DOHERTY, *AIChE J.*, **35**, 1592–1601 (1989).
46. PHAM, H.N., and M.F. DOHERTY, *Chem. Eng. Sci.*, **45**, 1845–1854 (1990).
47. KOVACH, III, J.W., and W.D. SEIDER, *Computers and Chem. Engng.*, **11**, 593 (1987).
48. SWARTZ, C.L.E., and W.E. STEWART, *AIChE J.*, **33**, 1977–1985 (1987).
49. GANI, R., and S.B. JØRGENSEN, *Computers and Chem. Engng.*, **18**, Suppl., S55 (1994).
50. SHEWCHUK, C.F., “Computation of Multiple Distillation Towers,” Ph.D. Thesis, University of Cambridge (1974).
51. MAGNUSSEN, T., M.L. MICHELSEN, and A. FREDENSLUND, *Inst. Chem. Eng. Symp. Series No. 56, Third International Symp. on Distillation*, Rugby, England (1979).
52. BEKIARIS, N., G.A. MESKI, C.M. RADU, and M. MORARI, *Ind. Eng. Chem. Res.*, **32**, 2023–2038 (1993).
53. BLACK, C., and D.E. DITSLER, *Advances in Chemistry Series*, ACS, Washington, D.C., Vol. 115, pp. 115 (1972).
54. BLACK, C., R.A. GOLDING, and D.E. DITSLER, *Advances in Chemistry Series*, ACS, Washington, D.C., Vol. 115, pp. 64–92 (1972).
55. BLACK, C., *Chem. Eng. Progress*, **76**(9), 78–85 (1980).
56. BLACK, C., *Ind. Eng. Chem.*, **50**, 403–412 (1958).
57. TERRILL, D.L., L.F. SYLVESTRE, and M.F. DOHERTY, *Ind. Eng. Chem. Proc. Des. Develop.*, **24**, 1062–1071 (1985).
58. ROBINSON, C.S., and E.R. GILLILAND, *Elements of Fractional Distillation*, 4th ed., McGraw-Hill, New York (1950).
59. BACKHAUS, A.A., U.S. Patent 1,400,849 (1921).
60. LEYES, C.E., and D.F. OTHMER, *Trans. AIChE*, **41**, 157–196 (1945).
61. BELCK, L.H., *AIChE J.*, **1**, 467–470 (1955).
62. MASAMOTO, J., and K. MATSUZAKI, *J. Chem. Eng. Japan*, **27**, 1–5 (1994).
63. AGREDA, V.H., and L.R. PARTIN, U.S. Patent 4,435,595 (March 6, 1984).
64. AGREDA, V.H., L.R. PARTIN, and W.H. HEISE, *Chem. Eng. Prog.*, **86**(2), 40–46 (1990).
65. SMITH, L.A., U.S. Patent 4,307,254 (Dec. 22, 1981).
66. SMITH, L.A., U.S. Patent 4,443,559 (April 17, 1984).
67. SMITH, L.A., U.S. Patent 4,978,807 (Dec. 18, 1990).
68. DEGARMO, J.L., V.N. PARULEKAR, and V. PINJALA, *Chem. Eng. Prog.*, **88**(3), 4350 (1992).
69. CHANG, Y.A., and J.D. SEADER, *Computers and Chem. Engng.*, **12**, 1243–1255 (1988).
70. VENKATARAMAN, S., W.K. CHAN, and J.F. BOSTON, *Chem. Eng. Progress*, **86**(8), 45–54 (1990).
71. SIMANDL, J., and W.Y. SVRCEK, *Computers and Chem. Engng.*, **15**, 337–348 (1991).
72. KANG, Y.W., Y.Y. LEE, and W.K. LEE, *J. Chem. Eng. Japan*, **25**, 649–655 (1992).
73. IZARRARAZ, A., G.W. BENTZEN, R. G. ANTHONY, and C.D. HOLLAND, *Hydrocarbon Processing*, **59**(6), 195 (1980).
74. REHFINGER, A., and U. HOFFMANN, *Chem. Eng. Sci.*, **45**, 1605–1617 (1990).
75. JACOBS, R., and R. KRISHNA, *Ind. Eng. Chem. Res.*, **32**, 1706–1709 (1993).
76. NIJHUIS, S.A., F.P.J.M. KERKHOF, and N.S. MAK, *Ind. Eng. Chem. Res.*, **32**, 2767–2774 (1993).
77. HAUAN, S., T. HERTZBERG, and K.M. LIEN, *Ind. Eng. Chem. Res.*, **34**, 987–991 (1995).
78. HANNAY, J.B., and J. HOGARTH, *Proc. Roy. Soc. (London) Sec. A*, **29**, 324 (1879).
79. WILLIAMS, D.F., *Chem. Eng. Sci.*, **36**, 1769–1788 (1981).
80. MCHUGH, M., and V. KRUKONIS, *Supercritical Fluid Extraction—Principles and Practice*, Butterworths, Boston (1986).
81. MCHUGH, M., and V. KRUKONIS, *Supercritical Fluid Extraction—Principles and Practice*, 2nd ed., Butterworth-Heinemann, Boston (1994).
82. TAKISHIMA, S., A. SAIKI, K. ARAI, and S. SAITO, *J. Chem. Eng. Japan*, **19**, 48–56 (1986).

83. INOMATA, H., A. KONDO, K. ARAI, and S. SAITO, *J. Chem. Eng. Japan*, **23**, 199–207 (1990).
84. DE FILLIPI, R.P., and J.E. VIVIAN, U.S. Patent 4,349,415 (1982).
85. KATZ, S.N., J.E. SPENCE, M.J. O'BRIAN, R.H. SKIFF, G.J. VOGEL, and R. PRASAD, U.S. Patent 4,911,941 (1990).
86. WONG, D.S.H., and S.I. SANDLER, *AIChE J.*, **38**, 671–680 (1992).
87. SANDLER, S.I., H. ORBEY, and B.-I. LEE, in S.I. Sandler, Ed., *Models for Thermodynamic and Phase Equilibria Calculations*, Marcel Dekker, New York, pp. 87–186 (1994).
88. KNAPP, H., R. DORING, L. OELLRICH, U. PLOCKER, and J.M. PRAUSNITZ, *Vapor-Liquid Equilibria for Mixtures of Low Boiling Substances*, Chem. Data Ser., Vol. VI, DECHEMA, pp. 771–793 (1982).
89. SHIBATA, S.K., and S.I. SANDLER, *Ind. Eng. Chem. Res.*, **28**, 1893–1898 (1989).
90. WONG, D.S.H., H. ORBEY, and S.I. SANDLER, *Ind. Eng. Chem. Res.*, **31**, 2033–2039 (1992).
91. GMEHLING, J., and U. ONKEN, *Vapor-Liquid Equilibrium Data Compilation*, DECHEMA Data Series, DECHEMA, Frankfurt (1977).
92. SKJOLD-JØRGENSEN, S., *Ind. Eng. Chem. Res.*, **27**, 110–118 (1988).
93. COLUSSI, I.E., M. FERMEGLIA, V. GALLO, and I. KIKIC, *Computers Chem. Engng.*, **16**, 211–224 (1992).
94. DOHERTY, M.F., and M.F. MALONE, *Conceptual Design of Distillation Systems*, McGraw-Hill, New York (2001).
95. STICHLMAIR, J.G., and J.R. FAIR, *Distillation Principles and Practices*, Wiley-VCH, New York (1998).
96. SIROLA, J.J., and S.D. BARNICKI, in R.H. Perry and D.W. Green, Eds., *Perry's Chemical Engineers Handbook*, 7th ed. McGraw-Hill, New York, pp. 13–54 to 13–85 (1997).
97. ECKERT, E., and M. KUBICEK, *Computers Chem. Eng.*, **21**, 347–350 (1997).
98. HOFFMASTER, W.R., and S. HAUAN, *AIChE J.*, **48**, 2545–2556 (2002).
99. LLANO-RESTREPO, M., and J. AGUILAR-ARIAS, *Computers Chem. Engng.*, **27**, 527–549 (2003).
100. FU, J., *AIChE J.*, **42**, 3364–3372 (1996).
101. HUSS, R.S., F. CHEN, M.F. MALONE, and M.F. DOHERTY, *Computers Chem. Engng.*, **27**, 1855–1866 (2003).

STUDY QUESTIONS

- 11.1. What is meant by enhanced distillation? When should it be considered?
- 11.2. What is the difference between extractive distillation and azeotropic distillation?
- 11.3. What is the difference between homogeneous and heterogeneous azeotropic distillation?
- 11.4. What are the main reasons for conducting reactive distillation?
- 11.5. What is a distillation boundary? Why is it important?
- 11.6. To what type of a distillation does a residue curve apply? What is a residue-curve map?
- 11.7. Is a residue curve computed from an algebraic or a differential equation? Does a residue curve follow the composition of the distillate or the residue?
- 11.8. Residue curves involve nodes. What is the difference between a stable and an unstable node? What is a saddle?
- 11.9. What is a distillation-curve map? How does it differ from a residue-curve map?
- 11.10. What is a region of feasible-product compositions? How is it determined? Why is it important?
- 11.11. Under what conditions can a distillation boundary be crossed by a material-balance line?
- 11.12. In extractive distillation, why is a large concentration of solvent required in the liquid phase? Why doesn't the solvent enter the column at the top tray?
- 11.13. Why is heterogeneous azeotropic distillation a more feasible technique than homogeneous azeotropic distillation?
- 11.14. What is meant by multiplicity? What kinds of multiplicity are there? Why is it important to obtain all multiple solutions when they exist?
- 11.15. In reactive distillation, does the reaction preferably take place in the vapor or in the liquid phase? Can a homogeneous or solid catalyst be used?
- 11.16. What happens to the solvent power of a compressed gas as it passes through the critical region? What happens to physical properties in the critical region?
- 11.17. Why is CO₂ a desirable solvent for SFE?

EXERCISES

Section 11.1

11.1. Approximate residue-curve map.

The *n*-hexane-methanol–methyl acetate system at 1 atm forms the following three binary azeotropes and one ternary azeotrope.

At 1 atm, the molecular weights and normal boiling points of the three components are:

Component	Molecular Weight	Boiling Point, °C
<i>n</i> -Hexane	86.17	69.0
Methanol	32.04	64.7
Methyl acetate	74.08	57.0

Binary azeotropes (all minimum boiling):

Mixture, A/B	Boiling Point, °C	Wt% A/B	Mol% A/B
<i>n</i> -Hexane/Methanol	50.6	72.1/27.9	49.0/51.0
<i>n</i> -Hexane/Methyl acetate	51.8	39.3/60.7	35.8/64.2
Methanol/Methyl acetate	53.5	19.0/81.0	35.2/64.8

Ternary azeotrope (minimum boiling):

Mixture, A/B/C	Boiling Point, °C	Wt% A/B/C	Mol% A/B/C
<i>n</i> -Hexane/ Methanol/ Methyl acetate	47.4	48.6/14.6/36.8	37.2/30.1/32.7

Sketch an approximate residue-curve map on a right-triangular diagram and indicate the distillation boundaries. Determine for each azeotrope and pure component whether it is a stable node, an unstable node, or saddle.

11.2. Calculation of a residue curve.

For the system in Exercise 11.1, use a process simulator with the UNIFAC equation to calculate a portion of a residue curve at 1 atm starting from a bubble-point liquid with 20 mol% *n*-hexane, 60 mol% methanol, and 20 mol% methyl acetate.

11.3. Calculation of a distillation curve.

For the same conditions as in Exercise 11.2, use a process simulator with the UNIFAC equation to calculate a portion of a distillation curve at 1 atm.

11.4. Distillation boundaries.

The acetone, benzene, and *n*-heptane system at 1 atm forms two binary azeotropes. Sketch a distillation curve map on an equilateral-triangle diagram, and indicate the distillation boundaries. Determine for each azeotrope and pure component whether it is a stable node, an unstable node, or saddle.

At 1 atm, the molecular weights and normal boiling points of the three components are:

Component	Molecular Weight	Boiling Point, °C
<i>n</i> -Heptane	100.2	98.4
Benzene	78.11	80.1
Acetone	58.08	56.5

Binary azeotropes (all minimum boiling):

Mixture, A/B	Boiling Point, °C	Wt% A/B	Mol% A/B
<i>n</i> -Heptane/Benzene	80.1	0.7/99.3	0.5/99.5
<i>n</i> -Heptane/Acetone	55.9	10.5/89.5	6.5/93.5
Benzene/Acetone	No azeotrope		

No ternary azeotrope

11.5. Calculation of a residue curve.

For the same ternary system as in Exercise 11.4, use a process simulator with UNIFAC to calculate a portion of a residue curve at 1 atm starting from a bubble-point liquid composed of 20 mol% acetone, 60 mol% benzene, and 20 mol% *n*-heptane.

11.6. Calculation of a distillation curve.

For the same conditions as in Exercise 11.5, use a process simulator with the UNIFAC equation to calculate a portion of a distillation curve at 1 atm.

11.7. Feasible-product-composition regions.

Develop the feasible-product-composition regions for the system of Figure 11.13, using feed F_1 .

11.8. Feasible-product-composition regions.

Develop the feasible-product-composition regions for the system of Figure 11.10 if the feed is 50 mol% chloroform, 25 mol% methanol, and 25 mol% acetone.

Section 11.2

11.9. Extractive distillation with ethanol.

Repeat Example 11.3, but with ethanol as the solvent. Use a process simulator with the UNIFAC method for K -values.

11.10. Extractive distillation with MEK.

Repeat Example 11.3, but with MEK as the solvent. Use a process simulator with the UNIFAC method for K -values.

11.11. Extractive distillation with toluene.

Repeat Example 11.3, but with toluene as the solvent. Use a process simulator with the UNIFAC method for K -values.

11.12. Extractive distillation with phenol.

Four hundred lbmol/h of an equimolar mixture of *n*-heptane and toluene at 200°F and 20 psia is to be separated by extractive distillation at 20 psia, using phenol at 220°F as the solvent, at a flow rate of 1,200 lbmol/h. Using a process simulator with the UNIFAC method for K -values, design a suitable two-column system to obtain reasonable product purities with minimal solvent loss.

Section 11.4

11.13. Pressure-swing distillation.

Repeat Example 11.5, using a process simulator with the UNIFAC method for K -values, for a feed of 100 mol/s of 55 mol% ethanol and 45 mol% benzene.

11.14. Pressure-swing distillation.

Determine the feasibility of separating 100 mol/s of a mixture of 20 mol% ethanol and 80 mol% benzene by pressure-swing distillation. If feasible, design such a system. Employ a process simulator with the UNIFAC method for K -values. First apply the FUG method to obtain initial estimates of stage and reflux ratio requirements. Then, complete the design with rigorous calculations.

11.15. Pressure-swing distillation.

Design a pressure-swing distillation system to produce 99.8 mol% ethanol for 100 mol/s of an aqueous feed containing 30 mol% ethanol. Employ a process simulator with the UNIFAC method for K -values using the procedure of Exercise 11.14.

Section 11.5

11.16. Homogeneous azeotropic distillation.

In Example 11.6, a mixture of benzene and cyclohexane is separated in a sequence of separation steps that begins with homogeneous azeotropic distillation using acetone as the entrainer. Using a process simulator with the Wilson equation for K -values, produce the best design you can.

11.17. Homogeneous azeotropic distillation.

Devise a separation sequence to separate 100 mol/s of an equimolar mixture of toluene and 2,5-dimethylhexane into nearly pure products. Include in the sequence a homogeneous azeotropic distillation column using methanol as the entrainer and determine a feasible design for that column. Use a process simulator with the UNIFAC method to compute K -values.

11.18. Homogeneous azeotropic distillation.

A mixture of 16,500 kg/h of 55 wt% methyl acetate and 45 wt% methanol is to be separated into 99.5 wt% methyl acetate and 99 wt% methanol. Use of one homogeneous azeotropic distillation column and one ordinary distillation column has been suggested. Possible entrainers are *n*-hexane, cyclohexane, and toluene. Determine feasibility of using *n*-hexane as the entrainer for the sequence. If feasible, use a process simulator with the UNIFAC method to estimate K -values to prepare a design. If not, consider one of the other two suggested entrainers. The following data are available.

The molecular weights and normal boiling points of the five components of interest are:

Component	Molecular Weight	Boiling Point, °C
Methyl acetate, A	74.08	57.1
Methanol, M	32.04	64.7
<i>n</i> -Hexane, H	86.17	69.0
Cyclohexane, C	84.16	80.7
Toluene, T	92.13	110.8

From the *Handbook of Chemistry and Physics*, the homogeneous binary azeotropes are:

Binary pair	Boiling Point, °C	Mol%
A-M	54.0	65.3, 34.7
A-H	51.8	64.2, 35.8
A-C	55.5	80.1, 19.9
M-T	63.7	88.3, 11.7

Also, heterogeneous binary azeotropes are formed by the pairs M-H and M-C. No azeotrope is formed with the pair A-T.

The following two homogeneous ternary azeotropes are formed. No ternary azeotrope is formed by A-M-T.

Ternary system	Boiling Point, °C	Mol%
A-M-H	45.0	24.5, 29.4, 46.1
A-M-C	50.8	40.7, 34.5, 24.8

Section 11.6

11.19. Heterogeneous azeotropic distillation.

Use a process simulator to design a three-column distillation sequence to separate 150 mol/s of an azeotropic mixture of ethanol and water at 1 atm into nearly pure ethanol and nearly pure water using heterogeneous azeotropic distillation with benzene as the entrainer. *K*-values are correlated well with the UNIQUAC method using the following values of $(u_{ij} - u_{ji})$:

$i \downarrow, j \rightarrow$	Water	Benzene	Ethanol
Water	----	719.890	405.036
Benzene	1795.85	----	764.780
Ethanol	-65.995	-85.507	----

Using a process simulator, the UNIQUAC method can be used to estimate all homogeneous and heterogeneous azeotropes.

11.20. Heterogeneous azeotropic distillation.

Use a process simulator to design a three-column distillation sequence to separate 120 mol/s of an azeotropic mixture of isopropanol and water at 1 atm into nearly pure isopropanol and nearly pure water using heterogeneous azeotropic distillation with a benzene entrainer. *K*-values are correlated well with the UNIQUAC method using the following values of $(u_{ij} - u_{ji})$:

$i \downarrow, j \rightarrow$	Water	Benzene	Isopropanol
Water	----	719.890	109.550
Benzene	1795.85	----	319.618
Isopropanol	300.190	54.883	----

Using a process simulator, the UNIQUAC method can be used to estimate all homogeneous and heterogeneous azeotropes.

11.21. Heterogeneous azeotropic distillation.

For the heterogeneous azeotropic distillation of Example 11.7, study of the effect of the number of stages and feed-stage location on product purities. Also consider the addition of an Aspen Plus MULT block and a design specification to automatically determine the make-up NPA flow rate, where the make-up is added to the reflux instead of to the feed.

Section 11.7

11.22. Reactive distillation.

Repeat Example 11.9, with the entire range of methanol feed-stage locations. Compare your results for isobutene conversion with the values shown in Figure 11.39.

11.23. Reactive distillation.

Repeat Exercise 11.22, but with activities, instead of mole fractions, in the reaction-rate expressions. Explain the difference in results, if any.

11.24. Reactive distillation.

Repeat Exercise 11.22, but with the assumption of chemical equilibrium on stages where catalyst is employed. Explain how the results differ from Figure 11.39.

Section 11.8

11.25. Supercritical-fluid extraction with CO₂.

Repeat Example 11.10, but with 10 equilibrium stages instead of 5. What is the effect of this change? Explain the results by means of the Kremser method.

11.26. Model for SFE of a solute from particles.

An application of supercritical extraction is the removal of solutes from particles of porous natural materials. Such applications include extraction of caffeine from coffee beans and extraction of ginger oil from ginger root. When CO₂ is used as the solvent, the rate of extraction is found to be independent of flow rate of CO₂ past the particles, but dependent upon the particle size. Develop a mathematical model for the rate of extraction consistent with these observations. What model parameter would have to be determined by experiment?

11.27. SFE of β-carotene with CO₂.

Cygnarowicz and Seider [*Biotechnol. Prog.*, **6**, 82–91 (1990)] present a process for supercritical extraction of β-carotene from water with CO₂, using the GC-EOS method of Skjold-Jørgensen to estimate phase equilibria. Repeat the calculations for their design using a process simulator with the PR EOS and the Wong-Sandler mixing rules. How do the designs compare?

11.28. SFE of acetone from water with CO₂.

Cygnarowicz and Seider [*Ind. Eng. Chem. Res.*, **28**, 1497–1503 (1989)] present a design for the supercritical extraction of acetone from water with CO₂ using the GC-EOS method of Skjold-Jørgensen to estimate phase equilibria. Repeat their design using a process simulator with the PR EOS and the Wong-Sandler mixing rules. How do the designs compare?

Rate-Based Models for Vapor–Liquid Separation Operations

§12.0 INSTRUCTIONAL OBJECTIVES

After completing this chapter, you should be able to:

- Write equations that model a nonequilibrium stage, where equilibrium is assumed only at the interface between phases.
- Explain component-coupling effects in multicomponent mass transfer.
- Explain the bootstrap problem and its application to distillation.
- Select methods for estimating transport coefficients and interfacial areas required for rate-based calculations.
- Explain differences among ideal vapor–liquid flow patterns employed for rate-based calculations.
- Use a process simulator to make rate-based calculations for distillation and other vapor–liquid separation problems.

Equations for equilibrium-based, continuous distillation models were first published by Sorel [1] in 1893. They consisted of total and component material balances around top and bottom sections of equilibrium stages, including a total condenser and a reboiler, and corresponding energy balances with provision for heat losses, which are important for small laboratory columns but not for insulated, industrial columns. Sorel used graphs of phase-equilibrium data instead of equations. Because of the complexity of Sorel's model, it was not widely applied until 1921. Then it was adapted to graphical-solution techniques for binary systems, first by Ponchon and then by Savarit, who used an enthalpy-concentration diagram. In 1925, a much simpler, but less-rigorous, graphical technique was developed by McCabe and Thiele. They eliminated the energy balances by assuming constant vapor and liquid molar flow rates, except across feed or sidestream withdrawal stages. When applicable, the McCabe–Thiele graphical method, presented in Chapter 7, is used, even today, for binary distillation, because it gives valuable insights into changes in phase compositions from stage to stage. McCabe–Thiele plots based on the two key components in multicomponent distillation are also useful to check for optimal feed-stage location.

Because some of Sorel's equations are nonlinear, it is not possible to obtain algebraic solutions unless simplifying assumptions are made. Smoker [2] did that in 1938 for the distillation of a binary mixture by assuming not only constant molar overflow, but also constant relative volatility. Smoker's equation is still useful for superfractionators involving close-boiling binary mixtures, where that assumption is close to being valid. In the early 1930s, two iterative numerical methods were developed for obtaining a solution to Sorel's

model for multicomponent mixtures. The Thiele–Geddes method [3] computes the distillate and bottoms compositions for a specified number of equilibrium stages, feed-stage location, reflux ratio, and distillate flow rate. The Lewis–Matheson method [4] computes the stages required and the feed-stage location for a specified reflux ratio and split between two key components. These two methods were widely used for the simulation and design of single-feed, multicomponent distillation columns prior to the 1960s.

Attempts in the late 1950s and early 1960s to adapt the Thiele–Geddes and Lewis–Matheson methods to digital computers had limited success. The breakthrough in computerization of stage-wise calculations occurred when Amundson and co-workers, starting in 1958, applied matrix algebra techniques. This led to successful computer-aided methods, based on sparse-matrix algebra, using Sorel's equilibrium-based model. The most useful of these models are presented in Chapter 10. Although occasionally the computations fail to converge, the methods are widely used and have become flexible, fast, and robust.

Methods presented in Chapters 10 and 11 assume that equilibrium is achieved at each stage with respect to both heat and mass transfer. The assumption of temperature equality for vapor and liquid phases leaving a stage is usually acceptable. An exception may occur when temperature changes significantly from stage to stage. However, for many industrial applications of distillation, and particularly of absorption and stripping, the assumption of equilibrium of exiting-phase compositions is not accurate. In general, exiting vapor-phase mole fractions are not related to exiting liquid-phase mole fractions by thermodynamic K -values. To overcome this limitation of equilibrium-based models, Lewis [5], in 1922,

proposed an overall stage efficiency for converting theoretical (equilibrium) stages to actual stages. Experimental laboratory and plant data show that efficiency varies, depending on the application, over a range of 5 to 120%. The highest efficiencies are for distillation in large-diameter single-liquid-pass trays because of a crossflow effect, whereas the lowest occur in absorption columns with high-viscosity, high-molecular-weight absorbents.

An improved procedure to account for nonequilibrium with respect to mass transfer was introduced by Murphree [6] in 1925. It incorporates the Murphree vapor-phase tray efficiency, $(E_{MV})_{i,j}$, directly into Sorel's model to replace the equilibrium equation based on the K -value. Thus,

$$K_{i,j} = y_{i,j}/x_{i,j} \quad (12-1)$$

is replaced by

$$(E_{MV})_{i,j} = (y_{i,j} - y_{i,j+1}) / (y_{i,j}^* - y_{i,j+1}) \quad (12-2)$$

where i refers to the component, and j the stage, with stages numbered down from the top. The * superscript designates the equilibrium value. This efficiency is the ratio of the actual change in vapor-phase mole fraction across a stage to the change that would occur if equilibrium were achieved. The equilibrium value, $y_{i,j}^*$ is obtained from (12-1), with substitution into (12-2) giving

$$(E_{MV})_{i,j} = (y_{i,j} - y_{i,j+1}) / (K_{i,j}x_{i,j} - y_{i,j+1}) \quad (12-3)$$

Equations (12-2) and (12-3) assume: (1) uniform vapor and liquid stream concentrations entering and exiting a tray; (2) complete mixing in the liquid flowing across the tray; (3) plug flow of the vapor up through the liquid; and (4) negligible resistance to mass transfer in the liquid.

Application of E_{MV} using empirical correlations has proved adequate for binary and close-boiling, ideal, and near-ideal multicomponent mixtures. However, deficiencies in the Murphree efficiency model for multicomponent mixtures have long been recognized. Murphree himself stated these deficiencies clearly for multicomponent mixtures and for cases where the efficiency is low. He even argued that theoretical plates should not be the basis of calculation for multicomponent mixtures.

For binary mixtures, values of E_{MV} are always positive and identical for the two components. However, for multicomponent mixtures, values of E_{MV} differ from component to component and from stage to stage. The independent values of E_{MV} make it necessary to force the sum of the mole fractions in the vapor phase to sum to 1, which introduces the possibility of negative values of E_{MV} . When using the Murphree vapor-phase efficiency, the temperatures of the exiting vapor and liquid phases are assumed identical and equal to the exiting-liquid bubble-point temperature. Because the vapor and liquid are not in equilibrium, the vapor temperature does not correspond to its dew point. It is even possible, algebraically, for the vapor temperature to correspond to an impossible value that is below its dew point.

Values of E_{MV} can be obtained from data or correlations, and are more likely to be Murphree vapor-point (rather than tray) efficiencies. These point values apply only to a particular location on the tray. To convert them to tray efficiencies, vapor and liquid flow patterns must be assumed after the manner of Lewis [7]. However, if vapor and liquid phases on a tray are completely mixed, point efficiency equals tray efficiency. Complete mixing on a tray is usually achieved in small Oldershaw columns, as discussed in §6.5.5.

In 1957, Toor [8] showed that diffusion in a ternary mixture is enormously more complex than in a binary mixture because of coupling among component concentration gradients, especially when components differ widely in molecular size, shape, and polarity. Toor showed that, in addition to diffusion due to a Fickian concentration driving force, gradient coupling could result in (1) diffusion against a driving force (reverse diffusion), (2) no diffusion even though a concentration driving force is present (diffusion barrier), and (3) diffusion with zero driving force (osmotic diffusion). Theoretical calculations by Toor and Burchard [9] predicted the possibility of negative values of E_{MV} in multicomponent systems, but E_{MV} for binary systems is restricted to 0–100%.

In 1977, Krishna et al. [10] extended the work of Toor and Burchard and showed that when the vapor mole-fraction driving force of component A is small compared to that of the other components, the transport rate of A is controlled by the other components, with the result that E_{MV} for A is anywhere from minus to plus ∞ . They confirmed this prediction by conducting experiments with the ethanol/*tert*-butanol/water system and obtained values of E_{MV} for *tert*-butanol ranging from –2,978% to +527%. In addition, E_{MV} for ethanol and water sometimes differed significantly.

Two other tray efficiencies are defined in the literature: the vaporization efficiency of Holland, which was first touted by McAdams, and the Hausen tray efficiency, which eliminates the assumption in E_{MV} that the exiting liquid is at its bubble point. The former cannot account for the Toor phenomena and can vary widely in a manner not ascribable to a particular component. The latter appears to be superior to E_{MV} , but is considerably more complicated and difficult to use and, thus, has not found many adherents.

Because of the difficulties in applying a tray efficiency to an equilibrium-stage model for multicomponent systems, development of a realistic, nonequilibrium transport- or **rate-based model** has long been a desirable goal. In 1977, Waggoner and Loud [11] developed a rate-based mass-transfer model limited to nearly ideal, close-boiling systems. However, an energy-transfer equation was not included (because thermal equilibrium would be closely approximated for a close-boiling mixture). The coupling of component mass-transfer rates was ignored.

In 1979, Krishna and Standart [12] showed the possibility of applying rigorous, multicomponent mass- and heat-transfer theory to calculations of simultaneous transport. This led to the development in 1985 by Krishnamurthy and Taylor [14] of the first rate-based computer-aided model for trayed and packed distillation columns and other continuous

separation operations. The theory is treated in detail by Taylor and Krishna [13]. Their model applies the two-film theory of mass transfer discussed in §3.7, with the assumption of phase equilibria at the interface, and provides options for vapor and liquid flow configurations, including plug flow and perfectly mixed flow, on each tray. The model does not require tray efficiencies or values of HETP. Instead, correlations of mass-transfer and heat-transfer coefficients are fashioned for the particular type of trays or packing employed. Taylor, Kooijman, and Hung [15] extended the model in 1994 to include (1) the effect of liquid-droplet entrainment in the vapor and occlusion of vapor bubbles in the liquid, (2) a column-pressure profile, (3) interlinking streams, and (4) axial dispersion in packed columns. Unlike the 1985 model, which required the user to specify the column diameter and tray geometry or packing size, the 1994 version includes a design mode that estimates column diameter for a specified fraction of flooding or pressure drop. Rate-based models are available in process simulators, including RateSep in the RadFrac model of Aspen Plus, SCDS with the mass-transfer option in CHEMCAD, and the nonequilibrium column option in ChemSep. Use of rate-based models is highly recommended for cases of low tray efficiencies (e.g., absorbers) and distillation of highly nonideal multicomponent systems.

§12.1 RATE-BASED MODEL

A schematic diagram of a nonequilibrium stage, consisting of a tray, a group of trays, or a segment of a packed section, is shown in Figure 12.1. Stages are numbered from the top down. The condenser, if present, is the first stage, even if it is a total condenser.

§12.1.1 Model Variables

Entering stage j , at pressure P_j , are molar flow rates of feed liquid F_j^L and/or feed vapor F_j^V with component i molar flow

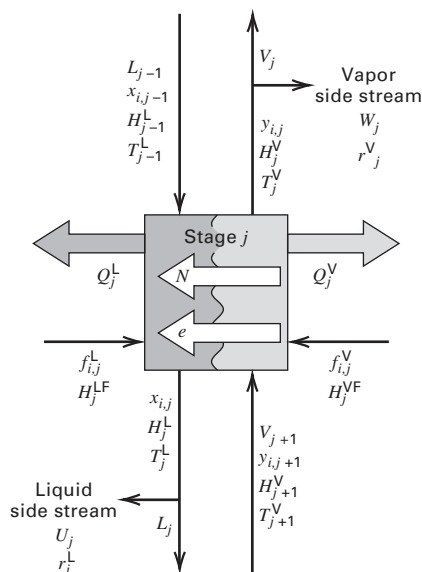


Figure 12.1 Nonequilibrium stage for rate-based method.

rates, $f_{i,j}^L$ and $f_{i,j}^V$, and stream molar enthalpies, H_j^{LF} and H_j^{VF} . Also leaving (+) or entering (–) the liquid and/or vapor phases at the stage are heat-transfer rates Q_j^V and Q_j^L , respectively. Entering stage j from the stage above is liquid molar flow rate L_{j-1} at temperature T_{j-1}^L and pressure P_{j-1} , with molar enthalpy H_{j-1}^L and component mole fractions $x_{i,j-1}$. Entering the stage from the stage below is vapor molar flow rate V_{j+1} at temperature T_{j+1}^V and pressure P_{j+1} , with molar enthalpy H_{j+1}^V and component mole fractions $y_{i,j+1}$. Within the stage, mass transfer of components occurs across the interface of the two phases at molar rates $N_{i,j}$ from the vapor phase to the liquid phase (+) or vice versa (–), and heat transfer occurs across the interface at rates e_j from the vapor phase to the liquid phase (+) or vice versa (–). Leaving the stage is liquid at temperature T_j^L and pressure P_j , with molar enthalpy H_j^L ; and vapor at temperature T_j^V and pressure P_j , with molar enthalpy H_j^V . A fraction, r_j^L , of the liquid exiting the stage may be withdrawn as a liquid sidestream at molar flow rate U_j , leaving the molar flow rate L_j to enter the stage below or to exit the column. A fraction, r_j^V , of the vapor exiting the stage may be withdrawn as a vapor sidestream at molar flow rate W_j , leaving the molar flow rate V_j to enter the stage above or to exit the column. If desired, entrainment, occlusion, interlink flows, a second immiscible liquid phase, and chemical reaction(s) can be included in the model.

§12.1.2 Model Equations

Recall that the equilibrium-stage model of §10.1 utilizes the $2C + 3$ MESH equations for each stage: C component mass balances, C phase-equilibria relations, two mole fraction summations, and one energy balance.

In the rate-based model, the mass and energy balances around each stage are replaced by separate balances for each phase. A stage can be a tray, a collection of trays, or a segment of a packed section. In residual form, the equations are as follows, where the residuals are on the LHSs and become zero when computations converge. When not converged, residuals are used to determine the proximity to convergence. The following set of rate-based equations is referred to as the MERSHQ equations.

Liquid-phase component material balance:

$$M_{i,j}^L \equiv (1 + r_j^L) L_j x_{i,j} - L_{j-1} x_{i,j-1} - f_{i,j}^L - N_{i,j}^L = 0, \quad i = 1, 2, \dots, C \quad (12-4)$$

Vapor-phase component material balance:

$$M_{i,j}^V \equiv (1 + r_j^V) V_j y_{i,j} - V_{j+1} y_{i,j+1} - f_{i,j}^V - N_{i,j}^V = 0, \quad i = 1, 2, \dots, C \quad (12-5)$$

Liquid-phase energy balance:

$$E_j^L \equiv (1 + r_j^L) L_j H_j^L - L_{j-1} H_{j-1}^L - \left(\sum_{i=1}^C f_{i,j}^L \right) H_j^{LF} + Q_j^L - e_j^L = 0 \quad (12-6)$$

Vapor-phase energy balance:

$$E_j^V \equiv (1 + r_j^V) V_j H_j^V - V_{j+1} H_{j+1}^V - \left(\sum_{i=1}^C f_{i,j}^V \right) H_j^{VF} + Q_j^V - e_j^V = 0 \quad (12-7)$$

where at the phase interface, I,

$$E_j^I \equiv e_j^V - e_j^L = 0 \quad (12-8)$$

Equations (12-4) and (12-5) are coupled by the component mass-transfer rates:

$$R_{i,j}^L \equiv N_{i,j} - N_{i,j}^L = 0, \quad i = 1, 2, \dots, C-1 \quad (12-9)$$

$$R_{i,j}^V \equiv N_{i,j} - N_{i,j}^V = 0, \quad i = 1, 2, \dots, C-1 \quad (12-10)$$

Mole-fraction summations for each phase are applied at the vapor-liquid interface:

$$S_j^{LI} \equiv \sum_{i=1}^C x_{i,j}^I - 1 = 0 \quad (12-11)$$

$$S_j^{VI} \equiv \sum_{i=1}^C y_{i,j}^I - 1 = 0 \quad (12-12)$$

A hydraulic equation for stage pressure drop is

$$H_j \equiv P_{j+1} - P_j - (\Delta P_j) = 0, \quad j = 1, 2, 3, \dots, N-1 \quad (12-13)$$

where the stage is assumed to be at mechanical equilibrium:

$$P_j^L = P_j^V = P_j \quad (12-14)$$

and ΔP_j is the gas-phase pressure drop from stage $j+1$ to stage j . Equation 12.13 is optional. It is included only when it is desired to compute one or more stage pressures from hydraulics. Phase equilibrium for each component is assumed to exist only at the phase interface:

$$Q_{i,j}^I \equiv K_{i,j} x_{i,j}^I - y_{i,j}^I = 0, \quad i = 1, 2, \dots, C \quad (12-15)$$

Because only $C-1$ equations are written for the component mass-transfer rates in (12-9) and (12-10), total phase material balances in terms of total mass-transfer rates, $N_{T,j}$, are added to the system:

$$M_{T,j}^L \equiv (1 + r_j^L) L_j - L_{j-1} - \sum_{i=1}^C f_{i,j}^L - N_{T,j} = 0 \quad (12-16)$$

$$M_{T,j}^V \equiv (1 + r_j^V) V_j - V_{j+1} - \sum_{i=1}^C f_{i,j}^V + N_{T,j} = 0 \quad (12-17)$$

where

$$N_{T,j} = \sum_{i=1}^C N_{i,j} \quad (12-18)$$

Equations (12-4), (12-5), (12-9), (12-10), (12-16), (12-17), and (12-18) contain terms for component mass-transfer

rates, estimated from diffusive and bulk-flow (convective) contributions. The former are based on interfacial area, average mole-fraction driving forces, and mass-transfer coefficients that account for component-coupling effects through binary-pair coefficients. Empirical equations are used for interfacial area and binary mass-transfer coefficients, based on correlations of data from bubble-cap trays, sieve trays, valve trays, random packings, and structured packings. The average mole-fraction driving forces for diffusion depend upon assumed vapor and liquid flow patterns. The simplest case is perfectly mixed flow on the tray for both phases, which simulates small-diameter, trayed columns. Countercurrent plug flow for vapor and liquid simulates a packed column with no axial dispersion.

Equations (12-6) to (12-8) contain heat-transfer rates. These are estimated from convective and enthalpy-flow contributions, where the former are based on interfacial area, average temperature-driving forces, and convective heat-transfer coefficients from the Chilton–Colburn analogy for the vapor phase (§3.5.2), and the penetration theory for the liquid phase (§3.6.2).

K -values in (12-15) are estimated from equation-of-state or activity-coefficient models discussed in Chapter 2. Tray or packed-segment pressure drops are estimated from suitable correlations.

§12.1.3 Degrees-of-Freedom Analysis

The total number of independent MERSHQ equations for each nonequilibrium stage, is $5C + 5$, as listed in Table 12.1. They apply for N stages—that is, $N_E = N(5C + 5)$ equations—in terms of $7NC + 14N + 1$ variables, listed in Table 12.2. The number of degrees of freedom is $N_D = N_V - N_E = (7N_C + 14N + 1) - (5NC + 5N) = 2NC + 9N + 1$.

Table 12.1 Summary of Independent Equations for Rate-Based Model

Equation	No. of Equations
$M_{i,j}^L$	C
$M_{i,j}^V$	C
$M_{T,j}^L$	1
$M_{T,j}^V$	1
E_j^L	1
E_j^V	1
E_j^I	1
$R_{i,j}^L$	$C-1$
$R_{i,j}^V$	$C-1$
S_j^{LI}	1
S_j^{VI}	1
H_j	(optional)
$Q_{i,j}^I$	C
Total	$5C + 5$

Table 12.2 List of Variables for Rate-Based Model

Variable Type No.	Variable	No. of Variables
1	No. of stages, N	1
2	$f_{i,j}^L$	NC
3	$f_{i,j}^V$	NC
4	T_j^{LF}	N
5	T_j^{VF}	N
6	P_j^{LF}	N
7	P_j^{VF}	N
8	L_j	N
9	$x_{i,j}$	NC
10	r_j^L	N
11	T_j^L	N
12	V_j	N
13	$y_{i,j}$	NC
14	r_j^V	N
15	T_j^V	N
16	P_j	N
17	Q_j^L	N
18	Q_j^V	N
19	$x_{i,j}^I$	NC
20	$y_{i,j}^I$	NC
21	T_j^I	N
22	$N_{i,j}$	NC
Total		$N_V = 7NC + 14N + 1$

If variable types 1 to 7, 10, 14, and 16 to 18 in Table 12.2 are specified, a total of $2NC + 9N + 1$ variables are assigned values and the degrees of freedom are totally consumed. The remaining $5C + 5$ independent variables in the $5C + 5$ equations are $x_{i,j}$, $y_{i,j}$, $x_{i,j}^I$, $y_{i,j}^I$, $N_{i,j}$, T_j^L , T_j^V , T_j^I , L_j , and V_j , which are the variables to be computed from the equations. Properties $K_{i,j}^L$, H_j^{LF} , H_j^{VF} , H_j^L and H_j^V are computed from thermodynamic correlations in terms of the remaining independent variables. Transport rates $N_{i,j}^L$, $N_{i,j}^V$, e_j^L , and e_j^V are from transport correlations and certain physical properties, in terms of the remaining independent variables. Stage pressures are computed from pressure drops, ΔP_j , stage geometry, fluid-mechanics equations, and physical properties, in terms of the remaining independent variables.

For a distillation column, it is preferable that Q_1^V (heat-transfer rate from the vapor in the condenser) and Q_N^L (heat-transfer rate to the liquid in the reboiler) are not specified. Instead, as in the case of a column with a partial condenser, L_1 (reflux rate) and L_N (bottoms flow rate) are substituted. These are referred to as **standard specifications** for ordinary distillation. For an adiabatic absorber or stripper, all Q_j^L and Q_j^V are set equal to 0, with no substitution of specifications.

§12.2 THERMODYNAMIC PROPERTIES AND TRANSPORT-RATE EXPRESSIONS

§12.2.1 Thermodynamic Properties

Rate-based models use the same K -value and enthalpy correlations as equilibrium-based models. However, K -values apply only at the equilibrium interface between vapor and liquid phases on trays or in packing. The K -value correlation, whether based on an equation-of-state or activity-coefficient model, is a function of interface temperature, interface compositions, and tray pressure. Enthalpies are evaluated at phase conditions as they exit a tray. For the equilibrium-based model, vapor is at the dew-point temperature and liquid is at the bubble-point temperature, where both temperatures are at the stage temperature. For the rate-based model, liquid is subcooled and vapor is superheated, so they are at different temperatures.

§12.2.2 Transport-Rate Expressions

Accurate enthalpies and, particularly, K -values are crucial to equilibrium-based models. For rate-based models, accurate predictions of heat-transfer rates and, particularly, mass-transfer rates are also required. These depend upon transport coefficients, interfacial area, and driving forces. It is critical that mass-transfer-rate models for multicomponent mixtures account for component-coupling effects through binary-pair coefficients.

The general forms for component mass-transfer rates across the vapor and liquid films, respectively, on a tray or in a packed segment, are as follows, where both diffusive and convective (bulk-flow) contributions are included:

$$N_{i,j}^V = a_j^I J_{i,j}^V + y_{i,j} N_{T,j} \quad (12-19)$$

$$\text{and} \quad N_{i,j}^L = a_j^I J_{i,j}^L + x_{i,j} N_{T,j} \quad (12-20)$$

where a_j^I is the total interfacial area for the stage and $J_{i,j}^P$ is the molar diffusion flux relative to the molar-average velocity, where P stands for the phase (V or L). For a binary mixture, as discussed in §3.7, these fluxes, in terms of mass-transfer coefficients, are

$$J_i^V = c_t^V k_i^V (y_i^V - y_i^I)_{\text{avg}} \quad (12-21)$$

$$\text{and} \quad J_i^L = c_t^L k_i^L (x_i^I - x_i^L)_{\text{avg}} \quad (12-22)$$

where c_t^P is total molar concentration of the phase, k_i^P is the mass transfer coefficient for a binary mixture based on a mole-fraction driving force, and the last factors in (12-21) and (12-22) are mean mole-fraction driving forces over the stage. The positive direction of mass transfer is assumed to be from the vapor to the liquid phase. From the definition of the molar diffusive flux:

$$\sum_{i=1}^C J_i = 0 \quad (12-23)$$

Thus, for the binary system (1, 2), $J_1 = -J_2$.

§12.2.3 Mass-Transfer Coupling

As discussed in detail by Taylor and Krishna [13], multi-component mass transfer is considerably more complex than binary mass transfer because of component-coupling effects. For example, for the ternary system (1, 2, 3), the fluxes for the first two components are

$$J_1^V = c_t^V \kappa_{11}^V (y_1^V - y_1^I)_{\text{avg}} + c_t^V \kappa_{12}^V (y_2^V - y_2^I)_{\text{avg}} \quad (12-24)$$

$$J_2^V = c_t^V \kappa_{21}^V (y_1^V - y_1^I)_{\text{avg}} + c_t^V \kappa_{22}^V (y_2^V - y_2^I)_{\text{avg}} \quad (12-25)$$

The flux for the third component is not independent of the other two, but is obtained from (12-23):

$$J_3^V = -J_1^V - J_2^V \quad (12-26)$$

In these equations, the binary-pair coefficients, κ^P , are complex functions related to inverse-rate functions described below and called the **Maxwell–Stefan mass-transfer coefficients**.

For the general multicomponent system (1, 2, ..., C), the independent fluxes for the first C-1 components are given in matrix form as

$$\mathbf{J}^V = c_t^V [\boldsymbol{\kappa}^V] (\mathbf{y}^V - \mathbf{y}^I)_{\text{avg}} \quad (12-27)$$

$$\mathbf{J}^L = c_t^L [\boldsymbol{\kappa}^L] (\mathbf{x}^I - \mathbf{x}^L)_{\text{avg}} \quad (12-28)$$

where \mathbf{J}^P , $(\mathbf{y}^V - \mathbf{y}^I)_{\text{avg}}$, and $(\mathbf{x}^I - \mathbf{x}^L)_{\text{avg}}$ are column vectors of length C-1 and $[\boldsymbol{\kappa}^P]$ is a $(C-1) \times (C-1)$ square matrix. The method for determining average mole-fraction driving forces depends, as discussed in §12.4, upon the flow patterns of the vapor and liquid phases.

The fundamental theory for multicomponent diffusion is that of Maxwell and Stefan, who, in the period from 1866 to 1871, developed the kinetic theory of gases. Their theory is presented most conveniently in terms of rate coefficients, \mathbf{B} , which are defined in reciprocal diffusivity terms [13]. Likewise, it is convenient to determine $[\boldsymbol{\kappa}^P]$ from a reciprocal mass-transfer coefficient function, \mathbf{R} , defined by Krishna and Standart [12]. For an ideal-gas solution:

$$[\boldsymbol{\kappa}^V] = [\mathbf{R}^V]^{-1} \quad (12-29)$$

For a nonideal-liquid solution:

$$[\boldsymbol{\kappa}^L] = [\mathbf{R}^L]^{-1} [\boldsymbol{\Gamma}^L] \quad (12-30)$$

where the elements of \mathbf{R}^P in terms of general mole fractions, z_i , are

$$R_{ii}^P = \frac{z_i}{k_{iC}^P} + \sum_{\substack{k=1 \\ k \neq i}}^C \frac{z_k}{k_{ik}^P} \quad (12-31)$$

$$R_{ij}^P = -z_i \left(\frac{1}{k_{ij}^P} - \frac{1}{k_{iC}^P} \right) \quad (12-32)$$

where j refers to the j th component and not the j th stage, and the values of k are binary-pair mass-transfer coefficients obtained from experimental data.

For a four-component vapor-phase system, the combination of (12-27) and (12-29) gives

$$\begin{bmatrix} J_1^V \\ J_2^V \\ J_3^V \end{bmatrix} = c_t^V \begin{bmatrix} R_{11}^V & R_{12}^V & R_{13}^V \\ R_{21}^V & R_{22}^V & R_{23}^V \\ R_{31}^V & R_{32}^V & R_{33}^V \end{bmatrix}^{-1} \begin{bmatrix} (y_1^V - y_1^I)_{\text{avg}} \\ (y_2^V - y_2^I)_{\text{avg}} \\ (y_3^V - y_3^I)_{\text{avg}} \end{bmatrix} \quad (12-33)$$

$$\text{with} \quad J_4^V = -(J_1^V + J_2^V + J_3^V) \quad (12-34)$$

and, for example, from (12-32) and (12-33), respectively:

$$R_{11}^V = \frac{y_1}{k_{14}^V} + \frac{y_2}{k_{12}^V} + \frac{y_3}{k_{13}^V} + \frac{y_4}{k_{14}^V} \quad (12-35)$$

$$R_{12}^V = -y_1 \left(\frac{1}{k_{12}^V} - \frac{1}{k_{14}^V} \right) \quad (12-36)$$

The term $[\boldsymbol{\Gamma}^L]$ in (12-30) is a $(C-1) \times (C-1)$ matrix of thermodynamic factors that corrects for nonideality, which often is a necessary correction for the liquid phase. When an activity-coefficient model is used:

$$\Gamma_{ij}^L = \delta_{ij} + x_i \left(\frac{\partial \ln \gamma_i}{\partial x_j} \right)_{T,P,x_k, k \neq j=1, \dots, C-1} \quad (12-37)$$

For a nonideal vapor, a $[\boldsymbol{\Gamma}^V]$ term can be included in (12-29), but this is rarely necessary. For either phase, if an equation-of-state model is used, (12-37) can be rewritten by substituting $\bar{\phi}_i$, the mixture fugacity coefficient, for γ_i . The term δ_{ij} is the Kronecker delta, which is 1 if $i = j$ and 0 if not. The thermodynamic factor is required because it is generally accepted that the fundamental driving force for diffusion is the gradient of the chemical potential rather than the mole fraction or concentration gradient.

When mass-transfer fluxes are moderate to high, an additional correction term is needed in (12-29) and (12-30) to correct for distortion of composition profiles. Taylor and Krishna [13] discuss this correction, which can have a serious effect on the results. The calculation of low mass-transfer flux, according to (12-19) to (12-32), is illustrated by the next example.

EXAMPLE 12.1 Multicomponent Mass-Transfer Rates.

This example is similar to Example 11.5.1 on page 283 of Taylor and Krishna [13]. The following results were obtained for tray n from a rate-based calculation of a ternary distillation at 14.7 psia, involving acetone (1), methanol (2), and water (3) in a 5.5-ft-diameter column using sieve trays with a 2-inch-high weir. Vapor and liquid phases are assumed to be completely mixed.

Component	y_n	y_{n+1}	y_n^I	K_n^I	x_n
1	0.2971	0.1700	0.3521	2.759	0.1459
2	0.4631	0.4290	0.4677	1.225	0.3865
3	0.2398	0.4010	0.1802	0.3673	0.4676
	1.0000	1.0000	1.0000		1.0000

The computed products of the gas-phase, binary mass-transfer coefficients and interfacial area, using the Chan–Fair correlation mentioned in §7.4.3, are as follows in lbmol/(h-unit mole fraction):

$$k_{12} = k_{21} = 1,955; \quad k_{13} = k_{31} = 2,407; \quad k_{23} = k_{32} = 2,797$$

(a) Compute the molar diffusion rates. (b) Compute the mass-transfer rates. (c) Calculate the Murphree vapor-tray efficiencies assuming the vapor and liquid phases are completely mixed.

Solution

Because rates instead of fluxes are given, the equations developed in this section are used with rates rather than fluxes.

(a) Compute the reciprocal rate functions, R , from (12-31) and (12-32), assuming linear mole-fraction gradients such that z_i can be replaced by $(y_i + y_i^1)/2$. Thus:

$$z_1 = (0.2971 + 0.3521)/2 = 0.3246$$

$$z_2 = (0.4631 + 0.4677)/2 = 0.4654$$

$$z_3 = (0.2398 + 0.1802)/2 = 0.2100$$

$$R_{11}^V = \frac{z_1}{k_{13}} + \frac{z_2}{k_{12}} + \frac{z_3}{k_{13}} = \frac{0.3246}{2,407} + \frac{0.4654}{1,955} + \frac{0.2100}{2,407} = 0.000460$$

$$R_{22}^V = \frac{z_2}{k_{23}} + \frac{z_1}{k_{21}} + \frac{z_3}{k_{23}} = \frac{0.4654}{2,797} + \frac{0.3246}{1,955} + \frac{0.2100}{2,797} = 0.000408$$

$$R_{12}^V = -z_1 \left(\frac{1}{k_{12}} - \frac{1}{k_{13}} \right) = -0.3246 \left(\frac{1}{1,955} - \frac{1}{2,407} \right) = -0.0000312$$

$$R_{21}^V = -z_2 \left(\frac{1}{k_{21}} - \frac{1}{k_{23}} \right) = -0.4654 \left(\frac{1}{1,955} - \frac{1}{2,797} \right) = -0.0000717$$

Thus, in matrix form:

$$[R^V] = \begin{bmatrix} 0.000460 & -0.0000312 \\ -0.0000717 & 0.000408 \end{bmatrix}$$

From (12-29), by matrix inversion:

$$[\kappa^V] = [R^V]^{-1} = \begin{bmatrix} 2,200 & 168.2 \\ 386.6 & 2,480 \end{bmatrix}$$

Because the off-diagonal terms in the preceding 2×2 matrix are much smaller than the diagonal terms, the effect of coupling in this example is small.

From (12-27):

$$\begin{bmatrix} J_1^V \\ J_2^V \end{bmatrix} = \begin{bmatrix} \kappa_{11}^V & \kappa_{12}^V \\ \kappa_{21}^V & \kappa_{22}^V \end{bmatrix} \begin{bmatrix} (y_1 - y_1^1) \\ (y_2 - y_2^1) \end{bmatrix}$$

$$J_1^V = \kappa_{11}^V (y_1 - y_1^1) + \kappa_{12}^V (y_2 - y_2^1) = 2,200(0.2971 - 0.3531) + 168.2(0.4631 - 0.4677) = -121.8 \text{ lbmol/h}$$

$$J_2^V = \kappa_{21}^V (y_1 - y_1^1) + \kappa_{22}^V (y_2 - y_2^1) = 383.6(0.2971 - 0.3521) + 2,480(0.4631 - 0.4677) = -32.7 \text{ lbmol/h}$$

From (12-23):

$$J_3^V = -J_1^V - J_2^V = 121.8 + 32.7 = 154.5 \text{ lbmol/h}$$

(b) From (12-19), but with diffusion and mass-transfer rates instead of fluxes:

$$N_1^V = J_1^V + z_1 N_T^V = -121.8 + 0.3246 N_T^V \quad (1)$$

Similarly:

$$N_2^V = -32.7 + 0.4654 N_T^V \quad (2)$$

$$N_3^V = 154.5 + 0.2100 N_T^V \quad (3)$$

To determine component mass-transfer rates, it is necessary to know the total mass-transfer rate for the tray, N_T^V . The problem of determining this quantity, when the diffusion rates, J , are known, is referred to as the **bootstrap problem** (p. 145 in Taylor and Krishna [13]). In chemical reaction with diffusion, N_T is determined by the stoichiometry. In distillation, N_T is determined by an energy balance, which gives the change in molar vapor rate across a tray. For the assumption of constant molar overflow, $N_T = 0$. In this example, that assumption is not valid, and the change is

$$N_T^V = V_{n+1} - V_n = -54 \text{ lbmol/h}$$

From (1), (2), and (3):

$$N_1^V = -121.8 + 0.3246(-54) = -139.4 \text{ lbmol/h}$$

$$N_2^V = -32.7 + 0.4654(-54) = -57.8 \text{ lbmol/h}$$

$$N_3^V = -154.5 + 0.2100(-54) = -143.2 \text{ lbmol/h}$$

(c) Values of the E_{MV} are obtained from (12-3), using K -values at phase-interface conditions:

$$E_{MV_i} = \frac{(y_{i,n} - y_{i,n+1})}{(K_{i,n}^1 x_{i,n} - y_{i,n+1})} \quad (4)$$

From (4):

$$E_{MV_1} = \frac{(0.2971 - 0.1700)}{[(2.759)(0.1459) - 0.1700]} = 0.547$$

$$E_{MV_2} = \frac{(0.4631 - 0.4290)}{[(1.225)(0.3865) - 0.4290]} = 0.767$$

$$E_{MV_3} = \frac{(0.2398 - 0.4010)}{[(0.3673)(0.4676) - 0.4010]} = 0.703$$

General forms for heat-transfer rates across vapor and liquid films of a stage are

$$e_j^V = a_j^I h^V (T^V - T^I) + \sum_{i=1}^C N_{i,j}^V \bar{H}_{i,j}^V \quad (12-38)$$

$$e_j^L = a_j^I h^L (T^I - T^L) + \sum_{i=1}^C N_{i,j}^L \bar{H}_{i,j}^L \quad (12-39)$$

where $\bar{H}_{i,j}^P$ are the partial molar enthalpies of component i for stage j and h^P are convective heat-transfer coefficients. The second terms on the RHS of (12-38) and (12-39) account for

the transfer of enthalpy by mass transfer. Temperatures T^V and T^L are the temperatures of vapor and liquid exiting the stage.

§12.3 METHODS FOR ESTIMATING TRANSPORT COEFFICIENTS AND INTERFACIAL AREA

Equations (12-31) and (12-32) require binary-pair mass-transfer coefficients for phase contacting devices, which must be estimated from empirical correlations of experimental data for different devices.

As discussed in §7.4.3, a number of semitheoretical tray models for absorption, stripping, and distillation have been published. They include the correlation of Hughmark [18] and the AIChE method [16] for bubble-cap trays; the correlation of Scheffe and Weiland [36] for Glitsch V-1 valve trays; and the correlations of Harris [17], Zuiderweg [19], Chan and Fair [20], Chen and Chuang [21], Garcia and Fair [22, 23], Syeda et al. [24], and Vennavelli et al. [25] for sieve trays.

The Vennavelli et al. modification of the Syeda et al. correlation is discussed in detail in §7.4.3.

Some mass-transfer correlations are presented in terms of the number of transfer units, N_V and N_L , where, by definition,

$$N_V \equiv k^V a h_f / u_s \quad (12-40)$$

$$N_L \equiv k^L a h_f z / (Q_L / W) \quad (12-41)$$

where a = interfacial area/volume of froth on the tray, h_f = froth height, u_s = superficial vapor velocity based on tray bubbling area, z = length of liquid-flow path across the bubbling area, Q_L = volumetric liquid flow rate, and W = weir length.

The interfacial area for a tray, a^I , is related to a by

$$a^I = a h_f A_b \quad (12-42)$$

where A_b = bubbling area.

Both k^P and a^I are from correlations in terms of N_V and N_L .

Empirical correlations for mass-transfer coefficients and interfacial-area density (area/packed volume) for random (dumped) packings, have been published by Onda, Takeuchi, and Okumoto [26] and Bravo and Fair [27]. For structured packings, the empirical correlations of Bravo, Rocha, and Fair for gauze packings [28] and for a wide variety of structured packings [29] are available. A semitheoretical correlation by Billet and Schultes [30], based on over 3,500 data points for more than 50 test systems and more than 70 different types of packings, is discussed in §6.8.3. It requires five packing parameters and is applicable to both random and structured packings.

Heat-transfer coefficients for the vapor film are usually estimated from the Chilton–Colburn analogy between heat and mass transfer (§3.5.2). Thus,

$$h^V = k^V \rho^V C_P^V (N_{Le})^{2/3} \quad (12-43)$$

where

$$N_{Le} = \left(\frac{N_{Sc}}{N_{Pr}} \right) \quad (12-44)$$

A penetration model (§3.6.2) is preferred for the liquid-phase film:

$$h^L = k^L \rho^L C_P^L (N_{Le})^{1/2} \quad (12-45)$$

Spagnolo et al. [37] give a more detailed heat-transfer model, specifically for sieve trays.

§12.4 VAPOR AND LIQUID FLOW PATTERNS

The simplest flow pattern corresponds to the assumption of perfectly mixed vapor and liquid. Under these conditions, mass-transfer driving forces in (12-27) and (12-28) are

$$(y^V - y^I)_{\text{avg}} = (y^V - y^I) \quad (12-46)$$

$$(x^I - x^L)_{\text{avg}} = (x^I - x^L) \quad (12-47)$$

where y^V and x^L are exiting-stage bulk mole fractions. These flow patterns are valid for Oldershaw laboratory columns and for industrial trayed towers with a short liquid flow path.

A plug-flow pattern for the vapor and/or liquid assumes that the phase moves through the froth without mixing. This requires that mass-transfer rates be integrated over the froth. An approximation of the integration is provided by Kooijman and Taylor [31], who assume constant mass-transfer coefficients and interface compositions. The resulting expressions for the average mole-fraction driving forces are the same as (12-46) and (12-47), except for a correction factor in terms of N^V or N^L included on the RHS of each equation. Plug-flow patterns are most applicable for packed towers. The perfectly mixed flow and plug-flow patterns are the two patterns presented by Lewis [7] to convert E_{OV} to E_{MV} , as discussed in §6.5. They represent the extreme situations in a trayed tower.

Except for small diameters, a partial liquid mixing model that includes a turbulent Peclet number is best for trayed towers. The Peclet number requires an estimate of the liquid eddy diffusivity. As discussed by Lockett [39], 11 correlations for the eddy diffusivity were proposed before 1986. Unfortunately, they differed widely when plotted against superficial velocity. In 1991, Bennett and Grimm [40] published a correlation for the liquid-phase eddy diffusivity on a sieve tray. Their correlation was based on the assumption that backmixing occurs by physical transport of droplet elements and was shown to be superior to previous correlations of sieve-tray data.

For reactive distillation, a rate-based multicell (or mixed-pool) model has proven useful. In this model, the liquid on the tray is assumed to flow horizontally across the tray through a series of perfectly mixed cells (perhaps 4 or 5). In the model of Higler, Krishna, and Taylor [38], which is available in the ChemSep program, the vapor phase is assumed to be perfectly mixed in each cell. If desired, cells for each tray can also be stacked in the vertical direction. Thus, a tray model might consist of a 5×5 cell arrangement, for a total of 25 perfectly mixed cells. It is assumed that the vapor streams leaving the topmost tray cells are collected and mixed before being divided to enter the cells on the next tray.

§12.5 METHOD OF CALCULATION

As summarized in Table 12.1, $N(5C + 5)$ equations must be solved for the rate-based model of Figure 12.1 when the pressure-drop equations are omitted. The equations contain the variables listed in Table 12.2. Other parameters in the equations are computed from these variables. When the number of equations is subtracted from the number of variables, the degrees of freedom is $2NC + 9N + 1$. If the total number of stages and all column feed conditions, including feed-stage locations ($2NC + 4N + 1$) variables are specified, the number of remaining degrees of freedom, using the variable designations in Table 12.2, is $5N$. A computer program for the rate-based model would generally require the user to specify these $2NC + 4N + 1$ variables. The degree of flexibility provided to the user in the selection of the remaining $5N$ variables depends on the particular rate-based computer algorithm, three of which are widely available: (1) ChemSep from R. Taylor and H. A. Kooijman, (2) RateSep in the Radfrac model of Aspen Plus, and (3) the mass-transfer option in SCDS of CHEMCAD. All these algorithms provide a wide variety of correlations for thermodynamic and transport properties and flexibility in the selection of the remaining $5N$ specifications. The basic $5N$ specifications are

$$r_j^L \text{ or } U_j, r_j^V \text{ or } W_j, P_j, Q_j^L, \text{ and } Q_j^V$$

However, substitutions can be made, as exemplified next for the ChemSep program.

§12.5.1 ChemSep Program (www.chemsep.org)

In this section, ChemSep, which introduced the rate-based method, is applied to illustrate applications to nonideal distillation and absorption. ChemSep provides three simulation cases: (1) Flash; (2) Equilibrium Column; and (3) Non-equilibrium Column. For each of the two Column cases, a large number of tables and graphs can be viewed and/or printed following a successfully converged run. In addition, the Non-equilibrium Column case, which applies to both trayed and packed towers, also includes the determination of column diameter, pressure drop, and efficiency, with a summary of operating limits. The Non-equilibrium Column case offers two options: a rate-based model and a stage-efficiency model. These two models require (1) the specification of the type of tray (bubble cap, sieve, or valve), for each set of trays, or packing (random or structured) for each packed-section height; (2) the selection of mass-transfer correlations for vapor and liquid phases; (3) the choice of vapor and liquid flow patterns, including mixed, dispersion (partially mixed), and plug; and (4) considerations of pressure drop, entrainment, and holdup. The column diameter is determined from a fraction of flooding or a maximum pressure drop. In addition, the tray layout is designed. The rate-based model computes actual trays. It then back-calculates Murphree vapor tray efficiencies. The stage-efficiency model computes nonequilibrium stages using the MESH equations for the equilibrium-stage model of Chapter 10 after replacing the K -value equilibrium equation (e.g., (10-2) with (12-3)). The latter equation is based

on the Murphree vapor tray efficiency calculated from (a) the selected mass-transfer correlations or (b) an overall tray efficiency determined from a suitable correlation, such as that of O'Connell (7-40) or (c) a constant value for the tray efficiency or a set of tray efficiency values selected by the user. For cases (b) and (c), the tray diameter and tray layout design are not needed, but they are determined.

The rate-based model of ChemSep applies multicomponent transport equations to trays or short heights (called segments) of packing. Partial condensers and reboilers are treated as equilibrium stages. The specification options include:

1. r_j^L and r_j^V : From each stage, either a liquid or a vapor sidestream can be specified as (a) a sidestream flow rate or (b) a ratio of the sidestream flow rate to the flow rate of the remaining fluid passing to the next stage:

$$r_j^L = U_j/L_j \text{ or } r_j^V = W_j/V_j \text{ as in Figure 12.1}$$

2. P_j : Four options are available, all requiring the pressure of the condenser, if any:
 - (a) Constant pressure for all stages in the tower and reboiler.
 - (b) Top and bottom tower pressures. Pressures of stages intermediate between top and bottom are obtained by linear interpolation.
 - (c) Top tower pressure, and specified pressure drop per stage to obtain remaining stage pressures.
 - (d) Top tower pressure, with stage pressure drops fixed, specified, or estimated by ChemSep from hydraulic correlations.
3. Q_j^L and Q_j^V : The heat duty must be specified for all stage heaters and coolers except the condenser and/or reboiler, if present. In addition, a heat loss for the tower that is divided equally over all stages can be specified. When a condenser (total without subcooling, total with subcooling, or partial) is present, one of the following specifications can replace the condenser heat duty: (a) molar reflux ratio; (b) condensate temperature; (c) distillate molar flow rate; (d) reflux molar flow rate; (e) component molar flow rate in distillate; (f) mole fraction of a component in distillate; (g) fractional recovery, from all feeds, of a component in the distillate; (h) molar fraction of all feeds to the distillate; and (i) molar ratio of two distillate components. For distillation, an often-used specification is the molar reflux ratio.

A reboiler may be partial (by far the most common), total with a vapor product, or total with a superheated vapor product. The following specification options can replace the reboiler heat duty: (a) molar boilup ratio; (b) reboiler temperature; (c) bottoms molar flow rate; (d) reboiled-vapor (boilup) molar flow rate; (e) component molar flow rate in bottoms; (f) mole fraction of a component in bottoms; (g) fractional recovery, from all feeds, of a component in the bottoms; (h) molar fraction of all feeds to the bottoms; and (i) molar ratio of two components in the bottoms. For distillation, an often-used specification is the molar bottoms flow rate, which must be estimated if it is not known.

The preceding number of optional specifications is considerable. However, in addition, ChemSep also provides “flexible” specifications that can substitute for the condenser and/or reboiler duties. These are advanced options supplied in the form of strings that contain values of certain allowable variables and/or combinations of these variables using the five common arithmetic operators (+, −, *, /, and exponentiation). The variables include stage variables (L , V , x , y , and T) and interface variables (x^I , y^I , and T^I) at any stage. Flow rates can be in mole or mass units.

Certain options and advanced options must be used with care because values might be specified that cannot lead to a converged solution. For example, with a simple distillation column of a fixed number of stages, N must be greater than the N_{\min} needed to achieve specified distillate and bottoms purities. As always, it is generally wise to begin a simulation with a standard pair of top and bottom specifications, such as reflux ratio and a bottoms molar flow rate that corresponds to the desired distillate rate. These specifications are almost certain to converge unless interstage liquid or vapor flow rates tend to zero somewhere in the column. A study of the calculated results will provide insight into possible limits in the use of other options.

The set of linear and nonlinear equations for the rate-based model is solved by the simultaneous-correction (SC) method in a manner similar to that developed by Naphtali and Sandholm for the equilibrium-based model described in §10.6. Thus, the variables and equations are grouped by stage so that the Jacobian matrix is of block-tridiagonal form. However, the equations for the rate-based model now number $5C + 6$ or $5C + 5$ per stage, depending on whether stage pressures are computed or specified, compared to just $2C + 1$ for the equilibrium-based method.

Calculations of transport coefficients and pressure drops require column diameter and dimensions of column internals. These may be specified or computed. In the latter case, default dimensions are selected for the internals, with column diameter computed from a specified value for percent of flooding for a trayed or packed column, or a specified pressure drop per unit height for a packed column.

Computing time per iteration for the rate-based model may be three or four times the computing time for the equilibrium-based model. The number of iterations may be two to three times that for the equilibrium-based model. Overall, the total computing time for the rate-based model is usually less than an order of magnitude greater than that for the equilibrium-based model. Computing time for the rate-based model is often less than 1 minute.

Like the Naphtali–Sandholm equilibrium-based method, the rate-based model utilizes mainly analytical partial derivatives in the Jacobian matrix and requires initial estimates of all variables. A method by Powers et al. [33] automatically generates these estimates. They involve the usual assumptions of constant molar overflow and a linear temperature profile. The initialization of the stage mole fractions is made by performing several iterations of the BP method using ideal K -values for the first iteration and nonideal K -values thereafter. Initial interface mole fractions are set equal to estimated

bulk values, and initial mass-transfer rates are arbitrarily set to values of $\pm 10^{-3}$ kmol/h, with the sign dependent upon the component K -value.

To prevent oscillations and promote convergence of the iterations, corrections to certain variables from iteration-to-iteration can be limited. Defaults are 10 K for temperature and 50% for flows. When a correction to a mole fraction would result in a value outside the feasible range of 0 to 1, the default correction is one-half of the step that would take the value to a limit. For very difficult problems, multiple-pass options are available.

Convergence of the SC method is determined from residuals of the functions, as in the Naphtali–Sandholm method, or from the corrections to the variables. ChemSep applies both criteria and terminates when either of the following are satisfied:

$$\left[\sum_{j=1}^N \sum_{k=1}^{N_j} f_{k,j}^2 \right]^{1/2} < \varepsilon \quad (12-48)$$

$$\sum_{j=1}^N \sum_{k=1}^{N_j} |\Delta X_{k,j}| / X_{k,j} < \varepsilon \quad (12-49)$$

where $f_{k,j}$ = residuals in Table 12.1, N = number of stages, N_j = number of equations for the j th stage, $X_{k,j}$ = unknown variables from Table 12.2, and ε = a small number with a default value of 10^{-4} . Unlike the Naphtali–Sandholm method, the residuals are not scaled. Accordingly, the second criterion is usually satisfied first.

From the results of a converged solution, it is highly desirable to back-calculate values of E_{MV} , component by component and tray by tray, from (12-3) for trayed columns, and HETP values for packed towers. ChemSep can also perform rate-based calculations for liquid–liquid extraction.

EXAMPLE 12.2 Extractive Distillation.

A mixture of n -heptane and toluene cannot be separated at 1 atm by ordinary distillation. Accordingly, an extractive distillation scheme with methyl ethyl ketone as a solvent is used. As part of an initial design study, use the rate-based model of ChemSep with the specifications listed in Table 12.3 to calculate a sieve-tray column.

Solution

The information in Table 12.3 was entered via the ChemSep menu and the program was executed. A converged solution was achieved in 8 iterations. The program initialized all of the variables. The predicted separation was as follows:

Component	Distillate, lbmol/h	Bottoms, lbmol/h
n -Heptane	54.87	0.13
Toluene	0.45	44.55
Methyl ethyl ketone	199.68	0.32

Predicted column profiles for pressure, liquid-phase temperature, total vapor and liquid flow rates, component vapor and liquid mole fractions, component mass-transfer rates, and values of E_{MV} are shown in Figure 12.2, where stages are numbered from the top down

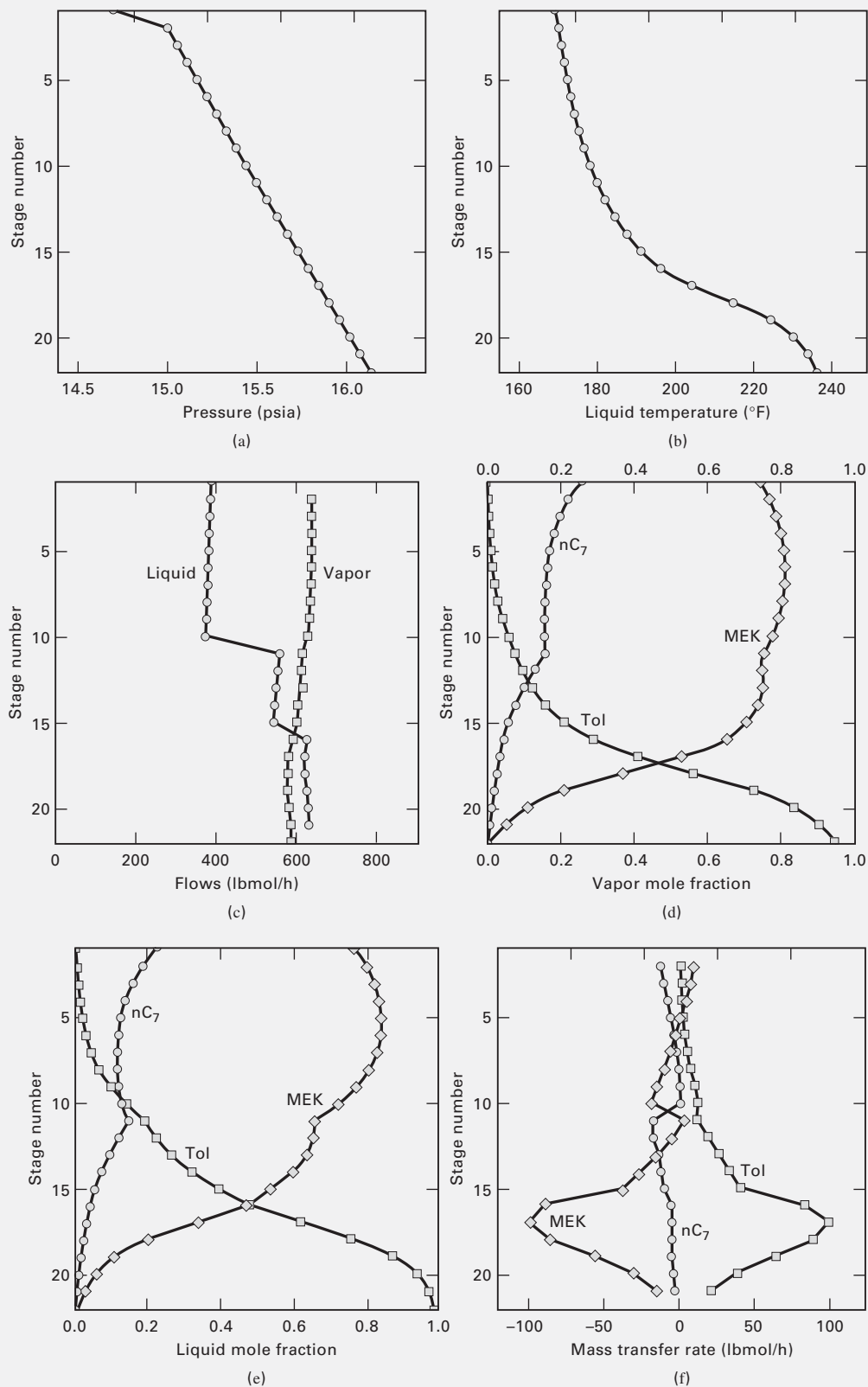


Figure 12.2 Column profiles for Example 12.2: (a) pressure profile; (b) liquid-phase temperature profile; (c) vapor and liquid flow rate profiles; (d) vapor mole-fraction profiles; (e) liquid mole-fraction profiles; (f) mass-transfer rate profiles. (*Continued*)

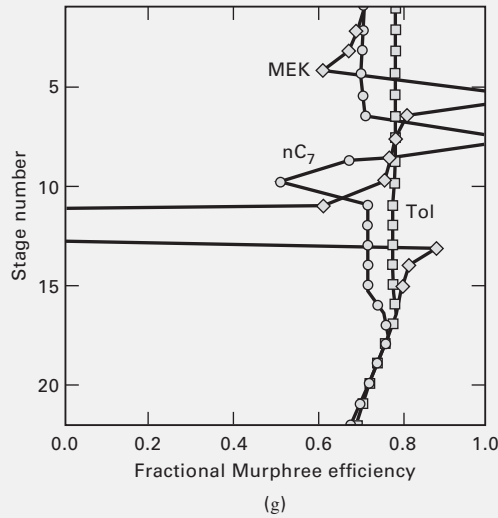


Figure 12.2 (Continued) (g) Murphree vapor-tray efficiencies.

Table 12.3 Specifications for Example 12.2

Total condenser delivering saturated liquid
Partial reboiler
Pressure at condenser outlet = 14.7 psia
Pressure at condenser inlet = 15.0 psia
Reflux ratio = 1.5
Bottoms flow rate = 45 lbmol/h
Total number of trays = 20
Feed 1 to Tray 10 from top:
55 lbmol/h of <i>n</i> -heptane
45 lbmol/h of toluene
100 lbmol/h of methyl ethyl ketone (MEK)
Saturated liquid at 20 psia
Feed 2 to Tray 15 from top:
100 lbmol/h of MEK
Saturated liquid at 20 psia
UNIFAC for liquid-phase activity coefficients
Chan–Fair correlation for mass-transfer coefficients
Plug flow for vapor
Mixed flow for liquid
85% of flooding
Tray spacing = 0.5 m (19.7 inches)
Weir height = 2 inches

and stages 2 to 21 are sieve trays. Back-calculated Murphree tray efficiencies are summarized as follows:

Component	Fractional Murphree Efficiencies	
	Range	Median
<i>n</i> -Heptane	0.52 to 1.10	0.73
Toluene	0.70 to 0.79	0.79
Methyl ethyl ketone	−3.23 to 1.14	0.76

The median values, based on experience, seem reasonable and give confidence in the rate-based method. The 20 trays are equivalent to approximately 15 equilibrium stages.

For sizing, the column is divided into three sections: 9 trays above the top feed, 5 trays from the top feed to the bottom feed, and 6 trays below the bottom feed. Computed column diameters are,

respectively, 1.75 m (5.74 ft), 1.74 m (5.71 ft), and 1.83 m (6.00 ft). Thus, a 1.83-diameter column is a reasonable choice. Average predicted pressure drop per tray is 0.06 psi. Computed heat-exchanger duties are condenser: 2.544 MW (8,686,000 Btu/h); and reboiler: 2.482 MW (8,475,000 Btu/h).

EXAMPLE 12.3 Packed Column Design.

Repeat Example 12.2 for a tower packed with FLEXIPAC® 2 structured packing, at 75% of flooding. The packing heights are as follows:

Section	Packing Height, ft
Above top feed	13
Between top and bottom feeds	6.5
Below bottom feed	6.5

Solution

Each 6.5 feet of packing was simulated by 50 segments. Because of the large number of segments, mixed flow is assumed for both vapor and liquid. Convergence was achieved in 26 iterations. The predicted separation, which is just slightly better than that in Example 12.2, is as follows:

Component	Distillate, lbmol/h	Bottoms, lbmol/h
<i>n</i> -Heptane	54.88	0.12
Toluene	0.40	44.60
Methyl ethyl ketone	199.72	0.28

The HETP profile is plotted in Figure 12.3. Median values for *n*-heptane, toluene, and methyl-ethyl ketone, respectively, are approximately 0.55 m (21.7 inches), 0.45 m (17.7 inches), and 0.5 m (19.7 inches). The HETP values for the ketone vary widely.

Predicted column diameters for the three sections, starting from the top, are 1.65, 1.75, and 1.85 m, which are very close to the predicted sieve-tray diameters.

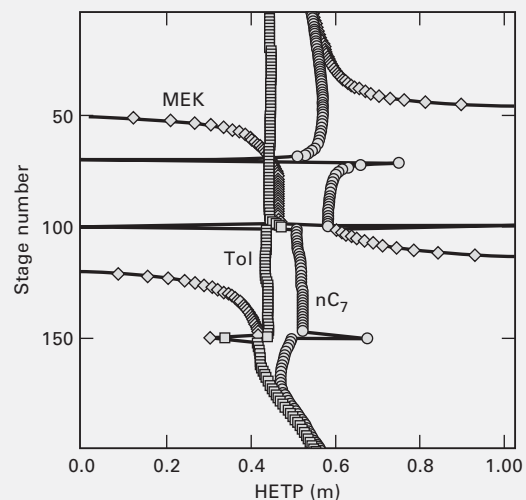


Figure 12.3 Column HETP profiles for Example 12.3.

EXAMPLE 12.4 Absorber Design.

Use the nonequilibrium column case of ChemSep to calculate the separation achieved in an absorber with 20 sieve trays operating at the conditions in Table 12.4. Use the default specifications for the tray design.

Table 12.4 Specifications for Example 12.4

Column top pressure = 182 psia
Column bottom pressure = 184 psia
Weir height = 2 inches
Vapor in plug flow
Liquid in dispersed flow using the Bennett-Grimm method
Chen–Chuang method for mass-transfer coefficients
Chilton–Colburn analogy for heat transfer
Soave–Redlich–Kwong method for K -values

Vapor feed at 126°F and 184 psia:

Component	lbmol/h
Hydrogen	218
Nitrogen	87
Methane	136
Ethane	139
Propane	118
Isobutane	6
<i>n</i> -Butane	2
Isopentane	43
<i>n</i> -Hexane	14
<i>n</i> -Heptane	4

Liquid absorbent feed at 100°F and 182 psia:

Component	lbmol/h
<i>n</i> -Dodecane	165
<i>n</i> -Tridecane	165

Solution

Initial estimates of the variables were provided automatically by the program. A total of 11 iterations were required. A column diameter of 3.48 feet was computed with a fraction of flooding between 50 and 67%. The converged product compositions were as follows:

Component	Lean Vapor, lbmol/h	Rich Oil, lbmol/h
Hydrogen	215.7	2.3
Nitrogen	85.5	1.5
Methane	130.5	5.5
Ethane	116.2	22.8
Propane	65.7	52.3
Isobutane	1.2	4.8
<i>n</i> -Butane	0.2	1.8
Isopentane	0.0	43.0
<i>n</i> -Hexane	0.0	14.0
<i>n</i> -Heptane	0.0	4.0
<i>n</i> -Dodecane	1.9	163.1
<i>n</i> -Tridecane	1.9	163.1
Total	618.9	478.1

Murphree and overall tray efficiencies vary from component to component and from tray to tray. For this absorber, of most interest is the overall tray efficiency for the key component, propane, whose absorption was $52.3/118 = 0.443$ or 44.3%. To obtain the overall tray efficiency for propane, equilibrium column calculations were made for a series of total equilibrium stages. The results pointed to an overall tray efficiency for propane of 28%.

As chemical engineers become more informed of the principles of mass transfer, and improved correlations for mass-transfer and heat-transfer coefficients are developed for trays and packings, use of rate-based models should accelerate, particularly for absorbers and nonideal mixtures. For best results, these models will also benefit from more studies of vapor and liquid flow patterns. More comparisons of rate-based models with industrial operating data are needed to gain confidence in the use of such models. Taylor, Kooijman, and Woodman [34], and Kooijman and Taylor [31] present some comparisons. Comparisons by Ovejero et al. [35], with distillation data obtained in a column packed with spheres and cylinders of known interfacial area, show very good agreement for three binary and two ternary systems.

§12.6 NOMENCLATURE**Latin Symbols**

A_b	tray bubbling area, (12-42)
a	tray froth interfacial area/froth volume, (12-40)
a_j^I	total stage interfacial area, (12-20)
c_t	total molar concentration, (12-22)
e	interface heat transfer rate on a stage, (12-6)
E	liquid and vapor phase energy balance residuals, (12-6) and (12-7)
f	feed component molar flow rates, (12-4):
$f_{k,j}$	residuals, (12-48)
H_j	stage pressure-drop residual, stage j , (12-13)
h	convective heat transfer coefficient, (12-39)
h_f	froth height on stage, (12-41)
J	molar diffusion flux, (12-19)
k	thermal conductivity, (12-43)
k_i	mass transfer coefficient for component i based on x or y driving force, (12-22)
M	liquid and vapor component material balance residuals, (12-4) and (12-5)
N_i	component mass transfer rate on a stage, Figure 12.1
N_T	total mass transfer rate on a stage, (12-18)
N_V, N_L	number of vapor or liquid transfer units, (12-40)
ΔP	tray pressure drop, (12-13)
Q^I	phase interface equilibrium residual, (12-15)
R	component mass-transfer rate residual, (12-9)
R	reciprocal mass-transfer coefficient function, (12-29)

r_j^V	vapor sidestream flow rate, (12-5)
r_j^L	liquid sidestream flow rate, (12-4)
S	component mole fraction residual, (12-11), (12-12)
U	molar liquid sidestream, molar flow, Figure 12.1
u_s	superficial vapor velocity based on bubbling area, (12-40)
W	molar vapor sidestream, molar flow, Figure 12.1
$X_{k,j}$	general residual, (12-49)
z	general or mixture mole fraction, (12-31)

Greek Symbol

κ^P	Maxwell-Stefan mass transfer coefficients, (12-24)
δ	Kronecker delta, (12-37)

SUMMARY

1. Rate-based models of multicomponent, multistage vapor-liquid separation operations became available in the late 1980s. These models are more accurate than equilibrium-based models.
2. Rate-based models incorporate rigorous procedures for component-coupling effects in multicomponent mass transfer.
3. The number of equations for a rate-based model is greater than that for an equilibrium-based model because separate balances are needed for each of the two phases. In addition, rate-based models are influenced by the geometry of the column internals. Correlations are used to predict mass-transfer and heat-transfer rates. Tray or packing

ε	tolerance, (12-49)
Γ	correction for non-ideality, (12-30)

Subscripts

T	total
---	-------

Superscripts

I	interface
L	liquid phase
P	phase L or V
V	vapor phase
—	partial molar

hydraulics are also incorporated into the rate-based model to enable prediction of column-pressure profiles. Phase equilibrium is assumed only at the phase interface.

4. Computing time for a rate-based model is not generally more than an order of magnitude greater than that for an equilibrium-based model.
5. RateSep in the RadFrac model of Aspen Plus, SCDS with the mass-transfer option in CHEMCAD, and the non-equilibrium column case in ChemSep all offer considerable flexibility in user specifications, so much so that inexperienced users can easily specify impossible conditions. Therefore, it is best to begin simulation studies with standard specifications.

REFERENCES

1. SOREL, E., *La rectification de l'alcool*, Paris (1893).
2. SMOKER, E.H., *Trans. AIChE*, **34**, 165 (1938).
3. THIELE, E.W., and R.L. GEDDES, *Ind. Eng. Chem.*, **25**, 290 (1933).
4. LEWIS, W.K., and G.L. MATHESON, *Ind. Eng. Chem.*, **24**, 496–498 (1932).
5. LEWIS, W.K., *Ind. Eng. Chem.*, **14**, 492 (1922).
6. MURPHREE, E.V., *Ind. Eng. Chem.*, **17**, 747–750, 960–964 (1925).
7. LEWIS, W.K., *Ind. Eng. Chem.*, **28**, 399 (1936).
8. TOOR, H.L., *AIChE J.*, **3**, 198 (1957).
9. TOOR, H.L., and J.K. BURCHARD, *AIChE J.*, **6**, 202 (1960).
10. KRISHNA, R., H.F. MARTINEZ, R. SREEDHAR, and G.L. STANDART, *Trans. I. Chem. E.*, **55**, 178 (1977).
11. WAGGONER, R.C., and G.D. LOUD, *Comput. Chem. Engng.*, **1**, 49 (1977).
12. KRISHNA, R., and G.L. STANDART, *Chem. Eng. Comm.*, **3**, 201 (1979).
13. TAYLOR, R., and R. KRISHNA, *Multicomponent Mass Transfer*, John Wiley & Sons, New York (1993).
14. KRISHNAMURTHY, R., and R. TAYLOR, *AIChE J.*, **31**, 449, 456 (1985).
15. TAYLOR, R., H.A. KOIJMAN, and J.-S. HUNG, *Comput. Chem. Engng.*, **18**, 205–217 (1994).
16. AIChE, *Bubble-Tray Design Manual*, New York (1958).
17. HARRIS, I.J., *British Chem. Engng.*, **10**(6), 377 (1965).
18. HUGHMARK, G.A., *Chem. Eng. Progress*, **61**(7), 97–100 (1965).
19. ZUIDERWEG, F.J., *Chem Eng. Sci.*, **37**, 1441 (1982).
20. CHAN, H., and J.R. FAIR, *Ind. Eng. Chem. Process Des. Dev.*, **23**, 814–827 (1984).
21. CHEN, G.X., and K.T. CHUANG, *Ind. Eng. Chem. Res.*, **32**, 701–708 (1993).
22. GARCIA, J.A. and FAIR, J.R., *Ind. Eng. Chem. Res.*, **39**, 1809–1817 (2000).
23. GARCIA, J.A. and FAIR, J.R., *Ind. Eng. Chem. Res.*, **39**, 1818–1825 (2000).
24. SYEDA, S. R., AFACAN, A., and CHUANG, K.T., *Chem. Eng. Res. and Design*, **85**(A2), 269–277 (2007).
25. VENNAVELLI, A.N., J.R. WHITELEY, and M.R. RESETARITS, *Ind. Eng. Chem. Res.*, **51**, 11458–11462 (2012).
26. ONDA, K., H. TAKEUCHI, and Y.J. OKUMOTO, *J. Chem. Eng. Japan*, **1**, 56–62 (1968).
27. BRAVO, J.L., and J.R. FAIR, *Ind. Eng. Chem. Process Des. Devel.*, **21**, 162–170 (1982).

28. BRAVO, J.L., J.A. ROCHA, and J.R. FAIR, *Hydrocarbon Processing*, **64**(1), 56–60 (1985).
29. BRAVO, J.L., J.A. ROCHA, and J.R. FAIR, *I. Chem. E. Symp. Ser.*, No. 128, A489–A507 (1992).
30. BILLET, R., and M. SCHULTES, *I. Chem. E. Symp. Ser.*, No. 128, B129 (1992).
31. KOOIJMAN, H.A., and R. TAYLOR, *Chem. Eng. J.*, **57**(2), 177–188 (1995).
32. FAIR, J.R., H.R. NULL, and W.L. BOLLES, *Ind. Eng. Chem. Process Des. Dev.*, **22**, 53–58 (1983).
33. POWERS, M.F., D.J. VICKERY, A. AREHOLE, and R. TAYLOR, *Comput. Chem. Engng.*, **12**, 1229–1241 (1988).
34. TAYLOR, R., H.A. KOOIJMAN, and M.R. WOODMAN, *I. Chem. E. Symp. Ser.*, No. 128, A415–A427 (1992).
35. OVEJERO, G., R. VAN GRIEKEN, L. RODRIGUEZ, and J.L. VALVERDE, *Sep. Sci. Tech.*, **29**, 1805–1821 (1994).
36. SCHEFFE, R.D., and R.H. WEILAND, *Ind. Eng. Chem. Res.*, **26**, 228–236 (1987).
37. SPAGNOLO, D.A., E.L. PLAICE, H.J. NEUBURG, and K.T. CHUANG, *Can. J. Chem. Eng.*, **66**, 367–376 (1988).
38. HIGLER, A., R. KRISHNA, and R. TAYLOR, *AIChE J.*, **45**, 2357–2370 (1999).
39. LOCKETT, M.J., *Distillation Tray Fundamentals*, Cambridge University Press, Cambridge (1986).
40. BENNETT, D.L. and H.J. GRIMM, *AIChE J.*, **37**, 589–596 (1991).

STUDY QUESTIONS

- 12.1. For binary distillation, what assumption did Smoker add to the McCabe–Thiele assumptions to obtain an algebraic solution?
- 12.2. What assumptions did Murphree make in the development of his tray efficiency equations?
- 12.3. For which situations does the Murphree efficiency appear to be adequate? What are its deficiencies?
- 12.4. What unusual phenomena did Toor discover for diffusion in a ternary mixture? Is a theory available to predict these phenomena?
- 12.5. In the rate-based model, is the assumption of phase equilibrium used anywhere? If so, where? Is it justified?
- 12.6. The rate-based model requires component mass-transfer coefficients, interfacial areas, and heat-transfer coefficients. How are these obtained?
- 12.7. What are component-coupling effects in mass-transfer-rate equations? Can they be appreciable?
- 12.8. Does the rate-based model account for the bulk-flow effect in mass transfer?
- 12.9. Can the rate-based model be applied to packed columns?
- 12.10. Are tray flow patterns important in rate-based models? What are the ideal flow-pattern models?

EXERCISES

Section 12.1

12.1. Entrainment and occlusion.

Modify the rate-based model of (12-4) to (12-18) to include entrainment and occlusion.

12.2. Addition of chemical reaction.

Modify the rate-based model of (12-4) to (12-18) to include a chemical reaction in the liquid phase under conditions of: (a) chemical equilibrium; (b) kinetic rate law.

12.3. Reducing equations in rate-based models.

Explain how the number of rate-based modeling equations can be reduced. Would this be worthwhile?

Section 12.2

12.4. Mass-transfer rates and tray efficiencies.

The following results were obtained at tray n from a rate-based calculation at 14.7 psia, for a ternary mixture of acetone (1), methanol (2), and water (3) in a sieve-tray column assuming that both phases are perfectly mixed.

Component	y_n	y_{n+1}	y_n^1	K_n^1	x_n
1	0.4913	0.4106	0.5291	1.507	0.3683
2	0.4203	0.4389	0.4070	0.900	0.4487
3	0.0884	0.1505	0.0639	0.3247	0.1830

The products of the computed gas-phase, binary mass-transfer coefficients, and interfacial area from the Chan–Fair correlations are as follows in units of lbmol/(h-unit mole fractions).

$$k_{12} = k_{21} = 1,750; k_{13} = k_{31} = 2,154; k_{23} = k_{32} = 2,503$$

The vapor rates are $V_n = 1,200$ lbmol/h and $V_{n+1} = 1,164$ lbmol/h. Determine: (a) component molar diffusion rates; (b) mass-transfer rates; (c) Murphree vapor-tray efficiencies.

12.5. Reciprocal rate functions.

Write all the expanded equations (12-31) and (12-32) for \mathbf{R}^P for a five-component system.

12.6. Perfectly mixed tray.

Repeat the calculations of Example 12.1 using 1 = methanol, 2 = water, and 3 = acetone. Are the results any different? If not, why not? Prove your conclusion mathematically.

Section 12.3

12.7. Mass-transfer coefficients for trays.

Compare and discuss the advantages and disadvantages of the available correlations for estimating binary-pair mass-transfer coefficients for trayed columns.

12.8. Mass-transfer coefficients for packings.

Discuss the advantages and disadvantages of the available correlations for estimating binary-pair mass-transfer coefficients for columns with random (dumped) and structured packings.

Section 12.4

12.9. Modeling flow patterns.

Discuss how the method of Fair, Null, and Bolles [32] might be used to model flow patterns in a rate-based model. How would the mole-fraction driving forces be computed?

Section 12.5

12.10. Distillation of a non-ideal ternary mixture.

A bubble-point mixture of 100 kmol/h of methanol, 50 kmol/h of isopropanol, and 100 kmol/h of water at 1 atm is sent to the 25th tray from the top of a 40-sieve-tray column equipped with a total condenser and partial reboiler, operating at a nominal pressure of 1 atm. If the reflux ratio is 5 and the bottoms flow rate is 150 kmol/h, determine the separation achieved if the UNIFAC method is used to estimate K -values and the Chan–Fair correlations are used for mass transfer. Assume that both phases are perfectly mixed on each tray and that operation is at about 80% of flooding.

12.11. Extractive distillation.

A sieve-tray column, operating at a nominal pressure of 1 atm, is used to separate a mixture of acetone and methanol by extractive distillation using water. The column has 40 trays with a total condenser and partial reboiler. The feed of 50 kmol/h of acetone and 150 kmol/h of methanol at 60°C and 1 atm enters Tray 35 from the top, while 50 kmol/h of water at 65°C and 1 atm enters Tray 5 from the top. Determine the separation for a reflux ratio of 10 and a bottoms flow rate of 200 kmol/h. Use the UNIFAC method for K -values and the AIChE method for mass transfer. Assume a perfectly mixed liquid and a vapor in plug flow on each tray, with operation at 80% of flooding. Determine the equilibrium stages (to the nearest stage) to achieve the same separation.

12.12. Distillation with dumped packing.

Repeat Exercise 12.10, if a column packed with 2-inch stainless steel Pall rings is used with 25 ft of rings above the feed and 15 ft below. Be sure to use sufficient segments for the calculations.

12.13. Distillation with structured packing.

Repeat Exercise 12.10, if a column with structured packing is used with 25 ft above the feed and 15 ft below. Be sure to use a sufficient number of segments.

12.14. Effect of percent flooding, weir height, and percent hole area.

Solve Exercise 12.10 for combinations of the following values of percent flooding, weir height, and % hole area: 40, 60, and 80%; 1, 2, and 3 inches; 6, 10, and 14%.

12.15. Effect of percent flooding on Murphree vapor tray efficiency.

The upper column of an air-separation system of the type shown in Exercise 7.39 contains 48 sieve trays and operates at a nominal pressure of 131.7 kPa. A feed at 80 K and 131.7 kPa enters the top plate at 1,349 lbmol/h with a composition of 97.868 mol% nitrogen, 0.365 mol% argon, and 1.767 mol% oxygen. A second feed enters tray 12 from the top at 83 K and 131.7 kPa at 1,832 lbmol/h with a composition of 59.7 mol% nitrogen, 1.47 mol% argon, and 38.83 mol % oxygen. The column has no condenser, but has a partial reboiler. Vapor distillate leaves the top plate at 2,487 lbmol/h, with remaining products leaving the reboiler as 50 mol% vapor and 50 mol% liquid. Assume ideal solutions. Determine the effect of flooding on the separation and the median E_{MV} for oxygen, using a rate-based model.

12.16. Extractive distillation in a sieve-tray column.

The following bubble-point, organic-liquid mixture at 1.4 atm is distilled by extractive distillation with the following phenol-rich solvent at 1.4 atm and the same temperature as the feed:

Component	Feed, kmol/h	Solvent, kmol/h
Methanol	50	0
<i>n</i> -Hexane	20	0
<i>n</i> -Heptane	180	0
Toluene	150	10
Phenol	0	800

The column has 30 sieve trays, with a total condenser and a partial reboiler. The solvent enters the fifth tray and the feed enters tray 15 from the top. The pressure in the condenser is 1.1 atm; the pressure at the top tray is 1.2 atm; and the pressure at the bottom is 1.4 atm. The reflux ratio is 5 and the bottoms rate is 960 kmol/h. Thermodynamic properties can be estimated with the UNIFAC method for the liquid phase and the SRK equation for the vapor phase. The Antoine equation is suitable for vapor pressure. Use a rate-based program to estimate the separation. Assume that the vapor and liquid are both well mixed and that the trays operate at 75% of flooding. Specify the Chan–Fair correlation for calculating mass-transfer coefficients. In addition, determine from the tray-by-tray results the average E_{MV} for each component (after discarding values much different than the majority). Try to improve the sharpness of the split by changing the feed and solvent entry tray locations. How can you increase the sharpness of the separation? List as many ideas as possible.

12.17. Equilibrium-and rate-based methods.

A bubble-cap tray absorber is designed to absorb 40% of the propane from a rich gas at 4 atm. The specifications for the entering rich gas and absorbent oil are as follows:

	Absorbent Oil	Rich Gas
Flow rate, kmol/s	11.0	11.0
Temperature, °C	32	62
Pressure, atm	4	4
Mole fraction:		
Methane	0	0.286
Ethane	0	0.157
Propane	0	0.240
<i>n</i> -Butane	0.02	0.169
<i>n</i> -Pentane	0.05	0.148
<i>n</i> -Dodecane	0.93	0

(a) Determine the number of equilibrium stages required and the splits of all components. (b) Determine the actual number of trays required and the splits and Murphree vapor-tray efficiencies of all components. Discuss and compare the equilibrium-based and rate-based results. What do you conclude?

12.18. Equilibrium-and rate-based methods.

A ternary mixture of methanol, ethanol, and water is distilled in a sieve-tray column to obtain a distillate with not more than 0.01 mol% water. The feed to the column is:

Flow rate, kmol/h	142.46
Pressure, atm	1.3
Temperature, K	316
Mole fractions:	
Methanol	0.6536
Ethanol	0.0351
Water	0.3113

Determine for a distillate rate of 93.10 kmol/h, a reflux ratio of 1.2, a condenser outlet pressure of 1.0 atm, and a top-tray pressure of 1.1 atm, using UNIFAC for activity coefficients: (a) number of equilibrium stages required and the corresponding split, if the feed enters at the optimal stage; and (b) number of actual trays required if the column operates at 85% of flooding and the feed is introduced to the optimal tray. Compare the split to that in part (a). (c) In addition, compute the component Murphree vapor-tray efficiencies. What do you conclude about the two methods of calculation?

12.19. Distillation in a packed bed.

Repeat Exercise 12.18 for a column packed with 2-inch stainless steel Pall rings.

12.20. Sizing a sieve-tray column.

It is required to absorb 96% of the benzene from a gas stream with absorption oil in a sieve-tray column at a nominal pressure of 1 atm. The feed conditions are as follows:

	Vapor	Liquid
Flow rate, kmol/s	0.01487	0.005
Pressure, atm	1.0	1.0
Temperature, K	300	300
Composition, mol fraction:		
Nitrogen	0.7505	0
Oxygen	0.1995	0
Benzene	0.0500	0.005
<i>n</i> -Tridecane (C ₁₃)	0	0.995

Tray geometry is as follows:

Tray spacing, m	0.5
Weir height, m	0.05
Hole diameter, m	0.003
Sheet thickness, m	0.002

Determine column diameter for 80% of flooding, the number of actual trays required, and the Murphree vapor-tray efficiency profile for benzene for the possible combinations of vapor and liquid flow patterns on a tray. Could the equilibrium-based method be used to obtain a reliable solution to this problem?

Chapter 13

Batch Distillation

§13.0 INSTRUCTIONAL OBJECTIVES

After completing this chapter, you should be able to:

- Derive the Rayleigh equation for a simple batch (differential) distillation and state the necessary assumptions.
- Calculate, by graphical and algebraic means for binary batch distillation, batch-still temperature, residue composition, and instantaneous and average distillate compositions as a function of time.
- Calculate for binary batch rectification, by modified McCabe–Thiele methods, residue and distillate compositions assuming equilibrium stages, no liquid holdup, and constant or variable reflux ratio to achieve constant distillate composition.
- Explain the importance of liquid holdup.
- Calculate, using rigorous equilibrium-stage methods with a process simulator, multicomponent, multistage batch rectification that includes a sequence of operating steps to obtain specified products.
- Apply the principles of optimal control to batch distillation.

A familiar example of a batch distillation is the laboratory apparatus shown in Figure 13.1. Here, a liquid mixture is charged to a **still pot** and heated to boiling. The vapor formed is continuously removed and condensed to produce a distillate. The compositions of the initial charge and distillate change with time. There is no steady state. The still temperature increases and the amount of lower-boiling components in the still pot decreases as distillation proceeds.

Batch operations can be used to advantage when:

1. The capacity of a facility is too small to permit continuous operation at a practical rate.
2. Seasonal or customer demands require distillation of different feedstocks with one unit to produce different products.
3. Several new products are to be produced with one distillation unit for evaluation by potential buyers.
4. Upstream process operations are batchwise and the compositions of feedstocks for distillation vary with time or from batch to batch.
5. The feed contains solids or materials that form solids, tars, or resin that can plug or foul a continuous distillation column.

§13.1 DIFFERENTIAL DISTILLATION

The simple, batch distillation apparatus in Figure 13.1 was first quantified by Lord Rayleigh [1] and is referred to as a **differential distillation**. There is no reflux. At any instant, vapor leaving the still pot with composition y_D is assumed to be in equilibrium with liquid (**residue**) in the still, which is assumed

to be perfectly mixed. For total condensation, $y_D = x_D$. The still pot is assumed to be the only equilibrium stage because there are no trays above the still pot. This apparatus is useful for separating wide-boiling mixtures.

The following nomenclature is used for variables that are a function of time, t , assuming that all compositions refer to a particular species in the multicomponent feed:

- D = instantaneous-distillate rate, mol/h
- Q_B = heat input rate to the still pot
- Q_C = heat output rate from the condenser
- V = instantaneous-overhead vapor rate, mol/h
- $y = y_D = x_D$ = mole fraction in instantaneous distillate leaving the still pot
- W = moles of liquid (residue) left in still
- $x = x_W$ = mole fraction in liquid (residue)
- 0 = subscript referring to $t = 0$

For any component in the mixture, the instantaneous rate of output = Dy_D is equal to the

$$\left. \begin{array}{l} \text{Instantaneous} \\ \text{rate of depletion} \\ \text{in the still} \end{array} \right\} = -\frac{d}{dt}(Wx_W) = -W\frac{dx_W}{dt} - x_W\frac{dW}{dt}$$

where distillate rate and, therefore, liquid-depletion rate in the still, depend on the heat-input rate, Q_B , to the still. Rearranging the above expression, a component material balance at any instant is

$$\boxed{\frac{d}{dt}(Wx_W) = W\frac{dx_W}{dt} + x_W\frac{dW}{dt} = -Dy_D} \quad (13-1)$$

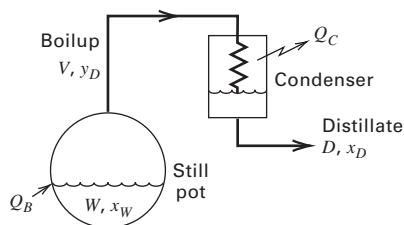


Figure 13.1 Differential (Rayleigh) distillation.

Multiplying (13-1) by dt :

$$Wdx_W + x_W dW = y_D(-Ddt) = y_D dW$$

since by total balance, $-Ddt = dW$. Separating variables and integrating from the initial charge condition of W_0 and x_{W_0} ,

$$\int_{x_{W_0}}^{x_W} \frac{dx_W}{y_D - x_W} = \int_{W_0}^W \frac{dW}{W} = \ln\left(\frac{W}{W_0}\right) \quad (13-2)$$

This is the Rayleigh equation, which was first applied to batch distillation of wide-boiling mixtures such as $\text{HCl-H}_2\text{O}$, $\text{H}_2\text{SO}_4\text{-H}_2\text{O}$, and $\text{NH}_3\text{-H}_2\text{O}$, where one stage is sufficient to achieve the desired separation. Without reflux, y_D and x_W are assumed to be in equilibrium, and (13-2) simplifies to

$$\int_{x_0}^x \frac{dx}{y-x} = \ln\left(\frac{W}{W_0}\right) \quad (13-3)$$

where x_{W_0} is replaced by x_0 .

Equation (13-3) is easily integrated when pressure is constant, temperature change in the still pot is relatively small (close-boiling mixture), and K -values are composition-independent. Then $y = Kx$, where if K is constant, (13-3) becomes

$$\ln\left(\frac{W}{W_0}\right) = \frac{1}{K-1} \ln\left(\frac{x}{x_0}\right) \quad (13-4)$$

For a binary mixture, if the relative volatility α , instead of K , is assumed constant, substitution of unsubscripted (7-3) into (13-3), followed by integration and simplification, gives

$$\ln\left(\frac{W_0}{W}\right) = \frac{1}{\alpha-1} \left[\ln\left(\frac{x_0}{x}\right) + \alpha \ln\left(\frac{1-x}{1-x_0}\right) \right] \quad (13-5)$$

If the equilibrium relationship $y = f\{x\}$ is graphical or tabular, integration of (13-3) can be performed graphically or numerically, as in the following three examples, which illustrate use of the Rayleigh equation for binary mixtures.

EXAMPLE 13.1 Differential Distillation at a Constant Boilup Rate.

A batch still is loaded with 100 kmol of an equimolar mixture of benzene and toluene. Make plots of (a) still temperature, (b) instantaneous vapor composition, (c) still pot (residue) composition, and (d) average total-distillate composition, all as a function of time. Assume a constant boilup rate, and, therefore, constant D of 10 kmol/h, and a constant α (benzene with respect to toluene) of 2.41 at a pressure of 101.3 kPa (1 atm).

Solution

Initially, $W_0 = 100$ kmol. Let the mole-fraction composition refer to the more volatile component, benzene, with $x_0 = 0.5$. Solving (13-5) for W at values of x from 0.5 in increments of 0.05, and determining corresponding values of time in hours from $t = (W_0 - W)/D$, the following table is generated:

t , h	2.12	3.75	5.04	6.08	6.94	7.66	8.28	8.83	9.35
W , kmol	78.85	62.51	49.59	39.16	30.59	23.38	17.19	11.69	6.52
$x = x_W$	0.45	0.40	0.35	0.30	0.25	0.20	0.15	0.10	0.05

Instantaneous-vapor composition, y , is obtained from a rearrangement of (4-10) to $y = \alpha x/[1 + (\alpha - 1)x]$. For $\alpha = 2.41$, $y = 2.41x/(1 + 1.41x)$. The average value of y_D or x_D over the time interval 0 to t is related to x and W at time t by combining overall component and total material balances to give

$$(x_D)_{\text{avg}} = (y_D)_{\text{avg}} = \frac{W_0 x_{W_0} - Wx}{W_0 - W} \quad (13-6)$$

Equation (13-6) is easier to apply than an equation that integrates the distillate composition.

To obtain the still temperature, T - x - y data for benzene-toluene at 101.3 kPa are given in Table 13.1. Computed temperature and compositions as a function of time are shown in Figure 13.2.

Table 13.1 Vapor-Liquid Equilibrium Data for Benzene (B)-Toluene (T) at 101.3 kPa

x_B	y_B	T , °C
0.100	0.208	105.3
0.200	0.372	101.5
0.300	0.507	98.0
0.400	0.612	95.1
0.500	0.713	92.3
0.600	0.791	89.7
0.700	0.857	87.3
0.800	0.912	85.0
0.900	0.959	82.7
0.950	0.980	81.4

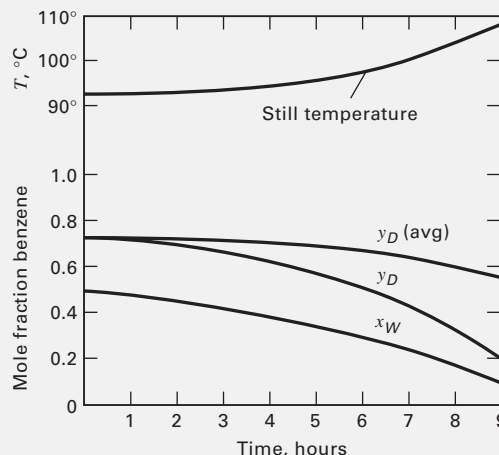


Figure 13.2 Distillation conditions for Example 13.1.

EXAMPLE 13.2 Differential Distillation Using Tabular Equilibrium Data.

Repeat Example 13.1, but instead of using $\alpha = 2.41$, use the vapor–liquid equilibrium data in Table 13.1 to solve the problem graphically or numerically with (13-3) rather than (13-5).

Solution

Equation (13-3) is solved by graphical integration by plotting $1/(y - x)$ versus x with a lower limit of $x_0 = 0.5$. Using the data of Table 13.1 for y as a function of x , points for the plot (in terms of benzene) are as follows:

x	0.5	0.4	0.3	0.2	0.1
$1/(y - x)$	4.695	4.717	4.831	5.814	9.259

The area under the curve from $x_0 = 0.5$ to a given value of x is equated to $\ln(W/W_0)$, and W is computed for $W_0 = 100$ kmol. In the region from $x_0 = 0.5$ to 0.3, the term $1/(y - x)$ changes only slightly; thus a numerical integration by the trapezoidal rule is readily made.

For $x = 0.5$ to 0.4:

$$\begin{aligned} \ln\left(\frac{W}{W_0}\right) &= \int_{0.5}^{0.4} \frac{dx}{y-x} \approx \Delta x \left[\frac{1}{y-x} \right]_{\text{avg}} \\ &= (0.4 - 0.5) \left(\frac{4.695 + 4.717}{2} \right) = -0.476 \\ W/W_0 &= 0.625, W = 0.625(100) = 62.5 \text{ kmol} \end{aligned}$$

For $x = 0.5$ to 0.3:

$$\begin{aligned} \ln\left(\frac{W}{W_0}\right) &= \int_{0.5}^{0.3} \frac{dx}{y-x} \approx \Delta x \left[\frac{1}{y-x} \right]_{\text{avg}} \\ &= (0.3 - 0.5) \left[\frac{4.695 + 4.717 + 4.717 + 4.831}{4} \right] = -0.948 \\ W/W_0 &= 0.388, W = 0.388(100) = 38.8 \text{ kmol} \end{aligned}$$

These two values of W are in good agreement with those in Example 13.1. A graphical integration from $x_0 = 0.4$ to $x = 0.1$ gives $W = 10.7$, which is approximately 10% less than the result in Example 13.1, which uses a constant value of the relative volatility.

The Rayleigh equation, (13-1), for differential distillation applies to any two components, i and j , of a multicomponent mixture. Thus, if M_i is the moles of i in the still pot,

$$\frac{dM_i}{dt} = \frac{d}{dt}(Wx_{W_i}) = -Dy_{D_i}$$

Then,
$$dM_i/dM_j = y_{D_i}/y_{D_j} \quad (13-7)$$

For constant $\alpha_{i,j} = y_{D_i}x_{W_j}/y_{D_j}x_{W_i}$, (13-7) becomes

$$dM_i/dM_j = \alpha_{i,j}(x_{W_i}/x_{W_j}) \quad (13-8)$$

Substitution of $M_i = Wx_{W_i}$ for both i and j into (13-8) gives

$$dM_i/M_i = \alpha_{i,j}dM_j/M_j \quad (13-9)$$

Integration from the initial-charge condition gives

$$\ln(M_i/M_{i_0}) = \alpha_{i,j} \ln(M_j/M_{j_0}) \quad (13-10)$$

The following example shows that (13-10) is useful for determining the effect of relative volatility on the separation achievable by differential distillation.

EXAMPLE 13.3 Effect of Relative Volatility in Differential Distillation.

The charge to a simple batch still consists of an equimolar, binary mixture of A and B. For values of $\alpha_{A,B}$ of 2, 5, 10, 100, and 1,000 and 50% vaporization of A, determine the mole fraction and percent vaporization of B in the total distillate.

Solution

For $\alpha_{A,B} = 2$ and $M_A/M_{A0} = 1 - 0.5 = 0.5$, (13-10) gives $M_B/M_{B0} = (M_A/M_{A0})^{1/\alpha_{A,B}} = (0.5)^{0.5} = 0.7071$. The vaporization of B = $(1 - 0.7071)(100) = 29.29\%$.

For 200 moles of charge, the amounts in the distillate are $D_A = (0.5)(0.5)(200) = 50$ mol and $D_B = (0.2929)(0.5)(200) = 29.29$ mol. Mole fraction of B in the total distillate = $29.29/(50 + 29.29) = 0.3694$.

Similar calculations for other values of $\alpha_{A,B}$ give:

$\alpha_{A,B}$	% Vaporization of B	Mole Fraction of B in Total Distillate
2	29.29	0.3694
5	12.94	0.2057
10	6.70	0.1182
100	0.69	0.0136
1,000	0.07	0.0014

These results show that a sharp separation between A and B for 50% vaporization of A is achieved only if $\alpha_{A,B} \geq 100$. Furthermore, the purity achieved depends on the percent vaporization of A. For $\alpha_{A,B} = 100$, with 90% of A vaporized, the mole fraction of B in the total distillate increases from 0.0136 to 0.0247. For this reason, it is common to conduct a binary, batch-distillation separation of LK and HK in the following manner:

1. Produce a distillate LK cut until the limit of impurity of the HK in the total distillate is reached.
2. Continue the batch distillation to produce an intermediate (slop) cut of impure LK until the limit of impurity of LK in the liquid remaining in the still is reached.
3. Empty the HK-rich cut from the still.
4. Recycle the intermediate (slop) cut to the next still charge.

For desired purities of the LK-HK cuts, the fraction of intermediate (slop) cut increases as the LK-HK relative volatility decreases.

§13.2 BINARY BATCH RECTIFICATION

For a sharp separation and/or to reduce the intermediate-cut fraction, a trayed or packed column is added between the still and the condenser to provide stages, as shown in Figure 13.3. Also, a reflux drum is added after the condenser. In addition, one or more drums are provided to collect distillate cuts. For a column of a given diameter, the molar vapor-boilup rate is fixed at a value safely below the column flooding point.

Two modes of operating a batch rectification are cited most frequently because they are the most readily modeled. The first is operation at a constant reflux rate or ratio (same as a constant distillate rate), while the second is operation at a constant distillate composition. With the former, the distillate composition varies with time; with the latter, the reflux ratio or distillate rate varies with time. The first mode is easily implemented because of the availability of rapidly responding flow-rate sensors. For the second mode, a rapidly responding composition sensor is required. In a third mode, referred to as the optimal-control mode, both reflux ratio (or distillate rate) and distillate composition are varied with time to maximize the amount of distillate, minimize operation time, and/or maximize profit. Constant reflux is discussed first, followed by constant composition. Optimal control is deferred to §13.7.

§13.2.1 Constant Reflux Operation

If R or D is fixed, instantaneous-distillate and pot-still bottoms compositions vary with time. Assume a trayed column with total condenser, negligible holdup of vapor and liquid in the condenser and column, phase equilibrium at each tray, and constant molar overflow. Then, (13-2) applies with $y_D = x_D$. The method of Smoker and Rose [2] facilitates the analysis using a McCabe–Thiele diagram.

Initially, the composition of the LK in the liquid in the still is the charge composition, x_{W_0} , which is 0.43 in the McCabe–Thiele diagram of Figure 13.4. If there are two theoretical stages (the still pot and one equilibrium stage), the initial distillate composition, x_{D_0} , at time 0 can be found by constructing an operating line of slope $L/V = (R/R + 1)$, such that exactly two stages are stepped off to the right from x_{W_0} to the $y = x$ line in Figure 13.4. After an arbitrary time, say, time 1, at still pot composition $x_W < x_{W_0}$, e.g., $x_W = 0.26$ in Figure 13.4, the instantaneous-distillate composition is x_D .

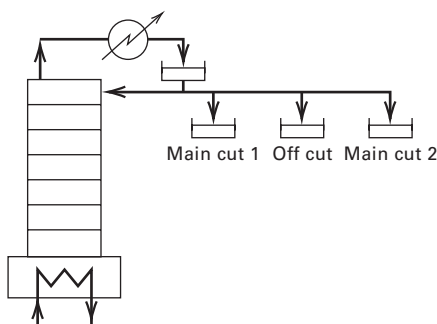


Figure 13.3 Batch rectification.

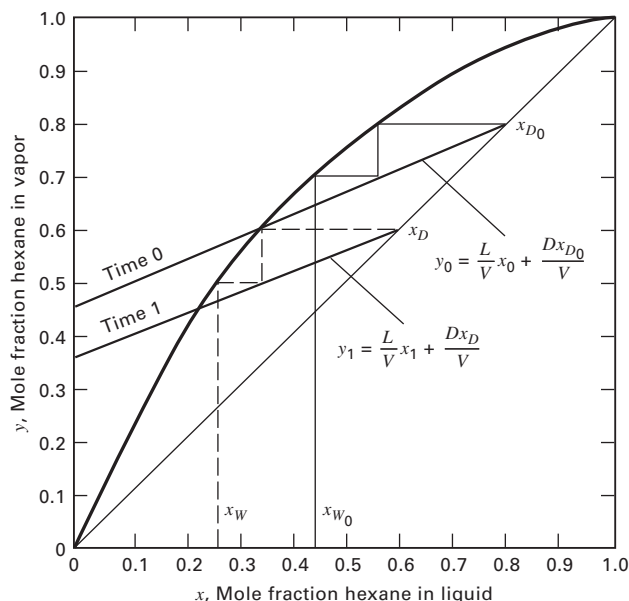


Figure 13.4 Batch binary distillation with fixed L/V and two theoretical stages.

In this manner, a time-dependent series of points for x_D as a function of x_W is established, with L/V and the number of stages held constant.

Equation (13-2) cannot be integrated analytically because the relationship between $y_D = x_D$ and x_W depends on L/V , the number of theoretical stages, and the phase-equilibrium relationship. However, (13-2) can be integrated graphically with pairs of values for $y_D = x_D$ and x_W obtained from the McCabe–Thiele diagram, as in Figure 13.4, for a series of operating lines of the same slope.

The time t required for this batch rectification can be computed by a total material balance based on a constant boilup rate V , to give an equation due to Block [3]:

$$t = \frac{W_0 - W_t}{V \left(1 - \frac{L}{V}\right)} = \frac{R + 1}{V} (W_0 - W_t) \quad (13-11)$$

With a constant-reflux policy, instantaneous-distillate purity is above specification at the beginning and below specification at the end of the run. By an overall material balance, the average mole fraction of LK in the accumulated distillate at time t is

$$x_{D_{\text{avg}}} = \frac{W_0 x_0 - W_t x_{W_t}}{W_0 - W_t} \quad (13-12)$$

EXAMPLE 13.4 Constant Reflux Operation.

A three-stage batch rectifier (first stage is the still pot) is charged with 100 kmol of a 20 mol% n -hexane in n -octane mixture. At a constant-reflux ratio of 1 ($L/V = 0.5$), how many moles of charge must be distilled for an average product composition of 70 mol% nC_6 ? The phase-equilibrium curve at column pressure is given in Figure 13.5. If the boilup rate is 10 kmol/h, calculate distillation time.

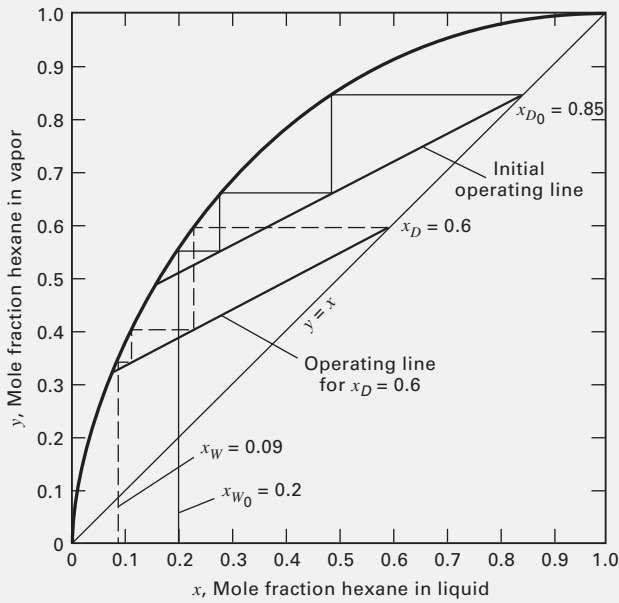


Figure 13.5 Solution to Example 13.4.

Solution

A series of operating lines and values of x_W are located by the trial-and-error procedure described earlier, as shown in Figure 13.5 for $x_{W_0} = 0.20$ and $x_W = 0.09$. Using Figure 13.5, the following table is developed:

$y_D = x_D$	0.85	0.60	0.5	0.35	0.3
x_W	0.2	0.09	0.07	0.05	0.035
$\frac{1}{y_D - x_W}$	1.54	1.96	2.33	3.33	3.77

The graphical integration is shown in Figure 13.6. Assuming a final value of $x_W = 0.1$, for instance, integration of (13-2) gives

$$\ln \frac{100}{W} = \int_{0.1}^{0.2} \frac{dx_W}{y_D - x_W} = 0.162$$

Hence, $W = 85$ and $D = 15$.

$$\text{From (13-12): } (x_D)_{\text{avg}} = \frac{100(0.20) - 85(0.1)}{(100 - 85)} = 0.77$$

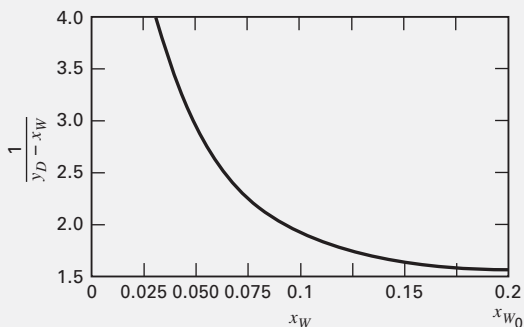


Figure 13.6 Graphical integration for Example 13.4.

The $(x_D)_{\text{avg}}$ is higher than the desired value of 0.70; hence, another x_W must be chosen. By trial, the correct answer is found to be $x_W = 0.06$, with $D = 22$, and $W = 78$, corresponding to a value of 0.25 for the integral. From (13-11), distillation time is $t = (1 + 1)(100 - 78)/10 = 4.4$ h. When differential distillation is used instead, Figure 13.5 shows that 70 mol% hexane distillate is not achievable because the initial distillate is only 56 mol% hexane.

§13.2.2 Constant Distillate Composition

The constant-reflux-ratio policy described in the previous section is easy to implement. For small batch-rectification systems, it may be the least expensive policy. A more optimal policy is to maintain a constant V but continuously vary R to achieve a constant x_D that represents the specified purity. This requires a more complex control system, including a composition sensor on the distillate, which may be justified only for large batch-rectification systems. Ellerbe [5] discusses other methods of operating batch columns.

Calculations for the policy of constant x_D can also be made with the McCabe–Thiele diagram, as described by Bogart [4] and illustrated in Example 13.5. The Bogart method assumes negligible liquid holdup and constant molar overflow. An overall material balance for the LK, at any time t , is given by a rearrangement of (13-12) at constant x_D , for W as a function of x_W :

$$W = W_0 \left[\frac{x_D - x_{W_0}}{x_D - x_W} \right] \quad (13-13)$$

Or for x_W as a function of W :

$$x_W = \frac{Wx_D - W_0(x_D - x_{W_0})}{W} \quad (13-14)$$

Differentiating (13-13) with respect to t for varying W and x_W gives

$$\frac{dW}{dt} = W_0 \frac{(x_D - x_{W_0})}{(x_D - x_W)^2} \frac{dx_W}{dt} \quad (13-15)$$

For constant molar overflow, the distillation rate is given by the rate of loss of charge, W :

$$-\frac{dW}{dt} = (V - L) = \frac{dD}{dt} \quad (13-16)$$

where D is now the amount of distillate, not the distillate rate. Substituting (13-16) into (13-15) and integrating:

$$t = \frac{W_0(x_D - x_{W_0})}{V} \int_{x_{W_t}}^{x_{W_0}} \frac{dx_W}{(1 - L/V)(x_D - x_W)^2} \quad (13-17)$$

For fixed values of W_0 , x_{W_0} , x_D , V , and the number of stages, the McCabe–Thiele diagram is used to determine values of L/V for a series of values of still pot composition between x_{W_0} and the final value of x_W . These values are then used with (13-17) to determine, by graphical or numerical integration, the time for rectification or the time to reach any still pot composition. The required number of stages can be estimated by assuming total reflux for the final value of x_W .

While rectification is proceeding, the instantaneous-distillate rate varies according to (13-16), which can be expressed in terms of L/V as

$$\frac{dD}{dt} = V(1 - L/V) \tag{13-18}$$

EXAMPLE 13.5 Constant Distillate Composition.

A three-stage batch still (boiler and the equivalent of two equilibrium plates) is charged with 100 kmol of a liquid containing an equimolar mixture of *n*-hexane and *n*-octane. A liquid distillate of 0.9 mole-fraction hexane is to be maintained by continuously adjusting the reflux ratio, while maintaining a distillate rate of 20 kmol/h. What should the reflux ratio be after one hour when the accumulated distillate is 20 kmol? Theoretically, when must distillate accumulation be stopped? Assume negligible holdup and constant molar overflow.

Solution

When the accumulated distillate = 20 kmol, $W = 80$ kmol, and the still residue composition with respect to the light-key is given by (13-14):

$$x_w = \frac{Wx_D - W_0(x_D - x_{w_0})}{W} = \frac{0.9(80) - 100(0.9 - 0.5)}{80} = 0.4$$

For $y_D = x_D = 0.9$, a series of operating lines of varying slope, $L/V = R/(R + 1)$, with three stages stepped off, is used to determine the corresponding still pot residue composition, x_w . By trial and error, Line 1 in Figure 13.7 is found for $x_w = 0.4$, corresponding to an $L/V = 0.22$. The reflux ratio = $(L/V)/[1 - (L/V)] = 0.282$. At the highest reflux rate possible, $L/V = 1$ (total reflux), and $x_w = 0.06$, according to the dashed-line construction shown in Figure 13.7. The corresponding time by material balance is $0.06(100 - 20t) = 50 - 20t(0.9)$. Solving, $t = 2.58$ h.

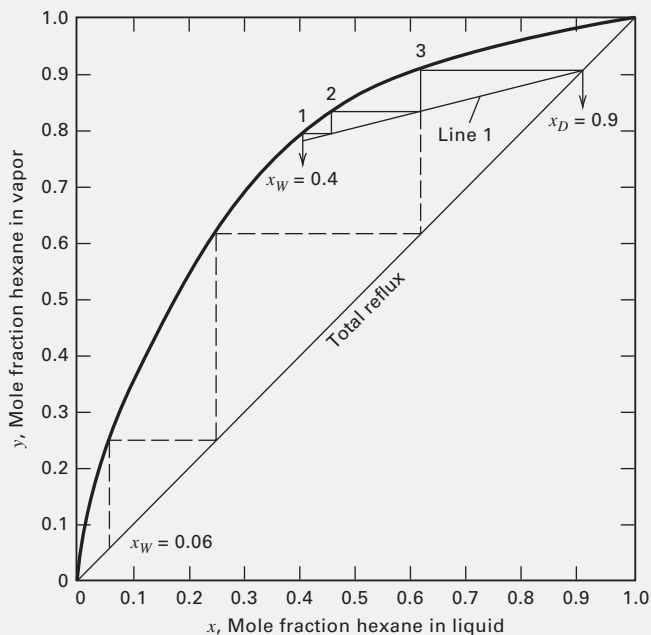


Figure 13.7 Solution to Example 13.5.

§13.3 BATCH STRIPPING AND COMPLEX BATCH DISTILLATION

A batch stripper consisting of a large accumulator (feed tank), a trayed or packed stripping column, and a reboiler is shown in Figure 13.8. The initial charge is placed in the accumulator rather than the reboiler. The mixture in the accumulator is fed to the top of the column and the bottoms cut is removed from the reboiler. A batch stripper is useful for removing small quantities of volatile impurities. For binary mixtures, the McCabe–Thiele construction applies, and the graphical methods in §13.2 can be modified to follow, with time, the change in composition in the accumulator and the corresponding instantaneous and average composition of the bottoms cut.

Figure 13.9 depicts a complex batch-distillation unit, described by Hasebe et al. [6], Barolo et al. [7], and Phimister and Seider [8,9], which permits considerable operating flexibility. The charge in the feed tank is fed to a suitable column location. Holdups in the reboiler and condenser are kept to a minimum. Products or intermediate cuts are withdrawn from the condenser, the reboiler, or both. In addition, the liquid in

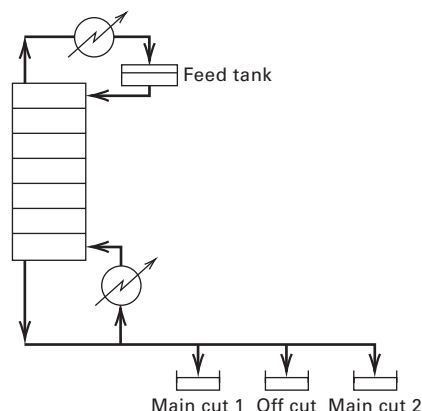


Figure 13.8 Batch stripping.

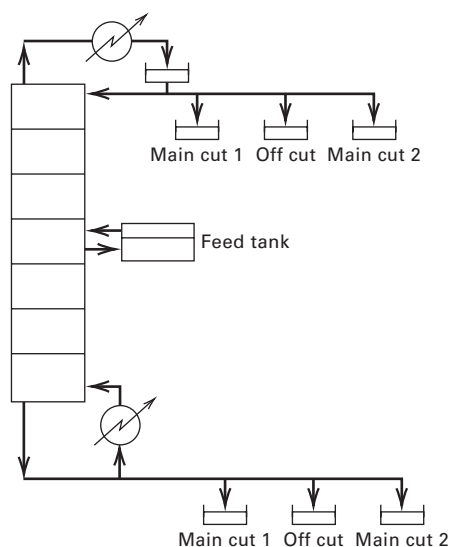


Figure 13.9 Complex batch distillation.

the column at the feed location can be recycled to the feed tank if it is desirable to make the composition in the feed tank close to the composition of liquid at the feed location.

§13.4 EFFECT OF LIQUID HOLDUP

Except at high pressure, vapor holdup in a batch-distillation rectifying column is negligible because of the small vapor density. However, the effect of liquid holdup on the trays and in the condensing and reflux system can be significant when the molar ratio of holdup to original charge is more than a few percent. This is especially true when a charge contains low concentrations of one or more of the components. The effect of holdup in a trayed column is greater than in a packed column because of the lower amount of holdup in the latter.

A batch rectifier is usually started up under total-reflux conditions for an initial period of time prior to the withdrawal of distillate. During this initial period, liquid holdup in the column increases and approaches a value that is reasonably constant for the remainder of the run. Because of the total-reflux concentration profile, the initial concentration of light components in the remaining charge to the still is less than in the original charge. At high liquid holdups, this causes the initial purity and degree of separation to be reduced from estimates based on methods that ignore liquid holdup. Liquid holdup can reduce the size of product cuts, increase the size of intermediate fractions that are recycled, increase the amount of residue, increase the batch-cycle time, and increase total energy input. Although approximate methods for predicting the effect of liquid holdup are available, the complexity of the holdup effect is such that it is best to use rigorous batch-distillation models described in §13.5 to study the effect on a case-by-case basis.

§13.5 STAGE-BY-STAGE METHODS FOR BATCH RECTIFICATION

Stage-by-stage temperature, flow rates, and composition profiles as a function of time are required for final design or simulation of multicomponent batch rectification. Such calculations involve the solution of **differential-algebraic equations (DAEs)**. The rigorous calculations are tedious, and must be carried out on a digital computer.

§13.5.1 Rigorous Model

Meadows [10] developed the first rigorous multicomponent batch-distillation model, based on assumptions of equilibrium stages; perfect mixing of liquid and vapor on each stage; negligible vapor holdup; constant-molar-liquid holdup, M , on a stage and in the condenser system; and adiabatic stages. Distefano [11] extended the model and developed a computer-based method for solving the equations. A more efficient method is described by Boston et al. [12].

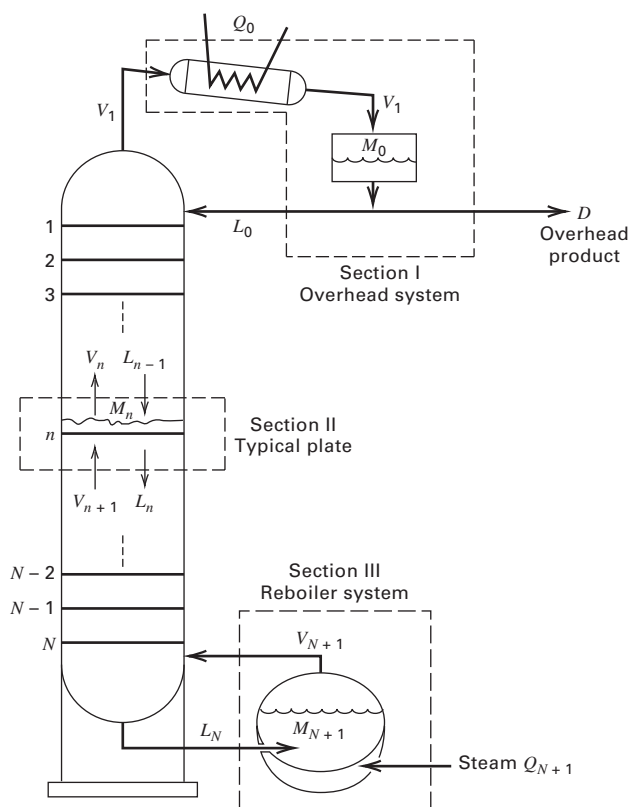


Figure 13.10 Multicomponent batch-rectification operation. [Reproduced from [11] with permission from John Wiley & Sons, Inc.]

Figure 13.10 shows the multicomponent batch-rectification operation modeled by Distefano. The unit consists of a partial reboiler (still pot), a column with N equilibrium stages or their equivalent in packing, and a total condenser with a reflux drum. Also included, but not shown in Figure 13.10, are a number of accumulator or receiver drums equal to the number of overhead product and intermediate cuts. When product purity specifications cannot be made for successive distillate cuts, then intermediate (waste or slop) cuts are necessary. These are usually recycled.

To initiate operation, feed is charged to the reboiler, to which heat is supplied. Vapor leaving stage 1 at the top of the column is condensed and passes to the reflux drum. At first, a total-reflux condition is established for a steady-state, fixed-overhead vapor flow rate. Depending upon the amount of liquid holdup in the column and in the condenser, the liquid amount and composition in the reboiler at total reflux differs from the original feed.

Starting at time $t = 0$, distillate flows from the reflux drum to a receiver (accumulator) at a constant molar flow rate, and a reflux ratio is established. The heat-transfer rate to the reboiler is adjusted to maintain the overhead-vapor molar flow rate. Model equations are derived for sections (I) the overhead condensing system, (II) column stages, and (III) the reboiler section, as illustrated in Figure 13.10. For Section I,

component material balances, a total material balance, and an energy balance are:

$$V_1 y_{i,1} - L_0 x_{i,0} - D x_{i,D} = \frac{d(M_0 x_{i,0})}{dt} \quad (13-19)$$

$$V_1 - L_0 - D = \frac{dM_0}{dt} \quad (13-20)$$

$$V_1 h_{V_1} - (L_0 + D) h_{L_0} = Q_0 + \frac{d(M_0 h_{L_0})}{dt} \quad (13-21)$$

where the derivative terms are accumulations due to holdup, M_0 , which is assumed to be perfectly mixed. Also, for phase equilibrium at Stage 1 of the column:

$$y_{i,1} = K_{i,1} x_{i,1} \quad (13-22)$$

The working equations are obtained by combining (13-19) and (13-22) to obtain a revised component material balance in terms of liquid-phase compositions, and by combining (13-20) and (13-21) to obtain a revised energy balance that does not include dM_0/dt . Equations for Sections II and III in Figure 13.10 are derived in a similar manner. The resulting working model equations for $t = 0^+$ are as follows, where i refers to component, j refers to the stage, and M is molar liquid holdup.

1. Component mole balances for the overhead-condensing system, column stages, and reboiler, respectively:

$$\frac{dx_{i,0}}{dt} = - \left[\frac{L_0 + D + \frac{dM_0}{dt}}{M_0} \right] x_{i,0} + \left[\frac{V_1 K_{i,1}}{M_0} \right] x_{i,1}, \quad i = 1 \text{ to } C \quad (13-23)$$

$$\begin{aligned} \frac{dx_{i,j}}{dt} = & \left[\frac{L_{j-1}}{M_j} \right] x_{i,j-1} - \left[\frac{L_j + K_{i,j} V_j + \frac{dM_j}{dt}}{M_j} \right] x_{i,j} \\ & + \left[\frac{K_{i,j+1} V_{j+1}}{M_j} \right] x_{i,j+1}, \quad i = 1 \text{ to } C, \quad j = 1 \text{ to } N \end{aligned} \quad (13-24)$$

$$\begin{aligned} \frac{dx_{i,N+1}}{dt} = & \left(\frac{L_N}{M_{N+1}} \right) x_{i,N} \\ & - \left[\frac{V_{N+1} K_{i,N+1} + \frac{dM_{N+1}}{dt}}{M_{N+1}} \right] x_{i,N+1}, \quad i = 1 \text{ to } C \end{aligned} \quad (13-25)$$

where $L_0 = RD$.

2. Total mole balances for the overhead-condensing system and column stages, respectively:

$$V_1 = D(R + 1) = \frac{dM_0}{dt} \quad (13-26)$$

$$L_j = V_{j+1} + L_{j-1} - V_j - \frac{dM_j}{dt}, \quad j = 1 \text{ to } N \quad (13-27)$$

3. Enthalpy balances around the overhead-condensing system, adiabatic column stages, and reboiler, respectively:

$$Q_0 = V_1 (h_{V_1} - h_{L_0}) - M_0 \frac{dh_{L_0}}{dt} \quad (13-28)$$

$$\begin{aligned} V_{j+1} = & \frac{1}{(h_{V_{j+1}} - h_{L_j})} \\ & \left[V_j (h_{V_j} - h_{L_j}) - L_{j-1} (h_{L_{j-1}} - h_{L_j}) + M_j \frac{dh_{L_j}}{dt} \right], \\ & j = 1 \text{ to } N \end{aligned} \quad (13-29)$$

$$\begin{aligned} Q_{N+1} = & V_{N+1} (h_{V_{N+1}} - h_{L_{N+1}}) - L_N (h_{L_N} - h_{L_{N+1}}) \\ & + M_{N+1} \left(\frac{dh_{L_{N+1}}}{dt} \right) \end{aligned} \quad (13-30)$$

4. Phase equilibrium on the stages and in the reboiler:

$$y_{i,j} = K_{i,j} x_{i,j}, \quad i = 1 \text{ to } C, \quad j = 1 \text{ to } N + 1 \quad (13-31)$$

5. Mole-fraction sums at column stages and in the reboiler:

$$\sum_{i=1}^C y_{i,j} = \sum_{i=1}^C K_{i,j} x_{i,j} = 1.0, \quad j = 0 \text{ to } N + 1 \quad (13-32)$$

6. Molar holdups in the condenser system and on the column stages, based on constant-volume holdups, G_j :

$$M_0 = G_0 \rho_0 \quad (13-33)$$

$$M_j = G_j \rho_j, \quad j = 1 \text{ to } N \quad (13-34)$$

where ρ is liquid molar density.

7. Variation of molar holdup in the reboiler, where M_{N+1}^0 is the initial charge to the reboiler:

$$M_{N+1} = M_{N+1}^0 - \sum_{j=0}^N M_j - \int_0^t D dt \quad (13-35)$$

Equations (13-23) through (13-35) constitute an **initial-value problem** for a system of ordinary differential and algebraic equations (DAEs). The total number of equations is $(2CN + 3C + 4N + 7)$. If variables $N, D, R = L_0/D, M_{N+1}^0$, and all G_j are specified, and if correlations are available for computing liquid densities, vapor and liquid enthalpies, and K -values, the number of unknown variables, distributed as follows, is equal to the number of equations.

$x_{i,j}$	$CN + 2C$
$y_{i,j}$	$CN + C$
L_j	N
V_j	$N + 1$
T_j	$N + 2$
M_j	$N + 2$
Q_0	1
Q_{N+1}	1
	<hr/>
	$2CN + 3C + 4N + 7$

Initial values at $t = 0$ for all these variables are obtained from the steady-state, total-reflux calculation, which depends only on values of N , M_{N+1}^0 , x_{N+1}^0 , G_j , and V_1 .

Equations (13-23) through (13-30) include first derivatives of $x_{i,j}$, M_j , and h_{Lj} . Except for M_{N+1} , derivatives of the latter two variables can be approximated with sufficient accuracy by incremental changes over the previous time step. If the reflux ratio is high, as it often is, the derivative of M_{N+1} can also be approximated in the same manner. This leaves only the $C(N+2)$ ordinary differential equations (ODEs) for the component material balances to be integrated in terms of the $x_{i,j}$ dependent variables.

§13.5.2 Rigorous Integration Method

The nonlinear equations (13-23) to (13-25) cannot be integrated analytically. Distefano [11] developed a solution method based on an investigation of 11 different numerical integration techniques that step in time. Of particular concern were the problems of **truncation error** and **stability**, which make it difficult to integrate the equations rapidly and accurately. Such systems of ODEs or DAEs constitute so-called **stiff systems** as described later in this section.

Local truncation errors result from using approximations for the functions on the RHS of the ODEs at each time step. These errors may be small, but they can grow through subsequent time steps, resulting in global truncation errors sufficiently large to be unacceptable. The number of significant digits in the computed dependent variables decrease as truncation errors become large. Truncation errors can be reduced by decreasing the time-step size.

Stability problems are much more serious. When instability occurs, the computed values of the dependent variables become totally inaccurate, with no significant digits at all. Reducing the time step does not eliminate instability until a time-step criterion, which depends on the numerical method, is satisfied. Even then, a further reduction in the time step is required to prevent oscillations of dependent variables.

Problems of stability and truncation error are conveniently illustrated by comparing results obtained by using the explicit- and implicit-Euler methods, both of which are first-order in accuracy, as discussed by Davis [15] and Riggs [16].

Consider the nonlinear, first-order ODE:

$$\frac{dy}{dt} = f\{t, y\} = ay^2te^y \quad (13-36)$$

for $y\{t\}$, where initially $y\{t_0\} = y_0$. The explicit- (forward) Euler method approximates (13-36) with a sequence of discretizations of the form

$$\frac{y_{k+1} - y_k}{\Delta t} = ay_k^2 t_k e^{y_k} \quad (13-37)$$

where Δt is the time step and k is the sequence index. The function $f\{t, y\}$ is evaluated at the beginning of the current time step. Solving for y_{k+1} gives the recursion equation:

$$y_{k+1} = y_k + ay_k^2 t_k e^{y_k} \Delta t \quad (13-38)$$

Regardless of the nature of $f\{t, y\}$ in (13-36), the recursion equation can be solved explicitly for y_{k+1} using results from the

previous time step. However, as discussed later, this advantage is counterbalanced by a limitation on the magnitude of Δt to avoid instability and oscillations.

The implicit- (backward) Euler method also utilizes a sequence of discretizations of (13-36), but the function $f\{t, y\}$ is evaluated at the end of the current time step. Thus:

$$\frac{y_{k+1} - y_k}{\Delta t} = ay_{k+1}^2 t_{k+1} e^{y_{k+1}} \quad (13-39)$$

Because the function $f\{t, y\}$ is nonlinear in y , (13-39) cannot be solved explicitly for y_{k+1} . This disadvantage is counterbalanced by unconditional stability with respect to selection of Δt . However, too large a value can result in unacceptable truncation errors.

When the explicit-Euler method is applied to (13-23) to (13-35) for batch rectification, as shown in the following example, the maximum value of Δt can be estimated from the maximum absolute eigenvalue, $|\lambda|_{\max}$, of the Jacobian matrix of (13-23) to (13-25). To prevent instability, $\Delta t_{\max} \leq 2/|\lambda|_{\max}$. To prevent oscillations, $\Delta t_{\max} \leq 1/|\lambda|_{\max}$. Applications of the explicit- and implicit-Euler methods are compared in the following batch-rectification example.

EXAMPLE 13.6 Selection of Time Step for a Batch Distillation.

One hundred kmol of an equimolar mixture of n -hexane (A) and n -heptane (B) is distilled at 15 psia in a batch rectifier consisting of a total condenser with a constant liquid holdup, M_0 , of 0.10 kmol; a single equilibrium plate with a constant liquid holdup, M_1 , of 0.01 kmol; and a reboiler. Initially the system is brought to the following total-reflux condition, with saturated liquid leaving the total condenser:

Stage	T , °F	x_A	K_A	K_B	M , kmol
Condenser	162.6	0.85935	—	—	0.1
Plate, 1	168.7	0.70930	1.212	0.4838	0.01
Reboiler, 2	178.6	0.49962	1.420	0.5810	99.89

Distillation begins ($t = 0$) with a reflux rate, L_0 , of 10 kmol/h and a distillate rate, D , of 10 kmol/h. Calculate the mole fractions of n -hexane and n -heptane at $t = 0.05$ h (3 min), at each of the three rectifier locations, assuming constant molar overflow and constant K -values for this small elapsed time period. Use explicit- and implicit-Euler methods to determine the influence of the time step, Δt .

Solution

Based on the constant molar overflow assumption, $V_1 = V_2 = 20$ kmol/h and $L_0 = L_1 = 10$ kmol/h. Using the K -values and liquid holdups given above, (13-23) to (13-25), with all $dM_j/dt = 0$, become as follows:

Condenser:

$$\frac{dx_{A,0}}{dt} = -200x_{A,0} + 242.4x_{A,1} \quad (1)$$

$$\frac{dx_{B,0}}{dt} = -200x_{B,0} + 96.76x_{B,1} \quad (2)$$

Plate:

$$\frac{dx_{A,1}}{dt} = 1,000x_{A,0} - 3,424x_{A,1} + 2,840x_{A,2} \quad (3)$$

$$\frac{dx_{B,1}}{dt} = 1,000x_{B,0} - 1,967x_{B,1} + 1,162x_{B,2} \quad (4)$$

Reboiler:

$$\frac{dx_{A,2}}{dt} = \left(\frac{10}{M_2}\right)x_{A,1} - \left(\frac{28.40}{M_2}\right)x_{A,2} \quad (5)$$

$$\frac{dx_{B,2}}{dt} = \left(\frac{10}{M_2}\right)x_{B,1} - \left(\frac{11.62}{M_2}\right)x_{B,2} \quad (6)$$

where

$$M_2\{t = t\} = M_2\{t = 0\} - (V_2 - V_1)t$$

Or

$$M_2 = 99.89 - 10t \quad (7)$$

Equations (1) through (6) can be grouped by component into the following two matrix equations:

Component A:

$$\begin{bmatrix} -200 & 242.2 & 0 \\ 1,000 & -3,424 & 2,840 \\ 0 & 10/M_2 & -28.40/M_2 \end{bmatrix} \cdot \begin{bmatrix} x_{A,0} \\ x_{A,1} \\ x_{A,2} \end{bmatrix} = \begin{bmatrix} dx_{A,0}/dt \\ dx_{A,1}/dt \\ dx_{A,2}/dt \end{bmatrix} \quad (8)$$

Component B:

$$\begin{bmatrix} -200 & 96.76 & 0 \\ 1,000 & -1,967 & 1,160 \\ 0 & 10/M_2 & -11.62/M_2 \end{bmatrix} \cdot \begin{bmatrix} x_{B,0} \\ x_{B,1} \\ x_{B,2} \end{bmatrix} = \begin{bmatrix} dx_{B,0}/dt \\ dx_{B,1}/dt \\ dx_{B,2}/dt \end{bmatrix} \quad (9)$$

Although (8) and (9) do not appear to be coupled, they are because at each time step, the sums $x_{A,j} + x_{B,j}$ do not equal 1. Accordingly, the mole fractions are normalized at each time step to force them to sum to 1. The initial eigenvalues of the Jacobian matrices, (8) and (9), are computed from MATLAB, using the **eig** function, with $M_2 = 99.89$ kmol:

	Component A	Component B
λ_0	-126.54	-146.86
λ_1	-3,497.6	-2,020.2
λ_2	-0.15572	-0.03789

It is seen that $|\lambda|_{\max} = 3,497.6$. Thus, for the explicit-Euler method, instability and oscillations can be prevented by choosing $\Delta t \leq 1/3,497.6 = 0.000286$ h.

If a $\Delta t = 0.00025$ h (just slightly smaller than the criterion) is selected, it takes $0.05/0.00025 = 200$ time steps to reach $t = 0.05$ h (3 min). No such restriction applies to the implicit-Euler method, but too large a Δt may result in an unacceptable truncation error.

Explicit-Euler Method

According to Distefano [11], the maximum step size for integration using an explicit method is nearly always limited by stability considerations, and usually the truncation error is small. Assuming this to be true for this example, the following results were obtained using

$\Delta t = 0.00025$ h with a spreadsheet program by converting (8) and (9), together with (7) for M_2 , to the form of (13-38). Only the results for every 40 time steps are given.

Time, h	Normalized Mole Fractions in Liquid for <i>n</i> -Hexane			Normalized Mole Fractions in Liquid for <i>n</i> -Heptane		
	Distillate	Plate	Still	Distillate	Plate	Still
0.01	0.8183	0.6271	0.4993	0.1817	0.3729	0.5007
0.02	0.8073	0.6219	0.4991	0.1927	0.3781	0.5009
0.03	0.8044	0.6205	0.4988	0.1956	0.3795	0.5012
0.04	0.8036	0.6199	0.4985	0.1964	0.3801	0.5015
0.05	0.8032	0.6195	0.4982	0.1968	0.3805	0.5018

To show the instability effect, a time step of 0.001 h (four times the previous time step) gives the following unstable results during the first five time steps to an elapsed time of 0.005 h. Also included are values at 0.01 h for comparison to the preceding stable results.

Time, h	Normalized Mole Fractions in Liquid for <i>n</i> -Hexane			Normalized Mole Fractions in Liquid for <i>n</i> -Heptane		
	Distillate	Plate	Still	Distillate	Plate	Still
0.000	0.85935	0.7093	0.49962	0.14065	0.2907	0.50038
0.001	0.859361	0.559074	0.499599	0.140639	0.440926	0.500401
0.002	0.841368	0.75753	0.499563	0.158632	0.24247	0.500437
0.003	0.852426	0.00755	0.499552	0.147574	0.99245	0.500448
0.004	0.809963	0.884925	0.499488	0.190037	0.115075	0.500512
0.005	0.874086	1.154283	0.499546	0.125914	-0.15428	0.500454
0.01	1.006504	0.999254	0.493573	-0.0065	0.000746	0.506427

Much worse results are obtained if the time step is increased 10-fold to 0.01 h, as shown in the following table, where at $t = 0.01$ h, a negative mole fraction has appeared.

Time, h	Normalized Mole Fractions in Liquid for <i>n</i> -Hexane			Normalized Mole Fractions in Liquid for <i>n</i> -Heptane		
	Distillate	Plate	Still	Distillate	Plate	Still
0.00	0.85935	0.7093	0.49962	0.14065	0.2907	0.50038
0.01	0.859456	-0.79651	0.49941	0.140544	1.796512	0.50059
0.02	2.335879	2.144666	0.497691	-1.33588	-1.14467	0.502309
0.03	1.284101	1.450481	0.534454	-0.2841	-0.45048	0.465546
0.04	1.145285	1.212662	0.895373	-0.14529	-0.21266	-7.95373
0.05	1.07721	1.11006	1.191919	-0.07721	-0.11006	-0.19192

Implicit-Euler Method

If (8) and (9) are converted to implicit equations like (13-39), they can be rearranged into a linear tridiagonal set for each component. For example, the equation for component A on the plate becomes

$$(1,000 \Delta t)x_{A,0}^{(k+1)} - (1 + 3,424 \Delta t)x_{A,1}^{(k+1)} + (2,840 \Delta t)x_{A,2}^{(k+1)} = -x_{A,1}^{(k)}$$

The two tridiagonal equation sets can be solved by the tridiagonal matrix algorithm of §10.4.1 or with a spreadsheet program using the iterative, circular-reference technique. For the implicit-Euler

method, the selection of the time step, Δt , is not restricted by stability considerations. However, too large a Δt can lead to unacceptable truncation errors. Normalized, liquid-mole-fraction results at $t = 0.05$ h for just component A are as follows for a number of choices of Δt , all of which are greater than the 0.00025 h used earlier to obtain stable and oscillation-free results with the explicit-Euler method. Included for comparison is the explicit-Euler result for $\Delta t = 0.00025$ h.

Time = 0.05 h:

Normalized Mole Fractions in Liquid for <i>n</i> -Hexane			
Δt , h	Distillate	Plate	Still
Explicit-Euler			
0.00025	0.8032	0.6195	0.4982
Implicit-Euler			
0.0005	0.8042	0.6210	0.4982
0.001	0.8042	0.6210	0.4982
0.005	0.8045	0.6211	0.4982
0.01	0.8049	0.6213	0.4982
0.05	0.8116	0.6248	0.4982

The preceding data show acceptable results with the implicit-Euler method using a time step of 40 times the Δt_{\max} for the explicit-Euler method.

Stiffness Problem

Another serious computational problem occurs when integrating the equations. Because the liquid holdups on the trays and in the condenser are small, the corresponding liquid mole fractions, $x_{i,j}$, respond quickly to changes. The opposite holds for the reboiler with its large liquid holdup. Hence, the required time step for accuracy is usually small, leading to a very slow response of the overall rectification operation. Systems of ODEs having this characteristic constitute **stiff systems**. For such a system, as discussed by Carnahan and Wilkes [17], an explicit method of solution must utilize a small time step for the entire period even though values of the dependent variables may all be changing slowly for a large portion of the time period. Accordingly, it is preferred to utilize a special implicit-integration technique developed by Gear [13,14] and others, as contained in the public-domain software package called ODEPACK (<http://www.netlib.org/odepack/>). Gear-type methods for stiff systems strive for accuracy, stability, and computational efficiency by using multistep, variable order, and variable-step-size implicit techniques. MATLAB contains four Solvers for stiff ODEs: ode15s, ode23s, ode23t, and ode23tb. The Solver, ode15s (<http://www.mathworks.com/help/MATLAB/ref/ode15s.html>) applies Gear's method and can also solve DAEs.

A commonly used measure of the degree of stiffness is the **eigenvalue** ratio $|\lambda|_{\max}/|\lambda|_{\min}$, where λ values are the eigenvalues of the Jacobian matrix of the set of ODEs. For the Jacobian matrix of (13-23) through (13-25), the Gerschgorin

circle theorem, discussed by Varga [18], can be employed to estimate the eigenvalue ratio. The maximum absolute eigenvalue corresponds to the component with the largest K -value and the tray with the smallest liquid molar holdup. When the Gerschgorin theorem is applied to a row of the Jacobian matrix based on (13-24),

$$|\lambda|_{\max} \leq \left[\left(\frac{L_{j-1}}{M_j} \right) + \left(\frac{L_j + K_{i,j}V_j}{M_j} \right) + \left(\frac{K_{i,j+1}V_{j+1}}{M_j} \right) \right] \\ \approx 2 \left[\frac{L_j + K_{i,j}V_j}{M_j} \right] \quad (13-40)$$

where i refers to the most-volatile component and j to the stage with the smallest liquid molar holdup. The minimum absolute eigenvalue almost always corresponds to a row of the Jacobian matrix for the reboiler. Thus, from (13-25):

$$|\lambda|_{\min} \leq \left[\left(\frac{L_N}{M_{N+1}} \right) + \left(\frac{V_{N+1}K_{i,N+1}}{M_{N+1}} \right) \right] \\ \approx \left[\frac{L_N + K_{i,N+1}V_{N+1}}{M_{N+1}} \right] \quad (13-41)$$

where i now refers to the least-volatile component and $N + 1$ is the reboiler stage. The largest value of the reboiler holdup is M_{N+1}^0 . The stiffness ratio, SR, is

$$SR = \frac{|\lambda|_{\max}}{|\lambda|_{\min}} \approx 2 \left(\frac{L + K_{\text{lightest}}V}{L + K_{\text{heaviest}}V} \right) \left(\frac{M_{N+1}^0}{M_{\text{tray}}} \right) \quad (13-42)$$

From (13-42), the stiffness ratio depends not only on the difference between tray and initial reboiler molar holdups, but also on the difference between K -values of the lightest (most volatile) and heaviest (least volatile) components.

Davis [15] states that $SR = 20$ is not stiff; $SR = 1,000$ is stiff; and $SR = 1,000,000$ is very stiff. For the conditions of Example 13.6, using (13-42),

$$SR \approx 2 \left[\frac{10 + (1.212)(20)}{10 + (0.581)(20)} \right] \left(\frac{100}{0.01} \right) = 31,700$$

which meets the criterion of a stiff problem. A modification of the computational procedure of Distefano [11], for solving (13-23) through (13-35), is as follows:

Initialization

1. Establish total-reflux conditions, based on vapor and liquid molar flow rates V_j^0 and L_j^0 . V_{N+1}^0 is the desired boilup rate or L_0^0 is based on the desired distillate rate and reflux ratio such that $L_0^0 = D(R + 1)$.
2. At $t = 0$, reduce L_0^0 to begin distillate withdrawal, but maintain the boilup rate established or specified for the total-reflux condition. This involves replacing all L_j^0 with $L_j^0 - D$. Otherwise, the initial values of all variables are those established for total reflux.

Time Step

3. In (13-23) to (13-25), replace liquid-holdup derivatives by total-material-balance equations:

$$\frac{dM_j}{dt} = V_{j+1} + L_{j-1} - V_j - L_j$$

Solve the resulting equations for liquid mole fractions using an appropriate implicit-integration technique and a suitable time step. Normalize the mole fractions at each stage if they do not sum to 1.

4. Compute a new set of stage temperatures and vapor-phase mole fractions from (13-32) and (13-31), respectively.
5. Compute liquid densities and holdups, and liquid and vapor enthalpies, from (13-33) and (13-34), and determine derivatives of enthalpies and liquid holdups with respect to time by forward-finite-difference approximations.
6. Compute a new set of liquid and vapor molar flow rates from (13-26), (13-27), and (13-29).
7. Compute the new reboiler molar holdup from (13-35).
8. Compute condenser and reboiler heat-transfer rates from (13-28) and (13-30).

Iteration to Completion of Operation

9. Repeat Steps 3 through 8 for additional time steps until the completion of a specified operation, such as a desired amount of distillate, mole fraction of a component in the distillate, etc.

New Operation

10. Dump the accumulated distillate into a receiver, change operating conditions, and repeat Steps 2 through 9. Terminate calculations following the final operation.

The foregoing procedure is limited to narrow-boiling feeds and the simple configuration shown in Figure 13.10. A more flexible and efficient method, designed to cope with stiffness, is that of Boston et al. [12], which uses a modified inside-out algorithm of the type discussed in §10.7. Their method can handle feeds ranging from narrow- to wide-boiling for nonideal-liquid solutions. In addition, their method permits multiple feeds, sidestreams, tray heat transfer, vapor distillate, and flexibility in operation specifications.

§13.5.3 BatchSep Model of Aspen Plus

In Aspen Plus, rigorous calculations for batch rectifiers are made with the BatchSep model. The column can consist of equilibrium stages or nonequilibrium stages with specified Murphree vapor efficiencies. The DAEs are solved by selecting a suitable integration method from a list consisting of Gear, Runge-Kutta 4th order, implicit-Euler, or explicit-Euler methods. Step sizes and tolerances can be specified or defaults

can be accepted. Condenser and Column pressure and holdup profiles, the number of stages, and the number of operation steps must be specified.

For operation step 1, a startup option is selected; either an empty column or total reflux. For subsequent operation steps, it is usually best to accept the conditions at the end of the previous step. For each operating step, the selection of two specification modes are necessary to satisfy the number of degrees of freedom. For the first mode, the options are reflux mass rate, reflux mole rate, reflux ratio, distillate mole flow rate, and distillate mass flow rate. For the second mode, the options include boilup mole rate, boilup mass rate, and reboiler duty. In addition, a stop option is specified for each operation step. These options include time and the many different variables associated with the distillate, receiver, or bottoms. For example, the first operation step can be stopped when the average mole fraction of the most volatile component in the receiver drops below a specified value.

BatchSep can also be used to conduct reactive batch distillation with specified kinetics and it can handle a second liquid phase.

As with continuous distillation, batch distillation calculations for some specifications are more easily converged than others. Some specifications may be impossible to achieve. Convergence is most likely to be attained by specifying the time for each operation step to stop. The results can then be analyzed and more desirable specifications selected for stopping the operation steps.

EXAMPLE 13.7 Batch Rectification Using BatchSep.

300 lbmoles of a mixture of 2 moles of methanol (M) to every mol of water (W) at 17 psia is charged to a batch rectifier consisting of a reboiler, a column with 15 trays, a total condenser, and one distillate accumulator (receiver). The molar liquid holdup of the condenser-reflux drum is 0.2 ft³ and the total molar liquid holdup for the 15 trays is 0.3 ft³. The pressure is 17 psia in the still pot, 15 psia in the condenser, and 15.5 psia on the top tray. The trays are assumed to be equivalent to equilibrium stages. Following the establishment of total reflux conditions, the column is operated at a constant boilup of 400 lbmol/h with a reflux ratio of 7. The operation is to be stopped when the average mole fraction of methanol in the accumulator drops to 0.90. Vapor-liquid equilibrium is modeled with the Wilson equation and the ideal gas law. Use the BatchSep model of Aspen Plus to determine lbmoles of methanol product, operation time after total reflux conditions are met, and composition of the bottoms residual.

Solution

The Aspen Plus flow sheet is shown in Figure 13.11. Stream 1 is the charge to still pot. The total condenser at the top of the column connects a reflux drum. Stream 2 is the final distillate product, which is sent to a receiver that is not shown. Stream 3 is the final bottoms residual product.

Gear's method was selected to solve the system of DAEs. Defaults were used for step sizes. The total charge was 171.5 ft³. Following establishment of total reflux, the mole fraction of methanol in the distillate stayed relatively constant at 0.9997 until

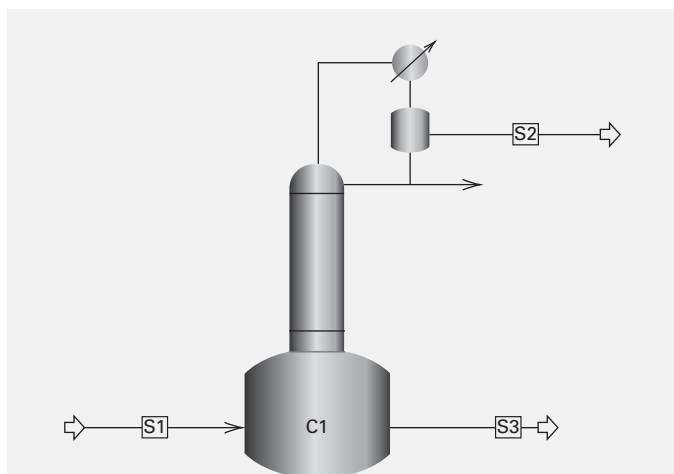


Figure 13.11 Aspen Plus flow sheet for Example 13.7.

at an elapsed time of 3.772 hours, it began to decrease. Finally after 4.244 hours, the average methanol mole fraction in the distillate receiver dropped to the specified value of 0.90. During the final 0.472 hours, the calculated methanol mole fraction in the receiver and the distillate vapor leaving the top tray were as follows:

Elapsed time, h	M mole fraction in the receiver	M mole fraction in the distillate vapor
3.772	0.9997	0.9087
3.815	0.9950	0.3810
3.900	0.9752	0.0025
3.986	0.9554	0.0004
4.072	0.9363	0.0000
4.158	0.9180	0.0000
4.244	0.9000	0.0000

The final accumulated distillate in the receiver consisted of 222.18 lbmol. The final bottoms residual was 77.82 lbmol of almost pure water.

§13.5.4 CC-BATCH Model of CHEMCAD

In the CHEMCAD process simulator, rigorous calculations for batch rectifiers are made with the CC-BATCH model. The column can consist of equilibrium stages or nonequilibrium stages with specified Murphree vapor efficiencies (Regular VLE model). Alternatively, rate-based calculations using mass-transfer correlations can be made with trays or packings. Solutions are converged by either an inside-out or simultaneous-correction method. If necessary, a damping factor less than the default of 1 can be specified and/or the convergence tolerance can be relaxed. Condenser and column pressure and holdup profiles are specified, as are the number of stages and number of operation steps.

For each operation step, a startup option is selected from either total reflux or from the column content existing from the previous operating step. For each operating step, a step size and recording frequency are specified. The selection of two

specification modes satisfies the number of degrees of freedom. For the first mode, the options are reflux mass rate, reflux mole rate, reflux ratio, condenser duty, distillate temperature, distillate mass fraction, and distillate mole fraction. For the second mode, the options are boilup mole rate, boilup mass rate, distillate mole rate, distillate mass rate, distillate volume rate, and reboiler duty. In addition, a stop option is specified for each operation step. These options include time and many different variables associated with the distillate, accumulator, or bottoms. For example, the first operation step can be stopped when the average mole fraction in the accumulator of the most volatile component drops below a specified value.

As with continuous distillation, batch distillation calculations for some specifications are more easily converged than others. Some specifications may be impossible to achieve. For CC-BATCH, convergence is most likely to be achieved by specifying the time for each operation step to stop. The results can then be analyzed to select more desirable specifications, particularly for stopping the operation steps.

EXAMPLE 13.8 Batch Rectification using CC-BATCH.

One hundred lbmol of 25 mol% benzene (B), 50 mol% monochlorobenzene (MCB), and 25 mol% *ortho*-dichlorobenzene (DCB) is distilled in a batch rectifier consisting of a reboiler, 10 equilibrium stages in the column, a reflux drum, and three distillate product accumulators. The condenser-reflux drum holdup is constant at 0.20 ft³, and each stage in the column has a liquid holdup of 0.02 ft³. Pressures are 18 psia in the reboiler and 16 psia in the reflux drum. Pressure drop in the condenser is 0.5 psia with a pressure drop of 1.5 psi in column. Following initialization at total reflux, the batch is distilled in three steps, each with a vapor boilup rate of 200 lbmol/h and a reflux ratio of 7. Thus, the distillate being sent to the accumulators is at a rate of 25 lbmol/h. Using the rigorous CC-BATCH method, assuming ideal solutions and the ideal gas law, determine the amounts and compositions of the accumulated distillate and reboiler holdup at the end of each step, and plots of the compositions of the (instantaneous) distillate, accumulator contents, and bottoms as a function of time.

For a perfect separation, and neglecting the initialization to total reflux, a one-hour operation would result in an accumulated product of 100% B. A subsequent two-hour operation would produce an accumulated product of 100% MCB, with a bottoms in the still pot of 100% DCB. For an initial set of operations, using three accumulators, with the second being a slop cut, assume the following:

- Step 1:** Terminate at 0.7 h.
- Step 2:** Terminate at 0.4 h.
- Step 3:** Terminate at 1.8 h.

Solution

Figure 13.12 shows the flow sheet for the batch distillation. The batch rectifier unit (1) and three accumulator drums (2, 3, and 4) are shown. It is not necessary to connect the three drums to the rectifier. Each stream leaving a drum is the accumulated product for the particular operation step. The time-step size for the calculations was reduced from the default value of 0.05 h to 0.02 h. The frequency for recording the step results was set for every 3 iterations.

The problem was executed successfully with both the inside-out and simultaneous-correction options. Results are given in Table 13.2, where it is seen that the accumulated distillate cut from Operation Step 1 is quite pure with respect to benzene (99.9 mol%). The slop cut from Step 2 is 65.2 mol% MCB. The cut from Step 3 is 91.6 mol% MCB, leaving a bottoms residual in the still pot of 99.7 mol% DCB. The slop cut from Step 2 contains 14.2% of B in the feed and 13.3% of MCB in the feed.

A plot of the instantaneous-distillate composition in mole fractions as a function of time, following the establishment of total reflux, is shown in Figure 13.13 for all three operation steps. Step 1 is completed at 0.7 h, Step 2 at 1.1 h, and Step 3 at 2.9 h. Note that there are periods of little change in composition and periods of rapid change. This type of plot is useful in developing alternative operation steps to obtain the most pure cuts for a given reflux ratio, while minimizing the amount of the slop cut(s).

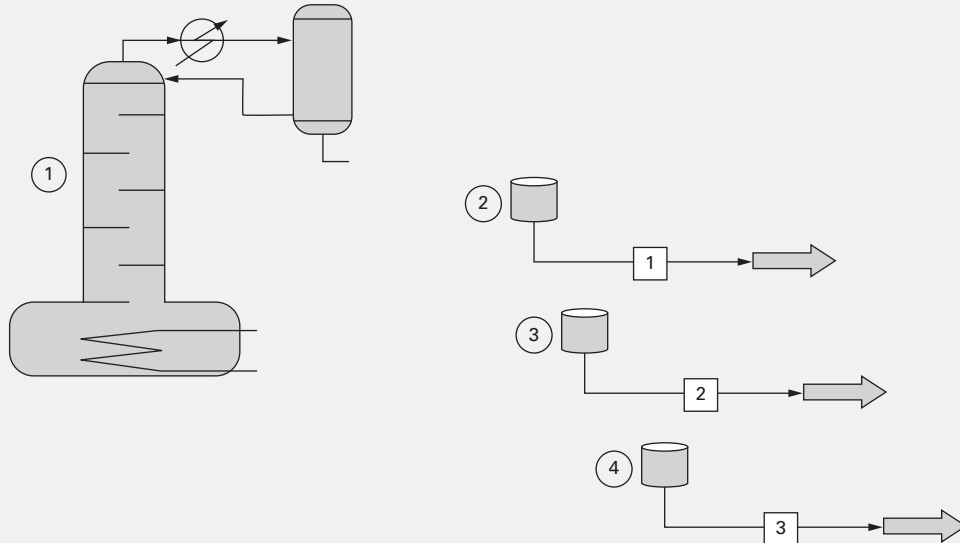


Figure 13.12 Flow sheet for batch distillation system of Example 13.8.

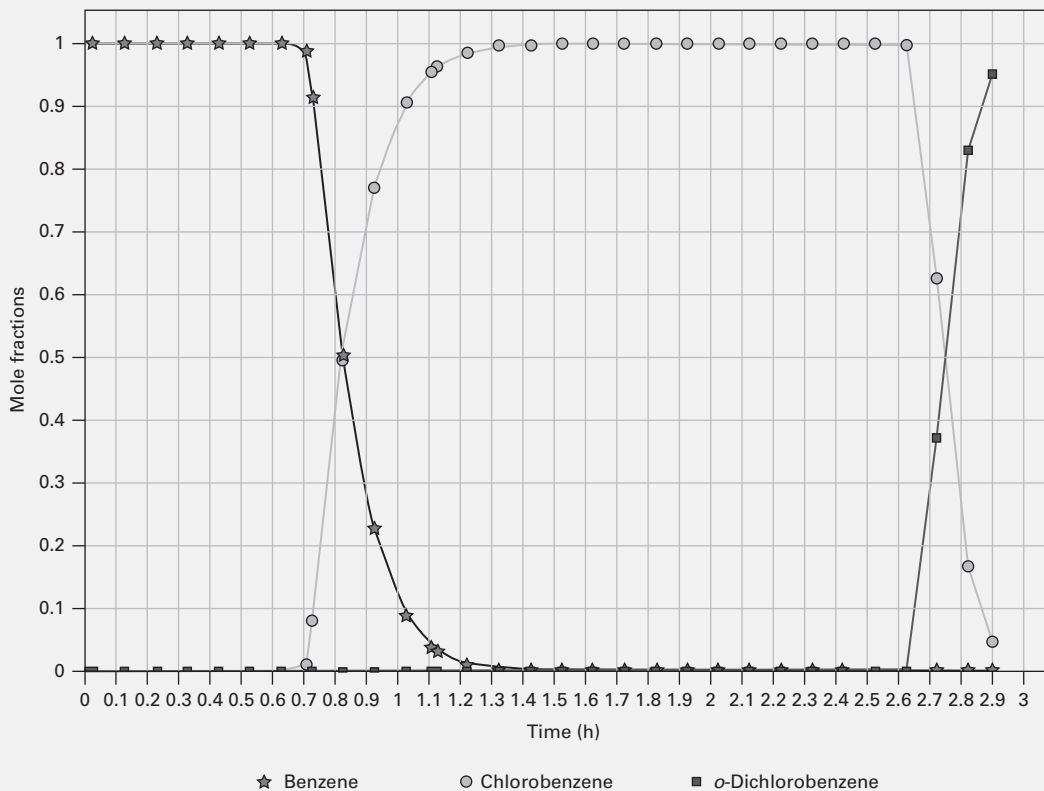


Figure 13.13 Instantaneous distillation composition as a function of time for the three operation steps in Example 13.8.

Figure 13.14 is a plot of the average composition in the accumulator drums as a function of time. Vertical lines separate the three drums. As shown, the most rapid change in composition occurs in the drum for Step 2. The rapid change during the last 0.2 h of Step 3

reduces the purity of the MCB in the accumulator. During the same interval of time, the purity of DCB in the bottoms residual (still pot) increases, as shown in Figure 13.15.

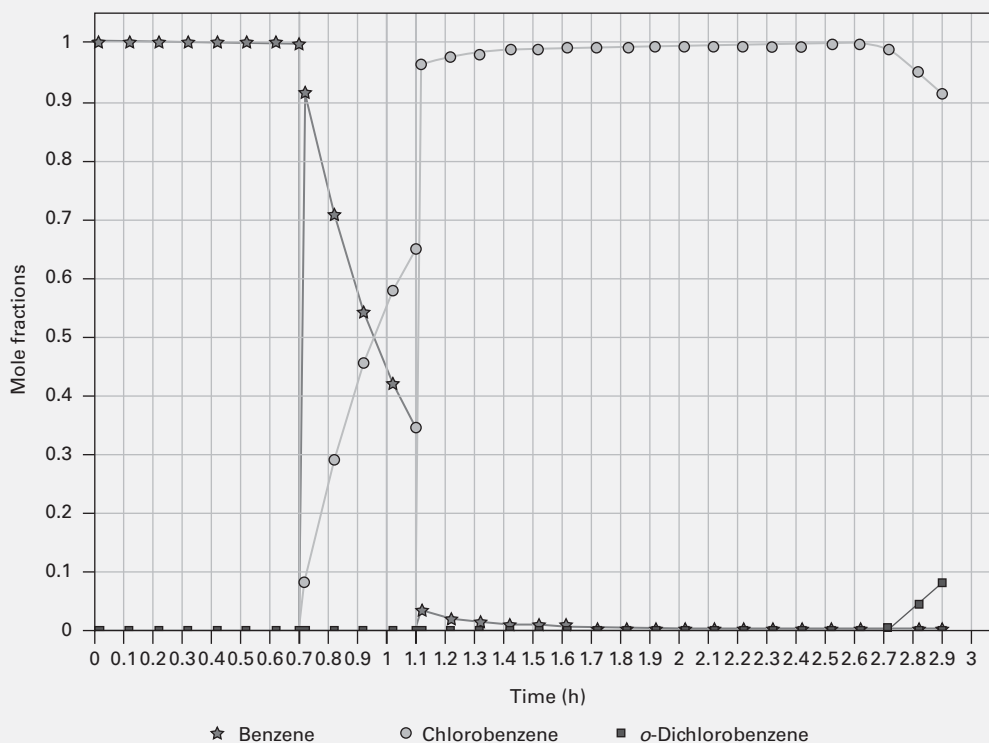


Figure 13.14 Average accumulator composition as a function of time for the three operation steps in Example 13.8.

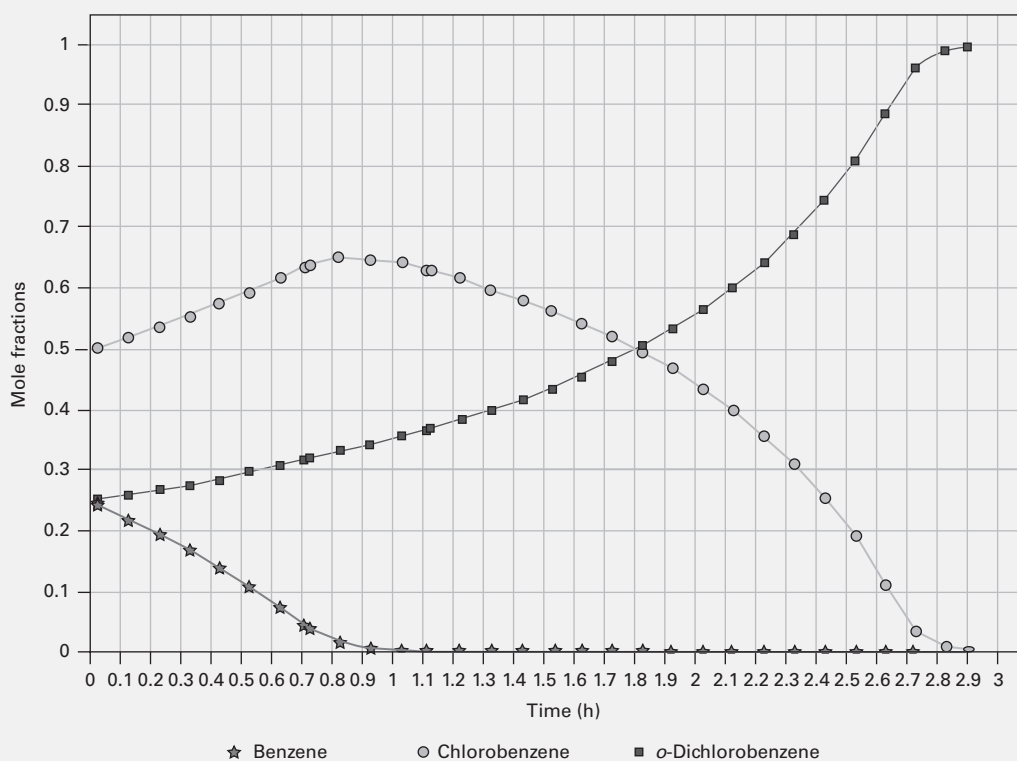


Figure 13.15 Average bottoms residual composition as a function of time for the three operation steps in Example 13.8.

Table 13.2 Results at the End of Each Operation Step for Example 13.9

	Operation Step		
	1	2	3
Operation time, h	0.7	0.4	1.8
Accumulation:			
Total lbmol	21.4	10.2	47.2
Mole fractions:			
B	0.999	0.348	0.002
MCB	0.001	0.652	0.916
DCB	0.000	0.000	0.082
Reboiler residual:			
Total lbmol	78.4	68.2	21.0
Mole fractions:			
B	0.044	0.001	0.000
MCB	0.637	0.632	0.003
DCB	0.319	0.367	0.997

To achieve a more optimal sequence of operation steps with CC-BATCH, it is usually necessary to make several runs, each using the plotted results to change the operating-step conditions for the operation steps and possibly use different reflux ratios for the steps.

§13.6 INTERMEDIATE-CUT STRATEGY

Luyben [19] points out that design of a batch-distillation process is complex because two aspects must be considered: (1) the products to be obtained and (2) the control method to be employed. Basic design parameters are the number of trays, the size of the charge to the still pot, the boilup ratio, and the reflux ratio as a function of time. Even for a binary feed, it may be necessary to take three products: a distillate rich in the most volatile component, a residue rich in the least volatile component, and an intermediate cut containing both components. If the feed is a ternary system, more intermediate cuts may be necessary. The next two examples demonstrate intermediate-cut strategies for binary and ternary feeds.

EXAMPLE 13.9 Intermediate Cuts.

One hundred kmol of an equimolar mixture of *n*-hexane (C6) and *n*-heptane (C7) at 1 atm is batch-rectified in a column with a total condenser. It is desired to produce two products, one with 95 mol% C6 and the other with 95 mol% C7. Neglect holdup and assume a boilup rate of 100 kmol/h. Also assume a constant reflux ratio; thus, the distillate composition will change with time. Determine a reasonable number of equilibrium stages and the effect of reflux ratio on the amount of intermediate cut.

Solution

To determine the number of equilibrium stages, a McCabe–Thiele diagram, based on SRK *K*-values, is used in the manner of Figures 13.4 and 13.5. For total reflux ($y = x$, 45° line), the minimum number of stages for a 95 mol% C6 from an initial feed of 50 mol% C6 is 3.1, where one stage is the boiler. For operation at twice R_{\min} , 5 stages plus the boiler are required.

Table 13.3 Batch Distillation of a C6–C7 Mixture

	Case 1	Case 2	Case 3	Case 4	Case 5
Reflux ratio	2	3	4	8	9.54
C6 product, kmol	15.1	36.0	42.4	49.2	50.0
C7 product, kmol	34.4	40.7	44.3	49.2	50.0
Intermediate cut, kmol	50.5	23.3	13.3	1.6	0.0
Mole fraction of C6 in intermediate cut	0.67	0.59	0.57	0.54	No intermediate cut
Total operation time, h	1.97	2.37	2.78	4.57	5.27

For each reflux ratio, the first product is the 95 mol% C6 distillate. At this point, if the residue contains less than 95 mol% C7, then in a second step, a second accumulation of distillate (the intermediate cut) is made until the residue achieves the desired 95 mol% C7 composition. The reflux ratio is held constant throughout. The results, using CC-BATCH of CHEMCAD, are given in Table 13.3. For no intermediate cut (by material balance), the C6 and C7 products must each be 50 lbmol at 95 mol% purity. From Table 13.3, this is achieved at a constant reflux ratio of 9.54, with an operating time of 5.27 hours.

For lower reflux ratios, an intermediate cut, whose amount increases as the reflux ratio decreases, is necessary. If the quantity of feed is much larger than the capacity of the still pot, the feed can be distilled in a sequence of charges. Then the intermediate cut for binary distillation of a batch can be recycled to the next batch. In this manner, each charge consists of fresh feed mixed with recycle intermediate cut. As discussed by Luyben [19], the composition of the intermediate cut is often not very different from the feed. This is confirmed in Table 13.3. If the number of stages is increased from 6, the reflux ratio for eliminating the intermediate cut can be reduced. For example, if 10 equilibrium stages are used, the reflux ratio can be reduced from 9.54 to approximately 6.

Intermediate-cut strategy for batch distillation of a ternary mixture, as discussed by Luyben [19], is considerably more complex, as shown in the following example.

EXAMPLE 13.10 Intermediate-Cut Strategy.

An equimolar ternary mixture of 150 kmol of C6, C7, and normal octane (C8) is to be distilled at 1 atm in a five-stage batch-rectification column with a boiler and a total condenser operating at a constant reflux ratio. It is desired to produce three products: distillates of 95 mol% C6 and 90 mol% C7, and a residue of 95 mol% C8. Neglect holdup and assume a boilup rate of 100 kmol/h. Thus, the distillate composition will change with time. Determine the effect of reflux ratio on the intermediate cuts, using CC-BATCH with the SRK EOS for *K*-values.

Solution

The difficulty in this ternary example lies in determining specifications for termination of the second cut. Unless *R* is high enough, it will be an intermediate cut. Suppose *R* is held constant at 4 and the intention is to terminate the second cut when the mole fraction of C7 in the instantaneous distillate reaches 90 mol% C7. Unfortunately,

Table 13.4 Batch Distillation of a C6–C7–C8 Mixture

	Case 1	Case 2
Reflux ratio	4	8
C6 product, kmol	35.85	46.70
First intermediate cut:		
Amount, kmol	42.16	16.67
Mole fraction C6	0.373	0.316
Mole fraction C7	0.602	0.672
C7 product:		
Amount, kmol		35.43
Mole fraction C6		0.011
Mole fraction C7	0.877 max	0.898
Second intermediate cut:		
Amount, kmol		4.38
Mole fraction C6		0.000
Mole fraction C7		0.523
C8 product, kmol		46.82
Total operation time, h		8.48

1 mol% C6. Acceptable results are almost achieved for the reflux ratio of 8, as shown in Table 13.4 and Figure 13.16, where desired purity of the C7 cut is 89.8 mol%. However, for a reflux ratio of 8, these results may not correspond to the optimal termination specification for the first intermediate cut. With a small adjustment in the reflux ratio, it may be possible to eliminate the second intermediate cut. These two considerations are the subject of Exercise 13.27.

Intermediate cuts and their recycle have been studied by a number of investigators, including Mayur, May, and Jackson [20]; Luyben [19]; Quintero-Marmol and Luyben [21]; Farhat et al. [22]; Mujtaba and Macchietto [23]; Diehl et al. [24]; and Robinson [25].

§13.7 OPTIMAL CONTROL BY VARIATION OF REFLUX RATIO

An operation policy in which the composition of the instantaneous distillate and, therefore, the accumulated distillate, is maintained constant is discussed in §13.2.2. This policy requires a variable reflux ratio and accompanying distillate rate. Although not as simple as the constant-reflux-ratio method of §13.2.1, it can be implemented with a rapidly responding composition (or surrogate) sensor and an associated reflux control system.

What is the optimal way to control a batch distillation: (1) constant reflux ratio, (2) constant distillate composition,

computer simulations show that only a value of 88 mol% C7 can be reached. Therefore, R is increased to 8. In addition, the third cut (the C7 product) is terminated when the mole fraction of C8 in that cut rises to 0.09 in the accumulator; and the second intermediate cut is terminated when the mole fraction of C8 in the residue rises to 0.95, the desired purity. Note that no purity specification has been placed on the C7 product. Instead, it has been assumed that the desired purity of 90 mol% C7 will be achieved with impurities of 9 mol% C8 and

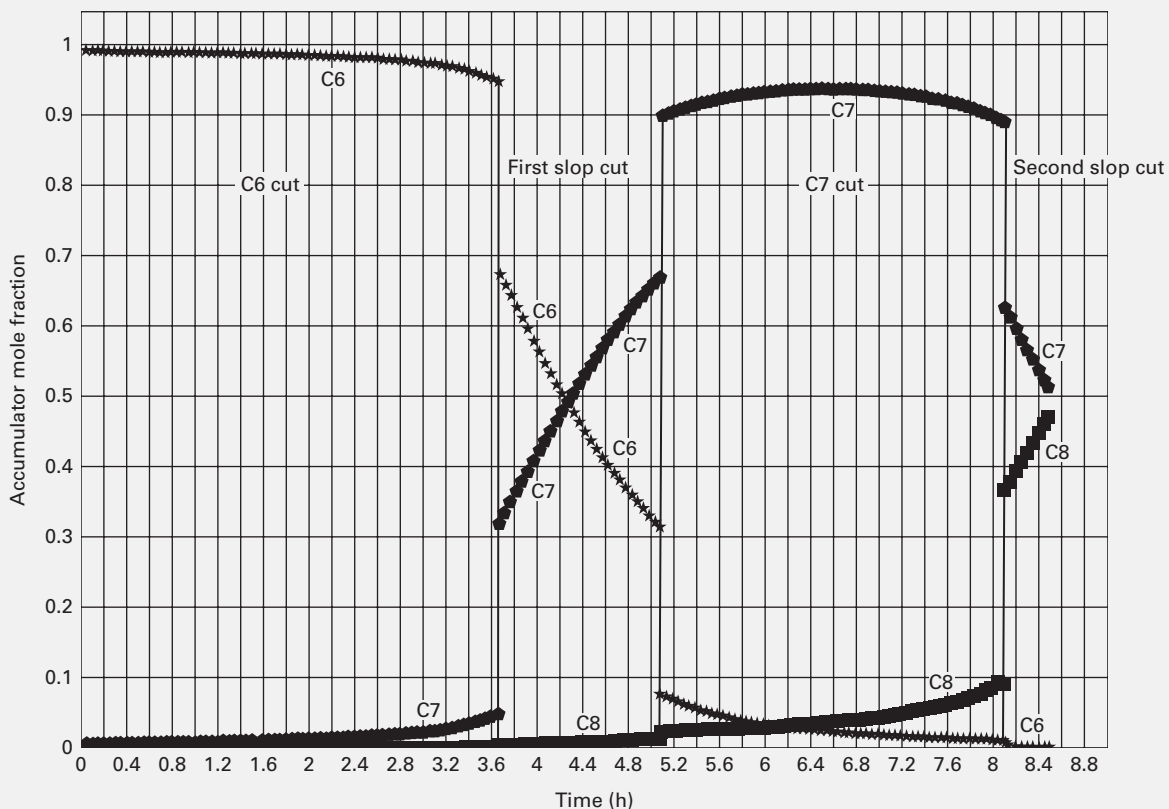


Figure 13.16 Ternary batch distillation with two intermediate (slop) cuts in Example 13.11.

or (3) some other means? With a process simulator, it is fairly straightforward to compare the first two methods. However, the results depend on the objective for the optimization. Diwekar [26] studied the following three objectives when the accumulated-distillate composition and/or the residual composition are/is specified:

1. Maximize the amount of accumulated distillate in a given time.
2. Minimize the time to obtain a given amount of accumulated distillate.
3. Maximize the profit. The next example compares the first two control policies with respect to their ability to meet the first two objectives.

EXAMPLE 13.11 Two Control Policies.

Repeat Example 13.9 under conditions of constant distillate composition and compare the results to those obtained at a constant reflux ratio of 4 with respect to both the amount of distillate and time of operation.

Solution

For Example 13.9, from Table 13.3 for a reflux ratio of 4, the amount of accumulated distillate during the first operation step is 42.4 kmol of 95 mol% C6. The time required for this cut, which is not listed in Table 13.3, is 1.98 hours. Using CC-BATCH, the operation specifications for a constant-composition operation are a boilup rate of 100 kmol/h, as in Example 13.9, with a constant instantaneous-distillate composition of 95 mol% C6. For the maximum distillate objective, the stop time for the first cut is 1.98 hours, as in Example 13.9. The amount of distillate obtained is 43.5 kmol, which is 2.6% higher than for operation at constant reflux ratio. The variation of reflux ratio with time for constant-composition control is shown in Figure 13.17, where the constant reflux ratio of 4 is also shown. The initial reflux ratio, 1.7, rises gradually at first and rapidly

at the end. At 1 hour, the reflux ratio is 4, while at 1.98 hours, it is 15.4. For constant composition control, 42.4 kmol of accumulated distillate are obtained in 1.835 hours, compared to 1.98 hours for reflux-ratio control. Constant composition control is more optimal, this time by almost 8%.

The maximization of distillate or minimization of operation time, as well as maximization of profit, can be achieved by using an **optimal-reflux-ratio policy**, as shown in studies by Converse and Gross [27], Coward [28, 29], and Robinson [25] for binary systems; by Robinson and Coward [30] and Mayur and Jackson [31] for ternary systems; and Diwekar et al. [32] for higher multicomponent systems. Often, this policy is intermediate between the constant-reflux-ratio and constant-composition controls in Figure 13.13 for Example 13.11. Generally, the optimal-reflux curve rises less sharply than that for the constant-distillate-composition control, with the result that savings in distillate, time, or money are highest for the more difficult separations. For relatively easy separations, savings for constant-distillate-composition control or optimal-reflux-ratio control may not be justified over the use of the simpler constant-reflux-ratio control.

Determination of optimal-reflux-ratio policy for complex operations requires a much different approach than that used for simpler optimization problems, which involve finding the optimal discrete values that minimize or maximize some objective with respect to an algebraic function. For example, in §7.3.7, a single value of the optimal reflux ratio for a continuous-distillation operation is found by plotting, as in Figure 7.21, the total annual cost versus R , and locating the minimum in the curve. Establishing the optimal reflux ratio as a function of time, $R\{t\}$, for a batch distillation, which is modeled with differential or integral equations rather than algebraic equations, requires optimal-control methods that

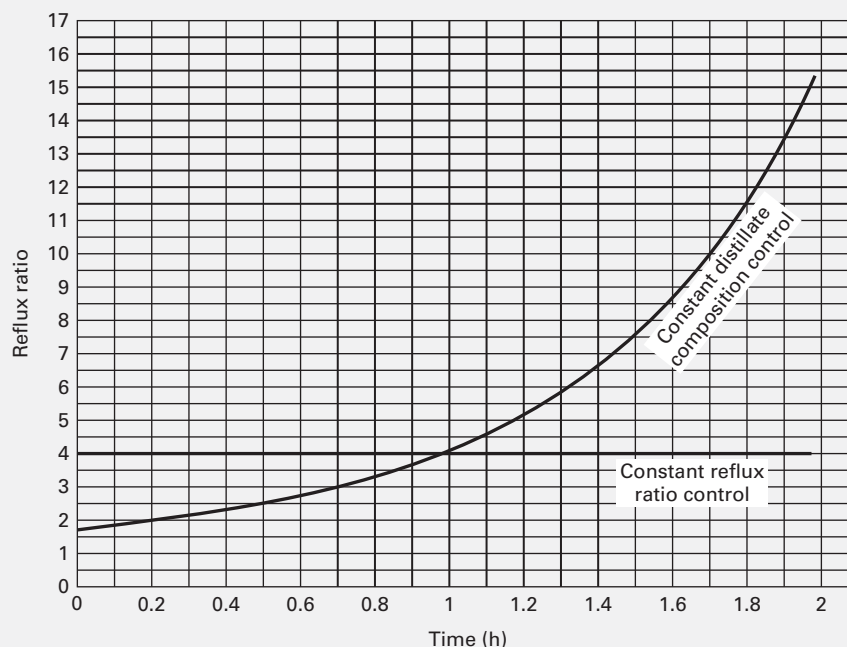


Figure 13.17 Binary batch distillation under distillate-composition control in Example 13.11.

include the calculus of variations, the maximum principle of Pontryagin, dynamic programming of Bellman, and non-linear programming. Diwekar [33] describes these methods in detail. Their development by mathematicians in Russia and the United States were essential for the success of their respective space programs.

CHAPTER 13 NOMENCLATURE

Abbreviations and Acronyms

SR stiffness ratio, (13-42)

Latin Symbols

G volume holdup, (13-33)

M_i moles of i in the pot still, Wx_i , (13-7)
 W moles of liquid in still (residue), (13-1)

Greek Symbols

λ eigenvalue, (13-40)

Subscripts

W residue, (13-1)
 0 initial value at $t=0$

Superscripts

k time-increment index, (13-22)

SUMMARY

1. The simplest case of batch distillation corresponds to the condensation of a vapor rising from a boiling liquid and is called differential or Rayleigh distillation. The vapor leaving the liquid surface is assumed to be in equilibrium with well-mixed liquid. The compositions of the liquid and vapor vary as distillation proceeds. The instantaneous vapor and liquid compositions can be computed as a function of time for a given vaporization rate.
2. A batch-rectifier system consists of a reboiler, a column with plates or packing that sits on top of the reboiler, a condenser, a reflux drum, and one or more distillate receivers.
3. For a binary system, a batch rectifier is usually operated at a constant reflux ratio or at a constant distillate composition. For either case, a McCabe–Thiele diagram can be used to follow the process, if constant molar overflow and negligible liquid holdups in trays (or packing), condenser, and reflux drum are assumed.
4. A batch stripper is useful for removing impurities from a charge. For complete flexibility, complex batch distillation utilizing both rectification and stripping can be employed.
5. Liquid holdup on the trays (or packing) and in the condenser and reflux drum influences the course of batch rectification and the size and composition of distillate cuts. The holdup effect is best determined by rigorous calculations for specific cases.
6. For accurate and detailed multicomponent batch-rectification compositions, the rigorous model of Distefano as implemented by Boston et al. is preferred. It accounts for liquid holdup and permits a sequence of operation steps to produce multiple distillate cuts. The model consists of algebraic and ordinary differential equations (DAE) that, when stiff, are best solved by Gear-type implicit-integration methods.
7. Two difficult aspects of batch distillation are (1) determination of the best set of operations for the production of the desired products and (2) determination of the optimal-control method to be used. The first, which involves the possibility that intermediate cuts may be necessary, is solved by computational studies using a batch distillation simulation program. The second, which requires consideration of the best reflux-ratio policy, is solved by optimal-control techniques.

REFERENCES

1. RAYLEIGH, J.W.S., *Phil. Mag. and J. Sci.*, Series 6, **4**(23), 521–537 (1902).
2. SMOKER, E.H., and A. ROSE, *Trans. AIChE*, **36**, 285–293 (1940).
3. BLOCK, B., *Chem. Eng.*, **68**(3), 87–98 (1961).
4. BOGART, M.J.P., *Trans. AIChE*, **33**, 139–152 (1937).
5. ELLERBE, R.W., *Chem. Eng.*, **80**(12), 110–116 (1973).
6. HASEBE, S., B.B. ABDUL AZIZ, I. HASHIMOTO, and T. WATANABE, *Proc. IFAC Workshop, London, Sept. 7–8, 1992*, p. 177.
7. BAROLO, M., G. GUARISE, S. RIENZI, and A. MACCHIETTO, *Ind. Eng. Chem. Res.*, **35**, 4612–4618 (1996).
8. PHIMISTER, J.R., and W.D. SEIDER, *Ind. Eng. Chem. Res.*, **39**, 1840–1849 (2000).
9. PHIMISTER, J.R., and W.D. SEIDER, *AIChE J.*, **46**, 1508–1520 (2000).
10. MEADOWS, E.L., *Chem. Eng. Progr. Symp. Ser. No. 46*, **59**, 48–55 (1963).
11. DISTEFANO, G.P., *AIChE J.*, **14**, 190–199 (1968).

12. BOSTON, J.F., H.I. BRITT, S. JIRAPONGPHAN, and V.B. SHAH, in R.H.S. Mah and W.D. Seider, Eds., *Foundations of Computer-Aided Chemical Process Design*, AIChE, Vol. II, pp. 203–237 (1981).
13. GEAR, C.W., *Comm. of the ACM*, **14**(3) 176–179 (1971).
14. GEAR, C.W., *Numerical Initial Value Problems in Ordinary Differential Equations*, Prentice-Hall, Englewood Cliffs, NJ (1971).
15. DAVIS, M.E., *Numerical Methods and Modeling for Chemical Engineers*, John Wiley & Sons, New York (1984).
16. RIGGS, J.B., *An Introduction to Numerical Methods for Chemical Engineers*, Texas Tech. Univ. Press, Lubbock, TX (1988).
17. CARNAHAN, B., and J.O. WILKES, “Numerical Solution of Differential Equations—An Overview,” in R.S.H. Mah and W.D. Seider, Eds., *Foundations of Computer-Aided Chemical Process Design*, Engineering Foundation, New York, Vol. I, pp. 225–340 (1981).
18. VARGA, R.S., *Matrix Iterative Analysis*, Prentice-Hall, Englewood Cliffs, NJ (1962).
19. LUYBEN, W.L., *Ind. Eng. Chem. Res.*, **27**, 642–647 (1988).
20. MAYUR, D.N., R.A. MAY, and R. JACKSON, *Chem. Eng. Journal*, **1**, 15–21 (1970).
21. QUINTERO-MARMOL, E., and W.L. LUYBEN, *Ind. Eng. Chem. Res.*, **29**, 1915–1921 (1990).
22. FARHAT, S., M. CZERNICKI, L. PIBOULEAU, and S. DOMENECH, *AIChE J.*, **36**, 1349–1360 (1990).
23. MUJTABA, I.M., and S. MACCHIETTO, *Comput. Chem. Eng.*, **16**, S273–S280 (1992).
24. DIEHL, M., A. SCHAFER, H.G. BOCK, J.P. SCHLODER, and D.B. LEINWEBER, *AIChE J.*, **48**, 2869–2874 (2002).
25. ROBINSON, E.R., *Chem. Eng. Journal*, **2**, 135–136 (1971).
26. DIWEKAR, U.M., *Batch Distillation—Simulation, Optimal Design and Control*, 2nd edition, CRC Press, Boca Raton, FL (2012).
27. CONVERSE, A.O., and G.D. GROSS, *Ind. Eng. Chem. Fundamentals*, **2**, 217–221 (1963).
28. COWARD, I., *Chem. Eng. Science*, **22**, 503–516 (1967).
29. COWARD, I., *Chem. Eng. Science*, **22**, 1881–1884 (1967).
30. ROBINSON, E.R., and I. COWARD, *Chem. Eng. Science*, **24**, 1661–1668 (1969).
31. MAYUR, D.N., and R. JACKSON, *Chem. Eng. Journal*, **2**, 150–163 (1971).
32. DIWEKAR, U.M., R.K. MALIK, and K.P. MADHAVAN, *Comput. Chem. Eng.*, **11**, 629–637 (1987).
33. DIWEKAR, U.M., *Introduction to Applied Optimization*, Kluwer Academic Publishers, Netherlands (2003).

STUDY QUESTIONS

- 13.1. How does batch distillation differ from continuous distillation?
- 13.2. When should batch distillation be considered?
- 13.3. What is differential (Rayleigh) distillation? How does it differ from batch rectification?
- 13.4. For what kinds of mixtures is differential distillation adequate?
- 13.5. What is the easiest way to determine the average composition of the distillate from a batch rectifier?
- 13.6. Which is easiest to implement: (1) the constant-reflux policy, (2) the constant-distillate-composition policy, or (3) the optimal-control policy? Why?
- 13.7. What is a batch stripper?
- 13.8. Can a batch rectifier and a batch stripper be combined? If so, what advantage is gained?
- 13.9. What effects does liquid holdup have on batch rectification?
- 13.10. What are the assumptions of the rigorous batch distillation model of Distefano?
- 13.11. Why is the Distefano model referred to as a differential-algebraic equation (DAE) system?
- 13.12. What is the difference between truncation error and stability?
- 13.13. How does the explicit-Euler method differ from the implicit method?
- 13.14. What is stiffness and how does it arise? What criterion can be used to determine the degree of stiffness, if any?
- 13.15. In the development of an operating policy (campaign) for batch distillation, what is done with intermediate (slop) cuts?
- 13.16. What are the common objectives of optimal control of a batch distillation, as cited by Diwekar?
- 13.17. What is varied to achieve optimal control?

EXERCISES

Section 13.1

13.1. Evaporation from a drum.

A bottle of pure *n*-heptane is accidentally poured into a drum of pure toluene in a laboratory. One of the laboratory assistants suggests that since heptane boils at a lower temperature than toluene, the following purification procedure can be used:

Pour the mixture (2 mol% *n*-heptane) into a simple still pot. Boil the mixture at 1 atm and condense the vapors until all heptane is boiled away. Obtain the pure toluene from the residue.

You, a chemical engineer with knowledge of vapor–liquid equilibrium, immediately realize that such a purification method will not work. (a) Indicate this by a curve showing the composition of the material remaining in the still pot after various quantities of the liquid have been distilled. What is the composition of the residue after 50 wt% of the original material has been distilled? What is the composition of the cumulative distillate? (b) When one-half of the heptane has been distilled, what is the composition of the cumulative

distillate and the residue? What weight percent of the original material has been distilled?

Equilibrium data at 1 atm [*Ind. Eng. Chem.*, **42**, 2912 (1949)] are:

Mole Fraction <i>n</i> -Heptane			
Liquid	Vapor	Liquid	Vapor
0.025	0.048	0.448	0.541
0.062	0.107	0.455	0.540
0.129	0.205	0.497	0.577
0.185	0.275	0.568	0.637
0.235	0.333	0.580	0.647
0.250	0.349	0.692	0.742
0.286	0.396	0.843	0.864
0.354	0.454	0.950	0.948
0.412	0.504	0.975	0.976

13.2. Differential distillation.

A mixture of 40 mol% isopropanol in water is distilled at 1 atm by differential distillation until 70 mol% of the charge has been vaporized (equilibrium data are given in Exercise 7.33). What is the composition of the liquid residue in the still pot and of the collected distillate?

13.3. Differential distillation.

A 30 mol% feed of benzene in toluene is to be distilled in a batch, differential-distillation operation. A product having an average composition of 45 mol% benzene is to be produced. Calculate the amount of residue, assuming $\alpha = 2.5$ and $W_0 = 100$.

13.4. Differential distillation.

A charge of 250 lb of 70 mol% benzene and 30 mol% toluene is subjected to differential distillation at 1 atm. Determine the compositions of the distillate and residue after 1/3 of the feed has been distilled. Assume Raoult's and Dalton's laws and obtain a y - x diagram using a process simulator.

13.5. Differential distillation.

A mixture containing 60 mol% benzene and 40 mol% toluene is subjected to differential distillation at 1 atm, under three different conditions:

1. Until the distillate contains 70 mol% benzene
2. Until 40 mol% of the feed is evaporated
3. Until 60 mol% of the original benzene leaves in the vapor

Using $\alpha = 2.43$, determine for each of the three cases: (a) number of moles in the distillate for 100 mol of feed; (b) compositions of distillate and residue.

13.6. Differential distillation.

Fifteen mol% phenol in water is to be differential-batch-distilled at 260 torr. What fraction of the batch is in the still pot when the total distillate contains 98 mol% water? What is the residue concentration?

Vapor-liquid data at 260 torr [*Ind. Eng. Chem.*, 17, 199 (1925)]:

x , wt% (H₂O):

1.54 4.95 6.87 7.73 19.63 28.44 39.73 82.99
89.95 93.38 95.74

y , wt% (H₂O):

41.10 79.72 82.79 84.45 89.91 91.05 91.15 91.86
92.77 94.19 95.64

13.7. Differential distillation with added feed.

A still pot is charged with 25 mol of benzene and toluene containing 35 mol% benzene. Feed of the same composition is supplied at a rate of 7 mol/h, and the heating rate is adjusted so that the liquid level in the still pot remains constant. If $\alpha = 2.5$, how long will it be before the distillate composition falls to 45 mol% benzene?

13.8. Differential distillation with continuous feed.

A system consisting of a still pot and a total condenser is used to separate A and B from a trace of nonvolatile material. The still pot initially contains 20 lbmol of feed of 30 mol% A. Feed of the same composition is supplied to the still pot at the rate of 10 lbmol/h, and the heat input is adjusted so that the total moles of liquid in the reboiler remain constant. No residue is withdrawn from the still pot. Calculate the time required for the composition of the overhead product to fall to 40 mol% A. Assume $\alpha = 2.50$.

Section 13.2**13.9. Batch rectification at constant reflux ratio.**

Repeat Exercise 13.2 for the case of batch distillation carried out in a two-equilibrium-stage column with $L/V = 0.9$.

13.10. Batch rectification at constant reflux ratio.

Repeat Exercise 13.3 assuming the operation is carried out in a three-equilibrium-stage column with $L/V = 0.6$.

13.11. Batch rectification at constant reflux ratio.

One kmol of an equimolar mixture of benzene and toluene is fed to a batch still containing three equivalent stages (including the boiler). The liquid reflux is at its bubble point, and $L/D = 4$. What is the average composition and amount of product when the instantaneous product composition is 55 mol% benzene? Neglect holdup and assume $\alpha = 2.5$.

13.12. Differential distillation and batch rectification.

The fermentation of corn produces a mixture of 3.3 mol% ethyl alcohol in water. If this mixture is batch distilled at 1 atm, calculate and plot the instantaneous-vapor composition as a function of mol% of batch distilled. If reflux with three theoretical stages (including the boiler) is used, what is the maximum purity of ethyl alcohol that can be produced by batch rectification?

Equilibrium data are given in Exercise 7.29.

13.13. Batch rectification at constant composition.

An acetone-ethanol mixture of 0.5 mole fraction acetone is to be separated by batch distillation at 101 kPa.

Vapor-liquid equilibrium data at 101 kPa are as follows:

	Mole Fraction Acetone									
y	0.16	0.25	0.42	0.51	0.60	0.67	0.72	0.79	0.87	0.93
x	0.05	0.10	0.20	0.30	0.40	0.50	0.60	0.70	0.80	0.90

- (a) Assuming an L/D of 1.5 times the minimum, how many stages should this column have if the desired composition of the distillate is 0.90 mole fraction acetone when the residue contains 0.1 mole fraction acetone?
- (b) Assume the column has eight equilibrium stages and the reflux rate is varied continuously so that the top product is maintained constant at 0.9 mole fraction acetone. Make a plot of the reflux ratio versus the still pot composition and the amount of liquid left in the still pot.
- (c) Assume the same distillation is carried out at constant reflux ratio (and varying product composition). A residue containing 0.1 and an (average) product containing 0.9 mole fraction acetone is desired. Calculate the total vapor generated. Which method of operation is more energy-intensive? Suggest operating policies other than constant reflux ratio and constant distillate compositions that lead to equipment or operating cost savings.

13.14. Batch rectification at constant composition.

Two thousand gallons of 70 wt% ethanol in water having a specific gravity of 0.871 is to be separated at 1 atm in a batch rectifier operating at a constant distillate composition of 85 mol% ethanol with a constant molar vapor boilup rate to obtain a residual wastewater containing 3 wt% ethanol. If the task is to be completed in 24 h, allowing 4 h for charging, start-up, shutdown, and cleaning, determine: (a) the number of theoretical stages; (b) the reflux ratio when the ethanol in the still pot is 25 mol%; (c) the instantaneous distillate rate in lbmol/h when the concentration of ethanol in the still pot is 15 mol%; (d) the lbmol of distillate product; and (e) the lbmol of residual wastewater. Vapor-liquid equilibrium data are given in Exercise 7.29.

13.15. Batch rectification at constant composition.

One thousand kmol of 20 mol% ethanol in water is to undergo batch rectification at 101.3 kPa at a vapor boilup rate of 100 kmol/h. If the column has six theoretical stages and the distillate composition

is to be maintained at 80 mol% ethanol by varying the reflux ratio, determine: (a) time in hours for the residue to reach an ethanol mole fraction of 0.05; (b) kmol of distillate obtained when the condition of part (a) is achieved; (c) minimum and maximum reflux ratios during the rectification period; and (d) variation of the distillate rate in kmol/h during the rectification period. Assume constant molar overflow, neglect liquid holdup, and obtain equilibrium data from Exercise 7.29.

13.16. Batch rectification for constant composition.

Five hundred lbmol of 48.8 mol% A and 51.2 mol% B with a relative volatility $\alpha_{A,B}$ of 2.0 is separated in a batch rectifier consisting of a total condenser, a column with seven theoretical stages, and a still pot. The reflux ratio is varied to maintain the distillate at 95 mol% A. The column operates with a vapor boilup rate of 213.5 lbmol/h. The rectification is stopped when the mole fraction of A in the still is 0.192. Determine the (a) rectification time and (b) total amount of distillate produced.

13.17. Batch rectification of ethanol and water.

A batch distillation system consisting of two equilibrium stages, a still pot, and a total condenser is to be used to distill 50 kmol of a 32/68 mole% ethanol/water (E/W) mixture at 1 atm and a constant reflux ratio $L/D = 2/3$. A final still pot composition of 4.5 mol% ethanol is desired. Find the average distillate composition and the amount of distillate collected. Equilibrium data are:

y_E	0.45	0.52	0.57	0.60	0.63	0.68	0.77	0.83
x_E	0.10	0.20	0.30	0.40	0.50	0.60	0.70	0.80

Section 13.3

13.18. Batch stripping at constant boilup ratio.

Develop a procedure similar to that of section §13.3 to calculate a binary batch stripping operation using the equipment arrangement of Figure 13.8.

13.19. Batch stripping at constant boilup ratio.

A three-equilibrium-stage batch stripper (one stage is the boiler) is charged to the feed tank (see Figure 13.8) with 100 kmol of 10 mol% *n*-hexane and 90 mol% *n*-octane. The boilup rate is 30 kmol/h. If a constant boilup ratio (V/L) of 0.5 is used, determine the instantaneous bottoms composition and the composition of the accumulated bottoms product at the end of 2 h of operation.

13.20. Batch distillation with a middle feed vessel.

Develop a procedure similar to that of §13.3 to calculate a complex, binary, batch-distillation operation using the equipment arrangement of Figure 13.9.

Section 13.4

13.21. Effect of holdup on batch rectification.

For a batch rectifier with appreciable column holdup: (a) Why is the charge to the still pot higher in the light component than at the start of rectification, assuming that total-reflux conditions are established before rectification? (b) Why will separation be more difficult than with zero holdup?

13.22. Effect of holdup on batch rectification.

For a batch rectifier with appreciable column holdup, why do tray compositions change less rapidly than they do for a rectifier with negligible column holdup, and why is the separation improved?

13.23. Effect of holdup on batch rectification.

Based on the statements in Exercises 13.21 and 13.22, why is it difficult to predict the effect of holdup?

Section 13.5

13.24. Batch rectification by rigorous method.

A charge of 100 lbmol of 35 mol% *n*-hexane, 35 mol% *n*-heptane, and 30 mol% *n*-octane is to be distilled at 1 atm in a batch rectifier, consisting of a still pot, a column, and a total condenser, at a constant boilup rate of 50 lbmol/h and a constant reflux ratio of 5. Before rectification begins, total-reflux conditions are established. Then, the following three operation steps are carried out to obtain an *n*-hexane-rich cut, an intermediate cut for recycle, an *n*-heptane-rich cut, and an *n*-octane-rich residue:

Step 1: Stop when the accumulated-distillate purity drops below 95 mol% *n*-hexane.

Step 2: Empty the *n*-hexane-rich cut produced in Step 1 into a receiver and resume rectification until the instantaneous-distillate composition reaches 80 mol% *n*-heptane.

Step 3: Empty the intermediate cut produced in Step 2 into a receiver and resume rectification until the accumulated-distillate composition reaches 4 mol% *n*-octane.

Consider conducting the rectification in two different columns, each with the equivalent of 10 theoretical stages, a still pot, and a total condenser reflux-drum liquid holdup of 1.0 lbmol. For each column, determine with a batch-distillation program in a process simulator assuming ideal solutions, S , the compositions and amounts in lbmol of each of the four products.

Column 1: A plate column with a total liquid holdup of 8 lbmol.

Column 2: A packed column with a total liquid holdup of 2 lbmol.

Discuss the effect of liquid holdup for the two columns. Are the results what you expected?

13.25. Rigorous batch rectification with holdup.

One hundred lbmol of 10 mol% propane, 30 mol% *n*-butane, 10 mol% *n*-pentane, and the balance *n*-hexane is to be separated in a batch rectifier equipped with a still pot, a total condenser with a liquid holdup of 1.0 ft³, and a column with the equivalent of eight theoretical stages and a total holdup of 0.80 ft³. The pressure in the condenser is 50.0 psia and column pressure drop is 2.0 psi. The rectification campaign, given as follows, is designed to produce cuts of 98 mol% propane and 99.8 mol% *n*-butane, a residual cut of 99 mol% *n*-hexane, and two intermediate cuts, one of which may be a relatively rich cut of *n*-pentane. All five operating steps are conducted at a molar vapor boilup rate of 40 lbmol/h. Use a batch-distillation program in a process simulator with the SRK EOS to determine the amounts and compositions of all cuts.

Step	Reflux Ratio	Stop Criterion
1	5	98% propane in accumulator
2	20	95% <i>n</i> -butane in instantaneous distillate
3	25	99.8% <i>n</i> -butane in accumulator
4	15	80% <i>n</i> -pentane in instantaneous distillate
5	25	99% <i>n</i> -hexane in the pot

How might you alter the operation steps to obtain larger amounts of the product cuts and smaller amounts of the intermediate cuts?

13.26. Stability and stiffness.

One hundred lbmol of benzene (B), monochlorobenzene (MCB), and *o*-dichlorobenzene (DCB) is distilled in a batch rectifier that has

a total condenser, a column with 10 theoretical stages, and a still pot. Following establishment of total reflux, the first operation step begins at a boilup rate of 200 lbmol/h and a reflux ratio of 3. At the end of 0.60 h, the following conditions exist for the top three stages in the column:

	Top Stage	Stage 2	Stage 3
Temperature, °F	267.7	271.2	272.5
V , lbmol/h	206.1	209.0	209.5
L , lbmol/h	157.5	158.0	158.1
M , lbmol	0.01092	0.01088	0.01087
Vapor Mole Fractions:			
B	0.0994	0.0449	0.0331
MCB	0.9006	0.9551	0.9669
DCB	0.0000	0.0000	0.0000
Liquid Mole Fractions:			
B	0.0276	0.0121	0.00884
MCB	0.9724	0.9879	0.99104
DCB	0.0000	0.0000	0.00012

In addition, still pot and condenser holdups at 0.6 h are 66.4 and 0.1113 lbmol, respectively. For benzene, use the preceding data with (13-24) and (13-27) to estimate the liquid-phase mole fraction of benzene leaving Stage 2 at 0.61 h by using the explicit-Euler method with a Δt of 0.01 h. If the result is unreasonable, explain why, with respect to stability and stiffness considerations.

13.27. Batch rectification of a ternary mixture.

One hundred kmol of 30 mol% methanol, 30 mol% ethanol, and 40 mol% *n*-propanol is charged at 120 kPa to a batch rectifier consisting of a still pot, a column with the equivalent of 10 equilibrium stages, and a total condenser. After establishing a total-reflux condition, the column begins a sequence of two operating steps, each for a duration of 15 h at a distillate flow rate of 2 kmol/h and a reflux ratio of 10. Thus, the two accumulated distillates are equal in moles to the methanol and ethanol in the feed. Neglect the liquid holdup in the condenser and column. The column pressure drop is 8 kPa, with a pressure drop of 2 kPa through the condenser. Using a batch distillation program in a process simulator with the UNIFAC method for liquid-phase activity coefficients, determine the composition and amount in kmol for the three cuts.

13.28. Batch rectification of a ternary mixture.

Repeat Exercise 13.27 with the following modification: add a third operating step. For all three steps, use the same distillate rate and reflux rate as in Exercise 13.27. Use the following durations for the three steps: 13 hours for Step 1, 4 hours for Step 2, and 13 hours for Step 3. The distillate from Step 2 will be an intermediate cut. Determine the mole-fraction composition and amount in kmol of each of the four cuts.

13.29. Batch rectification of a ternary mixture.

One hundred kmol of 45 mol% acetone, 30 mol% chloroform, and 25 mol% benzene is charged at 101.3 kPa to a batch rectifier consisting of a still pot, a column containing the equivalent of 10 equilibrium stages, and a total condenser. After establishing a total-reflux condition, the column will begin a sequence of two operating steps, each at a distillate flow rate of 2 kmol/h and a reflux ratio of 10. The durations will be 13.3 hours for Step 1 and 24.2 hours for Step 2. Neglect pressure drops and the liquid holdup. Using a batch distillation program, in a process simulator with the UNIFAC method for liquid-phase activity coefficients, determine the mole-fraction composition and amount in kmol of each of the three cuts.

Section 13.6

13.30. Reduction of intermediate cuts.

Using a batch distillation program in a process simulator, make the following modifications to the C6–C7–C8 distillation in Example 13.10: (a) Increase the reflux above 8 to eliminate the second intermediate cut. (b) Change the termination specification on the second step to reduce the amount of the first intermediate cut, without failing to meet all three product specifications.

Section 13.7

13.31. Batch rectification at conditions of varying pressure.

A hydrocarbon mixture comprised in mole fractions of, $C_3H_8 = 0.1$, $i-C_4H_{10} = 0.2$, and a heavy component of average composition $C_{10}H_{22} = 0.70$. is subject to batch vaporization at a constant temperature of 25°C and varying pressure until 1 mol% of the residue is $i-C_4H_{10}$. Determine the final pressure. What advantage might there be in controlling the vaporization by pressure rather than temperature? Vapor pressure for the components at 25°C are:

Component	Vapor Pressure, mm Hg
C_3	7,139
$i-C_4$	2,611
C_{10}	1.37

Membrane Separations

§14.0 INSTRUCTIONAL OBJECTIVES

After completing this chapter, you should be able to:

- Explain membrane processes in terms such as permeability, feed, sweep, retentate, permeate, and solute–membrane interactions.
- Distinguish effects on membrane mass transfer due to permeability, permeance, solute resistance, selectivity, concentration polarization, and fouling.
- Explain contributions to mass-transfer coefficients from membrane thickness and tortuosity; solute size, charge, and solubility.
- Differentiate between isotropic and anisotropic membranes and between dense and microporous membranes.
- Distinguish among microfiltration, ultrafiltration, nanofiltration, and reverse osmosis in terms of average pore size and unique role in purification.
- Describe four common membrane shapes and six common membrane modules.
- Distinguish among mass transfer through membranes by bulk flow, molecular diffusion, Knudsen diffusion, and solution diffusion.
- Explain four common idealized flow patterns in membrane modules.
- Differentiate between concentration polarization and membrane fouling, and explain how to minimize effects of each on membrane capacity and throughput.
- Calculate mass-transfer rates for dialysis and electrodialysis, reverse osmosis, gas permeation, and pervaporation.
- Explain osmosis and how reverse osmosis is achieved.

In a membrane-separation process, a mixture of two or more components is partially separated by means of a semipermeable barrier (the membrane) through which some species travel faster than others. The most general membrane process is shown in Figure 14.1, where the feed mixture is separated into a **retentate** (that part of the feed that does not pass through the membrane) and a **permeate** (that passes through the membrane). The feed, retentate, and permeate are usually liquid or gas. The barrier is most often a thin, nonporous, polymeric film, but may also be porous polymer, ceramic, or metal material, or even a liquid, gel, or gas. To maintain selectivity, the barrier must not dissolve, deform, disintegrate, or break. The optional sweep, shown in Figure 14.1, is a liquid or gas used to facilitate removal of the permeate. Industrially important membrane-separation operations are listed in Table 14.1.

In membrane separations: (1) the two products are usually miscible, (2) the separating agent is a semipermeable barrier, and (3) a sharp separation is often difficult to achieve. Thus, membrane separations differ in some respects from the more common separation operations of absorption, distillation, and liquid–liquid extraction.

Although membrane separations have been known for more than 100 years [1], large-scale applications have appeared only in the past 75 years. In the 1940s, porous fluorocarbons were

used to separate $^{235}\text{UF}_6$ from $^{238}\text{UF}_6$ [2]. In the mid-1960s, reverse osmosis with cellulose acetate was first used to desalinate seawater to produce potable water (drinkable water with less than 500 ppm by weight of dissolved solids) [3]. Commercial ultrafiltration membranes followed in the late 1960s. In 1979, Monsanto Chemical Company introduced a hollow-fiber polysulfone to separate gas mixtures—for example, to enrich hydrogen and carbon-dioxide-containing streams [4]. Commercialization of alcohol dehydration by pervaporation began in the late 1980s, as did the large-scale application of emulsion liquid membranes for removal of metals and organics from wastewater. Also in the 1980s, the application of membrane separations to bioprocesses emerged, particularly ultrafiltration to separate proteins and microfiltration to separate bacteria and yeast.

Replacement of more-common separation operations with membrane separations has the potential to save energy and lower costs. It requires the production of high-mass-transfer flux, defect-free, long-life membranes on a large scale and the fabrication of membranes into compact, economical modules of high surface area per unit volume. It also requires considerable pretreatment of process feeds and careful control of operating conditions to prevent membrane deterioration and avoid degradation of membrane functionality due to caking, plugging, and fouling.

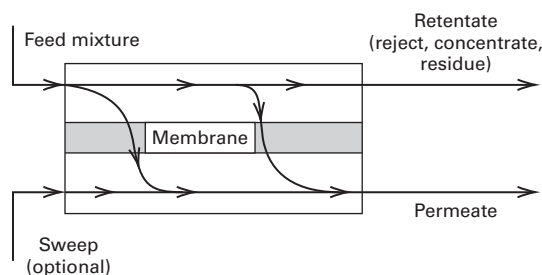


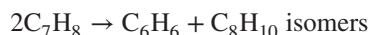
Figure 14.1 General membrane process.

Table 14.1 Industrial Membrane-Separation Processes

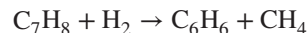
1. Reverse osmosis:
 - Desalinization of brackish water
 - Treatment of wastewater to remove a wide variety of impurities
 - Treatment of surface and groundwater
 - Concentration of foodstuffs
 - Removal of alcohol from beer
2. Dialysis:
 - Separation of nickel sulfate from sulfuric acid
 - Hemodialysis (removal of waste metabolites and excess body water, and restoration of electrolyte balance in blood)
3. Electrodialysis:
 - Production of table salt from seawater
 - Concentration of brines from reverse osmosis
 - Treatment of wastewaters from electroplating
 - Demineralization of cheese whey
 - Production of ultra-pure water for the semiconductor industry
4. Microfiltration:
 - Sterilization of liquids, gases, and parenteral drugs
 - Clarification and biological stabilization of beverages
 - Bacterial cell harvest and purification of antibiotics
 - Recovery of mammalian cells from cell culture broth
 - Transdermal patches to control rate of delivery of drugs
5. Ultrafiltration:
 - Preconcentration of milk before making cheese
 - Clarification of fruit juice
 - Purification of recombinant proteins and DNA, antigens, and antibiotics from clarified cell broths
 - Color removal from Kraft black liquor in papermaking
6. Pervaporation:
 - Dehydration of ethanol–water azeotrope
 - Removal of water from organic solvents
 - Removal of organics from water
7. Gas permeation:
 - Separation of CO₂ or H₂ from methane
 - Separation of uranium isotopes
 - Adjustment of the H₂/CO ratio in synthesis gas
 - Separation of air into nitrogen- and oxygen-enriched streams
 - Recovery of helium
 - Recovery of methane from biogas
 - Dehydration of compressed air
8. Liquid membranes:
 - Recovery of zinc from wastewater in the viscose fiber industry
 - Recovery of nickel from electroplating solutions

Industrial Example

A large-scale membrane process is in the manufacture of benzene from toluene, which requires the separation of hydrogen from methane. After World War II, during which large amounts of toluene were required to produce TNT (trinitrotoluene) explosives, petroleum refiners sought other markets for toluene. One was the use of toluene for manufacturing benzene, xylenes, and a number of other chemicals, including polyesters. Toluene can be catalytically disproportionated to benzene and xylenes in an adiabatic reactor with the feed entering at 950°F at a pressure above 500 psia. The main reaction is



To suppress coke formation, which fouls the catalyst, the reactor feed must contain a large fraction of hydrogen at a partial pressure of at least 215 psia. Unfortunately, the hydrogen takes part in a side reaction, the hydrodealkylation of toluene to benzene and methane:



Makeup hydrogen is usually not pure, but typically contains 15 mol% methane and 5 mol% ethane. Thus, the reactor effluent contains H₂, CH₄, C₂H₆, C₆H₆, unreacted C₇H₈, and C₈H₁₀ isomers. As shown in Figure 14.2a for the reactor section of the process, this effluent is cooled and partially condensed to 100°F at a pressure of 465 psia. At these conditions, a good separation between C₂H₆ and C₆H₆ is achieved in the flash drum. The vapor leaving the flash contains most of the H₂, CH₄, and C₂H₆, with the aromatic chemicals leaving in the liquid. The large amount of hydrogen in the flash-drum vapor should be recycled to the reactor, rather than sending it to a flare or using it as a fuel. However, if all of the vapor were recycled, methane and ethane would build up in the recycle loop, since no other exit is provided. Before the development of acceptable membranes for the separation of H₂ from CH₄ by gas permeation, part of the vapor stream was purged from the process, as shown in Figure 14.2a, to provide an exit for CH₄ and C₂H₆. With the introduction of a suitable membrane in 1979, it became possible to install membrane separators, as shown in Figure 14.2b.

Table 14.2 is the material balance of Figure 14.2b for a plant processing 7,750 barrels (42 gal/bbl) per day of toluene feed. The permeation membranes separate the flash vapor (stream S11) into a H₂-enriched permeate (S14, the recycled hydrogen), and a methane-enriched retentate (S12, the purge). The feed to the membrane system is 89.74 mol% H₂ and 9.26 mol% CH₄. No sweep gas is necessary. The permeate is enriched to 94.5 mol% H₂, and the retentate is 31.2 mol% CH₄. The recovery of H₂ in the permeate is 90%, leaving only 10% of the H₂ lost to the purge.

Before entering the membrane-separator system, the vapor is heated to at least 200°F (the dew-point temperature of the retentate) at a pressure of 450 psia (heater not shown). Because the hydrogen content in the feed is reduced in passing through the separator, the retentate becomes more concentrated in the heavier components. Without the heater, undesirable condensation would occur. The retentate leaves

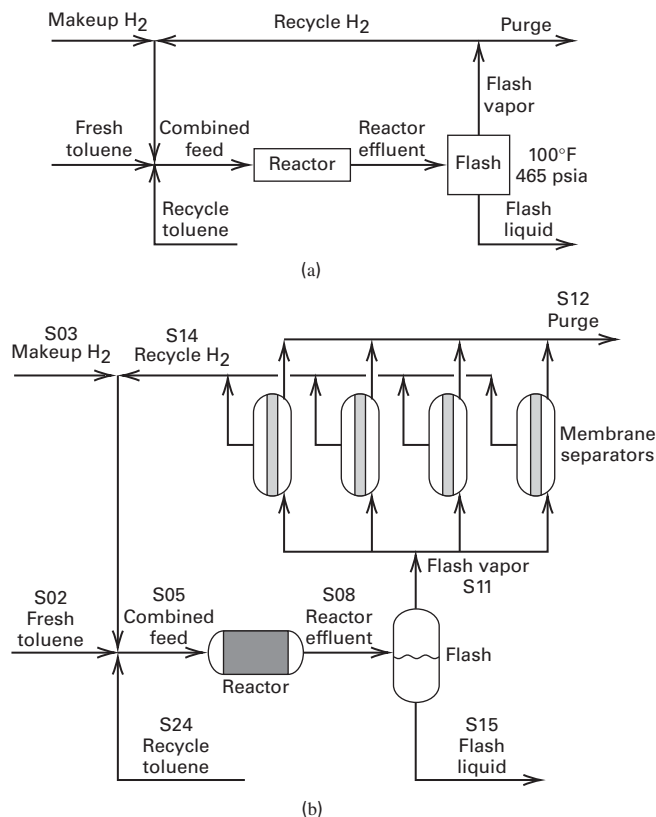


Figure 14.2 Reactor section of process to disproportionate toluene into benzene and xylene isomers. (a) Without a vapor-separation step. (b) With a membrane-separation step. Note: Heat exchangers, compressors, and pump not shown.

the separator at about the same temperature and pressure as the heated flash vapor. Recycle hydrogen permeate (S14) leaves at a pressure of 50 psia and a temperature lower than 200°F because of gas expansion. A disadvantage of the membrane process is the need to recompress the recycle hydrogen to the reactor inlet pressure.

The membrane is an aromatic polyamide polymer, 0.3- μm (micron) thick, with a nonporous layer in contact with the feed, and a much-thicker, porous support backing to give the membrane strength to withstand the pressure differential of $450 - 50 = 400$ psi. This large pressure difference is needed to force the hydrogen through the membrane, which is in the form of a spiral-wound module made from flat membrane sheets. The average flux of hydrogen through the membrane is 40 scfh (standard ft^3/h at 60°F and 1 atm) per

ft^2 of membrane surface area. From the material balance in Table 14.2, the H₂ transported through the membrane is

$$(1,685.1 \text{ lbmol/h})(379 \text{ scf/lbmol}) = 639,000 \text{ scfh}$$

The total membrane surface area required is $639,000/40 = 16,000 \text{ ft}^2$. The membrane is packaged in pressure-vessel modules of 4,000 ft^2 each. Thus, four modules in parallel are used.

Membrane separations are well developed for the applications listed in Table 14.1. Important progress is being made in developing new membrane applications, efficient membrane materials, and modules. Applications covering wider ranges of temperature and types of membrane materials are being investigated. Often, compared to other separation equipment, membrane separators are more compact, less capital intensive, and more easily operated, controlled, and maintained. However, membrane units are modular in construction, with many parallel units required for large-scale applications, in contrast to common separation techniques, where larger pieces of equipment are employed as plant size increases.

A key to an efficient and economical membrane-separation process is the membrane and how it is packaged to withstand large pressure differences. Research and development of membrane processes deals mainly with the discovery of suitably thin, selective membrane materials and their fabrication.

This chapter covers membrane materials and modules, the theory of transport through membranes, and the scale-up of membrane separators from experimental data. Emphasis is on dialysis, electro dialysis, reverse osmosis, gas permeation, and pervaporation. Microfiltration and ultrafiltration are applied mainly to biochemical separations and are not covered in this book. The theoretical principles apply as well to emerging but less-commercialized hybrid membrane processes such as membrane distillation, membrane gas absorption, membrane stripping, membrane solvent extraction, perstraction, and facilitated transport. The status of industrial membrane technology and applications are covered in depth by Baker [5] and in the handbook edited by Ho and Sirkar [6], which includes emerging processes.

§14.1 MEMBRANE MATERIALS

Originally, membranes were made from processed natural polymers such as cellulose and rubber; however, since 1930, many are custom-made synthetically by condensation reactions or from monomers by free-radical or ionic-catalyzed

Table 14.2 Material Balance for Toluene Disproportionation Plant; Flow Rates in lbmol/h for Streams in Reactor Section of Figure 14.2b

Component	S02	S03	S24	S14	S05	S08	S15	S11	S12
Hydrogen		269.0		1,685.1	1,954.1	1,890.6	18.3	1,872.3	187.2
Methane		50.5		98.8	149.3	212.8	19.7	193.1	94.3
Ethane		16.8			16.8	16.8	5.4	11.4	11.4
Benzene			13.1		13.1	576.6	571.8	4.8	4.8
Toluene	1,069.4		1,333.0		2,402.4	1,338.9	1,334.7	4.2	4.2
<i>p</i> -Xylene			8.0		8.0	508.0	507.4	0.6	0.6
Total	1,069.4	336.3	1,354.1	1,783.9	4,543.7	4,543.7	2,457.4	2,086.3	302.4

addition (chain) reactions. The resulting polymer is categorized as having (1) a long linear chain, such as linear polyethylene; (2) a branched chain, such as polybutadiene; (3) a three-dimensional, highly cross-linked structure typical of a condensation polymer like phenol–formaldehyde; or (4) a moderately cross-linked structure, such as butyl rubber or a partially cross-linked polyethylene. The linear-chain polymers soften with an increase in temperature, are soluble in organic solvents, and are referred to as **thermoplastic polymers**. At the other extreme, highly cross-linked polymers decompose at high temperature, are not soluble in organic solvents, and are referred to as **thermosetting polymers**. For polymeric membranes, a classification based on the arrangement or conformation of the polymer molecules is useful.

Polymers are **amorphous** or **crystalline**. The former refers to a polymer that is glass-like in appearance and lacks crystalline structure, whereas the latter refers to a polymer that is usually opaque and has a crystalline structure. If the temperature of a glassy polymer is increased to the **glass-transition temperature**, T_g , the polymer becomes **rubbery**. In rubbery polymers, portions of the chain can move and the backbone can rotate, resulting in high diffusion rates of the permeate. In glassy polymers, thermal motion of the polymer is largely curtailed, resulting in low permeate diffusion rates.

If the temperature of a crystalline polymer is increased to the **melting temperature**, T_m , the polymer melts. However, a thermosetting polymer never melts, it decomposes. Many polymers have both amorphous and crystalline regions—that is, a certain degree of crystallinity that varies from 5 to 90%, making it possible for some polymers to have both a T_g and a T_m . Glassy polymer membranes can operate below or above T_g ; crystalline polymer membranes must operate below T_m .

Table 14.3 lists **repeat units** and values of T_g and/or T_m for some of the many natural and synthetic polymers from which membranes have been fabricated. Included are crystalline, glassy, and rubbery polymers. Cellulose triacetate is the reaction product of cellulose and acetic anhydride. The repeat unit of cellulose is identical to that shown for cellulose triacetate, except that acetyl, Ac (CH_3CO), groups are replaced by H. The repeat units (**degree of polymerization**) in cellulose triacetate number ~ 300 . Triacetate is highly crystalline, of uniformly high quality, and hydrophobic.

Polyisoprene (natural rubber) is obtained from at least 200 different trees or plants found in the rubber-producing countries in Asia. Polyisoprene has a very low glass-transition temperature. Natural rubber has a degree of polymerization of from about 3,000 to 40,000 and is hard and rigid when cold, but soft, easily deformed, and sticky when hot. Depending on the temperature, it slowly crystallizes. To increase strength, elasticity, and stability of rubber, it is vulcanized with sulfur, a process that introduces cross-links.

Aromatic polyamides (also called aramids) are high-melting, crystalline polymers that have better long-term thermal stability and higher resistance to solvents than do aliphatic polyamides such as nylon. Some aromatic polyamides are easily fabricated into fibers, films, and sheets. The polyamide

structure shown in Table 14.3 is that of Kevlar, a du Pont trade name.

Polycarbonates, characterized by the presence of the $-\text{OCOO}-$ group in the chain, are mainly amorphous. The polycarbonate shown in Table 14.3 is an aromatic form, but aliphatic forms also exist. Polycarbonates differ from most other amorphous polymers in that they possess ductility and toughness below T_g . Because polycarbonates are thermoplastic, they can be extruded into various shapes, including films and sheets.

Polyimides are characterized by the presence of aromatic rings and heterocyclic rings containing nitrogen and attached oxygen. The structure shown in Table 14.3 is one of a number available. Polyimides are tough, amorphous polymers with high resistance to heat and excellent wear resistance. They can be fabricated into a wide variety of forms, including fibers, sheets, and films.

Polystyrene is a linear, amorphous, highly pure polymer of about 1,000 units of the structure shown in Table 14.3. Above a low T_g , which depends on molecular weight, polystyrene becomes a viscous liquid that is easily fabricated by extrusion or injection molding. Polystyrene can be annealed (heated and then cooled slowly) to convert it to a crystalline polymer with a melting point of 240°C . Styrene monomer can be copolymerized with other organic monomers, including acrylonitrile and butadiene to form acrylonitrile-butadiene-styrene (ABS) copolymers.

Polysulfones are synthetic polymers first introduced in 1966. The structure in Table 14.3 is just one of many, all of which contain the SO_2 group, which gives the polymers high strength. Polysulfones are easily spun into hollow fibers. Membranes of closely related polyethersulfone have also been commercialized.

Polytetrafluoroethylene is a straight-chain, highly crystalline polymer with a high degree of polymerization of the order of 100,000, giving it considerable strength. It possesses exceptional thermal stability and can be formed into films and tubing, as can polyvinylidene fluoride.

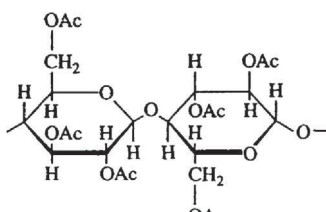
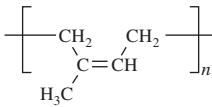
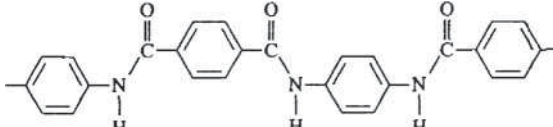
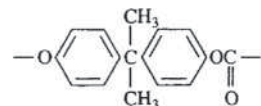
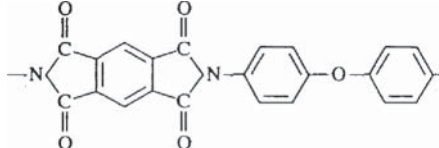
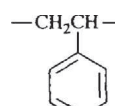
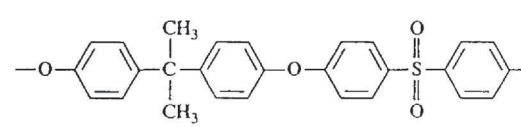
The details of membrane preparation techniques, organized by structure, are given by Baker [5].

To separate a binary chemical mixture, a polymer membrane must possess high permeance and a high permeance ratio for the two components being separated. The permeance for a given species diffusing through a membrane of given thickness is analogous to a mass-transfer coefficient, i.e., the flow rate of that species per unit cross-sectional area of membrane per unit driving force (concentration, partial pressure, etc.) across the membrane thickness. The molar transmembrane flux (flow rate per unit cross-sectional area of membrane) of species i is

$$N_i = \left(\frac{P_{M_i}}{l_M} \right) (\text{driving force}) = \bar{P}_{M_i} (\text{driving force}) \quad (14-1)$$

where \bar{P}_{M_i} is the **permeance**. In (14-1), l_M is the membrane thickness, and P_{M_i} is its **permeability**. The permeability is the fundamental property of the membrane material. The

Table 14.3 Common Polymers Used to Make Membrane Materials

Polymer	Type	Representative Repeat Unit	Glass-Transition Temp., °C	Melting Temp., °C
Cellulose triacetate	Crystalline			300
Polyisoprene (natural rubber)	Rubbery		-70	
Aromatic polyamide	Crystalline			275
Polycarbonate	Glassy		150	
Polyimide	Glassy		310-365	
Polystyrene	Glassy		74-110	
Polysulfone	Glassy		190	
Polytetrafluoroethylene (Teflon)	Crystalline	$-\text{CF}_2-\text{CF}_2-$		327

permeance depends upon the specific thickness of the membrane material and is defined as the ratio of the permeability of the membrane material to the membrane thickness.

Polymer membranes can be characterized as dense or microporous. In **dense, amorphous membranes**, pores of microscopic dimensions may be present, but they are generally less than a few Å (angstroms) in diameter. For this case, diffusing species must dissolve into the polymer and then diffuse through the polymer between the segments of the macromolecular chains. Diffusion can be difficult, but highly selective, for glassy polymers. If the polymer is partly crystalline, diffusion will occur almost exclusively through the amorphous regions, with the crystalline regions decreasing the diffusion area and increasing the diffusion path.

Microporous membranes contain interconnected pores and are categorized by their use in microfiltration (MF), ultrafiltration (UF), and nanofiltration (NF). The MF membranes, which have pore sizes of 200–100,000 Å, are used primarily to filter bacteria and yeast and provide cell-free suspensions. UF membranes have pore sizes of 10–200 Å and are used to separate low-molecular-weight solutes such as enzymes from higher-molecular-weight solutes like viruses or cell debris. NF membranes have pore sizes from 1 to 10 Å and can retain smaller molecules. NF membranes are used in reverse osmosis and pervaporation processes to purify liquids. The pores are formed by a variety of proprietary techniques, some of which are described by Baker [5]. Such techniques are valuable for producing isotropic (symmetric), microporous, crystalline

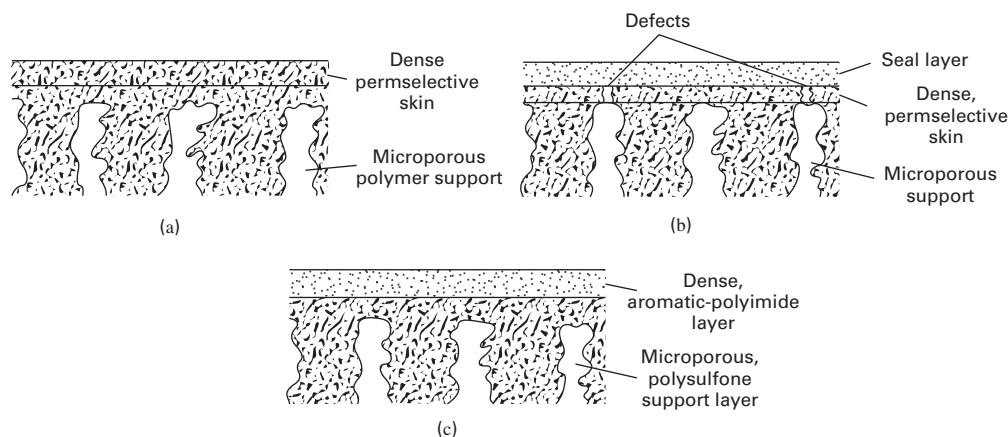


Figure 14.3 Anisotropic polymer membranes: (a) asymmetric, (b) caulked asymmetric, and (c) typical thin-film composite.

membranes. Permeability for microporous membranes is high, but selectivity is low for small molecules, due in part to pore-size distributions that can be variable and broad. However mixtures of molecules smaller and larger than the pore size may be separated almost perfectly by size.

The separation of small molecules is difficult. A high permeability is not compatible with a high separation factor. The beginning of the resolution of this dilemma occurred in 1963 with the fabrication by Loeb and Sourirajan [7] of an anisotropic, asymmetric membrane of cellulose acetate by a novel casting procedure. As shown in Figure 14.3a, the resulting membrane consists of a thin dense skin about 0.1–1.0 μm thick, called the **permselective** layer, formed over a much thicker microporous layer that provides support for the skin.

The flux rate of a species is controlled by the permeance of the very thin permselective skin. From (14-1), it is seen that the permeance of species i can be high because of the very small value of l_M , even though the permeability, P_{M_i} , is low because of the absence of pores. When large differences of P_{M_i} exist among molecules, both high permeance and high selectivity can be achieved with anisotropic membranes.

A very thin, isotropic membrane is subject to formation of minute holes in the permselective skin, which can render the membrane useless. A solution to the defect problem for an asymmetric polysulfone membrane was patented by Henis and Tripodi [8] of the Monsanto Company in 1980. They pulled silicone rubber, from a coating on the skin surface, into the defects by applying a vacuum. The resulting membrane, referred to as a **caulked membrane**, is shown in Figure 14.3b.

Wrasidlo [9] in 1977 introduced the thin-film composite membrane as an alternative to the asymmetric membrane. In the first application, shown in Figure 14.3c, a thin, dense film of polyamide polymer, 250 to 500 \AA in thickness, was formed on a thicker microporous polysulfone support. Today, both asymmetric and thin-film composites are fabricated by a variety of techniques.

Polymer membrane applications are usually limited to temperatures below 200°C and to mixtures that are chemically

inert. Operation at high temperatures and with chemically active mixtures requires membranes made of inorganic materials. These include microporous ceramics, metals, and carbon; and dense metals, such as palladium, that allow the selective diffusion of small molecules such as hydrogen and helium.

Examples of inorganic membranes are (1) asymmetric, microporous α -alumina tubes with 40–100 \AA pores at the inside surface and 100,000 \AA pores at the outside; (2) microporous glass tubes, whose pores may be filled with other oxides or the polymerization–pyrolysis product of trichloromethylsilane; (3) silica hollow fibers with 3–5 \AA pores; (4) porous ceramic, glass, or polymer materials coated with a thin, dense, palladium metal film just a few μm thick; (5) sintered metal; (6) pyrolyzed carbon; and (7) zirconia on sintered carbon. Extremely fine pores (< 10 \AA) are necessary to separate gas mixtures. Larger pores (> 50 \AA) are satisfactory for the separation of large molecules or solid particles from solutions containing small molecules.

EXAMPLE 14.1 Membrane Flux from Permeability.

A silica-glass membrane, 2- μm thick with pores < 10 \AA in diameter, has been developed for separating H_2 from CO at a temperature of 500°F. From laboratory data, the membrane permeabilities for H_2 and CO , respectively, are 200,000 and 700 Barrer, where the **Barrer**, a common unit for gas permeation, is defined by:

$$1 \text{ Barrer} = 10^{-10} \text{ cm}^3 (\text{STP})\text{-cm} / (\text{cm}^2\text{-s-cmHg})$$

where $\text{cm}^3 (\text{STP})/(\text{cm}^2\text{-s})$ is the volumetric transmembrane flux of the diffusing species in terms of standard conditions of 0°C and 1 atm; cm refers to the membrane thickness; and cmHg refers to the transmembrane partial-pressure driving force for the diffusing species.

The Barrer unit is named for R. M. Barrer, who published an early article [10] on diffusion in a membrane, followed by a widely referenced monograph on diffusion in and through solids [11].

If the transmembrane, partial-pressure driving forces for H_2 and CO , respectively, are 240 psi and 80 psi, calculate the transmembrane fluxes in $\text{kmol}/\text{m}^2\text{-s}$. Compare the H_2 flux to that for H_2 in the industrial application described at the beginning of this chapter.

Solution

At 0°C and 1 atm, 1 kmol of gas occupies $22.42 \times 10^6 \text{ cm}^3$. Also, $2 \mu\text{m}$ thickness = $2 \times 10^{-4} \text{ cm}$, and $1 \text{ cmHg } \Delta P = 0.1934 \text{ psi}$. Therefore, using (14.1):

$$N_{\text{H}_2} = \frac{(200,000)(10^{-10})(240/0.1934)(10^4)}{(22.42 \times 10^6)(2 \times 10^{-4})} = 0.0554 \frac{\text{kmol}}{\text{m}^2\text{-s}}$$

$$N_{\text{CO}} = \frac{(700)(10^{-10})(80/0.1934)(10^4)}{(22.42 \times 10^6)(2 \times 10^{-4})} = 0.000065 \frac{\text{kmol}}{\text{m}^2\text{-s}}$$

In the application discussed at the beginning of this chapter, the flux of H_2 for the polymer membrane is

$$\frac{(1685.1)(1/2.205)}{(16,000)(0.3048)^2(3600)} = 0.000143 \frac{\text{kmol}}{\text{m}^2\text{-s}}$$

Thus, the flux of H_2 through the ultra-microporous glass membrane is more than 100 times higher than the flux through the dense-polymer membrane. Large differences in molar fluxes through different membranes are common.

The following are useful factors for converting Barrer to SI and American Engineering units:

Multiply Barrer by 3.348×10^{-19} to obtain units of $(\text{kmol}\cdot\text{m})/(\text{m}^2\text{-s}\cdot\text{Pa})$.

Multiply Barrer by 5.584×10^{-12} to obtain units of $(\text{lbmol}\cdot\text{ft})/(\text{ft}^2\text{-h}\cdot\text{psi})$.

§14.2 MEMBRANE MODULES

Asymmetric and thin-film-composite anisotropic polymer-membrane materials are available in one or more of the three shapes shown in Figures 14.4a, b, and c. Flat sheets have typical dimensions of $1 \text{ m} \times 1 \text{ m} \times 200 \mu\text{m}$ thick, with a dense skin or a thin, dense layer of 500 to $5,000 \text{ \AA}$ in

thickness. Tubular membranes are typically 0.5 to 5.0 cm in diameter and up to 6 m long. The thin, dense layer is on the inside, as seen in Figure 14.4b, or on the outside tube surface. The porous tube support is fiberglass, perforated metal, or other suitable material. Very small-diameter hollow fibers, first reported by Mahon [12, 13] in the 1960s, are typically $42 \mu\text{m}$ i.d. $\times 85 \mu\text{m}$ o.d. $\times 1.2 \text{ m}$ long with a 0.1- to $1.0\text{-}\mu\text{m}$ thick dense skin. The hollow fibers shown in Figure 14.4c provide a large membrane surface area per unit volume. A honeycomb, monolithic element for inorganic oxide membranes is included in Figure 14.4d. Elements of hexagonal and circular cross section are available [14]. The circular flow channels are 0.3 to 0.6 cm in diameter, with a 20- to 40-mm-thick membrane layer. The hexagonal element in Figure 14.4d has 19 channels and is 0.85 m long. Both the bulk support and the thin membrane layer are porous, but the pores of the latter can be as small as 40 \AA .

The shapes in Figure 14.4 are incorporated into modules and cartridges, some of which are shown in Figure 14.5. Flat sheets used in plate-and-frame modules are circular, square, or rectangular in cross section. The sheets are separated by support plates that channel the permeate. In Figure 14.5a, a feed of brackish water flows across the surface of each sheet in the stack. Pure water is the permeate, while brine is the retentate.

Flat sheets are also fabricated into spiral-wound modules, as in Figure 14.5b. A laminate, consisting of two membrane sheets separated by spacers for the flow of feed and permeate, is wound around a central, perforated collection tube to form a module that is inserted into a pressure vessel. Feed flows axially in the channels created between the membranes by porous spacers. Permeate passes through the membrane, traveling inward in a spiral path to the central collection tube. From there, the permeate flows in either axial direction through and out of the tube. A typical spiral-wound module is 0.1–0.3 m in diameter and 3 m long. The four-leaf modification in Figure 14.5c minimizes permeate pressure drop because the permeate travel is less for the same membrane area.

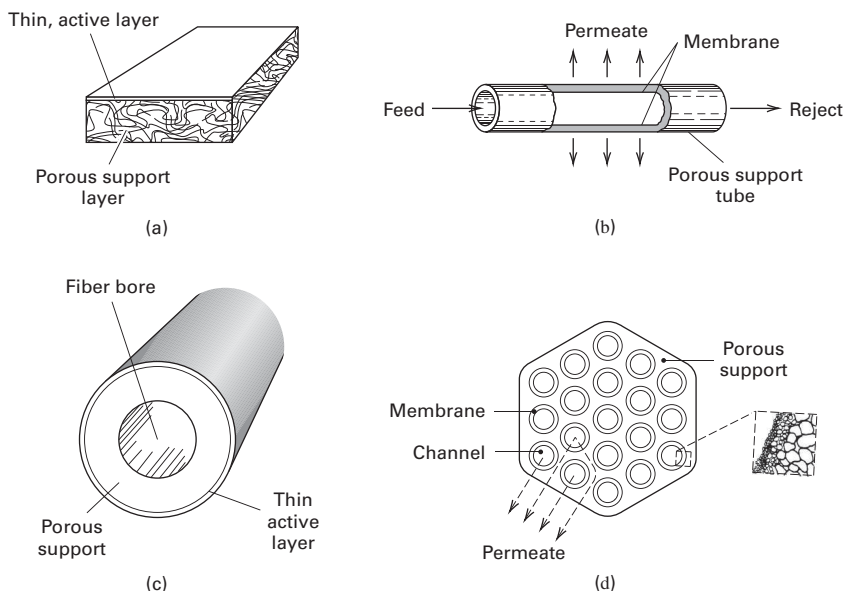


Figure 14.4 Common membrane shapes: (a) flat, asymmetric or thin-film composite sheet; (b) tubular; (c) hollow-fiber; (d) monolithic.

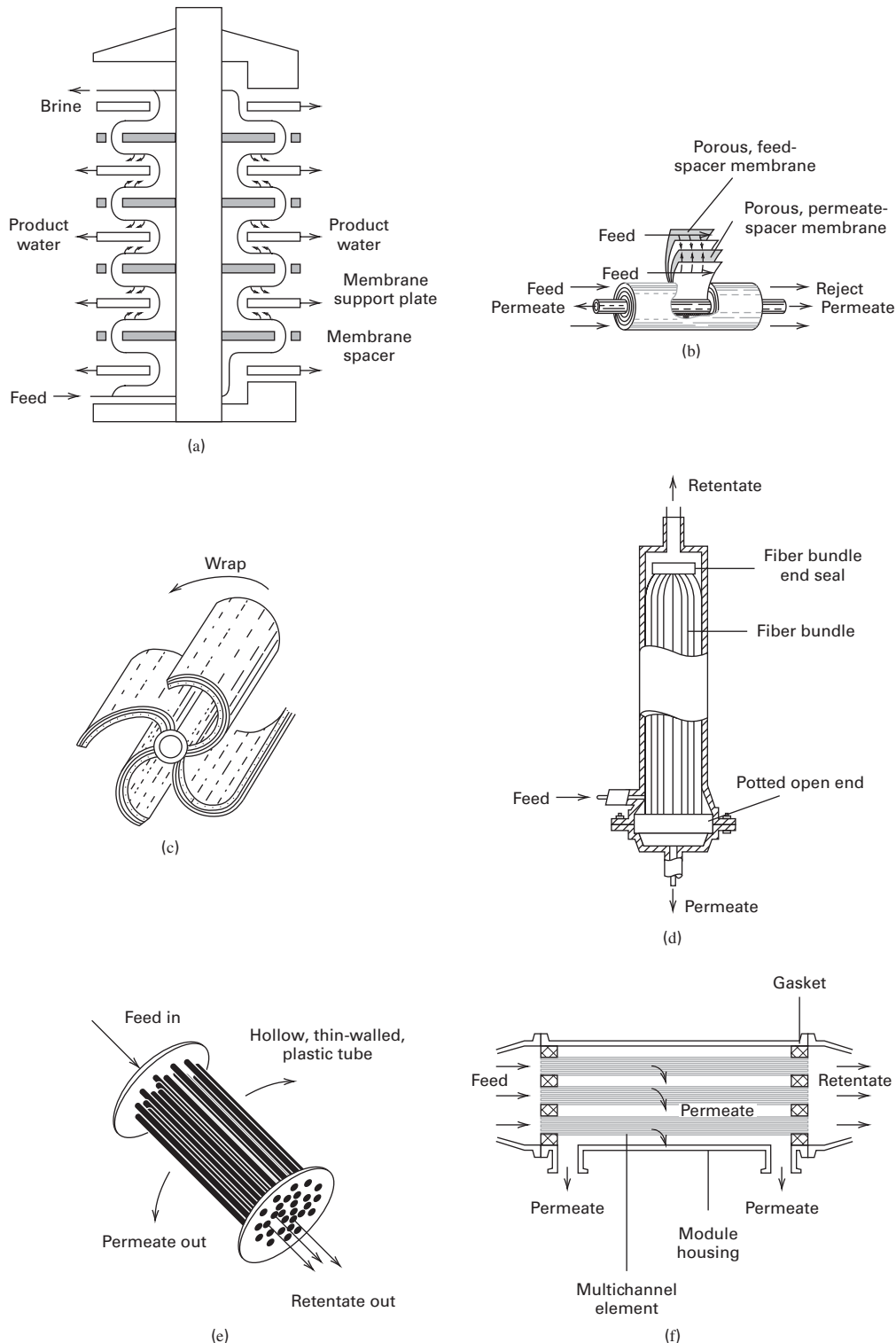


Figure 14.5 Common membrane modules: (a) plate-and-frame, (b) spiral-wound; (c) four-leaf spiral-wound; (d) hollow-fiber; (e) tubular; (f) monolithic.

Hollow-fiber modules for gas permeation and reverse osmosis are of two types, both resembling shell-and-tube exchangers. One type, shown in Figure 14.5d, is shell-fed. The permeate passes through the fiber wall into the tube side. The other type (not shown) is bore-fed into the tubes.

Permeate passes through the fiber wall into the shell side. Typically, the fibers are sealed at one end and embedded into a tube sheet with epoxy resin at the other end. A module might be 1 m long \times 0.1 to 0.25 m in diameter, and contain more than 1 million hollow fibers.

The tubular module in Figure 14.5e also resembles a heat exchanger, but the feed flows through the tubes. Permeate passes through the tube wall into the shell side of the module. Tubular modules contain up to 30 tubes.

The monolithic module in Figure 14.5f contains from 1 to 37 elements in a housing. Feed flows through the circular channels, and permeate passes through the membrane and porous support and into the open region between elements.

Table 14.4 is a comparison of the characteristics of four of the modules shown in Figure 14.5. The packing density is the membrane surface area per unit volume of module, for which hollow-fiber membrane modules are clearly superior.

The high cost and moderate packing density of the plate-and-frame module limits its use to high-value-added separations such as electrodialysis, pervaporation, cell broth clarification, and reverse osmosis where fouling can be a problem. The spiral-wound module is very popular for most applications because of its low cost and reasonable resistance to fouling. Tubular modules are used only for low-flow applications or when resistance to fouling and/or ease of cleaning is essential. Hollow-fiber modules, with their very high packing density and low cost, are popular when fouling and cleaning are minor considerations.

§14.3 MASS TRANSFER IN MEMBRANES

Membrane surface area requirements for a new application must ultimately be based on laboratory data. Nevertheless, because both the driving force and the permeability (or permeance) depend markedly on the mechanism of transport, it is important to understand the nature of transport in membranes to select an appropriate membrane process. This section deals with the theoretical aspects of mass-transfer processes that lead to proper choice of membrane. Applications to dialysis, reverse osmosis, gas permeation, and pervaporation are described.

Membranes can be macroporous, microporous, or dense (nonporous). Only microporous or dense membranes are permselective. Macroporous membranes are used to support thin microporous and dense membranes when significant pressure differences across the membrane are necessary to achieve high flux. The theoretical basis for mass transfer through microporous membranes is more highly developed than that for dense membranes, so porous-membrane transport is discussed first, with respect to bulk flow, liquid diffusion, and then gas diffusion. This is followed by nonporous (dense) membrane **solution-diffusion** transport, for liquid and gas mixtures. External mass-transfer resistances in the fluid films on either side of the membrane are treated where appropriate. It is important to note that, because of the range of pore sizes in membranes, the distinction between porous and nonporous membranes is not always obvious. The distinction can be made based only on the relative permeabilities for diffusion through pores and diffusion through the solid, amorphous regions of the membrane, respectively.

§14.3.1 Mass Transfer Through Porous Membranes

Mechanisms for transport of liquid and gas molecules through a porous membrane are depicted in Figures 14.6a, b, and c, where flow is downward. If the pore diameter is large compared to the molecular diameter and a pressure difference exists, bulk, convective flow through the pores occurs, as in Figure 14.6a. Bulk flow is undesirable because it is not permselective; therefore, no separation between feed components occurs. Permselective diffusion of components through the pores takes place if fugacity, activity, chemical-potential, concentration, or partial-pressure differences for components exist across the membrane, but the total pressure is the same on both sides of the membrane so no bulk flow occurs. Then a separation occurs, as shown in Figure 14.6b. If the pores are of

Table 14.4 Typical Characteristics of Membrane Modules

	Plate-and-Frame	Spiral-Wound	Tubular	Hollow-Fiber
Packing density, m ² /m ³	30 to 500	200 to 800	30 to 200	500 to 9,000
Resistance to fouling	Good	Moderate	Very good	Poor
Ease of cleaning	Good	Fair	Excellent	Poor
Relative cost	High	Low	High	Low
Main applications	D, RO, PV, UF, MF	D, RO, GP, UF, MF	RO, UF	D, RO, GP, UF

Note: D, dialysis; RO, reverse osmosis; GP, gas permeation; PV, pervaporation; UF, ultrafiltration; MF, microfiltration.

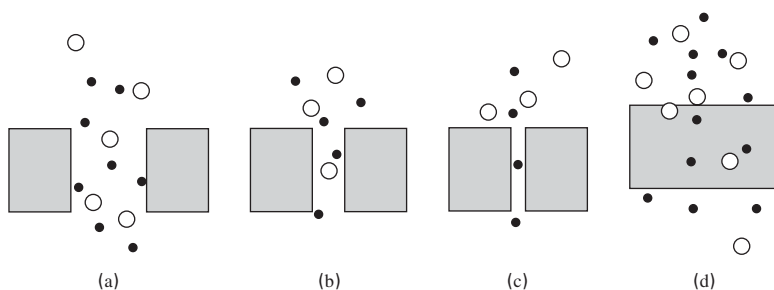


Figure 14.6 Mechanisms of mass transfer in membranes. (Flow is downward.) (a) bulk flow through pores; (b) diffusion through pores; (c) restricted diffusion through pores; (d) solution diffusion through dense membranes.

the order of molecular size for at least some of the components in the feed mixture, the diffusion of those components will be restricted (hindered) as shown in Figure 14.6c, resulting in an enhanced separation. Molecules larger than the pores are prevented from diffusing through the pores. This special case is highly desirable and is referred to as **size exclusion** or **sieving**. Another special case exists for gas diffusion in which the pore size and/or pressure (typically a vacuum) is such that the mean free path of the molecules is greater than the pore diameter, resulting in ballistic mass transfer via **Knudsen diffusion**, which depends on molecular weight. This is not shown in Figure 14.6.

Pore Resistance to Bulk Flow

Bulk flow is a pressure-driven flow of fluid through a semi-permeable barrier. Consider bulk flow of a fluid due to a pressure difference through an idealized straight, cylindrical pore. If the flow is laminar ($N_{Re} = Dv\rho/\mu < 2,100$), which is almost always true for small-diameter pores, flow velocity, v , given by the Hagen–Poiseuille law [15], is directly proportional to the transmembrane pressure drop, $P_0 - P_L$:

$$v = \frac{D^2}{32\mu L}(P_0 - P_L) \quad (14-2)$$

where D is pore diameter, large enough to pass all molecules; μ is fluid viscosity; and L is pore length. This results in a parabolic velocity profile for a Newtonian fluid. For a gas, the mean free path of the molecules is small compared to the pore diameter. If the membrane contains n such pores per unit cross section of membrane surface area normal to flow, the porosity (void fraction), ϵ , of the membrane is

$$\epsilon = n\pi D^2/4 \quad (14-3)$$

Then the superficial bulk-flow flux (mass velocity = mass flow/unit membrane area), N , through the membrane is

$$N = v\rho\epsilon = \frac{\epsilon\rho D^2}{32\mu l_M}(P_0 - P_L) = \frac{n\pi\rho D^4}{128\mu l_M}(P_0 - P_L) \quad (14-4)$$

where l_M is the membrane thickness and ρ and μ are fluid properties.

In real porous membranes, pores may not be cylindrical and straight, making it necessary to modify (14-4). Kozeny, in 1927, and Carman, in 1938, replaced cylindrical pores by a bundle of capillary tubes oriented at 45° to the surface. Ergun [16] extended this model by replacing, as a rough approximation, the pore diameter in (14-2) by the hydraulic diameter

$$d_H = 4 \left(\frac{\text{Volume available for flow}}{\text{Total pore surface area}} \right) = \frac{4 \left(\frac{\text{Total pore Volume}}{\text{Membrane volume}} \right)}{\left(\frac{\text{Total pore surface area}}{\text{Membrane volume}} \right)} = \frac{4\epsilon}{a_v} \quad (14-5)$$

where the membrane volume includes the volume of the pores. The specific surface area, a_v , which is the total pore surface

area per unit volume of just the membrane material (not including the pores), is

$$a_v = a/(1 - \epsilon) \quad (14-6)$$

Pore length is longer than the membrane thickness and can be represented by τl_M , where τ is a tortuosity factor > 1 . Substituting (14-5), (14-6), and the tortuosity factor into (14-4) gives

$$N = \frac{\rho\epsilon^2(P_0 - P_L)}{2(1 - \epsilon)^2 \tau a_v^2 \mu l_M} \quad (14-7)$$

In terms of a bulk-flow permeability, (14-7) becomes

$$N = \frac{P_M}{l_M}(P_0 - P_L) \quad (14-8)$$

where

$$P_M = \frac{\rho\epsilon^3}{2(1 - \epsilon)^2 \tau a_v^2 \mu} \quad (14-9)$$

Typically, τ is 2.5, whereas a_v is inversely proportional to the average pore diameter, giving it a wide range of values.

Equation (14-7) may be compared to the semi-theoretical Ergun equation [16], which represents the best fit of data for flow of a fluid through a packed bed:

$$\frac{P_0 - P_L}{l_M} = \frac{150\mu v_0(1 - \epsilon)^2}{D_p^2 \epsilon^3} + \frac{1.75\rho v_0^2(1 - \epsilon)}{D_p \epsilon^3} \quad (14-10)$$

where D_p is the mean particle diameter, v_0 is the superficial fluid velocity through the bed, and v_0/ϵ is the average velocity in the void space outside the particles. Equation (14-10) with just the first term on the RHS is the Kozeny–Carman equation. It applies to the laminar-flow region and is also known as Darcy's law. The second term applies to the turbulent region. For a spherical particle, the specific surface area is

$$a_v = \pi D_p^2 / (\pi D_p^3 / 6) \quad \text{or} \quad D_p = 6/a_v \quad (14-11)$$

Substitution of (14-11) into (14-10) for just the laminar-flow region, and rearrangement into the bulk-flow flux form gives

$$N = \frac{\rho\epsilon^3(P_0 - P_L)}{(150/36)(1 - \epsilon)^2 a_v^2 \mu l_M} \quad (14-12)$$

Comparing (14-12) to (14-7), it is seen that the term (150/36) in (14-12) corresponds to the term 2τ in (14-7), giving $\tau = 2.08$, which is reasonable. Accordingly, (14-12) can be used as a first approximation to the pressure drop for flow through a porous membrane when the pores are not straight cylinders. For gas flow, the density is taken as the average of the densities at the two membrane faces.

EXAMPLE 14.2 Pressure Drop Through a Membrane.

It is desired to pass water at 70°F through a supported polypropylene membrane, with a skin of 0.003-cm thickness and 35% porosity, at a volumetric flux of $200 \text{ m}^3/\text{m}^2$ membrane surface area/day. The pores can be considered straight cylinders of uniform diameter equal to $0.2 \text{ }\mu\text{m}$. If the pressure on the downstream side of the membrane

is 150 kPa, estimate the required pressure on the upstream side of the membrane. The pressure drop through the membrane support is negligible.

Solution

Equation (14-4) applies, where in SI units:

$$N/\rho = 200/(24)(3600) = 0.00232 \text{ m}^3/\text{m}^2\text{-s},$$

$$\varepsilon = 0.35, D_p = 0.2 \times 10^{-6} \text{ m}, l_M = 0.00003 \text{ m}, P_L = 150 \text{ kPa} = 150,000 \text{ Pa}, \mu = 0.001 \text{ Pa-s}$$

From a rearrangement of (14-4),

$$P_0 = P_L + \frac{32\mu l_M(N/\rho)}{\varepsilon D_p^2}$$

$$= 150,000 + \frac{(32)(0.001)(0.00003)(0.00232)}{(0.35)(0.2 \times 10^{-6})^2}$$

$$= 309,000 \text{ Pa} \quad \text{or} \quad 309 \text{ kPa}$$

Liquid Diffusion Through Pores

Consider diffusion through the pores of a membrane from a liquid feed to a sweep liquid when identical total pressures, but different component concentrations, exist on the two sides of the membrane. There is no bulk flow through the membrane due to lack of a pressure difference across the membrane. However, if species diffuse at different rates, a separation can be achieved. Assume the feed mixture is a liquid of solvent and solutes i . At concentrations sufficiently low to neglect solute-solute interactions, the transmembrane flux for each solute is given by a modified form of Fick's law (§3.1.1):

$$N_i = \frac{D_{e_i}}{l_M} (c_{i_0} - c_{i_L}) \quad (14-13)$$

where D_{e_i} is the effective diffusivity, and c_i is the concentration of i in the liquid in the pores at feed-side (0) and permeate-side (L) of the membrane. The effective diffusivity is

$$D_{e_i} = \frac{\varepsilon D_i K_{r_i}}{\tau} \quad (14-14)$$

where D_i is the molecular diffusion coefficient (diffusivity) of solute i in the solution, ε the volume fraction of pores in the membrane, τ the tortuosity, and K_{r_i} is a restrictive factor for the solute. The restrictive factor accounts for pore diameter, d_p , causing interfering collisions of diffusing solutes with the pore wall, when the ratio of molecular diameter, d_m , to pore diameter exceeds about 0.01. The restrictive factor, for a given solute, according to Beck and Schultz [17], is:

$$K_r = \left[1 - \frac{d_m}{d_p} \right]^4, \quad (d_m/d_p) \leq 1 \quad (14-15)$$

From (14-15), when $d_m/d_p = 0.01$, $K_r = 0.96$, but when $d_m/d_p = 0.3$, $K_r = 0.24$. When $d_m > d_p$, $K_r = 0$, and the solute cannot diffuse through the pore. This is the sieving

or size-exclusion effect in Figure 14.6c. As illustrated in the next example, transmembrane fluxes for liquids through microporous membranes are very small because effective solute diffusivities are low.

For solute molecules not subject to size exclusion, a useful selectivity ratio is defined as

$$S_{i,j} = \frac{D_i K_{r_i}}{D_j K_{r_j}} \quad (14-16)$$

This ratio is greatly enhanced by the effect of restrictive diffusion when the solutes differ widely in molecular weight and one or more molecular diameters approach the pore diameter. This is shown in the following example.

EXAMPLE 14.3 Solute Diffusion Through Membrane Pores.

Beck and Schultz [18] measured diffusion rates of urea and sugars, in aqueous solutions, in microporous mica membranes especially prepared to give almost-straight elliptical pores of almost uniform size. Based on the following data for a membrane and two solutes, estimate transmembrane fluxes for the two solutes in $\text{g}/\text{cm}^2\text{-s}$ at 25°C . Assume the aqueous solutions on either side of the membrane are sufficiently dilute that no multicomponent diffusional effects are present.

Membrane:

Material	Microporous
Thickness, μm	4.24
Average pore diameter, Angstroms	88.8
Tortuosity, τ	1.1
Porosity, ε	0.0233

Solutes (in aqueous solution at 25°C):

Solute	MW	$D_i \times 10^6$ cm^2/s	molecular diameter, $d_m, \text{\AA}$	g/cm^3	
				c_{i_0}	c_{i_L}
1 Urea	60	13.8	5.28	0.0005	0.0001
2 β -Dextrin	1135	3.22	17.96	0.0003	0.00001

Solution

Calculate the restrictive factor and effective diffusivity from (14-15) and (14-14), respectively.

For urea (1):

$$K_{r_1} = \left[1 - \frac{5.28}{88.8} \right]^4 = 0.783$$

$$D_{e_1} = \frac{(0.0233)(13.8 \times 10^{-6})(0.783)}{1.1} = 2.29 \times 10^{-7} \text{ cm}^2/\text{s}$$

For β -dextrin (2):

$$K_{r_2} = \left[1 - \frac{17.96}{88.8} \right]^4 = 0.405$$

$$D_{e_2} = \frac{(0.0233)(3.22 \times 10^{-6})(0.405)}{1.1} = 2.78 \times 10^{-8} \text{ cm}^2/\text{s}$$

Because of large differences in molecular size, effective diffusivities differ by an order of magnitude. From (14-16), selectivity is

$$S_{1,2} = \frac{(13.8 \times 10^{-6})(0.783)}{(3.22 \times 10^{-6})(0.405)} = 8.3$$

Next, calculate transmembrane fluxes from (14-13), noting that the given concentrations are at the two faces of the membrane. Concentrations in the bulk solutions on either side of the membrane may differ from concentrations at the faces, depending upon the magnitudes of external mass-transfer resistances in boundary layers adjacent to the two membrane faces.

For urea:

$$N_1 = \frac{(2.29 \times 10^{-7})(0.0005 - 0.0001)}{4.24 \times 10^{-4}} \\ = 2.16 \times 10^{-7} \text{ g/cm}^2\text{-s}$$

For β -dextrin:

$$N_2 = \frac{(2.768 \times 10^{-8})(0.0003 - 0.00001)}{4.24 \times 10^{-4}} \\ = 1.90 \times 10^{-8} \text{ g/cm}^2\text{-s}$$

Note that these fluxes are extremely low.

Gas Diffusion Through Porous Membranes

When the mixture on either side of a microporous membrane is a gas, rates of diffusion can be expressed in terms of Fick's law (§3.1.1). If pressure and temperature on either side of the membrane are equal and the ideal-gas law holds, (14-13) in terms of a partial-pressure driving force is:

$$N_i = \frac{D_{e_i} c_M}{Pl_M} (p_{i_0} - p_{i_L}) = \frac{D_{e_i}}{RTl_M} (p_{i_0} - p_{i_L}) \quad (14-17)$$

where c_M is the total gas-mixture molar concentration given as P/RT by the ideal-gas law and p is partial pressure.

For a gas, diffusion through a pore occurs by ordinary diffusion, as with a liquid, and/or in series with Knudsen diffusion when the pore diameter is very small and/or total pressure is low. In the Knudsen-flow regime, collisions occur primarily between gas molecules and the pore wall, rather than between gas molecules. In the absence of a bulk-flow effect or restrictive diffusion, (14-14) is modified to account for both diffusion mechanisms:

$$D_{e_i} = \frac{\varepsilon}{\tau} \left[\frac{1}{(1/D_i) + (1/D_{K_i})} \right] \quad (14-18)$$

where D_{K_i} is the Knudsen diffusivity, which from the kinetic theory of gases for a straight, cylindrical pore of diameter d_p is

$$D_{K_i} = \frac{d_p \bar{v}_i}{3} \quad (14-19)$$

where, if D_{K_i} is in cm^2/s , d_p is in cm, and \bar{v}_i is the average molecule velocity in cm/s given by

$$\bar{v}_i = (8RTg_c/\pi M_i)^{1/2} \quad (14-20)$$

where T is in K, M is molecular weight in kg_m/kmol , $R = 84,784 \text{ kg}_f\text{-cm/kmol-K}$, and $g_c = 980.7 \text{ kg}_m\text{-cm/kg}_f\text{-s}^2$. Combining (14-19) and (14-20) and simplifying,

$$D_{K_i} = 4,850 d_p (T/M_i)^{1/2} \quad (14-21)$$

When Knudsen flow predominates, as it often does for micropores, a selectivity based on the permeability ratio for species A and B is given from a combination of (14-1), (14-17), (14-18), and (14-21):

$$\frac{P_{M_A}}{P_{M_B}} = \left(\frac{M_B}{M_A} \right)^{1/2} \quad (14-22)$$

Except for gaseous species of widely differing molecular weights, the permeability ratio from (14-22) is not large, and the separation of gases by microporous membranes at low to moderate pressures that are equal on both sides of the membrane to minimize bulk flow is almost always impractical, as illustrated in the following example. However, during WWII, separation of the two UF_6 isotopes of by the U.S. government was accomplished by Knudsen diffusion, with a permeability ratio of only 1.0043, at Oak Ridge, Tennessee, using thousands of stages and acres of membrane surface. Tritium has also been separated from hydrogen in this manner.

EXAMPLE 14.4 Knudsen Diffusion.

A gas mixture of hydrogen (H) and ethane (E) is to be partially separated with a composite membrane having a 1- μm -thick porous skin with an average pore size of 20 \AA and a porosity of 30%. Assume $\tau = 1.5$. The pressure on either side of the membrane is 10 atm and the temperature is 100°C. Estimate permeabilities of the components in Barrer.

Solution

From (14-1), (14-17), and (14-18), the permeability can be expressed in $\text{mol-cm/cm}^2\text{-s-atm}$:

$$P_{M_i} = \frac{\varepsilon}{\tau RT} \left[\frac{1}{(1/D_i) + (1/D_{K_i})} \right]$$

where $\varepsilon = 0.30$, $R = 82.06 \text{ cm}^3\text{-atm/mol-K}$, $T = 373 \text{ K}$, and $\tau = 1.5$.

At 100°C, the ordinary diffusivity is given by $D_H = D_E = D_{H,E} = 0.86/P$ in cm^2/s with total pressure P in atm. Thus, at 10 atm, $D_H = D_E = 0.086 \text{ cm}^2/\text{s}$. Knudsen diffusivities are given by (14-21), with $d_p = 20 \times 10^{-8} \text{ cm}$.

$$D_{K_H} = 4,850 (20 \times 10^{-8}) (373/2.016)^{1/2} = 0.0132 \text{ cm}^2/\text{s}$$

$$D_{K_E} = 4,850 (20 \times 10^{-8}) (373/30.07)^{1/2} = 0.0342 \text{ cm}^2/\text{s}$$

For both components, diffusion is controlled mainly by Knudsen diffusion.

$$\text{For hydrogen: } \frac{1}{(1/D_H) + (1/D_{K_H})} = 0.0114 \text{ cm}^2/\text{s.}$$

$$\text{For ethane: } \frac{1}{(1/D_E) + (1/D_{K_E})} = 0.00329 \text{ cm}^2/\text{s.}$$

$$P_{M_H} = \frac{0.30(0.0114)}{(82.06)(373)(1.5)} = 7.45 \times 10^{-8} \frac{\text{mol-cm}}{\text{cm}^2\text{-s-atm}}$$

$$P_{M_E} = \frac{0.30(0.00329)}{(82.06)(373)(1.5)} = 2.15 \times 10^{-8} \frac{\text{mol-cm}}{\text{cm}^2\text{-s-atm}}$$

To convert to Barrer as defined in Example 14.1, note that

$$76 \text{ cmHg} = 1 \text{ atm and } 22,400 \text{ cm}^3 \text{ (STP)} = 1 \text{ mol}$$

$$P_{M_H} = \frac{7.45 \times 10^{-8}(22,400)}{(10^{-10})(76)} = 220,000 \text{ barrer}$$

$$P_{M_E} = \frac{2.15 \times 10^{-8}(22,400)}{(10^{-10})(76)} = 63,400 \text{ barrer}$$

§14.3.2 Transport Through Nonporous Membranes

Mass transfer through nonporous (dense) solid membranes is the predominant mechanism in membrane separators for reverse osmosis, gas permeation, and pervaporation (liquid and vapor). As indicated in Figure 14.6d, gas or liquid species absorb at the feed-side of the membrane, diffuse through the membrane, and desorb at the permeate-side.

Liquid diffusivities are several orders of magnitude less than gas diffusivities, and diffusivities of solutes in solids are a few orders of magnitude less than diffusivities in liquids. Thus, differences between diffusivities in gases and solids are enormous. For example, at 1 atm and 25°C, diffusivities in cm²/s for water are

Water vapor in air	0.25
Water in ethanol liquid	1.2×10^{-5}
Dissolved water in cellulose-acetate solid	1×10^{-8}

As might be expected, small molecules fare better than large molecules for diffusivities in solids. From the *Polymer Handbook* [19], diffusivities in cm²/s for several species in low-density polyethylene at 25°C are

Helium	6.8×10^{-6}
Hydrogen	0.474×10^{-6}
Nitrogen	0.320×10^{-6}
Propane	0.0322×10^{-6}

Regardless of whether a nonporous membrane is used to separate a gas or a liquid mixture, the **solution-diffusion model** of Lonsdale, Merten, and Riley [20] is used with experimental permeability data to design nonporous membrane separators. This model is based on Fick's law for diffusion through solid, nonporous membranes based on the driving force, $c_{i0} - c_{iL}$ shown in Figure 14.7b, where concentrations refer to solute dissolved in the membrane.

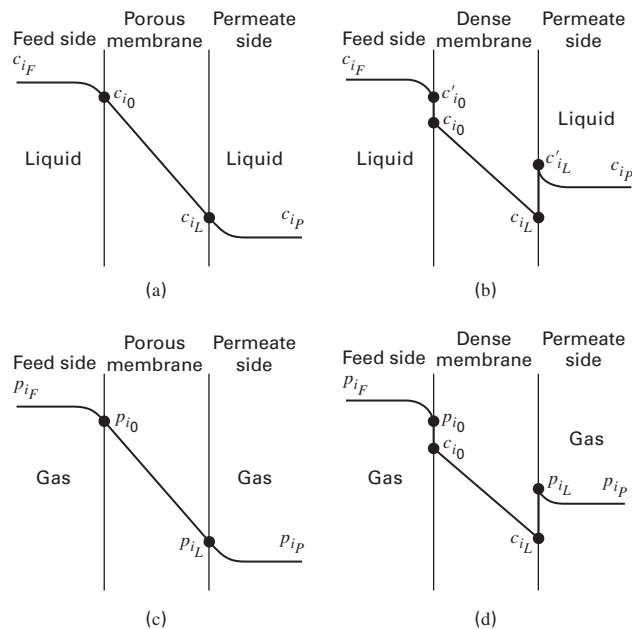


Figure 14.7 Concentration and partial-pressure profiles for solute transport through membranes. Liquid mixture with (a) a porous and (b) a nonporous membrane; gas mixture with (c) a porous and (d) a nonporous membrane.

Concentrations in the membrane are related to the concentrations or partial pressures in the fluid adjacent to the membrane faces by assuming thermodynamic equilibrium for the solute at the fluid–membrane interfaces. This assumption has been validated by Motamedian et al. [21] for permeation of light gases through dense cellulose acetate at up to 90 atm.

Solution-Diffusion for Liquid Mixtures

Figures 14.7a and b show typical solute-concentration profiles for liquid mixtures with porous and nonporous (dense) membranes. Solute concentration decreases across the membrane, and potentially on either side of the membrane, due to resistances in corresponding diffusive boundary layers or stagnant thin films.

For porous membranes, concentration profiles are continuous from the bulk-feed liquid to the bulk-permeate liquid because liquid is present continuously from one side to the other. The concentration c_{i0} is the same in the liquid feed just adjacent to the membrane surface and in the liquid just within the pore entrance. This is not the case for the nonporous membrane in Figure 14.7b. Solute concentration c'_{i0} is that in the feed liquid just adjacent to the upstream membrane surface, whereas c_{i0} is that in the membrane just adjacent to the upstream membrane surface. In general, c_{i0} is smaller than c'_{i0} but the two are related by a thermodynamic equilibrium partition coefficient K_{i0} defined by

$$K_{i0} = c_{i0}/c'_{i0} \quad (14-23)$$

Similarly, at the other face:

$$K_{i_L} = c_{i_L}/c'_{i_L} \quad (14-24)$$

Fick's law for the dense membrane of Figure 14.7b is:

$$N_i = \frac{D_i}{l_M} (c_{i_0} - c_{i_L}) \quad (14-25)$$

where D_i is the diffusivity of the solute in the membrane. If (14-23) and (14-24) are combined with (14-25), and the partition coefficient is assumed independent of concentration, such that $K_{i_0} = K_{i_L} = K_i$, the flux is

$$N_i = \frac{K_i D_i}{l_M} (c'_{i_0} - c'_{i_L}) \quad (14-26)$$

If the mass-transfer resistances in the two fluid boundary layers (films) are negligible:

$$N_i = \frac{K_i D_i}{l_M} (c_{i_F} - c_{i_P}) \quad (14-27)$$

In (14-26) and (14-27), $P_{M_i} = K_i D_i$ is the permeability for the solution-diffusion model, where K_i accounts for the solute solubility in the membrane and D_i accounts for diffusion through the membrane. Because D_i is generally very small, it is important that the membrane material have a large value for K_i and/or a small thickness.

D_i and K_i , and therefore P_{M_i} , depend on the solute and membrane. When solutes dissolve in a polymer membrane, it will swell, causing both D_i and K_i to increase. Other polymer-membrane factors that influence D_i , K_i , and P_{M_i} are listed in Table 14.5. However, the largest single factor is the chemical structure of the membrane polymer. Because of the many factors involved, it is important to obtain experimental permeability data for the membrane and feed mixture of interest. The effect of external mass-transfer resistances is considered later in this section.

Solution-Diffusion for Gas Mixtures

Figures 14.7c and d show typical solute profiles for gas mixtures with porous and nonporous membranes, including the

Table 14.5 Factors That Influence Permeability of Solutes in Dense Polymers

Factor	Value Favoring High Permeability
Polymer density	low
Degree of crystallinity	low
Degree of cross-linking	low
Degree of vulcanization	low
Amount of plasticizers	high
Amount of fillers	low
Chemical affinity of solute for polymer (solubility)	high

effect of external-fluid boundary layers. For a porous membrane, a continuous partial-pressure profile is shown. For the nonporous membrane, a concentration profile is shown within the membrane, where the solute is dissolved. Fick's law holds for transport through the membrane. Assuming that thermodynamic equilibrium exists at the fluid membrane interfaces, concentrations in Fick's law are related to partial pressures adjacent to the membrane faces by Henry's law in the form:

$$H_{i_0} = c_{i_0}/p_{i_0} \quad (14-28)$$

and

$$H_{i_L} = c_{i_L}/p_{i_L} \quad (14-29)$$

If it is assumed that H_i is independent of total pressure and concentration, and that temperatures are the same at both membrane faces:

$$H_{i_0} = H_{i_L} = H_i \quad (14-30)$$

Combining (14-25), (14-28), (14-29), and (14-30), the flux is

$$N_i = \frac{H_i D_i}{l_M} (p_{i_0} - p_{i_L}) \quad (14-31)$$

If the external mass-transfer resistances are neglected, $p_{i_F} = p_{i_0}$ and $p_{i_L} = p_{i_P}$, giving

$$N_i = \frac{H_i D_i}{l_M} (p_{i_F} - p_{i_P}) = \frac{P_{M_i}}{l_M} (p_{i_F} - p_{i_P}) \quad (14-32)$$

where

$$P_{M_i} = H_i D_i \quad (14-33)$$

Thus, permeability depends on both gas solubility in the membrane and its diffusivity when dissolved in the membrane. An acceptable rate of transport can be achieved only by using a very thin membrane and a high pressure on the feed side. The permeability of a gas through a polymer membrane is subject to factors listed in Table 14.5. Light gases do not interact with the polymer or cause it to swell. Thus, a light-gas permeant-polymer combination is readily characterized. Often both solubility and diffusivity are measured. An extensive tabulation is given in the *Polymer Handbook* [19]. Representative data at 25°C are given in Table 14.6. In general, diffusivity decreases and solubility increases with increasing molecular weight of the gas species, making it difficult to achieve a high selectivity. The effect of temperature over a modest increment of about 50°C can be represented for both solubility and diffusivity by Arrhenius equations. For example,

$$D = D_0 e^{-E_D/RT} \quad (14-34)$$

The modest effect of temperature on solubility may act in either direction. However, an increase in temperature can cause an increase in diffusivity, and a corresponding increase in permeability. Typical activation energies of diffusion in polymers, E_D , range from 15 to 60 kJ/mol.

Application of Henry's law to rubbery polymers is well accepted, particularly for low-molecular-weight penetrants,

Table 14.6 Coefficients for Gas Permeation in Polymers

	Gas Species					
	H ₂	O ₂	N ₂	CO	CO ₂	CH ₄
Low-density polyethylene:						
$D \times 10^6$	0.474	0.46	0.32	0.332	0.372	0.193
$H \times 10^6$	1.58	0.472	0.228	0.336	2.54	1.13
$P_M \times 10^{13}$	7.4	2.2	0.73	1.1	9.5	2.2
Polyethylmethacrylate:						
$D \times 10^6$	—	0.106	0.0301	—	0.0336	—
$H \times 10^6$	—	0.839	0.565	—	11.3	—
$P_M \times 10^{13}$	—	0.889	0.170	—	3.79	—
Polyvinylchloride:						
$D \times 10^6$	0.5	0.012	0.0038	—	0.0025	0.0013
$H \times 10^6$	0.26	0.29	0.23	—	4.7	1.7
$P_M \times 10^{13}$	1.3	0.034	0.0089	—	0.12	0.021
Butyl Rubber:						
$D \times 10^6$	1.52	0.081	0.045	—	0.0578	—
$H \times 10^6$	0.355	1.20	0.543	—	6.71	—
$PM \times 10^{13}$	5.43	0.977	0.243	—	3.89	—

Units are D in cm^2/s ; H in cm^3 (STP)/ cm^3 -Pa; P_M in cm^3 (STP)- cm/cm^2 -s-Pa.

but is less accurate for glassy polymers, for which alternative theories have been proposed. Foremost is the dual-mode model first proposed by Barrer and co-workers [22–24] after a comprehensive study of sorption and diffusion in ethyl cellulose. In this model, sorption of penetrant occurs by ordinary dissolution in polymer chains, as described by Henry's law, and by Langmuir sorption into holes or sites between chains of glassy polymers. According to this theory, when downstream pressure is negligible compared to upstream pressure, the permeability for Fick's law is given by

$$P_{M_i} = H_i D_i + \frac{D_{L_i} a b}{1 + b P} \quad (14-35)$$

where the second term refers to Langmuir sorption, with D_{L_i} = diffusivity of Langmuir-sorbed species, P = penetrant pressure, and a and b = Langmuir constants for sorption-site capacity and site affinity, respectively.

Koros and Paul [25] found that the dual-mode theory accurately represents data for CO₂ sorption in polyethylene terephthalate below its glass-transition temperature of 85°C. Above that temperature, the rubbery polymer obeys Henry's law. Mechanisms of diffusion for the Langmuir mode have been suggested by Barrer [26].

An ideal dense-polymer membrane has a high permeance, P_{M_i}/l_M , for the penetrant molecules and a high separation factor between components. The separation factor is defined similarly to relative volatility in vapor–liquid equilibrium:

$$\alpha_{A,B} = \frac{(y_A/x_A)}{(y_B/x_B)} \quad (14-36)$$

where y_i is the mole fraction in the permeate leaving the membrane, corresponding to partial pressure p_{i_p} in Figure 14.7d, while x_i is the mole fraction in the retentate on the feed side of the membrane, corresponding to partial pressure p_{i_f} in Figure 14.7d. However, unlike vapor–liquid equilibrium, y_i and x_i are not in equilibrium.

For separation of a binary gas mixture of A and B in the absence of external boundary layer or film mass-transfer resistances, transport fluxes are given by (14-32):

$$N_A = \frac{H_A D_A}{l_M} (p_{A_f} - p_{A_p}) = \frac{H_A D_A}{l_M} (x_A P_F - y_A P_P) \quad (14-37)$$

$$N_B = \frac{H_B D_B}{l_M} (p_{B_f} - p_{B_p}) = \frac{H_B D_B}{l_M} (x_B P_F - y_B P_P) \quad (14-38)$$

When no sweep gas is used, the ratio of fluxes N_A to N_B fixes the permeate composition, which is simply the ratio of y_A to y_B in the permeate gas. Thus,

$$\frac{N_A}{N_B} = \frac{y_A}{y_B} = \frac{H_A D_A (x_A P_F - y_A P_P)}{H_B D_B (x_B P_F - y_B P_P)} \quad (14-39)$$

If the downstream (permeate) pressure, P_P , is negligible compared to the upstream pressure, P_F , such that $y_A P_P \ll x_A P_F$ and $y_B P_P \ll x_B P_F$, (14-39) can be rearranged and combined with (14-36) to give an **ideal separation factor**:

$$\alpha_{A,B}^* = \frac{H_A D_A}{H_B D_B} = \frac{P_{M_A}}{P_{M_B}} \quad (14-40)$$

Thus, a high separation factor results from a high solubility ratio, a high diffusivity ratio, or both. The separation factor depends on both transport phenomena and thermodynamic equilibria.

When the downstream pressure is not negligible, (14-39) can be rearranged to obtain an expression for $\alpha_{A,B}$ in terms of pressure ratio, $r = P_P / P_F$, and mole fraction of A on the retentate side of the membrane. Combining (14-36), (14-40), and the definition of r with (14-39):

$$\alpha_{A,B} = \alpha_{A,B}^* \left[\frac{(x_B/y_B) - r\alpha_{A,B}}{(x_B/y_B) - r} \right] \quad (14-41)$$

Because $y_A + y_B = 1$ for a binary mixture, it is possible to substitute into (14-41) for x_B , the identity:

$$x_B = x_B y_A + x_B y_B$$

to give
$$\alpha_{A,B} = \alpha_{A,B}^* \left[\frac{x_B \left(\frac{y_A}{y_B} + 1 \right) - r\alpha_{A,B}}{x_B \left(\frac{y_A}{y_B} + 1 \right) - r} \right] \quad (14-42)$$

Combining (14-36) and (14-42) and replacing x_B with $1 - x_A$, the separation factor becomes:

$$\alpha_{A,B} = \alpha_{A,B}^* \left[\frac{x_A (\alpha_{A,B} - 1) + 1 - r\alpha_{A,B}}{x_A (\alpha_{A,B} - 1) + 1 - r} \right] \quad (14-43)$$

Equation (14-43) is an implicit equation for $\alpha_{A,B}$ in terms of the pressure ratio, r , and, x_A , which is readily solved for $\alpha_{A,B}$ by rearranging the equation into a quadratic form. In the limit when $r = 0$, (14-43) reduces to (14-40), where $\alpha_{A,B} = \alpha_{A,B}^* = P_{M_A}^*/P_{M_B}^*$.

Many investigators report values of $\alpha_{A,B}^*$. Table 14.7, taken from the *Membrane Handbook* [6], gives data at 35°C for various binary pairs with polydimethyl siloxane (PDMS), a rubbery polymer, and bisphenol-A-polycarbonate (PC), a glassy polymer. For the rubbery polymer, permeabilities are high, but separation factors are low. The opposite is true for a glassy polymer. For a given feed composition, the separation factor places limits on the achievable degree of separation.

Table 14.7 Ideal Membrane-Separation Factors of Binary Pairs for Two Membrane Materials

	PDMS, Silicon Rubbery Polymer Membrane	PC, Polycarbonate Glassy Polymer Membrane
$P_{M_{He}}$, barrer	561	14
α_{He, CH_4}^*	0.41	50
$\alpha_{He, C_2H_4}^*$	0.15	33.7
$P_{M_{CO_2}}$, barrer	4,550	6.5
α_{CO_2, CH_4}^*	3.37	23.2
$\alpha_{CO_2, C_2H_4}^*$	1.19	14.6
$P_{M_{O_2}}$, barrer	933	1.48
α_{O_2, N_2}^*	2.12	5.12

EXAMPLE 14.5 Air Separation by Gas Permeation

Air can be separated by gas permeation with dense-polymer membranes. In all cases, the membrane is more permeable to oxygen. A total of 20,000 scfm of air is compressed, cooled, and treated to remove moisture and compressor oil prior to being sent to a membrane separator at 150 psia and 78°F. Assume the air composition is 79 mol% N₂ and 21 mol% O₂. A low-density, thin-film composite polyethylene membrane with solubilities and diffusivities given in Table 14.6 is being considered.

If the membrane skin is 0.2 μm thick, calculate the material balance and membrane area, A_M , in ft² as a function of the cut, which is defined as

$$\theta = \text{cut} = \text{fraction of feed permeated} = \frac{n_P}{n_F} \quad (14-44)$$

where n = flow rate in lbmol/h and subscripts F and P refer, respectively, to feed and permeate. Assume 15 psia on the permeate side with perfect mixing on both sides of the membrane, such that compositions on both sides are uniform and equal to entering and exit compositions, respectively. Neglect pressure drop and mass-transfer resistances external to the membrane. Comment on the practicality of the membrane for making a reasonable separation.

Solution

Assume that standard conditions are 0°C and 1 atm (359 ft³/lbmol).

$$n_F = \text{Feed flow rate} = \frac{20,000}{359}(60) = 3,343 \text{ lbmol/h}$$

For the low-density polyethylene membrane, from Table 14.6, applying (14-33), and letting A = O₂ and B = N₂:

$$\begin{aligned} P_{M_B} &= H_B D_B = (0.228 \times 10^{-6})(0.32 \times 10^{-6}) \\ &= 0.073 \times 10^{-12} \text{ cm}^3 \text{ (STP)-cm/cm}^2 \text{-s-Pa} \end{aligned}$$

or, in AE units,

$$\begin{aligned} P_{M_B} &= \frac{(0.073 \times 10^{-12})(2.54 \times 12)(3600)(101,300)}{(22,400)(454)(14.7)} \\ &= 5.43 \times 10^{-12} \frac{\text{lbmol-ft}}{\text{ft}^2 \text{-h-psia}} \end{aligned}$$

Similarly, for oxygen:

$$P_{M_A} = 16.2 \times 10^{-12} \frac{\text{lbmol-ft}}{\text{ft}^2 \text{-h-psia}}$$

Permeance values are based on a 0.2 -μm (or 0.66 × 10⁻⁶ ft)-thick membrane skin.

From (14-1),

$$\bar{P}_{M_i} = P_M / l_M$$

$$\begin{aligned} \bar{P}_{M_B} &= 5.43 \times 10^{-12} / 0.66 \times 10^{-6} \\ &= 8.23 \times 10^{-6} \text{ lbmol/ft}^2 \text{-h-psia} \end{aligned}$$

$$\begin{aligned} \bar{P}_{M_A} &= 16.2 \times 10^{-12} / 0.66 \times 10^{-6} \\ &= 24.55 \times 10^{-6} \text{ lbmol/ft}^2 \text{-h-psia} \end{aligned}$$

Material-balance equations:

$$\text{For } N_2, \quad x_{F_B} n_F = y_{P_B} n_P + x_{R_B} n_R \quad (1)$$

where n = flow rate in lbmol/h and subscripts F , P , and R refer, respectively, to the feed, permeate, and retentate. Since $\theta = \text{cut} = n_P/n_F$, $(1 - \theta) = n_R/n_F$.

Note that if all components of the feed have a finite permeability. The cut, θ , can vary from 0 to 1. For a cut of 1, all of the feed becomes permeate and no separation is achieved. Substituting (14-44) into (1) gives

$$x_{R_B} = \frac{x_{F_B} - y_{P_B} \theta}{1 - \theta} = \frac{0.79 - y_{P_B} \theta}{1 - \theta} \quad (2)$$

Similarly, for O_2 ,

$$x_{R_A} = \frac{0.21 - y_{P_A} \theta}{1 - \theta} \quad (3)$$

Separation factor:

From the definition of the separation factor, (14-36), with well-mixed fluids, compositions are those of the retentate and permeate,

$$\alpha_{A,B} = \frac{y_{P_A}/x_{R_A}}{(1 - y_{P_A})/(1 - x_{R_A})} \quad (4)$$

Transport equations:

The transport of A and B through a membrane of area A_M , with partial pressures at exit conditions, can be written as

$$N_B = y_{P_B} n_P = A_M \bar{P}_{M_B} (x_{R_B} P_R - y_{P_B} P_P) \quad (5)$$

$$N_A = y_{P_A} n_P = A_M \bar{P}_{M_A} (x_{R_A} P_R - y_{P_A} P_P) \quad (6)$$

where A_M is the membrane area normal to flow, n_P , through the membrane. The ratio of (6) to (7) is y_{P_A}/y_{P_B} , and subsequent manipulations lead to (14-43),

where,

$$r = P_P/P_R = 15/150 = 0.1 \text{ and } \alpha_{A,B}^* = \alpha_{O_2,N_2} = \bar{P}_{M_{O_2}}/\bar{P}_{M_{N_2}} \\ = (24.55 \times 10^{-6})/(8.23 \times 10^{-6}) = 2.98$$

From (14-43):

$$\alpha_{A,B} = \alpha = 2.98 \left[\frac{x_{R_A} (\alpha - 1) + 1 - 0.1\alpha}{x_{R_A} (\alpha - 1) + 1 - 0.1} \right] \quad (7)$$

Equations (3), (4), and (7) contain four unknowns: x_{R_A} , y_{P_A} , θ , and $\alpha_{A,B} = \alpha$. The variable θ is bounded between 0 and 1, so values of θ are selected in that range. The other three variables are computed in the following manner. Combine (3), (4), and (7) to eliminate α and x_{R_A} . Solve the resulting nonlinear equation for y_{P_A} . Then solve (3) for x_{R_A} and (4) for α . Solve (6) for the membrane area, A_M . The following results are obtained:

θ	x_{R_A}	y_{P_A}	$\alpha_{A,B}$	A_M, ft^2
0.01	0.208	0.406	2.602	22,000
0.2	0.174	0.353	2.587	462,000
0.4	0.146	0.306	2.574	961,000
0.6	0.124	0.267	2.563	1,488,000
0.8	0.108	0.236	2.555	2,035,000
0.99	0.095	0.211	2.548	2,567,000

Note that the separation factor remains almost constant, varying by only 2%, with a value of about 86% of the ideal. The maximum permeate O_2 content (40.6 mol%) occurs with the smallest amount of permeate ($\theta = 0.01$). The maximum N_2 retentate content (90.5 mol%) occurs with the largest amount of permeate ($\theta = 0.99$). With a retentate equal to 60 mol% of the feed ($\theta = 0.4$), the N_2 retentate content has increased only from 79 to 85.4 mol%. Furthermore, the membrane area requirements are very large. The low-density polyethylene membrane is not a practical membrane for this separation. To achieve a reasonable separation, say, with $\theta = 0.6$ and a retentate of 95 mol% N_2 , it is necessary to use a membrane with an ideal separation factor of 5 and a higher O_2 permeance. For higher purities, a cascade of two or more stages is needed. These alternatives are developed in the next two subsections.

§14.3.3 Module Flow Patterns

In Example 14.5, perfect mixing, as shown in Figure 14.8a, was assumed. The three other idealized flow patterns shown, which have no mixing, have received considerable attention and are comparable to the idealized flow patterns used to design heat exchangers. These patterns are (b) countercurrent flow; (c) cocurrent flow; and (d) crossflow. For a given cut, θ , (14-44), the flow pattern can significantly affect the degree of separation and the membrane area. For flow patterns (b) to (d), fluid on the feed or retentate side of the membrane flows along and parallel to the upstream side of the membrane. For countercurrent and cocurrent flow, permeate fluid at a given location on the downstream side of the membrane consists of fluid that has just passed through the membrane at that location plus the permeate fluid flowing to that location. For crossflow, there is no flow of permeate fluid along the membrane surface. The permeate fluid that has just passed through the membrane at a given location is the only fluid there.

For a given module geometry, it is not obvious which idealized flow pattern to assume. This is particularly true for the spiral-wound module of Figure 14.5b. If the permeation rate is high, the fluid issuing from the downstream side of the membrane may continue to flow perpendicularly to the membrane surface until it finally mixes with bulk permeate fluid. In that case, the idealized crossflow pattern might be appropriate. Hollow-fiber modules are designed to approximate idealized countercurrent, cocurrent, or crossflow patterns. The hollow-fiber module in Figure 14.5d is approximated by a countercurrent-flow pattern.

Walawender and Stern [27] present methods for solving all four flow patterns of Figure 14.8, under assumptions of a binary feed of components A and B, with constant-pressure ratio, r , and constant ideal separation factor, $\alpha_{A,B}^*$. Exact analytical solutions are possible for perfect mixing (as in Example 14.5) and for crossflow; numerical solutions are necessary for countercurrent and cocurrent flow. A reasonably simple, but approximate, analytical solution for the crossflow case, derived by Naylor and Backer [28], is presented here.

Consider a module with the crossflow pattern shown in Figure 14.9, where subscript i refers to either component A or B. Feed passes across the upstream membrane surface in

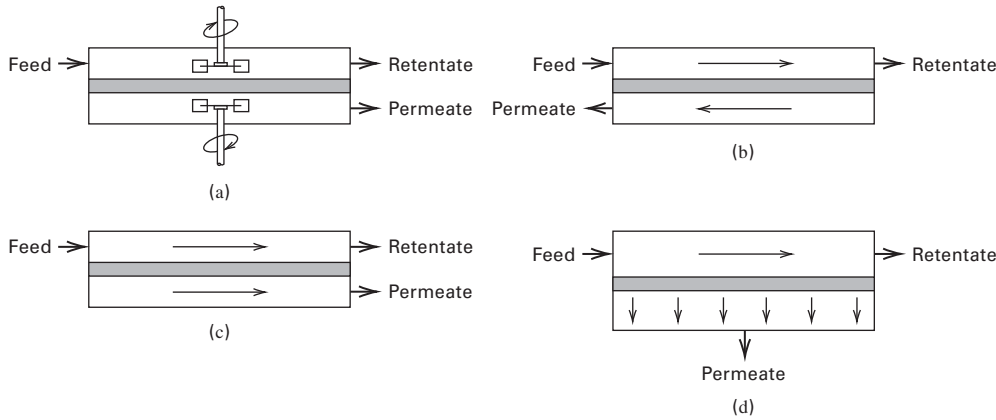


Figure 14.8 Idealized flow patterns in membrane modules: (a) perfect mixing; (b) countercurrent flow; (c) cocurrent flow; (d) crossflow.

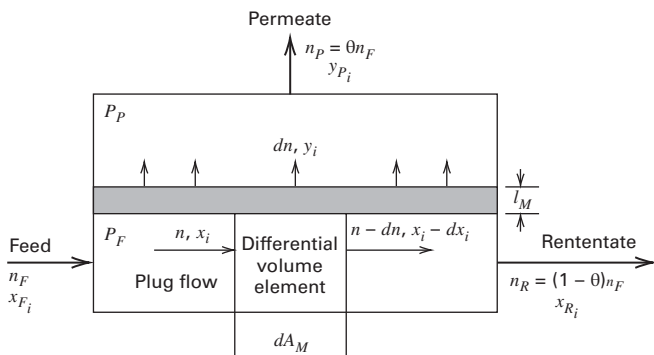


Figure 14.9 Crossflow model for membrane module.

plug flow with no longitudinal mixing. The pressure ratio, $r = P_P/P_F$, and the ideal separation factor, $\alpha_{A,B}^*$, are assumed constant. Boundary-layer or film mass-transfer resistances external to both sides of the membrane are assumed negligible. At the differential element, local mole fractions in the retentate and permeate are x_i and y_i , and the penetrant molar flux is dn/dA_M . Also, the local separation factor is given by (14-43) in terms of the local x_A , r , and $\alpha_{A,B}^*$. An alternative expression for the local permeate composition in terms of y_A , x_A , and r is obtained by combining (14-36) and (14-41):

$$\frac{y_A}{1 - y_A} = \alpha_{A,B}^* \left[\frac{x_A - r y_A}{(1 - x_A) - r(1 - y_A)} \right] \quad (14-45)$$

A material balance for A around the differential-volume element gives

$$y_A dn = d(n x_A) = x_A dn + n dx_A \quad \text{or} \quad \frac{dn}{n} = \frac{dx_A}{y_A - x_A} \quad (14-46)$$

which is identical in form to the Rayleigh equation (13-2) for batch differential distillation. If (14-36) is combined with (14-46) to eliminate y_A ,

$$\frac{dn}{n} = \left[\frac{1 + (\alpha - 1)x_A}{x_A(\alpha - 1)(1 - x_A)} \right] dx_A \quad (14-47)$$

where $\alpha = \alpha_{A,B}$. In Figure 14.9, subscript A in x_A and y_A is replaced by subscript i , e.g., x_i and y_i .

In the solution to Example 14.5, it was noted that $\alpha = \alpha_{A,B}$ is relatively constant over the entire range of cut, θ . Such is generally the case when the pressure ratio, r , is small. If the assumption of constant $\alpha = \alpha_{A,B}$ is made in (14-47) and integration is from the intermediate location of the differential element to the final retentate, that is, from n to n_R and from x_A to x_{R_A} , the result is

$$n = n_R \left[\left(\frac{x_A}{x_{R_A}} \right)^{\left(\frac{1}{\alpha-1} \right)} \left(\frac{1 - x_{R_A}}{1 - x_A} \right)^{\left(\frac{1}{\alpha-1} \right)} \right] \quad (14-48)$$

The mole fraction of A in the final permeate and the total membrane surface area are obtained by integrating the values obtained from solving (14-45) to (14-47):

$$y_{P_A} = \int_{x_{F_A}}^{x_{R_A}} y_A dn / \theta n_F \quad (14-49)$$

By combining (14-49) with (14-47), (14-48), and the definition of α , the integral in n can be transformed to an integral in x_A , which when integrated gives

$$y_{P_A} = x_{R_A}^{\left(\frac{1}{1-\alpha} \right)} \left(\frac{1 - \theta}{\theta} \right) \times \left[(1 - x_{R_A})^{\left(\frac{\alpha}{\alpha-1} \right)} \left(\frac{x_{F_A}}{1 - x_{F_A}} \right)^{\left(\frac{\alpha}{\alpha-1} \right)} - x_{R_A}^{\left(\frac{\alpha}{1-\alpha} \right)} \right] \quad (14-50)$$

where $\alpha = \alpha_{A,B}$ can be estimated from (14-43) by using $x_A = x_{F_A}$.

The differential rate of mass transfer of A across the membrane is given by

$$y_A dn = \frac{P_{M_A} dA_M}{l_M} [x_A P_F - y_A P_P] \quad (14-51)$$

from which the total membrane surface area can be obtained by integration:

$$A_M = \int_{x_{R_A}}^{x_{F_A}} \frac{l_M y_A dn}{P_{M_A} (x_A P_F - y_A P_P)} \quad (14-52)$$

Application of the crossflow model is illustrated in the next example.

EXAMPLE 14.6 Gas Permeation in a Crossflow Module.

For the conditions of Example 14.5, compute exit compositions for a spiral-wound module that approximates crossflow.

Solution

From Example 14.5: $\alpha_{A,B}^* = 2.98$; $r = 0.1$; $x_{F_A} = 0.21$

From (14-43), using $x_A = x_{F_A}$, $\alpha_{A,B} = \alpha = 2.60$

An overall module material balance for O₂ (A) gives

$$x_{F_A} n_F = x_{R_A} (1 - \theta) n_F + y_{P_A} \theta n_F \quad \text{or} \quad x_{R_A} = \frac{(x_{F_A} - y_{P_A} \theta)}{(1 - \theta)} \quad (1)$$

Solving (1) and (14-50) simultaneously with MATLAB gives the following results:

θ	x_{R_A}	y_{P_A}	Stage α_S
0.01	0.208	0.407	2.61
0.2	0.168	0.378	3.01
0.4	0.122	0.342	3.74
0.6	0.0733	0.301	5.44
0.8	0.0274	0.256	12.2
0.99	0.000241	0.212	1,120

Comparing these results to those of Example 14.5, it is seen that for crossflow, the permeate is richer in O₂ and the retentate is richer in N₂. Thus, for a given cut, θ , crossflow is more efficient than perfect mixing, as might be expected.

Included in the preceding table is the calculated degree of separation for the stage, α_S , defined on the basis of the mole fractions in the permeate and retentate exiting the stage by

$$(\alpha_{A,B})_S = \alpha_S = \frac{(y_{P_A}/x_{R_A})}{(1 - y_{P_A})/(1 - x_{R_A})} \quad (2)$$

The ideal separation factor, $\alpha_{A,B}^*$, is 2.98. Also, if (2) is applied to the perfect mixing case of Example 14.5, α_S is 2.603 for $\theta = 0.01$ and decreases slowly with increasing θ until at $\theta = 0.99$, $\alpha_S = 2.548$. Thus, for perfect mixing, $\alpha_S < \alpha^*$ for all θ . Such is not the case for crossflow. In the above table, $\alpha_S < \alpha^*$ for $\theta > 0.2$, and α_S increases with increasing θ . For $\theta = 0.6$, α_S is almost twice α^* .

Calculating the degree of separation of a binary mixture in a membrane module utilizing cocurrent- or countercurrent-flow patterns involves numerical solution of ODEs. These and computer codes for their solution are given by Walawender and Stern [27]. A representative solution is shown in Figure 14.10 for the separation of air (20.9 mol% O₂) for conditions of $\alpha^* = 5$ and $r = 0.2$. For a given cut, θ , it is seen that the best separation is with countercurrent flow. The curve for cocurrent flow lies between crossflow and perfect mixing. The computed crossflow case is a conservative estimate of membrane module performance. Stern et al. [29] extend the perfect mixing case for binary mixtures to multicomponent

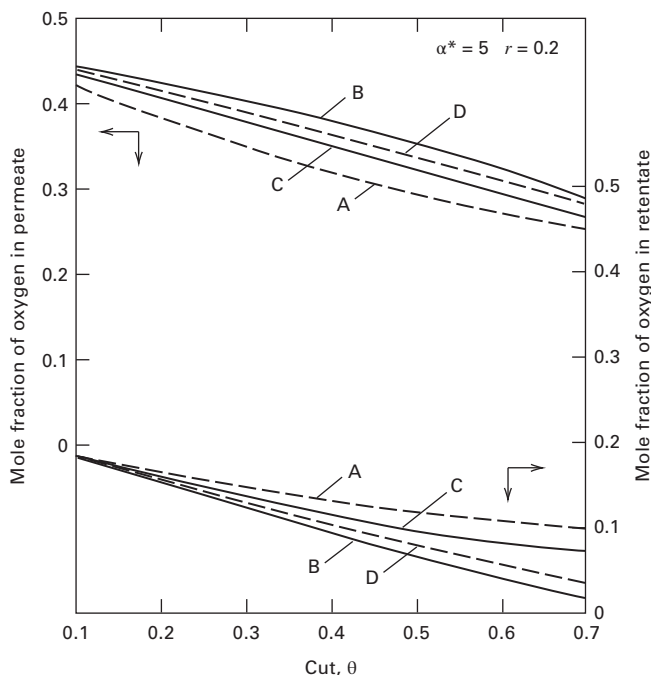


Figure 14.10 Effect of membrane module flow pattern on degree of separation of air. A, perfect mixing; B, countercurrent flow; C, cocurrent flow; D, crossflow.

mixtures. As with crossflow, countercurrent flow also offers the possibility of a separation factor for the stage, α_S , defined by (2) in Example 14.6, that is considerably greater than α^* .

§14.3.4 Cascades

A single membrane module or a number of such modules arranged in parallel or in series constitutes a single-stage membrane-separation process. The extent to which a feed mixture can be separated in a single stage is limited and determined by the separation factor, α . This factor depends, in turn, on module flow patterns; permeability ratio (ideal separation factor); cut, θ ; and the driving force for membrane mass transfer. To achieve a higher degree of separation than is possible with a single stage, a countercurrent cascade of membrane stages—such as used in distillation, absorption, stripping, and liquid–liquid extraction—or a hybrid process that couples a membrane separator with another type of separator must be devised. Membrane cascades, presented briefly in §5.4, are discussed next and illustrated with an example.

A countercurrent recycle cascade of membrane separators, similar to a distillation column, is depicted in Figure 14.11a. The feed enters at stage F, somewhere near the middle of the cascade. Permeate is enriched in components of high permeability in an enriching section, while the retentate is enriched in components of low permeability in a stripping section. The final permeate is withdrawn from stage 1, while the final retentate is withdrawn from stage N. For a cascade, additional factors that affect the degree of separation are number of stages and recycle ratio (permeate recycle rate/permeate product rate). As discussed by Hwang and Kammermeyer

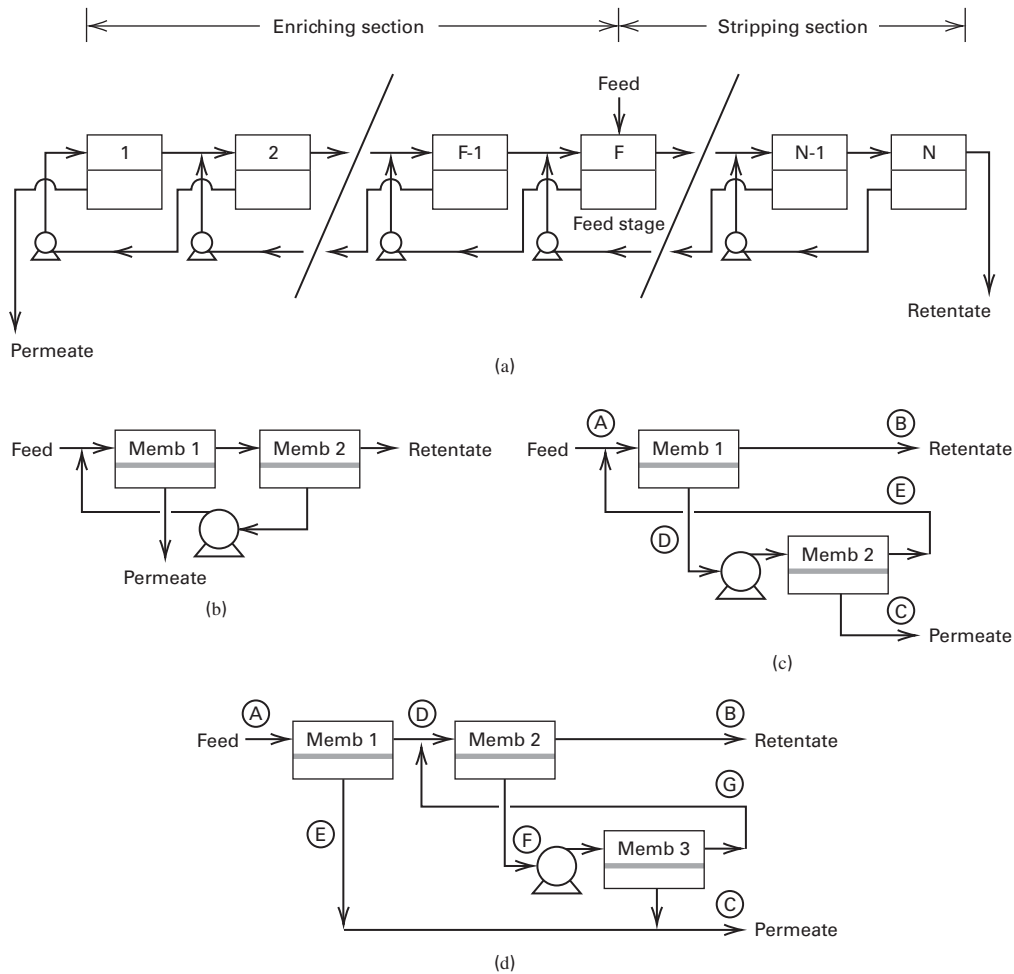


Figure 14.11 Countercurrent recycle cascades of membrane separators: (a) multiple-stage unit; (b) two-stage stripping cascade; (c) two-stage enriching cascade; (d) two-stage enriching cascade with additional pre-membrane stage.

[30], it is best to manipulate the cut and reflux rate at each stage so as to force compositions of the two streams entering each stage to be identical. For example, the composition of retentate leaving stage 1 and entering stage 2 would be identical to the composition of permeate flowing from stage 3 to stage 2. This corresponds to the least amount of entropy production for the cascade and, thus, the highest second-law efficiency. Such a cascade is referred to as “ideal.”

Calculation methods for cascades, as discussed by Hwang and Kammermeyer [30], utilize single-stage methods that depend upon the module flow pattern, as described in the previous section. The calculations are best carried out on a computer, but results for a binary mixture can be conveniently displayed on a McCabe–Thiele-type diagram of the type used for distillation in Chapter 7. For a membrane cascade, the component mole fraction in the permeate leaving each stage, y_i , is plotted against the mole fraction in the retentate leaving each stage, x_i . For a membrane cascade, the equilibrium curve becomes the selectivity curve in terms of the stage separation factor, α_S .

In Figure 14.11, it is assumed that pressure drop on the feed or upstream side of the membrane is negligible. Thus, only the permeate must be pumped to the next stage if a liquid, or

compressed if a gas. In the case of gas, compression costs are high. Thus, membrane cascades for gas permeation are often limited to just two or three stages, with the most common configurations shown in Figures 14.11b, c, and d.

Compared to one stage, the two-stage stripping cascade is designed to obtain a purer retentate, whereas a purer permeate is the goal of the two-stage enriching cascade. Addition of a pre-membrane stage, as shown in Figure 14.11d, may be attractive when feed concentration is low in the component to be passed preferentially through the membrane, desired permeate purity is high, separation factor is low, and/or a high recovery of the more permeable component is desired. Spillman [31] gives an example of the application of enrichment cascades for the removal of carbon dioxide from natural gas (simulated by methane) using cellulose-acetate membranes in spiral-wound modules that approximate cross-flow. The ideal separation factor, $\alpha_{\text{CO}_2, \text{CH}_4}^*$, is 21. Results of the calculations are given in Table 14.8 for a single stage (not shown in Figure 14.11), a two-stage enriching cascade (Figure 14.11c), and a two-stage enriching cascade with an additional pre-membrane stage (Figure 14.11d). Carbon dioxide flows through the membrane faster than methane. In all three cases, the feed is 20 million (MM) scfd of 7 mol%

Table 14.8 Separation of CO₂ and CH₄ with Membrane Cascades

Case 1: Single Membrane Stage:

	Stream		
	A Feed	B Retentate	C Permeate
Composition (mole%)			
CH ₄	93.0	98.0	63.4
CO ₂	7.0	2.0	36.6
Flow rate (million SCFD)	20.00	17.11	2.89
Pressure (psig)	850	835	10

Case 2: Two-Stage Enriching Cascade (Figure 14.1):

	Stream				
	A	B	C	D	E
Composition (mole%)					
CH ₄	93.0	98.0	18.9	63.4	93.0
CO ₂	7.0	2.0	81.0	36.6	7.0
Flow rate (million SCFD)	20.0	18.74	1.26	3.16	1.90
Pressure (psig)	850	835	10	10	850

Case 3: Two-Stage Enriching Cascade with Premembrane Stage (Figure 14.11d):

	Stream						
	A	B	C	D	E	F	G
Composition (mole%)							
CH ₄	93.0	98.0	49.2	96.1	56.1	72.1	93.0
CO ₂	7.0	2.0	50.8	3.9	43.9	27.9	7.0
Flow rate (million SCFD)	20.0	17.95	2.05	19.39	1.62	1.44	1.01
Pressure (psig)	850	835	10	840	10	10	850

CO₂ in methane at 850 psig (865 psia) and the retentate is 98 mol% methane. For each stage, the downstream (permeate-side) membrane pressure is 10 psig (25 psia). In Table 14.8, for all three cases, stream A is the feed, stream B is the final retentate, and stream C is the final permeate. Case 1 achieves a 90.2% recovery of methane. Case 2 increases that recovery to 98.7%. Case 3 achieves an intermediate recovery of 94.6%.

The following degrees of separation are computed from data given in Table 14.8:

Case	α_S for Membrane Stage		
	1	2	3
1	28	—	—
2	28	57	—
3	20	19	44

It is also possible to compute overall degrees of separation for the cascades, α_C , for cases 2 and 3, giving values of 210 and 51, respectively.

§14.3.5 External Mass-Transfer Resistances

Thus far, resistances to mass transfer on both sides of the membrane have been neglected. Thus, concentrations in the fluid at the upstream and downstream faces of the membrane

have been assumed equal to the respective bulk-fluid concentrations. When mass-transfer resistances external to the membrane are not negligible, gradients exist in the boundary layers adjacent to the membrane surfaces, as is illustrated for four cases in Figure 14.7. For given bulk-fluid concentrations, the presence of these resistances reduces the driving force for mass transfer and penetrant flux through the membrane.

Gas permeation by solution-diffusion (14-31) is slow compared to diffusion in gas boundary layers, so external mass-transfer resistances are negligible and $P_{i_F} = P_{i_0}$ and $P_{i_P} = P_{i_L}$ in Figure 14.7d. Because diffusion in liquid boundary layers is slow, concentration polarization, which is the accumulation of non-permeable species on the upstream surface of the membrane, cannot be neglected in membrane processes that involve liquids, such as dialysis, reverse osmosis, and pervaporation. Concentration polarization is of particular importance in reverse osmosis, where the effect can reduce the water flux and increase the salt flux, making it more difficult to obtain potable water.

Consider the membrane process in Figure 14.7a, involving liquids with a porous membrane. At steady state, the rate of mass transfer of a penetrating species, i , through the three resistances, assuming no change in area for mass transfer across the membrane, is:

$$N_i = k_{i_F}(c_{i_F} - c_{i_0}) = \frac{D_{e_i}}{l_M}(c_{i_0} - c_{i_L}) = k_{i_P}(c_{i_L} - c_{i_P})$$

where D_{e_i} is given by (14-14). If these three equations are combined to eliminate the intermediate concentrations, c_{i_0} and c_{i_L} , the result is:

$$N_i = \frac{c_{i_F} - c_{i_P}}{\frac{1}{k_{i_F}} + \frac{l_M}{D_{e_i}} + \frac{1}{k_{i_P}}} \quad (14-53)$$

The membrane process in Figure 14.7b, involves liquids with a nonporous membrane, for which the solution-diffusion mechanism, (14-26), applies for mass transfer through the membrane. At steady state, for constant mass-transfer area, the rate of mass transfer through the three resistances is:

$$N_i = k_{i_F}(c_{i_F} - c'_{i_0}) = \frac{K_i D_i}{l_M}(c'_{i_0} - c'_{i_L}) = k_{i_P}(c'_{i_L} - c_{i_P})$$

If these three equations are combined to eliminate the intermediate primed concentrations,

$$N_i = \frac{c_{i_F} - c_{i_P}}{\frac{1}{k_{i_F}} + \frac{l_M}{K_i D_i} + \frac{1}{k_{i_P}}} \quad (14-54)$$

where in (14-53) and (14-54), k_{i_F} and k_{i_P} are mass-transfer coefficients for the feed-side and permeate-side boundary layers. The three terms in the RHS denominator are the resistances to the mass flux. Mass-transfer coefficients depend on fluid properties, flow-channel geometry, and flow regime. In the laminar-flow regime, a long entry region may exist where the mass-transfer coefficient decreases with distance, L , from the entry of the membrane channel. Estimation of coefficients is complicated because of fluid velocities that change due to mass exchange between the two fluids. In (14-53) and (14-54), the membrane resistances, l_M/D_{e_i} and $l_M/K_i D_i$, respectively, can be replaced by l_M/P_{M_i} or \bar{P}_{M_i} .

Mass-transfer coefficients for channel flow can be obtained from the general empirical film-model correlation [32] for the Sherwood number:

$$N_{Sh} = k_i d_H / D_i = a N_{Re}^b N_{Sc}^{0.33} (d_H / L)^d \quad (14-55)$$

where $N_{Re} = d_H v \rho / \mu$, $N_{Sc} = \mu / \rho D_i$, d_H = hydraulic diameter, v = velocity, and L = length of the channel.

Expressions for d_H and values for constants a , b , and d are as follows:

Flow Regime	Flow Channel Geometry	d_H	a	b	d
Turbulent, ($N_{Re} > 10,000$)	Circular tube	D	0.023	0.8	0
	Rectangular channel	$2hw/(h+w)$	0.023	0.8	0
Laminar, ($N_{Re} < 2,100$)	Circular tube	D	1.86	0.33	0.33
	Rectangular channel	$2hw/(h+w)$	1.62	0.33	0.33

where w = width of channel, h = height of channel, L = length of channel, and D = inside diameter of channel.

EXAMPLE 14.7 Solute Flux Through a Membrane.

A dilute solution of solute A in solvent B is passed through a tubular-membrane separator, where the feed flows through the tubes. At a certain location, bulk solute concentrations on the feed and permeate sides are 5.0×10^{-2} kmol/m³ and 1.5×10^{-2} kmol/m³, respectively. The membrane vendor gives the permeance of the membrane for solute A as 7.3×10^{-5} m/s. If the tube-side Reynolds number is 15,000, the feed-side solute Schmidt number is 500, the diffusivity of the feed-side solute is 6.5×10^{-5} cm²/s, and the inside diameter of the tube is 0.5 cm, estimate the solute flux through the membrane if the mass-transfer resistance on the permeate side of the membrane is negligible.

Solution

Flux of the solute from the permeance form of (14-53) or (14-54):

$$N_A = \frac{c_{A_F} - c_{A_P}}{\frac{1}{k_{A_F}} + \frac{1}{\bar{P}_{M_A}} + 0}$$

$$c_{A_F} - c_{A_P} = 5 \times 10^{-2} - 1.5 \times 10^{-2} = 3.5 \times 10^{-2} \text{ kmol/m}^3 \quad (1)$$

$$\bar{P}_{M_A} = 7.3 \times 10^{-5} \text{ m/s}$$

From (14-55), for turbulent flow in a tube, since $N_{Re} > 10,000$:

$$\begin{aligned} k_{A_F} &= 0.023 \frac{D_A}{D} N_{Re}^{0.8} N_{Sc}^{0.33} \\ &= 0.023 \left(\frac{6.5 \times 10^{-5}}{0.5} \right) (15,000)^{0.8} (500)^{0.33} \\ &= 0.051 \text{ cm/s or } 5.1 \times 10^{-4} \text{ m/s} \end{aligned}$$

From (1),

$$N_A = \frac{3.5 \times 10^{-2}}{\frac{1}{5.1 \times 10^{-4}} + \frac{1}{7.3 \times 10^{-5}}} = 2.24 \times 10^{-6} \text{ kmol/s-m}^2$$

The fraction of the total resistance due to the membrane is

$$\frac{\frac{1}{7.3 \times 10^{-5}}}{\frac{1}{5.1 \times 10^{-4}} + \frac{1}{7.3 \times 10^{-5}}} = 0.875 \text{ or } 87.5\%$$

§14.3.6 Concentration Polarization and Fouling

Gases produced during electrolysis accumulate on and around the electrodes of the electrolytic cell, reducing the flow of electric current. This is referred to as polarization. A similar phenomenon, **concentration polarization**, occurs in membrane separators when the membrane is permeable to A, but relatively impermeable to B. Thus, molecules of B are carried by bulk flow to the upstream surface of the membrane, where they accumulate, causing their concentration at the surface of the membrane to increase in a **polarization layer**. The equilibrium concentration of B in this layer is reached when its back-diffusion to the bulk fluid on the feed-retentate side equals its bulk flow toward the membrane.

Concentration polarization is most common in pressure-driven membrane separations involving liquid mixtures, such as reverse osmosis and ultrafiltration, where it reduces the flux of A. The polarization effect can be serious if the concentration of B reaches its solubility limit on the membrane surface. Then, a precipitate of gel may form, causing fouling on the membrane surface or within membrane pores, resulting in a further reduction in the flux of A. Concentration polarization and fouling are most severe at high fluxes of A. Theory and an example of concentration polarization and fouling is given in §14.6 on reverse osmosis. The subject is covered in detail by Baker [5].

§14.4 DIALYSIS

In the dialysis process in Figure 14.12, the feed is liquid at pressure P_1 and contains solvent, solutes of type A, and solutes of type B and insoluble, but dispersed, colloidal matter. A sweep liquid or wash of the same solvent is fed at pressure P_2 to the other side of the membrane. The membrane is thin, with micropores of a size such that solutes of type A can pass through by a concentration-driving force. Solute of type B are larger in molecular size than those of type A and pass through the membrane only with difficulty or not at all. Colloids do not pass through the membrane. This transport of solutes through the membrane is called dialysis. With pressure the solvent may also pass through the membrane, but by a concentration driving force acting in the opposite direction. The transport of the solvent is called osmosis, which is discussed in §14.6. Solvent osmosis can be reduced or eliminated if $P_1 - P_2$ is higher than the osmotic pressure. The products of a dialysis unit (dialyzer) are a liquid **diffusate** (permeate) containing solvent, solutes of type A, and little or none of type B solutes; and a **dialysate** (retentate) of solvent, type B solutes, remaining type A solutes, and colloidal matter. Ideally, the dialysis unit would enable a perfect separation

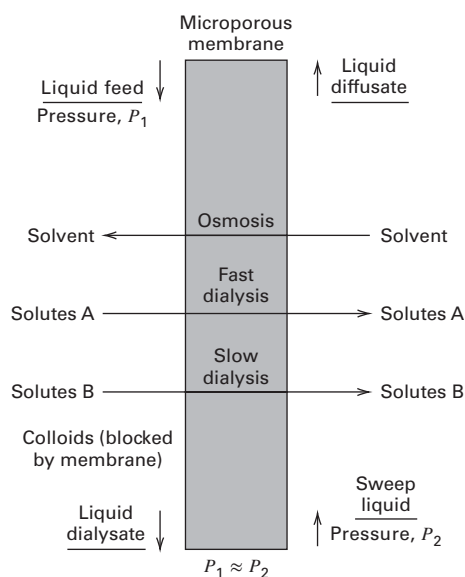


Figure 14.12 Dialysis.

between solutes of type A and solutes of type B and any colloidal matter. However, at best only a fraction of solutes of type A are recovered in the diffusate, even when solutes of type B do not pass through the membrane.

For example, when dialysis is used to recover sulfuric acid (type A solute) from an aqueous stream containing sulfate salts (type B solutes), the results obtained by Chamberlin and Vromen [33] are:

	Streams in		Streams out	
	Feed	Wash	Dialysate	Diffusate
Flow rate, gph	400	400	420	380
H ₂ SO ₄ , g/L	350	0	125	235
CuSO ₄ , g/L as Cu	30	0	26	2
NiSO ₄ , g/L as Ni	45	0	43	0

Thus, about 64% of the H₂SO₄ is recovered in the diffusate, accompanied by only 6% of the CuSO₄, and no NiSO₄.

Dialysis is closely related to other membrane processes that use other driving forces for separating liquid mixtures, including (1) reverse osmosis, which depends upon a transmembrane pressure difference for solute and/or solvent transport; (2) electrodialysis and electro-osmosis, which depend upon a transmembrane electrical-potential difference for solute and solvent transport, respectively; and (3) thermal osmosis, which depends upon a transmembrane temperature difference for solute and solvent transport.

Dialysis is attractive when concentration differences for the diffusing solutes of interest are large and permeability differences between those solutes and the other solute(s) and/or colloids are large. Although dialysis has been known since the work of Graham in 1861 [34], commercial applications of dialysis do not rival reverse osmosis and gas permeation. Nevertheless, dialysis has been used in separations, including (1) recovery of sodium hydroxide from a 17–20 wt% caustic viscose liquor contaminated with hemicellulose to produce a diffusate of 9–10 wt% caustic; (2) recovery of chromic, hydrochloric, and hydrofluoric acids from contaminating metal ions; (3) recovery of sulfuric acid from aqueous solutions containing nickel sulfate; (4) removal of alcohol from beer to produce a low-alcohol beer (near beer); (5) recovery of nitric and hydrofluoric acids from spent stainless steel pickle liquor; (6) removal of mineral acids from organic compounds; (7) removal of low-molecular-weight contaminants from polymers; and (8) purification of pharmaceuticals. Also of great importance is **hemodialysis**, in which urea, creatinine, uric acid, phosphates, and chlorides are removed from blood, without removing essential higher-molecular weight compounds and blood cells, in a device called an artificial kidney.

Microporous-membrane materials used in dialysis are usually hydrophilic and include cellulose, cellulose acetate, various acid-resistant polyvinyl copolymers, polysulfones, and polymethylmethacrylate. Typically they are less than 50 μm thick with pore diameters of 15 to 100Å. The most



Figure 14.13 Artificial kidney.
[Reproduced with permission of J.D. Seader.]

common membrane modules are plate-and-frame devices and hollow-fiber cartridges. Compact hollow-fiber **hemodialyzers**, such as the one shown in Figure 14.13, contain several thousand 200- μm -diameter fibers with a wall thickness of 20–30 μm and a length of 10–30 cm. Dialysis membranes can be thin because pressures on either side of the membrane are essentially equal. The differential rate of solute mass transfer across the membrane is

$$\boxed{dn_i = K_i(c_{i_F} - c_{i_P})dA_M} \quad (14-56)$$

where K_i is the overall mass-transfer coefficient, in terms of the three coefficients from the permeability form of (14-53):

$$\boxed{\frac{1}{K_i} = \frac{1}{k_{i_F}} + \frac{l_M}{P_{M_i}} + \frac{1}{k_{i_P}}} \quad (14-57)$$

Membrane area is determined by integrating (14-56), taking into account module flow patterns, bulk-concentration gradients, and individual mass-transfer coefficients in (14-57).

One of the oldest membrane materials used with aqueous solutions is porous cellophane, for which solute permeability is given by (14-14) with $P_{M_i} = D_{e_i}$ and $\bar{P}_{M_i} l_M$. If immersed, cellophane swells to about twice its dry thickness. The wet thickness should be used for l_M . Typical values of parameters in (14-13) to (14-15) for commercial cellophane are: wet thickness = $l_M = 0.004$ to 0.008 cm; porosity = $\varepsilon = 0.45$ to 0.60 ; tortuosity = $\tau = 3$ to 5 ; and pore diameter = $D = 30$ to 50 \AA .

If a solute does not interact with the membrane material, diffusivity, D_{e_i} in (14-14) is the ordinary molecular-diffusion coefficient, which depends only on solute and solvent properties and membrane porosity and tortuosity. In practice, the membrane may have another profound effect on solute diffusivity if membrane–solute interactions such as covalent, ionic, and hydrogen bonding; physical adsorption and chemisorption; and increases in membrane polymer flexibility occur. It is best to measure \bar{P}_{M_i} experimentally using process fluids.

Although transport of solvents, such as water, in a direction opposite to the solute can be described in terms of Fick's law, it is common to measure the solvent flux and report a so-called **water-transport number**, which is the ratio of the water flux to the solute flux, with a negative value indicating transport of solvent in the solute direction. The membrane can also interact with solvent and curtail solvent transport. Ideally, the water-transport number should be a small value, less than +1.0. Design parameters for dialyzers are best measured in

the laboratory using a batch cell with a variable-speed stirring mechanism on both sides of the membrane so that external mass-transfer resistances, $1/k_{i_F}$ and $1/k_{i_P}$ in (14-57), become negligible. Stirrer speeds $>2,000$ rpm may be required to minimize mass-transfer resistance and concentration polarization.

A common dialyzer is the plate-and-frame type of Figure 14.5a. For dialysis, the frames are vertical and a unit might contain 100 square frames, each $0.75 \text{ m} \times 0.75 \text{ m}$ on 0.6-cm spacing, equivalent to 56 m^2 of membrane surface. A typical dialysis rate for sulfuric acid is 5 lb/day-ft^2 . Recent dialysis units utilize hollow fibers of 200- μm inside diameter, 16- μm wall thickness, and 28-cm length, packed into a heat exchanger-like module to give 22.5 m^2 of membrane area in a volume that might be one-tenth of the volume of an equivalent plate-and-frame unit.

In a plate-and-frame dialyzer, the flow pattern is nearly countercurrent. Because total flow rates change little and solute concentrations are small, it is common to estimate solute transport rate by assuming a constant overall mass-transfer coefficient with a log-mean concentration-driving force. Thus, from (14-56):

$$n_i = K_i A_M (\Delta c_i)_{LM} \quad (14-58)$$

where K_i is from (14-57). This design method is used in the following example.

EXAMPLE 14.8 Recovery of H_2SO_4 by Dialysis.

A countercurrent-flow, plate-and-frame dialyzer is to be sized to process $0.78 \text{ m}^3/\text{h}$ of an aqueous solution containing 300 kg/m^3 of H_2SO_4 and smaller amounts of copper and nickel sulfates, using a wash water sweep of $1.0 \text{ m}^3/\text{h}$. It is desired to recover 30% of the acid at 25°C . From batch experiments with an acid-resistant vinyl membrane, in the absence of external mass-transfer resistances, a permeance of 0.025 cm/min for the acid and a water-transport number of +1.5 are measured. Membrane transport of copper and nickel sulfates is negligible. Experience with plate-and-frame dialyzers indicates that flow will be laminar and the combined external liquid-film mass-transfer coefficients will be 0.020 cm/min . Determine the membrane area in m^2 .

Solution

$$\begin{aligned} m_{\text{H}_2\text{SO}_4} \text{ in feed} &= 0.78(300) = 234 \text{ kg/h;} \\ m_{\text{H}_2\text{SO}_4} \text{ in feed transferred} &= 0.3(234) = 70 \text{ kg/h;} \\ m_{\text{H}_2\text{O}} \text{ transferred to dialysate} &= 1.5(70) = 105 \text{ kg/h;} \\ m_{\text{H}_2\text{O}} \text{ in entering wash} &= 1.0(1,000) = 1,000 \text{ kg/h;} \\ m_P \text{ leaving} &= 1,000 - 105 + 70 = 965 \text{ kg/h} \end{aligned}$$

For mixture densities, assume aqueous sulfuric acid solutions and from the appropriate table in *Perry's Chemical Engineers Handbook*:

$$\rho_F = 1,175 \text{ kg/m}^3; \quad \rho_R = 1,114 \text{ kg/m}^3; \quad \rho_P = 1,045 \text{ kg/m}^3;$$

$$m_F = 0.78(1,175) = 917 \text{ kg/h}; \quad m_R \text{ leaving} = 917 + 105 - 70$$

$$= 952 \text{ kg/h}$$

Sulfuric acid concentrations:

$$c_F = 300 \text{ kg/m}^3; \quad c_{\text{wash}} = 0 \text{ kg/m}^3$$

$$c_R = \frac{(234 - 70)}{950}(1,114) = 192 \text{ kg/m}^3$$

$$c_P = \frac{70}{965}(1,045) = 76 \text{ kg/m}^3$$

The log-mean driving force for H_2SO_4 with countercurrent flow of feed and wash is

$$(\Delta c)_{\text{LM}} = \frac{(c_F - c_P) - (c_R - c_{\text{wash}})}{\ln\left(\frac{c_F - c_P}{c_R - c_{\text{wash}}}\right)} = \frac{(300 - 76) - (192 - 0)}{\ln\left(\frac{300 - 76}{192 - 0}\right)}$$

$$= 208 \text{ kg/m}^3$$

The driving force is almost constant in the membrane module, varying only from 224 to 192 kg/m^3 .

From (14-57)

$$K_{\text{H}_2\text{SO}_4} = \frac{1}{\frac{1}{P_M} + \left(\frac{1}{k}\right)_{\text{combined}}} = \frac{1}{\frac{1}{0.025} + \frac{1}{0.020}}$$

$$= 0.0111 \text{ cm/min or } 0.0067 \text{ m/h}$$

From (14-58), using mass units instead of molar units:

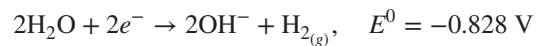
$$A_M = \frac{m_{\text{H}_2\text{SO}_4}}{K_{\text{H}_2\text{SO}_4}(\Delta_{\text{H}_2\text{SO}_4})_{\text{LM}}} = \frac{70}{0.0067(208)} = 50 \text{ m}^2$$

§14.5 ELECTRODIALYSIS

Electrodialysis dates back to the early 1900s, when electrodes and a direct current were used to increase the rate of dialysis. Since the 1940s, electrodialysis has become a process that differs from dialysis in many ways. Today, electrodialysis refers to an electrolytic process for separating an aqueous, electrolyte feed into concentrate and dilute or desalted water diluate by an electric field and ion-selective membranes. An electrodialysis process is shown in Figure 14.14, where the four ion-selective membranes are of two types arranged in an alternating-series pattern. The cation-selective membranes (C) carry a negative charge, and thus attract and pass positively charged ions (cations), while retarding negative ions (anions). The anion-selective membranes (A) carry a positive charge that attracts and permits passage of anions. Between each pair of membranes is a compartment. Both types of membranes are impervious to water. The net result is that both anions and cations are concentrated in compartments on the left side of A membranes, from which concentrate is withdrawn, and ions are depleted in compartments on the right side of A membranes from which the diluate is withdrawn. Compartment pressures are essentially equal. A direct-current voltage

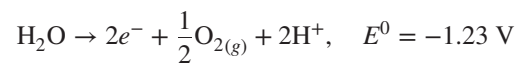
causes current to flow through the cell by ionic conduction from cathode to anode. Both electrodes are chemically neutral metals, with the anode being typically stainless steel and the cathode platinum-coated tantalum, niobium, or titanium. Thus, the electrodes are neither oxidized nor reduced.

The most easily oxidized species is oxidized at the anode and the most easily reduced species is reduced at the cathode. With inert electrodes, the result at the cathode is the reduction of water by the half reaction

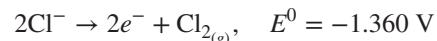


where E^0 is the standard electrical potential at 25°C for 1-M solution of ions and partial pressures of 1 atmosphere for the gaseous products.

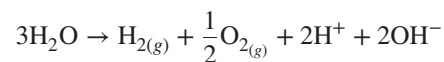
The oxidation half reaction at the anode is



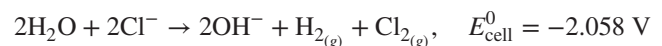
or, if chloride ions are present:



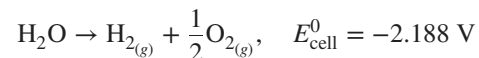
The corresponding overall cell reactions are:



or



The net reaction for the first case is



The electrode rinse solution that circulates through the compartments is typically acidic to neutralize the OH ions formed near the cathode and prevent precipitation of compounds such as CaCO_3 and $\text{Mg}(\text{OH})_2$.

The most widely used ion-exchange membranes for electrodialysis, first reported by Juda and McRae [35] in 1950, are (1) cation-selective membranes containing negatively charged groups fixed to a polymer matrix, and (2) anion-selective membranes containing positively charged groups fixed to a polymer matrix. The former, shown schematically in Figure 14.15, includes fixed anions, mobile cations (called counterions), and mobile anions (called co-ions). The latter are almost completely excluded from the polymer matrix by electrical repulsion, called the **Donnan effect**. For perfect exclusion, only cations are transferred through the membrane. In practice, the exclusion is better than 90%.

A cation-selective membrane may be made of polystyrene cross-linked with divinylbenzene and sulfonated to produce fixed sulfonate, $-\text{SO}_3^-$, anion groups. An anion-selective membrane of the same polymer contains quaternary ammonium groups such as $-\text{NH}_3^+$. Membranes are typically 0.01 to 0.20 mm thick and are reinforced for mechanical stability. The membranes are flat sheets, containing 30 to 50% water and have a network of pores too small to permit water transport.

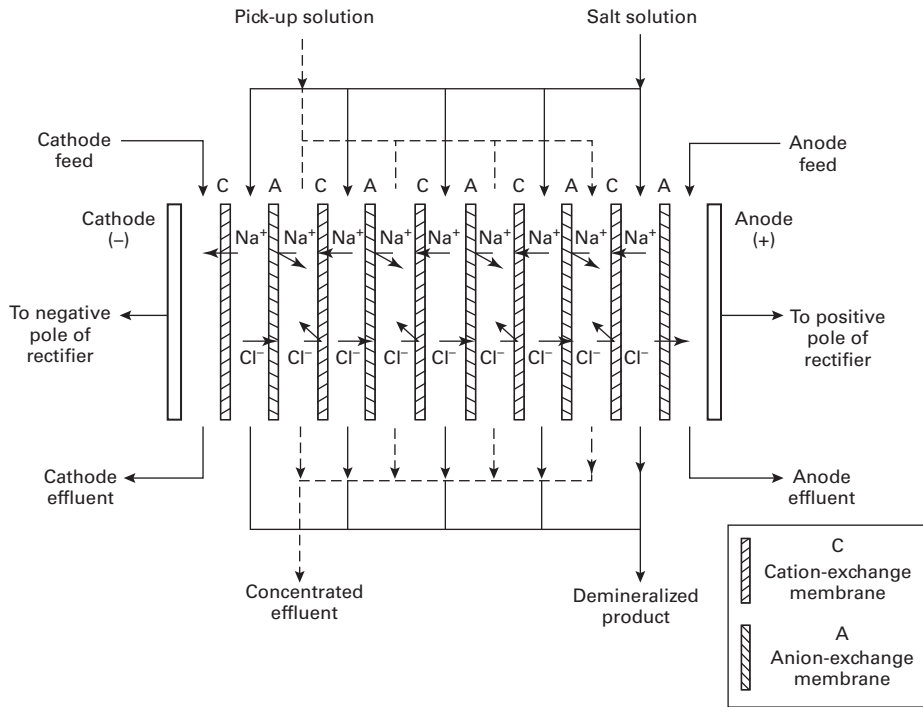


Figure 14.14 Schematic diagram of the electro dialysis process. [From R.W. Baker, *Membrane Technology and Applications*, 3rd Edition, John Wiley and Sons, Ltd. (2012) with permission.]

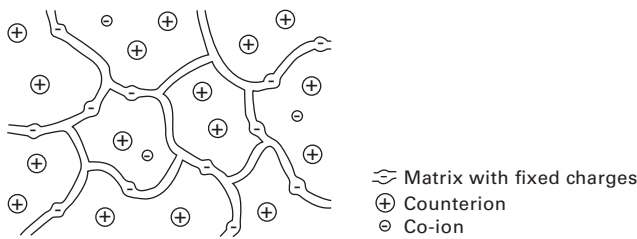


Figure 14.15 Cation-exchange membrane matrix.

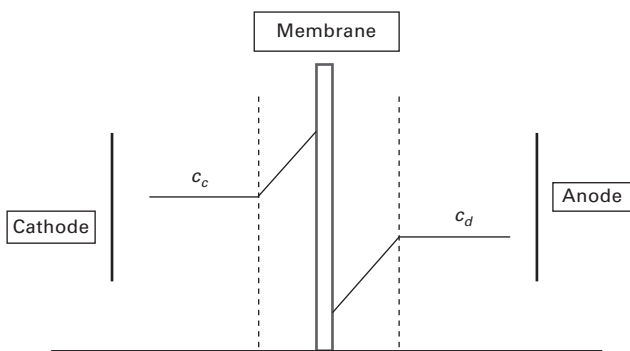


Figure 14.16 Concentration-polarization effects for a cation-exchange membrane.

A cell pair or unit cell contains one cation-selective membrane and one anion-selective membrane. A commercial electro dialysis system consists of a large stack of membranes in a plate-and-frame configuration, which, according to Applegate [2] and the *Membrane Handbook* [6], contains 100 to 600 cell pairs. In a stack, membranes of 0.4 to 1.5 m² surface area are separated by 0.5 to 2 mm with spacer gaskets. The total voltage or electrical potential applied across the

cell includes (1) electrode potentials, (2) overvoltages due to gas formation at the two electrodes, (3) voltage required to overcome the ohmic resistance of the electrolyte in each compartment, (4) voltage required to overcome the resistance in each membrane, and (5) voltage required to overcome concentration-polarization effects in the electrolyte solutions adjacent to the membrane surface.

For large stacks, the latter three voltage increments predominate and depend upon the current density (amps flowing through the stack per unit membrane surface area). A typical voltage drop across a cell pair is 0.5–1.5 V. Current densities are in the range of 5–50 mA/cm². Thus, a stack of 400 membranes (200 unit cells) of 1 m² surface area each might require 200 V at 100 A. Typically 50 to 90% of brackish water is converted to water, depending on concentrate recycle.

The concentration-polarization effect increases with increasing current density for a given membrane surface area. Figure 14.16 is a schematic of this effect for a cation-selective membrane, where c_c refers to cation concentration on the concentrate side and c_d refers to concentration on the dilute side. The maximum or limiting current density occurs when c_d at the membrane reaches zero. Typically, an electro dialysis cell is operated at 80% of the limiting current density, which is determined by experiment, as is the corresponding cell voltage or resistance.

The amount of gas formed at the electrodes at the ends of the stack are governed by **Faraday’s law of electrolysis**. One Faraday (96,520 coulombs) of electricity reduces at the cathode and oxidizes at the anode an equivalent of oxidizing and reducing agent corresponding to the transfer of 6.023×10^{23} (Avogadro’s number) electrons through wiring from the anode to the cathode. In general, it takes a large quantity of electricity to form appreciable quantities of gas in an electro dialysis process.

Of importance in design of an electro dialysis process are the membrane area and electrical-energy requirements, as discussed by Applegate [2] and Strathmann [36]. The membrane area is estimated from the current density, rather than from permeability and mass-transfer resistances, by applying Faradays law:

$$A_M = \frac{FQ\Delta c}{i\xi} \quad (14-59)$$

where A_M = total area of all cell pairs, m^2 ; F = Faraday's constant (96,520 amp-s/equivalent); Q = volumetric flow rate of diluate (potable water), m^3/s ; Δc = difference between feed and diluate ion concentration in equivalents/ m^3 ; i = current density, amps/ m^2 of a cell pair, usually about 80% of i_{max} ; and ξ = current efficiency < 1.00 .

The efficiency accounts for the fact that not all of the current is effective in transporting ions through the membranes. Inefficiencies are caused by a Donnan exclusion of less than 100%, some transfer of water through the membranes, current leakage through manifolds, etc. Power consumption is given by

$$P = IE \quad (14-60)$$

where P = power in watts; I = electric current flow through the stack in amps; and E = voltage across the stack. Electrical current is given by a rearrangement of (14-59),

$$I = \frac{FQ\Delta c}{n\xi} \quad (14-61)$$

where n is the number of cell pairs.

The main application of electro dialysis is to the desalination of brackish water in the salt-concentration range of 500 to 5,000 ppm (mg/L). Below this range, ion exchange is more economical, whereas above this range, to 50,000 ppm, reverse osmosis is preferred. However, electro dialysis cannot produce water with a very low dissolved-solids content because of the high electrical resistance of dilute solutions. Other applications include recovery of nickel and copper from electroplating rinse water; deionization of cheese whey, fruit juices, wine, milk, and sugar molasses; separation of salts, acids, and bases from organic compounds; and recovery of organic compounds from their salts. Bipolar membranes, prepared by laminating a cation-selective membrane and an anion-selective membrane back-to-back, are used to produce H_2SO_4 and $NaOH$ from a Na_2SO_4 solution.

EXAMPLE 14.9 Electro dialysis of Brackish Water.

Estimate membrane area and electrical-energy requirements for an electro dialysis process to reduce the salt ($NaCl$) content of 24,000 m^3/day of brackish water from 1,500 mg/L to 300 mg/L with a 50% conversion. Assume each membrane has a surface area of 0.5 m^2 and each stack contains 300 cell pairs. A reasonable current density is 5 mA/ cm^2 , and the current efficiency is 0.8 (80%).

Solution

Use (14-59) to estimate membrane area:

$$F = 96,520 \text{ A/equiv}$$

$$Q = (24,000)(0.5)/(24)(3,600) = 0.139 \text{ m}^3/\text{s}$$

$$MW_{NaCl} = 58.5; i = 5 \text{ mA/cm}^2 = 50 \text{ A/m}^2$$

$$\Delta c = (1,500 - 300)/58.5 = 20.5 \text{ mmol/L or } 20.5 \text{ mol/m}^3 \\ = 20.5 \text{ equiv/m}^3$$

$$A_M = \frac{(1)(96,520)(0.139)(20.5)}{(50)(0.8)} = 6,876 \text{ m}^2$$

Each stack contains 300 cell pairs with a total area of $0.5(300) = 150 \text{ m}^2$. Therefore, the number of stacks = $6,876/150 = 46$ in parallel. From (14-61), electrical current flow is given by

$$I = \frac{(96,500)(0.139)(20.5)}{(300)(0.8)} \\ = 1,146 \text{ A or } I/\text{stack} = 1,146/46 = 25 \text{ A/stack}$$

To obtain the electrical power, the average voltage drop across each cell pair is needed. Assume a value of 1 V. From (14-60) for 300 cell pairs:

$$P = (1,146)(1)(300) = 344,000 \text{ W} = 344 \text{ kW}$$

Additional energy is required to pump feed, recycle concentrate, and electrode rinse.

It is instructive to estimate the amount of feed that would be electrolyzed (as water to hydrogen and oxygen gases) at the electrodes. From the half-cell reactions presented earlier, half a molecule of H_2O is electrolyzed for each electron, or 0.5 mol H_2O is electrolyzed for each faraday of electricity.

$$1,146 \text{ amps} = 1,146 \text{ coulombs/s}$$

$$\text{or } (1,146)(3,600)(24) = 99,010,000 \text{ coulombs/day}$$

$$\text{or } 99,010,000/96,520 = 1,026 \text{ faradays/day}$$

This electrolyzes $(0.5)(1,026) = 513 \text{ mol/day}$ of water. The feed rate is 12,000 m^3/day , or

$$\frac{(12,000)(10^6)}{18} = 6.7 \times 10^8 \text{ mol/day}$$

Therefore, the amount of water electrolyzed is negligible.

§14.6 REVERSE OSMOSIS

Osmosis, from the Greek word for "push," refers to passage of a solvent, such as water, through a membrane that is much more permeable to solvent (A) than to solute(s) (B) (e.g., inorganic ions). The first recorded account of osmosis was in 1748 by Nolle, whose experiments were conducted with water, an alcohol, and an animal-bladder membrane. Osmosis is illustrated in Figure 14.17, where all solutions are at 25°C. In the initial condition (Figure 14.17a), seawater of approximately 3.5 wt% dissolved salts and at 101.3 kPa is in cell 1, while pure

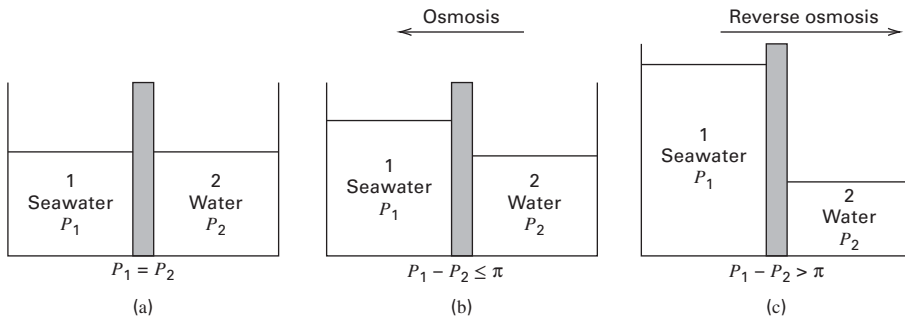


Figure 14.17 Osmosis and reverse osmosis phenomena: (a) initial condition; (b) at equilibrium after osmosis; (c) reverse osmosis.

water at the same pressure is in cell 2. The dense membrane is permeable to water, but not to dissolved salts. By osmosis, water passes from cell 2 to the seawater in cell 1, causing dilution of the dissolved salts. At equilibrium, the condition of Figure 14.17b is reached, wherein some pure water still resides in cell 2 and seawater, less concentrated in salt, resides in cell 1. Because of the higher head of solution in cell 1, pressure P_1 is now greater than pressure P_2 , in cell 2, with the difference, π , referred to as the **osmotic pressure**.

Osmosis is not a useful separation process because solvent is transferred in the wrong direction, resulting in mixing rather than separation. However, the direction of transport of solvent through the membrane can be reversed, as shown in Figure 14.17c, by applying a pressure, P_1 , in cell 1, that is higher than the sum of the osmotic pressure and pressure, P_2 , in cell 2: that is, $P_1 - P_2 > \pi$. Now water in the seawater is transferred to the pure water, and the seawater becomes more concentrated in dissolved salts. This phenomenon, called **reverse osmosis (RO)**, is used to partially remove solvent from a solute-solvent mixture. An important factor in developing a reverse-osmosis separation process is the osmotic pressure, π , of the feed mixture, which is proportional to the solute concentration. For pure water, $\pi = 0$.

In reverse osmosis, as shown in Figure 14.18, feed is a liquid at high pressure, P_1 , containing solvent (e.g., water) and solubles (e.g., inorganic salts and, perhaps, colloidal matter). No sweep liquid is used, but the other side of the membrane is maintained at a much lower pressure, P_2 . A dense membrane such as an acetate or aromatic polyamide, permselective for the solvent, is used. To withstand the large ΔP , the membrane must be thick. Accordingly, asymmetric or thin-wall composite membranes, having a thin, dense skin or layer on a thick, porous support, are needed. The products of reverse osmosis are a **permeate** of almost pure solvent and a **retentate** of solvent-depleted feed. A perfect separation between solvent and solute is not achieved, since only a fraction of the solvent is transferred to the permeate.

Reverse osmosis is widely used to desalinate and purify seawater, brackish water, and wastewater. Prior to 1980, multistage, flash distillation was the primary desalination process, but by 1990 this situation was dramatically reversed, making RO the dominant process for new construction. The dramatic

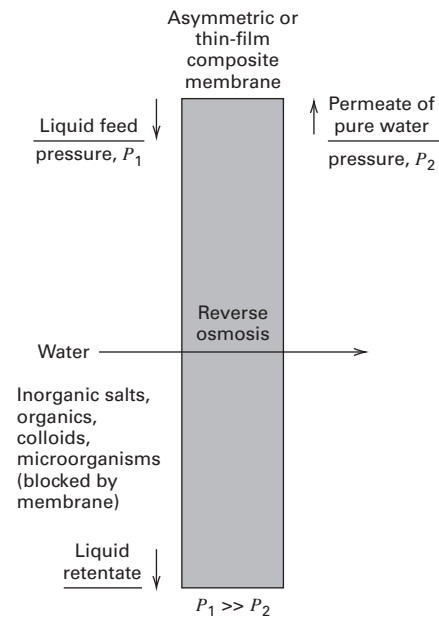


Figure 14.18 Reverse osmosis.

shift from a thermally driven process to a more economical, pressure-driven process was made possible by Loeb and Sourirajan [7], who developed an asymmetric membrane that allows pressurized water to pass through at a high rate, while almost preventing transmembrane flows of dissolved salts, organic compounds, colloids, and microorganisms. In 1980, an improved membrane for RO, developed by John E. Cadotte, was introduced by FilmTec (acquired by Dow Chemical in 1985). Known as FT30, it is now the predominate membrane material used for RO because of its high rejection of salts and dissolved organic compounds, and very stable, long-term operability. Today more than 1,000 RO desalting plants are producing more than 750,000,000 gal/day of potable water. One of the largest seawater RO plants, located in Ashkelon, Israel on the Mediterranean coast, produces 330,000 m³/day (84,500,000 gal/day), which is 13% of Israel's domestic consumer demand. The largest RO plant in the United States is in Tampa Bay, Florida, with a production rate of 25 million gpd (95,000 m³/day), enough to satisfy the drinking needs of 10% of the region.

RO for the desalination of water is accomplished mainly with spiral-wound and hollow-fiber membrane modules utilizing cellulose triacetate, cellulose diacetate, and aromatic polyamide membrane materials. Cellulose acetates are susceptible to biological attack, and to acidic or basic hydrolysis back to cellulose, making it necessary to chlorinate the feed water and control the pH to within 4.5–7.5. Polyamides are not susceptible to biological attack, and resist hydrolysis in the pH range of 4–11, but are attacked by chlorine.

The preferred membrane for the desalination of seawater, which contains about 3.5 wt% dissolved salts and has an osmotic pressure of 350 psia, is a spiral-wound, multileaf module of polyamide, thin-film composite operating at a feed pressure of 800 to 1,000 psia. With a transmembrane water flux of 9 gal/ft²-day (0.365 m³/m²-day), this module can recover 45% of the water at a purity of about 99.95 wt%. A typical module is 8 inches in diameter by 40 inches long, containing 365 ft² (33.9 m²) of membrane surface. However, the largest RO plants now use 16-inch diameter modules. Such modules resist fouling by colloidal and particulate matter, but seawater must be treated with sodium bisulfate to remove oxygen and/or chlorine.

For desalination of brackish water containing less than 0.5 wt% dissolved salts, hollow-fiber modules of high packing density, containing fibers of cellulose acetates or aromatic polyamides, are used if fouling is not serious. Because the osmotic pressure is much lower (<50 psi), feed pressures can be <250 psia and transmembrane fluxes may be as high as 20 gal/ft²-day.

Other uses of reverse osmosis, usually on a smaller scale than the desalination of water, include (1) treatment of industrial wastewater to remove heavy-metal ions, non-biodegradable substances, and other components of possible commercial value; (2) treatment of rinse water from electroplating processes to obtain a metal-ion concentrate and a permeate that can be reused as a rinse; (3) separation of sulfites and bisulfites from effluents in pulp and paper processes; (4) treatment of wastewater in dyeing processes; (5) recovery of constituents having food value from wastewaters in food-processing plants (e.g., lactose, lactic acid, sugars, and starches); (6) treatment of municipal water to remove inorganic salts, low-molecular-weight organic compounds, viruses, and bacteria; (7) dewatering of food products such as coffee, soups, tea, milk, orange juice, and tomato juice; and (8) concentration of amino acids and alkaloids. In such applications, membranes must have chemical, mechanical, and thermal stability to be competitive with other processes.

As with all membrane processes where feed is a liquid, three resistances to mass transfer must be considered: the membrane resistance and the two boundary-layer resistances on either side of the membrane. If the permeate is pure solvent, there is no film resistance on that side of the membrane.

Although the driving force for water transport is the concentration or activity difference in and across the membrane, common practice is to use a driving force based on osmotic pressure. Consider the reverse-osmosis process

of Figure 14.17c. At thermodynamic equilibrium, solvent chemical potentials or fugacities on the two sides of the membrane must be equal. Thus,

$$f_A^{(1)} = f_A^{(2)} \quad (14-62)$$

From definitions in Table 2.2, (14-62) can be rewritten in terms of activities:

$$a_A^{(1)} f_A^0 \{T, P_1\} = a_A^{(2)} f_A^0 \{T, P_2\} \quad (14-63)$$

For pure solvent, A, $a_A^{(2)} = 1$. For seawater, $a_A^{(1)} = x_A^{(1)} \gamma_A^{(1)}$. Substitution into (14-63) gives

$$f_A^0 \{T, P_2\} = x_A^{(1)} \gamma_A^{(1)} f_A^0 \{T, P_1\} \quad (14-64)$$

Standard-state, pure-component fugacities f^0 increase with increasing pressure. Thus, if $x_A^{(1)} \gamma_A^{(1)} < 1$, then from (14-64), $P_1 > P_2$. The pressure difference $P_1 - P_2$ is shown as a hydrostatic head in Figure 14.17b. It can be observed experimentally, and is defined as the osmotic pressure, π .

To relate π to solvent or solute concentration, the Poynting correction of (2-30) is applied. For an incompressible liquid of specific volume, v_A ,

$$f_A^0 \{T, P_2\} = f_A^0 \{T, P_1\} \exp \left[\frac{v_{AL} (P_2 - P_1)}{RT} \right] \quad (14-65)$$

Substitution of (14-64) into (14-65) gives

$$\pi = P_1 - P_2 = -\frac{RT}{v_{AL}} \ln \left(x_A^{(1)} \gamma_A^{(1)} \right) \quad (14-66)$$

Thus, osmotic pressure replaces activity as a thermodynamic variable.

For a mixture on the feed-retentate side of the membrane that is dilute in solute,

$$\gamma_A^{(1)} = 1$$

Also, $x_A^{(1)} = 1 - x_B^{(1)}$ and $\ln(1 - x_B^{(1)}) \approx -x_B^{(1)}$. Substitution into (14-66) gives

$$\pi = P_1 - P_2 = RT x_B^{(1)} / v_{AL} \quad (14-67)$$

Finally, since $x_B^{(1)} \approx n_B / n_A$, $n_A v_{AL} = V$, and $n_B / V = c_B$, (14-67) becomes

$$\pi \approx RT c_B \quad (14-68)$$

which was used in Exercise 1.6. For seawater, Applegate [2] suggests the approximate expression

$$\pi = 1.12T \sum \bar{m}_i \quad (14-69)$$

where π is in psia, T is in K, and $\sum \bar{m}_i$ is the summation of molarities of dissolved ions and nonionic species in the solution in mol/L. More exact expressions for π are those of Stoughton and Lietzke [38].

In the general case, when there are solutes on each side of the membrane, at equilibrium $(P_1 - \pi_1) = (P_2 - \pi_2)$. Accordingly, as discussed by Merten [37], the driving force for solvent transport through the membrane is $\Delta P - \Delta\pi$, and the rate of mass transport is

$$N_{H_2O} = \frac{P_{M_{H_2O}}}{l_M} (\Delta P - \Delta\pi) \quad (14-70)$$

where $\Delta P =$ hydraulic pressure difference across the membrane $= P_{feed} - P_{permeate}$, and $\Delta\pi =$ osmotic pressure difference across the membrane $= \pi_{feed} - \pi_{permeate}$. If the permeate is almost pure solvent, $\pi_{permeate} \approx 0$.

The flux of solute (e.g., salt), given by (14-26) in terms of membrane concentrations, is independent of ΔP across the membrane. Accordingly, the higher the ΔP , the purer the permeate water. Alternatively, the flux of salt may be conveniently expressed in terms of **salt passage, SP**,

$$SP = (c_{salt})_{permeate} / (c_{salt})_{feed} \quad (14-71)$$

Values of *SP* decrease with increasing ΔP . Salt rejection is given by $SR = 1 - SP$.

For brackish water of only 1,500 mg/L NaCl at 25°C, (14-69) predicts $\pi = 17.1$ psia. For seawater of 35,000 mg/L NaCl at 25°C, (14-69) predicts $\pi = 385$ psia, while Stoughton and Lietzke [38] give 368 psia. From (14-70), ΔP must be $> \Delta\pi$ for reverse osmosis to occur. For desalination of brackish water by RO, ΔP is typically 400–600 psi, while for seawater, it is 800–1,000 psi.

Feed water to an RO unit contains potential foulants, which must be removed prior to passage through the membrane unit; otherwise, performance and membrane life are reduced. Suspended solids and particulate matter are removed by screening and filtration. Colloids are flocculated and filtered. Scale-forming salts require acidification or water softening, and biological materials require chlorination or ozonation. Other organic foulants are removed by adsorption or oxidation.

Concentration polarization on the feed side of RO membranes is illustrated in Figure 14.19, where concentrations are

shown for water, c_w , and salt, c_s . Because of the high pressure, activity of water on the feed side is somewhat higher than that of near-pure water on the permeate side. This provides the driving force for water transport through the membrane. The flux of water to the membrane carries with it salt by bulk flow, but because the salt cannot readily penetrate the membrane, salt concentration adjacent to the surface of the membrane, c_{s_i} is $> c_{s_F}$. This difference causes mass transfer of salt by diffusion from the membrane surface back to the bulk feed. The back rate of salt diffusion depends on the mass-transfer coefficient for the boundary layer on the feed side. The lower the mass-transfer coefficient, the higher the value of c_{s_i} . This is important because it fixes the osmotic pressure, and influences the driving force for water transport according to (14-70).

Consider steady-state transport of water with back-diffusion of salt. A salt balance at the upstream membrane surface gives

$$N_{H_2O} c_{s_F} (SR) = k_s (c_{s_i} - c_{s_F})$$

Solving for c_{s_i} gives

$$c_{s_i} = c_{s_F} \left(1 + \frac{N_{H_2O} (SR)}{k_s} \right) \quad (14-72)$$

Values of k_s are estimated from (14-55). The concentration-polarization effect is seen to be most significant for high water fluxes and low mass-transfer coefficients.

A quantitative estimate of the importance of concentration polarization is derived by defining the concentration-polarization factor, Γ , by a rearrangement of the previous equation:

$$\Gamma \equiv \frac{c_{s_i} - c_{s_F}}{c_{s_F}} = \frac{N_{H_2O} (SR)}{k_s} \quad (14-73)$$

Values of *SR* are in the range of 0.97–0.995. If $\Gamma > 0.2$, concentration polarization may be significant, indicating a need for design changes to reduce Γ .

Feed-side pressure drop is also important because it causes a reduction in the driving force for water transport. Because of the complex geometries used for both spiral-wound and hollow-fiber modules, it is best to estimate pressure drops from experimental data. Feed-side pressure drops for spiral-wound modules and hollow-fiber modules range from 43 to 85 and 1.4 to 4.3 psi, respectively [6].

A schematic diagram of a reverse-osmosis for desalination is shown in Figure 14.20. The source of feed water may be a well or surface water, which is pumped through a series of pre-treatment steps to ensure a long membrane life. Of particular importance is pH adjustment. The pretreated water is fed by a high-pressure discharge pump to a parallel-and-series network of reverse-osmosis modules. The concentrate, which leaves the membrane system at a pressure that is 10–15% lower than the inlet pressure, is then routed through a power-recovery turbine, which reduces the net power consumption by 25–40%. The permeate, which may be 99.95 wt% pure water and about 50% of the feed water, is sent to a series of post-treatment steps to make it drinkable.

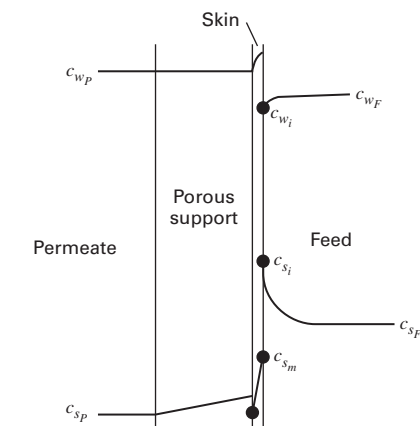


Figure 14.19 Concentration-polarization effects in reverse osmosis.

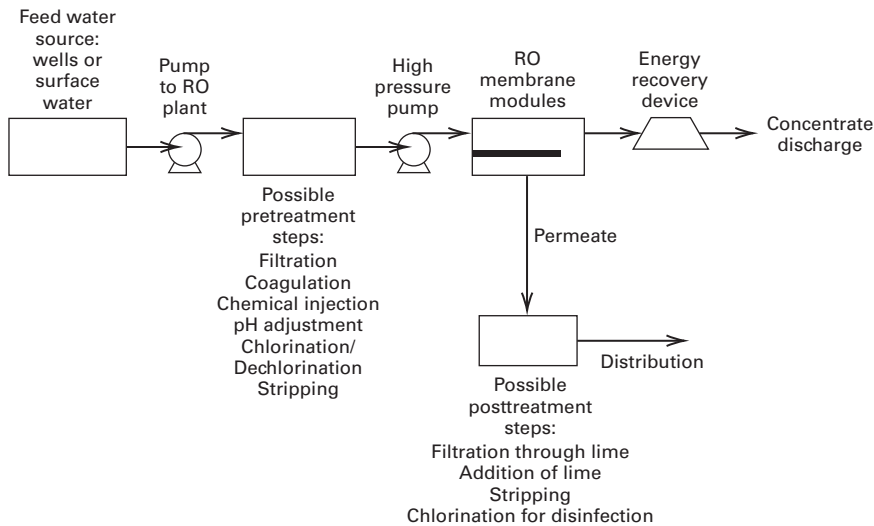


Figure 14.20 Reverse-osmosis process.

EXAMPLE 14.10 Polarization Factor in Reverse Osmosis.

At a certain point in a spiral-wound membrane, the bulk conditions on the feed side are 1.8 wt% NaCl, 25°C, and 1,000 psia, while bulk conditions on the permeate side are 0.05 wt% NaCl, 25°C, and 50 psia. For this membrane the permeance values are 1.1×10^{-5} g/cm²-s-atm for H₂O and 16×10^{-6} cm/s for the salt. If external mass-transfer resistances are negligible, calculate the flux of water in gal/ft²-day and the flux of salt in g/ft²-day. If $k_s = 0.005$ cm/s, estimate the polarization factor.

Solution

Bulk salt concentrations are

$$c_{sF} = \frac{1.8(1,000)}{58.5(98.2)} = 0.313 \text{ mol/L on feed side}$$

$$c_{sP} = \frac{0.05(1,000)}{58.5(99.95)} = 0.00855 \text{ mol/L on permeate side}$$

For water transport, using (14-69) for osmotic pressure and noting that dissolved NaCl gives 2 ions per molecule:

$$\Delta P = (1,000 - 50)/14.7 = 64.6 \text{ atm}$$

$$\pi_{\text{feed side}} = 1.12(298)(2)(0.313) = 209 \text{ psia} = 14.2 \text{ atm}$$

$$\pi_{\text{permeate side}} = 1.12(298)(2)(0.00855) = 5.7 \text{ psia} = 0.4 \text{ atm}$$

$$\Delta P - \Delta \pi = 64.6 - (14.2 - 0.4) = 50.8 \text{ atm}$$

$$P_{M_{\text{H}_2\text{O}}}/l_M = 1.1 \times 10^{-5} \text{ g/cm}^2\text{-s-atm}$$

From (14-70),

$$N_{\text{H}_2\text{O}} = (1.1 \times 10^{-5})(50.8) = 0.000559 \text{ g/cm}^2\text{-s}$$

$$\text{or } \frac{(0.000559)(3,600)(24)}{(454)(8.33)(1.076 \times 10^{-3})} = 11.9 \text{ gal/ft}^2\text{-day}$$

For salt transport:

$$\Delta c = 0.313 - 0.00855 = 0.304 \text{ mol/L or } 0.000304 \text{ mol/cm}^3$$

$$P_{M_{\text{NaCl}}}/l_M = 16 \times 10^{-6} \text{ cm/s}$$

From (14-26):

$$N_{\text{NaCl}} = 16 \times 10^{-6}(0.000304) = 4.86 \times 10^{-9} \text{ mol/cm}^2\text{-s}$$

$$\text{or } \frac{(4.86 \times 10^{-9})(3,600)(24)(58.5)}{1.076 \times 10^{-3}} = 22.8 \text{ g/ft}^2\text{-day}$$

The flux of salt is much smaller than the flux of water.

To estimate the concentration-polarization factor, first convert the water flux through the membrane into the same units as the salt mass-transfer coefficient, k_s , i.e., cm/s:

$$N_{\text{H}_2\text{O}} = \frac{0.000559}{1.00} = 0.000559 \text{ cm/s}$$

From (14-71), the salt passage is

$$SP = 0.00855/0.313 = 0.027$$

Therefore, the salt rejection = $SR = 1 - 0.027 = 0.973$.

From (14-73), the concentration-polarization factor is

$$\Gamma = \frac{0.000559(0.972)}{0.005} = 0.011$$

This small value indicates that polarization is not significant.

§14.7 GAS PERMEATION

Figure 14.21 shows gas permeation (GP) through a thin membrane, where feed gas, at high pressure P_1 , contains some low-molecular-weight species (MW < 50) to be separated from small amounts of higher-molecular-weight species. Usually a sweep gas is not needed, but the other side of the membrane is maintained at a much lower pressure, P_2 , often near ambient, to provide an adequate driving force.

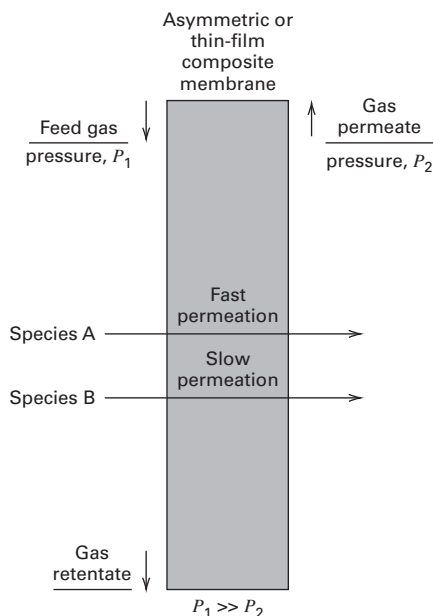


Figure 14.21 Gas permeation.

The membrane, often dense but sometimes microporous, is permselective for the low-molecular-weight species A. If the membrane is dense, these species are absorbed at the surface and then transported through the membrane by one or more mechanisms. Permselectivity depends on both membrane absorption and transport rate. Mechanisms are formulated in terms of a partial-pressure or fugacity driving force using the solution-diffusion model of (14-32). The products are a permeate enriched in A and a retentate enriched in B. A near-perfect separation is generally not achievable. If the membrane is microporous, pore size is extremely important because it is necessary to block the passage of species B. Otherwise, unless molecular weights of A and B differ appreciably, only a very modest separation is achievable, as was discussed in connection with Knudsen diffusion, (14-21). Since the early 1980s, applications of GP with dense polymeric membranes have increased dramatically. Major applications are listed in Table 14.1. The largest industrial gas permeation process is the separation of N_2 from air (nitrogen generator).

Gas permeation competes with absorption, pressure-swing adsorption, and cryogenic distillation. Advantages of gas permeation, as cited by Spillman and Sherwin [39], are low capital investment, ease of installation, ease of operation, absence of rotating parts, high process flexibility, low weight and space requirements, and low environmental impact. In addition, if the feed gas is already at high pressure, a gas compressor is not needed, thus no utilities are required.

Since 1986, the most rapidly developing industrial application for GP has been air separation, for which available membranes have separation factors for O_2 with respect to N_2 of 3 to 7. However, product purities are economically limited to a retentate of 95–99.9% N_2 and a permeate of 30–45% O_2 .

In the future, if highly selective membranes can be developed, gas permeation will be used to separate close-boiling hydrocarbon mixtures such as ethylene from ethane and possibly close boiling organic vapor mixtures.

Gas permeation also competes favorably for H_2 recovery because of high separation factors. The rate of permeation of H_2 through a dense polymer membrane is more than 30 times that for N_2 . GP can achieve a 95% recovery of 90% pure H_2 from a feed gas containing 60% H_2 .

Early applications of GP used nonporous membranes of cellulose acetates and polysulfones, which are still predominant, although polyimides, polyamides, polycarbonates, polyetherimides, sulfonated polysulfones, Teflon, polystyrene, and silicone rubber are also finding applications for temperatures to at least 70°C. High-performance polymers for the separation of mixtures of O_2 and N_2 include polytrimethylsilylpropyne, tetrabromobisphenol A polycarbonate, polytert-butylacetylene, Vectra polyester, polytriazole, and polypyrrolone, with separation factors for these polymers varying from 2.0 to 15.3.

Although plate-and-frame and tubular modules have been used for gas permeation (e.g., the separation of helium from natural gas), almost all large-scale applications use spiral-wound or hollow-fiber modules because of their higher packing density. Commercial membrane modules for gas permeation are available from many suppliers. Feed-side pressure is typically 300 to 500 psia, but is as high as 1,650 psia. Typical refinery applications involve feed-gas flow rates of 20 million scfd, but flow rates as large as 300 million scfd have been reported [40]. When the feed contains condensables, it may be necessary to preheat the feed gas to prevent condensation as the retentate becomes richer in the high-molecular-weight species. For high-temperature applications where polymers cannot be used, membranes of glass, carbon, and inorganic oxides are available, but are limited in their selectivity.

For dense membranes, external mass-transfer resistances or concentration-polarization effects are generally negligible, and (14-32) with a partial-pressure driving force can be used to compute the rate of membrane transport. As discussed in §14.3.3 on module flow patterns, the appropriate partial-pressure driving force depends on the flow pattern. Cascades are used to increase degree of separation.

Progress is being made in the prediction of permeability of gases in glassy and rubbery homopolymers, random copolymers, and block copolymers. Teplyakov and Meares [41] present correlations at 25°C for the diffusion coefficient, D_i , and solubility, S , applied to 23 different gases for 30 different polymers. Predicted values for glassy polyvinyltrimethylsilane (PVTMS) and rubbery polyisoprene are listed in Table 14.9. D and S values agree with data to within $\pm 20\%$ and $\pm 30\%$, respectively.

Gas-permeation separators are claimed to be relatively insensitive to changes in feed flow rate, feed composition, and loss of membrane surface area [42]. This claim is tested in the following example.

Table 14.9 Predicted Values of Diffusivity and Solubility of Light Gases in a Glassy and a Rubbery Polymer

Permeant	$D_i \times 10^{11}$, m ² /s	$S \times 10^4$, mol/m ³ -Pa	P_M , Barrer
Polyvinyltrimethylsilane (Glassy Polymer)			
He	470	0.18	250
Ne	87	0.26	66
Ar	5.1	1.95	30
Kr	1.5	6.22	29
Xe	0.29	20.6	18
Rn	0.07	69.6	15
H ₂	160	0.54	250
O ₂	7.6	1.58	37
N ₂	3.8	0.84	9
CO ₂	4.0	13.6	160
CO	3.7	1.28	14
CH ₄	1.9	3.93	22
C ₂ H ₆	0.12	30.2	10
C ₃ H ₈	0.01	98.1	2.8
C ₄ H ₁₀	0.001	347	1.2
C ₂ H ₄	0.23	17.8	12
C ₃ H ₆	0.038	77.6	9
C ₄ H ₈	0.0052	293	4.5
C ₂ H ₂	0.58	16.8	32
C ₃ H ₄ (m)	0.17	138.1	70
C ₄ H ₆ (e)	0.053	318.5	50
C ₃ H ₄ (a)	0.15	186.5	83
C ₄ H ₆ (b)	0.03	226.1	20
Polyisoprene (Rubber-like Polymer)			
He	213	0.06	35
Ne	77.4	0.08	18
Ar	14.6	0.58	25
Kr	7.2	1.78	25
Xe	2.7	5.68	45
Rn	1.2	18.7	64
H ₂	109	0.17	54
O ₂	18.4	0.47	26
N ₂	12.2	0.26	10
CO ₂	12.6	3.80	140
CO	12.1	0.38	14
CH ₄	8.0	1.14	27
C ₂ H ₆	3.3	8.13	79
C ₃ H ₈	1.6	25.4	123
C ₄ H ₁₀	1.5	86.4	390
C ₂ H ₄	4.3	4.84	62
C ₃ H ₆	2.7	20.3	163
C ₄ H ₈	1.5	73.3	333
C ₂ H ₂	5.7	4.64	80
C ₃ H ₄ (m)	4.1	35.3	433
C ₄ H ₆ (e)	2.9	79.6	690
C ₃ H ₄ (a)	4.5	47.4	640
C ₄ H ₆ (b)	3.4	40.0	410

Note: m, methylacetylene; e, ethylacetylene; a, allene; b, butadiene.

EXAMPLE 14.11 Recovery of H₂ by Gas Permeation.

The feed to a membrane separator consists of 500 lbmol/h of a mixture of 90% H₂ (H) and 10% CH₄ (M) at 500 psia. Permeance values based on a partial-pressure driving force are

$$\bar{P}_{MH} = 3.43 \times 10^{-4} \text{ lbmol/h-ft}^2\text{-psi}$$

$$\bar{P}_{MM} = 5.55 \times 10^{-5} \text{ lbmol/h-ft}^2\text{-psi}$$

Flow patterns in the separator are such that the permeate side is well mixed and the feed side is in plug flow. The pressure on the permeate side is constant at 20 psia, and there is no feed-retentate side pressure drop. (a) Compute the membrane area and permeate purity if 90% of the hydrogen is transferred to the permeate. (b) For the membrane area determined in part (a), calculate the permeate purity and hydrogen recovery if (1) the feed rate is increased by 10%, (2) the feed composition is reduced to 85% H₂, and (3) 25% of the membrane area becomes inoperative.

Solution

The following independent equations apply to all parts of this example. Component material balances:

$$n_{iF} = n_{iR} + n_{iP}, \quad i = H, M \quad (1,2)$$

Dalton's law of partial pressures:

$$P_k = p_{H_k} + p_{M_k}, \quad k = F, R, P \quad (3,4,5)$$

Partial-pressure–mole relations:

$$p_{H_k} = P_k n_{H_k} / (n_{H_k} + n_{M_k}), \quad k = F, R, P \quad (6,7,8)$$

Solution-diffusion transport rates are obtained using (14-32), assuming a log-mean partial-pressure driving force based on the exiting permeate partial pressures on the downstream side of the membrane because of the assumption of perfect mixing.

$$n_{iP} = \bar{P}_{Mi} A_M \left[\frac{p_{iF} - p_{iR}}{\ln \left(\frac{p_{iF} - p_{iP}}{p_{iR} - p_{iP}} \right)} \right], \quad i = H, M \quad (9,10)$$

Thus, a system of 10 equations has the following 18 variables:

$$\begin{matrix} A_M & n_{HF} & n_{MF} & P_F & P_R & P_P \\ \bar{P}_{MH} & n_{HR} & n_{MR} & p_{HF} & p_{HR} & p_{HP} \\ \bar{P}_{MM} & n_{HP} & n_{MP} & p_{MF} & p_{MR} & p_{MP} \end{matrix}$$

To solve the equations, eight variables must be fixed. For all parts of this example, the following five variables are fixed:

$$\begin{aligned} &\bar{P}_{MH} \text{ and } \bar{P}_{MM} \text{ given above} \\ &P_F = 500 \text{ psia}; \quad P_R = 500 \text{ psia}; \quad P_P = 20 \text{ psia} \end{aligned}$$

For each part, three additional variables must be fixed.

- (a) $n_{H_F} = 0.9(500) = 450$ lbmol/h
 $n_{M_F} = 0.1(500) = 50$ lbmol/h
 $n_{H_P} = 0.9(450) = 405$ lbmol/h

Solving Equations (1)–(10) above, using, MATLAB, the results are:

$A_M = 3.370$ ft²
 $n_{M_P} = 20.0$ lbmol/h; $n_{H_R} = 45.0$ lbmol/h; $n_{M_R} = 30.0$ lbmol/h
 $p_{H_F} = 450$ psia; $p_{M_F} = 50$ psia; $p_{H_R} = 300$ psia
 $p_{M_R} = 200$ psia; $p_{H_P} = 19.6$ psia; $p_{M_P} = 0.94$ psia

- (b) Calculations are made in a similar manner using Equations (1)–(10). Results for parts (1), (2), and (3) are:

	Part		
	(1)	(2)	(3)
Fixed:			
n_{H_F} , lbmol/h	495	425	450
n_{M_F} , lbmol/h	55	75	50
A_m , ft ²	3,370	3,370	2,528
Calculated, in lbmol/h:			
n_{H_P}	424.2	369.6	338.4
n_{M_P}	18.2	25.9	11.5
n_{H_R}	70.8	55.4	111.6
n_{M_R}	36.8	49.1	38.5
Calculated, in psia:			
p_{H_F}	450	425	450
p_{M_F}	50	75	50
p_{H_R}	329	265	372
p_{M_R}	171	235	128
p_{H_P}	19.18	18.69	19.34
p_{M_P}	0.82	1.31	0.66

From the above results:

	Part			
	(a)	(b1)	(b2)	(b3)
Mol% H ₂ in permeate	95.3	95.9	93.5	96.7
% H ₂ recovery in permeate	90	85.7	87.0	75.2

It is seen that when the feed rate is increased by 10% (Part b1), H₂ recovery drops about 5%, but the permeate purity is maintained. When the feed composition is reduced from 90% to 85% H₂ (Part b2), H₂ recovery decreases by about 3% and permeate purity decreases by about 2%. With 25% of the membrane area inoperative (Part b3), H₂ recovery decreases by about 15%, but the permeate purity is about 1% higher. Overall, percentage changes in H₂ recovery and purity are less than the percentage changes in feed flow rate, feed composition, and membrane area, thus confirming the insensitivity of gas-permeation separators to changes in operating conditions.

§14.8 PERVAPORATION

Figure 14.22 depicts pervaporation (PV), which differs from dialysis, reverse osmosis, and gas permeation in that the phase on one side of the membrane is different from that on the other. Feed to the membrane module is a liquid mixture at pressure P_1 , which is high enough to maintain a liquid phase as the feed begins to be depleted of species A and B to produce liquid retentate. A composite membrane is used that is selective for species A, but with some finite permeability for species B. The dense, thin-film side of the membrane is in contact with the liquid side. The retentate is enriched in species B. Generally, a sweep fluid is not used on the other side of the membrane, but a pressure P_2 , which may be a vacuum, is held at or below the dew point of the permeate, causing it to vaporize. Vaporization may occur near the downstream face such that the membrane operates with two zones, a liquid-phase and a vapor-phase zone, as shown in Figure 14.22. Alternatively, the vapor phase may exist only on the permeate side of the membrane. The vapor permeate is enriched in species A. Overall permeabilities of species A and B depend on solubilities and diffusion rates. Generally, solubilities cause the membrane to swell.

The term **pervaporation** is a combination of the words “permselective” and “evaporation.” It was first reported in 1917 by Kober [43], who studied several experimental techniques for removing water from albumin–toluene solutions. The economic potential of PV was shown by Binning et al. [44] in 1961, but commercial applications were delayed until the mid-1970s, when suitable membrane materials became available. Major commercial applications

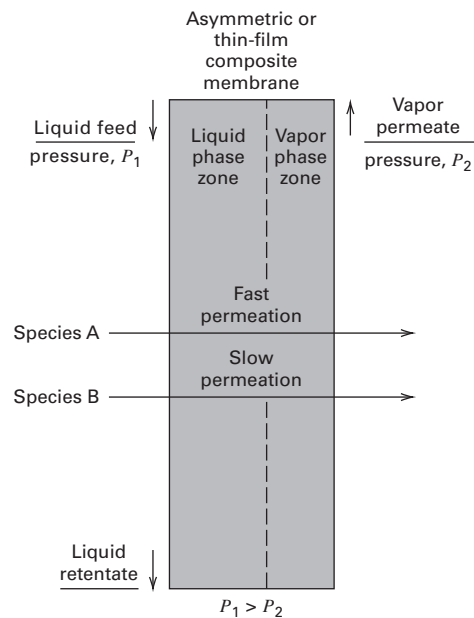


Figure 14.22 Pervaporation.

now include (1) dehydration of ethanol; (2) dehydration of other organic alcohols, ketones, and esters; and (3) removal of dissolved organics from water. The separation of close-boiling organic mixtures like benzene-cyclohexane is receiving much attention. Applications to the separation of other hydrocarbon and organic mixtures at elevated temperatures will require advanced membranes and modules.

Pervaporation is favored when the feed solution is dilute in the main permeant because sensible heat of the feed mixture provides the permeant enthalpy of vaporization. If the feed is rich in the main permeant, a number of membrane stages may be needed, with a small amount of permeant produced per stage and reheating of the retentate between stages. Even when only one membrane stage is sufficient, the feed liquid may be preheated.

Many pervaporation schemes have been proposed [6], with three important ones shown in Figure 14.23. A hybrid process for integrating distillation with pervaporation to produce 99.5 wt% ethanol from a feed of 60 wt% ethanol is shown in Figure 14.23a. Feed is sent to a distillation column operating

at near-ambient pressure, where a bottoms product of nearly pure water and an ethanol-rich distillate of 95 wt% is produced. The distillate purity is limited by the 95.6 wt% ethanol-water azeotrope. The distillate is sent to a pervaporation unit, where a permeate of 25 wt% alcohol and a retentate of 99.5 wt% ethanol is produced. The permeate vapor is condensed under vacuum and recycled to the distillation column. Figure 14.24 from Baker [5] shows the dramatic difference in separability by pervaporation as compared to distillation. For pervaporation, compositions refer to a liquid feed (abscissa) and a vapor permeate (ordinate) at 60°C for membranes of PVA, CTA, and Anionic Polyelectrolyte under vacuum. There is no limitation on ethanol purity, and the separation index is high for feeds of > 90 wt% ethanol.

A pervaporation process for dehydrating dichloroethylene (DCE) is shown in Figure 14.23b. The liquid feed, which is DCE saturated with water (0.2 wt%), is preheated to 90°C at 0.7 atm and sent to a PVA membrane system, which produces a retentate of almost pure DCE (< 10 ppm H₂O) and a permeate vapor of 50 wt% DCE. Following condensation, the two

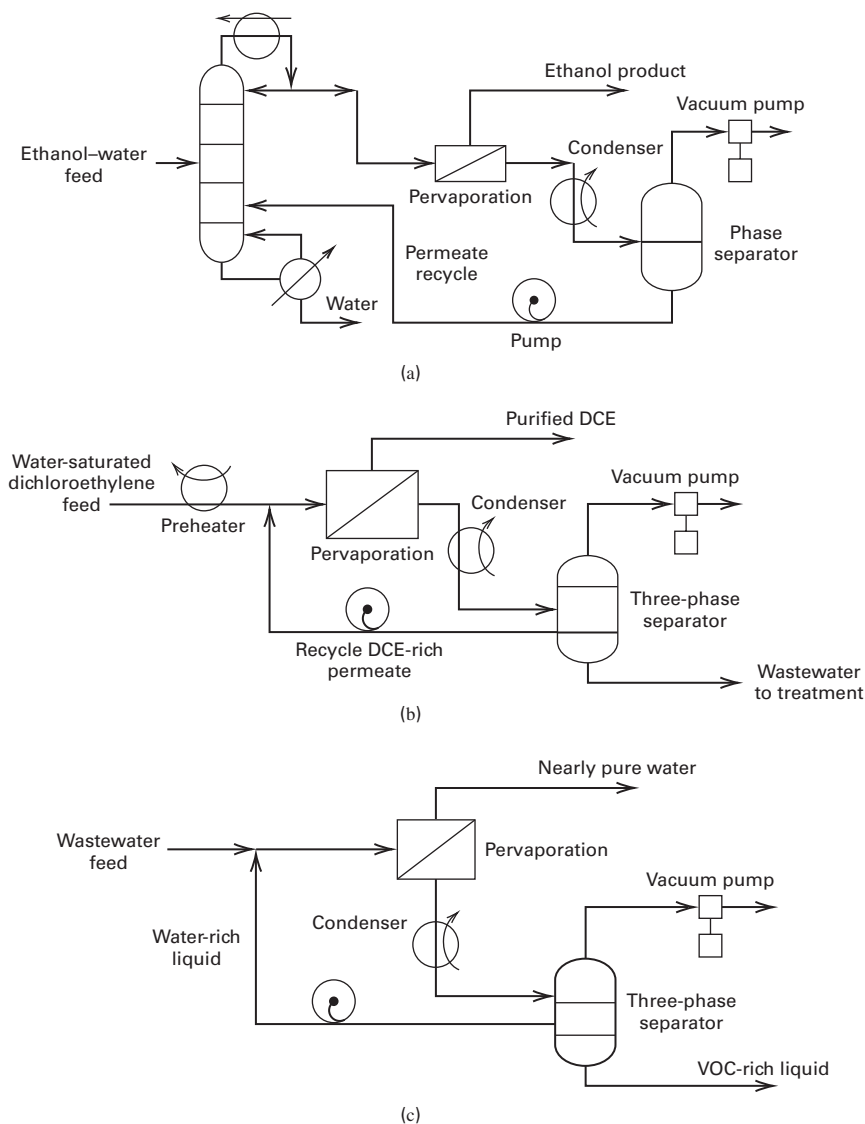


Figure 14.23 Pervaporation processes. (a) Hybrid process for removal of water from ethanol. (b) Dehydration of dichloroethylene. (c) Removal of volatile organic compounds (VOCs) from wastewater.

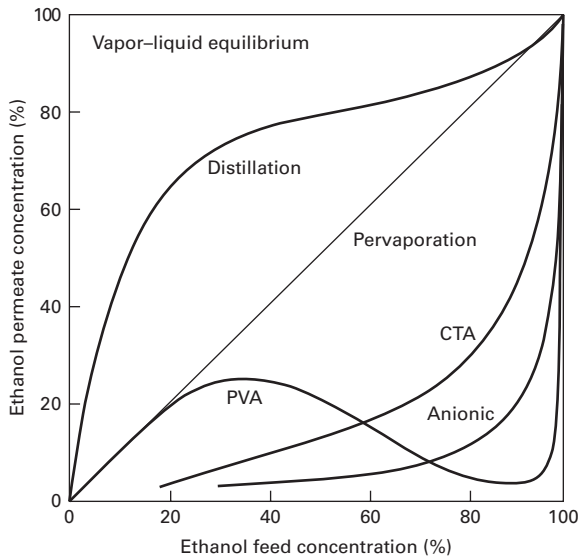


Figure 14.24 Comparison of ethanol–water separabilities for distillation and pervaporation with three different membranes. [Reproduced from [5] with permission of John Wiley and Sons.]

resulting liquid phases are separated, with the DCE-rich phase recycled and the water-rich phase sent to an air stripper, steam stripper, adsorption unit, or hydrophobic, pervaporation membrane system for residual DCE removal.

For removal of VOCs (e.g., toluene and trichloroethylene) from wastewater, pervaporation with hollow-fiber modules of silicone rubber can be used, as shown in Figure 14.23c. The retentate is almost pure water (<5 ppb of VOCs) and the permeate, after condensation, is (1) a water-rich phase that is recycled to the membrane system and (2) a nearly pure VOC phase.

A pervaporation module may operate with heat transfer or adiabatically, with the enthalpy of vaporization supplied by feed enthalpy. Consider the adiabatic pervaporation of a binary liquid mixture of A and B. Ignore heat of mixing. For an enthalpy datum temperature of T_0 , an enthalpy balance, in terms of mass flow rates m , liquid sensible heats C_P , and heats of vaporization ΔH^{vap} , gives

$$\begin{aligned} & (m_{A_F} C_{P_A} + m_{B_F} C_{P_B}) (T_F - T_0) \\ &= [(m_{A_F} - m_{A_P}) C_{P_A} + (m_{B_F} - m_{B_P}) C_{P_B}] (T_R - T_0) \\ &+ (m_{A_P} C_{P_A} + m_{B_P} C_{P_B}) (T_P - T_0) + m_{A_P} \Delta H_A^{\text{vap}} \\ &+ m_{B_P} \Delta H_B^{\text{vap}} \end{aligned} \quad (14-74)$$

where enthalpies of vaporization are evaluated at T_P . After collection of terms, (14-74) reduces to

$$\begin{aligned} & (m_{A_F} C_{P_A} + m_{B_F} C_{P_B}) (T_F - T_R) \\ &= (m_{A_P} C_{P_A} + m_{B_P} C_{P_B}) (T_P - T_R) \\ &+ (m_{A_P} \Delta H_A^{\text{vap}} + m_{B_P} \Delta H_B^{\text{vap}}) \end{aligned} \quad (14-75)$$

Permeate temperature, T_P , is the dew point at the permeate vacuum upstream of the condenser. The retentate temperature is computed from (14-75).

Membrane selection is critical in the commercial application of PV. For water permeation, hydrophilic membrane materials are preferred. For example, a three-layer composite membrane is used for the dehydration of ethanol, with water being the main permeating species. The support layer is porous polyester, which is cast on a microporous polyacrylonitrile or polysulfone membrane. The final layer, which provides the separation, is dense PVA, 0.1 μm in thickness. This composite combines chemical and thermal stability with adequate permeability. Hydrophobic membranes, such as silicone rubber and Teflon, are preferred when organics are the permeating species.

Commercial membrane modules for PV are almost exclusively of the plate-and-frame type because of the need for gasketing materials that are resistant to organic solvents and the ease of providing heat exchange for vaporization and high-temperature operation. Hollow-fiber modules are used for removal of VOCs from wastewater. Because feeds are generally clean and operation is at low pressure, membrane fouling and damage is minimal, resulting in a useful membrane life of 2–4 years.

Models for transport of permeant through a membrane by pervaporation have been proposed, based on the solution-diffusion concept. They assume equilibrium between the upstream liquid and the upstream membrane surface, and between the downstream vapor and its membrane side. Membrane transport follows Fick's law, with a permeant concentration gradient as the driving force. However, because of phase change and nonideal-solution feed, simple equations like (14-56) for dialysis and (14-32) for gas permeation are inadequate.

A convenient PV model is that of Wijmans and Baker [46], who express the driving force for permeation in terms of a partial-vapor-pressure difference. Because pressures on both sides of the membrane are low, the gas phase follows the ideal-gas law. Therefore, at the upstream membrane surface (1), permeant activity for component i is

$$a_i^{(1)} = f_i^{(1)} / f_i^{(0)} = p_i^{(1)} / P_i^s \quad (14-76)$$

where P_i^s is the vapor pressure at the feed temperature. Liquid on the upstream side of the membrane is generally nonideal. From Table 2.1:

$$a_i^{(1)} = \gamma_i^{(1)} x_i^{(1)} \quad (14-77)$$

Combining (14-76) and (14-77):

$$p_i^{(1)} = \gamma_i^{(1)} x_i^{(1)} P_i^s \quad (14-78)$$

On the vapor side of the membrane (2), partial pressure is

$$p_i^{(2)} = y_i^{(2)} P_P^{(2)} \quad (14-79)$$

Thus, the driving force can be expressed as

$$\gamma_i^{(1)} x_i^{(1)} P_i^s - y_i^{(2)} P_P^{(2)}$$

The corresponding permeant flux, after dropping unnecessary superscripts, is

$$N_i = \frac{P_{M_i}}{l_M} (\gamma_i x_i P_i^s - y_i P_P) \quad (14-80)$$

or

$$N_i = \bar{P}_{M_i} (\gamma_i x_i P_i^s - y_i P_P) \quad (14-81)$$

where γ_i and x_i refer to feed-side liquid, P_i^s is the vapor pressure at the feed-side temperature, y_i is the mole fraction in the permeant vapor, and P_P is total permeant pressure. Unlike gas permeation, where P_{M_i} depends mainly on permeant, polymer, and temperature, the permeability for pervaporation depends also on the concentrations of permeants in the polymer, which can be large enough to cause swelling and cross-diffusion. It is thus best to back-calculate and correlate permeant flux with feed composition at a given feed temperature and permeate pressure. Because of nonideal effects, selectivity can be a strong function of feed concentration and permeate pressure, causing inversion of selectivity, as illustrated next.

EXAMPLE 14.12 Pervaporation for Purification of Ethanol.

Wesslein et al. [45] present the following experimental data for the pervaporation of liquid mixtures of ethanol (1) and water (2) at a feed temperature of 60°C for a permeate pressure of 76 mmHg, using a commercial polyvinylalcohol membrane:

wt% Ethanol		Total Permeation Flux, kg/m ² -h
Feed	Permeate	
8.8	10.0	2.48
17.0	16.5	2.43
26.8	21.5	2.18
36.4	23.0	1.73
49.0	22.5	1.46
60.2	17.5	0.92
68.8	13.0	0.58
75.8	9.0	0.40

At 60°C, vapor pressures are 352 and 149 mmHg for ethanol and water, respectively.

Liquid-phase activity coefficients at 60°C for the ethanol (1)–water (2) system are given by van Laar equations (§2.7.1):

$$\ln \gamma_1 = 1.6276 \left[\frac{0.9232x_2}{1.626x_1 + 0.9232x_2} \right]^2$$

$$\ln \gamma_2 = 0.9232 \left[\frac{1.6276x_1}{1.6276x_1 + 0.9232x_2} \right]^2$$

Calculate permeance for water and ethanol from (14-81).

Solution

For the first row of data, mole fractions in the feed, x_i , and permeate, y_i , with $MW_1 = 46.07$ and $MW_2 = 18.02$, are

$$x_1 = \frac{0.88/46.07}{0.088 + \frac{(1.0 - 0.088)}{18.02}} = 0.0364$$

$$x_2 = 1.0 - 0.0364 = 0.9636$$

$$y_1 = \frac{0.10/46.07}{\frac{0.10}{46.07} + \frac{0.90}{18.02}} = 0.0416$$

$$y_2 = 1.0 - 0.0416 = 0.9584$$

Activity coefficients for the feed mixture are

$$\gamma_1 = \exp \left\{ 1.6276 \left[\frac{0.9232(0.9636)}{1.6276(0.0364) + 0.9232(0.9636)} \right]^2 \right\} = 4.182$$

$$\gamma_2 = \exp \left\{ 0.9232 \left[\frac{1.6276(0.0364)}{1.6276(0.0364) + 0.9232(0.9636)} \right]^2 \right\} = 1.004$$

From the total mass flux, component molar fluxes are

$$N_1 = \frac{(2.48)(0.10)}{46.07} = 0.00538 \frac{\text{kmol}}{\text{h} \cdot \text{m}^2}$$

$$N_2 = \frac{(2.48)(0.90)}{18.02} = 0.1239 \frac{\text{kmol}}{\text{h} \cdot \text{m}^2}$$

From (14-81), permeance values are

$$\bar{P}_{M_1} = \frac{0.00538}{(4.182)(0.0364)(352) - (0.0416)(76)}$$

$$= 0.000107 \text{ kmol/h} \cdot \text{m}^2 \cdot \text{mmHg}$$

$$\bar{P}_{M_2} = \frac{0.1239}{(2.004)(1.0 - 0.364)(149) - (1.0 - 0.0416)(76)}$$

$$= 0.001739 \text{ kmol/h} \cdot \text{m}^2 \cdot \text{mmHg}$$

Results for other feed conditions are computed in a similar manner:

wt% Ethanol		Activity Coefficient in Feed		Permeance, kmol/h-m ² -mmHg	
Feed	Permeate	Ethanol	Water	Ethanol	Water
8.8	10.0	4.182	1.004	1.07 × 10 ⁻⁴	1.74 × 10 ⁻³
17.0	16.5	3.489	1.014	1.02 × 10 ⁻⁴	1.62 × 10 ⁻³
26.8	21.5	2.823	1.038	8.69 × 10 ⁻⁵	1.43 × 10 ⁻³
36.4	23.0	2.309	1.077	6.14 × 10 ⁻⁵	1.17 × 10 ⁻³
49.0	22.5	1.802	1.158	4.31 × 10 ⁻⁵	1.10 × 10 ⁻³
60.2	17.5	1.477	1.272	1.87 × 10 ⁻⁵	8.61 × 10 ⁻⁴
68.8	13.0	1.292	1.399	7.93 × 10 ⁻⁶	6.98 × 10 ⁻⁴
75.8	9.0	1.177	1.539	3.47 × 10 ⁻⁶	6.75 × 10 ⁻⁴

The PVA membrane is hydrophilic. As concentration of ethanol in the feed liquid increases, sorption of feed liquid by the membrane decreases, reducing polymer swelling. As swelling is reduced, the permeance of ethanol decreases more rapidly than that of water, thus increasing selectivity for water. For example, selectivity for water can be defined as

$$\alpha_{2,1} = \frac{(100 - w_1)_P / (w_1)_P}{(100 - w_1)_F / (w_1)_F}$$

where w_1 = weight fraction of ethanol. For cases of 8.8 and 75.8 wt% ethanol in the feed, the selectivities for water are, respectively, 0.868 (more selective for ethanol) and 31.7 (more selective for water).

CHAPTER 14 NOMENCLATURE

Abbreviations and Acronyms

A	anion selective membrane, Figure 14.14
C	cation selective membrane, Figure 14.14
GP	gas permeation, Section 14.7
MF	microfiltration, Section 14.1
NF	nanofiltration, Section 14.1
PV	pervaporation, Section 14.8
RO	reverse osmosis, Section 14.6
UF	ultrafiltration, Section 14.1

Latin Symbols

A_M	membrane area, (14-5) in Example 14.5
a_v	specific surface area, (14-5)
c_M	total molar concentration of a gas mixture, (14-17)
c_i	solute concentrations at various locations, (14-13)
Δc	difference in ion concentrations, (14-59)
c_s	salt concentration, (14-72)
c_w	water concentration, Figure 14.19
D	pore diameter, (14-2)
D_i	solute diffusivity in a membrane, (14-25)
D_p	particle diameter, (14-10)
D_e	effective diffusivity, (14-13)
D_L	Langmuir diffusivity of sorbed species, (14-35)
d_H	hydraulic diameter, (14-5)
d_m	molecular diameter, (14-5)
d_p	pore diameter, (14-5)
E	voltage, (14-60)
E_D	activation energy, (14-34)
E°	standard electrical potential, Section 14.5
F	Faraday's constant, (14-59)
$f^{(0)}$	standard state fugacity, (14-76)
I	electric current, (14-60)
i	current density (current/unit area), (14-59)
K	overall mass transfer coefficient, (14-56)
K_r	solute restrictive factor, (14-14)

K_i	solute solubility in membrane, (14-27)
k	mass-transfer coefficient, (14-54)
\bar{m}	summation of molarities, (14-69)
m	mass flow rate, (14-74)
N	flux, mass flow/unit area, (14-4)
n	number of cell pairs, (14-61)
P	electrical power, (14-60)
P_M	permeability, (14-1)
\bar{P}_M	permeance = permeability/unit membrane thickness, (14-1)
Q	diluate volumetric flow rate, (14-59)
r	pressure ratio, P_p/P_F , (14-41)
$S_{i,j}$	selectivity ratio, (14-16)
SP	salt passage, (14-71)
SR	salt rejection, (14-71)
v_0	superficial liquid velocity through the bed, (14-10)

Greek Symbols

α	separation factor, (14-36)
α^*	ideal separation factor, (14-40)
Γ	polarization factor, (14-73)
ξ	current efficiency, (14-61)
θ	fraction of feed permeated, (14-44)
π	osmotic pressure, (14-66)

Subscripts

L	outside membrane surface, Fig. 14.7
M	membrane, (14-51)
0	feed membrane surface, Figure 14.7
P	permeate, Figure 14.7
R	retentate, Example 14.5

Superscripts

c	concentrate side, Figure 14.16
d	dilute side, Figure 14.16

SUMMARY

1. Separation of liquid and gas mixtures with membranes is an emerging separation operation. Applications began accelerating in the 1980s. The products of separation are retentate and permeate.
2. The key to an efficient and economical membrane-separation process is the membrane. It must have good permeability, high selectivity, solute compatibility, high capacity, stability, freedom from fouling, a long life, and a reasonable cost.
3. Commercialized membrane-separation processes include dialysis, electrodialysis, reverse osmosis, gas permeation, pervaporation, ultrafiltration, and microfiltration.
4. Membranes for commercial separation processes are natural or synthetic, and glassy or rubbery polymers cast as a

film from a solvent mixture. However, for high-temperature (>200°C) operations with chemically reactive mixtures, ceramics, metals, and carbon find applications.

5. For high permeability and selectivity, dense, nonporous membranes are preferred. For mechanical integrity, membranes 0.1–1.0 μm thick are incorporated as a surface layer or film on a thicker, porous asymmetric or composite membrane.
6. To achieve a high surface area per unit volume, membranes are fabricated into spiral-wound or hollow-fiber modules. Less surface area per volume is available in plate-and-frame, tubular, and monolithic modules.
7. Permeation through a membrane occurs by many mechanisms. For a microporous membrane, mechanisms include bulk flow (no selectivity), liquid and gas diffusion, Knudsen diffusion, restrictive diffusion, sieving, and surface diffusion. For a nonporous membrane, a solution-diffusion mechanism applies.
8. Flow patterns in membrane modules have a profound effect on overall permeation rates. Idealized flow patterns for which theory has been developed include perfect mixing, countercurrent flow, cocurrent flow, and crossflow. To overcome separation limits of a single membrane module stage, modules can be arranged in series and/or parallel cascades.
9. In gas permeation, film mass-transfer resistances on either side of the membrane are usually negligible compared to the membrane resistance. For separation of liquid mixtures, external mass-transfer effects and concentration polarization can be significant.
10. Component mass-transfer fluxes through a membrane can be formulated as the product of two terms: (1) permeance

\bar{P}_{M_i} , which is the ratio of the permeability, P_{M_i} , to the membrane thickness, l_M ; and (2) a driving force based on concentration, partial pressure, fugacity, or activity.

11. In dialysis of a liquid mixture, a microporous membrane is used to separate small solutes of type A from the solvent and larger solutes of type B. The driving force is the concentration difference across the membrane. Transport of solvent can be minimized by adjusting pressure differences across the membrane to equal osmotic pressure.
12. In electrodialysis, a series of alternating cation- and anion-selective membranes are used with a direct-current voltage across an outer anode and an outer cathode to concentrate an electrolyte.
13. In reverse osmosis, the solvent of a liquid mixture is selectively transported through a dense membrane. By this means, seawater can be desalinated. The driving force for solvent transport is fugacity difference, which is commonly expressed in terms of $\Delta P - \Delta\pi$, where π is the osmotic pressure.
14. In gas permeation, mixtures of gases are separated by differences in permeation rates through dense membranes. The driving force for each component is its partial-pressure difference, Δp_i , across the membrane. Both permeance and permeability depend on membrane absorptivity for the particular gas species and species diffusivity. Thus, $P_{M_i} = H_i D_i$.
15. In pervaporation, a liquid mixture is separated with a dense membrane by a vacuum on the permeate side of the membrane so as to evaporate the permeate. The driving force may be approximated as a fugacity difference expressed by $(\gamma_i x_i P_i^s - y_i P_p)$. Permeability varies with concentration because of membrane swelling.

REFERENCES

1. LONSDALE, H.K., *J. Membrane Sci.*, **10**, 81 (1982).
2. APPLGATE, L.E., *Chem. Eng.*, **91**(12), 64–89 (1984).
3. HAVENS, G.G., and D.B. GUY, *Chem. Eng. Progress Symp. Series*, **64**(90), 299 (1968).
4. BOLLINGER, W.A., D.L. MACLEAN, and R.S. NARAYAN, *Chem. Eng. Progress*, **78**(10), 27–32 (1982).
5. BAKER, R.W., *Membrane Technology and Applications*, 3rd edition, John Wiley & Sons, New York, NY (2012).
6. HO, W.S.W., and K.K. SIRKAR, Eds., *Membrane Handbook*, Van Nostrand Reinhold, New York (1992).
7. LOEB, S., and S. SOURIRAJAN, *Advances in Chemistry Series*, Vol. **38**, *Saline Water Conversion II* (1963).
8. HENIS, J.M.S., and M.K. TRIPODI, U.S. Patent 4,230,463 (1980).
9. WRASIDLO, W.J., U.S. Patent 3,951,815 (1977).
10. BARRER, R.M., *J. Chem. Soc.*, 378–386 (1934).
11. BARRER, R.M., *Diffusion in and through Solids*, Cambridge Press, London (1951).
12. MAHON, H.I., U.S. Patent 3,228,876 (1966).
13. MAHON, H.I., U.S. Patent 3,228,877 (1966).
14. HSIEH, H.P., R.R. BHAVE, and H.L. FLEMING, *J. Membrane Sci.*, **39**, 221–241 (1988).
15. BIRD, R.B., W.E. STEWART, and E.N. LIGHTFOOT, *Transport Phenomena*, John Wiley & Sons, New York, pp. 42–47 (1960).
16. ERGUN, S., *Chem. Eng. Progress*, **48**, 89–94 (1952).
17. BECK, R.E., and J.S. SCHULTZ, *Science*, **170**, 1302–1305 (1970).
18. BECK, R.E., and J.S. SCHULTZ, *Biochim. Biophys. Acta*, **255**, 273 (1972).
19. BRANDRUP, J., E.H. IMMERGUT, and E.A. GRULKE, Eds., *Polymer Handbook*, 4th ed., Wiley Interscience, New York (2003).
20. LONSDALE, H.K., U. MERTEN, and R.L. RILEY, *J. Applied Polym. Sci.*, **9**, 1341–1362 (1965).
21. MOTAMEDIAN, S., W. PUSCH, G. SENDELBACH, T.-M. TAK, and T. TANIOKA, *Proceedings of the 1990 International Congress on Membranes and Membrane Processes*, Chicago, Vol. **II**, pp. 841–843 (1990).
22. BARRER, R.M., J.A. BARRIE, and J. SLATER, *J. Polym. Sci.*, **23**, 315–329 (1957).
23. BARRER, R.M., and J.A. BARRIE, *J. Polym. Sci.*, **23**, 331–344 (1957).
24. BARRER, R.M., J.A. BARRIE, and J. SLATER, *J. Polym. Sci.*, **27**, 177–197 (1958).

25. KOROS, W.J., and D.R. PAUL, *J. Polym. Sci., Polym. Physics Edition*, **16**, 1947–1963 (1978).
26. BARRER, R.M., *J. Membrane Sci.*, **18**, 25–35 (1984).
27. WALAWENDER, W.P., and S.A. STERN, *Separation Sci.*, **7**, 553–584 (1972).
28. NAYLOR, R.W., and P.O. BACKER, *AIChE J.*, **1**, 95–99 (1955).
29. STERN, S.A., T.F. SINCLAIR, P.J. GAREIS, N.P. VAHLDIECK, and P.H. MOHR, *Ind. Eng. Chem.*, **57**(2), 49–60 (1965).
30. HWANG, S.-T., and K.L. KAMMERMEYER, *Membranes in Separations*, Wiley-Interscience, New York, pp. 324–338 (1975).
31. SPILLMAN, R.W., *Chem. Eng. Progress*, **85**(1), 41–62 (1989).
32. STRATHMANN, H., “Membrane and Membrane Separation Processes,” in *Ullmann’s Encyclopedia of Industrial Chemistry*, VCH, FRG, Vol. **A16**, p. 237 (1990).
33. CHAMBERLIN, N.S., and B.H. VROMEN, *Chem. Engr.*, **66**(9), 117–122 (1959).
34. GRAHAM, T., *Phil. Trans. Roy. Soc. London*, **151**, 183–224 (1861).
35. JUDA, W., and W.A. MCRAE, *J. Amer. Chem. Soc.*, **72**, 1044 (1950).
36. STRATHMANN, H., *Sep. and Purif. Methods*, **14**(1), 41–66 (1985).

37. MERTEN, U., *Ind. Eng. Chem. Fundamentals*, **2**, 229–232 (1963).
38. STOUGHTON, R.W., and M.H. LIETZKE, *J. Chem. Eng. Data*, **10**, 254–260 (1965).
39. SPILLMAN, R.W., and M.B. SHERWIN, *Chemtech*, 378–384 (June 1990).
40. SCHELL, W.J., and C.D. HOUSTON, *Chem. Eng. Progress*, **78**(10), 33–37 (1982).
41. TEPLYAKOV, V., and P. MEARES, *Gas Sep. and Purif.*, **4**, 66–74 (1990).
42. ROSENZWEIG, M.D., *Chem. Eng.*, **88**(24), 62–66 (1981).
43. KOBER, P.A., *J. Am. Chem. Soc.*, **39**, 944–948 (1917).
44. BINNING, R.C., R.J. LEE, J.F. JENNINGS, and E.C. MARTIN, *Ind. Eng. Chem.*, **53**, 45–50 (1961).
45. WESSLEIN, M., A. HEINTZ, and R.N. LICHTENTHALER, *J. Membrane Sci.*, **51**, 169 (1990).
46. WIJMANS, J.G., and R.W. BAKER, *J. Membrane Sci.*, **79**, 101–113 (1993).
47. RAUTENBACH, R., and R. ALBRECHT, *Membrane Processes*, John Wiley & Sons, New York (1989).
48. RAO, M.B., and S. SIRCAR, *J. Membrane Sci.*, **85**, 253–264 (1993).

STUDY QUESTIONS

- 14.1. What are the two products from a membrane separation called? What is a sweep?
- 14.2. From what kinds of materials are membranes made? Can a membrane be porous or nonporous? What forms pores in polymer membranes?
- 14.3. What is the basic equation for computing the rate of mass transfer through a membrane? Explain each of the four factors in the equation and how they can be exploited to obtain high rates of mass transfer.
- 14.4. What is the difference between permeability and permeance? How are they analogous to diffusivity and the mass-transfer coefficient?
- 14.5. For a membrane separation, is it usually possible to achieve both a high permeability and a large separation factor?
- 14.6. What are the three mechanisms for mass transfer through a porous membrane? Which are the best mechanisms for making a separation? Why?
- 14.7. What is the mechanism for mass transfer through a dense (nonporous) membrane? Why is it called solution-diffusion?

Does this mechanism work if the polymer is completely crystalline? Explain.

- 14.8. How do the solution-diffusion equations differ for liquid transport and gas transport? How is Henry’s law used in solution-diffusion for gas transport? Why are the film resistances to mass transfer on either side of the membrane for gas permeation often negligible?
- 14.9. What are the four idealized flow patterns in membrane modules? Which is the most effective? Which is the most difficult to calculate?
- 14.10. What is osmosis? Can it be used to separate a liquid mixture? How does it differ from reverse osmosis? For what type of mixtures is it well suited?
- 14.11. Can a near-perfect separation be made with gas permeation? If not, why not?
- 14.12. What is pervaporation?

EXERCISES

Section 14.1

14.1. Differences between membrane separations and other separations.

Explain, as completely as you can, how membrane separations differ from (a) absorption and stripping; (b) distillation; (c) liquid–liquid extraction; (d) extractive distillation.

14.2. Barrer units for permeabilities.

For the commercial application of membrane separators discussed at the beginning of this chapter, calculate the permeabilities of hydrogen and methane in Barrer units.

14.3. Membrane separation of N_2 from CH_4 .

A new asymmetric, polyimide polymer membrane has been developed for the separation of N_2 from CH_4 . At 30°C, permeance values are 50,000 and 10,000 Barrer/cm for N_2 and CH_4 , respectively. If this new membrane is used to perform the separation in Figure 14.25,

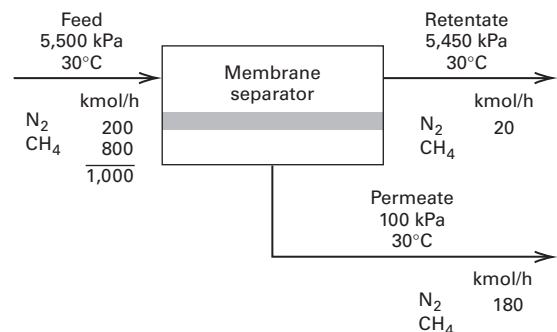


Figure 14.25 Data for Exercise 14.3.

determine the membrane surface area in m^2 , and the kmol/h of CH_4 in the permeate. Base the driving force for diffusion on the arithmetic average of the partial pressures of the entering feed and the exiting retentate, with the permeate-side partial pressures at exit condition.

Section 14.2

14.4. Characteristics of a hollow-fiber module.

A hollow-fiber module has 4,000 ft^2 of membrane surface area based on the size of the fibers, which are $42 \mu m$ i.d. \times $85 \mu m$ o.d. \times 1.2 m long each. Determine the (a) number of hollow fibers in the module; (b) diameter of the module, assuming the fibers are on a square spacing of $120 \mu m$ center-to-center; and (c) membrane surface area per unit volume of module (packing density) m^2/m^3 . Compare your result with that in Table 14.4.

14.5. Geometry of a membrane module.

A spiral-wound module made from a flat sheet of membrane material is 0.3 m in diameter and 3 m long. If the packing density (membrane surface area/unit module volume) is $500 m^2/m^3$, what is the center-to-center spacing of the membrane in the spiral, assuming a collection tube 1 cm in diameter?

14.6. Characteristics of a monolithic element.

A monolithic membrane element of the type shown in Figure 14.4d contains 19 flow channels of 0.5 cm in inside diameter by 0.85 m long. If 9 of these elements are in a cylindrical module of the type in Figure 14.5f, determine values for (a) module volume in m^3 and (b) packing density in m^2/m^3 . Compare your value with those for other membrane modules in Table 14.4.

Section 14.3

14.7. Porous membrane with pressure differential.

Water at $70^\circ C$ passes through a polyethylene membrane of 25% porosity with an average pore diameter of $0.3 \mu m$ and an average tortuosity of 1.3. The pressures on the downstream and upstream sides of the membrane are 125 and 500 kPa, respectively. Estimate the flux of water in m^3/m^2 -day.

14.8. Knudsen flow in a membrane.

A porous-glass membrane, with an average pore diameter of 40 \AA , is used to separate light gases at $25^\circ C$ when Knudsen flow may be dominant. The pressures are 15 psia downstream and not >120 psia upstream. The membrane has been calibrated with pure helium gas, giving a constant permeability of 117,000 Barrer. Experiments with pure CO_2 give a permeability of 68,000 Barrer. Assuming that helium is in Knudsen flow, predict the permeability of CO_2 . Is it in agreement with the experimental value? If not, suggest an explanation. Reference: Kammermeyer, K., and L.O. Rutz, *C.E.P. Symp. Ser.*, **55**(24), 163–169 (1959).

14.9. Partial condensation and surface diffusion.

Two mechanisms for the gas transport through a porous membrane not discussed in §14.3 or illustrated in Figure 14.6 are (1) partial condensation in the pores by some components of the gas mixture to the exclusion of other components, and subsequent transport of the condensed molecules through the pore, and (2) selective adsorption on pore surfaces of some components and subsequent surface diffusion across the pores. In particular, Rao and Sircar [48] have found that the latter mechanism provides a potentially attractive means for separating hydrocarbons from hydrogen for low-pressure gas streams. In porous-carbon membranes with continuous pores 4–15 \AA in diameter, little pore void space is available for Knudsen diffusion of hydrogen when the hydrocarbons are selectively adsorbed.

Typically, the membranes are not more than $5 \mu m$ in thickness. Measurements at 295.1 K of permeabilities for five pure components and a mixture of the five components are as follows:

Component	Permeability, Barrer		mol% in the Mixture
	As a Pure Gas	In the Mixture	
H_2	130	1.2	41.0
CH_4	660	1.3	20.2
C_2H_6	850	7.7	9.5
C_3H_8	290	25.4	9.4
nC_4H_{10}	155	112.3	19.9
Total			100.0

A refinery waste gas mixture of the preceding composition is to be processed through such a porous-carbon membrane. If the pressure of the gas is 1.2 atm and an inert sweep gas is used on the permeate side such that partial pressures of feed-gas components on that side are close to zero, determine the permeate composition on a sweep-gas-free basis when the composition on the upstream pressure side of the membrane is that of the feed gas. Explain why the component permeabilities differ so much between pure gas and the gas mixture.

14.10. Module flow pattern and membrane area.

A mixture of 60 mol% propylene and 40 mol% propane at a flow rate of 100 lbmol/h and at $25^\circ C$ and 300 psia is to be separated with a polyvinyltrimethylsilane polymer (see Table 14.9 for permeabilities). The membrane skin is $0.1 \mu m$ thick, and spiral-wound modules are used with a pressure of 15 psia on the permeate side. Calculate the material balance and membrane area in m^2 as a function of the cut (fraction of feed permeated) for (a) perfect-mixing flow pattern and (b) crossflow pattern.

14.11. Membrane area for gas permeation.

Repeat part (a) of Exercise 14.10 for the two-stage stripping cascade and two-stage enriching cascade shown in Figure 14.11. However, select just one set of reasonable cuts for the two stages of each case so as to produce 40 lbmol/h of final retentate.

14.12. Concentration polarization in dialysis.

Repeat Example 14.7 with the following changes: tube-side Reynolds number = 25,000; tube inside diameter = 0.4 cm; permeate-side mass-transfer coefficient = 0.06 cm/s . How important is concentration polarization?

14.13. Gas permeation through a rubber stopper.

Carbon dioxide at 2 atm and $25^\circ C$ is stored in a cylinder with a flat, circular plug stopper of vulcanized rubber, 3 cm thick and 2 cm^2 in area. Experimental data at $25^\circ C$ give the solubility of CO_2 in rubber as 0.90 cm^3 (at $0^\circ C$ and 1 atm)/ cm^3 of rubber/atm CO_2 and the diffusivity of CO_2 in rubber at $0.11 \times 10^{-5} \text{ cm}^2/\text{s}$, independent of pressure. Neglecting mass transfer resistances in the gas on either side of the stopper and a pressure of 1 atm outside of the cylinder, calculate rate of loss of CO_2 from the cylinder in mol/s.

14.14. Liquid diffusion through a porous membrane.

At one face of 0.3-cm thick sintered silica is an aqueous solution of 0.1-M KCl. Calculate the rate of diffusion of KCl through the silica into pure water at the other face. Neglect mass-transfer resistances on either side of the silica. The diffusivity of KCl is $1.87 \times 10^{-5} \text{ cm}^2/\text{s}$. The silica porosity is 0.3 and the tortuosity is 2.2. Assume a restrictive factor of 1.0. Calculate the diffusion rate of KCl in mol/s- cm^2 of silica surface area. Neglect diffusion of water through the membrane.

14.15. Knudsen diffusion.

Pure hydrogen at 1 atm and $100^\circ C$ diffuses through 0.6-cm thick plugs into pure nitrogen. In one case, the plug has straight pores of 130 \AA in diameter. In the second case, the pores are straight with a diameter of $18.3 \times 10^{-4} \text{ cm}$. The mean-free path of hydrogen is

1,400 Å. From Table 3.2, the diffusivity of hydrogen through nitrogen at 25°C and 1 atm is 0.784 cm²/s. Assuming that no nitrogen flows through the pores, calculate the flux of hydrogen in mol/s-cm² of pore cross-sectional area for each of the two cases.

Section 14.4

14.16. Dialysis to separate Na₂SO₄.

An aqueous process stream of 100 gal/h at 20°C contains 8 wt% Na₂SO₄ and 6 wt% of a high-molecular-weight substance (A). This stream is processed in a continuous countercurrent-flow dialyzer using a pure water sweep of the same flow rate. The membrane is a microporous cellophane with pore volume = 50%, wet thickness = 0.0051 cm, tortuosity = 4.1, and pore diameter = 31 Å. The molecules to be separated have the following properties:

	Na ₂ SO ₄	A
Molecular weight	142	1,000
Molecular diameter, Å	5.5	15.0
Diffusivity, cm ² /s × 10 ⁵	0.77	0.25

Calculate the membrane area in m² for only a 10% transfer of A through the membrane, assuming no transfer of water. What is the % recovery of the Na₂SO₄ in the diffusate? Use log-mean concentration-driving forces and assume the mass-transfer resistances on each side of the membrane are each 25% of the total mass-transfer resistances for Na₂SO₄ and A.

14.17. Removal of HCl by dialysis.

A dialyzer is to be used to separate 300 L/h of an aqueous solution containing 0.1-M NaCl and 0.2-M HCl. Laboratory experiments with the microporous membrane to be used give the following values for the overall mass-transfer coefficient K_i in (14-56) for a log-mean concentration-driving force:

	K_i , cm/min
Water	0.0025
NaCl	0.021
HCl	0.055

Determine the membrane area in m² for 90, 95, and 98% transfer of HCl to the diffusate. For each case, determine the complete material balance in mol/h for a sweep of 300 L/h.

Section 14.5

14.18. Desalinization by electrodialysis.

An total of 86,000 gal/day of an aqueous solution of 3,000 ppm of NaCl is to be desalinized to 400 ppm by electrodialysis, with a 40% conversion. The process will be conducted in four stages, with three stacks of 150 cell pairs in each stage. The fractional desalinization will be the same in each stage and the expected current efficiency is 90%. The applied voltage for the first stage is 220 V. Each cell pair has an area of 1,160 cm². Calculate the current density in mA/cm², the current in A, and the power in kW for the first stage. Reference: Mason, E.A., and T.A. Kirkham, *C.E.P. Symp. Ser.*, 55(24), 173–189 (1959).

Section 14.6

14.19. Reverse osmosis of seawater.

A reverse-osmosis plant is used to treat 30,000,000 gal/day of seawater at 20°C containing 3.5 wt% dissolved solids to produce 10,000,000 gal/day of potable water, with 500 ppm of dissolved

solids and the balance as brine containing 5.25 wt% dissolved solids. The feed-side pressure is 2,000 psia, while the permeate pressure is 50 psia. A single stage of spiral-wound membranes is used that approximates crossflow. If the total membrane area is 2,000,000 ft², estimate the permeance for water and the salt passage.

14.20. Reverse osmosis with multiple stages.

A reverse-osmosis process is to be designed to handle a feed flow rate of 100 gpm. Three designs have been proposed that differ in the percent recovery of potable water from the feed:

Design 1: A single stage consisting of four units in parallel to obtain a 50% recovery

Design 2: Two stages in series with respect to the retentate (four units in parallel followed by two units in parallel)

Design 3: Three stages in series with respect to the retentate (four units in parallel followed by two units in parallel followed by a single unit)

Draw the three designs and determine the percent recovery of potable water for Designs 2 and 3.

14.21. Concentration of Kraft black liquor by two-stage reverse osmosis.

Production of paper requires a pulping step to break down wood chips into cellulose and lignin. In the Kraft process, an aqueous solution known as white liquor and consisting of dissolved inorganic chemicals such as Na₂S and NaOH is used. Following removal of the pulp (primarily cellulose), a solution known as weak Kraft black liquor (KBL) is left, which is regenerated to recover white liquor for recycle. In this process, a 15 wt% (dissolved solids) KBL is concentrated to 45 to 70 wt% by multiple-effect evaporation. It is suggested that reverse osmosis be used to perform an initial concentration to 25 wt%. Higher concentrations may not be feasible because of the high osmotic pressure, which at 180°F and 25 wt% solids is 1,700 psia. Osmotic pressure for other conditions can be scaled with (14-69) using wt% instead of molality.

A two-stage RO process, shown in Figure 14.26, has been proposed to carry out this initial concentration for a feed rate of 1,000 lb/h at 180°F. A feed pressure of 1,756 psia is to be used for the first stage to yield a permeate of 0.4 wt% solids. The feed pressure to the second stage is 518 psia to produce water of 300 ppm dissolved solids and a retentate of 2.6 wt% solids. Permeate-side pressure for both stages is 15 psia. Equation (14-70) can be used to estimate membrane area, where the permeance for water can be taken as 0.0134 lb/ft²-hr-psi in conjunction with an arithmetic mean osmotic pressure for plug flow on the feed side. Complete the material balance for the process and estimate the required membrane areas for each stage. Reference: GOTTSCHLICH, D.E., and D.L. ROBERTS. *Final Report* DE91004710, SRI International, Menlo Park, CA, Sept. 28, 1990.

14.22. Osmotic pressure.

Many years before freeze drying was used, fruit juices were concentrated by immersion in brine solutions of membrane packaged

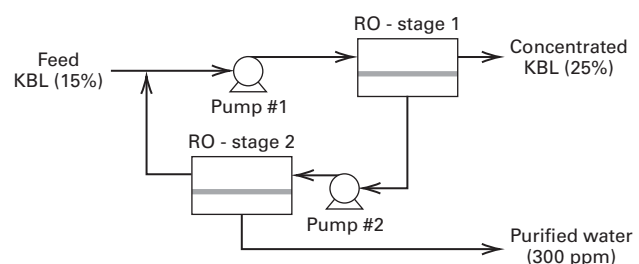


Figure 14.26 Data for Exercise 14.21.

juice. A fruit juice containing 1 weight percent dissolved sucrose (MW = 342) is to be concentrated at 10°C by reverse osmosis using a brine containing 35 g of NaCl (MW = 58.5) per 100 g water. The membrane is a plastic bag permeable to water but not to salt or sucrose. Calculate the difference in osmotic pressure at the beginning of the reverse osmosis process.

Section 14.7

14.23. Recovery of VOCs by gas permeation.

Gas permeation can be used to recover VOCs (volatile organic compounds) from air at low pressures using a highly selective membrane. In a typical application, 1,500 scfm (0°C, 1 atm) of air containing 0.5 mol% acetone (A) is fed to a spiral-wound membrane module at 40°C and 1.2 atm. A liquid-ring vacuum pump on the permeate side establishes a pressure of 4 cmHg. A silicone-rubber, thin-composite membrane with a 2- μ m-thick skin gives permeabilities of 4 Barrer for air and 20,000 Barrer for acetone.

If the retentate is to contain 0.05 mol% acetone and the permeate is to contain 5 mol% acetone, determine the membrane area required in m², assuming crossflow. References: (1) Peinemann, K.-V., J.M. Mohr, and R.W. Baker, *C.E.P. Symp. Series*, **82**(250), 19–26 (1986); (2) Baker, R.W., N. Yoshioka, J.M. Mohr, and A.J. Khan, *J. Membrane Sci.*, **31**, 259–271 (1987).

14.24. Separation of air by gas permeation.

Separation of air into N₂ and O₂ is widely practiced. Cryogenic distillation is most economical for processing 100 to 5,000 tons of air per day, while pressure-swing adsorption is favorable for 20 to 50 tons/day. For small-volume users requiring less than 10 tons/day, gas permeation finds applications, where for a single stage, either an oxygen-enriched air (40 mol% O₂) or 98 mol% N₂ can be produced. It is desired to produce a permeate of 5 tons/day (2,000 lb/ton) of 40 mol% oxygen and a retentate of nitrogen, ideally of 90 mol% purity, by gas permeation. Assume pressures of 500 psia (feed side) and 20 psia (permeate). Two companies who can supply the membrane modules have provided the following data:

	Company A	Company B
Module type	Hollow-fiber	Spiral-wound
\bar{P}_M for O ₂ , Barrer/ μ m	15	35
$\bar{P}_{M_{O_2}} / \bar{P}_{M_{N_2}}$	3.5	1.9

Determine the required membrane area in m² for each company. Assume that both module types approximate crossflow.

14.25. Removal of CO₂ and H₂S by permeation.

A joint venture has been underway for several years to develop a membrane process to separate CO₂ and H₂S from high-pressure, sour natural gas. Typical feed and product conditions are:

	Feed Gas	Pipeline Gas
Pressure, psia	1,000	980
Composition, mol%:		
CH ₄	70	97.96
H ₂ S	10	0.04
CO ₂	20	2.00

To meet these conditions, the following hollow-fiber membrane material targets have been established:

	Selectivity
CO ₂ —CH ₄	50
H ₂ S—CH ₄	50

where selectivity is the ratio of permeabilities. $P_{M_{CO_2}} = 13.3$ Barrer, and membrane skin thickness is expected to be 0.5 μ m. Make calculations to show whether the targets can realistically meet the pipeline-gas conditions in a single stage with a reasonable membrane area. Assume a feed-gas flow rate of 10×10^3 scfm (0°C, 1 atm) with crossflow. Reference: Stam, H., in L. Cecille and J.-C. Toussaint, Eds., *Future Industrial Prospects of Membrane Processes*, Elsevier Applied Science, London, pp. 135–152 (1989).

14.26. Separation of air with a low-density membrane.

A 0.1- μ m thick, low-density polyethylene membrane with properties given in Table 14.6 is to separate 37,000 m³ (at 25°C, 1 atm)/h of air (79 mol% N₂, 21 mol% O₂) into enriched O₂ (A) and enriched N₂ (B). The pressure on the feed-retentate side of the membrane is constant at 10 atm. The pressure on the permeate side is constant at 1 atm. Assume perfect mixing on both sides of the membrane and neglect the mass-transfer resistances in the gases on both sides of the membrane. Calculate the membrane surface area required and the mole-fraction compositions of the retentate and permeate for a cut fraction, θ , of 0.4.

Section 14.8

14.27. Separation by pervaporation.

Pervaporation is to be used to separate ethyl acetate (EA) from water. The feed rate is 100,000 gal/day of water containing 2.0 wt% EA at 30°C and 20 psia. The membrane is dense polydimethylsiloxane with a 1- μ m-thick skin in a spiral-wound module that approximates crossflow. The permeate pressure is 3 cmHg. The total measured membrane flux at these conditions is 1.0 L/m²-h with a separation factor given by (14-36) of 100 for EA with respect to water. A retentate of 0.2 wt% EA is desired for a permeate of 45.7 wt% EA. Determine the required membrane area in m² and the feed temperature drop. Reference: Blume, I., J.G. Wijans, and R.W. Baker, *J. Membrane Sci.*, **49**, 253–286 (1990).

14.28. Permeances for pervaporation.

For a temperature of 60°C and a permeate pressure of 15.2 mmHg, Wesslein et al. [45] measured a total permeation flux of 1.6 kg/m²-h for a 17.0 wt% ethanol-in-water feed, giving a permeate of 12 wt% ethanol. Otherwise, conditions were those of Example 14.12. Calculate the permeances of ethyl alcohol and water for these conditions. Also, calculate the selectivity for water.

14.29. Second stage of a pervaporation process.

Separation of benzene (B) from cyclohexane (C) by distillation at 1 atm is impossible because of a minimum-boiling-point azeotrope at 54.5 mol% benzene. However, extractive distillation with furfural is feasible. For an equimolar feed, cyclohexane and benzene products of 98 and 99 mol%, respectively, can be produced. Alternatively, the use of a three-stage pervaporation process, with selectivity for benzene using a polyethylene membrane, has received attention, as discussed by Rautenbach and Albrecht [47]. Consider the second stage of this process, where the feed is 9,905 kg/h of 57.5 wt% B at 75°C. The retentate is 16.4 wt% benzene at 67.5°C and the permeate is 88.2 wt% benzene at 27.5°C. The total permeate mass flux is 1.43 kg/m²-h and selectivity for benzene is 8. Calculate flow rates of retentate and permeate in kg/h and membrane surface area in m².

Adsorption, Ion Exchange, and Chromatography

§15.0 INSTRUCTIONAL OBJECTIVES

After completing this chapter, you should be able to:

- Explain why a few grams of porous adsorbent can have an adsorption area as large as a football field.
- Differentiate between chemisorption and physical adsorption.
- Explain how ion-exchange resins function.
- Compare the three major expressions (called isotherms) used for correlating adsorption-equilibria data.
- List steps involved in adsorption of a solute, and which ones may control the rate of adsorption.
- Describe major modes for contacting adsorbents with fluids containing solute(s) to be adsorbed.
- Describe major methods for regenerating adsorbent.
- Calculate vessel size or residence time for the major modes of slurry adsorption.
- List the assumptions for ideal fixed-bed adsorption and explain the concept of width of mass-transfer zone.
- Explain the concept of breakthrough in fixed-bed adsorption.
- Calculate bed height, bed diameter, and cycle time for fixed-bed adsorption.
- Compute separations for a simulated-moving-bed operation.
- Calculate rectangular and Gaussian-distribution pulses in chromatography.

Adsorption, ion exchange, and chromatography are **sorption** operations in which components of a fluid phase (**solutes**) are selectively transferred to insoluble, rigid particles suspended in a vessel or packed in a column. Sorption, a general term introduced by J.W. McBain [*Phil. Mag.*, **18**, 916–935 (1909)], includes selective transfer to the surface and/or into the bulk of a solid or liquid. In a sorption process, the sorbed solutes are referred to as **sorbate**, and the sorbing agent is the **sorbent**.

Sorption of a gas into a liquid and penetration of fluid species into a nonporous membrane are absorption operations. Absorbed solutes are referred to as absorbate, whereas the liquid or solid containing the absorbate is the absorbent. Absorption in liquids was described in Chapter 6. Absorption into nonporous membranes was described in Chapter 14.

In the **adsorption** process in Figure 15.1a, molecules, or atoms or ions, in a gas or liquid, diffuse to the surface of a solid, where they bond with the solid surface or are held by weak intermolecular forces. Adsorbed solutes are referred to as **adsorbate**, whereas the solid material is the **adsorbent**. To achieve a large surface area for adsorption per unit volume, porous solid particles with small-diameter, interconnected pores are used, with adsorption occurring on the surface of the pores.

In an **ion-exchange** process, as in Figure 15.1b, ions of positive charge (**cations**) or negative charge (**anions**) in a liquid solution, usually aqueous, replace dissimilar and displaceable ions, called counterions, of the same charge

contained in a solid **ion exchanger**, which also contains immobile, insoluble, and permanently bound Poynting correction **co-ions** of the opposite charge. Thus, ion exchange can be cation or anion exchange. Water softening by ion exchange involves a cation exchanger, in which a reaction replaces calcium ions with sodium ions:



where R is the ion exchanger and subscripts (aq) and (s) refer to aqueous and solid phases, respectively. The exchange of ions is reversible and does not cause any permanent change to the solid ion-exchanger structure. Thus, it can be used and reused unless fouled by organic compounds in the liquid feed that attach to exchange sites on and within the ion exchange resin.

The ion-exchange concept can be extended to the removal of essentially all inorganic salts from water by a two-step **dem-inalization** process or **deionization**. In step 1, a cation resin exchanges hydrogen ions for cations such as calcium, magnesium, and sodium. In step 2, an anion resin exchanges hydroxyl ions for strongly and weakly ionized anions such as sulfate, nitrate, chloride, and bicarbonate. The hydrogen and hydroxyl ions combine to form water. Regeneration of the cation and anion resins is usually accomplished with sulfuric acid and sodium hydroxide, respectively.

In **chromatography**, one or more dissolved species are selectively separated from other components in the fluid phase by interaction with a species-selective sorbent. The sorbent may be a solid adsorbent; an insoluble, nonvolatile liquid

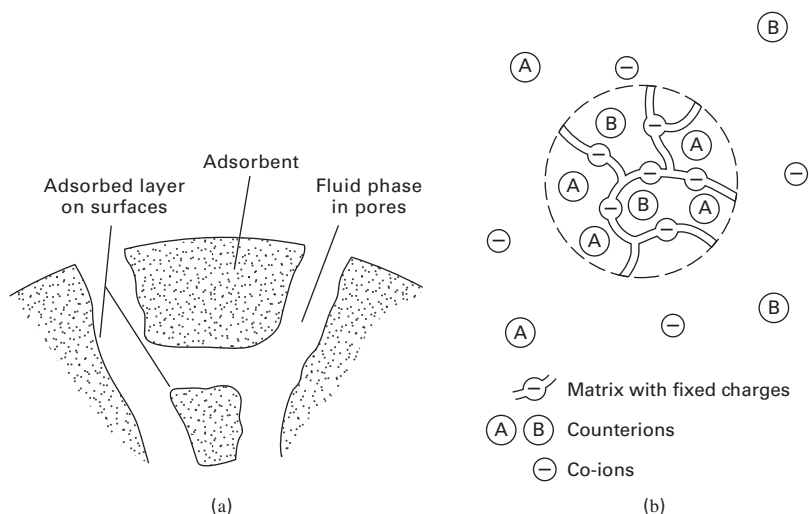


Figure 15.1 Sorption operations with solid-particle sorbents. (a) Adsorption. (b) Ion exchange.

adsorbent contained in the pores of a granular solid support; or an ion exchanger. Time-dependent chromatography may be carried out in three modes. In elution or **differential chromatography**, the solutes to be separated move through the chromatographic separator, with an inert, eluting fluid, at different rates because of different sorption affinities during repeated sorption-desorption cycles. Differential chromatography is used to achieve high-purity separations of closely related species. In “on-off” or **frontal chromatography**, one or more solutes preferentially adsorb to the stationary phase while fluid carries un-adsorbed components through the separator. Regeneration may occur by changing the thermodynamic state at the adsorbent surface (e.g., temperature, pressure, fluid composition). Alternatively, the sorbate may be displaced by mass action, as in ion exchange or by a more strongly adsorbed species as in **displacement chromatography**.

During adsorption, ion exchange, and frontal chromatography, the solid separating agent becomes saturated or nearly saturated with the molecules, atoms, or ions transferred from the fluid. To recover the sorbed substances and allow the sorbent to be reused, the sorbent is regenerated by desorbing the sorbed substances. Accordingly, these two operations are carried out in a cyclic manner. In differential chromatography, regeneration occurs continuously, but at changing locations in the separator.

Adsorption processes may be classified as **purification** or **bulk separation**, depending on the concentration in the feed of the components to be adsorbed. Although there is no sharp dividing concentration, Keller [1] has suggested 10 wt%. Early applications of adsorption involved only purification. Adsorption with charred wood to improve the taste of water has been known for centuries. Decolorization of liquids by adsorption with bone char and other materials has been practiced for at least five centuries. Adsorption of gases by a solid (charcoal) was first described by C.W. Scheele in 1773.

Commercial applications of bulk separation by gas adsorption began in the early 1920s, but did not escalate until

the 1960s, following inventions by Milton [2] of synthetic molecular-sieve zeolites, which provide high adsorptive selectivity, and by Skarstrom [3] of the **pressure-swing cycle**, which made possible a fixed-bed, cyclic gas-adsorption process. The commercial separation of liquid mixtures by adsorption also began in the 1960s, following the invention by Broughton and Gerhold [4] of the **simulated moving bed** for adsorption.

Uses of ion exchange date back to the time of Moses, who, while leading his followers out of Egypt, sweetened the bitter waters of Marah with a tree [Exodus 15:23–26]. In ancient Greece, Aristotle observed that the salt content of water was reduced when it percolates through certain sands. Studies of ion exchange were published in 1850 by both Thompson and Way, who experimented with cation exchange in soils before the discovery of ions.

The first major application of ion exchange occurred over 100 years ago for water treatment to remove calcium and other ions responsible for water hardness. Initially, the ion exchanger was a porous, natural, mineral zeolite containing silica. In 1935, synthetic, insoluble, polymeric-resin ion exchangers were introduced. Today they dominate water-softening and deionizing applications. Ion exchange and filtration units for domestic water purification are on the shelves of hardware stores.

Since the 1903 invention of chromatography by M. S. Tswett [5], a Russian botanist, it has found widespread use as an analytical, preparative, and industrial technique. Tswett separated a mixture of structurally similar yellow and green chloroplast pigments in leaf extracts by dissolving the extracts in carbon disulfide and passing the solution through a column packed with chalk particles. The pigments were separated by color; hence, the name chromatography, which was coined by Tswett in 1906 from the Greek *chroma*, meaning “color,” and *graphe*, meaning “writing.” Chromatography has revolutionized laboratory chemical analysis of liquid and gas mixtures. Commercial applications described by Bonmati et al. [6] and Bernard et al. [7] began in the 1980s.

Industrial Example

Pressure-swing gas adsorption is used for air dehydration and for partial separation of air into nitrogen and oxygen. Figure 15.2 shows a flow sheet for the dehydration of compressed air as described by White and Barkley [8]. The unit consists of two fixed-bed adsorbers, each 12.06 cm in diameter and packed with 11.15 kg of 3.3-mm-diameter Alcoa F-200 activated-alumina beads to a height of 1.27 m. The external porosity (void fraction) of the bed is 0.442 and the alumina-bead bulk density is 769 kg/m^3 .

The unit operates on a 10-minute cycle, with 5 minutes for adsorption of water vapor and 5 minutes for regeneration, which consists of depressurization, purging of the water vapor, and a 30 s repressurization. While one bed is adsorbing, the other bed is being regenerated. The adsorption (drying) step takes place with air entering at 21°C and 653.3 kPa (6.45 atm) with a flow rate of 1.327 kg/minute, passing through the bed with a pressure drop of 2.386 kPa. The dew-point temperature of the air at system pressure is reduced from 11.2 to -61°C by the adsorption process. During the 270 s purge period, about one-third of the dry air leaving one bed is directed to the other bed as a downward-flowing purge to regenerate the adsorbent. The purge is exhausted at a pressure of 141.3 kPa. Thus, the pressure swings from about 650 to 140 kPa. By conducting the purge flow countercurrently to the entering airflow, the highest degree of water-vapor desorption is achieved.

Other equipment shown in Figure 15.2 includes an air compressor, an aftercooler, piping and valving to switch the beds from one step in the cycle to the other, a coalescing filter to remove aerosols from the entering air, and a particulate filter to remove adsorbent fines from the exiting dry air. If dry air is needed at a lower pressure, an air turbine can be installed to recover energy while reducing air pressure.

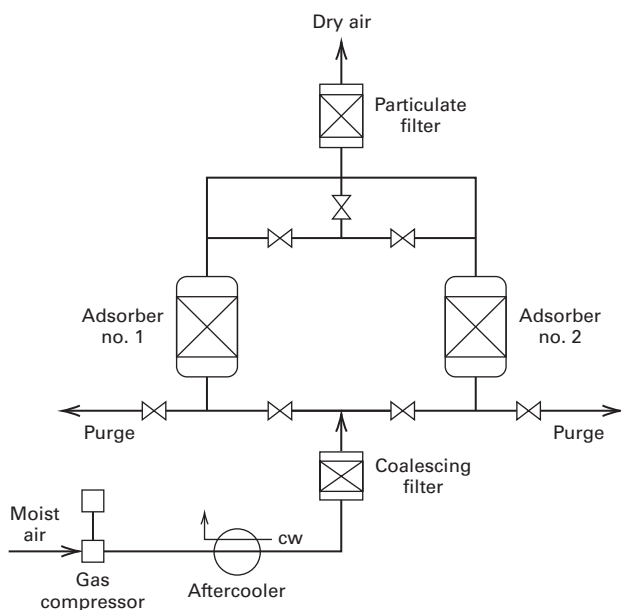


Figure 15.2 Pressure-swing adsorption for the dehydration of air.

During the 5-minute adsorption period of the cycle, the capacity of the adsorbent for water must not be exceeded. In this example, the water content of the air is reduced from $1.27 \times 10^{-3} \text{ kg H}_2\text{O/kg air}$ to the very low value of $9.95 \times 10^{-7} \text{ kg H}_2\text{O/kg air}$. To achieve this exiting water-vapor content, only a small fraction of the adsorbent capacity is utilized during the adsorption step, with most of the adsorption occurring in the first 0.2 m of the 1.27-m bed height.

Important progress is being made in bulk, adsorptive separation of gas and liquid mixtures by development of adsorbent stationary phases with improved selectivity, increased throughput, and more-efficient operation cycles. Hybrid systems that combine adsorption with membrane, centrifugation, and other separation operations have been introduced. The three sorption operations addressed in this chapter have found many applications, as given in Table 15.1, compiled from listings in Rousseau [9].

This chapter discusses (1) sorbents, including their equilibrium, sieving, transport, and kinetic properties with respect to solutes removed from solutions; (2) techniques for conducting cyclic operations; and (3) equipment configuration and design. Both equilibrium-stage and rate-based models are developed. Although emphasis is on adsorption, basic principles of ion exchange, and chromatography are also presented. More detailed treatments of adsorption operations are given by Rousseau [9] and Ruthven [10].

§15.1 SORBENTS

To be suitable for commercial use, a sorbent should have (1) high selectivity to enable sharp separations; (2) high capacity to minimize amount of sorbent; (3) favorable kinetic and transport properties for rapid sorption; (4) chemical and thermal stability, including extremely low solubility in the contacting fluid to preserve the amount of sorbent and its properties; (5) hardness and mechanical strength to prevent crushing and erosion; (6) a free-flowing tendency for ease of filling or emptying vessels; (7) high resistance to fouling for long life; (8) no tendency to promote undesirable chemical reactions; (9) capability of being regenerated when used with commercial feedstocks containing trace quantities of high-MW species that are strongly sorbed and difficult to desorb; and (10) low cost.

§15.1.1 Adsorbents

Most solids adsorb species from gases and liquids, but few naturally occurring solids have a sufficient selectivity and capacity to qualify as candidates for commercial adsorbents. Of importance is a large specific surface area (area per unit volume), which is achieved by manufacturing techniques, like sintering together sub-micron sized particles, which results in solids with a microporous structure. Pore sizes are usually given in angstroms, Å; nanometers, nm; or micrometers (microns), μm ; which are related to meters, m, and millimeters, mm, by:

$$1 \text{ m} = 10^2 \text{ cm} = 10^3 \text{ mm} = 10^6 \mu\text{m} \text{ (microns)} = 10^9 \text{ nm} \\ = 10^{10} \text{ \AA} \text{ (angstroms)}$$

Table 15.1 Industrial Applications of Sorption Operations**1. Adsorption**

Gas purifications with removal of:

- organics from vent streams
- SO₂ from vent streams
- sulfur compounds from gas streams
- water vapor from air and other gas streams
- solvents and odors from air
- NO_x from N₂
- CO₂ from natural gas

Gas bulk separations:

- N₂/O₂
- H₂O/ethanol
- Acetone/vent streams
- C₂H₄/vent streams
- Normal paraffins/isoparaffins, aromatics
- CO, CH₄, CO₂, N₂, A, NH₃, H₂

Liquid purifications with removal of:

- H₂O from organic solutions
- organics from H₂O
- odors and taste bodies from H₂O
- sulfur compounds from organic solutions
- colorizing agents

Liquid bulk separations:

- Normal paraffins/isoparaffins
- Normal paraffins/olefins
- p*-xylene/other C₈ aromatics
- p*- or *m*-cymene/other cymene isomers
- p*- or *m*-cresol/other cresol isomers
- Fructose/dextrose, polysaccharides

2. Ion Exchange

- water softening
- water demineralization
- water dealkalization
- decolorization of sugar solutions
- recovery of uranium from acid leach solutions
- recovery of antibiotics from fermentation broths
- recovery of vitamins from fermentation broths

3. Chromatography

- separation of monomeric sugars
- separation of perfume ingredients
- separation of C₄–C₁₀ normal- and iso-paraffins

Hydrogen and helium atoms are approximately 1 Å in size. By the International Union of Pure and Applied Chemistry (IUPAC) definitions, a **micropore** is <20 Å, a **mesopore** is 20–500 Å, and a **macropore** is >500 Å. Commercial adsorbents are granules, spheres, cylindrical pellets, flakes, and/or particles, with diameters ranging from 20 μm to 1.2 cm and specific surface areas from 300 to 1,200 m²/g. Thus, a few grams of adsorbent can have a surface area equal to that of a football field (120 × 53.3 yards or 5,350 m²)! This large area is made possible by a particle porosity from 30 to 85 vol% with pore diameters from 10 to 200 Å. To quantify this,

consider a cylindrical pore of diameter d_p and length L . The surface area-to-volume ratio is

$$S/V = \pi d_p L / (\pi d_p^2 L / 4) = 4/d_p \quad (15-1)$$

If the fractional particle porosity is ϵ_p and the particle density is ρ_p , the **specific surface area**, S_g , in area per unit mass of adsorbent is

$$S_g = 4\epsilon_p / \rho_p d_p \quad (15-2)$$

For example, if ϵ_p is 0.5, ρ_p is 1 g/cm³ = 1 × 10⁶ g/m³, and d_p is 20 Å (20 × 10⁻¹⁰ m), (15-2) gives $S_g = 1,000$ m²/g.

Depending upon the forces between fluid molecules and solid molecules, adsorption may be **physical adsorption** (van der Waals adsorption) or **chemisorption** (activated adsorption). Physical adsorption from a gas occurs when intermolecular attractive forces between solid and gas molecules are greater than those between gas molecules. In effect, the resulting adsorption is like condensation, which is exothermic. The magnitude of the heat of adsorption can be > or < than heat of vaporization, and changes with amount of adsorption.

Physical adsorption occurs rapidly, and may result in a monomolecular (unimolecular) layer, or two or more layers thick (multimolecular). If unimolecular, it is reversible. As physical adsorption takes place, it begins as a monolayer, becomes multilayered, and then, if the pores are close to the size of the molecules, capillary condensation occurs. The amount adsorbed in the capillaries at equilibrium depends on the direction from which equilibrium is approached. Less capillary adsorption occurs if adsorption equilibrium is approached by raising (rather than lowering) the partial pressure or concentration of the species being adsorbed. This phenomenon is called **adsorption hysteresis**. The adsorbate density is of the order of magnitude of the liquid rather than the vapor. Accordingly, maximum capacity of a porous adsorbent is related more to pore volume than to surface area. However, for gases at temperatures above their critical temperature, adsorption is confined to a monolayer.

Chemisorption involves the formation of chemical bonds (as in a chemical reaction) between adsorbent and adsorbate in a monolayer, often with a release of heat larger than the heat of vaporization. Because of its chemical-reaction nature, chemisorption from a gas generally takes place only at temperatures greater than 200°C and may be slow and irreversible. Commercial adsorbents rely on physical adsorption to achieve separations; solid catalysts rely on chemisorption to catalyze chemical reactions. This chapter deals only with physical adsorption.

Adsorption from liquids is more difficult to measure or describe. When the fluid is a gas, the amount of gas adsorbed in a confined space is determined from the measured decrease in total pressure. For a liquid, no simple procedure for determining the extent of adsorption from a pure liquid exists; consequently, experiments must be conducted using liquid mixtures. When porous particles of adsorbent are immersed in a liquid mixture, the pores, if sufficiently larger in diameter than the

liquid molecules, fill with liquid. At equilibrium, because of differences in the extent of physical adsorption among liquid molecules, composition of the liquid in the pores differs from that of bulk liquid surrounding adsorbent particles. The observed exothermic heat effect is referred to as the **heat of wetting**, which is much smaller than the heat of adsorption for a gas. As with gases, the extent of equilibrium adsorption of a given solute increases with concentration and decreases with temperature. Chemisorption also occurs with liquids.

Table 15.2 lists, for six major types of solid adsorbents: the nature of the adsorbent and representative values of the mean pore diameter, d_p ; particle porosity (internal void fraction), ε_p ; particle density, ρ_p ; and specific surface area, S_g . In addition, for some adsorbents, the capacity for adsorbing water vapor at a partial pressure of 4.6 mmHg in air at 25°C is listed, as taken from Rousseau [9]. Not included is specific pore volume, V_p , which is given by

$$V_p = \varepsilon_p / \rho_p \quad (15-3)$$

Also not included in Table 15.2, but of interest when the adsorbent is used in fixed beds, are bulk density, ρ_b , and bed porosity (external void fraction), ε_b , which are related by

$$\varepsilon_b = 1 - \frac{\rho_b}{\rho_p} \quad (15-4)$$

In addition, the true solid particle density (also called the crystalline density), ρ_s , can be computed from a similar expression:

$$\varepsilon_p = 1 - \frac{\rho_p}{\rho_s} \quad (15-5)$$

Surface Area and the BET Equation

Specific surface area of an adsorbent, S_g , is measured by adsorbing gaseous nitrogen, using the well-accepted **BET method** (Brunauer, Emmett, and Teller [11]). Typically, the BET apparatus operates at the normal boiling point of N_2

(−195.8°C) by measuring the equilibrium volume of pure N_2 physically adsorbed on several grams of adsorbent at a number of different values of the total pressure in a vacuum of 5 to 250 mmHg. Brunauer, Emmett, and Teller derived an equation to model adsorption by allowing for the formation of multimolecular layers. They assumed the heat of adsorption during monolayer formation (ΔH_{ads}) is constant and that heat effects associated with subsequent layers is equal to the heat of condensation (ΔH_{cond}). The BET equation is

$$\frac{P}{v(P_0 - P)} = \frac{1}{v_m c} + \frac{(c - 1)}{v_m c} \left(\frac{P}{P_0} \right) \quad (15-6)$$

where P = total pressure, P_0 = vapor pressure of adsorbate at test temperature, v = volume of gas adsorbed at STP (0°C, 760 mmHg), v_m = volume of monomolecular layer of gas adsorbed at STP, and c = a constant related to the heat of adsorption $\approx \exp[(\Delta H_{\text{cond}} - \Delta H_{\text{ads}})/RT]$.

Experimental data for v as a function of P are plotted, according to (15-6), as $P/[v(P_0 - P)]$ versus P/P_0 , from which v_m and c are determined from the slope and intercept of the best straight-line fit of the data. The value of S_g is then computed from

$$S_g = \frac{\alpha v_m N_A}{V} \quad (15-7)$$

where N_A = Avogadro's number = 6.023×10^{23} molecules/mol, V = volume of gas per mole at STP conditions (0°C, 1 atm) = 22,400 cm³/mol, and α is surface area per adsorbed molecule. If spherical molecules arranged in close two-dimensional packing are assumed, the projected surface area is:

$$\alpha = 1.091 \left(\frac{M}{N_A \rho_L} \right)^{2/3} \quad (15-8)$$

where M = molecular weight of the adsorbate, and ρ_L = density of the adsorbate in g/cm³, taken as the liquid at the test temperature.

Although the BET surface area may not always represent the surface area available for adsorption of a particular

Table 15.2 Representative Properties of Commercial Porous Adsorbents

Adsorbent	Nature	Pore Diameter d_p , Å	Particle Porosity, ε_p	Particle Density ρ_p , g/cm ³	Surface Area S_g , m ² /g	Capacity for H ₂ O Vapor at 25°C and 4.6 mmHg, wt% (Dry Basis)
Activated alumina	Hydrophilic, amorphous	10–75	0.50	1.25	320	7
Silica gel:	Hydrophilic/hydrophobic, amorphous					
Small pore		22–26	0.47	1.09	750–850	11
Large pore		100–150	0.71	0.62	300–350	—
Activated carbon:	Hydrophobic, amorphous					
Small pore		10–25	0.4–0.6	0.5–0.9	400–1200	1
Large pore		>30	—	0.6–0.8	200–600	—
Molecular-sieve carbon	Hydrophobic	2–10	—	0.98	400	—
Molecular-sieve zeolites	Polar-hydrophilic, crystalline	3–10	0.2–0.5	1.4	600–700	20–25
Polymeric adsorbents	Hydrophilic to hydrophobic	30–400	0.4–0.55	0.3–1.0	50–700	—

molecule, the BET test is reproducible and widely used to characterize adsorbents.

Pore Volume and Distribution

Specific pore volume in units of cm^3 of pore volume/g of adsorbent, is determined for a small mass of adsorbent, m_p , by measuring the volumes of helium, V_{He} , and mercury, V_{Hg} , displaced by the adsorbent. Helium is not adsorbed, but fills the pores. At ambient pressure, mercury cannot enter the pores because of unfavorable interfacial tension and contact angle. Specific pore volume, V_p , is then determined from

$$V_p = (V_{\text{Hg}} - V_{\text{He}})/m_p \quad (15-9)$$

Particle density is

$$\rho_p = \frac{m_p}{V_{\text{Hg}}} \quad (15-10)$$

and true solid density is

$$\rho_s = \frac{m_p}{V_{\text{He}}} \quad (15-11)$$

Particle porosity is then obtained from (15-3) or (15-5).

Distribution of pore volumes over the range of pore size is of great importance in adsorption. It is measured by mercury porosimetry for large-diameter pores ($> 100 \text{ \AA}$); by gaseous-nitrogen desorption for pores of 15–250 \AA in diameter; and by molecular sieving, using molecules of different diameter, for pores $< 15 \text{ \AA}$ in diameter. In mercury porosimetry, the extent of mercury penetration into the pores is measured as a function of applied hydrostatic pressure. A force balance along the axis of a straight pore of circular cross section for the pressure and interfacial tension between mercury and the adsorbent surface gives the following equation:

$$d_p = -\frac{4\sigma_1 \cos \theta}{P} \quad (15-12)$$

where for mercury, $\sigma_1 =$ interfacial tension = 0.48 N/m and $\theta =$ contact angle = 140° . With these values, (15-12) becomes

$$d_p(\text{\AA}) = \frac{21.6 \times 10^5}{P(\text{psia})} \quad (15-13)$$

Thus, forcing mercury into a 100- \AA -diameter pore requires a pressure of 21,600 psia.

The nitrogen desorption method for determining pore-size distribution in the 15–250- \AA -diameter range is an extension of the BET method for measuring specific surface area. By increasing nitrogen pressure above 600 mmHg, multilayer adsorbed films reach the point where they bridge the pore, resulting in capillary condensation. At $P/P_0 = 1$, the entire pore volume is filled with nitrogen. Then, by reducing the pressure in steps, nitrogen is desorbed selectively, starting with larger pores. This selectivity occurs because of the effect of pore diameter on vapor pressure of the condensed phase in the pore, as modeled by the Kelvin equation:

$$P_p^s = P^s \exp\left(-\frac{4\sigma v_L \cos \theta}{RTd_p}\right) \quad (15-14)$$

where $P_p^s =$ vapor pressure of liquid in pore, $P^s =$ the normal vapor pressure of liquid on a flat surface, $\sigma =$ surface tension of liquid in pore, and $v_L =$ molar volume of liquid in pore.

Vapor pressure of the condensed phase in the pores is less than its normal vapor pressure for a flat surface. The effect of d_p on P_p^s can be significant. For example, for liquid nitrogen at -195.8°C , $P^s = 760$ torr, $\sigma = 0.00827$ N/m, $\theta = 0$, and $v_L = 34.7$ cm^3/mol . Equation (15-14) then becomes

$$d_p(\text{\AA}) = 17.9/\ln(P^s/P_p^s) \quad (15-15)$$

From (15-15) for $d_p = 30 \text{ \AA}$, $P_p^s = 418$ torr, a reduction in vapor pressure of almost 50%. At 200 \AA , the reduction is only about 10%. At 418 torr pressure, only pores less than 30 \AA in diameter remain filled with liquid nitrogen. For greater accuracy in applying the Kelvin equation, a correction is needed for the thickness of the adsorbed layer. This correction is discussed in detail by Satterfield [12]. For a monolayer, this thickness for nitrogen is about 0.354 nm, corresponding to a P/P_0 in (15-6) of between 0.05 and 0.10. At $P/P_0 = 0.60$ and 0.90, the adsorbed thicknesses are 0.75 and 1.22 nm, respectively. The correction is applied by subtracting twice the adsorbed thickness from d_p in (15-14) and (15-15).

EXAMPLE 15.1 Particle Porosity.

Using data from Table 15.2, determine the volume fraction of pores in silica gel (small-pore type) filled with adsorbed water vapor when its partial pressure is 4.6 mmHg and the temperature is 25°C . At these conditions, the partial pressure is considerably below the water vapor pressure of 23.75 mmHg. In addition, determine whether the amount of water adsorbed is equivalent to more than a monolayer, if the area of an adsorbed water molecule is given by (15-8) and the specific surface area of the silica gel is $830 \text{ m}^2/\text{g}$.

Solution

Take 1 g of silica gel particles as a basis. From (15-3) and data in Table 15.2, specific pore volume = $V_p = 0.47/1.09 = 0.431 \text{ cm}^3/\text{g}$. From the capacity value in Table 15.2, amount of adsorbed water = $0.11/(1 + 0.11) = 0.0991 \text{ g}$. Assume density of adsorbed water is 1 g/cm^3 , volume of adsorbed water = 0.0991 cm^3 , fraction of pores filled with water = $0.0991/0.431 = 0.230$, and surface area of 1 g = 830 m^2 . From (15-8):

$$\alpha = 1.091 \left[\frac{18.02}{(6.023 \times 10^{23})(1.0)} \right]^{2/3} = 10.51 \times 10^{-16} \text{ cm}^2/\text{molecule}$$

$$\begin{aligned} \text{Number of H}_2\text{O molecules adsorbed} &= \frac{(0.0991)(6.023 \times 10^{23})}{18.02} \\ &= 3.31 \times 10^{21} \end{aligned}$$

$$\begin{aligned} \text{Number of H}_2\text{O molecules in a monolayer for } 830 \text{ m}^2 \\ &= \frac{830(100)^2}{10.51 \times 10^{-16}} = 7.90 \times 10^{21} \end{aligned}$$

Therefore, only 3.31/7.90 or 42% of one monolayer is adsorbed.

Activated Alumina

The four most widely used adsorbents in increasing order of commercial usage are activated alumina, silica gel, carbon (activated and molecular-sieve), and molecular-sieve zeolites in Table 15.2, activated alumina, Al_2O_3 , which includes activated bauxite, is made by removing water from hydrated colloidal alumina. It has a moderately high S_g , with an affinity for water sufficient to dry gases to less than 1 ppm moisture. Because of this, activated alumina is widely used for removal of water from gases and liquids.

Silica Gel

SiO_2 , made from colloidal silica, is incompressible and has a high S_g and high affinity for water and other polar compounds. Related silicate adsorbents include magnesium silicate, calcium silicate, various clays, Fuller's earth, and diatomaceous earth. Silica gel is also desirable for water removal. Surface derivitization with long-chain, bonded alkanes followed by end-capping provides selective adsorption of hydrophobic species. Small-pore and large-pore types are available.

Activated Carbon

Partial oxidation of coconut shells, fruit nuts, wood, coal, lignite, peat, petroleum residues, and bones produces activated carbon. Macropores within the carbon particles help transfer molecules to the micropores. Two commercial grades are available, one with large pores for processing liquids and one with small pores for gas adsorption. As shown in Table 15.2, activated carbon is relatively hydrophobic and has a large surface area. Accordingly, it is widely used for purification and separation of gas and liquid mixtures containing nonpolar and weakly polar organic compounds, which adsorb more strongly than water. In addition, the bonding strength of adsorption on activated carbon is low, resulting in a low heat of adsorption and ease of regeneration.

Molecular-Sieve Carbon

Unlike activated carbon, which has pore diameters starting from 10 Å, molecular-sieve carbon (MSC) has pores ranging from 2 to 10 Å, making it possible to separate N_2 from air. In one process, small pores are made by depositing coke in the pore mouths of activated carbon.

Molecular-Sieve Zeolites

As shown in Figure 15.3, most adsorbents have a range of pore sizes, where the cumulative pore volume is plotted against

pore diameter. Exceptions are molecular-sieve zeolites. These are crystalline, inorganic polymers of aluminosilicates and alkali or alkali-earth elements, such as Na, K, and Ca, with the stoichiometric, unit-cell formula $\text{M}_{x/m}[(\text{AlO}_2)_x(\text{SiO}_2)_y]z\text{H}_2\text{O}$. The M is the cation with valence m , z is the number of water molecules in each unit cell, and x and y are integers such that $y/x \geq 1$. The cations balance the charge of the AlO_2 groups, each having a net charge of -1 . To activate the zeolite, the water molecules are removed by raising the temperature or pulling a vacuum. This leaves the remaining atoms spatially intact in interconnected, cage-like structures with six identical window apertures each of from 3.8 to about 10 Å, depending on the cation and crystal structure. These apertures act as sieves, which permit small molecules to enter the crystal cage, but exclude large molecules. Thus, compared to other types of adsorbents, molecular-sieve zeolites are highly selective because all apertures in the crystal have the same size.

Properties and applications of five of the most commonly used molecular-sieve zeolites are given in Table 15.3, from Ruthven [13]. Zeolites separate not only by molecular size and shape, but also by polarity, so they can also separate molecules of similar size. Zeolites have circular or elliptical apertures. Adsorption in zeolites is a selective and reversible filling of the crystal cages, so cage volume is a pertinent factor. Although natural zeolite minerals have been known for more than 200 years, molecular-sieve zeolites were first synthesized by Milton [2], using reactive materials at temperatures of 25–100°C.

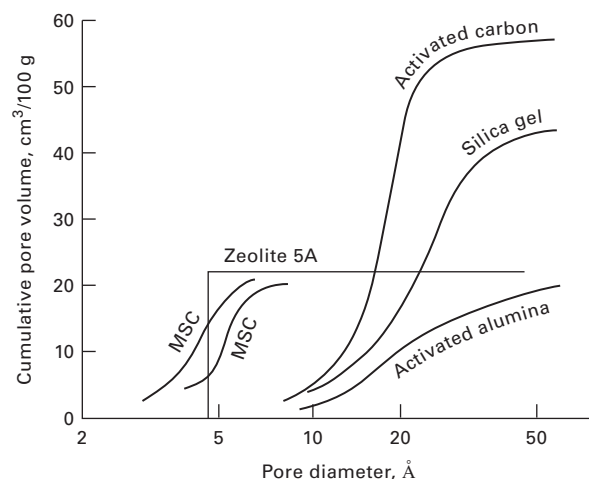


Figure 15.3 Representative cumulative pore-size distributions of adsorbent.

Table 15.3 Properties and Applications of Molecular-Sieve Zeolites

Designation	Cation	Unit-Cell Formula	Aperture Size, Å	Typical Applications
3A	K^+	$\text{K}_{12}[(\text{AlO}_2)_{12}(\text{SiO}_2)_{12}]$	2.9	Drying of reactive gases
4A	Na^+	$\text{Na}_{12}[(\text{AlO}_2)_{12}(\text{SiO}_2)_{12}]$	3.8	H_2O , CO_2 removal; air separation
5A	Ca^{2+}	$\text{Ca}_5\text{Na}_2[(\text{AlO}_2)_{12}(\text{SiO}_2)_{12}]$	4.4	Separation of air; separation of linear paraffins
10X	Ca^{2+}	$\text{Ca}_{43}[(\text{AlO}_2)_{86}(\text{SiO}_2)_{106}]$	8.0	Separation of air; removal of mercaptans
13X	Na^+	$\text{Na}_{86}[(\text{AlO}_2)_{86}(\text{SiO}_2)_{86}]$	8.4	

A type A zeolite is shown in Figure 15.4a as a three-dimensional structure of silica and alumina tetrahedra, each formed by four oxygen atoms surrounding a silicon or aluminum atom. Oxygen and silicon atoms have two negative and four positive charges, respectively, causing the tetrahedra to build uniformly in four directions. Aluminum, with a valence of 3, causes the alumina tetrahedron to be negatively charged. The added cation provides the balance. In Figure 15.4a, an octahedron of tetrahedra with six faces is evident, with one near-circular window aperture at each face. A type X zeolite is shown in Figure 15.4b. This unit-cell structure results in a larger window aperture. Zeolites are treated in monographs by Barrer [14] and Breck [15].

Polymeric Adsorbents

Of increasing commercial importance are polymeric adsorbents. Typically, they are spherical beads from 0.02 to 0.5 mm in diameter. Synthetic polymer adsorbents are often made from microspheres about 10^{-4} mm in diameter consisting of vinylpyridine or copolymers of styrene or ethylvinylbenzene

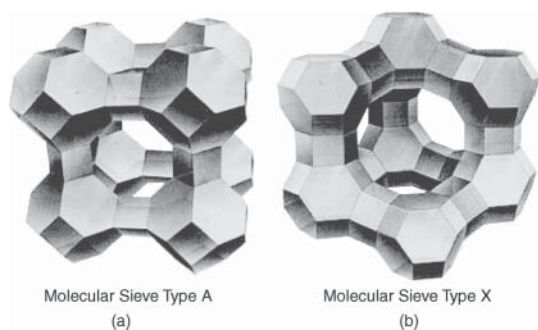


Figure 15.4 Structures of molecular-sieve zeolites: (a) Type A unit cell. (b) Type X unit cell.

with divinylbenzene. These are used to adsorb nonpolar organics from aqueous solutions. Polymerized acrylic esters can adsorb polar solutes. Synthetic polymer adsorbents can be regenerated by leaching with organic solvents. Natural polymer adsorbents are formed from hydrophilic, hydrogel-forming polymers like agarose, large-pore dextran, and microcrystalline cellulose. Their rigidity can be improved by substitution and cross linking.

§15.1.2 Ion Exchangers

The first ion exchangers were naturally occurring inorganic aluminosilicates (zeolites) used in experiments in the 1850s to exchange ammonium ions in fertilizers with calcium ions in soils. Industrial water softeners using zeolites were introduced about 1910, but they were unstable in the presence of mineral acids. Adams and Holmes [16] solved the instability problem in 1935 when they synthesized the first organic-polymer, ion-exchange resins by the polycondensation of phenol and aldehydes. Depending upon the phenolic group, the resin contains either sulfonic ($-\text{SO}_3^-$) or amine ($-\text{NH}_3^+$) groups for the reversible exchange of cations or anions. Today, the most widely used ion exchangers are synthetic, organic-polymer resins based on styrene- or acrylic-acid-type monomers, as described by D'Alelio in U.S. Patent 2,366,007 (Dec. 26, 1944).

Ion-exchange resins are generally solid gels in spherical or granular form, which consist of (1) a three-dimensional polymeric network, (2) ionic functional groups attached to the network, (3) **counterions**, and (4) a solvent. Strong-acid, cation-exchange resins and strong-base, anion-exchange resins that are fully ionized over the entire pH range are based on the copolymerization of styrene and a cross-linking agent, divinylbenzene, to produce the three-dimensional, cross-linked structure shown in Figure 15.5a. The degree of

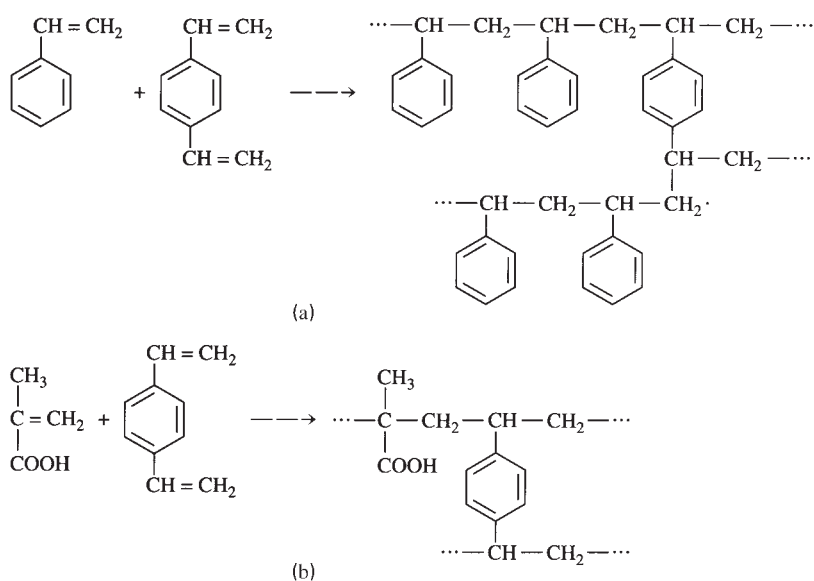


Figure 15.5 Ion-exchange resins: (a) Resin from styrene and divinylbenzene; (b) Resin from acrylic and methacrylic acid.

cross-linking is governed by the ratio of divinylbenzene to styrene. Weak-acid, cation exchangers are sometimes based on the copolymerization of acrylic acid and methacrylic acid, as shown in Figure 15.5b. These two cross-linked copolymers swell in the presence of organic solvents and have no ion-exchange properties.

To convert the copolymers to water-swallowable gels with ion-exchange properties, ionic functional groups are added to the polymeric network by reacting copolymers with various chemicals. For example, if the styrene-divinylbenzene copolymer is sulfonated, as shown in Figure 15.6a, the cation-exchange resin, shown in Figure 15.6b, is obtained with ($-\text{SO}_3^-$) groups permanently attached to the polymeric network to give a negatively charged matrix and exchangeable, mobile, positive hydrogen ions (cations). The hydrogen ion can be exchanged on an equivalent basis with other cation **counterions**, such as Na^+ , Ca^{2+} , K^+ , or Mg^{2+} to maintain charge neutrality of the polymer. For example, two H^+ ions are exchanged for one Ca^{2+} ion. The liquid whose ions are being exchanged also contains other ions of unlike charge, such as Cl^- for a solution of NaCl , where Na^+ is exchanged. These other ions are called **co-ions**. Often the liquid treated is H_2O , which dissolves to some extent in the resin and causes it to swell. Other solvents, such as methanol, are also soluble in the resin. If the styrene-divinylbenzene copolymer is chloromethylated and aminated, a strong-base,

anion-exchange resin is formed, as shown in Figure 15.6c, which can exchange Cl^- ions for other anions, such as OH^- , HCO_3^- , SO_4^{2-} , and NO_3^- .

Commercial ion exchangers in the H, Na, and Cl form are available under the trade names of AmberliteTM, DuoliteTM, DowexTM, Ionac[®], and Purolite[®], typically in the form of spherical beads from 40 μm to 1.2 mm in diameter. When saturated with water, the beads have typical moisture contents from 40 to 65 wt%. When water-swollen, $\rho_p = 1.1\text{--}1.5 \text{ g/cm}^3$. When packed into a vessel, $\rho_b = 0.560\text{--}0.96 \text{ g/cm}^3$ with ϵ_b of 0.35–0.40.

Before water is demineralized by ion exchange, potential organic foulants must be removed. As discussed by McWilliams [17], this can be accomplished by coagulation, clarification, prechlorination, and use of ion-exchanger traps that exchange inorganic anions for anionic organic molecules.

The maximum ion-exchange capacity of a strong-acid cation or strong-base anion exchanger is stoichiometric, based on the number of equivalents of mobile charge in the resin. Thus, 1 mol H^+ is one equivalent, whereas 1 mol Ca^{2+} is two equivalents. Exchanger capacity is usually quoted as eq/kg of dry resin or eq/L of wet resin. Wet capacity depends on resin water content and degree of swelling, whereas dry capacity is fixed. For copolymers of styrene and divinylbenzene, maximum capacity is based on the assumption that each benzene ring in the resin contains one sulfonic-acid group.

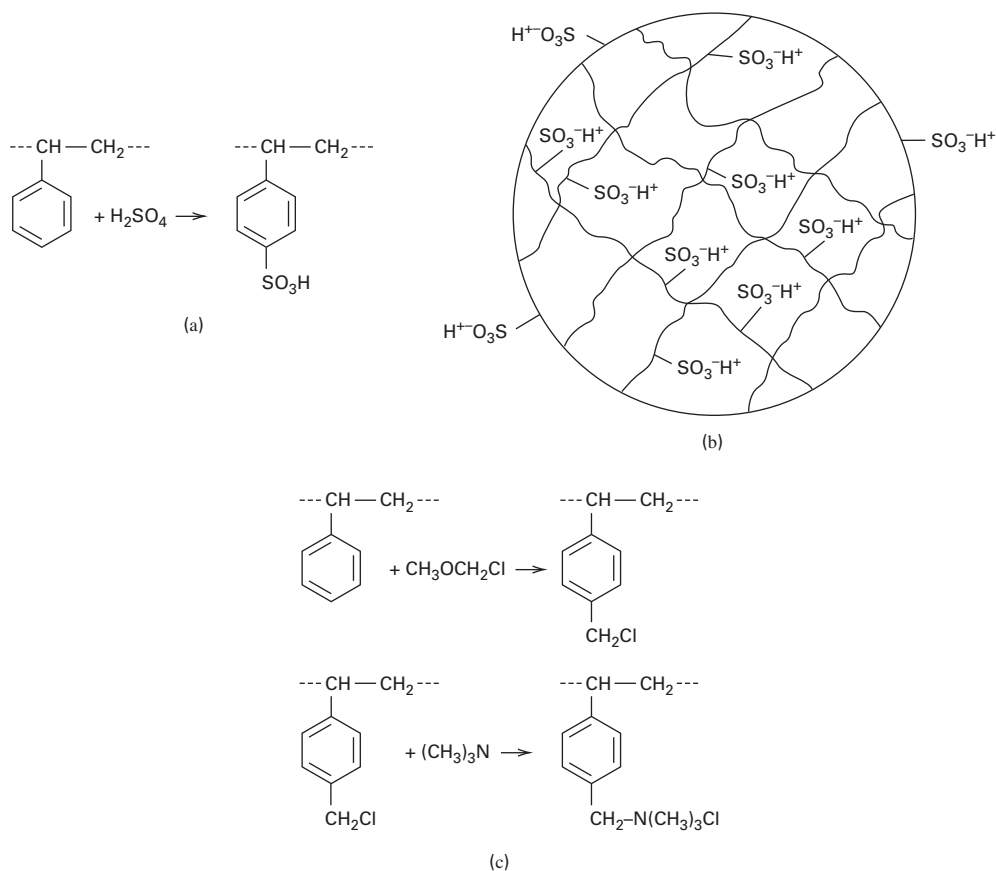


Figure 15.6 Introducing ionic functional groups into resins. (a) Sulfonation to a cation exchanger. (b) Fixed and mobile ions in a cation exchanger. (c) Chloromethylation and amination to an anion exchanger.

EXAMPLE 15.2 Ion-Exchange Capacity.

A commercial ion-exchange resin is made from 88 wt% styrene and 12 wt% divinylbenzene. Estimate the maximum ion-exchange capacity in eq/kg resin (same as meq/g resin).

Solution

Basis: 100 g of resin before sulfonation.

	MW	g	gmol
Styrene	104.14	88	0.845
Divinylbenzene	130.18	<u>12</u>	<u>0.092</u>
Total		100	0.937

Sulfonation at one location on each benzene ring requires 0.937 mol of H₂SO₄ to attach a sulfonic acid group (MW = 81.07) and split out one water molecule. This is 0.937 equivalent, with a weight addition of 0.937(81.07) = 76 g. Total dry weight of sulfonated resin = 100 + 76 = 176 g maximum ion-exchange capacity, or

$$\frac{0.937}{(176/1,000)} = 5.3 \text{ eq/kg(dry)}$$

Depending on the extent of cross-linking, resins from copolymers of styrene and divinylbenzene are listed as having actual capacities of from 3.9 (high degree of cross-linking) to 5.5 (low degree of cross-linking). Although a low degree of cross-linking favors dry capacity, almost every other ion-exchanger property, including wet capacity and selectivity, is improved by cross-linking, as discussed by Dorfner [18].

§15.1.3 Sorbents for Chromatography

Sorbents (called **stationary phases**) for chromatographic separations consist primarily of a supporting silica, alumina, or polymer substrate that may be bonded with alkane and/or derivatized with various functional groups. Figure 15.7 shows a classification of analytical chromatographic systems taken from Sewell and Clarke [19]. A mixture to be separated can be injected into a carrier fluid to form the **mobile phase**, which may be a liquid (**liquid chromatography**) or a gas (**gas chromatography**). Vaporization of a liquid by a carrier gas, to give a gas mixture as the mobile phase, is common. An ideal carrier fluid is inert and does not interact with the sorbent or feed. Gas carriers commonly behave more ideally than liquid carriers (solvents) which often interact and must be selected to effect the desired sorbent distribution and separation.

The stationary sorbent phase is a solid, a liquid supported on or bonded to a solid, or a gel. With a porous-solid adsorbent, the mechanism of separation is adsorption. If an ion exchange mechanism is desired, a synthetic, polymer ion exchanger is used. With a polymer gel or a microporous solid, a separation based on **exclusion** (sieving), can be operative. **Partition chromatography** uses liquid-supported or bonded stationary phases, where the mechanism is absorption into the liquid. The liquid stationary phase is chemically bonded

to the solid substrate to avoid stripping or dissolution of the stationary liquid by the mobile liquid phase.

In chromatography columns >1 mm inside diameter, sorbents in the form of particles are commonly flow- or pressure-packed to form an adsorptive bed. Packed beds have begun being displaced by monolithic and membrane packing materials that decrease pressure drop, replace packed column porosity with sorptive area, and increase throughput. In capillary columns <0.5 mm inside diameter, sorbent typically coats the inside wall, forming a wall-coated, open-tubular (WCOT) column. If the coating is a layer of fine particulate support material to which a liquid adsorbent is added, the column is a support-coated, open-tubular (SCOT) column. If the wall is coated with a porous adsorbent only, the column is a porous-layer, open-tubular (PLOT) column.

Sorbent applied to the surface of glass, plastic, or aluminum sheets supports **thin-layer** (or planar) **chromatography**. Sorbent applied to a sheet of cellulose material is used in **paper chromatography**. Column back-pressure at operational flow rates is used to classify liquid chromatography as **low pressure** (50.8–76.1 psi; 0.35–0.525 MPa), **medium pressure** (ca. 150 psi; 1 MPa), or **high pressure** (> hundreds of psi; tens of MPa). Automated packed-bed liquid chromatography that employs gradient pumping, sample injection, in-line detection, fraction collection, and other peripherals is called **high-performance liquid chromatography** (HPLC).

Porous alumina and silica gel substrates are widely used chromatographic adsorbents. Carbon, magnesium oxide, and carbonate substrates are less common. Alumina, a polar adsorbent, is preferred for separating components that are weakly or moderately polar. More polar compounds are more selectively retained by alumina in a column and elute later than less polar species. Alumina is a basic adsorbent, preferentially retaining acidic compounds. Silica gel is less polar than alumina and is an acidic adsorbent, preferentially retaining basic compounds, such as amines. Carbon is a nonpolar (apolar) stationary phase with the highest attraction for nonpolar molecules.

Adsorbent-type sorbents are better suited for separation of a mixture on the basis of chemical type (e.g., olefins, esters, acids, aldehydes, alcohols) than for separation of individual members of a homologous series. For the latter, **partition chromatography**—wherein an inert-solid support, often silica gel, is coated with a liquid phase—is preferred. For **gas chromatography**, that liquid must be nonvolatile. For **liquid chromatography**, the stationary liquid phase must be insoluble in the mobile phase, but since this is difficult to achieve, the stationary liquid phase is usually bonded to the solid support. An example of a bonded phase is the result of reacting silica with a chlorosilane. Both monofunctional and bifunctional silanes are used, as shown in Figure 15.8, where R is a methyl (CH₃) group and R' is a hydrocarbon chain (C₆, C₈, or C₁₈) where the terminal CH₃ group is replaced with a polar group, such as –CN or –NH₂. If the resulting stationary phase is more polar than the mobile phase, it is **normal-phase chromatography**; otherwise, it is **reverse-phase chromatography**.

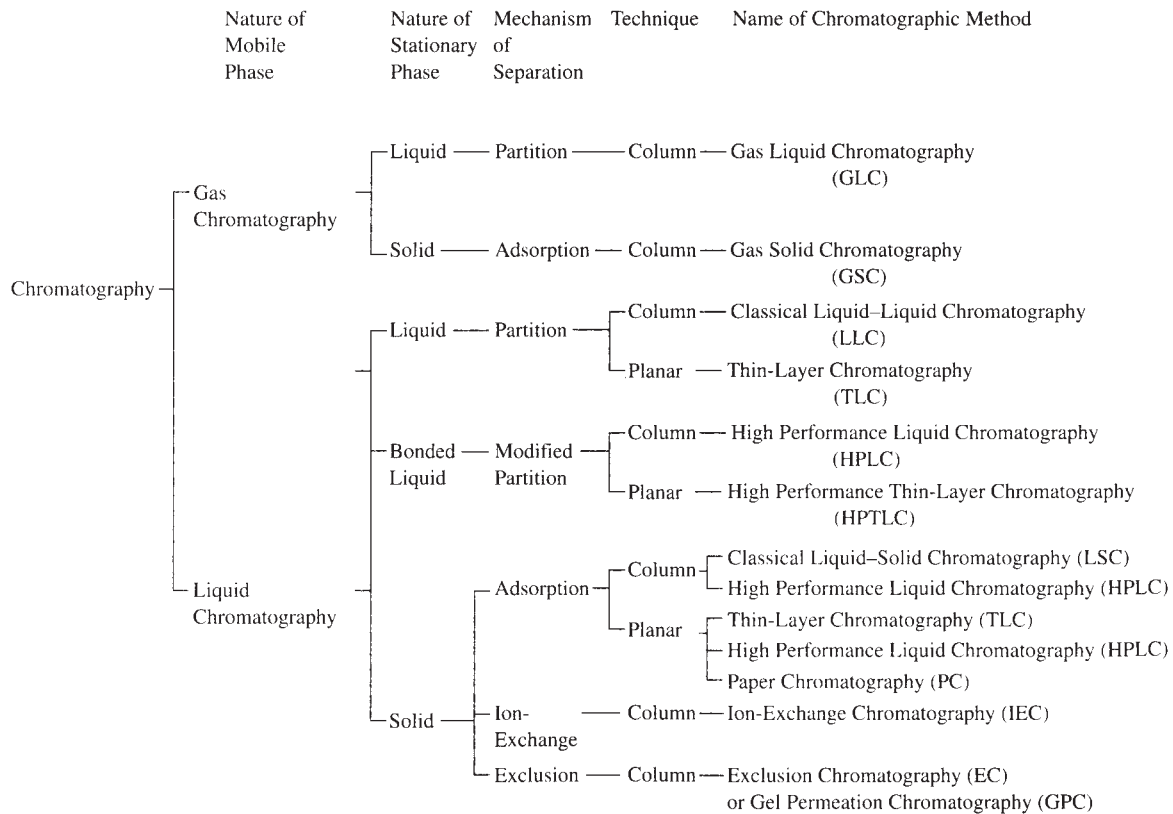


Figure 15.7 Classification of analytical chromatographic systems.

[Reproduced from [19] with permission of John Wiley & Sons, New York, © Thames Polytechnic.]

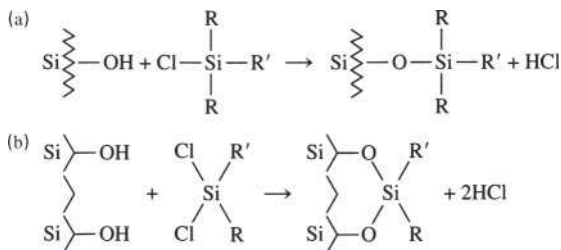


Figure 15.8 Bonded phases from the reaction of surface silanol groups with (a) monofunctional and (b) bifunctional chlorosilanes.

In liquid chromatography, selection of the solvent carrier of the mobile phase influences the order of elution of solutes. Solvent polarity is matched to that of the solutes, and more-polar adsorbents are used for less-polar solutes while less-polar adsorbents are used for more-polar solutes.

EXAMPLE 15.3 Chromatography Mode.

For the separation of each of the following mixtures, select an appropriate mode of chromatography from Figure 15.7: (a) gas mixture of O_2 , CO , CO_2 , and SO_2 ; (b) vaporized mixture of anthracene, phenanthrene, pyrene, and chrysene; and (c) aqueous solution containing Ca^{2+} and Ba^{2+} .

Solution

- (a) Use gas–solid chromatography, with a gas mobile phase and a solid-adsorbent stationary phase.
- (b) Use partition or gas–liquid chromatography, with a gas mobile phase and a bonded liquid coating on a solid for the stationary phase.
- (c) Use ion-exchange chromatography, with a liquid as the mobile phase and polymer resin beads as the stationary phase.

§15.2 EQUILIBRIUM CONSIDERATIONS

In adsorption, a dynamic equilibrium is established as a solute distributes between the fluid carrier and the solid surface. This is expressed in terms of (1) **concentration** (if the fluid is a liquid) or **partial pressure** (if the fluid is a gas) of the adsorbate in the fluid and (2) **solute loading** on the adsorbent, expressed as mass, moles, or volume of adsorbate per unit mass or per unit BET adsorbent surface area. Unlike vapor–liquid and liquid–liquid equilibria, where phase distributions are always described in the form of K -values, fluid–solid adsorption equilibria is less developed. It is necessary to obtain equilibrium data for a particular solute, or mixture of solutes and/or solvent, and the solid-adsorbent material of interest. If the data are taken over a range of fluid concentrations at a constant

temperature, a plot, called an **adsorption isotherm**, is made of adsorbent solute loading versus solute concentration or partial pressure in the fluid. This equilibrium isotherm places a limit on the extent to which a solute is adsorbed from a specific fluid mixture on a given adsorbent for one set of conditions. As described in the following subsections, the nature of the isotherms depends upon whether gas or liquid solutes are adsorbed. The rate of solute adsorption is discussed in Section 15.3.

§15.2.1 Pure-Gas Adsorption

Figure 15.9 from Brunauer et al. in [20, 21] shows five experimental physical-adsorption isotherms for pure gases. The simplest isotherm is Type I, which corresponds to unimolecular adsorption, characterized by a maximum limit in the amount adsorbed. This type describes gases at temperatures above their critical temperature. The more complex Type II isotherm is associated with multimolecular BET adsorption and is observed for gases at temperatures below their critical temperature and for pressures below, but approaching, the saturation pressure. The heat of adsorption for the first adsorbed layer is greater than that for the succeeding layers,

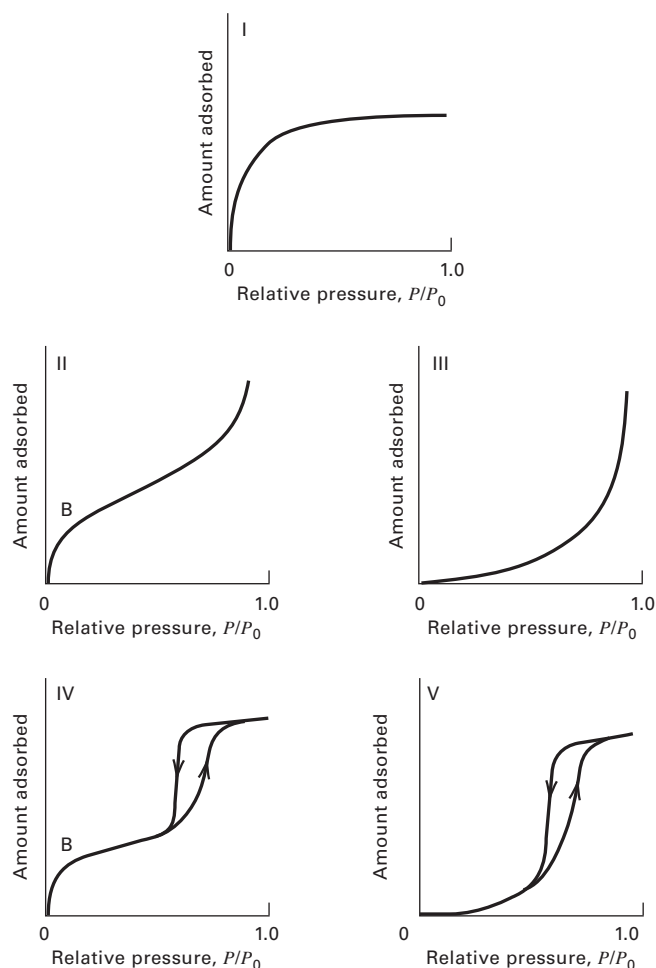


Figure 15.9 Brunauer's five types of adsorption isotherms. (P/P_0 = total pressure/vapor pressure.)

each of which is assumed to have a heat of adsorption equal to the heat of condensation. Both Types I and II are desirable isotherms, exhibiting strong adsorption.

Type III isotherm in Figure 15.9 is undesirable because the extent of adsorption is low except at high pressures. According to BET theory, it corresponds to multimolecular adsorption where heat of adsorption of the first layer is less than that of succeeding layers. Fortunately, this type of isotherm is rare, an example being adsorption of iodine vapor on silica gel. In the limit, as heat of adsorption of the first layer approaches zero, adsorption is delayed until the saturation pressure is approached.

Derivation of the BET equation (15-6) assumes that an infinite number of molecular layers can be adsorbed, thus precluding the possibility of capillary condensation. In a development by Brunauer et al. [20] before the development of the BET equation, the number of layers is restricted by pore size. Capillary condensation is assumed to occur at a reduced vapor pressure in accordance with the Kelvin equation (15-14). The resulting equation is complex, but predicts observed adsorption isotherms of Types IV and V in Figure 15.9, where the maximum extent of adsorption occurs before the saturation pressure is reached. Types IV and V are the capillary-condensation versions of Types II and III, respectively.

As shown in Figure 15.9, hysteresis occurs in multimolecular adsorption regions for isotherms of Types IV and V. The upward adsorption branch of the hysteresis loop is due to simultaneous, multimolecular adsorption and capillary condensation. Only the latter occurs during the downward desorption branch. Hysteresis can also occur in any isotherm when strongly adsorbed impurities are present. Measurements of pure-gas adsorption require adsorbents with clean pore surfaces, which is achieved by pre-evacuation.

Linear Isotherm

Figure 15.10 shows physical-adsorption data of Titoff [22] for ammonia gas on charcoal, as discussed by Brunauer [21]. The five adsorption isotherms of Figure 15.10 cover pressures from vacuum to almost 800 mmHg and temperatures from -23.5 to 151.5°C . For ammonia, the normal boiling point is -33.3°C and the critical temperature is 132.4°C . For the lowest-temperature isotherm, up to 160 cm^3 (STP) of ammonia per gram of charcoal is adsorbed, which is equivalent to $0.12\text{ g NH}_3/\text{g charcoal}$. All five isotherms are of Type I, as shown in Figure 15.9. When the amount adsorbed is low ($<25\text{ cm}^3/\text{g}$), isotherms are almost linear, and a form of Henry's law, called the **linear isotherm**, is obeyed:

$$q = kp \quad (15-16)$$

where q is equilibrium loading or amount adsorbed of a given species/unit mass of adsorbent; k is an empirical, temperature-dependent constant for the component; and p is the partial pressure of the species. As temperature increases, the amount adsorbed decreases because of Le Chatelier's principle for an exothermic process.

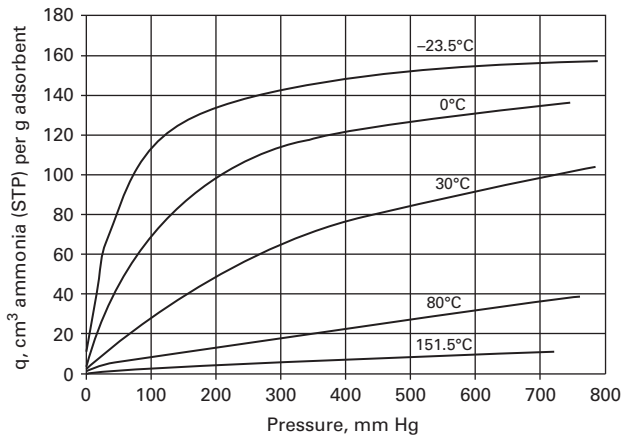


Figure 15.10 Adsorption isotherms for NH_3 on charcoal.

As discussed by Brunauer [21], other useful representations of the data are obtained by making crossplots of Figure 15.10 to obtain adsorption isobars and adsorption isosteres (adsorbed volumes). The latter curves for constant amounts adsorbed resemble vapor-pressure plots, for which the adsorption form of the Clausius–Clapeyron vapor-pressure equation applies

$$\frac{d \ln p}{dT} = \frac{-\Delta H_{\text{ads}}}{RT^2} \quad (15-17)$$

or

$$\frac{d \log p}{d(1/T)} = \frac{-\Delta H_{\text{ads}}}{2.303RT} \quad (15-18)$$

Equations (15-17) and (15-18) are used to determine the exothermic heat of adsorption. For the data in Figure 15.10, $-\Delta H_{\text{ads}}$ is initially 7,300 cal/mol, but decreases as the amount adsorbed increases, reaching 6,100 cal/mol at 100 cm^3/g . These values can be compared to the heat of vaporization of NH_3 , which at 30°C is 4,600 cal/mol.

Adsorption-isotherm data for 18 different pure gases and a variety of solid adsorbents are analyzed by Valenzuela and Myers [23]. In Figure 15.11, adsorption isotherms for a given pure gas at fixed temperature vary markedly with the adsorbent. For propane vapor at 25–30°C and pressures up to 101.3 kPa, the highest specific adsorption is with Columbia G-grade activated carbon, while the lowest is with Norton Z-900H, a zeolite molecular sieve. Columbia G-grade activated carbon has about twice the adsorbate capacity of Cabot Black Pearls activated carbon. Their compilation of data also show that for a given adsorbent, loading depends strongly on the gas. This is illustrated in Table 15.4 for a temperature of 38°C and a pressure range of 97.9 to 100 kPa from the data of Ray and Box [24] for Columbia L activated carbon. Included in the table are normal boiling points and critical temperatures. As might be expected, the species are adsorbed in approximately the inverse order of volatility.

Correlation of experimental gas adsorption isotherms is the subject of numerous articles and books. As summarized by Yang [25], approaches have ranged from empirical to

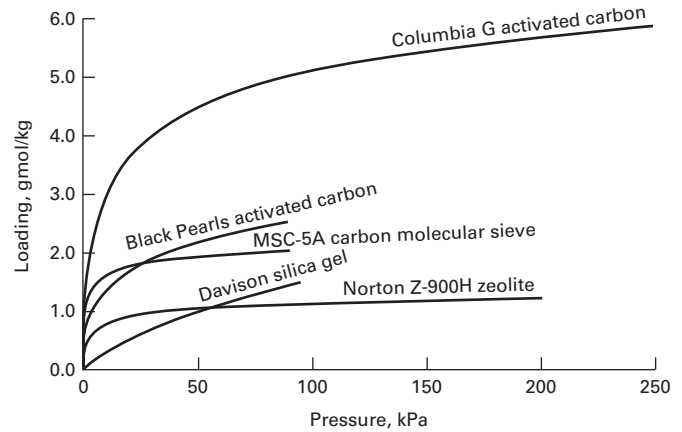


Figure 15.11 Adsorption isotherms for pure propane vapor at 298–303 K.

Table 15.4 Comparison of Equilibrium Adsorption of Pure Gases on 20–40 mesh Columbia L Activated Carbon Particles ($S_g = 1,152 \text{ m}^2/\text{g}$) at 38°C and $\sim 1 \text{ atm}$

Pure gas	q , mol/kg	T_b , °F	T_c , °F
H_2	0.0241	−423.0	−399.8
N_2	0.292	−320.4	−232.4
CO	0.374	−313.6	−220.0
CH_4	0.870	−258.7	−116.6
CO_2	1.64	−109.3	87.9
C_2H_2	2.67	−119	95.3
C_2H_4	2.88	−154.6	48.6
C_2H_6	3.41	−127.5	90.1
C_3H_6	4.54	−53.9	196.9
C_3H_8	4.34	−43.7	216.0

theoretical. In practice, the classic equations of Freundlich and Langmuir, discussed next, are dominant because of their simplicity and ability to correlate Type I isotherms.

Freundlich Isotherm

The equation attributed to Freundlich [26], but which according to Mantell [27], was devised earlier by Boedeker and van Bemmelen, is empirical and nonlinear in pressure:

$$q = kp^{1/n} \quad (15-19)$$

where k and n are temperature-dependent constants for a particular component and adsorbent. The constant, n , lies in the range of 1 to 5, and for $n = 1$, (15-19) reduces to the linear isotherm (15-16). Experimental q – p isothermal data can be fitted to (15-19) by a nonlinear curve fit or by converting (15-19) to the following linear form, and using a graphical method or a linear-regression program to obtain k and n :

$$\log q = \log k + (1/n) \log p \quad (15-20)$$

In the graphical method, data are plotted as $\log q$ versus $\log p$; the best straight line through the data has a slope of

$(1/n)$ and an intercept of $\log k$. In general, k decreases, while n increases with increasing temperature, approaching a value of 1 at high temperatures. Although (15-19) is empirical, it can be derived by assuming a heterogeneous surface with a nonuniform distribution of heat of adsorption (Brunauer [21]). The Freundlich equation does not predict a maximum loading, as shown in Figure 15.9 for a Type I isotherm. Instead, loadings continue to increase with increasing solute concentration or partial pressure, as shown in Figure 15.11 for Columbia G.

Langmuir Isotherm

The Langmuir equation [28] predicts Type I isotherms with a maximum loading. It is derived from mass-action kinetics, assuming that chemisorption is the reaction. Let the surface of the pores of the adsorbent be homogeneous ($\Delta H_{\text{ads}} = \text{constant}$), with negligible interaction forces between adsorbed molecules. If θ is the fraction of surface covered by adsorbed molecules, $(1-\theta)$ is the fraction of bare surface, and the net rate of adsorption is the difference between the rate of adsorption on the bare surface and the rate of desorption on the covered surface:

$$dq/dt = k_a p(1 - \theta) - k_d \theta \quad (15-21)$$

where k_a and k_d are the adsorption and desorption kinetic constants, and p is the partial pressure of the solute. At equilibrium, $dq/dt = 0$ and (15-21) reduces to

$$\theta = \frac{Kp}{1 + Kp} \quad (15-22)$$

where $K = k_a/k_d$ is the adsorption-equilibrium constant and

$$\theta = q/q_m \quad (15-23)$$

where q_m is the maximum loading corresponding to complete surface coverage. Thus, the Langmuir adsorption isotherm is restricted to a monomolecular layer. Combining (15-23) with (15-22) results in the **Langmuir isotherm**:

$$q = \frac{Kq_m p}{1 + Kp} \quad (15-24)$$

At low pressures, if $Kp \ll 1$, (15-24) reduces to the linear isotherm, (15-16), while at high pressures where $Kp \gg 1$, $q = q_m$. At intermediate pressures, (15-24) is nonlinear in pressure. Although originally devised by Langmuir for chemisorption, (15-24) is widely applied to physical-adsorption data.

In (15-24), K and q_m are treated as constants obtained by fitting the nonlinear equation to experimental data or by employing the following linearized form, numerically or graphically:

$$\frac{p}{q} = \frac{1}{q_m K} + \frac{p}{q_m} \quad (15-25)$$

Using (15-25), the best straight line is drawn through a plot of p/q versus p , giving a slope of $(1/q_m)$ and an intercept of $1/(q_m K)$. Theoretically, K should change rapidly with temperature but q_m should not, because it is related through v_m by (15-7) to S_g . The choice between the nonlinear Freundlich and Langmuir isotherms depends on whether the experimental adsorption isotherm predicts an asymptotic limit for q at high pressure or not.

Other Adsorption Isotherms

Valenzuela and Myers [23] fit isothermal, pure-gas adsorption data to the three-parameter isotherms of Toth:

$$q = \frac{mp}{(b + p^t)^{1/t}} \quad (15-26)$$

where m , b , and t are constants for a given adsorbate-adsorbent system and temperature.

Honig and Reyerson devised the three-constant UNILAN equation:

$$q = \frac{n}{2s} \ln \left[\frac{c + pe^s}{c + pe^{-s}} \right] \quad (15-27)$$

where n , s , and c are the constants for a given system and temperature. The Toth and UNILAN isotherms reduce to the Langmuir isotherm for $t = 1$ and $s = 0$, respectively.

EXAMPLE 15.4 Freundlich and Langmuir Isotherms.

Data for the equilibrium adsorption of pure methane gas on activated carbon (PCB from Calgon Corp.) at 296 K were obtained by Ritter and Yang [34]:

q , cm ³ (STP) of CH ₄ /g carbon	45.5	91.5	113	121	125	126	126
$P = p$, psia	40	165	350	545	760	910	970

Fit the data to: (a) the Freundlich isotherm, and (b) the Langmuir isotherm. Which isotherm provides a better fit? Do the data give a reasonable fit to the linear isotherm?

Solution

Using the linearized forms of the isotherm equations, a spreadsheet or MATLAB can be used to do a linear regression:

- (a) Using (15-20), $\log k = 1.213$, $k = 16.34$, $1/n = 0.3101$, and $n = 3.225$. Thus, the Freundlich equation is:

$$q = 16.34p^{0.3101}$$

- (b) Using (15-25), $1/q_m = 0.007301$, $q_m = 137.0$, $1/(q_m K) = 0.5682$, and $K = 0.01285$. Thus, the Langmuir equation is

$$q = \frac{1.760p}{1 + 0.01285p}$$

The predicted values of q from the two isotherms are:

p , psia	q , cm ³ (STP) of CH ₄ /g Carbon		
	Experimental	Freundlich	Langmuir
40	45.5	51.3	46.5
165	91.5	79.6	93.1
350	113	101	112
545	121	115	120
760	125	128	124
910	126	135	126
970	126	138	127

The Langmuir isotherm fits the data significantly better than the Freundlich isotherm. Average percent deviations in q are 1.01% and 8.64%, respectively. One reason for the better Langmuir fit is the trend to an asymptotic value for q at the highest pressures. Clearly, the data do not fit a linear isotherm.

§15.2.2 Gas Mixtures and Extended Isotherms

Commercial applications of physical adsorption involve mixtures rather than pure gases. If adsorption of all components except one (A) is negligible, then adsorption of A is estimated from its pure-gas adsorption isotherm using the partial pressure of A. If adsorption of two or more components in the mixture is significant, the situation is complicated. Experimental data show that one component can increase, decrease, or have no influence on adsorption of another, depending on interactions of adsorbed molecules. A simple theoretical treatment is the extension of the Langmuir equation by Markham and Benton [29], who neglect interactions and assume that the only effect is the reduction of the vacant surface area for the adsorption of A because of adsorption of other components. For a binary gas mixture of A and B, let θ_A = fraction of surface covered by A and θ_B = fraction of surface covered by B. Then, $(1 - \theta_A - \theta_B)$ = fraction of vacant surface. At equilibrium:

$$(k_A)_d p_A (1 - \theta_A - \theta_B) = (k_A)_d \theta_A \quad (15-28)$$

$$(k_B)_d p_B (1 - \theta_A - \theta_B) = (k_B)_d \theta_B \quad (15-29)$$

Solving these equations simultaneously, and combining results with (15-23), gives

$$q_A = \frac{(q_A)_m K_A p_A}{1 + K_A p_A + K_B p_B} \quad (15-30)$$

$$q_B = \frac{(q_B)_m K_B p_B}{1 + K_A p_A + K_B p_B} \quad (15-31)$$

where $(q_i)_m$ is the maximum amount of adsorption of species i for coverage of the entire surface. Equations (15-30) and

(15-31) are readily extended to a mixture of j components:

$$q_i = \frac{(q_i)_m K_i p_i}{1 + \sum_j K_j p_j} \quad (15-32)$$

In a similar fashion, as shown by Yon and Turnock [30], the Freundlich and Langmuir equations can be combined to give the following extended relation for gas mixtures:

$$q_i = \frac{(q_i)_0 K_i p_i^{1/n_i}}{1 + \sum_j K_j p_j^{1/n_j}} \quad (15-33)$$

where $(q_i)_0$ is the maximum loading, which may differ from $(q_i)_m$ for a monolayer. Equation (15-33) represents data for nonpolar, multicomponent mixtures in molecular sieves reasonably well. Broughton [31] has shown that both the extended-Langmuir and Langmuir-Freundlich equations lack thermodynamic consistency. Therefore, (15-32) and (15-33) are frequently referred to as **nonstoichiometric** isotherms. Nevertheless, for practical purposes, their simplicity often makes them the isotherms of choice.

Both (15-32) and (15-33) are also referred to as **constant-selectivity equilibrium** equations because they predict a separation factor (selectivity), $\alpha_{i,j}$, for each pair of components, i, j , in a mixture that is constant for a given temperature and independent of mixture composition. For example, (15-32) gives

$$\alpha_{ij} = \frac{q_i/q_j}{p_i/p_j} = \frac{(q_i)_m K_i}{(q_j)_m K_j}$$

As with vapor-liquid and liquid-liquid phase equilibria for three or more components, data for binary and multicomponent gas-solid adsorbent equilibria are scarce and less accurate than corresponding pure-gas data. Valenzuela and Myers [23] include experimental data on adsorption of gas mixtures from 9 published studies on 29 binary systems, for which pure-gas-adsorption isotherms were also obtained. They also describe procedures for applying the Toth and UNILAN equations to multicomponent mixtures based on the ideal-adsorbed-solution (IAS) theory of Myers and Prausnitz [32]. Unlike the extended-Langmuir equation (15-32), which is explicit in the amount adsorbed, the IAS theory, though more accurate, is not explicit and requires an iterative solution procedure. Additional experimental data for higher-order (ternary and/or higher) gas mixtures are given by Miller, Knaebel, and Ikels [33] for 5A molecular sieves and by Ritter and Yang [34] for activated carbon. Yang [25] presents a discussion of mixture adsorption theories, together with comparisons of these theories with mixture data for activated carbon and zeolites. The data on zeolites are the most difficult to correlate, with the statistical thermodynamic model (SSTM) of Ruthven and Wong [35] giving the best results.

EXAMPLE 15.5 Extended-Langmuir Isotherm.

The experimental work of Ritter and Yang, cited in Example 15.4, also includes adsorption isotherms for pure CO and CH₄ and a binary mixture of CH₄ (A) and CO (B). Ritter and Yang give the following Langmuir constants for pure A and B at 294 K:

	q_m , cm ³ (STP)/g	K , psi ⁻¹
CH ₄	133.4	0.01370
CO	126.1	0.00624

Use these constants with the extended-Langmuir equation to predict the specific adsorption volumes (STP) of CH₄ and CO for a vapor mixture of 69.6 mol% CH₄ and 30.4 mol% CO at 294 K and a total pressure of 364.3 psia. Compare the results with the following experimental data of Ritter and Yang:

Total volume adsorbed, cm ³ (STP)/g	114.1
Mole fractions in adsorbate:	
CH ₄	0.867
CO	0.133

Solution

$$p_A = y_A P = 0.696(364.3) = 253.5 \text{ psia}$$

$$p_B = y_B P = 0.304(364.3) = 110.8 \text{ psia}$$

From (15-30):

$$q_A = \frac{133.4(0.0137)(253.5)}{1 + (0.0137)(253.5) + (0.00624)(110.8)} = 89.7 \text{ cm}^3(\text{STP})/\text{g}$$

$$q_B = \frac{126.1(0.00624)(110.8)}{1 + (0.0137)(253.5) + (0.00624)(110.8)} = 16.9 \text{ cm}^3(\text{STP})/\text{g}$$

The total amount adsorbed = $q = q_A + q_B = 89.7 + 16.9 = 106.6 \text{ cm}^3(\text{STP})/\text{g}$, which is 6.6% lower than the experimental value. Mole fractions in the adsorbate are $x_A = q_A/q = 89.7/106.6 = 0.841$ and $x_B = 1 - 0.841 = 0.159$. These adsorbate mole fractions deviate from the experimental values by 0.026. For this example, the extended-Langmuir isotherm gives reasonable results.

§15.2.3 Liquid Adsorption

When porous adsorbent particles are immersed in a confined pure gas, the pores fill with adsorbed gas. The amount of adsorbed gas is determined by the decrease in total pressure. With a liquid, the pressure does not change, and no simple experimental procedure has been devised for determining the extent of adsorption of a pure liquid. If the liquid is a homogeneous binary mixture, it is customary to designate one component the solute (1) and the other the solvent (2). The assumption made is that the change in composition of the bulk liquid in contact with the porous solid is due entirely to adsorption of the solute; solvent adsorption is thus tacitly assumed not to occur. If the liquid mixture is

dilute in solute, the consequences are not serious. If, however, experimental data are obtained over the entire concentration range, the distinction between solute and solvent is arbitrary and the resulting adsorption isotherms, as discussed by Kipling [36], can exhibit curious shapes, unlike those obtained for pure gases or gas mixtures. To illustrate this, let n^0 = total moles of binary liquid contacting the adsorbent, m = mass of adsorbent, x_1^0 = mole fraction of solute before contact with adsorbent, x_1 = mole fraction of solute in the bulk solution after adsorption equilibrium is achieved, and q_1^e = apparent moles of solute adsorbed per unit mass of adsorbent.

A solute material balance, assuming no adsorption of solvent and a negligible change in the total moles of liquid mixture, gives

$$q_1^e = \frac{n^0(x_1^0 - x_1)}{m} \quad (15-34)$$

If isothermal data are obtained over the entire concentration range, processed with (15-34), and plotted as adsorption isotherms, the resulting curves are not as shown in Figure 15.12a. Instead, curves of the type in Figures 15.12b and c are obtained, where negative adsorption appears to occur as in Figure 15.12c. Such isotherms are best referred to as **composite isotherms** or **isotherms of concentration change**, as suggested by Kipling [36]. Likewise, adsorption loading, q_1^e , of (15-34) is more correctly referred to as **surface excess**.

Under what conditions are composite isotherms of the shapes in Figures 15.12b and c obtained? This is shown by examples from Kipling in Figure 15.13, where various combinations of hypothetical adsorption isotherms for solute (A) and solvent (B) are shown together with resulting composite isotherms. When the solvent is not adsorbed, as seen in Figure 15.13a, a composite curve without negative adsorption is obtained. In all other cases of Figure 15.13, negative values of surface excess appear.

Valenzuela and Myers [23] tabulate literature values for equilibrium adsorption of 25 different binary-liquid mixtures. With one exception, all 25 mixtures give composite isotherms of the shapes shown in Figures 15.12b and c. The exception is a mixture of cyclohexane and *n*-heptane with silica gel, for which surface excess is almost negligible ($0 \pm 0.05 \text{ mmol/g}$) from $x_1 = 0.041$ to 0.911. They also include literature references to 354 binary sets, 25 ternary sets, and 3 sets of data for higher-order liquid mixtures.

When data for the binary mixture are available only in the dilute region, solvent adsorption, if any, may be constant, and all changes in total amount adsorbed are due to the solute. In that case, the adsorption isotherms are of the form of Figure 15.12a, which resembles the shape obtained with pure gases. It is then common to fit the data with concentration forms of the Freundlich (15-19) or Langmuir (15-24) equations:

$$q = kc^{1/n} \quad (15-35)$$

$$q = \frac{Kq_m c}{1 + Kc} \quad (15-36)$$

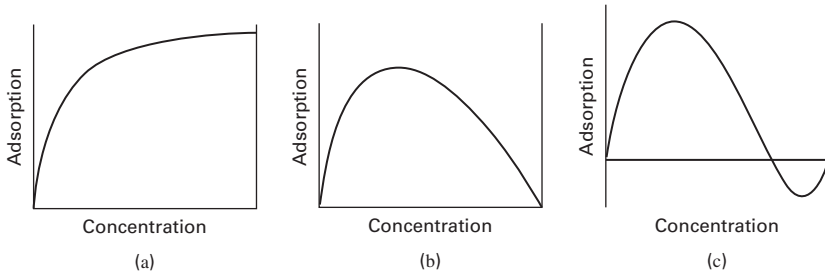


Figure 15.12 Representative isotherms of concentration change for liquid adsorption.

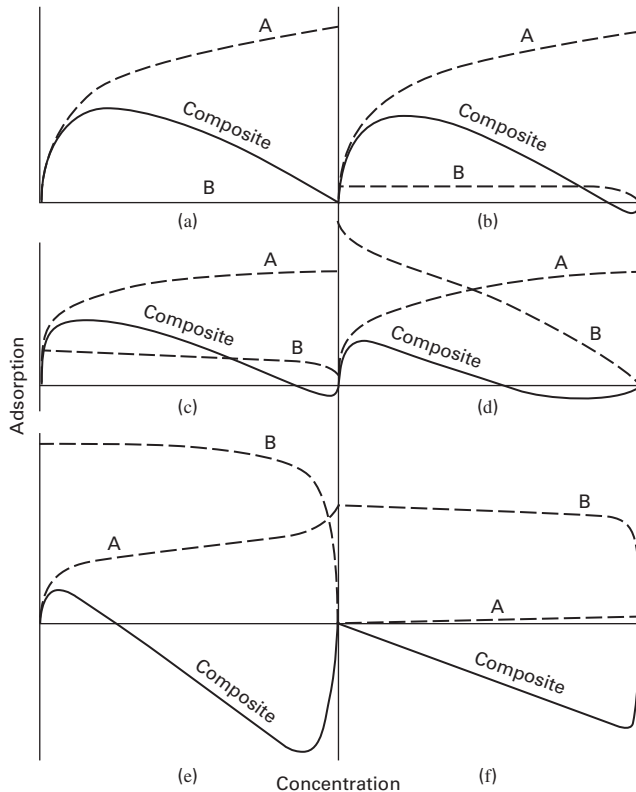


Figure 15.13 Origin of various types of composite isotherms for binary-liquid adsorption.

[Reproduced from Kipling [36].]

Candidate systems for this case are small amounts of organics dissolved in water and small amounts of water dissolved in hydrocarbons. For liquid mixtures dilute in two or more solutes, multicomponent adsorption may be estimated from a concentration form of the extended-Langmuir equation (15-32) based on constants, q_m and K , obtained from experiments on single solutes. However, when solute-solute interactions are suspected, it may be necessary to determine constants from multicomponent data. As with gas mixtures, the concentration form of (15-32) also predicts constant selectivity for each pair of components in a mixture.

EXAMPLE 15.6 Adsorption of VOCs.

Small amounts of VOCs in water can be removed by adsorption. Generally, two or more VOCs are present. An aqueous stream containing small amounts of acetone (1) and propionitrile (2) is to be treated with activated carbon. Single-solute equilibrium data from Radke and Prausnitz [37] have been fitted to the Freundlich and Langmuir isotherms, (15-35) and (15-36), with the average deviations indicated, for solute concentrations up to 50 mmol/L:

Acetone in Water (25°C):		Absolute Average Deviation of q , %
$q_1 = 0.141c_1^{0.597}$	(1)	14.2
$q_1 = \frac{0.190c_1}{1 + 0.146c_1}$	(2)	27.3
Propionitrile in water (25°C):		
$q_2 = 0.138c_2^{0.658}$	(3)	10.2
$q_2 = \frac{0.173c_2}{1 + 0.0961c_2}$	(4)	26.2

where q_i = amount of solute adsorbed, mmol/g, and c_i = solute concentration in aqueous solution, mmol/L.

Use these single-solute results with an extended Langmuir-type isotherm to predict the equilibrium adsorption in a binary-solute, aqueous system containing 40 and 34.4 mmol/L, respectively, of acetone and propionitrile at 25°C with the same adsorbent. Compare the results with the following experimental values from Radke and Prausnitz [37]:

$$q_1 = 0.715 \text{ mmol/g}; q_2 = 0.822 \text{ mmol/g}; \text{ and } q_{\text{total}} = 1.537 \text{ mmol/g}$$

Solution

From (15-32), the extended liquid-phase Langmuir isotherm is

$$q_i = \frac{(q_i)_m K_i c_i}{1 + \sum_j K_j c_j} \quad (1)$$

From (2), $(q_1)_m = 0.190/0.146 = 1.301 \text{ mmol/g}$.

From (4), $(q_2)_m = 0.173/0.0961 = 1.800 \text{ mmol/g}$.

From (5):

$$q_1 = \frac{1.301(0.146)(40)}{1 + (0.146)(40) + (0.0961)(34.4)} = 0.749 \text{ mmol/g}$$

$$q_2 = \frac{1.800(0.0961)(34.4)}{1 + (0.146)(40) + (0.0961)(34.4)} = 0.587 \text{ mmol/g}$$

Summing, $q_{\text{total}} = 1.336 \text{ mmol/g}$.

Compared to experimental data, the percent deviations for q_1 , q_2 , and q_{total} , respectively, are 4.8%, -28.6%, and -13.1%. Better agreement is obtained by Radke and Prausnitz using IAS theory. It is expected that a concentration form of (15-33) would also give better agreement, but that requires that the single-solute data be refitted for each solute to a Langmuir–Freundlich isotherm of the form

$$q = \frac{q_0 K c^{1/n}}{1 + K c^{1/n}} \quad (2)$$

§15.2.4 Ion-Exchange Equilibria

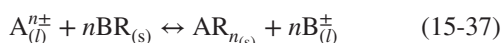
Ion exchange differs from adsorption in that one sorbate (a counterion) is exchanged for a solute ion, the process being governed by a reversible, stoichiometric, chemical-reaction equation. Thus, selectivity of the ion exchanger for one counterion over another may be just as important as the ion-exchanger capacity. Accordingly, the law of mass action is used to obtain an equilibrium ratio rather than to fit data to a sorption isotherm such as the Langmuir or Freundlich equation.

As discussed by Anderson [38], two cases are important. In the first, the counterion, initially in the ion, is exchanged with a counterion from an acid or base solution, e.g.,



Hydrogen ions leaving the exchanger immediately react with hydroxyl ions to form water, leaving no counterion on the right-hand side of the reaction. Accordingly, ion exchange continues until the aqueous solution is depleted of sodium ions or the exchanger is depleted of hydrogen ions.

In the second, more-common, case, the counterion being transferred from exchanger to fluid remains as an ion. For example, exchange of counterions A and B is expressed by:



where A and B must be either cations (positive charge) or anions (negative charge). For this case, at equilibrium, a chemical-equilibrium constant based on the law of mass action can be defined:

$$K_{\text{A,B}} = \frac{q_{\text{AR}_n} c_{\text{B}}^{n\pm}}{q_{\text{BR}}^n c_{\text{A}}^{n\pm}} \quad (15-38)$$

where molar concentrations c and q refer to the liquid and ion-exchanger phases, respectively. The constant, $K_{\text{A,B}}$ is not a rigorous equilibrium constant because (15-38) is in terms of concentrations instead of activities. Although it could be corrected by including activity coefficients, it is used in the form shown, with $K_{\text{A,B}}$ referred to as a **molar selectivity coefficient** for A displacing B. For the resin phase, concentrations are in equivalents per unit mass or unit bed volume of ion

exchanger. For the liquid, concentrations are in equivalents per unit volume of solution. For dilute solutions, $K_{\text{A,B}}$ is constant for a given pair of counterions and a given resin.

When exchange is between two counterions of equal charge, (15-38) reduces to a simple equation in terms of equilibrium concentrations of A in the liquid solution and in the ion-exchange resin. Because of (15-37), the total concentrations, C and Q , in equivalents of counterions in the solution and the resin, remain constant during the exchange. Accordingly:

$$c_i = Cx_i/z_i \quad (15-39)$$

$$q_i = Qy_i/z_i \quad (15-40)$$

where x_i and y_i are equivalent fractions, rather than mole fractions, of A and B, such that

$$x_{\text{A}} + x_{\text{B}} = 1 \quad (15-41)$$

$$y_{\text{A}} + y_{\text{B}} = 1 \quad (15-42)$$

and z_i = valence of counterion i . Combining (15-38) with (15-42) gives, for counterions A and B of equal charge,

$$K_{\text{A,B}} = \frac{y_{\text{A}}(1 - x_{\text{A}})}{x_{\text{A}}(1 - y_{\text{A}})} \quad (15-43)$$

At equilibrium, x_{A} and y_{A} are independent of total equivalent concentrations C and Q . Such is not the case when the two counterions are of unequal charge, as in the exchange of Ca^{2+} and Na^+ . A derivation for this general case gives

$$K_{\text{A,B}} = \left(\frac{C}{Q}\right)^{n-1} \frac{y_{\text{A}}(1 - x_{\text{A}})^n}{x_{\text{A}}(1 - y_{\text{A}})^n} \quad (15-44)$$

Thus, for unequal counterion charges, $K_{\text{A,B}}$ depends on the ratio C/Q and on the ratio of charges, n , as defined in (15-37).

When $K_{\text{A,B}}$ data for a system of counterions with a particular ion exchanger are not available, the method of Bonner and Smith [39], as modified by Anderson [38], is used for screening purposes or preliminary calculations. In this method, $K_{\text{A,B}}$ is

$$K_{i,j} = K_i/K_j \quad (15-45)$$

where values for relative molar selectivities K_i and K_j are given in Table 15.5 for cations with an 8% cross-linked, strong-acid

Table 15.5 Relative Molar Selectivities, K , for Cations with 8% Cross-Linked Strong-Acid Resin

Li^+	1.0	Zn^{2+}	3.5
H^+	1.3	Co^{2+}	3.7
Na^+	2.0	Cu^{2+}	3.8
NH_4^+	2.6	Cd^{2+}	3.9
K^+	2.9	Be^{2+}	4.0
Rb^+	3.2	Mn^{2+}	4.1
Cs^+	3.3	Ni^+	3.9
Ag^+	8.5	Ca^{2+}	5.2
UO_2^{2+}	2.5	Sr^{2+}	6.5
Mg^{2+}	3.3	Pb^{2+}	9.9
		Ba^{2+}	11.5

Table 15.6 Approximate Relative Molar Selectivities, K , for Anions with Strong-Base Resins

I ⁻	8	OH ⁻ (Type II)	0.65
NO ₃ ⁻	4	HCO ₃ ⁻	0.4
Br ⁻	3	CH ₃ COO ⁻	0.2
HSO ₄ ⁻	1.6	F ⁻	0.1
NO ₂ ⁻	1.3	OH ⁻ (Type I)	0.05–0.07
CN ⁻	1.3	SO ₄ ²⁻	0.15
Cl ⁻	1.0	CO ₃ ²⁻	0.03
BrO ₃ ⁻	1.0	HPO ₄ ²⁻	0.01

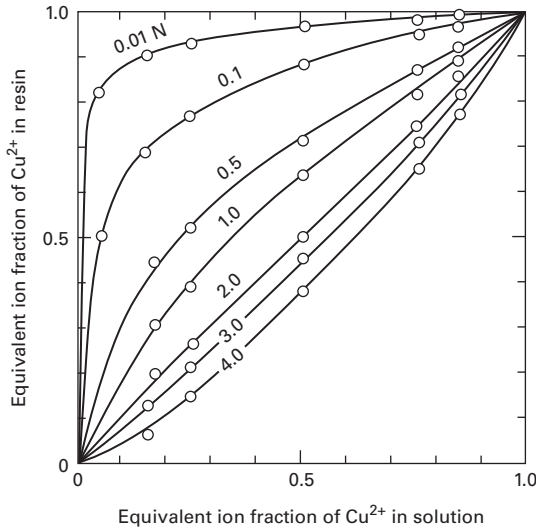


Figure 15.14 Isotherms for ion exchange of Cu²⁺ and Na⁺ on Dowex 50-X8 as a function of total normality in the bulk solution. [Reproduced from [45] with permission of Springer Science + Business Media B.V.]

resin, and in Table 15.6 for anions with strong-base resins. For values of K in these tables, the units of C and Q are, respectively, eq/L of solution and eq/L of bulk bed volume of water-swelled resin.

A typical cation-exchange resin of the sulfonated styrene-divinylbenzene type, such as Dowex 50, as described by Bauman and Eichhorn [40] and Bauman, Skidmore, and Osmun [41], has an exchangeable ion capacity of 5 ± 0.1 meq/g of dry resin. As shipped, water-wet resin might contain 41.4 wt% water. Thus, wet capacity is $5(58.6/100) = 2.9$ meq/g of wet resin. If bulk density of a drained bed of wet resin is 0.83 g/cm^3 , bed capacity is 2.4 eq/L of resin bed.

A separation factor, $SP = S_{A,B}$, which ignores the valence of the exchanging ions, can be defined for an equilibrium stage. For binaries in terms of equivalent ionic fractions:

$$S_{A,B} = \frac{y_A(1 - x_A)}{x_A(1 - y_A)} \quad (15-46)$$

which is identical to (15-43). Data for an exchange between Cu²⁺ (A) and Na⁺ (B) (counterions of unequal charge) with Dowex 50 cation resin over a wide range of total-solution normality at ambient temperature are shown in terms of y_A and x_A in Figure 15.14, from Subba Rao and David [42]. At low

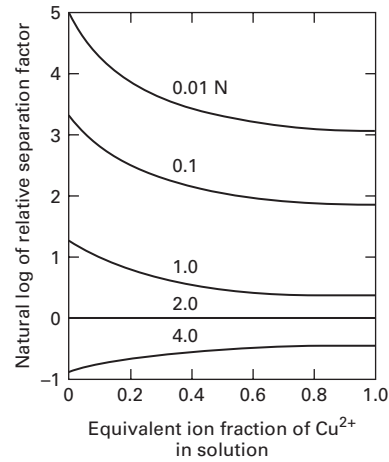


Figure 15.15 Relative separation factor of Cu²⁺ and Na⁺ for ion exchange on Dowex 50-X8 as a function of total normality in the bulk solution. [Reproduced from [45] with permission of Springer Science + Business Media B.V.]

total-solution concentration, the resin is highly selective for copper ion, whereas at high total-solution concentration, the selectivity is reversed to slightly favor sodium ions. A similar trend was observed by Selke and Bliss [43, 44] for exchange between Ca²⁺ and H⁺ using a similar resin, Amberlite IR-120. Selectivity sensitivity is shown dramatically in Figure 15.15, from Myers and Byington [45], where the natural logarithm of the separation factor, $S_{\text{Cu}^{2+}, \text{Na}^+}$, as computed from data of Figure 15.14 with (15-46), is plotted as a function of equivalent ionic fraction, $x_{\text{Cu}^{2+}}$. For dilute solutions of Cu²⁺, $S_{\text{Cu}^{2+}, \text{Na}^+}$ ranges from 0.5 at a total concentration of 4-N to 60 at 0.01-N. In terms of $K_{\text{Cu}^{2+}, \text{Na}^+}$ of (15-44), with $n = 2$, the corresponding variation is only from 0.6 to 2.2.

EXAMPLE 15.7 Ion-Exchange Equilibrium.

An Amberlite IR-120 ion-exchange resin similar to that of Example 15.2, but with a maximum ion-exchange capacity of 4.90 meq/g of dry resin, is used to remove cupric ion from a waste stream containing 0.00975-M CuSO₄ (19.5 meq Cu²⁺/L solution). The spherical resin particles range in diameter from 0.2 to just over 1.2 mm. The equilibrium ion-exchange reaction is of the divalent-monovalent type:



As ion exchange takes place, the meq of cations in the aqueous solution and in the resin remain constant.

Experimental measurements by Selke and Bliss [43, 44] show an equilibrium curve like Figure 15.14 at ambient temperature. It is markedly dependent on total equivalent concentration of the aqueous solution, with the following equilibrium data for cupric ions with a 19.5 meq/L solution:

c , meq Cu ²⁺ /L solution	0.022	0.786	4.49	10.3
q , meq Cu ²⁺ /g resin	0.66	3.26	4.55	4.65

These data follow a highly nonlinear isotherm.

- (a) From the data, compute the molar selectivity coefficient, K , at each value of c for Cu^{2+} and compare it to the value estimated from (15-45) using Table 15.5.
- (b) Predict the milliequivalents of Cu^{2+} exchanged at equilibrium from 10 L of 20 meq Cu^{2+}/L , using 50 g of dry resin with 4.9 meq of H^+/g .

Solution

- (a) Selke and Bliss do not give a value for the resin capacity, Q , in eq/L of bed volume. Assume a value of 2.3. From (15-44):

$$K_{\text{Cu}^{2+}, \text{H}^+} = \left(\frac{C}{Q} \right) \frac{y_{\text{Cu}^{2+}}(1 - x_{\text{Cu}^{2+}})^2}{x_{\text{Cu}^{2+}}(1 - y_{\text{Cu}^{2+}})^2}$$

where $C/Q = 0.0195/2.3 = 0.0085$.

$$x_{\text{Cu}^{2+}} = c_{\text{Cu}^{2+}}/19.5 \quad \text{and} \quad y_{\text{Cu}^{2+}} = q_{\text{Cu}^{2+}}/4.9$$

Using the above values of c and q from Selke and Bliss:

q , meq Cu^{2+}/g	$x_{\text{Cu}^{2+}}$	$y_{\text{Cu}^{2+}}$	$K_{\text{Cu}^{2+}, \text{H}^+}$
0.66	0.00113	0.135	1.35
3.26	0.0403	0.665	1.15
4.55	0.230	0.929	4.04
4.65	0.528	0.949	1.30

The average value of K is 2.0. Values in Table 15.5 when substituted into (15-45) predict $K_{\text{Cu}^{2+}, \text{H}^+} = 3.8/1.3 = 2.9$, which is higher.

- (b) Assume a value of 2.0 for $K_{\text{Cu}^{2+}, \text{H}^+}$ with $Q = 2.3$ eq/L. The total-solution concentration, c , is 0.02 eq/L. Equation (15-44) becomes

$$2.0 = \left(\frac{0.02}{2.3} \right) \frac{y_{\text{Cu}^{2+}}(1 - x_{\text{Cu}^{2+}})^2}{x_{\text{Cu}^{2+}}(1 - y_{\text{Cu}^{2+}})^2} \quad (1)$$

Initially, the solution contains $(0.02)(10) = 0.2$ equivalent of cupric ion with $x_{\text{Cu}^{2+}} = 1.0$. Let a = equivalents of Cu exchanged. Then, at equilibrium, by material balance:

$$x_{\text{Cu}^{2+}} = \frac{0.02 - (a/10)}{0.02} \quad (2)$$

$$y_{\text{Cu}^{2+}} = \frac{(a/50)}{0.0049} \quad (3)$$

Substitution of (2) and (3) into (1) gives

$$2.0 = 0.0087 \frac{\left[\frac{(a/50)}{0.0049} \right] \left[1 - \frac{0.02 - (a/10)}{0.02} \right]^2}{\left[\frac{0.02 - (a/10)}{0.02} \right] \left[1 - \frac{(a/50)}{0.0049} \right]^2} \quad (4)$$

Solving (4), a nonlinear equation for a with MATLAB, gives 0.1887 eq of Cu exchanged. Thus, $0.1887/[(0.020)(10)] = 0.944$ or 94.4% of the cupric ion is exchanged.

Equilibria in Chromatography

As discussed in §15.1.3, separation by chromatography involves many sorption mechanisms, including adsorption on porous solids, absorption or extraction (partitioning) in liquid-supported or bonded solids, and ion transfer in ion-exchange in resins. Thus, at equilibrium, depending upon the sorption mechanism, equations such as (15-19), (15-24), (15-32), and (15-33) for gas adsorption; (15-35) and (15-36) for liquid adsorption; (6-37) to (6-40) for gas absorption; (8-1) for liquid extraction; and (15-38), (15-43), and (15-44) for ion exchange apply.

At equilibrium, the distribution (partition) constant for solute, i , is

$$K_i = q_i/c_i \quad (15-47)$$

where q is concentration in the stationary phase and c is concentration in the mobile phase. Solutes with the highest equilibrium constants will elute from the chromatographic column at a slower rate than solutes with smaller constants.

§15.3 KINETIC AND TRANSPORT RATE CONSIDERATIONS

The design of adsorption, ion exchange, and chromatographic units involves multiple kinetic and mass-transfer steps. For example, consider adsorption in a column packed with porous adsorbent particles, as shown in Figure 15.16, adapted from Athalye et al. [46]. Mass transfer of solute occurs by a series of four rate-limiting processes.

1. Solute is transported along the axis of the column by bulk flow (convection) and parallel to the axis by dispersion through interstices (voids) of the bed of adsorptive particles.

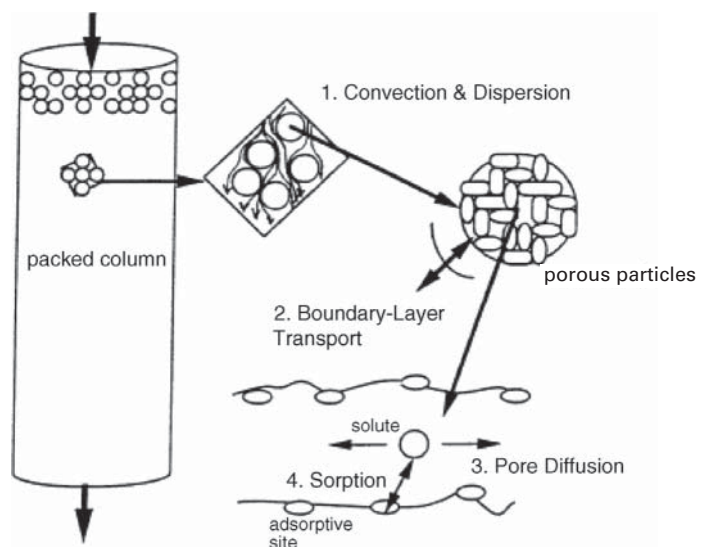


Figure 15.16 Transport-rate processes in adsorption.

2. Solute moves from bulk flow to the outer surface of an adsorbent particle through a thin, stagnant film or boundary layer via external (interphase) solute mass transfer.
3. Solute diffuses within quiescent, fluid-filled pores and to the inner surfaces of the internal porous structure via internal (intrapphase) solute mass transfer.
4. Solute adsorbs to the internal pore surfaces of the adsorbent.

Adsorbed solute may also move via surface diffusion along the internal porous surface of the adsorbent particle.

For chemisorption, which involves bond formation, or biospecific (e.g., antibody-antigen) interactions, the rate of the fourth kinetic step may be slow and even controlling. For physical adsorption, however, Step 4 is rapid relative to Steps 1–3 and is often considered instantaneous because it depends only on the collision frequency and orientation of the molecules with the pore surface. Thus, consideration is often limited to the first three steps.

During regeneration of the adsorbent, the reverse of the four steps occurs, where Step 4, physical desorption, is considered instantaneous. Adsorption and desorption are accompanied by heat transfer because of exothermic heat of adsorption and endothermic heat of desorption. These are often negligible for liquid sorption. Mass transfer external to the particle is limited to convection, dispersion, and boundary layer transport, but heat transfer external to the particle also occurs by these mechanisms as well as by thermal radiation between particles when the fluid is a gas, and by conduction at points of contact by adjacent particles. Conduction and radiation also transfer heat within the particles, in addition to conductive and convective heat transfer by fluid within the pores.

Consider a fixed bed of adsorbent particles in which solute concentration and temperature change continuously with time and location. For a given particle at a particular time, profiles of temperature and solute concentration in the fluid are as shown in Figures 15.17a and b for adsorption and desorption, respectively, where subscripts *b* and *s* refer to bulk fluid and particle outer surface, respectively. The fluid concentration gradient is usually steepest within the particle, whereas the temperature gradient is usually steepest in the boundary layer surrounding the particle. Thus, while resistance to heat transfer is mainly external to the adsorbent particles, the primary resistance to mass transfer resides within the adsorbent particle. All gradients in Figure 15.17 approach asymptotic values at end points.

§15.3.1 External Transport

Rates of convective mass and heat transfer between the outer surface of a particle and surrounding bulk fluid during an adsorption process are represented by

$$\text{rate of mass transfer of } i = n_i = k_c A (c_{b_i} - c_{s_i}) \quad (15-48)$$

$$\text{rate of heat transfer} = q = hA(T_s - T_b) \quad (15-49)$$

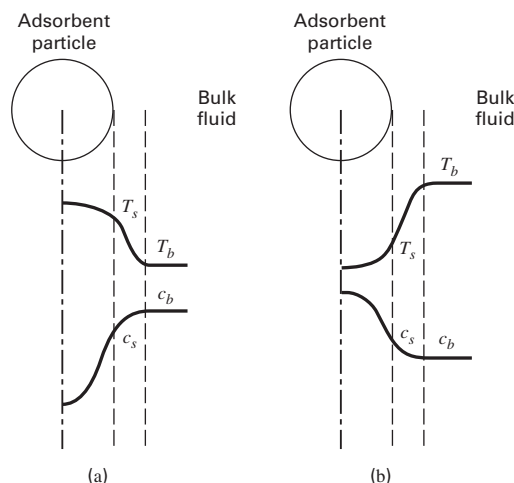


Figure 15.17 Solute concentration and temperature profiles for a porous adsorbent particle surrounded by a fluid: (a) adsorption (b) desorption.

where k_c = mass-transfer coefficient based on concentration units and A is the area for mass and heat transfer.

For a spherical particle surrounded by an infinite, quiescent fluid, mass- and heat-transfer coefficients are small. Assume an insoluble, solid, spherical particle of radius R_p and diameter $D_p = 2R_p$, suspended in an infinite-fluid medium. The radial distance out from the center of the particle is r . The particle is heated so that, at steady state, its surface temperature is constant at T_s . The fluid is quiescent (no free convection) and radiation is ignored, so heat transfer through the fluid is by conduction. The thermal conductivity, k , of the fluid is constant, and temperature far from the particle is T_b . Fourier's second law of heat conduction in the fluid, for spherical coordinates, is

$$\frac{d}{dr} \left(kr^2 \frac{dT}{dr} \right) = 0 \quad (15-50)$$

for $r \geq R_p$, where r is the radial distance from the center of the particle. The boundary conditions are

$$T\{r = R_p\} = T_s \quad (15-51)$$

$$T\{r = \infty\} = T_b \quad (15-52)$$

If (15-50) is integrated twice with respect to r :

$$T = -\frac{C_1}{r} + C_2 \quad (15-53)$$

where C_1 and C_2 are integration constants. Substitution of the boundary conditions, (15-51) and (15-52), results in an expression for the temperature profile in the fluid surrounding the particle:

$$\frac{T - T_b}{T_s - T_b} = \frac{R_p}{r}, \quad r \geq R_p \quad (15-54)$$

The heat flux at the particle's outer surface is given by Fourier's first law of heat conduction applied to the fluid adjacent to the particle outer surface:

$$\frac{q}{A} \Big|_{r=R_p} = -k \frac{dT}{dr} \Big|_{r=R_p} \quad (15-55)$$

From (15-54):

$$\left. \frac{dT}{dr} \right|_{r=R_p} = -\frac{(T_s - T_b)}{R_p} \quad (15-56)$$

Applying Newton's law of cooling for the heat flux at the outer surface of the particle:

$$\left. \frac{q}{A} \right|_{r=R_p} = h(T_s - T_b) \quad (15-57)$$

where h is the heat-transfer coefficient.

Combining (15-55) to (15-57):

$$h = k/R_p \quad (15-58)$$

which rearranges into a Nusselt number:

$$N_{Nu} = hD_p/k = 2 \quad (15-59)$$

A similar development for convective mass transfer using Fick's laws of diffusion gives

$$N_{Sh_i} = k_{c_i}D_p/D_i = 2 \quad (15-60)$$

where D_i is the diffusivity of component i in the mixture.

When the fluid is not quiescent, but flows past a particle, convection increases the convective mass- and heat-transfer coefficients above the values computed from (15-59) and (15-60). Furthermore, transport coefficients now vary around the particle periphery, the largest value occurring where the fluid first impinges on the particle. Correlations of transport data are usually developed for coefficients averaged over the surface of the particle. Typical correlations are those of Ranz and Marshall [47] for Nusselt numbers as high as 30 and Sherwood numbers to 160:

$$N_{Nu} = 2 + 0.60N_{Re}^{1/2}N_{Pr}^{1/3} \quad (15-61)$$

$$N_{Sh_i} = 2 + 0.60N_{Re}^{1/2}N_{Sc_i}^{1/3} \quad (15-62)$$

where from Table 3.9,

$$N_{Pr} = \text{Prandtl number} = C_p\mu/k$$

$$N_{Sc_i} = \text{Schmidt number} = \mu/\rho D_i$$

$$N_{Re} = \text{Reynolds number} = D_p G/\mu$$

where D_p is the characteristic length and G is the mass flow per unit area (mass velocity).

All fluid properties are evaluated at the average temperature of the film. Equations (15-61) and (15-62) reduce to (15-59) and (15-60), respectively, when G is zero.

When particles are packed in a bed, fluid-flow patterns are difficult to model, and single-particle correlations (15-61) and (15-62) cannot be used to estimate average external-transport coefficients for the particles. Ranz [48] showed that equations of the same form as (15-61) and (15-62) correlate external-transport data for beds packed with spherical particles. However, most early investigators, starting with Gamson et al. [49], developed correlations in the form of

the Chilton and Colburn j -factors [50], given in Table 3.9 and discussed in §3.5.

$$j_D = N_{StM}N_{Sc}^{2/3} = f\{N_{Re}\} \quad (15-63)$$

$$j_H = N_{St}N_{Pr}^{2/3} = f\{N_{Re}\} \quad (15-64)$$

where from Table 3.9,

$$N_{StM} = k_c\rho/G \quad \text{and} \quad N_{St} = h/C_pG$$

where different Reynolds number functions apply to different regions. Various forms of the Reynolds number have been used, including $D_p G/\mu$ and $D_p G/\epsilon_b\mu$, in attempts to account for bed void fraction, ϵ_b , where G is the superficial mass velocity based on the empty-bed cross-sectional area, and G/ϵ_b (a larger value) is the effective mass velocity through the void region of the bed. Notable among correlations of this type are those of Sen Gupta and Thodos [51], Petrovic and Thodos [52], and Dwivedi and Upadhyay [53].

A study by Wakao and Funazkri [54] reanalyzed 37 sets of previously published mass-transfer data, with Sherwood-number corrections for axial dispersion. The resulting correlation, which represents a return to the form of (15-62), is

$$N_{Sh_i} = 2 + 1.1N_{Re}^{1/2}N_{Sc_i}^{1/3} \quad (15-65)$$

The data cover Schmidt numbers of 0.6 to 70,600, Reynolds numbers of 3 to 10,000, and particle diameters from 0.6 to 17.1 mm. Particle shapes include spheres, short cylinders, flakes, and granules. By analogy, the corresponding equation for fluid-particle convective heat transfer in packed beds is

$$N_{Nu} = 2 + 1.1N_{Re}^{1/2}N_{Pr}^{1/3} \quad (15-66)$$

When (15-65) and (15-66) are used with beds packed with nonspherical particles, D_p is the equivalent diameter of a spherical particle. The following suggestions have been proposed for computing equivalent diameters from particle geometry. These suggestions may be compared to a short cylinder with diameter, D , equal to length, L .

1. D_p = diameter of a sphere with the same external surface area:

$$\pi D_p^2 = \pi DL + \pi D^2/2$$

$$\text{and} \quad D_p = (DL + D^2/2)^{0.5} = 1.225D$$

2. D_p = diameter of a sphere with the same volume:

$$\pi D_p^3/6 = \pi D^2L/4 \quad \text{and} \quad D_p = (3D^2L/2)^{1/3} = 1.145D$$

3. D_p = 4 times the hydraulic radius, r_H , where for a packed bed,

$$4r_H = 6/a_v$$

a_v = external particle surface area/volume of particle
Thus,

$$a_v = \frac{\pi DL + \pi D^2/2}{\pi D^2L/4} = \frac{6}{D} \quad \text{and} \quad D_p = 4r_H = \frac{6D}{6} = 1.0D$$

The hydraulic radius concept is equivalent to replacing D_p in the Reynolds number by $\psi D'_p$, where ψ is sphericity and D'_p is given by Suggestion 2: The sphericity is defined by:

$$\psi = \frac{\text{Surface area of a sphere of same volume as particle}}{\text{Surface area of particle}}$$

For a cylinder of $D = L$,

$$\psi = \frac{\pi D_p^2}{\pi D L + 2 \left(\frac{\pi D^2}{4} \right)} = \frac{\pi (1.145 D)^2}{\frac{3}{2} \pi D^2} = 0.874$$

and $\psi D'_p = (0.874)(1.145 D) = D$, the diameter of the cylinder.

Suggestions 2 and 3 are widely used. Suggestion 3 is conveniently applied to crushed particles of irregular surface and isotropic shape, but with no obvious longer or shorter dimension. In that case, D'_p is taken as the size of the particle and the sphericity is approximately 0.65, as discussed by Kunii and Levenspiel [55].

EXAMPLE 15.8 External Transport Coefficients in a Packed Bed.

Acetone vapor in a nitrogen stream is removed by adsorption in a fixed bed of activated carbon. At a location in the bed where the pressure is 136 kPa, the bulk gas temperature is 297 K, and the bulk mole fraction of acetone is 0.05, estimate the external gas-to-particle mass-transfer coefficient for acetone and the external particle-to-gas heat-transfer coefficient. Additional data are:

Average particle diameter = 0.0040 m

Gas superficial molar velocity = 0.00352 kmol/m²-s

Solution

Because the temperature and composition are known only for the bulk gas and not at the particle external surface, gas properties at bulk gas conditions are used. From the CHEMCAD process simulator, relevant properties for use in (15-65) and (15-66) are:

Viscosity = $\mu = 0.0000165$ Pa-s (kg/m-s); Density = $\rho = 1.627$ kg/m³

Thermal conductivity = $k = 0.0240$ W/m-K = 0.024×10^{-3} kJ/m-K-s

Heat capacity at constant pressure = 31.45 kJ/kmol-K

Molecular weight = $M = 29.52$

Thus, specific heat $C_p = 31.45/29.52 = 1.065$ kJ/kg-K

Other parameters are:

Gas mass velocity $G = 0.00352(29.52) = 0.1039$ kg/m²-s

Assume $\psi = 0.65$; therefore, $D_p = 0.65(0.004) = 0.0026$ m

The acetone gas diffusivity, D_i , in nitrogen at 297 K and 136 kPa is 0.085×10^{-4} m²/s; independent of composition and

$$N_{Re} = D_p G / \mu = 0.0026(0.1039) / (0.0000165) = 16.4$$

$$N_{Sc} = \mu / \rho D_i = 0.0000165 / (1.627)(0.000085) = 1.19$$

$$N_{Pr} = C_p \mu / k = (1.065)(0.0000165) / (0.000024) = 0.73$$

From (15-65):

$$N_{Sh} = 2 + 1.1(16.4)^{0.6} (1.19)^{1/3} = 8.24$$

From (15-65), the mass-transfer coefficient for acetone is

$$\begin{aligned} k_{c_i} &= N_{Sh}(D_i/D_p) = 8.24(0.000085/0.0026) \\ &= 0.027 \text{ m/s} = 0.088 \text{ ft/s} \end{aligned}$$

From (15-66):

$$\begin{aligned} N_{Nu} &= 2 + 1.1(16.4)^{0.6} (0.73)^{1/3} = 7.31 \\ h &= N_{Nu}(k/D_p) = 7.31(0.0240/0.0026) \\ &= 67.5 \text{ W/m}^2\text{-K or } 11.9 \text{ Btu/h-ft}^2\text{-}^\circ\text{F} \end{aligned}$$

§15.3.2 Internal Transport

Porous, adsorbent particles have a sufficiently high, effective thermal conductivity that temperature gradients within the particle are usually negligible. However, internal (intraparticle) mass transfer in the particle is the largest resistance to equilibrium solute partitioning between fluid carrier and stationary phases, and must be considered. Mechanisms for mass transfer in the pores are analogous to those described for porous membranes in §14.3. However, in membranes, transport of solute occurs through the membrane, whereas in sorption, net solute transport occurs radially inward into the interior of the particle during sorption and radially outward from the interior in desorption.

Internal transport in porous particles may be described like that for catalytic chemical reactions in porous catalyst pellets. The first pore model was that of Thiele [56], who considered a first-order, isothermal, irreversible reaction on the surface of a single, straight, cylindrical pore closed at one end. Thiele's treatment was extended to a porous spherical pellet by Wheeler [57], who utilized an effective diffusivity, D_e , for sorption.

Consider the porous spherical pellet in Figure 15.18, where fluid concentration, c , refers to the solute. A material balance

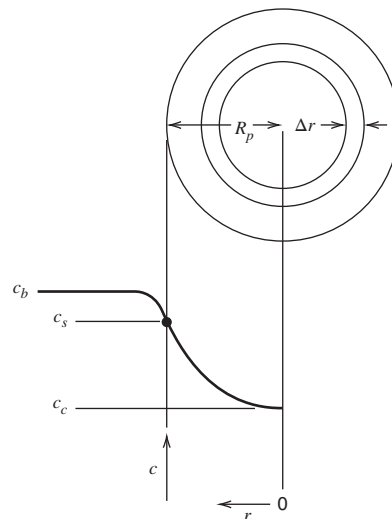


Figure 15.18 Solute concentration profile in adsorbent particle.

in moles or mass per unit time over a spherical-shell volume of thickness Δr involves diffusion of solute into the shell at radius $r + \Delta r$, adsorption within the shell, and diffusion out at radius r . Using Fick's first law:

$$4\pi(r + \Delta r)D_e \left. \frac{\partial c}{\partial r} \right|_{r+\Delta r} = 4\pi r^2 \Delta r \frac{\partial q}{\partial t} + 4\pi r^2 D_e \left. \frac{\partial c}{\partial r} \right|_r \quad (15-67)$$

Dividing by $4\pi\Delta r$, taking the limit as $\Delta r \rightarrow 0$, and collecting terms,

$$D_e \left(\frac{\partial^2 c}{\partial r^2} + \frac{2}{r} \frac{\partial c}{\partial r} \right) = \frac{\partial q}{\partial t} \quad (15-68)$$

where q is the amount adsorbed per unit volume of porous pellet and effective diffusivity D_e applies to the entire spherical-shell surface area even though only about 50% of it is available as pores for diffusion. For liquid-phase diffusion in the pores, the effective diffusivity is given by (14-14), in terms of volume fraction of pellet pores, solute molecular diffusivity in the fluid within the pore, pore tortuosity, and a possible restrictive factor for large solute molecules. For gas-phase diffusion in pores, the effective diffusivity is given by (14-18), which accounts for possibility of Knudsen diffusion, with diffusivity D_K for very small pore diameters and/or low total pressures. Although (14-14) and (14-18) strictly apply only to equimolar counterdiffusion, they can be used as an approximation for unimolecular diffusion of solute molecules dilute in carrier fluids. A diffusion mechanism not accounted for directly in (14-18) is that of surface diffusion along the pore wall due to a concentration gradient of adsorbate (adsorbed solute) along the wall.

Fick's first law for diffusion through a fluid in a pore is

$$n_i = -D_i A (dc_i/dx) \quad (15-69)$$

where n_i is the molar rate of ordinary diffusion of i through a fluid in the x -direction, perpendicular to cross-sectional area, A , for diffusivity, D_i , and concentration, c_i , in moles/unit volume of fluid. A modified Fick's first law applies to surface diffusion, as suggested by Schneider and Smith [58]. Thus,

$$(n_i)_s = -(D_i)_s A_s (c_i)_s / dx \quad (15-70)$$

where A_s is the pore surface area, $(c_i)_s$ is the surface concentration of adsorbate in moles/unit surface area, and $(D_i)_s$ is the surface diffusivity as defined by (15-70).

For convenience, (15-70) is converted to the flux form of (15-69) so that the two diffusion mechanisms can be combined in a single transport rate equation. In flux form, (15-69) is

$$N_i = n_i/A = -D_i (dc_i/dx) \quad (15-71)$$

The corresponding flux form of (15-70) is obtained by dividing both sides by pore cross-sectional area and converting surface concentration, $(c_i)_s$, in moles/unit surface area to the loading, q , in mol/g of adsorbate, by using the product of pore

surface/pore volume times the reciprocal of the adsorbent particle density times the particle porosity.

$$(N_i)_s = -(D_i)_s \frac{\rho_p}{\epsilon_p} \left(\frac{dq_i}{dx} \right) \quad (15-72)$$

Substituting linear adsorption, $q_i = K_i c_i$, into (15-72) and adding the result to (15-71), the total flux is

$$N_i = - \left[D_i + (D_i)_s \frac{\rho_p K_i}{\epsilon_p} \right] \frac{dc_i}{dx} \quad (15-73)$$

In terms of the effective diffusivity employed in (15-68):

$$D_e = \frac{\epsilon_p}{\tau} \left\{ \left[\frac{1}{1/D_i + 1/D_K} \right] + (D_i)_s \frac{\rho_p K_i}{\epsilon_p} \right\} \quad (15-74)$$

Equation (15-74) should be used with caution, because, as discussed by Riekert [59], tortuosity, τ , for pore-volume diffusion may not be the same as for surface diffusion.

Based on the study by Sladek, Gilliland, and Baddour [60], values of surface diffusivity of light gases for physical adsorption are typically from 5×10^{-3} to 10^{-6} cm²/s, the larger values applying to cases of a low differential heat of adsorption. For nonpolar adsorbates, the surface diffusivity in cm²/s may be estimated from the following correlation [60],

$$D_s = 1.6 \times 10^{-2} \exp[-0.45(-\Delta H_{\text{ads}})/mRT] \quad (15-75)$$

where $m = 2$ for conducting adsorbents such as carbon and $m = 1$ for insulating adsorbents.

EXAMPLE 15.9 Effective Diffusivity in Porous Silica Gel.

Porous silica gel particles 1.0 mm in diameter, with a particle density of 1.13 g/cm³, a porosity of 0.486, an average pore radius of 11 Å, and a tortuosity of 3.35 are used to adsorb propane from helium. At 100°C, diffusion in the pores is controlled by both Knudsen and surface diffusion. Estimate the effective diffusivity. The differential heat of adsorption is -5,900 cal/mol. At 100°C, the adsorption constant (for a linear isotherm) is 19 cm³/g.

Solution

Pore diameter, d_p , = 22 Å = 22×10^{-10} m = 22×10^{-8} cm.

Molecular weight of propane, M_i , = 44.06.

From (14-21), the Knudsen diffusivity for propane is

$$D_K = 4,850 (22 \times 10^{-8}) (373/44.06)^{1/2} = 3.7 \times 10^{-3} \text{ cm}^2/\text{s}$$

From (15-75), using $m = 1$,

$$D_s = 1.6 \times 10^{-2} \exp\{(-0.45)(5,900)/[(1)(1.987)(373)]\} \\ = 4.45 \times 10^{-4} \text{ cm}^2/\text{s}$$

Equation (15-67) reduces to $D_e = (\epsilon_p/\tau)D_K + (\rho_p K/\tau)D_s$

$$= (0.486/3.35)(3.17 \times 10^{-3}) + (1.13)(19)(4.45 \times 10^{-4})/3.35 \\ = 0.46 \times 10^{-3} + 2.85 \times 10^{-3} = 3.31 \times 10^{-3} \text{ cm}^2/\text{s}$$

Schneider and Smith [58] report a value of $1.22 \times 10^{-3} \text{ cm}^2/\text{s}$ for D_e with a value of 0.88×10^{-3} for the contribution of surface diffusion. Thus, the estimated contribution from surface diffusion is high by a factor of about 3. In either case, the contribution due to surface diffusion is large. A review of surface diffusion is given by Kapoor, Yang, and Wong [61].

§15.3.3 Mass Transfer in Ion Exchange and Chromatography

As discussed by Helfferich [62], two major mass-transfer resistances occur in ion exchange: the external mass-transfer resistance due to the boundary layer surrounding the ion-exchange bead and the internal diffusional resistance due to the resin bead. Either or both can be rate-controlling; in either case, the resin bead diameter is an important factor. In general, external mass-transfer is rate-controlling at very low exchange-ion concentrations, say below 0.01-N, whereas internal mass transfer (particle diffusion) controls at high concentrations (say above 1.0-N). It has also been observed that a large separation factor, as defined by (15-46), favors external mass-transfer control, and that divalent ions diffuse more slowly through the resin than monovalent ions. Usually, the rate-determining step is not the chemical reaction between exchanging ions and resin.

The external mass-transfer coefficient for flow of fluid through a fixed bed of ion-exchange resin is obtained from the same relation, (15-65), used for fixed-bed adsorption. For internal mass transfer, it is customary to assume the ion-exchange resin bead is a single quasi-homogeneous phase and that diffusivity of the diffusing ion is constant at a given temperature. Then, (15-68) can be used, where D_e is a diffusivity determined by experiments. These depend on: (1) ion size and charge, with smaller, monovalent ions diffusing faster; (2) degree of cross-linking and resin swelling, with larger diffusivities favored by swelling and less cross-linking; and (3) temperature.

Diffusivity measurements in ion-exchange resins have been made with isotopes of the ions to obtain self-diffusion coefficients independent of ion concentration. Typical data are those of Soldano [63], shown in Figure 15.19 for Na^+ , Zn^{2+} , and Y^{3+} in a sulfonated styrene-divinylbenzene cation exchanger at 0.2 and 25°C. Note that order-of-magnitude diffusivities for small molecules are:

- 0.1 cm^2/s in the gas phase
- $1 \times 10^{-5} \text{ cm}^2/\text{s}$ in the liquid phase
- $1 \times 10^{-7} \text{ cm}^2/\text{s}$ in polymers

Figure 15.19 demonstrates that diffusivities depend on the degree of cross-linking and ionic charge. Values are much less than those found in liquids, especially for divalent and trivalent ions, which have diffusivities even smaller than those for small molecules in polymers.

For chromatography in packed beds, equations (15-65) and (15-66), if necessary, may be used to determine external mass

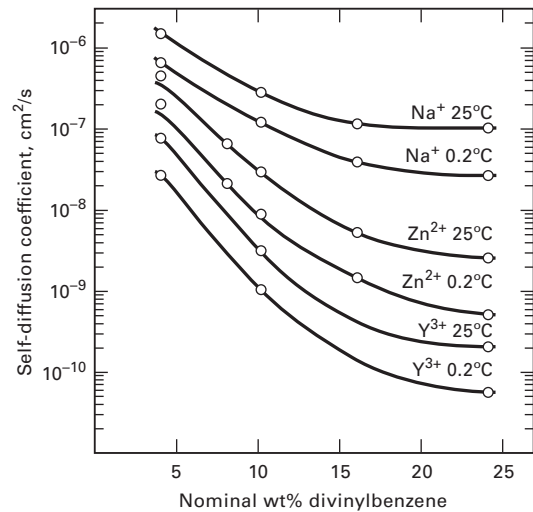


Figure 15.19 Self-diffusion coefficients for cations in a resin as a function of cross-linking with divinylbenzene. [Reproduced from Soldano [63].]

and heat transport coefficients, respectively. Where internal mass transfer resistance is negligible (e.g., for relatively slow percolation velocities and/or monolithic or stacked membrane stationary phases) the rate for convective dispersion must be considered. Appropriate relations are discussed in §15.3.2 of the third edition of this book. If a coated flat plate or a tube with a coated inner wall is used, correlations discussed in Chapter 3 are applicable. In some cases, entry regions of finite length exist, particularly for laminar flow, such that transport coefficients vary with axial location, decrease with length, and eventually approach an asymptotic value. For internal sorbent diffusion, Fick's second law applies, and the effective diffusivity depends on factors discussed in §15.3.2.

§15.4 EQUIPMENT FOR SORPTION OPERATIONS

A variety of configurations and operating procedures are employed for commercial sorption-separation equipment due mainly to the wide range of sorbent particle sizes and the need, in most applications, to regenerate the solid sorbent.

§15.4.1 Adsorption

For adsorption, Table 15.7 lists widely used equipment and operations. The devices are classified into the three operating modes in Figure 15.20. In **slurry adsorption**, shown in Figure 15.20a, a powdered adsorbent such as activated carbon, of $d_p < 1 \text{ mm}$, is added with water to an agitated tank to form a slurry. The internal resistance to mass transfer within the pores of small particles is small. However, even with good stirring, the external resistance to mass transfer from bulk liquid to the external surface of the adsorbent particles may not be small because small particles tend to move with the liquid. Thus, the rate of adsorption may be controlled by

Table 15.7 Commercial Methods for Adsorption Separations

Phase Condition of Feed	Contacting Device	Adsorbent Regeneration Method	Main Application
Liquid	Slurry in an agitated vessel	Adsorbent discarded	Purification
Liquid	Fixed bed	Thermal reactivation	Purification
Liquid	Simulated moving bed	Displacement purge	Bulk separation
Gas	Fixed bed	Thermal swing (TSA)	Purification
Gas	Combined fluidized bed–moving bed	Thermal swing (TSA)	Purification
Gas	Fixed bed	Inert-purge swing	Purification
Gas	Fixed bed	Pressure swing (PSA)	Bulk separation
Gas	Fixed bed	Vacuum swing (VSA)	Bulk separation
Gas	Fixed bed	Displacement purge	Bulk separation

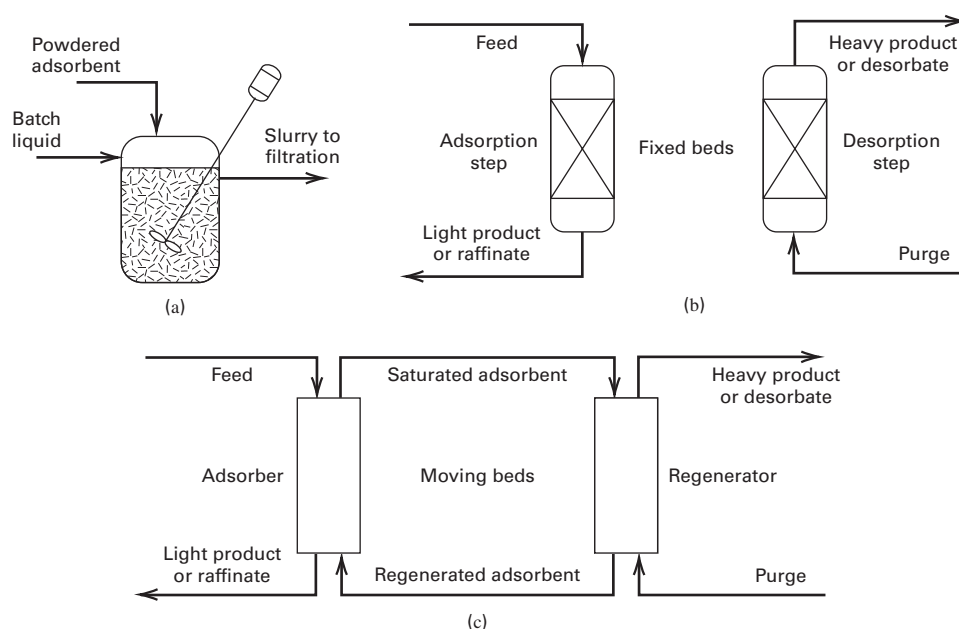


Figure 15.20 Contacting modes for adsorption and ion exchange: (a) Stirred-tank, slurry operation; (b) Cyclic fixed-bed, batch operation; (c) Continuous countercurrent operation.

external mass transfer. The main application of this operation is removal of small amounts of large, dissolved molecules, such as coloring agents, from water. Spent adsorbent, which is removed from the slurry by sedimentation or filtration, is discarded because it is difficult to desorb large molecules. The slurry system, also called **contact filtration**, can be operated continuously.

Fixed-bed adsorption with a cyclic-batch operating mode, shown in Figure 15.20b, is widely used with either liquid or gas feeds. Adsorbent particle sizes range from 0.05 to 1.2 cm. Both bed pressure drop and solute mass-transfer rate increase with decreasing particle size. The optimal particle size is determined mainly from these two considerations. To avoid jiggling, fluidizing the bed, or blowing out fines during adsorption, the feed flow is often downward. For removal of small amounts of dissolved hydrocarbons from water, spent adsorbent is removed from the vessel and reactivated thermally at high temperature or discarded. Fixed-bed adsorption, also called **percolation**, is used for removal of dissolved organic compounds from water. For purification

or bulk separation of gases, the adsorbent is almost always regenerated in-place by one of the five methods listed in Table 15.7 and considered next.

In **thermal (temperature)-swing-adsorption (TSA)**, the adsorbent is regenerated by desorption at a temperature higher than used during adsorption, as shown in Figure 15.21. Bed temperature is increased by (1) heat transfer from heating coils located in the bed, followed by pulling a moderate vacuum; or (2) more commonly, by heat transfer from an inert, non-adsorbing, hot purge gas, such as steam. Following desorption, the bed is cooled before adsorption is resumed. Because bed heating and cooling requires hours, a typical cycle time for TSA is hours to days. Therefore, if the quantity of adsorbent in the bed is to be reasonable, TSA is practical only for purification involving small adsorption rates.

In **pressure-swing adsorption (PSA)**, adsorption takes place at an elevated pressure, whereas desorption occurs at near-ambient pressure, as shown in Figure 15.21. PSA is used for bulk separations because the bed can be depressurized and repressurized rapidly, making it possible to operate at cycle

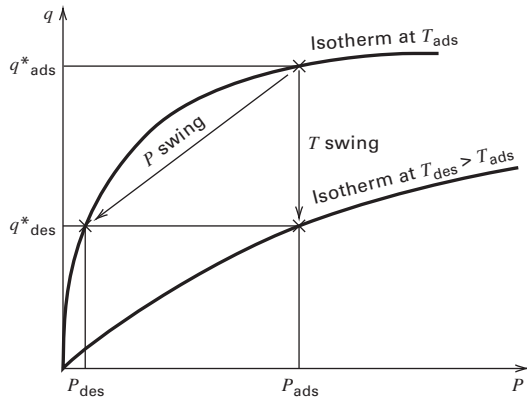


Figure 15.21 Schematic representation of pressure-swing and thermal-swing adsorption.

times of seconds to minutes. Because of these short times, the beds need not be large even when a substantial fraction of the feed gas is adsorbed. If adsorption takes place at near-ambient pressure and desorption under vacuum, the cycle is sometimes referred to as **vacuum-swing adsorption (VSA)**.

PSA and VSA are widely used for air separation. If a zeolite molecular-sieve adsorbent is used, equilibrium is rapidly established and nitrogen is preferentially adsorbed. Non-adsorbed, high pressure product gas is a mixture of oxygen and argon with a small amount of nitrogen. Alternatively, if a carbon molecular-sieve adsorbent is used, the particle diffusivity of oxygen is about 25 times that of nitrogen. As a result, the selectivity of adsorption is controlled by mass transfer, and oxygen is preferentially adsorbed. The resulting high-pressure product is nearly pure nitrogen. In both cases, the adsorbed gas, which is desorbed at low pressure, is impure. For the separation of air, large plants use VSA because it is more energy-efficient than PSA. Small plants often use PSA because the cycle is simpler.

In **displacement-purge (displacement-desorption) cycles**, a strongly adsorbed purge gas is used to displace adsorbed species. Another step is then required to recover the purge gas. Displacement-purge cycles are viable only where TSA, PSA, and VSA cannot be used because of pressure or temperature limitations. One application is separation of medium-MW linear paraffins ($C_{10}-C_{18}$) from branched-chain and cyclic hydrocarbons by adsorption on 5A zeolite. Ammonia, which is separated from the paraffins by flash vaporization, is used as the purge.

In an **inert-purge-swing regeneration**, desorption is at the same temperature and pressure as the adsorption step, because the gas used for purging is non-adsorbing (inert) or only weakly adsorbing. This method is used only when the solute is weakly adsorbed, easily desorbed, and of little or no value. The purge gas must be inexpensive so that it does not have to be purified before recycle.

Most commercial adsorption applications involve fixed beds that cycle between adsorption and desorption. Thus, compositions, temperature, and/or pressure at a given bed location vary with time. Alternatively, a continuous, countercurrent

operation, where such variations do not occur, can be envisaged, as shown in Figure 15.20c and discussed by Ruthven and Ching [65]. A difficulty with this scheme is the need to circulate solid adsorbent in a moving bed to achieve steady-state operation. The first commercial application of countercurrent adsorption and desorption was the moving bed used by the Hypersorption process for recovery, by adsorption on activated carbon, of light hydrocarbons from various gas streams in petroleum refineries, as discussed by Berg [66]. Only a few units were installed because of problems with adsorbent attrition, difficulties in regenerating the adsorbent when heavier hydrocarbons in the feed gas were adsorbed, and unfavorable economics compared to distillation. Newer adsorbents with a much higher resistance to attrition and possible applications to more difficult separations are reviving interest in moving-bed units.

A fluidized bed can be used instead of a fixed bed for adsorption and a moving bed for desorption, as shown in Figure 15.22, provided that particles are attrition-resistant. In the adsorption section, sieve trays are used with raw gas passing up through the perforations and fluidizing the adsorbent. The fluidized particles flow like a liquid across the tray, into the downcomer, and onto the tray below. In the

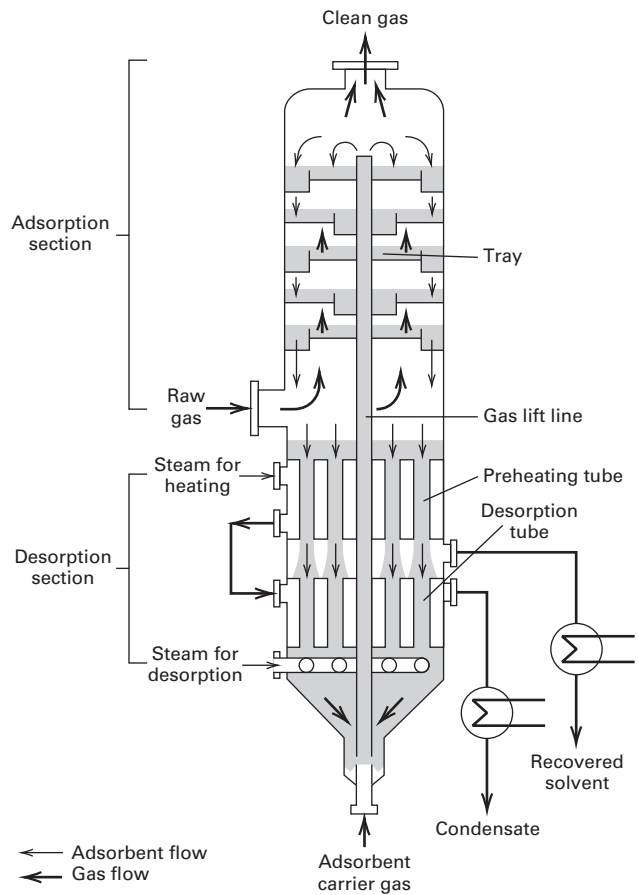


Figure 15.22 Purasiv™ process with a fluidized bed for adsorption and moving bed for desorption.

[Reproduced from [64] with permission of the American Institute of Chemical Engineers.]

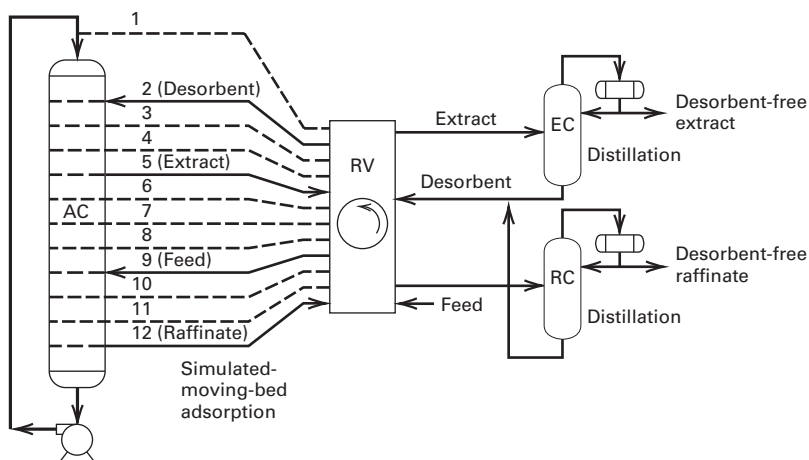


Figure 15.23 Sorbex hybrid simulated-moving-bed process for bulk separation. AC, adsorbent chamber; RV, rotary valve; EC, extract column; RC, raffinate column.

[Reproduced from [67] with permission of the American Institute of Chemical Engineers.]

food industry, this type of tray is rotated. From the adsorption section, the solids pass to the desorption section, where, as moving beds, they first flow down through preheating tubes and then through desorption tubes. Steam is used for indirect heating in both sets of tubes and for stripping in the desorption tubes. Moving beds, rather than fluidized beds on trays, are used in desorption because the stripping-steam flow rate is insufficient for fluidizing the solids. At the bottom of the unit, the regenerated solids are picked up by a carrier gas, which flows up through a gas-lift line to the top, where the solids settle out on the top tray to repeat the adsorption cycle. Keller [64] reports that this configuration, which was announced in 1977, is used in more than 50 units worldwide to remove small amounts of solvents from air. Other applications of TSA include removal of moisture, CO_2 , and pollutants from gas streams.

A successful countercurrent adsorption system for commercial separation of liquid mixtures is the simulated-moving-bed system for the UOP Sorbex process. As shown in Figure 15.23, it is a hybrid system with two added distillation columns. As described by Broughton [67], the bed is held stationary in one column, which is equipped with a number (perhaps 12) of liquid feed entry and discharge locations. By using a rotary valve (RV) to shift the locations of feed entry, **desorbent** entry, **extract (adsorbed)** removal, and **raffinate (nonadsorbed)** removal, countercurrent movement of solids is simulated by a downward movement of liquid. For the valve positions shown in Figure 15.23, Lines 2 (entering desorbent), 5 (exiting extract), 9 (entering feed), and 12 (exiting raffinate) are operational, with all other numbered lines closed. Liquid is circulated down through and, externally, back up to the top of the column by a pump. Ideally, an infinite number of entry and exit locations exist and the valve would continuously change the four operational locations. Since this is impractical, a finite number of locations are used and valve changes are made periodically.

In Figure 15.23, when the valve is moved to the next position, Lines 3, 6, 10, and 1 become operational. Thus, raffinate removal is relocated from the bottom to the top of the bed. Thus, the bed has no top or bottom. Humphrey and Keller [68] cite 100 commercial Sorbex installations. Applications

include separations of *p*-xylene from C8 aromatics; *n*-paraffins from branched and cyclic hydrocarbons; olefins from paraffins; *p*- or *m*-cymene (or cresol) from cymene (or cresol) isomers; and fructose from dextrose and polysaccharides.

§15.4.2 Ion Exchange

Ion exchange employs the same modes of operation as adsorption. Although use of fixed beds, as in Figure 15.20b in a cyclic operation is most common, stirred tanks are used for batch contacting, with an attached strainer or filter to separate resin beads from the solution after equilibrium is approached. Agitation is mild to avoid resin attrition, but sufficient to achieve suspension of resin particles.

To increase resin utilization and achieve high efficiency, efforts have been made to develop continuous, countercurrent contactors, two of which are shown in Figure 15.24. The Higgins contactor [69] operates as a moving, packed bed by using intermittent hydraulic pulses to move incremental portions of the bed from the ion-exchange section up, around, and down to the backwash region, down to the regenerating section, and back up through the rinse section to the ion-exchange section to repeat the cycle. Liquid and resin move countercurrently. The Himsley contactor [70] has a series of trays on which the resin beads are fluidized by upward flow of liquid. Periodically the flow is reversed to move incremental amounts of resin from one stage to the stage below. The batch of resin at the bottom is lifted to the wash column, then to the regeneration column, and then back to the top of the ion-exchange column for reuse.

§15.4.3 Chromatography

Operation modes for industrial-scale chromatography are of three major types (Ganetsos and Barker [71]). The first, and most common, is a transient mode that is a scaled-up version of an analytical chromatograph, referred to as batch, elution, or **differential chromatography**. Packed columns of diameter up to 4.6 m and packed heights to 12 m have been reported. As shown in Figure 15.25 and discussed by Wankat [72], a recycled solvent or carrier gas is fed continuously into a sorbent-packed column. The feed mixture and recycle is

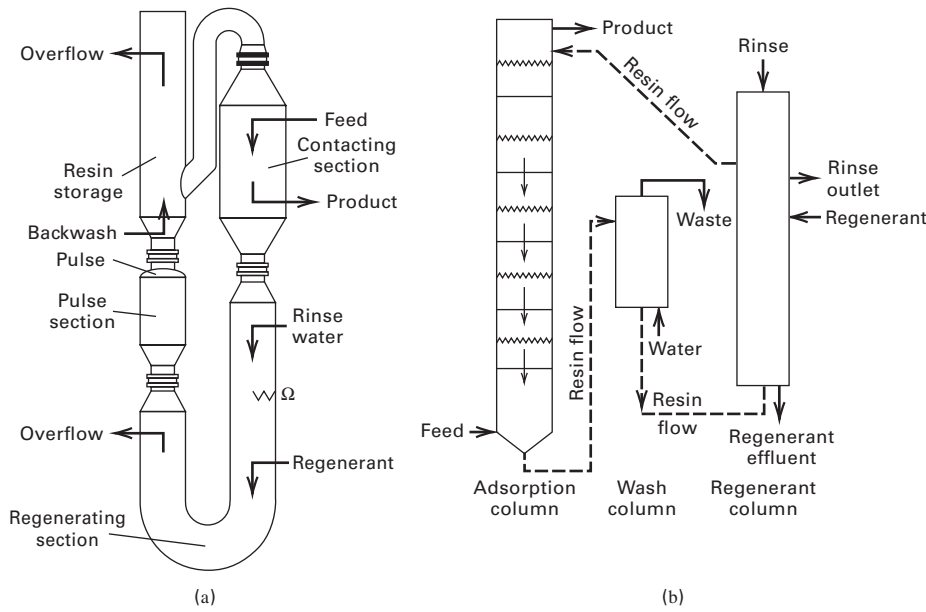


Figure 15.24 Continuous countercurrent ion-exchange contactors. (a) Higgins moving packed-bed process. (b) Himsley fluidized-bed process.

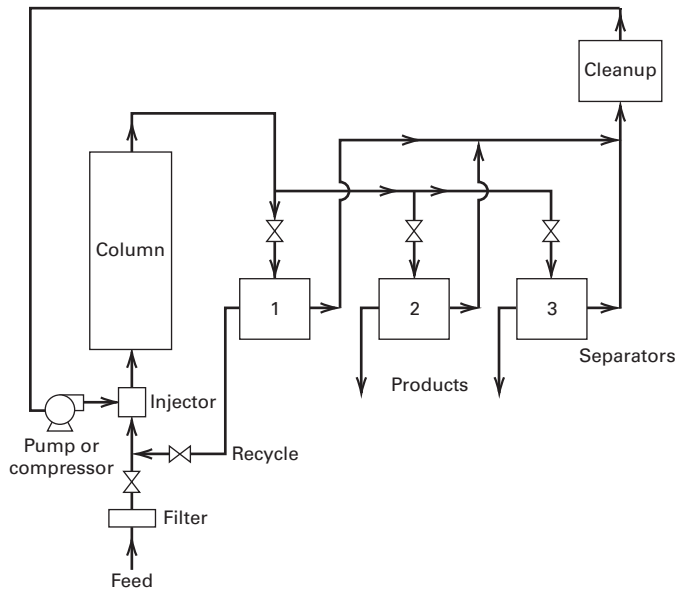


Figure 15.25 Large-scale, batch elution chromatography process.

pulsed into the column by an injector. A timer or detector (not shown) splits the column effluent by residence time, sending it to different separators (condensers, evaporators, distillation columns, etc.). Each separator is designed to remove a particular feed component from the carrier fluid. An additional cleanup step is required to purify the carrier fluid before it is recycled to the column. Separator 1 produces no product because it handles an effluent pulse containing carrier fluid and two or more feed components, which are recovered and recycled to the column. Thus, the batch chromatograph operates somewhat like a batch-distillation column, producing a nearly pure cut for each component in the feed and slop cuts for recycle. The system shown in Figure 15.25 is designed to separate a binary system. If three more separators are added, the system can separate a five-component feed into five products.

The second operational mode is on-off or **frontal chromatography**. The mobile phase (gas or liquid) containing solute(s) is fed continuously to a packed chromatographic bed until the adsorbed solute content in the entire bed approaches saturation. Whereupon, desorbing mobile phase(s) is/are applied to the bed to desorb captured solute(s). Desorbing phases often consist of an isocratic step, or gradient change in solvent composition that changes the pH, ionic strength, or polarity within quiescent fluid-filled pores. This change induces desorption of solute(s) adsorbed from the original feed. Repetition of the adsorption/desorption cycle is often interspersed by a cleaning step in order to maximize packed bed capacity.

The third operational mode is **displacement chromatography**. Following near-saturation of a packed bed with adsorbed solute(s) loaded from a mobile feed phase, a similar mobile phase is applied to the bed, except that it contains a solute (the displacing agent) whose affinity for the adsorbent exceeds that of adsorbed solute(s). The displacing agent produces consecutive zones of eluting solutes, in order of lowest to highest affinity for the stationary packed resin. Displaced solute concentrations in these zones exceeds that for corresponding solutes in the feed solution. Thus, use of a displacing agent both purifies and concentrates solute(s) in a dilute feed. Upon removal of the displacer by an appropriate change in fluid phase composition, the load/elute process may be repeated.

§15.5 SLURRY AND FIXED-BED ADSORPTION SYSTEMS

In this section, design procedures are presented and illustrated by example for the most common sorption operations, including three modes of slurry adsorption; thermal-swing adsorption; pressure-swing adsorption; continuous, countercurrent adsorption; simulated-moving-bed systems; and an ion-exchange cycle.

§15.5.1 Slurry Adsorption (Contact Filtration)

Three modes of adsorption from a liquid in an agitated vessel are of interest. First is the **batch mode**, in which a batch of liquid is contacted with a batch of adsorbent for a period of time, followed by discharge of the slurry from the vessel, and filtration to separate solids from liquid. The second is a **continuous mode**, in which liquid and adsorbent are continuously added to and removed from the agitated vessel. In the third, **semi-batch** or **semi-continuous mode**, liquid is continuously fed, then removed from the vessel, where it is contacted with adsorbent, which is retained in the vessel contacting zone until it is nearly spent.

Design models for batch, continuous, and semicontinuous modes are developed next, followed by an example of their applications. In all models, the slurry is assumed to be perfectly mixed in the turbulent regime to produce a fluidized-like bed of sorbent. Perfect mixing is approached by using a liquid depth of from one to two vessel diameters, four vertical wall baffles, and one or two marine propellers or pitched blade turbines on a vertical shaft. With proper impeller speed, axial flow achieves complete suspension. For semi-continuous operation, a clear liquid region is maintained above the suspension for liquid withdrawal.

Because small particles are used in slurry adsorption and the relative velocity between particles and liquid in an agitated slurry is low (small particles tend to move with the liquid), the rate of adsorption is assumed to be controlled by external, rather than internal, mass transfer.

Batch Mode

The rate of solute adsorption, as controlled by external mass transfer, is

$$-\frac{dc}{dt} = k_c a (c - c^*) \quad (15-76)$$

where c is the solute concentration in the bulk liquid; c^* is the concentration in equilibrium with the adsorbent loading, q ; k_c is an external liquid-phase mass-transfer coefficient; and a is external surface area of adsorbent per unit volume of liquid. Starting from feed concentration, c_F , the instantaneous bulk concentration, c , at time t , is related to the instantaneous adsorbent loading, q , by material balance:

$$c_F Q = cQ + qS \quad (15-77)$$

where the adsorbent is assumed to be initially free of adsorbate, Q is the liquid volume (assumed to remain constant for dilute feeds), and S is the mass of adsorbent. Equilibrium concentration, c^* , is given by an appropriate adsorption isotherm: a linear isotherm using concentration in place of partial pressure (15-16), Langmuir isotherm (15-36), or Freundlich isotherm (15-35). For example, a rearrangement of the latter gives

$$c^* = (q/k)^n \quad (15-78)$$

To solve (15-76) and (15-77) for c and q as a function of time, starting from c_F at $t = 0$, (15-77) is combined with an

equilibrium isotherm, for example, (15-78), to eliminate q . The resulting equation is combined with (15-76) to eliminate c^* to give an ODE for c in t , which is integrated analytically or numerically. Values of q are obtained from (15-77).

If the equilibrium is represented by a linear isotherm,

$$c^* = q/k \quad (15-79)$$

an analytical integration gives

$$c = \frac{c_F}{\beta} [\exp(-k_c a \beta t) + \alpha] \quad (15-80)$$

where

$$\beta = 1 + \frac{Q}{Sk} \quad (15-81)$$

$$\alpha = \frac{Q}{Sk} \quad (15-82)$$

As contact time approaches ∞ , adsorption equilibrium is approached. For the linear isotherm, from (15-80), or combining (15-77) with $c = c^*$ and (15-79):

$$c\{t = \infty\} = c_F \alpha / \beta \quad (15-83)$$

Continuous Mode

When both liquid and solids flow continuously through a perfectly mixed vessel, (15-76) converts to an algebraic equation because, as in a perfectly mixed reaction vessel (CSTR), concentration c throughout the vessel is equal to the outlet concentration, c_{out} . In terms of vessel residence time, t_{res} :

$$\frac{c_F - c_{\text{out}}}{t_{\text{res}}} = k_c a (c_{\text{out}} - c^*) \quad (15-84)$$

or, rearranging,

$$c_{\text{out}} = \frac{c_F + k_c a t_{\text{res}} c^*}{1 + k_c a t_{\text{res}}} \quad (15-85)$$

Equation (15-77) becomes

$$c_F Q = c_{\text{out}} Q + q_{\text{out}} S \quad (15-86)$$

where Q and S are now flow rates. An appropriate adsorption isotherm relates c^* to q_{out} . For a linear isotherm, (15-79) becomes $c^* = q_{\text{out}}/k$, which when combined with (15-86) and (15-85) to eliminate c^* and q_{out} , gives

$$c_{\text{out}} = c_F \left(\frac{1 + \gamma \alpha}{1 + \gamma + \gamma \alpha} \right) \quad (15-87)$$

where α is given by (15-82) and

$$\gamma = k_c a t_{\text{res}} \quad (15-88)$$

The corresponding q_{out} is given by rearranging (15-86):

$$q_{\text{out}} = \frac{Q(c_F - c_{\text{out}})}{S} \quad (15-89)$$

For a nonlinear adsorption isotherm, such as (15-35) or (15-36), (15-84) and (15-86) are combined with the isotherm equation, but it may not be possible to express the result explicitly in q_{out} . Then, as in Example 15.10, a numerical solution is required.

Semi-continuous Mode

The most difficult mode to model is the semi-continuous mode, where adsorbent is retained in the vessel, but feed liquid enters and exits the vessel at a fixed, continuous flow rate. Both concentration, c , and loading, q , vary with time. With perfect mixing, the outlet concentration is given by (15-85), where t_{res} is the liquid residence time in the suspension, and c^* is related to q by an appropriate adsorption isotherm. Variation of q in the batch of solids is given by (15-76), rewritten in terms of the change in q , rather than c :

$$S \frac{dq}{dt} = k_c a (c_{\text{out}} - c^*) t_{\text{res}} Q \quad (15-90)$$

where, for this mode, S is the batch mass of adsorbent in suspension and Q is the steady, volumetric-liquid flow rate.

Both (15-90) and (15-85) involve c^* , which can be replaced by a function of instantaneous q by selecting an appropriate isotherm. The resulting two equations are combined to eliminate c_{out} , and the resulting ODE is then integrated analytically or numerically, with MATLAB, to obtain q as a function of time, from which c_{out} as a function of time can be determined from (15-85) and the isotherm. The time-average value of c_{out} is then obtained by integration of c_{out} with respect to time. These steps are illustrated in Example 15.10. For a linear isotherm, the derivation is left as an exercise.

EXAMPLE 15.10 Three Modes of Slurry Adsorption.

An aqueous solution containing 0.010 mol phenol/L is to be treated at 20°C with activated carbon to reduce the concentration of phenol to 0.00057 mol/L. The adsorption-equilibrium data are well fitted to the Freundlich equation:

$$q = 2.16c^{1/4.35} \quad (1)$$

or rearranging,

$$c^* = (q/2.16)^{4.35} \quad (2)$$

where q and c are in mmol/g and mmol/L, respectively. In terms of kmol/kg and kmol/m³, (2) becomes

$$c^* = (q/0.01057)^{4.35} \quad (3)$$

All three modes of slurry adsorption are to be considered. From the results of Example 4.9, the minimum amount of adsorbent is 5 g/L of solution. Laboratory experiments with adsorbent particles 1.5 mm in diameter in a well-agitated vessel have confirmed that the rate of adsorption is controlled by external mass transfer with $k_c = 5 \times 10^{-5}$ m/s. Particle surface area is 5 m²/kg of particles.

(a) Using twice the minimum amount of adsorbent in an agitated vessel operated in the batch mode, determine the time in seconds to reduce phenol content to the desired value. (b) For operation in the continuous mode with twice the minimum amount of adsorbent, determine the required residence time in seconds. Compare it to the batch time of part (a). (c) For semi-continuous operation with 1,000 kg of activated carbon, a liquid feed rate of 10 m³/h, and a liquid residence time equal to 1.5 times the value computed in part (b), determine the run time to obtain a composite liquid product with the desired phenol concentration. Do you believe the results are reasonable?

Solution

(a) Batch mode:

$$\begin{aligned} S/Q &= 2(5) = 10 \text{ g/L} = 10 \text{ kg/m}^3; \quad k_c a = 5 \times 10^{-5}(5)(10) \\ &= 2.5 \times 10^{-3} \text{ s}^{-1}; \quad c_F = 0.010 \text{ mol/L} = 0.010 \text{ kmol/m}^3 \end{aligned}$$

From (15-77),

$$q = \frac{c_F - c}{S/Q} = \frac{0.010 - c}{10} \quad (4)$$

Substituting (4) into (3),

$$c^* = \left(\frac{0.010 - c}{0.01057} \right)^{4.35} \quad (5)$$

Substituting (1) into (15-76),

$$-\frac{dc}{dt} = 2.5 \times 10^{-3} \left[c - \left(\frac{0.010 - c}{0.01057} \right)^{4.35} \right] \quad (6)$$

where $c = c_F = 0.010$ kmol/m³ at $t = 0$, and t for $c = 0.00057$ kmol/m³ is wanted. By numerical integration using the ode45 function in MATLAB, $t = 1,140$ s.

(b) Continuous mode:

Equation (15-84) applies, where all quantities are the same as those determined in part (a) and $c_{\text{out}} = 0.00057$ kmol/m³. Thus

$$t_{\text{res}} = \frac{c_F - c_{\text{out}}}{k_c a (c_{\text{out}} - c^*)}$$

where c^* is given by (3) with $q = q_{\text{out}}$, and q_{out} is obtained from (15-86). Thus,

$$t_{\text{res}} = \frac{0.010 - 0.00057}{2.5 \times 10^{-3} \left[0.00057 - \left(\frac{0.010 - 0.00057}{0.01057} \right)^{4.35} \right]} = 6,950 \text{ s}$$

This is appreciably longer than the batch residence time of 1,140 s. In the batch mode, the concentration-driving force for external mass transfer is initially $(c - c^*) = c_F = 0.010$ kmol/m³ and gradually declines to a final value, at 1,140 s, of

$$(c - c^*) = c_{\text{final}} - \left(\frac{0.010 - c_{\text{final}}}{0.01057} \right)^{4.35} = 0.000543 \text{ kmol/m}^3$$

For the continuous mode the concentration-driving force for external mass transfer is always at the final batch value of 0.000543 kmol/m³, which here is very small.

(c) Semi-continuous mode:

Equation (15-90) applies with: $S = 1,000$ kg; $c_F = 0.010$ kmol/m³; $Q = 10$ m³/h; $t_{\text{res}} = 10,425$ s; $k_c a = 2.5 \times 10^{-3}$ s⁻¹; c^* is given in terms of q by (3); and c_{out} is given by (15-85). Combining (15-90), (3), and (15-85) to eliminate c^* and c_{out} gives, after simplification,

$$\frac{dq}{dt} = \left(\frac{\gamma}{1 + \gamma} \right) \frac{Q}{S} \left[c_F - \left(\frac{q}{0.01057} \right)^{4.35} \right] \quad (7)$$

where γ is given by (15-88) and t is the time the adsorbent remains in the vessel. For values of γ , Q/S , and c_F equal, respectively, to 26.06, 0.01 m³/h-kg, and 0.010 kmol/m³, (7) reduces to

$$\frac{dq}{dt} = 0.00963 \left[0.010 - \left(\frac{q}{0.01057} \right)^{4.35} \right] \quad (8)$$

Table 15.8 Results for Part (c), Semicontinuous Mode, of Example 15.10

Time t , h	q , kmol/kg	kmol/m ³	
		c_{out}	c_{cum}
0.0	0.0	0.000370	0.000370
5.0	0.000481	0.000371	0.000370
10.0	0.000962	0.000398	0.000375
15.0	0.001440	0.000535	0.000401
15.7	0.001506	0.000570	0.000407
20.0	0.001905	0.000928	0.000476
21.0	0.001995	0.001052	0.000501
22.0	0.002084	0.001195	0.000529
23.0	0.002172	0.001356	0.000561
23.2	0.002189	0.001390	0.000568
23.3	0.002197	0.001407	0.000572

where t is in hours and q is in kmol. By numerical integration of (8) using the ode45 function of MATLAB, starting from $q = 0$ at $t = 0$, q is obtained as a function of t as given in Table 15.8. Included are corresponding values of c_{out} computed from (15-85) combined with (3) to eliminate c^* , giving

$$c_{\text{out}} = \frac{c_F + \gamma(q/0.01057)^{4.35}}{1 + \gamma} = \frac{0.010 + 26.06(q/0.01057)^{4.35}}{27.06}$$

Also included in Table 15.8 are the cumulative values of c for the liquid effluent that exits the vessel during the period from $t = 0$ to $t = t$, as obtained by integrating c_{out} with respect to time:

$$c_{\text{cum}} = \int_0^t c_{\text{out}} dt/t.$$

From Table 15.8, it is seen that the loading, q , increases almost linearly during the first 10 h, while the instantaneous phenol concentration, c_{out} , in the exiting liquid remains almost constant. At 15.7 h, instantaneous c_{out} has increased to the specified value of 0.00057 kmol/m³, but c_{cum} is only 0.000407 kmol/m³. Therefore, the operation must continue. Finally, at between 23.2 and 23.3 h, c_{cum} reaches 0.00057 kmol/m³ and the operation is terminated. During operation, the vessel contains 1,000 kg or 2 m³ of adsorbent particles. With a liquid residence time of almost 3 h, the vessel must contain 10(3) = 30 m³. Thus, the vol% solids in the vessel is 6.7. This is reasonable. If adsorbent in the vessel is doubled, the time is doubled.

§15.5.2 Fixed-Bed Adsorption (Percolation)

In the continuous and semi-continuous operation modes of slurry adsorption, the liquid exiting the vessel always contains un-adsorbed solute. If a fixed bed is used, it is possible to obtain a nearly solute-free liquid or gas effluent until the adsorbent in the bed approaches saturation. Fixed beds are used frequently for gas purification and bulk separation.

Ideal Fixed-Bed Adsorption

Consider the flow of a fluid containing an adsorbable solute through a fixed bed of adsorbent. Assume: (1) external and internal mass-transfer resistances are very small; (2) plug flow

is achieved; (3) axial dispersion is negligible; (4) adsorbent is initially adsorbate-free; and (5) the adsorption isotherm begins at the origin. Then local equilibrium between fluid and adsorbent is achieved instantaneously. As shown in Figure 15.26, a shock-like wave, called a **stoichiometric front**, forms. It moves as a sharp adsorbate concentration front through the bed and is referred to as an **ideal (local equilibrium) fixed-bed adsorption**. Upstream of the front, adsorbent is saturated with adsorbate and the concentration of solute in the fluid is that of the feed, c_F . Loading on the adsorbent is the q_F in equilibrium with c_F . Length (height) and weight of the bed section upstream of the front are LES and WES, respectively, where ES refers to the equilibrium section or **equilibrium zone**.

In the upstream region, the adsorbent is spent. Downstream of the stoichiometric front and in the exit fluid, concentration of solute in the fluid is zero, and the adsorbent is adsorbate-free. In this section, length and weight are LUB and WUB, respectively, where UB refers to unused bed.

After a time period, called the **stoichiometric time**, the wave front reaches the end of the bed and the solute concentration in the effluent rises to the inlet value, c_F . No further adsorption is possible because the bed is spent. This is referred to as the **breakpoint** and the ideal wave front is a **breakthrough curve**.

For ideal fixed-bed adsorption, location of the concentration wave front L in Figure 15.26, as a function of time, is determined by material balance and adsorption equilibrium. At equilibrium, the loading is in equilibrium with the feed and is designated by $q_F = f\{c_F\}$, where $f\{c_F\}$ is given by an adsorption isotherm. Before breakthrough occurs, feed solute = adsorbate, as given by:

$$Q_F c_F t_{\text{ideal}} = q_F S L_{\text{ideal}} / L_B \quad (15-91)$$

where Q_F is volumetric feed flow rate, c_F is solute concentration in the feed, q_F is loading per unit mass of adsorbent in equilibrium with the feed concentration, S is total mass of adsorbent in the bed, L_B is bed length, and t_{ideal} is the time for an ideal front to reach $L_{\text{ideal}} < L_B$. Thus,

$$L_{\text{ideal}} = \text{LES} = \frac{Q_F c_F t_{\text{ideal}} L_B}{q_F S} \quad (15-92)$$

$$\text{LUB} = L_B - \text{LES} \quad (15-93)$$

$$\text{WES} = S \frac{\text{LES}}{L_B} \quad (15-94)$$

$$\text{WUB} = S - \text{WES} \quad (15-95)$$

Nonideal Fixed-Bed Adsorption

In a nonideal fixed-bed adsorber, assumptions leading to (15-91) are not valid. Internal transport resistance and, in some cases, external transport resistance are finite. Axial dispersion can also be significant, particularly at low flow rates in shallow beds. Local equilibrium between fluid and adsorbent is not achieved instantaneously, and broad concentration fronts like those in Figure 15.27 develop with time. In

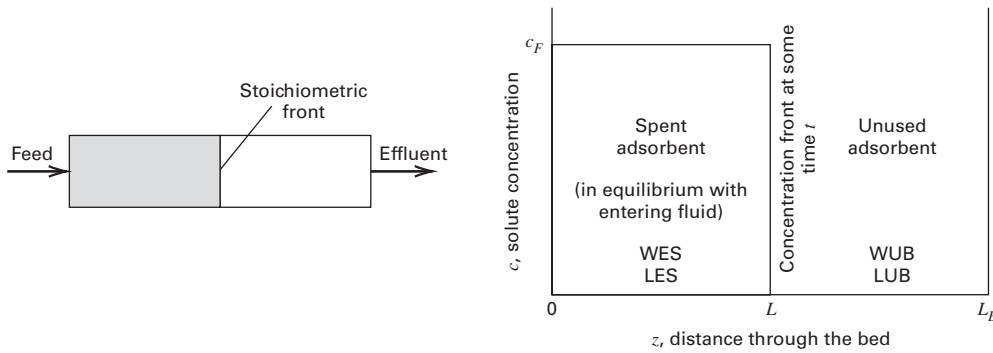


Figure 15.26 Stoichiometric (equilibrium) concentration front for ideal fixed-bed adsorption.

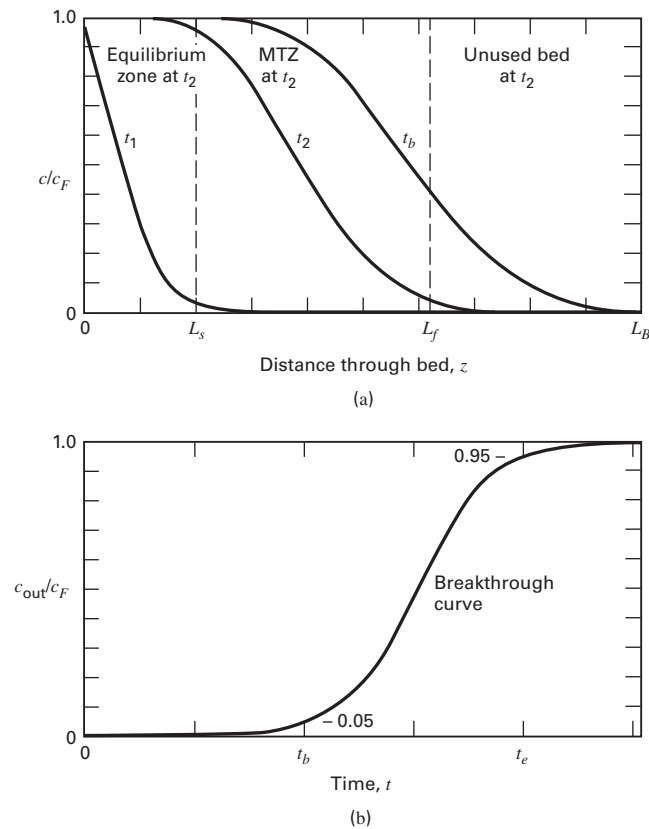


Figure 15.27 Solute wave fronts in a fixed-bed adsorber with mass-transfer effects. (a) Concentration–distance profiles. (b) Breakthrough curve.

Figure 15.27a, typical fluid solute concentration profiles are given as a function of distance through the bed at increasing times t_1 , t_2 , and t_b from initiation of flow through the bed. At t_1 , no part of the bed is saturated. At t_2 , the bed is almost saturated for a distance L_s . At L_f , the bed is almost clean. Beyond L_f , little mass transfer occurs at t_2 and the adsorbent is still mostly unused. The region between L_s and L_f is called the **mass-transfer zone**, MTZ at t_2 , where adsorption takes place.

Because it is difficult to determine where the MTZ zone begins and ends, L_f can be taken where $c/c_F = 0.05$, with L_s at $c/c_F = 0.95$. From time t_2 to time t_b , the S-shaped front moves through the bed. At t_b , the leading point of the MTZ just reaches the breakthrough point. Rather than using

$c/c_F = 0.05$, the breakthrough concentration can be the minimum detectable or maximum allowable solute concentration in the effluent fluid.

Figure 15.27b is a typical plot of the ratio of the outlet-to-inlet solute concentration in the fluid as a function of time from the start of flow. The S-shaped curve is the **breakthrough curve**. Prior to t_b , the outlet solute concentration is less than some maximum permissible value, say, $c_{\text{out}}/c_F = 0.05$. At t_b , this value is reached, adsorption is discontinued, and regeneration is initiated or the spent adsorbent is discarded. If adsorption were to be continued for $t > t_b$, the outlet solute concentration would rise rapidly, to approach the inlet concentration as the outlet end of the bed became saturated. The time to reach $c_{\text{out}}/c_F = 0.95$ is t_e .

The breakthrough-curve steepness determines the bed length. For the ideal case, with a stoichiometric wave front, (15-91) applies and the bed is totally utilized before breakthrough occurs. As the width of the breakthrough curve and the corresponding MTZ width increases, less and less bed capacity can be utilized. The situation is further complicated by the fact that steepness of the concentration profiles shown in Figure 15.27a can increase or decrease with time, depending on the shape of the adsorption isotherm, as shown by DeVault [73].

Consider a nonideal case with finite external and internal mass-transfer resistances. But, retain the assumptions of negligible axial dispersion and plug flow, with the added stipulation of constant interstitial fluid velocity, u , through the bed. The superficial fluid velocity is $\varepsilon_b u$, where ε_b is the external bed void fraction. A solute mass balance for the fluid flowing through an adsorption bed of cross-sectional area, A_b and differential length, Δz , for a differential-time duration, dt , gives

$$\varepsilon_b u A_b c|_z = \varepsilon_b u A_b c|_{z+\Delta z} + \varepsilon_b A_b \Delta z \frac{\partial c}{\partial t} + (1 - \varepsilon_b) A_b \Delta z \frac{\partial \bar{q}}{\partial t}$$

Dividing by $\varepsilon_b A_b \Delta z$ and taking the limit as $\Delta z \rightarrow 0$ gives the partial differential equation (PDE) for the change in the bulk fluid solute concentration, c , with time and location in the bed:

$$u \frac{\partial c}{\partial z} + \frac{\partial c}{\partial t} + \frac{(1 - \varepsilon_b)}{\varepsilon_b} \frac{\partial \bar{q}}{\partial t} = 0 \quad (15-96)$$

where \bar{q} is the volume-average adsorbate loading per unit mass. It accounts for the variation of q throughout the adsorbent particle, due to internal mass-transfer resistance, by

averaging the rate of adsorption over the adsorbent particle. The volume-average adsorbate loading for a spherical particle is given by

$$\bar{q} = \frac{3}{R_p^3} \int_0^{R_p} r^2 q dr \quad (15-97)$$

where R_p is the radius of the adsorbent particle and r is the radial distance from the center of the particle.

Equation (15-68) gives the solute concentration in the fluid within the pores of an adsorbent particle. Equations (15-68) and (15-96) are coupled by the continuity condition at the particle surface:

$$D_e \left(\frac{\partial c}{\partial r} \right)_{R_p} = k_c (c - c_{R_p}) \quad (15-98)$$

where k_c is the external mass-transfer coefficient and D_e is the effective diffusivity in the particle, as discussed in §15.3. The simultaneous solution of (15-96) to (15-98) and (15-68) is a formidable task, which can be avoided by using the linear-driving-force (LDF) model formulated by Glueckauf and Coates [74, 75] and discussed in detail by Yang [25] and Ruthven [10]. This model is widely used to simulate and design fixed-bed adsorbers. It is based on the following relation, which replaces (15-68) and (15-98):

$$\frac{\partial \bar{q}}{\partial t} = k(q^* - \bar{q}) = kK(c - c^*) \quad (15-99)$$

where q^* is the adsorbate loading in equilibrium with solute concentration, c , in the bulk fluid; c^* is the solute concentration in equilibrium with average loading \bar{q} ; k is an overall mass-transfer coefficient, which includes both external- and internal-transport resistances; and K is the adsorption-equilibrium constant for a linear adsorption isotherm of the form $q = Kc$. A suitable relationship for the factor kK is

$$\frac{1}{kK} = \frac{R_p}{3k_c} + \frac{R_p^2}{15D_e} \quad (15-100)$$

where the first RHS term represents the external mass-transfer resistance, $k_c a_v$, since for a sphere, surface area/unit volume, a_v , is given by

$$4\pi R_p^2 / \left[\frac{4}{3}\pi R_p^3 \right] = 3/R_p$$

The second RHS term in (15-100) is the internal resistance, which was first developed by Glueckauf [75], but can also be derived by assuming a parabolic adsorbate loading profile in the particle, as shown by Liaw et al. [76].

The analytical solution of (15-96) with the LDF mass-transfer model, is summarized by Ruthven [10] and discussed by Klinkenberg [77] for the case where initially the bed is free of adsorbed solute. The solution was first obtained by Anzelius [78] in terms of Bessel functions for the analogous problem of heating or cooling a packed bed of depth z with a fluid. A useful approximate solution is that of Klinkenberg [79]:

$$\frac{c_f}{c_F} \approx \frac{1}{2} \left[1 + \operatorname{erf} \left(\sqrt{\tau} - \sqrt{\xi} + \frac{1}{8\sqrt{\tau}} + \frac{1}{8\sqrt{\xi}} \right) \right] \quad (15-101)$$

where

$$\xi = \frac{kKz}{u} \left(\frac{1 - \varepsilon_b}{\varepsilon_b} \right) = \text{Dimensionless distance coordinate} \quad (15-102)$$

$$\tau = k \left(t - \frac{z}{u} \right) = \text{Dimensionless time coordinate corrected for displacement} \quad (15-103)$$

$$\operatorname{erf}(-x) = -\operatorname{erf}(x) \quad (15-104)$$

$$\operatorname{erf}(x) = \frac{2}{\sqrt{\pi}} \int_0^x e^{-\eta^2} d\eta \quad (15-105)$$

where ξ and τ are coordinate transformations for z and t , which convert the equations to a much simpler form. The approximation (15-101) is accurate to $< 0.6\%$ error for $\xi > 2.0$. The $\operatorname{erf}(x)$, which is included in most spreadsheet programs, is 0.0 at $x = 0$ and asymptotically approaches 1.0 for $x > 2.0$, where x is a dummy variable.

Klinkenberg [79] also includes the following approximate solution for profiles of solute concentration in equilibrium with the average sorbent loading:

$$\frac{c^*}{c_F} = \frac{\bar{q}}{q_F^*} \approx \frac{1}{2} \left[1 + \operatorname{erf} \left(\sqrt{\tau} - \sqrt{\xi} - \frac{1}{8\sqrt{\tau}} - \frac{1}{8\sqrt{\xi}} \right) \right] \quad (15-106)$$

where $c^* = \bar{q}/K$ and $c^*/c_F = \bar{q}/q_F^*$, where q_F^* is the loading in equilibrium with c_F .

EXAMPLE 15.11 Breakthrough Curves Using the Klinkenberg Equations.

Air at 70°F and 1 atm, containing 0.9 mol% benzene, enters a fixed-bed adsorption tower at 23.6 lb/min. The tower has an inside diameter of 2 ft and is packed to a height of 6 ft with 735 lb of 4 × 6 mesh silica gel (SG) particles with a 0.26 cm effective diameter and an external void fraction of 0.5. The adsorption isotherm for benzene has been determined to be linear for the conditions of interest:

$$q = Kc^* = 5,120c^* \quad (1)$$

where q = lb benzene adsorbed per ft³ of silica gel particles, and c^* = equilibrium concentration of benzene in the gas, in lb benzene per ft³ of gas.

Mass-transfer experiments simulating conditions in the 2-foot-diameter bed fit the linear-driving-force (LDF) model of (15-99):

$$\frac{\partial \bar{q}}{\partial t} = 0.206K(c - c^*) \quad (2)$$

where time is in minutes and 0.206 is the constant k in min⁻¹, which includes resistances both in the gas film and in the adsorbent pores, with the latter resistance dominant.

Using the approximate concentration-profile equations of Klinkenberg [77], compute a set of breakthrough curves and the time when the benzene concentration in the exiting air rises to 5% of the inlet. Assume isothermal, isobaric operation. Compare breakthrough time with time predicted by the ideal equilibrium model.

Solution

For the ideal equilibrium model, the breakthrough curve is vertical, and the bed becomes completely saturated with benzene at the feed concentration, c_F .

MW of entering gas = $0.009(78) + 0.991(29) = 29.44$
 Density of entering gas = $(1)(29.44)/(0.730)(530) = 0.076 \text{ lb/ft}^3$
 Gas flow rate = $23.6/0.0761 = 310 \text{ ft}^3/\text{min}$
 Benzene flow rate in entering gas = $(23.6/29.44)(0.009)(78) = 0.562 \text{ lb/min}$

$$c_F = \frac{0.562}{310} = 0.00181 \text{ lb benzene/ft}^3 \text{ of gas}$$

From (1),

$$q = 5,120(0.00181) = 9.27 \frac{\text{lb benzene}}{\text{ft}^3 \text{ SG}}$$

The total adsorption of benzene at equilibrium

$$= \frac{9.27(3.14)(2)^2(6)(0.5)}{4} = 87.3 \text{ lb}$$

Time of operation = $87.3/0.562 = 155 \text{ min}$

For the actual nonideal fixed-bed operation, taking into account external and internal mass-transfer resistances, from (15-102) and (15-103),

$$\xi = \frac{(0.206)(5,120)z}{u} \left(\frac{1 - 0.5}{0.5} \right) = 1,055 z/u$$

$$u = \text{interstitial velocity} = \frac{310}{0.5 \left(\frac{3.14 \times 2^2}{4} \right)} = 197 \text{ ft/min} \quad (3)$$

$$\xi = \frac{1,055}{197} z = 5.36z, \text{ where } z \text{ is in ft.}$$

When $z = \text{bed height} = 6 \text{ ft}$, $\xi = 32.2$ and

$$\tau = 0.206 \left(t - \frac{z}{197} \right) \quad (4)$$

For $t = 155 \text{ min}$ (the ideal time), and $z = 6 \text{ ft}$. Using (4), $\tau = 32$.

Thus, breakthrough curves should be computed from (15-101) for values of τ and ξ no greater than about 32. For example, when $\xi = 32.2$ (exit end of the bed), and $\tau = 30$, which corresponds to a time $t = 145.7 \text{ minutes}$, the concentration of benzene in the exiting gas, from (15-101), is

$$\begin{aligned} \frac{c}{c_F} &= \frac{1}{2} \left[1 + \operatorname{erf} \left(30^{0.5} - 32.2^{0.5} + \frac{1}{8(30)^{0.5}} + \frac{1}{8(32.2)^{0.5}} \right) \right] \\ &= \frac{1}{2} [1 + \operatorname{erf}(-0.1524)] = \frac{1}{2} \operatorname{erfc}(0.1524) \\ &= 0.4147 \text{ or } 41.47\% \end{aligned}$$

This far exceeds the specification of $c/c_F = 0.05$ or 5% at the exit. Thus, the time of operation of the bed is considerably less than the ideal time of 155 min.

Figure 15.28 shows breakthrough curves computed from (15-101) over a range of the dimensionless time, τ , for values

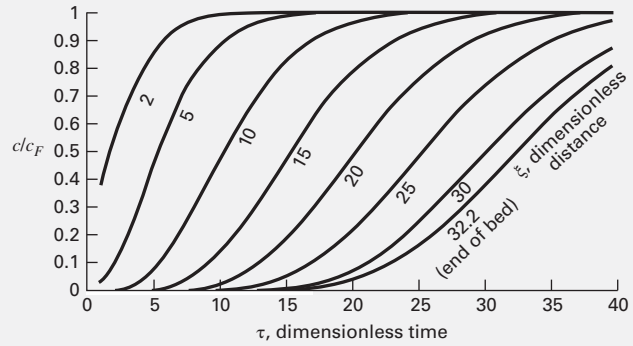


Figure 15.28 Gas concentration breakthrough curves for Example 15.11.

of the dimensionless distance, ξ , of 2, 5, 10, 15, 20, 25, 30, and 32.2, where the last value corresponds to the bed exit. For $c/c_F = 0.05$ and $\xi = 32.2$, τ is seen to be nearly 20.

From a rearrangement of (4), with $z = 6 \text{ ft}$, the time to breakthrough is $t = 20/0.206 + 5/197 = 97.1 \text{ minutes}$, which is 62.3% of the ideal time.

Equation (15-101) can be used to compute the bulk concentration of benzene at various locations in the bed. For example, for $\tau = 20$, the results are as follows:

ξ	$z, \text{ ft}$	c/c_F
2	0.373	1.00000
5	0.932	0.99948
10	1.863	0.97428
15	2.795	0.82446
20	3.727	0.53151
25	4.658	0.25091
30	5.590	0.08857
32.2	6.000	0.05158

The fractional adsorbent loading, at various positions in the bed, can be computed from (15-106), using $q = 5,120c$. Figure 15.29 is a plot of the results for τ , while tabular results are given in the next table below the plot. The maximum loading corresponds to $c = c_F$. Thus, $q_{\max} = 9.28 \text{ lb benzene/ft}^3$ of SG. As expected, the curves in Figure 15.29 are displaced to the right from the curves of Figure 15.28.

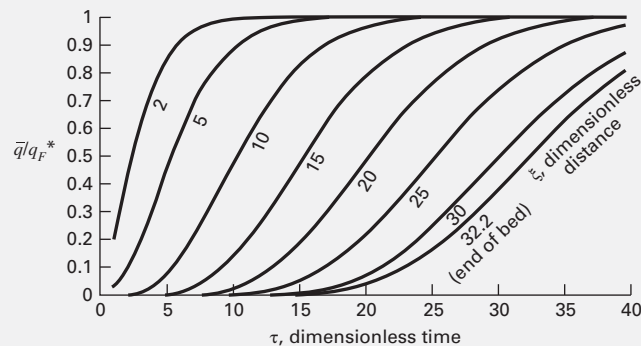
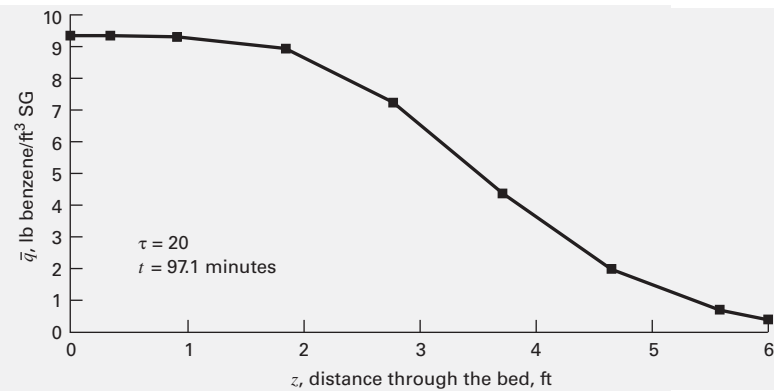


Figure 15.29 Adsorbent loading breakthrough curves for Example 15.11.


Figure 15.30 Adsorbent loading profile for Example 15.11.

ξ	z , ft	$\frac{c^*}{c_F} = \frac{\bar{q}}{q_F^*}$	\bar{q} , lb benzene/ft ³ SG
2	0.373	0.99998	9.28
5	0.932	0.99883	9.27
10	1.863	0.96054	8.91
15	2.795	0.77702	7.21
20	3.727	0.46849	4.35
25	4.658	0.20571	1.909
30	5.590	0.06769	0.628
32.2	6.000	0.03827	0.355

Values of \bar{q} are plotted in Figure 15.30 and integrated over the bed length to obtain the average bed loading:

$$\bar{q}_{\text{avg}} = \int_0^6 \bar{q} dz / 6$$

The result is 5.72 lb benzene/ft³ of SG, which is 61.6% of the maximum loading based on inlet benzene concentration.

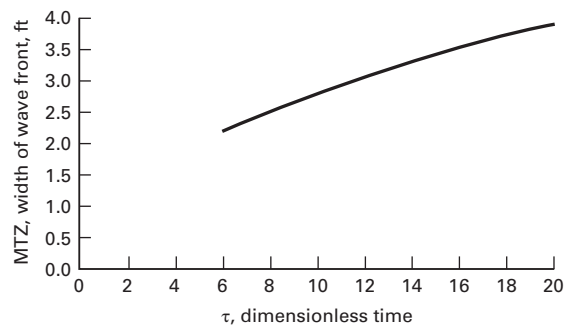
If the bed height were increased by a factor of 5, to 30 ft ($\xi = 161$), the ideal time of operation would be 780 min or 13 h. With mass-transfer effects taken into account, as before, the dimensionless operating time to breakthrough is computed to be $\tau = 132$, or breakthrough time from (4) is

$$t = \frac{132}{0.206} + \frac{30}{197} = 641 \text{ minutes}$$

which is 82.2% of the ideal time. This represents a substantial increase in bed utilization.

Effect of Adsorption Isotherm on the Solute Concentration Wave-Front Pattern

Figure 15.28 shows that as the dimensionless distance, ξ , through the bed increases, the solute concentration wave front broadens. This is shown quantitatively, for Example 15.11, in Figure 15.31 in a plot of the width of the MTZ as a function of dimensionless time up to a value of $\tau = 20$ (where the front breaks through the 6-ft-long bed). MTZ broadening increases from ~ 2 feet at $\tau = 6$ to ~ 4 feet at $\tau = 20$. The rate of broadening slows as τ increases; however, calculation for a deeper bed showed that broadening persisted even at $\tau = 100$.


Figure 15.31 Broadening of wavefront in Example 15.11.

This is a typical result with a linear adsorption isotherm (curve A in Figure 15.32a) or with an unfavorable Type III isotherm (curve C in Figure 15.32a). A favorable Type I Langmuir or Freundlich isotherm (curve B in Figure 15.32a) rapidly diminishes wave-front broadening to produce a “self-sharpening” wave front, as illustrated in Figure 15.32b.

The wave broadening effect has been evaluated by DeVault [73] and others. A semi-quantitative explanation of its cause can be described using an equation for the velocity of the solute concentration wave front, u_c , derived as follows. Assume that (15-96) applies for the variation of solute concentration, c , as a function of time and location in the fixed bed. However, assume the internal mass-transfer resistance in the adsorbent particles is negligible so that \bar{q} can be replaced with q . By the chain rule:

$$\frac{\partial q}{\partial t} = \frac{\partial q}{\partial c} \frac{\partial c}{\partial t} \quad (15-107)$$

By the rules of implicit partial differentiation,

$$u_c = \left(\frac{\partial z}{\partial t} \right)_c = - \frac{\left(\frac{\partial c}{\partial t} \right)}{\left(\frac{\partial c}{\partial z} \right)} \quad (15-108)$$

Combining (15-96) with (15-107) and (15-108) gives:

$$u_c = \frac{u}{1 + \left(\frac{1 - \epsilon_b}{\epsilon_b} \right) \frac{dq}{dc}} \quad (15-109)$$

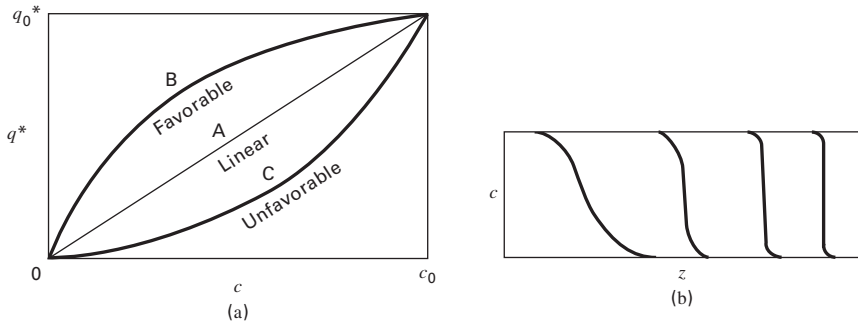


Figure 15.32 Effect of shape of isotherm on sharpness of concentration wavefront. (a) Isotherm shapes. (b) Self-sharpening wavefront caused by a favorable adsorption isotherm.

This is the solute velocity of the concentration wave front in terms of interstitial fluid velocity, u , and slope, dq/dc , of the adsorption isotherm. If dq/dc is constant, the wave front moves at a constant value.

In general, wave velocity, u_c , is much less than interstitial velocity, u , and the superficial fluid velocity, $u_s = \epsilon u$. For example, suppose $\epsilon_b = 0.5$ and the equilibrium adsorption isotherm is $q = 5,000c$. Then $dq/dc = 5,000$ and from (15-109), $u_c/u = 0.0002$. If u is 3 ft/s, the superficial fluid velocity is 1.5 ft/s, and the velocity of the solute concentration wave front is only 0.0006 ft/s. If the bed were 6 ft in height, it would take 2.78 h for the concentration wave front to pass through the bed compared to 2 s for the fluid to pass through the bed.

Using (15-109), for a curved adsorption isotherm, regions of the wave front at a higher concentration move at a velocity different from regions at a lower concentration. For a linear isotherm (curve A in Figure 15.32a), the MTZ width and wave pattern remain constant. For a Freundlich or Langmuir isotherm (curve B in Figure 15.32a) high-concentration regions move faster than low-concentration regions, and the wavefront steepens with time until a **constant-pattern wave front** (CPF) develops, as shown in Figure 15.32b. For the unfavorable type of isotherm (Curve C in Figure 15.29a), low-concentration regions travel faster and wave fronts increasingly broaden with time. Cooney and Lightfoot [80] proved the existence of an asymptotic wave-front solution. Sircar and Kumar [81] developed analytical solutions for CPF and Cooney [82] estimated CPF profiles and breakthrough curves for Freundlich and Langmuir isotherms.

Scale-Up for Constant-Pattern Front

When the constant-pattern-front assumption is valid, it becomes possible to determine the length of a full-scale adsorbent bed from breakthrough curves obtained in laboratory experiments. This widely used technique is described by Collins [83] for purification applications. The adsorbent bed is considered to be the sum of two sections: (1) LES, the length of the ideal fixed-bed adsorber, plus (2) LUB, an additional length that depends on the observed width of the MTZ and the shape of the c/c_F profile within that zone. The total required bed length is

$$L_B = LES + LUB \quad (15-110)$$

The ideal, fixed-bed adsorber contribution, LES, is determined by material balance from the amount of solute in the

feed for time = 0 to ideal breakthrough time, t_b , and equilibrium loading on the adsorbent for the solute concentration given by the adsorption isotherm. Thus,

$$c_F Q_F t_b = q_F \rho_b (\text{bed volume}) = q_F \rho_b A_B (\text{LES})$$

which rearranges to:

$$\text{LES} = \frac{c_F Q_F t_b}{q_F \rho_b A_B} \quad (15-111)$$

where Q_F is the volumetric feed rate.

LUB is determined from experimental laboratory data for the same feed composition and superficial velocity to be used for the commercial adsorber. The data must include the time, t_b , when breakthrough first occurs, and time, t_e , when the adsorbent in the bed is spent, as shown in Figure 15-27b. To determine LUB, the data for an experimental bed of length, L_e , are plotted as c_{out}/c_F versus time. An equivalent time-to-breakthrough for an ideal bed, t_s , is located such that in Figure 15.33, area A is equal to area B. The ideal wave front velocity is L_e/t_s , and

$$\text{LUB} = \text{Ideal wavefront velocity} \times (t_s - t_b) = \frac{L_e}{t_s} (t_s - t_b) \quad (15-112)$$

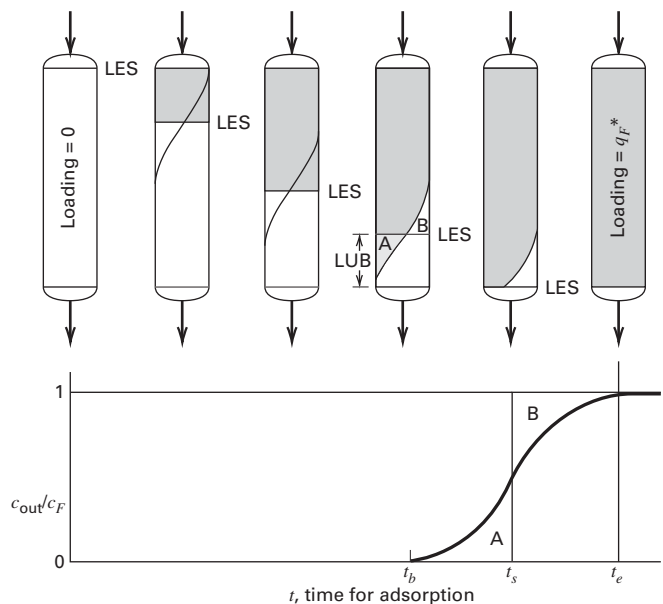


Figure 15.33 Determination of equivalent ideal bed length, t_s

Instead of positioning the stoichiometric front for equal areas as in Figure 15.33, the LUB can be determined from the experimental breakthrough-curve by computing t_s from

$$t_s = \int_0^{t_e} \left(1 - \frac{c}{c_F}\right) dt \quad (15-113)$$

If, in Figure 15.33, t_s is located midway between t_b and t_e , such that the shape of the experimental breakthrough curve below area B is equivalent to the curve above area A , then $LUB = MTZ/2$, i.e., one-half of the width of the mass-transfer zone. In the absence of experimental breakthrough data, a conservative estimate of MTZ is 4 ft.

The following example illustrates the Collins scale-up method.

EXAMPLE 15.12 Scale-Up for Fixed-Bed Adsorption.

Collins [83] reports the experimental data below for water-vapor adsorption from nitrogen in a fixed bed of 4A molecular sieves. Bed depth = 0.88 ft, $T = 83^\circ\text{F}$, $P = 86$ psia, $G =$ entering gas molar velocity = 29.6 lbmol/h-ft², entering water content = 1,440 ppm (by volume), initial adsorbent loading = 1 lb/100 lb sieves, and bed bulk density = 44.5 lb/ft³. For the entering gas moisture content, c_F , the equilibrium loading, q_F , equals 0.186 lb H₂O/lb solid.

c_{out} , ppm (by volume)	Time, h	c_{out} , ppm (by volume)	Time, h
<1	0–9.0	650	10.8
1	9.0	808	11.0
4	9.2	980	11.25
9	9.4	1,115	11.5
33	9.6	1,235	11.75
80	9.8	1,330	12.0
142	10.0	1,410	12.5
238	10.2	1,440	12.8
365	10.4	1,440	13.0
498	10.6		

Determine the bed height required for a commercial unit to be operated at the same temperature, pressure, and entering gas mass velocity and water content to obtain an exiting gas with no more than 9 ppm (by volume) of water vapor with a breakthrough time of 20 h.

Solution

$$c_F = \frac{1,440(18)}{106} = 0.02592 \text{ lb H}_2\text{O/lbmol N}_2$$

$$G = \frac{Q_F}{\pi D^2/4} = 29.6 \text{ lbmol N}_2/\text{h-ft}^2 \text{ of bed cross-section}$$

Initial moisture content of bed = 0.01 lb H₂O/lb solid.

From (15-111), revised for a gas flow rate based on the lbmol of N₂ instead of volume in ft³ of N₂,

$$LES = \frac{c_F G t}{q_F \rho_b} = \frac{(0.02592)(29.6)(20)}{(0.186 - 0.01)(44.5)} = 1.96 \text{ ft}$$

Use the integration method to obtain LUB. From the experimental data:

Take $t_e = 12.8$ h (1,440 ppm) and $t_b = 9.4$ h (9 ppm).

By numerical integration of breakthrough-curve data, using (15-113), $t_s = 10.93$ h.

$$\text{From (15-112), } LUB = \frac{0.88}{10.93}(10.93 - 9.40) = 0.12 \text{ ft}$$

$$\text{From (15-110), } L_B = 1.96 + 0.12 = 2.08 \text{ ft.}$$

$$\text{The bed utilization is } \frac{1.96}{2.08} \times 100\% = 94.2\%$$

Alternatively, an approximate calculation can be made. Let t_b , the beginning of breakthrough, be 5% of the final ppm, or 0.05(1,440) = 72 ppm. Using the experimental data, this corresponds to $t_b = 9.76$ h. Let t_e , the end of breakthrough, be 95% of the final ppm, or 0.95(1,440) = 1,370 ppm, corresponding to $t_e = 12.25$ h. Let t_s = the midpoint or $(9.76 + 12.25)/2 = 11$ h. The ideal wave-front velocity = $L_e/t_s = 0.88/11 = 0.08$ ft/h. From (15-112), $LUB = 0.08(11 - 9.76) = 0.1$ ft. $MTZ = 0.2$ ft and $L_B = 1.96 + 0.1 = 2.06$ ft.

§15.5.3 Temperature (Thermal)-Swing Adsorption (TSA)

As in Figure 15.34, temperature-swing adsorption (TSA), in its simplest configuration, is carried out with two fixed beds in parallel, operating cyclically. While one bed is adsorbing solute at near-ambient temperature, $T_1 = T_{\text{ads}}$, the other bed is regenerated by desorbing adsorbate at a higher temperature, $T_2 = T_{\text{des}}$, at which the equilibrium adsorbate loading is much less for a given concentration of solute in the fluid. Although the desorption step might be accomplished in the absence of a purge fluid by simply vaporizing the adsorbate, re-adsorption of some solute vapor would occur upon cooling the bed. Thus, it is best to remove the desorbed adsorbate with a purge. The desorption temperature is high, but not so high as to cause deterioration of the adsorbent. TSA is best applied to the removal of contaminants present at low concentrations in the feed fluid. In that case, nearly isothermal adsorption and desorption is achieved.

An ideal TSA cycle involves four steps: (1) adsorption at T_1 to breakthrough, (2) heating of the bed to T_2 , (3) desorption at T_2 to a low adsorbate loading, and (4) cooling of the bed to T_1 . Practical cycles do not operate with isothermal steps. Instead, Steps 2 and 3 are combined for the regeneration part of the cycle, with the bed being simultaneously heated and desorbed with preheated purge gas until the temperature of the effluent approaches that of the inlet purge. Steps 1 and 4 may also be combined because, as discussed in detail by Ruthven [10], the thermal wave precedes the MTZ front. Thus, adsorption takes place at essentially the feed-fluid temperature.

The heating and cooling steps cannot be accomplished instantaneously because of the relatively low thermal conductivity of the adsorbent particles in the bed. Although heat transfer can be done indirectly from jackets surrounding the beds or from coils located within the beds, bed temperature changes are more readily achieved by preheating or precooling a purge fluid, as shown in Figure 15.34. The purge fluid can be a portion of the feed or effluent, or some other fluid. The purge fluid can also be used in the desorption step. When

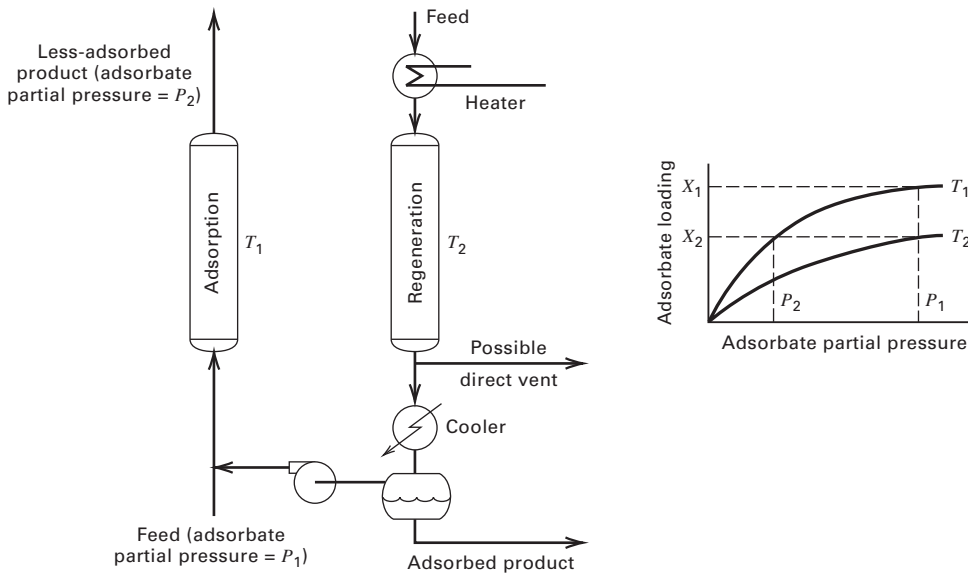


Figure 15.34 Temperature-Swing Adsorption.

the adsorbate is valuable and easily condensed, the purge fluid might be a non-condensable gas. When the adsorbate is valuable, but not easily condensed, and is essentially insoluble in water, steam may be used as the purge fluid, followed by condensation of the steam to separate it from the desorbed adsorbate. When the adsorbate is not valuable, fuel and/or air can be used as the purge fluid, followed by incineration of the adsorbent. Often the amount of purge used in the regeneration step is much less than the amount of feed to the bed in the adsorption step. In Figure 15.34, the feed fluid is a gas. The spent bed is heated and regenerated with preheated feed gas, which is then cooled to condense the desorbed adsorbate.

Because of the time to heat and cool a fixed bed, cycle times for TSA are long, usually hours or days. Longer cycle times require longer bed lengths, which result in a greater percent bed utilization during adsorption. However, a **lead-trim-bed**

arrangement of two absorbing beds in series should be considered when the MTZ width is an appreciable fraction of bed length such that bed capacity is poorly utilized. When the lead bed is spent, it is switched to regeneration. At this time, the trim bed has an MTZ occupying a considerable portion of the bed, and that bed becomes the lead bed, with a regenerated bed becoming the trim bed. In this manner, only a fully spent bed is switched to regeneration and three beds are used. If the feed flow rate is high, beds in parallel may be required.

Adsorption is usually conducted with the feed fluid flowing downward. Desorption can be either downward or upward, but the upward direction is preferred because it is more efficient. Consider the loading fronts shown in Figure 15.35 for regeneration counter-flow to adsorption. Although the bed is shown horizontal, it must be positioned vertically. The feed fluid flows down, entering at the left and leaving at the right. At

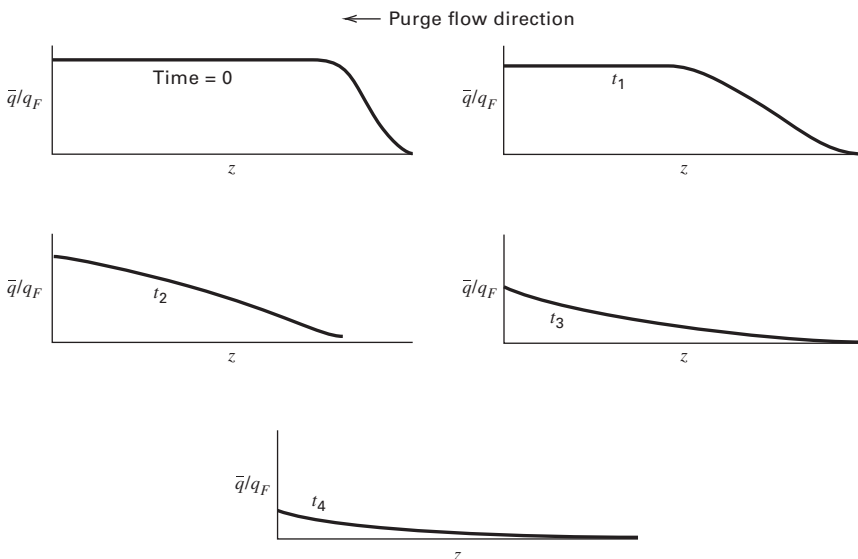


Figure 15.35 Sequence of loading profiles during countercurrent regeneration.

time $t = 0$, breakthrough has occurred, with a loading profile as shown at the top, where the MTZ is about 25% of the bed. If the purge fluid for regeneration also flows downward (entering at the left), the adsorbate will move through the unused portion of the bed, and some desorbed adsorbate will be re-adsorbed in the unused section and then desorbed a second time. If counter-flow regeneration is used, the unused portion of the bed is never in contact with desorbed adsorbate.

During a countercurrent regeneration step, the loading profile changes progressively with time, from time = 0 to t_4 as shown in Figure 15.35. The right-side end of the bed, where purge enters, is desorbed first. After regeneration, residual loading may be uniformly zero or, more likely, finite and nonuniform, as shown for time, t_4 , at the bottom of Figure 15.35. If the latter, then the useful cyclic capacity, called the **delta loading**, is as shown in Figure 15.36.

The Klinkenberg equations, (15-101) and (15-106), are not valid for calculations of the concentration and loading profiles during desorption because the loading is not uniform at the beginning of desorption. A numerical solution for the desorption step can be obtained using a procedure discussed by Wong and Niedzwiecki [84]. Although their method was developed for adsorption, it is readily applied to desorption. In the absence of axial dispersion and for constant fluid velocity, (15-96) and (15-99) can be rewritten as:

$$u \frac{\partial \phi}{\partial z} + \frac{\partial \phi}{\partial t} + \frac{(1 - \epsilon_b)}{\epsilon_b} kK(\phi - \psi) = 0 \quad (15-114)$$

$$\frac{\partial \psi}{\partial t} = k(\phi - \psi) \quad (15-115)$$

where $\phi = c/c_F$ (15-116)

$$\psi = \bar{q}/q_F^* \quad (15-117)$$

and c_F and q_F^* are taken at the beginning of the adsorption step. Boundary conditions are:

At $t = 0$: $\phi = \phi\{z\}$ at the end of the adsorption step and $\psi = \psi\{z\}$ at the end of the adsorption step, where, for counter-flow desorption, it is best to let z start from the bed

bottom (called z') and increase in the direction of purge-gas flow. Thus, u in (15-114) is positive.

At $z' = 0$: $\phi = 0$ (no solute in the entering purge gas) and $\psi = 0$.

Partial differential equations (15-114) and (15-115) in independent variables z and t can be converted to a set of ordinary differential equations (ODEs) in independent variable t by the method of lines (MOL), which was first applied to parabolic PDEs by Rothe in 1930, as discussed by Liskovets [85], and subsequently to elliptic and hyperbolic PDEs. The MOL is developed by Schiesser [86]. The lines refer to the z' -locations of the ODEs. To obtain the set of ODEs, the z' -coordinate is divided into N increments or $N + 1$ grid points that are usually evenly spaced, with 20 increments being sufficient. Letting i be the index for each grid point in z' , starting from the end where the purge gas enters, and discretizing $\partial\phi/\partial z'$, (15-114) and (15-115) become

$$\frac{d\phi_i}{dt} = -u \left(\frac{\Delta\phi}{\Delta z'} \right)_i - \left(\frac{1 - \epsilon_b}{\epsilon_b} \right) kK(\phi_i - \psi_i) \quad i = 1, N + 1 \quad (15-118)$$

$$\frac{d\psi_i}{dt} = k(\phi_i - \psi_i) \quad i = 1, N + 1 \quad (15-119)$$

where initial conditions ($t = 0$) for ϕ_i and ψ_i are as given above. Before first-order ODEs (15-118) and (15-119) can be integrated, a suitable approximation for $(\Delta\phi/\Delta z')$ must be provided. In general, for a moving-wave front problem of the hyperbolic type as in adsorption and desorption, the simple central difference

$$\left(\frac{\Delta\phi}{\Delta z'} \right)_i \approx \frac{\phi_{i+1} - \phi_{i-1}}{2\Delta z'} \quad (15-120)$$

is not adequate. Wong and Niedzwiecki [84] found that a five-point, biased, upwind, finite-difference approximation, used by Schiesser [86], is very effective. This approximation, which is derived from a Taylor's series analysis, places emphasis on conditions upwind of the moving front. At an interior grid point:

$$\left(\frac{\Delta\phi}{\Delta z'} \right)_i \approx \frac{1}{12\Delta z'} [-\phi_{i-3} + 6\phi_{i-2} - 18\phi_{i-1} + 10\phi_i + 3\phi_{i+1}] \quad (15-121)$$

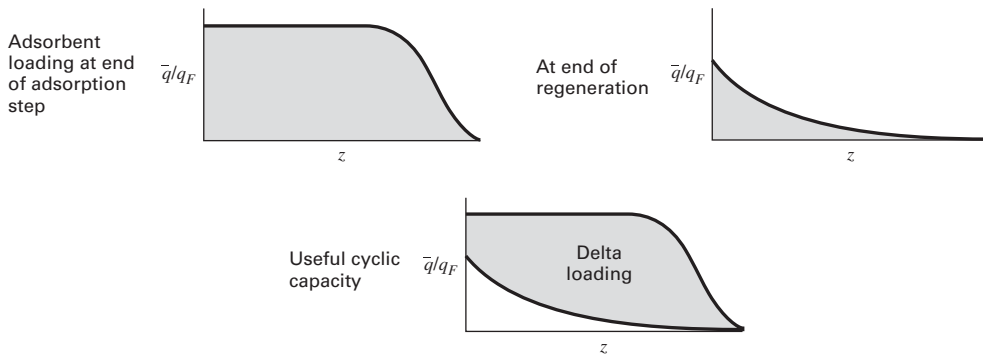


Figure 15.36 Delta loading for regeneration step.

Note that the coefficients of the ϕ -factors, inside the square brackets, sum to 0. At the last grid point, $N + 1$, where the purge gas exits, (15-121) is replaced by

$$\left(\frac{\Delta\phi}{\Delta z'}\right)_{N+1} \approx \frac{1}{12\Delta z'} [3\phi_{N-3} + 16\phi_{N-2} + 36\phi_{N-1} - 48\phi_N + 25\phi_{N+1}] \quad (15-122)$$

For the first three node points, the following approximations replace (15-121):

$$\left(\frac{\Delta\phi}{\Delta z'}\right)_1 \approx \frac{1}{12\Delta z'} [-25\phi_1 + 48\phi_2 - 36\phi_3 + 16\phi_4 - 3\phi_5] \quad (15-123)$$

$$\left(\frac{\Delta\phi}{\Delta z'}\right)_2 \approx \frac{1}{12\Delta z'} [-3\phi_1 - 10\phi_2 + 18\phi_3 - 6\phi_4 + \phi_5] \quad (15-124)$$

$$\left(\frac{\Delta\phi}{\Delta z'}\right)_3 \approx \frac{1}{12\Delta z'} [\phi_1 - 8\phi_2 + 0\phi_3 + 8\phi_4 - \phi_5] \quad (15-125)$$

Because values of ϕ_1 (at $z' = 1$) are given as a boundary condition, (15-123) is not needed.

Equations (15-118) to (15-125) with boundary conditions for ϕ_1 and ψ_1 , constitute a set of $2N$ ODEs as an initial-value problem, with t as the independent variable. Values of ϕ_i and ψ_i at the different axial locations can change with t at vastly different rates. For example, suppose in Figure 15.35 for desorption fronts, the bed length, L , is divided into 20 equal-length increments (21 points in ψ_i and ϕ_i) starting from the right-hand side where the purge gas enters. It is seen that initially, ψ_{21} , where the purge gas exits, is not changing at all, while ψ_5 is changing rapidly. Near the end of the desorption step, ψ_{21} is changing rapidly, while ψ_5 is not. Identical observations hold for ϕ_i . This type of response, referred to as **stiffness**, is described by Schiesser [87] and Press et al. [88]. If attempts are made to integrate the ODEs with simple Euler or Runge-Kutta methods, not only are truncation errors encountered, but, with time, values of ϕ_i and ψ_i go through enormous instability, characterized by wild swings between large and impossible positive and negative values. Even if the length is divided into more than 20 increments and very small time steps are used, instability is often encountered. The subject of stiffness is also discussed in Section 13.5.2.

Integration of a stiff set of ODEs is most efficiently carried out by variable-order, variable-step-size implicit methods first developed by Gear [89] and included in a widely available software package called ODEPACK, described by Byrne and Hindmarsh [90]. MATLAB contains a collection of seven solvers for systems of ODES. For stiff systems, ode15s is often the solver of choice.

EXAMPLE 15.13 Thermal-Swing Adsorption.

In Example 15.11, benzene is adsorbed from air at 70°F and 1 atm onto silica gel in a 6-ft-long fixed-bed adsorber. Breakthrough occurs at close to 97.1 minutes for $\phi = 0.05$. At that time, values of $\phi = c/c_F$ and $\psi = \bar{q}/q_F^*$ in the bed are distributed as follows, where z' is measured backward from the bed exit for the adsorption step. These results were obtained numerically using the method of lines with equations (15-118) to (15-125), and are in close agreement with the Klinkenberg solution given in Example 15.11.

z' , ft	$\phi = c/c_F$	$\psi = \bar{q}/q_F^*$
0.0	0.05227	0.03891
0.3	0.07785	0.05913
0.6	0.11314	0.08776
0.9	0.16008	0.12690
1.2	0.22017	0.17850
1.5	0.29394	0.24387
1.8	0.38042	0.32310
2.1	0.47678	0.41459
2.4	0.57825	0.51469
2.7	0.67861	0.61786
3.0	0.77108	0.71728
3.3	0.84969	0.80603
3.6	0.91057	0.87858
3.9	0.95281	0.93207
4.2	0.97848	0.96690
4.5	0.99172	0.98636
4.8	0.99731	0.99531
5.1	0.99921	0.99857
5.4	0.99987	0.99960
5.7	1.00000	1.00000
6.0	1.00000	1.00000

If the bed is regenerated isothermally with pure air at 1 atm and 145°F, and benzene desorption during the heat-up period is neglected, determine the loading, \bar{q} , profile at times of 15, 30, and 60 minutes for air stripping at interstitial velocities of: (a) 197 ft/minute, and (b) 98.5 ft/minute. At 145°F and 1 atm, the adsorption isotherm, in the same units as in Example 15.11, is

$$q = 1,000c^* \quad (1)$$

giving an equilibrium loading of about 20% of that at 70°F. Assume that k is unchanged from the value of 0.206 in Example 15.11.

Solution

This problem was solved by the method of lines, with 20 increments in z' , using a stiff ODE function. Derivative functions were (15-118) to (15-122) and (15-124) to (15-125). The computed loading profiles are plotted in Figures 15.37a and b, for desorption interstitial velocities of 197 and 98.5 ft/minute, where z is distance from the feed gas inlet end for adsorption. The curves are similar to those in Figure 15.27. For the 197-ft/minute case, desorption is almost complete at 60 minutes with less than 1% of the bed still loaded

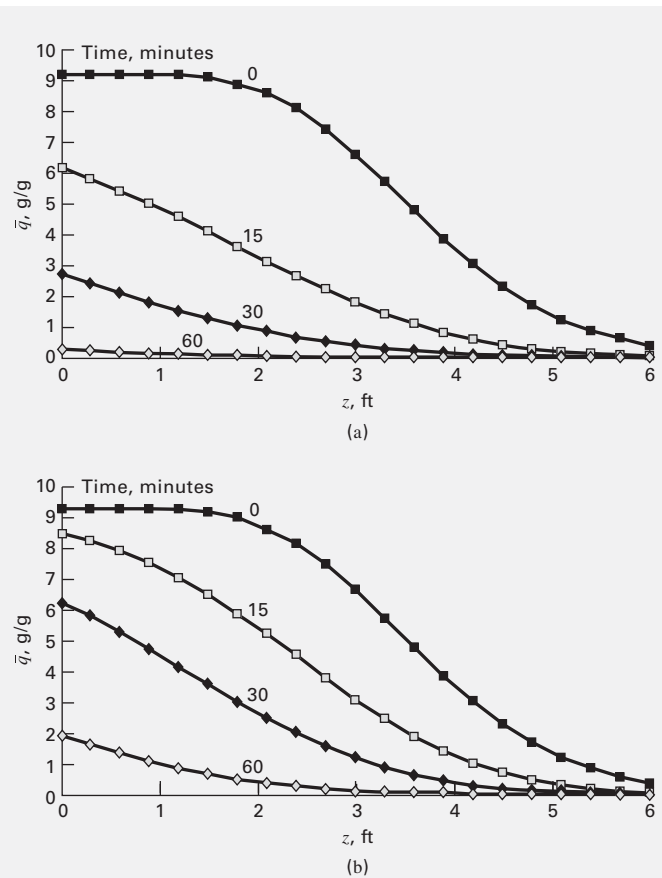


Figure 15.37 Regeneration loading profiles for Example 15.13. (a) Regeneration air interstitial velocity = 197 ft/min. (b) Regeneration air interstitial velocity = 98.5 ft/min.

with benzene. If this velocity were used, this would allow $97.1 - 60 = 37.1$ minutes for heating and cooling the bed before and after desorption. For the 98.5 ft/minute case at 60 minutes, about 5% of the bed is still loaded with benzene. This may be acceptable, but the resulting adsorption step would take a little longer because initially, the bed would not be clean. Several cycles are required to establish a cyclic steady state, whose development is considered in the next section, on pressure-swing adsorption.

§15.5.4 Pressure-Swing Adsorption (PSA)

Pressure-swing adsorption (PSA) and vacuum-swing adsorption (VSA), in their simplest configurations, are carried out with two fixed beds in parallel, operating in a cycle, as in Figure 15.38. Unlike TSA, where thermal means is used to effect the separation, PSA and VSA use mechanical work to increase the pressure or create a vacuum, as is illustrated in Figure 15.21. Unlike TSA, which can be used to purify gases or liquids, PSA and VSA are used only with gases, because a change in pressure has little or no effect on equilibrium loading for liquid adsorption. PSA was originally used only for purification, as in the removal of moisture from air by the “heatless drier,” invented by C.W. Skarstrom in 1960 to compete with TSA. However, by

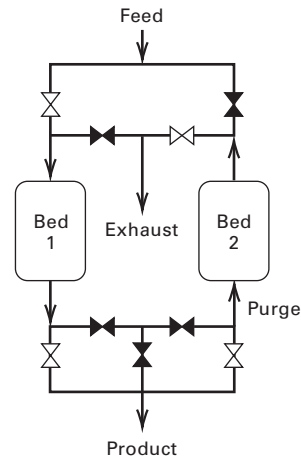


Figure 15.38 Pressure-swing-adsorption cycle.

the early 1970s, PSA was being applied to bulk separations such as the partial separation of air to produce either nitrogen or oxygen and to the removal of impurities and pollutants from other gas streams. PSA can also be used for vapor recovery, as discussed and illustrated by Ritter and Yang [91].

A typical sequence of steps in the Skarstrom cycle, operating with two beds, is shown in Figure 15.39, where t_c is the cycle time. Each bed operates alternately in two half-cycles of equal duration: (1) pressurization followed by adsorption, and (2) depressurization (blowdown) followed by a purge. The feed gas is used for pressurization, while a portion of the effluent product gas is used for purge. Thus, in Figure 15.39, while adsorption is taking place in Bed 1, part of the gas leaving Bed 1 is routed to Bed 2 to purge that bed in a direction counter to the direction of flow of the feed gas during the adsorption step. When moisture is to be removed from air, the dry-air product is produced during the adsorption step in each of the two beds. In Figure 15.39, the adsorption and purge steps represent less than 50% of the total cycle time. In many commercial applications of PSA, these two steps consume a much greater fraction of the cycle time because pressurization

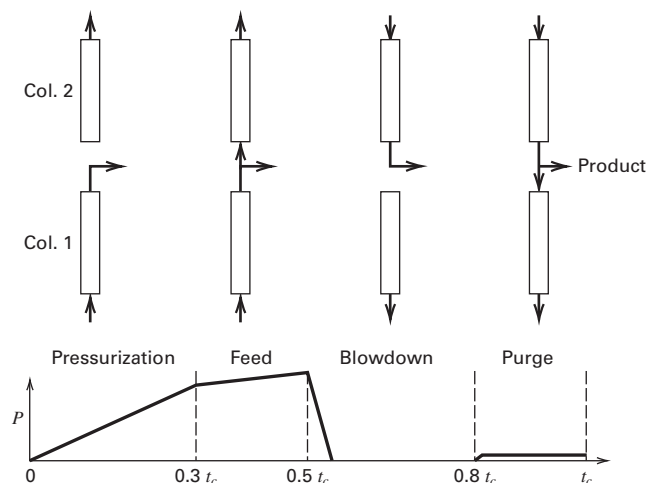


Figure 15.39 Sequence of cycle steps in PSA.

and blowdown can be completed rapidly. Therefore, cycle times for PSA and VSA are short, typically seconds to minutes. Thus, small beds have relatively large throughputs. With the valving shown in Figure 15.38, the entire cyclic sequence can be programmed to operate automatically. With some valves open and others closed, as in Figure 15.38, adsorption takes place in Bed 1 and purge takes place in Bed 2. During the second half of the cycle, the valve openings and beds are switched.

Since the introduction of the Skarstrom cycle, improvements have been made to increase product purity, product recovery, adsorbent productivity, and energy efficiency, as discussed by Yang [25] and by Ruthven, Farooq, and Knaebel [92]. Among these modifications are use of:

1. three, four, or more beds;
2. a pressure-equalization step in which both beds are equalized in pressure following the purge of one bed and adsorption in the other;
3. pretreatment or guard beds to remove strongly adsorbed components that might interfere with the separation of other components;
4. purge with a strongly adsorbing gas; and
5. an extremely short cycle time to approach isothermal operation, if a longer cycle causes an undesirable increase in temperature during adsorption and an undesirable decrease in temperature during desorption.

Separations by PSA and VSA are controlled by adsorption equilibrium or adsorption kinetics, where the latter refers to mass transfer external and/or internal to the adsorbent particle. Both types of control are important commercially. For the separation of air with zeolites, adsorption equilibrium is the controlling factor, with nitrogen more strongly adsorbed than oxygen and argon. For air with 21% oxygen and 1% argon, oxygen of about 96% purity can be produced. When carbon molecular sieves are used, oxygen and nitrogen have almost the same adsorption isotherms, but the effective diffusivity of

oxygen is much larger than that of nitrogen. Consequently, a nitrogen product of very high purity (>99%) can be produced.

PSA and VSA cycles have been modeled successfully for both equilibrium and kinetic-controlled cases, with models and computational procedures similar to those used for TSA. The models are particularly useful for optimizing cycles. Of particular importance in PSA and TSA is the determination of the cyclic steady state. In TSA, following the desorption step, the regenerated bed is usually clean. Thus, a cyclic steady state is closely approached in one cycle. In PSA and VSA, this is often not the case, and complete regeneration is seldom achieved or necessary. It is only required to attain a cyclic steady state whereby the product obtained during the adsorption step has the desired purity. At cyclic steady state, the difference between a loading profile after adsorption and desorption is equal to the solute in the feed. Starting with a clean bed, the attainment of a cyclic steady state for a fixed cycle time may require tens or hundreds of cycles.

Consider an example of cyclic steady state from a study by Mutasim and Bowen [93] on the removal of ethane and carbon dioxide from nitrogen with 5A zeolite, at ambient temperature with adsorption and desorption for 3 minutes each at 4 bar and 1 bar, respectively, in beds 0.25 m in length. Figures 15.40a and b show the computed development of the loading and gas concentration profiles at the end of each adsorption step for ethane, starting from a clean bed. At the end of the first cycle, the bed is still clean beyond about 0.11 m. By the end of the 10th cycle, a cyclic steady state has almost been attained, with a clean bed existing only near the very end of the bed. Experimental data points for ethane loading at the end of 10 cycles agree reasonably well with the computed profile from a mathematical model.

Modeling of PSA and VSA cycles is carried out with the same equations as for TSA. However, the assumptions of negligible axial diffusion and isothermal operation may not be valid. For each cycle, the pressurization and blowdown steps are often ignored and the initial conditions for adsorption and desorption are the final conditions for the desorption

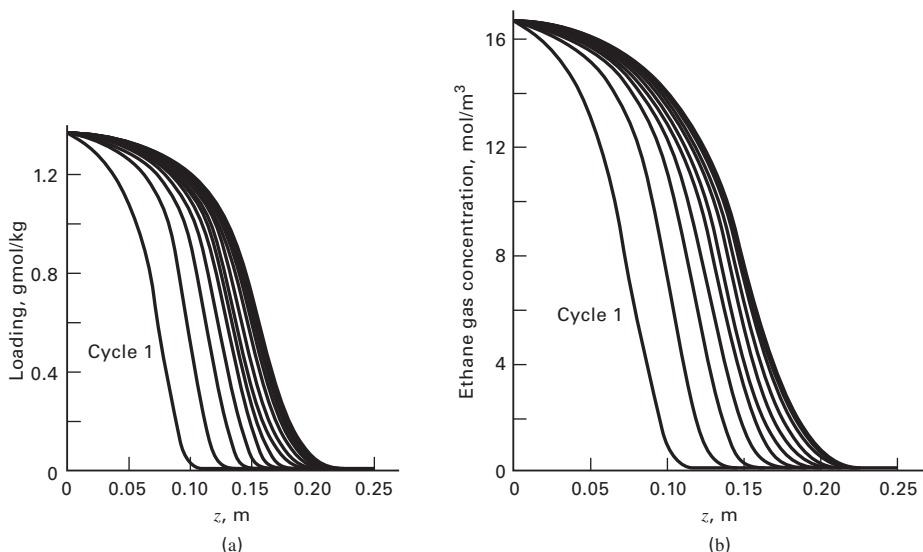


Figure 15.40 Development of cyclic steady-state profiles. (a) Loading profiles for first 11 cycles. (b) Ethane gas concentration profiles for first 16 cycles.

and adsorption steps, respectively, of the previous cycle. Rigorous calculations are best made with Aspen Adsorption, which is not included in Aspen Plus, but is a core element of AspenONE. Aspen Adsorption can handle complex gas and liquid adsorption processes including TSA, PSA, and VSA. Options include: rate-based and equilibrium-based models; addition of axial dispersion; cylindrical and radial beds; and specification of cycle steps, with consideration of cyclic steady state.

§15.6 CONTINUOUS, COUNTERCURRENT ADSORPTION SYSTEMS

Slurry and fixed-bed modes of adsorption, shown in Figures 15.20a and b, are traditional modes of adsorber operation. A third mode of operation, shown in Figure 15.20c, is a continuous, countercurrent, moving-bed operation, often referred to as a true-moving-bed (TMB) system. It has an important advantage because, as in a heat exchanger, an absorber, and other separation cascades, countercurrent flow maximizes the average driving force for transport. In adsorption, this increases the efficiency of adsorbent use, giving lower capital and operating costs.

§15.6.1 True and Simulated Moving Bed Systems

In Figure 15.20c, the fluid feed is separated with two sections: an adsorber and a regenerator (desorber). The solid adsorbent particles move through the two sections of the system. However, as discussed in detail by Ruthven and Ching [65] and Wankat [94], the advantage of countercurrent operation can be achieved without movement of the adsorbent particles by a simulated-moving-bed (SMB) operation. A widely used implementation of an SMB is shown in Figure 15.23, wherein adsorbent particles remain fixed in a bed. The SMB can be used for purification or bulk separation.

Operation of a simulated moving bed is best understood by studying the two representations of a four-section system and the accompanying fluid composition profile in Figure 15.41. The feed to be separated is a binary mixture of A and B. A desorbent, D, is used for regeneration. The schematic representation in Figure 15.41a shows a TMB, with circulation of solid adsorbent S down through four dense-bed sections in a closed cycle. Figure 15.41b represents an SMB system, made up of four sections divided into 12 fixed-bed subsections, shown as rectangles, with periodic movement of fluid inlet and outlet ports, shown as circles. The sections in Figure 15.41a are sometimes referred to as zones, and the fixed-bed subsections in Figure 15.41b are often referred to as beds and sometimes columns. In the equivalent TMB case of Figure 15.41a, fluid of changing composition with respect to feed components A and B, and desorbent D, flows upward through the downward-flowing adsorbent beds. From the top of Section IV, fluid rich in D is recirculated to Section I. Fluid feed is shown as a binary mixture of A and B, which enters between Sections II and III. Component A is more strongly

adsorbed than D, which is more strongly adsorbed than B. The desired result is that A is almost completely separated from B. However, appreciable amounts of D may appear in both the B-rich raffinate and A-rich extract. Thus, makeup D is added to the recirculated fluid.

Each of the four sections in Figure 15.41a performs a different primary function. More detail follows for the case where D, as well as A and B, are adsorbed. A typical component composition profile is shown in Figure 15.41c.

Section I: Desorb A. Entering S contains adsorbed A and D. Ideally, entering fluid is nearly pure D. Exiting S contains adsorbed D. Exiting fluid is A and D, part of which is withdrawn as A-rich extract.

Section II: Desorb B. Entering S contains adsorbed A, B, and D. Entering fluid is A and D. Exiting S contains adsorbed A and D. Exiting fluid is A, B, and D.

Section III: Adsorb A. Entering S contains adsorbed B and D. Entering fluid is A, B, and D from Section II and fresh feed of A and B. Exiting S contains adsorbed A, B, and D. Exiting fluid is B and D, part of which is withdrawn as B-rich raffinate.

Section IV: Adsorb B. Entering S contains adsorbed D. Entering fluid is B and D. Exiting S contains adsorbed B and D. Ideally, exiting fluid is nearly pure D.

The steady-state separation achieved by the TMB in Figure 15.41a is close approximation to that achieved by the SMB, shown for a commercial Sorbex system in Figure 15.23 and by a simpler representation in Figure 15.41b. In both figures, it is seen that four sections are provided with a total of 12 ports for fluid feeds to enter, or fluid products to exit. In Figure 15.41b, it is clear that ports divide each section into subsections, four for Section I, three for Section II, three for Section III, and two for Section IV. As each section is divided into more subsections (thereby adding more ports), the SMB system more closely approaches the separation achieved in the corresponding TMB. In Figure 15.41b, only ports 2, 6, 9, and 12 are open. After an increment of time (called the switching time or port-switching interval, t^* , those ports are closed and 3, 7, 10, and 1 are opened. In this manner, the ports are closed and opened in sequence in the direction shown. By periodically shifting feed and product positions by one port position in the direction of fluid flow, movement of solid adsorbent in the opposite direction within the sections is simulated. Because of stream additions and withdrawals between sections, flow rates in each of the four sections are different. Figure 15.23 shows a pump for controlling the fluid flow rate at the bottom of the SMB. Although sections are switched, the pump is not. Therefore, the pump must be programmed for four different flow rates depending on the section to which the pump is currently connected.

A number of models have been developed for designing and analyzing SMBs. These include: (1) TMB equilibrium-stage model using a McCabe–Thiele-type analysis, (2) TMB local adsorption-equilibrium model, (3) TMB rate-based model,

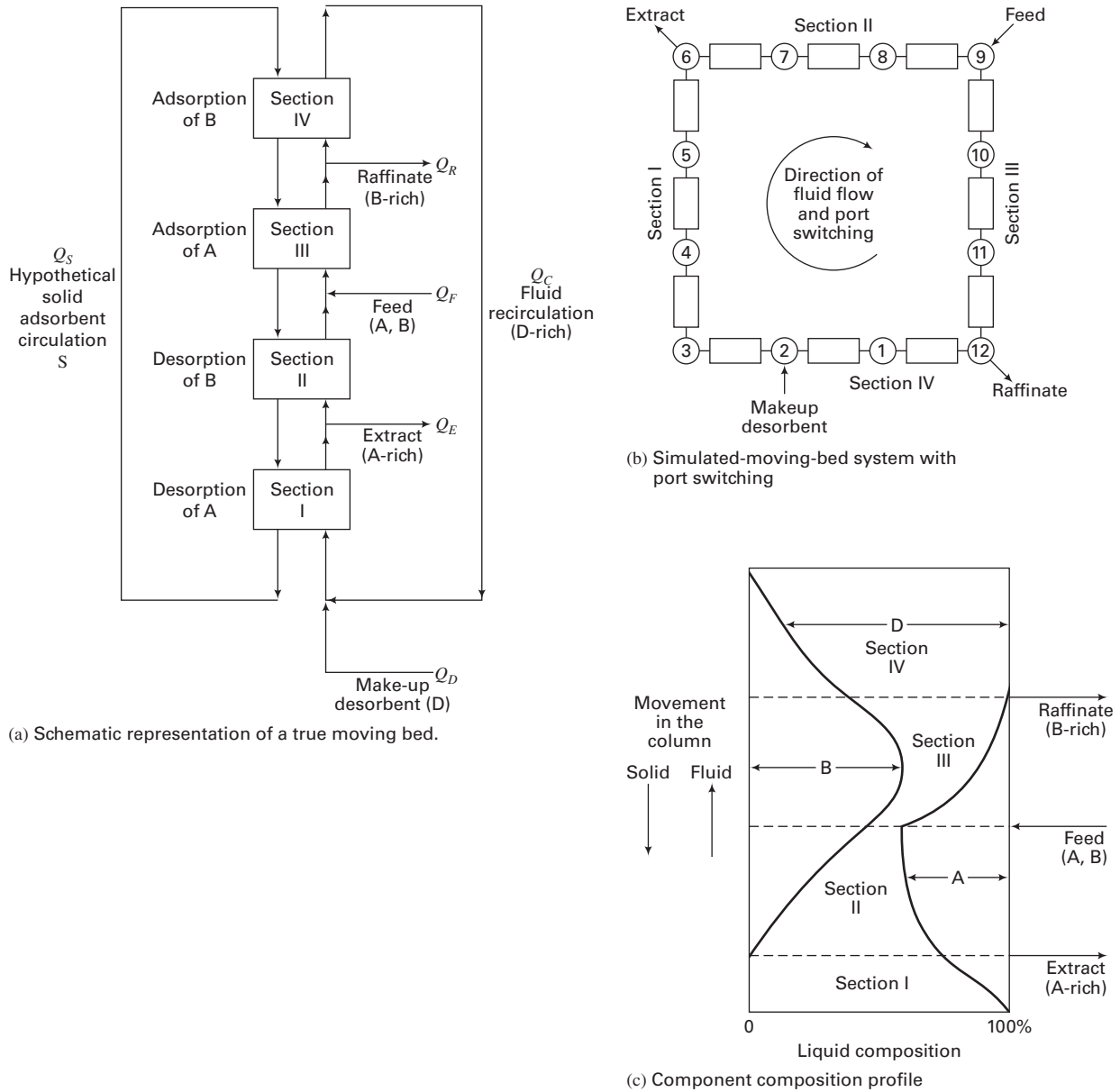


Figure 15.41 Four-section TMB and SMB systems.

and (4) SMB rate-based model. The first three assume steady-state conditions with continuous countercurrent flows of fluid and solid adsorbent, approximating SMB operation with a TMB. The SMB rate-based model applies to transient operation for start-up, approach to a cyclic steady state, and shut-down. The simplest of the four approaches is the TMB equilibrium-stage model, but it is difficult to apply to multicomponent systems with nonlinear adsorption-equilibrium isotherms. The TMB local adsorption-equilibrium model, although ignoring the effects of axial dispersion and fluid-particle mass transfer, has proved useful for establishing reasonable operating flow rates in multiple sections of an SMB because its behavior is often determined largely by adsorption equilibria. For a linear adsorption isotherm,

Wankat [95] has successfully applied this method to SMBs with large numbers of sections for feeds dilute in solutes.

Methods for solving the TMB local adsorption equilibrium model for multicomponent systems, including concentrated mixtures, with nonlinear adsorption isotherms, have been presented by a number of investigators. They include Storti et al. [96], who extended the pioneering work of Rhee, Aris, and Amundson [97] for a single section to the commonly used four-section unit, and Mazzotti et al. [98] for multicomponent systems. For a final design, rigorous rate-based models are preferred. These models, which account for axial dispersion in the bed, particle-fluid mass-transfer resistances, and nonlinear adsorption isotherms, are available in the program Aspen Chromatography, which is not included in Aspen Plus, but is a

core element of AspenONE. Aspen Chromatography is useful for both TMB steady-state operation and SMB dynamic operation. The local adsorption equilibrium and rate-based models are described next, followed by illustrative examples, two of which are solved using Aspen Chromatography. Equations are given for four-section units, but are readily extended to more sections.

Steady-State Local Adsorption Equilibrium TMB Model

The TMB model describes continuous, steady-state, multi-component adsorption with countercurrent flow of the fluid and solid adsorbent, as shown in Figure 15.42 for a single section of height Z of a multisection system, subject to these assumptions:

- One-dimensional plug flow of both phases with no channeling
- Constant volumetric flow rates, of Q for the liquid and Q_S for the solid
- Constant external void fraction, ϵ_b , of the solids bed
- Negligible axial dispersion and particle-fluid mass transfer resistances
- Local adsorption equilibrium between solute concentrations, c_i , in the bulk liquid and adsorption loading, q_i , on the solid
- Isothermal and isochoric conditions

For a differential-bed thickness, dz , where component i undergoes mass transfer between the two phases, the mass balance is:

$$Q \frac{dc_i}{dz} - S \frac{dq_i}{dz} = 0 \tag{15-126}$$

Boundary conditions are

$$z = 0, c_i = c_{i,in} \quad \text{and} \quad z = Z, q_i = q_{i,in}$$

The solution to (15-126) depends on the equilibrium adsorption isotherm. Typically, when the fluid is a liquid dilute in solutes, a linear isotherm, $q_i = K_i c_i$, is used, where q_i is on

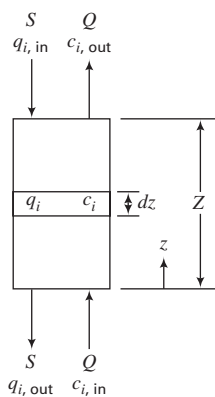


Figure 15.42 TMB local-adsorption-equilibrium model for a single section.

a particle volume basis so that K_i is dimensionless. For the bulk separation of liquid mixtures, where concentrations of the feed components and desorbent are not small, a nonlinear, extended-Langmuir equilibrium-adsorption isotherm of the constant-selectivity form, Example 15.6, is appropriate:

$$q_i = \frac{(q_i)_m K_i c_i}{1 + \sum_j K_j c_j} \tag{15-127}$$

In either case, the solution of Rhee, Aris, and Amundson [97], when extended to multiple (e.g., four) sections, as by Storti et al. [96], predicts constant component concentrations in each section, but with discontinuities at either one or both section boundaries. Typical concentration profiles are shown in Figure 15.43 for a four-solute system (1, 2, 3, and 4), where a set of stationary rectangular (shock-like) waves of constant concentration exists in the fluid phase in each section. The concentration profile for the desorbent (component 5) is not shown. Note that the concentrations of the four solutes for this local equilibrium assumption are negligible in Sections I and IV, where only desorbent is present.

Local equilibrium theory is useful to determine approximate values of required solid adsorbent and fluid flow rates in each section of a TMB in order to achieve a perfect separation of two solutes. The description of the method, first developed by Ruthven and Ching [99] and extended by Zhong and Guiochon [100], is facilitated by applying local adsorption-equilibrium theory to the simple case of the separation of a feed dilute in binary solutes, A and B. Assume diluent, D, does not adsorb and Henry’s law governs adsorption equilibrium, with $K_A > K_B$ (i.e., A is more strongly adsorbed). First, a set of flow-rate ratios, m_j , one for each section, j , are defined:

$$m_j = \frac{Q_j}{Q_S} = \frac{\text{volumetric fluid phase flow rate}}{\text{volumetric solid particle phase flow rate}} \tag{15-128}$$

For conditions of local adsorption equilibrium, the following necessary and sufficient conditions at each section for complete separation are

$$K_A < m_I < \infty \tag{15-129}$$

$$K_B < m_{II} < K_A \tag{15-130}$$

$$K_B < m_{III} < K_A \tag{15-131}$$

$$0 < m_{IV} < K_B \tag{15-132}$$

Constraint (15-130) ensures that net flow rates of components A and B will be positive (upward) in section I. Constraint (15-132) ensures that the net flow rates of components A and B will be negative (downward) in Section IV. Constraints (15-130) and (15-131) are most important because they ensure sharpness of the separation. They cause net flow rates of A and B to be negative (downward) and positive (upward), respectively, in the two central sections II and III. Inequality

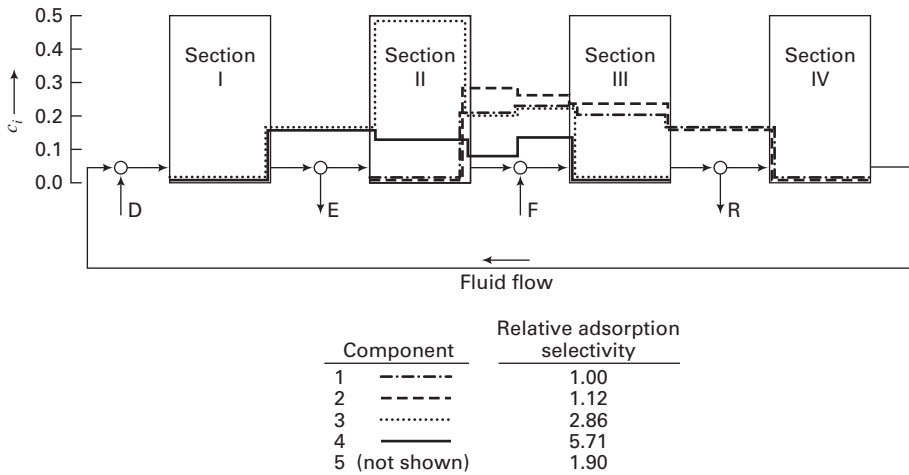


Figure 15.43 Typical solute-concentration profiles for local adsorption equilibrium in a four-section unit.

constraints (15-129) to (15-132) may be converted to equality constraints with a safety margin, β .

$$Q_1/Q_S = K_A\beta \quad (15-133)$$

$$(Q_1 - Q_E)/Q_S = K_B\beta \quad (15-134)$$

$$(Q_1 - Q_E + Q_F)/Q_S = K_A/\beta \quad (15-135)$$

$$(Q_1 - Q_E + Q_F - Q_R)/Q_S = K_B/\beta \quad (15-136)$$

Solving (15-133) to (15-136) by eliminating Q_1 gives

$$Q_S = \frac{Q_F}{K_A/\beta - K_B\beta} \quad (15-137)$$

$$Q_E = Q_S(K_A - K_B)\beta \quad (15-138)$$

$$Q_R = Q_S(K_A - K_B)/\beta \quad (15-139)$$

Then, using (15-133),

$$Q_1 = Q_C + Q_D = Q_S Q_A \beta \quad (15-140)$$

Therefore,
$$Q_C = Q_S K_A \beta - Q_D \quad (15-141)$$

where Q_C = fluid recirculation rate before adding makeup desorbent. By an overall material balance,

$$Q_D = Q_E + Q_R - Q_F \quad (15-142)$$

Restrictions on flow-rate ratios, m_{II} and m_{III} in inequality constraints (15-130) and (15-131), are conveniently represented by the **triangle method** of Storti et al. [101], as shown in Figure 15.44. If values of m_{II} and m_{III} within the triangular region are selected, a perfect separation is possible. However, if $m_{II} < K_B$, some B will appear in the extract; if $m_{III} > K_A$, some A will appear in the raffinate. If $m_{II} < K_B$ and $m_{III} > K_A$, extract will contain some B and raffinate will contain some A.

The permissible range for safety margin, β , in (15-133) to (15-139) is determined from inequality constraints (15-130) and (15-131). Let

$$\gamma_{i,j} = \frac{m_j}{K_i} = \frac{Q_j}{Q_S K_i} \quad (15-143)$$

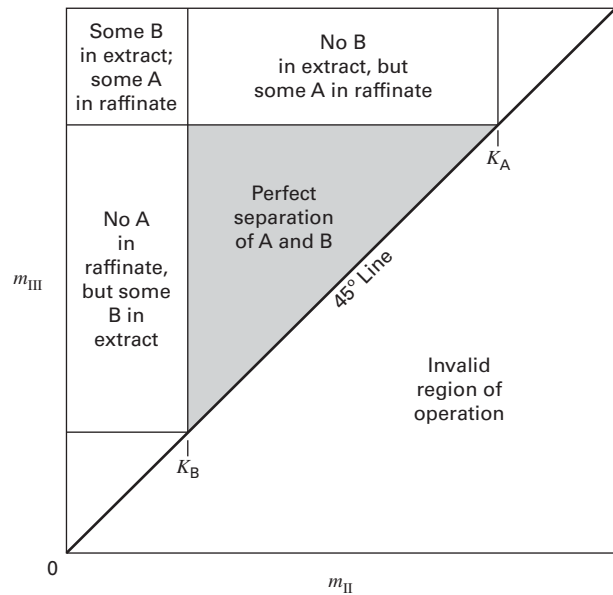


Figure 15.44 Triangle method for determining necessary values of flow rate ratios.

In Section II, it is required that $\gamma_{A,II} > 1$ and $\gamma_{B,II} < 1$. In terms of safety margin, β , (15-143) is used to give corresponding equalities, $Q_{II}/Q_S = K_A/\beta$ and $Q_{II}/Q_S = K_B\beta$, assuming equal β in all four sections. Equating these two equalities for the same safety margin gives $\beta = \sqrt{K_A/K_B}$, which is the maximum value of β for a perfect separation, the minimum value being 1.0. Above the maximum value of β , some sections will encounter negative fluid flow rates. Below a β value of 1.0, a perfect separation will not be achieved. As the value of β increases from minimum to maximum, fluid flow rates in the sections increase, often exponentially. Thus, estimation of operating flow rates is generally carried out using a value of β close to, but above, 1.0, e.g., 1.05 (unless this exceeds the maximum value of β). Note that as the separation factor, K_A/K_B , approaches 1.0, not only does the separation become more difficult, but also, the permissible range of β becomes

smaller. In the triangle method, of Figure 15.44, the upper left corner of the triangle corresponds to $\beta = 1$, while the maximum value of β occurs when $m_{II} = m_{III}$, which falls on the 45° line between the values K_A and K_B . Extensions of the above binary procedures for estimating operating flow rates to cases of both constant selectivity Langmuir adsorption isotherms and to more complex nonlinear isotherms are given by Mazzotti et al. [102] and for multicomponent systems by Mazzotti et al. [98]. With nonlinear adsorption isotherms, the right triangle of Figure 15.44 is distorted to a shape with one or more curved sides.

EXAMPLE 15.14 Operation with a TMB for Steady-State, Local Adsorption Equilibrium Conditions.

Fructose (A) is separated from glucose (B) in a four-section SMB unit. The aqueous feed of 1.667 mL/min contains 0.467 g/min of A, 0.583 g/min of B, and 0.994 g/min of water. For the adsorbent and expected concentrations and temperature of the operation, Henry's law holds, with constants of $K_A = 0.610$ and $K_B = 0.351$ for fluid concentrations in g/mL and loadings in g/mL of adsorbent particles. Water is assumed not to adsorb. Estimate operating flow rates in mL/min to achieve a perfect separation of fructose from glucose for a TMB. Note that the extract will contain fructose, while the raffinate will contain glucose. Conversion of the results to SMB operation will be made in Example 15.15.

Solution

Equations (15-137) to (15-142) apply. The minimum value of β is 1.0, while the maximum value is $\sqrt{K_A/K_B} = \sqrt{0.610/0.351} = 1.32$. Calculations are most conveniently carried out with a spreadsheet. With reference to Figure 15.41 for the case of a TMB, the results for values of $\beta = 1.0, 1.05, 1.20$ are:

	Volumetric Flow Rates, mL/min		
	$\beta = 1.0$	$\beta = 1.05$	$\beta = 1.20$
Feed, Q_F	1.667	1.667	1.667
Solid particles, Q_S	6.436	7.848	19.132
Extract, Q_E	1.667	2.134	5.946
Raffinate, Q_R	1.667	1.936	4.129
Recirculation, Q_C	2.259	2.624	5.596
Makeup desorbent, Q_D	1.667	2.403	8.408
Q_I	3.926	5.027	14.004
Q_{II}	2.259	2.893	8.058
Q_{III}	3.926	4.560	9.725
Q_{IV}	2.259	2.624	5.596

Note that the lowest section fluid flow rates, Q_I to Q_{IV} , correspond to $\beta = 1.0$. At $\beta = 1.2$, section fluid flow rates, as well as the adsorbent particles flow rate, become significantly higher. The most concentrated products (extract and raffinate) and the smallest flow rate of makeup desorbent are also achieved with the lowest β value.

Steady-State TMB Model

This model assumes plug flow at isothermal, isobaric, and constant-fluid-velocity conditions in each section j ($j = 1$ to 4). For each component i ($i = 1$ to C) the following equations apply, where each section begins at $z = 0$, where the fluid enters, and ends at $z = L_j$. Unlike the previous local adsorption-equilibrium model, axial dispersion and fluid-particle mass transfer are taken into account.

1. Mass-balance equation for solute i in bulk fluid phase f , in section j :

$$-D_{L_j} \frac{d^2 c_{i,j}}{dz^2} + u_{f_j} \frac{dc_{i,j}}{dz} + \frac{(1 - \epsilon_b)}{\epsilon_b} J_{i,j} = 0 \quad (15-144)$$

where the first term accounts for axial dispersion with eddy diffusivity D_L , J is solute mass-transfer flux between the bulk fluid phase and the sorbate in the pores of the solid, and u_f is the interstitial fluid velocity, where for an adsorbent bed of cross-sectional area, A_b ,

$$u_{f_j} = \frac{Q_j}{\epsilon_b A_b} \quad (15-145)$$

2. Mass-balance equation for the sorbate, s , on the solid phase:

$$u_s \frac{d\bar{q}_{i,j}}{dz} - J_{i,j} = 0 \quad (15-146)$$

where u_s is the true moving-solid velocity given by

$$u_s = \frac{Q_S}{(1 - \epsilon_b)A_b} \quad (15-147)$$

3. Fluid-to-solid mass transfer:

$$J_{i,j} = k_{i,j}(q_{i,j}^* - \bar{q}_{i,j}) \quad (15-148)$$

4. Adsorption isotherm (e.g., the multicomponent, extended-Langmuir equation)

$$q_{i,j}^* = f\{\text{all } c_{i,j}\} \quad (15-149)$$

This system of $4C$ second-order ODEs and $4C$ first-order ODEs, together with the algebraic equations for mass-transfer rates and adsorption equilibria, requires $12C$ boundary conditions, i.e., $3C$ for each section. At the entrance, $z = 0$, to each section, a boundary condition that accounts for axial dispersion is required. This has been discussed extensively in the literature, e.g., Danckwerts [103]. Used most often is

$$u_{f_j}(c_{i,j,0} - c_{i,j}) = -\epsilon_b D_{L_j} \frac{dc_{i,j}}{dz} \quad (15-150)$$

where $c_{i,j,0}$ is the concentration of component i entering ($z = 0$) section j .

For continuity of bulk fluid concentrations and sorbate loadings in moving from one section to another, the following boundary conditions apply at adjacent sections:

At Sections I and II where extract is withdrawn:

$$c_{i,I,z=L_j} = c_{i,II,z=0} \quad (15-151)$$

$$q_{i,I,z=L_j} = q_{i,II,z=0} \quad (15-152)$$

At Sections III and IV where raffinate is withdrawn:

$$c_{i,III,z=L_j} = c_{i,IV,z=0} \quad (15-153)$$

$$q_{i,III,z=L_j} = q_{i,IV,z=0} \quad (15-154)$$

At Sections II and III where the feed enters:

$$c_{i,III,z=0} = \frac{Q_{II}}{Q_{III}} c_{i,II,z=L_{II}} + \frac{Q_F}{Q_{III}} c_{i,F} \quad (15-155)$$

$$q_{i,II,z=L_j} = q_{i,III,z=0} \quad (15-156)$$

At Sections IV and I where makeup desorbent enters:

$$c_{i,I,z=0} = \frac{Q_{IV}}{Q_I} c_{i,IV,z=L_{IV}} + \frac{Q_D}{Q_I} c_{i,D} \quad (15-157)$$

$$q_{i,IV,z=L_j} = q_{i,I,z=0} \quad (15-158)$$

where the volumetric fluid flow rates, which change from section to section, are subject to

$$Q_I = Q_{IV} + Q_D \quad (15-159)$$

$$Q_{II} = Q_I - Q_E \quad (15-160)$$

$$Q_{III} = Q_{II} + Q_F \quad (15-161)$$

$$Q_{IV} = Q_{III} - Q_E \quad (15-162)$$

It is important to note that for an SMB, solid particles do not flow down through the unit, but are retained in stationary beds in each section. To obtain the same true velocity difference between the fluid and solid particle phase, the upward fluid velocity in the SMB must be the sum of the absolute true velocities in the upward-moving fluid and downward-moving solid particle phases in the TMB. Thus, using (15-145) and (15-147),

$$(Q_j)_{SMB} = (Q_j)_{TMB} + \left(\frac{\epsilon_b}{1 - \epsilon_b} \right) (Q_S)_{TMB} \quad (15-163)$$

The TMB model can be solved by a number of techniques, as discussed by Constantinides and Mostoufi [104], with the Newton shooting method being preferred. An example of the application of the steady-state TMB model is given after the next subsection that treats dynamic SMB models.

Dynamic SMB Model

Equations for this model are subject to the same assumptions as for the steady-state TMB model. Changes in the equations permit the model to take into account time of operation, t , and to use a fluid velocity relative to the stationary solid particles. In addition, equations now must be written for each bed subsection (also referred to as a column), k , between adjacent ports, as shown in Figure 15.41b. The revised equations are

1. Mass-balance equation for solute i in bulk fluid phase f , in subsection k :

$$\frac{\partial c_{i,k}}{\partial t} - D_{L_k} \frac{\partial^2 c_{i,k}}{\partial z^2} + u_{f_k} \frac{\partial c_{i,k}}{\partial z} + \frac{(1 - \epsilon_b)}{\epsilon_b} J_{i,k} = 0 \quad (15-164)$$

2. Mass-balance equation for the sorbate, s , on the solid phase:

$$\frac{\partial \bar{q}_{i,k}}{\partial t} - J_{i,k} = 0 \quad (15-165)$$

where the interstitial fluid velocity for SMB operation is related to that for TMB operation at a particular location by

$$(u_f)_{SMB} = (u_f)_{TMB} + |(u_s)|_{TMB} \quad (15-166)$$

SMB and TMB models are further connected by an equation that relates the solid velocity in the TMB model to a port-switching time, t^* , and bed height between adjacent ports, L_k , for use in this SMB model:

$$u_s = \frac{L_k}{t^*} \quad (15-167)$$

Boundary conditions for the TMB model apply to SMB models. In addition, initial conditions are needed for fluid concentrations, $c_{i,k}$, and sorbate loadings, $\bar{q}_{i,k}$, throughout the adsorbent beds; e.g., at $t = 0$, $c_{i,k} = 0$ and $\bar{q}_{i,k} = 0$.

The SMB model, which involves PDEs, rather than ODEs, is much more difficult to solve than the steady-state TMB, because it involves moving concentration fronts. In Aspen Chromatography, the dynamic SMB equations are solved by discretizing the first- and second-order spatial terms of the PDEs to obtain a large set of ODEs and algebraic equations, which constitute a DAE (differential algebraic equations) system. A number of discretization or differencing methods are provided. Each complete cycle of the SMB model provides a different result, which ultimately leads to a cyclic steady state. Studies have shown that if the number of bed subsections per section is at least four and the number of cycles is 10 or more, the steady-state TMB result closely approximates the SMB result. Therefore, if only steady-state results are of interest, the simpler steady-state TMB model is best employed.

All four models can be used for gas or liquid feeds, with the latter being the most widely applied to industrial separations. Regardless of the model used for design of an SMB (dynamic SMB or steady-state TMB), the information required is:

1. Flow rate and feed composition (binary of A and B, or multicomponent).
2. Adsorbent, S, and desorbent, D.
3. Nominal bed operating temperature, T , and pressure, P .
4. Adsorption isotherm for all components, with known constants at the bed operating conditions.
5. Desired separation, which may be purity (on a desorbent-free basis) or desired recovery of the most strongly adsorbed component in the extract.

Not initially known, but required before calculations can be made, are:

6. Total bed height and inside diameter of the adsorption column.
7. Amount of adsorbent in the column.
8. Desorbent recirculation rate.
9. Flow rates of extract and raffinate.
10. Overall mass-transfer coefficients for transport of solutes between bulk fluid and sorbate layer on the adsorbent.
11. Eddy diffusivity for axial dispersion.
12. Spacing of inlet and outlet ports.

Guidance on initial values for items 6, 10, and 11 is sometimes provided in patents for similar separations. For example, for the separation of xylene mixtures using para diethylbenzene as desorbent, Minceva and Rodrigues [105] suggest:

- Molecular-sieve zeolite adsorbent with a spherical particle diameter, d_p , between 0.25 and 1.00 mm and a particle density, ρ_p , of 1.39 g/cm³
- Operating temperature between 140°C and 185°C with an operating pressure sufficient to maintain a liquid phase
- Liquid interstitial velocity, u_f , between 0.4 and 1.2 cm/s
- Four sections with 8 to 24 subsections (beds)

For a commercial-size unit, the following are suggested:

- Bed height, L_k , in each subsection from 40 to 120 cm
- An estimate of the overall mass-transfer coefficient, $k_{i,j}$, for solute transport between bulk fluid and sorbate layer on the adsorbent
- An axial diffusivity, D_L , defined in terms of a Peclet number, where

$$N_{Pe} = \frac{u_f(\text{characteristic length})}{D_L} \quad (15-168)$$

Characteristic lengths equal to bed depth or particle diameter have been used. Most common for TMB and SMB is bed depth, with Peclet numbers in the 1000–2000 range.

EXAMPLE 15.15 Operation with an SMB.

Use the results of the fructose-glucose separation of Example 15.14, for $\beta = 1.05$, with the steady-state TMB model of Aspen Chromatography to estimate product compositions obtained with the following laboratory-size SMB unit:

Number of sections = 4

Number of subsections (beds) in each section (column) = 2

All bed diameters = 2.54 cm

All bed heights = 10 cm

Bed void fraction = 0.40

Particle diameter = 500 microns (0.5 mm)

Overall mass-transfer coefficient for A and B = 10 min⁻¹

Peclet number high enough that axial dispersion is negligible

Solution

To use Aspen Chromatography, the recirculating liquid flow rate for a TMB must be converted to an SMB using (15-163), and the solid particle flow rate must be converted to a port-switching time given by (15-167). From (15-163), using the results for $\beta = 1.05$ in Example 15.14,

$$(Q_C)_{SMB} = 2.624 + \left(\frac{0.40}{1 - 0.40} \right) 7.848 = 7.856 \text{ mL/min}$$

The total liquid rate in Section I of the SMB is

$$(Q_1)_{SMB} = (Q_C)_{SMB} + Q_D = 7.856 + 2.403 = 10.259 \text{ mL/min}$$

This is the maximum volumetric flow rate in the SMB and it is of interest to calculate the corresponding interstitial fluid velocity. From (15-145),

$$\begin{aligned} (u_f)_{SMB} &= \frac{(Q_1)_{SMB}}{\varepsilon_b A_b} = \frac{10.259}{0.40 \left[\frac{3.14(2.54)^2}{4} \right]} \\ &= 5.06 \text{ cm/min} = 0.0844 \text{ cm/s} \end{aligned}$$

This fluid velocity is low, but it corresponds to a desirable bed diameter-to-particle diameter ratio of 2.54/0.05 = 49. To increase fluid velocity to, say, 0.4 cm/s, the bed diameter would be decreased to 1.17 cm, giving a bed diameter-to-particle diameter of 23, which would still be acceptable.

From (15-147), the true velocity of the solid particles in each bed is

$$u_s = \frac{Q_s}{(1 - \varepsilon_b)A_b} = \frac{7.848}{(1 - 0.40) \left[\frac{3.14(2.54)^2}{4} \right]} = 2.58 \text{ cm/min}$$

From (15-167), port-switching time for subsection bed height, L , of 10 cm is,

$$t^* = \frac{L}{u_s} = \frac{10}{2.58} = 3.88 \text{ min}$$

The following results were obtained with Aspen Chromatography for a steady-state TMB:

	Feed	Desorbent	Extract	Raffinate
Flow rate, mL/min	1.667	2.403	2.134	1.936
Concentrations, g/L:				
Fructose	280.0	0.0	211.6	12.7
Glucose	350.0	0.0	8.4	295.3
Water	596.0	996.0	861.7	795.8
Mass fraction on water-free basis:				
Fructose	0.444		0.962	0.040
Glucose	0.556		0.038	0.960

As seen in the table, a reasonably sharp separation between fructose and glucose is achieved. In Exercise 15.34, modifications to the input data are studied in an attempt to improve separation sharpness.

EXAMPLE 15.16 Recovery of Paraxylene in an SMB.

Minceva and Rodrigues [105] consider the industrial-scale separation of paraxylene (PX) from a liquid mixture of other C_8 aromatics (ethylbenzene, EB, metaxylene, MB, and orthoxylene, OX) in a four-section SMB. Feed to the unit is 1,450 L/min with a composition in wt% of 14.0 EB, 49.7 MX, 12.7 OX, and 23.6 PX. The adsorbent is a molecular-sieve zeolite with a particle density of 1.39 g/cm³ and a particle diameter of 0.092 cm that packs a bed with an external void fraction of 0.39. The desorbent is paradiethylbenzene (PDEB). With reference to Figure 15.41, the number of subsections is 6, 9, 6, and 3, respectively, in Sections I to IV. The height of each bed subsection is 1.135 m, with a bed diameter of 4.117 m. The operation takes place at 180°C and a pressure above 12 bar, sufficient to prevent vaporization. At these conditions, the extended liquid-phase Langmuir adsorption isotherm (see Example 15.6) correlates adsorption equilibrium, yielding the following constants. Note that this is a constant-selectivity isotherm; therefore, the selectivity relative to paradiethylbenzene is tabulated.

Component	q_m , mg/g	K , cm ³ /mg	Selectivity
Paraxylene	130.3	1.0658	0.9969
Paradiethylbenzene	107.7	1.2935	1.0000
Ethylbenzene	130.3	0.3067	0.2689
Metaxylene	130.3	0.2299	0.2150
Orthoxylene	130.3	0.1884	0.1762

The desorbent does not have the most desirable equilibrium adsorption property because its selectivity does not lie between that of paraxylene and the other C_8 components of the feed. The overall mass-transfer coefficient between sorbate and bulk fluid, in (15-148), is 2 min⁻¹ for each component. For axial dispersion, assume a Peclet number of 700 in (15-168) with a characteristic length equal to the bed height.

Using Aspen Chromatography with the TMB model as an approximation of the SMB, determine steady-state flow rates and

compositions of extract and raffinate, together with the composition profiles in the four sections for the following operating conditions:

Extract flow rate = 1,650 L/min

Raffinate flow rate = 2,690 L/min

Circulation flow rate, $(Q_C)_{SMB}$, before adding makeup DPEB = 5,395 L/min

Port-switching interval, $t^* = 1.15$ min

Solution

By an overall material balance, the DPEB makeup flow rate is

$$Q_D = Q_E + Q_R - Q_F = 1,650 + 2,690 - 1,450 = 2,890 \text{ L/min}$$

From the switching time, using (15-167), with a 1.135-m bed height,

$$u_s = 1.135/1.15 = 0.987 \text{ m/min} = 98.7 \text{ cm/min}$$

The adsorbent bed cross-sectional area, $A_b = 3.14(4.117)^2/4 = 13.31 \text{ m}^2$

From (15-147), the volumetric flow rate of the solid particles in the TMB is

$$Q_S = u_s(1 - \epsilon_b)A_b = 0.987(1 - 0.39)(13.31) = 8.014 \text{ m}^3/\text{min} \\ = 8,014 \text{ L/min}$$

Liquid flow rates in the four sections are as follows, where both $(Q_j)_{SMB}$ and $(Q_j)_{TMB}$ flow rates are included, where the former are computed by material balance and the latter from (15-163). For example,

$$(Q_1)_{SMB} = (Q_C)_{SMB} + Q_D = 5,395 + 2,890 = 8,285 \text{ L/min}$$

$$(Q_1)_{TMB} = (Q_1)_{SMB} - [0.39/(1 - 0.39)]Q_S \\ = 8,285 - 0.639(8,014) = 3,164 \text{ L/min}$$

Section in Figure 15.45	$(Q_j)_{SMB}$, L/min	$(Q_j)_{TMB}$, L/min
I	8,285	3,164
II	6,635	1,514
III	8,085	2,964
IV	5,395	274

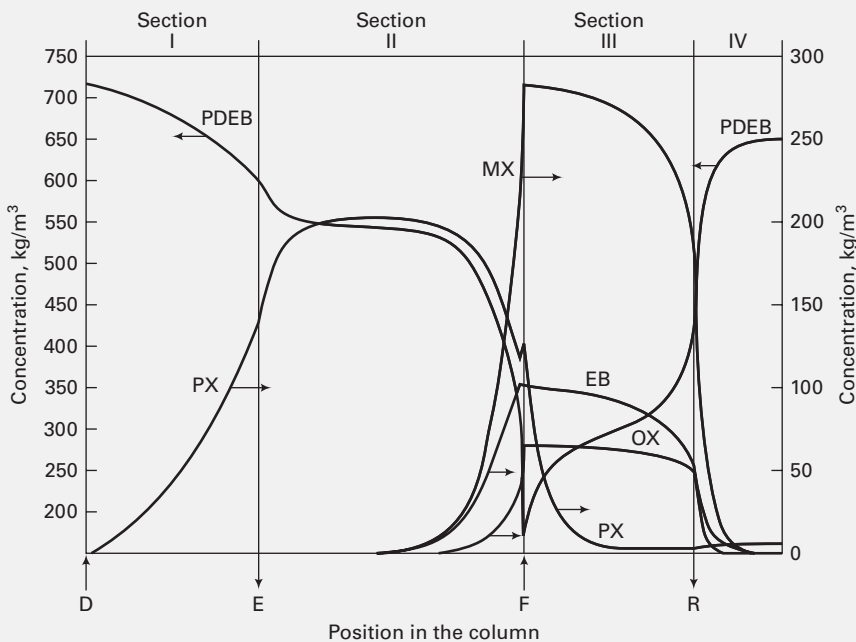


Figure 15.45 Concentration profiles in the liquid for SMB of Example 15.16.

Results of the Aspen Chromatography calculations for the steady-state TMB model, but on an SMB basis are:

Wt% of Component	Feed	Desorbent	Extract	Raffinate
Ethylbenzene	14.0	0.0	0.00	7.63
Metaxylene	49.7	0.0	0.00	27.09
Orthoxylene	12.7	0.0	0.00	6.92
PDEB	0.0	100.0	80.79	57.85
Paraxylene	23.6	0.0	19.21	0.51

Note that an excellent separation between paraxylene and the other feed components is achieved. However, both the extract and raffinate contain a substantial fraction of desorbent, PDEB. The desorbent in both products is recovered by the hybrid SMB-distillation process shown in Figure 15.23. Component concentration profiles in the four sections, as computed by Aspen Chromatography, are shown in Figure 15.45. In Sections I and III particularly, the profiles differ considerably from the flat profile predictions of the simple, local-equilibrium TMB model. The circulating desorbent is predicted to be essentially pure PDEB.

§15.7 ION-EXCHANGE CYCLE

Although ion exchange has a wide range of applications, water softening with gel resins continues to be the major one. Usually a fixed bed is used, which is operated in a cycle of four steps: (1) loading, (2) displacement, (3) regeneration, and (4) washing. The solute ions removed from water in the loading step are mainly Ca^{2+} and Mg^{2+} , which are absorbed by resin while an equivalent amount of Na^+ is transferred from resin to water as feed solution flows down through the bed. If mass transfer is rapid, the solution and resin are at equilibrium at all points in the bed. With a divalent ion (e.g., Ca^{2+}) replacing a monovalent ion (e.g., Na^+), the equilibrium expression is given by (15-44), where A is the divalent ion. If $(Q/C)^{n-1} K_{A,B} \gg 1$, equilibrium for the divalent ion is very favorable (see Figure 15.32a) and a self-sharpening front of the type shown in Figure 15.32b develops. In that case, which is common, ion exchange is well approximated using simple stoichiometric or shock-wave front theory for adsorption, assuming plug flow. As the front moves down through the bed, the resin behind (upstream) the front is in equilibrium with the feed composition. Ahead (downstream) of the front, water is essentially free of the divalent ion(s). Breakthrough occurs when the front reaches the end of the bed.

Suppose the only cations in the feed are Na^+ and Ca^{2+} . Then, from (15-44):

$$K_{\text{Ca}^{2+}, \text{Na}^+} \left(\frac{Q}{C} \right) = \frac{y_{\text{Ca}^{2+}} (1 - x_{\text{Ca}^{2+}})^2}{x_{\text{Ca}^{2+}} (1 - y_{\text{Ca}^{2+}})^2} \quad (15-169)$$

where Q is total concentration of the two cations in the resin, in eq/L of bed of wet resin, and C is total concentration of the two ions in the solution, in eq/L of solution. One mole of Na^+ is 1 equivalent, while 1 mole of Ca^{2+} is 2 equivalents. The quantities y_i and x_i are equivalent (rather than mole) fractions. From Table 15.5, using (15-45), the molar selectivity factor is

$$K_{\text{Ca}^{2+}, \text{Na}^+} = 5.2/2.0 = 2.6$$

For a given loading step during water softening, values of Q and C remain constant. Thus, for a given equivalent fraction, $x_{\text{Ca}^{2+}}$ in the feed, (15-169) is solved for the equilibrium $y_{\text{Ca}^{2+}}$. By material balance, for a given bed volume, the time u_L for the loading step is computed. The loading wave-front velocity is $u_L = L/t_L$ where L is the height of the bed. Equivalent fractions ahead of and behind the loading front are shown in Figure 15.46a. Typically, feed-solution superficial mass velocities are about 15 gal/h-ft², but can be much higher at the expense of larger pressure drops.

At the end of the loading step, the bed voids are filled with feed solution, which must be displaced from the bed. This is best done with a regeneration solution, which is usually a concentrated salt solution that flows upwards through the bed. Thus, the displacement and regeneration steps are combined. Following displacement, mass transfer of Ca^{2+} from the resin beads to the regenerating solution takes place while an equivalent amount of Na^+ is transferred from the solution to the resin. In order for equilibrium to be favorable for regeneration with Na^+ , it is necessary for $(Q/C) K_{\text{Ca}^{2+}, \text{Na}^+} \ll 1$. In that case, which is just the opposite for loading, the wave front during regeneration sharpens quickly into a shock-like wave. This criterion can be satisfied by using a saturated salt solution to give a large value for C .

During displacement and regeneration, two concentration waves move through the bed. The first is the displacement front; the second, the regeneration front. For plug flow and negligible mass-transfer resistance, the resin and solution are in equilibrium at all locations in the bed. Again (15-169) is used to solve for the equilibrium equivalent fractions, which are shown for the displacement and regeneration steps in Figure 15.46b. The displacement time, t_D , is determined from

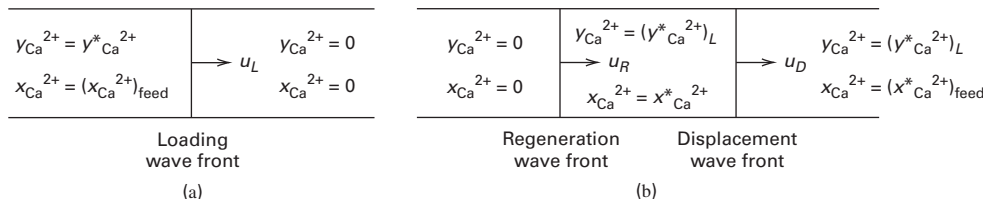


Figure 15.46 Ion exchange in a cyclic operation with a fixed bed. (a) Loading step. (b) Displacement and regeneration steps.

the interstitial velocity, u_D , of the fluid during displacement:

$$t_D = L/u_D \quad (15-170)$$

Regeneration time, t_R , is determined by material balance, from which the regeneration wave-front velocity is $u_R = L/t_R$. In general, the mass velocity of the regeneration solution is less than that of the feed solution. The cycle is completed by displacing, with water, the salt solution in the bed voids. The cycle calculations are illustrated by the following example. Calculations can also be made with Aspen Chromatography.

EXAMPLE 15.17 Ion-Exchange Cycle.

Hard water, containing 500 ppm (by weight) of magnesium carbonate and 50 ppm of NaCl, is to be softened at 25°C in an existing fixed bed of gel resin with a cation capacity of 2.3 eq/L of bed volume. The bed is 8.5 ft in diameter and packed to a height of 10 ft, with a wetted-resin void fraction of 0.38. During the loading step, the recommended throughput is 15 gal/min-ft². During displacement, regeneration, and washing, the flow rate is reduced to 1.5 gal/min-ft². The displacement and regeneration solutions are water saturated with NaCl (26 wt%). Determine: (a) flow rate of feed solution in L/min, (b) loading time to breakthrough in hours, (c) loading wavefront velocity in cm/min, (d) flow rate of regeneration solution in L/min, (e) displacement time in hours, and (f) additional time for regeneration in hours.

Solution

Molecular weight, M , of $\text{MgCO}_3 = 83.43$

$$\begin{aligned} \text{Concentration of MgCO}_3 \text{ in feed} &= \frac{500(1,000)}{83.43(1,000,000)} \\ &= 0.006 \text{ mol/L or } 0.012 \text{ eq/L} \end{aligned}$$

M of NaCl = 58.45

$$\begin{aligned} \text{Concentration of NaCl in feed} &= \frac{50(1,000)}{58.45(1,000,000)} \\ &= 0.000855 \text{ mol/L or eq/L} \end{aligned}$$

(a) Bed cross-section area = $3.14(8.5)^2/4 = 56.7 \text{ ft}^2$.
Feed-solution flow rate = $15(56.7) = 851 \text{ gpm}$ or $3,219 \text{ L/min}$

(b) Behind the loading wave front:

$$x_{\text{Mg}^{2+}} = \frac{0.012}{0.012 + 0.000855} = 0.9335$$

Since no NaCl in the feed is exchanged:

$$C = 0.012 \text{ eq/L and } Q = 2.3 \text{ eq/L}$$

From Table 15.5,

$$K_{\text{Mg}^{2+}, \text{Na}^+} = 3.3/2 = 1.65$$

From (15-169), for Mg^{2+} instead of Ca^{2+} as the exchanging ion, with $x_{\text{Mg}^{2+}} =$ that of the feed from Figure 15.46a:

$$1.65 \left(\frac{2.3}{0.012} \right) = \frac{y_{\text{Mg}^{2+}}(1 - 0.9335)^2}{0.9335(1 - y_{\text{Mg}^{2+}})^2}$$

Solving: $y_{\text{Mg}^{2+}} = 0.9961$. Thus, sodium ion is displaced from the resin almost completely.

Bed volume = $(56.7)(10) = 567 \text{ ft}^3$ or $16,060 \text{ L}$

Total bed capacity = $2.3(16,060) = 36,940 \text{ eq}$

Mg^{2+} absorbed by resin = $0.9961(36,940) = 36,796 \text{ eq}$

Mg^{2+} entering bed in feed solution = $0.012(3,219) =$

38.63 eq/min

$$t_L = \frac{36,796}{38.63} = 953 \text{ minutes or } 15.9 \text{ h}$$

(c) $u_L = L/t_L = 10/953 = 0.0105 \text{ ft/min}$ or 0.320 cm/min .

(d) Flow rate of regeneration solution = $(1.5/15)(3,219) = 321.9 \text{ L/min}$.

(e) Displacement time = time for 321.9 L/min to displace liquid in the voids. Void volume = $0.38(16,060) = 6,103 \text{ L}$ and $t_D = 6103/321.9 = 19 \text{ min}$

(f) For a 26 wt% NaCl solution at 25°C, density from *Perry's Chemical Engineers' Handbook* = 1.19443 g/cm^3 .

Flow rate of Na^+ in regeneration solution

$$= \frac{321.9(1,000)(1.19443)(0.26)}{58.45} = 1,710 \text{ eq/min}$$

NaCl concentration in regenerating solution = $1,710/321.9 =$

$5.31 \text{ eq/L} = c_R$

From (15-169), noting conditions in Figure 15.46:

$$\frac{Q}{c_R} K_{\text{Mg}^{2+}, \text{Na}^+} = 1.65 \left(\frac{2.3}{5.31} \right) = 0.715$$

This is less than 1, but not much less than 1. Therefore, the regeneration wave front may not sharpen rapidly. Assume a shock-wave-like front anyway.

From (15-169),

$$0.715 = \frac{0.9998(1 - x_{\text{Mg}^{2+}})^2}{x_{\text{Mg}^{2+}}(1 - 0.9998)^2}$$

Solving:

$$x_{\text{Mg}^{2+}} = 0.999763$$

This means that downstream of the regeneration wave front, but upstream of the displacement wave front, the liquid contains very few sodium ions.

§15.8 CHROMATOGRAPHIC SEPARATIONS

Separation of multicomponent mixtures into more than two products usually requires more than one separation device. For example, if a four-component mixture (A, B, C, D) is to be separated by distillation into pure products, a sequence of three trayed columns is almost always used. If the order of decreasing volatility is A, B, C, and D, the first column might produce a distillate of nearly pure A; the second column a distillate of nearly pure B; and the third column a distillate of nearly pure C and a bottoms of nearly pure D. Four other sequences are possible, depending upon the selection of the split for each column.

Chromatography is one of the few separation techniques that can separate a multicomponent mixture into nearly pure components in a single device, generally a column packed with

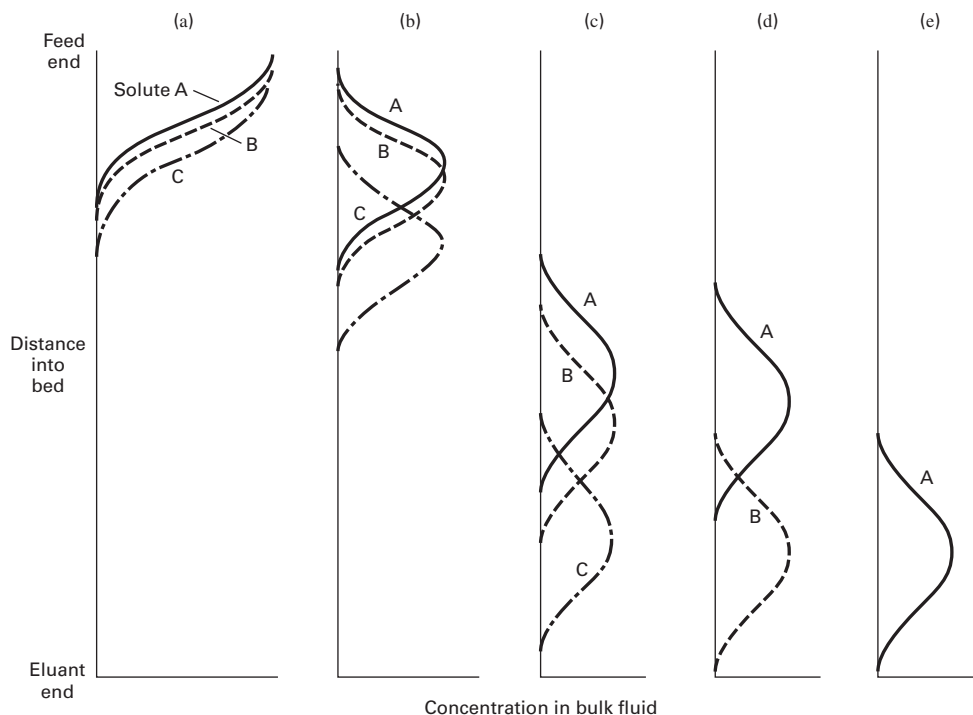


Figure 15.47 Movement of concentration waves during separation in a chromatographic column.

a suitable sorbent. The degree of separation depends upon column length, differences in component affinities for the sorbent, and the composition and flow rate of the eluting fluid.

As an example of what is called elution, batch, or differential chromatography, consider a mixture of three components, A, B, and C, in order of decreasing affinity for the sorbent, S. If the separation is achieved by adsorption, then A is the most strongly adsorbed. A feed mixture, insufficient to load the sorbent, is introduced as a pulse into the feed end of the packed chromatographic column. The resulting initial concentrations for the three components are shown in Figure 15.47a, where most of the bed remains clean of adsorbates. An **elutant**, such as a carrier gas or solvent that has little or no affinity for the sorbent, is now introduced continuously into the feed end of the bed, causing the three components to desorb, with C desorbing most readily. However, as the desorbed components are carried down the bed by the elutant into cleaner regions of the bed, the components are successively re-adsorbed and then re-desorbed to produce three waves, as shown in Figure 15.47b. Because of differences in affinities for the sorbent, the three waves, which initially overlap considerably, gradually overlap less (Figure 15.47c), and finally, if the column is long enough, become completely separated, as in Figure 15.47d and e. In that case, the components are **eluted** from the column, one at a time. In Figure 15.47e, all components but A have been eluted. As the separated waves elute, the area under each component wave is proportional to the mass of the component moving through the packed column.

Differential chromatography is limited to a batch process in which the feed is introduced as pulses into an elutant carrier gas or solvent, which then contacts the sorbent. All feed

components have affinities for the sorbent, but the elutant does not. Chromatography in the broader sense, as mentioned by Ruthven [10], refers to any separation process involving partitioning of components between a flowing fluid and a solid adsorbent (or a solid-supported liquid absorbent). The previously presented simulated-moving-bed (SMB) system, which uses a circulating desorbent that may also partition, may be viewed as a chromatographic process.

§15.8.1 Equilibrium-Based Chromatography with Linear Isotherm

A simple and useful wave theory for differential chromatography is based on isothermal conditions, with plug flow, negligible axial dispersion, and local equilibrium everywhere. This theory, when developed for adsorption, results in the stoichiometric wave-front shown in Figure 15.26. For chromatography, where solutes are pulsed into the column, the wave pulse in Fig 15.48a, rather than a wave-front, results. For a stoichiometric (equilibrium) wave, the pulse is a square wave rather than the Gaussian-like waves shown in Figure 15.47. Gaussian waves result when (1) axial dispersion occurs, (2) mass-transfer resistances are important, (3) radial variations of the fluid velocity occur, and/or (4) solute pulses are not square waves.

If the sorbent is nonporous, like a gel, and the adsorption isotherm is linear ($q = Kc$) for each solute i , then (15-109) applies and each solute wave velocity, u_i , in terms of the interstitial fluid velocity, u , is given by

$$u_i = \frac{u}{1 + \frac{1-\epsilon_b}{\epsilon_b} K_i} \quad (15-171)$$

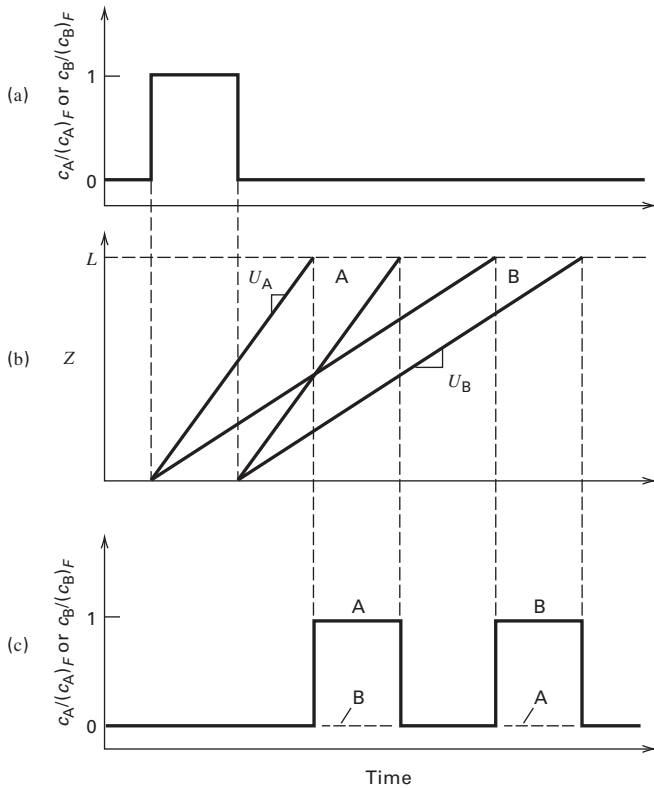


Figure 15.48 Ideal solute wave pulses in a chromatographic column.

This equation applies to both the leading and trailing edges of the feed pulse and was used by Wankat [106] to produce solute movement diagrams. When the elutant is dilute in solutes, such that the sorption equilibrium constants depend only on temperature, (15-171) applies independently to each solute. For a strongly sorbed solute, such as B in Figure 15.48b, K is large, and the second term in the denominator dominates, so that solute moves through the bed much slower than elutant. For a weakly sorbed solute, such as A in Figure 15.48b, K is small and the denominator is not much greater than one, so its velocity may not be significantly smaller than the elutant velocity.

In Figure 15.48b, the wave velocities of both the leading and trailing edges of the wave pulses are constant, with $u_A > u_B$. For each solute, the pulse time to move through a column of length L is $t_i = L/u_i$. The wave pulse of A reaches the end of the column in less time than the B wave pulse. In Figure 15.48c, the product-concentration ratios, c_A/c_{A_F} and c_B/c_{B_F} , are shown at the end of the bed as a function of time. The widths of these product waves are identical to the widths of the feed pulses, as illustrated in the following example. This simple equilibrium-wave pulse theory for linear isotherms can be used to obtain an approximate estimate of the separation achievable in a chromatographic column. Unfortunately, the estimate is not conservative when computing necessary column lengths, because the pulses broaden due to rate-limiting mass transfer resistances illustrated in Figure 15.16 and described in §15.3. This will be described in greater detail after the following example.

EXAMPLE 15.18 Separation by Pulse Chromatography.

An aqueous solution of 3 g/cm³ each of glucose (G), sucrose (S), and fructose (F) is to be separated in a chromatographic column, packed with an ion-exchange resin of the calcium form. In the range of expected solute concentrations, the sorption isotherms are linear and independent, with $q_i = K_i c_i$, where q_i is in grams sorbate per 100 cm³ resin and c_i is in grams solute per 100 cm³ solution. From experiments:

Solute	K
Glucose	0.26
Sucrose	0.40
Fructose	0.66

The superficial solution velocity, u_s , is 0.031 cm/s and bed void fraction is 0.39. If a 500-second pulse, t_p , of feed is followed by elution with pure water, what length of column packing is needed to separate the three solutes if sorption equilibrium is assumed? How soon after the first pulse begins can a second 500-second pulse begin?

Solution

Interstitial solution velocity = $u_s/\epsilon_b = 0.031/0.39 = 0.0795$ cm/s
Wave velocity for glucose from (15-171):

$$u_G = \frac{0.0795}{1 + \left(\frac{1-0.39}{0.39}\right)(0.26)} = 0.0565 \text{ cm/s}$$

Similarly,

$$u_S = 0.0489 \text{ cm/s} \quad \text{and} \quad u_F = 0.0391 \text{ cm/s}$$

The smallest difference in wave velocities is between glucose and sucrose. Therefore, the separation between these two waves determines the column length. The minimum column length, assuming equilibrium, corresponds to the time at which the trailing edge of the glucose wave pulse, together with the leading edge of the sucrose wave pulse, leaves the column. Thus, if t_p is the duration of the first pulse and L is the length of the packing:

$$t_p + \frac{L}{u_G} = \frac{L}{u_S} \quad (1)$$

$$\text{Thus, } 500 + \frac{L}{0.0565} = \frac{L}{0.0489}$$

Solving, length of packing, $L = 182$ cm. The glucose just leaves the column at

$$500 + \frac{182}{0.0565} = 3,718 \text{ s}$$

The locations of the three wave fronts in the column at 3,718 s are shown in Figure 15.49. The time at which the second pulse

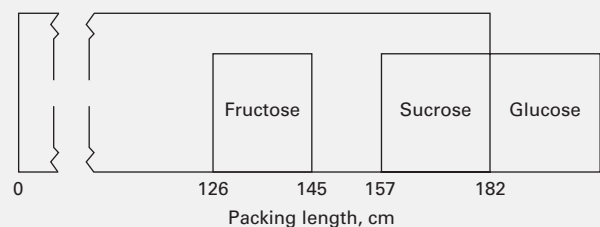


Figure 15.49 Locations of solute waves of first pulse for Example 15.20 at 3,718 s.

begins is determined so that the trailing edge of the first fructose wave pulse just leaves the column as the second pulse of glucose begins to leave the column. This time, based on the fructose, is $500 + 182/0.0391 = 5,155$ s. It takes the leading edge of a glucose wave $182/0.0565 = 3,220$ s to pass through the column. Therefore, the second pulse can begin at $5,155 - 3,220 = 1,935$ s. This establishes the following ideal cycle: pulse: 500 s, elute: 1,435 s, pulse: 500 s, elute: 1,435 s, etc. In the real case, where we account for mass-transfer resistance, as shown in the next example, the column will have to be longer.

§15.8.2 Rate-Based Chromatography with Linear Isotherm

A plot of solute concentrations in the elutant as a function of time is a **chromatogram**. When mass-transfer resistances, axial dispersion, and/or other nonideal phenomena are not negligible, the solute concentrations in a chromatogram will not appear as square waves, but will exhibit the wave shapes in Figure 15.50. Carta [107] developed analytical solutions for chromatographic response to periodic injections of rectangular feed pulses, taking into account mass-transfer resistances for solute mixtures having linear, independent adsorption isotherms. Carta's solution for the linear driving force (LDF) approximation is readily applied to the determination of the necessary length of packing and frequency of feed pulses for the chromatographic separation of a feed mixture.

For each solute in the feed, (15-96) is assumed to apply, along with the linear driving force approximation (15-99), the linear isotherm, and (15-100) for the overall mass-transfer resistance for each solute. For periodic, rectangular feed pulses, the boundary conditions for feed pulses of duration, t_F , each followed by an elution period of duration, t_E , are for each solute concentration, $c_i\{z, t\}$:

Initial condition:

$$\text{At } t = 0, c_i\{z, 0\} = 0 \quad (15-172)$$

Feed pulse:

$$\begin{aligned} \text{At } z = 0, c_i\{0, t\} &= (c_i)_F, \\ \text{for } (j-1)(t_F + t_E) < t < j(t_F + t_E) - t_E \end{aligned} \quad (15-173)$$

Elution period:

$$\text{At } z = 0, c_i\{0, t\} = 0, \quad \text{for } j(t_F + t_E) - t_E < t < j(t_F + t_E) \quad (15-174)$$

where $j = 1, 2, 3, \dots$ is an index that accounts for the periodic nature of the feed and elution pulses. Thus, with $j = 1$, the feed pulse takes place from $t = 0$ to $t = t_F$ and the elution pulse is from t_F to $t_F + t_E$.

Carta solved the linear system of (15-96), (15-99), and (15-100) for conditions (15-172) to (15-174) by the Laplace transform method to obtain the following dimensionless series solution, which is applied to each solute in the feed pulse:

$$\begin{aligned} X = \frac{r_F}{2r} + \frac{2}{\pi} \sum_{m=1}^{\infty} \left[\frac{1}{m} \exp\left(-\frac{m^2 n_f}{m^2 + r^2}\right) \sin\left(\frac{m\pi r_F}{2r}\right) \right. \\ \left. \times \cos\left(\frac{m\theta_f}{r} - \frac{m\pi r_F}{2r} - \frac{m\beta n_f}{r} - \frac{mr n_f}{m^2 + r^2}\right) \right] \quad (15-175) \end{aligned}$$

where

$$X = c/c_F \quad (15-176)$$

$$r = \frac{k}{2\pi K}(t_F + t_E) \quad (15-177)$$

$$r_F = \frac{k}{\pi K} t_F \quad (15-178)$$

$$n_f = \frac{(1 - \varepsilon_b)kz}{\varepsilon_b u} \quad (15-179)$$

$$\theta_f = kt/K \quad (15-180)$$

$$\beta = \frac{\varepsilon_b}{(1 - \varepsilon_b)K} \quad (15-181)$$

$$K = q/c \quad (15-182)$$

and where

$$k = \frac{1}{\frac{R_p}{3k_c} + \frac{R_p^2}{15D_e}} \quad (15-183)$$

When nonlinear adsorption isotherms such as the Freundlich equation (15-35), the Langmuir equation (15-36), or extensions thereof to multicomponent mixtures [e.g., concentration forms of (15-32) or (15-33)] are necessary, the analytical solution of Carta is not applicable. However, the method of lines, using five-point, biased, upwind finite-difference approximations, as described earlier in the section on thermal-swing adsorption, can be used to obtain numerical solutions.

EXAMPLE 15.19 Calculation of a Chromatogram.

Use Carta's equation with the following properties to compute the chromatogram for the conditions of Example 15.18 with a packing length of 182 cm. Does a significant overlap of peaks result?

Property	Glucose	Sucrose	Fructose
K	0.26	0.40	0.66
D_e , cm ² /s	1.1×10^{-8}	1.8×10^{-8}	2.8×10^{-8}
k_c , cm/s	5.0×10^{-3}	5.0×10^{-3}	5.0×10^{-3}

$\varepsilon_b = 0.39$, $R_p = 0.0025$ cm, $u = 0.0795$ cm/s
 $z = 182$ cm, $t_E = 2,000$ s, and $t_F = 500$ s

Solution

Values of k and the computed dimensionless parameters from (15-177) to (15-181) and (15-183) are as follows:

	Glucose	Sucrose	Fructose
r	40.22	42.66	40.06
r_F	16.09	17.07	16.03
n_f	94.13	153.6	238.0
θ_f	0.1011 t	0.1072 t	0.1007 t
β	2.459	1.598	0.9687
k , s ⁻¹	0.0263	0.0429	0.0665

where t is in seconds

Values of $X = c/c_F$ are computed using these parameters with (15-175) for values of time, t , in the neighborhood of times for the equilibrium-based waves. The resulting chromatogram for glucose is shown in Figure 15.50a, compared to the equilibrium rectangular wave (shown as a thin line) determined in Example 15.18 using (15-171). The areas under the two curves should be identical. The equilibrium-based wave appears to be centered in time within the mass-transfer-based wave.

Figure 15.50b, contains the complete computed chromatogram for the three carbohydrates. It is seen that the effect of mass transfer is to cause the peaks to overlap significantly. To obtain a sharp separation, it is necessary to lengthen the column or reduce the feed pulse time, t_F .

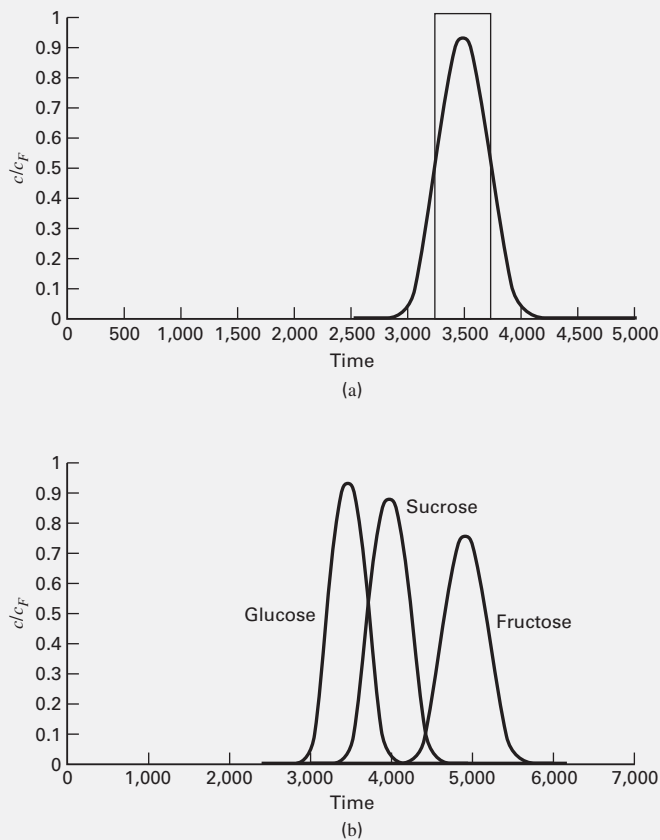


Figure 15.50 Computed chromatograms for Example 15.19. (a) Comparison of ideal to nonideal wave for fructose. (b) Computed chromatogram for nonideal eluant.

CHAPTER 15 NOMENCLATURE

Abbreviations and Acronyms

BET	Brunauer–Emmett–Teller equation, (15-6)
IAS	ideal absorbed solution, Section 15.2.2
LDF	linear driving force approximation, (15-99)
LES	length of bed upstream of the front, (15-92)
LUB	length of unused bed, (15-93)
MTZ	mass-transfer zone, Figure 15.27
PSA	pressure swing adsorption, Section 15.5.4

SMB	simulated moving bed, Section 15.6
SP	separation factor, (15-46)
TMB	true moving-bed system, Section 15.6
TSA	thermal-swing adsorption, Section 15.5.3
VSA	vacuum-swing adsorption, Section 15.5.4
WES	weight of bed upstream of the front, (15-94)
WUB	weight of unused bed, (15-95)

Latin Symbols

A	pore cross-sectional area, (15-69)
A_b	adsorbent bed cross-sectional area, above (15-96)
A_s	pore surface area, (15-70)
a	external surface area of adsorbent/volume of liquid, (15-76)
a	external particle surface area/volume of particle, Section 15.3.1
C	total solution ion concentration, (15-39)
c	solute concentration, (15-35); constant in the BET equation (15-6)
D_p	particle diameter, (15-59)
D_i	molecular diffusivity, (15-60)
$(D_i)_s$	surface diffusivity, (15-70)
D_e	effective diffusivity, (15-68)
D_L	axial eddy diffusivity, (15-144)
D_K	Knudsen diffusivity, (15-74)
d_p	pore diameter, (15-1)
G	superficial (empty vessel) gas mass flow/cross-sectional area, (15-64)
ΔH_{ads}	heat of monolayer adsorption, (15-17)
ΔH_{cond}	heat of condensation for more than a monolayer, Section 15.1.1
$J_{i,j}$	mass transfer flux of component i in section j , (15-144)
K	adsorption equilibrium constant, (15-22)
$K_{A,B}$	molar selectivity coefficient, (15-38)
$K_{i,j}$	relative molar selectivities, K_i/K_j , (15-45)
k	overall mass-transfer coefficient for external and internal particle transport resistances, (15-99)
k_a	rate of adsorption, (15-21)
k_d	rate of desorption, (15-21)
k_c	convective external mass transfer coefficient, (15-48)
$k_{i,j}$	fluid-to-solid mass-transfer coefficient, (15-148)
L	pore length, (15-1)
L_B	bed length, (15-91)
L_e	experimental bed length, (15-112)
L_j	section length, above (15-144)
L_k	bed height between adjacent ports, (15-167)
L_{ideal}	length of ideal stoichiometric front, (15-91)

m_p	mass of adsorbent, (15-9)
n^o	total moles of binary liquid contacting the adsorbent, (15-34)
n_i	molar rate of diffusion of i , (15-69)
P_0	vapor pressure of adsorbate in BET equation, (15-6)
P_p^s	vapor pressure of liquid in a pore, (15-15)
Q	liquid volume, (15-77); volumetric liquid flow rate, (15-86)
Q_F	volumetric feed-flow, (15-91)
Q_S	volumetric flow rate of solid, above (15-126)
q	amount adsorbed (loading) per unit mass of adsorbent, (15-16)
q_F	loading per unit mass of adsorbent in equilibrium with feed concentration, (15-91)
R_p	radius of spherical particle, (15-51)
r	radial distance from the particle center, (15-67)
S	pore surface area, (15-1); mass of adsorbent, (15-77); adsorbent flow rate, (15-86); solid adsorbent circulation rate, Figure 15.41
S_g	specific surface area, (15-2)
$S_{A,B}$	separation factor, (15-46)
T_s	surface temperature, (15-51)
T_b	bulk temperature, (15-52)
t	time
u	interstitial fluid velocity, (15-96)
u_s	superficial velocity, (15-146)
V	pore volume (15-1)

V_p	specific pore volume, (15-3)
X	c/c_F , (15-176)
x_i	equivalent fraction, (15-39)
y_i	equivalent fraction, (15-40)
z	bed height, Example 15.11

Greek Symbols

ϵ_b	external void fraction of bed, (15-96)
ϵ_p	particle porosity, (15-2)
ξ	dimensionless distance, (15-102)
ψ	sphericity, Section 15.3.1; parameter (15-117)
τ	interstitial tortuosity factor, (15-74); dimensionless time, (15-103)
ρ_b	bulk density, (15-4)
ρ_p	particle density, (15-2)
ρ_s	crystalline (true) particle density, (15-5)
θ	surface fraction covered, (15-21)
ϕ	parameter, (15-116)

Subscript

f	bulk fluid phase, (15-164)
k	subsection, (15-164)

Superscripts

n	stoichiometric coefficient, (15-38)
*	at equilibrium, (15-76)

SUMMARY

- Sorption is a generic term for the selective transfer of a solute from the bulk of a liquid or gas to the surface and/or into the bulk of a solid or liquid. Thus, sorption includes adsorption and absorption. The sorbed solute is the sorbate.
- For commercial applications, a sorbent should have high selectivity, high capacity, rapid solute transport rates, stability, strength, and ability to be regenerated. An adsorbent should have small pores to give a large surface area per unit volume.
- Physical adsorption of pure gases and gas mixtures is easily measured; adsorption of pure liquids and liquid mixtures is not.
- Widely used adsorbents are carbon (activated and molecular-sieve), molecular-sieve zeolites, silica gel, and activated alumina.
- The most widely used ion exchangers are water-swallowable, solid gel resins based on the copolymerization of styrene and a cross-linking agent such as divinylbenzene. They can be cation or anion exchangers. Ions are exchanged stoichiometrically on an equivalent basis. Thus, Ca^{2+} is exchanged for 2Na^+ .
- Sorbents for chromatographic separations are typically solid, or liquid adsorbents supported on or bonded to an inert solid, or gel.
- The most commonly used adsorption isotherms for gases and liquids are linear, Freundlich, and Langmuir. The latter asymptotically approaches the linear isotherm at low concentrations, and at high concentration gives an asymptotic value representing maximum surface coverage. For mixtures, extended versions of the isotherms are available.
- Ion-exchange equilibrium is represented by an equilibrium constant based on the law of mass action. For dilute conditions in chromatography, a linear equilibrium isotherm can be employed.
- For physical adsorption, the rate is almost instantaneous after solutes reach the sorbing surface. Thus, only external and internal mass-transfer resistances need be considered. External mass-transfer coefficients are obtained from correlations like the Chilton–Colburn j -factor type.

Internal mass transfer is based on a modified Fick's first law using an effective diffusivity that depends on such factors as particle porosity, pore tortuosity, bulk molecular diffusivity, surface diffusivity, and pore restrictions. Diffusivities in ion-exchange resin gels depend strongly on the degree of cross-linking of the resin.

10. Sorption systems include slurries in various modes of operation, fixed-bed, and simulated, continuous, counter-current units. When sorbent regeneration is necessary, the system is operated on a cycle. For fixed beds, the common cycles are temperature-swing adsorption (TSA) and pressure-swing adsorption (PSA). Ion exchange includes a displacement regeneration step, using a displacement fluid. In chromatography, adsorption and regeneration take place in the same column.
11. The adsorption isotherm is of great importance because it relates, at equilibrium, the concentration of the solute in the fluid to its loading as a sorbate in and/or on the sorbent. Most commonly, the overall rate of adsorption is expressed in the form of a linear driving force (LDF) model, where the driving force is the difference between bulk concentration and concentration in equilibrium with the loading. The coefficient in the LDF equation is a combined overall mass-transfer coefficient and area for sorption.
12. In ideal, fixed-bed operation, solute-sorbate equilibrium between the flowing fluid and static bed is assumed everywhere. For plug flow and negligible axial dispersion, the result is a sharp concentration front that moves like a shock wave (stoichiometric front) through the bed. Upstream of the front, the sorbent is spent and in equilibrium with the feed mixture. Downstream, the sorbent is free of sorbate. The stoichiometric front travels through the bed at a much slower velocity than the interstitial feed velocity. The time for the front to reach the end of the bed is the breakthrough time.
13. When mass-transfer effects are included, the concentration front broadens into an S-shaped curve such that at breakthrough only a portion of the sorbent is fully loaded. When mass-transfer coefficients and sorption isotherms are known, these curves can be computed with Klinkenberg's equations. When shapes of experimental concentration fronts exhibit a constant pattern, because of favorable adsorption equilibrium, commercial-size beds can be scaled-up from breakthrough data by the method of Collins.

14. Thermal-swing adsorption (TSA) is used to remove small concentrations of solutes from gas and liquid mixtures. Adsorption is carried out at ambient temperature and desorption at an elevated temperature. Because bed heating and cooling between adsorption and desorption is not instantaneous, TSA cycles are long, typically hours or days. The desorption step, starting with a partially loaded bed, can be computed by the method of lines, using a stiff integrator.
15. Pressure-swing adsorption (PSA) is used to separate air and enrich hydrogen-containing streams. Adsorption is carried out at an elevated or ambient pressure, whereas desorption occurs at ambient pressure or in a vacuum; the latter is called vacuum-swing adsorption (VSA). Because pressure swings can be made rapidly, PSA cycles are short, typically seconds or minutes. It is not necessary to regenerate the bed completely, but if not, a number of the initial cycles are needed to approach a cyclic steady-state operation.
16. Although continuous, countercurrent adsorption with a moving bed is difficult to achieve successfully in practice, an SMB system is popular, particularly for separation of solutes in dilute aqueous solutions and for bulk-liquid separations. Design procedures for SMB systems require solution of differential-algebraic equations (DAEs).
17. Design calculations for ion-exchange operations are based on an equilibrium assumption for the loading and regeneration steps.
18. In batchwise, elution chromatography, feed is periodically pulsed into a column packed with sorbent. Between feed pulses, an elutant is passed through the column, causing the less strongly sorbed solutes to move through the column more rapidly than more strongly sorbed solutes. If the column is long enough, a multicomponent feed can be completely separated, with solutes eluted one by one from the column. In the absence of mass-transfer resistances, a rectangular feed pulse is separated into individual solute rectangular pulses, whose position-time curves are readily established. When mass-transfer effects are important, rectangular pulses become Gaussian distribution curves that are predicted by the analytical solution of Carta, provided that a linear adsorption isotherm applies and axial dispersion is negligible.

REFERENCES

1. KELLER, G.E. II, in *Industrial Gas Separations*, T.E. WHYTE, Jr., C.M. YON, and E.H. WAGNER, eds., ACS Symposium Series No. 223, American Chemical Society, Washington, D.C., p. 145 (1983).
2. MILTON, R.M., U.S. Patents 2,882,243 and 2,882,244 (1959).
3. SKARSTROM, C.W., U.S. Patent 2,944,627 (1960).
4. BROUGHTON, D.B., and C.G. GERHOLD, U.S. Patent 2,985,589 (May 23, 1961).
5. ETTRE, L.S., and A. ZLATKIS, Eds., *75 Years of Chromatography—A Historical Dialog*, Elsevier, Amsterdam (1979).
6. BONMATI, R.G., G. CHAPELET-LETOURNEUX, and J.R. MARGULIS, *Chem. Engr.*, **87**(6), 70–72 (1980).
7. BERNARD, J.R., J.P. GOURLIA, and M.J. GUTTIERREZ, *Chem. Engr.*, **88**(10), 92–95 (1981).
8. WHITE, D.H., Jr. and P.G. BARKLEY, *Chem. Eng. Progress*, **85**(1) 25–33 (1989).

9. ROUSSEAU, R.W., Ed., *Handbook of Separation Process Technology*, Wiley-Interscience, New York (1987).
10. RUTHVEN, D.M., *Principles of Adsorption and Adsorption Processes*, John Wiley and Sons, New York (1984).
11. BRUNAUER, S., P.H. EMMETT, and E. TELLER, *J. Am. Chem. Soc.*, **60**, 309 (1938).
12. SATTERFIELD, C.N., *Heterogeneous Catalysis in Practice*, McGraw-Hill, New York (1980).
13. RUTHVEN, D.M., in *Kirk-Othmer Encyclopedia of Chemical Technology*, Vol. 1, 4th ed., Wiley-Interscience, New York (1991).
14. BARRER, R.M., *Zeolites and Clay Minerals as Sorbents and Molecular Sieves*, Academic Press, New York (1978).
15. BRECK, D.W., *Zeolite Molecular Sieves*, John Wiley and Sons, New York (1974).
16. ADAMS, B.A., and E.L. HOLMES, *J. Soc. Chem. Ind.*, **54**, 1–6T (1935).
17. MCWILLIAMS, J.D., *Chem. Engr.*, **85**(12), 80–84 (1978).
18. DORFNER, K., *Ion Exchangers, Properties and Applications*, 3rd ed., Ann Arbor Science, Ann Arbor, MI (1971).
19. SEWELL, P.A., and B. CLARKE, *Chromatographic Separations*, John Wiley and Sons, New York (1987).
20. BRUNAUER, S., L.S. DEMING, W.E. DEMING, and E. TELLER, *J. Am. Chem. Soc.*, **62**, 1723–1732 (1940).
21. BRUNAUER, S., *The Adsorption of Gases and Vapors*, Vol. I, *Physical Adsorption*, Princeton University Press (1943).
22. TITOFF, A., *Z. Phys. Chem.*, **74**, 641 (1910).
23. VALENZUELA, D.P., and A.L. MYERS, *Adsorption Equilibrium Data Handbook*, Prentice-Hall, Englewood Cliffs, NJ (1989).
24. RAY, G.C., and E.O. BOX, Jr. *Ind. Eng. Chem.*, **42**, 1315–1318 (1950).
25. YANG, R.T., *Gas Separation by Adsorption Processes*, Butterworths, Boston (1987).
26. FREUNDLICH, H., *Z. Phys. Chem.*, **73**, 385–423 (1910).
27. MANTELL, C.L., *Adsorption*, 2nd ed., McGraw-Hill, New York, p. 25 (1951).
28. LANGMUIR, J., *J. Am. Chem. Soc.*, **37**, 1139–1167 (1915).
29. MARKHAM, E.C., and A.F. BENTON, *J. Am. Chem. Soc.*, **53**, 497–507 (1931).
30. YON, C.M., and P.H. TURNOCK, *AICHE Symp. Series*, **67**(117), 75–83 (1971).
31. BROUGHTON, D.B., *Ind. Eng. Chem.*, **40**, 1506–1508 (1948).
32. MYERS, A.L., and J.M. PRAUSNITZ, *AICHE J.*, **11**, 121–127 (1965).
33. MILLER, G.W., K.S. KNAEBEL, and K.G. IKELS, *AICHE J.*, **33**, 194–201 (1987).
34. RITTER, J.A., and R.T. YANG, *Ind. Eng. Chem. Res.*, **26**, 1679–1686 (1987).
35. RUTHVEN, D.M., and F. WONG, *Ind. Eng. Chem. Fundam.*, **24**, 27–32 (1985).
36. KIPLING, J.J., *Adsorption from Solutions of Nonelectrolytes*, Academic Press, London (1965).
37. RADKE, C.J., and J.M. PRAUSNITZ, *AICHE J.*, **18**, 761–768 (1972).
38. ANDERSON, R.E., “Ion-Exchange Separations,” in *Handbook of Separation Techniques for Chemical Engineers*, 2nd ed., P.A. Schweitzer, Ed., McGraw-Hill, New York (1988).
39. BONNER, O.D., and L.L. SMITH, *J. Phys. Chem.* **61**, 326–329 (1957).
40. BAUMAN, W.C., and J. EICHORN, *J. Am. Chem. Soc.*, **69**, 2830–2836 (1947).
41. BAUMAN, W.C., J.R. SKIDMORE, and R.H. OSMUN, *Ind. Eng. Chem.*, **40**, 1350–1355 (1948).
42. SUBBA RAO, H.C., and M.M. DAVID, *AICHE Journal*, **3**, 187–190 (1957).
43. SELKE, W.A., and H. BLISS, *Chem. Eng. Prog.*, **46**, 509–516 (1950).
44. SELKE, W.A., and H. BLISS, *Chem. Eng. Prog.*, **47**, 529–533 (1951).
45. MYERS, A.L., and S. BYINGTON, in *Ion Exchange: Science and Technology*, A.E. Rodrigues, Ed., Martinus Nijhoff, Boston, **107**, 119–145 (1986).
46. ATHALYE, A.J., S.J. GIBBS, and E.N. LIGHTFOOT, *J. Chromatogr.*, **589**, 71–85 (1992).
47. RANZ, W.E., and W.R. MARSHALL, Jr. *Chem. Eng. Prog.*, **48**, 141–146 and 173–180 (1952).
48. RANZ, W.E., *Chem. Eng. Prog.*, **48**, 247–253 (1952).
49. GAMSON, B.W., G. THODOS, and O.A. HOUGEN, *Trans. AICHE*, **39**, 1–35 (1943).
50. CHILTON, T.H., and A.P. COLBURN, *Ind. Eng. Chem.*, **26**, 1183–1187 (1934).
51. SEN GUPTA, A., and G. Thodos, *AICHE J.*, **9**, 751–754 (1963).
52. PETROVIC, L.J., and G. THODOS, *Ind. Eng. Chem. Fundamentals*, **7**, 274–280 (1968).
53. DWIVEDI, P.N., and S.N. UPADHAY, *Ind. Eng. Chem. Process Des. Dev.*, **16**, 157–165 (1977).
54. WAKAO, N., and T. FUNAZKRI, *Chem. Eng. Sci.*, **33**, 1375–1384 (1978).
55. KUNII, D., and O. LEVENSPIEL, *Fluidization Engineering*, 2nd ed., Butterworth-Heinemann, Boston, Chap. 3 (1991).
56. THIELE, E.W., *Ind. Eng. Chem.*, **31**, 916–920 (1939).
57. WHEELER, A., *Advances in Catalysis*, Vol. **3**, Academic Press, New York, pp. 249–327 (1951).
58. SCHNEIDER, P., and J.M. SMITH, *AICHE J.*, **14**, 886–895 (1968).
59. RIEKERT, L., *AICHE J.*, **31**, 863–864 (1985).
60. SLADEK, K.J., E.R. GILLILAND, and R.F. BADDOUR, *Ind. Eng. Chem. Fundam.*, **13**, 100–105 (1974).
61. KAPOOR, A., R.T. YANG, and C. WONG, “Surface Diffusion,” *Catalyst Reviews*, **31**, 129–214 (1989).
62. HELFFERICH, F., *Ion Exchange*, McGraw-Hill, New York (1962).
63. SOLDANO, B.A., *Ann. NY Acad. Sci.*, **57**, 116–124 (1953).
64. RUTHVEN, D.M., and C.B. CHING, *Chem. Eng. Sci.*, **44**, 1011–1038 (1989).
65. KELLER, G.E., “Separations: New Directions for an Old Field,” *AICHE Monograph Series*, **83**(17) (1987).
66. BERG, C., *Trans. AICHE*, **42**, 665–680 (1946).
67. BROUGHTON, D.B., *Chem. Eng. Progress*, **64**(8), 60–65 (1968).
68. HUMPHREY, J.L., and G.E. KELLER II, *Separation Process Technology*, McGraw-Hill, New York (1997).
69. HIGGINS, I.R., and J.T. ROBERTS, *Chem. Engr. Prog. Symp. Ser.*, **50**(14), 87–92 (1954).
70. HIMSLEY, A., Canadian Patent 980, 467 (Dec. 23, 1975).
71. GANETSOS, G., and P.E. BARKER, Ed., *Preparative and Production Scale Chromatography*, Marcel Dekker, New York (1993).
72. WANKAT, P.C., Chapter 14 in Rousseau, R.W., Ed., *Handbook of Separation Process Technology*, Wiley-Interscience, New York (1987).
73. DEVULT, D., *J. Am. Chem. Soc.*, **65**, 532–540 (1943).
74. GLUECKAUF, E., *Trans. Faraday Soc.*, **51**, 1540–1551 (1955).
75. GLUECKAUF, E., and J.E. COATES, *J. Chem. Soc.*, 1315–1321 (1947).

76. LIAW, C.H., J.S.P. WANG, R.A. GREENKORN, and K.C. CHAO, *AIChE J.*, **25**, 376–381 (1979).
77. KLINKENBERG, A., *Ind. Eng. Chem.*, **46**, 2285–2289 (1954).
78. ANZELIUS, A., Z., *Angew. Math u. Mech.*, **6**, 291–294 (1926).
79. KLINKENBERG, A., *Ind. Eng. Chem.*, **40**, 1992–1994 (1948).
80. COONEY, D.O., and E. N. LIGHTFOOT, *IEC Fundamentals*, **4**, 233–236 (1965).
81. SIRCAR, S., and K. KUMAR, *Ind. Eng. Chem. Process Des. Dev.*, **22**, 271–280 (1983).
82. COONEY, D.O., *Chem. Eng. Comm.*, **91**, 1–9 (1990).
83. COLLINS, J.J., *Chem. Eng. Prog. Symp. Ser.* 63 (74), 31–35 (1967).
84. WONG, Y.W., and J.L. NIEDZWIECKI, *AIChE Symposium Series*, **78** (219), 120–127 (1982).
85. LISKOVETS, O.A., *Differential Equations* (a translation of *Differentsial'nye Uravneniya*) **1**, 1308–1323 (1965).
86. SCHIESSER, W.E., *The Numerical Method of Lines Integration of Partial Differential Equations*, Academic Press, San Diego (1991).
87. SCHIESSER, W.E., *Computational Mathematics in Engineering and Applied Science*, CRC Press, Boca Raton, FL (1994).
88. PRESS, W.H., S.A., TEUKOLSKY, W.T. VETTERLING, and B.P. FLANNERY, *Numerical Recipes, 3rd Edition: The Art of Scientific Computing*, Cambridge University Press, Cambridge (2007).
89. GEAR, C.W., *Numerical Initial Value Problems in Ordinary Differential Equations*, Prentice-Hall, Englewood Cliffs, NJ (1971).
90. BYRNE, G.D., and A.C. HINDMARSH, *J. Comput. Phys.*, **70**, 1–62 (1987).
91. RITTER, J.A., and R.T. YANG, *Ind. Eng. Chem. Res.*, **30**, 1023–1032 (1991).
92. RUTHVEN, D.M., S. FAROOQ, and K.S. KNAEBEL, *Pressure-Swing Adsorption*, VCH, New York (1994).
93. MUTASIM, Z.Z., and J.H. BOWEN, *Trans. I. Chem. E.*, **69**, Part A, 108–118 (March 1991).
94. WANKAT, P.C., *Large-Scale Adsorption and Chromatography*, Vols. I and II, CRC Press, Inc., Boca Raton (1986).
95. WANKAT, P.C., *Ind. Eng. Chem. Res.*, **40**, 6185–6193 (2001).
96. STORTI, G., M. MASI, S. CARRA, and M. MORBIDELLI, *Chem. Eng. Sci.*, **44**, 1329 (1989).
97. RHEE, H.-K., R. ARIS, and N.R. AMUNDSON, *Phil. Trans. Royal Soc. London, Series A*, **269** (No. 1194), 187–215 (Feb. 5, 1971).
98. MAZZOTTI, M., G. STORTI, and M. MORBIDELLI, *AIChE Journal*, **40**, 1825–1842 (1994).
99. RUTHVEN, D.M., and C.B. CHING, *Chem. Eng. Sci.*, **44**, 1011–1038 (1989).
100. ZHONG, G., and G. GUIOCHON, *Chem. Eng. Sci.*, **51**, 4307–4319 (1996).
101. STORTI, G., M. MAZZOTTI, M. MORBIDELLI, and S. CARRA, *AIChE Journal*, **39**, 471–492 (1993).
102. MAZZOTTI, M., G. STORTI, and M. MORBIDELLI, *J. Chromatography A*, **769**, 3–24 (1997).
103. DANCKWERTS, P.V., *Chem. Eng. Sci.*, **2**, 1 (1953).
104. CONSTANTINIDES, A., and N. MOSTOUFI, *Numerical Methods for Chemical Engineers with MATLAB Applications*, Prentice Hall PTR, Upper Saddle River, NJ (1999).
105. MINCEVA, M. and A. E. RODRIGUES, *Ind. Eng. Chem. Res.*, **41**, 3454–3461 (2002).
106. WANKAT, P.C., *Rate-Controlled Separations*, Elsevier Applied Science, New York (1990).
107. CARTA, G., *Chem. Eng. Sci.*, **43**, 2877–2883 (1988).

STUDY QUESTIONS

- 15.1. In adsorption operations, what are the adsorbate and the adsorbent?
- 15.2. How is a large surface area for adsorption achieved?
- 15.3. What is meant by ion exchange? How does ion exchange differ from deionization?
- 15.4. What kinds of sorbents are used in chromatography?
- 15.5. In adsorption processes, what distinguishes a purification from a bulk separation?
- 15.6. What three inventions made possible the bulk separation of mixtures by adsorption?
- 15.7. What is meant by regeneration?
- 15.8. What are some of the features of an effective adsorbent?
- 15.9. Can the specific surface area of an adsorbent be estimated from its average pore diameter? If so, what equation is used and under what assumptions is it derived?
- 15.10. Why is it easy to measure the amount of adsorption of a pure gas, but difficult to measure adsorption from a pure liquid?
- 15.11. Name five of the most important commercial adsorbents? What is the distinguishing feature of molecular-sieve zeolites?
- 15.12. For what is the BET equation used? Does it assume physical or chemical adsorption? Does it assume monomolecular or multimolecular layer adsorption?
- 15.13. What experimental techniques can be used to measure pore-size distribution?
- 15.14. What kinds of materials are most commonly used as ion exchangers?
- 15.15. Describe the different chromatographic methods?
- 15.16. How is it possible to use a liquid sorbent in chromatography?
- 15.17. What is meant by loading in adsorption?
- 15.18. What is an adsorption isotherm? How can the heat of adsorption be determined from a series of isotherms?
- 15.19. What is capillary condensation? What effect does it have on an adsorption isotherm?
- 15.20. In Figure 15.9, which isotherm(s) is (are) favorable and which unfavorable?
- 15.21. What is the equation for a linear adsorption (also called Henry's law)?
- 15.22. What is the major difference between the shapes of the isotherms predicted by the Freundlich and Langmuir isotherms? Which one is based on theory?
- 15.23. What is meant by an extended adsorption isotherm?
- 15.24. What makes the determination of an equation for an adsorption isotherm of a binary or multicomponent liquid mixture difficult, leading to weird-shaped curves as shown in Figure 15.13?
- 15.25. Why is the maximum loading of an ion exchanger fixed? What fixes it?
- 15.26. Does the valences of the ions being exchanged influence the equilibrium expression? How?

- 15.27. What are the four steps that occur during the adsorption of a solute from a gas or liquid mixture? Which step is almost instantaneous such that equilibrium can be assumed?
- 15.28. Within the particle, why are mass and heat transfer not analogous?
- 15.29. For mass transfer outside a spherical particle, what is the smallest value of the Sherwood number? What is the basis for this value?
- 15.30. What is the recommended equation for predicting the external mass-transfer coefficient for flow through a packed bed of particles?
- 15.31. What mechanisms of internal mass transfer must be considered for gas adsorption?
- 15.32. What is the difference between slurry adsorption (contact filtration) and fixed-bed adsorption (percolation)? When should each be considered and not considered?
- 15.33. How do pressure-swing and thermal-swing adsorption differ?
- 15.34. What are inert-purge swing and displacement purge?
- 15.35. How does VSA differ from PSA?
- 15.36. What is meant by a simulated countercurrent adsorption system?
- 15.37. What are the three common modes for conducting slurry adsorption? Which mode requires the smallest residence time for the liquid feed? What controls the rate of slurry adsorption, external or internal mass transfer?
- 15.38. What is ideal fixed-bed adsorption? What assumptions are necessary for it to apply? What is meant by the stoichiometric front? What is meant by breakthrough?
- 15.39. What is a mass-transfer zone (MTZ) and what causes it? Is it desirable? If not, why not?
- 15.40. For fixed-bed adsorption, what is the difference between the superficial velocity, interstitial velocity, and the concentration wave velocity? Which is the largest and which is the smallest?
- 15.41. What is the linear driving-force (LDF) model of Glueckauf? Why is it so useful?
- 15.42. What is the Klinkenberg approximation? Why is it useful in computing concentration and loading profiles, and breakthrough curves for fixed-bed adsorption?
- 15.43. What is the Collins technique for sizing a fixed-bed adsorption vessel?
- 15.44. Describe a typical thermal-swing adsorption cycle.
- 15.45. What is meant by the delta loading?
- 15.46. What is the basis for the method of lines for solving partial differential equations?
- 15.47. Why are cycle times for TSA much larger than for PSA?
- 15.48. Describe the steps in the Skarstrom cycle.
- 15.49. Why can the Skarstrom cycle be completed in seconds or minutes?
- 15.50. What is the difference between a true-moving-bed (TMB) system and a simulated-moving-bed (SMB) system?
- 15.51. Why is it difficult to carry out a continuous, countercurrent adsorption process using a TMB system?
- 15.52. Under what conditions is a circulating desorbent used to separate a binary mixture by a SMB system?
- 15.53. How is port switching used in an SMB system?
- 15.54. Why are sections used in an SMB system?
- 15.55. How is the triangle method used to determine flow-rate ratios in a TMB unit?
- 15.56. What are the assumptions made in the steady-state TMB model?
- 15.57. How does the dynamic SMB model differ from the TMB model?
- 15.58. Can axial dispersion be significant in SMB systems?
- 15.59. Describe a typical ion exchange cycle.
- 15.60. In batch, elution chromatography, what causes different solutes to pass through the chromatography column with different residence times?
- 15.61. In batch, elution chromatography, what is the difference between the equilibrium wave pulse theory and the rate-based theory?

EXERCISES

Section 15.1

15.1. Adsorbent characteristics.

Porous particles of activated alumina have a BET surface area of $310 \text{ m}^2/\text{g}$, $\epsilon_p = 0.48$, and $\rho_p = 1.30 \text{ g/cm}^3$. Determine: (a) V_p in cm^3/g ; (b) ρ_s , in g/cm^3 ; and (c) d_p in \AA .

15.2. Surface area of molecular sieves.

Carbon molecular sieves are available from a Japanese manufacturer in two forms:

	Form A	Form B
Pore volume, cm^3/g	0.18	0.38
Average pore diameter	5 \AA	2.0 μm

Estimate S_g of each form in m^2/g .

15.3. Characteristics of silica gel.

Representative properties of small-pore silica gel are: $d_p = 24 \text{ \AA}$, $\epsilon_p = 0.47$, $\rho_p = 1.09 \text{ g/cm}^3$, and $S_g = 800 \text{ m}^2/\text{g}$. (a) Are these values reasonably consistent? (b) If the adsorption capacity for water vapor

at 25°C and 6 mmHg partial pressure is 18% by weight, what fraction of a monolayer is adsorbed?

15.4. Specific surface area from BET data.

The following data were obtained in a BET apparatus for adsorption equilibrium of N_2 on silica gel (SG) at -195.8°C . Estimate S_g in m^2/g of silica gel. How does your value compare with that in Table 15.2?

N_2 Partial Pressure, torr	Volume of N_2 Adsorbed in cm^3 (0°C , 1 atm) per gram SG
6.0	6.1
24.8	12.7
140.3	17.0
230.3	19.7
285.1	21.5
320.3	23.0
430	27.7
505	33.5

15.5. Maximum ion-exchange capacity.

Estimate the maximum ion-exchange capacity in meq/g resin for an ion-exchange resin made from 8 wt% divinylbenzene and 92 wt% styrene.

Section 15.2**15.6. Adsorption isotherms and heat of adsorption.**

Shen and Smith [*Ind. Eng. Chem. Fundam.*, **7**, 100–105 (1968)] measured equilibrium-adsorption isotherms at four temperatures for benzene vapor on silica gel having the following properties: $S_g = 832 \text{ m}^2/\text{g}$, $V_p = 0.43 \text{ cm}^3/\text{g}$, $\rho_p = 1.13 \text{ g/cm}^3$, and average $d_p = 22 \text{ \AA}$. The adsorption data are:

Partial Pressure of Benzene, atm	Moles Adsorbed/g Gel $\times 10^5$			
	70°C	90°C	110°C	130°C
5.0×10^{-4}	14.0	6.7	2.6	1.13
1.0×10^{-3}	22.0	11.2	4.5	2.0
2.0×10^{-3}	34.0	18.0	7.8	3.9
5.0×10^{-3}	68.0	33.0	17.0	8.6
1.0×10^{-2}	88.0	51.0	27.0	16.0
2.0×10^{-2}	—	78.0	42.0	26.0

(a) For each temperature, obtain a best fit of the data to (1) linear, (2) Freundlich, and (3) Langmuir isotherms. Which isotherm(s), if any, fit(s) the data reasonably well? (b) Do the data represent less than a monolayer of adsorption? (c) From the data, estimate the heat of adsorption. How does it compare to the heat of vaporization (condensation) of benzene?

15.7. Adsorption-equilibria data.

The separation of propane (C_3) and propylene (C_3^-) is accomplished by distillation, but at the expense of more than 100 trays and a reflux ratio greater than 10. Consequently, the use of adsorption has been investigated in a number of studies. Jarvelin and Fair [*Ind. Eng. Chem. Res.*, **32**, 2201–2207 (1993)] measured adsorption-equilibrium data at 25°C for three different zeolite molecular sieves (ZMSs) and activated carbon. The data were fitted to the Langmuir isotherm with the following results:

Adsorbent	Sorbate	q_m	K
ZMS 4A	C_3	0.226	9.770
	C_3^-	2.092	95.096
ZMS 5A	C_3	1.919	100.223
	C_3^-	2.436	147.260
ZMS 13X	C_3	2.130	55.412
	C_3^-	2.680	100.000
Activated carbon	C_3	4.239	58.458
	C_3^-	4.889	34.915

where q and q_m are in mmol/g and p is in bar. (a) Which component is most strongly adsorbed by each adsorbent? (b) Which adsorbent has the greatest capacity? (c) Which adsorbent has the greatest selectivity? (d) Based on equilibrium considerations, which adsorbent is best?

15.8. Fitting zeolite data to isotherms.

Ruthven and Kaul [*Ind. Eng. Chem. Res.*, **32**, 2047–2052 (1993)] measured adsorption isotherms for a series of gaseous aromatic hydrocarbons on well-defined crystals of NaX zeolite over ranges of temperature and pressure. For 1,2,3,5-tetramethylbenzene at

547 K, the following equilibrium data were obtained with a vacuum microbalance:

q , wt%	7.0	9.1	10.3	10.8	11.1	11.5
p , torr	0.012	0.027	0.043	0.070	0.094	0.147

Obtain a best fit of the data to the linear, Freundlich, and Langmuir isotherms, with q in mol/g and pressure in atm. Which isotherm gives the best fit?

15.9. Fitting adsorption data to isotherms.

Lewis, Gilliland, Chertow, and Hoffman [*J. Am. Chem. Soc.*, **72**, 1153–1157 (1950)] measured adsorption equilibria for propane (C_3), propylene (C_3^-), and binary mixtures thereof on activated carbon and silica gel. Adsorbate capacity was high on carbon, but selectivity was poor. Selectivity was high on silica gel, but capacity was low. For silica gel ($751 \text{ m}^2/\text{g}$), the pure-component data below were obtained at 25°C:

Propane		Propylene	
P , torr	q , mmol/g	P , torr	q , mmol/g
11.1	0.0564	34.2	0.3738
25.0	0.1252	71.4	0.7227
43.5	0.1980	91.6	0.7472
71.4	0.2986	194.3	1.129
100.0	0.3850	198.3	1.168
158.9	0.5441	271.5	1.401
227.5	0.7020	353.2	1.562
304.2	0.843	550.7	1.918
387.0	1.010	555.2	1.928
468.0	1.138	760.6	2.184
569.0	1.288		
677.8	1.434		
775.0	1.562		

The following mixture data were measured with silica gel at 25°C, over a pressure range of 752–773 torr:

Total Pressure, torr	Millimoles of Mixture Adsorbed/g	y_{C_3} , Mole Fraction in Gas Phase	x_{C_3} , Mole Fraction in Adsorbate
769.2	2.197	0.2445	0.1078
760.9	2.013	0.299	0.2576
767.8	2.052	0.4040	0.2956
761.0	2.041	0.530	0.2816
753.6	1.963	0.5333	0.3655
766.3	1.967	0.5356	0.3120
754.0	1.974	0.6140	0.3591
753.6	1.851	0.6220	0.5550
754.0	1.701	0.6252	0.7007
760.0	1.686	0.7480	0.723
—	2.180	0.671	0.096
760.0	1.993	0.8964	0.253
760.0	1.426	0.921	0.401

(a) Fit the pure-component data to Freundlich and Langmuir isotherms. Which gives the best fit? Which component is most strongly adsorbed? (b) Use the results of the Langmuir fits in part (a) to predict binary-mixture adsorption using the extended-Langmuir equation, (15-32). Are the predictions adequate? (c) Ignoring the

pure-component data, fit the binary-mixture data to the extended-Langmuir equation, (15-32). Is the fit better than that obtained in part (b)? (d) Ignoring pure-component data, fit the binary mixture data to the extended-Langmuir–Freundlich equation, (15-33). Is the fit adequate? Is it better than that in part (c)? (e) For the binary-mixture data, compute the relative selectivity, $\alpha_{C_3, C_3} = y_{C_3} (1 - x_{C_3}) / [x_{C_3} (1 - y_{C_3})]$, for each condition. Does α_{C_3, C_3} vary widely or is the assumption of a constant value reasonable?

15.10. Adsorption isotherms.

As shown in Figure 15.10, adsorption is strongly influenced by temperature. Given below are data provided by a supplier of BPL carbon for adsorption of gaseous *n*-hexane, in a table of *V*, volume adsorbed in cm³ liquid/100 g carbon, with corresponding values of $T/V[\log_{10}(f_s/f)]$, where *T* is in K, *f* is the hydrocarbon fugacity in mm Hg, and *f_s* is the fugacity in mmHg of the saturated liquid. An adsorption process is carried out at 760 mm Hg with a gas containing hexane at a concentration of 0.2 mol% for temperatures of 20°C and 40°C. Calculate the equilibrium capacity of the bed in g of hexane/g carbon at each temperature. The vapor pressure of hexane at 20°C is 120 mm Hg and at 40°C it is 276 mm Hg. Hexane liquid density is 0.615 g/cm³ and MW = 86.17.

<i>V</i> , cm ³ liquid /100 g BPL	$T/V[\log_{10}(f_s/f)]$
40.0	2.5
27.0	5.0
10.0	10.0
3.5	15.0
1.2	20.0

15.11. Extended-Langmuir–Freundlich isotherm.

In Example 15.6, pure-component, liquid-phase adsorption data are used with the extended-Langmuir isotherm to predict a binary-solute data point. Use the mixture data below to obtain the best fit to an extended-Langmuir–Freundlich isotherm of the form

$$q_i = \frac{(q_0)_i k_i c_i^{1/n_i}}{1 + \sum_j k_j c_j^{1/n_j}} \quad (1)$$

Data for binary-mixture adsorption on activated carbon (1,000 m² /g) at 25°C for acetone (1) and propionitrile (2) solutes in water are as follows. Water is assumed not to adsorb.

Solution Concentration, mol/L		Loading, mmol/g	
<i>c</i> ₁	<i>c</i> ₂	<i>q</i> ₁	<i>q</i> ₂
5.52E – 5	7.46E – 5	0.0192	0.0199
6.14E – 5	7.71E – 5	0.0191	0.0198
1.06E – 4	1.35E – 4	0.0308	0.0320
1.12E – 4	1.46E – 4	0.0307	0.0319
3.03E – 4	2.32E – 3	0.0378	0.263
3.17E – 4	2.34E – 3	0.0378	0.264
3.25E – 4	3.89E – 4	0.0644	0.0672
1.42E – 3	1.58E – 3	0.161	0.169
1.42E – 3	1.61E – 3	0.161	0.169
1.43E – 3	1.60E – 3	0.161	0.169
2.09E – 3	3.84E – 4	0.250	0.0390
2.17E – 3	3.85E – 4	0.251	0.0392
4.99E – 3	5.24E – 3	0.291	0.307
5.06E – 3	5.31E – 3	0.288	0.305

7.41E – 3	2.42E – 2	0.237	0.900
7.52E – 3	2.47E – 2	0.236	0.896
2.79E – 2	7.59E – 3	0.802	0.251
4.00E – 2	3.44E – 2	0.715	0.822
4.02E – 2	3.42E – 2	0.717	0.834

15.12. Liquid mixture adsorption data.

Sircar and Myers [*J. Phys. Chem.*, **74**, 2828–2835 (1970)] measured liquid-phase adsorption at 30°C for a binary mixture of cyclohexane (1) in ethyl alcohol (2) on activated carbon. Assuming no adsorption of ethyl alcohol, (15-34) gives these results:

<i>x</i> ₁	<i>q</i> ₁ ^e , mmol/g	<i>x</i> ₁	<i>q</i> ₁ ^e , mmol/g
0.042	0.295	0.440	0.065
0.051	0.485	0.470	0.000
0.072	0.517	0.521	–0.129
0.148	0.586	0.537	–0.362
0.160	0.669	0.610	–0.643
0.213	0.661	0.756	–1.230
0.216	0.583	0.848	–1.310
0.249	0.595	0.893	–1.180
0.286	0.532	0.920	–1.230
0.341	0.383	0.953	–0.996
0.391	0.192	0.974	–0.470

(a) Plot the data as *q*₁^e against *x*₁. Explain the shape of the curve. (b) In what concentration region does the Freundlich isotherm fit the data? Determine the constants in the Freundlich isotherm.

15.13. Fitting liquid adsorption-equilibrium data.

Both the adsorptive removal of small amounts of toluene from water and small amounts of water from toluene are important in the process industries. Activated carbon is particularly effective for removing soluble organic compounds (SOCs) from water. Activated alumina is effective for removing soluble water from toluene. Fit each of the following two sets of equilibrium data for 25°C to the Langmuir and Freundlich isotherms. For each case, which isotherm provides a better fit? Can a linear isotherm be used?

Toluene (in Water) with Activated Carbon		Water (in Toluene) with Activated Alumina	
<i>c</i> , mg/L	<i>q</i> , mg/g	<i>c</i> , ppm (by Weight)	<i>q</i> , g/100g
0.01	12.5	25	1.9
0.02	17.1	50	3.1
0.05	23.5	75	4.2
0.1	30.3	100	5.1
0.2	39.2	150	6.5
0.5	54.5	200	8.2
1	90.1	250	9.5
2	70.2	300	10.9
5	125.5	350	12.1
10	165	400	13.3

15.14. Ion exchange and regeneration.

Derive (15-44) and use it to solve the following problem. Sulfate ion is to be removed from 60 L of water by exchanging it with chloride ion on 1 L of a strong-base resin with relative molar selectivities listed in Table 15.6 and an ion-exchange capacity of 1.2 eq/L of resin. The water to be treated has a sulfate-ion concentration

of 0.018 eq/L and a chloride-ion concentration of 0.002 eq/L. Following the attainment of equilibrium ion exchange, the treated water will be removed and the resin will be regenerated with 30 L of 10 wt% aqueous NaCl. (a) Write the ion-exchange reaction. (b) Determine the value of $K_{\text{SO}_4^{2-}, \text{Cl}^-}$. (c) Calculate equilibrium concentrations $c_{\text{SO}_4^{2-}}$, c_{Cl^-} , $q_{\text{SO}_4^{2-}}$, and q_{Cl^-} in eq/L for the initial ion exchange step. (d) Calculate the concentration of Cl^- in eq/L for the regenerating solution. (e) Calculate $c_{\text{SO}_4^{2-}}$, c_{Cl^-} , $q_{\text{SO}_4^{2-}}$, and q_{Cl^-} upon reaching equilibrium in the regeneration step. (f) Are the separations sufficiently selective?

15.15. Equivalent fractions for ion exchange.

Silver ion in methanol was exchanged with sodium ion using Dowex 50 cross-linked with 8% divinylbenzene by Gable and Stroebel [*J. Phys. Chem.*, **60**, 513–517 (1956)]. The molar selectivity coefficient was found to vary somewhat with the equivalent fraction of Na^+ in the resin as follows:

x_{Na^+}	0.1	0.3	0.5	0.7	0.9
$K_{\text{Ag}^+, \text{Na}^+}$	11.2	11.9	12.3	14.1	17.0

If the wet capacity of the resin is 2.5 eq/L and the resin is initially saturated with Na^+ , calculate the equilibrium equivalent fractions if 50 L of 0.05-M Ag^+ in methanol is treated with 1 L of wet resin.

15.16. Recovery of glycerol by ion exclusion.

Ion exclusion is a process that uses ion-exchange resins to separate nonionic organic compounds from ionic species contained in a polar solvent, usually water. The resin is presaturated with the same ions as in the solution, thus eliminating ion exchange. However, in the presence of the polar solvent, resins undergo considerable swelling by absorbing the solvent. Experiments have shown that a nonionic solute will distribute between the bulk solution and solution within the resin, while only ions exchange.

A feed solution of 1,000 kg contains 6 wt% NaCl, 35 wt% glycerol, and 47 wt% water. It is to be treated with Dowex-50 ion-exchange resin in the sodium form, after prewetting with water, to recover 75% of the glycerol. The data for the glycerol distribution coefficient,

$$K_d = \frac{\text{mass fraction in solution inside resin}}{\text{mass fraction in solution outside resin}}$$

are from Asher and Simpson [*J. Phys. Chem.*, **60**, 518–521 (1956)]:

Mass Fraction Glycerol in Solution Outside Resin	K_d	
	6 wt% NaCl	12 wt% NaCl
0.10	0.75	0.91
0.20	0.80	0.93
0.30	0.83	0.95
0.40	0.85	0.97

If the prewetted resin contains 40 wt% water, determine the kg of resin (dry basis) required.

Section 15.3

15.17. External transport coefficients in a fixed-bed.

Benzene vapor in an air stream is adsorbed in a fixed bed of 4×6 mesh silica gel packed to an external void fraction of 0.5. The bed is 2 ft in diameter and air flow is 25 lb/minute (benzene-free basis). At a bed location where pressure is 1 atm, temperature is

70°F, and the benzene mole fraction is 0.005, estimate the external gas-to-particle mass-transfer and heat-transfer coefficients.

15.18. External transport coefficients in a fixed bed.

Water vapor in an air stream is to be adsorbed in a 12.06-cm-diameter column packed with 3.3-mm-diameter Alcoa F-200 activated-alumina beads with external porosity of 0.442. At a location in the bed where the pressure is 653.3 kPa, temperature is 21°C, gas flow rate is 1.327 kg/minute, and dew-point temperature is 11.2°C, estimate the external gas-to-particle mass-transfer and heat-transfer coefficients.

15.19. Effective diffusivity of acetone.

For the conditions of Example 15.8, estimate the effective diffusivity of acetone vapor in the pores of activated carbon whose properties are: $\rho_p = 0.85 \text{ g/cm}^3$, $\epsilon_p = 0.48$, average $d_p = 25 \text{ \AA}$, and tortuosity = 2.75. Consider bulk and Knudsen diffusion, but ignore surface diffusion.

15.20. Effective diffusivity of benzene vapor.

For the conditions of Exercise 15.17, estimate the effective diffusivity of benzene vapor in the pores of silica gel with the following properties: $\rho_p = 1.15 \text{ g/cm}^3$, $\epsilon_p = 0.48$, average $d_p = 30 \text{ \AA}$, and tortuosity = 3.2. Consider all mechanisms of diffusion. The adsorption-equilibrium constant is given in Example 15.11, and the differential heat of adsorption is $-11,000 \text{ cal/mol}$.

15.21. Effective diffusivity of water vapor.

Using data in Exercise 15.18, estimate the effective diffusivity of water vapor in the pores of activated alumina with the following properties: $\rho_p = 1.38 \text{ g/cm}^3$, $\epsilon_p = 0.52$, average $d_p = 60 \text{ \AA}$, and tortuosity = 2.3. Consider all mechanisms of diffusion except surface diffusion.

Section 15.5

15.22. Comparison of slurry adsorption modes.

Adsorption, with activated carbon made from bituminous coal, of soluble organic compounds (SOCs), to purify surface and ground-water is a proven technology, as discussed by Stenzel [*Chem. Eng. Prog.*, **89**(4), 36–43 (1993)]. The less-soluble organic compounds, such as chlorinated organic solvents and aromatic solvents, are the more strongly adsorbed. Water containing 3.3 mg/L of trichloroethylene (TCE) is to be treated with activated carbon to obtain an effluent with only 0.01 mg TCE/L. At 25°C, adsorption-equilibrium data for TCE on activated carbon are correlated with the Freundlich equation:

$$q = 67c^{0.564} \quad (1)$$

where q = mg TCE/g carbon and c = mg TCE/L solution.

TCE is to be removed by slurry adsorption using powdered activated carbon with an average d_p of 1.5 mm. In the absence of any laboratory data on mass-transfer rates, assume the small-particle absorption rate is controlled by external mass transfer with a Sherwood number of 30. Particle surface area is $5 \text{ m}^2/\text{kg}$. The molecular diffusivity of TCE in low concentrations in water at 25°C is $1.02 \times 10^{-5} \text{ cm}^2/\text{s}$ from the Wilke–Chang equation in Chapter 3. (a) Determine the minimum amount of adsorbent needed. (b) For operation in the batch mode with twice the minimum amount of adsorbent, determine the time to reduce TCE content to the desired value. (c) For operation in the continuous mode using twice the minimum amount of adsorbent, obtain the required residence time. (d) For operation in the semi-continuous mode at a feed rate of 50 gpm and for a liquid residence time equal to 1.5 times that computed in part (c), determine the amount of activated carbon to give a reasonable vol% solids in the tank and a run time of not less than 10 times the liquid residence time.

15.23. Comparison of slurry adsorption modes.

Repeat Exercise 15.22 for water containing 0.324 mg/L of benzene (B) and 0.630 mg/L of *m*-xylene (X). Adsorption isotherms at 25°C for these low concentrations are independent and given in the same units as in Exercise 15.22 as

$$q_B = 32 c_B^{0.428} \quad (1)$$

$$q_X = 125 c_X^{0.333} \quad (2)$$

The SOC concentrations are to be reduced to 0.002 mg/L each. The molecular diffusivity for both benzene and *m*-xylene is $1.04 \times 10^{-5} \text{ cm}^2/\text{s}$.

15.24. Comparison of slurry adsorption modes.

Repeat Exercise 15.22 for water containing 0.223 mg/L chloroform whose concentration is to be reduced to 0.010 mg/L. The adsorption isotherm at 25°C is given by $q = 10 c^{0.564}$ in the same units as in Exercise 15.22. The molecular diffusivity for chloroform at low concentrations in water is $1.13 \times 10^{-5} \text{ cm}^2/\text{s}$.

15.25. Intraparticle diffusion resistance.

The volume-average adsorbate loading of a spherical particle is given by (15-97). Show that a parabolic adsorbate loading profile proposed by Liaw et al., [76], $q = a_0 + a_1 r + a_2 r^2$, may be used to obtain a transport-rate resistance term for intraparticle diffusion for a thermodynamic driving force given by the difference between the solute concentration on the particle at its outer surface ($r = R_p$) and the volume-average adsorbate loading. Prove this by equating the rate of accumulation of adsorbate within the particle to Fick's first law for diffusion into the particle evaluated at the particle outer surface.

15.26. MTZ concept.

Three fixed-bed adsorbers containing 10,000 lb of granules of activated carbon ($\rho_b = 30 \text{ lb}/\text{ft}^3$) each are to be used to treat 250 gpm of water containing 4.6 mg/L of 1,2-dichloroethane (D) to reduce the concentration to less than 0.001 mg/L. Each carbon bed has a height equal to twice its diameter. Two beds are to be placed in series so that when Bed 1 (the lead bed) becomes saturated with D at the feed concentration, that bed is removed. Bed 2 (the trailing bed), which is partially saturated at this point, depending upon the width of the MTZ, becomes the lead bed, and previously idle Bed 3 takes the place of Bed 2. While Bed 1 is off-line, its spent carbon is removed and replaced with fresh carbon. The spent carbon is incinerated. The equilibrium adsorption isotherm for D is given by $q = 8 c^{0.57}$, where q is in mg/g and c is in mg/L. Once the cycle is established, how often must the carbon bed be replaced? What maximum MTZ width allows saturated loading of the lead bed?

15.27. MTZ concept.

The fixed-bed adsorber arrangement of Exercise 15.26 is to be used to treat 250 gpm of water containing 0.185 mg/L of benzene (B) and 0.583 mg/L of *m*-xylene (X). However, because the two solutes may have considerably different breakthrough times, more than two operating beds in series may be needed. Adsorption isotherms are given in Exercise 15.23, where q is in mg/g and c is in mg/L. From laboratory measurements, widths of the mass-transfer zones are estimated to be $\text{MTZ}_B = 2.5 \text{ ft}$ and $\text{MTZ}_X = 4.8 \text{ ft}$. Once the cycle is established, how often must the carbon be replaced?

15.28. Comparison of models.

Air at 80°F, 1 atm, 80% relative humidity, and a superficial velocity of 100 ft/minute passes through a 5-ft-high bed containing 2.8-mm-diameter spherical particles of silica gel ($\rho_b = 39 \text{ lb}/\text{ft}^3$). The adsorption-equilibrium isotherm for water vapor at 80°F is given by

$$q_{\text{H}_2\text{O}} = 15.9 p_{\text{H}_2\text{O}}$$

where q is in lb H₂O/lb gel and p is in atm. The overall mass-transfer coefficient can be estimated from (15-100), using an effective diffusivity of $0.05 \text{ cm}^2/\text{s}$, and with k_c estimated from (15-65) using the diffusivity of water vapor in air as $0.26 \text{ cm}^2/\text{s}$, the density of the gas as $0.0727 \text{ lb}/\text{ft}^3$, and the gas viscosity as $1.75 \times 10^{-5} \text{ kg}/\text{m}\cdot\text{s}$.

Using the approximate concentration-profile equations of Klinkenberg, compute a set of breakthrough curves and determine the time when the exiting-air humidity reaches 0.0009 lb H₂O/lb dry air. Assume isothermal and isobaric operation. Compare the breakthrough time with the time for the equilibrium model. At breakthrough, what is the approximate width of the mass-transfer zone? What is the average loading of the bed at breakthrough?

15.29. Treatment of wastewater by fixed-bed adsorption.

A train of four 55-gallon canisters of activated carbon is to be used to reduce the nitroglycerine (NG) content of 400 gph of wastewater from 2,000 ppm by weight to less than 1 ppm. Each canister has a diameter of 2 ft and holds 200 lb activated carbon ($\rho_b = 32 \text{ lb}/\text{ft}^3$). Each canister is also equipped with a liquid-flow distributor to promote plug flow through the bed. The effluent from the first canister is monitored so that when a 1-ppm threshold of NG is reached, that canister is removed from the train and a fresh canister is added to the end of the train. The spent carbon is mixed with coal for use as a fuel in a coal-fired power plant at the process site. Using the following pilot-plant data, estimate how many \$700 canisters are needed each month and the monthly cost.

Pilot-plant data:

Tests with the 55-gallon canister used in the commercial process: water rate = 10 gpm; NG content in feed = 1,020 ppm by weight.

Breakthrough correlation:

$t_B = 3.90 L - 2.05$, where t_B = time, h, at breakthrough of the 1-ppm threshold and L = bed depth of carbon in ft.

15.30. Sizing of fixed-bed adsorption unit.

Air at a flow rate of 12,000 scfm (60°F, 1 atm) containing 0.5 mol% ethyl acetate (EA) and no water vapor is to be treated with activated carbon (C) ($\rho_b = 30 \text{ lb}/\text{ft}^3$) with an equivalent particle diameter of 0.011 ft in a fixed-bed adsorber to remove EA. Subsequently the EA is stripped from C by steam at 230°F. Based on the following data, determine the diameter and height of the carbon bed, assuming adsorption at 100°F and 1 atm and a time to breakthrough of 8 h with a superficial gas velocity of 60 ft/minute. If the bed height-to-diameter ratio is unreasonable, what change in design basis would you suggest?

Adsorption isotherm data (100°F) for EA:

p^{EA} , atm	q , lb EA/lb C	p^{EA} , atm	q , lb EA/lb C
0.0002	0.125	0.0020	0.227
0.0005	0.164	0.0050	0.270
0.0010	0.195	0.0100	0.304

Breakthrough data at 100°F and 1 atm for EA in air at a gas superficial velocity of 60 ft/minute in a 1-ft dry bed:

Mole Fraction EA in Effluent	Time, Minutes	Mole Fraction EA in Effluent	Time, Minutes
0.00005	60	0.00100	95
0.00010	66	0.00250	120
0.00025	75	0.00475	160
0.00050	84		

15.31. Scale-up of laboratory data for fixed-bed adsorption.

A small laboratory fixed bed 10.16 cm in diameter and 16 cm in length, containing 600 g of activated carbon (C), has been used to adsorb *n*-butanol (B) from air containing 365 ppm of B. Measurements of the effluent concentration in terms of c_{out}/c_F as function of time t are:

c_{out}/c_F	0.0019	0.003	0.008	0.018	0.04	0.07	0.15	0.24	0.66	0.81	0.94	1.00
t , hr	5	5.5	6	6.5	7	7.5	8	8.5	10	11	12	13

Other pertinent data are: entering superficial gas velocity, $u_s = 58$ cm/s; $T = 25^\circ\text{C}$; $P = 737$ mm Hg; bed porosity, $\varepsilon = 0.456$; average particle diameter, $d_p = 0.37$ cm; and butanol MW = 74.12 g/mol.

A cylindrical vessel with an inside diameter of 2 ft and a height of 5 ft is available to conduct the adsorption on an industrial scale. The vessel can be packed with carbon to a 4 ft height. Plot the laboratory data and determine: (a) the mass velocity of the gas as it enters the bed in g gas/cm²-h, (b) the equilibrium loading of the carbon laboratory bed in g B/g C, and (c) the fraction of the laboratory bed utilized in the experiment if the breakthrough time is taken at $c_{\text{out}}/c_F = 0.05$. For the industrial application calculate: (d) the gas flow rate in kg/h for the same entering superficial velocity used in the laboratory experiment, (e) the fraction of the industrial bed that can be utilized; and (f) the estimated breakthrough time in h.

15.32. Desorption of benzene.

In Examples 15.11 and 15.13, benzene is adsorbed from air at 70°F in a 6-ft-high bed of silica gel and then stripped with air at 145°F. If the bed height is changed to 30 ft, the following data are obtained for breakthrough at 641 minutes for the adsorption step:

z , ft	$\phi = c/c_F$	$\psi = \bar{q}/q_F^*$	z , ft	$\phi = c/c_F$	$\psi = \bar{q}/q_F^*$
15	1.000	1.000	23	0.722	0.701
16	0.999	0.999	24	0.599	0.575
17	0.997	0.997	25	0.468	0.444
18	0.992	0.990	26	0.343	0.321
19	0.978	0.975	27	0.235	0.217
20	0.951	0.944	28	0.150	0.137
21	0.901	0.890	29	0.090	0.081
22	0.825	0.808	30	0.050	0.044

If the bed is regenerated isothermally with pure air at 1 atm and 145°F, and the desorption of benzene during the heat-up period is neglected, determine the loading, \bar{q} , profile at a time sufficient to remove 90% of the benzene from the 30-ft bed if an interstitial pure air velocity of 98.5 ft/minute is used. Values of k and K at 145°F are given in Example 15.11.

Section 15.6**15.33. Simulated moving bed.**

A dilute feed of 3-phenyl-1-propanol (A) and 2-phenyl ethanol (B) in a 60/40 wt% ratio methanol–water mixture is to be fed to a four-section laboratory SMB to separate A from B. The feed rate is 0.16 mL/minute, with 0.091 g/L of A and 0.115 g/L of B. The desorbent is the 60/40 wt% methanol–water mixture. For this dilute

mixture of A and B and the adsorbent to be used, a linear adsorption isotherm applies, with $K_A = 2.36$ and $K_B = 1.40$. Assume that neither methanol nor water adsorb. The external void fraction, ε_b , of the adsorbent beds is 0.572. A switching time of 10 minutes is to be used. Using the steady-state, local-composition TMB model for a perfect separation of A from B with $\beta = 1.15$, estimate initial values for the volumetric flow rates of the extract, raffinate, desorbent, and solid particles. Convert the value of the recirculation rate for the TMB to that for the SMB and compute the resulting volumetric-liquid flow rates in each of the four sections.

15.34. Steady-State TMB.

In the steady-state TMB run of Example 15.15, results from application of the steady-state, local-equilibrium TMB model in Example 15.14, were used with a β of 1.05 to establish flow rates of the raffinate, extract, makeup desorbent, recirculation, and solid particles so as to approach a perfect separation between fructose and glucose. While the separation was not perfect, it was reasonably good. What results are achieved in Example 15.15 if the overall mass-transfer coefficients approach infinity?

Section 15.7**15.35. Softening of hard water.**

Repeat Example 15.17, except for a feed containing 400 ppm (by weight) of CaCl₂ and 50 ppm of NaCl.

Section 15.8**15.36. Equilibrium model for a chromatographic column.**

An aqueous solution, buffered to a pH of 3.4 by sodium citrate and containing 20 mol/m³ each of glutamic acid, glycine, and valine, is separated in a chromatographic column packed with Dowex 50W-X8 in the sodium form to a depth of 470 mm. The resin is 0.07 mm in diameter and packs to a bed void fraction of 0.374. Equilibrium data follow a linear law, as in Example 15.18, with the following dimensionless constants determined by Takahashi and Goto [*J. Chem. Eng. Japan*, 24, 121123 (1991)]:

Solute	K
Glutamic acid	1.18
Glycine	1.74
Valine	2.64

The superficial solution velocity is 0.025 cm/s. Using equilibrium theory, what pulse duration achieves complete separation? What is the time interval between elution and the second pulse?

15.37. Mass-transfer resistances in a chromatographic column.

Repeat Exercise 15.36 using Carta's equation to account for mass transfer with the following effective diffusivities:

Solute	D_e , cm ² /s
Glutamic acid	1.94×10^{-7}
Glycine	4.07×10^{-7}
Valine	3.58×10^{-7}

Assume $k_c = 1.5 \times 10^{-3}$ cm/s. Establish a cycle of feed pulses and elution periods that will give the desired separation.

Answers to Selected Exercises

Chapter 1

- 1.6 2,750 kPa
1.11(b) 80.8%
1.12(b) 96.08%
1.15(b) 98.8%

Chapter 2

- 2.3(b) 0.00257
2.7 427 kg/m³
2.16 2,060 kJ/h
2.17 924,000 Btu/h
2.18(e) 3.05%
2.19(b) 4,883,000 Btu/h

Chapter 3

- 3.2 991 lb/day
3.4(a) 2,260 h
3.8(a) 1.91×10^{-7} mol/s-cm²
3.14 0.218 cm
3.17 2.1×10^{-5} cm²/s
3.20(c) 169,500 h
3.24 4.4 cm
3.26(a) 2.54×10^{-6} kmol/s-m²
3.27 3.73 m
3.28(d) 380 s
3.30 3.44×10^{-5} kmol/s-m²
3.33(b) 4.08 s
3.35(b) 1.24×10^{-4} mol/s-cm²-atm

Chapter 4

- 4.1(c) $4C + 10$
4.3(d) $C + 3$
4.11 4
4.12(b) 196 kJ/kg of feed
4.27 126 psia
4.31 211°F
4.37(c) 65% of nC_8
4.39(a) -61°F
4.48(a) 4.4 kg, (b) 504 kg
4.58 99.96%
4.60 97.73%

Chapter 5

- 5.3(c) 85.5%
5.4(e) 13.1 g
5.5(b) 74.3%, (e) 100%
5.6(d) 1,748 kg
5.9(b) 7,169 kg/h
5.10(b) 2,766 kg/h
5.13 Need 5 more specs
5.19 Need 5 more specs

- 5.21 $N_D = 19$
5.23(c) $2(N + M) + C + 16$
5.25(c) $2(N + M) + C + 15$

Chapter 6

- 6.7(a) 1.74
6.9(b) 9 to 10 stages
6.12 165 lbmol/h
6.16 0.005 ppm DCA
6.23(b) 375,000 gpm
6.25 3.56 ft
6.28 1.15 m
6.30(b) 6.0 ft

Chapter 7

- 7.9(a) 90.4%, (c) 8
7.13(b) 10 + reboiler
7.14 0.90 and 0.28 for benzene
7.15(b) 43.16 kmol/h
7.21 8 + reboiler
7.23 20 stages + reboiler, feed at 17 from top
7.25 63.49 kmol
7.27 9 to 10 trays + reboiler
7.29(d) 26 plates + reboiler
7.31(b) 4 + reboiler
7.33(c) 8
7.35 32 + reboiler, feeds at 17 and 27 from the top
7.40(c) 55.9%
7.46(a) 14.7 and 21.2 ft

Chapter 8

- 8.11(a) 233 kg/h, (b) 5
8.13 2.5 stages
8.15 5 stages
8.17 5 stages
8.23(b) 64 kg/h, (c) 142,000 kg/h
8.26 139,000 lb/h
8.28(a) 0.32 mm, (c) 1,234 ft²/ft³
8.30(a) 81 rpm, (b) 5.6 Hp, (c) 0.53 mm, (d) 2,080 ft²/ft³, (e) 0.202 ft/h, (f) 26.3

Chapter 9

- 9.4 28.3 stages
9.5(a) 7.1, (b) 5.3, (c) 2.3
9.7 8.4 stages
9.11 272.8 kmol/h reflux rate
9.17(c) 1.175, (e) 6 or 7 from top

Chapter 10

- 10.4 0.3674, 0.2939, 0.1917
10.5 -16.67, -33.333, -33.333, -33.333, -33.333

- 10.7(a)** 1.0, 4.0
10.8(a) 0.2994, 0.9030
10.10 $x_1 = -2.62161$, $x_2 = 3.72971$
10.16 Stage 8 or 9
10.18 Reb. duty = 1,014,000 Btu/h
10.20 Cond. duty = 1,002,600 Btu/h
10.22 Reb. duty = 3,495,000 Btu/h
10.28 14.00
10.35 Reb. duty = 4,470,000 Btu/h
10.37 5 to 6 stages

Chapter 11

- 11.9** 57 stages, 70 mol/s solvent, 7 ft diam.
 for extractive colm.
11.16 100 stages, 115 kmol/h methanol, $R = 10$

Chapter 12

- 12.17(a)** 15, **(b)** 20 trays
12.18(a) 24, feed to stage 20 from the condenser
12.19 23 m above, 4 m below

Chapter 13

- 13.1(b)** 29.9 wt% distilled
13.3 57.9 moles
13.7 2.14 h
13.9 0, 0.571 isopropanol
13.10 35 lbmol
13.11 0.548 kmol distilled
13.13(a) 9 stages
13.15(a) 7.28 h
13.16(a) 4.60 h
13.25(a) 22.8 h, **(b)** 50.6 lbmol

- 13.28** 26, 8, 26, 40 kmol
13.29 26.6, 48.4, 25 kmol

Chapter 14

- 14.3** 48,800 m², 281 kmol/h
14.5 2 mm
14.7 41,700 m³/m²-day
14.11 Case 1 195 m²/stage, permeate = 60 lbmol/h
14.16 545 m², 65% recovery
14.18 73 amp/m², 25.6 amp
14.20 75% recovery for Des. 2
14.23 548,000 ft²
14.25 197,000 ft² for crossflow
14.28 EtOH permeance = 4.62×10^{-5} kmol/h-m²-mm Hg

Chapter 15

- 15.1(a)** 0.369 cm³/g, **(b)** 2.5 g/cm³, 47.6 angstroms
15.3(b) 0.87
15.4 52.1 m²/g
15.5 5.35 meq/g
15.14(b) 0.15
15.16 4,170 kg dry resin
15.17 0.0741 m/s and 170.1 J/m²-s-K
15.20 0.0054 cm²/s
15.22(a) 0.66 g/L, **(b)** 12.2 h
15.23(c) 1,845 h
15.26 13.8 days
15.27 279 days
15.28 679 min ideal, 451 min actual, 2.6 ft
15.29 84 cannisters
15.41 660 s, 1,732 s

Index

- A**
- Absorption (absorber), 6, 8, 137
 - applications, 139
 - chemical (reactive), 180–182
 - design considerations, 143–144
 - equipment, 138–143
 - graphical design method, 144–148
 - industrial example, 137–138
 - Kremser method, 148–151
 - rigorous equilibrium-based methods, 284–297
 - rigorous rate-based methods, 368–380
 - stage (plate, tray) efficiency, 154–160
 - Absorption factor, 149
 - Acentric factor, 23
 - Activity, 17–18
 - Activity coefficient, 17–18
 - Activity coefficient models, 30
 - binary interaction parameters, 29
 - NRTL, 30, 32–33, 137
 - UNIFAC, 30, 34–35, 137
 - UNIQUAC, 30, 33–34, 137
 - Wilson, 30–32
 - Adiabatic flash, 96
 - Adsorbate loading, 483
 - Adsorbents, 455, 457–458
 - activated alumina, 455, 457
 - activated carbon, 455, 457
 - molecular-sieve carbon, 455–458
 - molecular-sieve zeolites, 455, 457–458
 - polymeric, 455, 458
 - silica gel, 455, 457
 - Adsorbent properties, 453–456
 - BET equation, 455–456
 - pores, 454–456
 - porosity, 454–456
 - specific pore volume, 455
 - specific surface area, 454–456
 - Adsorption (adsorber), 7, 451–458, 462–467, 470–502
 - applications, 454
 - bulk separation, 452
 - chemisorption, 454–455, 464
 - countercurrent, 476–478
 - displacement purge, 476–477
 - equipment, 475–478
 - fixed-bed, 476, 482–487
 - fluidized-bed, 476–478
 - gas, 105, 452–453, 462–470
 - industrial example, 453
 - kinetics, 464, 493
 - liquid, 103, 466–467
 - monomolecular, 454–455, 464
 - moving-bed (simulated), 476, 478, 494–500
 - multimolecular, 454–455, 462
 - physical, 454–455, 462, 465, 471
 - pressure-swing, 16, 476–477, 492–494
 - regeneration, 471, 476–477, 483, 488–490, 493–494
 - scale-up, 487–488
 - simulated moving-bed, 476, 478, 494–500
 - slurry, 475–476, 479–481
 - thermal-swing, 476–477, 488–491
 - transport, 470–474
 - external, 471–473
 - internal, 473–474
 - true moving bed (TMB), 494–495
 - local-equilibrium model, 496, 502
 - triangle method, 497–498
 - vacuum-swing, 476–477, 492
 - Adsorption equilibrium, 103, 461–467
 - constant-selectivity, 467, 496, 498
 - extended isotherms, 466
 - Freundlich isotherm, 463–465
 - Henry's law (linear isotherm), 462, 496
 - isotherms of concentration change, 466–467
 - Langmuir isotherm, 464–465
 - Toth, 464
 - UNILAN, 464
 - Agitated columns for extraction, 235–238
 - axial dispersion, 235
 - design, 239–243
 - superficial velocities in, 258–259
 - Amagat's law, 30
 - Analogies, 68–72
 - Chilton-Colburn, 70
 - Churchill-Zajic, 71–72
 - Friend-Metzner, 70–71
 - Prandtl, 70
 - Reynolds, 69–70
 - Anion, 432–433, 468
 - Anode, 432–433
 - Antoine equation, extended, 21
 - Availability, 37–39
 - Axial dispersion (backmixing), 235
 - Azeotropes, 31–32, 123
 - estimating all, 326
 - heterogeneous, 93
 - homogeneous, 93
 - maximum-boiling, 31–32, 92
 - minimum-boiling, 31–32, 92
 - ternary, 328
 - Azeotropic distillation, 320, 334, 339–351
- B**
- Balances
 - availability (exergy), 37–39
 - energy, 38
 - entropy, 38
 - material (mole or mass), 9
 - Batch distillation, 385–403
 - advantages of, 466
 - constant distillate composition, 470–471
 - constant reflux, 469–470
 - complex, 471–472
 - differential, 466–471
 - holdup, effect of, 472
 - rigorous model, 474–476
 - Rayleigh, 466–468
 - stripping, 471–472
 - Barrer unit, 413–414
 - Billet-Shultes correlations
 - holdup, 169–170
 - mass transfer, 177–179
 - Binodal curve, 244
 - Blasius equation, 64
 - Block-flow diagram, 2
 - Boilup, 6, 122, 197
 - Boilup ratio, 195, 197
 - Bubble cap, 139–141
 - Bubble-cap columns, 141
 - Bubble point, 90, 97
 - Bubble-point (BP) method, 286, 294–295
 - Bulk-flow in mass transfer, 47, 49
- C**
- Carman-Kozeny (Kozeny-Carman) equation, 417
 - Carrier, 231

- Cascades, 118–125
 cocurrent, 119
 countercurrent, 120
 crosscurrent, 119–120
 liquid–liquid, 119–121
 membrane, 123–124
 single-section, 119–121
 two-section, 121–123
 vapor–liquid, 121–123
- Case
 design, 127
 simulation, 127
- Catalytic distillation, 420
- Cathode, 432–433
- Cation, 432–433, 468
- Chemical potential, 16, 18
- Chromatography, 451–452, 460–461, 475, 478–479, 503–506
 applications, 454
 bonded phase, 460
 equilibria, 470
 equilibrium-based model, 505–504
 equilibrium wave pulse theory, 505
 equipment, 478–479
 gas, 460–461
 high-performance liquid, 460–461
 liquid, 460–461
 mobile phase, 460
 rate-based model, 506
 stationary phase, 452–453, 460, 470
- Chilton-Colburn analogy, 70
j-factors, 68
- Churchill-Zajic analogy, 71–72
- Cloud-point titration, 99
- Co-ion, 432–433
- Components
 distribution of, 271–272, 278–279
 key, 9, 345–346
 recovery of, 9
- Composition, measures of, 11
 mass ratio, 98
 molality, 11
 molarity, 11
 mole %, 11
 mole ratio, 105
 normality, 11
 ppb, 11
 ppm, 11
 volume %, 11
 weight %, 11
- Compressibility factor, 23
- Concentration polarization, 428–430, 433, 437
- Condenser, 172
 duty, 206
 type, selection of, 204
- Continuity equation, 162
- Continuous phase, 233
- Convergence pressure, 25
- Corresponding states, law of, 23
- Counter ion, 519
- Critical solution temperature, 243
- D**
- Dalton's law, 17, 146
- Darcy's law, 503
- Decanter, 234
- Degrees of freedom analysis, 88, 94, 125–132
 elements, 126, 128
 separation cascades, 127, 129–130
 rigorous models, for, 289–290
 stream variables, 126
- Density, liquid
 Rackett equation, 21
- Derived thermodynamic properties, 25–27
- Design variables, 126
- Desublimation, 106
- Dew point, 90, 97
- Dialysis, 7, 430–431
 applications, 409
- Diabatic stages, 122
- Diffusion, 46–50, 102
 anisotropic materials, in, 47
 eddy (turbulent), 46–47, 69
 equimolar counterdiffusion (EMD), 48
 Fick's first law, 47
 Fick's second law, 59
 Knudsen, 57, 417, 419, 439
 forced, 46
 ordinary (concentration), 46
 pressure, 46
 thermal, 46
 multicomponent, 371
 mutual, 47
 pores, in, 57, 418–419, 454–456
 restrictive, 464
 steady-state, 47–51
 surface, 57, 471, 474
 unimolecular diffusion (UMD), 49–50
 unsteady state, 58–59
 velocities, 48
- Diffusivity (diffusion coefficient), 51–58
 binary, 51
 effective, in porous solid, 57, 418–419, 474
- Fuller-Schettler-Giddings equation, 51–52
- gas mixture, 51–53
- Hayduk-Minhas equation, 54
- high pressure, 52
 mass, 61
 momentum, 61
 Nernst-Haskell equation, 56
 restrictive factor, 418, 464
 self, 51
 Stokes-Einstein equation, 53
 tortuosity, 57, 417–418, 474
 Vignes equation, 55
 Wilke-Chang equation, 53
- Dimensionless groups in transport, 68
 Eotvos number, 258
 Froude number, 254
 Nusselt number, 62, 68
 Peclet number, 61, 68
 Peclet number for mass transfer, 61, 68
 Power number, 253
 Prandtl number, 61, 68
 Reynolds number, 61, 68, 170, 179
 Schmidt number, 61, 68, 190
 Sherwood number, 62, 68
 Stanton number, 68, 69
 Stanton number for mass transfer, 68, 70
 Weber number, 256
- Discontinuous (dispersed) phase, 233
- Distillation, 5, 8, 11, 171–176
 azeotropic, 320, 339–351
 batch, 385–403
 binary, 385–390
 multicomponent, 391–401
 binary, 191–219, 466–472
 applications, 192–193
 industrial example, 191–193
 McCabe-Thiele method, 193–208
 packed column design, 216–219
 HETP method, 217
 HTU method, 217–219
 design considerations, 193
 efficiency, stage (plate), 208–215
 Drickamer-Bradford correlation, 209
 flow patterns, effect, 369, 371, 375
 liquid flow-path length, 155, 160, 210
 Lockhart-Leggett correlation, 209–210
 Murphree, 157–160
 vapor efficiency, 158–160
 vapor-point efficiency, 158
 O'Connell correlation, 154–155, 209–210
 operating pressure, 203–204
 overall, 154, 209–210
 performance data, 154–155, 208
 scale-up, 160, 215

- Syeda et al. method, 210–214
 Vennavelli et al. method, 211–214
 enhanced, 320
 extractive, 320, 332–334
 heterogeneous azeotropic, 320, 339–342
 homogeneous, azeotropic, 320, 343–347
 multicomponent
 approximate methods, 171–176, 267
 batch, 391–401
 distribution of nonkey components, 278–279
 feed-stage location, 277–278
 Fenske-Underwood-Gilliland (FUG) method, 267–280
 Gilliland correlation for stages and reflux, 276–277
 key components, selection of, 267–269
 Kirkbride equation for feed-stage location, 276–277
 minimum reflux ratio by Underwood equations, 273–276
 minimum stages by Fenske equation, 270–272
 operating pressure, selection of, 269–270
 pinch points, 273
 rigorous methods,
 Amundson-Pontinen method, 286
 Boston-Sullivan method, 286, 304–309
 Bubble-point (BP) method, 286, 294–295
 Burningham-Otto method, 286, 295
 convergence criteria, 290, 295
 equation tearing, 286, 291
 equilibrium-stage model, 284–286
 Fredenslund-Gmehling-Rasmussen method, 297
 Friday-Smith analysis, 286, 294–295
 Goldstein-Stanfield method, 297
 Inside-out method, 304–308
 Lewis-Matheson method, 286
 MESH equations, 285–287, 290–291, 295, 297, 304
 Naphtali-Sandholm method, 297–300
 Newton-Raphson method, 286, 291, 293, 295, 298
 Simultaneous-correction method, 297–300
 Sum-rates (SR) method, 286–287, 294–295
 Theta method of Holland et al., 286
 Thiele-Geddes method, 286
 Thomas algorithm, 291–292
 tridiagonal matrix algorithm, 284, 291–292
 Wang-Henke (BP) method, 286, 294–295
 phase contacting methods, 5
 pressure-swing, 320, 337–338
 product-composition region, feasible, 330–332
 rate-based model, 368–380
 Krishna, et al., 369–370, 373–375
 Taylor, et al., 369, 373–375
 reactive, 320, 352–353
 Chang-Seader method, 353
 residue curve, 323–324
 residue curve map, 323–324, 326–330
 salt, 320, 335–337
 sequences,
 direct, 322–323
 indirect, 322–323
 Distillation boundary, 323, 326, 328, 330
 Distillation curve, 322, 329
 Distillation curve map, 329
 Distribution ratio (coefficient), 32, 98, 241
 Donnan effect (exclusion), 432
 Dortmund Data Bank (DDB) software package (DDBST), 16, 31, 34
 Downcomer, 160–162
 flooding, 161
 Drag coefficient, 68
- E**
 Eddy diffusivities, 46–47
 Efficiency, stage
 Murphree tray, 157–160
 Overall of Lewis, 154, 449
 Electrodialysis, 432–434
 applications, 409
 Electrolysis, 432–434
 Electrolyte solution models, 36
 Energy balance, 38
 Energy-separating agent (ESA), 4
 Enhanced Distillation, 320–357
 Enhancement factor, 182
 Enthalpy
 ideal gas, 20
 liquid, 20
 nonideal gas, 26
 of vaporization, 21, 26
 Entrainer, 320, 339
 Entrainment, 196
 flooding, 161–162
 Entropy
 balance, 37–38
 ideal gas, 20
 irreversible increase in, 38
 liquid, 20, 26
 nonideal gas, 26
 production, 38
 Eotvos number, 258
 Equation-of-state (EOS), 23
 formulation of K -value, 18
 Equation-of-state models, 23–27
 Benedict-Webb-Rubin (BWR), 24
 GC-EOS (Skjold-Jorgensen), 362
 generalized, 24
 ideal-gas law, 24
 Lee-Kessler-Plöcker (LKP), 24
 mixing rules, 24
 Peng-Robinson (PR), 24–25
 Redlich-Kwong (RK), 24–25
 Soave-Redlich-Kwong (SRK), 24–25
 Equation tearing, 286, 291
 Equilibrium, thermodynamic,
 chemical (reaction), 87
 physical (phase), 16–19, 87
 Equilibrium curve, 91
 Equilibrium stage, 4
 Equipment
 absorption, 138–143
 adsorption, 475–478
 distillation, 196–200
 liquid-liquid extraction, 233–240
 membranes, 414–416
 stripping, 144, 146, 148–200
 Ergun equation, 417
 Euler method, 393
 Exergy, 37–38
 Excess thermodynamic functions, 28, 34
 Extensive variables, 93–94, 125–126
 Extraction (extractor), 6
 liquid-liquid, 6, 8, 231–259
 solvent, 231, 240–242
 ternary, 231
 supercritical-fluid, 357, 359
 Extraction factor, 165
 Extractive distillation, 320, 332, 334
 applications, 332
 solvent, 320
 Extract phase, 241
 Extract reflux, 251–252

F

F-factor, 176
 Fanning friction factor, 64, 68, 70–71
 Faraday's law, 433–434
 Feasible product composition region, 322–323, 330–332
 Feed-stage location
 Fenske equation, 270–272
 Kirkbride equation, 276–277
 McCabe-Thiele method, 198–199
 optimal, 2071
 Fenske equation, 270–272
 Fenske-Underwood-Gilliland method, 267–280
 Fick's law, 47, 504–509, 529–530
 Film theory
 film theory of Nernst, 73–74
 penetration theory, 74
 surface-renewal theory, 75
 Film thickness, 76
 Fixed-bed adsorption (Percolation), 476, 482–487
 breakthrough, 482–483
 constant-pattern front, 487
 favorable adsorption isotherm, 486–487
 ideal (local) equilibrium, 483
 Klinkenberg approximations, 484
 linear driving force (LDF), 484, 506
 mass-transfer zone (MTZ), 483, 488
 stoichiometric front, 482–483
 Flash calculations, 93–97
 adiabatic, 96
 isothermal, 94–96
 non-adiabatic, 96
 percent vaporization, 96
 two-phase, 93–97
 three-phase, 107–108
 Flash drum, 216
 Flash vaporization, 4, 93–97
 adiabatic, 96
 isothermal, 94–96
 Flooding, 198, 215–218
 packed column, 173–175
 Strigle correlation, 173–174
 Kister-Gill correlation, 173–174
 plate column
 downcomer, 161–162
 entrainment, 161–163
 Fair correlation, 162
 Free-energy models, 29–34
 Freundlich adsorption isotherm, 463–465
 Friction factor, 64, 68
 Fanning, 64, 68, 70–71
 Friday-Smith analysis, 286, 294–295
 Friend-Metzner analogy, 70–71

Froude number, 170, 179, 327

FUG method, 267–280

Fugacity, 17–18, 148
 partial, 18

Fugacity coefficient, 17–18
 partial, 181

G

Gamma-phi formulation of *K*-value, 18

Gas absorption, 104

Gas-liquid system, 104

Gas permeation, 7, 421–428, 438–440
 applications, 409

Gas-solid system, 105–107

Gaussian elimination, 368

Gibbs free-energy

 models, 29–34

 NRTL, 30, 32–33

 UNIQUAC, 30, 33–34

 Wilson, 30–32

Gibbs' phase rule, 88–89

Gilliland correlation, 276–267

Glass-transition temperature, 411

Glassy polymers, 411

Graesser raining-bucket contactor, 238

Group methods, 148

 Kremser method, 148–150

H

Half reaction, 432

Hayduk-Minhas equation, 54

Heat-transfer coefficient, 61–62

Heavy key, 9, 117, 172

Henry's law, 19, 73, 76, 105, 206

Heterogeneous azeotrope, 93

Heterogeneous azeotropic distillation, 320, 343–347

HETP (HETS), 154, 164, 167, 175–176, 258–259

Holdup

 packed columns, liquid–liquid, 254

 packed columns, vapor–liquid, 169–170

Hollow-fiber membrane module, 414–416

Homogeneous azeotrope, 93

Homogeneous azeotropic distillation, 320, 339–342

HTU, 166–167, 175, 217–218

Hunter-Nash extraction method, 243–250

Hybrid systems, 161, 170, 175–176, 528

Hydraulic diameter, 179

Hydrogen bonds, 27–28

Hydrotrope, 337

I

Ideal-gas properties, 18, 20

Ideal *K*-value, 18–19

Ideal mixtures, 20

Ideal solutions, 17–20

Impellers, 233–234

Industrial Examples

 absorption, 137–138

 adsorption, 453

 binary distillation, 191–193

 liquid–liquid extraction, 231–232

 membrane separation, 409–410

Inside-out method, 304–308

 MESH equations, 305

Intensive variables, 88, 94, 125–126

Interfacial tension force, 235, 239, 243

Ion exchange, 451, 454, 458–459,

 468–469, 502–503

 applications, 454

 equilibria, 468–469

 equipment, 478–479

Ion exchanger, 451–452, 458–459

Isothermal flash, 94–96

J

Jacobian matrix, 298

j-factors of Chilton and Colburn, 68

K

Karr reciprocating-plate column, 238

Key components in distillation,

 9, 345–346

Kinetic energy ratio (of Sherwood), 162, 173

Kirkbride equation, 276–277

Knudsen diffusion, 57, 417, 419, 439

Kremser group method, 148–150, 356–359

 absorption, 148–150

 equation, 149

 plot, 150

 stripping, 149, 356–357

K-values, 17–19

 expressions (forms)

 activity coefficient, 18, 29–34

 electrolyte solution models, 36

 equation-of-state, 18, 23–27

 Henry's law, 19, 144–145, 206

 ideal, 18–19

 modified Raoult's law, 19

 polymer solution models, 39

 Poynting correction, 19

 PSRK model, 35

 Raoult's law, 18–19, 206

 solubility-based, 19

 selection of a model, 37

Kuhni extraction column, 237–238

- L**
- Langmuir adsorption isotherm, 464–465
 - Lee-Kessler-Plöcker method, 24
 - Light key, 9, 117
 - Liquid adsorption, 103
 - Liquid-liquid equilibrium coefficient, 18–19
 - Liquid-liquid equilibrium stage, 98, 102
 - multicomponent system, 101–102
 - ternary system, 98–101
 - Liquid-liquid extraction, 6, 8, 165–167, 231
 - applications, 233
 - design considerations, 239–243
 - equipment, 233–238
 - advantages and disadvantages, 239
 - HETS, 258–259
 - maximum loading, 238–239, 258–259
 - maximum size, 239
 - scale-up, 252
 - selection of, 238–240
 - graphical design methods
 - Hunter-Nash method, 243–250
 - minimum and maximum solvent rate, 247–248
 - operating points and lines, 344–247
 - right-triangle method, 250–251
 - industrial example, 231–232
 - preferred to distillation, when, 233
 - reflux, extract and raffinate, 251–252
 - rigorous design methods, 309–310
 - isothermal sum-rates method, 309–310
 - ternary, 243–251
 - Liquid-liquid miscibility boundaries, 98–100, 244
 - Liquid-solid equilibrium, 102, 103
 - Loading of adsorbate in adsorbent, 483–484
 - Loading point in packed columns, 169
 - Local composition concept, 30–31
 - Longitudinal mixing (dispersion), 159, 300, 334–337
 - Lost work, 37–38
- M**
- McCabe-Thiele method for binary distillation, 193–208
 - boilup, 6, 122, 197
 - condenser duty, 206
 - condenser type, 204
 - constant molar overflow assumption, 196
 - equilibrium curve, 196
 - equilibrium stages, number of, 199–200
 - feed line (*q*-line), 198–199
 - feed preheat, 207
 - feed-stage location, 198–199
 - heavy key, 193–194
 - light key, 193–194
 - minimum number of stages, 200–201
 - minimum reflux ratio, 201
 - multiple feeds, 226
 - Murphree efficiency, use of, 225
 - open steam, 226
 - operating lines, 196–197
 - perfect separation, 201
 - reboiler duty, 206
 - reboiler type, 206
 - reflux, subcooled, 207–208
 - reflux ratio, 196
 - sidestreams, 227
 - Marangoni interface effect, 76, 309, 330
 - Mass-mean diameter, 652
 - Mass-separating agent (MSA), 6
 - Mass transfer, 7, 46–47, 60–62
 - adsorption, in, 568–572
 - boundary layer, 64–66
 - bulk-flow effect, 46–47, 49
 - coefficient, 62
 - extraction, for, 255–258
 - individual, 62, 78, 158, 176
 - membranes, in, 416–424
 - overall, 76–78, 107–111, 157–158
 - volumetric, 166, 175–176, 220
 - driving forces, 78
 - droplet (particle), for,
 - external, 255–258, 568–570
 - internal, 255–258, 571–572
 - fluid-fluid interface, at
 - film theory of Nernst, 73–74
 - penetration theory of Higbe, 74
 - surface renewal theory of Danckwerts, 75
 - fully developed flow, in, 65–66
 - interfacial area, 371–372, 375
 - laminar flow, 60–67
 - boundary layer on a flat plate, 64–65
 - falling liquid film, 60–64
 - fully developed flow in a tube, 65–67
 - entry region, 66
 - Graetz solution 66
 - Hagen-Poiseuille equation 66
 - Leveque solution, 68
 - large driving force, case of, 79–80
 - liquid-liquid extraction columns, 234–240
 - Marangoni effect, 76
 - mechanisms, 46
 - membranes, in, 416–429
 - multicomponent, 372–373
 - bootstrap problem, 374
 - Maxwell-Stefan equations, 373
 - packed bed, 140, 164, 216–217, 235
 - particle, for
 - external, 330–331, 568–570
 - internal, 330–331, 571–572
 - penetration depth, 59
 - rate, 68
 - turbulent flow, in, 68–72
 - Chilton-Colburn analogy, 70
 - Churchill-Zajic analogy, 71–72
 - Friend-Metzner analogy, 70–71
 - Reynolds analogy, 69–70
 - two-film theory of Whitman, 76–78, 237–238
 - Material balance, 9
 - Maximum-boiling azeotropes, 31–32, 92
 - Melting temperature, polymer, 411
 - Membrane cascades, 123–124, 426–428
 - Membrane materials, 410–413
 - asymmetric, 413–414
 - carbon, 413
 - caulked asymmetric, 413
 - ceramics, 413
 - inorganic, 413
 - metals, 413
 - polymers, 410–413
 - amorphous, 411
 - crystalline, 411–412
 - melting temperature, 411
 - degree of polymerization, 411
 - glassy, 411–412
 - glass-transition temperature, 411–412
 - permselective layer (skin), 413, 416
 - repeat units, 411
 - rubbery, 411–412
 - thermoplastic, 411
 - thermosetting, 411
 - thin-layer composite, 498–499
 - transport in, 502–509
 - Membrane modules, 414–416
 - flow patterns in, 424–426
 - cocurrent flow, 424–426
 - countercurrent flow, 424–426
 - crossflow, 424–426
 - perfect mixing, 424–426

- Membrane modules, (*continued*)
 hollow-fiber, 414–416
 monolithic, 414–416
 plate-and-frame, 414–416
 spiral-wound, 414–416
 tubular, 414–416
- Membrane separations, 7, 408–444
 applications, 409
 cut, 423
 dialysis, 7, 430–431
 electrodialysis, 432–434
 gas permeation, 7, 421–428, 438–440
 industrial example, 409–410
 osmosis, 434
 pervaporation, 7, 441–444
 reverse osmosis, 7, 434–437
- Membranes, transport in, 416–423
 bulk flow, 417
 external resistances, 428–429
 gas diffusion, 419
 ideal separation factor, 422–423
 Knudsen diffusion, 417, 419, 439
 liquid diffusion, 418
 restricted (hindered) diffusion, 418
 separation factor, 422
 sieving (size exclusion), 417–418
 solution-diffusion, 82, 421–423
- MESH equations, 285–287, 290–291, 295, 297, 304
- Method of lines (MOL), 490, 506
- Minimum-boiling azeotrope, 31–32, 92
- Minimum number of equilibrium stages, 200–201, 347–348
- Minimum reflux ratio, 201–202, 349–353
- Minimum work of separation, 38
- Mixer-settlers, 233–234, 252–258
 design and scale-up, 252–258
 drop size, 256–257
 flat-blade turbine, use of, 233–234, 253
 interfacial area, 256–257
 mass transfer, 255–258
 minimum impeller rate of rotation, 254
 Murphree dispersed-phase efficiency, 255–258
 power consumption, 253–254
 mixing rules, 24–25, 361–362
 Wong-Sandler, 362
- Models, 138
 equilibrium-based, 138
 rate-based, 138, 368–380
 rigorous,
- Molecular-sieve carbon, 455, 457
- Molecular-sieve zeolites, 455–458
- Molecules, classification of, 28
- Momentum diffusivity, 68
- Moving-bed adsorber, 476, 478, 494–500
- Multiple solutions (multiplicity), 347
- Murphree efficiencies, 157–159, 255
 extraction, 255
 Gerster et al. flow integration, 159
 Lewis flow integration, 158
- N**
- Nernst-Haskell equation, 56
- Newton-Raphson method, 286, 291, 293, 295, 298
- Newton's law of cooling, 61, 569
- Nodes, 326
 saddle, 326
 stable, 325
 unstable, 325
- Nonideal liquid solutions, 27–29
- Nonkey components in distillation, 272
- NRTL equation, 32–33, 55–56
- NTU, 167–168, 336–337
- Number of transfer units (NTU), 167–168
- Nusselt number, 62, 68, 568–570
- O**
- Occlusion, 139
- ODEPACK, 491
- Oldershaw column, 160
- Oldshue-Rushton column, 236
- Operating lines
 Hunter-Nash method, 245–247
 McCabe-Thiele method, 196–197
- Optimal control of batch distillation, 401–403
 slop (intermediate) cuts, 387, 400
 variation of reflux ratio, 389–390
- Osmosis, 434
- Osmotic pressure, 435–435
- P**
- Packed column (tower), 164–180, 235
 diameter, 175
 distributor, 140–141
F-factor, 176
 flooding, 173–175
 height, 164
 HETP (HETS), 164, 166–168, 175–176
 HTU, 166–167, 175–179
 liquid holdup, 169–170
 loading, 169–170
 preloading, 170
 mass transfer, 175–179, 568–570
 Billet-Schultes correlations, 177–179
 NTU, 166–168
 packings, 141–143, 171–172
 pressure drop, 173–174
 rate-based method, 164–179
 redistributor, 141
- Packings, 141–142, 1781–172
 random (dumped), 141–142
 characteristics, 171–172
 structured (arranged, ordered), 142–143
 characteristics, 172
- Parachor, 54–55
- Partial condensation, 4
- Partial vaporization, 4
- Particle density, 454–456
- Particle porosity, 454–456
- Partition coefficient, 17
- Patched solutions, 63, 67
- Peclet number for heat transfer, 61, 68
- Peclet number for mass transfer, 61, 68, 213–214, 336
- Penetration theory of Higbe, 74
- Peng-Robinson (PR) equation, 24–25
 binary interaction coefficient, 25
- Perforated trays, 139, 141
- Permeability, 498, 507–509, 526
- Permeance, 498
- Permeate, 7, 493
- Pervaporation, 7, 441–444
 applications, 409
- Phase equilibria, 16–19, 88, 94, 102, 107
 gas-liquid, 104
 gas-solid, 105–107
 liquid-liquid, 19, 58, 97–102
 solid-liquid, 19, 138–144
 thermodynamic quantities, 18
 vapor-liquid, 17–20, 88–97
- Phase equilibrium ratio (*K*-value), 16–17
- Phase splitting, 30, 33
- Pinch points in distillation, 273
- Plait point, 100, 244
- Podbielniak centrifugal extractor, 238
- Poynting-correction, 19
- Polymer membranes, 410–413
 dense (nonporous), 412–413
 macroporous, 416
 microporous, 416, 419
- Polymer solution models, 36
- Pore-size distribution, 456
- Power number, 253
- Prandtl analogy, 69
- Prandtl number, 61, 68

- Predictive models
 Predictive Peng-Robinson UNIFAC, 36
 PSRK, 35
 UNIFAC, 34–35
 VTPR, 36
- Pressure, operating, 203–204, 347
- Pressure drop
 packed column, 169–175
 trayed tower, 164
- Pressure-swing adsorption (PSA), 16, 476–477, 492–494
- Pressure-swing distillation, 401, 419–420
- Process, chemical, 4
 auxiliary operations, 1
 batch, 1
 continuous, 1
 key operations, 1
 semicontinuous, 1
- Process-flow diagram, 2
- Processes, industrial chemical, 1–3
- Process simulators, 1
- Product composition region, feasible, 330–332
- PSRK model for K -values, 35
- Pumparounds, 287
- Q**
 q -line, 91, 198–199
- R**
 Rachford-Rice method, 94–96
 Rackett liquid-density equation, 21
 Raffinate phase, 6, 241
 Random-walk motion, 47
 Raoult's law, 18–19, 122–123, 148, 206
 deviations from, 28
 modified, 19, 123, 128, 194, 206
 Rate-based model, 164, 216, 368–380
 mass and heat transfer, 369
 packed column method, 164–179, 216–219, 376
 plate column method, 375
 RDC (rotating disk column), 237
 Reactive distillation, 320, 352–353
 Reboiler
 duty, 206
 selection of, 206
 Rectifying section, 196–197
 Recycle technique, 6
 Redlich-Kwong (RK) equation, 24–25, 42–46
 Reduced conditions, 23
 Reference (datum) state
 component, 23
 elemental, 23
- Reflux, 6, 194–195
 extract, 251–252
 ratio, 196
 minimum, 201, 202, 349–352
 optimal, 207
- Reflux drum, 216
- Rejection, 435, 437
- Relative selectivity, 18
- Relative volatility, 18, 90–92
- Residence-time distribution, 75
- Residue curve, 323–324
- Residue curve map, 323–324, 326–330
 nodes, 407
 saddle, 407
 stable, 406
 unstable, 406
- Resins, ion exchange, 458, 475
- Retentate, 7, 493
- Reverse osmosis, 7, 434–438
 applications, 409
- Reynolds analogy, 69–70
- Reynolds number, 61, 68, 170, 179, 253, 257
- Rigorous equilibrium-stage models
 Aspen Plus, 287
 CHEMCAD, 287–289
 ChemSep, 289
 steps, 296
 initialization, 296
 iteration, 296
 damping and acceleration, 296
 convergence, 296
- Rotating-disk column, 237
- RTL (Graesser raining-bucket contactor), 238
- Rubbery polymers, 439–440
- S**
 Salt distillation, 320, 335–337
 Salting in and salting out, 336
 Salt passage, 437
 Saturated liquid, 90
 Saturated vapor, 90
 Sauter mean diameter, 256, 652
 Scale-up, 215
 Scheibel columns, 236
 Schmidt number, 61, 68, 240, 331
 Second-law analysis, 37–39
 Second-law efficiency, 38–39
 Separation methods, 4–8
 barrier, 7
 force field or gradient, 7
 general, 4
 phase addition, 6–7
 phase creation, 4–6
 Separations, 1
 cost as a function of concentration, 8
 feasible, 8
 industrial methods, 1–3
 influencing factors, 21
 Influencing properties, 4
 parallel units, need for, 8
 specifications for, 125–127
 staging, ease of, 8
 technological maturity, 8
 use maturity, 8
 Separation sequences, 11
 Separation specifications, 9
 component recoveries, 9
 product purities, 9
 Separation techniques, 3
 phase creation, 4
 phase addition, 6
 barrier, 7
 external fields, 7
 Settler (decanter), 233–234, 252
 Sherwood number, 62–68
 average, 63, 65
 extraction, 257
 local, 65–66
 packed beds, 472–473
 single particle, 471–472
 Sieve-tray columns, 138–141, 235
 flow regimes, 138–140
 Silica gel, 455, 457
 Simulated moving-bed adsorber, 476, 478, 494–500
 Simultaneous-correction method, 297–300
 Single-section cascade, 118–119
 Single-stage equilibrium, 94
 Slop (intermediate) cuts, 387, 400
 Slurry adsorption (contact filtration), 475–476, 479–481
 batch mode, 578
 continuous mode, 578
 semicontinuous mode, 578–579
 Soave-Redlich-Kwong (SRK) equation, 24–25
 Solute, 137, 231
 Solution-diffusion, 416, 420–423
 Solutropy, 136, 244
 Solvent, 118, 231
 ideal, 240–241
 selection by group interactions, 241–242
 Sorel distillation model, 368–369
 Sorbate, 451–452
 Sorbents, 451, 453–458
 Sorption, 451
 Sphericity, 473
 Spiral-wound membrane modules, 414–416, 424
 Spray tower (column), 140, 234–235

- Stage
 Stage efficiency
 Murphree point, 158–159
 Murphree tray, 157–160, 489
 Overall (Lewis), 154–155, 160
 Drickamer-Bradford correlation, 155
 O'Connell correlation, 155
 performance data, 156
 Stanton number for heat transfer, 68–69
 Stanton number for mass transfer, 68, 70
 Stiff differential equations, 393, 491
 Euler implicit method, 393
 stiffness ratio, 365
 Stream variables, 126
 Stripping (stripper), 9, 12, 137, 146, 148–150
 design considerations, 143–144
 equipment, 138–143
 graphical design method, 144–147
 equilibrium curve, 146
 minimum stripping vapor flow rate, 146
 number of equilibrium stages, 146–147
 operating line, 146
 stage efficiency, 154–155
 Kremser algebraic design method, 148–150, 356–357
 operating conditions, 144
 rigorous design methods, 374–378, 380–393
 Stripping agent, 144
 Stripping factor, 149
 Stripping section, 122, 172, 197
 Sum-rates (SR) method, 286–287, 294–295
 Supercritical-fluid extraction, 320, 357–362
 Superficial velocity, 228
 Surface diffusion, 471, 474
 Surface renewal theory of Danckwerts, 75
- T**
 Temperature
 infinite surroundings, 38
 reference (datum), 20, 23
- Ternary liquid-liquid phase diagrams, 99–101, 242–243
 classes (type I and II), 242–243
 equilateral triangular, 99–101, 242–243
 right triangular, 250–251
- Thermal diffusivity, 69
- Thermodynamic properties
 departure equations, 26
 derived functions, 25–26
 excess functions, 34
 ideal mixtures, 20
 nonideal mixtures, 27–29
- Thermodynamics, 27
- Theorem of corresponding states, 23
- Thermal-swing adsorption (TSA), 476–477, 488–491
- Three-phase flash, 107–108
- Tie-line, 100, 107, 242, 244
- Tortuosity, 57, 504
- Transfer units, height of
 individual, 167, 176
 overall, 166–167, 176
- Transfer units, number of
 individual, 167
 overall, 166–167, 256
- Tray (plate), 139, 141, 300
 bubble-cap, 139–141
 diameter, 161–163
 entrainment, 161–163
 Fair correlation, 162
F-factor, 176
 foaming, 162
 flooding, 161–163
 downcomer, 161
 entrainment, 161
 Fair correlation, 162
 high-capacity, 163
 interfacial area, 165
 liquid flow passes, number of, 155–156
 mass transfer, 157–160
 perforated (sieve), 139–141
 pressure drop, 140, 164
 regimes of contacting, 138–140
 residence time, 140
 sieve, 139–141
 spacing, 161–162
 stable operation, limits, 161
 turndown ratio, 163, 176
 ultimate capacity, Stupin-Kister, 163
 valve, 139–141
- Trayed (plate) tower (column), 138–141
 height, 160
 Tray spacing, 161–162
- Tridiagonal matrix, 284, 291–292
- Turndown ratio, 163–176
- Two-section cascade, 118–119, 121–123, 193
- Two-film theory of Whitman, 76–78
 gas (vapor)–liquid case, 76–78
 liquid–liquid case, 78
- T*-*y*-*x* plot, 90
- U**
 Underwood equations, 273–275
 UNIFAC equation, 34–35
 UNIQUAC equation, 30, 33–34
 Upcomer, 235
- V**
 Valve cap, 139–141
 Valve-tray columns, 139–141
 Vapor-liquid-liquid system, 107–108
 Vapor pressure data, 22
 Velocity
 flooding, 161–163, 173
 interstitial, 483, 487
 superficial, 169
- Volume, molar, 20–21
- Vortex, 253–254
- VPE (vibrating-plate extractor), 238
- W**
 Water softening, 452, 502
 Weber number, 1791, 330
 Weeping, 139–140, 161
 Wilke-Chang equation, 53
 Wilson equation, 30–32
- Work
 lost, 37–39
 minimum, 38–39
- Y**
y-*x* plot, 90
- Z**
 Zeolites, 455, 457–458
 Zeotropic system, 89, 402

Physical Constants

Universal (ideal) gas law constant, R

$$1.987 \text{ cal/mol-K or Btu/lbmol-}^\circ\text{F}$$

$$8315 \text{ J/kmol-K or Pa-m}^3\text{/kmol-K}$$

$$8.315 \text{ kPa-m}^3\text{/kmol-K}$$

$$0.08315 \text{ bar-L/mol-K}$$

$$82.06 \text{ atm-cm}^3\text{/mol-K}$$

$$0.08206 \text{ atm-L/mol-K}$$

$$0.7302 \text{ atm-ft}^3\text{/lbmol-}^\circ\text{R}$$

$$10.73 \text{ psia-ft}^3\text{/lbmol-}^\circ\text{R}$$

$$1544 \text{ ft-lb}_f\text{/lbmol-}^\circ\text{R}$$

$$62.36 \text{ mmHg-L/mol-K}$$

$$21.9 \text{ in. Hg-ft}^3\text{/lbmol-}^\circ\text{R}$$

Atmospheric pressure (sea level)

$$101.3 \text{ kPa} = 101,300 \text{ Pa} = 1.013 \text{ bar}$$

$$760 \text{ torr} = 29.92 \text{ in. Hg}$$

$$1 \text{ atm} = 14.696 \text{ psia}$$

Avogadro's number

$$6.022 \times 10^{23} \text{ molecules/mol}$$

Boltzmann constant

$$1.381 \times 10^{-23} \text{ J/K-molecule}$$

Faraday's constant

$$96490 \text{ charge/g-equivalent}$$

Gravitational acceleration (sea level)

$$9.807 \text{ m/s}^2 = 32.174 \text{ ft/s}^2$$

Joule's constant (mechanical equivalent of heat)

$$4.184 \text{ J/cal}$$

$$778.2 \text{ ft-lb}_f\text{/Btu}$$

Planck's constant

$$6.626 \times 10^{-34} \text{ J-s/molecule}$$

Speed of light in vacuum

$$2.998 \times 10^8 \text{ m/s}$$

Stefan-Boltzmann constant

$$5.671 \times 10^{-8} \text{ W/m}^2\text{-K}^4$$

$$0.1712 \times 10^{-8} \text{ Btu/h-ft}^2\text{-}^\circ\text{R}^4$$

WILEY END USER LICENSE AGREEMENT

Go to www.wiley.com/go/eula to access Wiley's ebook EULA.